LLR.20071004.0002

QA: NA

TDR-WIS-PA-000014 REV 00

October 2007

TSPA Information Package for the Draft Supplemental Environmental Impact Statement

Prepared for:
U.S. Department of Energy
Office of Civilian Radioactive Waste Management
Office of Repository Development
1551 Hillshire Drive
Las Vegas, Nevada 89134-6321

Prepared by:
Sandia National Laboratories
OCRWM Lead Laboratory for Repository Systems
1180 Town Center Drive
Las Vegas, Nevada 89144

Under Contract Number
DE-AC04-94AL85000

DISCLAIMER

This report was prepared as an account of work sponsored by an agency of the United States Government. Neither the United States Government nor any agency thereof, nor any of their employees, nor any of their contractors, subcontractors or their employees, makes any warranty, express or implied, or assumes any legal liability or responsibility for the accuracy, completeness, or any third party's use or the results of such use of any information, apparatus, product, or process disclosed, or represents that its use would not infringe privately owned rights. Reference herein to any specific commercial product, process, or service by trade name, trademark, manufacturer, or otherwise, does not necessarily constitute or imply its endorsement, recommendation, or favoring by the United States Government or any agency thereof or its contractors or subcontractors. The views and opinions of authors expressed herein do not necessarily state or reflect those of the United States Government or any agency thereof.

QA: NA

TSPA Information Package for the Draft Supplemental Environmental Impact Statement

TDR-WIS-PA-000014 REV 00

October 2007

CONTENTS

CONTENTS (Continued)

Page

CONTENTS (Continued)

Page

CONTENTS (Continued)

Page

CONTENTS (Continued)

Page

CONTENTS (Continued)

CONTENTS (Continued)

Page

CONTENTS (Continued)

Page

FIGURES

FIGURES (Continued)

Page

FIGURES (Continued)

FIGURES (Continued)

FIGURES (Continued)

Page

FIGURES (Continued)

FIGURES (Continued)

FIGURES (Continued)

FIGURES (Continued)

FIGURES (Continued)

FIGURES (Continued)

Page

FIGURES (Continued)

Page

TABLES

TABLES (Continued)

TABLES (Continued)

Page

TABLES (Continued)

TABLES (Continued)

TABLES (Continued)

TABLES (Continued)

TABLES (Continued)

EXECUTIVE SUMMARY

ES1. SCOPE

ES1.1 Introduction

The *Total System Performance Assessment–Supplemental Environmental Impact Statement Information Package* (TSPA-SEIS) for the Draft SEIS describes the method, structure, validation or confidence building, and application of a computational model of the performance of the repository system, the Total System Performance Assessment Model, that was developed to support the SEIS. The TSPA-SEIS is part of the evaluation of a geologic repository for safe disposal of spent nuclear fuel (SNF) and high-level radioactive waste (HLW) at Yucca Mountain. The TSPA-SEIS is one of an iterative series of performance assessments conducted during the progress of the Yucca Mountain Project. The TSPA-SEIS evaluates the ability of the repository to adequately isolate nuclear waste meeting standards for exposure during the first 10,000 years following repository closure according to the NRC Proposed Rule 10 CFR 63.311(a)(1) [DIRS 178394], and additional standards until the period of geologic stability (approximately one million years after repository closure) according to NRC Proposed Rule 10 CFR 63.311(a)(2) [DIRS 178394]). Figure ES-1 shows the Yucca Mountain area and the entrance to the underground facilities, which will become part of the repository after a license to construct the repository is granted. Figure ES-2 shows a timeline of the major legislative and regulatory actions bearing on the Yucca Mountain Project from 1980 to the present. Among the regulatory mandates of NRC Proposed Rule 10 CFR Part 63 [DIRS 178394] is the requirement to demonstrate, by means of risk-informed assessment, the reasonable expectation of waste isolation after closure of the repository (10 CFR 63.304 [DIRS 180319]).

The TSPA-SEIS for the draft SEIS evaluates the performance of engineered and natural components of the Yucca Mountain repository system for the expected natural conditions prevailing at the Yucca Mountain site (referred to as the Nominal Scenario Class), considers the effect on repository performance of unexpected early failure of the engineered components of the repository system, and evaluates the impact on repository performance due to natural disruptive events, such as igneous activity and seismic events. The development of the process models, submodels, and other components included in the TSPA-SEIS can be found in the supporting analysis model reports that are referenced in appropriate sections of this report. The technical basis for the TSPA-SEIS includes field, laboratory, and natural-analogue data obtained during the conduct of the Yucca Mountain Site Characterization phase of the project.

ES1.2 Governing Regulations

The TSPA-SEIS supports evaluations of the performance of the Yucca Mountain repository system under the relevant postclosure regulatory requirements promulgated in NRC Proposed Rule 10 CFR 63, Subparts E and L [DIRS 178394] and [DIRS 180319]. The TSPA-SEIS was also used to address the criteria related to postclosure performance described in *Yucca Mountain Review Plan, Final Report* (NRC 2003 [DIRS 163274], Section 2.2), and agreement items associated with the NRC's Key Technical Issues (Reamer 2001 [DIRS 158380], Attachment 1). The TSPA-SEIS serves as part of the overall U.S. Department of Energy (DOE) strategy to

provide for the safe disposal of SNF and HLW, a process comprising the following five steps, as illustrated by Figure ES-3:

Step 1: Define the goals and boundary conditions of the TSPA-SEIS, according to regulations promulgated by the U.S. government.

Step 2: Develop the design for the Yucca Mountain repository so that the repository will meet the regulatory standards, including the contributions to repository performance of both natural and engineered barriers to radionuclide migration from the repository.

Step 3: Identify and evaluate features, events, and processes (FEPs) potentially relevant to the long-term performance of a waste-disposal repository, screen the identified FEPs, and use relevant FEPs to establish scenario classes for use in assessing estimated repository performance.

Step 4: Develop and use the TSPA-SEIS to estimate repository performance.

Step 5: Analyze and interpret the results of the model simulations of repository performance with respect to the performance measures established by the regulations.

The draft TSPA-SEIS addresses Step 4 of that process, as informed by the preceding steps, to provide information for Step 5, which describes the results.

In particular, the draft TSPA-SEIS calculates:

a) Annual doses to the REMI from releases from the undisturbed Yucca Mountain disposal system (NRC Proposed Rule 10 CFR 63.311)

b) Annual doses to the REMI to the REMI from releases from Yucca Mountain disposal system resulting from human intrusion (NRC Proposed Rule 10 CFR 63.321)

c) Levels of radioactivity in the representative volume of groundwater of 3,000 acre ft. (NRC Proposed Rule 10 CFR 63.331).

ES2. TOTAL SYSTEM PERFORMANCE ASSESSMENT METHODOLOGY

The general TSPA process adopted by the DOE follows the methodology developed by Cranwell et al. (1990 [DIRS 101234], Sections 2 and 3). Over time, the methodology has been enhanced, including input from the NRC, and applied to numerous projects by various international organizations involved in radioactive waste management. Figure ES-4 shows the major steps in the performance assessment (PA) modeling process. Previous PAs and related supplemental analyses of the performance of the Yucca Mountain repository were conducted to meet various regulatory milestones, following the publication of the Nuclear Waste Policy Amendments Act of 1987, Public Law No. 100-203 [DIRS 100016]. The Yucca Mountain TSPAs have been iterative, with each succeeding PA building on and extending the scope and results of the

previous TSPAs by incorporating both an improved understanding of the processes affecting performance and, through additional field observations and laboratory analyses, better identification and quantification of the parameters used in the TSPAs. Figure ES-5 illustrates the evolution of the TSPA iterations for the Yucca Mountain Project. The most recent TSPA documents were the *Total System Performance Assessment for the Site Recommendation,* TDR-WIS-PA-000001 REV 00 ICN 01 (CRWMS M&O 2000 [DIRS 153246]) and the application of the Total System Performance Assessment-Site Recommendation (TSPA-SR) Model to the *Total System Performance Assessment – Analyses for Disposal of Commercial and DOE Waste Inventories at Yucca Mountain – Input to Final Environmental Impact Statement and Site Suitability Evaluation,* REV 00 ICN 02 (Williams 2001 [DIRS 157307]).

The TSPA-SEIS is built on the foundation of the earlier PAs and enhanced by updated analyses of the processes affecting Yucca Mountain and the design elements of the repository, including a comprehensive consideration of the FEPs that are relevant to repository system performance. The previous comprehensive TSPA model used for simulating repository performance was the TSPA-SR/Final Environmental Impact Statement (FEIS) model, which adapted, but did not fundamentally change, the TSPA-SR model, *Total System Performance Assessment for the Site Recommendation,* TDR-WIS-PA-000001 REV 00 ICN 01 (CRWMS M&O 2000 [DIRS 153246]) to analyze the specific requirements of the Final Environmental Impact Statement and the impacts of the final rules of the U.S. Environmental Protection Agency and the NRC that regulate the disposal of SNF and HLW (*Total System Performance Assessment – Analyses for Disposal of Commercial and DOE Waste Inventories at Yucca Mountain – Input to Final Environmental Impact Statement and Site Suitability Evaluation,* REV 00 ICN 02 (Williams 2001 [DIRS 157307])).

Figure ES-6 represents the TSPA process as a pyramid. The foundation of the pyramid consists of a system characterization involving assimilation of the information collected by scientists and engineers involved in site characterization and engineering design. The repository system and site characterization provides information regarding waste properties, facility design, regional geology, regional hydrology, and environmental characteristics of the Yucca Mountain site. The broad foundation of the pyramid represents the more than 20-year body of knowledge, collected in the field and in the laboratory, regarding the Yucca Mountain repository system. These data were used to identify the set of possible FEPs that may be part of and affect the performance of the repository system. This body of knowledge also provides the basis for the second stage of the TSPA pyramid.

The next stage of the TSPA pyramid consists of the development and testing of models that include the retained FEPs, and their outcomes regarding repository performance. The models consist of sets of hypotheses, assumptions, simplifications, and idealizations that, together, describe the essential aspects of a system or subsystem of the repository relative to performance. An example of such a model is a model that describes the movement of water and dissolved radionuclides by diffusive flow in rock pores or by advective flow in fracture openings in the unsaturated bedrock surrounding the repository and through the saturated zone (SZ) below the repository. Because the TSPA process deals with future outcomes and includes uncertainty in both process descriptions and parameter values, an essential element of the TSPA process is to capture uncertainty in probabilistic analyses that represent likely outcomes, based on the best available values of the models' parameters and the processes involved.

The next stage of the PA pyramid involves development of abstracted models. These abstractions are progressive simplifications of the detailed models of physical and chemical processes to more compact, efficient numerical models. Abstractions consist of statistical or mathematical abstractions, including look-up tables, equations representing response surfaces, probability distributions, linear transfer functions, or reductions of model dimensionality. The abstractions used to analyze the projected evolution through time of the various components of the repository system are compact but still capture the salient features of the process models, along with their associated uncertainties.

The top level of the PA pyramid consists of the integrated total system models. The total system model is a numerical model that is used to simulate the integrated behavior of the entire Yucca Mountain repository system. The TSPA-SEIS incorporates the abstracted detailed models and that describe the TSPA-SEIS components, and their submodels, from their development to their implementation, including information from the analysis model reports. The abstractions and associated process models and submodels describing various repository attributes in a series of analysis model reports form the technical basis for the TSPA-SEIS.

The attributes of both natural and engineered systems comprising the total repository system, as illustrated on Figure ES-7 include:

- Limited water entering emplacement drifts and coming into contact with the waste packages (WPs) and, subsequently, the waste forms
- Prolonged lifetimes of WPs and drip shields (DSs)
- Gradual and limited radionuclide mobilization and release from the repository's engineered barrier system (EBS)
- Retarded radionuclide transport by means of retardation and dilution in natural hydrogeologic systems after release from the EBS
- Low mean annual dose to receptors, even considering potential disruptive events.

Use of the TSPA-SEIS to simulate Yucca Mountain repository behavior and project future outcomes is aided by the development of scenario classes to assist in the analysis of repository performance and provide the framework for the TSPA-SEIS analyses. The TSPA-SEIS is structured to address a specific set of scenario classes that span the range of possible FEPs for both expected conditions and disruptive events. The TSPA-SEIS scenario classes, which represent a range of future outcomes, include the Nominal (undisturbed) Scenario Class, the Early Failure Scenario Class, and two disruptive event scenario classes, the Igneous Scenario Class and the Seismic Scenario Class.

This document contains references to the supporting analysis model reports for the model abstractions that are included in the TSPA-SEIS. Other information from the documents supporting the process models and their abstractions are included in the electronic GoldSim model file for the TSPA-SEIS, along with additional references to the parameter values and distributions of parameter values that are incorporated in the TSPA-SEIS.

ES3. TSPA-SEIS DEVELOPMENT PROCESS

The TSPA-SEIS was developed to support the evaluation of a geologic repository for the safe disposal of SNF and HLW at Yucca Mountain, Nevada. The TSPA-SEIS was developed to analyze the ability of the natural and engineered systems of the Yucca Mountain repository to isolate nuclear waste from the biosphere. The TSPA-SEIS evaluates repository performance for the first 10,000 years following repository closure and for the period of geologic stability, understood at NRC Proposed Rule 10 CFR 302 to be one million years after repository closure.

ES3.1 Features, Events and Processes Analysis

The development of the TSPA-SEIS for the Yucca Mountain repository system began, as is shown on Step 3 of Figure ES-3, with a thorough analysis and screening of the FEPs that could affect repository performance after closure. The results of the FEPs analyses led to the development of process models and abstractions that address the attributes necessary to allow the TSPA-SEIS to assess repository safety, and to determine whether or not the repository meets regulatory standards. These process models and their abstractions considered FEPs that could affect the Yucca Mountain repository system and, in turn, FEPs that could be affected by the presence of the repository.

Figure ES-8 is a schematic representation of the development of the TSPA-SEIS and describes, for analysis purposes, the repository system divided into individual model components. Each individual model component represents a major process or set of processes of the total repository system. Figure ES-9 shows the model component areas as well as the disruptive events scenario classes that are included in analyses of repository performance. Figure ES-10 shows the principal components and supporting submodels of the Yucca Mountain repository system.

ES3.2 Development of the Scenario Classes

A scenario is a well-defined, connected sequence of FEPs that describes a possible future condition of the repository system. A scenario class is a set of related scenarios that share sufficient similarities that they can usefully be aggregated for the purposes of screening or analysis. The objective of scenario development for the TSPA-SEIS Model is to define a limited set of scenario classes that are representative of the range of future FEPs that are potentially relevant to the licensing of the facility.

The TSPA-SEIS approach focuses on a set of scenario classes that are distinguished by initiating events. The Nominal Scenario Class includes all possible future outcomes except those initiated by early failure of the drip shields or waste packages, and igneous or seismic activity. The Igneous Scenario Class includes all possible future outcomes initiated by igneous activity; and the Seismic Scenario Class includes all possible futures initiated by seismic activity. In addition to the analyses of the Scenario Classes, the TSPA-SEIS also simulates a Human Intrusion Scenario according to the scenario and criteria described in NRC Proposed Rule 10 CFR 63.322 ([DIRS 180319]).

Modeling cases are used in the TSPA-SEIS to represent scenario classes and to calculate estimates of performance measures for the repository system. The model for TSPA-SEIS starts with the Nominal Scenario Class, which incorporates all expected FEPs describing the

fundamental processes at work under ambient conditions without disruptive events, as well as possible changes to those processes.

The Early Failure Modeling Cases address FEPs that describe early waste package (WP) and drip shield (DS) failure due to manufacturing and material defects and pre-emplacement operations, including improper heat treatment of the WPs.

The Igneous Intrusion Modeling Case addresses the FEPs for the possibility that magma, in the form of a dike, could intrude into repository drifts, destroying DSs and WPs in those drifts intruded by the magma, exposing the waste forms to percolating water that could mobilize radionuclides from the waste forms and transport the radionuclides through the UZ and SZ to the reasonably maximally exposed individual (RMEI). The Volcanic Eruption Modeling Case addresses FEPs that describe a volcanic conduit (or conduits) that invades the repository, destroys WPs, and erupts at the land surface. The volcanic eruption disperses volcanic tephra and entrained waste under atmospheric conditions, and deposits the contaminated tephra on land surfaces where the contaminated tephra becomes subject to redistribution by soil and near-surface hydrogeologic processes.

Seismic disruption of the repository is addressed by two modeling cases that analyze possible seismic disruption of the repository and its effect on repository performance. The Seismic Ground Motion (GM) Modeling Case addresses FEPs concerning damage to WPs and DSs due to vibrating ground motion. The Seismic Fault Displacement (FD) Modeling Case includes the effects of fault displacement on WPs and DSs. FEPs that describe localized corrosion of WPs and DSs are also included in this modeling case because fault displacement could cause disruption of the DSs associated with damaged WPs. Disruption of the DSs could result in the possibility of crown seepage that, in turn, could induce localized corrosion. This modeling case includes advection and diffusion of mobilized radionuclides out of the WP breaches.

The TSPA-SEIS considers a human intrusion scenario in a stylized calculation that simulates a future drilling operation in which an intruder drills a land-surface borehole using a drilling apparatus operating under the common techniques and practices currently employed in exploratory drilling for groundwater in the region around Yucca Mountain. During drilling, the drilling apparatus directly intersects a degraded DS and WP causing a release of waste and continues subsequently into the SZ underlying Yucca Mountain. The TSPA-SEIS simulated a human intrusion scenario occurring approximately 200,000 years after repository closure.

ES3.3 Incorporation of Uncertainty

Uncertainty and variability in the expected behavior of the Yucca Mountain repository system requires that TSPA-SEIS analyses be probabilistic in order to capture the full range of potential outcomes.

Uncertainty in the TSPA-SEIS is characterized as either epistemic or aleatory uncertainty where:

- **Epistemic Uncertainty**, also referred to as "reducible" uncertainty, concerns the state of uncertainty in knowledge about a parameter value due to limited data or alternative interpretations of the available data. Epistemic uncertainty can be reduced, in principle,

using the results of experimental testing and additional data collection. However, given the complexity of nature and the variability observed over time and space in natural phenomena, there are practical limits below which many uncertainties cannot be reduced, neither is their reduction necessary once there is a sound technical basis for finding that a proposed system is likely to be sufficiently safe to allow moving forward to the next phase of its development. Scientific work continues at a significant level until the final closure and sealing of the repository, allowing safety evaluations to be informed by new information and repeated in advance of subsequent decision-points in the repository's life.

- **Aleatory Uncertainty,** also referred to as "irreducible" uncertainty, concerns whether or not there is a chance occurrence of a feature, event, or process. No amount of exploratory work will allow determining whether or not a chance event will or will not occur at any given time, but determining a range of likelihoods-of-occurrence for a given timeframe is generally supportable through using various formalized means for combining scientific insights from experts in the field.

The TSPA-SEIS utilizes multiple realizations to calculate future outcomes using distributions of values for uncertain parameters that may be important to performance, rather than deterministic or single-value calculations for each parameter in the repository system. The model realizations are performed using various combinations of parameter values obtained from the parameter-value distributions in the TSPA Input Database, where each of the combinations of parameter values is representative of a subset of the full range of potential outcomes. These probabilistic analyses thus reflect an appropriate range of process behaviors or parameter values, or both, of the inherently variable Yucca Mountain repository system, given that complete knowledge of the system is not attainable.

ES3.4 Natural and Engineered Model Components

The TSPA-SEIS of the Yucca Mountain repository system is based on several natural and engineered model components. These principal model components of the TSPA-SEIS function as follows (Figure ES-9):

- UZ Flow describes fluid flow through the unsaturated welded and nonwelded tuffs above and below the repository.

- The EBS Environment describes the coupled processes in the environment surrounding and within the engineered elements of the repository.

- WP and DS Degradation describes the responses of these engineered systems to heat, humidity, seepage, and the geochemical environment of the EBS.

- Waste Form Degradation and Mobilization describes the degradation and dissolution of the waste forms and the release of radionuclides from the WPs.

- EBS Flow and Transport describes the flow of water and the transport of radionuclides from the repository to the UZ below the repository.

- UZ Transport describes the transport of radionuclides released from the repository through the UZ below the repository to the SZ.

- SZ Flow and Transport describes water flow and radionuclide transport from beneath the repository and downgradient through saturated rocks and alluvium, to the RMEI.

- Biosphere describes the biologic uptake of radionuclides, including inhalation, ingestion, and water consumption by humans at the site of the RMEI; the biosphere model component also includes consumption of bio-accumulated radionuclides in plants and animal food products.

- In addition, the TSPA-SEIS considers disruptive events and describes the potential effects on the repository and the surrounding environment in response to igneous and seismic events.

ES3.5 Alternative Conceptual Models

A conceptual model is a set of working hypotheses and assumptions that provide an acceptable description of a system for its intended purpose. Because the TSPA process deals with future outcomes and includes uncertainty in both process descriptions and parameter values, there may be several alternative conceptual models (ACMs) that provide reasonable descriptions of a particular system or subsystem. Considering ACMs helps build confidence that plausible changes in modeling assumptions or simplifications will not change conclusions regarding subsystem and total-system performance. Each model component and submodel discussion includes a summary evaluation of ACMs. Since ACMs must be compatible with all known data and established facts, their number is limited. Typically, when the two or more models exist for the same phenomena and data, the more conservative one from a total-system perspective has been chosen for implementation. Another approach is to assign probabilities to each ACM and probabilistically bring them into the calculations according to their relative frequencies, but this approach places a greater demand on knowledge and adds complexity that is avoided by the more conservative approach.

ES3.6 Configuration Management for the TSPA-SEIS

The TSPA-SEIS describes how the supporting parameter values, along with the process-model abstractions, representing many different aspects of the Yucca Mountain repository system, were integrated into one comprehensive PA model, and used to estimate future repository performance. Appropriate restrictions were built into the TSPA-SEIS during its development to help ensure that the process-model abstractions were used only within their range of applicability.

The numerical abstractions of the process models were integrated in the TSPA-SEIS using software called GoldSim. The GoldSim software implements the TSPA-SEIS and simulates repository performance and calculates potential dose to the RMEI. The software used for the TSPA-SEIS is subject to the Yucca Mountain Project Quality Assurance program and controlled through the Software Configuration Management system to ensure that calculations are traceable to controlled software. The TSPA-SEIS simulations are conducted on computers and servers in

a controlled environment. The TSPA-SEIS simulations are recorded, and the results are stored in the Yucca Mountain Technical Data Management System.

A number of software codes were implemented to support the development of the TSPA-SEIS. Some of these codes were used to provide supporting information, and some codes were directly implemented in the TSPA-SEIS using the GoldSim simulation software. Supporting software codes, including process models, were developed and operated externally before running the TSPA-SEIS. Software codes directly implemented as dynamically linked libraries (DLLs) in the TSPA-SEIS are generally referred to as abstractions and are run within the TSPA-SEIS. All software codes used to support the TSPA-SEIS are qualified and are under configuration control. Each qualified software code is uniquely identified with the software name, tracking number, version number, hardware platform, and operating system under which the code was qualified. All software documentation, including the software media, is linked to the unique tracking number.

Input parameter values are controlled through the TSPA Input Database. The database supports the TSPA-SEIS by providing the parameter values and distributions of these parameter values necessary for the TSPA analysis of the repository. The TSPA Input Database categorizes, stores, and retrieves fixed and distributed values of the TSPA-SEIS parameters, and allows qualified, authorized analysts to review and update parameter values. The TSPA Input Database has strict user controls, featuring read and write access and audit trails that ensure the security, integrity, and traceability of the information used in the TSPA-SEIS analyses.

The TSPA-SEIS handles both the multiple-realization requirement and the maximum size of individual coupled submodels. The GoldSim software fulfills these requirements using an efficient solver that minimizes run time for each individual realization. The Monte Carlo sampling structure in GoldSim allows the software to simultaneously run multiple realizations, then reassembles the results from these realizations into an ensemble result from the entire probabilistic run. Further, GoldSim acts as a driver, or integration software, that can couple other large pieces of software for those process models and submodels that were not converted to response surfaces, but are run concurrently in the TSPA-SEIS. A separate software code, EXDOC 2.0 (EXDOC_LA V. 2.0. 2007 [DIRS 182102]), uses the GoldSim results to compute mean and median potential dose histories.

ES4. YUCCA MOUNTAIN SITE DESCRIPTION

The Yucca Mountain repository system consists of natural and engineered systems that together will ensure the safe disposal of radioactive materials. The following provides a brief overview of the Yucca Mountain site and context for the development of the TSPA-SEIS.

The characteristics of the natural systems at Yucca Mountain that affect repository performance include climate, site geology, and site hydrogeology. The characteristics of the site geology and hydrogeology that affect repository performance include groundwater flow through the UZ and SZ, radionuclide transport, and disruptive events caused by igneous and seismic activity (BSC 2004 [DIRS 169734]). The Yucca Mountain repository system lies in the Great Basin physiographic province. Characteristics of the natural system at Yucca Mountain that aid in repository performance include a semiarid climate, relatively stable site geology, a deep water

table, and limited groundwater flow through the UZ and SZ. The Yucca Mountain area has a low incidence of large magnitude seismic activity, and volcanic activity in the Yucca Mountain region has declined through recent geologic time as described in *Igneous Activity at Yucca Mountain: Technical Basis for Decision Making,* (NRC 2007 [DIRS 182132], Sections 2 and 3).

ES4.1 Physiographic Setting and Topography

Yucca Mountain is located within a transition zone between the northern boundary of the Mojave Desert and the southern boundary of the Great Basin Desert. The topography in this region is characterized by isolated, long and narrow, roughly north-south-trending mountain ranges and broad intervening valleys (Figure ES-11). The topography in the Yucca Mountain vicinity was shaped by erosional processes on the eastward-sloping ridge of the mountains, and along faults and fault scarps that have created a series of washes downcut to varying degrees into different bedrock formations (Figure ES-12).

ES4.2 Climate

Current climatic conditions for the repository site and the Yucca Mountain region are discussed in *Yucca Mountain Site Description* (BSC 2004 [DIRS 169734], Section 6.3). The Yucca Mountain Project environmental program collected site climate and meteorological data using a network of nine automated weather stations (BSC 2004 [DIRS 169734], Section 7.1.3.2). The climate data show that the mountains west of Yucca Mountain cause a rain shadow effect causing the present-day Nevada climate to be semiarid to arid, with dry winds and low precipitation. The climatic factors that most affect water-transport processes in the Yucca Mountain UZ are solar radiation-intensity flux; diurnal and seasonal temperature cycles; relative humidity; and precipitation, in the form of either rain or snow as well as extended periods of drought.

ES4.3 Geology

Yucca Mountain is an uplifted, block-faulted ridge of alternating layers of Miocene age welded and nonwelded volcanic tuffs. The major Yucca Mountain geologic units are the volcanic tuff formations of the Paintbrush Group, the Calico Hills Formation, and the Crater Flat Group. For purposes of hydrogeologic studies, including infiltration, *Yucca Mountain Site Description,* (BSC 2004 [DIRS 169734], Tables 3-1, 3-5, and 7-1)) provides a separate stratigraphic nomenclature based on the degree of welding and hydrologic property distributions. The major hydrogeologic units are divided into the Tiva Canyon welded; the Paintbrush nonwelded, which consists primarily of the Yucca Mountain and Pah Canyon members and interbedded tuffs; the Topopah Spring welded; the Calico Hills nonwelded; and the Crater Flat undifferentiated units (Ortiz et al. 1985 [DIRS 101280], pp. 7 to 14, Table 1). Figure ES-13 shows the spatial relationship of the major hydrogeologic units of the UZ in both perspective, and north-south and east-west cross-sectional views.

ES4.4 Regional Tectonic Setting

Igneous Activity at Yucca Mountain: Technical Basis for Decision Making, (NRC 2007 [DIRS 182132], Section 2) describes the tectonic setting in terms of the geologic framework or structural geologic configuration (or both) of the different rock masses in the Yucca Mountain

vicinity. The overall tectonic setting of the Great Basin physiographic province, including Yucca Mountain, is extensional, generally consisting of fault-bounded basins and mountain ranges that have been modified by volcanic activity during the past 15 million years. Typically, faults in the Great Basin include normal and strike-slip faults that reflect the extensional deformation caused by plate tectonic interactions at the western margin of the North American continent. The structural geology of Yucca Mountain and its vicinity is dominated by north-stretching normal faults with movement down to the west (Figures ES-14 and ES-15). Some of the faults on Figure ES-14 show evidence of quaternary activity (i.e., within the last 1.8 million years). Figure ES-15 shows that Yucca Mountain is a large eastward tilting block bounded by the Solitario Canyon fault to the west and the Bow Ridge fault to the east.

ES4.5 Local Volcanism

Two types of volcanism have occurred in the Yucca Mountain region. An early phase of Miocene silicic volcanism in the southwestern Nevada volcanic field culminated between 11.8 and 12.4 million years ago, with the eruption of four voluminous ash-flow tuffs of about 1,000 km^3 each (*Igneous Activity at Yucca Mountain: Technical Basis for Decision Making,* (NRC 2007 [DIRS 182132], Section 3.2.1; Sawyer et al. 1994 [DIRS 100075], pp. 1311 and 1312). One of the silicic ash-flow tuffs that erupted from the Timber Mountain Caldera Complex (Figure ES-16) is the Topopah Spring Tuff, which forms the repository horizon planned for waste emplacement. Yucca Mountain is an uplifted, erosional remnant of these ash-flow tuff deposits.

Small-volume basaltic volcanism continued into the Quaternary Period. In terms of eruption volume, the 15-million-year history of volcanism in the region is viewed as a magmatic system that peaked between 11 and 13 million years ago, with the eruption of over 5,000 km^3 of ash-flow tuffs. Following this peak of eruptive activity, relatively minor volumes of basalt have erupted in the last 11 million years (BSC 2004 [DIRS 169989], Section 6.1.1.1). Considered in terms of total eruption volume, frequency of eruptions, and duration of volcanism, basaltic volcanic activity in the region, including Yucca Mountain, defines one of the least active basaltic volcanic fields in the western United States (e.g., *Synthesis of Volcanism Studies for the Yucca Mountain Site Characterization Project* (CRWMS M&O 1998 [DIRS 105347], Chapter 2)).

ES4.6 Hydrology

ES4.6.1 Surface Hydrology

Yucca Mountain is located in the Amargosa River drainage basin, which is the major tributary drainage area to Death Valley (Figure ES-11). Stream flow from Yucca Mountain is captured by local drainages to the Amargosa River. The Amargosa River and its tributaries are ephemeral streams that are dry most of the time, with surface water-flow occurring rarely in direct response to precipitation. In some cases, groundwater discharges at springs in stream channels. During episodic flooding, flow occurs along the Amargosa River and flows to and fills much of the Death Valley playa to depths of 0.3 m (1 ft) or more (Miller 1977 [DIRS 105462], p. 18). During periods of cooler and wetter climate periods, such as 140,000 to 175,000 years ago, Death Valley was filled with water to depths of 175 m. Throughout the Yucca Mountain region

and the Death Valley basin, perennial flow is only observed downgradient from spring discharges and around the margins of playas, where the groundwater discharges at land surface.

ES4.6.2 Groundwater Hydrology

Yucca Mountain is located in the Death Valley Regional Groundwater System (Figure ES-17). Groundwater below Yucca Mountain and in the surrounding region flows generally south toward discharge areas in the Amargosa Desert and Death Valley. The area around Yucca Mountain is in the central subregion of the Death Valley Regional Groundwater System, which has three groundwater basins: Pahute Mesa-Oasis Valley, Ash Meadows, and Alkali Flat-Furnace Creek. The primary sources of groundwater recharge are infiltration on Pahute Mesa, Rainier Mesa, Timber Mountain, and Shoshone Mountain to the north, and the Grapevine and Funeral Mountains to the south (Figures ES-11 and ES-17). Recharge in the immediate Yucca Mountain vicinity is low, consisting of water reaching Fortymile Wash (Figure ES-17), as well as precipitation that infiltrates into the subsurface.

ES5. THE REPOSITORY SUBSURFACE FACILITY AND ENGINEERED BARRIER SYSTEM

ES5.1 Layout

Note: The following information regarding the repository subsurface facility and the EBS describes the design analyzed by the TSPA-SEIS, and may be updated. The design layout of the Yucca Mountain repository subsurface facility is illustrated on Figure ES-18 and aspects of the design are described in *Total System Performance Assessment Data Input Package for Requirements Analysis for TAD Canister and Related Waste Package Overpack Physical Attributes Basis for Performance Assessment* (SNL 2007 [DIRS 179394]) and in *Total System Performance Assessment Data Input Package for Requirements Analysis for Subsurface Facilities* (SNL 2007 [DIRS 179466], Table 4-1, Parameter Number 01-02). The waste emplacement drifts will be excavated to a diameter of 5.5 m and a nominal length of 600 m (actual lengths will range from 355 to 808 m), using a tunnel boring machine. Emplacement drifts will accommodate the 70,000 metric tons of heavy metal waste inventory scheduled for emplacement in the repository and are planned with a uniform spacing of 81 m between their centerlines. Each emplacement drift will have a capacity of approximately 100 WPs. An area in the southern section of the repository will be constructed to allow for contingencies during emplacement. The emplacement drift area will be excavated in the Topopah Spring Tuff upper lithophysal unit, Topopah Spring Tuff middle nonlithophysal unit, Topopah Spring Tuff lower lithophysal unit, and the Topopah Spring Tuff crystal-poor lower nonlithophysal unit of the repository host horizon. Eighty percent of the excavation will be in the lower lithophysal unit. The lithophysal rock units contain numerous cavities (lithophysal) of varying size and, consequently, high porosities. The nonlithophysal rock units are highly fractured, and, are characterized by fewer cavities, lower porosities, and have longer fractures than the lithophysal rock units.

ES5.2 Engineered Barrier System

The principal features of the EBS are a titanium-alloy DS and a two-layer WP to contain the waste. Figure ES-19 is a cross-section illustration of an emplacement drift and the major components of the EBS. The EBS includes ground support, a corrosion-resistant waste-emplacement supporting pallet, and an invert at the base of the drift filled with crushed welded tuff, which will have a steel infrastructure.

ES5.2.1 Ground Support

The repository subsurface ground-support system will be used to maintain drift stability in lithophysal and nonlithophysal rocks. Ground support will consist of friction-type, nongrouted rock bolts and a perforated steel sheet covering the upper 240 degrees of the drift-wall circumference above the invert. The perforations in the steel-sheet liner will provide flexural strength and allow air circulation for moisture removal behind the perforated sheet. Cementitious materials will not be used for the emplacement drifts ground support because of uncertainties related to potential chemical effects on the long-term performance of the repository. However, cement may be used in the turnouts from the access ways to the emplacement drifts.

ES5.2.2 Drip Shield

The emplacement drifts will be equipped with titanium interlocking DSs designed to reduce the effects of rockfall and seepage dripping on the WPs. The linked DSs will form a single continuous barrier for the entire length of each emplacement drift. The DSs will be fabricated from Titanium Grade 7 plates, with Titanium Grade 24 for structural support, and Alloy 22 for the base plates, which will prevent direct contact between titanium and the steel members of the invert.

ES5.2.3 Waste Package

The WPs will consist of an outer shell and an inner shell. The 25-mm-thick outer shell will be composed of corrosion-resistant Alloy 22. The 50-mm-thick stainless-steel inner shell will serve three functions: (1) the inner shell will provide structural strength to resist rockfall, support the internal waste form components, allow the WPs to be supported by the emplacement pallets, and facilitate handling; (2) the inner shell will provide radiation shielding to reduce the exterior surface contact dose rate; and (3) the inner shell will provide limited containment for the radioactive waste inside the WPs, although the TSPA-SEIS analyses do not consider this containment. The CSNF reference WPs also contain stainless steel transport aging and disposal canister that is 25-mm-thik and designed to hold 21 pressurized water reactor or 44 BWR SNF assemblies. The co-disposed (CDSP) WP is designed to contain five defense HLW glass canisters surrounding a central canister of DOE owned spent nuclear fuel (DSNF).

ES5.2.4 Emplacement Pallet

An emplacement pallet will support each WP emplaced in the repository. The emplacement pallets will prevent the WPs from coming in contact with the invert and any invert moisture. The emplacement pallet will be constructed of Alloy 22, a material that will provide long-term corrosion resistance and will provide that an identical material will be in contact with the WP

outer shell. The emplacement pallets will be annealed to remove stresses from welding and fabrication and minimize the potential for corrosion.

ES5.2.5 Invert

The invert will provide support for the WP emplacement pallets and the DSs. The invert will consist of a steel support structure and a crushed welded tuff ballast derived from the repository host rock. The ballast will be placed in and around the steel invert infrastructure to an elevation just below the top of the pallets' longitudinal and transverse support beams. The invert ballast will be compacted to prevent long-term settlement.

ES5.2.6 Waste Form

CSNF is composed of uranium oxide and the majority of DSNF consists of uranium oxide. HLW will be mixed and solidified in a high-temperature, lanthanum borosilicate glass for storage in stainless-steel canisters. Following breaching of the CSNF WPs and CDSP WPs and exposure of the waste to water infiltrating the WPs, the waste forms will be subject to aqueous dissolution and release of radionuclides. All waste forms will release radionuclides at different rates depending on their integrity and the solubility of the constituents of the waste.

ES5.2.7 Waste Form Cladding

SNF generally is encased in a metallic protective cladding. After the cladding is breached, the waste forms can degrade and release radionuclides to the EBS environment. The TSPA-SEIS takes no barrier credit for CSNF cladding. In addition, DSNF cladding is considered to be failed upon receipt. Therefore, the TSPA-SEIS does not take credit for waste-form cladding.

ES5.2.8 Emplacement Drift

The WPs will be placed in 5.5-m diameter, circular emplacement drifts that will serve to enhance the role of the natural barriers and the EBS. The presence of the circular underground drifts will result in the formation of a capillary barrier at the drifts' walls during the thermal and ambient postclosure periods. In addition, the decay heat from the waste in the WPs will lead to the development of a dry-out zone around the drifts that will help to prevent percolation from reaching the repository during the thermal period. The effectiveness of the drifts in providing a barrier will depend on the strength of the capillary pressure close to the drifts, host-rock permeability, the local percolation flux above the drifts, the temperature of the rock near the walls of the drifts, and the shape of the drift openings.

ES5.2.9 Internal Waste Package Components

The WPs will have internal steel components consisting primarily of steel basket guides-and basket tubes, the steel canisters for HLW and DSNF, and the stainless-steel inner WP liners. These internal steel components are expected to degrade to iron oxyhydroxides following WP failure. These iron oxyhydroxides degradation products could potentially sorb radionuclides released from the degradation of the waste forms.

ES5.2.10 Thermal Loading and Waste Package Spacing

The WPs will be placed in the emplacement drifts in a line-load configuration, with a WP-to-WP spacing of approximately 10 cm, and a line-averaged heat load of 1.45 kW/m. Preclosure forced ventilation will be active for at least 50 years from the start of emplacement, continuing until 50 years after the last WP is emplaced.

ES6. NATURAL AND ENGINEERED BARRIERS

The repository horizon is a minimum of 200 m beneath the land surface, with a mean depth from the surface of approximately 300 m. The waste forms are solids (with minor gaseous constituents). Unless there is a volcanic eruption, the primary means for the radioactive constituents of the waste to reach the biosphere will be along groundwater pathways. The waste forms will pose minimal risks to humans, unless all of the following processes were to occur:

- Breaching of the WPs
- Exposure of the waste forms to water
- Dissolution of the waste forms releasing radionuclides into the water
- Release of dissolved or colloid-associated radionuclides from the repository and subsequent aqueous transport of the radionuclides to the SZ
- Natural or pumped discharge of radionuclide-containing water from the SZ
- Biosphere uptake of released radionuclides by humans or any part of the food chain.

Three repository subsystems constitute barriers to radionuclide transport from the repository to the natural environment. The engineered components and natural processes of the Yucca Mountain repository system that are expected to combine to provide long-term waste isolation and act as barriers to radionuclide release, flow, and transport are:

- The Upper Natural Barrier–Limits water movement in the UZ above the repository
- The EBS–Limits water movement and radionuclide transport within and through the repository
- The Lower Natural Barrier–Retards water movement and radionuclide transport through the UZ below the repository, and radionuclide transport through the SZ aquifers, hinders radionuclide transport, and limits subsequent uptake by the biosphere.

ES6.1 The Upper Natural Barrier

Figure ES-20 illustrates the key concepts associated with water movement in the UZ at Yucca Mountain. The source of water in the UZ at the repository horizon is precipitation at the land surface (SNL 2007 [DIRS 175177], Section 6.1.4). Climate controls the range of precipitation and land surface temperature conditions. Three potential climate states, present-day, monsoon,

and glacial-transition, are identified as likely during the first 10,000 years after repository closure, as illustrated on Figure ES-21. The present-day climate state is equivalent to the relatively warm present-day climate state. The monsoon climate state is characterized by hot summers, with higher summer rainfall relative to the present-day climate. The glacial-transition climate state has cooler and wetter summers and winters relative to the present-day climate state. Climate forecasting indicates that, during the next 10,000 years at Yucca Mountain, the present-day climate may persist for 600 years, followed by a warmer and wetter monsoon climate for 1,400 years, followed by a cooler and wetter glacial-transition climate for the remaining 8,000 years of the next 10,000 years (BSC 2004 [DIRS 170002], Table 6-1)). The climate from 10,000 years after repository closure to the period of geologic stability, defined as 1,000,000 years in NRC Proposed Rule 10 CFR 63.302 [DIRS 178394], is based on specifications regarding deep percolation rates provided in NRC Proposed Rule 10 CFR 63.342(c)(2) [DIRS 178394].

Precipitation on the surface of Yucca Mountain that does not run off, evaporate, or transpire, infiltrates downward through the soil horizon and into the matrix and fractures in the bedrock. The net infiltration flowing downward to the UZ, the percolation flux, provides the water for groundwater flow and transport that could allow radionuclide transport from the repository to the water table. Net infiltration is spatially and temporally variable and higher on side slopes and ridge tops where bedrock is exposed.

ES6.2 The Engineered Barrier System

The EBS includes the engineered components and the physical and chemical environment surrounding and within the engineered elements of the repository. Figure ES-19 illustrates the primary components of the EBS are the WPs containing the waste, the DSs that protect the WPs from dripping water and falling rocks, and the crushed-tuff invert and support structures beneath the WPs and DSs. The barrier functions of the EBS are to isolate the waste forms from migrating water and chemical conditions leading to mobilization of the radionuclides in the waste forms. The EBS helps divert water from the UZ above the repository to the invert, and to the UZ below the repository. The WP and DS Degradation Model Component simulates the response of these engineered systems to heat, humidity, seepage, geochemical environment, and moisture. The Waste Form Degradation and Mobilization Model Component simulates the dissolution of the waste forms and the amount of water released from breached WPs. The EBS Flow and Transport Model Component simulates the flux of fluid and radionuclides from the repository to the UZ below the repository.

ES6.2.1 Water Movement and Radionuclide Transport Within and Through the Engineered Barrier System

Figure ES-22 illustrates the key concepts associated with thermal-hydrologic (TH) processes affecting the EBS, including water vapor movement around the drifts, in the post-closure environment. WP and DS temperatures will be elevated, and some WPs and DSs may approach the boiling point of water immediately after emplacement. However, the heat output from the SNF and HLW will decline continuously because of radioactive decay. Heat output from the WPs will be at a maximum during the nominally 50-year preclosure period, but the emplacement drifts will be ventilated to remove most of the heat (SNL 2007 [DIRS 181383], Section 6.1.4).

However, the warming of ventilation air will ensure that preclosure conditions will have relatively low humidity. At permanent closure of the repository, ventilation will cease, and a small zone of boiling to above boiling conditions is expected to form. At the same time, a condensation zone is expected to develop outside the boiling zone, resulting in continuous drainage of condensate and percolation in the near-drift region (SNL 2007 [DIRS 181383], Sections 6.1.3 and 6.1.4). However, the variable end-to-end WP spacing coupled with the nonuniform heat output from CSNF and CDSP WPs, makes it likely there will be direct flow toward cooler areas and around the drifts rather than through the drifts. In the drifts, vaporized water will tend to move away from hotter regions within the drifts and condense at cooler locations on the drift walls. The condensed water would then be available to drip directly onto an underlying DS (SNL 2007 [DIRS 181383], Section 6.1.4).

The titanium DSs will provide exceptional structural strength and corrosion resistance in saline environments that may evolve on the DS surfaces. The DSs will shield the WPs from damage due to rockfall as the emplacement drifts degrade over time. The titanium DSs are expected to degrade by general corrosion, a slow process. Except for a limited number of early failure, the first DS failure is not projected to occur until between 260,000 and 310,000 years after repository closure.

The temperature of the WP surfaces, the chemistry of the water in contact with the WP surfaces, mechanical stress, and the degradation characteristics of Alloy 22 and stainless steel will affect the degradation rates of the WPs. Degradation of the WPs because of general corrosion is not expected during the preclosure period. During the postclosure dry-out period, drift-wall temperatures are expected to be greater than the boiling point of seepage water. During this time, potential high-temperature modes of degradation include SCC, dry oxidation, and localized corrosion in response to deliquescence formed by hygroscopic minerals in dust deposited on the WPs and DSs as described in *Engineered Barrier System: Physical and Chemical Environment* (SNL 2007 [DIRS 177412], Section 6.10). Three main types of WP degradation were considered under nominal conditions-general corrosion, SCC, and seepage induced localized corrosion. An additional corrosion process, microbially induced corrosion, was considered to provide enhanced general corrosion on the WP. The TSPA-SEIS also included mechanical failure of the DS and WP in the Seismic Scenario Class. Failure mechanisms that the analyses considered included collapse of the DS, SCC, and rupture of DS and WP. Under nominal conditions the time of the first breach of a WP ranges from 100,000 years to 1 million years, with breaches caused by SCC in the weld of the outer closure lid. General corrosion failures would occur after 400,000 years.

Water vapor can enter the WP by diffusion when WP failure is by SCC and by advection when failure is by general corrosion or rupture. Once water contacts the waste form degradation will begin. Following degradation and the start of dissolution of the waste forms, the concentrations of dissolved radionuclides in the water in the WPs will depend on their solubility limits. In case of high solubility limits, the concentration will depend on the waste form degradation rate. In addition, some radionuclides may attach to mobile colloids in the water. Radionuclides released from the solid waste forms into the solution will be available for transport. Figure ES-23 illustrates radionuclide transport through the EBS as either dissolved species or adsorbed onto colloidal particles. Radionuclide transport through the EBS will depend upon the distribution of water on the waste form surfaces, and between the waste form surfaces and the outer edges of the

degraded WPs. If water has dripped into the WPs through general corrosion breach, there could be advective transport of radionuclides to the edges of the WPs. If water has not dripped into the WPs, then diffusive radionuclide transport could occur in an assumed continuous, interconnected water film.

Radionuclides may be transported through the invert by advection if there is mobile seepage water, or by diffusion through the water into the pores of the invert materials. The radionuclides transported through the invert would ultimately be released to the fractures and matrix of the UZ below the repository, as shown on Figure ES-23. The dissolved and colloidally attached radionuclides will then be available for transport through the matrix and fractures in the UZ rock and ultimately released to the SZ.

The TSPA-SEIS simulates the release of radionuclides from the repository, depending on:

- The degradation rates of the engineered barriers
- The dissolution rates of the waste forms
- The solubilities of the radionuclides
- Whether or not the released radionuclides are dissolved or attached to colloids
- Whether or not the radionuclides are sorbed onto corrosion products or invert material, or both
- The rate and volume of water flowing through the engineered barriers
- The assumed existence of continuous water-film pathways allowing diffusion.

ES6.2.2 Water and Water-Vapor Movement around the Engineered Barrier System

The heat generated by the decay of waste will result in elevated rock temperatures for thousands of years after emplacement (SNL 2007 [DIRS 181383], Section 6.1.2, Figure 6.1-1). For the TSPA-SEIS repository design concept, these temperatures will be high enough, in most locations, to cause boiling conditions in the vicinity of the drifts, thus giving rise to local water redistribution and altered groundwater flow paths in the UZ. As water approaches within a distance of one to several meters above the ceiling, or crown, of an emplacement drift, changing conditions may affect the amount of water that can drip into the drifts. In the early postclosure period, the water in the vicinity of the drifts will first encounter a dry-out zone. Under boiling conditions, water reaching the dry-out zone will vaporize, thus preventing liquid water from reaching the drifts. Vaporized water will tend to move away from the drifts and through the permeable fracture network, driven primarily by the altered pressure conditions caused by boiling. In cooler regions away from the drifts, the water vapor will condense in the cooler fractures, where it will have the potential to drain either toward the heat source from above, or migrate around the drifts to the UZ below the heated drifts. In addition, water percolating through the repository horizon will be partly diverted around the repository drifts, reducing the amount of liquid water available to enter the drifts. The development of a capillary barrier in the

rocks around the drifts may prevent dripping altogether, but this process is not simulated in the evaluations of repository performance.

There may be considerable spatial and temporal variability of the TH conditions in and around the repository (SNL 2007 [DIRS 181383], Section 8.1). The spatial variability will be caused by heterogeneity in the rock properties and variations in the ambient percolation flux. In addition, differences in the thermal output of different WPs may cause a range of TH conditions in the repository. For example, cooler regions are expected along the edges of the repository and near low-thermal output WPs. The temporal variability in water movement around the drifts is caused, in the short-term, by the thermal output of the waste. Eventually, the waste heat output will decline, resulting in hundreds of years of drying, and several thousand years of cooling and rewetting of the bedrock surrounding the drifts. Percolation encountering the dry-out zone could still be prevented from dripping into the drifts because of the capillary conditions in the bedrock matrix. The rate of water dripping into an emplacement drift is expected to be considerably less than the local percolation rate, because the dry-out zone around the drift is expected to reduce liquid water flow, potentially preventing water from reaching the drift walls for a considerable period. The modeling approach to these phenomena in the long-term repository safety calculations is conservative, however, and percolations is allowed to reach and even enter drifts soon after the boiling front is not longer in the rock.

ES6.3 Lower Natural Barrier

ES6.3.1 Flow and Transport in the Unsaturated Zone below the Repository

Figures ES-23 and ES-24 illustrate radionuclide transport of the dissolved or colloidally attached radionuclides released from the EBS to the UZ beneath the repository. Radionuclide transport within the UZ is expected to be principally by advection, but matrix diffusion and colloid-facilitated transport are considered as well. The effectiveness of these transport mechanisms will depend on sorption/desorption and precipitation processes and radioactive decay. In the welded tuff units, advection of liquid water through fracture networks is expected to dominate radionuclide transport. Advection is also an important mechanism for transport between fractures and the rock matrix, especially at interfaces between nonwelded and welded tuff units, where there will likely be transitions between dominant advective fracture flow and dominant diffusive matrix flow. Dominant fault-and-fracture flow in welded tuffs will provide relatively short transport times through these units, whereas dominant matrix flow in the vitric nonwelded tuffs will result in much longer transport times. Mass transfer between fractures and the tuff matrix may play an important role in transport within Yucca Mountain and the transfer of radionuclides from fractures to the matrix may retard the overall transport of radionuclides to the water table. Also, variable flow paths, such as through perching horizons, may affect the direction, distance, and time of radionuclide transport.

Sorption describes the combination of chemical interactions between dissolved solutes and solid phases such as immobile rock matrix or colloids, including adsorption, ion exchange, surface complexation, and chemical precipitation. Radionuclide transport in the UZ will also likely involve colloid-facilitated transport. Radioactive decay will lead to stable decay products that will decrease radionuclide concentrations exponentially with time. Chain decay will add additional complexity to the mix of transported material because of the ingrowth of radionuclide

daughter products created from the decay of parent radionuclides. Further, some daughter products may have different sorption characteristics than their parent radionuclides and may be have different transport characteristics.

Because the characteristics of the natural environment, along with the processes controlling transport, are variable in space and time, radionuclide transport will also be variable. Part of the temporal variability may involve long-term climatic changes that not only will change the percolation flux, but could also cause the water table beneath Yucca Mountain to rise due to wetter climates, or fall in response to drier climates.

ES6.3.2 Flow and Radionuclide Transport through the Saturated Zone to the Biosphere

Radionuclides transported through the UZ below the repository will be released to the saturated zone beneath the repository. Figure ES-25 illustrates the key concepts associated with flow and transport in the saturated zone beneath and downgradient from the Yucca Mountain site, as well as the pathways by which dissolved radionuclides may come into contact with the biosphere, including potential human uptake of and exposure to radionuclides.

Radionuclides reaching the SZ will be subject to flow and transport processes in the general direction of groundwater flow to the southeast, and then to the south and southwest. The groundwater flow processes determine the rate of water movement within the SZ and the flow paths through which groundwater is likely to travel. The groundwater flow paths extend from where the radionuclides may enter the SZ through volcanic tuff and alluvium to the boundary of the controlled area, as defined according to NRC Proposed Rule 10 CFR 63.302 [DIRS 180319].

Advective transport will be determined by the rate of groundwater flow and the effective porosity of the media through which the flow occurs and processes that relate to interactions between the dissolved or colloidal radionuclides and the aquifer materials. Dispersive processes will be affected by the effective porosity of the host rock and by small-scale velocity heterogeneities that allow some dissolved constituents to travel faster, or slower, than the average advective transport time.

Dissolved radionuclide transport may be retarded by diffusion from fractures into the rock matrix. The effectiveness of matrix diffusion in retarding radionuclide transport will depend on the diffusive properties of the matrix and the degree of spacing between the flowing fracture zones.

Some radionuclides that are potentially important to repository performance may be sorbed by the matrix of the SZ rocks. Carbon, technetium, and iodine do not sorb (SNL 2007 [DIRS 181650], Sections 6.5.3.1, 6.6.2, 6.6.2(a), 6.7.1, and 6.7.1(a)) and are modeled considering only advection, dispersion, and matrix diffusion processes. Other radionuclides, such as neptunium, uranium, and plutonium, will be sorbed to varying degrees onto colloids, which could subsequently diffuse into the matrix pores of fractured tuffs and alluvium (SNL 2007 [DIRS 181650], Sections 6.5.2, 6.7.1, 6.7.1(a), and 8.1)). The stronger the sorption, the longer the radionuclide transport time compared with advective-dispersive transport times.

The time for radionuclides to reach any specified point in the SZ downgradient from the repository, such as the boundary of the controlled area, described as 18-km in the primary

direction of groundwater flow (10 CFR Part 63 (66 FR 55732 [DIRS 180319], III Public Comments and Responses, p. 55750)), will depend primarily on the groundwater velocity and the potential retardation of radionuclides by sorption on the mineral surfaces within the bedrock or alluvial aquifers of the SZ.

Radionuclides in the SZ downgradient from the repository could enter biosphere pathways, including uptake by the local human population. The principal biosphere pathways to humans consist of the following:

- Direct consumption of water containing dissolved radionuclides
- Consumption of crops produced using water containing dissolved radionuclides
- Consumption of meat or dairy products from livestock watered with contaminated water or fed with contaminated crops, or both
- Direct exposure to contaminated soil
- Inhalation of dust that may contain attached radionuclides.

ES7. GENERAL DESCRIPTION OF THE TSPA-SEIS

The development of the TSPA-SEIS began with the identification and screening of the relevant FEPs that could affect the performance of the repository. The FEPs that were screened in were used to develop scenario classes for the TSPA-SEIS analyses. Figure ES-8 is a schematic representation of the development of the TSPA-SEIS showing the individual model components of the repository system. Figure ES-9 shows the hierarchy of the abstractions and submodels of the TSPA-SEIS. Each of the following individual model components represents a major aspect of the total repository system.

ES7.1 Model Components for the Nominal Scenario Class Modeling Case

The Nominal Scenario Class modeling case for the TSPA-SEIS encompasses all screened-in FEPs except those FEPs related to early failure and igneous or seismic activity. The Nominal Scenario Class modeling case includes the important effects and system perturbations caused by climate change and repository heating that are projected to occur after repository closure. In addition, the Nominal Scenario Class modeling case considers that the WPs and DSs will be subject to EBS environments, and will degrade with time until they are breached and expose the waste forms to percolating groundwater. The degraded waste forms will release and mobilize radionuclides for transport out of the emplacement drifts. Radionuclides released from the emplacement drifts will be transported through the UZ below the repository by percolating groundwater and ultimately released to the SZ where they will be available for groundwater flow and transport to the accessible environment. The TSPA-SEIS's calculated annual dose to the RMEI also includes FEPs associated with the biosphere.

ES7.1.1 Unsaturated Zone Flow

The UZ Flow Model Component of the TSPA integrates five processes that contribute to flow in the UZ as shown on Figures ES-8 and ES-9: climate, infiltration, mountain-scale UZ flow, drift seepage, drift-wall condensation, and drift-scale coupled processes. The UZ Flow Model Component defines the temporal and spatial distribution of water flow from the ground surface through the unsaturated tuffs above and below the repository horizon, and the temporal and spatial distribution of seepage into the waste emplacement drifts. Figure ES-20 provides a conceptual illustration of the mountain-scale flow processes at Yucca Mountain. Water at the repository horizon is derived from precipitation in the form of rainfall and snow at the land surface above the repository. Long-term temporal variability is included in the TSPA-SEIS by specifying four successive climate states: present-day, monsoon, glacial-transition, and a long-term climate based on specifications regarding deep percolation rates provided in NRC Proposed Rule 10 CFR 63.342(c)(2) [DIRS 178394] (Figure ES-21).

ES7.1.2 Engineered Barrier System Environment

The EBS Environment Model Component encompasses environments that may affect the performance of the EBS including the mountain-scale TH environment and the chemical environment within the emplacement drifts as shown on Figures ES-8, ES-9, and ES-10. These environments are important to repository performance because they help determine the degradation rates of the EBS components, quantities, and species of mobilized radionuclides, as well as the transport of radionuclides and fluids through the emplacement drifts and into the UZ below the repository. Figure ES-20 shows the position of the repository drifts and WPs with respect to the Yucca Mountain flow system. Water percolating into the repository environment will be affected by heat from the emplaced waste and waste heat and geochemical processes and conditions will determine the chemical environment of the EBS.

ES7.1.3 Waste Package and Drip Shield Degradation

The WPs and DSs will be the primary engineered components of the EBS (Figure ES-26). The EBS Model Component describes the degradation of the WPs and DSs as a function of time, presence of water, and repository location (see Figures ES-8, ES-9, and ES-10). The EBS Model Component simulates: general corrosion of the WPs and DSs; general corrosion and localized corrosion of the WP outer surface; SCC of the DSs and WPs; microbially influenced corrosion on the WP outer surface; and early WP failure.

ES7.1.4 Waste Form Degradation and Mobilization

The Waste Form Degradation and Mobilization Model Component simulates waste-form degradation and the release of CSNF, DSNF, and HLW radionuclide inventories (Figure ES-27). Figure ES-28 shows the mechanisms related to CSNF, as well as the concentrations of dissolved and colloidal radionuclides released from the waste forms to the EBS Transport Submodel. The Waste Form Degradation and Mobilization Model Component accounts for: in-package water chemistry; matrix degradation rates for CSNF, DSNF, and HLW forms; radionuclide solubilities; and the types and concentrations of waste form and in-drift colloids.

ES7.1.5 Engineered Barrier System Flow and Transport

The EBS Flow and Transport Model Component calculates the rate of radionuclide release from the EBS to the UZ, which is determined by seepage into the emplacement drifts, condensation on the drift walls, WP and DS degradation, the presence of water films on in-package internals, waste-form degradation, and the TH environment of the EBS. The EBS Flow and Transport Model Component simulates the rate of water flow through the EBS, diffusive and advective transport, sorption, and colloid-facilitated transport.

ES7.1.6 Unsaturated Zone Transport

The UZ Radionuclide Transport Model Component describes the migration of radionuclides from the EBS and through the UZ to the water table. Consistent with the Mountain-Scale UZ Flow Submodel, the conceptual model for UZ transport (Figure ES-24) simulates coupled advective and diffusive transport through fracture and matrix continua using a dual-continuum approach. The UZ Radionuclide Transport Model Component simulates: advective, dispersive and diffusive transport; sorption; colloid retardation, filtration, and exclusion; radioactive decay and ingrowth; and changes in water-level elevation.

ES7.1.7 Saturated Zone Flow and Transport

The SZ Flow and Transport Model Component simulates the transport of radionuclides from their introduction at the water table below the repository to the regulatory boundary 18-km downgradient from the Yucca Mountain repository (10 CFR Part 63 (66 FR 55732 [DIRS 180319], III Public Comments and Responses, p. 55750)). Radionuclides are transported through the SZ either as solutes or sorbed to colloids. The SZ Flow and Transport Model Component simulates: advection, dispersion, and diffusion in fractures; matrix diffusion; colloid retardation; and exclusion and sorption (Figure ES-25).

ES7.1.8 Biosphere

The Biosphere Model Component simulates radionuclide transport in the biosphere and the resulting exposure of the RMEI to radionuclides released from the repository after closure (Figure ES-29). The TSPA-SEIS includes the two dominant mechanisms of radionuclide release to the biosphere: (1) release through the SZ via groundwater and (2) release through the air by ash dispersal from a volcanic eruption.

ES7.2 Model Components for the Early Failure Scenario Class

The Early Failure Scenario Class addresses FEPs that describe the potential for DS and WP early failure in the absence of disruptive events. The early-failure scenarios include DSs and WPs that fail prematurely due to material defects or improper manufacturing conditions or pre-emplacement operations and practices, such as improper heat treatment or welding flaws. Early DS and WP failures are analyzed using the Drip Shield Early Failure (EF) Modeling Case and the Waste Package Early Failure (EF) Modeling Case. The Early Failure Modeling Cases address FEPs that describe the potential for DS and WP early failure that could affect repository performance in the absence of disruptive events. The Drip Shield EF Modeling Case analyzes the possibility that DSs could fail prematurely, thus failing to protect the underlying WPs from

seepage and possible localized corrosion. The Waste Package EF Modeling Case analyzes WPs that fail prematurely due to material defects, manufacturing errors, or pre-emplacement operations and practices, such as improper heat treatment or welding flaws that could affect WP performance and longevity.

ES7.2.1 Drip Shield Early Failure Modeling Case

Section 6.1.6 of *Analysis of Mechanisms for Early Waste Package/Drip Shield Failure* (SNL 2007 [DIRS 178765]) identified numerous potential mechanisms that could result in the early failure of DSs. The following mechanisms were identified as potentially leading to early DS failure in TSPA-SEIS analyses:

- Improper heat treatment
- Base metal selection flaws
- Improper weld filler material
- Emplacement errors.

The probabilities of occurrence for the four DS early failure mechanisms were combined to develop a probability distribution for the rate of occurrence of undetected defects in DSs, where an undetected defect was assumed to result in early failure of a DS. The occurrence of undetected defects is assumed to be independent between DSs, and, therefore, DS early failure is also independent between DSs. The DS Early Failure modeling case considers DSs as associated with the waste forms in CSNF and CDSP WPs. Also, the TSPA-SEIS uses the simplifying assumption that each DS early failure affects a single WP, and removes the overlying DS as a barrier to seepage at the time of repository closure, thus allowing the full volume of seepage to contact the affected WP. The TSPA-SEIS then assumes that a WP beneath an early-failed DS experiences localized corrosion, completely compromising the WP outer barrier at the time of repository closure, thus allowing both advective and diffusive transport of radionuclides.

ES7.2.2 Waste Package Early Failure Modeling Case

Section 6.1.6 of *Analysis of Mechanisms for Early Waste Package/Drip Shield Failure* (SNL 2007 [DIRS 178765]) identified numerous potential mechanisms that could result in the early failure of WPs. The following mechanisms were identified as potentially leading to early WP failure in TSPA-SEIS analyses:

- Weld flaws
- Improper heat treatment of the outer corrosion barrier (OCB)
- Improper heat treatment of OCB lid
- Improper stress relief of OCB lid (low plasticity burnishing)
- WP mishandling damage
- Improper base metal selection
- Improper weld filler material.

The TPSA-SEIS model calculates the characteristics of weld flaws using distributions for the size and number of potentially undetected weld flaws based on industrial analogue studies, which are then used to form the per WP closure weld volume and weld thickness. The TSPA-SEIS

simulates the critical flaw orientation probability and an applicable depth factor to model where undetected flaws might remain and might result in SCC that could penetrate the WP closure welds.

The analysis of the other early WP failure mechanisms determined that the occurrence of an undetected defect could result in early failure of a WP. The probability distribution for the rate of occurrence of undetected defects is equivalent to a probability distribution for the rate of WP early failures. The occurrence of undetected defects is assumed to be independent between WPs; therefore, WP early failure is also independent between WPs regardless of the type of WP.

ES7.3 Model Components for the Disruptive Events Scenario Classes

Igneous events and seismic activity are possible sources of repository disruption. The TSPA-SEIS assumes that igneous activity will cause EBS damage from magma intersecting and intruding into the repository drifts, and/or from an unlikely eruption from a volcanic vent passing through the repository. Seismic activity in the form of vibratory ground motion and/or fault displacement will disrupt DSs resulting and allow dripping water to contact WPs, and that could lead to localized corrosion of the WP outer barrier.

The modeling cases described below do not mention the likelihood of these events. Rater, these descriptions indicate how such an event is considered in the TSPA-SEIS if it were to occur.

ES7.3.1 Igneous Scenario Class Modeling Cases

ES7.3.1.1 Igneous Intrusion Modeling Case

The Igneous Intrusion Modeling Case describes the performance of the repository system if igneous activity disrupts the repository. The Igneous Intrusion Modeling Case assumes that a dike intersects the repository and destroys DSs and WPs in those drifts intruded by magma, exposing the waste forms to percolating water and mobilizing radionuclides for transport out of the repository, down through the UZ to the SZ, and then to the accessible environment as shown on Figure ES-30. The Igneous Intrusion Modeling Case uses the following model components to simulate repository performance, given that a certain number of WPs are destroyed by the intrusion:

- UZ Flow
- EBS Environment
- WP and DS Degradation
- Waste Form Degradation and Mobilization
- EBS Flow and Transport
- UZ Transport
- SZ Flow and Transport
- Biosphere.

ES7.3.1.2 Volcanic Eruption Modeling Case

The Volcanic Eruption Modeling Case simulates the fraction of igneous events in which a volcanic eruption through the repository also occurs. In this case, waste from WPs intersected by flowing magma is transported to the land surface through one or more eruptive conduits, and tephra and entrained waste are discharged into the atmosphere, transported by wind currents, and deposited at the land surface as shown on Figure ES-31. The Volcanic Eruption Modeling Case also evaluates the fluvial and eolian redistribution of the contaminated tephra deposited on the land surface using the tephra redistribution code FAR. The TSPA-SEIS uses the following processes and model components to calculate repository system performance for the Volcanic Eruption Modeling Case:

- Volcanic interaction with the repository
- Atmospheric transport
- Tephra redistribution
- Biosphere.

ES7.3.2 Seismic Scenario Class Modeling Cases

The Seismic Scenario Class evaluates repository performance for seismic activity that disrupts the repository drifts and the EBS and uses the same TSPA-SEIS components as the Nominal Scenario Class to evaluate the mobilization and transport of radionuclides exposed to seeping water, release from the EBS, transport in the UZ, and transport in the SZ to the location of the RMEI. The effects of seismic events are taken into account in the EBS but not in the natural system. The Seismic Scenario Class modeling cases simulate damage to DSs and WPs as a function of the magnitude of a seismic event, including Ground Motion and Fault Displacement modeling cases using mean hazard curves for peak ground velocity (PGV) and fault displacement to estimate mean annual dose conditional on event occurrence. Each mean hazard curve is defined as the mean estimate or average of a distribution of hazard curves, and typically represents the 80th or greater percentile of the distribution because the average is dominated by the larger values of the distribution.

The Seismic Scenario Class modeling cases use the following model components to estimate total system performance:

- UZ Flow
- EBS Environment
- WP and DS Degradation
- Waste Form Degradation and Mobilization
- EBS Flow and Transport
- UZ Transport
- SZ Flow and Transport
- Biosphere.

ES7.3.2.1 Ground Motion Modeling Case

The Seismic GM Modeling Case includes WPs that fail solely due to ground motion damage from a seismic event. The Seismic GM Modeling Case uses nominal processes because nominal corrosion processes can affect the repository's susceptibility to damage during a seismic ground motion event.

The TSPA-SEIS simulates the effects of vibratory ground motion on both lithophysal and nonlithophysal rock using rockfall analyses. Rockfall, the large rock blocks that could be ejected from the nonlithophysal units of the repository horizon during vibratory ground motion, could fill emplacement drifts during the period of geologic stability. The drifts in the lithophysal zone are predicted to collapse into small fragments with particle sizes of centimeters to decimeters, whereas the large blocks in nonlithophysal zones may be shaken loose from the drift walls and fall onto DSs. Drift collapse could lead to increased temperature and relative humidity of the outer surface of WPs in lithophysal regions, where rubble filling the collapsed drift could form a thermal blanket covering the WPs. Drift collapse could also affect seepage flux and drift-wall condensation in the emplacement drifts in the lithophysal zones.

ES7.3.2.2 Fault Displacement Modeling Case

The Seismic FD Modeling Case includes only those WPs that fail due to fault displacement damage from known and hypothetical faults in the repository. The projected number of WPs that could fail due to fault displacement is a small fraction of the total number of WPs in the repository. A fault displacement that occurs in an emplacement drift may cause one portion of a drift to be displaced vertically or horizontally relative to an adjacent section, possibly causing shearing of an overlying WP and DS if the fault displacement exceeds the available clearance in the EBS. The TSPA-SEIS simulates fault displacement for an intact DS within 10,000 years after repository closure, and for a late-time response after a DS failure leads to rubble surrounding a WP. The TSPA-SEIS simulates direct shear failure of a WP if fault displacement exceeds one-quarter of the outer diameter of the WP OCB (about 0.4 meters to 0.5 meters) allowing advective flow through the sheared WPs. This failure condition is due to an extremely low-frequency, high-amplitude fault displacement, corresponding to an annual exceedence frequency of less than or equal to 2.5×10^{-7} per year.

ES7.4 TSPA Input Database

The TSPA Input Database provides the parameter values and distributions of parameter values necessary for TSPA-SEIS. All input data including the parameter values and their distributions are stored and controlled. The TSPA-SEIS was developed concurrently with the supporting models and analyses, and tracks and ensures traceability of data and data sources. The TSPA Input Database also categorizes and stores fixed and distributed values of the TSPA-SEIS parameters under strict user controls that ensure the security, integrity, and traceability of the information used in the TSPA-SEIS analyses using signed and catalogued Parameter Entry Forms.

ES8. VERIFICATION/VALIDATION OF THE TOTAL SYSTEM PERFORMANCE ASSESSMENT CODE

Note: This work was not completed at the time the draft TSPA-SEIS was published.

Procedures IM-PRO-003, *Software Management* Section 6.9.12 and SCI-PRO-006, *Models*, Section 6.3, respectively, were utilized to support verification and validation of the TSPA-SEIS, providing confidence that the TSPA-SEIS adequately represents the physical processes in the repository system, and properly transfers outputs between the TSPA-SEIS's modules and submodels. Figure ES-32 provides an illustration of the major activities conducted for TSPA-SEIS validation. The model validation activities provide confidence in the TSPA-SEIS and its results. Using these activities ensures that the TSPA-SEIS is valid for its intended use of calculating mean annual dose and other performance measures with respect to radionuclide releases from the repository and compliance with NRC proposed rule 10 CFR Part 63, Subparts E and L [DIRS 178394 and DIRS 180319].

ES8.1 Model Validation Strategy

Note: This work was not completed at the time the draft TSPA-SEIS was published.

A typical model validation compares the model's results with experimental measurements and/or field observations. However, such measurements are impossible to obtain for the TSPA-SEIS at the temporal and spatial scales of interest for postclosure repository performance. Therefore, the TSPA-SEIS was validated using several methods ensuring that the calculated results apply during the next 10,000 years after repository closure, and during the period of geologic stability, nominally 1,000,000 years after repository closure (NRC Proposed Rule 10 CFR 63.302 [DIRS 178394]).

The TSPA-SEIS inputs were checked, controlled, and documented to maintain traceability and transparency. Confidence in the methodology of and inputs to the TSPA-SEIS is provided through:

- Selection of input parameters and/or input data from validated supporting analysis model reports
- Model calibration activities and/or evaluation of the initial boundary conditions for the TSPA-SEIS, establishing model convergence
- Evaluation of the impacts of uncertainties on model results.

These three activities demonstrate that: (1) the TSPA-SEIS's input parameter values from source documents, as well as those parameter values that are calculated by the TSPA-SEIS, are correctly propagated throughout the model; (2) the TSPA-SEIS is stable in terms of the number of realizations, the length of model timesteps and spatial discretization; and (3) that the uncertainty in model inputs is propagated through and correctly accounted for in the TSPA-SEIS.

The following three post-development methods were used to demonstrate TSPA-SEIS validation with respect to intended use and desired level of confidence:

- Corroboration of TSPA-SEIS results with data acquired from the laboratory, field experiments, analogue studies, or other relevant observations not previously used to develop or calibrate the model
- Independent technical review by experts independent of the development and checking processes, and interdisciplinary review of the model documentation
- Corroboration of abstraction or submodel results to the results of the validated mathematical models from which the abstraction or submodel was derived, including corroboration with results of auxiliary analyses to provide additional confidence.

ES8.2 Computer Code and Input Verification

Note: This work was not completed at the time the draft TSPA-SEIS was published.

The verification of computer codes from outside sources and model inputs used in the TSPA-SEIS included: (1) verification of the integrated system software, GoldSim, the software platform on which the TSPA-SEIS is based; (2) verification of DLLs from source documents and DLLs that are generated within the TSPA-SEIS; and (3) verification of model inputs from the TSPA Input Database. Submodels from source analysis model reports were verified by comparing submodel results calculated by the TSPA-SEIS with the results in the analysis model reports. Coupling between submodels was examined by verifying that the information generated by one submodel was input correctly to successive submodels, and that the information never exceeded the applicable range of validity of the next successive submodel. The following model verification activities apply and demonstrate that incorporation of information and submodels from other sources into the TSPA-SEIS has not altered the validity of the information, the submodels, or both.

- The TSPA-SEIS software GoldSim was qualified per a well defined process following program procedure SCI-PRO-002.
- Outputs from DLLs from other sources, including analysis model reports and data tracking numbers, were correctly replicated in the TSPA-SEIS.
- Outputs from DLLs calculated within the TSPA-SEIS were found to be within established acceptance criteria (e.g., within 5 percent).
- Individual submodels were validated in their respective analysis model reports.
- Results from submodels within the TSPA-SEIS were compared to results contained in analysis model reports and were found to agree within selected acceptance criteria (e.g., within 5 percent).

- Feeds from one submodel to another submodel were found to be correctly transferred, and these feeds either did not exceed the valid range of the successive submodel or the values used were fixed within the range or at the upper bound of the range of the successive submodel.

- Inputs from the TSPA Input Database were verified to correspond with source data.

ES8.3 Stability Testing

Note: This work was not completed at the time the draft TSPA-SEIS was published.

The stability of the model was evaluated in the following areas:

- Statistical stability, including replicated sampling
- Temporal stability
- Spatial stability
- Stability of the number of realizations.

The TSPA-SEIS model calculates a range of projected annual doses for each epistemic realization, a range determined by aleatory uncertainty for any given epistemic uncertainty value. This technical approach follows advice given by the regulatory agency in its publications, and reflects the internationally accepted way to conduct complex, long-term analyses of this type.

The output of interest from these types of calculations is typically labeled as the mean (or median or 95th/5th percentiles) of the projected annual dose, or just annual dose. But the approach to each calculation fits the specific modeling case at hand. Section 6.1.2.4 describes the calculation of projected annual dose for each modeling case. In general, the calculation involves numerical evaluation of one or more integrals. Because each modeling case addresses different aleatory uncertainties, the methods of calculating projected annual dose differ for each modeling case. Figure ES-33 illustrates numerical accuracy of the calculated mean annual dose for the Nominal Modeling Case considering Latin Hypercube sampling sizes of 300 and 1,000 realizations. The important point is that no instability in the means are shown whether the selected sample size is 300 or 1,000 realizations, therefore, 300 realizations provide a sufficiently robust mean value.

The temporal discretization of the TSPA-SEIS affects its ability to predict the future behavior of water and radionuclide movement. Timestep size was evaluated for the Early Failure WP, Igneous Intrusion, and Seismic GM Modeling Cases because of its effect on radionuclide mobilization and transport. The degree of stability shown in the graphical comparisons of the results of the stability analysis, see Figure ES-34, indicated that a statistical comparison of time-step changes was not necessary.

The TSPA-SEIS deals with the variability associated with spatial discretization of the various model domains which operate at different scales with spatially dependent information. The TSPA-SEIS also represents different TH histories bounded by percolation subregions. The spatial discretization utilized in the TSPA-SEIS accounts for the variable scales of the submodels and provides stable results that include the spatial variability in the predicted TH histories. This is discussed in greater detail below.

The stability of the TSPA-SEIS simulations depends on whether or not the number of Monte Carlo realizations adequately quantifies the uncertainty in the estimate of mean annual dose. Several statistical methods were employed to evaluate the stability and reliability of the TSPA-SEIS. Separate tests were conducted for the Nominal, Early Failure, Igneous, and Seismic Scenario Class modeling cases. These modeling cases were run with from 300 to 2,000 realizations to determine the optimal number that would yield stable results. The Seismic FD Modeling Case was not tested because it always has about two orders of magnitude lower annual dose than the Seismic GM Modeling Case.

Additional analyses were conducted for the UZ Transport and the Localized Corrosion Submodels. The maximum number of particles specified in the finite element, heat and mass transfer code (FEHM) using the particle-tracking technique to simulate radionuclide transport. FEHM was run with from 500,000 up to 900,000 particles to evaluate the results for mean annual dose and mass flux from the UZ and SZ for select the number of particles necessary to provide consistent output. The Localized Corrosion Initiation Analysis was tested for consistency using a two-stage analysis to account for both epistemic and aleatory uncertainty. The two tests yielded the same stable results regardless of the size of number of iterations.

A comparison of mean-value dose histories for the Seismic Scenario Class with the Seismic GM Modeling Case (2,000 realizations) for the same temporal discretization as shown for the Igneous Intrusion Modeling Case shows that the results of the Seismic GM Modeling Case are also insensitive to timestep discretization, except at times before approximately 600 years (Figure ES-34).

The TSPA-SEIS quantifies both aleatory and epistemic uncertainty associated with the repository's natural and engineered systems. Part of the aleatory uncertainty addressed by the TSPA-SEIS deals with spatial variability. Different discretization sequences were compared to one another to determine the simplest discretization for the TSPA-SEIS. The influence of spatial variability on the stability of the results of the TSPA-SEIS Model depends on the spatial discretization sequence and the selection of the most representative environmental conditions for the EBS.

The TSPA-SEIS Model deals with uncertainty due to variability associated with spatial discretization of the various model domains. The TSPA-SEIS Model utilizes different spatial scales from the Mountain-Scale UZ Flow, EBS TH Environment, UZ Transport, and SZ Flow and Transport abstractions. The TSPA-SEIS Model's spatial domain is derived from subdividing the repository into percolation subregions at the EBS Submodel level using a subset of the comprehensive TH dataset provided by the MSHTM process model to represent the different TH histories bounded by a particular percolation subregion.

The TSPA-SEIS Model, in conjunction with the MSTHM Process Model Abstraction, implements its own spatial discretization scheme to accommodate the use of the comprehensive TH dataset. This scheme involves the discretization of the repository domain into a specified number of subregions based upon percolation flux, and each subregion's TH conditions are characterized by a subset of the comprehensive TH dataset that is meant to be representative of the TH conditions everywhere within that specific percolation subregion.

Spatially discretizing the repository into subregions is a balance between a minimum number of subregions that would adequately capture the variability of the EBS TH environment across the repository footprint. The TSPA-SEIS Model uses five repository percolation subregions to maximize the ability of the TSPA-SEIS Model to include spatial effects when sensitivity analyses and alternative scenarios were analyzed.

ES8.4 Uncertainty Characterization Reviews

10 CFR 63.114 (a) (2) [DIRS 178394] requires that a repository performance assessment include an appropriate treatment of parameter uncertainty and variability. A technical review team analyzed the TSPA-model for consistency, defensibility, and traceability with respect to uncertainty and variability characterizations in several formal reviews of the uncertainty of a number of key TSPA-SEIS input parameters and their associated abstractions. The technical reviews focused on: (1) confirming that the parameter representations appropriately reflect the major sources of uncertainty and/or variability, (2) verifying that the probability distributions were derived using sound statistical methods and interpretations, and (3) ensuring model parameter probability distributions are reasonable and defensible, and do not underestimate dose risk. One result of the reviews was that fifteen probability distributions were subsequently corrected, modified, or independently derived to improve their treatment of uncertainty and variability. These updates were included in the information provided to TSPA.

The reviews included a risk-based ranking of TSPA-SEIS scenario classes and modeling cases to focus the reviews on the most important component model abstractions for the Nominal Scenario Class excluding early failures and disruptive processes and events, the Early Failure Scenario Class, the Igneous Scenario Class, and the Seismic Scenario Class.

Based on the comparison of probability-weighted dose calculations, the following ranking (from highest to lowest) of the scenario modeling cases was obtained:

1. Seismic Scenario Class, Seismic GM Modeling Case
2. Igneous Scenario Class, Igneous Intrusion Modeling Case
3. Igneous Scenario Class, Volcanic Eruption Modeling Case
4. Early Failure Scenario Class, WP and DS Early Failure Modeling Cases
5. Seismic Scenario Class, Seismic FD Modeling Case
6. Nominal Scenario Class, Nominal Modeling Case.

The magnitudes of the projected dose risk indicated that the first three modeling cases by far dominated the projected total dose for 10,000 years. The analysis provided a list of key TSPA-SEIS parameters whose uncertainty or variability would have the greatest influence on the mean and variance of the dose distribution for the various components of the TSPA-SEIS.

ES8.5 Surrogate Waste Form Validation

The waste forms included in the TSPA-SEIS are limited to CSNF (stainless steel and zirconium-based Zircaloy cladding), DSNF surrogates, and HLW. This was done because there are 11 categories of DSNF, and their individual representation in the TSPA-SEIS would dramatically increase simulation time. The naval spent fuel (Category 1) in the TSPA-SEIS is represented by Zircaloy-clad CSNF. The remaining DSNF (Categories 2 through 11) is

represented by a single DOE surrogate spent fuel that has a radionuclide inventory that is the weighted average of the radionuclide inventories of Categories 2 through 11. The dissolution rate of the DOE surrogate spent fuel is instantaneous, based on the rapid dissolution of Category 7 DSNF (i.e., uranium metal). The analyses show that the use of surrogates to represent naval spent fuel and Categories 2 through 11 of DSNF is appropriate. The analyses of naval spent fuel for the Nominal Modeling Case, the Igneous Intrusion Modeling Case, and the Volcanic Eruption Modeling Case show that the mean annual dose from naval spent fuel is bounded by annual dose calculated for the Zircaloy-clad CSNF surrogate. The results of Categories 2 through 11 DSNF show that the DOE surrogate spent fuel used in the TSPA-SEIS is a reasonable representation of the weighted sum of these categories of DSNF.

ES8.6 Auxiliary Analyses

A number of auxiliary analyses were also conducted to support confidence of the modeling results and to evaluate the conservatism of the TSPA-SEIS. They provided useful information during the development of the model to confirm the reasonableness of the TSPA-SEIS.

ES8.7 Confidence Building: Natural Analogues

Corroboration of the results of the TSPA-SEIS can be gained, in part, through comparison with natural analogues. Natural analogue results were used in the validation process for the model components and submodels for several of the analysis model reports supporting the TSPA-SEIS. The natural analogues relevant to the Yucca Mountain repository are discussed in *Natural Analogue Synthesis Report* (BSC 2004 [DIRS 169218]), and include natural analogues to materials intended for use in the Yucca Mountain repository as well as the results of some investigations of analogues to geologic processes. The information from natural analogues has contributed to the understanding of drift stability; degradation of the waste forms and elements of the EBS; seepage; UZ flow and transport; coupled processes; SZ transport; the biosphere; and disruptive events, such as volcanism and seismic events. Natural analogue information was used in the development of the supporting submodels of the TSPA-SEIS as provided by the analysis model reports. The use of natural analogues helps ensure that these submodels are grounded in reality, and provides confidence that the TSPA-SEIS provides reasonable results. In addition to the confidence provided in general by the examples of natural analogues on a qualitative basis, performance comparisons with two selected analogues, the Cerro Negro volcanic eruption and the Nopal I uranium mine at Peña Blanca, provide additional confidence in the TSPA-SEIS.

The ASHPLUME software was used to simulate ash-fall thickness from the 1995 eruption of the Cerro Negro volcano. The results show that the ASHPLUME can reasonably predict the ash-fall distribution and ash-fall thickness from the eruption of a basaltic cinder cone volcano similar to Cerro Negro (Figure ES-35). The Cerro Negro ash-fall-calculation method was used to simulate eruptive releases of ash from volcanic vents in the vicinity of the Yucca Mountain repository or from a volcanic vent passing through the repository and resulting in WP destruction and aerial distribution of waste particles containing radionuclides.

Radionuclide transport by groundwater is the most likely off-site transport pathway for the Yucca Mountain repository. The Peña Blanca natural analogue site (Figure ES-36) offers a unique opportunity to examine the groundwater flow and transport of uranium and some of its

daughter products in a climatic and geologic setting very similar to that of Yucca Mountain. Both the Peña Blanca and Yucca Mountain sites are set in volcanic tuff in an oxidizing UZ, and are in similar desert environments. Figure ES-37 shows the geologic structure at the Nopal I mine and the position of the ore deposit above the water table. The Nopal I mine at Peña Blanca was originally comprised of uraninite, which is chemically similar to nuclear fuel. The Nopal I deposit was analyzed using a modified version of the metal-fuel dissolution submodel used in the TSPA-SEIS. The observed uranium concentrations at observation wells PB1, PB2, PB3, and PB4, shown on Figure ES-38, indicate that radionuclides released from the Nopal I uranium deposit appear to have been retarded by the natural geologic system. The results of field investigations at the Nopal I mine and analyses of rock and water samples demonstrate the ability of natural systems to provide a sink for radionuclides released from the deposit.

ES8.8 Summary of Technical Reviews

Technical reviews of performance assessment models form an important part of model validation. During the past decade, the Yucca Mountain Project has developed successive TSPA models as well as accompanying input process models, all of which have been subject to technical reviews as part of their validation. The comments from the technical reviews have been addressed to the extent practicable, and the TSPA modeling has been updated accordingly.

ES9. SYSTEM PERFORMANCE ANALYSES

The TSPA-SEIS was used to perform system performance analyses in the form of calculations of mean and median annual dose for modeling cases representing nominal conditions, early DS and WP failures, and disruptive events. The PA analyses also address both the individual and groundwater protection requirements of NRC Proposed Rule 10 CFR 63.311[DIRS 178394] and 10 CFR 63.331 [DIRS 180319], respectively. All GoldSim files for calculated mean annual dose and other calculated values determined for these modeling cases presented in this section can be found in output DTN: MO0708TSPASEIS.000.

ES9.1 Results of the Scenario Class Modeling Case Simulations

The TSPA-SEIS was used to assess total system performance of a repository system for seven modeling cases and the human intrusion scenario. The analyses provide projected annual dose to the RMEI for 10,000 years after repository closure and for the period of geologic stability as specified in NRC Proposed Rule 10 CFR 63.303 [DIRS 178394]. The analyses account for uncertainties in the representations of FEPs that could affect the annual dose. The performance assessment analyses address the effect of alternative parameters, submodels, and approaches to FEPs. The calculations are probabilistic in the sense that the results are for multiple realizations, carried out using sampled values from the probability distributions for the values of the uncertain model parameters.

There are more than 200 radionuclides in the analyzed waste inventory. It would be impractical for DOE to model all of these radionuclides in a total system performance assessment (TSPA).The analysis for this Repository SEIS used a reduced set of radionuclides. The number of radionuclides to be analyzed was determined by a screening analysis. Thus, the purpose of the radionuclide screening analysis is to remove from further consideration (screen out)

radionuclides that are unlikely to significantly contribute to radiation dose to the RMEI. The remaining nuclides (those screened in) are recommended for consideration in TSPA modeling. The radionuclide screening analysis was recently revised to incorporate updated radionuclide inventory and screening factor data (DIRS 177424-SNL 2007, all). This screening analysis determined that 32 radionuclides could potentially contribute an important fraction of the dose to the RMEI. This set of radionuclides forms the basis for the analysis this chapter discusses. However, it is noted that the TSPA simulations presented in this Repository SEIS for the first 10,000 years after closure were not based on the revised version of the radionuclide screening analysis and 32 radionuclides, but on 29 important radionuclides identified in the previous version of the screening analysis (DIRS 160059-BSC 2002, all). In the revised version of the screening analysis, three additional radionuclides, chlorine-36, selenium-79, and tin-126, were screened in for postclosure analysis. Although these three additional radionuclides were not included in the assessment of postclosure repository performance for the first 10,000 years after repository closure, they were included in the post-10,000 year assessment. The exclusion of the three identified radionuclides from the analysis of the first postclosure time period did not have a significant impact to projected dose. Based on the post-10,000 year total annual dose assessment, these three radionuclides would make the following estimated contributions to total mean annual dose to the RMEI for the first 10,000 years after repository closure: 0.02 millirem (chlorine-36), 0.01 millirem (selenium-79), and 0.000001 millirem (tin-126) for a total annual mean contribution of 0.03 millirem.

Following are projected annual dose histories for the scenario class modeling cases used to simulate repository performance. The projected annual dose calculated for the individual modeling cases are presented on Figures ES-39 to ES-52. The following describes these results by modeling case.

ES9.1.1 Nominal Modeling Case

The results for this modeling case show zero mean annual dose for the first 10,000 years because no waste packages are estimated to fail (by general corrosion, localized corrosion, or stress corrosion cracking) in this period. The first waste package failure (by nominal stress corrosion cracking) would occur at approximately 30,000 years, and the drip shields would begin to fail by general corrosion at approximately 260,000 years. As shown in Figure ES-39, the projected estimated mean and median annual doses would be 0.5 and 0.3 millirem, respectively, for the post-10,000-year period. Figure ES-40 shows the radionuclides that dominate the estimate of projected mean annual dose for the Nominal Scenario Case. The main contributors to mean annual dose would be the highly soluble and mobile radionuclides iodine-129 and technetium-99.

ES9.1. 2 Early Failure Scenario Class Modeling Cases

The Early Failure Class Modeling Cases includes features, events, and processes that relate to early WP and DS failure due to manufacturing, material defects, or preemplacement operations that would include improper heat treatment. In addition, the Early Failure Scenario Class includes all features, events, and processes in the Nominal Scenario Class.

ES9.1.2.1 Drip Shield Early Failure Modeling Case

The defective drip shields were modeled as being failed at the time of repository closure, assuming coincident early WP failure. Figure ES-41 shows the annual dose histories for the first 10,000 years after closure and the post-10,000-year period. The estimated doses account for aleatory uncertainty for characteristics of the early failed drip shields such as the number of early failed drip shields, types of waste package under failed drip shields, and their locations in the repository. The mean, median, and 5th- and 95th-percentile curves in this plot show the uncertainty in the magnitude of the projected annual dose due to epistemic uncertainty from incomplete knowledge of the behavior of the physical system. The calculations for the first 10,000-years show a projected mean annual dose of approximately 0.0003 millirem at 2,000 years. The mean annual dose then decreases steadily and is less than 0.0003 millirem for the post-10,000 year period up to 1 million years.

Figure ES-42 shows the radionuclides contributing most to the total mean annual dose during the first 2,000 years after repository closure are soluble and mobile radionuclides, in particular technetium-99, iodine-129, and carbon-14. During the post-10,000-year period, plutonium-239, and plutonium-240, and neptunium-237 dominate the mean annual dose.

ES9.1.2.2 Waste Package Early Failure Modeling Case

The WPs are assumed to be failed at the time of repository closure but the DSs would degrade by general corrosion and fail in accordance with the Nominal Scenario Class Modeling Case (Figure ES-43). The estimated dose accounts for aleatory uncertainty in the number of early failed WPs, types of early failed WPs, and their locations in the repository. The mean, median, and 5th- and 95th-percentile curves in Figure ES-43 reflect the epistemic uncertainty in the estimated mean annual dose.

The calculated mean annual dose is about 0.004 millirem at about 9,800 years and then increases due to the 10,000-year climate change. The estimated mean and median annual doses are about 0.2 and 0.006 millirem, respectively, before 15,000 years with a gradual decrease thereafter. Figure ES-44 shows that in the first 10,000 years after closure, the more soluble and mobile radionuclides technetium-99, iodine-129, and carbon-14, dominate the estimate of mean annual dose. During the post-10,000-year period, plutonium-239, and plutonium-240, and neptunium-237 dominate the mean annual dose.

ES9.1.3 Igneous Scenario Class Modeling Cases

The Igneous Scenario Class includes all features, events, and processes in the Nominal Scenario Class and includes the set of features, events, and processes specific to igneous disruption. The Igneous Scenario Class consists of two modeling cases: (1) the Igneous Intrusion Modeling Case that represents a magma dike that intrudes into the repository causing subsequent release of radionuclides to the groundwater in the UZ, and (2) the Volcanic Eruption Modeling Case that represents a hypothetical volcanic eruption from a volcanic conduit that passes through the repository and emerges at the land surface with the release of radionuclides to the atmosphere.

ES9.1.3.1 Igneous Intrusion Modeling Case

After a magmatic dike intersects the repository, radionuclide release and transport away from the repository would be similar to the Nominal Modeling Case for radionuclide release and transport. All of the DSs and WPs would be damaged, exposing the waste forms to percolating groundwater with subsequent degradation, radionuclide mobilization, and transport through the UZ to the SZ. The Igneous Intrusion modeling case takes no credit for water diversion by the remnants of the drip shield, waste package, or cladding.

Figure ES-45 shows estimated mean annual dose histories which account for aleatory uncertainty in the igneous intrusion such as the number of future events and the time at which they may occur. The mean, median, and 5th- and 95th-percentile curves in Figure ES-45 indicate epistemic uncertainty in incomplete knowledge of the behavior of the physical system during and after the disruptive event. The calculated mean annual dose for 10,000 years after closure is less than 0.06 millirem, and 1.3 millirem for the post-10,000-year period. The median projected annual dose for the post-10,000-year period is less than 0.4 millirem.

Figure ES-46a shows that technetium-99 and iodine-129 dominate the estimate of the mean for the first 4,000 years and plutonium-239, technetium-99, and plutonium-240 dominate the estimate of the mean for the 10,000-year postclosure period. Figure ES-46b shows that plutonium-239 in both dissolved and colloidal forms would dominate the estimate of the mean for the next 170,000 years, and radium-226, plutonium-242, and neptunium-237 would dominate the estimate of the mean for the remainder of the post-10,000-year period.

ES9.1.3.2 Volcanic Eruption Modeling Case

The volcanic eruption at Yucca Mountain is from an igneous dike that that would rise through the Earth's crust and intersect one or more repository drifts and an eruptive conduit forming somewhere along the dike would feed a volcanic eruption. Waste packages in the direct path of the conduit would be destroyed, and the waste in those packages would be entrained in the eruption. Contaminated volcanic ash would be erupted, and transported in the atmosphere. The RMEI would receive a radiation dose from inhalation and exposure to the contaminated ash.

Figure ES-47 shows the estimated mean annual dose for first 10,000 years after closure, and the post-10,000-year period. The dose considers aleatory uncertainty in the number of WPs intersected by the eruption, the fraction of waste packages intersected that are ejected, eruption power, wind direction, and wind speed and epistemic uncertainty due to incomplete knowledge of the behavior of the physical system during and after the disruptive event. The mean annual dose for 10,000 years after closure is less than 0.0002 millirem, decreasing to less than 0.0001 millirem for the post-10,000 year period.

Figure ES-48 shows the radionuclides that dominate the estimate of mean annual dose for this scenario are the short-lived radionuclides cesium-137 and plutonium-238, which are significant contributors at early times, but their contributions would decrease rapidly because of radioactive decay. At 300 years, americium-241 would dominate the mean annual dose, but its contribution would diminish rapidly after about 1,000 years due to decay. These short-lived radionuclides would be able to reach the location of the RMEI by relatively rapid atmospheric transport. After 1,000 years, plutonium-239 and -240 would become dominant contributors until approximately

100,000 years after closure when radium-226 and thorium-229 become the primary dose contributors for the remainder of the post-10,000-year period.

ES9.1.4 Seismic Scenario Class Modeling Cases

The Seismic Scenario Class represents the direct effects of vibratory ground motion and fault displacement associated with seismic activity including the effects of the seismic hazard on DSs and WPs. The Seismic Scenario Class modeling cases include seismic-related changes in seepage, waste package degradation, and flow in the EBS. The Seismic Scenario Class estimates the mean annual dose due to a presumed seismic event and takes into account the post-event processes that affect system performance. The Seismic Scenario Class is represented by two modeling cases, the Seismic Ground Motion Modeling Case and the Seismic Fault Displacement Modeling Case.

ES9.1.4.1 Ground Motion Modeling Case

The Seismic Ground Motion represents DSs and WPs that fail from mechanical damage associated with seismic vibratory ground motion leading to: stress corrosion cracking, tearing or rupture, localized corrosion, and collapse of drip shield supports. Figure ES-49 presents estimated mean annual dose histories for the Seismic Ground Motion Modeling Case for the first 10,000 years after closure and the post-10,000-year period. The mean annual dose takes into account aleatory uncertainty associated with the number of events, times of events, and events' peak ground velocities.

The mean, median, and 5th- and 95th-percentile dose histories on Figure ES-49 show uncertainty in the value of the mean annual dose and consider epistemic uncertainty due to incomplete knowledge of the behavior of the physical system during and after the disruptive event. This figure shows that the highest projected mean annual dose for 10,000 years after closure is approximately 0.2 millirem. The median annual dose for the 1-million-year period is less than 0.5 millirem. The spikes in the results correspond to the occurrence of seismic events of sufficient magnitude to cause damage to the waste packages.

The results in Figure ES-50 show that technetium-99, carbon-14, and iodine-129, and plutonium-239 dominate the estimate of the mean for 10,000 years after closure. Figure ES-50 shows that radionuclides technetium-99, iodine-129, selenium-79, and plutonium-239/radium-226 would dominate the estimate. The mean annual dose due to carbon-14 would decrease completely by 100,000 years because of radioactive decay. The codisposal waste packages would be the primary waste packages damaged during 10,000 years after closure because the commercial spent nuclear fuel waste packages are stronger and more failure-resistant. The commercial spent nuclear fuel waste packages will be more robust than codisposal waste packages because they include two inner stainless-steel vessels instead of one: the inner vessel and its lids similar to the codisposal waste packages, and an additional stainless-steel TAD canister. The predominant mechanism that would cause damage to codisposal and commercial spent nuclear fuel waste packages would be through stress-corrosion cracking resulting in diffusive releases of radionuclides. Diffusive transport of dissolved radionuclides through the cracks contributes significantly to the total estimated mean annual dose.

ES9.1.4.2 Fault Displacement Modeling Case

The Seismic Fault Displacement Modeling Case includes disruption of waste packages and drip shields by the displacement of faults, as well as local corrosion failure of waste packages exposing WPs to flow through drip shield breaches. Figure ES-51 shows the mean annual dose histories for the Seismic Fault Displacement Modeling Case for the first 10,000 years after closure and post-10,000-year period. The projected dose accounts for aleatory uncertainty for characteristics for the number of disrupted drip shields and waste packages. The mean, median, and 5th- and 95th-percentile curves on Figure ES-51 show uncertainty in the value of the mean annual dose, taking into account epistemic uncertainty from incomplete knowledge of the behavior of the physical system during and after the disruptive event. These figures show that the mean annual dose for 10,000 years after closure is less than 0.002 millirem and for the post-10,000-year period is approximately 0.02 millirem. The median projected dose for the post-10,000-year period is approximately 0.01 millirem.

The results in Figure ES-52 show the radionuclides that contribute most to the estimate of mean annual dose. Figure ES-52a shows that plutonium-239, iodine-129, and plutonium-240 dominate the estimate of the mean annual dose for 10,000 years after closure. Figure ES-52b shows that plutonium-239, radium-226, and technicium-99 dominate the mean at 100,000 years and plutonium-242, radium-226, and neptunium-237 dominate the mean for the remainder of the post-10,000-year period.

ES9.2. Total Mean Annual Dose to the Reasonably Maximally Exposed Individual for the Repository System

Figure ES-53 shows an estimate of the total repository system performance obtained by adding together the total mean annual dose histories for the Drip Shield EF, Waste Package EF, Igneous Intrusion, Volcanic Eruption, Seismic GM, and Seismic FD Modeling Cases. The Nominal Modeling Case has zero annual dose during the 10,000 years after repository closure and does not contribute to total mean annual dose during that time. Figure ES-53 shows that the Seismic GM and Igneous Intrusion Modeling Cases provide the largest contributions to the maximum estimated mean annual dose.

Retention of radionuclides by the EBS arises from the containment provided by the WPs. In the Waste Package EF Modeling Case, only a small number of WPs are expected to be breached. In the Igneous Intrusion Modeling Case, a larger number of WPs can be breached, but the low probability of breaching means that the expected containment of radionuclides will continue to be substantial. In the Seismic GM Modeling Case, a seismic event can result in failure of all WPs in the repository. However, because the breaches of the WPs are expected to consist of small cracks, the amount of breached area also will be small. Therefore, the low probability of seismic events that can cause breaches in WPs means that there will continue to be substantial containment of radionuclides in the Seismic GM Modeling Case.

The subsystem performance analyses provided by the TSPA-SEIS also indicate retention of radionuclides by the EBS by sorption of actinides on corrosion products in the WPs, and diffusion of radionuclides into these corrosion products, and in the drift invert materials. Irreversible sorption of plutonium and americium onto the corrosion product solid phases results

in a reduction in the release of these radionuclides from the repository system. In the Early Failure and Seismic GM Modeling Cases, advective transport of radionuclides within the WPs is precluded and slow diffusive transport limits the annual release of radionuclides from the WPs and the EBS. The diffusivity of colloids is a factor of 100 lower than that for solutes, limiting release of radionuclides irreversibly bound to colloids relative to the release of dissolved radionuclides. The lower natural barrier reduces the amount of radionuclides that can reach the RMEI in 10,000 years and provides substantial dispersion in the transport of radionuclides, reducing the annual release of radionuclides from the lower natural barrier.

The subsystem performance analyses indicate that the most important factors determining the estimate of the total mean annual dose for the Early Failure Modeling Cases and the Seismic GM Modeling Case are the breaching of WPs, in-package solubility of radionuclides such as uranium and neptunium, irreversible sorption of plutonium and americium onto corrosion products, in-package diffusion, and delay and dispersion in the SZ. These analyses indicate that the most important factors determining the estimate of the total mean annual dose for the Igneous Intrusion Modeling Case are seepage into emplacement drifts, the number of breached WPs and DSs, in-package solubility of radionuclides such as uranium and neptunium, irreversible sorption of plutonium and americium onto corrosion products, colloid concentration limits, and delay and dispersion in the SZ.

ES9.3 Effects of Annual Dose on Postclosure Individual and Groundwater Protection Standards

ES9.3.1 Individual Protection Standard

The results of the TSPA-SEIS include calculations of the mean annual dose to the RMEI in any year during the next 10,000 years after repository closure. The postclosure individual protection standard is 15 millirem/year (NRC Proposed Rule 10 CFR 63.311 [DIRS 178394]). The TSPA-SEIS results, shown on Figure ES-53, show that the highest projected mean and median annual doses to the RMEI are estimated to be about 0.2 millirem and 0.1 millirem, respectively. These results demonstrate that the total mean annual dose (NRC Proposed Rule 10 CFR 63.303 [DIRS 178394]) to the RMEI in any year during the next 10,000 years after repository closure is less than the individual protection standard at 10 CFR 63.331 [DIRS 180319]. Figure ES-53 shows that the highest projected mean and median annual doses after 10,000 year postclosure but within the period of geologic stability are estimated to be about 2.3 millirem and 0.9 millirem, respectively. These highest projected mean dose values are below the individual protection limit of 350 millirem.

ES9.3.2 Groundwater Protection Standard

The groundwater protection standard at 10 CFR 63.331 [DIRS 180319] stipulates that the releases of radionuclides in groundwater at the location of the RMEI should not cause the level of radioactivity in the representative water volume of 3,000 acre-ft of water per NRC Proposed Rule 10 CFR 63.332(a)(3) [DIRS 180319] to exceed the regulatory standards. However, the TSPA-SEIS results can be used with other information to compare repository performance to the groundwater protection standard at 10 CFR 63.331 [DIRS 180319].

The analyses of groundwater protection were made considering only likely processes and events. For the purposes of these analyses, likely processes and events are those that have a probability of occurrence in 10,000 years greater than 10 percent.

Figure ES-54 shows the estimates of groundwater protection performance measures taken from the simulation for the Early Failure Modeling Cases and the Seismic GM Modeling Case. The first groundwater protection performance measure is the maximum concentration of ^{226}Ra and ^{228}Ra in the representative volume of 3,000 acre-ft/yr of water. The second groundwater protection performance measure is gross alpha activity (excluding radon and uranium) in that volume (Figure ES-55). The third is the amount of beta- and photon-emitting radionuclides in the groundwater, expressed in terms of annual dose to the whole body or any organ of a human receptor resulting from drinking two liters of this water per day (Figure ES-56).

ES9.4. Human Intrusion

To address the second requirement of the human intrusion standard (40 CFR 197.25(b)), DOE conducted a TSPA-SEIS calculation for the drilling intrusion scenario. The Department used a probabilistic approach analogous to that used to evaluate conformance with the individual protection and groundwater protection standards, to evaluate the dose *risk* for the human intrusion standard. It performed dose calculations for all environmental pathways, as 40 CFR 197.25(c) specifies.

Figure ES-57 shows the mean, median, and 5th- and 95th-percentile values for the annual individual doses for the post-10,000-year period that could result from a human intrusion 200,000 years after repository closure for the set of 300 epistemic realizations. Estimates of WP degradation and the ability to drill through a degraded WP using current technology suggested that at about 200,000 years, sufficient thickness would have been lost to general corrosion to allow current technology to penetrate a WP. The values in Figure ES-57 represent the dose from a single waste package, and are not combinations of releases from other waste packages that would fail due to other processes. The mean and median annual individual doses from human intrusion are estimated to be less than 0.01 millirem and occur approximately 4,000 years after intrusion. These results indicate that the repository would be sufficiently robust and resilient to limit releases from human intrusion to values well below the individual protection standard for human intrusion of 350-millirem annual individual dose to the RMEI for intrusions in the post-10,000-year period. The regulations exclude the calculation of a potential dose to the hypothetical driller.

ES9.5. Uncertainty/Sensitivity Results

For different time frames in the analysis, different epistemic parameters emerge as important to the overall uncertainty in the results. Table ES-1 lists summary results of the sensitivity analysis. The important parameters, which the table lists, are as follows:

- *IGRATE.* This parameter is the probability of an igneous event, which is the annual frequency, as a cumulative distribution function, of an intersection of the repository by a volcanic dike. It was assumed that an igneous intrusion event would destroy all drip

shields and waste packages and, therefore, they would offer no barrier to seepage and radionuclide transport.

- *SCCTHRP.* This parameter is the residual stress threshold for the Alloy-22 waste package outer barrier. If the residual stress in the waste package outer barrier exceeded this threshold value, stress corrosion cracks could form, which could allow radionuclides to migrate from the waste package. The primary causes of residual stresses in the waste package outer barrier would be low-frequency, high-peak ground velocity seismic ground motions, which could cause impacts from waste package to waste package, from waste package to emplacement pallet, and from waste package to drip shield. These impacts could cause dynamic loads that dented the waste package, which could result in structural deformation with residual stresses that make the material susceptible to stress corrosion cracking.

- *WDGCA22.* This parameter relates to the temperature dependence for the general corrosion rate of the Alloy 22 waste package outer barrier. It determines the magnitude of this temperature dependence and directly influences the short-term and long-term general corrosion rates of the Alloy 22; the larger this value the higher the earlier general corrosion rates during the thermal period and the lower the long-term corrosion rates when the repository temperatures are near the ambient in- situ temperature.

The parameters in Table ES-1 that most affect the total uncertainty in the TSPA-SEIS model are factors that would govern degradation of the waste packages or the rate at which igneous intrusion would destroy all waste packages.

Table ES-1. Top-Ranking Uncertainty Importance Parameters

Time after closure (years)	Two most important parameters	
3,000	SCCTHRP	IGRATE
5,000	SCCTHRP	IGRATE
10,000	SCCTHRP	IGRATE
125,000	IGRATE	SCCTHRP
250,000	WDGCA22	IGRATE
500,000	IGRATE	WDGCA22
1,000,000	IGRATE	WDGCA22

Source: DTN: MO0708TSPASEIS.000

ES10. SUMMARY OF THE RESULTS OF THE TSPA-SEIS

The TSPA-SEIS was applied to the assessment of total system performance of the Yucca Mountain repository based on FEPs that could affect total system performance. The TSPA-SEIS analyses incorporate uncertainty in input data and submodel performance and use the validated TSPA-SEIS. All parameter values and ranges of parameter values used to calculate mean annual dose and other calculated values determined for the six TSPA-SEIS cases can be found in output DTN: MO0708TSPASEIS.000.

The TSPA-SEIS simulation/analysis periods cover 10,000 years after repository closure and the 1,000,000-year period of geologic stability. The 10,000-year simulations are extended to an

additional 10,000 years to assess whether or not the trends present at the end of 10,000 years continue, or if uncertainties in the 10,000-year results affect the overall conclusions regarding the 10,000-year performance period and beyond. The analyses results showed that the period between 10,000 years to 20,000 years after repository closure did not display any significant changes to the trends observed from 0 to 10,000 years, providing confidence in the conclusions reached regarding the 10,000-year period.

The TSPA-SEIS results demonstrate that the projected highest mean dose to the RMEI in any year during the next 10,000 years after repository closure is less than the individual protection standard at 10 CFR 63.331 and its Table 1 [DIRS 180319], which describes the limits on radionuclides in the representative volume. The TSPA-SEIS analyses also indicate the performance of the repository system provides significant protection to groundwater. The results show concentrations of in the groundwater are likely to be well below groundwater protection standards at 10 CFR 63.331 [DIRS 173164]. Likewise, the results suggest the mean annual drinking water dose to any organ and to the whole body from beta-and photon-emitting radionuclides is likely to be well below the applicable standards.

Thus, the physiographic setting, topography, climate, area geology, and soil characteristics are favorable for restricting the amount of infiltration of precipitation into the subsurface at the repository location. This along with rock characteristics, ambient and perturbed subsurface environmental conditions, and geometry of emplacement drifts tend to further limit the amount of liquid water available to enter drifts. Features of the waste form and other components of the engineered system, physical limitations on solubility of radionuclides, and subsurface geology and hydrology further limit the release, rate of release, and transport of radionuclides to the saturated zone beneath the repository. Only a small fraction of radionuclide inventory is projected to be released from the EBS, move down through the unsaturated zone beneath the repository and enter the saturated zone. Sorption and diffusion of radionuclides into the UZ further reduces the amount. Once the migrating radionuclides enter the saturated zone, the performance assessment indicates the characteristics of the rock, soil, and the hydrologic and geochemical environmental factors further reduce the transport and rate of transport of the radionuclides to the accessible environment. Even with incorporation of disruptive events, the repository system evaluation indicates it will perform in a manner that protects the future human populations of the area with a high degree of confidence.

INTENTIONALLY LEFT BLANK

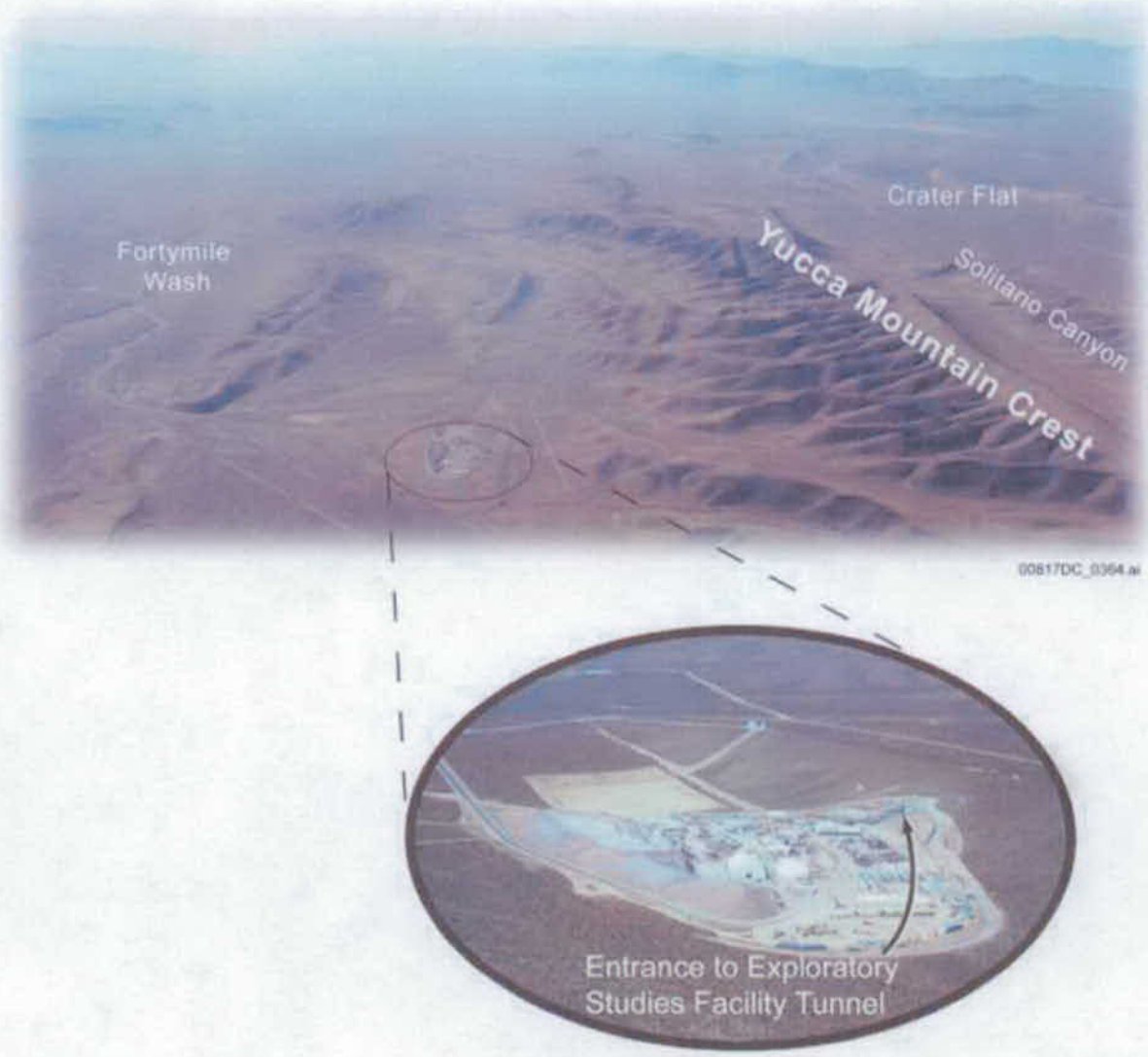

Figure ES-1. Yucca Mountain Area

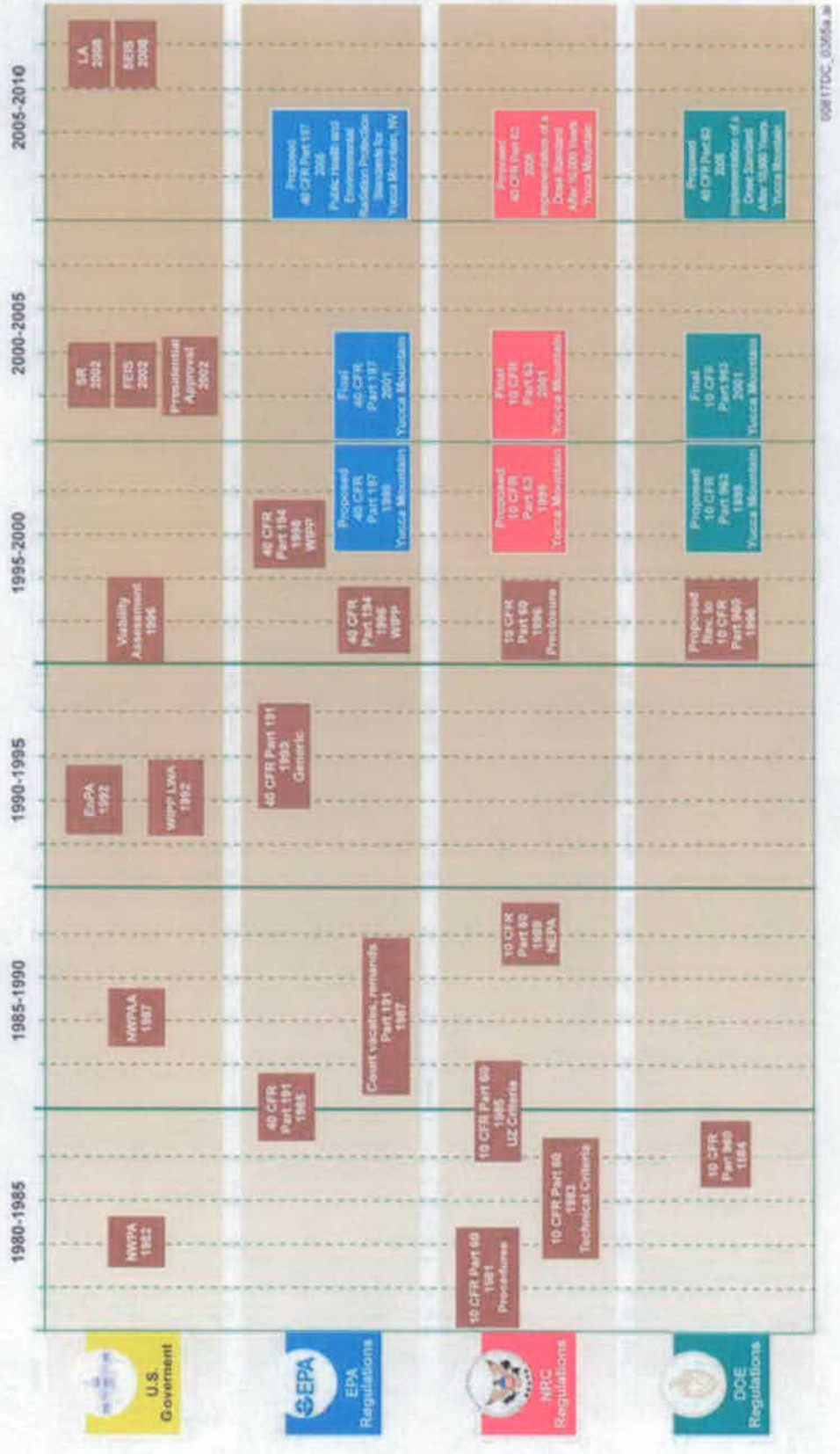

Figure ES-2. Timeline of Legislative and Regulatory Events: 1980 to 2010

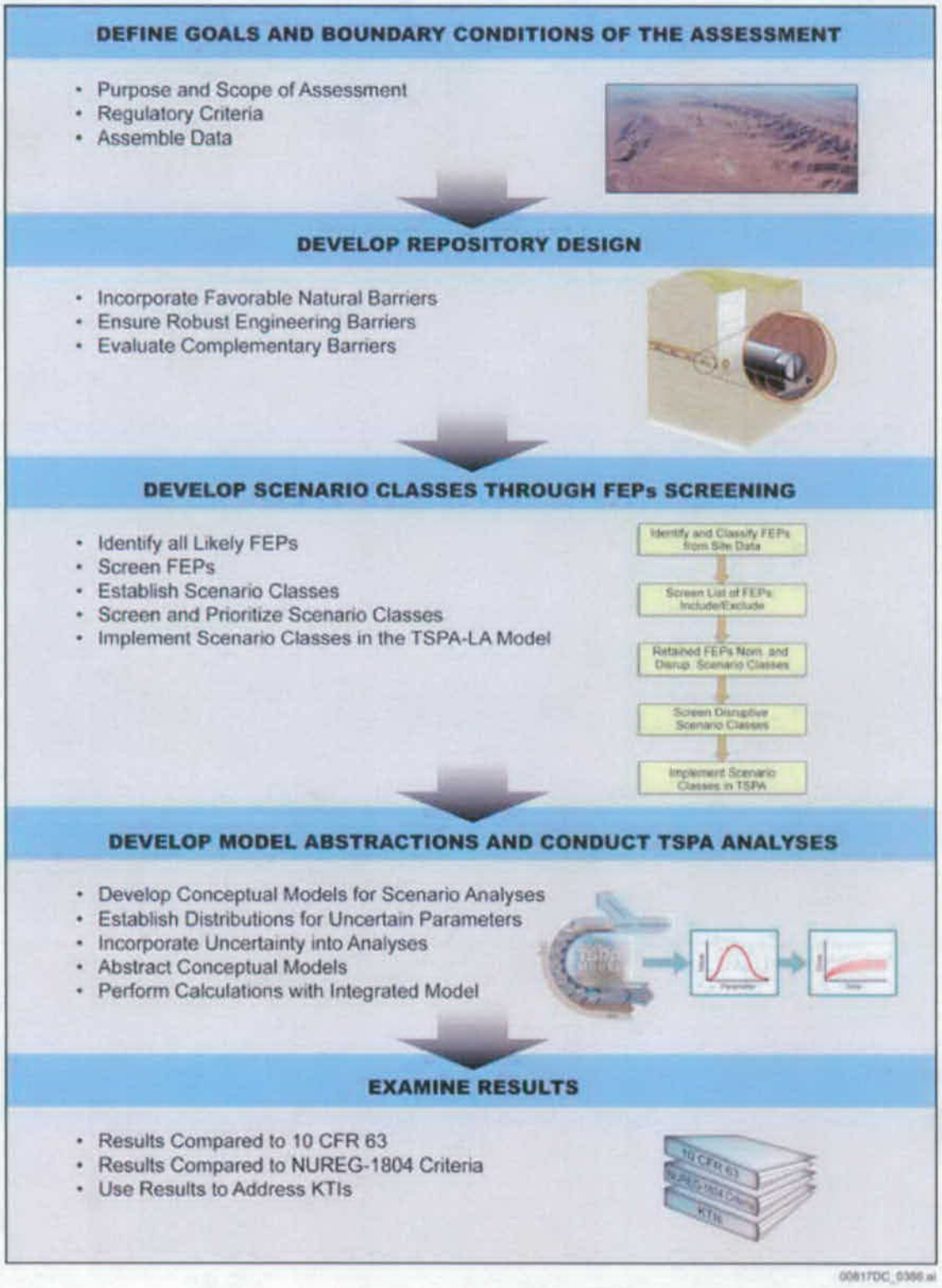

Figure ES-3. Structure of the Process of the TSPA-SEIS

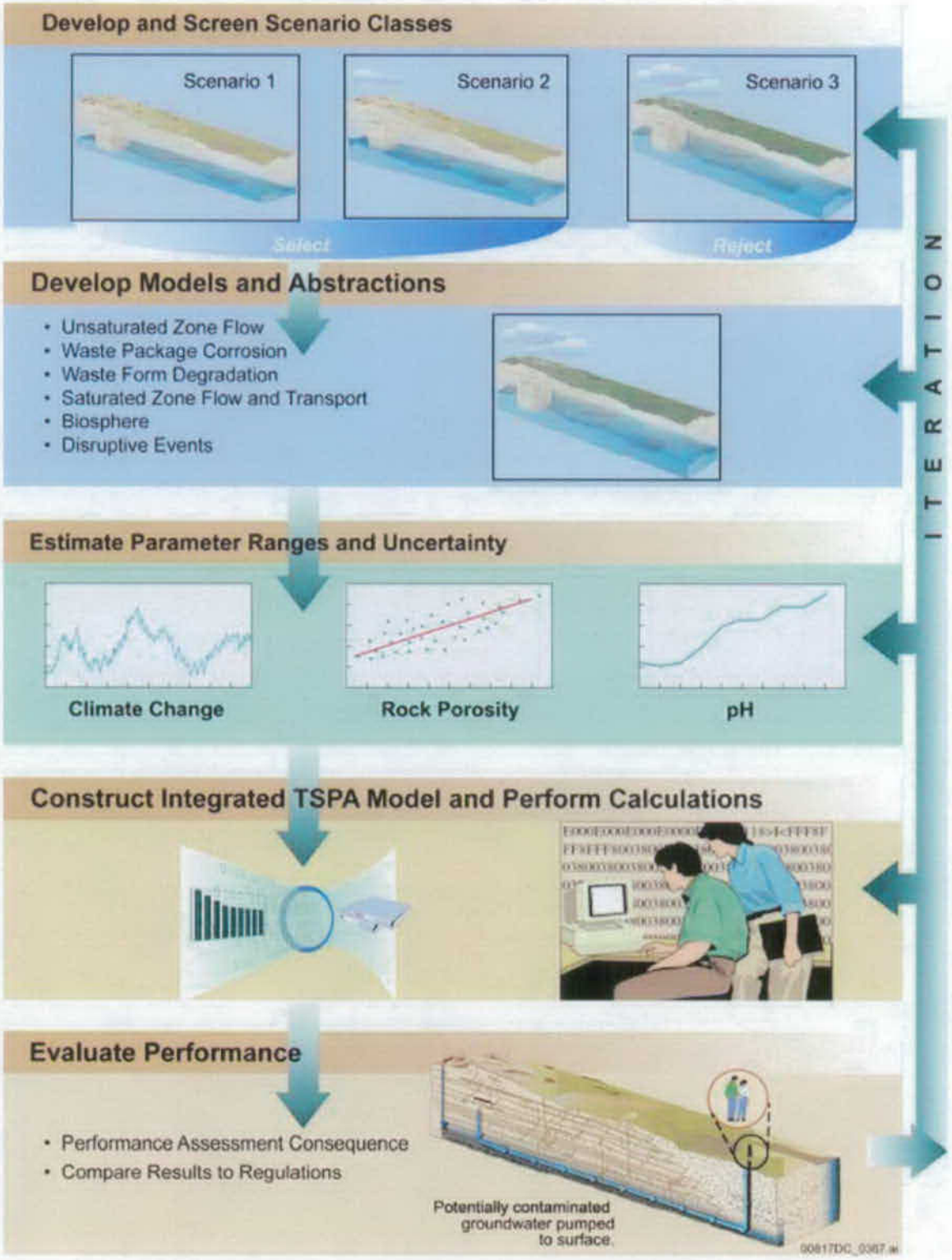

Figure ES-4. Major Steps in a Generic Performance Assessment

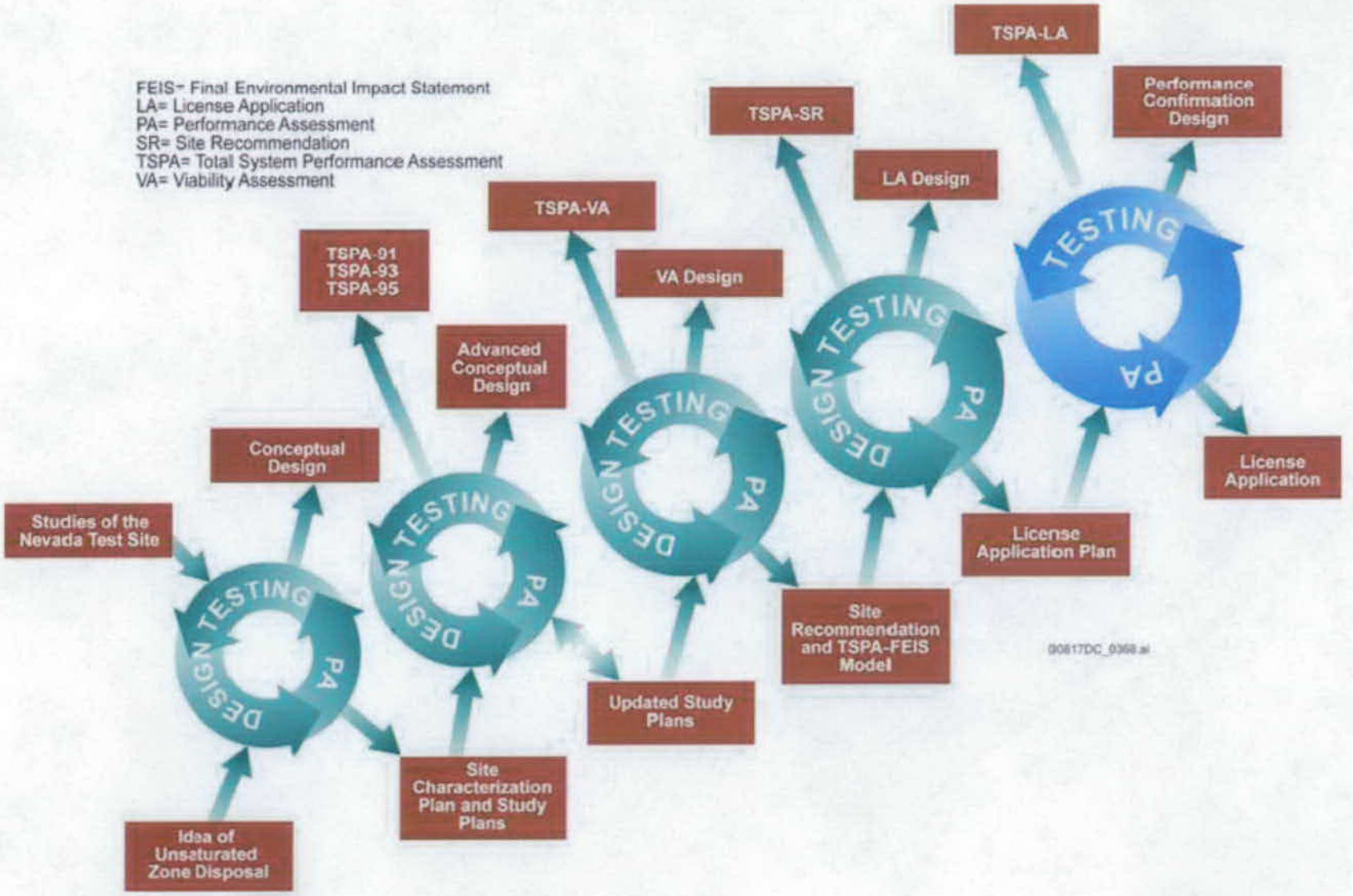

Figure ES-5. Iterative Application of the TSPA Process

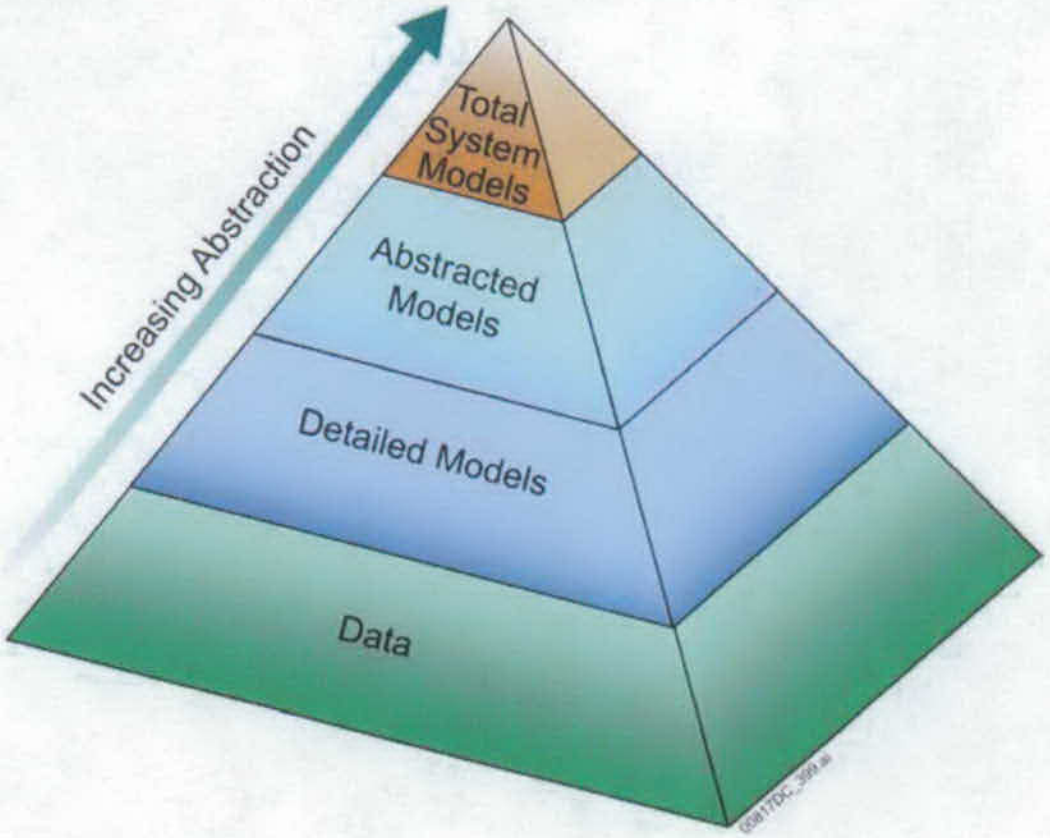

Figure ES-6. Performance Assessment Pyramid Showing the Steps Involved in Developing a Total System Model

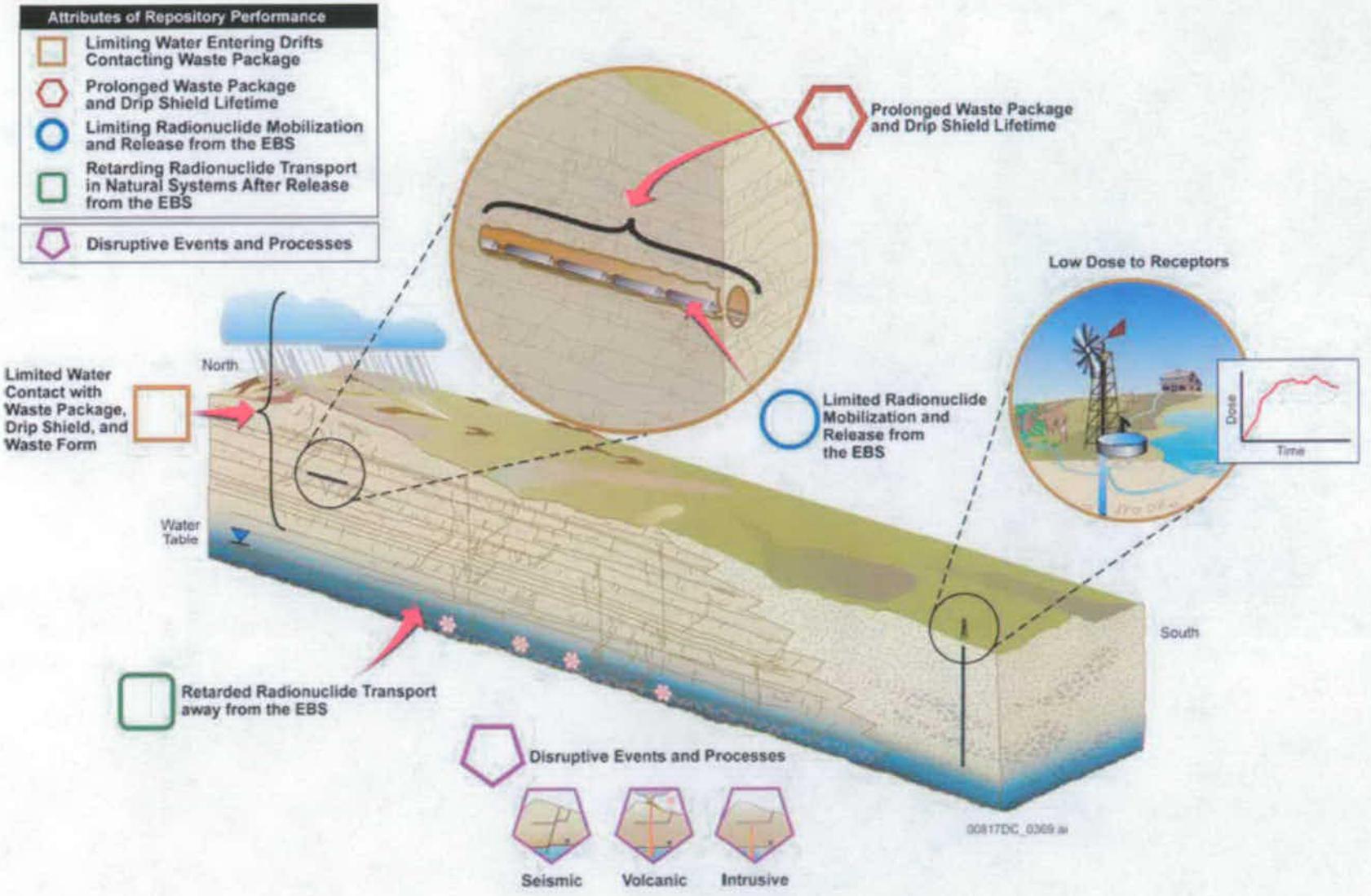

Figure ES-7. Schematic of Attributes of Repository Performance

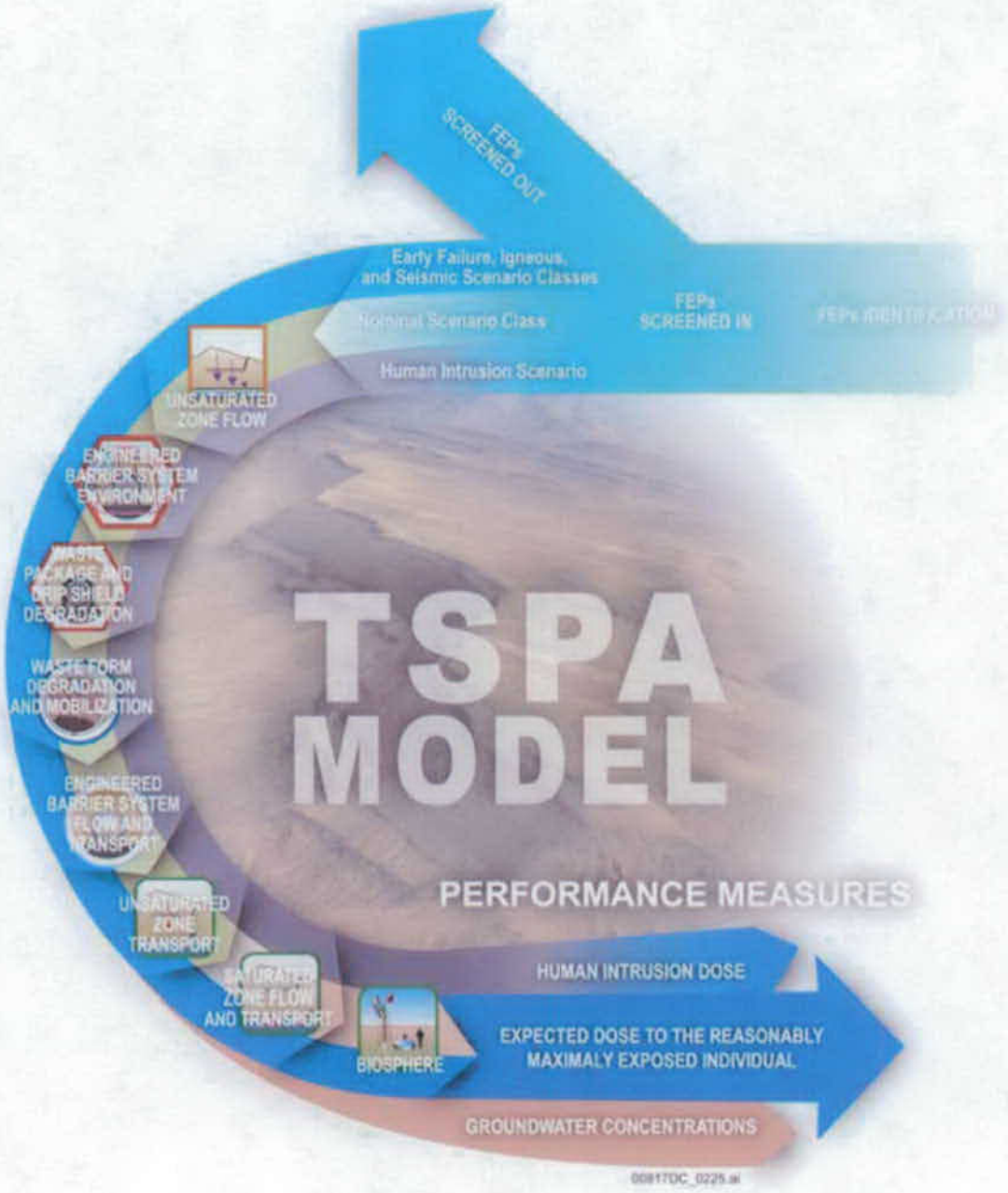

Figure ES-8. Schematic Representation of the Development of the TSPA-SEIS Model, Including the Nominal, Igneous, and Seismic Scenario Classes

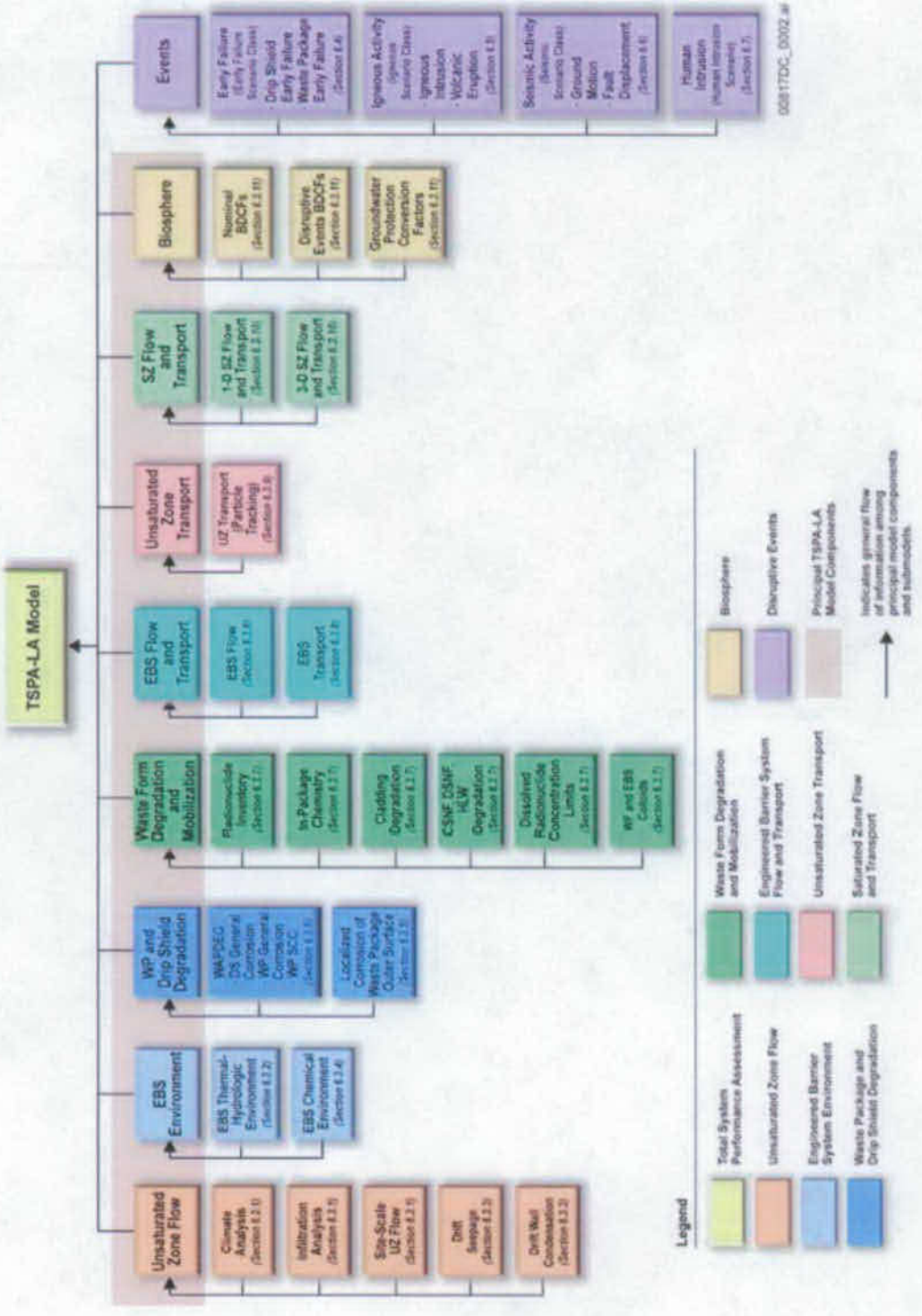

Note: Structure of the TSPA-SEIS is similar to the TSPA-LA Model.

Figure ES-9. TSPA-SEIS Principal Model Components and Submodels

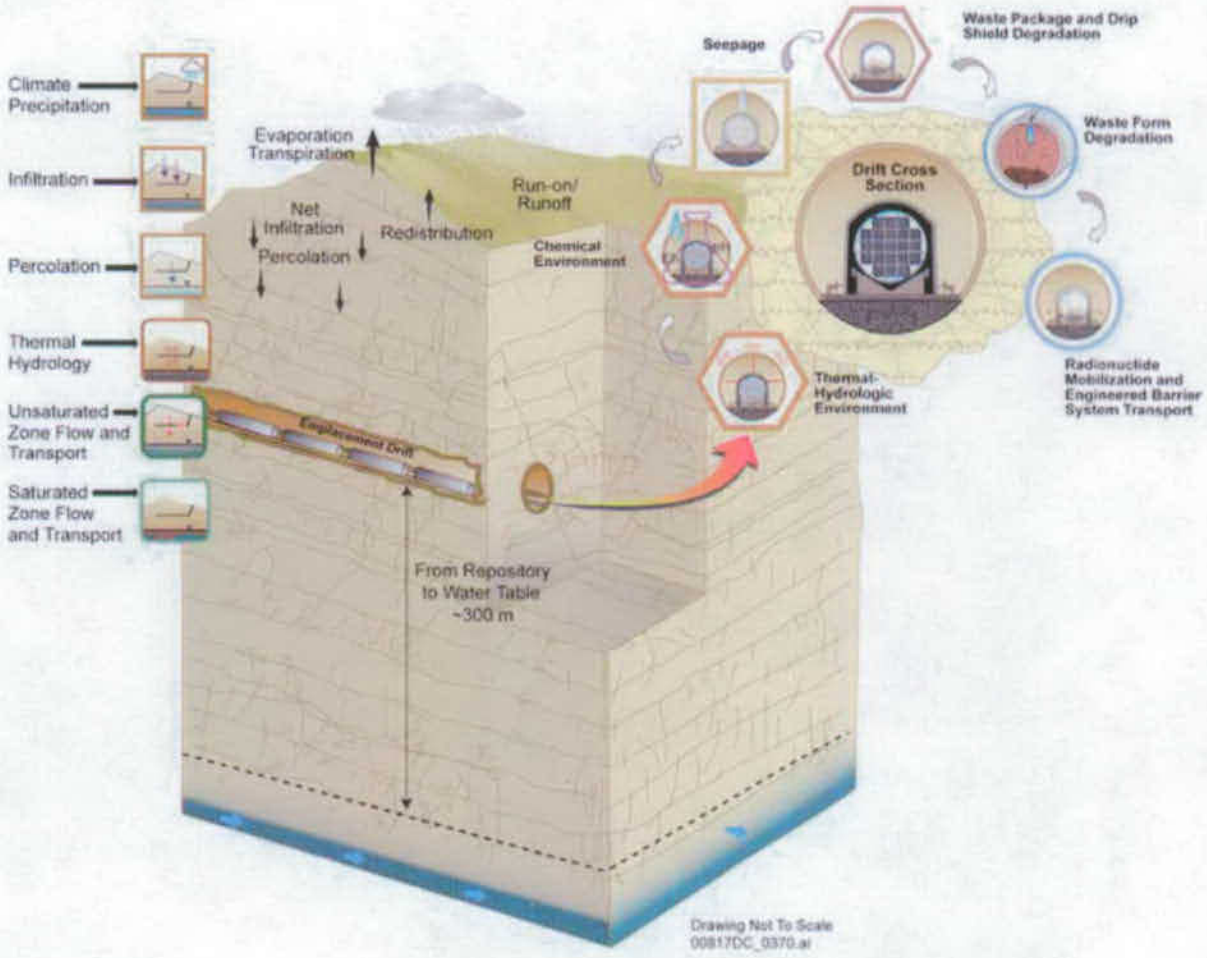

Figure ES-10. Principal Components of the Yucca Mountain Repository System

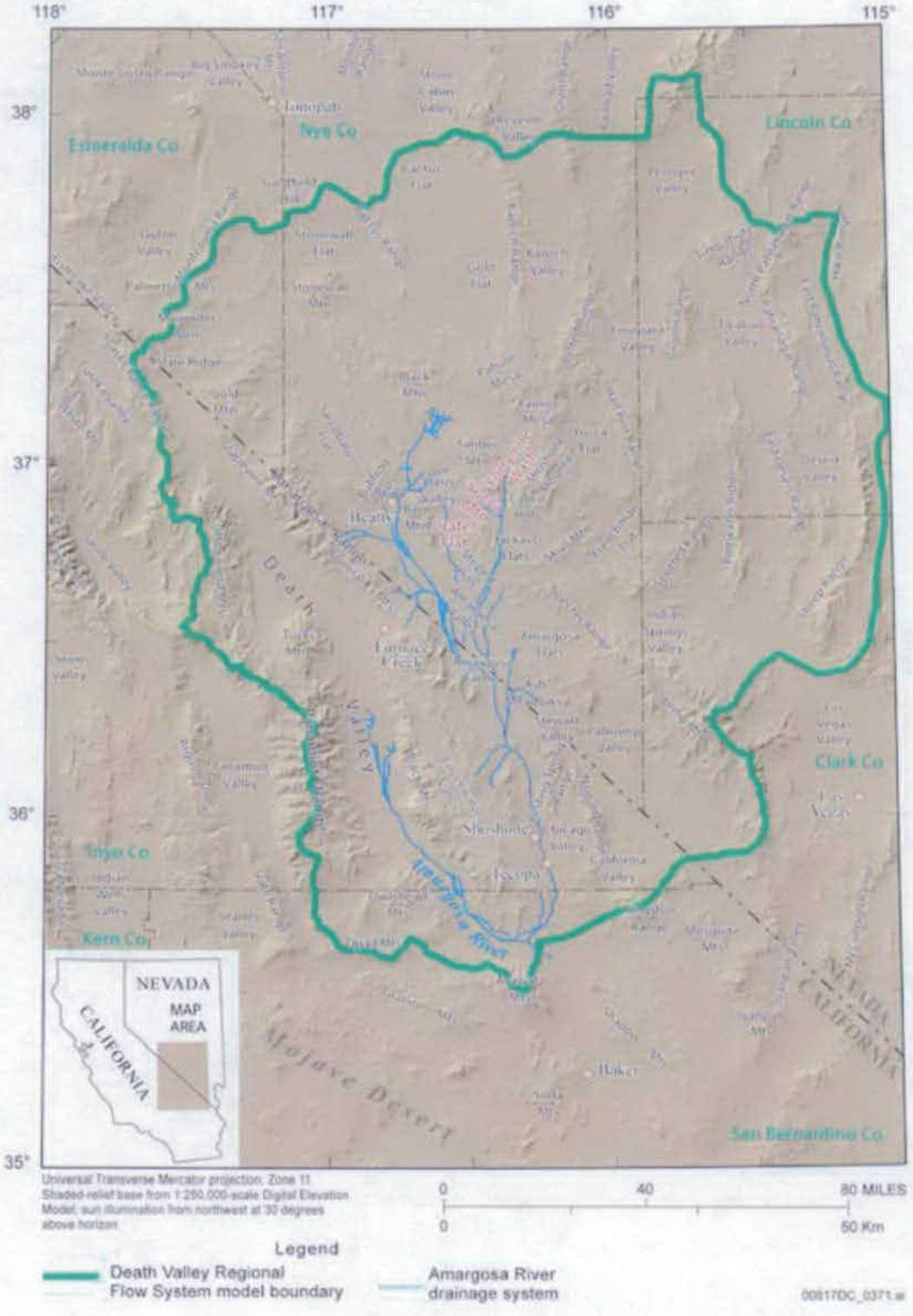

Source: Modified from (BSC 2004 [DIRS 169734], Figure 8-2)

Figure ES-11. Geographic and Prominent Topographic Features of the Death Valley Region

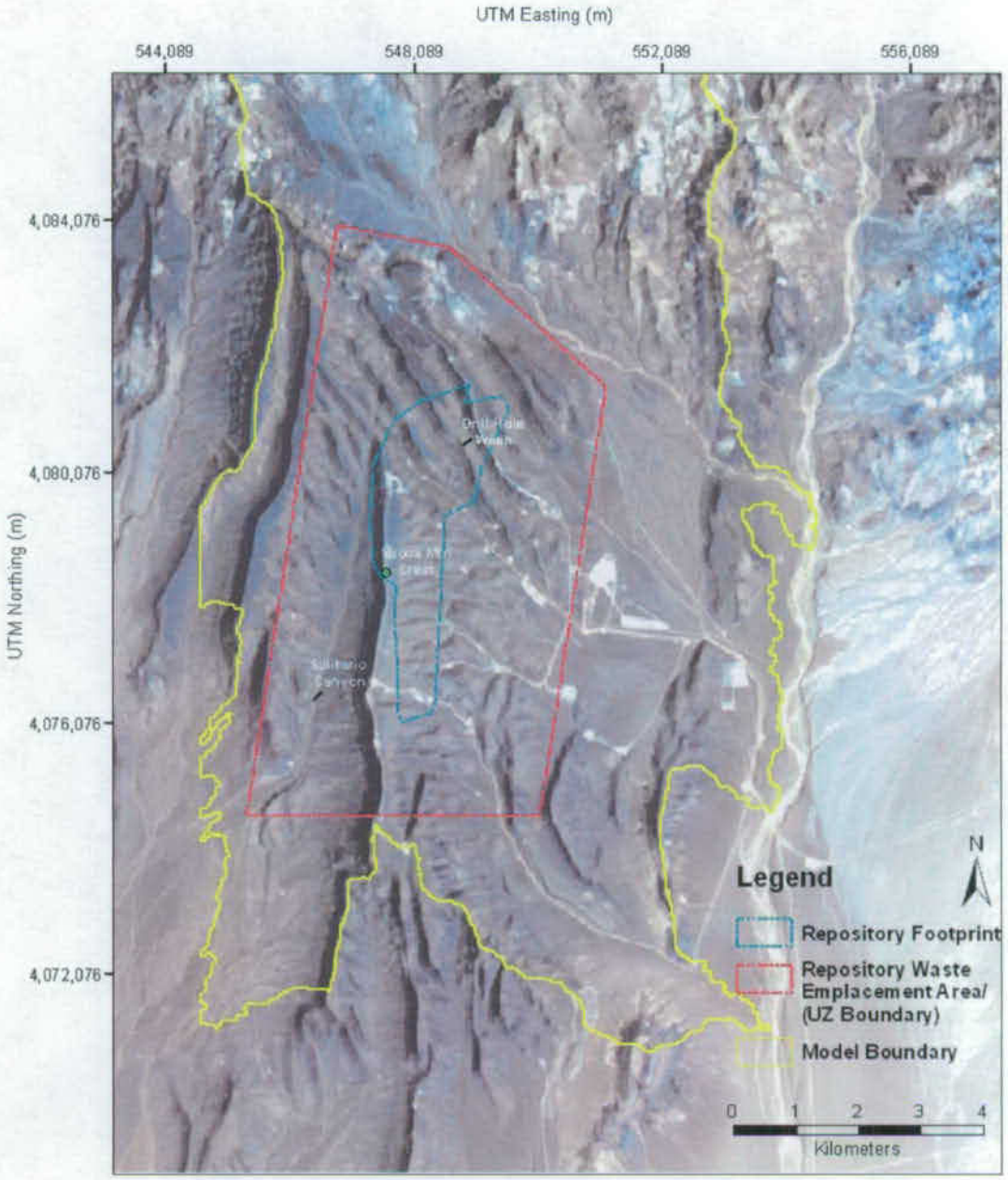

Source: Modified from SNL 2007 [DIRS 174294], Figure 6.5.2.1-1.

NOTE: The model boundary is the same as the 1999 unsaturated zone flow model domain of the TSPA-SR.

Figure ES-12. Topographic Map of the Yucca Mountain Site Showing in Slope Characteristics

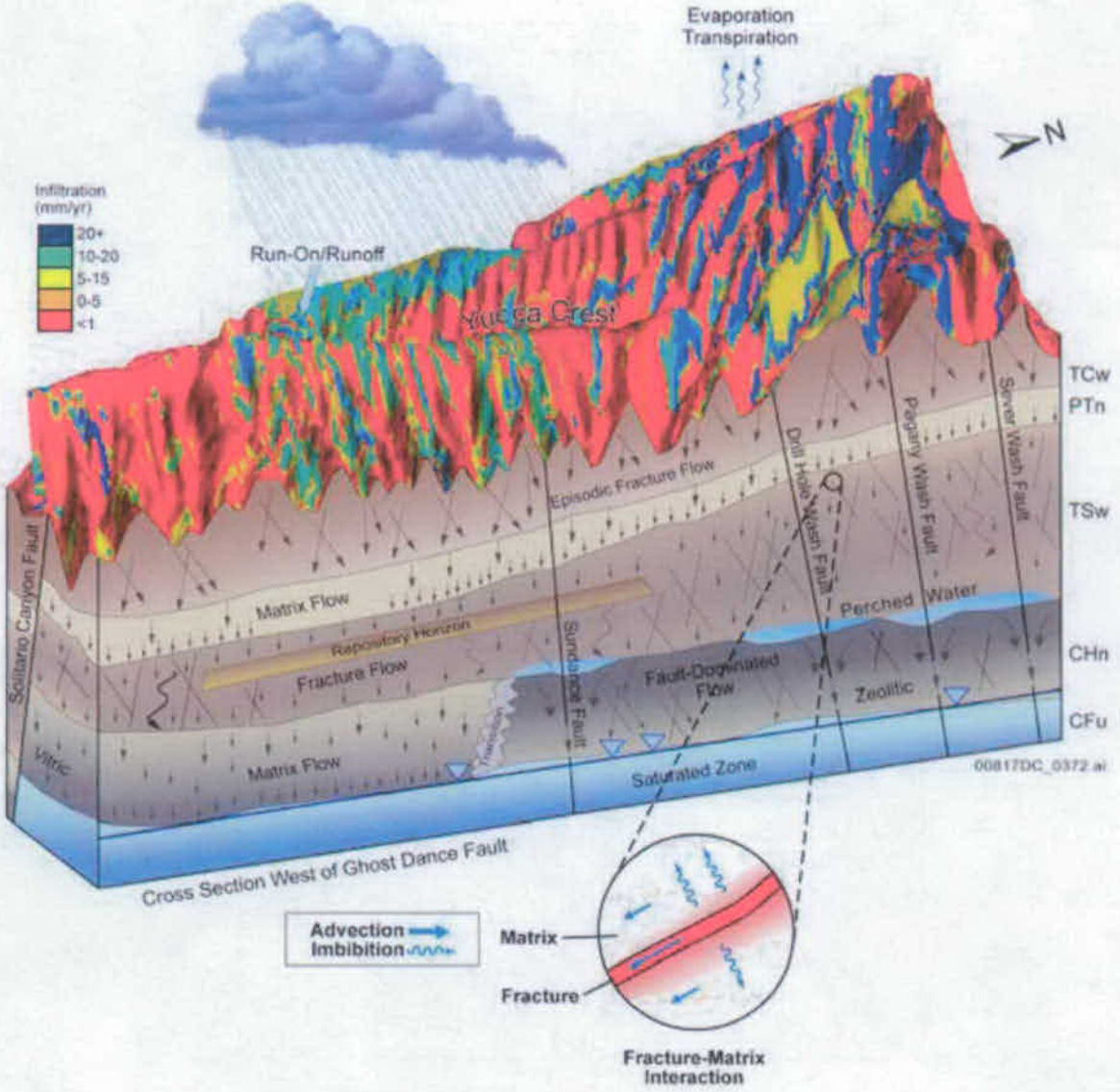

Source: Modified from BSC 2004 [DIRS 170035], Figure 6-1.

Figure ES-13. Overall Water Flow Behavior in the Unsaturated Zone, Including the Relative Flux Magnitudes of Fracture and Matrix Flow Components in the Different Hydrogeologic Units

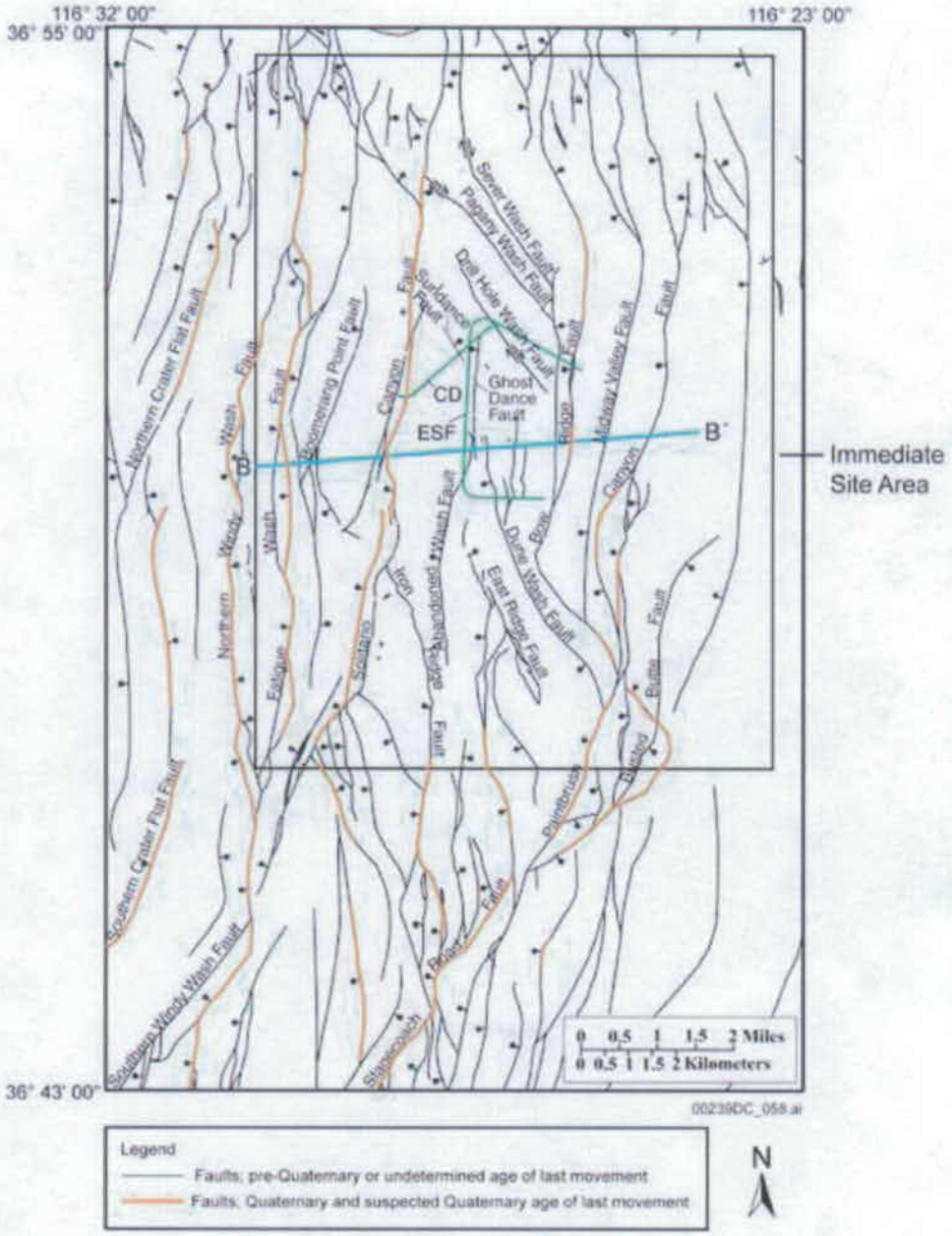

Source: Modified from BSC 2004 [DIRS 169734], Figure 3-20.

NOTES: The following faults have demonstrable Quaternary activity: Northern Crater Flat fault, Southern Crater Flat fault, Northern Windy Wash fault, Southern Windy Wash fault, Fatigue Wash fault, Solitario Canyon fault, Iron Ridge fault, Bow Ridge fault, Paintbrush Canyon fault, and Stagecoach Road fault. All faults are shown with solid lines, although many segments are concealed or inferred.

Symbols and acronyms: bar and bell: downthrown side of fault; arrows: relative direction of strike-slip movement; ESF = Exploratory Studies Facility (green line); CD = Cross-Drfit; blue line: approximate location of section on Figure ES-15.

Figure ES-14. Distribution of Faults in the Yucca Mountain Site Area and Adjacent Areas to the South and West

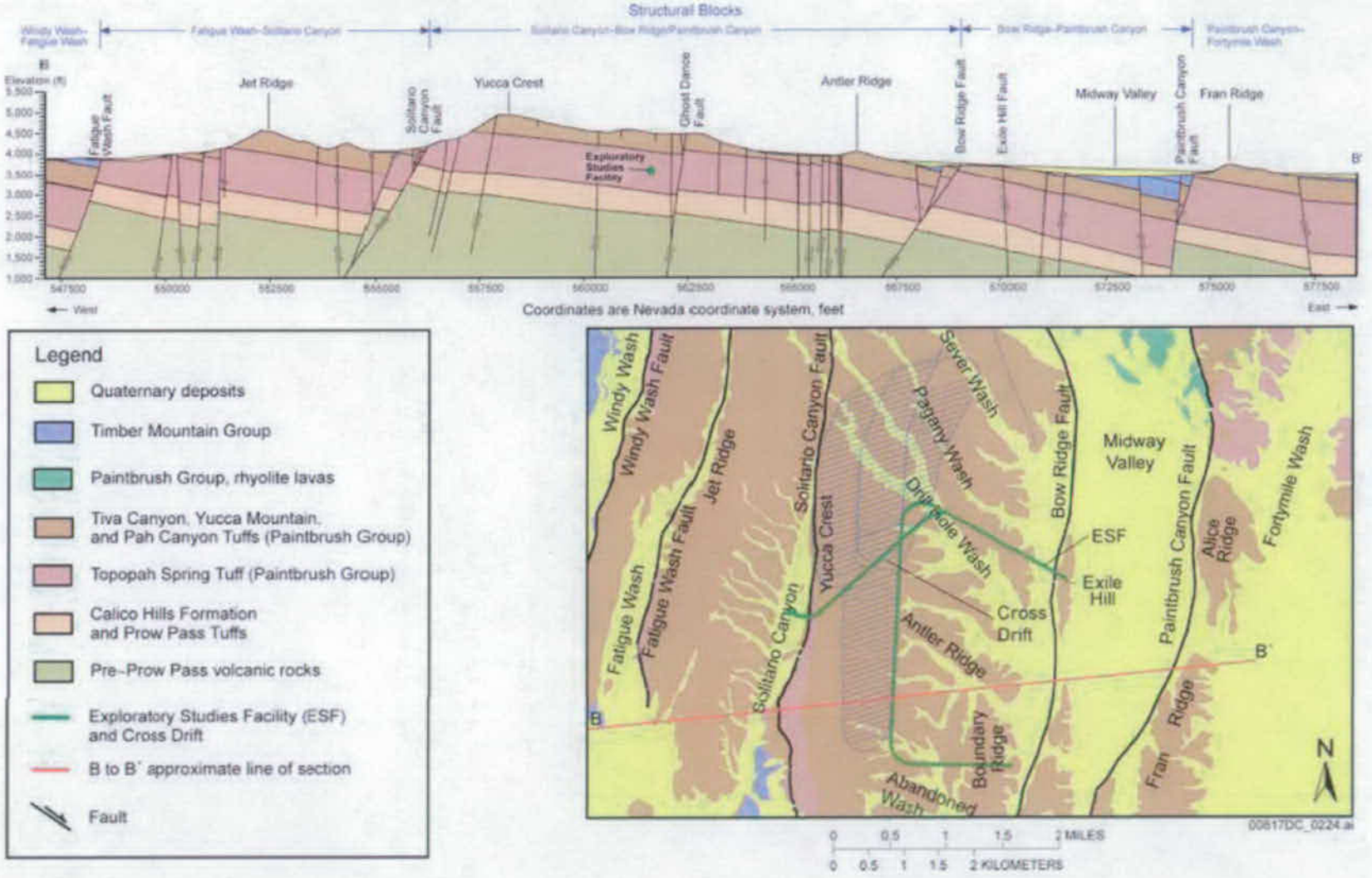

Source: Simplified from Day et al. 1998 [DIRS 100027], Cross Section B-B'

NOTE: ESF = Exploratory Studies Facility, location of intersection along the approximate line of section, also shown on Figure ES-14.

Figure ES-15. East-West Structure Section across Yucca Mountain Site Area

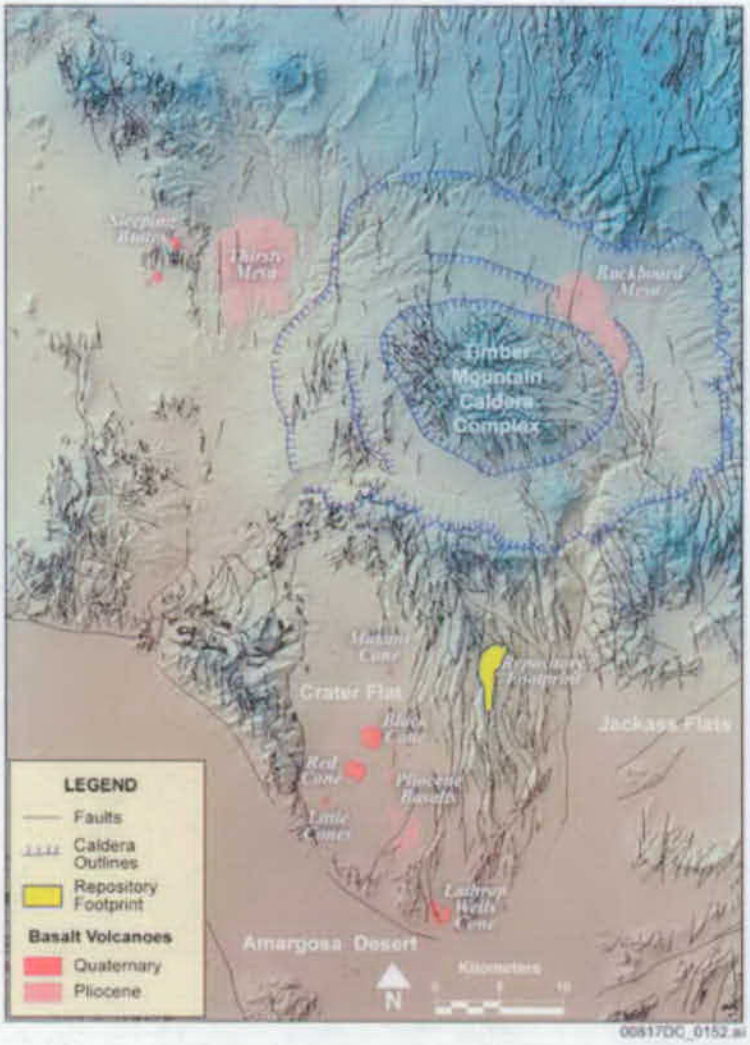

Source: Modified from CRWMS M&O 1998 [DIRS 123196], Figure 2.1

Figure ES-16. Location and Age of Post-Miocene (less than 5.3 million years) Volcanoes (or clusters where multiple volcanoes have indistinguishable ages) in the Yucca Mountain Region

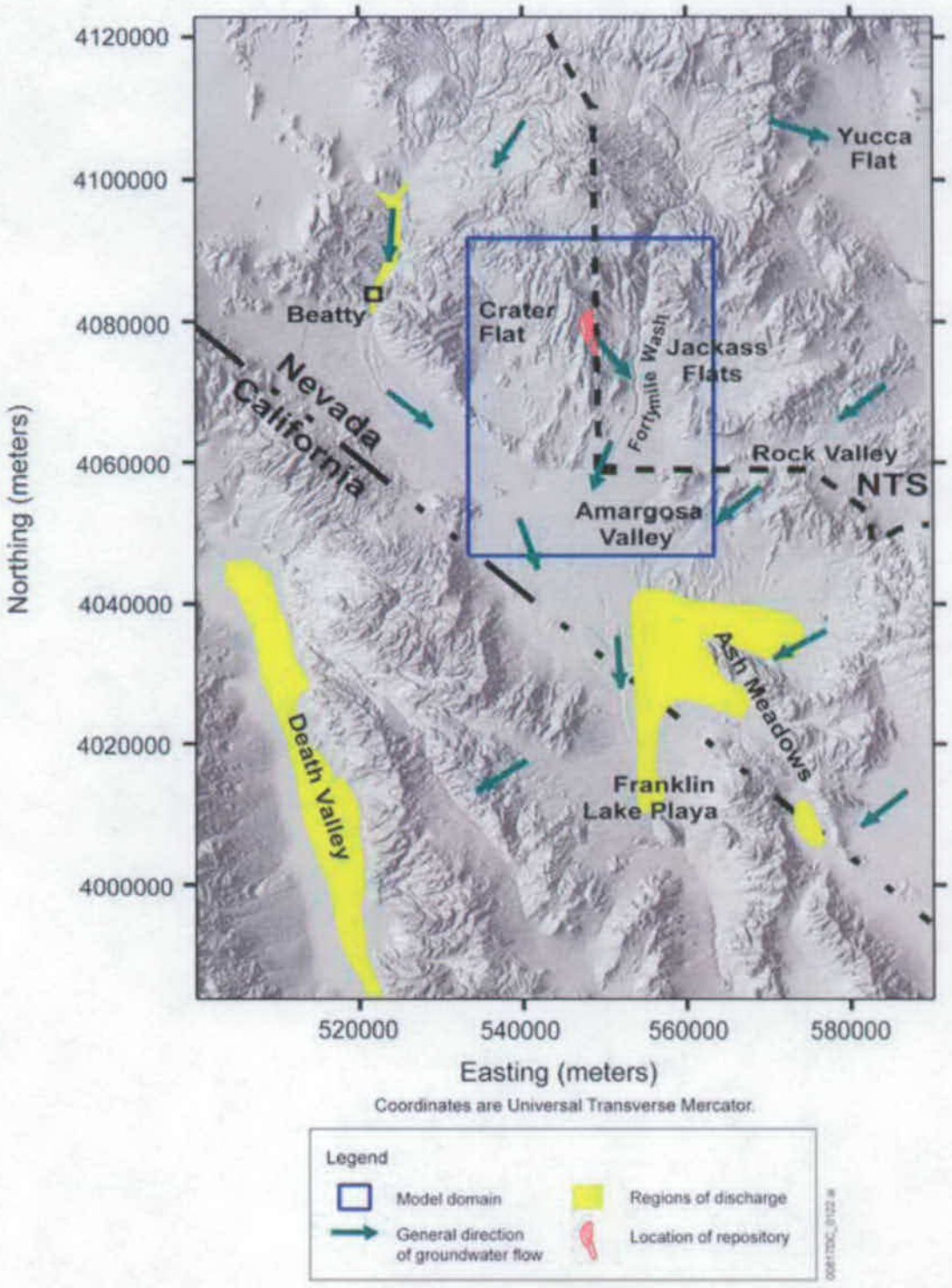

Source: Compiled from BSC 2004 [DIRS 169734], Figures 8-2, 8-5, and 8-6

Figure ES-17. Regional Map of the Saturated Zone Flow System Showing Direction of Flow and Outline of the 3-D Saturated Zone Site-Scale Flow Model Domain

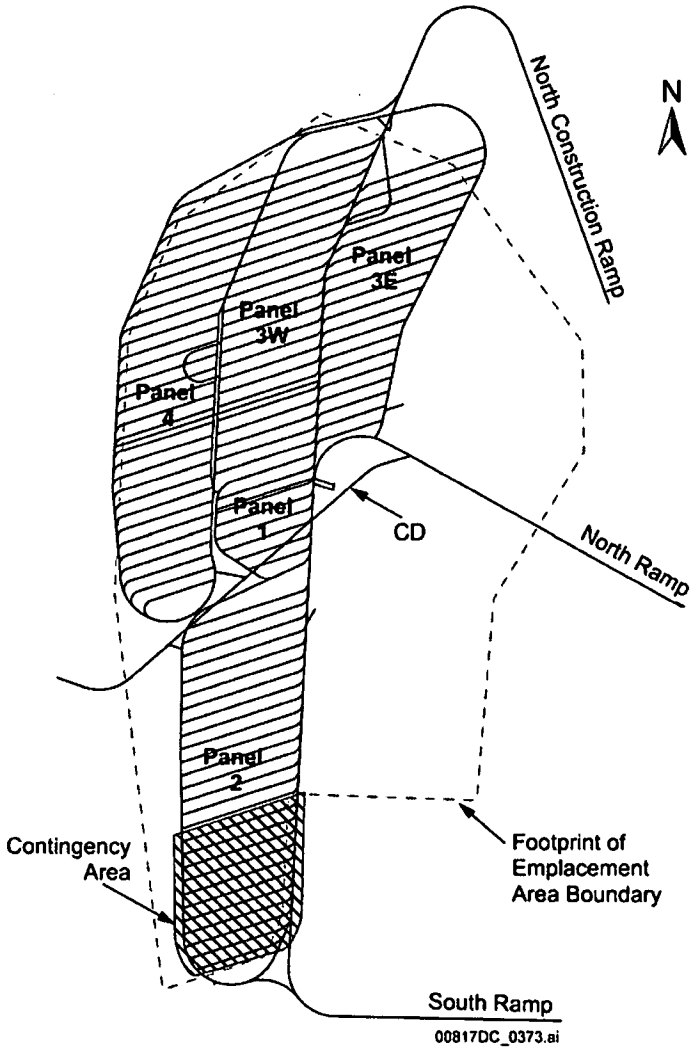

Source: Modified from SNL 2007 [DIRS 179466], Table 4-1, Parameter 01-02.

NOTE: CD = Cross Drift.

Figure ES-18. Subsurface Facility Layout

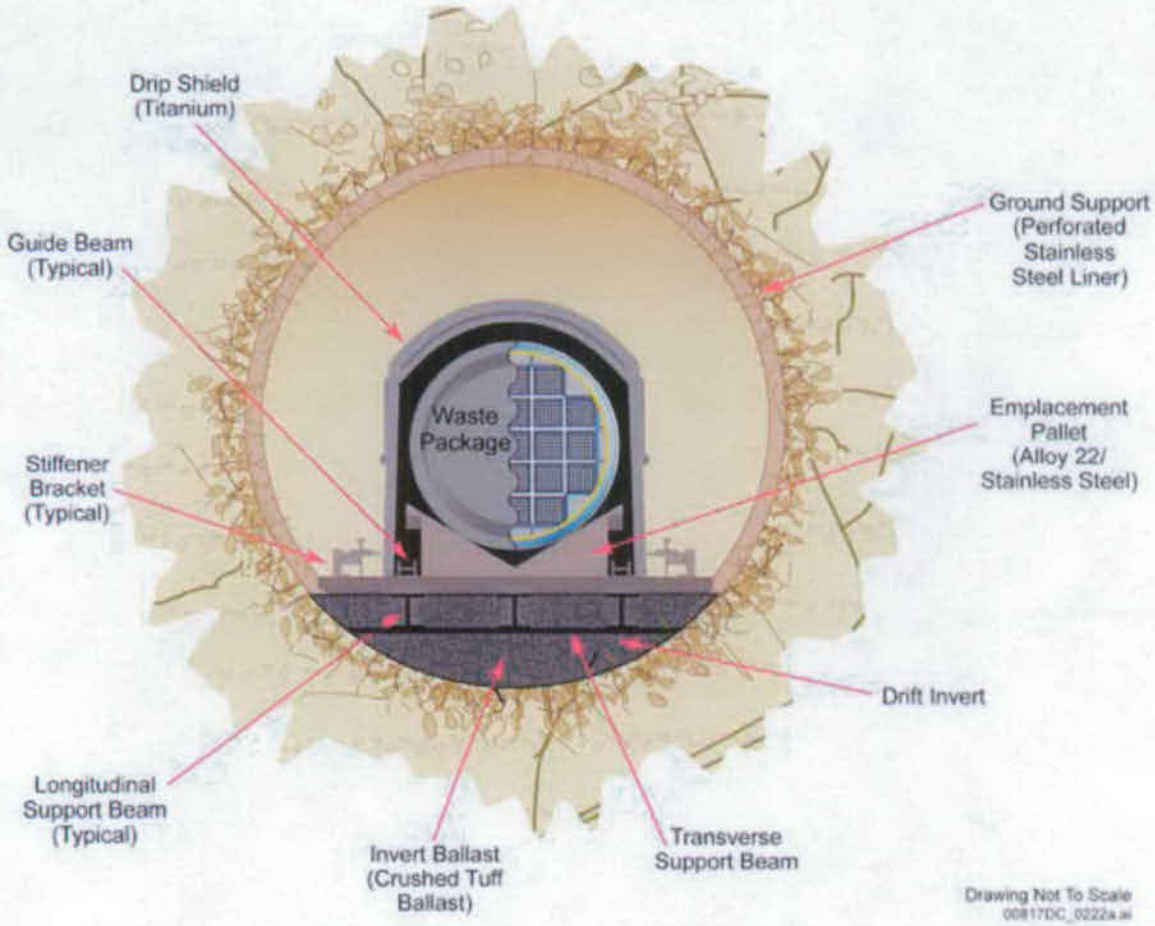

Source: Modified from SNL 2007 [DIRS 179354], Figure 4-1.

Figure ES-19. Cross-Section Illustration of the EBS

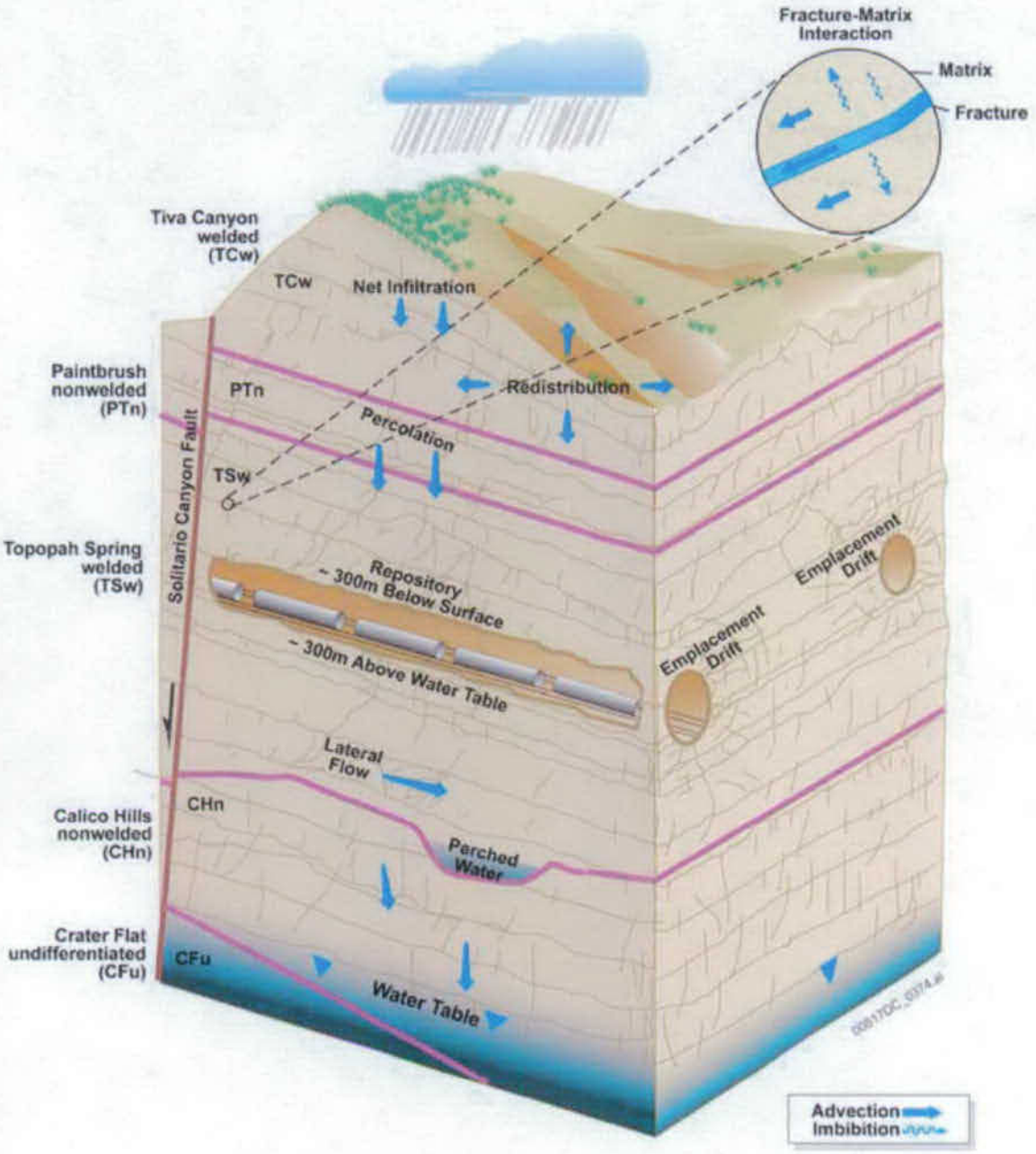

Figure ES-20. Conceptual Drawing of Mountain-Scale Flow Processes

Present-Day Climate

Yucca Mountain:
Regional Meteorological Stations

Monsoon Climate

Lower-bound analogue: Yucca Mountain
Upper-bound analogue: Nogales, AZ
Higher precipitation and temperature
than present-day climate

Glacial-Transition Climate

Lower-bound analogue: Delta, UT
Upper-bound analogue: Spokane, WA
Higher precipitation and lower
temperature than present-day climate

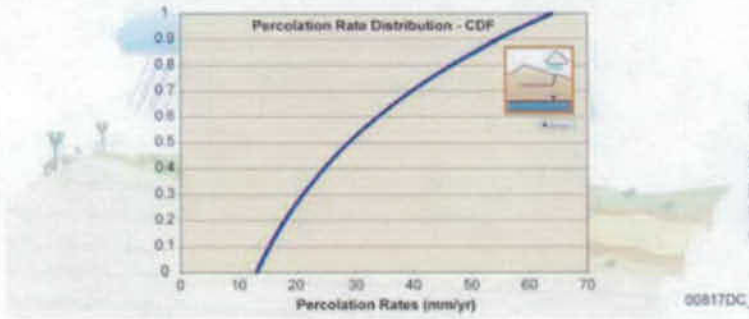

Post-10,000 Year Climate

Sampled value based on a log-uniform
probability distribution for deep percolation
rates from 13 to 64 mm/yr
(10 CFR 63.324(c)(2) [DIRS 178394])

Figure ES-21. Illustration of the Four Climate States Used in the TSPA-SEIS Model and the Present-Day Analogues of the Present-Day, Monsoon, and Glacial-Transition Climates

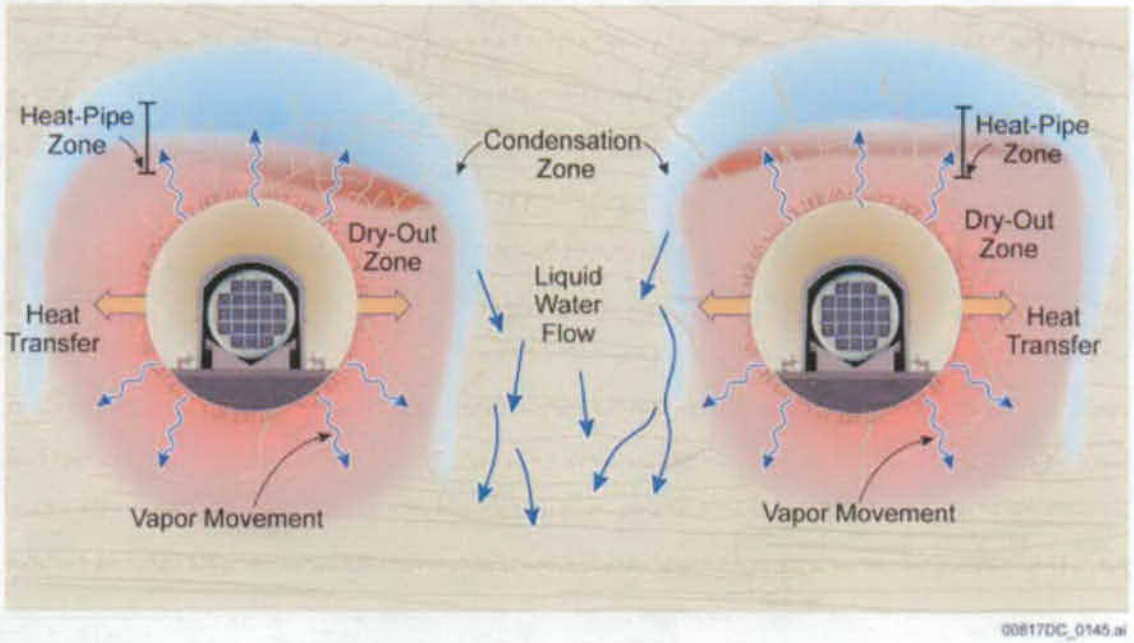

Source: Modified from BSC 2004 [DIRS 169734], Figure 5-81

Figure ES-22. Schematic Illustration (not to scale) of Thermal-Hydrologic Processes in the Vicinity of the Emplacement Drifts Due to Repository Heating

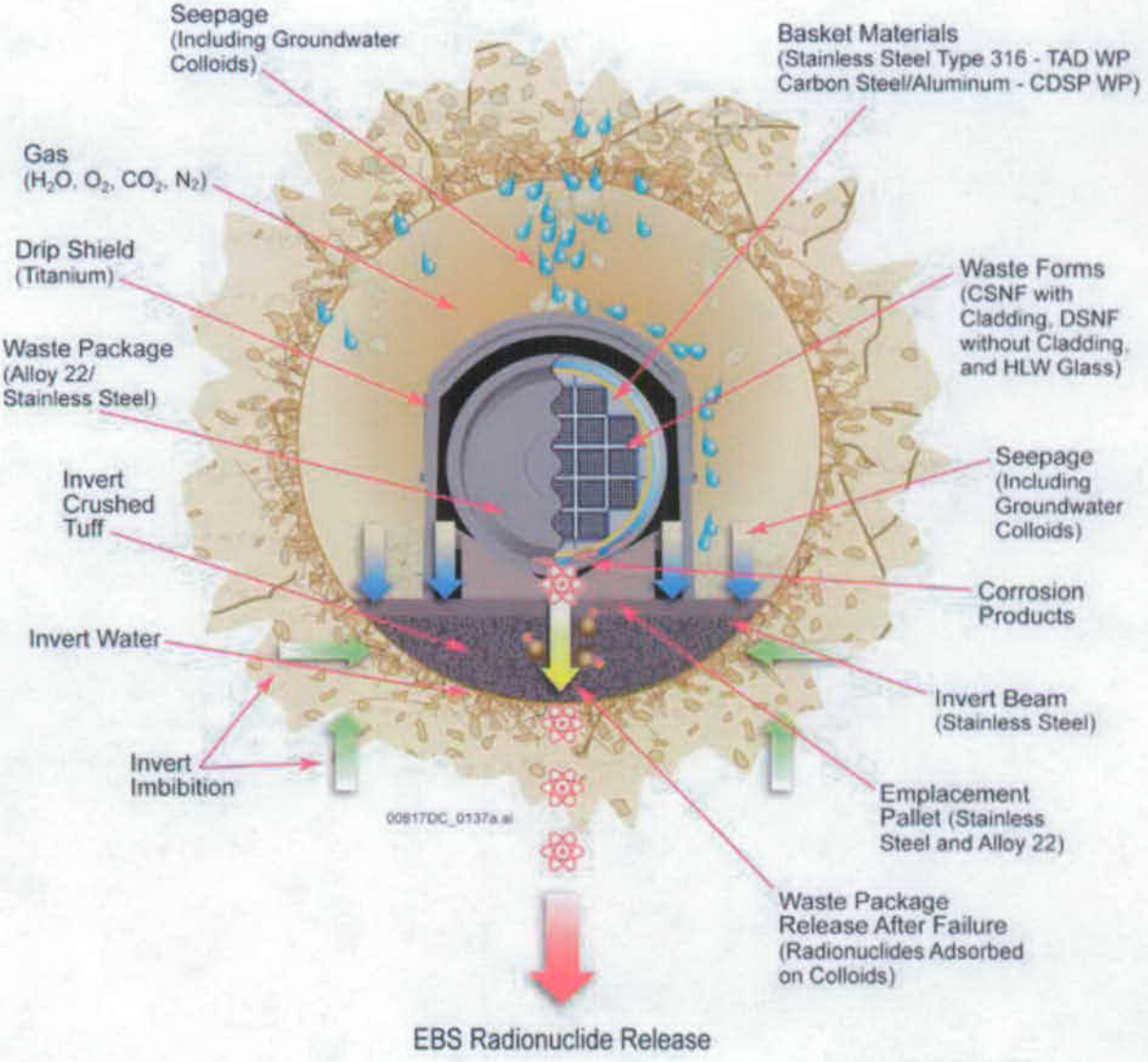

NOTE: Discussion and analysis of the features and processes illustrated on this figure can be found in *EBS Radionuclide Transport Abstraction* (SNL 2007 [DIRS 177407]), Section 6.1.1, Figure 6.1-1).

Figure ES-23. General EBS Design Features and Materials, Water Movement, and Drift Degradation

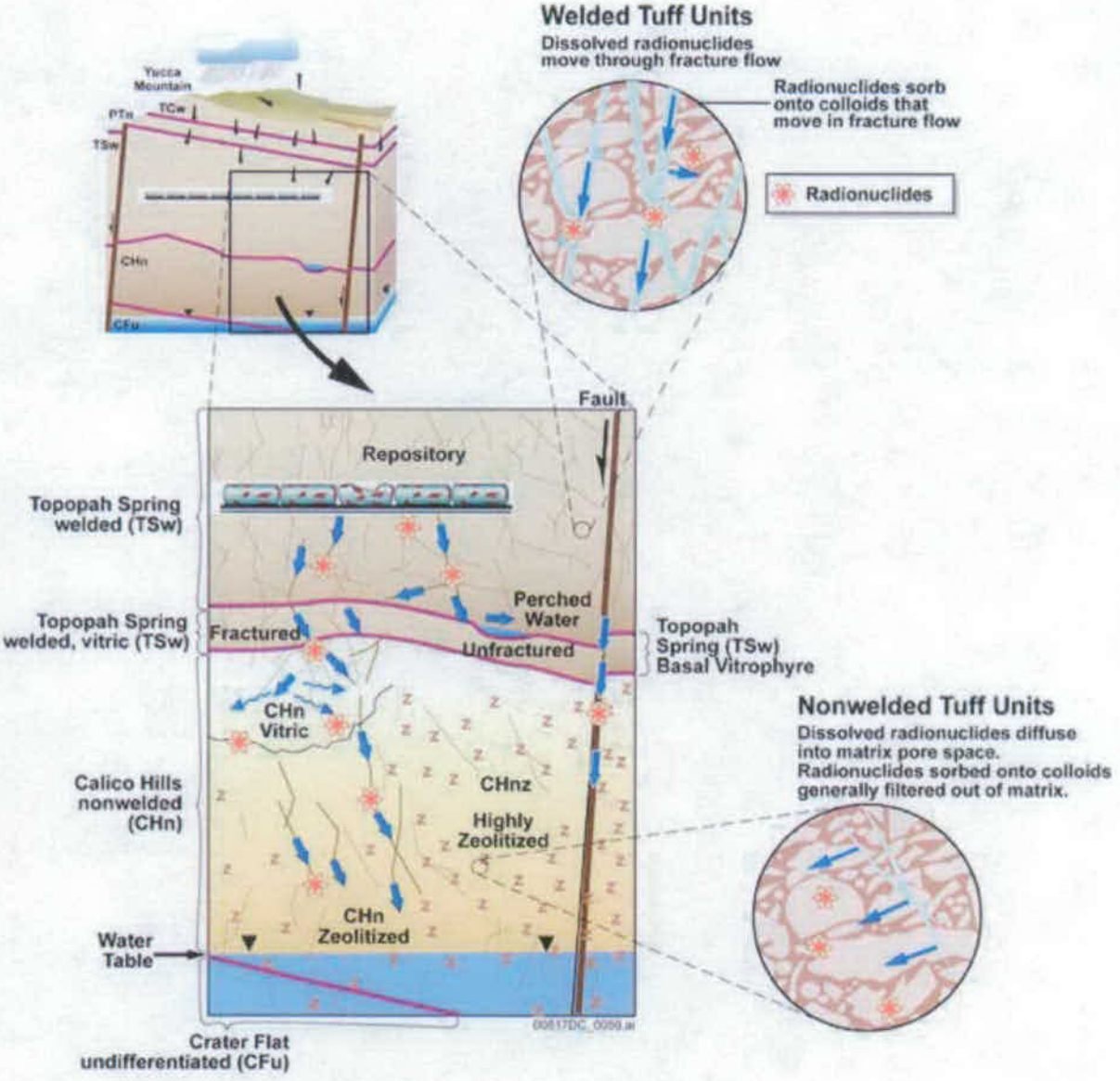

Figure ES-24. Conceptual Drawing of Unsaturated Zone Transport Processes

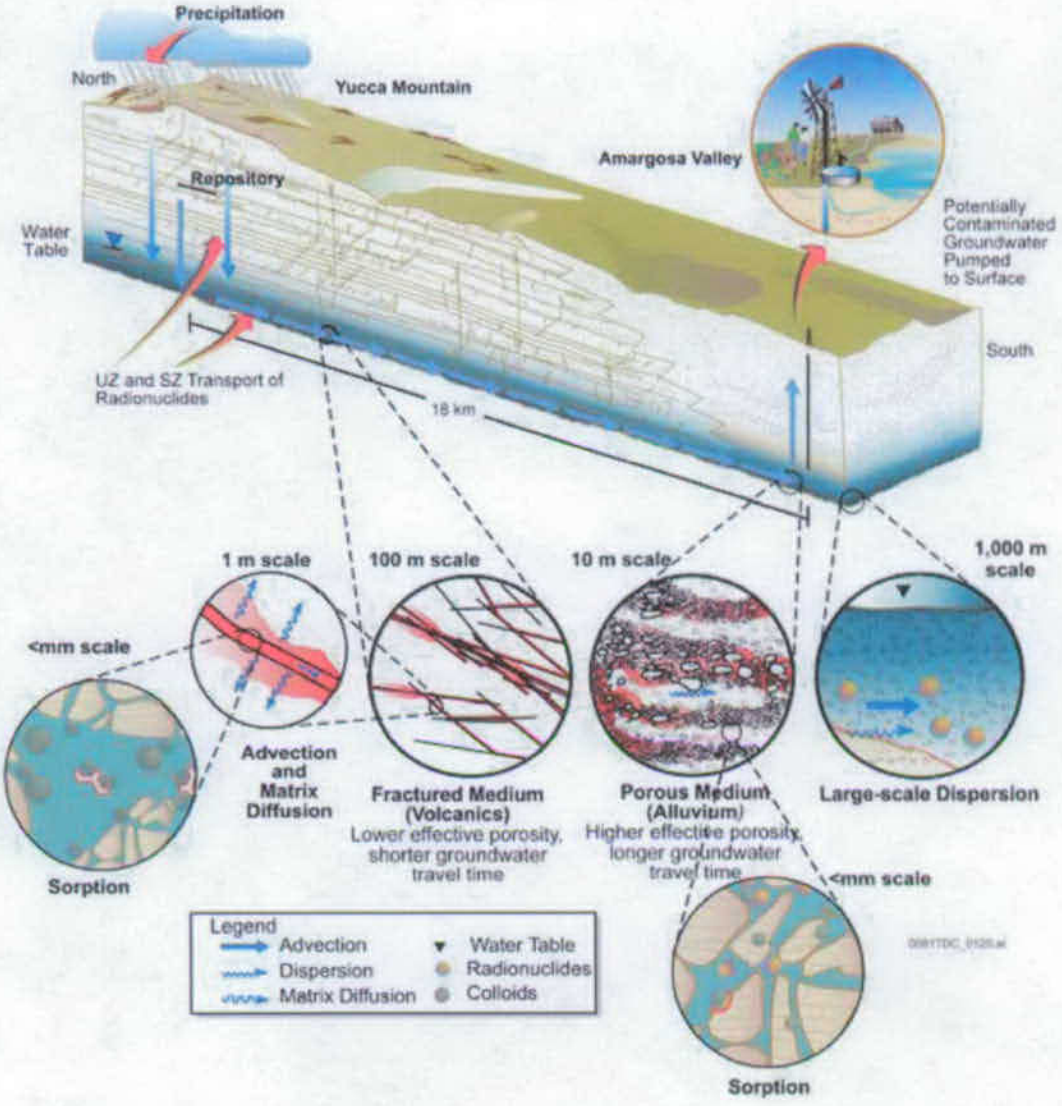

Figure ES-25. Conceptualization of Features and Processes Important to Saturated Zone Transport

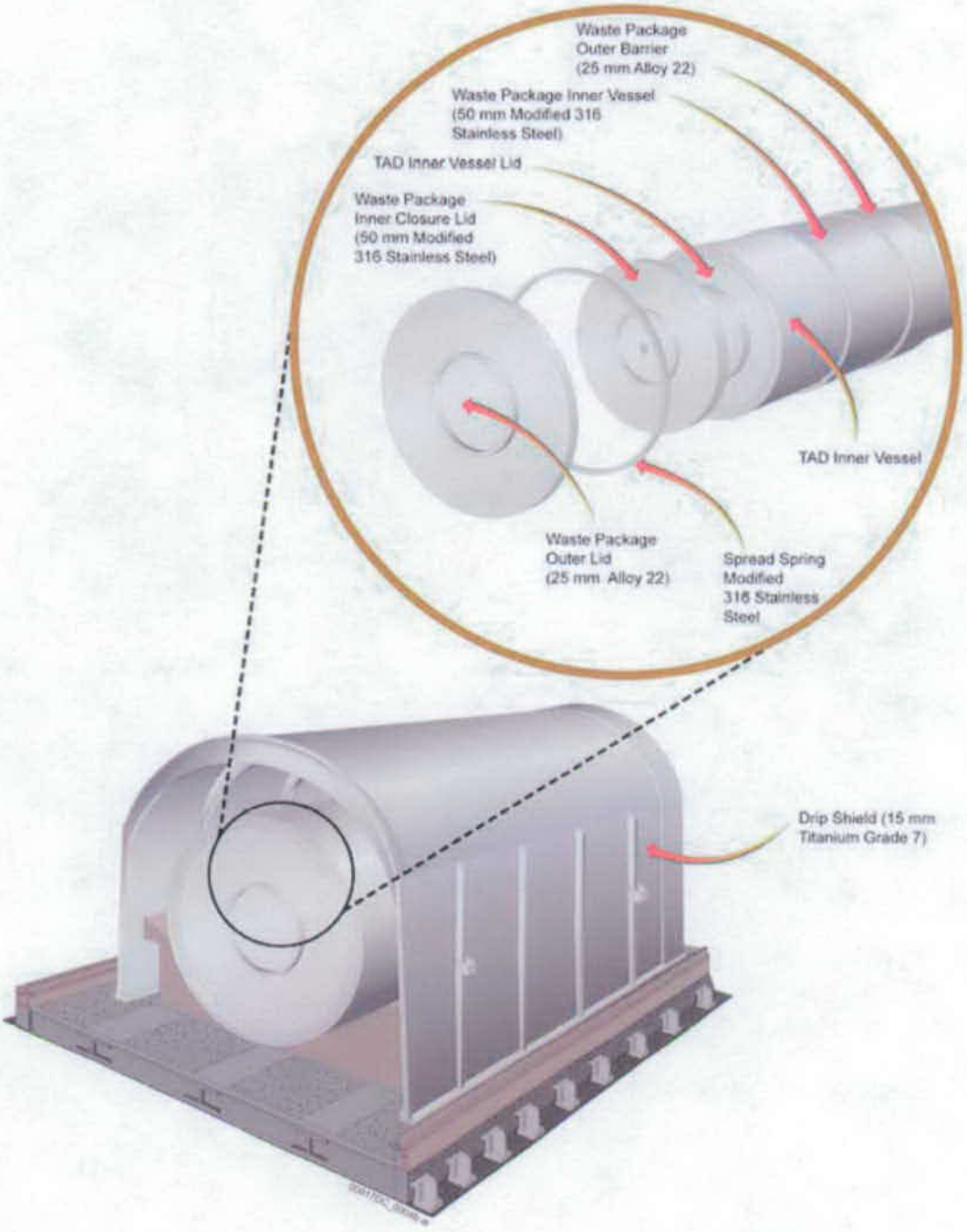

NOTE: Discussion and analysis of the waste package design used in the TSPA-SEIS can be found in *WAPDEG Analysis of Waste Package and Drip Shield Degradation* (BSC 2004 [DIRS 169996], Section 6.3.2, Figures 2 and 4).

Figure ES-26. Schematic Design of the Drip Shield and Waste Package Emphasizing the Waste Package Closure Lids

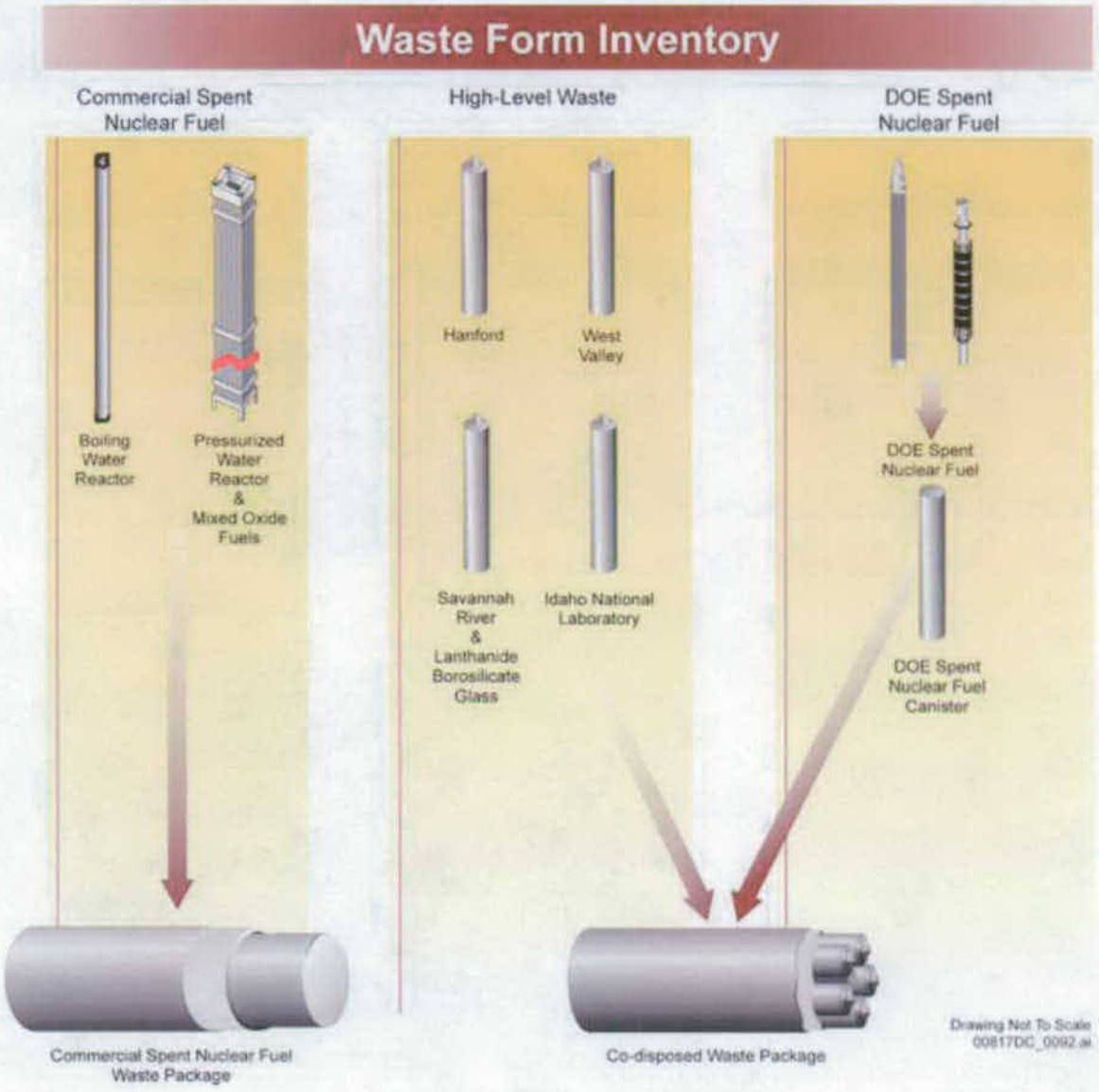

Source: Modified from SNL 2007 [DIRS 180472], Figure 6-1.

NOTE: For modeling purposes, the naval fuels are treated as commercial spent nuclear fuel.

Figure ES-27. Three Waste Types Grouped into Two Representative Waste Packages: CSNF and CDSP WPs

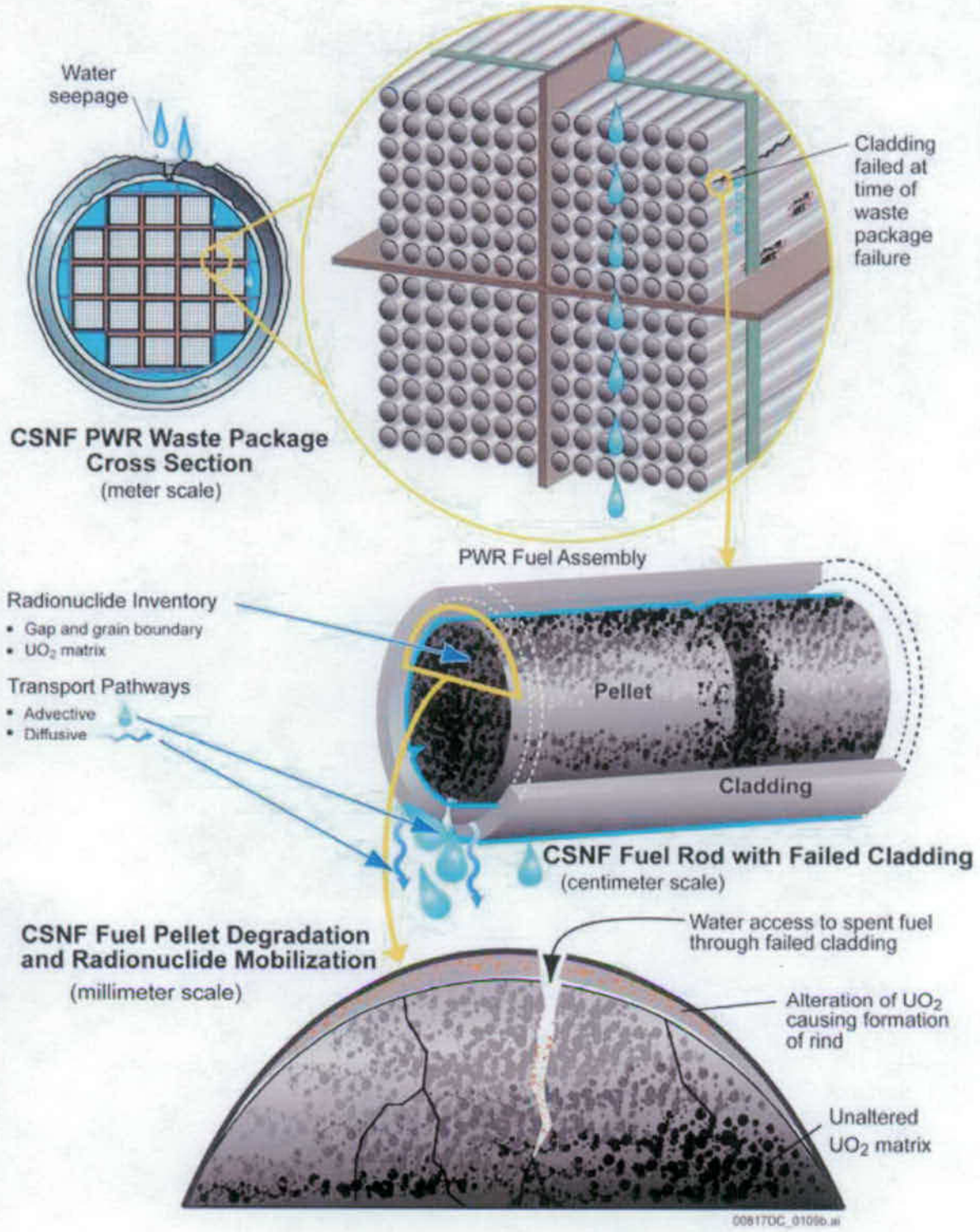

Figure ES-28. Schematic of CSNF Waste Form Degradation Mechanisms at Various Scales

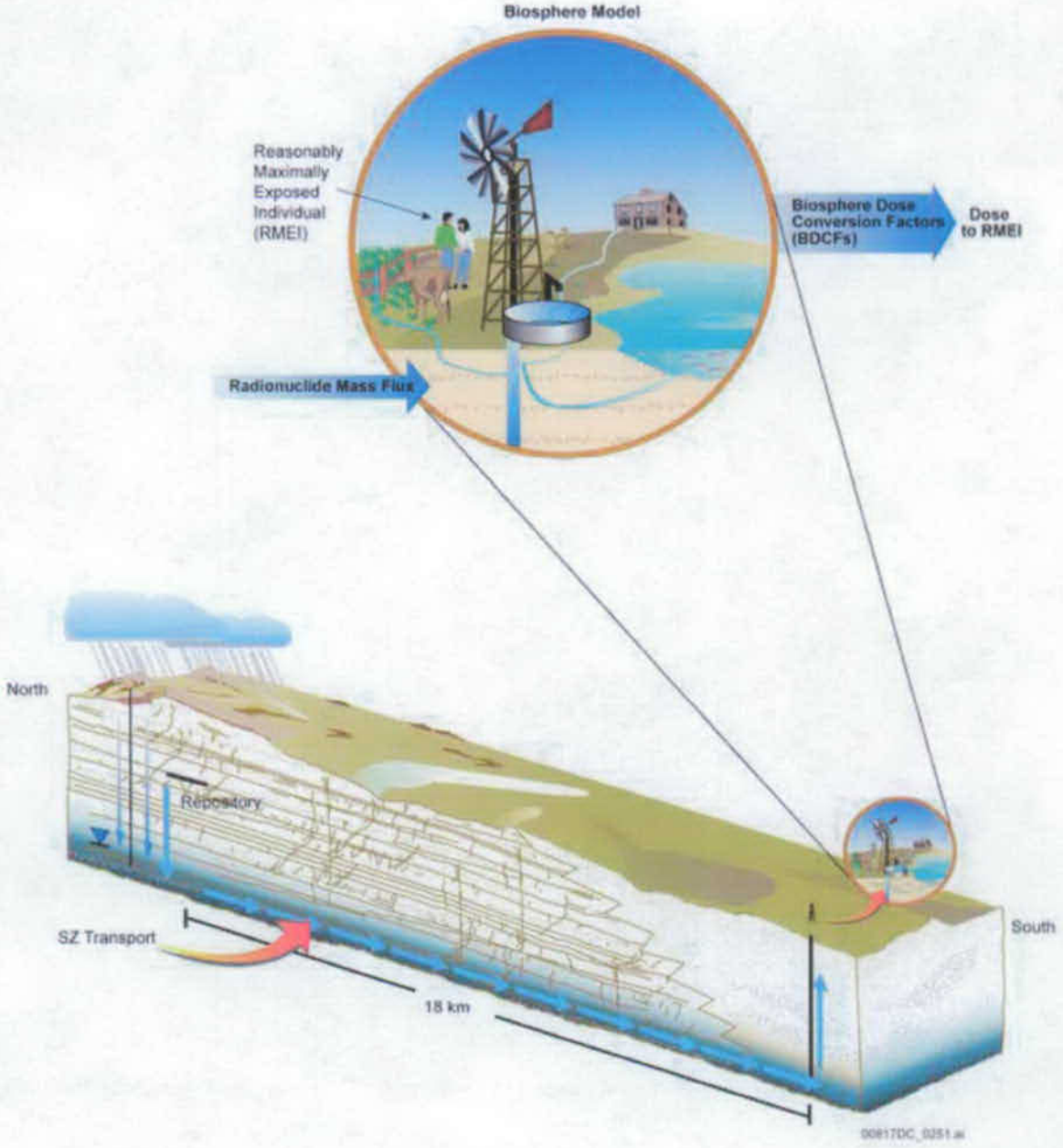

Figure ES-29. Overview of the Biosphere Groundwater Scenario Showing Groundwater Transport of Radionuclides and Uptake by the RMEI

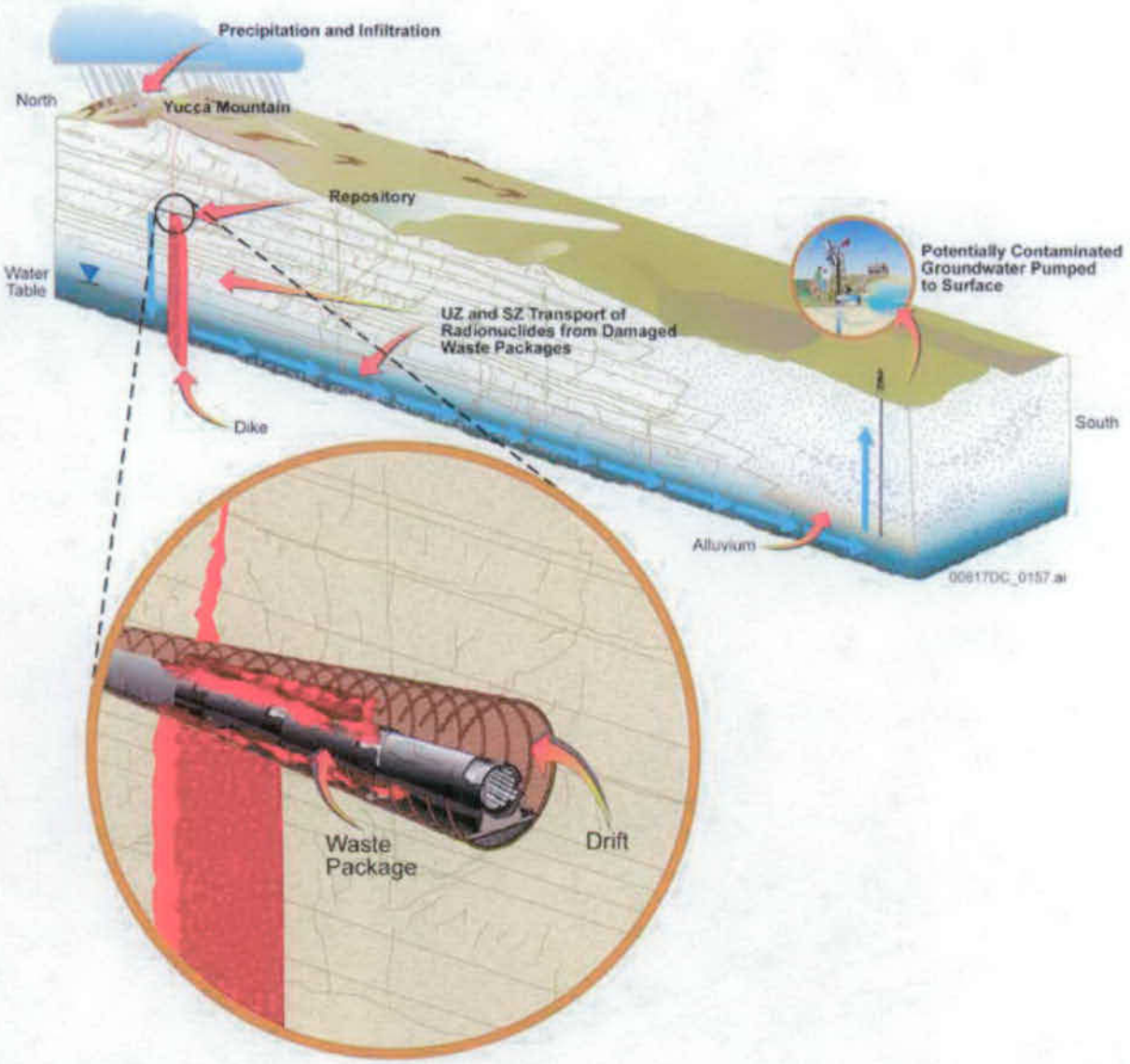

Figure ES-30. Schematic Diagram of the Intersection of an Igneous Dike with the Repository and Waste Packages

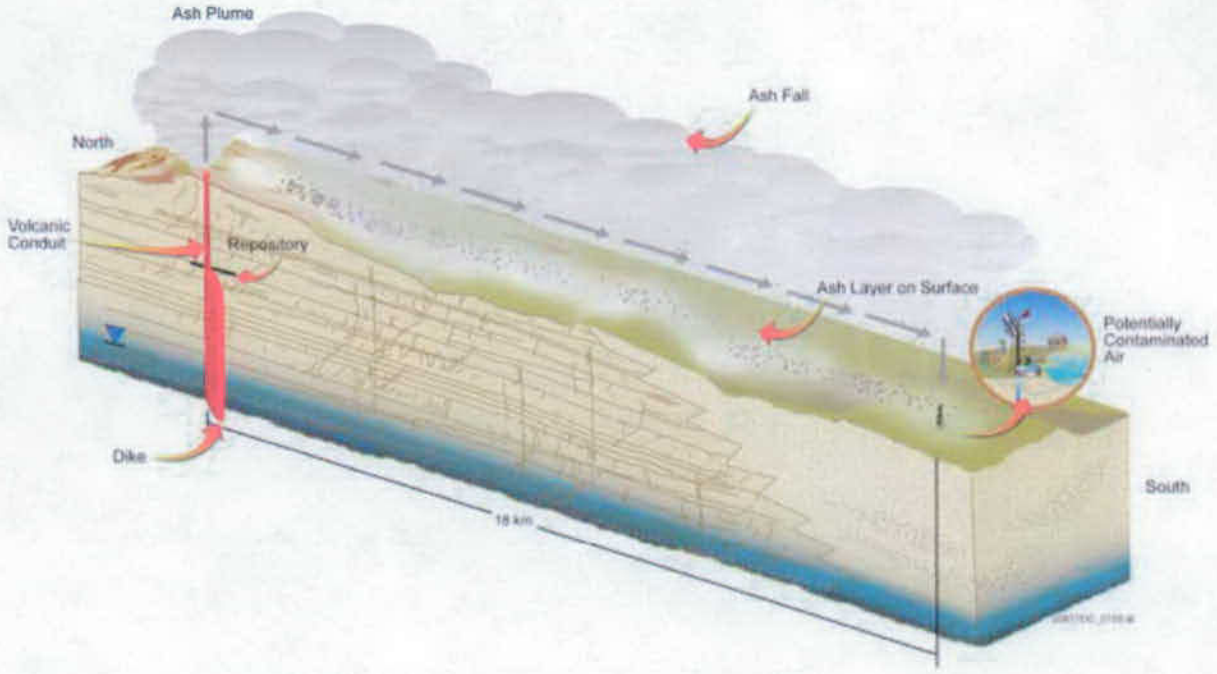

Figure ES-31. Schematic Representation of a Volcanic Eruption at Yucca Mountain, Showing Transport of Radioactive Waste in a Tephra Plume

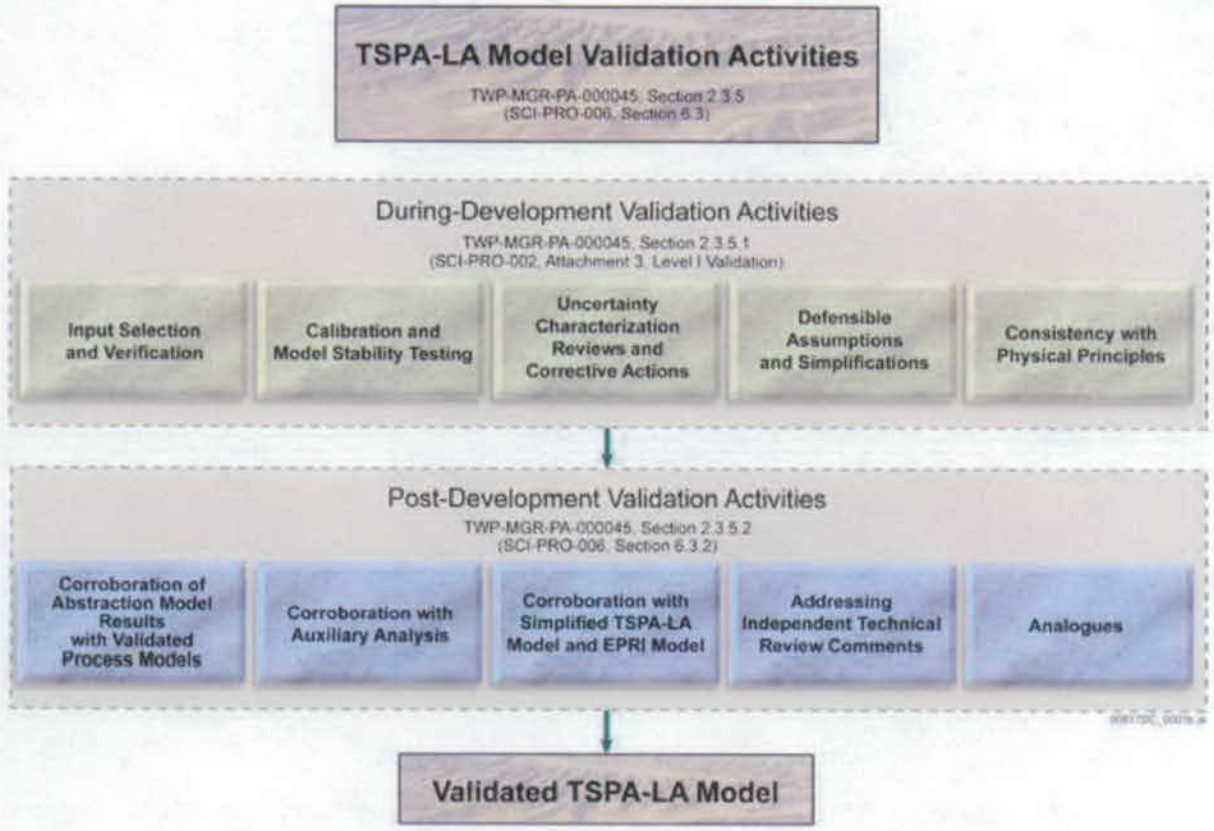

Note: Validation activities completed for the TSPA-LA, also apply for the TSPA-SEIS

Figure ES-32. Model Validation Approach

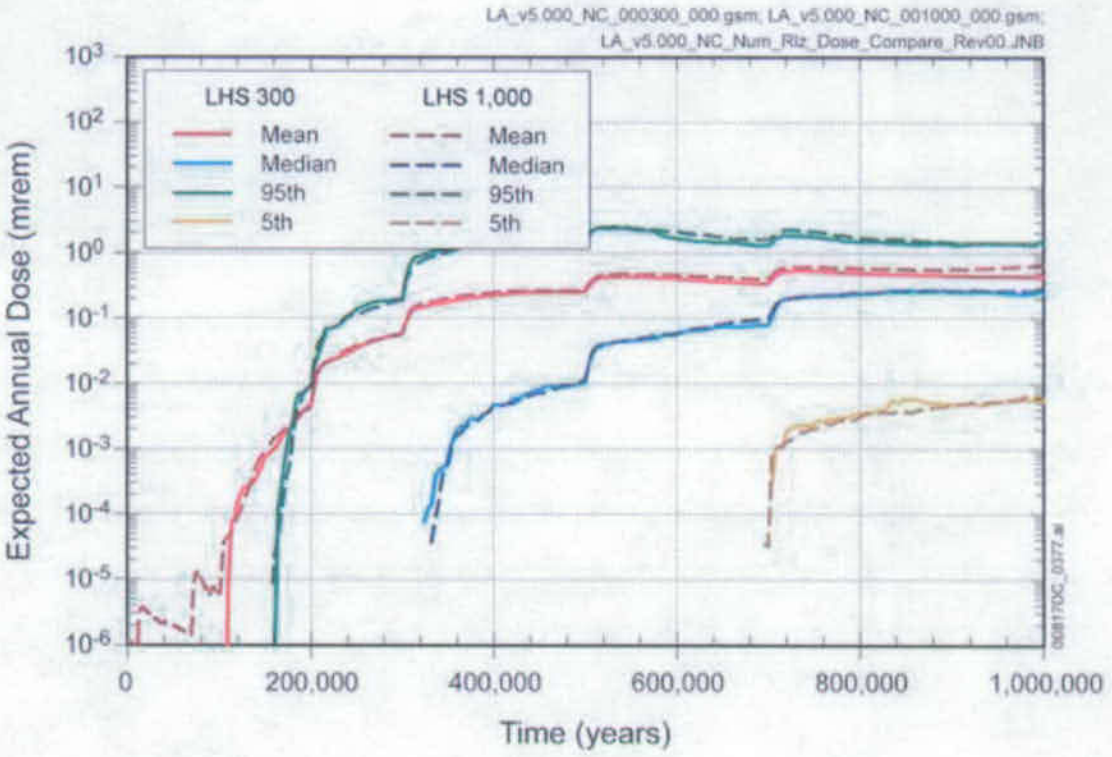

Figure ES-33. Uncertainty in Mean Annual Dose for the Nominal Modeling Case, Latin Hypercube Sampling Sizes of 300 and 1,000

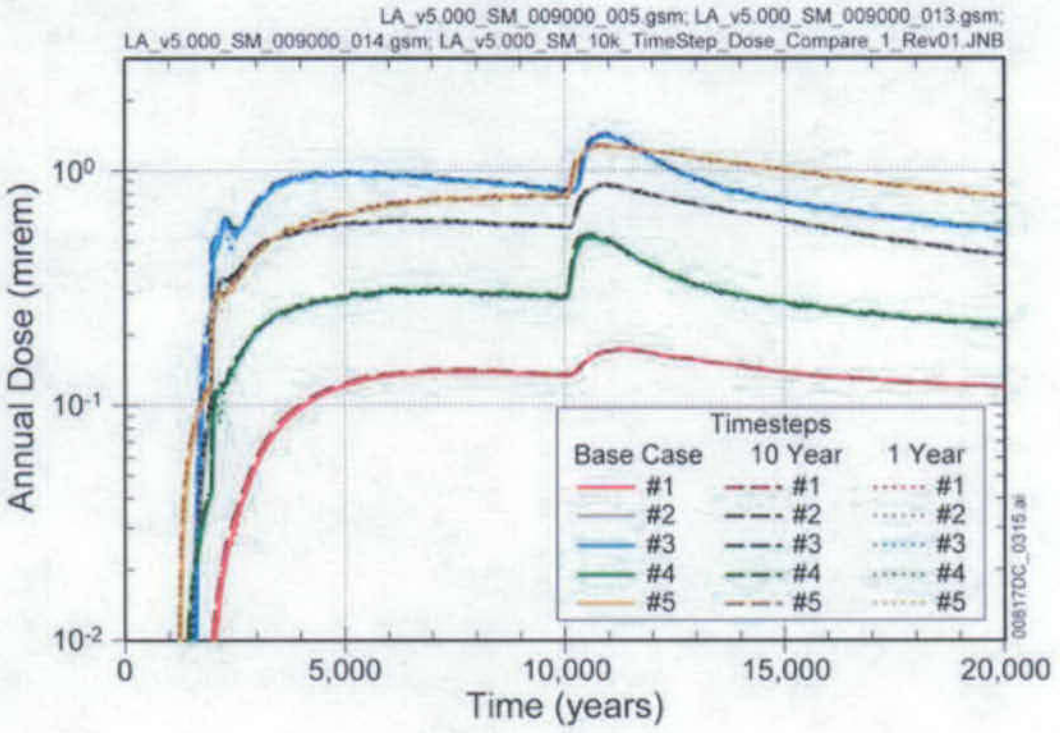

Figure ES-34. Annual Dose from a Seismic Ground Motion Event at 1,000 Years with Damage Fraction 10^{-6}, for Three Timestep Schemes

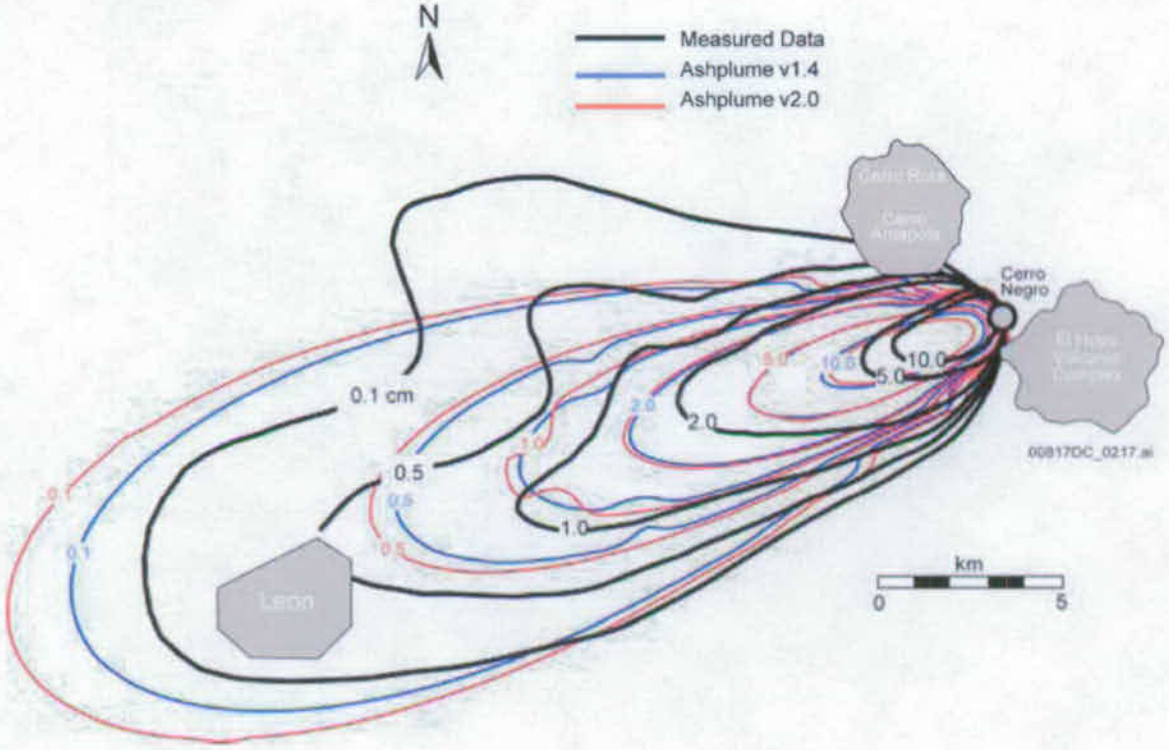

Source: SNL 2007 [DIRS 177431], Appendix L

Figure ES-35. Comparison of Ash Fall at Cerro Negro with ASHPLUME Simulated Results

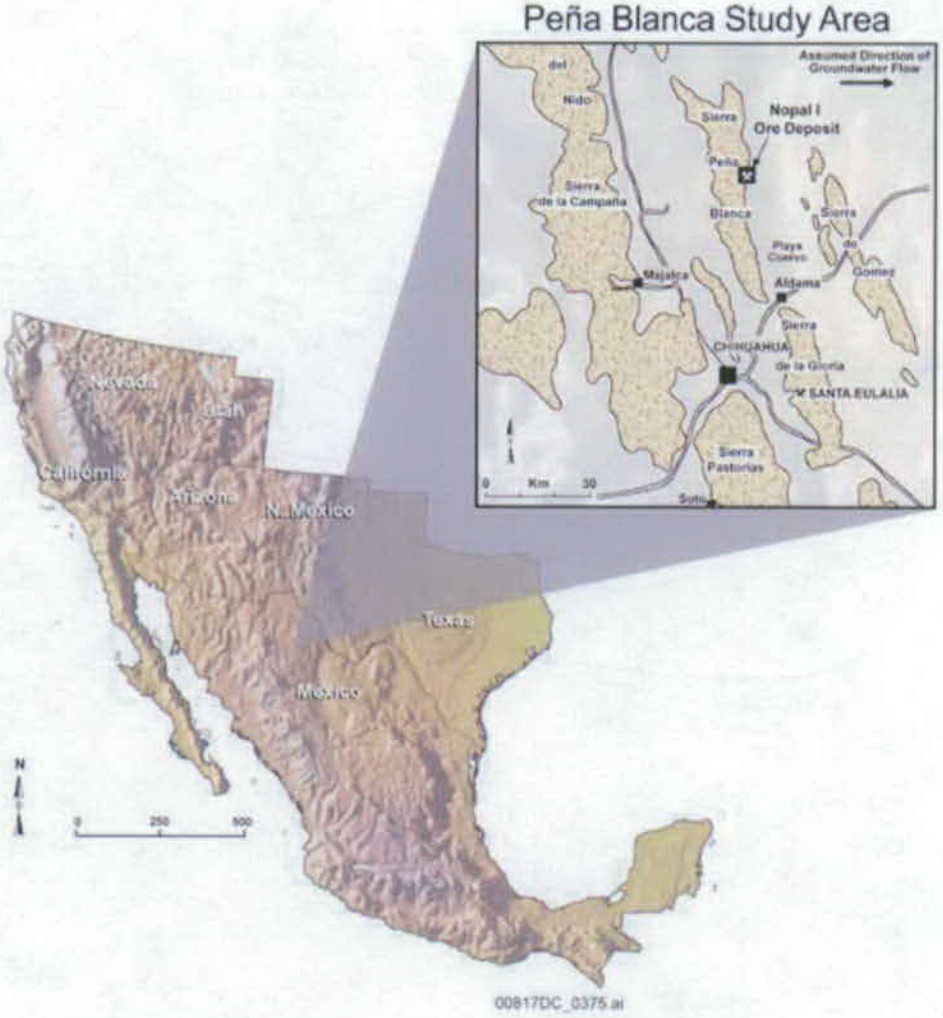

Source: Modified from George-Aniel et al. 1991 [DIRS 105636], Figure 1

Figure ES-36. Location of Peña Blanca Nopal I Ore Deposit in the Sierra Peña Blanca

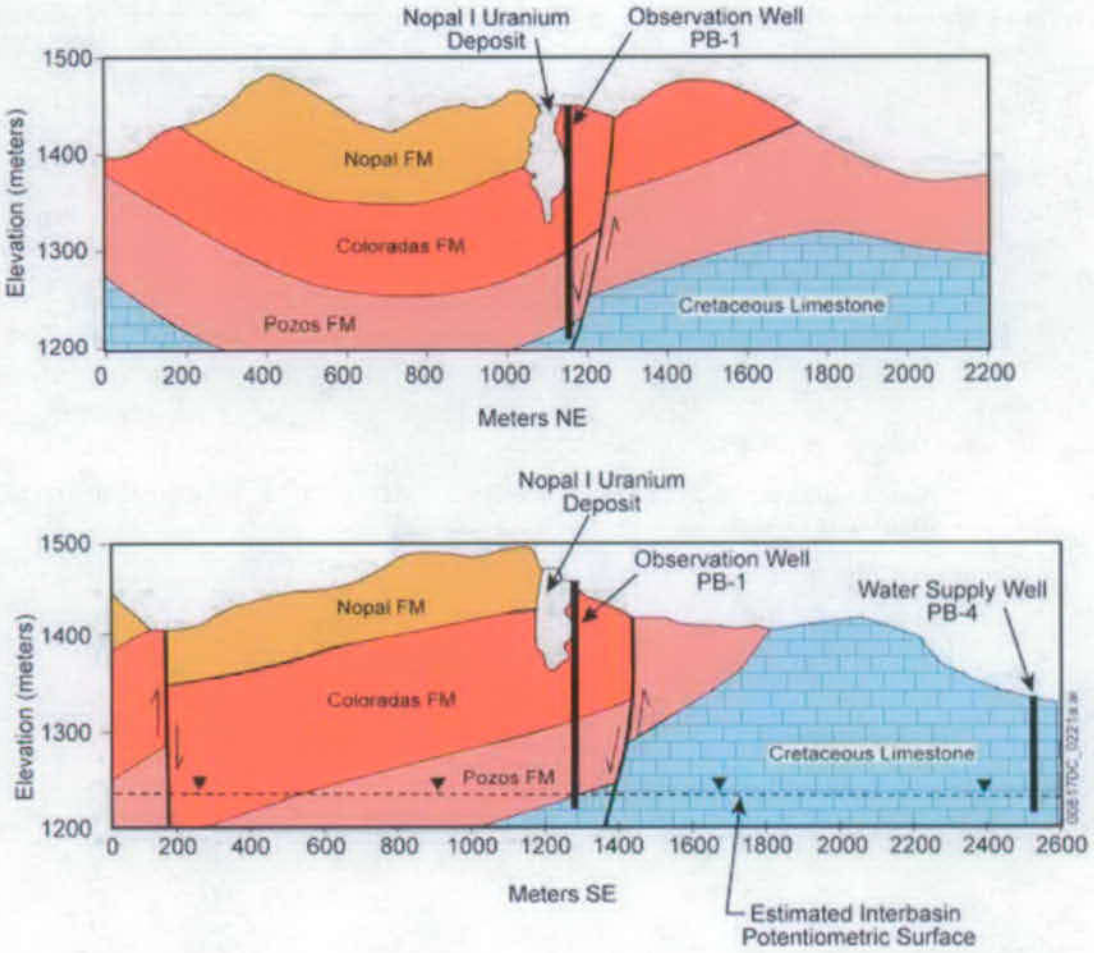

Source: Modified from Pearcy et al. 1993 [DIRS 151774], p. 1-4

Figure ES-37. Geologic Characterization of Nopal 1 Ore Body

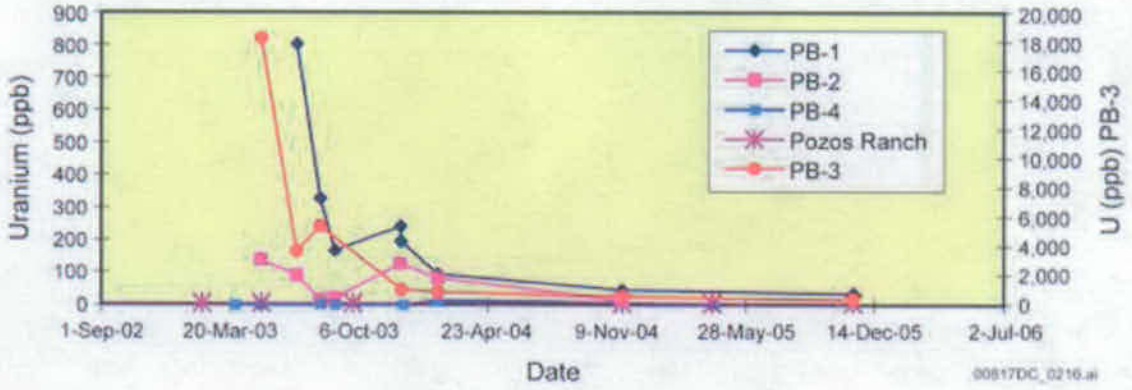

Source: Data from Goldstein et al. [DIRS 181364], p. 217.

Figure ES-38. Uranium Concentration Determined in Groundwater Samples from Wells at and Near the Nopal I Ore Deposit

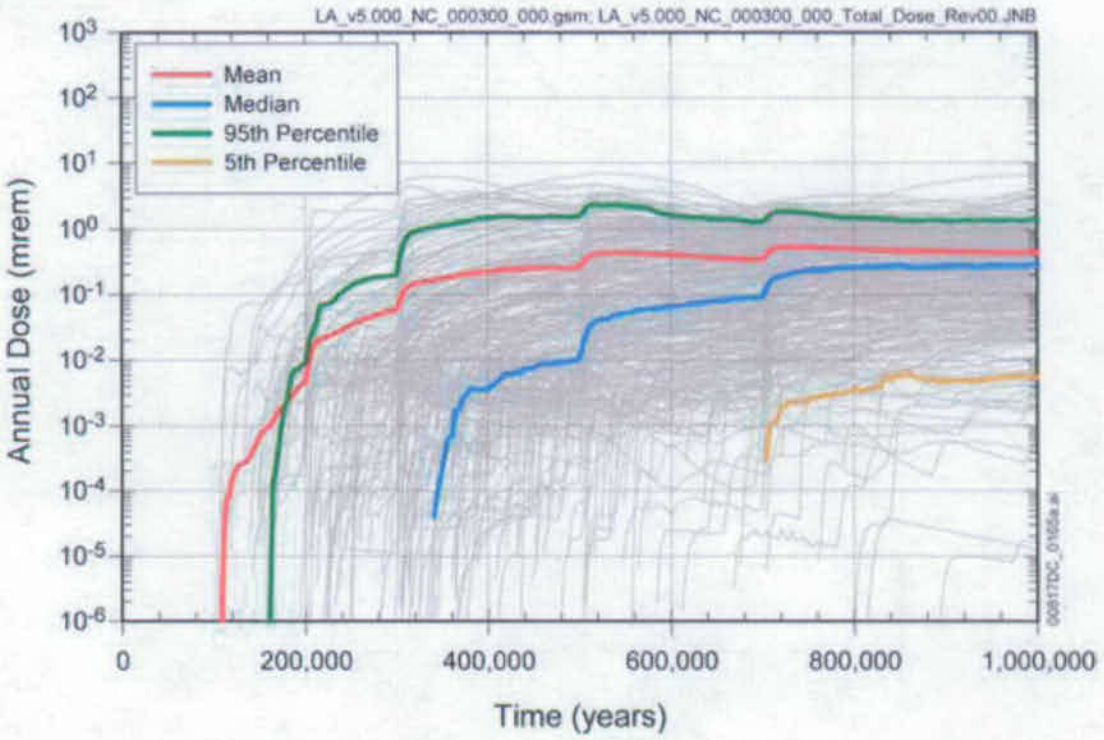

Figure ES-39. Projected Annual Dose for the Nominal Scenario Class Modeling Case for the Post-10,000-Year Period

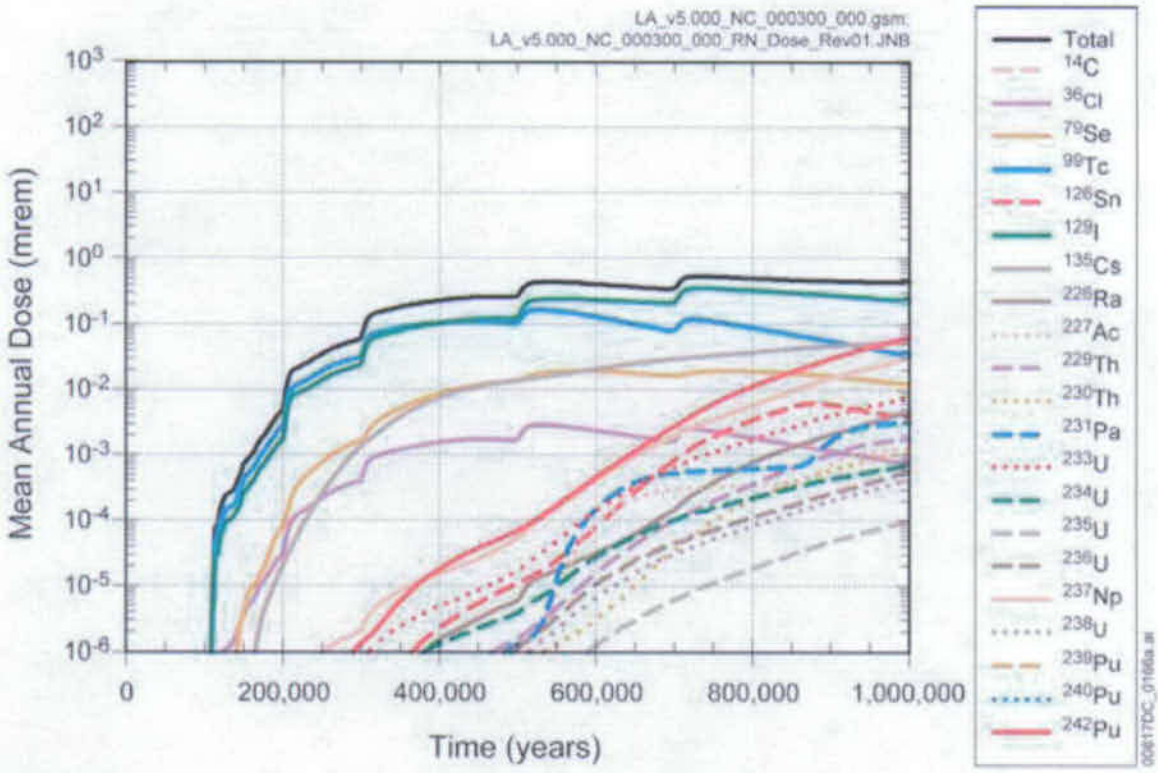

Figure ES-40. Mean Annual Dose Histories of Major Radionuclides for the Nominal Scenario Class Modeling Case for the Post-10,000-Year Period

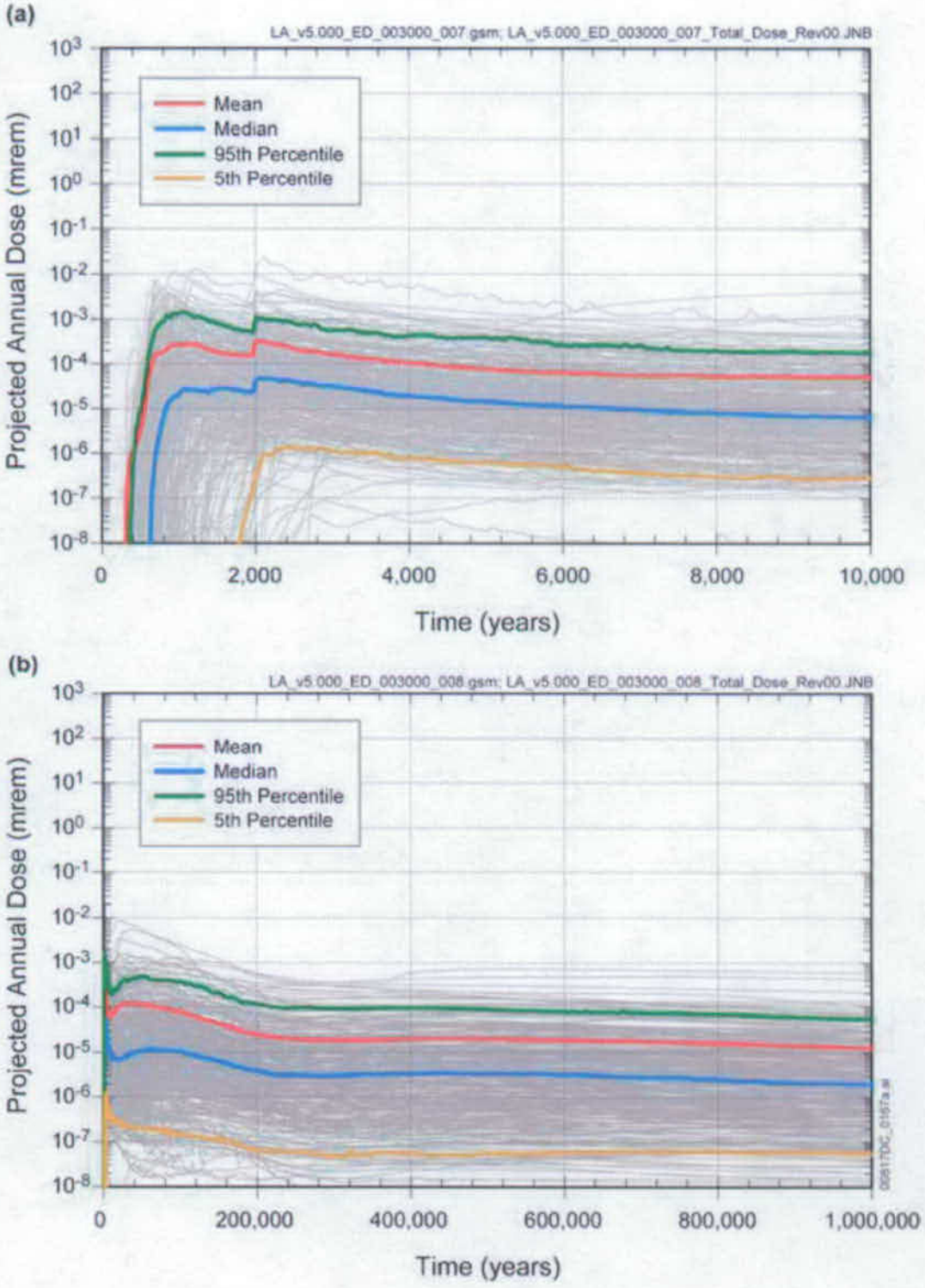

Figure ES-41. Projected Annual Dose for the Drip Shield Early Failure Modeling Case for (a) the First 10,000 Years after Repository Closure and (b) Post-10,000-Year Period

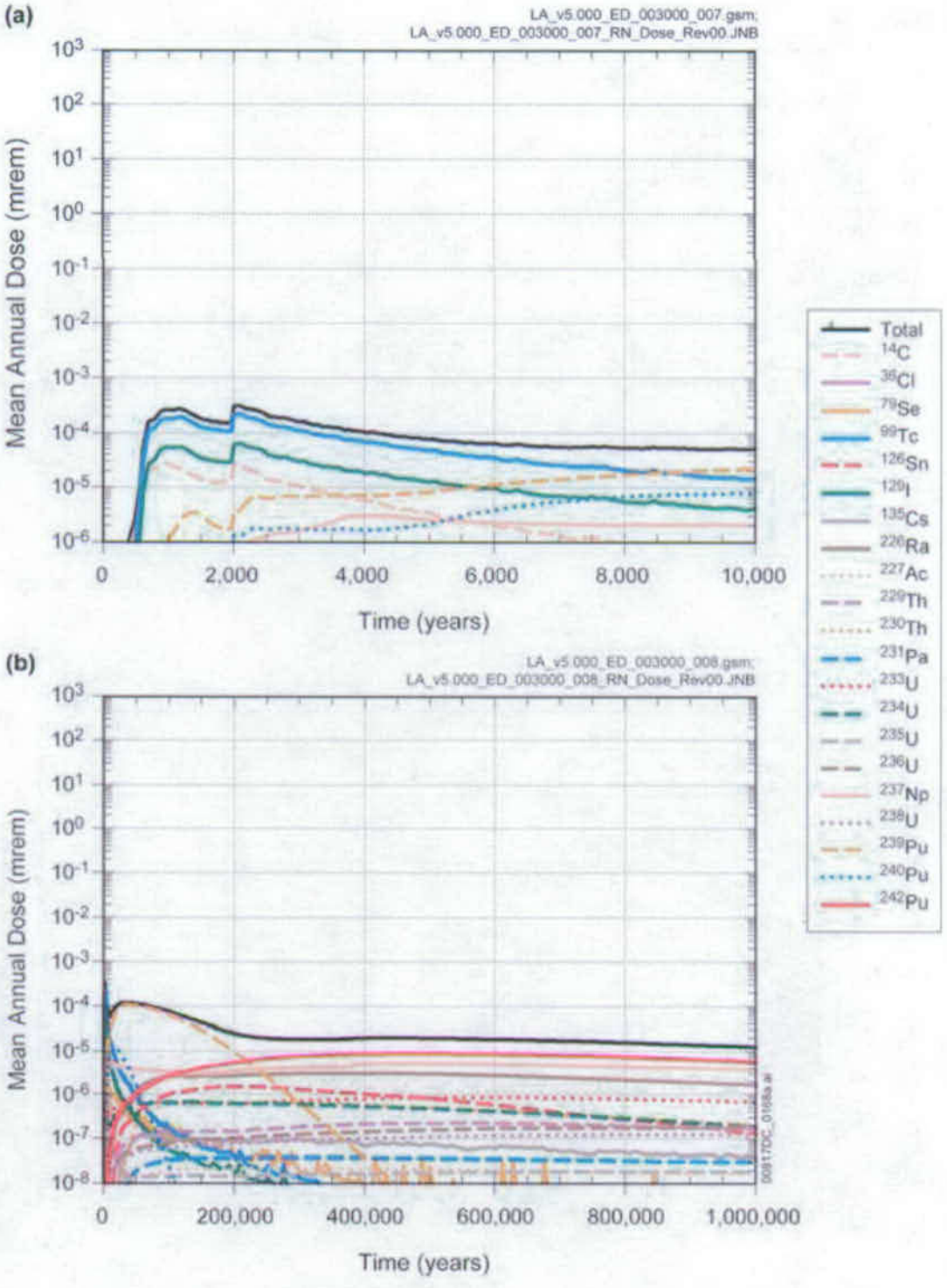

Figure ES-42. Mean Annual Dose Histories of Major Radionuclides for the Drip Shield Early Failure Modeling Case for (a) the First 10,000 Years after Repository Closure and (b) Post-10,000-Year Period

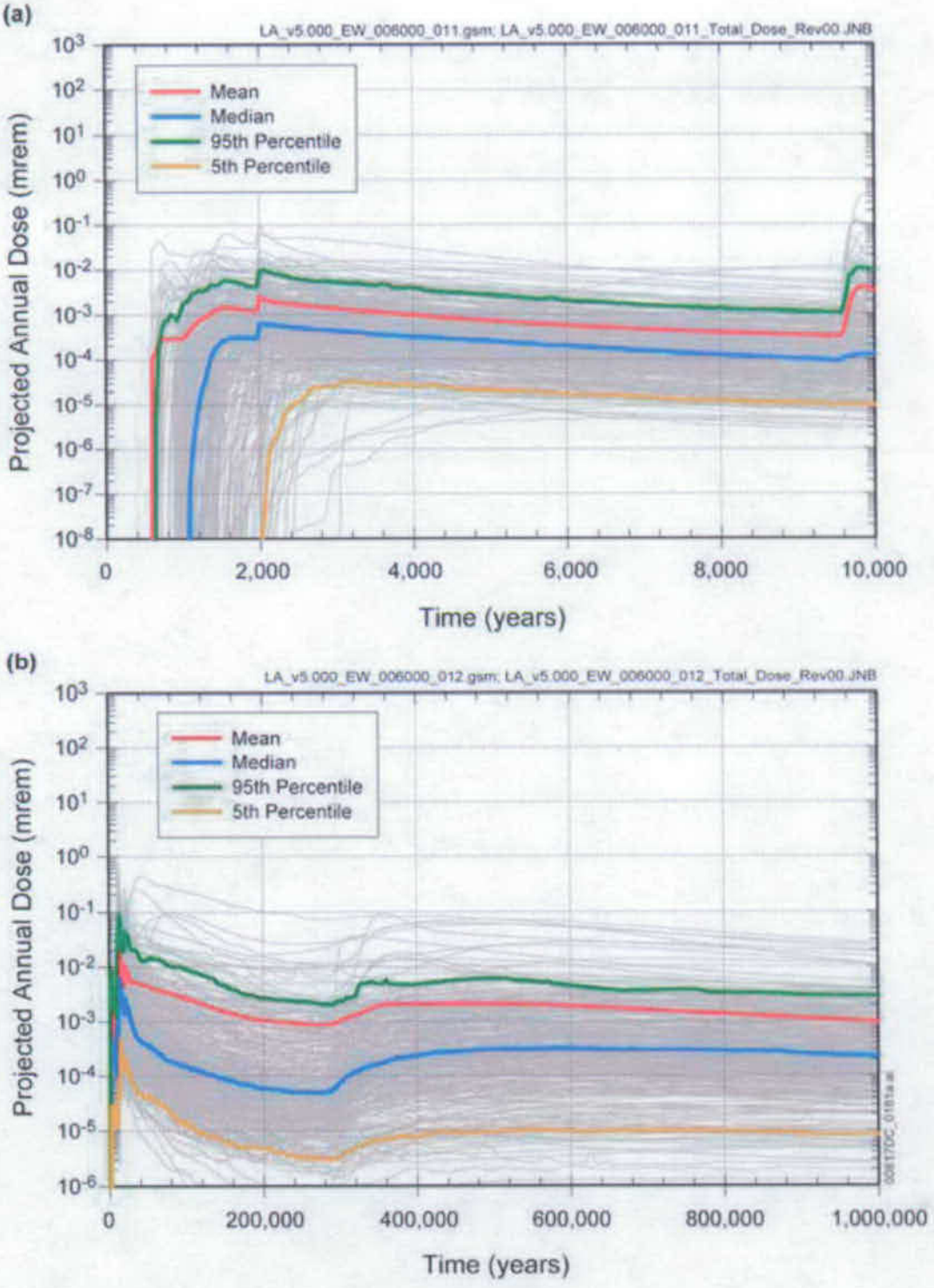

Figure ES-43. Projected Annual Dose for the Waste Package Early Failure Modeling Case (a) the First 10,000 Years after Repository Closure and (b) Post-10,000-Year Period

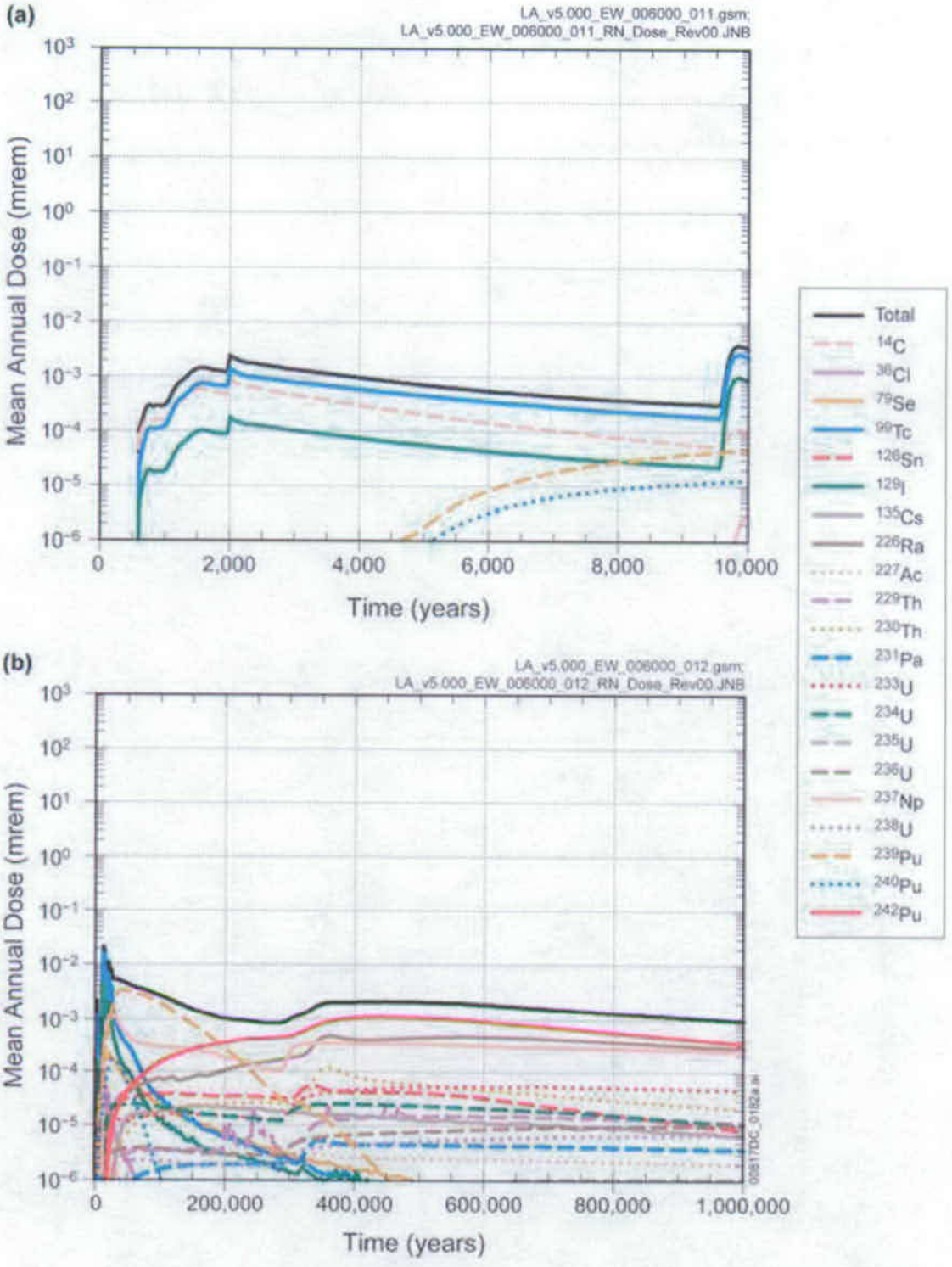

Figure ES-44. Mean Annual Dose Histories of Major Radionuclides for the Waste Package Early Failure Modeling Case for (a) the First 10,000 Years after Repository Closure and (b) Post-10,000-Year Period

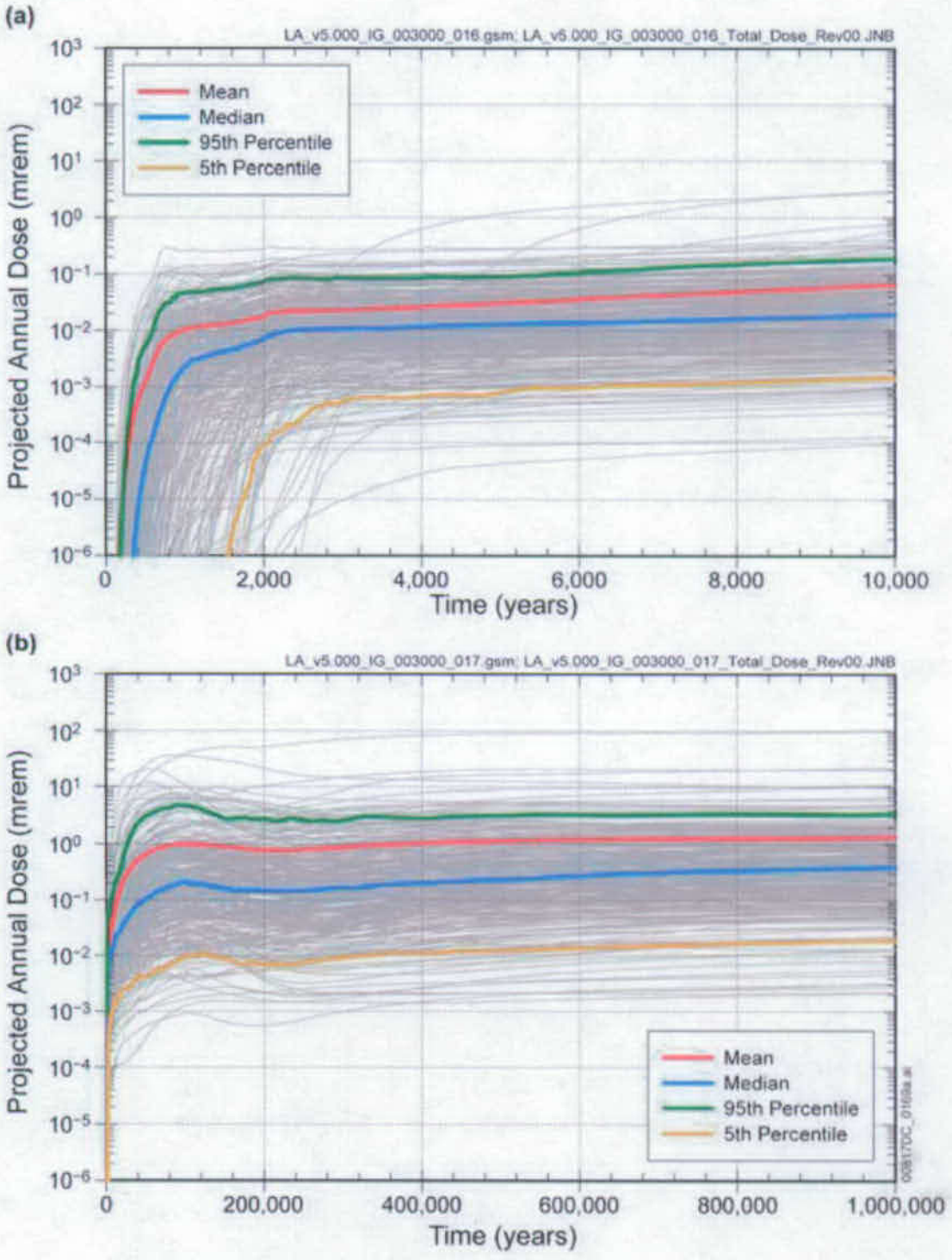

Figure ES-45. Projected Annual Dose for the Igneous Intrusion Modeling Case for (a) the First 10,000 Years after Repository Closure and (b) Post-10,000-Year Period

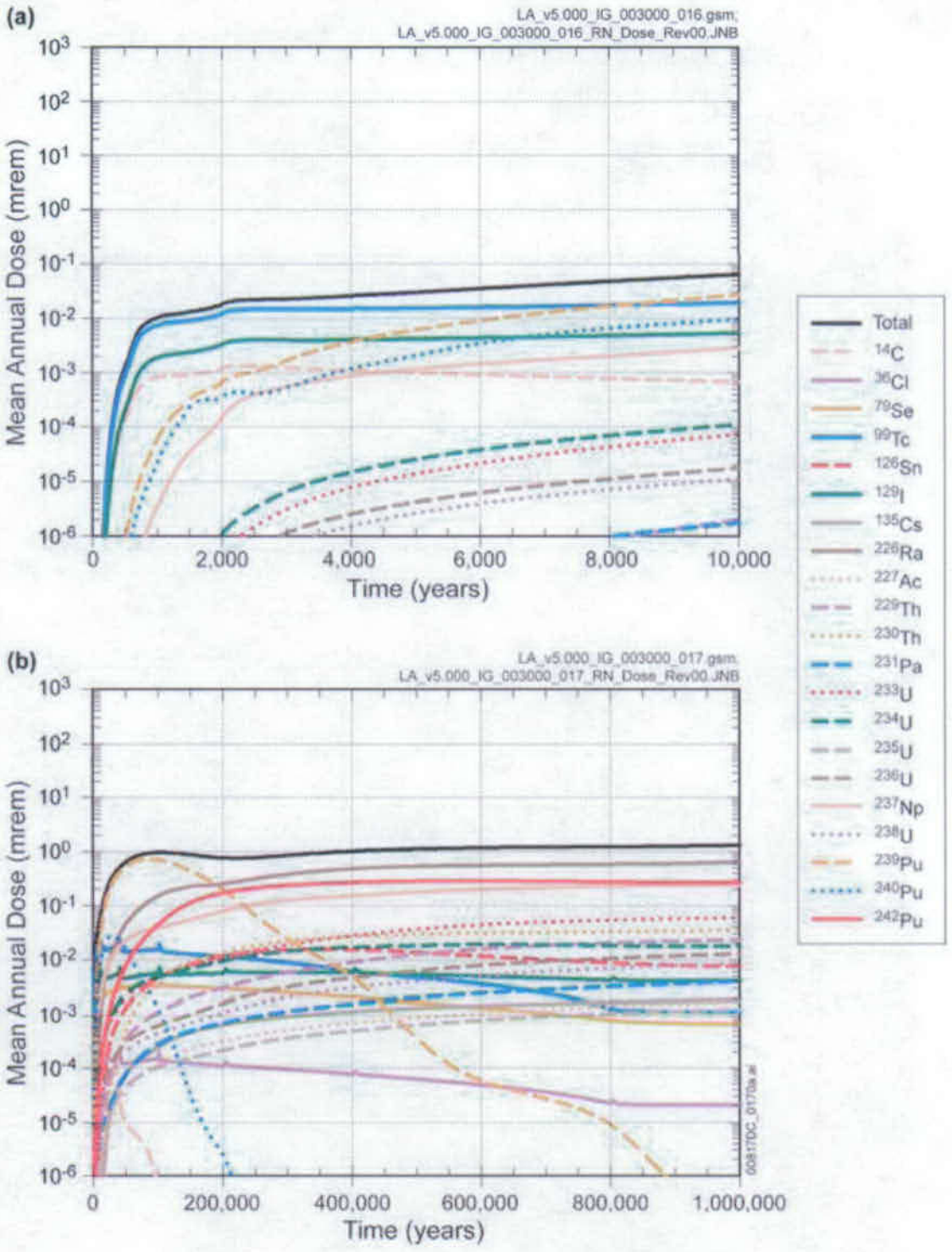

Figure ES-46. Mean Annual Dose Histories of Major Radionuclides for the Igneous Intrusion Modeling Case for (a) the First 10,000 Years after Repository Closure and (b) Post-10,000-Year Period

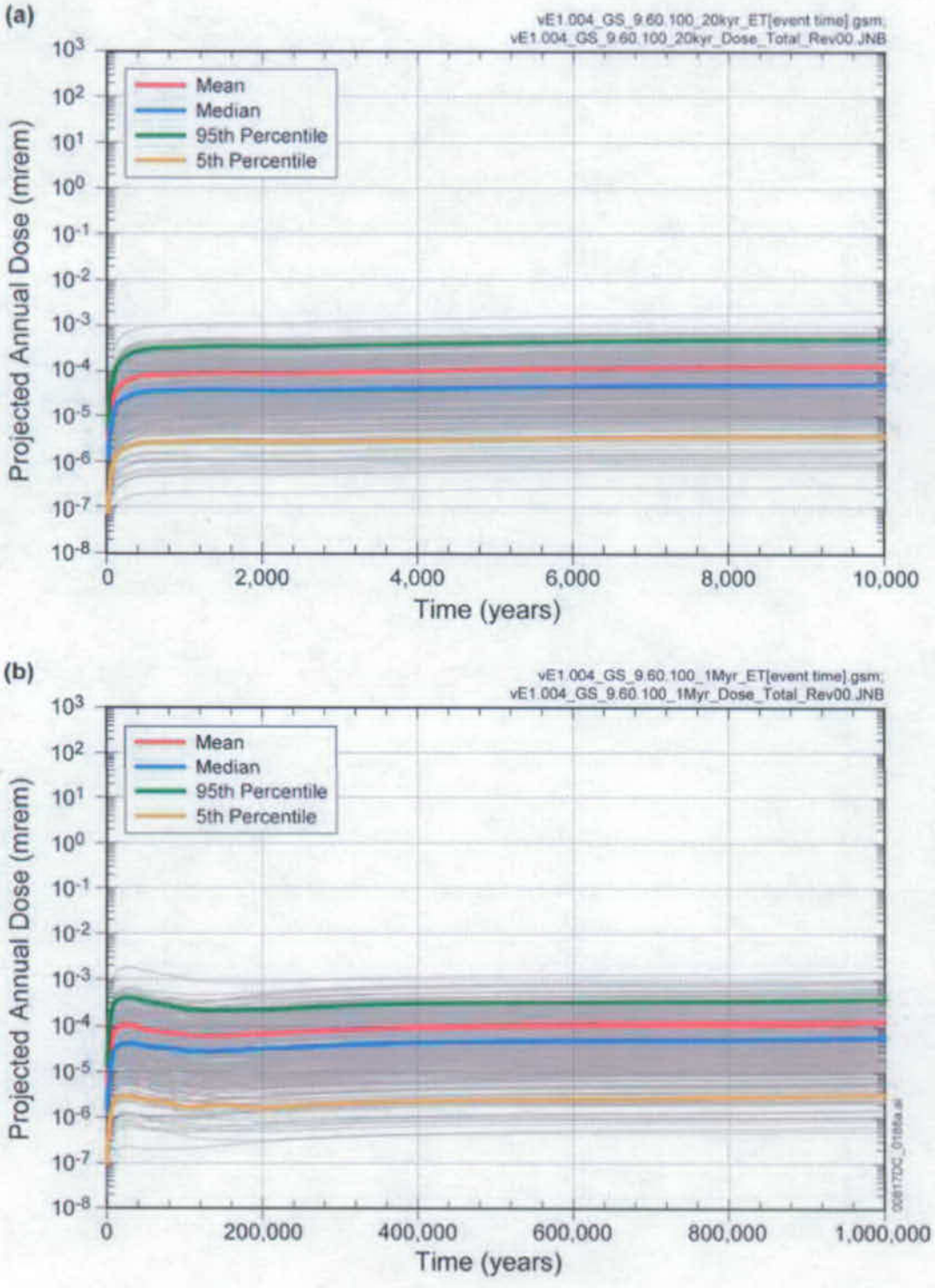

Figure ES-47. Projected Annual Dose for the Volcanic Eruption Modeling Case for (a) the First 10,000 Years after Repository Closure and (b) Post-10,000-Year Period

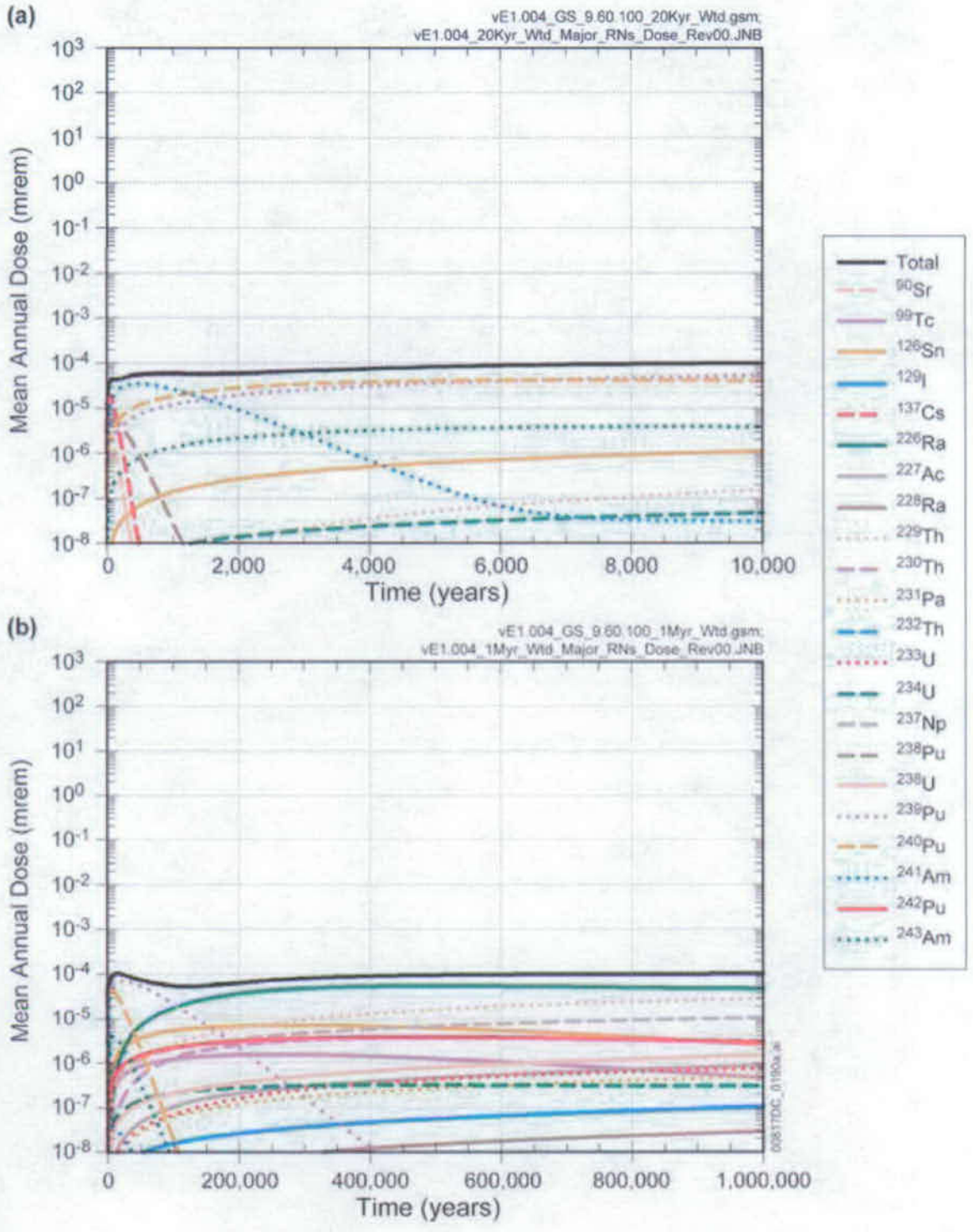

Figure ES-48. Mean Annual Dose Histories of Major Radionuclides for the Volcanic Eruption Modeling Case for (a) the First 10,000 Years after Repository Closure and (b) Post-10,000-Year Period

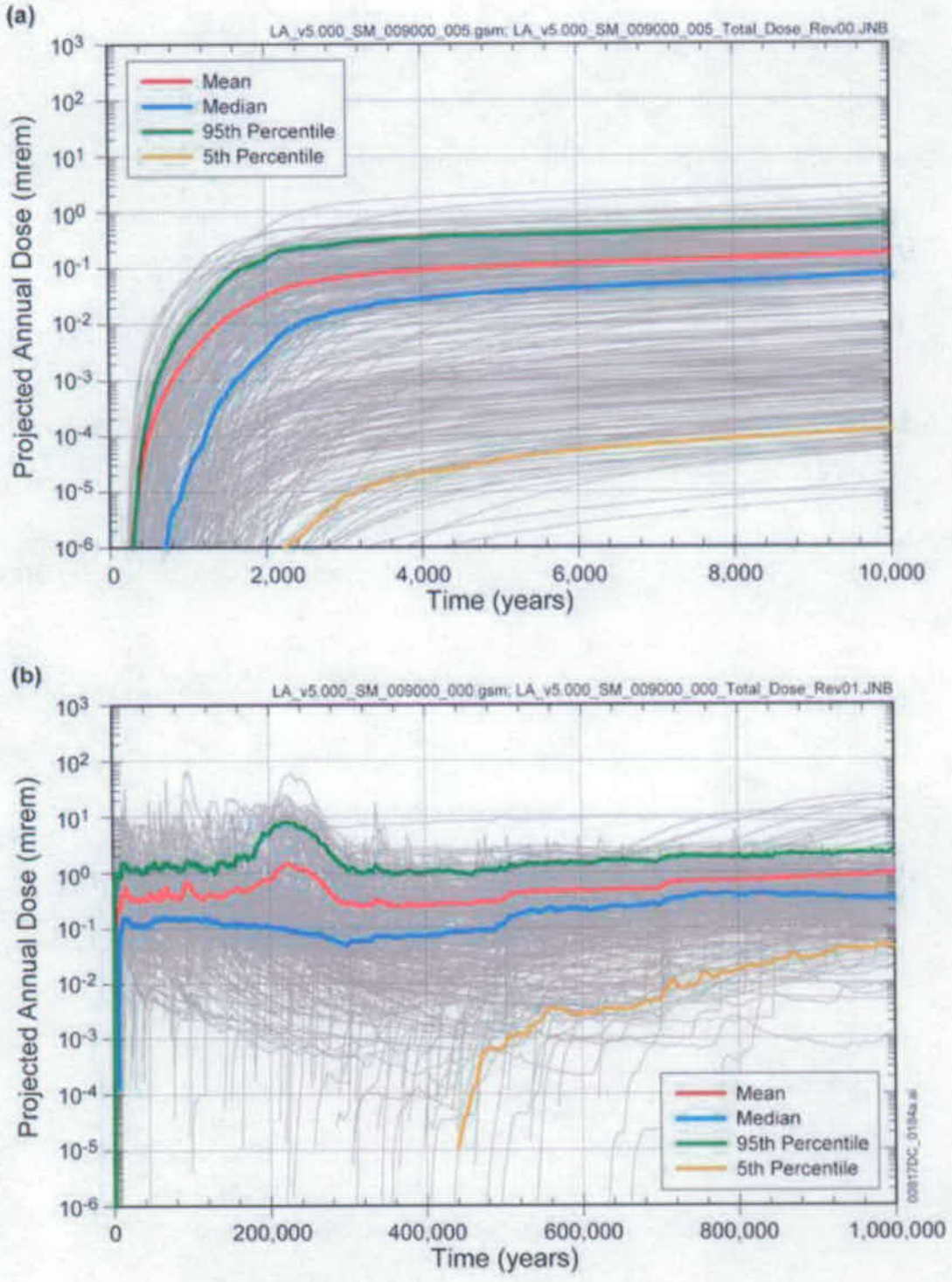

Figure ES-49. Projected Annual Dose for the Seismic Ground Motion Modeling Case for (a) the First 10,000 Years after Repository Closure and (b) Post-10,000-Year Period

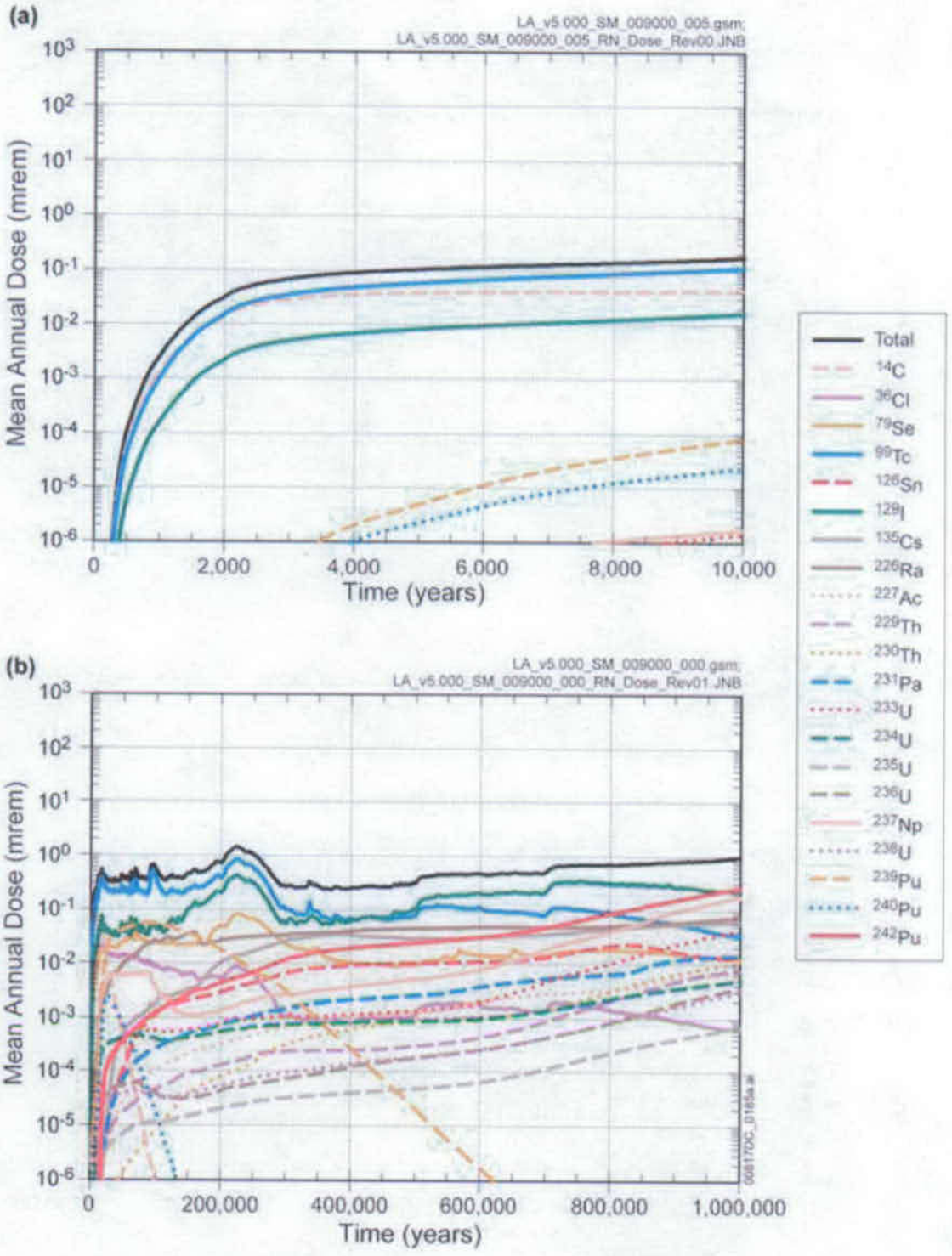

Figure ES-50. Mean Annual Dose Histories of Major Radionuclides for the Seismic Ground Motion Modeling Case for (a) the First 10,000 Years after Repository Closure and (b) Post-10,000-Year Period

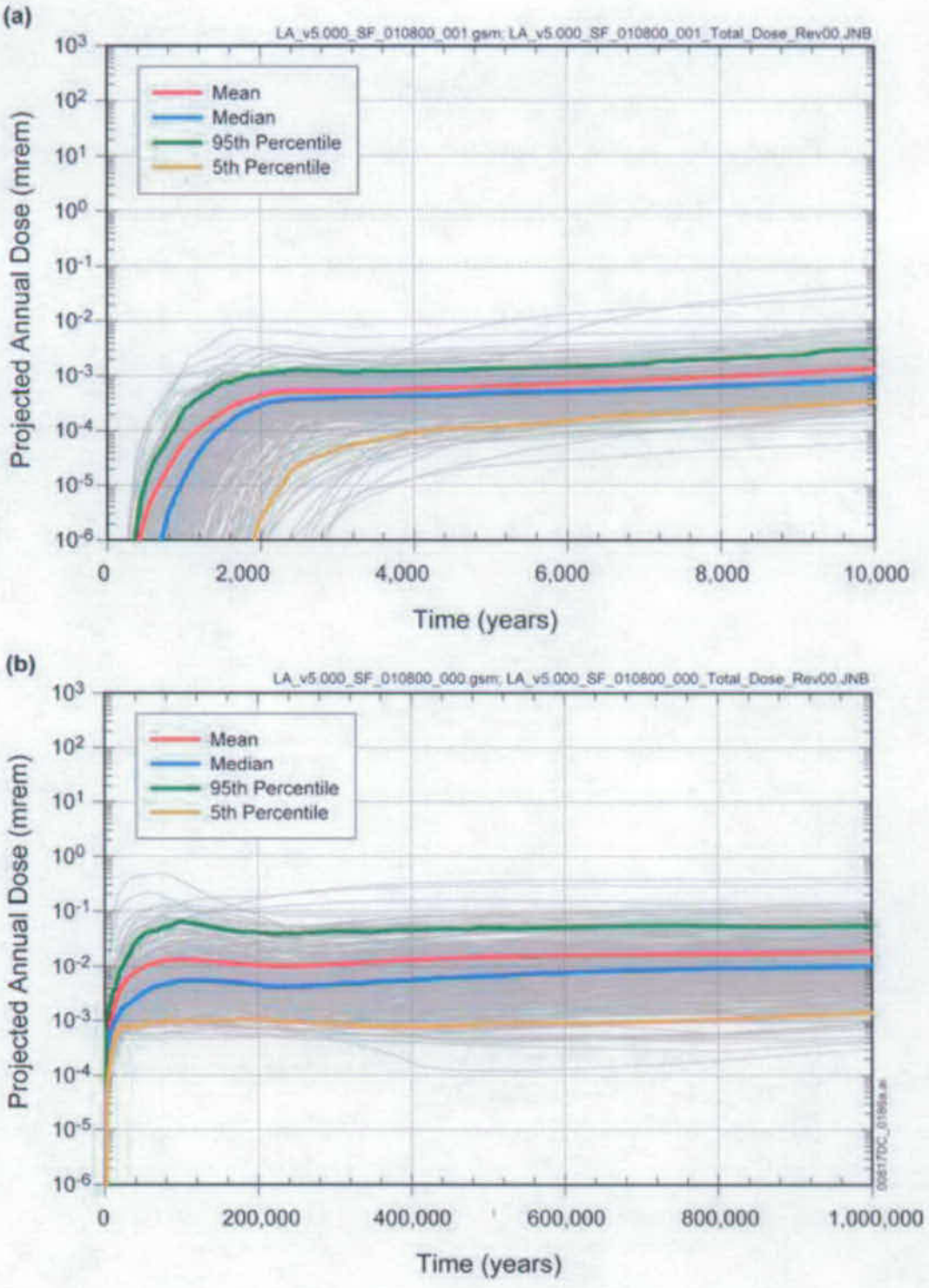

Figure ES-51. Projected Annual Dose for the Seismic Fault Displacement Modeling Case for the (a) First 10,000 Years after Repository Closure and (b) Post-10,000-Year Period

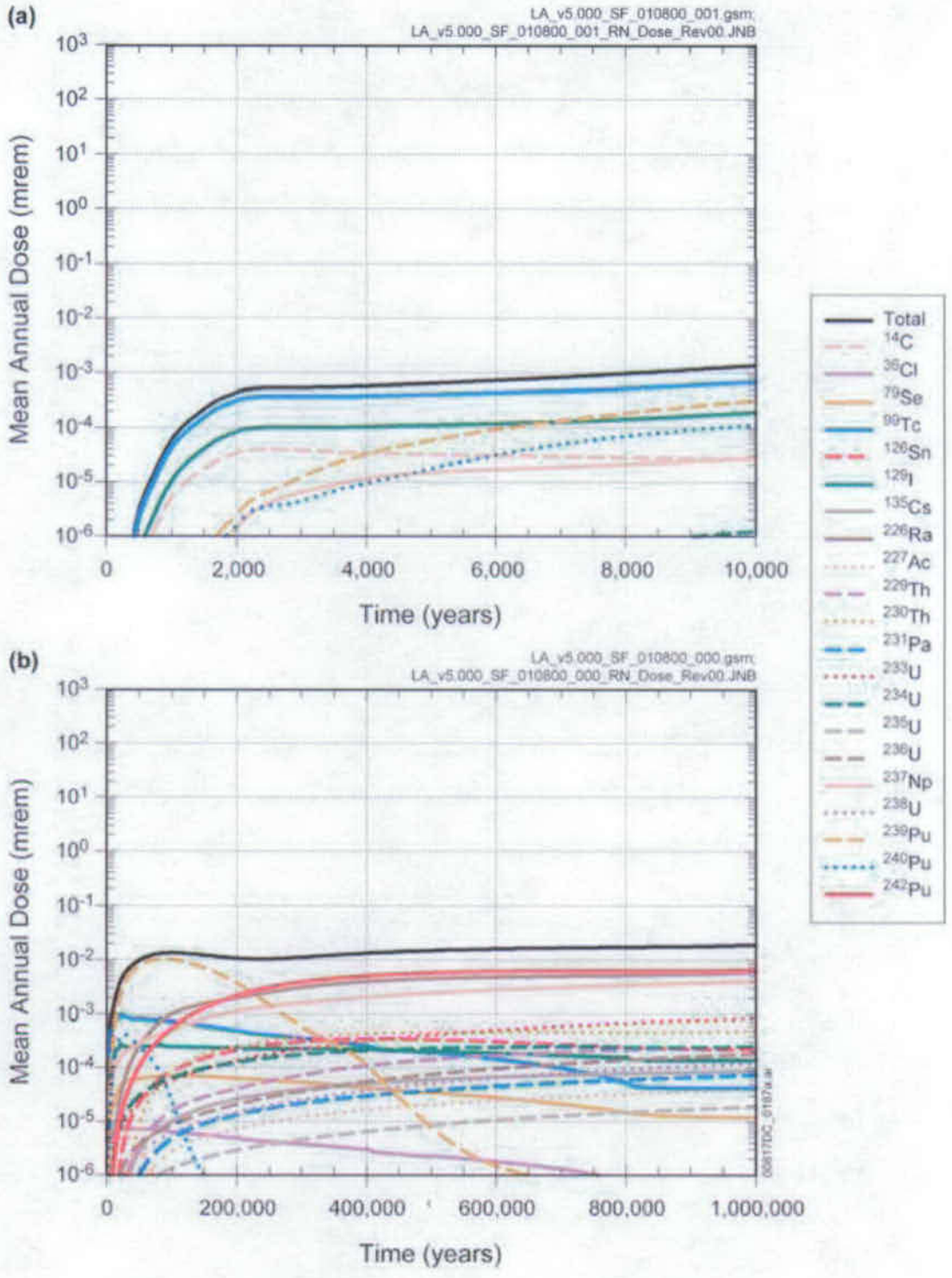

Figure ES-52. Mean Annual Dose Histories of Major Radionuclides for the Seismic Fault Displacement Modeling Case for the (a) First 10,000 Years after Repository Closure and (b) Post-10,000-Year Period

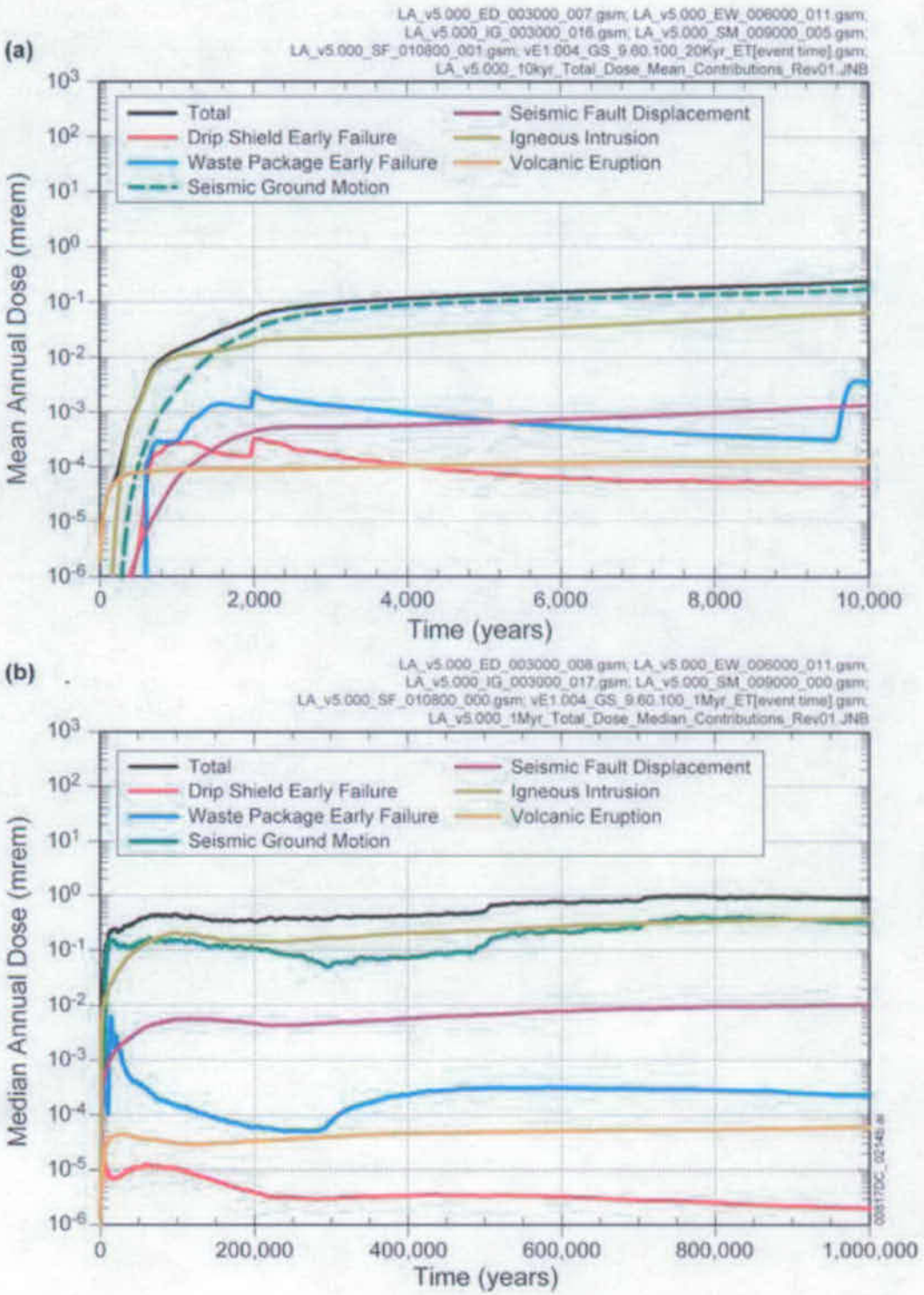

Figure ES-53. Total Mean Annual Dose and Median Annual Doses for Each Modeling Case for (a) the First 10,000 Years after Repository Closure and (b) Post-10,000-Year Period

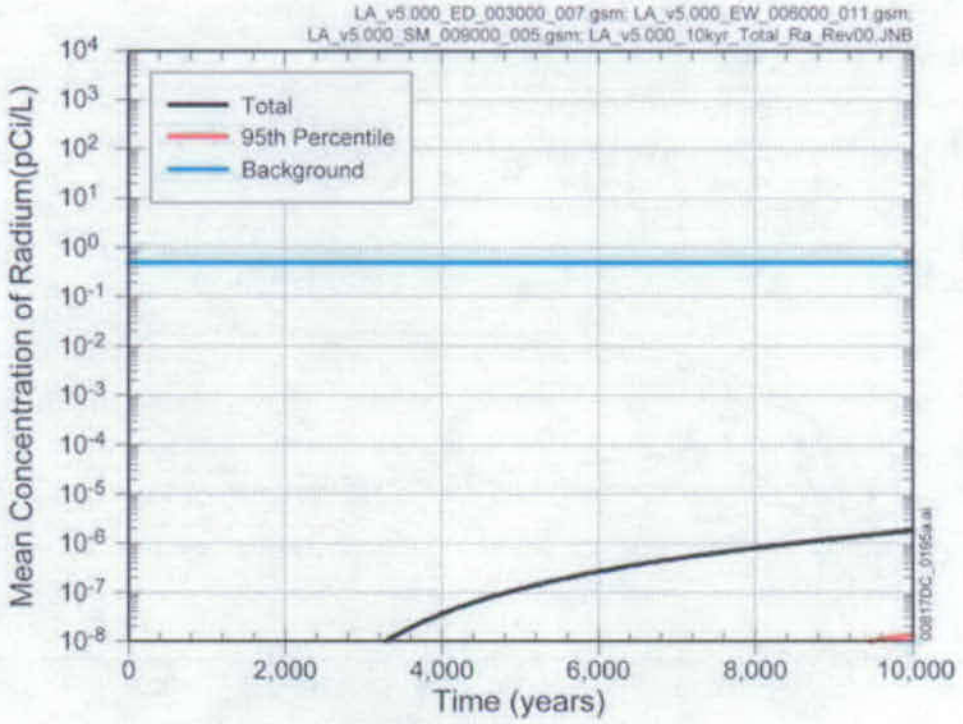

Figure ES-54. Combined Radium-226 and -228 Activity Concentrations, Excluding Natural Background, for Likely Features, Events, and Processes Using Nominal, Early failure, and Seismic Ground Motion Damage Processes

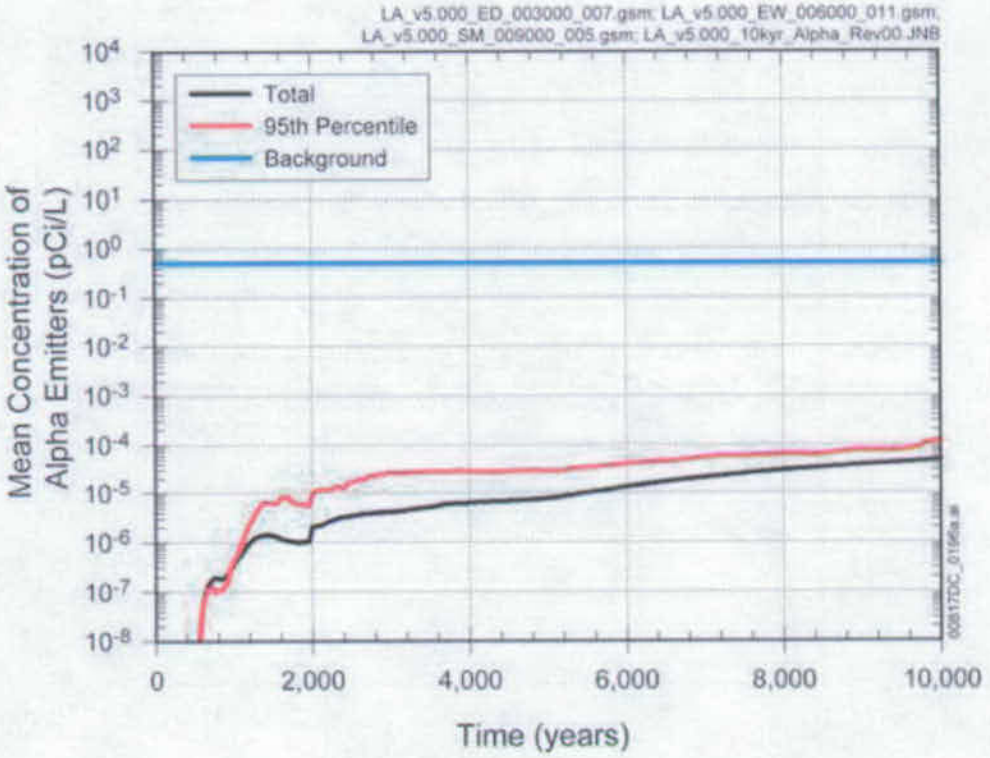

Figure ES-55. Combined Activity Concentrations of All Alpha Emitters (including Radium-226 but without radon and uranium isotopes), Excluding Natural Background, for Likely Features, Events, and Processes Using Nominal, Early Failure, and Seismic Ground Motion Damage Processes

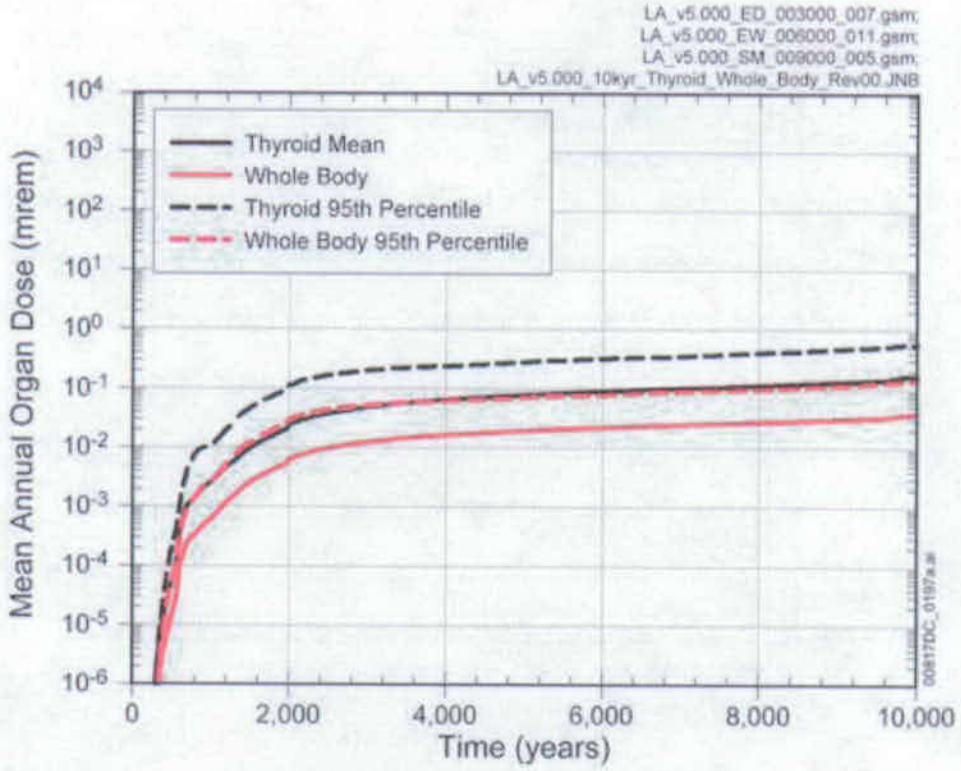

Figure ES-56. Mean Annual Drinking Water Dose from Combined Beta and Photon Emitters for Likely Features, Events, and Processes using the Nominal, Early Failure, and Seismic Ground Motion Damage Processes

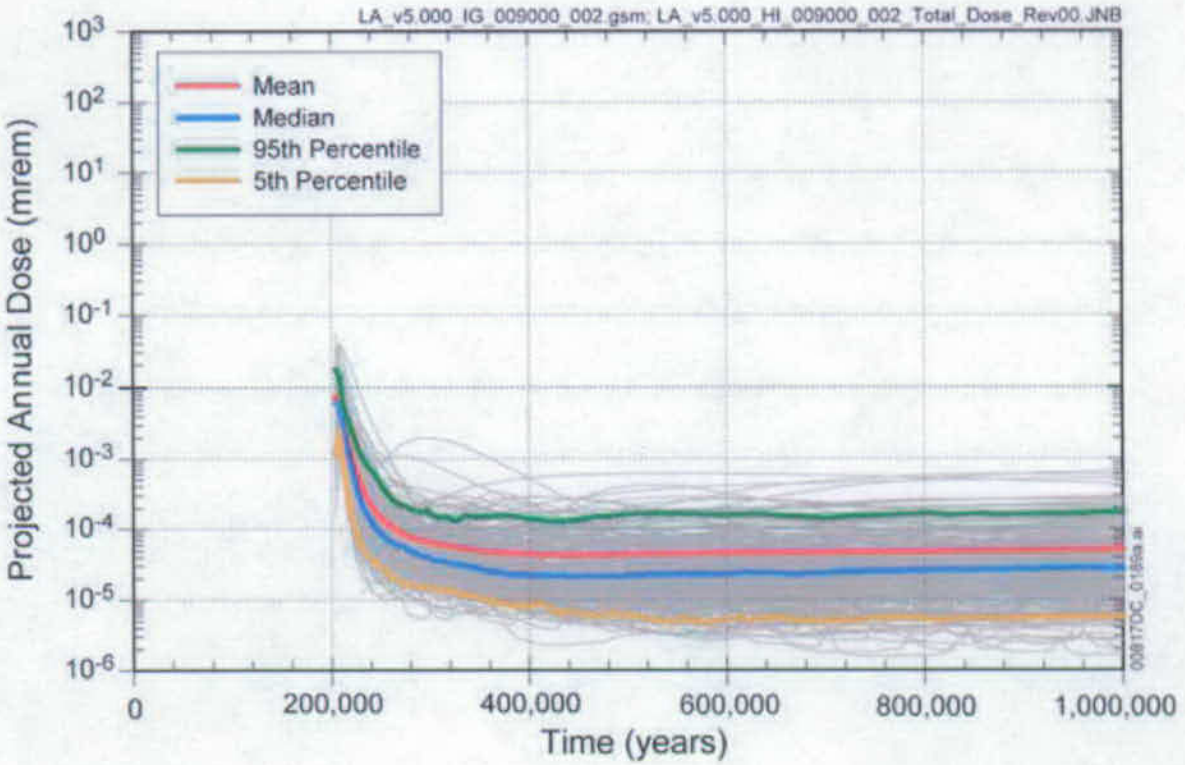

Figure ES-57. Projected Annual Individual Dose at the RMEI Location from Human Intrusion 200,000 Years after Repository Closure

INTENTIONALLY LEFT BLANK

1. PURPOSE

The *Total System Performance Assessment Model–Supplemental Environmental Impact Statement Information Package* describes the methodology, structure, validation, and application of the Total System Performance Assessment for the Supplemental Environmental Impact Statement (TSPA-SEIS) Model that has been developed to support the Draft SEIS for construction of a geologic repository for the safe disposal of spent nuclear fuel (SNF) and high-level radioactive waste (HLW) at Yucca Mountain, Nevada. The TSPA-SEIS is one of a series of iterative performance assessments (PAs) conducted over the life of the Yucca Mountain Project. The TSPA-SEIS evaluates the ability of the repository to adequately isolate nuclear waste following repository closure, as described in the NRC Proposed Rule 10 CFR Part 63, [DIRS 178394] and [DIRS 180319].

1.1 INTRODUCTION

The TSPA-SEIS was developed to analyze the ability of the natural and engineered systems of the Yucca Mountain repository to isolate nuclear waste following repository closure. PAs and related supplemental analyses of the Yucca Mountain repository have been conducted following the publication of the Nuclear Waste Policy Amendments Act of 1987, Public Law No. 100-203 [DIRS 100016]. Total System Performance Assessments (TSPAs) of the Yucca Mountain repository have been iterative and periodically updated, each succeeding assessment building on and extending the scope and results of the previous TSPA. The iterative PAs incorporate both an improved understanding of the processes affecting repository performance and, through additional field observations and laboratory analyses, better identification and quantification of the values of the parameters used in the TSPAs. The most recent TSPA document applied the TSPA methodology to the Final Environmental Impact Statement for the Yucca Mountain repository (Williams 2001 [DIRS 157307]).

The TSPA-SEIS evaluates the potential consequences of nuclear waste disposal at Yucca Mountain in terms of dose to potential receptors. The analyses presented in this document demonstrate the validity of the TSPA-SEIS in terms of its ability to represent the natural and engineered systems in and around the repository environment and the effects of possible disruptive events that could affect the performance of the Yucca Mountain repository system.

1.1.1 Governing Regulations

Final rules from the U.S. Environmental Protection Agency (EPA) and NRC concerning the disposal of waste at Yucca Mountain are not yet available, but analyses described in this report have been designed and executed consistent with the expectation that the final rules will be identical in all regards to the proposed rules. The discussion in this section is consistent with that expectation.

The conceptual structure of the TSPA-SEIS and analysis of the Yucca Mountain repository, as presented in this document, is based on regulatory requirements in the NRC Proposed Rule 10 CFR Part 63 [DIRS 178394] and [DIRS 180319]. In proposed 10 CFR Part 63 [DIRS 178394], the NRC Proposed Rule adopts the EPA Proposed Rule at 40 CFR Part 197, Subpart B, [DIRS 177357] regarding public health and safety standards for radioactive material for the

Yucca Mountain repository. The core requirement in NRC Proposed Rule 10 CFR Part 63 [DIRS 178394] and [DIRS 180319] that ultimately gives rise to the conceptual structure of the TSPA-SEIS is the individual protection standard at 10 CFR 63.311 [DIRS 178394] specifying the dose standard for the reasonably maximally exposed individual (RMEI):

> "(a) DOE must demonstrate, using performance assessment, that there is a reasonable expectation that the reasonably maximally exposed individual receives no more than the following annual dose from releases from the undisturbed Yucca Mountain disposal system:
>
> (1) 0.15 mSv (15 mrem) for 10,000 years following disposal; and
>
> (2) 3.5 mSv (350 mrem) after 10,000 years, but within the period of geologic stability.
>
> (b) DOE's performance assessment must include all potential environmental pathways of radionuclide transport and exposure."

The NRC proposed rule requires that an application for a license to operate an HLW disposal facility at Yucca Mountain include a PA analysis as described at 10 CFR 63.113 [DIRS 180319] and 10 CFR 63.114 [DIRS 178394]. The proposed rule at 10 CFR 63.113 [DIRS 180319] describes the PA objectives for the geologic repository after permanent closure and 10 CFR 63.114(a) [DIRS 178394] states that any PA prepared in compliance with 10 CFR 63.113 [DIRS 180319] must:

> "(1) Include data related to the geology, hydrology, and geochemistry (including disruptive processes and events) of the Yucca Mountain site, and the surrounding region to the extent necessary, and information on the design of the engineered barrier system used to define, for 10,000 years after disposal, parameters and conceptual models used in the assessment.
>
> (2) Account for uncertainties and variabilities in parameter values, for 10,000 years after disposal, and provide for the technical basis for parameter ranges, probability distributions, or bounding values used in the performance assessment.
>
> (3) Consider alternative conceptual models of features and processes, for 10,000 years after disposal, that are consistent with available data and current scientific understanding and evaluate the effects that alternative conceptual models have on the performance of the geologic repository.
>
> (4) Consider only features, events, and processes consistent with the limits on performance assessment specified at § 63.342.
>
> (5) Provide the technical basis for either inclusion or exclusion of specific features, events, and processes in the performance assessment. Specific features, events, and processes must be evaluated in detail if the magnitude and time of the resulting radiological exposures to the reasonably maximally exposed individual, or radionuclide releases to the

accessible environment, for 10,000 years after disposal, would be significantly changed by their omission.

(6) Provide the technical basis for either inclusion or exclusion of degradation, deterioration, or alteration processes of engineered barriers in the performance assessment, including those processes that would adversely affect the performance of natural barriers. Degradation, deterioration, or alteration processes of engineered barriers must be evaluated in detail if the magnitude and time of the resulting radiological exposures to the reasonably maximally exposed individual, or radionuclide releases to the accessible environment, for 10,000 years after disposal, would be significantly changed by their omission.

(7) Provide the technical basis for models used to represent the 10,000 years after disposal in the performance assessment, such as comparisons made with outputs of detailed process-level models and/or empirical observations (e.g., laboratory testing, field investigations, and natural analogs).

(b) Any performance assessment used to demonstrate compliance with § 63.113 for the period of time after 10,000 years through the period of geologic stability must be based on the performance assessment specified in paragraph (a) of this section."

Thus, the requirements state that any PA used to demonstrate compliance with the regulations should include a site description, considerations of uncertainty, alternative conceptual models (ACMs), and a features, events, and processes (FEPs) analysis as described at proposed rule 10 CFR 63.114 [DIRS 178394]. Further, the FEPs identified as pertinent to the repository were screened for the postclosure 10,000 year compliance period as specified at proposed rule 10 CFR 63.342(a) [DIRS 178394], "DOE's performance assessments conducted to show compliance with §§ 63.111(a)(1), 63.321(b)(1), and 63.331 shall not include consideration of very unlikely features, events, or processes, *i.e.*, those that are estimated to have less than one chance in 10,000 of occurring within 10,000 years of disposal (less than one chance in 1,000,000 per year)." The NRC proposed rule at 10 CFR 63.114(a)(2) [DIRS 178394] requires the PA to include concepts related to uncertainty in the estimates of the values of the parameters used in the TSPA-SEIS. The uncertainties used to provide the estimates of parameter values for the TSPA-SEIS address: (1) uncertainty in the epistemic or subjective sense related to knowledge about the appropriateness of assumptions used in an analysis, (2) spatial variability, and (3) uncertainty in the aleatory sense related to events that may or may not occur in the future. The regulation indicates that a PA analysis shall calculate outcome in terms of dose to the RMEI but include an uncertainty analysis that evaluates "how uncertainty in parameter values affects uncertainty in the estimate of dose" (10 CFR 63 [DIRS 180319], Supplementary Information III, Section 3.1).

The U.S. Department of Energy (DOE) must demonstrate, using a PA, that there is a reasonable expectation that, for 10,000 years following disposal, the RMEI receives no more than an annual dose of 15 mrem from releases from the undisturbed Yucca Mountain disposal system. DOE analysis must include all potential pathways of radionuclide transport and exposure. The NRC Proposed Rule at 10 CFR 63.303 [DIRS 178394] also adopts the EPA performance measures quoted from EPA Proposed Rule 40 CFR 197.13 [DIRS 177357] as follows:

> "(a) The NRC will determine compliance based upon the arithmetic mean of the projected doses from DOE's performance assessments for the period within 10,000 years after disposal."
>
> "(b) NRC will determine compliance based upon the median of the projected doses from DOE's performance assessments for the period after 10,000 years of disposal and through the period of geologic stability:"

The TSPA-SEIS calculates dose to the RMEI from the simulated release of radioactive materials from the Yucca Mountain repository to the accessible environment, as specified at 66 FR 32074 ([DIRS 155216], p. 32133). The RMEI is located in the accessible environment where the groundwater path of the highest concentration of the contaminant plume would cross the southernmost boundary of the controlled area of the repository (at a latitude of 36° 40′ 13.6661″ North). This location is approximately 18 km from the repository footprint [DIRS 180319], III Public Comments and Responses, 3.5, p. 55750).

The NRC Proposed Rule at 10 CFR 63.305(b) [DIRS 180319] also describes specifications which indicate that: (1) the reference biosphere should incorporate FEPs consistent with present conditions in the Yucca Mountain region; (2) the PA should not project future demographic or biosphere conditions other than climate; (3) the PA should include reasonable assumptions about future geologic, hydrologic, and climatic conditions that could affect future conditions at the Yucca Mountain disposal site after repository closure; and (4) the PA should include biosphere pathways consistent with arid or semiarid conditions. Regarding climate, the NRC Proposed Rule at 10 CFR 63.342(c)(2) [DIRS 178394] states that,

> "DOE must assess the effects of climate change. The climate change analysis may be limited to the effects of increased water flow through the repository as a result of climate change, and the resulting transport and release of radionuclides to the accessible environment. The nature and degree of climate change may be represented by constant climate conditions. The analysis may commence at 10,000 years after disposal and shall extend to the period of geologic stability. The constant value to be used to represent climate change is to be based on a log-uniform probability distribution for deep percolation rates from 13 to 64 mm/year (0.5 to 2.5 inches/year)."

The NRC Proposed Rule at 10 CFR 63.303(b) [DIRS 178394] states that, "Compliance is based upon the median of the projected doses from DOE's performance assessments for the period after 10,000 years of disposal and through the period of geologic stability for: . . ." The National Academy of Sciences considers the period of geologic stability at Yucca Mountain as approximately one million years (National Research Council 1995 [DIRS 100018], p. 72). To comply with this stipulation in the regulation, the TSPA-SEIS provides analyses that provide estimates of repository performance for one million years, where one million years is considered to be the period of geologic stability. According to the NRC Proposed Rule at 10 CFR 63.302 [DIRS 178394], "Period of geologic stability means the time during which the variability of geologic characteristics and their future behavior in and around the Yucca Mountain site can be bounded, that is, they can be projected within a reasonable range of possibilities. This period is defined to end at one million years after disposal." The one-million-year analyses are thus

consistent with the NRC Proposed Rule at 10 CFR 63.342 [DIRS 178394] and the EPA Proposed Rule at 40 CFR 197.25 [DIRS 177357]. The TSPA-SEIS developed for the FEPs screened for the 10,000 year time period was also applied to the one-million-year time period of geologic stability.

The NRC proposed rule also requires DOE to assess a human intrusion scenario and 10 CFR 63.321 [DIRS 178394] provides the individual protection standard for the human intrusion scenario as follows:

> "(a) DOE must determine the earliest time after disposal that the waste package would degrade sufficiently that a human intrusion (see § 63.322 [DIRS 180319]) could occur without recognition by the drillers.
>
> (b) DOE must demonstrate that there is a reasonable expectation that the reasonably maximally exposed individual receives, as a result of human intrusion, no more than the following annual dose:
>
> (1) 0.15 mSv (15 mrem) for 10,000 years following disposal; and
>
> (2) 3.5 mSv (350 mrem) after 10,000 years, but within the period of geologic stability.
>
> (c) DOE's analysis must include all potential environmental pathways of radionuclide transport and exposure, subject to the requirements at § 63.322 [DIRS 180319]."

1.1.2 Total System Performance Assessment Methodology

The TSPA process is represented on Figure 1-1 as a series of pyramid levels. Figure 1-2 separates the levels of the TSPA pyramid showing the information flow, the reports, and the feedback loops involved in the development of the TSPA-SEIS. The foundation of the TSPA pyramid consists of a repository-system characterization involving the assimilation of the information collected by scientists and engineers involved in site characterization and engineering design. The repository system and regional characterization entails data collection regarding waste properties and design of the repository facilities, as well as the regional geology, regional hydrology, and environmental characteristics of the Yucca Mountain site. The broad foundation of the pyramid represents the more than 20-year body of knowledge collected in the field and in the laboratory regarding the repository system. This accumulated body of knowledge was used to identify the set of possible FEPs that may affect the repository system after repository closure and also provide the basis for the second stage of the TSPA pyramid. The TSPA-SEIS is built on the family of analyses of the identified FEPs, including analyses related to the exclusion of FEPs that are either very unlikely, are not required for regulatory reasons, or that have a low impact on performance (Section 1.1.1).

The next stage of the TSPA pyramid consists of the development and testing of detailed models used to conceptually describe retained and probable FEPs and their outcomes regarding repository performance. The detailed conceptual models consist of sets of hypotheses, assumptions, simplifications, and idealizations that, together, describe the essential aspects of a system or subsystem of the repository relative to its performance. Model conceptualization

identifies and selects FEPs that collectively comprise the scenarios considered in the conceptual models. An example of such a model or set of interconnected models is the description of the movement of water molecules and dissolved radionuclides by diffusive flow in rock pores or by advective flow in fracture openings in the unsaturated bedrock surrounding and below the repository and through the saturated zone (SZ) below the repository. Furthermore, because the TSPA process deals with future outcomes and includes uncertainty in both process descriptions and parameter values, there may be more than one ACM that provides a reasonable description of a particular system or subsystem. Therefore, the development and documentation of the supporting analyses are essential elements of the TSPA process. The supporting analyses capture uncertainty in probabilistic analyses that represent likely outcomes, based on the best available parameter values and the processes involved. This information serves as the foundation and source of input for the TSPA-SEIS. The documentation of the processes involved in the incorporation of uncertainty, the evaluation of ACMs, the treatment of conservatism, and the evaluation of FEPs in the supporting analyses provides input to the TSPA-SEIS.

The next stage of the TSPA pyramid involves the development of mathematical representations or abstractions of the conceptual models of the FEPs or scenarios, or both, that contribute to overall repository performance. The mathematical models consist of quantitative expressions of the process models developed in such a way that they can be used together to simulate repository performance. The mathematical models might include algebraic expressions, ordinary differential, partial differential, or integral equations characterizing accepted conservation laws, such as the conservation of mass, energy, or momentum, as well as appropriate constitutive equations that describe material behavior in the domain of the conceptual model. An example of one of the process models abstracted in mathematical and numerical form is a model describing the flow of water infiltrating at land surface and then percolating through the unsaturated zone (UZ) above the water table. Such a model would incorporate equations describing fluid flow and probable fluid interactions between the rock matrix and fractures in the rock, as well as descriptions of any other hydrologic, physical, and chemical processes needed to describe how water flows throughout the rock mass of the UZ.

The TSPA-SEIS includes a numerical representation of water flow through Yucca Mountain as an abstraction consisting of a series of statistical or mathematical expressions, including look-up tables, equations representing response surfaces, probability distributions, linear transfer functions, or reductions of model dimensionality. These inputs developed by the abstraction process were either implemented directly into the TSPA-SEIS or through a series of simplifying steps, depending upon the relative complexity or importance, or both, of the FEPs being abstracted. This abstraction, or progressive simplification of the conceptual models to more compact and usable numerical models, is the essence of this level of the TSPA pyramid. The models eventually used to analyze the projected evolution through time of the various components of the repository system are abstracted models that capture the salient features of the process models, along with their associated uncertainties.

The top level of the TSPA pyramid consists of the integrated total system model. The total system model is a numerical model used to simulate the behavior of the Yucca Mountain repository system. The TSPA-SEIS incorporates the abstracted process models and/or the

analyses that describe the model components and their submodels from their development to their implementation. Together these form the basis for the TSPA-SEIS.

The TSPA-SEIS integrates conceptual, mathematical, and computational models of the relevant FEPs that may affect repository performance as informed by site-specific information, relevant laboratory data, and natural analogues that assist in building the confidence in the long-term processes evaluated in TSPA-SEIS analyses. The TSPA-SEIS approach provides for an analysis of the repository system that appropriately incorporates parameter distributions used to quantify uncertainty. Incorporating this uncertainty in multiple stochastic realizations of the TSPA-SEIS produces a long-term projection of repository performance. The simulations of repository performance thus provide a means for the defensible analysis of system behavior, incorporating process models and parameters based on scientific observations. The TSPA-SEIS then uses the parameter values and process models to assess the capability of the Yucca Mountain Repository System to comply with applicable radiation-protection standards contained in the governing regulations.

The use of the TSPA-SEIS to simulate Yucca Mountain repository behavior and project future outcomes is aided by the development of scenario classes to assist in repository performance analyses. A scenario class is a set of related scenarios, incorporating groups of possible FEPs, that describe possible future repository conditions and share sufficient similarities that can be aggregated for performance analysis. The TSPA-SEIS scenario classes represent a wide range of future outcomes, including the Nominal (undisturbed), the Early Failure, Igneous, and Seismic Scenario Classes, as well as a Human Intrusion Scenario.

The TSPA-SEIS builds on the family of analyses related to FEPs. The resulting TSPA-SEIS includes the results of analyses of the FEPs that were screened and included in the TSPA-SEIS development process. In addition, the TSPA-SEIS development was affected by the exclusion of FEPs that are either very unlikely, are not required for regulatory reasons, or that have a low impact on performance.

Probabilistic simulations provide a useful tool for the SEIS process and address issues raised by previous TSPAs conducted for the Yucca Mountain repository. The TSPA-SEIS also provides results useful in addressing questions raised by internal and external reviews, such as those conducted by the U.S. Nuclear Waste Technical Review Board and the Performance Assessment International Review Team (OECD and IAEA 2002 [DIRS 158098]).

1.1.3 Treatment of Uncertainty

The TSPA-SEIS incorporates uncertainty in parameter values and event occurrence. Uncertainty in the TSPA-SEIS is characterized as either epistemic or aleatory uncertainty according to the following definitions (Hoffman and Hammonds 1994 [DIRS 107502]:

- **Epistemic Uncertainty**—Epistemic uncertainty pertains to the state of uncertainty in the state of knowledge concerning parameter values because there are limited data or there are alternative interpretations of the available data. The state of knowledge about the exact value of the parameter can increase through testing and data collection. Therefore, epistemic uncertainty can also be referred to as 'reducible uncertainty.'

- **Aleatory Uncertainty**—Aleatory uncertainty concerns whether or not there is a chance of occurrence of a feature, event, or process. For example, there can be uncertainty about whether or not a volcanic disruption can occur or not occur. Aleatory uncertainty may also be referred to as 'irreducible uncertainty' because no amount of knowledge will determine whether or not a chance event will or will not occur.

Maintaining a separation between aleatory and epistemic uncertainty strongly affects the design of the PA analyses conducted with the TSPA-SEIS. It may also strongly affect the design of individual TSPA-SEIS submodels. However, it is not always useful or enlightening to strictly maintain this separation for all parameters. For example, in the TSPA-SEIS, UZ flow is modeled as occurring as an epistemically uncertain constant rate during each climate period, rather than as dependent on the aleatory uncertainty in future rainfall. The aleatory uncertainty in rainfall is accounted for in the calculation of the distribution of UZ flow rates. The separation of parameter uncertainty into aleatory or epistemic uncertainty may or may not occur for any one particular variable, but the processes employed will help ensure that appropriate supporting analyses are included. The TSPA-SEIS and the manner in which the two forms of parameter uncertainty are handled will ensure that the distributions of parameter values reflect how the underlying model is used in the TSPA-SEIS analyses.

1.2 TSPA-SEIS DEVELOPMENT PROCESS

The TSPA-SEIS analyses were conducted in a probabilistic framework. The TSPA-SEIS was used to calculate estimates of repository performance, including expected annual dose to receptors, groundwater concentrations at selected distances from the repository, and effects of disruptive events. The calculated results are consistent with the abstraction model inputs provided by analyses of the processes governing flow and transport of radionuclides expected to be released from the repository upon failure of the waste packages (WPs) containing SNF and HLW. The TSPA-SEIS uses Monte Carlo simulation techniques to address the uncertainty and/or variability in the values of the input parameters of the model. The TSPA-SEIS provides multiple realizations of the model's output by sampling input parameter values from assigned probability distributions spanning their defined ranges. To assist in TSPA-SEIS validation, several hundred to more than 1,000 realizations were simulated to ensure stochastic convergence and stability of the results. The simulations of each realization provided time histories of the annual dose or other performance measures. These results were analyzed for uncertainty and sensitivity with respect to the values of the input parameters at both total system and subsystem levels

1.2.1 Features, Events, and Processes Analysis

The development of the TSPA-SEIS includes the identification and screening of FEPs that could affect the repository for up to one-million years after repository closure. The FEPs that were screened in were used to develop scenario classes for the TSPA-SEIS analyses. Figure 1-3 is a schematic representation of the development of the TSPA-SEIS and describes, for analysis purposes, the repository system divided into individual model components. Each individual model component represents a major process or set of processes of the total repository system. Figure 1-3 shows the model component areas as well as the scenario classes that were used to

analyze repository performance under all expected conditions identified in the FEPs analysis, including a possible human intrusion into the repository.

1.2.2 Development of the Scenario Classes

The processes included in the principal model components in the TSPA-SEIS shown on Figure 1-3 were combined to evaluate the repository system performance for four scenario classes, seven modeling cases, and a stylized analysis of possible human intrusion into the repository. The underlying TSPA-SEIS incorporates all FEPs describing the fundamental processes governing repository performance under undisturbed conditions and additional FEPs that describe disruptive events, as well as possible changes to those fundamental processes. The Nominal Scenario Class encompasses all processes affecting the integrity of the WPs containing SNF and HLW in the absence of disruptive events. These processes include WP degradation because of corrosion mechanisms, including general corrosion (GC), stress corrosion cracking (SCC), localized corrosion (LC), and microbially influenced corrosion (MIC). The Early Failure Scenario Class addresses FEPs that describe the potential for drip shield (DS) and WP early failure in the absence of disruptive events. The early-failure scenarios include DSs and WPs that fail prematurely due to material defects or improper manufacturing conditions or pre-emplacement operations and practices, such as improper heat treatment or welding flaws. Early DS and WP failures are analyzed using the Drip Shield Early Failure (EF) Modeling Case and the Waste Package Early Failure (EF) Modeling Case.

The TSPA-SEIS includes two scenario classes that address the possibility that disruptive events may occur at or near the repository and that these events may affect repository performance. The Igneous Scenario Class comprises two modeling cases that address FEPs that describe igneous activity that could affect the repository. The Igneous Intrusion Modeling Case includes FEPs that account for the possibility that a dike containing magma could intrude into the repository and disrupt repository performance. The Igneous Intrusion Modeling Case includes all nominal flow-and-transport processes involving radionuclides after their release from WPs affected by an igneous intrusion. The Igneous Scenario Class also includes the Volcanic Eruption Modeling Case that addresses FEPs that describe a volcanic conduit(s) that invades the repository, destroys WPs, and erupts at land surface. The volcanic eruption disperses volcanic tephra and entrained waste into the atmosphere and deposits the contaminated tephra on land surfaces where the contaminated tephra becomes subject to redistribution by near-surface hydrogeologic processes.

The TSPA-SEIS also includes a Seismic Scenario Class, which is used to analyze possible seismic disruption of the repository and the disruption's effect on repository performance. The Seismic Scenario Class considers two modeling cases: (1) the Seismic Ground Motion Modeling Case addresses FEPs concerning damage to WPs, DSs, and commercial spent nuclear fuel (CSNF) due to vibratory ground motion; and (2) the Seismic Fault Displacement Modeling Case addresses the effects of fault displacement (FD) on WPs and DSs. The modeling cases simulate the degraded performance of damaged DSs and the release of radionuclides from WPs that are damaged due to seismic events. The transport of released radionuclides will be simulated using all the nominal processes that apply.

The NRC Proposed Rule at 10 CFR 63.322 [DIRS 180319] requires DOE to assess a human intrusion scenario, and 10 CFR 63.321 [DIRS 178394] provides the performance standard for the human intrusion scenario. The TSPA-SEIS considered the human intrusion scenario in a calculation that simulates a future drilling operation. The human intrusion scenario considers an intruder drilling a land-surface borehole using a drilling apparatus operating under the common techniques and practices currently employed in exploratory drilling for groundwater in the region around Yucca Mountain. While drilling a borehole, the drilling apparatus directly intersects a degraded WP and continues subsequently into the SZ underlying Yucca Mountain. The human intrusion causes the subsequent compromise and release of waste in the penetrated WP. The TSPA-SEIS simulated the human intrusion scenario occurring approximately 200,000 years after repository closure.

1.2.3 Incorporation of Uncertainty

The TSPA-SEIS contains over 300 parameters with uncertain parameter values that are described by probability distributions. In some cases, if there was significant uncertainty in parameters values, the TSPA-SEIS uses conservative estimates of the parameter values so as not to bias the results toward potentially optimistic projections of total system performance. The goal of the TSPA-SEIS is to provide a defensible quantification of the uncertainty in parameter values using probability distributions.

The parameter-value distributions were identified, considered, and evaluated using the most recent and relevant information about the repository system that was available from all sources. This information was used to quantify uncertainties in parameter values; provide insights for updating conceptual and numerical models, submodels, and abstractions; and provide additional lines of evidence about the possible future behavior of the repository. To the extent possible, the information has been incorporated in the TSPA-SEIS database.

The process used to evaluate unquantified uncertainties in parameter values contained in the parameter-valued distributions involved: (1) identifying the unquantified uncertainties to be evaluated; (2) developing more representative, quantified descriptions of those uncertainties; and (3) evaluating the implications of those newly quantified uncertainties with respect to repository performance. The impacts of these representations of parameter values to previously unquantified uncertainties were then evaluated using revised process models and supplemental TSPA-SEIS analyses using the revised uncertainty treatments. The results were documented accordingly in the TSPA-SEIS database.

Therefore, the TSPA-SEIS approach provides for an analysis of the repository system that appropriately incorporates distributions of parameter values that are, in turn, used to quantify uncertainty. The uncertainty and variability in the expected behavior of the repository system requires that the TSPA-SEIS analyses be probabilistic in order to capture the full range of possible future outcomes. Incorporating this uncertainty in multiple stochastic realizations of the TSPA-SEIS produces a probabilistic long-term projection of repository performance. Therefore, the TSPA-SEIS incorporates multiple realizations using distributions of values for uncertain parameters, rather than deterministic calculations using identified and assumed single values for each parameter in the repository system. The model realizations are performed many times using many combinations of the distributed parameter values, where each of the combinations of

parameter values is representative of a subset of the full range of future outcomes. Given that complete knowledge of the repository system cannot be attained, the probabilistic analyses obtained with the TSPA-SEIS reflect an appropriate range of process behaviors or parameter values, or both, of the repository system.

1.2.4 Alternative Conceptual Models

ACMs are a means to specifically acknowledge model form uncertainty. An ACM is a set of working hypotheses and assumptions that provide an acceptable description of a system for the intended purpose. Because the TSPA process deals with future outcomes and includes uncertainty in both process descriptions and parameter values, there may be several ACMs that provide reasonable descriptions of a particular system or subsystem. Considering ACMs helps to build confidence that plausible changes in modeling assumptions or simplifications will not change conclusions regarding subsystem and total system performance. Also, ACMs are used to ensure that the nominal model adequately captures the range of plausible and reasonable uncertainty in the conceptual model of the repository system. Each model component and submodel discussion in Section 6.3 includes a summary evaluation of ACMs.

1.2.5 Configuration Management for the TSPA-SEIS

The development of the TSPA-SEIS required organization, control, and accountability. Configuration control was implemented for software, input parameter values, and model architecture. The result is enhanced transparency and traceability for the TSPA-SEIS.

A number of software codes were implemented to support the development of the TSPA-SEIS. Some of these codes were used to provide supporting information and some codes were directly implemented in the TSPA-SEIS using the GoldSim simulation software (GoldSim V. 9.60.100 STN: 10344-9.60-01 [DIRS181903]). Supporting software codes, including process models, were developed and operated externally before running the TSPA-SEIS. Software codes directly implemented in the TSPA-SEIS are generally referred to as abstractions and are run within the TSPA-SEIS. All software codes used to support the TSPA-SEIS are qualified and are under configuration control. Each qualified code is in SCM and is uniquely identified with a tracking number. The SCM database also includes information on the software name, version, hardware platform, and operating system under which the code was qualified. All software documentation, including the software media, is linked to this tracking number.

Input parameter values are controlled through the TSPA Input Database. The database supports the TSPA-SEIS by providing the parameter values and distributions necessary for the PA analysis of the repository. The TSPA Input Database categorizes, stores, and retrieves fixed and distributed values of the TSPA-SEIS parameters, and allows qualified, authorized analysts to review and update the values. The TSPA Input Database has strict user controls, featuring read and write access and audit trails that ensure the security, integrity, and traceability of the information used in the TSPA-SEIS analyses.

The TSPA-SEIS integrates several model components and submodels to simulate the performance of the repository. A numerical representation is used to implement the TSPA-SEIS with GoldSim software. The inputs used by this numerical representation of the TSPA-SEIS are

obtained from controlled sources maintained by the Office of Civilian Radioactive Waste Management (OCRWM) data and information systems, such as OCRWM Program Documents, the Technical Data Management System (TDMS), the Technical Information Center, or other available sources such as NRC Proposed Rule 10 CFR Part 63 [DIRS 178394] and [DIRS 180319].

The TSPA-SEIS was designed and developed to run in a reasonable time on readily available computer hardware, using appropriate software. However, the size and complexity of the TSPA-SEIS makes it subject to some hardware limitations, including the number of realizations needed to provide reasonable results. The TSPA-SEIS was tested and provided stable results that met the validation criteria in the areas of statistical and temporal stability, spatial variability, and discretization.

The probabilistic, multiple-realization requirement necessitates that the hardware configuration have several hundred nodes. Each node is a separate processor capable of running one realization of the TSPA-SEIS. Each individual node, or central processing unit, was purchased with the largest hardware, with 3.2 gigahertz (GHz) processor speed, 3 or 4 gigabytes (GB) of random access memory (RAM) per processor, and high-speed hard drives to access virtual memory. The TSPA-SEIS uses individual central processing units with 32-bit Intel Xeon processors, which have a maximum allowable process size of 3 GB using the flexible 32-bit Windows 2003 operating system. The UZ Transport Submodel was designed to maximize the use of the 3 GB process size. More information on the hardware platform for the TSPA-SEIS is provided in Section 3.0.

The TSPA-SEIS handles both the multiple-realization requirement and the maximum size of individual coupled submodels. The GoldSim software fulfilled all of these requirements, having an efficient solver that minimized its run time for each individual realization. The Monte Carlo sampling structure in GoldSim allows the software to simultaneously run multiple realizations by distributing the realizations to individual nodes on the (approximately) 750-node TSPA-SEIS's Computational Cluster, then reassemble the results from these realizations into an ensemble result from the entire probabilistic run. Further, GoldSim acts as a driver, or integration software, that can couple other large pieces of software for those process models and submodels that were not converted to response surfaces, but are run concurrently in the TSPA-SEIS. Examples of such software include WP degradation software, UZ transport software, FEHM, seepage software (SEEPAGEDLL_LA V. 1.3. STN: 11076-1.3-00 [DIRS 180318]), and SZ transport software (SZ_CONVOLUTE V. 3.10.01. STN: 10207-3.10.01-00 [DIRS 181060]). Because of GoldSim's ability to run each submodel software in its own process space (particularly GoldSim itself and FEHM), it can maximize the use of the computer memory, subject to a soft limitation on the amount of virtual memory that should be used on any particular node (i.e., it is generally faster to run processes in 3 or 4 GB of RAM per processor than to run on the hard disk virtual memory).

1.3 YUCCA MOUNTAIN SITE DESCRIPTION

The Yucca Mountain repository system consists of natural and engineered systems that together will ensure the safe disposal of radioactive materials. The following information is provided as a general overview of the Yucca Mountain site, giving a context for the development of the TSPA-

SEIS that is discussed in detail in the remainder of this document. The understanding and analysis of FEPs relevant to postclosure performance is described in the supporting analyses that contain the abstractions used as input to the TSPA-SEIS. Detailed information on the direct inputs to the TSPA-SEIS is provided in Section 6 with full references and traceability.

The characteristics of the natural systems at Yucca Mountain that affect repository performance include climate, site geology, and site hydrogeology. The characteristics of the site geology and hydrogeology that affect repository performance include groundwater flow through the UZ and SZ, radionuclide transport, and disruptive events caused by igneous and seismic activity. This section provides a brief description of the current understanding of the Yucca Mountain natural system and the repository design. Information on Yucca Mountain site characteristics, along with descriptions of field and laboratory investigations conducted at Yucca Mountain, can be found in *Yucca Mountain Site Description* (BSC 2004 [DIRS 169734]), which contains comprehensive descriptions of the repository site and the surrounding region.

1.3.1 Physiographic Setting and Topography

Yucca Mountain is located within a transition zone between the northern boundary of the Mojave Desert and the southern boundary of the Great Basin Desert. The topography is characterized by isolated, long and narrow, roughly north-south-trending mountain ranges and broad intervening valleys (Figure 1-4). The surface elevations above the repository site are approximately 1,400 m above mean sea level. The ridgetops are generally flat to gently sloping, with soils 0.5- to 2-m thick. Terraces and channels are located at lower elevations of the primary washes and have thinner soil cover in the upper washes and thicker soil cover further downgradient. Yucca Mountain is a generally north-to-south-trending ridge with a relatively gentle eastward slope and a steep, westward facing escarpment. The topography in the Yucca Mountain vicinity is shaped by erosional processes on the eastward-sloping ridge of the mountain and along faults and fault scarps that have created a series of washes downcut to varying degrees into different bedrock layers. Slopes are locally steep on the west-facing escarpments eroded along the faults and in some of the valleys that cut into the more gentle eastward-facing dip slopes. Narrow valleys and ravines are cut in bedrock; wider valleys are covered by alluvial deposits, with terraces cut by intermittent streams. Locally, small sandy alluvial fans extend down the lower slopes and spread out on the valley floors. East of the Yucca Mountain crest, drainage is into Fortymile Wash. West of the crest, streams flow southwestward down fault-controlled canyons and discharge into Crater Flat (Figure 1-4). The topography is different to the south and north of Drill Hole Wash. The washes south of Drill Hole Wash trend eastward, are relatively short (less than 2 km), and have erosional channels with gently sloping sides (Figure 1-5). The washes north of Drill Hole Wash trend northwest and are relatively longer (3 to 4 km) because they are controlled by fault features and have steeper side slopes. A more detailed description of the topographic features of Yucca Mountain can be found in *Yucca Mountain Site Description* (BSC 2004 [DIRS 169734], Section 7.1).

1.3.2 Climate and Precipitation

In general, the present-day Nevada climate is characterized as semiarid to arid, with dry winds and low precipitation. The Pacific side of the mountain system to the west of Nevada causes a rain shadow effect, which in turn, causes moisture-loaded winds traveling east from the Pacific

Ocean to rise, cool, and drop precipitation on the Pacific mountain system. The climatic factors affecting water-transport processes in the UZ at Yucca Mountain are solar radiation flux, diurnal and seasonal temperature cycles, relative humidity, and precipitation, in the form of either rain or snow, as well as extended periods of drought. The Yucca Mountain Project environmental program collected site meteorological data using a network of nine automated weather stations (*Yucca Mountain Site Description* (BSC 2004 [DIRS 169734], Section 7.1.3.2). Current climatic conditions for the site and the Yucca Mountain region are discussed in detail in *Yucca Mountain Site Description* (BSC 2004 [DIRS 169734], Section 6.3).

The analysis of data from 114 weather stations measuring precipitation in the Yucca Mountain region, providing at least eight years of complete records, indicates a strong positive correlation between average annual precipitation and station elevation (BSC 2004 [DIRS 169734], Figure 7-7). These results indicate that the zones of maximum precipitation are likely to correspond to the zones of higher elevations in the mountain ranges. Average annual precipitation over the area of the Nevada Test Site ranges from a maximum of 370 mm in the Belted Range to a minimum of 100 mm in the Amargosa Desert. Annual precipitation in the Yucca Mountain vicinity ranges from a minimum of about 100 mm at low elevations along the southern boundary of the repository area to a maximum in excess of 300 mm at high elevations in the north (BSC 2004 [DIRS 169734], Figure 7-6)).

1.3.3 Geology

1.3.3.1 Surficial Deposits

The dominant surficial deposits in the general vicinity of Yucca Mountain are fluvial sediments and fluvial debris-flow deposits found in basins, washes, and alluvial fans. These deposits have varying degrees of soil development and thickness and have a gravelly texture, with rock fragments constituting between 20 and 80 percent of the total volume (BSC 2004 [DIRS 169734], Section 3.3.7.2). The deposits range from 100-m thick in the valleys to less than 30-m thick in the mouths of the washes. Halfway up the washes, alluvial fill generally is less than 15-m deep in the center of the channels and well-developed, cemented, calcium-carbonate soil horizons are common. On the more stable surfaces, generally on the ridgetops, soils are 0.5- to 2-m thick with a high clay content. Overall, the thickness of surficial deposits was classified into 4 categories: 0 to less than 0.5 m, 0.5 m to less than 3.0 m, 3.0 m to less than 6.0 m, and greater than or equal to 6.0 m, which encompass about 50 percent, 5 percent, 5 percent, and 40 percent of the site area, respectively (BSC 2004 [DIRS 169734], Section 3.3.7). Soil thickness tends to be well correlated to local topography, with the upland areas generally having thin soils and the lower washes and alluvial fans having thicker soils (surficial materials). The deeper deposits are present on the shallower slopes of the ridges, in washes, and underlying alluvial fans, whereas the deposits on the steeper side slopes, if present, consist of colluvium from rock slides. Soil storage capacity is determined mostly by soil thickness and porosity. Detailed information regarding the soils at Yucca Mountain can be found in *Yucca Mountain Site Description* (BSC 2004 [DIRS 169734], Section 3.3.7).

The maximum erosion during the first 10,000 years after repository closure is expected to be on the order of centimeters (BSC 2004 [DIRS 169734], Section 3.4.6), which is within the range of existing surface elevation irregularities, and would not affect the processes in the hundreds of

meters of UZ at Yucca Mountain. Similar conditions can be expected to be in effect throughout the one-million-year period of geologic stability (NRC Proposed Rule 10 CFR 63 ([DIRS 178394]). Therefore, the effects of soil erosion on infiltration are considered negligible and are reasonably excluded from the TSPA-SEIS calculations.

1.3.3.2 Bedrock Geology

Yucca Mountain is an uplifted, block-faulted ridge of alternating layers of welded and nonwelded volcanic tuffs of Miocene age. The major Yucca Mountain geologic units are the volcanic tuff formations of the Paintbrush Group (Tp), the Calico Hills Formation (Tac), and the Crater Flat Group (Tc). The lithostratigraphic nomenclature divides the Paintbrush Group into the Tiva Canyon (Tpc), Yucca Mountain (Tpy), Pah Canyon (Tpp), and Topopah Spring (Tpt) tuffs. The Crater Flat Group is divided into the Prow Pass (Tcp), Bullfrog (Tcb), and Tram (Tct) tuffs. For the purposes of hydrogeologic studies, including infiltration, a separate stratigraphic nomenclature was developed based on the degree of welding and the distribution of the hydrologic properties of the hydrogeologic units (BSC 2004 [DIRS 169734], Tables 3-1, 3-5, and 7-1). The main geologic units are divided into the Tiva Canyon welded (TCw), the Paintbrush nonwelded (PTn) (consisting primarily of the Yucca Mountain and Pah Canyon members and the interbedded tuffs), the Topopah Spring welded (TSw), the Calico Hills nonwelded (CHn), and the Crater Flat undifferentiated (CFu) units (Ortiz et al. 1985 [DIRS 101280]). Figure 1-6 shows the spatial relationship of the geologic units of the UZ in both perspective and east-west cross-sectional views.

1.3.3.3 Tectonics

1.3.3.3.1 Tectonic Setting

Tectonic setting refers to the geologic framework or structural configuration of the different rock masses in the Yucca Mountain vicinity. The overall tectonic setting of the Great Basin physiographic province generally consists of fault-bounded basins and mountain ranges (including Yucca Mountain) that have been modified by volcanic activity during the past 15 million years. Typically, faults in this setting include normal and strike-slip faults that reflect the extensional deformation caused by the tectonic interactions of crustal plates at the western margin of the North American continent. Studies of the extensional tectonics in the central Basin and Range tectonic province (Snow and Wernicke 2000 [DIRS 159400]) conclude that approximately 250 to 300 km of extension have occurred by a west-northwest motion of the Sierra Nevada block away from the Colorado Plateau, at rates initially as great as 2 cm/yr, and at 1.5 to 1 cm/yr during the last 5 million years. Research suggests that most of the current extension, as indicated by strain measurements and seismicity, is concentrated along the eastern and western margins of the Basin and Range tectonic province (Thatcher et al. 1999 [DIRS 119053]; Martinez et al. 1998 [DIRS 159031]).

1.3.3.3.2 Structural Geology

The structural geology of Yucca Mountain and its vicinity (BSC 2004 [DIRS 169734], Section 3.5) is dominated by a series of north-striking normal faults (Figure 1-7), along which Tertiary volcanic rocks were tilted and displaced hundreds of meters. Movement occurred

during a period of extensional deformation in the middle-to-late Miocene time, but has continued at a low level into the Quaternary Period, which consists of the last 1.8 million years before the present. These faults extend through the Yucca Mountain vicinity and divide the site area into several blocks, each of which is further deformed by minor faults. Block-bounding faults within the Yucca Mountain site area are spaced from 1 to 6 km apart and include, from east to west, the Paintbrush Canyon, Bow Ridge, Solitario Canyon-Iron Ridge, Fatigue Wash, and Windy Wash faults (BSC 2004 [DIRS 169734], Section 3.5)) (Figures 1-7 and 1-8), which commonly dip from 50° to 80° to the west. Displacements along these block-bounding faults are mainly dip-slip, down-to-the-west, with subordinate strike-slip or oblique-slip components of movement exhibited along some faults. Numerous intrablock faults occur within the individual structural blocks, representing local adjustments in response to the stress created, for the most part, by the large displacements that took place along the block boundaries (BSC 2004 [DIRS 169734], Section 3.5).

1.3.3.3.3 Volcanism

Two types of volcanism have occurred in the Yucca Mountain region. An early phase of Miocene silicic volcanism in the southwestern Nevada volcanic field culminated between 11.8 and 12.4 million years ago with the eruption of 4 voluminous ash-flow tuffs of about 1,000 km^3 each (Sawyer et al. 1994 [DIRS 100075], pp. 1311 and 1312). One of the silicic ash-flow tuffs that erupted from the Timber Mountain Caldera Complex (Figure 1-9) is the Topopah Spring Tuff, which forms the horizon that will be used for waste emplacement. Yucca Mountain is an uplifted, erosional remnant of these voluminous ash-flow tuff deposits.

The early caldera-forming, silicic volcanism was approximately coincident with the major period of crustal extension, which occurred primarily between 13 and 9 million years ago (Sawyer et al. 1994 [DIRS 100075], pp. 1314 and 1316). The onset of basaltic volcanism in the Yucca Mountain region occurred as extension rates waned during the latter part of the caldera-forming period of silicic volcanism. Small-volume basaltic volcanism continued into the Quaternary Period. In terms of eruption volume, the 15-million year history of volcanism in the Yucca Mountain region is viewed as a magmatic system that peaked between 13 and 11 million years ago, with the eruption of more than 5,000 km^3 of ash-flow tuffs. Following this peak of eruptive activity, volcanism has been in decline, characterized by eruptions of relatively minor volumes of basalt since 11 million years ago (BSC 2004 [DIRS 169989], Section 6.2). Approximately 99.9 percent of the volume of the southwestern Nevada volcanic field erupted about 7.5 million years ago, culminating with the eruption of tuffs from the Stonewall Mountain volcanic center, which is the last active caldera system of the southwestern Nevada volcanic field. The last 0.1 percent of eruptive volume of the volcanic field consists of basalt that erupted since 7.5 million years ago (BSC 2004 [DIRS 169989], Section 6.2). Considered in terms of total eruption volume, frequency of eruptions, and duration of volcanism, basaltic volcanic activity in the Yucca Mountain region comprises one of the least active basaltic volcanic fields in the western United States (e.g., *Synthesis of Volcanism Studies for the Yucca Mountain Site Characterization Project* (CRWMS M&O 1998 [DIRS 105347], Chapter 2)).

Post-caldera basalts in the Yucca Mountain region can be divided into 2 episodes: Miocene eruptions, between approximately 9 and 7.3 million years before present, and post-Miocene eruptions, between approximately 4.8 and 0.08 million years ago. The time interval of about

2.5 million years between these episodes is the longest hiatus of basaltic eruptive activity in the Yucca Mountain region during the last 9 million years (CRWMS M&O 1998 [DIRS 105347], Chapter 2). This eruptive hiatus also marks a distinct shift in the locus of post-caldera basaltic volcanism to the southwest in the Yucca Mountain region (BSC 2004 [DIRS 169989], Section 6.2). Thus, the Miocene basalts and post-Miocene basalts are both temporally and spatially distinct.

1.3.4 Hydrogeology

1.3.4.1 Surface Hydrology

Yucca Mountain is located in the Amargosa River drainage basin, which is the major tributary drainage area to Death Valley (Figure 1-4). Streamflow from Yucca Mountain can extend from local drainages to the Amargosa River and then to Death Valley. The Amargosa River and its tributaries are ephemeral streams that are dry most of the time, with surface water flow rarely occurring in direct response to precipitation. In some cases, groundwater discharges at springs in stream channels. During episodic flooding, flow occurs along the Amargosa River, filling much of Death Valley to depths of 0.3 m or more (Miller 1977 [DIRS 105462], p. 18). During periods in which the climate has been cooler and wetter, such as 140,000 to 175,000 years ago, Death Valley was filled with water to depths of 175 m (BSC 2004 [DIRS 170002], Section 6.2, p. 6-6). The entire Death Valley drainage basin and several closed drainage basins are hydrologically interconnected through the groundwater system (D'Agnese et al. 1997 [DIRS 100131], Figure 9, pp. 20 and 22). About 10,000 km^2 of watershed area drain directly into Death Valley (Miller 1977 [DIRS 105462], p. 18). The Amargosa River drains almost 9,100 km^2 north and east of Death Valley. Like the streams, the playas are mainly ephemeral and contain water only after heavy runoff periods, and perennial flow is only observed downgradient from spring discharges and around the margins of playas and saltpans, where the groundwater discharges to the land surface.

1.3.4.2 Groundwater Hydrology

Yucca Mountain is located within the larger Death Valley Regional Groundwater System (Figure 1-4). The groundwater flow system of the Death Valley region is complex, involving many local groundwater systems. There is groundwater movement between aquifers in some areas. In other areas, low-permeability confining units support artesian conditions. The groundwater below Yucca Mountain and in the surrounding region flows generally south toward discharge areas in the Amargosa Desert and Death Valley. The area around Yucca Mountain is in the central subregion of the Death Valley Regional Groundwater System, which consists of the Pahute Mesa-Oasis Valley, Ash Meadows, and Alkali Flat-Furnace Creek groundwater basins. The primary sources of groundwater recharge to the regional system are infiltration on Pahute Mesa, Rainier Mesa, Timber Mountain, and Shoshone Mountain to the north, and the Grapevine and Funeral Mountains to the south (Figure 1-4). Recharge in the immediate Yucca Mountain vicinity is low, consisting of water reaching Fortymile Wash (Figure 1-4), as well as precipitation that infiltrates into the subsurface.

1.4 DESIGN OF YUCCA MOUNTAIN REPOSITORY SUBSURFACE FACILITIES

Following is a description of the design and layout of the repository subsurface facility and engineered barrier system (EBS). Descriptions of the repository subsurface facility are found in *Total System Performance Assessment Data Input Package for Requirements Analysis for TAD Canister and Related Waste Package Overpack Physical Attributes Basis for Performance Assessment* (SNL 2007 [DIRS 179394]) and in *Total System Performance Assessment Data Input Package for Requirements Analysis for Subsurface Facilities* (SNL 2007 [DIRS 179466]).

1.4.1 Repository Layout

The layout of the subsurface facility is illustrated on Figure 1-10 (SNL 2007 [DIRS 179466],Table 4-1, Parameter Number 01-02). The emplacement drifts will be excavated using a tunnel boring machine to a diameter of 5.5 m; with a nominal length of 600 m (actual lengths will range from 355 to 808 m). Emplacement drifts will be excavated in a sequence of 4 panels, which will contain 70,000 metric tons of heavy metal waste. Emplacement drifts will be arranged with a uniform spacing of 81 m between their centerlines. The repository design used in the TSPA-SEIS calls for approximately 100 WPs to be placed in a single emplacement drift with a nominal length of 600 m. There is an area in the southern section of the repository that will be constructed to allow for contingencies during waste emplacement. The repository's host-rock units contain both lithophysal and nonlithophysal units. The lithophysal rock units are characterized by numerous cavities (lithophysae), which result in high porosities. The lithophysal rock units are highly fractured and the fractures have short trace lengths. In contrast, the nonlithophysal rock units are characterized by few cavities, lower porosities, and fractures with generally longer trace lengths. A total of 4.5 percent of the emplacement drift area will be excavated in the upper lithophysal unit (Tptpul), 12.4 percent in the middle nonlithophysal unit (Tptpmn), 80.5 percent in the lower lithophysal unit (Tptpll), and 2.6 percent in the lower nonlithophysal unit (Tptpln) of the repository host horizon (SNL 2007 [DIRS 179466], Table 4-1, Parameter Number 01-01).

1.4.2 Features of the Engineered Barrier System

The subsurface facility system includes ground support, such as rock bolts, steel liner, cement, and wire mesh. The EBS design (SNL 2007 [DIRS 179354], Figure 4-1) includes a DS, a two-layer WP, a corrosion-resistant emplacement pallet (made of Alloy 22 and stainless steel on which the WPs will be placed), and an invert, consisting of a steel support structure and crushed, welded tuff, at the base of the emplacement drifts. The TSPA-SEIS analysis of the EBS did not include the degradation of the subsurface facility system's ground-support material because the FEPs, including 2.1.06.01.0A, 2.1.06.02.0A, and 2.1.06.04.0A, were excluded because of low consequence. Figure 1-11 presents a cross-section illustration of an emplacement drift and the major components of the EBS. The following provides a more detailed description of each of the EBS components and repository thermal loading.

1.4.2.1 Drip Shield

The DSs will be composed of a titanium alloy. The highly corrosion-resistant nature of titanium has been demonstrated by long-term experiments conducted on a range of metal titanium alloys in wells in corrosive brines at the Salton Sea geothermal field in California. In addition, the mineral Rutile, TiO_2, which will form the passive film on the titanium DS, has been observed to have long-term geologic stability (BSC 2004 [DIRS 169218], Section 7.2.1). These characteristics support the selection of titanium alloys for the construction of a corrosion-resistant DS for the EBS.

The function of the DSs is to reduce the effect of rockfall and dripping on the WPs. The DSs are designed to link together, forming a single continuous barrier for the entire length of the emplacement drifts. The DSs will be fabricated from Titanium Grade 7 plates, with Titanium Grade 24 for structural support. The base plates will be composed of Alloy 22 to prevent direct contact between titanium and the steel members of the invert.

1.4.2.2 Waste Package

WPs consist of an outer layer and an inner layer (Figure 1-11). The outer layer is 20-mm thick corrosion-resistant Alloy 22. The WPs will be solution-annealed to minimize the possibility of SCC, and the outer closure weld will be stress mitigated using either laser peening or controlled plasticity burnishing. The inner layer is 50-mm thick stainless steel and serves 3 functions. First, the inner layer provides structural strength to resist rockfall, to support the internal waste form components, to allow the WPs to be supported by the emplacement pallets, and to facilitate handling. Second, the inner layer provides radiation shielding to reduce the exterior surface contact dose rate. Third, because of sorption of radionuclides on corrosion products from the degradation of the inner layer, it acts as a limited containment part of the EBS barrier for the radioactive waste inside the WPs. The TSPA-SEIS analyzes a configuration-design WP containing 21-pressurized water reactor SNF assemblies. Roughly the same size WP can also accommodate 44 of the smaller, boiling water reactor SNF assemblies, a combination of 5 HLW glass canisters surrounding a central canister of DOE SNF (DSNF), or a naval SNF canister (SNL 2007 [DIRS 181383], Table 5.4-1[a]).

1.4.2.3 Emplacement Pallet

An emplacement pallet will support each WP (Figure 1-11). The emplacement pallets are designed to prevent the WPs from coming in contact with the invert of the emplacement drifts and, therefore, prevent direct exposure to invert moisture or materials that may induce accelerated corrosion of the WPs. The material supporting the WPs will consist of Alloy 22, providing long-term corrosion resistance and an identical material in contact with the outer surfaces of the WPs. To reduce the possibility of SCC, the emplacement pallets will also be annealed to remove stresses from welding and fabrication.

1.4.2.4 Invert

The invert will provide support for the WP emplacement pallets and the DSs. The invert consists of two components: a steel invert structure and a crushed tuff fill. The granular crushed tuff will be composed of crushed welded tuff produced from the excavation of the repository's

underground openings with the tunnel boring machines, and will be placed in and around the steel invert structure to an elevation just below the top of the longitudinal and transverse support beams. The crushed tuff will be compacted to prevent long-term settlement.

1.4.2.5 Waste Form

SNF consists of fuel removed from nuclear reactors after its useful heat-generating capacity has been spent. The TSPA-SEIS analyzes the disposal of WPs containing CSNF and WPs referred to as co-disposed (CDSP) WPs, containing both DSNF and HLW. CSNF consists primarily of uranium oxide, some of which has been enriched with surplus plutonium to create a mixed-oxide fuel (MOX). DSNF is fuel associated with DOE's defense programs and research and development programs. The majority of DSNF consists of uranium oxide. However, there are 11 categories of DSNF representing a variety of uranium-based waste forms. HLW consists of by-products of nuclear reactions, material generated during fuel preparation and reprocessing, and sludges and residues recovered from nuclear-waste storage tanks. HLW will be mixed and solidified in a high-temperature, lanthanum borosilicate glass for storage in stainless-steel canisters. CDSP WPs typically contain five HLW canisters surrounding one DSNF canister.

Following breaching of the CSNF WPs and CDSP WPs and exposure of the fuel, the waste forms will be subject to aqueous dissolution at various rates followed by release of radionuclides to the EBS.

1.4.2.6 Waste Form Cladding

Nuclear fuel generally consists of stacked pellets of uranium-based fuel encased in a metallic protective cladding. However, for ther PA analyses, the TSPA-SEIS assumes that CSNF cladding is failed at the time the WPs are breached. In addition, DSNF cladding is in poor condition and is considered to be failed upon receipt. Therefore, the TSPA-SEIS does not take credit for spent-fuel cladding.

1.4.2.7 Emplacement Drift

The nuclear waste will be placed in 5.5-m diameter, circular emplacement drifts excavated with tunnel boring machines. The drifts will serve to enhance the role of the natural barriers and the EBS due to two processes: (1) the formation of a capillary barrier at the drifts' walls that will be active during the thermal and ambient postclosure periods, and (2) the formation of a dry-out zone helping to prevent percolation from reaching the repository during the thermal period. The effectiveness of these processes depends on the strength of the capillary pressure in the fractures close to the drift, the host rock's permeability close to the drifts, the local percolation flux above the drifts, the temperature of the rock near the drifts' walls, and the shape of the drift openings.

1.4.2.8 Internal Waste Package Components

The WPs will have internal steel components consisting primarily of carbon-steel basket guides and basket tubes, steel canisters for HLW and DSNF, and stainless-steel inner WP liner. All these internal steel components are expected to degrade to iron oxyhydroxides upon exposure to water and repository atmospheric conditions following WP failure. These degradation products could potentially sorb radionuclides released from the degradation of the waste forms.

1.4.3 Waste Emplacement Approach

WPs will be placed in the emplacement drifts in a line-load configuration with a WP-to-WP spacing of approximately 10 cm, and a line-averaged heat load of 1.45 kW/m per 12 WPs (SNL 2007 [DIRS 179354], Table 4-4, Parameter Numbers 05-02 and 05-03). Preclosure ventilation will be activated for at least 50 years from the start of waste emplacement.

1.5 GENERAL DESCRIPTION OF THE TSPA-SEIS

The development of the TSPA-SEIS began with the identification and screening of all FEPs that could affect the repository (Section 1.2.1) and a mapping to the GoldSim model file. The FEPs that were screened in were used to develop the scenario classes for the TSPA-SEIS analyses (Section 1.2.2). Figure 1-3 is a schematic representation of the development of the TSPA-SEIS. The Figure illustrates how the TSPA-SEIS, for analysis purposes, divides the repository system into individual model components. Each individual model component represents a major process or set of processes of the total repository system. Figure 1-3 indicates these model component areas as well as the scenario classes that are included in analyses of repository performance.

GoldSim software integrates the model components and submodels of the TSPA-SEIS allowing simulation of repository performance for each realization of uncertain parameters. GoldSim manages the flow of information between and among the external process models, the model components and submodels, and the abstractions provided to the TSPA-SEIS. A separate software code, EXDOC 2.0, uses GoldSim results to compute mean and median dose. The principal model components of the TSPA-SEIS are described in the following sections.

1.5.1 Model Components and Modeling Case for the Nominal Scenario Class

The TSPA-SEIS is based on the Nominal Scenario Class, which incorporates all expected FEPs to describe the most likely fundamental processes at work under ambient conditions, as well as possible changes to those processes after repository closure. The Nominal Scenario Class represents the most likely FEPs under the expected natural conditions prevailing at the repository. The Nominal Scenario Class describes WP failure during expected repository performance without the occurrence of early failure of EBS components or of disruptive events. The Nominal Scenario Class includes a single modeling case, the Nominal Modeling Case, that addresses FEPs that describe WP degradation due to corrosion mechanisms including GC, SCC, LC, and MIC. The TSPA-SEIS components for the Nominal Modeling Case are the nominal modeling components, namely:

- UZ Flow
- EBS Environment
- WP and DS Degradation
- Waste Form Degradation and Mobilization
- EBS Flow and Transport
- UZ Transport
- SZ Flow and Transport
- Biosphere.

1.5.1.1 Unsaturated Zone Flow

The UZ Flow Model Component defines the temporal and spatial distribution of water flow from the ground surface through the unsaturated tuffs above and below the repository horizon and the temporal and spatial distribution of water dripping into the waste emplacement drifts. The UZ Flow Model Component of the TSPA-SEIS integrates five processes that contribute to flow in the UZ. These processes include: climate-induced precipitation, infiltration, mountain-scale UZ flow, drift seepage, and drift-scale coupled processes. Figure 1-12 provides a conceptual illustration of the Yucca Mountain mountain-scale flow processes. The UZ Flow Model Component provides a representation of the hydrogeologic processes above and below the repository. Water that reaches the repository horizon has its source in precipitation at the land surface above the repository. This precipitation occurs in the form of rainfall and snow. The temporal variability in precipitation that occurs is included in the TSPA-SEIS by specifying four successive climate states: present-day climate and three future climate states (Figure 1-13). The climate from 10,000 years after repository closure to the period of geologic stability is based on specifications regarding deep percolation rates described in NRC Proposed Rule 10 CFR 63.342(c) ([DIRS 178394]) (Sections 1.1.1 and 1.6.1).

1.5.1.2 Engineered Barrier System Environment

The EBS Environment Model Component includes the EBS mountain-scale thermal-hydrology and the EBS chemical environments within the emplacement drifts. These environments are important to repository performance because they help determine the degradation rates of EBS components, quantities and species of mobilized radionuclides, and transport of radionuclides and fluids through the repository and drifts, and their release into the UZ below the repository. Figure 1-12 shows the position of the repository drifts and WPs with respect to the flow system within Yucca Mountain. The percolation moving into the repository environment will be affected by heat from the emplaced waste. The waste heat and geochemical processes and conditions will determine the EBS chemical environment.

1.5.1.3 Waste Package and Drip Shield Degradation

Together, the WPs and DSs are the key engineered components of the EBS (Figure 1-14). The WP and DS Degradation Model Component describes the degradation of the WPs and DSs as a function of time, presence of water, and repository location. The WP and DS Degradation Model Component is described in Section 6.3.5. The WP and DS Degradation Model Component includes the implementation of WAPDEG.DLL (WAPDEG V. 4.07 [DIRS 161240]) within GoldSim and supporting submodel implementations. The WP and DS Degradation Model Component accounts for the following degradation processes: GC of the DSs; GC and LC of the outer surfaces of the WPs; SCC of the WPs; MIC on the outer surfaces of the WPs; and early WP failure.

1.5.1.4 Waste Form Degradation and Mobilization

The Waste Form Degradation and Mobilization Model Component establishes the radionuclide inventories for the CSNF WPs, co-disposed WPs, and HLW waste forms (Figure 1-15), and calculates the rates of degradation of these waste forms. Figure 1-16 provides an overview of the

mechanisms included in the Waste Form Degradation and Mobilization Model Component, as well as the concentrations of radionuclides released from the CSNF waste forms to the EBS Transport Submodel. The Waste Form Degradation and Mobilization Model Component accounts for the following processes and conditions: in-package water chemistry, matrix degradation rates for CSNF, DSNF, and HLW waste forms, radionuclide solubilities, and the types and concentrations of waste form and in-drift colloids.

1.5.1.5 Engineered Barrier System Flow and Transport

The EBS Flow and Transport Model Component calculates the rate of radionuclide release from the EBS to the UZ. This quantity is determined by seepage into the emplacement drifts, condensation on the drift walls, WP and DS degradation, the presence of water films on in-package internals, and the EBS thermal-hydrologic (TH) environment (Figure 1-17). The EBS Flow and Transport Model Component accounts for the following processes: the rate of water flow through the EBS, diffusive and advective transport, sorption, and colloid-facilitated transport.

1.5.1.6 Unsaturated Zone Transport

The UZ Radionuclide Transport Model Component describes the migration of radionuclides from the EBS of the repository, through the UZ, to the water table. Consistent with the Mountain-Scale UZ Flow Submodel, the conceptual model for UZ transport (Figure 1-18) uses a dual-continuum representation to couple advective and diffusive transport through fracture and matrix continua. The UZ Transport Model Component accounts for the following processes: advective, dispersive, and diffusive transport, sorption, colloid retardation, filtration, and exclusion, radioactive decay and ingrowth, and change in water-level elevation.

1.5.1.7 Saturated Zone Flow and Transport

The SZ Flow and Transport Model Component evaluates the transport of radionuclides from their introduction at the water table below the repository to the regulatory boundary 18 km downgradient from the Yucca Mountain repository (Figure 1-19). Radionuclides move through the SZ either as solutes or sorbed to colloids. The SZ Flow and Transport Model Component accounts for the following processes: advection and dispersion, matrix diffusion, colloid retardation and exclusion, and sorption.

1.5.1.8 Biosphere

The Biosphere Model Component evaluates radionuclide transport in the biosphere and the resulting exposure of the RMEI (NRC Proposed Rule 10 CFR 63.312 [DIRS 180319]) for releases of radioactive material after closure of the repository (Figure 1-19). The Biosphere Model Component analyzes two dominant mechanisms of radionuclide release to the biosphere: (1) release through the SZ via groundwater, and (2) release through the air by ash dispersal from a volcanic eruption. These two release mechanisms correspond to the two modes by which radionuclides may be introduced into the biosphere.

1.5.2 Model Components and Modeling Cases for the Early Failure Scenario Class

The Early Failure Scenario Class addresses FEPs that describe WP failures due to materials and/or manufacturing defects or pre-emplacement operations and practices that could affect the performance of the EBS. The Early Failure Modeling Cases address FEPs that describe the potential for DS and WP early failure that could affect repository performance in the absence of disruptive events. The Drip Shield EF Modeling Case analyzes the possibility that DSs could fail prematurely, thus failing to protect the underlying WPs from seepage and possible LC. The Waste Package EF Modeling Case analyzes WPs that fail prematurely due to material defects, manufacturing errors, or pre-emplacement operations and practices, such as improper heat treatment or welding flaws that could affect WP performance and longevity. The TSPA-SEIS components for the Early Failure Scenario Class modeling cases are the nominal modeling components namely:

- UZ Flow
- EBS Environment
- WP and DS Degradation
- Waste Form Degradation and Mobilization
- EBS Flow and Transport
- UZ Transport
- SZ Flow and Transport
- Biosphere.

The Early Failure FEPs are addressed by specifying initial conditions for the TSPA-SEIS, which represent WPs and/or DSs that experience early failure.

1.5.3 Model Components and Modeling Cases for the Igneous Scenario Class

The Igneous Scenario Class addresses FEPs that describe igneous activity that could affect repository performance. The Igneous Scenario Class includes the Igneous Intrusion Modeling Case that addresses the FEPs for the unlikely possibility that magma, in the form of a dike, could intrude into the repository and disrupt expected repository performance. The Igneous Scenario Class also includes a Volcanic Eruption Modeling Case that addresses FEPs that describe a volcanic conduit that invades the repository, destroys WPs, and erupts at the land surface. The volcanic eruption disperses volcanic tephra and entrained waste under atmospheric conditions and deposits the contaminated tephra on land surfaces where the contaminated tephra becomes subject to redistribution by soil and near-surface hydrogeologic processes.

1.5.3.1 Igneous Intrusion Modeling Case

The Igneous Intrusion Modeling Case assumes that a dike intersects the repository and destroys DSs and WPs in those drifts intruded by magma, exposing the waste forms to percolating water and mobilizing radionuclides that may then be transported out of the repository and down through the UZ to the SZ, and then transported to the accessible environment. The TSPA-SEIS uses the following model components to calculate total system performance for the Igneous Intrusion Modeling Case:

- UZ Flow
- EBS Environment
- WP and DS Degradation
- Waste Form Degradation and Mobilization
- EBS Flow and Transport
- UZ Transport
- SZ Flow and Transport
- Biosphere.

Prior to the time of the first intrusion, the TSPA-SEIS for the Igneous Intrusion Modeling Case is the same as the model for the Nominal Modeling Case. The TSPA-SEIS changes the representation of the EBS components (WPs and DSs) at the time of the first intrusion to represent damage to the EBS caused by the intrusion of magma. The TSPA-SEIS assumes that the entire repository is damaged at the time of the first intrusion and that subsequent intrusions cause no significant additional damage.

1.5.3.2 Volcanic Eruption Modeling Case

The Volcanic Eruption Modeling Case represents the fraction of igneous intrusions in which a volcanic eruption also occurs. In this case, waste from WPs is transported to the land surface through one or more eruptive conduits, and tephra and entrained waste are discharged into the atmosphere, transported by wind currents, and deposited at land surface. The Volcanic Eruption Modeling Case also evaluates the fluvial and eolian redistribution of contaminated tephra deposited on the land surface. The TSPA-SEIS uses the following processes and model components to calculate repository system performance for the Volcanic Eruption Modeling Case:

- Volcanic interaction with the repository
- Atmospheric transport
- Tephra redistribution
- Biosphere.

The TSPA-SEIS does not include any nominal processes other than radionuclide decay prior to the occurrence of an eruptive event.

1.5.4 Model Components and Modeling Cases for the Seismic Scenario Class

The Seismic Scenario Class evaluates repository performance in the event of seismic activity capable of disrupting repository emplacement drifts and the engineered components of the EBS through ground motion (GM) and FD. The Seismic Scenario Class includes damage to DSs and WPs as a function of the magnitude of a seismic event. Radionuclides in breached WPs may be mobilized and transported out of the repository, transported through the UZ to the SZ, and then to the accessible environment. The TSPA-SEIS uses the following model components to estimate total system performance for the Seismic Scenario Class:

- UZ Flow
- EBS Environment

- WP and DS Degradation
- Waste Form Degradation and Mobilization
- EBS Flow and Transport
- UZ Transport
- SZ Flow and Transport
- Biosphere.

The Seismic Scenario Class includes two modeling cases. The Seismic GM Modeling Case and the Seismic FD Modeling Case. The Seismic GM Modeling Case addresses FEPs concerning damage due to vibratory GM, which include:

- SCC of the DS due to rockfall
- Potential buckling and/or rupture of the DS due to accumulated rockfall and dynamic loading during seismic events
- Potential SCC damage and/or rupture of WPs due to seismic events
- Diffussion and/or advection of mobilized radionuclides from failed or ruptured WPs.

The Seismic FD Modeling Case addresses FEPs that describe damage due to fault displacement, including rupture of WPs and the overlying DS components. FEPS that describe LC are also included in both Seismic Modeling Cases because rupture of the DS leads to the possibility of crown-seepage induced LC of WPs.

Prior to the first seismic event, the TSPA-SEIS for the Seismic GM Modeling Case is the same as the model for the Nominal Modeling Case. After the first seismic event, rockfall may affect seepage into a drift, damage to DS components may affect seepage contacting WPs, and damage to WPs may result in radionuclide release. Rockfall and damage may accumulate as additional seismic events occur, increasing the effects on flow and transport processes. Seismic events that include FD will affect an uncertain number of WPs. Subsequent FD events will not increase damage to WPs already damaged by preceding FD events, although additional WPs may be damaged. If a WP is damaged by an FD event, the overlying DS is considered to be ruptured and is no longer a barrier to seepage.

1.5.5 Model Components for the Human Intrusion Scenario

The TSPA-SEIS considers a stylized Human Intrusion Scenario based on a simulated future exploratory drilling operation that penetrates the repository. The scenario considers a drilling operation that utilizes the most sophisticated drilling apparatus currently available. Using current technology, if the drilling apparatus encountered a WP, it would easily be detected by a driller because of the combination of the WP or DS resistance to penetration and the presence of metal in the drilling cuttings. Encountering DSs or WPs would not only alert the driller to the presence of non-natural materials, but the strength of the DSs and WPs would be enough to prevent the penetration of the WP by the drilling apparatus. However, if the drilling apparatus were to directly intersect a degraded WP, and the borehole were deepened to the SZ, then the borehole could become an avenue for aqueous waste transport. The stylized scenario at NRC

Proposed Rule at 10 CFR 63.322 [DIRS 180319] supposes that waste from the penetrated WP is transported to the SZ and available to the RMEI. Because only a degraded WP would be penetrated, the TSPA-SEIS for the Human Intrusion Scenario would include simulation of nominal processes until the time of the WP penetration. However, following the penetration, only the waste transported down the borehole would be evaluated for dose to the RMEI, and the waste transport would be simulated by only the SZ and biosphere model components. Therefore, the Human Intrusion Scenario Modeling Case would involve the following TSPA-SEIS components:

- UZ Flow
- EBS Environment
- WP and DS Degradation
- Waste Form Degradation and Mobilization
- SZ Flow and Transport
- Biosphere.

1.6 CONCEPTUAL DESCRIPTION OF PROCESSES RELEVANT TO AN EVALUATION OF POSTCLOSURE PERFORMANCE IN THE ABSENCE OF DISRUPTIVE EVENTS

The following sections describe processes relevant to the evaluation of repository system performance. Information relevant to the technical basis for this conceptual description can be found in *Yucca Mountain Site Description* (BSC 2004 [DIRS 169734], Sections 6, 7, and 8).

Because the repository horizon will be approximately greater than 200 m beneath the land surface (SNL 2007 [DIRS 179466], Table 4-1, Parameter Number 01-06) and the waste forms are solids (with minor gaseous constituents), the primary means for the mobile radioactive constituents of the waste forms to reach the biosphere, in the absence of an unlikely volcanic eruption, will be along groundwater pathways. The waste forms will pose minimal risks to humans, unless all of the following processes were to occur:

- The WPs are breached.
- The waste forms are exposed to water.
- Radionuclides within the waste forms are dissolved in the water.
- Dissolved or colloid-associated radionuclides are released from the repository and transported with the water in the SZ.
- Radionuclide-containing water is discharged, either naturally or at a pumping well, from the SZ.
- Humans or any part of the food chain uses water containing the released radionuclides.

The following sections describe how these processes might occur and how the major components and processes of the Yucca Mountain repository system could act to affect long-term waste isolation. The discussion is divided into five topics:

- Water movement in the unsaturated tuffs above the repository in the upper natural barrier
- Water and water vapor movement around the repository drifts
- Water movement and radionuclide transport within and through the EBS
- Water movement and radionuclide transport through the unsaturated tuffs, below the repository
- Water movement and radionuclide transport through the SZ aquifers and biosphere.

1.6.1 Water Movement in the Unsaturated Tuffs above the Repository

The following concepts are excerpted from *UZ Flow Models and Submodels* (SNL 2007 [DIRS 175177], Section 6.1.4). Figure 1-12 illustrates the key concepts associated with water movement in the UZ at Yucca Mountain. The source of water in the UZ at the repository horizon is precipitation at the land surface. Climate will control the range of precipitation and land surface temperature conditions. Four potential climate periods, present-day, monsoon, glacial-transition, and a post-10,0000-year climate, were identified as being likely from repository closure to the period of geologic stability (Figure 1-13). The present-day climate state is equivalent to the current climate in the Yucca Mountain area as determined from regional meteorological stations. The monsoon climate state is characterized by hot summers, with increased summer rainfall relative to the present-day climate. The glacial-transition climate state has cooler and wetter summers and winters, relative to the present-day climate state. Climate forecasting indicates that, during the next 10,000 years at Yucca Mountain following repository closure, the present-day interglacial climate may persist for 400 to 600 years, followed by a warmer and wetter monsoon climate for 900 to 1,400 years, followed by a cooler and wetter glacial-transition climate for the remaining 8,000 to 8,700 years (BSC 2004 [DIRS 170002], Section 6.6 and Table 6-1). Per the NRC Proposed Rule at 10 CFR 63.342(c)(2) ([DIRS 178394]), the post-10,000-year climate after repository closure until the period of geologic stability will be a sampled value based on a log-uniform probability distribution for deep percolation rates from 13 to 64 mm/year.

A large portion of the precipitation on the Yucca Mountain land surface either runs off into the washes that are cut into the mountain, evaporates from the surface, or transpires from the native plants in the area. The remaining water infiltrates downward through the soil horizon and into the rock. The net amount of total precipitation that infiltrates is called net infiltration. Net infiltration is the source of percolation flux within the UZ, and it provides the water for flow and transport mechanisms that may move radionuclides from the repository to the water table and into the SZ. Net infiltration is spatially and temporally variable because of the nature of the storm events that supply precipitation, and because of the variation in soil cover and topography. Infiltration is believed to be high on side slopes and ridgetops, where bedrock crops out and fracture flow in the bedrock is able to move moisture away from zones of active evapotranspiration.

The net infiltration moves downward through the UZ, driven primarily by gravity. The downward movement of water in the UZ is called percolation flux. Percolation flux in the unsaturated fractured tuffs occurs in the rock matrix and in the fractures of the rock. Generally, the welded tuff layers have more of the total flux within the fractures because the permeability of the matrix is low, whereas the nonwelded lithologic layers have greater total flux within the matrix. Water flows through the welded and densely fractured TCw unit mainly through fractures. Within the more porous PTn unit, most of the water flows through the matrix, where the high storage capacity causes a dampening of the infiltration pulses. Small amounts of flowing water preferentially flow along faults that cut through the PTn. Unsaturated flow in the TSw unit occurs primarily through fractures. In addition, some lateral diversion of water occurs as it moves downward from the soil horizon through the UZ. This lateral diversion is caused by the eastward dip of the geologic strata and heterogeneities in the rock because of the different permeabilities of the welded and nonwelded tuffs between land surface and the repository horizon.

1.6.2 Water and Water Vapor Movement around the Repository Drifts

Figure 1-20 illustrates the key concepts anticipated to be associated with water movement around the repository drifts after waste emplacement at Yucca Mountain. Water is one of the principal determining factors of: (1) corrosion of the EBS, (2) waste dissolution, and (3) radionuclide transport from the repository to the accessible environment. The amount and chemical composition of water seeping into waste-emplacement drifts will affect the long-term performance of the repository system.

In the UZ, percolating water encountering a large underground opening will be partly diverted around the cavity. This effect would reduce the amount of liquid water that could enter a waste-emplacement drift or prevent dripping altogether and is due to the formation of a capillary barrier around the cavity. Moreover, during the early stages after closure, the heat from decaying radionuclides will likely vaporize water that approaches the waste-emplacement drifts. The presence of a capillary barrier and a zone of vaporization would limit the amount of water that could potentially contact the WPs.

The heat generated by the decay of radioactive wastes is anticipated to result in elevated rock temperatures in the repository environment for thousands of years after emplacement (SNL 2007 [DIRS 181383], Figure 6.1-1). For the TSPA-SEIS repository design concept, these temperatures will be high enough, in most locations, to cause boiling conditions in the vicinity of the drifts, thus giving rise to local water redistribution and altered flow paths. Conditions one to several meters above the ceilings of the emplacement drifts could change in several ways that could affect the amount of water seeping into the drifts. Within 50 years after repository closure, the water will first encounter a dry-out zone above the repository drifts. Under boiling conditions, water reaching the dry-out zone would vaporize, thus preventing liquid water from reaching the drifts. Water vapor would tend to move away from the drifts and through the permeable fracture network, driven primarily by a pressure increase caused by boiling. In cooler regions away from the drifts, the vapor would condense in the fractures, where it could drain either toward the heat source from above or shed around the drifts into the zone below the heat source. Condensed water could also imbibe from fractures into the matrix, leading to increased liquid saturation in the rock matrix.

For the TSPA-SEIS repository design concept, the dry-out zone around drifts may extend from a few to more than 25 m from the walls of the drifts. Boiling conditions in the rock are anticipated to range from no boiling to boiling for over 2,000 years after emplacement (SNL 2007 [DIRS 181383], Section 8.2[a] and Table 6.3-39), reflecting the spatial and temporal variability of possible TH conditions in the repository system. The spatial variability would be caused by heterogeneity in the rock properties and variations in the ambient percolation flux. In addition, differences in the thermal output of different WPs could cause a range of TH conditions in the repository environment. For example, cooler regions are expected along the edges of the repository and near low-thermal output WPs. The temporal variability in water movement around the drifts could be caused, in the short-term, by the thermal output of the wastes that will eventually decline to minimal values. Hundreds of years of drying and several thousand years of cooling and rewetting are anticipated. In the long-term, water movement will be controlled by the climatic variability (BSC 2004 [DIRS 170002], Sections 6.6) and percolation flux at the repository horizon. If water ultimately penetrates the dry-out zone as the repository cools and reaches the immediate vicinity of the walls of the drifts, most of it will still be prevented from seeping into the drift because of the capillary barrier effect.

The characteristics of the rock around the repository openings may change with time. The fracture permeability could increase because of mechanical stress relaxation following the construction of the repository drifts, and ultimately, the drifts could collapse. The fracture permeability may also change because of rock thermal expansion and mineral precipitation. The capillarity of the fractures could either increase or decrease because of these same processes. However, these changes are not expected to significantly affect seepage into emplacement drifts.

In summary, the rate of water dripping into an emplacement drift is expected to be significantly less than the local percolation rate because of the following:

- The dry-out zone around the drifts will reduce liquid water flow while the temperatures in the drifts are elevated, potentially preventing water from reaching the drift surfaces.
- The capillary barrier will divert water around the drifts.

1.6.3 Water Movement and Radionuclide Transport within and through the Engineered Barrier System

Figures 1-21 and 1-17 illustrate the key concepts associated with TH processes, including water movement within the drifts and water contacting the WPs that may experience water dripping from the walls of the emplacement drifts.

The heat output from the SNF and HLW will decline continuously because of radioactive decay. WP heat output will be highest during the nominal 50-year preclosure period, but the emplacement drifts will be ventilated to remove most of the heat (SNL 2007 [DIRS 179466], Table 4-2). Temperatures of the WPs and DSs will be elevated, and some WPs and DSs may approach the boiling point of water immediately after emplacement, depending on ventilation. However, the warming of ventilation air will ensure that preclosure conditions will be relatively dry with low humidity. At permanent closure, ventilation will cease. The temperature of the drift-wall rock will be below boiling initially, but will increase sharply within a few decades

(SNL 2007 [DIRS 179466], Table 4-2). The maximum postclosure temperatures of a WP and DS at any location will be determined by the history of heat output from the waste, the resistance to dissipation of heat in the host rock, heat transfer from the WPs to the DSs and to the walls of the drifts, and the relationship to other nearby heat sources.

Vaporized water within the drifts will tend to move away from hotter regions within the drifts and will condense at cooler locations on the walls of the drifts or in the adjacent rock. Some of this condensed water could then drip directly onto an underlying DS or move along the walls of the drifts to the invert.

Evaporation of dripping water could result in the evolution of highly saline brines on the surfaces of the DSs. The dominant degradation mode of the titanium DSs may be by GC. Because this process is anticipated to be very slow, DS failure is not expected to occur during the 10,000-year period after repository closure. Therefore, the integrity of the DSs could reduce any damage to WPs in the event of rockfall as the emplacement drifts degrade over time.

Significant degradation of the WPs is not expected during the preclosure period. In the postclosure dry-out regime, when drift-wall temperatures are greater than the boiling point of seepage water, potentially relevant high-temperature modes of degradation include SCC, dry oxidation, and LC. In the transition regime, the temperatures of the walls of the drifts are estimated to be approximately equal to the boiling point of the seepage water, and evaporation could cause seepage waters to become concentrated on the surfaces of the WPs if the DSs were to fail. These concentrated brines could result in LC of the WPs. In lower temperature regions, seepage waters could enter the drifts, but the thermal driving force for LC would be less and GC, SCC, and MIC may lead to WP failure.

The temperatures of the surfaces of the WPs, the chemistry of the water in contact with the surfaces of the WPs, the mechanical stress, and the degradation characteristics of the metals themselves will affect the degradation rates of Alloy 22 and stainless steel (no credit is taken for the stainless-steel portions of the WPs relative to the corrosion failure of the WPs). Because these environmental parameters are spatially variable, and because the metal fabrication could be variable, WP degradation is also expected to be variable in space and time. Although degradation will occur, WPs are not anticipated to be breached during the first 10,000 years after repository closure. The only exceptions may be a small number of potential early WP failures because of manufacturing defects.

Until a WP has been sufficiently degraded to allow an opening to form through its two metallic liners, there is no potential for water to come into contact with the waste forms. During this period, the waste forms are completely contained within the WPs. If there is a breach of a WP, some of the water vapor or dripping water could enter a WP.

Figure 1-17 illustrates the key concepts associated with water moving into the WPs and contacting the waste forms. Figure 1-17 also illustrates the transport of radionuclides through the EBS. These radionuclides may be mobilized as either dissolved species or they may be adsorbed onto colloids.

Water may enter breached CSNF WPs and contact the waste forms, which are assumed to have failed cladding. CDSP WPs will contain HLW glass placed in stainless-steel pour canisters and DSNF fuel assemblies in stainless-steel canisters. Because DSNF aluminum or Zircaloy cladding may or may not be fully intact, DSNF is modeled as not having any cladding.

The rate at which radionuclides may be released from the repository will depend on the following:

- Degradation rates of the components of the EBS
- Dissolution rate of the waste forms
- The form of the released radionuclides (colloidal versus dissolved)
- Sorption of radionuclides onto corrosion products and invert material
- The solubility of the radionuclides
- The rate of water movement and volume of water that flows or diffuses through the EBS.

1.6.4 Water Movement and Radionuclide Transport through the Unsaturated Tuffs below the Repository

Figure 1-18 illustrates the key concepts associated with water movement in the unsaturated rocks beneath the repository and the migration and transport of radionuclides in these rocks. After the dissolved or colloidally attached radionuclides are released into the UZ beneath the repository, they may be transported with the water to the SZ.

Radionuclide transport within the UZ is strongly related to UZ flow through advective transport. Advective transport (advection) refers to the movement of dissolved or colloidal materials because of the bulk flow of fluid. In the welded units, advection through fractures is expected to dominate transport, mainly because liquid water largely flows through fracture networks in these units. Advection is also an important mechanism for transport between fractures and matrix, especially at interfaces between nonwelded and welded units where there is a transition between dominant matrix flow and dominant fracture flow, respectively.

Liquid water flow paths below the repository horizon will affect advective transport of released radionuclides, particularly in perched water bodies, where lateral transport of radionuclides is likely to occur. Dominant fault-and-fracture flow provides relatively short transport times for transport to the water table, whereas dominant matrix flow leads to much longer transport times. In addition to advection, radionuclide transport within the UZ will be affected by several other mechanisms, such as matrix diffusion, sorption, colloid-facilitated transport, and radioactive decay. Matrix diffusion refers to solute transport from fracture networks to surrounding matrix blocks resulting from molecular diffusion. Mass transfer between fractures and matrix may play an important role in transport within Yucca Mountain. Because flow velocity in the matrix is much slower than in fractures, the transfer of radionuclides from fractures to the matrix by matrix diffusion could retard the overall transport of radionuclides to the water table.

The transport of radionuclides may also be affected by sorption and colloid attachment. Sorption describes a combination of chemical interactions between dissolved radionuclides and the solid phases (immobile rock matrix or colloids), including adsorption, ion exchange, surface complexation, and chemical precipitation. Radionuclide transport in the UZ also involves a colloid-facilitated transport mechanism. Colloids are particles small enough to become suspended (and thus transportable) in a liquid. Radionuclides can be sorbed onto colloids. Unlike the sorption of radionuclides to the rock matrix, however, the radionuclides sorbed on colloids are potentially mobile.

Radioactive decay can also affect the concentration of radionuclides during transport through the UZ. For simple decay, radionuclide concentration decreases exponentially with time, thereby creating stable decay products. Chain decay adds additional complexity because of the ingrowth of new radionuclides created from the decay of a parent radionuclide. Daughter products from chain decay may have different sorption characteristics than their parent radionuclides, therefore exhibiting different modes of transport.

Because each of the characteristics of the natural environment and the processes controlling transport are variable in space and time, radionuclide transport is also variable. Part of the temporal variability relates to long-term climatic changes that not only affect the percolation flux through the repository system but could also cause the water table beneath Yucca Mountain to rise during wetter climates or fall during drier climates.

1.6.5 Water Movement and Radionuclide Transport through the Saturated Zone Aquifers to the Biosphere

Radionuclides that are transported through the UZ below the emplacement drifts are released to the SZ beneath the repository. Figure 1-22 illustrates the key concepts associated with water movement and the transport of radionuclides in the SZ beneath and downgradient from the Yucca Mountain site. Figure 1-22 also illustrates the pathways by which dissolved radionuclides and colloids may come into contact with the biosphere.

When radionuclides released from the repository reach the SZ, they will be transported laterally within the SZ. The general direction of groundwater flow in the SZ is to the southeast, and then to the south and southwest. The processes that affect the performance of the SZ barrier include both groundwater flow and radionuclide transport processes. The groundwater flow processes determine the rate of water movement within the SZ and the flow paths. Dissolved radionuclides diffuse from fractures in which they are advectively transported and into the matrix, which has little advective flux and tends to slow the transport time of these species. The effectiveness of this process depends on the diffusive properties of the matrix and the degree of spacing between the flowing fracture zones. Larger diffusion coefficients or smaller spacing between flowing fracture zones result in slower transport times within the fractured rock.

Many radionuclides that are potentially important to repository performance may be sorbed within the matrix of the rock mass. The degree of sorption depends on the individual radionuclide. Carbon, technetium, and iodine are not sorbed (SNL 2007 [DIRS 181650], Sections 6.5.3.1 and 6.7.1) and are transported considering only advection, dispersion, and matrix diffusion processes. Other radionuclides, such as neptunium, uranium,

and plutonium, are sorbed in the matrix of the fractured tuffs and alluvium (SNL 2007 [DIRS 181650], Section 6.7.1). The stronger the sorption, the longer the radionuclide transport time compared with advective-dispersive transport times.

The TSPA-SEIS calculates the time for radionuclides to reach the boundary of the controlled area (10 CFR 63.302 [DIRS 180319]) downgradient from the repository. The time required depends primarily on the groundwater velocity and the retardation of radionuclides that may sorb on the mineral surfaces within the volcanic or alluvial aquifers.

If radionuclides were to reach a location downgradient from the repository where water is being pumped from the aquifer, the potential exists for radionuclides to come into contact with humans through biosphere pathways. The TSPA-SEIS calculates dose to the RMEI based on an annual water demand of 3,000 acre-feet.

The principal biosphere pathways to humans consist of the following:

- Direct consumption of water containing dissolved radionuclides
- Consumption of crops produced using water containing dissolved radionuclides
- Watering of livestock with contaminated water or feeding of livestock with contaminated crops, or both, and the subsequent consumption of meat, milk, or eggs
- Raising fish in contaminated water and subsequent consumption of the fish
- Direct exposure to contaminated soil
- Inhalation of dust that may contain attached radionuclides
- Inhalation of aerosols from evaporative coolers.

1.7 CONCEPTUAL DESCRIPTION OF PROCESSES RELEVANT TO AN EVALUATION OF POSTCLOSURE PERFORMANCE AFTER THE OCCURRENCE OF DISRUPTIVE EVENTS

Section 1.6 describes processes relevant to repository performance in response to nominal conditions. The following sections describe processes relevant to the evaluation of repository system performance likely to occur in response to natural disruptive events that may affect the repository system. Natural disruptive events that may affect the repository include igneous intrusion intersecting the repository, volcanic eruption from a volcanic vent that intersects the repository, seismic activity that produces vibratory ground motion affecting the repository and the EBS, and potential seismic activity, including fault displacement that affects the repository and the EBS.

As described in Section 6.1, the primary means for radionuclide transport to the biosphere, in the absence of an unlikely volcanic eruption, will be along groundwater pathways. If disruptive events occur and if these events affect the EBS, the disrupted parts of the EBS will transport radionuclides through the UZ using the nominal processes described in Section 6.3. The following sections describe how these processes might differ from those described in Section 1.6 because of disruptive events.

1.7.1 Water Movement in the Unsaturated Tuffs above the Repository

Figure 1-12 illustrates the key concepts associated with water movement in the UZ at Yucca Mountain. Disruptive events are not expected to affect precipitation at the land surface, which is the source of water in the UZ at the repository horizon (SNL 2007 [DIRS 175177], Section 6.1.4). The climate states incorporated in the TSPA-SEIS are the same for all modeling cases and scenario classes (Section 1.6.1).

1.7.2 Water Movement around the Repository Drifts

As described in Section 1.6.2, in the absence of disruptive events, the rate and chemical composition of seepage into the repository's emplacement drifts is expected to be substantially less than the local percolation rate because of the early-time dry-out zone around the drifts that will reduce liquid water flow while the temperatures in the drifts are elevated, and the strength of the capillary barrier around the drifts. In addition, changes in mechanical stress coupled with the mechanical properties of the rock surrounding the repository will eventually cause drifts to collapse and alter the quantity and location of seepage.

The Seismic Scenario Class modeling cases include disruptive events in which there are expected changes in the UZ above the repository that will affect the factors controlling seepage into the drifts. The principal changes to these modeling cases are expected to be in the distribution and quantity of seepage as described in *Seepage Model for PA Including Drift Collapse* (BSC 2004 [DIRS 167652], Section 6.6). Seepage into the repository depends on the integrity of the drifts, the surface area of the drifts, the value of capillary strength, and whether or not a drift lies in the lithophysal or non-lithophysal zone. The more degraded a drift becomes, the more seepage enters the repository. Seismic disruptive events will degrade the repository drifts by causing a loss of integrity of the walls and ceiling of the emplacement drifts. In general, the greater that loss of integrity, the greater the seepage. The most extreme variance in seepage into the repository drifts is expected to occur when a seismic event triggers complete collapse of the repository drifts in the lithophysal zone, increasing the seepage to the value of the percolation flux with no assumed physical retardation of seepage. Collapse of the non-lithophysal areas of the drifts will also increase seepage but not to the value expected for the lithophysal zones.

1.7.3 Water Movement and Radionuclide Transport within and through the Engineered Barrier System

Section 1.6.3 illustrates and describes the TH processes related to the movement of seepage water within the drifts and seepage contacting WPs under the influence of nominal processes. The disruptive events expected to have the most influence on aqueous geochemical processes in the repository environment are seismic events and a possible igneous intrusion that enters the repository drifts. There are two modeling cases that analyze responses to seismic events and one modeling case that is concerned with an igneous intrusion into the repository.

Section 1.7.2 briefly describes the disruption of the pattern of seepage into the repository that can occur in response to seismic events. In addition, rock and seepage responses to seismic events can affect fluid flow within the EBS after seismic activity. Enhanced seepage into the repository, coupled with disruption of the EBS, could enhance LC, WP and DS degradation, and

waste-form degradation processes in the EBS as described in Section 1.6.3. Further, water flow in rubble in the repository in response to seismically influenced rockfall would encounter little resistance because of the relatively high porosity and permeability of the rubble. However, the repository invert is not expected to be as disrupted under the seismic modeling cases. Therefore, although there could be enhanced degradation and release of waste from the EBS following seismic GM or FD, transport of waste following liberation from the WPs would follow nominal processes through the invert, the UZ below the repository, and the SZ. Two modeling cases simulate the effects of seismic activity on the repository: the Seismic GM Modeling Case and the Seismic FD Modeling Case, as described in Section 1.5.4.

The rate at which radionuclides may be released from the repository due to seismic activity will depend on the following:

- The number and extent of WP damage
- Dissolution rate of the waste forms in the failed WPs
- Whether or not the released radionuclides are dissolved or colloidally attached
- Whether or not the released radionuclides are sorbed onto corrosion products and invert material
- The solubility of the released radionuclides.

The Igneous Intrusion Modeling Case simulates the number of WPs damaged and failed when portions of the repository are affected by magma that reaches the repository environment through a dike that breaches the repository. This modeling case assumes that for any drift intersected by a dike, all WPs in the drift will be failed by contact with magma. All waste from the failed WPs will be incorporated in the cooled magma or otherwise available for transport. After the waste is released from the WPs, transport out of the repository and through the UZ below the repository and the SZ will be subject to nominal processes.

The rate at which radionuclides released from the failed WPs may be released from the repository will depend on the following:

- Whether or not and at what rate the radionuclides released from the failed WPs are available to be dissolved
- Whether or not the released radionuclides are dissolved or colloidally attached
- Whether or not and at what rate the radionuclides released from the failed WPs are available for sorption onto corrosion products and invert material
- The solubility of the released radionuclides
- The rate of water movement and volume of water that flows or diffuses through the cooled magma and/or the damaged EBS.

1.7.4 Water Movement and Radionuclide Transport through the Unsaturated Tuffs below the Repository

Section 1.6.3 illustrates and describes the processes related to the movement of water and transport of radionuclides released from the repository under the influence of nominal processes. The principal difference between the nominal scenarios and scenarios that include disruptive events is the impetus for the release of radionuclides from the WPs and waste forms. Section 1.7.3 describes the factors relevant to the mobilization of radionuclides as a result of disruptive events. After disruptive events have mobilized radionuclides as a result of igneous or seismic events, radionuclide transport of dissolved or colloidal materials within and through the UZ will be governed by the same nominal processes described in Section 1.6.4. The TSPA-SEIS treats SZ flow and transport in the same way for both the Nominal Modeling Case and modeling cases that include disruptive events.

1.7.5 Water Movement and Radionuclide Transport through the Saturated Zone Aquifers to the Biosphere

Section 1.6.3 illustrates and describes the processes related to the movement of water and transport of radionuclides released from the repository under the influence of nominal processes. Section 1.7.3 describes the factors relevant to the mobilization of radionuclides after disruptive events. Section 1.7.4 describes radionuclide transport of dissolved or colloidal materials by nominal processes within and through the UZ after release from the EBS by disruptive events. In a similar way, radionuclide transport of dissolved and colloidal materials through the SZ to the biosphere will be governed by the same nominal processes described in Section 1.6.5. The TSPA-SEIS treats SZ flow and transport in the same way for both the Nominal Modeling Case and modeling cases that include disruptive events.

1.7.6 Atmospheric Transport and Redeposition of Radionuclides

The Volcanic Eruption Modeling Case in the TSPA-SEIS considers a post-eruption situation where volcanic ash has already been deposited on the ground surface. This eruption phase is evaluated in Section 6.4.2.5 to show that the probability-weighted annual dose during the eruption is much lower than the probability-weighted mean annual dose for after the eruption.

The Volcanic Eruption Modeling Case simulates the fate and transport of radionuclides deposited at land surface as a result of a volcanic eruption. The volcanic eruption includes waste from a number of WPs that are failed when portions of the repository are affected by a volcanic conduit that intersects the repository environment. The Volcanic Eruption Modeling Case does not include evaluation of the annual dose received during the volcanic eruption phase when the ash is transported and dispersed in the atmosphere. The Volcanic Eruption Modeling Case assumes that for any drift intersected by a volcanic conduit, all WPs in the drift will be failed by contact with magma. All waste from the failed WPs will be directly released by a volcanic eruption at land surface that sends the waste and tephra from the eruption into the atmosphere.

The atmospheric transport and dispersal of tephra and waste particles entrained in the eruptive cloud released during the volcanic eruption is described in *Atmospheric Dispersal and Deposition of Tephra from a Potential Volcanic Eruption at Yucca Mountain, Nevada* (SNL

2007 [DIRS 177431]). The dispersal and deposition is simulated using ASHPLUME (ASHPLUME_DLL_LA V. 2.1. STN: 11117-2.1-01 [DIRS 180147]). The ASHPLUME conceptual model accounts for incorporation and entrainment of waste fuel particles associated with a hypothetical volcanic eruption through the repository and downwind transport of contaminated tephra. ASHPLUME describes the conceptual model in mathematical terms to predict radioactive waste/ash deposition on land surface.

The waste inventory in the CSNF and CDSP WPs hit by the magma provide the radionuclides in the waste-contaminated ash. The contaminated ash, with consideration of radionuclide decay, is transported through the atmosphere and redistributed on interchannel divides and distributary channels at land surface. The ash redistribution model redistributes tephra through erosion and subsequent deposition of waste-contaminated ash. The Volcanic Eruption Modeling Case includes submodels for the processes affecting the release of radionuclides associated with the volcanic eruption, and implements the submodels for the calculation of mean annual dose from the redistributed contaminated tephra at the location of the RMEI. These submodels use the redistribution submodel to provide the calculated radionuclide concentrations in the tephra or in the soil/tephra mixture as the radioactive source term for calculating annual dose to the RMEI. The biosphere component of the TSPA-SEIS contains the appropriate biosphere dose conversion factors (BDCFs) to calculate the annual dose associated with the radioactive source by multiplying radionuclide concentrations by the volcanic ash BDCFs. The TSPA-SEIS uses mean tephra and waste concentrations and the percentages of the initial volumetric concentrations of waste and tephra to calculate source term multipliers for the following potential exposure pathways during soil removal, and for the residual tephra for the interchannel divides and distributary channels:

- Ingestion and radon exposure
- Long-term inhalation exposure
- Short-term inhalation exposure.

1.8 CONSERVATISMS AND LIMITATIONS RELATED TO THE TSPA-SEIS

1.8.1 Conservatisms Incorporated in the TSPA-SEIS

The submodels incorporated into the TSPA-SEIS are representations of the repository system. The guiding principles during the development of these submodels were to: (1) ensure that representations were not optimistic (i.e., leading to an underestimation of the dose results), and (2) incorporate all included FEPs. Although these representations were developed to be as realistic as possible, some conservative (reasonable and technically defensible based on supporting analyses) representations were required for complete development of the TSPA-SEIS. These conservatisms and models are appropriate and within the regulatory guidelines for the TSPA-SEIS effort, as found in NRC Proposed Rule 10 CFR Part 63 ([DIRS 178394] and [DIRS 180319]). Conservatisms incorporated in the TSPA-SEIS, if present, are not functions of the TSPA process, but are a result of the approach, methodology, and assumptions used in the abstractions found in the supporting analyses and process models described therein.

The NRC Proposed Rule at 10 CFR 63.114(a)(2) [DIRS 178394] requires that a PA:

> "Account for uncertainties and variabilities in parameter values, for 10,000 years after disposal, and provide for the technical basis for parameter ranges, probability distributions, or bounding values used in the performance assessment."

Also, NRC Proposed Rule 10 CFR 63.304 [DIRS 180319] requires that the ranges of parameters and performance-assessment calculations provide a "Reasonable Expectation" of repository performance in the following way:

> *"Reasonable expectation* means that the Commission is satisfied that compliance will be achieved based upon the full record before it. Characteristics of reasonable expectation include that it:
>
> 1. Requires less than absolute proof because absolute proof is impossible to attain for disposal due to the uncertainty of projecting long-term performance;
>
> 2. Accounts for the inherently greater uncertainties in making long-term projections of the performance of the Yucca Mountain disposal system;
>
> 3. Does not exclude important parameters from assessments and analyses simply because they are difficult to precisely quantify to a high degree of confidence; and
>
> 4. Focuses performance assessments and analyses on the full range of defensible and reasonable parameter distributions rather than only upon extreme physical situations and parameter values."

Accordingly, because 10 CFR 63.304(4) [DIRS 180319] does not preclude the use of conservative parameter values, the approach used for the TSPA-SEIS was to use full ranges of 'reasonable and defensible' distributions of estimates of parameter values that also could include conservative estimates of their values as provided by the supporting analyses. The TSPA-SEIS approach integrates the abstraction models developed in the supporting analyses to describe the relevant FEPs and appropriately propagate uncertainty in these abstractions. The TSPA-SEIS embodies all the assumptions, limitations, differences, and conservatisms of the underlying abstractions, process models, and related analyses.

The intended purpose of the TSPA-SEIS is to provide a defensible basis for an evaluation for compliance with the adopted postclosure regulatory standards (e.g., NRC Proposed Rule 10 CFR Part 63 [DIRS 178394] and [DIRS 180319]). Defensibility included, but was not limited to, reasonable and technically defensible conservative estimates of expected dose or other performance measures. The development of the TSPA-SEIS employed the following measures in providing defensible estimates of repository performance:

- Providing the best available estimates of parameter values, covering their ranges of uncertainty, including conservative estimates where appropriate.

- Documenting the full range of uncertainty and sensitivity analyses and other supporting analyses conducted to evaluate the significance of alternative assumptions to provide confidence in the overall results.

- Providing probabilistic estimates of mean dose, including conservative approaches only where knowledge of a process is limited.

The TSPA-SEIS includes an assemblage of the best available estimates of the parameters and parameter values, including, only when necessary, conservative estimates of parameter values and conservative assumptions related to the underlying process models and submodels. The TSPA-SEIS then uses this information to calculate the best available estimate of repository performance. The descriptions of the TSPA-SEIS components in Section 6.3 include the conservatisms applicable to each of the model components and include, as applicable, conservative values in the ranges of estimates of parameters values.

The preparation for the TSPA-SEIS involved the development of parameter-value distributions to account for uncertainty in parameter values. The TSPA process includes a Parameter Review Team that is responsible for evaluating parameter uncertainty, including the use of conservative parameter values. The Parameter Review Team meets with the authors of each supporting analysis, process model, and submodel that served to develop inputs to the TSPA-SEIS. The Parameter Review Team's goal was to develop realistic parameter-value distributions that appropriately characterize uncertainty. However, in cases where there was insufficient information available to support realistic characterizations, subject matter experts (SMEs) and the Parameter Review Team jointly concurred on conservative treatments of uncertainty.

1.8.2 Limitations of the TSPA-SEIS

Constraints that influence the TSPA-SEIS relate to the physical system, computer software, computer hardware, input data and knowledge, and limitations of the process models. The physical system is constrained by the given initial conditions, which reflect the complexity of the systems and processes being analyzed. Assessing the performance of a nuclear waste repository, which is sited in the UZ geologic setting at Yucca Mountain, involves numerous coupled physical and chemical processes. The constraints evolve through time, for example, with the gathering of additional scientific data and with advances in computer hardware and software.

The primary limitations on the TSPA-SEIS are described in the following sections. The TSPA-SEIS was tested to determine the impact of its limitations, such as conservatisms and inconsistencies, described below. Evaluation of this testing indicated that the model's limitations had a minimal effects on the results calculated with the TSPA-SEIS. Therefore, the limitations described below do not affect the utility of the TSPA-SEIS for achieving its intended purpose of providing a defensible evaluation of repository performance in compliance with applicable regulatory standards.

1.8.2.1 Software Limitations

The TSPA-SEIS uses GoldSim software. The GoldSim software has the following general capabilities:

- Addresses variability and uncertainty by using Monte Carlo simulation
- Superimposes the occurrence and consequences of discrete events onto continuously varying systems
- Uses model 'containers' that facilitate the simulation of large, complex systems
- Dynamically links external process models and/or abstractions directly to the GoldSim software
- Directly exchanges information between any Open Database Connectivity compliant database and the software.

Despite these attractive capabilities, the GoldSim software has limitations regarding the number of realizations that it can perform, its inability to resample the distributions of uncertain parameters during a realization, the discretization of temporal and spatial domains, and its ability to simulate certain complex processes, such as irreversible sorption. Because of these types of limitations in the framework of the GoldSim software, implementation of the TSPA-SEIS required the use of alternative processes configured to imitate certain processes or phenomena. For example, GoldSim utilizes the radioactive decay model to mimic the process of irreversible sorption. Other examples of this process are presented in Section 6.3 in the discussions of the implementations of the TSPA-SEIS components. The limitations of the GoldSim software do not affect its ability to achieve its intended purpose of providing a defensible evaluation of repository performance in compliance with applicable regulatory standards.

When developing and integrating the process models that comprise the model components of the TSPA-SEIS, hardware and software limitations were an important consideration in the model abstraction process. Hardware limitations include the speed and number of computer processors available, while software limitations include limits on the size of individual processes and threads in a 32-bit operating system. For Yucca Mountain, the judgment of scientists involved in developing the TSPA-SEIS is that the computational size and efficiency of the underlying process models do not allow direct coupling of most process models. Examples include the process-level TH, thermal-hydrologic-chemical (THC), UZ flow, and biosphere models. Some process models, such as EBS transport, have been built directly into the TSPA-SEIS but most have been abstracted in one form or another, as described in Section 6. The decoupled process models were run separately and converted to abstractions, such as response surfaces and look-up tables, which serve as direct input to the TSPA-SEIS.

1.8.2.2 Computational Limitations

The regulatory requirement to include the effects of model and data uncertainty in the PA of the repository means that the TSPA-SEIS must have the capability of modeling the repository

system in a probabilistic fashion, which involves multiple realizations of the reasonably expected future system behavior. Furthermore, there must be a sufficient number of model realizations of system behavior to produce a stable estimate of the mean annual dose. This probabilistic requirement thus places a constraint on the size of the TSPA-SEIS and the run time for simulations of repository performance using the hardware configuration described in Section 1.2.5.

The software and hardware constraints discussed in Section 1.2.5 affected the size of the various pieces of the TSPA-SEIS during development, including the number of nodes in the three-dimensional UZ flow fields, the number of particles per radionuclide used in the UZ Transport Model Component, the number of unique radionuclides in all parts of the TSPA-SEIS and software, and also the spatial discretization of the EBS. In particular, of all the processes modeled in the TSPA-SEIS, radionuclide transport through the EBS was the only process modeled directly with subroutines in GoldSim software, rather than as an external process model that provided direct input to the TSPA-SEIS in the form of a look-up table or response surface. Radionuclide transport through the EBS was modeled with the GoldSim contaminant transport module. The object-oriented nature of the GoldSim software can place limitations on the number of representative WPs or source term environments that can be modeled for waste-form mobilization, chemical conditions, and EBS transport. For example, the spatial discretization used to evaluate LC will be distributed among five percolation subregions, and up to 500 WP locations for each percolation subregion, repeating the same number for CSNF and CDSP WPs. In addition, GC calculations will be limited to 500 WP locations in each percolation subregion.

Thus, a constraint on the TSPA-SEIS's suite of software integrated with GoldSim is a limit on the number of release environments for the purposes of waste-form degradation and radionuclide mobilization/transport, specifically with respect to spatial variability in chemical conditions (solubility and sorption) and thermal conditions (temperature and relative humidity). The total number of unique release or source term environments in the TSPA-SEIS is ten for any one realization. To accommodate this limitation consistent with regulatory constraints, some variability was treated as uncertainty in the TSPA-SEIS because the overall mean of the calculated dose includes both system uncertainty and variability. However, the computational and hardware limitations described above do not affect the ability of the TSPA-SEIS to achieve its intended purpose of providing a defensible evaluation of compliance with applicable regulatory standards.

1.8.2.3 Data Limitations

The TSPA-SEIS utilizes a large amount and variety of field and laboratory data. Source documents for these data, cited in Section 4 and elsewhere in this report, describe the limitations in these data, indicate where additional data could lead to further refinements of the process models and submodels, and provide the bases for the conclusion that the currently available data supporting the TSPA-SEIS are defensible and suitable for their intended use. The limitations on the field and laboratory data used in the TSPA-SEIS do not affect the utility of the model for achieving its intended purpose of providing a defensible evaluation of repository performance in compliance with applicable regulatory standards.

1.8.2.4 Process Model Limitations

The TSPA-SEIS is a representation of the total repository system, including both natural and engineered components. The model components shown on Figure 1-3 are represented by separate process models, which were based on an analysis of FEPs affecting postclosure repository performance. In most cases, these process models are mathematical representations of physical and chemical processes that will occur in the natural and engineered systems over the life of the repository. The principal investigators who have developed these process models have also developed abstractions, or simplifications, of the process models to be used in the TSPA-SEIS. The abstraction models may be response surfaces, one-dimensional or two-dimensional look-up tables, or software linked to GoldSim as dynamically linked libraries (DLLs). The abstraction models capture the principal features of the process models. Therefore, the TSPA-SEIS is subject to the limitations of the supporting process models. However, although the TSPA-SEIS is subject to the limitations of the process models and submodels contained in supporting analyses, these limitations do not affect the ability of the TSPA-SEIS to achieve its intended purpose of providing a defensible evaluation of repository performance in compliance with applicable regulatory standards.

1.8.2.5 Other Limitations of the TSPA-SEIS

In addition to the limitations related to software, computational constraints, data, and process models that are discussed in the previous sections, there are the following additional limitations that derive from choices made in the design and implementation of the TSPA-SEIS.

Conservatism—The decision to implement reasonable and technically defensible conservative approaches, may cause the TSPA-SEIS to tend to underestimate the overall performance of the repository system or its model components. This limitation does not affect the utility of the TSPA-SEIS for achieving its intended purpose of providing a defensible evaluation of compliance with applicable regulatory standards, because the TSPA-SEIS tends to overestimate, rather than underestimate, radionuclide releases from the repository system and subsequent doses to the RMEI. However, effects of conservative assumptions at the model component level should be considered in interpretations of the realistic behavior of the repository system and its components. Not all conservative assumptions made at the model component level necessarily result in conservative outcomes at the system level: conservatisms that have the potential to increase radionuclide release (or dose) may have little or no impact on overall performance if the model component or process model in which the conservatisms are applied result in only a minor contribution to performance. At any level within the repository system modeled with the TSPA-SEIS, conservative assumptions may tend to mask the relative importance of other processes or parameters, and conclusions regarding the importance, or lack thereof, of aspects of the TSPA-SEIS should be understood as having been made consistent with the conservatisms embedded in the model.

Some abstractions used in the TSPA-SEIS are based on process level models that are limited to conditions under which Darcy's law and its extensions and generalizations are applicable. These abstractions are limited in the TSPA-SEIS to situations in which the differential equations describing fluid flow can be uncoupled from those that describe the mass transport of colloids or dissolved species in the UZ, SZ, and through the EBS, including corrosion products and the

invert. The uncoupling is appropriate as long as the density and viscosity of the fluids in the TSPA-SEIS do not change with concentration in such a manner as to significantly alter the flow fields. The analysis examines solubility and dissolved radionuclide concentrations calculated during the compliance analyses using the TSPA-SEIS. Density and viscosity values reported for solutions with comparably high concentrations of uranium indicate that the use of Darcy's law and the uncoupling of flow and transport equations under the condition commonly encountered in the TSPA-SEIS are reasonable and appropriate for the model's intended use.

The TSPA-SEIS utilizes some numerical model abstractions from process level models that are limited to conditions under which Fick's first law of diffusion is applicable. This is true for describing diffusive transport in the UZ, SZ, and through the EBS, including the WPs, corrosion products, and the invert. Fick's first law states that mass transport is proportional to the concentration gradient and mass is transported from high to low concentration in such a way as to tend to minimize the gradient. The second and third order effects can contribute to additional diffusive mass transfer under unique situations such as thermal diffusion, pressure diffusion, and external forced diffusion (e.g., under an imposed electrical current). The models invoked in the TSPA-SEIS either directly or indirectly are limited to situations dominated by ordinary concentration diffusion. Fick's law for mass transport is as fundamental as Fourier's law of heat conduction, which states that the flow of heat by conduction is proportional to the temperature gradient.

Period of performance—The TSPA-SEIS results presented in this report are limited to postclosure performance objectives specified at NRC Proposed Rule 10 CFR 63.113 [DIRS 180319] and are suitable for comparison with the proposed 10,000-year regulatory standard and the period of geologic stability per NRC Proposed Rule 10 CFR 63.303(b) [DIRS 178394].

Limitations inherent in mathematical modeling and uncertainty analysis—Because the TSPA-SEIS represents complex natural or engineered systems, insights that can be drawn from the model's calculations are limited to those based on processes that have been included in the model. Processes that have been omitted from the TSPA-SEIS, either through the FEP screening process (Section 6.1.3) or through simplifications made as part of the abstraction process (Section 6.3), are not evaluated in detail. This limitation is inherent in mathematical models that simplify complex systems to allow predictive analysis, and does not affect the utility of the model for achieving its intended purpose of providing a defensible evaluation of compliance with applicable regulatory standards. Insights into processes that have been omitted from the TSPA-SEIS or simplified through the abstraction process can be obtained by consulting underlying reports describing analyses that document the FEP screening process and the development of relevant process models, as cited in Section 6.

Similarly, conclusions drawn from sensitivity and uncertainty analyses are dependent on the design of the TSPA-SEIS and the treatment of uncertainty in its inputs. Because the TSPA-SEIS is based on Monte Carlo uncertainty analysis, the results are sensitive only to those processes and parameters that are included in the model. Sensitivity to uncertainty in parameter values will be directly related to both the roles of the parameters in the mathematical models, and to the distribution of values assigned to the parameters to represent uncertainty. Parameters for which no uncertainty is assigned will not appear as important in the results of standard sensitivity analyses, regardless of their function in the TSPA-SEIS.

In some instances, modeling cases were developed to intentionally implement unrealistic assumptions about the performance of specific model components, or that use assumptions that go beyond the range of uncertainty assigned to specific input parameters. Interpretation of these analyses, provides useful insights into some aspects of subsystem performance, but requires recognition of a fundamental limitation: model results obtained by using the TSPA-SEIS outside of its intended range, or outside the range of its model components and input parameters, should not be interpreted as providing a realistic or reasonable estimate of system or subsystem performance.

1.9 DESCRIPTION OF THE TOTAL SYSTEM PERFORMANCE ASSESSMENT MODEL/ANALYSIS FOR THE SEIS

The *Total System Performance Assessment Model/Analysis – SEIS Information Package* describes how the supporting parameters and parameter values, along with process-model abstractions representing many different aspects of the repository system, were integrated into one comprehensive model to describe the total repository system.

Figure 1-23 shows the principal model components of the TSPA-SEIS and the hierarchy of the submodels that support and/or are contained within these model components. References to the documents that describe the development of model components and submodels used to analyze the repository system, and/or provide direct inputs to the TSPA-SEIS, can be found in Table 1-1 and in the list of references for this document. Section 6.1.4 describes the overall approach used to assemble the representations of the individual model components and their submodels into a description of the entire repository system. Descriptions of the model components and submodels used in the TSPA-SEIS, and the scientific bases for these model components and submodels, are presented in Section 6.3.

The TSPA-SEIS documentation consists of three key information sources: (1) the *Total System Performance Assessment Model/Analysis – SEIS Information Package* (i.e., this report), (2) the numerical model files within the GoldSim model file, and (3) the TSPA-SEIS database. GoldSim allows all linked operations of the abstracted process models and submodels to perform complex calculations, thereby incorporating the natural geochemical and hydrogeologic processes and engineered-design elements of the repository. There are several GoldSim model files developed and documented herein. Nominally, the discussion in this document will refer to the GoldSim model file, meaning all related model files.

TSPA-SEIS Analysis Time Period—Two time periods were used for the analysis of repository performance. NRC Proposed Rule 10 CFR 63.311 ([DIRS 178394]) states the following:

> "(a) DOE must demonstrate, using performance assessment, that there is a reasonable expectation that the reasonably maximally exposed individual receives no more than the following annual dose from releases from the undisturbed Yucca Mountain disposal system:
>
> (1) 0.15 mSv (15 mrem) for 10,000 years following disposal; and

> (2) 3.5 mSv (350 mrem) after 10,000 years, but within the period of geologic stability indicates that performance assessment cover a compliance period of 10,000 years after repository closure."

The TSPA-SEIS analyses presented in this document satisfy the 10,000-year requirement of the NRC proposed rule. However, the analyses that extend the analysis period to 20,000 years postclosure allow evaluation of whether or not the trends present at the end of 10,000 years continue, or if uncertainties in results affect the conclusions regarding the 10,000-year performance period and beyond. These results closure do not display any significant changes to the trends observed from 0 to 10,000 years, providing confidence in the conclusions reached regarding the 10,000-year performance period.

The time period for the TSPA-SEIS analyses presented in this document to satisfy the 'period of geologic stability' requirement at 10 CFR 63.311a (2) [DIRS 180319] is one million years after repository closure. The one-million-year analyses comply with NRC Proposed Rule 10 CFR 63.302 ([DIRS 178394]), which indicates that, "This period is defined to end at one million years after disposal." The one-million-year analyses are thus consistent with the proposed NRC Proposed Rule 10 CFR 63.342 ([DIRS 178394]) and the EPA Proposed Rule 40 CFR 197.25 ([DIRS 177357]). The graphical representations of the TSPA-SEIS show the mean annual dose to the REMI observed during the one-million-year postclosure time period.

1.10 DOCUMENT ORGANIZATION

The GoldSim model file contains in-depth descriptions of the submodels and descriptions of their implementation. Direct inputs to the TSPA-SEIS are readily available in the TSPA-SEIS parameter database, the controlled source for the direct inputs to the GoldSim model file. The database allows the user to review most parameter values by accessing a single source location.

This report provides a road map to the information required to use the TSPA-SEIS, including detailed information regarding direct inputs, parameters, and submodel descriptions, as required to describe the TSPA-SEIS calculations, and to trace the sources of the TSPA-SEIS's direct inputs. As appropriate, the document contains appropriate references to source information.

Section 1: Purpose—Section 1 describes the FEPs process that led to the development of the scenario classes used in analyzing the performance of the repository system. Section 1 also describes the regulatory framework for the TSPA-SEIS as well as an overview of the natural and engineered barriers in the repository system, including site-description information, descriptions of the elements of the EBS, processes affecting water movement through the UZ and SZ, descriptions of the model components, and a general description of the architecture of the TSPA-SEIS.

Section 2: Quality Assurance—Section 2 describes the applicable quality assurance (QA) procedures of the *Quality Assurance Requirements and Description* (QARD) (DOE 2007 [DIRS 182051]), along with descriptions and references to the methods used for the electronic management of information.

Section 3: Use of Software—Section 3 lists and briefly describes the software used in the development of the TSPA-SEIS. The primary software used to run the TSPA-SEIS is GoldSim. Analysis of the results developed with the TSPA-SEIS is aided by the use of additional postprocessing software. Section 3 identifies and briefly describes all auxiliary software and software routines that were developed for the TSPA-SEIS, including those developed external to, and incorporated into, the TSPA-SEIS.

Section 4: Inputs—Section 4 identifies the direct inputs used in the TSPA-SEIS, either by direct tabulations included in this document or through linkage to the appropriate sections of the GoldSim model file or TSPA-SEIS database. Section 4 also identifies all applicable criteria, codes, and standards.

Section 5: Assumptions—Section 5 lists the assumptions directly used to perform the TSPA-SEIS analyses along with their bases. Section 5 also includes key assumptions from supporting documents that are used in the TSPA-SEIS.

Section 6: Model Description—Section 6 describes the TSPA-SEIS representation of the repository system, presents the scenario classes being analyzed, describes the modeling cases used to analyze the scenario classes, and provides references to the applicable sections of the TSPA-SEIS, the GoldSim model file, and supporting analyses. Section 6 includes detailed descriptions of the conceptual models, mathematical formulations, implementations of the submodels in the TSPA-SEIS, conservatisms, and ACMs.

INTENTIONALLY LEFT BLANK

Table 1-1. Principal Documents that Support the TSPA-SEIS

Topic	Title	Document Identifier
UZ Flow		
Climate	*Future Climate Analysis*	ANL-NBS-GS-000008 [DIRS 170002]
Infiltration	*Simulation of Net Infiltration for Present-Day and Potential Future Climates*	MDL-NBS-HS-000023 [DIRS 174294]
Mountain-Scale UZ Flow	*UZ Flow Models and Submodels*	MDL-NBS-HS-000006 [DIRS 175177]
Drift Seepage	*Abstraction of Drift Seepage*	MDL-NBS-HS-000019 [DIRS 181244]
	In-Drift Natural Convection and Condensation	MDL-EBS-MD-000001 [DIRS 181648]
	Seepage Model for PA Including Drift Collapse	MDL-NBS-HS-000002 [DIRS 167652]
EBS Environment		
EBS Thermal-Hydrologic	*Multiscale Thermohydrologic Model*	ANL-EBS-MD-000049 [DIRS 181383]
EBS Chemical Environment	*Engineered Barrier System: Physical and Chemical Environment*	ANL-EBS-MD-000033 [DIRS 177412]
WP and DS Degradation		
WP, GC, and LC	*General Corrosion and Localized Corrosion of the Drip Shield Barrier*	ANL-EBS-MD-000004 [DIRS 180778]
WP, GC, and LC	*General Corrosion and Localized Corrosion of Waste Package Outer Barrier*	ANL-EBS-MD-000003 [DIRS 178519]
	Stress Corrosion Cracking of Waste Package Outer Barrier and Drip Shield Material	ANL-EBS-MD-000005 [DIRS 181953]
	Analysis of Mechanisms for Early Waste Package/Drip Shield Failure	ANL-EBS-MD-000076 [DIRS 178765]
Waste Form Degradation and Mobilization		
Radionuclide Inventory	*Initial Radionuclide Inventories*	ANL-WIS-MD-000020 [DIRS 180472]
In-Package Chemistry	*In-Package Chemistry Abstraction*	ANL-EBS-MD-000037 [DIRS 180506]
Cladding Degradation	*Cladding Degradation Summary for LA*	ANL-WIS-MD-000021 [DIRS 180616]
Waste Form Degradation	*CSNF Waste Form Degradation: Summary Abstraction*	ANL-EBS-MD-000015 [DIRS 169987]
	Defense HLW Glass Degradation Model	ANL-EBS-MD-000016 [DIRS 169988]
	DSNF and Other Waste Form Degradation Abstraction	ANL-WIS-MD-000004 [DIRS 172453]
Dissolved Radionuclide Concentration Limits	*Dissolved Concentration Limits of Elements with Radioactive Isotopes*	ANL-WIS-MD-000010 [DIRS 177418]

Table 1-1. Principal Documents that Support the TSPA-SEIS (Continued)

Topic	Title	Document Identifier
Waste Form and EBS Colloids	*Waste Form and In-Drift Colloids-Associated Radionuclide Concentrations: Abstraction and Summary*	MDL-EBS-PA-000004 [DIRS 177423]
EBS Flow and Transport		
EBS Flow and Transport	*EBS Radionuclide Transport Abstraction*	ANL-WIS-PA-000001 [DIRS 177407]
UZ Transport		
UZ Particle Tracking	*Particle Tracking Model and Abstraction of Transport Processes*	MDL-NBS-HS-000020 [DIRS 181006]
	Calibrated UZ Properties	ANL-NBS-HS-000058 [DIRS 179545]
	Radionuclide Transport Models Under Ambient Conditions	MDL-NBS-HS-000008 [DIRS 177396]
Transport Interface	*Drift-Scale Radionuclide Transport*	MDL-NBS-HS-000016 [DIRS 170040]
SZ Flow and Transport		
SZ Convolute	*Saturated Zone Flow and Transport Model Abstraction*	MDL-NBS-HS-000021 [DIRS 181650]
1-D SZ Transport		
SZ Flow and Transport		
Biosphere		
Biosphere	*Biosphere Model Report*	MDL-MGR-MD-000001 DIRS [177399]
Disruptive Events		
Seismic Activity	*Seismic Consequence Abstraction*	MDL-WIS-PA-000003 [DIRS 176828]
Igneous Intrusion Modeling Case	*Number of Waste Packages Hit by Igneous Intrusion*	ANL-MGR-GS-000003 [DIRS 177432]
	Dike/Drift Interactions	MDL-MGR-GS-000005 [DIRS 177430]
	Characterize Framework for Igneous Activity at Yucca Mountain, Nevada	ANL-MGR-GS-000001 [DIRS 169989]
Volcanic Eruption Modeling Case	*Atmospheric Dispersal and Deposition of Tephra from a Potential Volcanic Eruption at Yucca Mountain, Nevada*	MDL-MGR-GS-000002 [DIRS 177431]
	Redistribution of Tephra and Waste by Geomorphic Processes Following a Potential Volcanic Eruption at Yucca Mountain, Nevada	MDL-MGR-GS-000006 [DIRS 179347]
	Characterize Framework for Igneous Activity at Yucca Mountain, Nevada	ANL-MGR-GS-000001 [DIRS 169989]

Source: *Technical Work Plan for: Total System Performance Assessment FY 07-08 Activities* (SNL 2007 [DIRS 179605], Table 1-1)

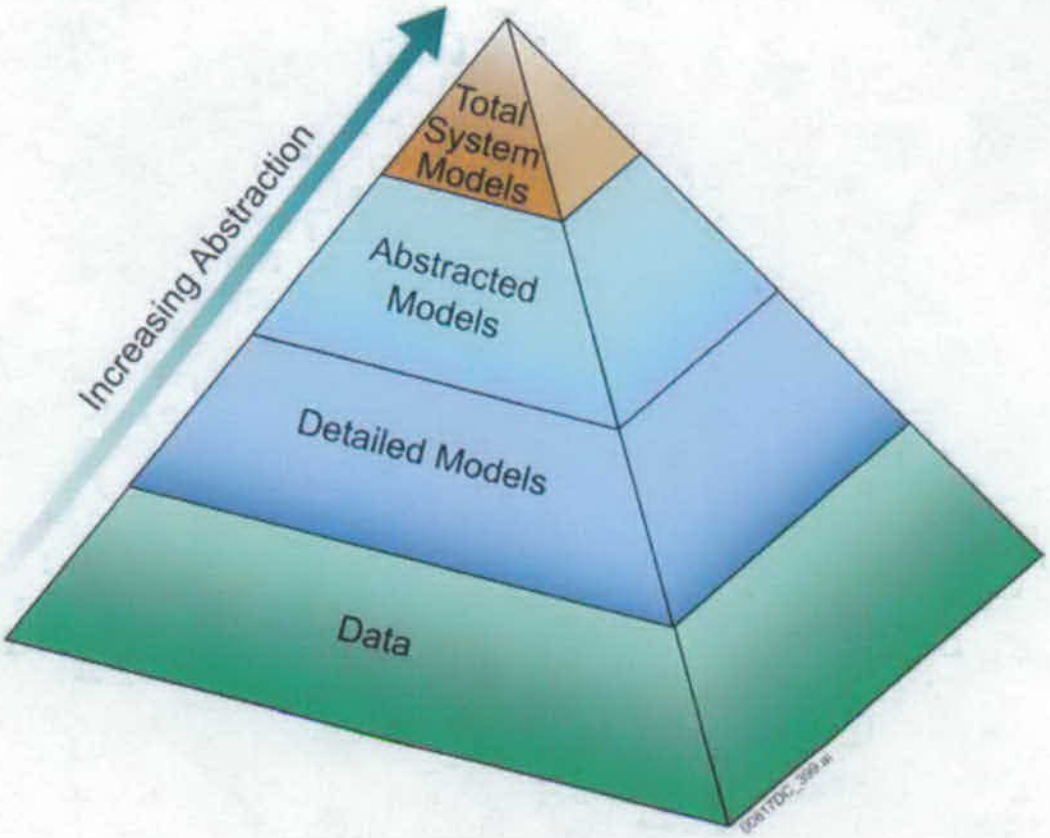

Figure 1-1. Performance Assessment Pyramid Showing the Steps Involved in Developing a Total System Model

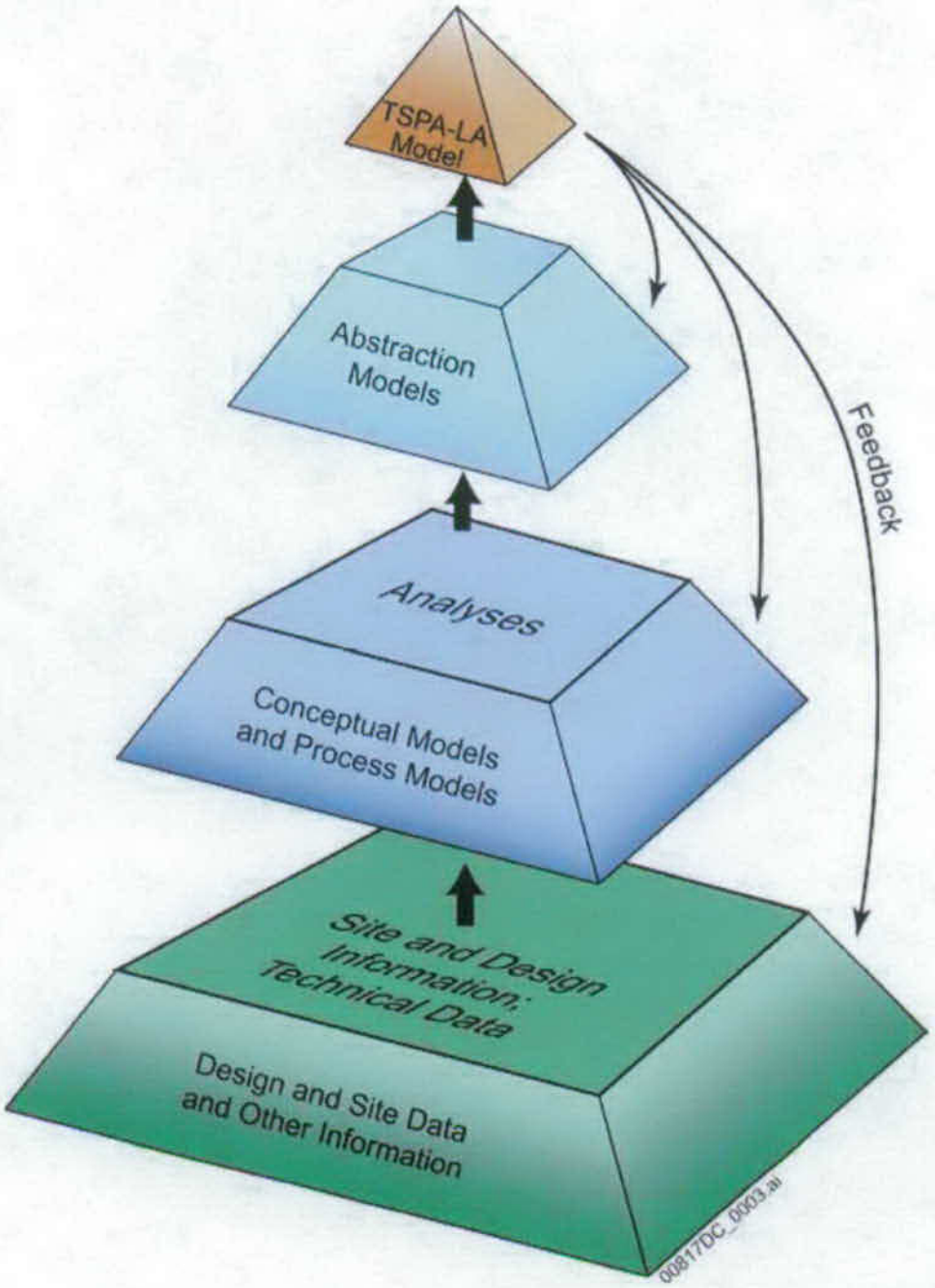

Figure 1-2. Performance Assessment Pyramid Showing How Detailed Underlying Information Builds the Technical Basis for the TSPA-SEIS

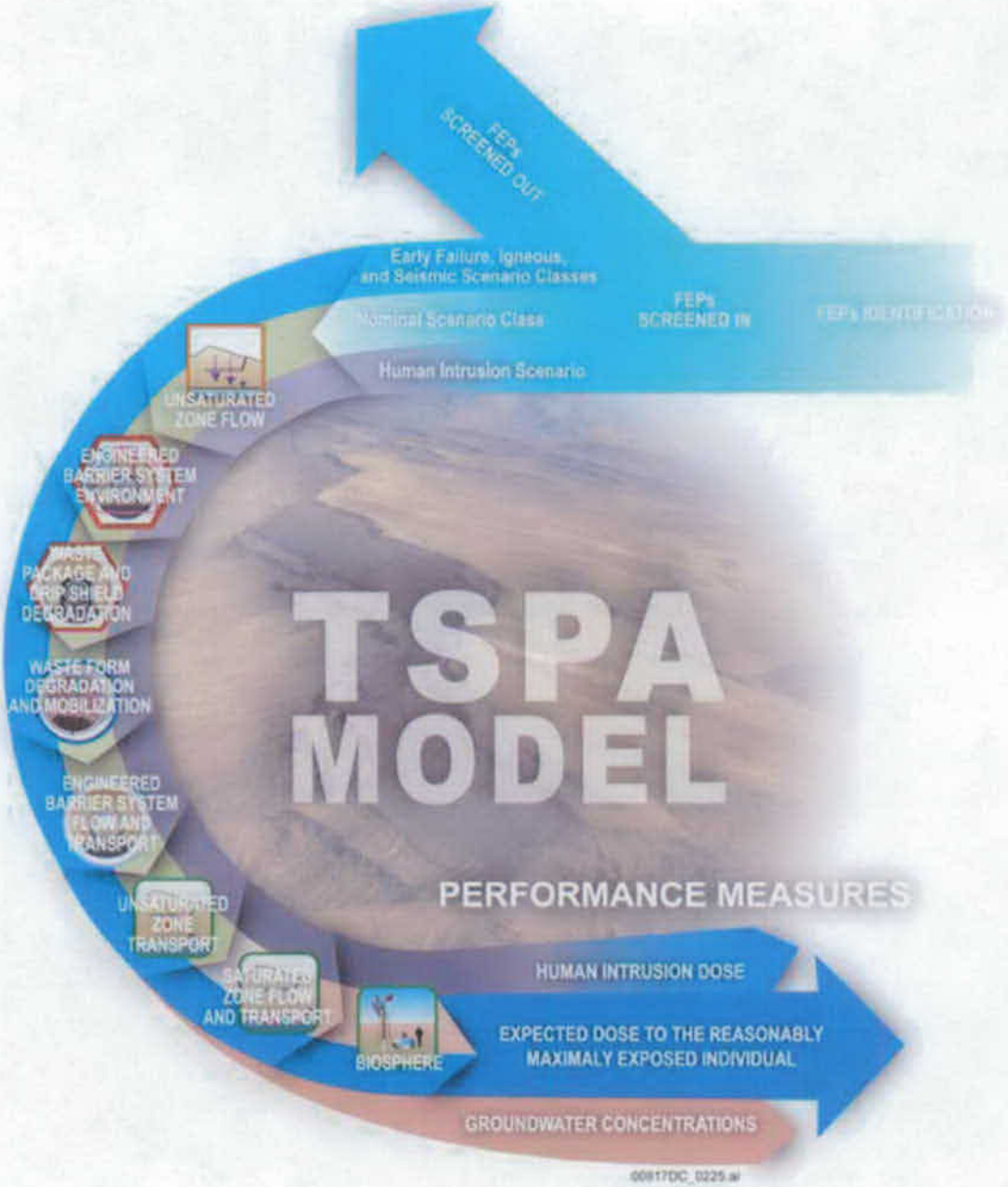

Figure 1-3. Schematic Representation of the Development of the TSPA-SEIS, Including the Nominal, Igneous, and Seismic Scenario Classes

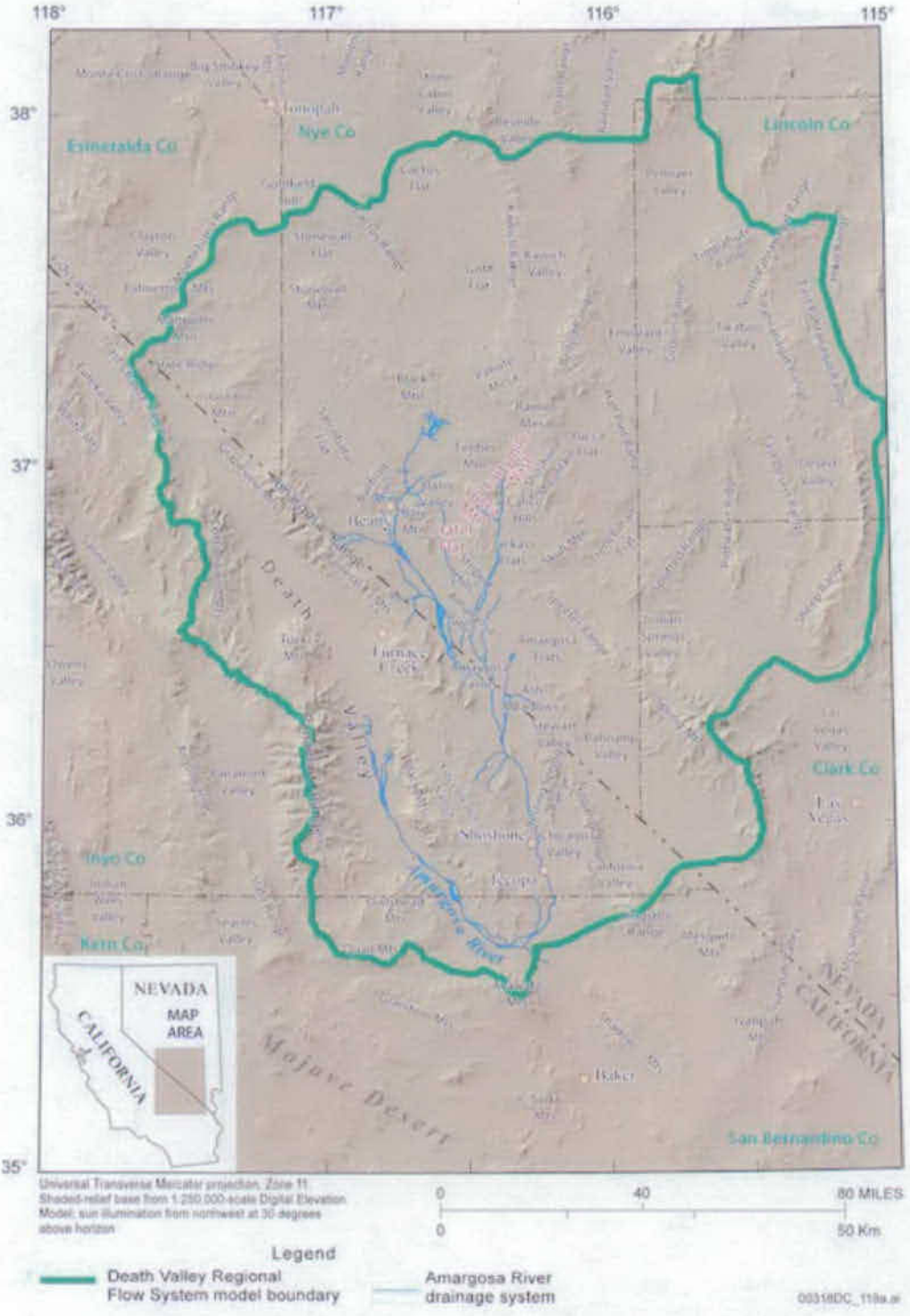

Source: Modified from BSC 2004 [DIRS 169734], Figure 8-2

Figure 1-4. Geographic and Prominent Topographic Features of the Death Valley Region

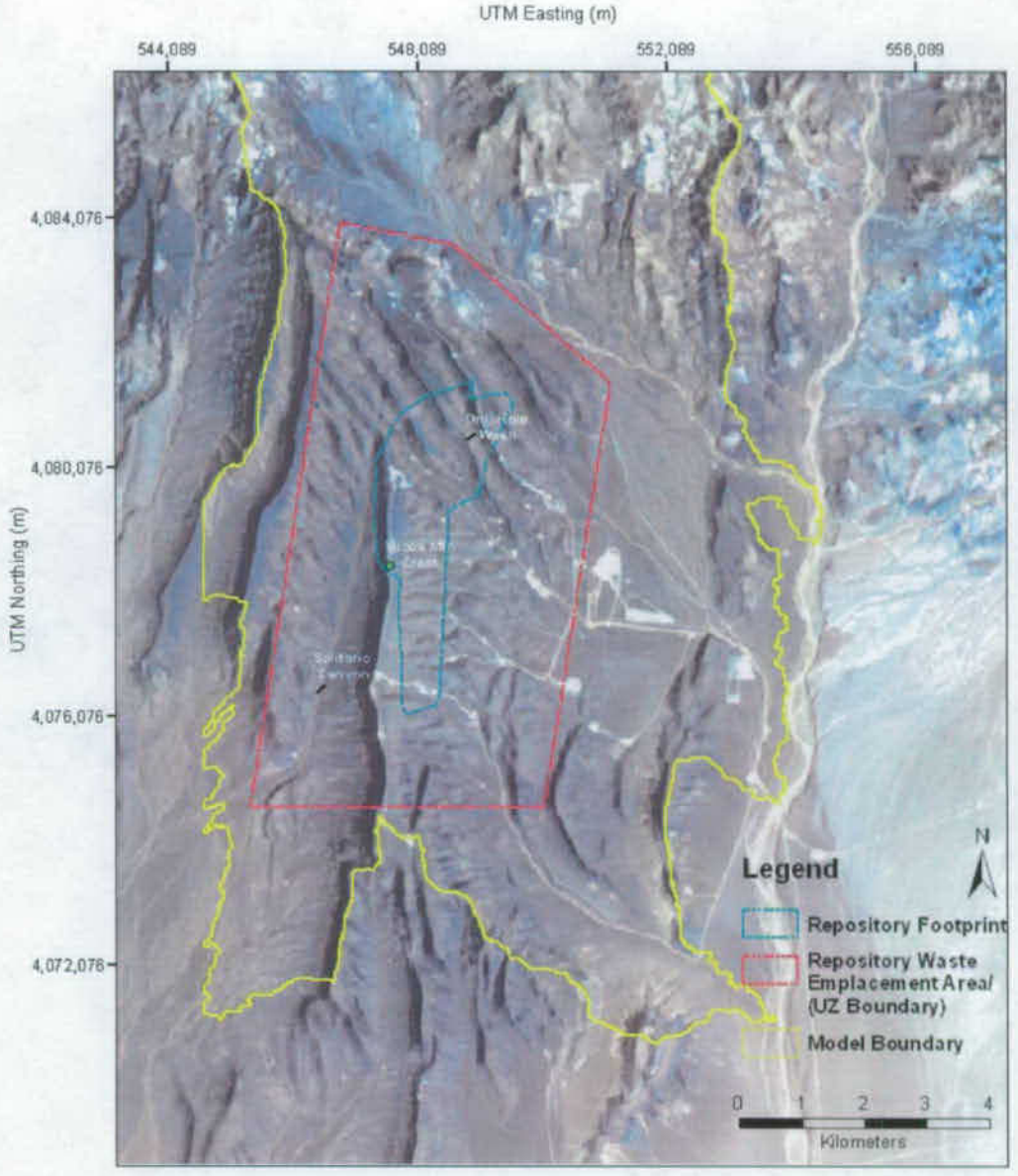

Source: Modified from SNL 2007 [DIRS 174294], Figure 6.5.2.1-1.

NOTE: The model boundary is the same as the 1999 unsaturated zone flow model domain of the TSPA-SR.

Figure 1-5. Topographic Map of the Yucca Mountain Site Showing Differences in Slope Characteristics North and South of Drill Hole Wash

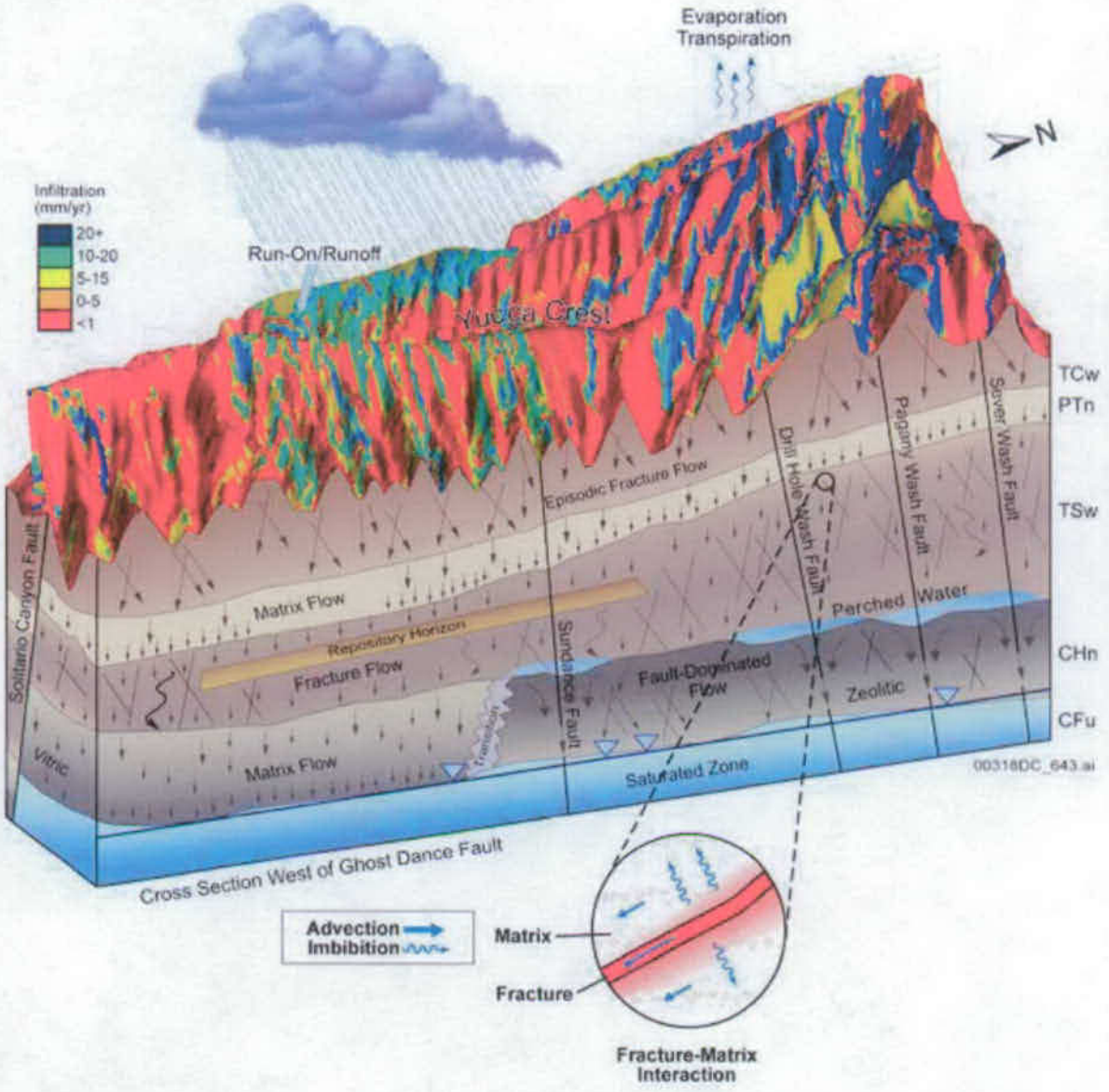

Source: Modified from BSC 2004 [DIRS 170035], Figure 6-1

Figure 1-6. Overall Water Flow Behavior in the Unsaturated Zone, Including the Relative Flux Magnitudes of Fracture and Matrix Flow Components in the Different Hydrogeologic Units

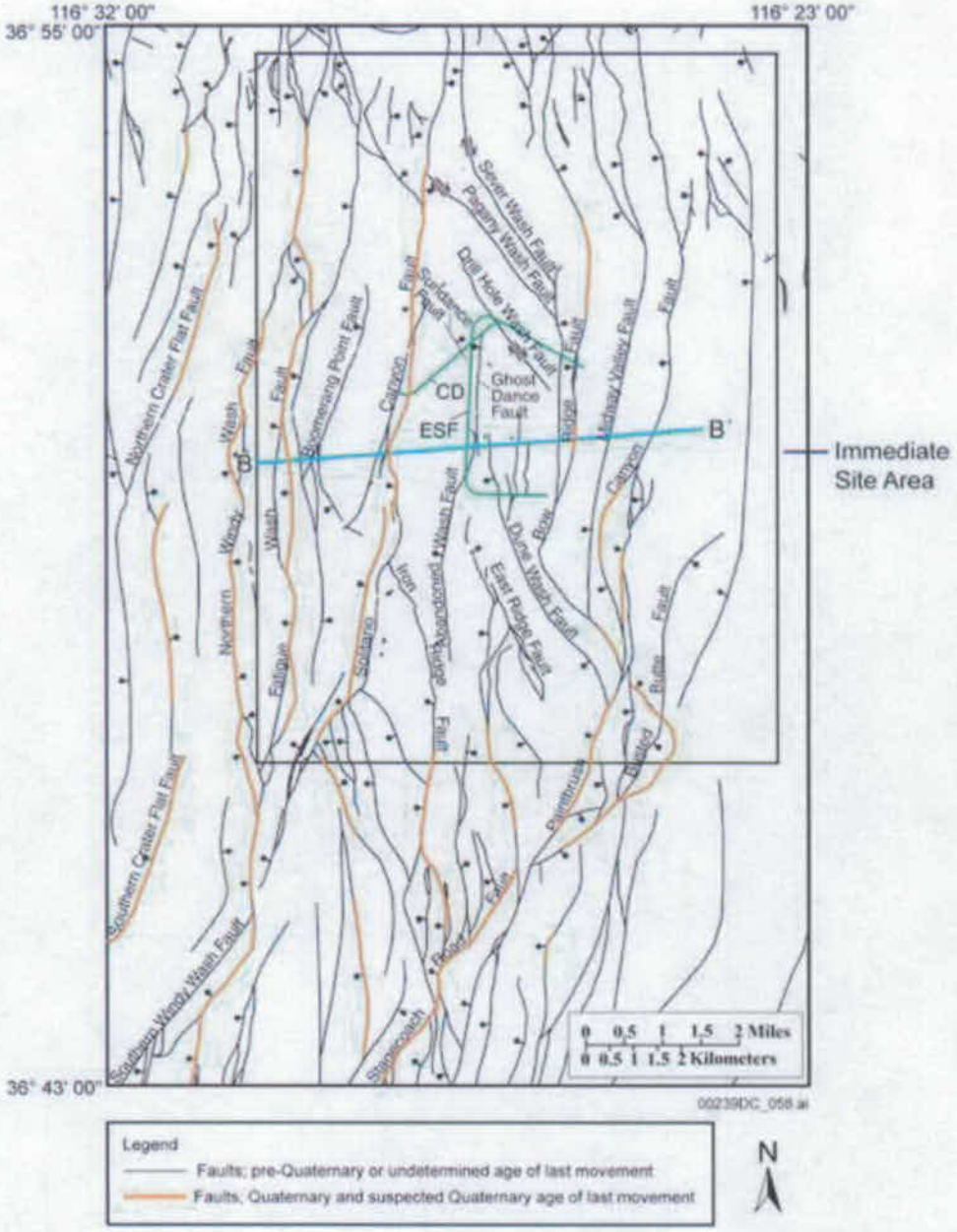

Source: Modified from BSC 2004 DIRS 169734], Figure 3-20

NOTES: The following faults have demonstrable Quaternary activity: Northern Crater Flat Fault, Southern Crater Flat Fault, Northern Windy Wash Fault, Southern Windy Wash Fault, Fatigue Wash Fault, Solitario Canyon Fault, Iron Ridge Fault, Bow Ridge Fault, Paintbrush Canyon Fault, and Stagecoach Road Fault. All faults are shown with solid lines, although many segments are concealed or inferred.

Symbols and acronyms: bar and bell: downthrown side of fault; arrows: relative direction of strike-slip movement; ESF = Exploratory Studies Facility (green line); CD = Cross-Drift; blue line: approximate location of line of section shown on Figure 1-8.

Figure 1-7. Distribution of Faults in the Yucca Mountain Site Area and Adjacent Areas to the South and West

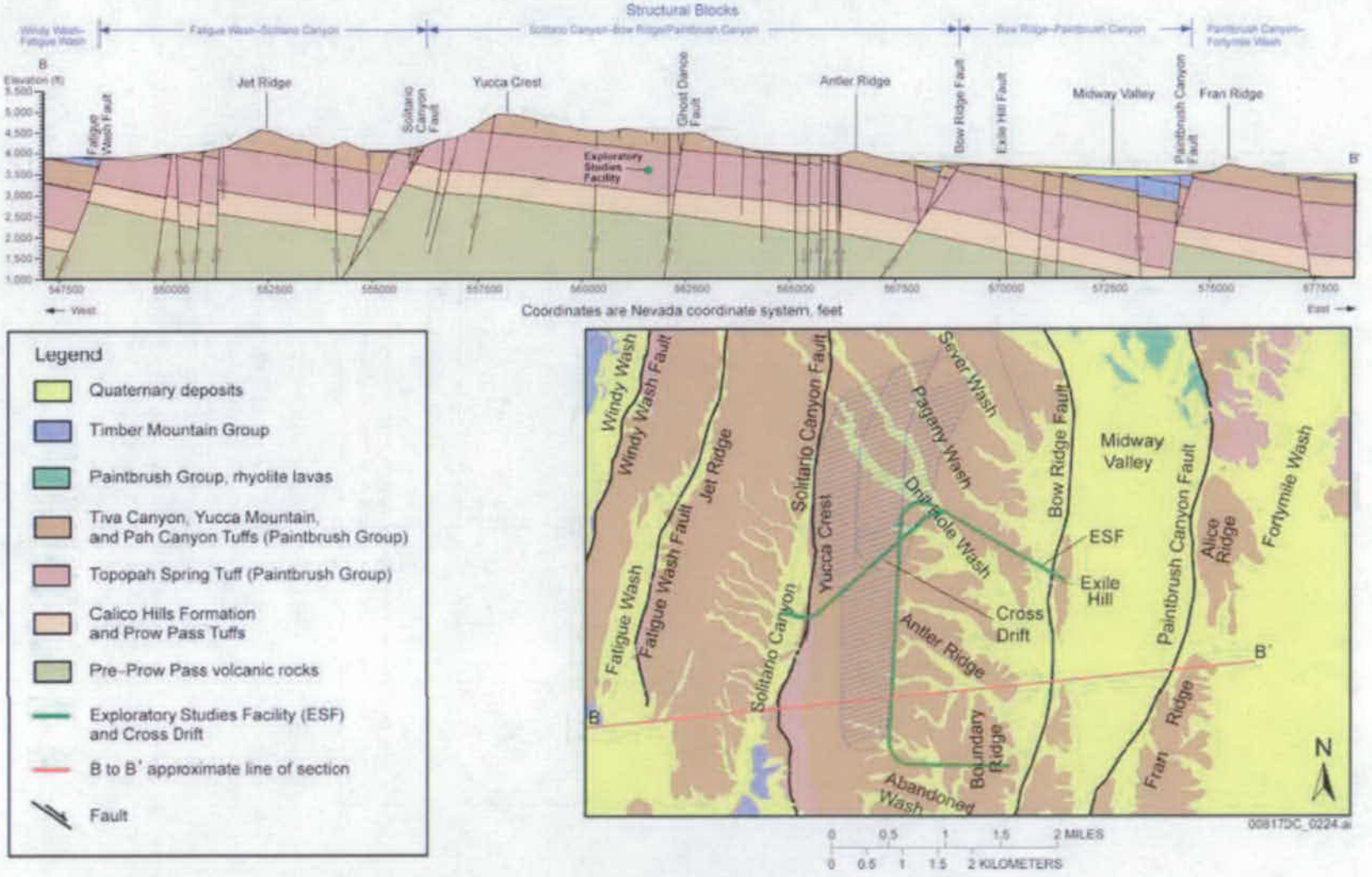

Source: Simplified from Day et al. 1998 [DIRS 100027], Cross Section B-B'

NOTE: ESF = Exploratory Studies Facility, location of intersection along the approximate line of section, also shown on Figure 1-7.

Figure 1-8. East-West Structure Section across Yucca Mountain Site Area

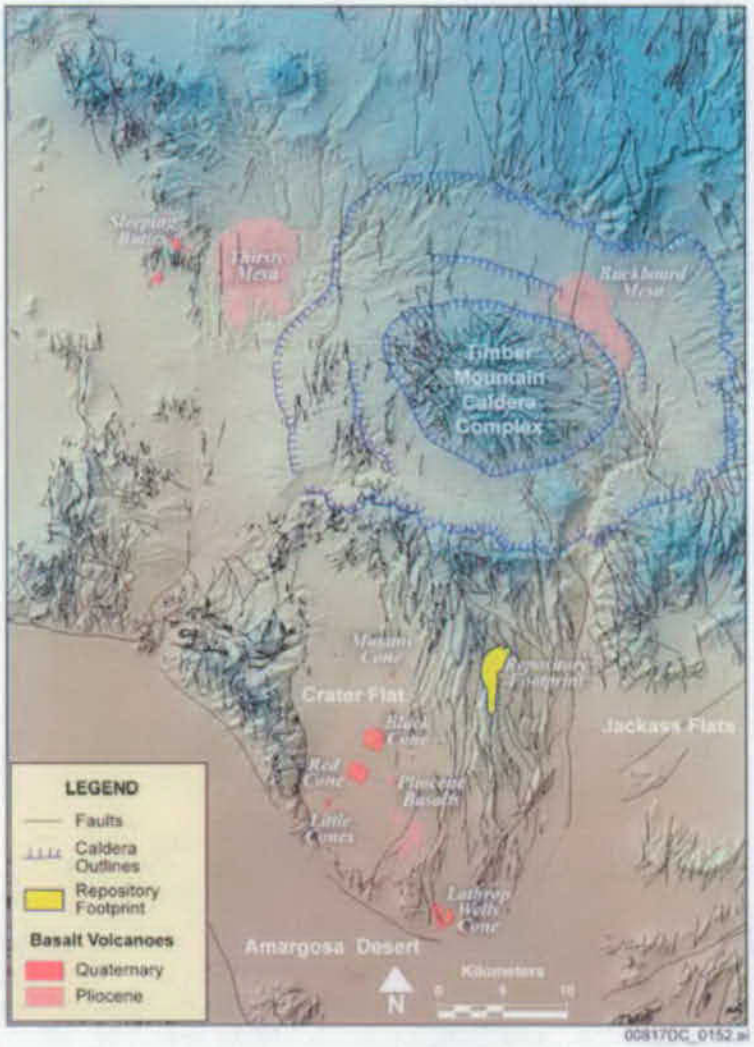

Source: Modified from CRWMS M&O 1998 [DIRS 123196], Figure 2.1

Figure 1-9. Location and Age of Post-Miocene (less than 5.3 million years) Volcanoes (or clusters where multiple volcanoes have indistinguishable ages) in the Yucca Mountain Region

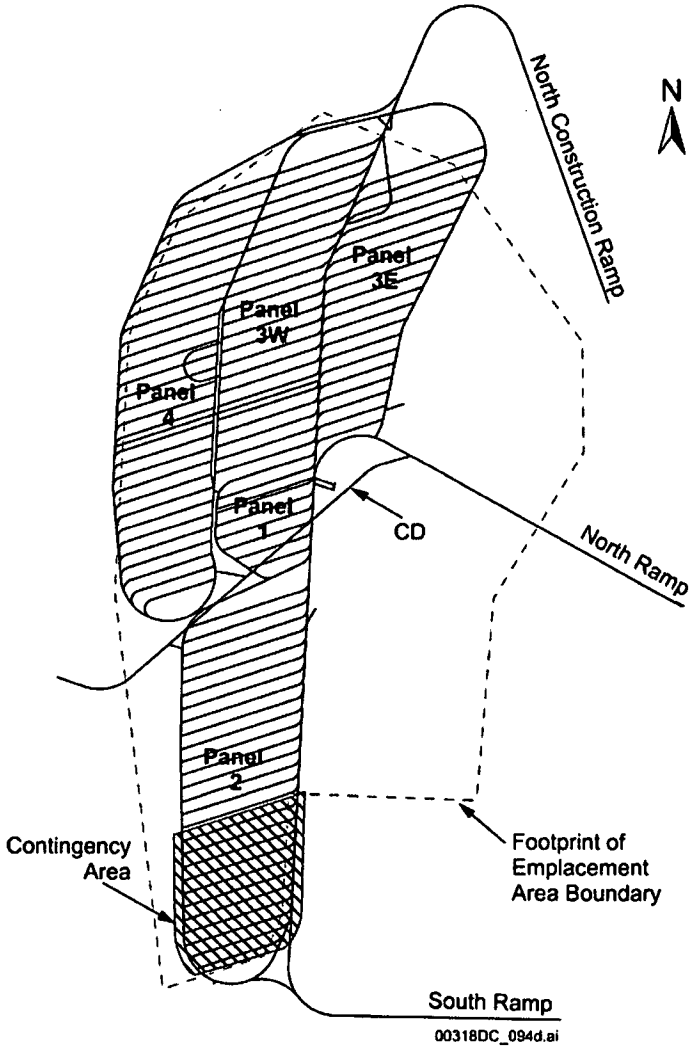

Source: Modified from SNL 2007 [DIRS 179466], Table 4-1, Parameter 01-02.

NOTE: CD = Cross Drift.

Figure 1-10. Subsurface Facility Layout

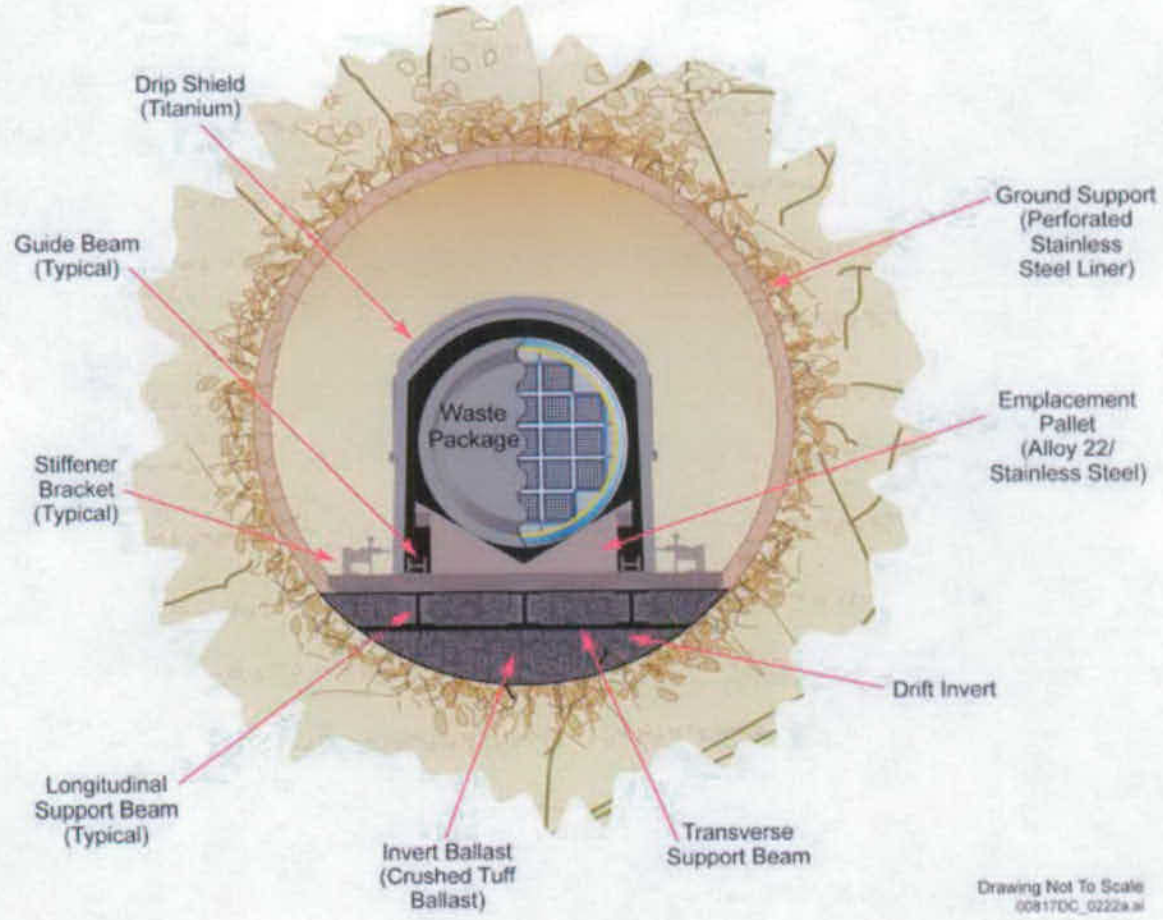

Source: Modified from SNL 2007 [DIRS 179354], Figure 4-1.

Figure 1-11. Cross Section Illustration of the Engineered Barrier System

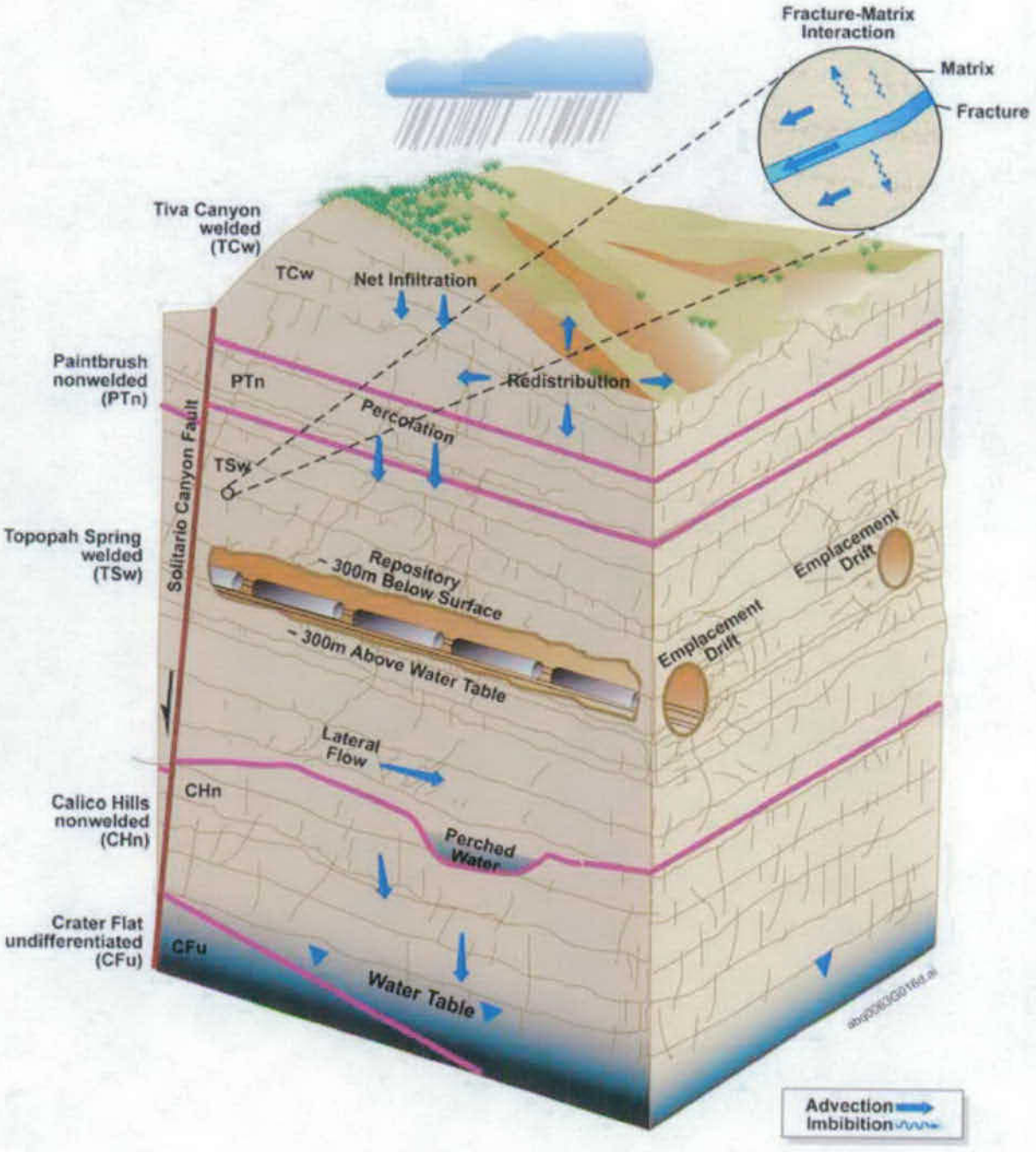

Figure 1-12. Conceptual Drawing of Mountain-Scale Flow Processes

Present-Day Climate

Yucca Mountain:
Regional Meteorological Stations

Monsoon Climate

Lower-bound analogue: Yucca Mountain
Upper-bound analogue: Nogales, AZ
Higher precipitation and temperature
than present-day climate

Glacial-Transition Climate

Lower-bound analogue: Delta, UT
Upper-bound analogue: Spokane, WA
Higher precipitation and lower
temperature than present-day climate

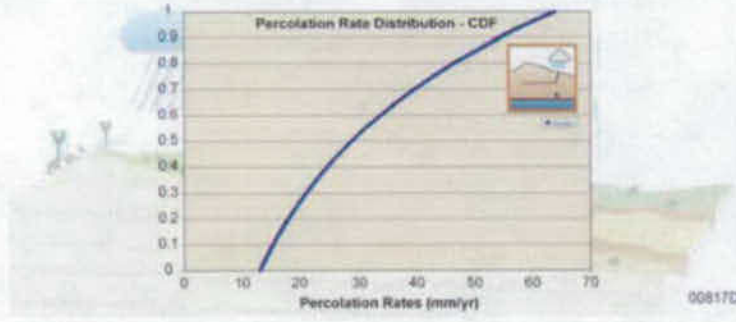

Post-10,000 Year Climate

Sampled value based on a log-uniform
probability distribution for deep percolcation
rates from 13 to 64 mm/yr
(10 CFR 63.324(c)(2) [DIRS 178394])

Figure 1-13. Illustration of the Four Climate States Used in the TSPA-SEIS and Present-Day Analogues of the Present-Day, Monsoon, and Glacial-Transition Climates

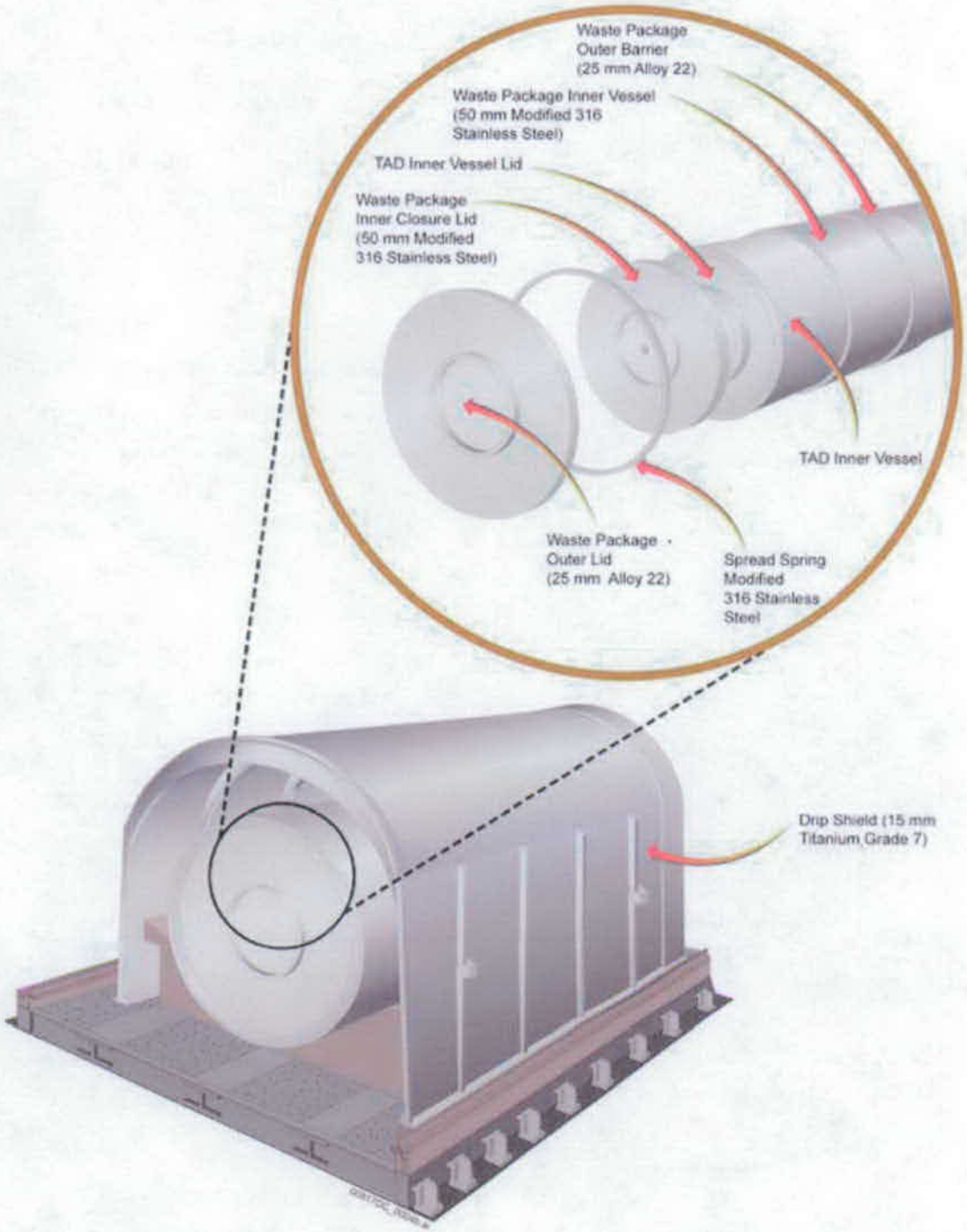

Figure 1-14. Schematic Design of the Drip Shield and Waste Package

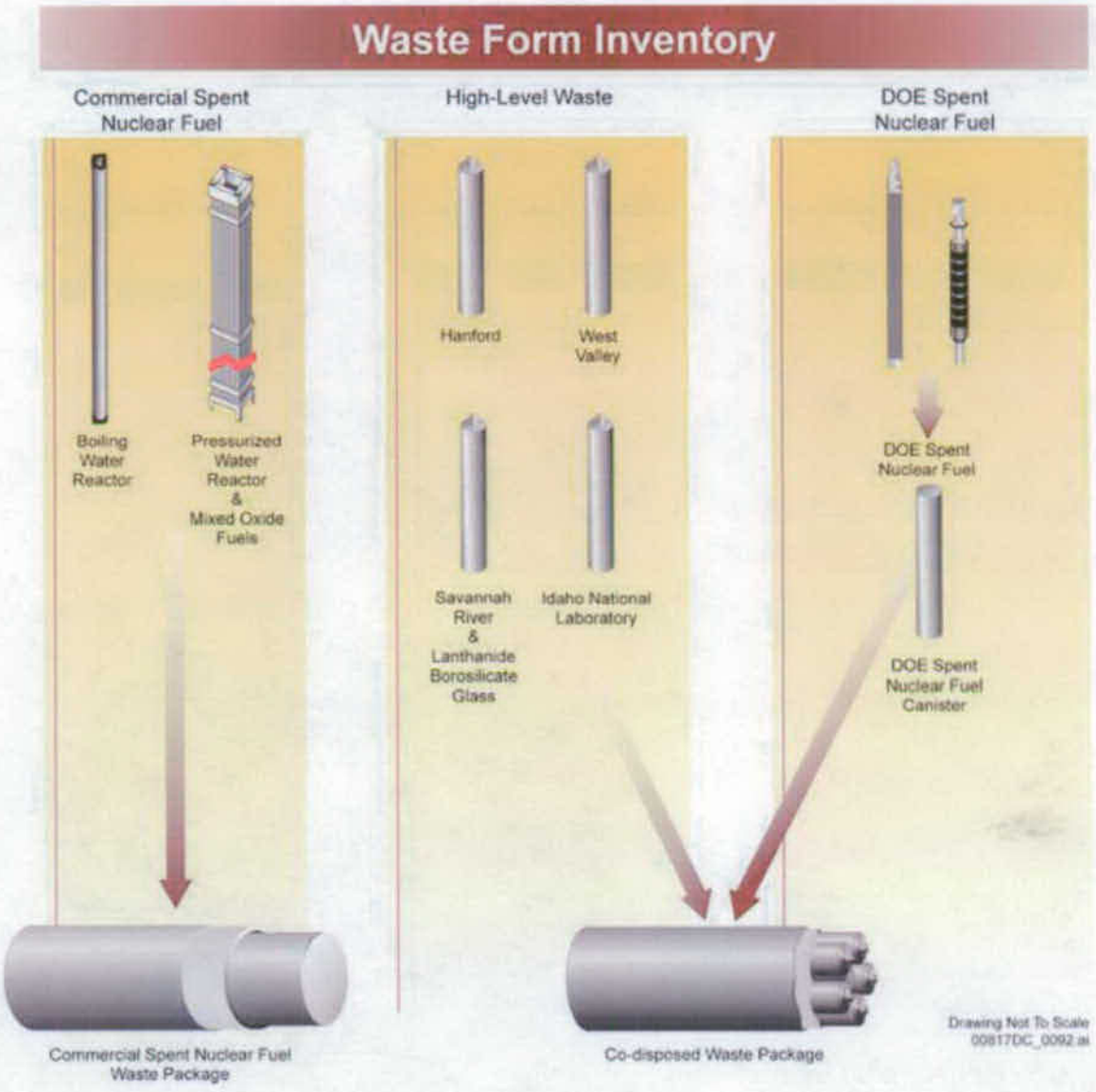

Source: Modified from SNL 2007 [DIRS 180472], Figure 6-1

NOTE: For modeling purposes, the naval fuels are treated as CSNF.

Figure 1-15. Three Waste Types Grouped into Two Representative Waste Packages: CSNF and CDSP WPs

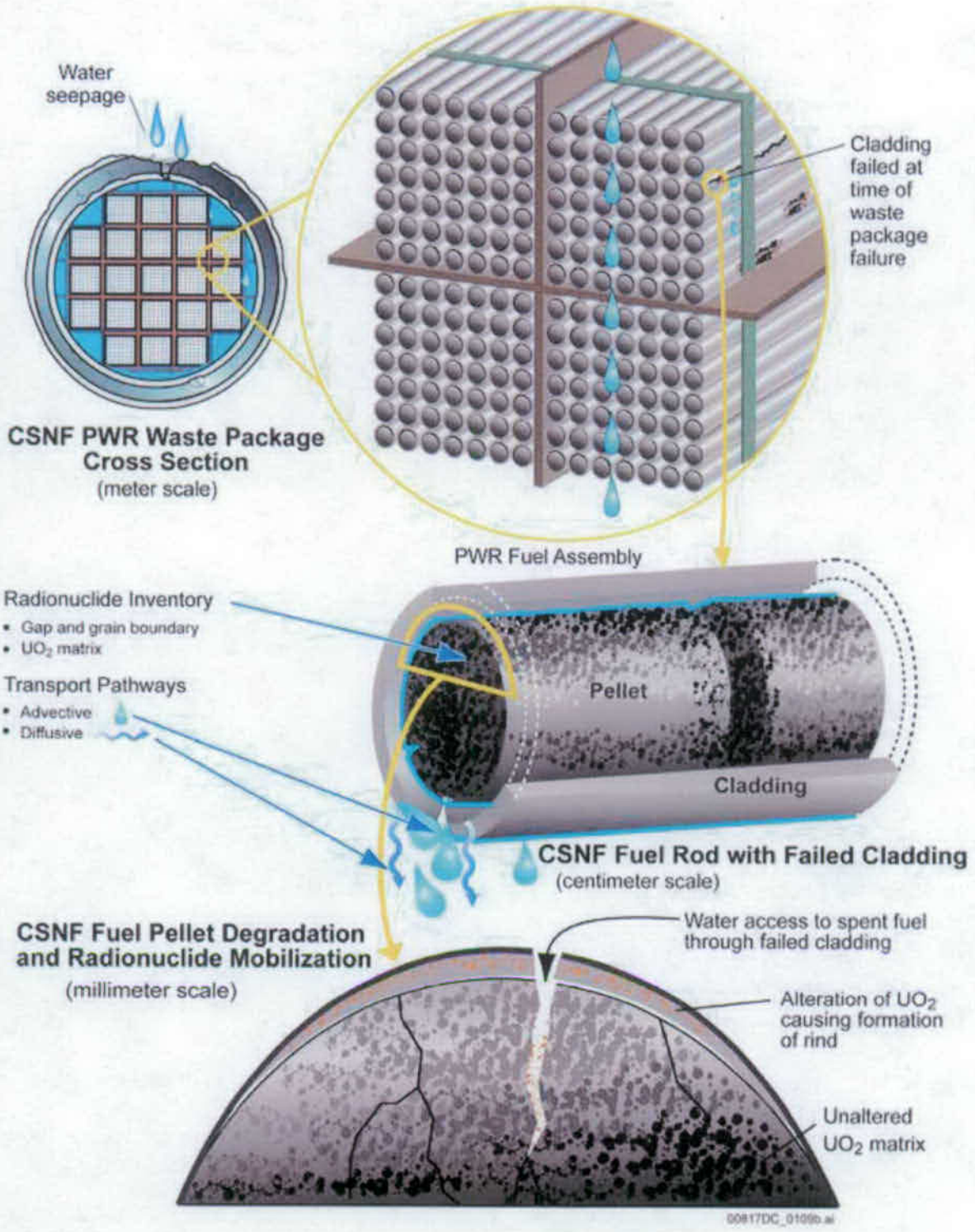

Figure 1-16. Schematic of CSNF Waste Form Degradation Mechanisms at Various Scales

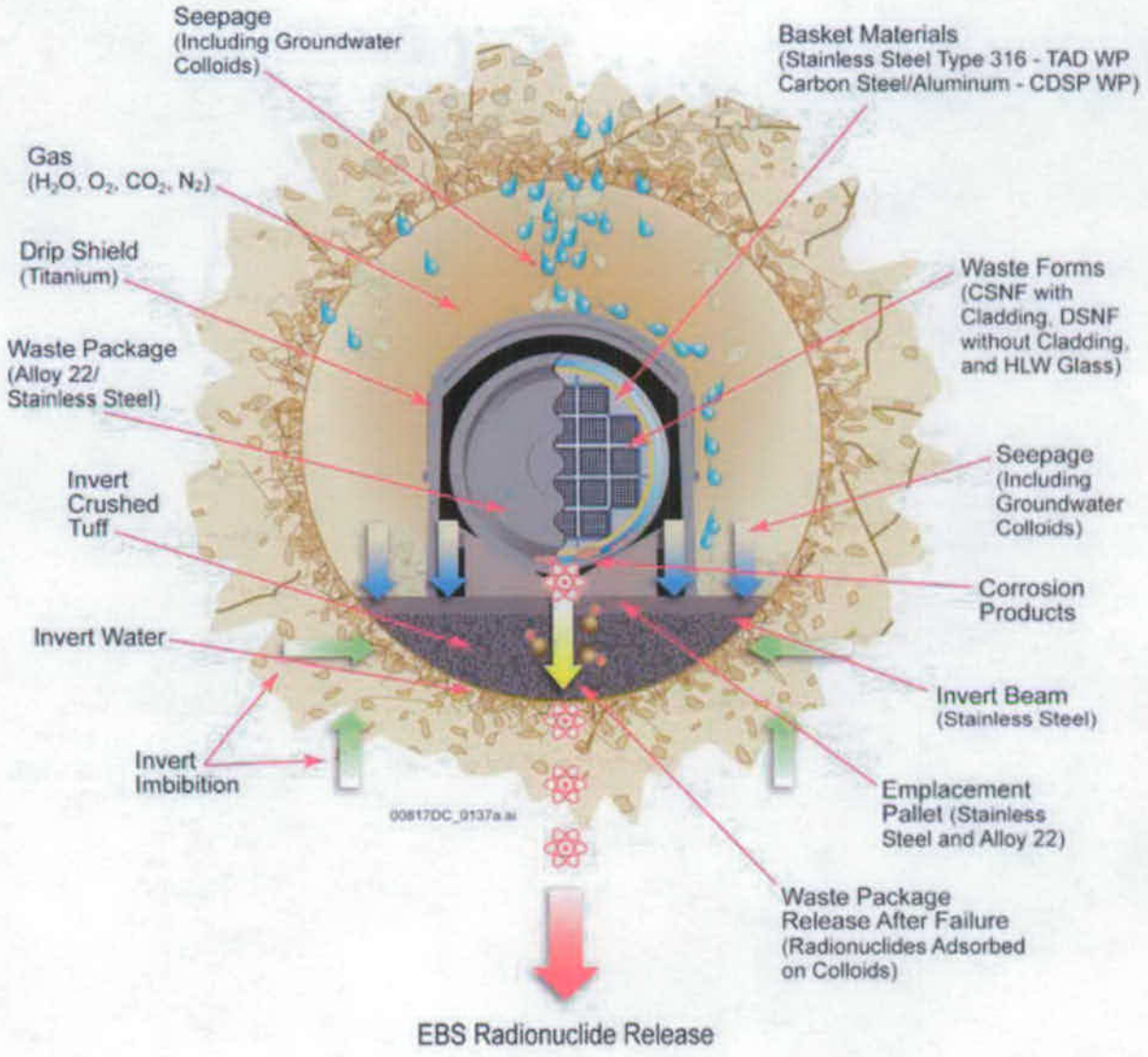

NOTE: Discussion and analysis of the features and processes illustrated on this figure can be found in *EBS Radionuclide Transport Abstraction* (SNL 2007 [DIRS 177407], Section 6.1.1, Figure 6.1-1).

Figure 1-17. General EBS Design Features and Materials, Water Movement, and Drift Degradation

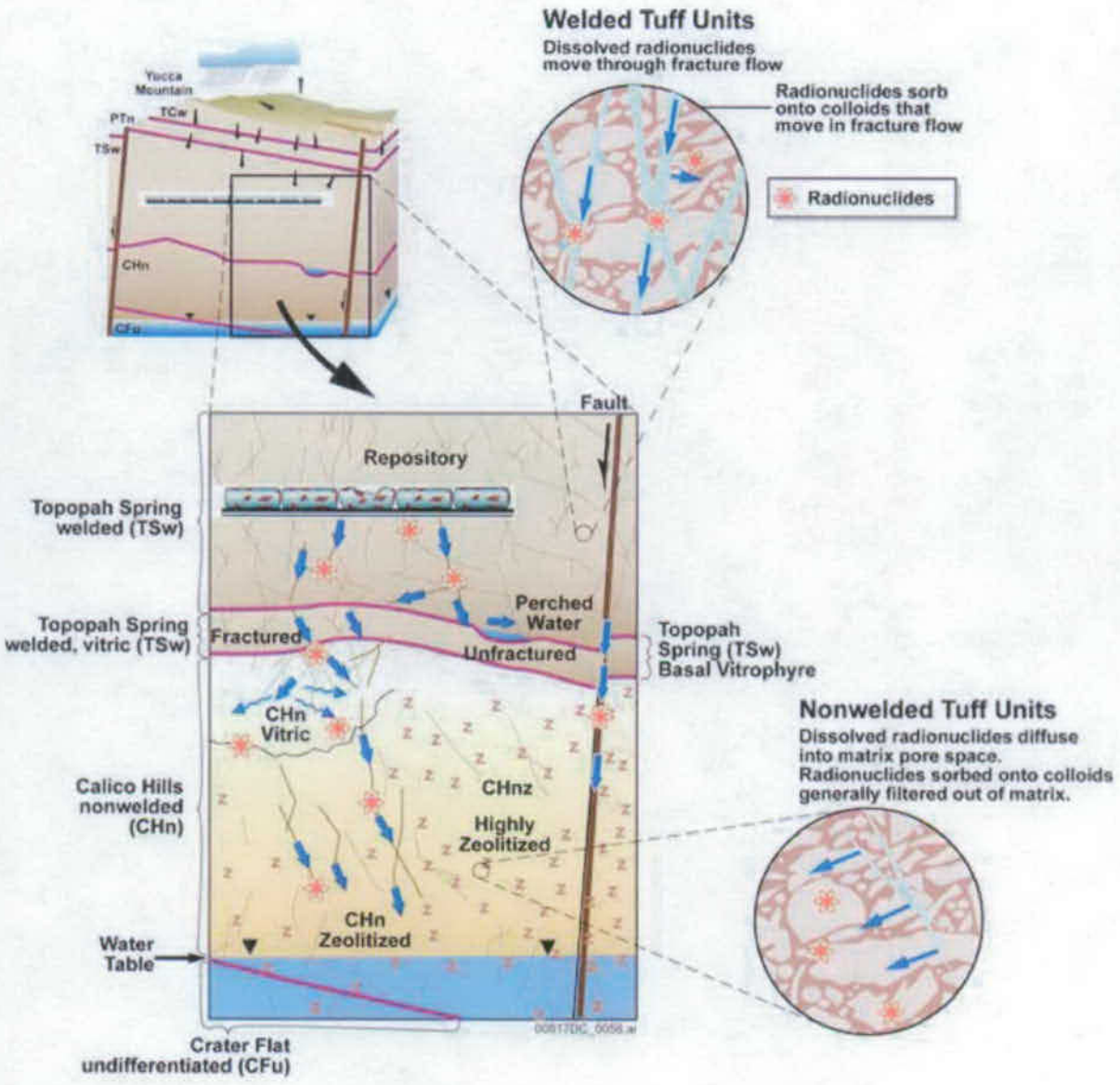

Figure 1-18. Conceptualization of Unsaturated Zone Transport Processes

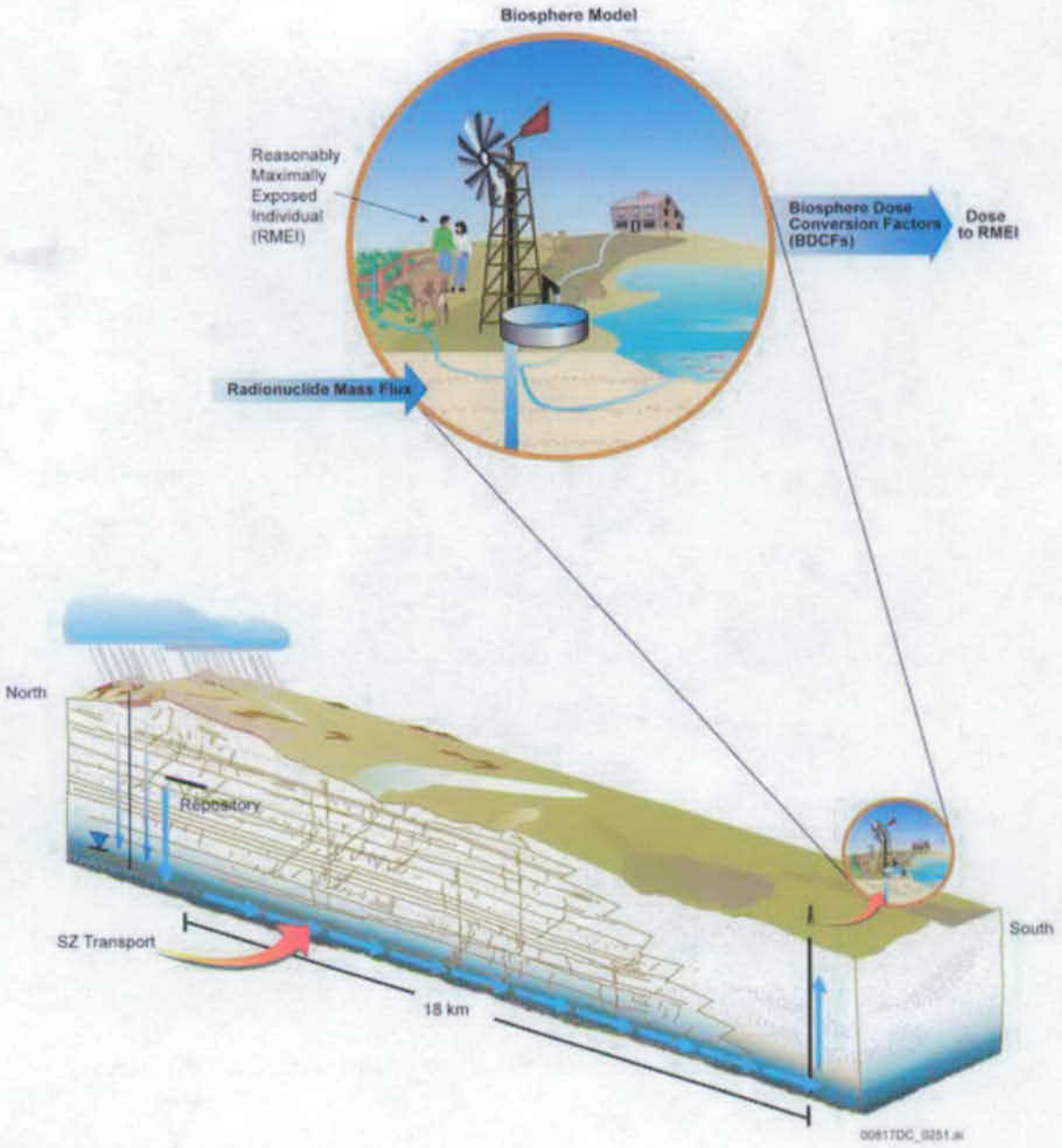

Figure 1-19. Overview of the Biosphere Groundwater Scenario Showing Groundwater Transport of Radionuclides and Uptake by the RMEI

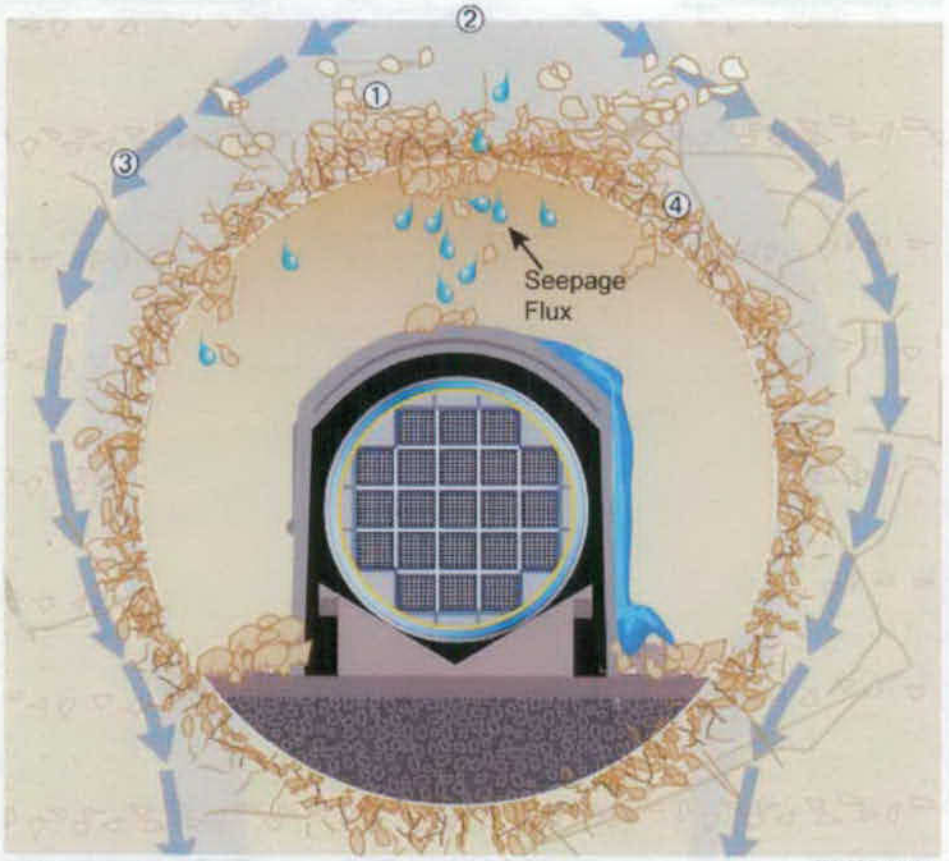

Source: Modified from SNL 2007 [DIRS 181244], Figure 6.3-1

Figure 1-20. Schematic Illustration of the Processes Affecting Ambient Drift Seepage

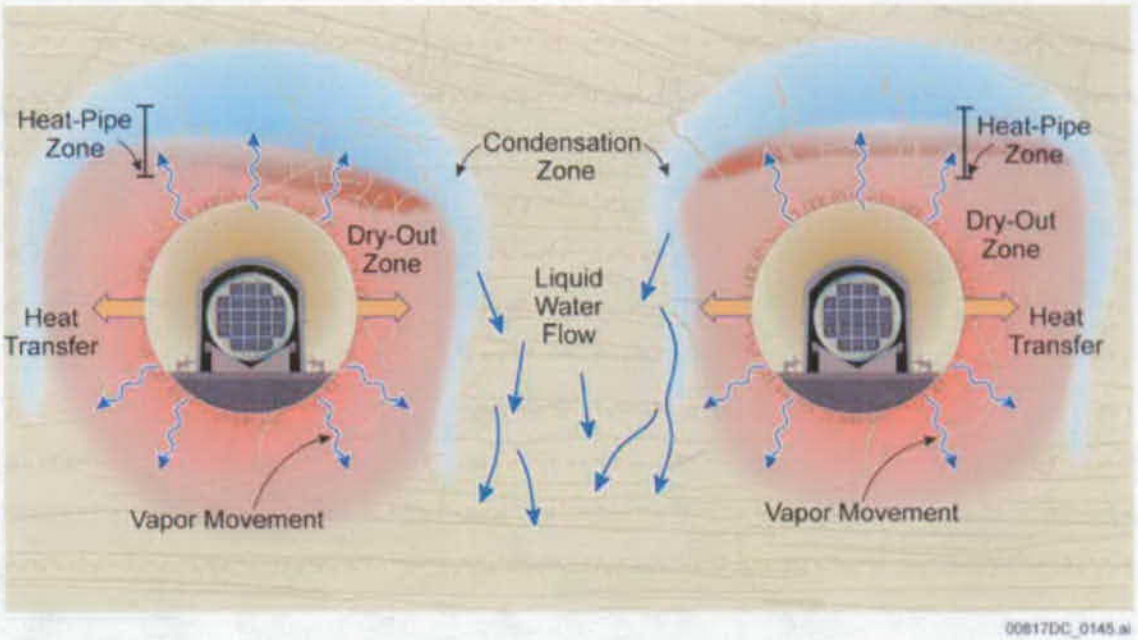

Source: Modified from BSC 2004 [DIRS 169734], Figure 5-81

Figure 1-21. Schematic Illustration (not to scale) of Thermal-Hydrologic Processes in the Vicinity of the Emplacement Drifts Due to Repository Heating

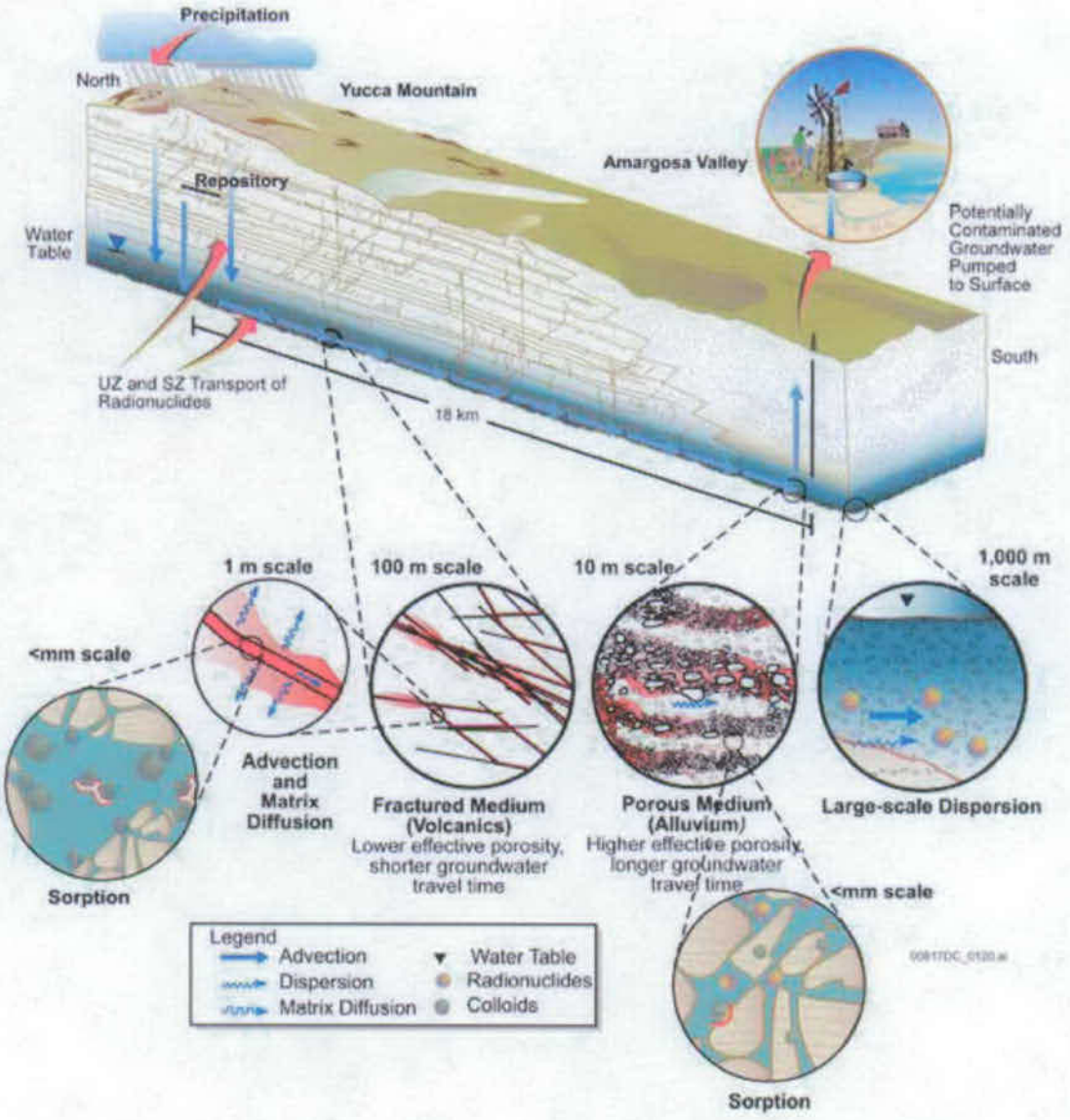

Figure 1-22. Conceptualization of Features and Processes Important to Saturated Zone Transport

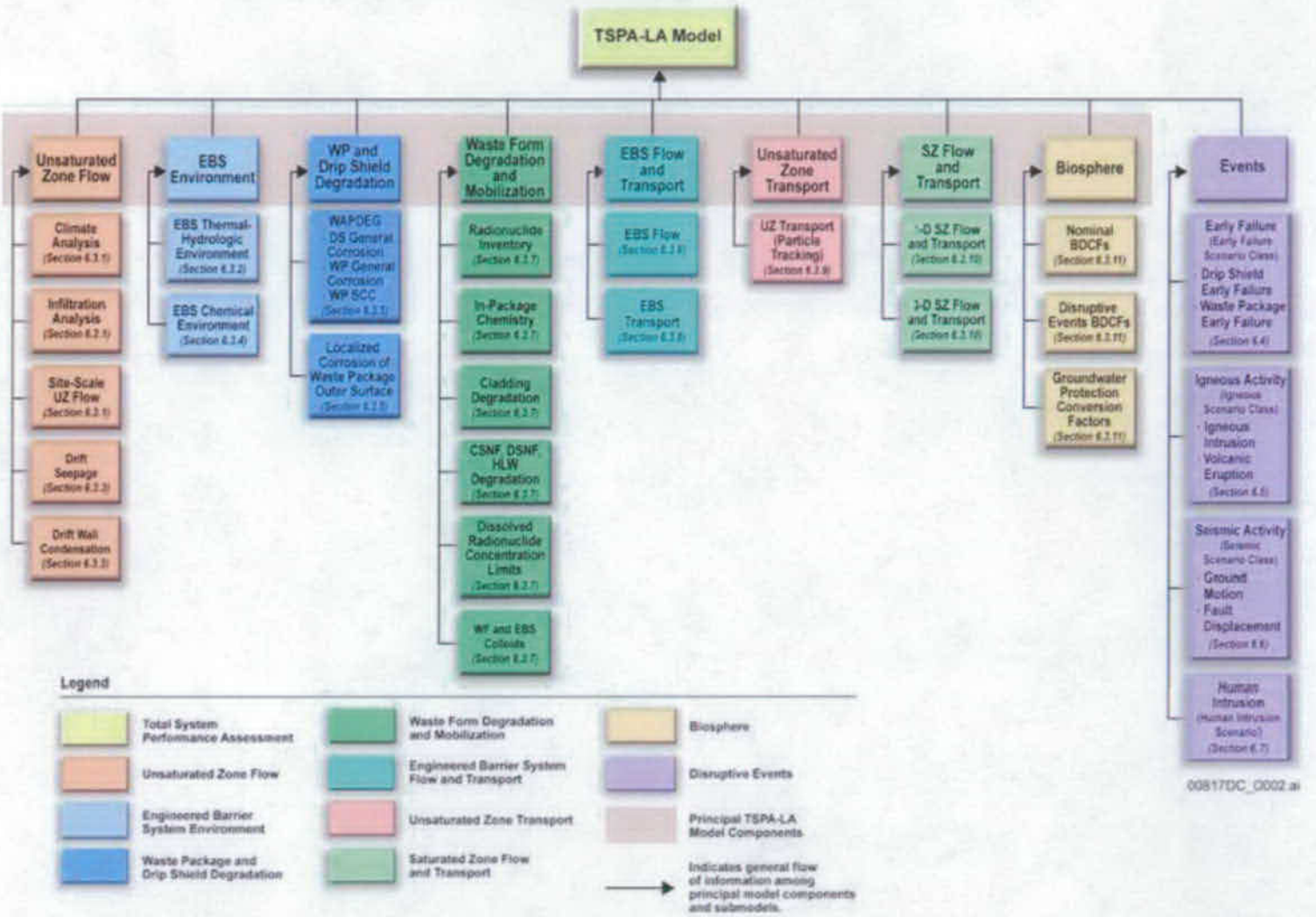

Note: Structure of the TSPA-SEIS Model is similar to the TSPA-LA Model

Figure 1-23.TSPA-SEIS Principal Model Components and Submodels

INTENTIONALLY LEFT BLANK

2. QUALITY ASSURANCE

The OCRWM QA program is first codified and implemented in the *Quality Assurance Requirements and Description* (QARD) (DOE 2007 [DIRS 182051]). The QARD (DOE 2007 [DIRS 182051]) applies to this technical product.

2.1 CONFIGURATION MANAGEMENT

The development of the TSPA-SEIS required organization, control, and accountability. In the language of Configuration Management, this translated into implementing the following four processes:

- **Configuration Identification**—This is the unique identification of all the items to be managed in the system. Configuration identification consists of selecting the items to be managed and recording their functional and physical characteristics.

- **Configuration Change Control**—This is the mechanism used to approve or disapprove all proposed changes to the system that is being managed. Configuration change control ensures that changes to any configuration items are approved and controlled so that consistency among components is maintained.

- **Configuration Status Accounting**—This is used to ensure that information contained in the status accounting system, documents the evolution of the TSPA-SEIS in a transparent and traceable manner.

- **Review**—The review process checks the configuration items to verify that they are uniquely identified, described and managed in the system.

The software development procedures (i.e., IM-PRO-003, *Software Management*; IM-PRO-004, *Qualification of Software*; IM-PRO-005, *Software Independent Verification and Validation*; and IM-PRO-006, *Software Independent Verification and Validation of Legacy Code*) implement these Configuration Management processes for software development. However, to efficiently manage the development of the TSPA-SEIS, the same configuration management processes (e.g., Configuration Identification and Configuration Change Control) mentioned previously, were used in the form of workplace controls. Summaries of the controls placed on software development, model development, and input development are provided in the sections that follow.

2.1.1 Configuration Management of Software

All software codes used to support the TSPA-SEIS were qualified in accordance with project software development procedures. These procedures establish the roles and responsibilities for the organizations responsible for implementing the four configuration management processes described previously. The first three processes below were administered by the SCM organization. The fourth process below was administered by the Software Independent Verification and Validation organization.

1. **Configuration Identification**—Each piece of software and its supporting documentation was uniquely identified with a software tracking number (STN) and document number, respectively.

2. **Configuration Change Control**—After software was qualified in accordance with the software development procedures and placed on the software baseline, only then approved changes were made.

3. **Configuration Status Accounting**—This process kept track of the status of software during software development and operations. The following are examples of the items tracked: (a) descriptions of the primary function of the software; (b) versions of documents and media; (c) software users; (d) software status, such as active, retired, or canceled; and (e) descriptions of operating platforms and systems.

4. **Review**—The details of the review process are established in IM-PRO-005, *Software Independent Verification and Validation* (LP-SI.13Q-BSC, *Software Independent Verification and Validation,* and AP-SI.3Q, *Software Independent Verification and Validation*, for earlier code qualifications). This review ensures that software requirements are adequately written and traced through the software documentation and that each requirement is verified by validation testing. Additionally, the review ensures that the documentation is reviewed by a qualified individual without recourse to the originator.

The specific codes used in the TSPA-SEIS are discussed in detail in Section 3. Section 3 also expands the discussion of the SCM functions mentioned in Items 1 through 3.

2.1.2 Configuration Management of the Development of the TSPA-SEIS

The development of the TSPA-SEIS required modifications from time to time for a number of reasons. This section presents the management control system that was implemented to track and maintain a record of these changes, as illustrated on Figure 2-1.

New or revised analysis and/or model reports were developed for the TSPA-SEIS. During the development of new or revised analysis and/or model reports, the TSPA Analysts consulted with the SMEs to define the technical output of their analysis and/or model reports for use in the TSPA-SEIS. Draft information, such as preliminary data tracking numbers (DTNs) and preliminary TSPA Data Input Packages, was provided for initial implementation and inserted into the TSPA-SEIS. This information included relevant process models, model abstractions,

and submodels that are contained in the analysis and/or model reports. The appropriate SMEs have reviewed the results of the initial implementation to ensure that the implementation is consistent with each SME's intent. Discrepancies were addressed by changing the implementation of the submodels or model abstractions in the TSPA-SEIS and/or by changing the supporting analyses and/or model reports and/or DTNs prior to their approval.

In addition, new or revised analysis and/or model reports developed for the TSPA-SEIS were reviewed by the TSPA Department according to SCI-PRO-003, *Document Review*. Part of this review determined whether or not changes to the TSPA-SEIS were needed and if the changes were within the TSPA-SEIS development scope and schedule.

Internal TSPA-SEIS changes, such as a change in model logic to select specific parameters for individual modeling cases, were identified as part of TSPA-SEIS development. The TSPA Department Manager reviewed and approved changes to the TSPA-SEIS development scope and schedule to accomplish required revisions to the analyses and/or model reports and/or the TSPA-SEIS inputs developed by the analysis and/or model reports. Changes outside the TSPA-SEIS development scope and schedule elevated the issue(s) to the appropriate management level for resolution. Management approval of changes to the TSPA-SEIS were based in part on whether or not a change was necessary to comply with regulatory requirements, regardless of the final input feed date for the requested change, or whether the TSPA-SEIS was finalized or frozen for performing TSPA-SEIS analyses.

Changes to the TSPA-SEIS were tracked by the TSPA Department. Figure 2-2 shows the TSPA Model Change Approval Form used to track the changes to the TSPA-SEIS. During the development stage of the TSPA-SEIS, TSPA Analysts were required to obtain written approvals from the TSPA Department Manager, TSPA Model Calculations Lead, and TSPA Configuration Management Lead, to change and/or introduce, new process models, model abstractions, or parameters into the TSPA-SEIS. The written authorization specified the source(s) (e.g., analysis and/or model reports, DTNs) of the process models, analyses models, model abstractions, or input parameters.

Another important aspect regarding the control of the TSPA-SEIS is ensuring consistent, well-documented inputs. The supporting organizations provide abstractions and technical product output to the TSPA-SEIS according to a scope and schedule review. The most recent scope and schedule reviews were led by the Performance Assessment System Integration Team. The reviews resulted in the addition of detailed requirements and specifications to the technical work plans for each work package containing an analysis and/or model report. Additional requirements were incorporated into revisions to the TWPs that specified content for FEPs, ACMs, parameters, and characterization of uncertainty for the TSPA-SEIS.

The detailed plan for the systematic treatment of uncertainty in support of the TSPA-SEIS supporting documents was intimately linked to this overall strategy of placing more management emphasis and control on the development of inputs to the TSPA-SEIS. These additional product management emphases and controls included:

- A consistent model hierarchy and structure supporting the TSPA-SEIS architecture

- A consistent treatment and documentation of model abstractions supporting the TSPA-SEIS
- A consistent treatment and documentation of ACMs
- A consistent treatment and documentation of FEPs included in the TSPA-SEIS, as well as how the FEPs were included and where their inclusion was documented
- A consistent evaluation of the definition and performance of the natural and engineered barriers of the repository system and the basis for the projection of barrier performance
- A consistent evaluation of parameter uncertainty and how that uncertainty is propagated through the model hierarchy to the TSPA-SEIS and how the significance of that uncertainty is evaluated
- A consistent documentation of how the TSPA-SEIS components and submodels are integrated and how the information flows between the submodels and the analyses, including roadmaps of information supporting the TSPA-SEIS
- A consistent basis for determining the appropriate amount of confidence required for model validation
- A consistent evaluation of the parameter values that were used to develop parameter distributions and why those parameter values are sufficient to capture the range of possible observations.

The above emphases determined much of the content of the analysis and/or model reports that support the TSPA-SEIS and postclosure safety case for presentation in the LA. These analysis and/or model reports remain the primary supporting documentation for the TSPA-SEIS. Updated TWPs for each of the supporting analysis and/or model reports ensured that the scope was assigned appropriately (i.e., FEP by FEP, model by model, and parameter by parameter).

The more detailed scope definitions that resulted from the above process yielded a much more consistent and comprehensive treatment of, not only parameter uncertainty, but also FEP uncertainty and ACM uncertainty. The process also allowed for early definition of the scope and content of the TSPA-SEIS within the context of the document, as agreed to in several Total System Performance Assessment Integration Key Technical Issue agreements. This more detailed scope definition has allowed the authors of analysis and/or model report authors to focus on the key performance-related aspects of their models and analyses in a more risk-informed way.

Physical Control of Files—The TSPA-SEIS input files, DLLs, and the database were controlled by their storage in a set of controlled subdirectories on the TSPA file server.

Input Files—Input files for the TSPA-SEIS were stored in a controlled subdirectory on the TSPA file server. Read access to this subdirectory was limited to the TSPA Department staff. Write access was limited to the TSPA-SEIS Configuration Management staff and the System

Administrator. The TSPA-SEIS Configuration Management staff established a baseline list of files. Any subsequent changes to the input files were documented as changes to the baseline list.

DLLs—DLLs for the TSPA-SEIS were obtained from SCM and installed in a controlled subdirectory on the TSPA file server by the TSPA-SEIS Configuration Management staff. Read access to this subdirectory was limited to the TSPA Department staff. Write access was limited to the TSPA-SEIS Configuration Management staff and the System Administrator. The TSPA-SEIS Configuration Management staff established a baseline list of DLLs, and any subsequent changes to the DLLs were documented by the TSPA-SEIS Configuration Management staff as changes to the baseline list.

Input Parameters—Both fixed-value and uncertain input parameters for the TSPA-SEIS were controlled in the TSPA Input Database described in Section 4.4. The database was stored in a controlled subdirectory on the TSPA file server. Read access to this subdirectory was limited to the TSPA Department staff. Write access was limited to the TSPA-SEIS Configuration Management staff and System Administrator. Changes to the database were controlled via the change control and checking process used for the TSPA-SEIS.

Change Control and Checking—Table 2-1 summarizes the forms, checklists, descriptions, and logs used to manage the change control and checking of the TSPA-SEIS.

The TSPA-SEIS GoldSim model file was checked by qualified individuals assigned by the TSPA Model Calculations Lead. The checker is usually another TSPA Analyst who was not involved in modifying the model file or input file(s).

Two types of checks were performed on updated versions of the TSPA-SEIS GoldSim model file: implementation checking and conceptual model checking. Implementation checking verifies that all of the changes to the TSPA-SEIS file and/or external files were performed correctly. Conceptual model checking considers whether the TSPA-SEIS implementation correctly reproduces the conceptual process model or model abstraction from the associated analysis and/or model report, submodel, or scientific analysis.

Implementation Checking—Implementation Checking was completed by reviewing the changes identified by the analyst in a checklist similar to Figure 2-3 and then documenting completion to the following steps in a second checklist similar to Figure 2-4. The primary steps involved in Implementation Level checking included:

- Checking modified GoldSim elements against their source information to verify that they were changed correctly
- Verification that the input links of added elements were correct
- Verification that the output links of added parameters were correct
- Checking that the links to and from any deleted elements were appropriately reconnected

- Verification (by inspecting source references for changes) that each change to an external file was correct.

Concept Level Checking – The Concept Level Checking process considers whether the changes to the TSPA-SEIS correctly reflect conceptual model changes using a checklist similar to Figure 2-5. The conceptual description includes a general description of changes made to the TSPA-SEIS. Any development and testing work to support changes to the TSPA-SEIS were documented in the conceptual description.

Any differences between the results of the initial and modified modeling case(s) were explained and properly documented by the checker and/or analysts in terms of the changes made to the TSPA-SEIS.

The details of the Implementation and Concept checks are described in a series of Desk Guides used by the TSPA Department.

2.1.3 Configuration Management for the TSPA-SEIS Input

The TSPA-SEIS was developed by making incremental changes to the TSPA Final Environmental Impact Statement Model (Williams 2001 [DIRS 157307]). Each of these incremental changes had a set of input files and parameters that were saved and/or archived on the designated TSPA Department server. The DLLs and their associated input files were not embedded in the TSPA-SEIS file but were saved or archived separately as file sets, whereas the input parameters used for each TSPA-SEIS run, were captured in each of the incremental TSPA-SEIS files and in the final TSPA-SEIS file, upon which this document is based. The TSPA-SEIS file and all associated inputs were submitted to the TDMS database in accordance with TST-PRO-001, *Submittal and Incorporation of Data/Technical Information to the Technical Data Management System.*

The input files are the files that are necessary to run each of the DLLs. The DLL input files used during the development of the TSPA-SEIS were numbered (e.g., Input File Set 1, Input File Set 2, and so on). The Input File Set used for each model change was documented on the TSPA-SEIS Change Approval Form (Figure 2-2). An electronic copy of each file set was saved on the designated TSPA Department file server.

The TSPA Input Database, which is described in Section 4.7, is electronically linked at run time to the TSPA-SEIS. The TSPA Input Database is a controlled warehouse of all of the input parameters used to run the TSPA-SEIS. An important configuration management feature of the TSPA Input Database is that the TSPA Input database supports the independent verification of every value used in the TSPA-SEIS. For example, a TSPA Analyst is assigned the task of verifying that for a given parameter value or set of values, the reference information used to find the value is within the reference. Once the TSPA Analyst has confirmed the value in the database is the same as the value in the reference, then the TSPA Analyst clicks a verification button in the TSPA Database for the given parameter, thereby indicating that the parameter is verified. If the parameter value or reference information is edited, then the TSPA Input Database indicates that the parameter is no longer verified. The TSPA Input Database verification feature

ensures that any preliminary input parameters are confirmed to be consistent with the formal reference such as an analysis and/or model report or DTN.

The parameter values are obtained from controlled sources maintained by the project data and information systems, such as project documents, TDMS, and Technical Information Center. The TDMS database is a project-wide database, whereas the TSPA Input Database is used only for the TSPA-SEIS. Each of the parameter sets used in the TSPA Input Database has a DTN to provide the link to the TDMS database or a reference to the controlled source of the information, such as an analysis and/or model report. The TDMS maintains the qualification status of all of its contents. In closing, the TSPA Model inputs are controlled and well documented by using the TSPA Input Database. Additional details on the control and documentation of the sources of the data can be found in Section 4.

INTENTIONALLY LEFT BLANK

Table 2-1. Configuration Control Documents for the TSPA-SEIS

Figure Number	Name	Purpose
2-2	TSPA-SEIS Change Approval Form	Provides management control of all changes to the TSPA-SEIS. Summarizes the extent of the change.
2-3	TSPA-SEIS Changes Checklist	Initiated by the TSPA analyst. Documents the specific changes made to the TSPA-SEIS (parameter checking). Checker uses this list of changes to check.
NA	Conceptual Description	Provides overview of the changes that were incorporated into the TSPA-SEIS. May also include development and checking work that was performed to support the change.
2-4	TSPA-SEIS Implementation Checklist	Documents the answers to parameter check questions. Conceptual checking and Configuration Management check.
NA	GoldSim Version Report (Run Log)	Provides record of specific changes made to the GoldSim model file (generated by GoldSim).
2-5	TSPA-SEIS Concept Checklist	Documents the answers to concept check questions.

INTENTIONALLY LEFT BLANK

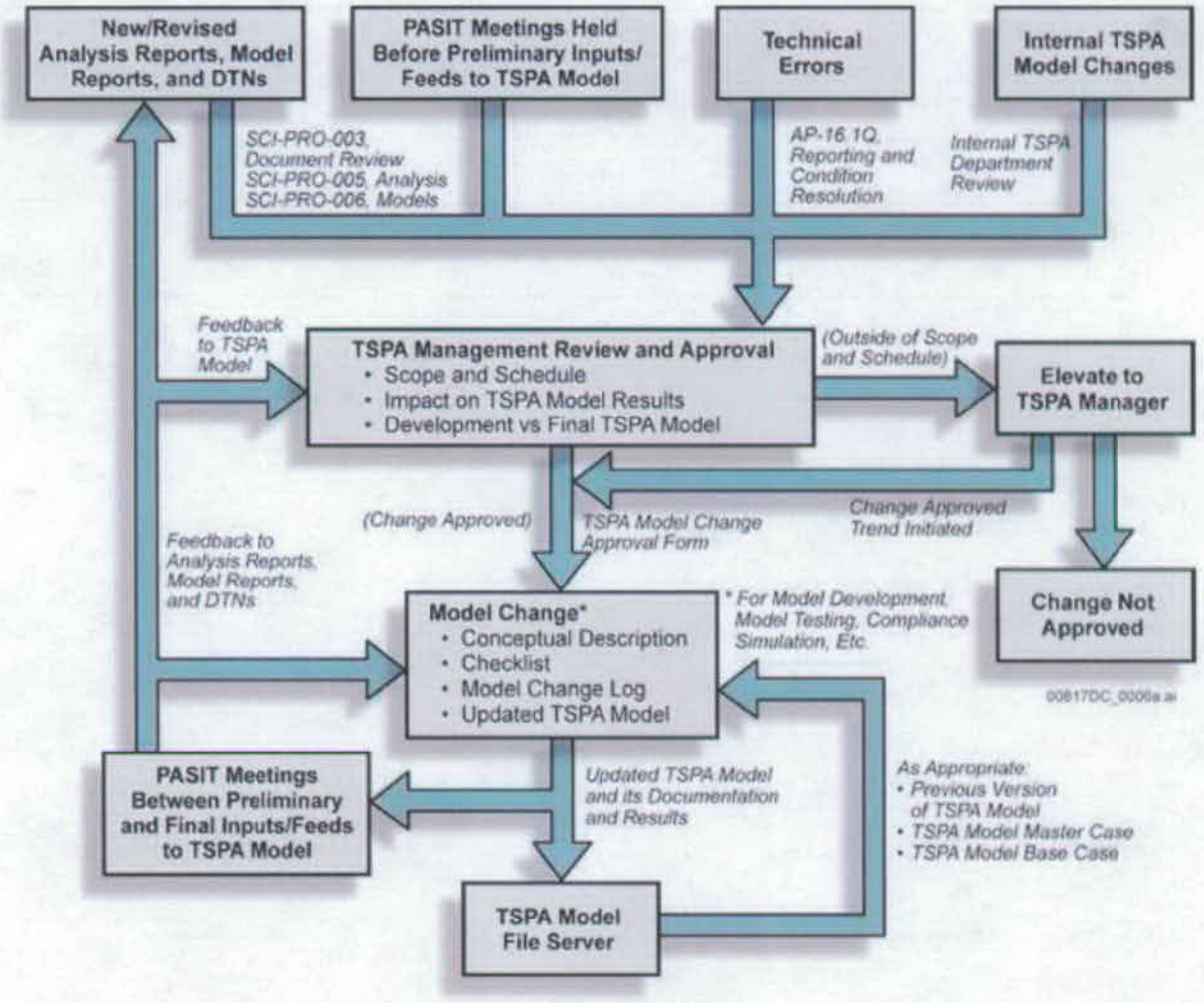

Figure 2-1. Flowchart Illustrating the Management Control Process for the TSPA-SEIS

TSPA Analyst:	Date:
Input File Set:	DLL Set:
Change to TSPA Database?	Change due to Parameter Source?
Change Number:	Model Version:
Basis for Proposed Change:	
Description of Proposed Change:	
Model Freeze Date:	Expected Change Date:
Modeling Stage: ___ Development ___ Production ___ Post-production	

Reviewer Signatures	Date	Approval (yes/no)
TSPA Model Calculations Lead		
TSPA Configuration Management Lead		
TSPA Department Manager		
Performance Assessment Manager		
Comments Attached? No		

00817DC_0007.ai

Figure 2-2. Example of the TSPA-SEIS Change Approval Form

Model ID:				
TSPA Analyst:		Date:		
Checker:		Date:		
Parameter, Element, etc.	Location	Description of Change	Comment / Resolution	Correct? Y/N /Initials
Background color denotes changes are made within the **Epistemic_Params** submodel				
Background color denotes changes are made within the **Aleatory_Params** submodel				
Background color denotes changes are made within the **EBS_Submodel** submodel				

00817DC_0006.ai

Figure 2-3. Example of the TSPA-SEIS Change Checklist

Model ID:			TSPA Analyst Name: Signature:
Checker Name: Signature:			Date:
No.	Check Questions	Y, N, or NA	Notes
1.00	**Master Case Folder**		
1.01	Are the change approval form(s) included? (Both the word file and the signed PDF file)		
1.02	Is the conceptual description file included? (Both the word file and the signed PDF.)		
1.03	Is the version report included?		
1.04	Is the Master Case Change Checklist file included? (Both the word file and the signed PDF)		
1.05	Is the Master Case GoldSim file included without results?		
1.06	Are all other files, if any, placed in the Additional_Information directory (including all external files modified for the Master Case and all Base Cases)?		
2.00	**Nominal Base Case Directory or Directories**		
2.01	Is/are the GoldSim file(s) included with results?		
2.02	Is/are the Change Checklist file(s) included? (Both the word file and the signed PDF file)		
2.03	Is/are the version report(s) included?		
2.04	Do all entries in the version report(s) match the checklist(s)?		
2.05	If there are any additional files associated with the Nominal Base Case(s), is/are they located in the Additional_Information directory?		
2.06	Compared to the Master Case, are there any additional scenario specific changes, other than simulation settings, required to run the Nominal Base Case(s) from the Master Case?		
3.00	**Human Intrusion Base Case Directory or Directories**		
3.01	Is/are the GoldSim file(s) included with results?		
3.02	Is/are the Change Checklist file(s) included? (Both the word file and the signed PDF file)		
3.03	Is/are the version report(s) included?		
3.04	Do all entries in the version report(s) match the checklist(s)?		
3.05	If there are any additional files associated with the Human Intrusion Case(s), is/are they located in the Additional_Information directory?		
3.06	Compared to the Master Case, are there any additional scenario specific changes, other than simulation settings, required to run the Nominal Base Case(s) from the Master Case?		
4.00	**Early Failure Base Case Directory or Directories**		
4.01	Is/are the GoldSim file(s) included with results?		
4.02	Is/are the Change Checklist file(s) included? (Both the word file and the signed PDF file)		
4.03	Is/are the version report(s) included?		
4.04	Do all entries in the version report(s) match the checklist(s)?		
4.05	If there are any additional files associated with the Early Failure Case(s), is/are they located in the Additional_Information directory?		
4.06	Compared to the Master Case, are there any additional scenario specific changes, other than simulation settings, required to run the Nominal Base Case(s) from the Master Case?		

00817DC_0009.ai

Figure 2-4. Example of the TSPA-SEIS Implementation Checklist

Model ID:	TSPA Analyst Name: Signature:
Checker Name: Signature:	Date:

No.	Check Questions	Y, N, or NA	Notes
5.00	**Igneous Base Case Directory or Directories**		
5.01	Is/are the GoldSim file(s) included with results?		
5.02	Is/are the Change Checklist file(s) included? (Both the word file and the signed PDF file)		
5.03	Is/are the version report(s) included?		
5.04	Do all entries in the version report(s) match the checklist(s)?		
5.05	If there are any additional files associated with the Igneous Base Case, are they located in the Additional_Information directory?		
5.06	Compared to the Master Case, are there any additional scenario specific changes, other than simulation settings, required to run the Igneous Base Case(s) from the Master Case?		
6.00	**Seismic Base Case Directories**		
6.01	Is/are the GoldSim file(s) included with results?		
6.02	Is/are the Change Checklist file(s) included? (Both the word file and the signed PDF file)		
6.03	Is/are the version report(s) included?		
6.04	Do all entries in the version report(s) match the checklist(s)?		
6.05	If there are any additional files associated with the Seismic Base Case(s), are they located in the Additional_Information directory?		
6.06	Compared to the Master Case, are there any additional scenario specific changes, other than simulation settings, required to run the Seismic Base Case(s) from the Master Case?		
7.00	**Change Control Check**		
7.01	Does/Do the Change Approval Form(s) need to be revised to address additional scope discovered during version change?		
7.02	Does the Master Case originate from the previous Master Case?		
7.03	Are all input file transfers controlled by the Input Database and associated file elements?		
7.04	Are all DLL file transfers controlled by the Input Database and associated file elements?		
7.05	Was the Master Case versioned before the Base Cases were run?		
7.06	Was a database download performed before running the Base Cases?		
7.07	If this Master Case requires changes to an external file, are copies of the modified files placed in the Additional_Information directory for the Master Case?		
7.08	Is the Master Case checklist consistent with the Master Case Goldsim version report?		
7.09	Are all changes associated with input changes and conceptual model changes documented with sufficient source information in the checklist? (i.e. TMRB proposal #, DTN change, error log entry, new AMR etc.)		
7.10	Are the Base Case checklists consistent with the Base Case Goldsim version reports?		

00817DC_0010.ai

Figure 2-4. Example of the TSPA-SEIS Implementation Checklist (Continued)

Model ID:			TSPA Analyst Name: Signature:
Checker Name: Signature:			Date:
No	Check Questions	Y, N, or NA	Notes
8.00	**Element Level Check**		
8.01	Are all new inputs, if any, added to the Input Database? Are new input elements connected to the Input Database?		
8.02	Have all changed/added Goldsim elements been checked against their source information to verify that they were changed correctly?		
8.03	If a cloned element was changed, was the changed element and at least one of its clones checked to be identical?		
8.04	Are the input links of added elements correct?		
8.05	Are the output links of added parameters correct?		
8.06	Are the links to and from any deleted elements appropriately reconnected?		
8.07	Are all changes to external files correct?		
9.00	**Conceptual Level Check**		
9.01	Is the conceptual description consistent with the change approval form?		
9.02	Is the Master Case Change Checklist consistent with the conceptual description?		
9.03	Are all conceptual model changes made in the Master Case?		
9.04	Is mass conserved within each major subsystem?		
9.05	Can each entry in the GoldSim run log be shown to have no/negligible impact on the run?		
10.00	**Error Tracking**		
10.01	Are there any model errors in this case that will be addressed in a future version of the model?		
10.02	Are errors noted by 10.01 adequately described in the error log, including a proposed correction?		
10.03	Are there any previously logged model errors addressed in this case?		
10.04	If errors noted by 10.03 are addressed in this case, is their treatment adequately documented in this case's conceptual description and Master Case checklist		
10.05	If errors noted by 10.03 are addressed in this case, has the error log entry been updated to reflect that the correction has been made?		

00817DC_0011.ai

Figure 2-4. Example of the TSPA-SEIS Checking Implementation Checklist (Continued)

Concept Analyst Checklist for TSPA Model Version:			
Analyst (name): Analyst (sig): Date:		Checker (name): Checker (sig): Date:	
1.00	**Conceptual Level Check**	**Y,N, or n/a**	**Notes**
1.01	Is the objective adequately and clearly stated?		
	Are the conceptual descriptions sufficiently detailed to:		
1.02	Understand it's purpose?		
1.03	Explain what is intended to be done?		
1.04	Explain how it is intended to be done?		
1.05	Explain why it is being done?		
1.06	Properly designed for each relevant scenario?		
1.07	Does the implementation address the conceptual design in detail and intent for each scenario?		
1.08	Does the conceptual design, it's implementation, and analysis of results accomplish the stated purpose?		
1.09	Does the modified portion of the model respond appropriately to its inputs?		
1.10	Do the model components downstream from the modifications respond appropriately?		
1.11	Are model inputs and outputs within their specified ranges?		
1.12	Can the final dose results be explained in terms of upstream parameters (e.g., waste package/drip shield failure curves, seepage flow, pH, solubilities, EBS release rates)?		
1.13	Did the modification(s) invalidate or bring into question assumptions of an upstream or downstream conceptual model?		
1.14	Is the model implemented correctly for all scenario classes?		
1.15	Are there any unintended behaviors that cannot be explained?		
1.16	Is there additional work needed or outstanding issues generated as a result of this work?		

00817DC_0033.ai

Figure 2-5. Example of the TSPA-SEIS Concept Checklist

INTENTIONALL LEFT BLANK

3. USE OF SOFTWARE

A number of software codes were implemented to support the development of the TSPA-SEIS. Some of the software codes were used to provide supporting information and some were directly implemented in the TSPA-SEIS using the GoldSim simulation software code. Supporting software codes, including process models, were developed and operated externally before running the TSPA-SEIS. Software codes directly implemented in the TSPA-SEIS are generally referred to as abstractions and are run within the TSPA-SEIS. All software codes used to support the TSPA-SEIS are qualified and have been placed under the control of SCM per IM-PRO-003, *Software Management*. Each qualified software code is in SCM and uniquely identified with a tracking number. The SCM database also includes information on the software name, version, hardware platform, and operating system under which the software code was qualified. All software documentation, including the software media, is linked to this tracking number.

The software codes used to support the TSPA-SEIS are listed in Table 3-1 along with their unique STNs. The TSPA-SEIS was developed over several months; as a result, several versions of the software codes (e.g., GoldSim, SEEPAGE, and FEHM) are identified here in Section 3 because they were used for the development and prototyping of the model. The software codes used in the TSPA-SEIS that are used to develop the results and conclusions are identified in Table 3-1 and individually discussed in Section 6. Brief descriptions of the primary function(s) of the software codes are also provided in Sections 3.1 through 3.22. The software codes used to support the TSPA-SEIS were selected because they were either developed specifically for use with the TSPA-SEIS or considered to be the most suitable software codes on the Yucca Mountain Project Software Baseline. As a result, there are no limitations on the outputs of any of the software codes used to support the TSPA-SEIS. All software codes used for the TSPA-SEIS were qualified in accordance with the procedures that were in place at the time of their qualification.

Qualification documentation for each software code is available in SCM as well as the Records Processing Center. All software codes were obtained from SCM, were appropriate for use in this analysis, and each was used within the software's range of validation. Unless noted otherwise, the software codes described below are directly linked to the GoldSim software code used during the TSPA-SEIS analyses.

Installation of Qualified TSPA Software Codes on TSPA Department Computers—The installation process for each software code listed in this section was followed to ensure that there was a proper, qualified (i.e., in accordance with governing project procedures and controlled by SCM) installation by personnel authorized by SCM. Because installation procedures have changed during the course of developing the TSPA-SEIS, the installation process is described in one of the following types of documents: Installation Test Process, Software Management Report, or User Information Document.

In order to run the TSPA-SEIS, two types of installations were performed: the GoldSim installation and supporting DLL installations. The installations for GoldSim and callable DLL software routines have the following similarities: (1) both types of installations are qualified, (2) both document the installations using a procedurally required form called a Software User

Request, and (3) both collect the objective evidence of the installation and forward it to SCM. SCM then submits the installation documentation to the Records Processing Center.

One key difference between GoldSim and the callable DLLs is that GoldSim is installed on all master computers, remote processors, and local (desktop) computers, whereas DLLs are only installed on a single computer identified as the PA_Cronus. The PA_Cronus is a TSPA computer that serves as a file server to all the other computers in the TSPA Department. The single installation of the DLLs on the PA_Cronus is possible because of the nature of the GoldSim qualification.

When GoldSim was qualified, the qualification process verified and tested that the DLLs, input files, and database parameters were obtained from the PA_Cronus file server and properly distributed to remote processors as part of the GoldSim distributed processing environment.

In summary, the TSPA-SEIS was run on TSPA- Department distributed processing network computers using qualified installations of GoldSim and the DLLs.

TSPA Computing Environment—The computer system utilized for the TSPA-SEIS is based on a TSPA-wulf personal computer cluster consisting of more than 752 processors (Figure 3-1) with 6 to 16 GB of RAM available to each processor (note that TSPA-wulf is a TSPA phrase that refers to building a supercomputer by interconnecting a cluster of off-the-shelf personal computers). Realizations are fed from a central server to the processors to accomplish the distributed processing. When this report was prepared, run time for the TSPA-SEIS was approximately two hours for each realization.

This system has evolved and become more powerful with each successive iteration of the TSPA-SEIS. The numbers of processors utilized, processor speed, and physical memory have increased by an order of magnitude. This allows the TSPA-SEIS to incorporate more detail and provide rapid turnaround as analyses are developed. The architecture of the computing environment is shown on Figure 3-1. The system has 30 master servers for distributing jobs or analyses. A large file server contains storage for input and output files and the TSPA-SEIS Input Database. The system has a backup power supply and is capable of remote access, if necessary.

3.1 INTRODUCTION

The sections that follow identify the following types of information: 1) name of software; 2) brief description of software; 3) relationship to TSPA-SEIS (i.e., used for model development only, model development and final model, or final model only); 4) location of software documentation; and 5) statement regarding use of code within range of validation. The sections are listed in alphabetical order. The tables that contain the software documents are numbered to match the section number in which they are described.

3.2 ASHPLUME_DLL_LA

3.2.1 Description of Software

All versions of ASHPLUME_DLL_LA used in the TSPA-SEIS documented in this report have the following general capabilities:

- Are called from another program that conforms to the external interface method and function calls described in *User's Guide, GoldSim Probabilistic Simulation Environment* (GoldSim Technology Group 2007 [DIRS 181727]) listed in Table 3-8
- Provide GoldSim with the ability to perform calculations not included in the standard capabilities of GoldSim
- Calculate the waste and ash areal depositional densities on the ground surface from a hypothetical volcanic eruption through the repository (Section 6.5.2)
- Transfer information back and forth to the GoldSim software running the TSPA-SEIS.

3.2.2 Relationship to the TSPA-SEIS

ASHPLUME_DLL_LA V2.0 (STN: 11117-2.0-00 [DIRS 181034]) was used for the TSPA-SEIS development.

ASHPLUME_DLL_LA V2.1 (STN: 11117-2.1-00 [DIRS 181035]) was used for the TSPA-SEIS development and TSPA-SEIS validation and analysis cases.

ASHPLUME_DLL_LA V2.1 (STN: 11117-2.1-01 [DIRS 181036]) was used for the TSPA-SEIS development and TSPA-SEIS validation and analysis cases.

3.2.3 Software Documentation

The software documents for the versions of ASHPLUME_DLL_LA mentioned in Section 3.2.2 are listed in Table 3-2.

3.2.4 Range of Validation

- The range of validation for the versions of ASHPLUME_DLL_LA listed in Section 3.2.2 are defined by the documented functionality (i.e., requirements) and range(s) of acceptable inputs. The requirements are located in the respective requirements documents listed in Table 3-2. The range(s) of acceptable inputs are discussed in the respective design and user documents listed in Table 3-2.

3.3 CWD

3.3.1 Description of Software

All versions of CWD used in the TSPA-SEIS documented in this report have the following general capabilities:

- Are called from another program that conforms to the external interface method and function calls described in *User's Guide, GoldSim Probabilistic Simulation Environment* (GoldSim Technology Group 2007 [DIRS 181727]) listed in Table 3-8
- Provide GoldSim with the ability to perform calculations not included in the standard capabilities of GoldSim
- Implement the abstraction results of the probability of occurrence and size of manufacturing defects in the closure lid welds of the Alloy 22 WP outer surface
- Transfer information back and forth to the GoldSim software running the TSPA-SEIS.

3.3.2 Relationship to the TSPA-SEIS

CWD V2.0 (STN: 10363-2.0-00 [DIRS 162809]) was used for the TSPA-SEIS development and TSPA-SEIS validation and analysis cases.

CWD V2.0 (STN: 10363-2.0-01 [DIRS 181037]) was used for the TSPA-SEIS development and TSPA-SEIS validation and analysis cases.

3.3.3 Software Documentation

The software documents for the versions of CWD mentioned in Section 3.3.2 are listed in Table 3-3.

3.3.4 Range of Validation

- The range of validation for the versions of CWD listed in Section 3.3.2 are defined by the documented functionality (i.e., requirements) and range(s) of acceptable inputs. The requirements are located in the respective requirements documents listed in Table 3-3. The range(s) of acceptable inputs are discussed in the respective design and user documents listed in Table 3-3.

3.4 EXDOC_LA

3.4.1 Description of Software

EXDOC_LA V2.0 (STN: 11193-2.0-00 [DIRS 182102]) calculates the expected dose, conditional of a disruptive event happening.

3.4.2 Relationship to the TSPA-SEIS

EXDOC_LA V2.0 was used for the TSPA-SEIS development and TSPA-SEIS validation and analysis cases.

A controlled version of EXDOC_LA V2.0 was used prior to a qualified version.

3.4.3 Software Documentation

The software documents for EXDOC_LA V2.0 are listed in Table 3-4.

3.4.4 Range of Validation

- The range of validation for the version of EXDOC_LA listed in Section 3.4.2 is defined by the documented functionality (i.e., requirements) and range(s) of acceptable inputs. The requirements are located in the requirements document listed in Table 3-4. The range(s) of acceptable inputs are discussed in the design and user documents listed in Table 3-4.

3.5 FAR

3.5.1 Description of Software

All versions of FAR used in the TSPA-SEIS documented in this report have the following general capabilities:

- Are called from another program that conforms to the external interface method and function calls described in *User's Guide, GoldSim Probabilistic Simulation Environment* (GoldSim Technology Group 2007 [DIRS 181727]) listed in Table 3-8
- Provide GoldSim with the ability to perform calculations not included in the standard capabilities of GoldSim
- Implement the Fortymile Wash volcanic ash redistribution (Section 6.5.2) into the TSPA-SEIS
- Transfer information back and forth to the GoldSim software running the TSPA-SEIS.

3.5.2 Relationship to the TSPA-SEIS

FAR V1.1 (STN: 11190-1.1-00 [DIRS 180002]) was used for the TSPA-SEIS development.

FAR V1.2 was used for the TSPA-SEIS validation and analysis cases.

A controlled version of FAR V1.2 was used prior to a qualified version.

3.5.3 Software Documentation

The software documents for the versions of FAR mentioned in Section 3.5.2 are listed in Table 3-5.

3.5.4 Range of Validation

- The range of validation for the versions of FAR listed in Section 3.5.2 are defined by the documented functionality (i.e., requirements) and range(s) of acceptable inputs. The requirements are located in the respective requirements documents listed in Table 3-5. The range(s) of acceptable inputs are discussed in the respective design and user documents listed in Table 3-5.

3.6 FEHM

3.6.1 Description of Software

All versions of FEHM used in the TSPA-SEIS documented in this report have the following general capabilities:

- Are called from another program that conforms to the external interface method and function calls described in the *User's Guide, GoldSim Probabilistic Simulation Environment* (GoldSim Technology Group 2007 [DIRS 181727]) listed in Table 3-8
- Provide GoldSim with the ability to perform calculations not included in the standard capabilities of GoldSim
- Calculate the transport of radionuclides through the UZ
- Transfer information back and forth to the GoldSim software running the TSPA-SEIS.

3.6.2 Relationship to the TSPA-SEIS

FEHM V2.23 (STN: 10086-2.23-00 [DIRS 173139]) was used for the TSPA-SEIS development.

FEHM V2.24-01 (STN: 10086-2.24-01-00 [DIRS 179419]) was used for the TSPA-SEIS validation and analysis cases.

3.6.3 Software Documentation

The software documents for the versions of FEHM mentioned in Section 3.6.2 are listed in Table 3-6.

3.6.4 Range of Validation

- The range of validation for the versions of FEHM listed in Section 3.6.2 are defined by the documented functionality (i.e., requirements) and range(s) of acceptable inputs. The requirements are located in the respective requirements documents listed in Table 3-6.

The range(s) of acceptable inputs are discussed in the respective design and user documents listed in Table 3-6.

3.7 GETTHK_LA

3.7.1 Description of Software

GetThk_LA V1.0 (STN: 11229-1.0-00 [DIRS 181040]) has the following general capabilities:

- Is called from another program that conforms to the external interface method and function calls described in the *User's Guide, GoldSim Probabilistic Simulation Environment* (GoldSim Technology Group 2007 [DIRS 181727]) listed in Table 3-8
- Provides GoldSim with the ability to perform calculations not included in the standard capabilities of GoldSim
- Reads WAPDEG output for Seismic Scenario Class and calculates statistics (Section 6.6)
- Transfers information back and forth to the GoldSim software running the TSPA-SEIS.

3.7.2 Relationship to the TSPA-SEIS

GetThk_LA V1.0 was used for the TSPA-SEIS validation and analysis cases.

3.7.3 Software Documentation

The software documents for GetThk_LA V1.0 are listed in Table 3-7.

3.7.4 Range of Validation

- The range of validation for the version of GetThk_LA listed in Section 3.7.2 is defined by the documented functionality (i.e., requirements) and range(s) of acceptable inputs. The requirements are located in the respective requirements documents listed in Table 3-7. The range(s) of acceptable inputs are discussed in the respective design and user documents listed in Table 3-7.

3.8 GOLDSIM

3.8.1 Description of Software

All versions of GoldSim used in the TSPA-SEIS documented in this report have the following general capabilities:

- Address the inherent variability and uncertainty that is present in real-world systems by using Monte Carlo simulation

- Superimpose the occurrence and consequences of discrete events onto continuously varying systems
- Build top-down models using hierarchical containers that facilitate the simulation of large, complex systems that are easy to understand and navigate
- Dynamically link external programs or spreadsheets directly to the GoldSim software
- Directly exchange information between any Open Database Connectivity (ODBC)-compliant (Yucca Mountain Structered) database and GoldSim.

3.8.2 Relationship to the TSPA-SEIS

GoldSim V9.60.100 (STN: 10344-9.60-01 [DIRS 181903]) was used for the TSPA-SEIS development.

GoldSim V9.60.100 (STN: 10344-9.60.100-00 [DIRS 181903]) was used for the TSPA-SEIS development and TSPA-SEIS validation and analysis cases.

A controlled version of GoldSim V9.60.100 was used prior to a qualified version.

3.8.3 Software Documentation

The software documents for the versions of GoldSim mentioned in Section 3.8.2 are listed in Table 3-8.

3.8.4 Range of Validation

- The range of validation for the versions of GoldSim listed in Section 3.8.2 are defined by the documented functionality (i.e., requirements) and range(s) of acceptable inputs. The requirements are located in the respective requirements documents listed in Table 3-8. The range(s) of acceptable inputs are discussed in the respective design and user documents listed in Table 3-8.

3.9 INTERPZDLL_LA

3.9.1 Description of Software

All versions of InterpZdll_LA used in the TSPA-SEIS documented in this report have the following general capabilities:

- Are called from another program that conforms to the external interface method and function calls described in *User's Guide, GoldSim Probabilistic Simulation Environment* (GoldSim Technology Group 2007 [DIRS 181727]) listed in Table 3-8
- Provide GoldSim the ability to perform calculations not included in the standard capabilities of GoldSim

- Provide interpolation capabilities for the EBS Chemical Environment Submodel of the TSPA-SEIS (Section 6.3.4)

- Transfer information back and forth to the GoldSim software running the TSPA-SEIS.

3.9.2 Relationship to the TSPA-SEIS

InterpZdll_LA V1.0 (STN: 11107-1.0-00 [DIRS 167885]) was used for the TSPA-SEIS development and TSPA-SEIS validation and analysis cases.

InterpZdll_LA V1.0 (STN: 11107-1.0-01 [DIRS 181043]) was used for the TSPA-SEIS development and TSPA-SEIS validation and analysis cases.

3.9.3 Software Documentation

The software documents for the versions of InterpZdll_LA mentioned in Section 3.9.2 are listed in Table 3-9.

3.9.4 Range of Validation

- The range of validation for the versions of InterpZdll_LA listed in Section 3.9.2 are defined by the documented functionality (i.e., requirements) and range(s) of acceptable inputs. The requirements are located in the respective requirements documents listed in Table 3-9. The range(s) of acceptable inputs are discussed in the respective design and user documents listed in Table 3-9.

3.10 WAPDEG

3.10.1 Description of Software

All versions of WAPDEG used in the TSPA-SEIS documented in this report have the following general capabilities:

- Are called from another program that conforms to the external interface method and function calls described in *User's Guide, GoldSim Probabilistic Simulation Environment* (GoldSim Technology Group 2007 [DIRS 181727]) listed in Table 3-8

- Provide GoldSim with the ability to perform calculations not included in the standard capabilities of GoldSim

- Implement the GC, SCC, and MIC Abstractions used in the TSPA-SEIS

- Calculate DS and WP failure profiles

- Transfer information back and forth to the GoldSim software running the TSPA-SEIS.

3.10.2 Relationship to the TSPA-SEIS

WAPDEG V4.07 (STN: 10000-4.07-00 [DIRS 161240]) was used for the TSPA-SEIS development and TSPA-SEIS validation and analysis cases.

WAPDEG V4.07 (STN: 10000-4.07-01 [DIRS 181064]) was used for the TSPA-SEIS development and TSPA-SEIS validation and analysis cases.

3.10.3 Software Documentation

The software documents for the versions of WAPDEG mentioned in Section 3.10.2 are listed in Table 3-10.

3.10.4 Range of Validation

- The range of validation for the versions of WAPDEG listed in Section 3.10.2 are defined by the documented functionality (i.e., requirements) and range(s) of acceptable inputs. The requirements are located in the respective requirements documents listed in Table 3-10. The range(s) of acceptable inputs are discussed in the respective design and user documents listed in Table 3-10.

3.11 MFCP_LA

3.11.1 Description of Software

All versions of MFCP_LA used in the TSPA-SEIS documented in this report have the following general capabilities:

- Are called from another program that conforms to the external interface method and function calls described in *User's Guide, GoldSim Probabilistic Simulation Environment* (GoldSim Technology Group 2007 [DIRS 181727]) listed in Table 3-8
- Provide GoldSim with the ability to perform calculations not included in the standard capabilities of GoldSim
- Control the selection of input files for various DLLs that are part of the TSPA-SEIS
- Transfer information back and forth to the GoldSim software running the TSPA-SEIS.

3.11.2 Relationship to the TSPA-SEIS

MFCP_LA V1.0 (STN: 11071-1.0-00 [DIRS 167884]) was used for the TSPA-SEIS development and TSPA-SEIS validation and analysis cases.

MFCP_LA V1.0 (STN: 11071-1.0-01 [DIRS 181045]) was used for the TSPA-SEIS development and TSPA-SEIS validation and analysis cases.

3.11.3 Software Documentation

The software documents for the versions of MFCP_LA mentioned in Section 3.11.2 are listed in Table 3-11.

3.11.4 Range of Validation

- The range of validation for the versions of MFCP_LA listed in Section 3.11.2 are defined by the documented functionality (i.e., requirements) and range(s) of acceptable inputs. The requirements are located in the respective requirements documents listed in Table 3-11. The range(s) of acceptable inputs are discussed in the respective design and user documents listed in Table 3-11.

3.12 MKTABLEAND MKTABLE_LA

3.12.1 Description of Software

All versions of MkTable and MkTable_LA used in the TSPA-SEIS documented in this report have the following general capabilities:

- Are called from another program that conforms to the external interface method and function calls described in *User's Guide, GoldSim Probabilistic Simulation Environment* (GoldSim Technology Group 2007 [DIRS 181727]) listed in Table 3-8
- Provide GoldSim with the ability to perform calculations not included in the standard capabilities of GoldSim
- Control the selection of input files for various DLLs that are part of the TSPA-SEIS
- Transfer information back and forth to the GoldSim software running the TSPA-SEIS.

3.12.2 Relationship to the TSPA-SEIS

MkTable V1.00 (STN: 10505-1.00-00 [DIRS 174528]) was used for the TSPA-SEIS development.

MkTable_LA V1.0 (STN: 11217-1.0-00 [DIRS 181047]) was used for the TSPA-SEIS development and TSPA-SEIS validation and analysis cases.

MkTable_LA V1.0 (STN: 11217-1.0-01 [DIRS 181048]) was used for the TSPA-SEIS development and TSPA-SEIS validation and analysis cases.

3.12.3 Software Documentation

The software documents for the versions of MkTable_LA mentioned in Section 3.12.2 are listed in Table 3-12.

3.12.4 Range of Validation

- The range of validation for the versions of MkTable_LA listed in Section 3.12.2 are defined by the documented functionality (i.e., requirements) and range(s) of acceptable inputs. The requirements are located in the respective requirements documents listed in Table 3-12. The range(s) of acceptable inputs are discussed in the respective design and user documents listed in Table 3-12.

3.13 MVIEW

3.13.1 Description of Software

MVIEW V4.0 (STN: 10072-4.0-00 [DIRS 181049]) is a stand-alone executable program that transforms text output describing numeric model geometry and numeric model output into two-dimensional and three-dimensional visual representations.

3.13.2 Relationship to the TSPA-SEIS

MVIEW V4.0 is not part of the TSPA-SEIS. Rather, MVIEW is used to interpret the results of the TSPA-SEIS using two-dimensional and three-dimensional visual representations. MVIEW V4.0 is also used to statistically analyze the TSPA-SEIS output.

3.13.3 Software Documentation

The software documents for MVIEW 4.0 are listed in Table 3-13.

3.13.4 Range of Validation

- The range of validation for the version of MVIEW listed in Section 3.13.2 is defined by the documented functionality (i.e., requirements) and range(s) of acceptable inputs. The requirements are located in the requirements document listed in Table 3-13. The range(s) of acceptable inputs are discussed in the design and user documents listed in Table 3-13.

3.14 PASSTABLE1D_LA

3.14.1 Description of Software

All versions of PassTable1D_LA used in the TSPA-SEIS documented in this report have the following general capabilities:

- Are called from another program that conforms to the external interface method and function calls described in *User's Guide, GoldSim Probabilistic Simulation Environment* (GoldSim Technology Group 2007 [DIRS 181727]) listed in Table 3-8

- Provide GoldSim with the ability to perform calculations not included in the standard capabilities of GoldSim

- Read one-dimensional tabular information from an input file and pass that information into GoldSim in a format that is compatible with the external definition of a one-dimensional look-up table element

- Support the evaluation of LC on the WPs.

3.14.2 Relationship to the TSPA-SEIS

PassTable1D_LA V1.0 (STN: 11142-1.0-00 [DIRS 169130]) was used for the TSPA-SEIS development.

PassTable1D_LA V1.0 (STN: 11142-1.0-01 [DIRS 181050]) was used for the TSPA-SEIS development.

PassTable1D_LA V2.0 (STN: 11142-2.0-00 [DIRS 181051] was used for the TSPA-SEIS development and TSPA-SEIS validation and analysis cases.

3.14.3 Software Documentation

The software documents for the versions of PassTable1D_LA mentioned in Section 3.14.2 are listed in Table 3-14.

3.14.4 Range of Validation

- The range of validation for the versions of PassTable1D_LA listed in Section 3.14.2 are defined by the documented functionality (i.e., requirements) and range(s) of acceptable inputs. The requirements are located in the respective requirements documents listed in Table 3-14. The range(s) of acceptable inputs are discussed in the respective design and user documents listed in Table 3-14.

3.15 PASSTABLE3D_LA

3.15.1 Description of Software

All versions of PassTable3D_LA used in the TSPA-SEIS documented in this report have the following general capabilities:

- Are called from another program that conforms to the external interface method and function calls described in *User's Guide, GoldSim Probabilistic Simulation Environment* (GoldSim Technology Group 2007 [DIRS 181727]) listed in Table 3-8

- Provide GoldSim with the ability to perform calculations not included in the standard capabilities of GoldSim

- Read three-dimensional tabular information from an input file and pass that information into GoldSim in a format that is compatible with the external definition of a three-dimensional look-up table element

- Support the evaluation of LC on the WPs (Sections 6.3.5).

3.15.2 Relationship to the TSPA-SEIS

PassTable3D_LA V1.0 (STN: 11143-1.0-00 [DIRS 168980]) was used for the TSPA-SEIS development and TSPA-SEIS validation and analysis cases.

PassTable3D_LA V1.0 (STN: 11143-1.0-01 [DIRS 181052]) was used for the TSPA-SEIS development and TSPA-SEIS validation and analysis cases.

PassTable3D_LA V2.0 (STN 11143-2.0-00 [DIRS 182556]) was used for the TSPA-SEIS development and TSPA-SEIS validation and analysis cases.

3.15.3 Software Documentation

The software documents for the versions of PassTable3D_LA mentioned in Section 3.15.2 are listed in Table 3-15.

3.15.4 Range of Validation

The range of validation for the versions of PassTable3D_LA listed in Section 3.15.2 are defined by the documented functionality (i.e., requirements) and range(s) of acceptable inputs. The requirements are located in the respective requirements documents listed in Table 3-15. The range(s) of acceptable inputs are discussed in the respective design and user documents listed in Table 3-15.

3.16 PREWAP_LA

3.16.1 Description of Software

PREWAP_LA V1.1 (STN: 10939-1.1-00 [DIRS 181053]) has the following general capabilities:

- Implements the processing of output files produced by the Multiscale Thermal-Hydrologic Abstraction software, MSTHAC V7.0 (STN: 10419-7.0-00 [DIRS 164274]).
- Processes files from MSTHAC V7.0 as input for DLLs (e.g., WAPDEG) (STN: 10000-4.07-00 [DIRS 161240]), which are components of the TSPA-SEIS.

3.16.2 Relationship to the TSPA-SEIS

PREWAP_LA V1.1 was used for the TSPA-SEIS development and TSPA-SEIS validation and analysis cases.

3.16.3 Software Documentation

The software documents for PREWAP_LA V1.1 are listed in Table 3-16.

3.16.4 Range of Validation

- The range of validation for the version of PREWAP_LA listed in Section 3.16.2 is defined by the documented functionality (i.e., requirements) and range(s) of acceptable inputs. The requirements are located in the requirements document listed in Table 3-16. The range(s) of acceptable inputs are discussed in the design and user documents listed in Table 3-16.

3.17 SCCD

3.17.1 Description of Software

All versions of SCCD used in the TSPA-SEIS documented in this report have the following general capabilities:

- Are called from another program that conforms to the external interface method and function calls described in *User's Guide, GoldSim Probabilistic Simulation Environment* (GoldSim Technology Group 2007 [DIRS 181727]) listed in Table 3-8
- Provide GoldSim with the ability to perform calculations not included in the standard capabilities of GoldSim
- Implement the abstraction results of the stress and stress-intensity factor profiles in the closure-lid welds of the Alloy 22 WP outer surface
- Transfer information back and forth to the GoldSim software running the TSPA-SEIS.

3.17.2 Relationship to the TSPA-SEIS

SCCD V2.01 (STN: 10343-2.01-00 [DIRS 181157]) was used for the TSPA-SEIS development and TSPA-SEIS validation and analysis cases.

SCCD V2.01 (STN: 10343-2.01-01 [DIRS 181054]) was used for the TSPA-SEIS development and TSPA-SEIS validation and analysis cases.

3.17.3 Software Documentation

The software documents for the versions of SCCD mentioned in Section 3.17.2 are listed in Table 3-17.

3.17.4 Range of Validation

- The range of validation for the versions of SCCD listed in Section 3.17.2 are defined by the documented functionality (i.e., requirements) and range(s) of acceptable inputs. The requirements are located in the respective requirements documents listed in Table 3-17. The range(s) of acceptable inputs are discussed in the respective design and user documents listed in Table 3-17.

3.18 SEEPAGEDLL_LA

3.18.1 Description of Software

All versions of SEEPAGEDLL_LA used in the TSPA-SEIS documented in this report have the following general capabilities:

- Are called from another program that conforms to the external interface method and function calls described in *User's Guide, GoldSim Probabilistic Simulation Environment* (GoldSim Technology Group 2007 [DIRS 181727]) listed in Table 3-8
- Provide GoldSim with the ability to perform calculations not included in the standard capabilities of GoldSim
- Implement the Drift Seepage Abstraction (Section 6.3.3.1.2) into the TSPA-SEIS
- Transfer information back and forth to the GoldSim software running the TSPA-SEIS.

3.18.2 Relationship to the TSPA-SEIS

SEEPAGEDLL_LA V1.2 (STN: 11076-1.2-00 [DIRS 173435]) was used for the TSPA-SEIS development.

SEEPAGEDLL_LA V1.3 (STN: 11076-1.3-00 [DIRS 180318]) was used for the TSPA-SEIS development and TSPA-SEIS validation and analysis cases.

SEEPAGEDLL_LA V1.3 (STN: 11076-1.3-01 [DIRS 181058]) was used for the TSPA-SEIS development and TSPA-SEIS validation and analysis cases.

3.18.3 Software Documentation

The software documents for the versions of SEEPAGEDLL_LA mentioned in Section 3.18.2 are listed in Table 3-18.

3.18.4 Range of Validation

- The range of validation for the versions of SEEPAGEDLL_LA listed in Section 3.18.2 are defined by the documented functionality (i.e., requirements) and range(s) of acceptable inputs. The requirements are located in the respective requirements documents listed in Table 3-18. The range(s) of acceptable inputs are discussed in the respective design and user documents listed in Table 3-18.

3.19 SOILEXP_LA

3.19.1 Description of Software

SOILEXP_LA V1.0 (STN: 10933-1.0-00 [DIRS 167883]) has the following general capabilities:

- Is called from another program that conforms to the external interface method and function calls described in *User's Guide, GoldSim Probabilistic Simulation Environment* (GoldSim Technology Group 2007 [DIRS 181727]) listed in Table 3-8
- Provides GoldSim with the ability to perform calculations not included in the standard capabilities of GoldSim
- Calculates the cumulative redistribution factors used to calculate the radionuclide concentration in volcanic ash after it is deposited
- Transfers information back and forth to the GoldSim software running the TSPA-SEIS model.

3.19.2 Relationship to the TSPA-SEIS

SOILEXP_LA V1.0 was used for TSPA-SEIS development.

3.19.3 Software Documentation

The software documents for SoilExp_LA V1.0 are listed in Table 3-19.

3.19.4 Range of Validation

- The range of validation for the version of SoilExp_LA listed in Section 3.19.2 is defined by the documented functionality (i.e., requirements) and range(s) of acceptable inputs. The requirements are located in the requirements document listed in Table 3-19. The range(s) of acceptable inputs are discussed in the design and user documents listed in Table 3-19.

3.20 SZ_CONVOLUTE

3.20.1 Description of Software

All versions of SZ_Convolute used in the TSPA-SEIS documented in this report have the following general capabilities:

- Are called from another program that conforms to the external interface method and function calls described in *User's Guide, GoldSim Probabilistic Simulation Environment* (GoldSim Technology Group 2007 [DIRS 181727]) listed in Table 3-8
- Provide GoldSim with the ability to perform calculations not included in the standard capabilities of GoldSim
- Calculate the radionuclide mass-flux rates in accordance with the three-dimensional SZ Flow and Transport Abstraction (Section 6.3.10)
- Transfer information back and forth to the GoldSim software running the TSPA-SEIS.

3.20.2 Relationship to the TSPA-SEIS

SZ_Convolute V3.0 (STN: 10207-3.0-00 [DIRS 164180]) was used for the TSPA-SEIS development.

SZ_Convolute V3.0 (STN: 10207-3.10.01-00 [DIRS 181060]) was used for the TSPA-SEIS development and TSPA-SEIS Model validation and analysis cases.

3.20.3 Software Documentation

The software documents for the versions of SZ_Convolute mentioned in Section 3.20.2 are listed in Table 3-20.

3.20.4 Range of Validation

- The range of validation for the versions of SZ_Convolute listed in Section 3.20.2 are defined by the documented functionality (i.e., requirements) and range(s) of acceptable inputs. The requirements are located in the respective requirements documents listed in Table 3-20. The range(s) of acceptable inputs are discussed in the respective design and user documents listed in Table 3-20.

3.21 TSPA_INPUT_DB

3.21.1 Description of Software

All versions of TSPA_Input_DB used in the TSPA-SEIS documented in this report are a Microsoft Access database that is used as a quality-controlled storage area for the TSPA-SEIS input parameters. The parameter values are maintained as originally entered (i.e., no

manipulations or post-processing of the parameter values are performed). The database is capable of interfacing via ODBC for automated download to the TSPA-SEIS.

3.21.2 Relationship to the TSPA-SEIS

TSPA_Input_DB V2.2 (STN: 10931-2.2-00 [DIRS 181061]) was used for the TSPA-SEIS development and TSPA-SEIS validation and analysis cases.

TSPA_Input_DB V2.2 (STN: 10931-2.2-01 [DIRS 181062]) was used for the TSPA-SEIS validation and analysis cases.

3.21.3 Software Documentation

The software documents for the versions of the TSPA_Input_DB mentioned in Section 3.21.2 are listed in Table 3-21.

3.21.4 Range of Validation

- The range of validation for the versions of TSPA_Input_DB listed in Section 3.21.2 are defined by the documented functionality (i.e., requirements) and range(s) of acceptable inputs. The requirements are located in the respective requirements documents listed in Table 3-21. The range(s) of acceptable inputs are discussed in the respective design and user documents listed in Table 3-21.

3.22 EXEMPT SOFTWARE USED

Exempt software was also used in developing the TSPA-SEIS. Where applicable, the information (i.e., formula and list of inputs) required per procedure for transparency is included in the respective information documenting the software.

INTENTIONALLY LEFT BLANK

Table 3-1. TSPA-SEIS Software Codes

Code	Version	Software Tracking Number	Operating System	DIRS Number
ASHPLUME_DLL_LA[a1]	2.0	STN: 11117-2.0-00	Windows 2000	DIRS 181034
ASHPLUME_DLL_LA[a2]	2.1	STN: 11117-2.1-00	Windows 2000	DIRS 181035
ASHPLUME_DLL_LA[a2]	2.1	STN: 11117-2.1-01	Windows 2003	DIRS 180147
CWD[a2]	2.0	STN: 10363-2.0-00	Windows 2000	DIRS 162809
CWD[a2]	2.0	STN: 10363-2.0-01	Windows 2003	DIRS 181037
EXDOC_LA[b1]	2.0	STN: 11193-2.0-00	Windows 2000 Windows 2003 Windows XP	182102
FAR[a1]	1.1	STN: 11190-1.1-00	Windows 2000 Windows 2003	DIRS 180002
FAR[a2]	1.2	STN: 11190-1.2-00	Windows 2000 Windows 2003	182225
FEHM[a1]	2.23	STN: 10086-2.23-00	Windows 2000	DIRS 173139
FEHM[a2]	2.24-01	STN: 10086-2.24-01-00	Windows 2000 Windows 2003 Windows XP	DIRS 179419
GetThk_LA[a2]	1.0	STN: 11229-1.0-00	Windows 2000 Windows 2003	DIRS 181040
GoldSim[a1]	9.60	STN: 10344-9.60-00	Windows 2000 Windows 2003 Windows XP	DIRS 181041
GoldSim[a2]	9.60.100	STN: 10344-9.60-01	Windows 2000 Windows 2003 Windows XP	DIRS 180224
InterpZdll_LA[a2]	1.0	STN: 11107-1.0-00	Windows 2000	DIRS 167885
InterpZdll_LA[a2]	1.0	STN: 11107-1.0-01	Windows 2003	DIRS 181043
MFCP_LA[a2]	1.0	STN: 11071-1.0-00	Windows 2000	DIRS 167884
MFCP_LA[a2]	1.0	STN: 11071-1.0-01	Windows 2003	DIRS 181045
MkTable[a1]	1.00	STN: 10505-1.00-00	Windows 2000	DIRS 174528
MkTable_LA[a2]	1.0	STN: 11217-1.0-00	Windows 2000	DIRS 181047
MkTable_LA[a2]	1.0	STN: 11217-1.0-01	Windows 2003	DIRS 181048
MView[b1]	4.0	STN: 10072-4.0-01	Windows XP	DIRS 181049
PassTable1D_LA[a1]	1.0	STN: 11142-1.0-00	Windows 2000	DIRS 169130
PassTable1D_LA[a1]	1.0	STN: 11142-1.0-01	Windows 2003	DIRS 181050
PassTable1D_LA[a2]	2.0	STN: 11142-2.0-00	Windows 2000 Windows 2003	DIRS 181051
PassTable3D_LA[a1]	1.0	STN: 11143-1.0-00	Windows 2000	DIRS 168980
PassTable3D_LA[a1]	1.0	STN: 11143-1.0-01	Windows 2003	DIRS 181052

Table 3-1. TSPA-SEIS Software Codes(Continued)

Code	Version	Software Tracking Number	Operating System	DIRS Number
PassTable3D_LA [a2]	2.0	STN: 11143-2.0-00	Windows 2000 Windows 2003	 182556
PREWAP_LA[b1]	1.1	STN: 10939-1.1-00	Windows 2000	DIRS 181053
SCCD[a2]	2.01	STN: 10343-2.01-00	Windows 2000	DIRS 181157
SCCD[a2]	2.01	STN: 10343-2.01-01	Windows 2003	DIRS 181054
SEEPAGEDLL_LA[a1]	1.2	STN: 11076-1.2-00	Windows 2000	DIRS 173435
SEEPAGEDLL_LA[a2]	1.3	STN: 11076-1.3-00	Windows 2000	DIRS 180318
SEEPAGEDLL_LA[a2]	1.3	STN: 11076-1.3-01	Windows 2003	DIRS 181058
SoilExp_LA [a1]	1.0	STN: 10933-1.0-00	Windows 2000	DIRS 167883
SZ_Convolute[a1]	3.0	STN: 10207-3.0-00	Windows 2000	DIRS 164180
SZ_Convolute[a2]	3.10.01	STN: 10207-3.10.01-00	Windows 2000/ Windows 2003	DIRS 181060
TSPA_Input_DB[a2]	2.2	STN: 10931-2.2-00	Windows 2000	DIRS 181061
TSPA_Input_DB[a2]	2.2	STN: 10931-2.2-01	Windows 2003	DIRS 181062
WAPDEG[a2]	4.07	STN: 10000-4.07-00	Windows 2000	DIRS 181774
WAPDEG[a2]	4.07	STN: 10000-4.07-01	Windows 2003	DIRS 181064

[a1] Codes are used only for TSPA-SEIS development.

[a2] Codes used in the TSPA-SEIS that are used for TSPA-SEIS development and to develop results and conclusions.

[b1] Code is a pre- or post-processor that does not require GoldSim to run codes that are used for TSPA-SEIS development and to develop results and conclusions.

[b2] Code is a pre- or post-processor that does not require GoldSim to run codes that are used only for TSPA-SEIS development.

Table 3-2. ASHPLUME_DLL_LA Software Documents

Version 2.0 Windows 2000 (STN: 11117-2.0-00)			
Description	**Document ID**	**DIRS Number**	**Tracking Number**
Requirements Document (RD)	11117-RD-2.0-00	DIRS 167601	MOL.20031212.0438
Design Document (DD)	11117-DD-2.0-00	DIRS 167603	MOL.20031212.0439
User Manual (UM)	11117-UM-2.0-00	DIRS 167607	MOL.20031212.0444
Installation Test Process (ITP)	11117-ITP-2.0-00	DIRS 167606	MOL.20031212.0440
Validation Test Process (VTP)	11117-VTP-2.0-01	DIRS 167604	MOL.20031212.0441
Validation Test Report (VTR)	11117-VTR-2.0-00	DIRS 166506	MOL.20031212.0443
Version 2.1 Windows 2000 (STN: 11117-2.1-00)			
Description	**Document ID**	**DIRS Number**	**Tracking Number**
Requirements Document (RD)	11117-RD-2.1-00	DIRS 181073	MOL.20061106.0385
Design Document (DD)	11117-DD-2.1-00	DIRS 181075	MOL.20061106.0387
User Information Document (UID)	11117-UID-2.1-00	DIRS 181076	MOL.20070102.0242
Software Validation Report (SVR)	11117-SVR-2.1-00-WIN2000	DIRS 181077	MOL.20070102.0246
Version 2.1 Windows 2003 (STN: 11117-2.1-01)			
Description	**Document ID**	**DIRS Number**	**Tracking Number**
Requirements Document (RD)	Same as above	NA	NA
Design Document (DD)	Same as above	NA	NA
User Information Document (UID)	Same as above	NA	NA
Software Validation Report (SVR)	11117-SVR-2.1-01-WIN2003	DIRS 181275	MOL.20070223.0261

Table 3-3. CWD Software Documents

Version 2.0 Windows 2000 (STN: 10363-2.0-00)			
Description	**Document ID**	**DIRS Number**	**Tracking Number**
Software Management Report (SMR)	10363-SMR-2.0-00	DIRS 167564	MOL.20030501.0182
Version 2.0 Windows 2003 (STN: 10363-2.0-01)			
Description	**Document ID**	**DIRS Number**	**Tracking Number**
Software Management Report (SMR)	Same as above	NA	NA
Software Validation Report (SVR)	10363-SVR-2.0-01	DIRS 181079	MOL.20070209.0021

Table 3-4. EXDOC_LA Software Documents

Version 2.1 Windows 2000 (STN: 11193-2.0-00)			
Description	**Document ID**	**DIRS Number**	**Tracking Number**
Requirements Document (RD)	11193-RD-2.0-01	DIRS 182906	MOL.20070723.0260
Design Document (DD)	11193-DD-2.0-01	DIRS 182907	MOL.20070723.0262
User Information Document (UID)	11193-UID-2.0-00	DIRS 182908	MOL.20070723.0264
Software Validation Report (SVR)	11193-SVR-2.0-00-2000	DIRS 182909	MOL.20070723.0266
Software Validation Report (SVR)	11193-SVR-2.0-00-2003	DIRS 182910	MOL.20070723.0268
Software Validation Report (SVR)	11193-SVR-2.0-00-WINXP	DIRS 182911	MOL.20070723.0270

Table 3-5. FAR Software Documents

Version 1.1 Windows 2000 and Windows 2003 (STN:11190-1.1-00)			
Description	**Document ID**	**DIRS Number**	**Tracking Number**
Requirements Document (RD)	11190-RD-1.1-00	DIRS 181080	MOL.20070322.0326
Design Document (DD)	11190-DD-1.1-00	DIRS 181081	MOL.20070322.0328
User Information Document (UID)	11190-UID-1.1-00	DIRS 181084	MOL.20070417.0336
Software Validation Report (SVR)	11190-SVR-1.1-00-WIN2000	DIRS 181085	MOL.20070417.0338
Software Validation Report (SVR)	11190-SVR-1.1-00-WIN2003	DIRS 181087	MOL.20070417.0340
Version 1.2 Windows 2000 AND 2003 (STN: 11190-1.20-00)			
Description	**Document ID**	**DIRS Number**	**Tracking Number**
Requirements Document (RD)	11190-RD-1.2-00	DIRS	MOL.
Design Document (DD)	11190-DD-1.2-00	DIRS	MOL.
User Information Document (UID)	11190-UID-1.2-00	DIRS	MOL.
Software Validation Report (SVR)	11190-SVR-1.2-00-WIN2000	DIRS	MOL.
Software Validation Report (SVR)	11190-SVR-1.2-00-WIN2003	DIRS	MOL.

Table 3-6. FEHM Software Documents

Version 2.23 Windows 2000 (STN: 10086-2.23-00)			
Description	**Document ID**	**DIRS Number**	**Tracking Number**
Requirements Document (RD)	10086-RD-2.23-00	DIRS 174616	MOL.20050301.0040
Design Document (DD)	10086-DD-2.23-00	DIRS 173440	MOL.20050301.0043
User Information Document (UID)	10086-UID-2.23-00	DIRS 173441	MOL.20050301.0046
Software Validation Report (SVR)	10086-SVR-2.23-00-WIN2000	DIRS 173442	MOL.20050301.0049
Version 2.24-01 Windows 2000 and 2003 (STN: 10086-2.24-01)			
Description	**Document ID**	**DIRS Number**	**Tracking Number**
Requirements Document (RD)	10086-RD-2.24-00-00	DIRS 181094	MOL.20061127.0272
Design Document (DD)	10086-DD-2.24-01-00	DIRS 181095	MOL.20070309.0032
User Information Document (UID)	10086-UID-2.24-01-00	DIRS 181096	MOL.20070309.0037
Software Validation Report (SVR)	10086-SVR-2.24-01-00-WIN2000	DIRS 181097	MOL.20070309.0047
Software Validation Report (SVR)	10086-SVR-2.24-01-00-WIN2003	DIRS 181098	MOL.20070309.0045

Table 3-7. GetThk_LA Software Documents

Version 1.0 Windows 2000 and 2003 (STN: 11229-1.0-00)			
Description	**Document ID**	**DIRS Number**	**Tracking Number**
Requirements Document (RD)	11229-RD-1.0-00	DIRS 181100	MOL.20060915.0163
Design Document (DD)	11229-DD-1.0-00	DIRS 181101	MOL.20060915.0165
User Information Document (UID)	11229-UID-1.0-00	DIRS 181102	MOL.20060915.0169
Software Validation Report (SVR)	11229-SVR-1.0-00-WIN2000	DIRS 181104	MOL.20060915.0173
Software Validation Report (SVR)	11229-SVR-1.0-00-WIN2003	DIRS 181105	MOL.20060915.0171

Table 3-8. GoldSim Software Documents

Version 9.60 Windows 2000, Windows 2003, and Windows XP (STN: 10344-9.60-00)			
Description	**Document ID**	**DIRS Number**	**Tracking Number**
Requirements Document (RD)	10344-RD-9.60-00	DIRS 181106	MOL.20070416.0330
Design Document (DD)	10344-DD-9.60-01	DIRS 181107	MOL.20070416.0338
User Information Document (UID)	10344-UID-9.60-00	DIRS 181108	MOL.20070416.0339
User's Guide, GoldSim Probabilistic Simulation Environment, V. 9.60	NA	DIRS 181727	TIC: 259221
Software Validation Report (SVR)	10344-SVR-9.60-00-WIN2000	DIRS 181109	MOL.20070416.0341
Software Validation Report (SVR)	10344-SVR-9.60-00-WIN2003	DIRS 181110	MOL.20070416.0343
Software Validation Report (SVR)	10344-SVR-9.60-00-WINXP	DIRS 181111	MOL.20070416.0345
Version 9.60.100 Windows 2000, Windows 2003, and Windows XP (STN: 10344-9.60.100-00)			
Description	**Document ID**	**DIRS Number**	**Tracking Number**
Requirements Document (RD)	Same as above	NA	NA
Design Document (DD)	Same as above	NA	NA
User Information Document (UID)	Same as above	NA	NA
User's Guide, GoldSim Probabilistic Simulation Environment, V. 9.60	Same as above	NA	NA
Software Validation Report (SVR)	10344-SVR-9.60-01-WIN2000	DIRS 182913	MOL.20070711.0250
Software Validation Report (SVR)	10344-SVR-9.60-01-WIN2003	DIRS 182914	MOL. 20070711.0252
Software Validation Report (SVR)	10344-SVR-9.60-01-WINXP	DIRS 182915	MOL. 20070711.0254

Table 3-9. InterpZdll_LA Software Documents

Version 1.0 Windows 2000 (STN: 11107-1.0-00)			
Description	**Document ID**	**DIRS Number**	**Tracking Number**
Software Management Report (SMR)	11107-SMR-1.0-00	DIRS 168988	MOL.20040130.0403
Version 1.0 Windows 2003 (STN: 11107-1.0-01)			
Description	**Document ID**	**DIRS Number**	**Tracking Number**
Software Management Report (SMR)	Same as above	NA	NA
Software Validation Report (SVR)	11107-SVR-1.0-01-WIN2003	DIRS 181092	MOL.20070220.0471

Table 3-10. WAPDEG Software Documents

Version 4.07 Windows 2000 (STN:10000-4.07-00)			
Description	**Document ID**	**DIRS Number**	**Tracking Number**
Requirements Document (RD)	10000-RD-4.07-00	DIRS 167545	MOL.20030409.0228
Design Document (DD)	10000-DD-4.07-00	DIRS 167547	MOL.20030409.0229
User Manual (UM)	10000-UM-4.07-00	DIRS 162606	MOL.20030409.0233
Installation Test Plan (ITP)	10000-ITP-4.07-01	DIRS 167548	MOL.20030409.0231
Validation Test Plan (VTP)	10000-VTP-4.07-00	DIRS 167542	MOL.20030409.0232
Validation Test Report (VTR)	10000-VTR-4.07-00	DIRS 167554	MOL.20030409.0234
Version 4.07 Windows 2003 (STN:10000-4.07-01)			
Description	**Document ID**	**DIRS Number**	**Tracking Number**
Requirements Document (RD)	Same as above	NA	NA
Design Document (DD)	Same as above	NA	NA
Validation Test Plan (VTP)	Same as above	NA	NA
Installation Test Plan (ITP)	Same as above	NA	NA
User Manual (UM)	Same as above	NA	NA
Software Validation Report (SVR)	10000-SVR-4.07-01-WIN2003	DIRS 181141	MOL.20070417.0371

Table 3-11. MFCP_LA Software Documents

Version 1.0 Windows 2000 (STN: 11071-1.0-00)			
Description	**Document ID**	**DIRS Number**	**Tracking Number**
Software Management Report (SMR)	11071-SMR-1.0-00	DIRS 167597	MOL.20030529.0258
Version 1.0 Windows 2003 (STN: 11071-1.0-01)			
Description	**Document ID**	**DIRS Number**	**Tracking Number**
Software Management Report (SMR)	Same as above	NA	NA
Software Validation Report (SVR)	11071-SVR-1.0-01-WIN2003	DIRS 181113	MOL.20061218.0126

Table 3-12. MKTABLE/MkTable_LA Software Documents

Version 1.00 Windows 2000 (STN:10505-1.00-00)			
Description	**Document ID**	**DIRS Number**	**Tracking Number**
Software Management Report (SMR)	10505-SMR-1.00-00	DIRS 167572	MOL.20010712.0055
Version 1.0 Windows 2000 (STN:11217-1.0-00)			
Description	**Document ID**	**DIRS Number**	**Tracking Number**
Requirements Document (RD)	11217-RD-1.0-00	DIRS 181114	MOL.20060413.0349
Design Document (DD)	11217-DD-1.0-00	DIRS 181115	MOL.20060413.0351
User Information Document (UID)	11217-UID-1.0-00	DIRS 181116	MOL.20060413.0354
Software Validation Report (SVR)	11217-SVR-1.0-00-WIN2000	DIRS 181117	MOL.20060413.0357
Version 1.0 Windows 2003 (STN: 11217-1.0-01)			
Description	**Document ID**	**DIRS Number**	**Tracking Number**
Requirements Document (RD)	Same as above	NA	NA
Design Document (DD)	Same as above	NA	NA
User Information Document (UID)	Same as above	NA	NA
Software Validation Report (SVR)	11217-SVR-1.0-01-WIN2003	DIRS 181118	MOL.20070208.0274

Table 3-13. MVIEW Software Documents

Version 1.0 XP (STN: 10072-4.0-01)			
Description	**Document ID**	**DIRS Number**	**Tracking Number**
Requirements Document (RD)	10072-RD-4.0-01	DIRS 174593	MOL.20050712.0023
Design Document (DD)	10072-DD-4.0-00	DIRS 174594	MOL.20050712.0025
User Information Document (UID)	10072-UID-4.0-00	DIRS 174595	MOL.20050712.0027
Software Validation Report (SVR)	10072-SVR-4.0-01-WINXP	DIRS 181119	MOL.20070417.0382

Table 3-14. PassTable1D_LA Software Documents

Version 1.0 Windows 2000 (STN: 11142-1.0-00)			
Description	**Document ID**	**DIRS Number**	**Tracking Number**
Software Management Report (SMR)	11142-SMR-1.0-00	DIRS 168978	MOL.20040310.0105
Version 1.0 Windows 2003 (STN: 11142-1.0-01)			
Description	**Document ID**	**DIRS Number**	**Tracking Number**
Software Management Report (SMR)	Same as above	NA	NA
Software Validation Report (SVR)	11142-SVR-1.0-01-WIN2003	DIRS 181120	MOL.20061218.0107
Version 2.0 Windows 2003 (STN: 11142-2.0-01)			
Description	**Document ID**	**DIRS Number**	**Tracking Number**
Requirements Document (RD)	11142-RD-2.0-01	DIRS 181121	MOL.20070420.0357
Design Document (DD)	11142-DD-2.0-01	DIRS 181122	MOL.20070420.0359
User Information Document (UID)	11142-UID-2.0-00	DIRS 181123	MOL.20070420.0361
Software Validation Report (SVR)	11142-SVR-2.0-00-WIN2000	DIRS 181124	MOL.20070420.0363
Software Validation Report (SVR)	11142-SVR-2.0-00-WIN2003	DIRS 181125	MOL.20070420.0365

Table 3-15. PassTable3D_LA Software Documents

Version 1.0 Windows 2000 (STN: 11143-1.0-00)			
Description	**Document ID**	**DIRS Number**	**Tracking Number**
Software Management Report (SMR)	11143-SMR-1.0-00	DIRS 168981	MOL.20040317.0127
Version 1.0 Windows 2003 (STN: 11143-1.0-01)			
Description	**Document ID**	**DIRS Number**	**Tracking Number**
Software Management Report (SMR)	Same as above	NA	NA
Software Validation Report (SVR)	11143-SVR-1.0-01-WIN2003	DIRS 181126	MOL.20070208.0286
Version 2.0 Windows 2000 and 2003 (STN: 11143-2.0-00)			
Description	**Document ID**	**DIRS Number**	**Tracking Number**
Requirements Document (RD)	11143-RD-2.0-00	DIRS 182916	MOL.20070816.0245
Design Document (DD)	11143-DD-2.0-00	DIRS 182917	MOL. 20070816.0247
User Information Document (UID)	11143-UID-2.0-00	DIRS 182918	MOL. 20070816.0252
Software Validation Report (SVR)	11143-SVR-2.0-00-WIN2000	DIRS 182919	MOL. 20070816.0254
Software Validation Report (SVR)	11143-SVR-2.0-00-WIN2003	DIRS 182920	MOL. 20070816.0256

Table 3-16. PREWAP_LA Software Documents

Version 1.1 Windows 2000 (STN: 10939-1.1-00)			
Description	**Document ID**	**DIRS Number**	**Tracking Number**
Requirements Document (RD)	10939-RD-1.1-00	DIRS 181127	MOL.20060418.0163
Design Document (DD)	10939-DD-1.1-00	DIRS 181128	MOL.20060418.0165
User Information Document (UID)	10939-UID-1.1-00	DIRS 181129	MOL.20060418.0169
Software Validation Report (SVR)	10939-SVR-1.1-00-WIN2000	DIRS 181130	MOL.20060418.0171

Table 3-17. SCCD Software Documents

Version 2.01 Windows 2000 (STN: 10343-2.01-00)			
Description	**Document ID**	**DIRS Number**	**Tracking Number**
Software Management Report (SMR)	10343-SRR-2.01-00	DIRS 152499	MOL.20010205.0113
Version 2.01 Windows 2003 (STN: 10343-2.01-00)			
Description	**Document ID**	**DIRS Number**	**Tracking Number**
Software Management Report (SMR)	Same as above	NA	NA
Software Validation Report (SVR)	10343-SVR-2.01-00-WIN2003	DIRS 181277	MOL.20070209.0013

Table 3-18. SEEPAGEDLL_LA Software Documents

Version 1.2 Windows 2000 (STN:11076-1.2-00)			
Description	**Document ID**	**DIRS Number**	**Tracking Number**
Requirements Document (RD)	11076-RD-1.2-00	DIRS 173465	MOL.20050406.0437
Design Document (DD)	11076-DD-1.2-00	DIRS 173464	MOL.20050406.0440
User Information Document (UID)	11076-UID-1.2-00	DIRS 173463	MOL.20050406.0425
Software Validation Report (SVR)	11076-SVR-1.2-00	DIRS 173462	MOL.20050406.0429
Version 1.3 Windows 2000 (STN:11076-1.3-00)			
Description	**Document ID**	**DIRS Number**	**Tracking Number**
Requirements Document (RD)	11076-RD-1.3-00	DIRS 181131	MOL.20060525.0294
Design Document (DD)	11076-DD-1.3-00	DIRS 181132	MOL.20060525.0296
User Information Document (UID)	11076-UID-1.3-00	DIRS 181133	MOL.20060525.0300
Software Validation Report (SVR)	11076-SVR-1.3-00-WIN2000	DIRS 181134	MOL.20060525.0302
Version 1.3 Windows 2003 (STN: 11076-1.3-01)			
Description	**Document ID**	**DIRS Number**	**Tracking Number**
Requirements Document (RD)	Same as above	NA	NA
Design Document (DD)	Same as above	NA	NA
User Information Document (UID)	Same as above	NA	NA
Software Validation Report (SVR)	11076-SVR-1.3-01-WIN2003	DIRS 181135	MOL.20070223.0249

Table 3-19. SoilExp_LA Software Documents

Version 1.0 Windows 2000 (STN: 10933-1.0-00)			
Description	**Document ID**	**DIRS Number**	**Tracking Number**
Requirements Document (RD)	10933-SMR-1.0-00	DIRS 168977	MOL.20040227.0046

Table 3-20. SZ_Convolute Software Documents

Version 3.0 Windows 2000 (STN:10207-3.0-00)			
Description	**Document ID**	**DIRS Number**	**Tracking Number**
Requirements Document (RD)	10207-RD-3.0-00	DIRS 167587	MOL.20030717.0478
Design Document (DD)	10207-DD-3.0-00	DIRS 167588	MOL.20030717.0479
User Manual (UM)	10207-UM-3.0-00	DIRS 167591	MOL.20030717.0483
Installation Test Process (ITP)	10207-ITP-3.0-00	DIRS 167590	MOL.20030717.0480
Validation Test Process (VTP)	10207-VTP-3.0-00	DIRS 167589	MOL.20030717.0481
Validation Test Report (VTR)	10207-VTR-3.0-00	DIRS 167593	MOL.20030717.0484
Version 3.10.01 Windows 2000 and Windows 2003 (STN:10207-3.10.01-01)			
Description	**Document ID**	**DIRS Number**	**Tracking Number**
Requirements Document (RD)	10207-RD-3.10-00	DIRS 181284	MOL.20061106.0218
Design Document (DD)	10207-DD-3.10-00	DIRS 181286	MOL.20061106.0219
User Information Document (UID)	10207-UID-3.10-00	DIRS 181288	MOL.20070223.0313
Software Validation Report (SVR)	10207-SVR-3.10.01-00-WIN2000	DIRS 181289	MOL.20070501.0392
Software Validation Report (SVR)	10207-SVR-3.10.01-00-WIN2003	DIRS 181290	MOL.20070501.0394

Table 3-21. TSPA_Input_DB Software Documents

Version 2.2 Windows 2000 (STN:10931-2.2-00)			
Description	**Document ID**	**DIRS Number**	**Tracking Number**
Requirements Document (RD)	10931-RD-2.0-00	DIRS 173449	MOL.20050131.0427
Design Document (DD)	10931-DD-2.0-00	DIRS 173450	MOL.20050131.0430
User Information Document (UID)	10931-UID-2.2-00	DIRS 181137	MOL.20060222.0419
Software Validation Report (SVR)	10931-SVR-2.2-00-WIN2000	DIRS 181139	MOL.20060222.0422
Version 2.2 Windows 2003 (STN:10931-2.2-01)			
Description	**Document ID**	**DIRS Number**	**Tracking Number**
Requirements Document (RD)	Same as above	NA	NA
Design Document (DD)	Same as above	NA	NA
User Information Document (UID)	Same as above	NA	NA
Software Validation Report (SVR)	10931-SVR-2.2-01-WIN2003	DIRS 181140	MOL.20061011.0198

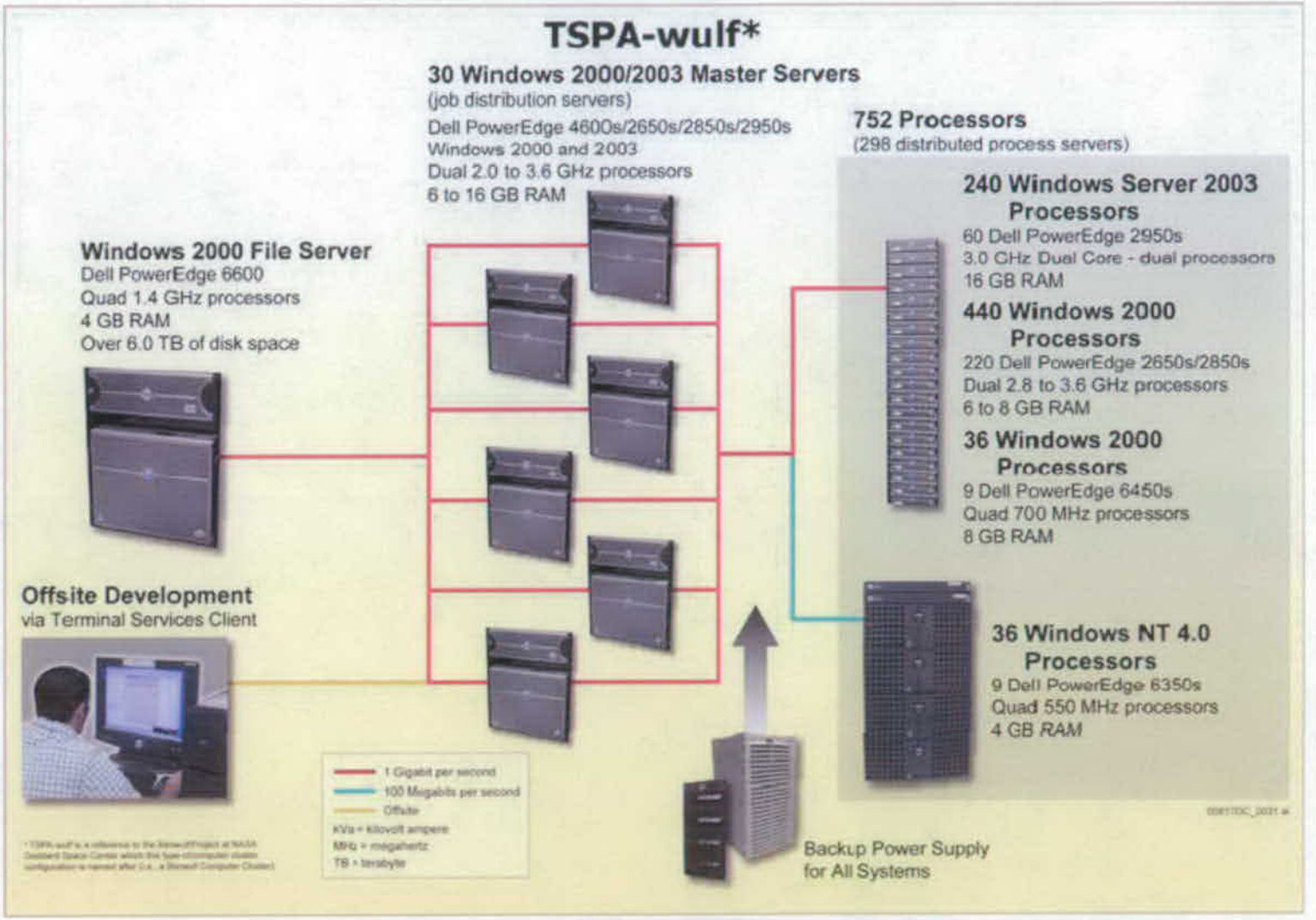

Figure 3-1. Hardware Configuration for TSPA-SEIS

INTENTIONALLY LEFT BLANK

4. INPUTS

The TSPA-SEIS integrates several model components and submodels to simulate the performance of the repository. A numerical representation was used to implement the model with GoldSim software (see Table 3-1 for specific versions used). Inputs used by this numerical representation of the TSPA-SEIS were obtained from controlled sources maintained by the OCRWM data and information systems, such as the Controlled Documents Information System, TDMS, Technical Information Center, and other available sources such as NRC Proposed Rule 10 CFR Part 63 [DIRS 178394 and 180319]. Figure 4-1 provides an overview of the information flow for the TSPA-SEIS development and analysis. This figure illustrates the control of information as it flows from initial data collection and generation to external process models, to the GoldSim software, and finally to the TSPA-SEIS output that is submitted to the TDMS.

This section provides descriptions of the TSPA-SEIS inputs, criteria, codes and standards, and the TSPA Input Database. Model inputs consist of both direct and indirect inputs per SCI-PRO-004, *Managing Technical Product Inputs.*

4.1 DIRECT INPUTS

Direct inputs are only those parameters and their values that are used by the TSPA-SEIS to develop results and conclusions presented in this report. This information is stored in the TSPA Input Database described in Section 4.7. Table 4-1 lists the direct inputs and associates each with a reference (source) and a Parameter Entry Form (PEF) number. The respective PEF (see Section 4.4 for an overview of PEFs) contains a list and descriptions of the parameters used as input and their sources.

When a direct input is referenced from an analysis and/or model report rather than a DTN, Table 4-1 lists the document title, document identifier (DI) number, revision number, and Document Input Reference System (DIRS) reference number for the analysis and model report. Similarly, when a direct input is referenced from an analysis and/or model report output DTN, Table 4-1 lists the DI, document title, DTN, and DIRS reference number for the DTN. In these cases, the DI and document title are listed to provide the connection to the analysis and/or model report that generated the DTN. The revision number for the analysis and/or model report is deliberately not shown because the Technical Database Information Form (TDIF) for the DTN will indicate the current analysis and/or model report revision number that is the source of the DTN.

In some instances, parameters are incorporated into input files or DLLs. The parameters that fall into these categories are specifically identified in the TSPA Input Database described in Section 4.7. Consequently, not all parameters in the TSPA Input Database are direct inputs, as defined by SCI-PRO-004. Thus, the PEFs containing these parameters are not presented in Table 4-1. For example, PEF 80 contains parameters that are actually all of the DLLs identified in the TSPA Input Database and used in the TSPA-SEIS.

4.2 TSPA-SEIS GENERATED PARAMETERS

The TSPA-SEIS requires the generation of many parameters (often incorporated into large data files) that are created by preprocessing methods (i.e., created prior to running the TSPA-SEIS).

These parameters are captured in output DTNs along with explanations for how they were generated.

4.3 PARAMETER ENTRY FORMS

All parameter names, parameter values, and parameter references used in support of the TSPA-SEIS are documented in PEFs and contained in the TSPA Input Database. PEFs document both parameters that were downloaded from the TSPA Input Database and parameters that were entered directly into the TSPA-SEIS. Figure 4-2 provides an overview of the PEF development and update process.

Concurrent with the TSPA-SEIS development, inputs changed as analysis and/or model reports and DTNs were revised. These changes caused some PEFs to be added and others were retired from further use. As a result, some PEF numbers do not appear in Table 4-1.

Generally, PEFs provide the following information:

- List of parameters, parameter descriptions, parameter values, and references
- Directions or roadmaps to the location(s) of the information in the references
- Explanations of any transformations, files, or parameters created by a TSPA analyst
- Signatures documenting that inputs were appropriately selected from analysis and/or model reports and used in the TSPA-SEIS.

The PEF contains signature lines for purposes of approval as represented on Figure 4-2. Approvals indicate the following:

- The Parameter Team Lead indicates that the PEF contains appropriate information, including the list of parameters, parameter descriptions, references where the parameters were obtained, and roadmaps describing the location of the parameters within the references.
- The TSPA analyst indicates that the PEF contains the parameters (and their associated parameter values) used as direct input to the TSPA-SEIS and any conversions made to the parameter values necessary for model input.
- The SME indicates that the PEF accurately represents the parameters (and their associated parameter values) and the references intended for TSPA-SEIS input. SMEs are generally the principal investigators that are most knowledgeable about the input parameters and their uncertainties for use in the TSPA-SEIS.
- The database administrator indicates that the parameters and parameter values are available in the TSPA Input Database in the appropriate formats defined by the software documents listed in Table 3-21.

4.4 TRACEABILITY OF INPUTS

Traceability of inputs is provided by using one or more of the following tools:

- **DIRS Database**—DIRS is a database that contains the technical product input sources, such as direct and indirect inputs and their status.

- **TSPA Input Database**—The TSPA Input Database (Section 4.7) provides detailed information for each parameter, such as parameter name, parameter description and type, source reference, parameter value, and verification status. When the database is downloaded into the TSPA-SEIS, this traceability information is embedded in the TSPA-SEIS as a model element.

- **Table 4-1**—Table 4-1 lists all direct inputs used in the TSPA-SEIS and associates each direct input with a PEF.

- **PEFs**—The PEFs collectively contain all parameters used as input to the TSPA-SEIS. Each PEF references the specific locations of the parameters within a reference document or DTN to aid in the traceability of the direct inputs. The original signed PEFs are in the records package for this document; however, the TSPA Input Database can be used to generate any PEF, as described in Section 4.7.

- **TSPA-SEIS**—The TSPA Input Database information is embedded in the TSPA-SEIS file (e.g., parameter name, type of parameter, source reference, and parameter value).

4.5 CRITERIA

In NRC Proposed Rule 10 CFR 63.102(j) [DIRS 180319], the NRC requires the DOE to complete "a performance assessment to quantitatively estimate radiological exposures to the reasonably maximally exposed individual at any time during the compliance period." The TSPA-SEIS was developed to meet this requirement.

4.6 CODES AND STANDARDS

No codes or standards are required for this document other than those identified in Section 4.5.

4.7 TSPA INPUT DATABASE

This section provides a summary of the TSPA Input Database. Additional detail on its design and operation can be found in the software documents listed in Section 3. The TSPA Input Database supports the TSPA-SEIS by providing the parameter values and distributions necessary for the PA analysis of the repository. The database is used to categorize, store, and retrieve fixed and distributed values of the TSPA-SEIS parameters. The database is programmed with user controls featuring read and write access and audit trails. These controls were designed to ensure the security, integrity, and traceability of the information used in the TSPA-SEIS analyses. The following sections provide a brief overview of:

- Database structure
- Database operation login
- Database forms
  -Parameter Identification Form (PIF)
  -Parameter Documentation Form (PDF)
  -Parameter Value Entry Form (PVEF)
  -PEF Information Entry Form
  -Parameter Verification Form (PVF).
- Database reports
- Database support of GoldSim.

4.7.1 Database Structure

The TSPA Input Database was developed using a commercially available desktop database manager, Microsoft Access 2000. It is a multi-user, Microsoft Windows based, relational database solution that allows data entry, viewing, and querying, as well as report preparation. The TSPA Input Database was designed and qualified in accordance with IM-PRO-004, *Qualification of Software*. The software documents listed in Table 3-21 provide details of the software design and implementation of the database. In a relational database, related information can be stored in separate tables, reducing the likelihood of redundant entries. Referential integrity relationships among tables in the TSPA Input Database are used where there is information in one table that must refer to information in another table.

Figure 4-3 illustrates the structured framework (schema) of the TSPA Input Database and the relationships among the three fundamental elements of data flow and data storage in the database. The three principal operational elements of the database are the PIF, parameter documentation form, and parameter value entry form. Each of these three database elements appears as a separate interactive screen image when the database is electronically accessed. The relationship line between these elements, (Figure 4-3) automatically enforces database referential integrity by creating a foreign key constraint on the related tables. In this manner, parameter information is not duplicated across multiple tables.

4.7.2 Database Operation Login

The initial point of entry to the TSPA Input Database is the login screen, which contains a password entry feature to control access of authorized users. (Note: the database that is included with the electronic version of this document does not have password entry because it is read-only.) Each authorized user is assigned a user name, and each user name has an established password and user level. The user level (i.e., 1, 2, or 3) determines user privileges. A Level 1 user is allowed to perform data entry and updates but is not allowed to perform data verifications. A Level 2 user is allowed to view data and perform data verifications. A Level 3 user has read-only privileges.

4.7.3 Parameter Identification Form

Following login into the TSPA Input Database, the PIF (Figure 4-4) appears as the first interactive, menu-driven screen image. The PIF serves as the primary means to view existing parameters and to enter new parameters into the database. All parameters have an associated PIF accessible by selecting a parameter name from the list on the left side of the PIF. The database ensures that each parameter is assigned a unique parameter name and parameter identification. The PIF presents the PEF number that the parameter is assigned, a description of the parameter, and other attributes. The Primary Model Location field identifies the location in which the parameter is first introduced into the TSPA-SEIS as a data element. In contrast, the Other Locations field identifies the other locations in which the parameter is introduced into the TSPA-SEIS. These locations are often difficult to ascertain due to the complexity of the model and should be viewed as general assignments.

4.7.4 Parameter Documentation Form

The parameter documentation form (Figure 4-5) is accessible from the PIF via the Documentation button. This form presents the reference information from which the parameter was obtained. The appearance of the parameter documentation form differs depending on the parameter type recorded on the PIF. For example, if the parameter type is file, two additional fields are displayed. The File Element Pathway field contains the external file pathway to the controlled data file, and the Document Signature field contains the associated audit-tracking signature number. This information is required by the GoldSim software in order to perform external file and DLL transfers. For details, see *User's Guide, GoldSim Probabilities Simulation Environment* (GoldSim Technology Group 2007 [DIRS 181727]). The effective date on the form indicates the date the parameter was entered into the TSPA Input Database. Finally, the parameter documentation form contains a hyperlink to the Automated Technical Data Tracking system to provide access directly to the DTN from which the parameters were obtained.

4.7.5 Parameter Value Entry Form

The parameter value entry from (Figure 4-6) is accessible from the parameter documentation form via the Value button. This form presents the parameter value(s). The appearance of the parameter value entry form differs depending on the parameter type recorded on the PIF. Each parameter type has a corresponding parameter value format. In addition, each parameter value has a unique component identification. For data tables, each row of data has its own component identification. For one-dimensional and two-dimensional data tables and multiple-row stochastic values, two separate forms are required. Figure 4-6 is an example of a parameter value entry form for the 1-D Table parameter type, with multiple-row stochastic values. A sequential code is assigned to each row of values in the input tables. This code is read by the GoldSim software to ensure that downloads from the TSPA Input Database are performed in the correct order.

4.7.6 Parameter Entry Form Information Entry Form

The PEF Information Entry Form (Figure 4-7) is accessible from the PIF via the Enter PEF Information button. For each PEF number, this form presents the name of the analyst(s),

roadmap information, and PEF revision history. The contents and purpose of the PEF are described in more detail in Section 4.3.

4.7.7 Parameter Verification Form

The parameter verification form (Figure 4-8) is accessible from the PIF form, parameter documentation form, and parameter value entry form via the Verify button. This form presents the checker's name, date and time of verification, and any checker comments. The Editing History field shows all users and the dates and times for modifications made to the parameter information. The verification status is cleared when any parameter form is modified that affects a parameter. A cleared verification status indicates that the parameter needs to be reverified. Before downloading parameter values to the TSPA-SEIS for a PA analysis, each parameter undergoes verification to ensure that all information was correctly and completely entered. Only users with the appropriate, controlled access to the TSPA Input Database can perform data verification (Section 4.7.2).

4.7.8 Database Reports

TSPA Input Database reports are accessible from the PIF via the Report button. The following reports can be produced:

- **Alphabetized Parameter Listing**—This report is an alphabetic list of all parameters and includes parameter description, primary model location, PEF number, and reference information.
- **Parameter Listing by Analyst(s)**—This report lists all parameters for a specified TSPA analyst. The report is grouped by PEF number and primary model location and includes parameter description, input type, other model locations, reference information, and verification status.
- **Complete Parameter Listing by PEF**—This report lists all parameters by PEF number and includes parameter description, units, type, distribution, primary model location, and reference information. A count of parameter entries is displayed for each PEF grouping and for the entire database.
- **Print a PEF**—This report displays the PEF information for a selected PEF number and includes TSPA analyst, roadmap, and revision history; all parameters associated with the PEF parameter description; reference information; and any associated To Be Verified (TBV) references. A count of the total number of parameter entries for the PEF is printed at the end of the parameter listing.
- **List by All Locations in TSPA-SEIS**—This report lists all parameters associated with the specified TSPA-SEIS location which includes both primary and other locations. The list includes PEF number, parameter description, input type, reference information, and whether the model location is primary. The number of parameter entries for the TSPA-SEIS location requested is reported at the end of the list.

- **List by Primary Locations in TSPA-SEIS**—This report lists all parameters associated with the specified primary model location and is grouped by reference document. The report includes parameter description, PEF number, and any associated DTN(s).
- **Report and DTN Listings**—This report lists all references cited in the PEFs and includes analysis and/or model reports by DI and document title and all associated DTNs.
- **DI–PEF List**—This report lists all parameters grouped by PEF for the selected DI. The information presented includes parameter description, primary model location, and input type. The end of each DI list includes a count of the number of PEFs and parameter entries.
- **List All Data**—This report lists all information about the selected parameter, including the parameter values.
- **List by Input Type**—This report lists all parameters associated with the selected input type. The information presented includes PEF, parameter description, primary model location, and reference information. The number of parameter entries is reported at the end of the report.

4.7.9 Database Support of GoldSim

The TSPA Input Database serves as the quality-controlled repository for the input parameters before the parameter values are downloaded to the TSPA-SEIS. The database is designed to interface with GoldSim, via ODBC, for automated downloads to the TSPA-SEIS. Upon download of the database to the TSPA-SEIS, designated content from the database is embedded in a model element.

The TSPA Input Database download provides two primary functions: (1) insures the most recent data are being used, and (2) insures that the correct DLLs and input files are moved from a controlled directory to the directory for the current GoldSim run.

INTENTIONALLY LEFT BLANK

Table 4-1. Direct Inputs

Line #	Document_ID	Reference_Document	Document DIRS	DTN	DTN DIRS	PEF
1	10 CFR 63	10 CFR 63. Energy: Disposal of High-Level Radioactive Wastes in a Geologic Repository at Yucca Mountain, Nevada	180319	NA	NA	81
	70 FR 53313	Implementation of a Dose Standard After 10,000 Years	178394	NA	NA	90
2	ANL-EBS-MD-000003	*General Corrosion and Localized Corrosion of Waste Package Outer Barrier*	NA	MO0703PAGENCOR.001_R4	182029	5
3	ANL-EBS-MD-000003	*General Corrosion and Localized Corrosion of Waste Package Outer Barrier*	NA	MO0703PAGENCOR.001_R4	182029	7
	ANL-EBS-MD-000003	*General Corrosion and Localized Corrosion of Waste Package Outer Barrier*	NA	MO0703PAGENCOR.001_R4	182029	85
4	ANL-EBS-MD-000003	*General Corrosion and Localized Corrosion of Waste Package Outer Barrier*	NA	MO0703PAGENCOR.001_R4	182029	117
5	ANL-EBS-MD-000004	*General Corrosion and Localized Corrosion of the Drip Shield*	NA	SN0704PADSGCMT.001_R2	182122	3
6	ANL-EBS-MD-000004	*General Corrosion and Localized Corrosion of the Drip Shield*	NA	SN0704PADSGCMT.002_R2	182188	105
7	ANL-EBS-MD-000005	*Stress Corrosion Cracking of Waste Package Outer Barrier and Drip Shield Materials*	NA	MO0702PASTRESS.002_R2	180514	4
8	ANL-EBS-MD-000015	*CSNF Waste Form Degradation: Summary Abstraction*	NA	MO0404ANLSF001.001_R0	169007	31
9	ANL-EBS-MD-000015 REV 02	*CSNF Waste Form Degradation: Summary Abstraction*	169987	NA	NA	82
10	ANL-EBS-MD-000016	*Defense HLW Glass Degradation Model*	NA	MO0502ANLGAMR1.016_R0	172830	32

Table 4-1. Direct Inputs (Continued)

Line #	Document_ID	Reference_Document	Document DIRS	DTN	DTN DIRS	PEF
11	ANL-EBS-MD-000033	*Engineered Barrier System: Physical and Chemical Environment*	NA	SN0701PAEBSPCE.001_R1	180523	75
12	ANL-EBS-MD-000033	*Engineered Barrier System: Physical and Chemical Environment*	NA	SN0701PAEBSPCE.002_R0	179425	76
13	ANL-EBS-MD-000033	*Engineered Barrier System: Physical and Chemical Environment*	NA	SN0703PAEBSPCE.006_R2	181571	77
14	ANL-EBS-MD-000033	*Engineered Barrier System: Physical and Chemical Environment*	NA	SN0703PAEBSPCE.007_R1	180177	78
14.5	ANL-EBS-MD-000033	*Engineered Barrier System: Physical and Chemical Environment*	NA	SN0706PAEBSPCE.016_R0	181837	104
	ANL-EBS-MD-000033 Rev 06	*Engineered Barrier System: Physical and Chemical Environment*	177412	NA	NA	119
15	ANL-EBS-MD-000037	*In-Package Chemistry Abstraction*	NA	MO0502SPAINPCA.000_R0	172893	79
16	ANL-EBS-MD-000037	*In-Package Chemistry Abstraction*	NA	SN0702PAIPC1CA.001_R2	180451	12
16.5	ANL-EBS-MD-000037	*In-Package Chemistry Abstraction*	NA	SN0702PAIPC1CA.001_R2	180451	102
17	ANL-EBS-MD-000049	*Multiscale Thermohydrologic Model*	NA	LL0702PA027MST.082_R0	179590	15
18	ANL-EBS-MD-000049	*Multiscale Thermohydrologic Model*	NA	LL0702PA027MST.082_R0	179590	86
19	ANL-EBS-MD-000049	*Multiscale Thermohydrologic Model*	NA	LL0703PA011MST.006_R0	179853	16
20	ANL-EBS-MD-000049	*Multiscale Thermohydrologic Model*	NA	LL0703PA012MST.007_R0	179854	17
21	ANL-EBS-MD-000049	*Multiscale Thermohydrologic Model*	NA	LL0703PA013MST.008_R0	179855	18
22	ANL-EBS-MD-000049	*Multiscale Thermohydrologic Model*	NA	LL0703PA014MST.009_R0	179856	19
23	ANL-EBS-MD-000049	*Multiscale Thermohydrologic Model*	NA	LL0703PA015MST.010_R0	179857	20
24	ANL-EBS-MD-000049	*Multiscale Thermohydrologic Model*	NA	LL0703PA016MST.011_R0	179858	21
25	ANL-EBS-MD-000049	*Multiscale Thermohydrologic Model*	NA	LL0703PA017MST.012_R0	179859	22
25.1	ANL-EBS-MD-000049	*Multiscale Thermohydrologic Model*	NA	LL0703PA026MST.013_R0	179981	50
26	ANL-EBS-MD-000049	*Multiscale Thermohydrologic Model*	NA	LL0703PA034MST.016_R0	179982	23
28	ANL-EBS-MD-000049	*Multiscale Thermohydrologic Model*	NA	LL0703PA035MST.017_R0	179985	24
29	ANL-EBS-MD-000049	*Multiscale Thermohydrologic Model*	NA	LL0703PA036MST.018_R0	179986	25
30	ANL-EBS-MD-000049	*Multiscale Thermohydrologic Model*	NA	LL0703PA037MST.019_R0	179989	26

Table 4-1. Direct Inputs (Continued)

Line #	Document_ID	Reference_Document	Document DIRS	DTN	DTN DIRS	PEF
31	ANL-EBS-MD-000049	*Multiscale Thermohydrologic Model*	NA	LL0703PA038MST.020_R0	179992	27
32	ANL-EBS-MD-000049	*Multiscale Thermohydrologic Model*	NA	MO0505SPAROCKM.000_R0	173893	28
33	ANL-EBS-MD-000049	*Multiscale Thermohydrologic Model*	NA	MO0703PAHYTHRM.000_R1	182093	29
34	ANL-EBS-MD-000076	*Analysis of Mechanisms for Early Waste Package/Drip Shield Failure*	NA	MO0701PASHIELD.000_R2	180508	2
35	ANL-EBS-MD-000076	*Analysis of Mechanisms for Early Waste Package/Drip Shield Failure*	NA	MO0701PASHIELD.000_R2	180508	118
36	ANL-MGR-GS-000001	*Characterize Framework for Igneous Activity at Yucca Mountain, Nevada*	NA	LA0307BY831811.001_R0	164713	60
37	ANL-MGR-GS-000003	*Number of Waste Packages Hit by Igneous Intrusion*	NA	SN0701PAWPHIT.001_R2	182961	61
37.5	ANL-MGR-GS-000003	*Number of Waste Packages Hit by Igneous Intrusion*	NA	SN0701PAWPHIT.001_R2	182961	800
38	ANL-MGR-GS-000003	*Number of Waste Packages Hit by Igneous Intrusion*	NA	SN0701PAWPHIT1.001_R2	182961	30
39	ANL-NBS-GS-000008	*Future Climate Analysis*	NA	GS000308315121.003_R0	151139	33
40	ANL-NBS-HS-000031	*Saturated Zone Colloid Transport*	NA	LA0303HV831352.003_R0	165624	84
40.5	ANL-NBS-HS-000058	*Calibrated Unsaturated Zone Properties*	NA	LB0610UZDSCP30.001	179180	116
41	ANL-WIS-MD-000004 REV 04	*DSNF and Other Waste Form Degradation Abstraction*	172453	NA	NA	83
42	ANL-WIS-MD-000010	*Dissolved Concentration Limits of Elements with Radioactive Isotopes*	NA	MO0702PADISCON.001_R0	179358	9
43	ANL-WIS-MD-000010	*Dissolved Concentration Limits of Elements with Radioactive Isotopes*	NA	MO0702PAFLUORI.000_R1	181219	10
44	ANL-WIS-MD-000010	*Dissolved Concentration Limits of Elements with Radioactive Isotopes*	NA	MO0704PASOLCAP.000_R0	180389	11
45	ANL-WIS-MD-000020	*Initial Radionuclides Inventory*	NA	MO0702PASTREAM.001_R0	179925	72
46	ANL-WIS-MD-000020	*Initial Radionuclides Inventory*	NA	MO0702PASTREAM.001_R0	179925	113
47	ANL-WIS-MD-000020	*Initial Radionuclide Inventory*	NA	SN0310T0505503.004_R0	168761	74
48	ANL-WIS-MD-000021	*Cladding Degradation Summary for*	NA	MO0411SPACLDDG.003_R1	180755	1

Table 4-1. Direct Inputs (Continued)

Line #	Document_ID	Reference_Document	Document DIRS	DTN	DTN DIRS	PEF
		LA				
48.5	ANL-WIS-MD-000021 Rev 03 ADD 01	*Cladding Degradation Summary for LA*	180616	NA	NA	92
49	ANL-WIS-PA-000001	*EBS Radionuclide Transport Abstraction*	NA	SN0703PAEBSRTA.001_R1	183217	59
49.5	NA	*Fundamentals of Heat and Mass Transfer*	163337	NA	NA	47
50	MDL-EBS-MD-000001	*In-Drift Natural Convection and Condensation*	NA	MO0703PAEVSIIC.000_R2	181990	73
51	MDL-EBS-MD-000001	*In-Drift Natural Convection and Condensation*	NA	MO0702PALOVERT.000_R2	180377	70
52	MDL-EBS-MD-000001	*In-Drift Natural Convection and Condensation*	NA	MO0702PALV010K.000_R2	180376	71
52.5	MDL-EBS-MD-000001Rev 00 ADD 01	*In-Drift Natural Convection and Condensation*	181648	NA	NA	99
53	MDL-EBS-PA-000004	*Waste Form and In-Drift Colloids-Associated Radionuclide Concentrations: Abstraction and Summary*	NA	MO0701PACSNFCP.000_R1	180439	53
54	MDL-EBS-PA-000004	*Waste Form and In-Drift Colloids-Associated Radionuclide Concentrations: Abstraction and Summary*	NA	MO0701PAGLASWF.000_R1	180393	54
55	MDL-EBS-PA-000004	*Waste Form and In-Drift Colloids-Associated Radionuclide Concentrations: Abstraction and Summary*	NA	MO0701PAGROUND.000_R0	179310	55
56	MDL-EBS-PA-000004	*Waste Form and In-Drift Colloids-Associated Radionuclide Concentrations: Abstraction and Summary*	NA	MO0701PAIRONCO.000_R1	180440	56

Table 4-1. Direct Inputs (Continued)

Line #	Document_ID	Reference_Document	Document DIRS	DTN	DTN DIRS	PEF
57	MDL-EBS-PA-000004	*Waste Form and In-Drift Colloids-Associated Radionuclide Concentrations: Abstraction and Summary*	NA	MO0701PAKDSUNP.000_R1	180392	57
58	MDL-EBS-PA-000004	*Waste Form and In-Drift Colloids-Associated Radionuclide Concentrations: Abstraction and Summary*	NA	MO0701PASORPTN.000_R1	180391	58
59	MDL-MGR-GS-000002	*Atmospheric Dispersal and Deposition of Tephra from a Potential Volcanic Eruption at Yucca Mountain, Nevada*	NA	LA0612DK831811.001_R1	179987	62
60	MDL-MGR-GS-000002	*Atmospheric Dispersal and Deposition of Tephra from a Potential Volcanic Eruption at Yucca Mountain, Nevada*	NA	LA0702PADE03GK.002_R1	179980	63
61	MDL-MGR-GS-000002	*Atmospheric Dispersal and Deposition of Tephra from a Potential Volcanic Eruption at Yucca Mountain, Nevada*	NA	MO0408SPADRWSD.002_R0	171751	64
62	MDL-MGR-GS-000005	*Dike/Drift Interactions*	NA	LA0702PADE01EG.001_R0	179495	13
63	MDL-MGR-GS-000005	*Dike/Drift Interactions*	NA	LA0702PADE01EG.002_R0	179496	14
64	MDL-MGR-GS-000006	*Redistribution of Tephra and Waste by Geomorphic Processes Following a Potential Volcanic Eruption at Yucca Mountain, Nevada*	NA	MO0605SPAFORTY.000_R1	182281	65
65	MDL-MGR-GS-000006	*Redistribution of Tephra and Waste by Geomorphic Processes Following a Potential Volcanic Eruption at Yucca Mountain, Nevada*	NA	MO0702PAFARDAT.001_R3	182578	66
66	MDL-MGR-GS-000006	*Redistribution of Tephra and Waste by Geomorphic Processes Following a Potential Volcanic Eruption at Yucca Mountain, Nevada*	NA	MO0704PASCOURD.000_R1	182149	87
67	MDL-MGR-MD-000001	*Biosphere Model Report*	NA	MO0702PAGBDCFS.001_R0	179327	67

Table 4-1. Direct Inputs (Continued)

Line #	Document_ID	Reference_Document	Document DIRS	DTN	DTN DIRS	PEF
68	MDL-MGR-MD-000001	*Biosphere Model Report*	NA	MO0702PAGWPROS.001_R0	179328	68
69	MDL-MGR-MD-000001	*Biosphere Model Report*	NA	MO0702PAVBPDCF.000_R0	179330	69
70	MDL-NBS-HS-000006	*UZ Flow Models and Submodels*	NA	LB0612PDFEHMFF.001_R0	179296	38
71	MDL-NBS-HS-000006	*UZ Flow Models and Submodels*	NA	LB0701GTFEHMFF.001_R0	179160	39
72	MDL-NBS-HS-000006	*UZ Flow Models and Submodels*	NA	LB0701MOFEHMFF.001_R0	179297	40
73	MDL-NBS-HS-000006	*UZ Flow Models and Submodels*	NA	LB0702PAFEM10K.002_R0	179507	43
74	MDL-NBS-HS-000006	*UZ Flow Models and Submodels*	NA	LB0701PAWFINFM.001_R0	179283	42
75	MDL-NBS-HS-000008	*Radionuclide Transport Models Under Ambient Conditions*	NA	LB0701PAKDSESN.001_R0	179299	41
76	MDL-NBS-HS-000008	*Radionuclide Transport Models Under Ambient Conditions*	NA	LB0702PAUZMTDF.001_R1	180776	46
77	MDL-NBS-HS-000008	*Radionuclide Transport Models Under Ambient Conditions*	NA	LA0408AM831341.001_R0	171584	34
78	MDL-NBS-HS-000019	*Abstraction of Drift Seepage*	NA	LB0702PASEEP01.001_R0	179511	44
79	MDL-NBS-HS-000019	*Abstraction of Drift Seepage*	NA	LB0702PASEEP02.001_R1	181635	45
80	MDL-NBS-HS-000019	*Abstraction of Drift Seepage*	NA	LB0407AMRU0120.001_R0	173280	37
81	MDL-NBS-HS-000020	*Particle Tracking Model and Abstraction of Transport Processes*	NA	LA0701PANS02BR.003_R2	180497	35
82	MDL-NBS-HS-000020	*Particle Tracking Model and Abstraction of Transport Processes*	NA	LA0702PANS02BR.001_R1	180322	36
82.5	MDL-NBS-HS-000020	*Particle Tracking Model and Abstraction of Transport Processes*	NA	LA0702PANS02BR.001_R1	180322	114
83	MDL-NBS-HS-000020	*Particle Tracking Model and Abstraction of Transport Processes*	NA	MO0704PAFEHMBR.001_R2	180526	48
84	MDL-NBS-HS-000020	*Particle Tracking Model and Abstraction of Transport Processes*	NA	MO0704PAFEHMBR.001_R2	180526	101
85	MDL-NBS-HS-000020	*Particle Tracking Model and Abstraction of Transport Processes*	NA	MO0704PAPTTFBR.002_R0	180442	49
	MDL-NBS-HS-000020 Rev 02 ADD 01	*Particle Tracking Model and Abstraction of Transport Processes*	181006	NA	NA	100

Table 4-1. Direct Inputs (Continued)

Line #	Document_ID	Reference_Document	Document DIRS	DTN	DTN DIRS	PEF
86	MDL-NBS-HS-000021	*Saturated Zone Flow and Transport Model Abstraction*	NA	SN0702PASZFTMA.001_R0	179504	51
87	MDL-NBS-HS-000021	*Saturated Zone Flow and Transport Model Abstraction*	NA	SN0702PASZFTMA.002_R0	179494	52
87.5	MDL-NBS-HS-000021	*Saturated Zone Flow and Transport Model Abstraction*	NA	SN0702PASZFTMA.002_R0	179494	89
87.6	MDL-NBS-HS-000021 Rev 03	*Saturated Zone Flow and Transport Model Abstraction*	181650	NA	NA	128
88	MDL-WIS-PA-000003	*Seismic Consequence Abstraction*	NA	MO0703PASEISDA.002_R4	183156	6
90	TDR-TDIP-ES-000005 Rev 00	*Total System Performance Assessment Data Input Package for No Commercial Spent Nuclear Fuel Cladding Credit*	180648	NA	NA	92
91	TDR-TDIP-ES-000006 Rev 00	*Total System Performance Assessment Data Input Package for Requirements Analysis for TAD Canister and Related Waste Package Overpack Physical Attributes Basis for Performance Assessment*	179394	NA	NA	109
92	TDR-TDIP-ES-000009 Rev 00	*Total System Performance Assessment Data Input Package for Requirements Analysis for DOE SNF/HLW and Navy SNF Waste Package Overpack Physical Attributes Basis for Performance Assessment*	179567	NA	NA	110

INTENTIONALLY LEFT BLANK

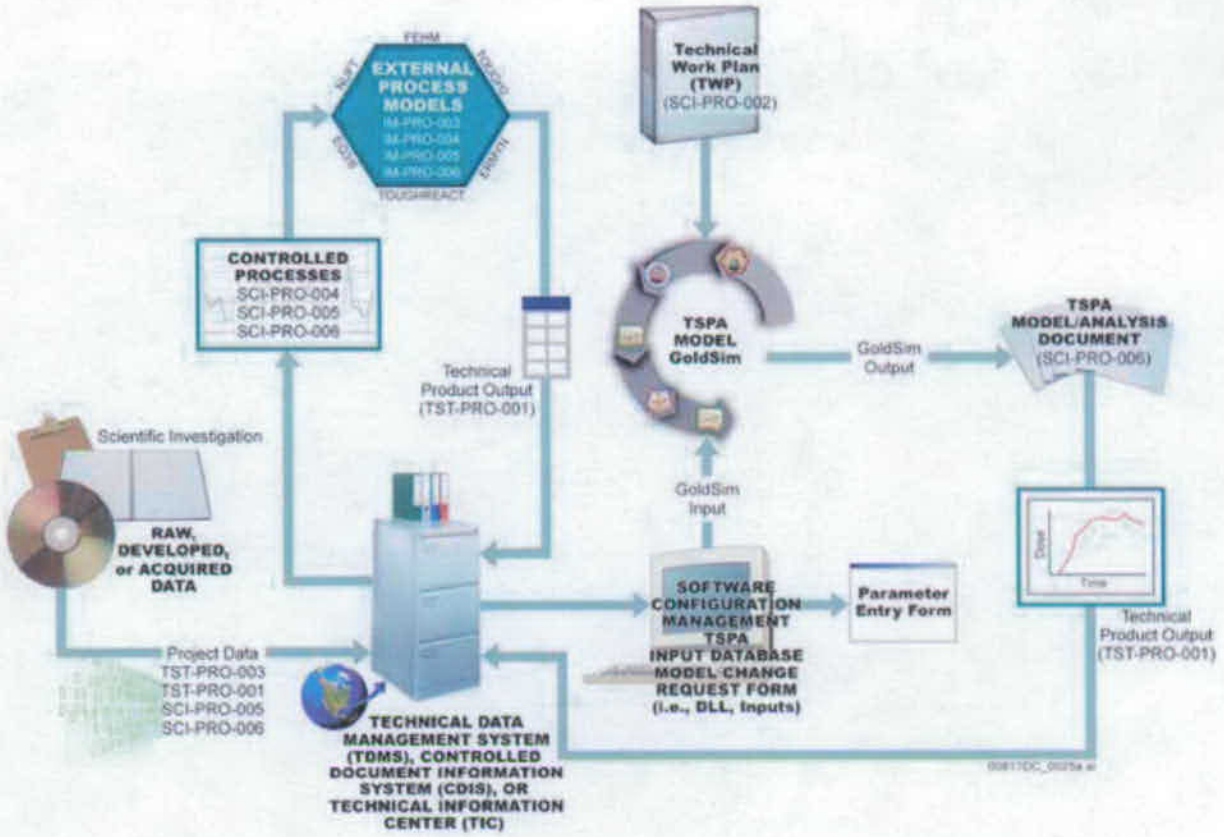

Figure 4-1. Control of Information for TSPA-SEIS Development and Analysis

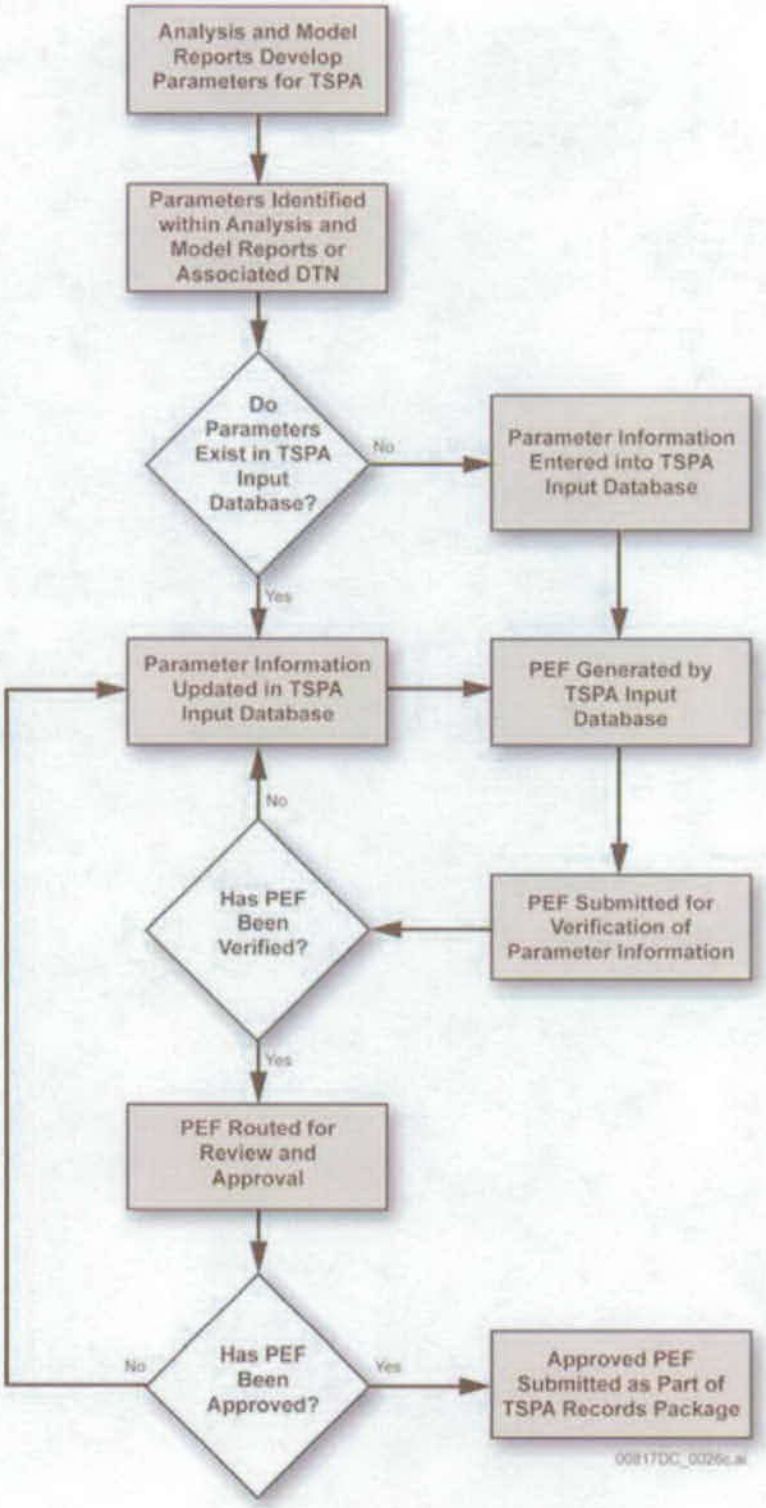

Figure 4-2. Development and Revision of Parameter Entry Forms

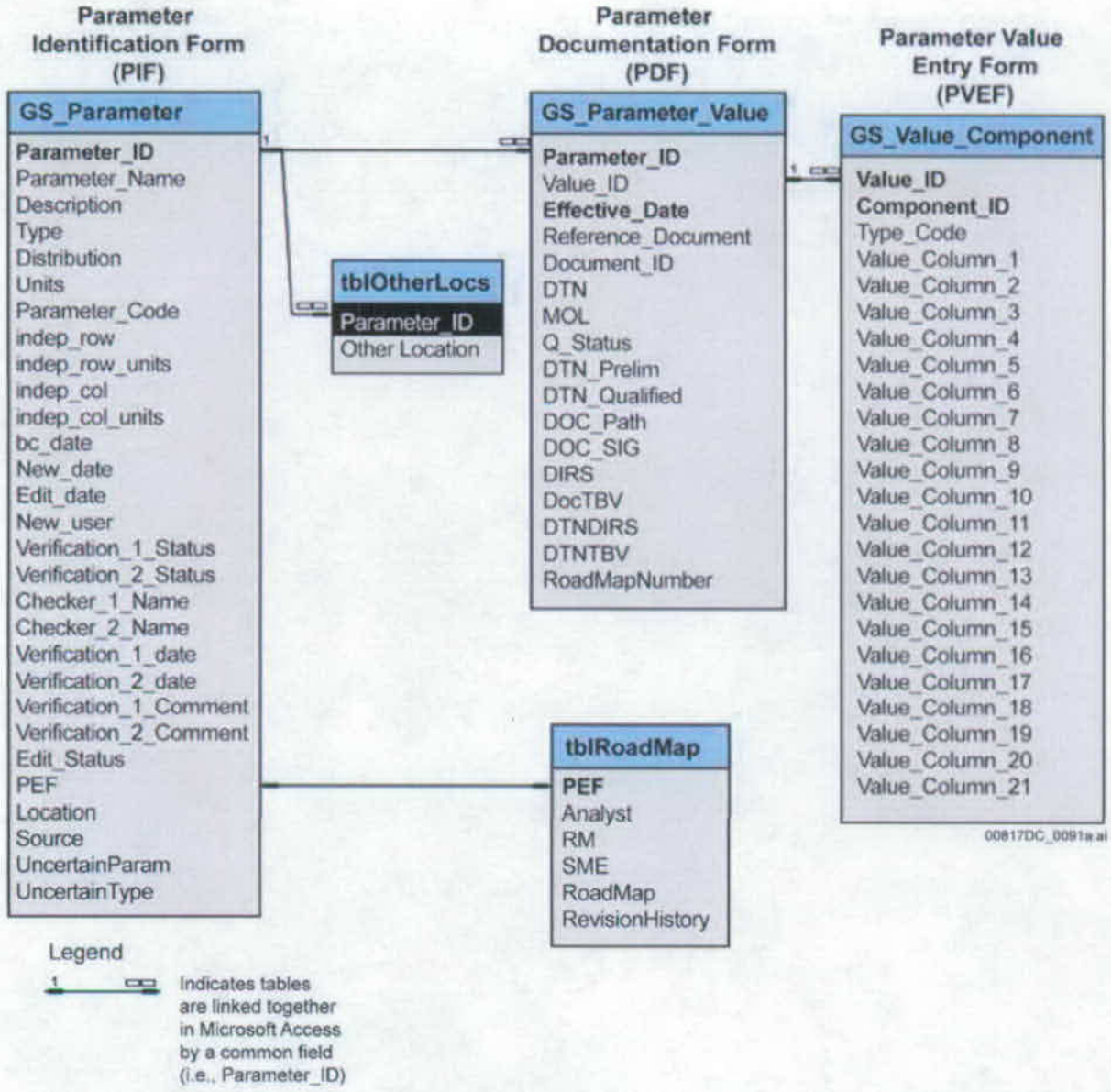

NOTE: These tables are described in detail in the TSPA Input Database documents listed in Section 3.

Figure 4-3. Structural Framework (Schema) for the TSPA Input Database Showing Relationships between Tables

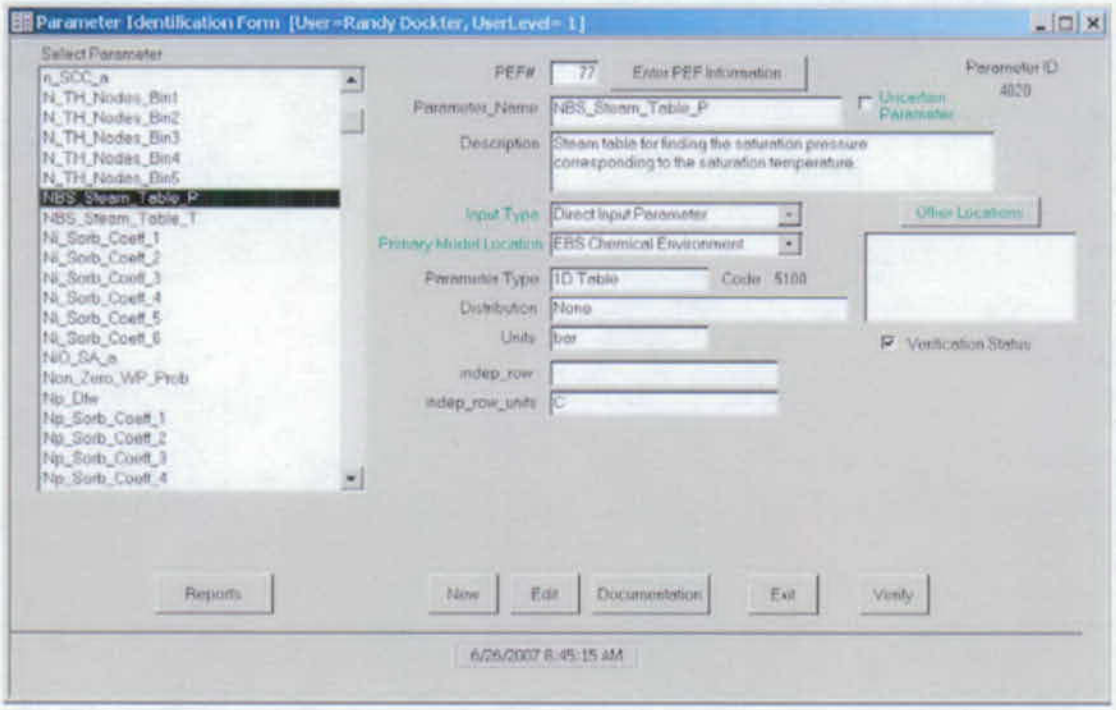

Figure 4-4. Example of a Parameter Identification Form for the TSPA Input Database

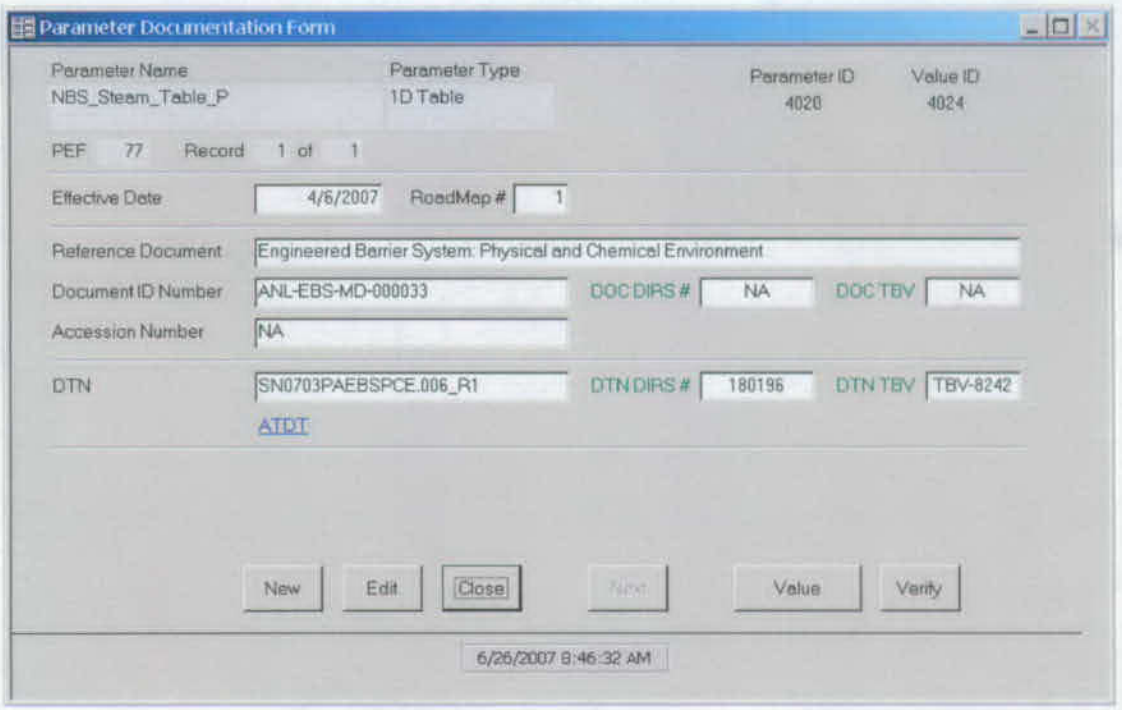

Figure 4-5. Example of a Parameter Documentation Form for the TSPA Input Database

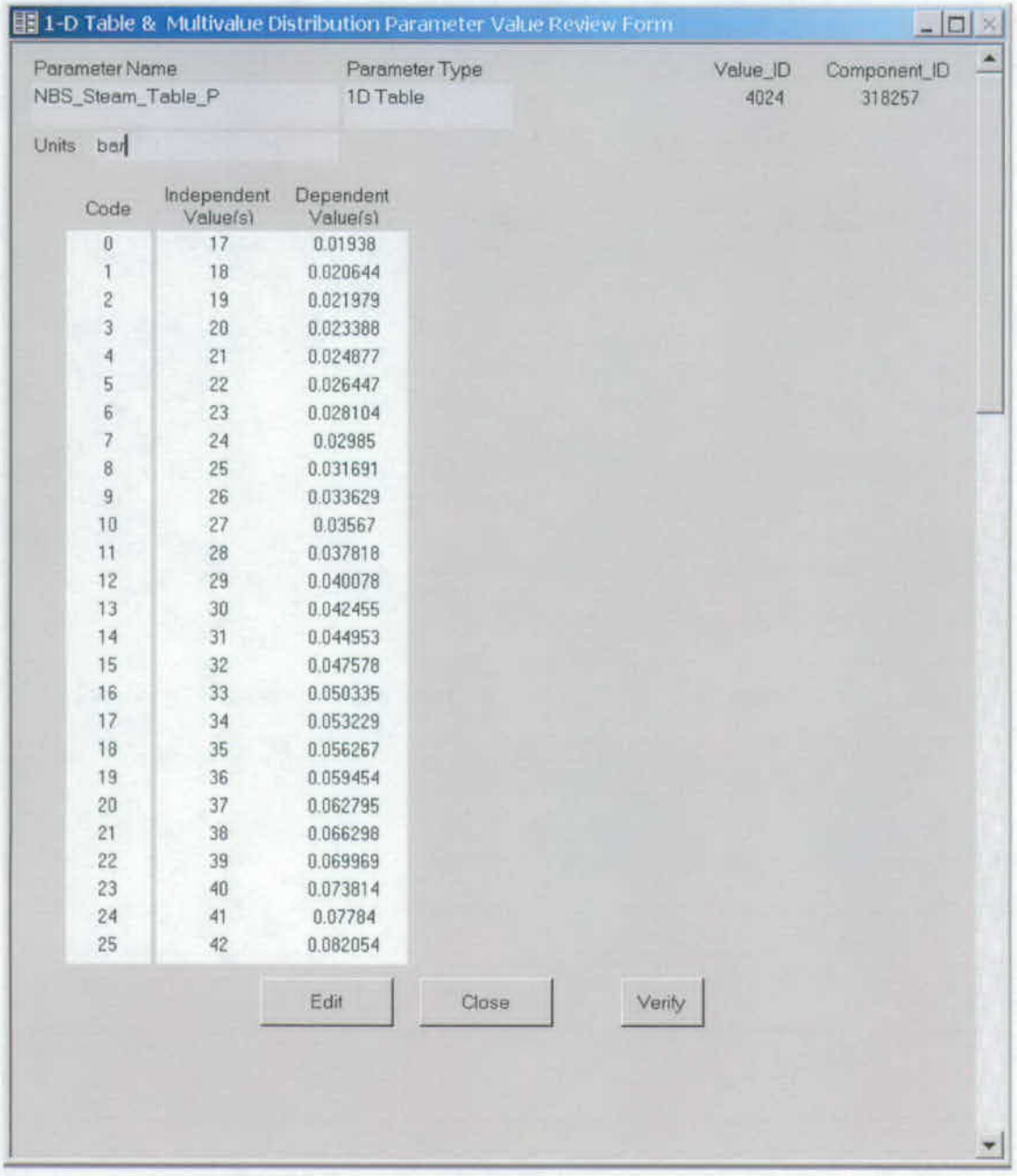

Figure 4-6. Example of a Parameter Value Entry Form for a One-Dimensional Data Table in the TSPA Input Database

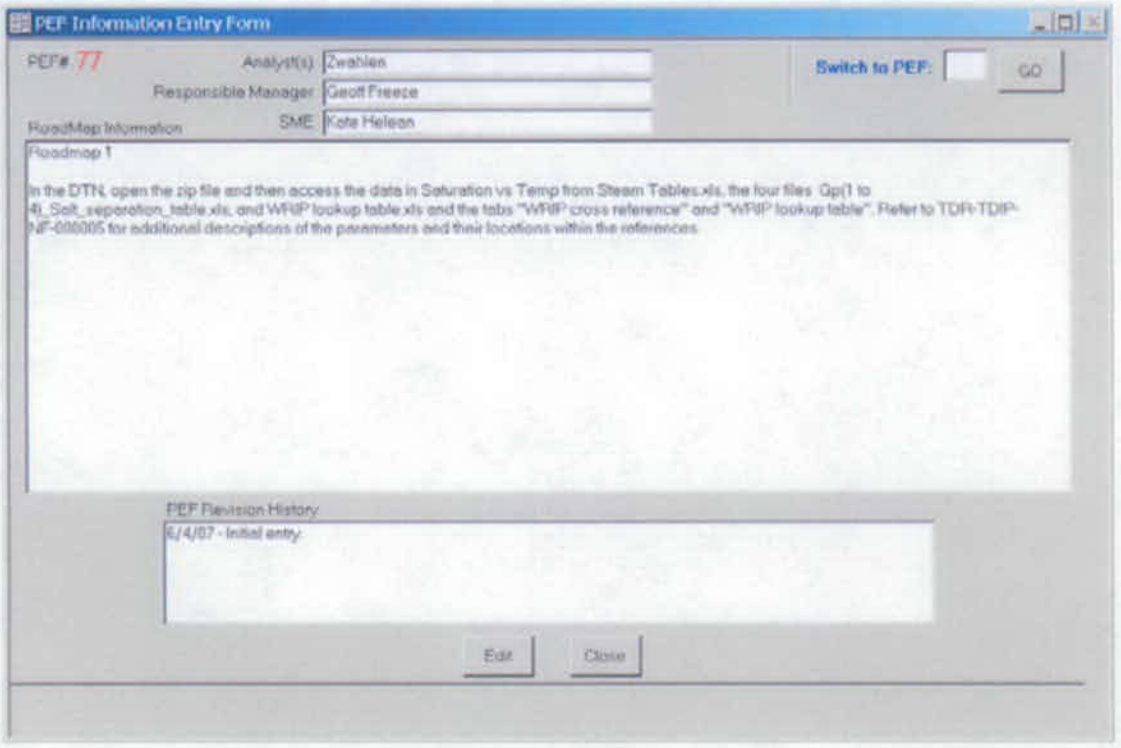

Figure 4-7. Example of a PEF Information Entry Form in the TSPA Input Database

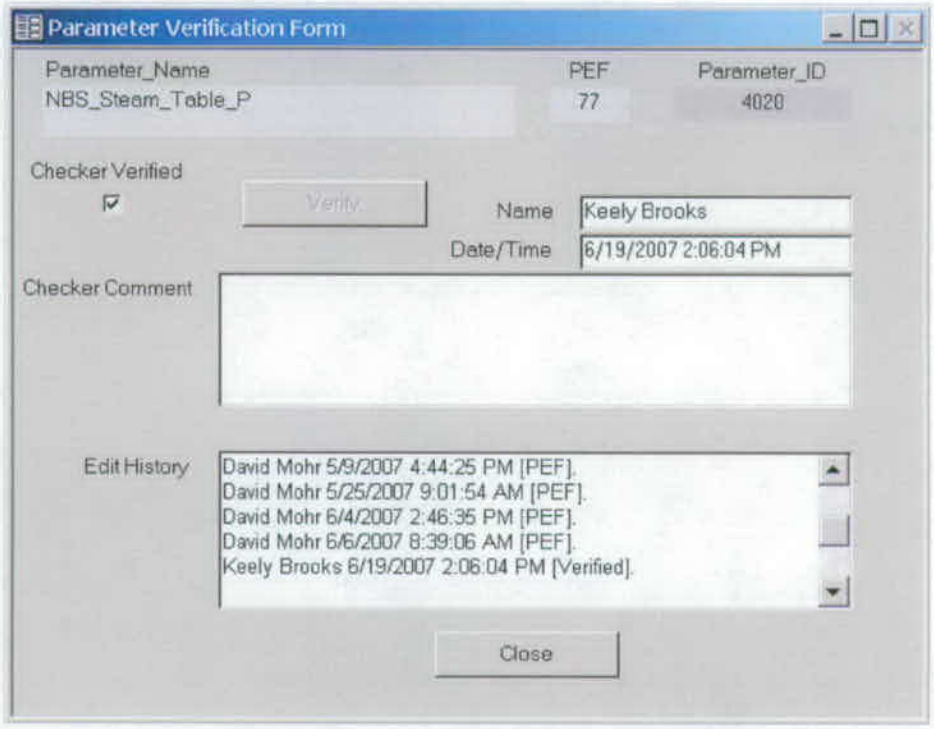

Figure 4-8. Example of a Parameter Verification Form for the TSPA Input Database

5. ASSUMPTIONS

Section 5 presents assumptions for the TSPA-SEIS. The assumptions are as defined and described in SCI-PRO-006, *Models,* Attachment I, Definitions: "***Assumption***–A statement or proposition that is taken to be true or representative in the absence of direct confirming data or evidence, or those estimations, approximations, and/or limitations made during model development (such as when expanding the range of variables to achieve conservatism)." The TSPA-SEIS was developed by integrating assumptions, process models, abstractions, and the results of analyses documented in other project documents.

The assumptions that support the TSPA-SEIS consist of a subset of the assumptions from supporting analyses that, in turn, support the TSPA-SEIS. The list of assumptions from the supporting analyses that are documented below was developed by the TSPA staff in a series of deliberative meetings that considered the technical bases for these assumptions. The assumptions below were judged to be either required by SCI-PRO-006 or represent assumptions not covered in Section 6.3 that describe the technical bases for the TSPA-SEIS and its submodels. In addition, Section 6.1.4 describes how the process models and submodels from the supporting analyses were integrated into the TSPA-SEIS and the reasoning behind that integration. Modeling implementation decisions (i.e., assumptions) covered in Section 6.3 are not included here because they are not considered essential to the understanding of the results of the TSPA-SEIS.

The assumptions from supporting analyses provide the conceptual underpinning of the TSPA-SEIS and show the key supporting results of these analyses that were assimilated into the TSPA-SEIS. In addition, when the supporting analyses provide ranges of conditions, the TSPA-SEIS makes reasonable, and technically defensible conservative assumptions regarding those ranges of conditions to avoid providing over-optimistic estimates of repository performance.

These assumptions are organized by scenario class, beginning with the Nominal Scenario Class and followed by the Early Failure Scenario Class, the Igneous Scenario Class, and the Seismic Scenario Class. In addition, Section 5.5 includes the assumptions for the Human Intrusion Scenario. Because the assumptions from supporting analyses were not changed in applying them to the TSPA-SEIS, the bases for these assumptions are described in the supporting analyses or are included in the descriptions of the following assumptions. Sections 6.3.1 to 6.7 discuss the conservatisms assumed to apply to the TSPA-SEIS components and scenario classes.

5.1 NOMINAL SCENARIO CLASS

5.1.1 Unsaturated Zone Flow

- **Assumption**—Climate changes can be considered in an approximate way by imparting an instantaneous jump from one steady-state flow field to another, with a corresponding rise or fall in the water table representing the base of the UZ Transport Model Component. Shorter-term transients, such as wet and dry years or individual storm events, are assumed to be adequately captured with a model that assumes such transients can be averaged to obtain a long-term, effective, steady-state climate.

Basis—This assumption and its rationale/basis are described in *Particle Tracking Model and Abstraction of Transport Processes* (SNL 2007 [DIRS 181006], Section 5, Assumption 6).

Supports Total System Performance Assessment Model/Analysis for the SEIS in: Section 6.3.1.3

Assumption—The effect of uncertainty regarding the influence of the duration of climate periods on repository performance is negligible and, for simulation purposes, the range of durations estimated for the present-day climate state and the monsoon climate state can be simplified to the longest predicted duration of each climate state. For the present-day climate, a duration range of 400 to 600 years is projected, and only the longest duration of 600 years is simulated in the TSPA-SEIS. The monsoon climate period is predicted to have a duration of between 900 to 1,400 years. The TSPA-SEIS simulations use a duration of 1,400 years for the monsoon climate state.

Basis—The effect on performance is negligible based on the impact that the ranges of the durations of these climate periods have on total infiltration that is applied to the Site-Scale UZ Flow Process Model. The difference of estimated total infiltration when using the minimum climate durations as compared to the maximum projected durations of these climate periods is only about 3 percent during the 10,000-year simulation period (Section 6.3.1.2). When considering the minimum and maximum transition times, the small impact of these maximum climate-period durations on the amount of total infiltration is not likely to have a significant effect on radionuclide releases from the repository or the travel times of these radionuclides to the RMEI.

Supports Total System Performance Assessment Model/Analysis for the SEIS in: Section 6.3.1.2

Assumption—Per regulatory guidance, with the exception of factors related to geology, hydrology, and climate, and for the purposes of performance assessment, future conditions at the Yucca Mountain site are assumed to be the same as current conditions.

Basis—This assumption is described at NRC Proposed Rule 10 CFR 63.305(c) [DIRS 178394].

Supports Total System Performance Assessment Model/Analysis for the SEIS in: Section 6.3.1.2

5.1.2 Engineered Barrier System Environment

Assumption—It is assumed that the NFC (near field chemistry) model results, calculated using averaged rock properties (mineralogy, porosity, saturation, grain density) for the four repository host units to evaluate the degree of water-rock interaction, and thermal properties for the Tptpll (Topapah Spring Tuff lower lithophysal unit) lithologic unit to model development and evolution of the thermal field, are applicable to all lithologies intersected by the repository drifts.

Basis—This assumption and its rationale/basis are described in *Engineered Barrier System: Physical and Chemical Environment* (SNL 2007 [DIRS 177412], Section 5.2.1).

Supports Total System Performance Assessment Model/Analysis for the SEIS in: Section 6.3.2.2

Assumption—The NFC/P&CE (physical and chemical environment) model simulations using the four starting waters adequately represent all possible seepage waters.

Basis—This assumption and its rationale/basis are described in *Engineered Barrier System: Physical and Chemical Environment* (SNL 2007 [DIRS 177412], Section 5.2.2).

Supports Total System Performance Assessment Model/Analysis for the SEIS in: Section 6.3.4.2

Assumption—The ambient percolation-flux distribution above the repository horizon is assumed to be unaffected by mountain-scale, repository heat-driven, TH effects. Therefore, the estimated repository-scale percolation-flux distribution is assumed to be the percolation-flux distribution from the PTn to the upper Topopah Spring welded tuff (TSw) UZ Flow Model Component layer.

Basis—This assumption and its rationale/basis are described in *Multiscale Thermohydrologic Model* (SNL 2007 [DIRS 181383], Section 5.1.2).

Supports Total System Performance Assessment Model/Analysis for the SEIS in: Section 6.3.2.1

Assumption—The entire WP inventory of the repository is assumed to be emplaced at the same time.

Basis—This assumption and its rationale/basis are described in *Multiscale Thermohydrologic Model* (SNL 2007 [DIRS 181383], Section 5.2.3).

Supports Total System Performance Assessment Model/Analysis for the SEIS in: Section 6.3.2.1

Assumption—The EBS is assumed to be in a state of local metastable equilibrium. All aqueous and gas constituents in the TSPA-SEIS achieve and maintain local equilibrium, and most mineral phases achieve and maintain local equilibrium upon saturation. Because the reaction rates of some minerals likely to form under the Yucca Mountain geochemical conditions are slower than the scale of the modeled processes in the TSPA-SEIS, these minerals would not precipitate despite local conditions of saturation or supersaturation. However, using the assumption of metastable equilibrium, the TSPA-SEIS can be used to make steady-state predictions for nonequilibrium conditions concerning mineral stability with respect to relative humidity, provided the appropriate inputs are used.

Basis—This assumption and its rationale/basis are described in *In-Drift Precipitates/Salts Model* (SNL 2007 [DIRS 177411], Section 5.2) and applied in Section 6.6.2.6 with respect to local equilibrium and in Section 6.6.3.3 with respect to relative humidity.

Supports Total System Performance Assessment Model/Analysis for the SEIS in: Section 6.3.2.2

5.1.3 Waste Form Degradation and Mobilization

Assumption—The zirconium-based (Zircaloy) and stainless-steel spent-fuel cladding is assumed to split instantly along the length of a fuel rods at the time of WP failure. Therefore cladding does not retard radionuclide release and transport in the TSPA-SEIS.

Basis—This assumption and its rationale/basis are described in *Cladding Degradation Summary for LA* (SNL 2007 [DIRS 180616], Section 5.3).

Supports Total System Performance Assessment Model/Analysis for the SEIS in: Section 6.3.7.3.1

Assumption—Plutonium and americium are either associated irreversibly (or embedded) and with DOE-owned high-level waste glass colloids or totally reversibly.

Basis—This assumption and its rationale/basis are described in *Waste Form and In-Drift Colloids-Associated Radionuclide Concentrations: Abstraction and Summary* (SNL 2007 [DIRS 177423], Section 5.4[a]).

Supports Total System Performance Assessment Model/Analysis for the SEIS in: Section 6.3.7.6.2

Assumption—It is assumed that physical filtration and gravitational settling of colloids will not occur within the WPs and repository drifts.

Basis–This assumption and its rationale/basis are described in *EBS Radionuclide Transport Abstraction* (SNL 2007 [DIRS 177407], Section 5.7).

Supports Total System Performance Assessment Model/Analysis for the SEIS in: Section 6.3.7.6

5.1.4 Engineered Barrier System Flow and Transport

Assumption—It is assumed that the seepage locations in the emplacement drifts are random with respect to the locations of the WPs, but after seepage occurs, its location does not change with time. It is also assumed that fragments of the DSs that may rest on WPs, or fallen rock that may rest on DSs or WPs, do not divert any seepage flux. In addition, it is assumed that all seepage into the emplacement drifts falls on the crowns of the DSs, and in the absence of a DS, all seepage falls on the crowns of the WPs.

Basis—This assumption and its rationale/basis are described in *EBS Radionuclide Transport Abstraction* (SNL 2007 [DIRS 177407], Section 5.1).

Supports Total System Performance Assessment Model/Analysis for the SEIS in: Section 6.3.6.1

Assumption—It is assumed that there is no evaporation of the seepage water from the surfaces of the DSs.

Basis—This assumption and its rationale/basis are described in *EBS Radionuclide Transport Abstraction* (SNL 2007 [DIRS 177407], Section 5.2).

Supports Total System Performance Assessment Model/Analysis for the SEIS in: Sections 6.3.6.1 and 6.3.6.4.1

Assumption—It is assumed that evaporation of water from the surface or interior of a WP does not occur.

Basis—This assumption and its rationale/basis are described in *EBS Radionuclide Transport Abstraction* (SNL 2007 [DIRS 177407], Section 5.3).

Supports Total System Performance Assessment Model/Analysis for the SEIS in: Sections 6.3.6.1 and 6.3.6.4.1

Assumption—The TSPA-SEIS assumes that a thin film of adsorbed water is always present on the surfaces of internal WP components and corrosion products in a breached WP below the boiling point of water (100°C). This water film is assumed to be continuous, and to behave as a bulk liquid, thus allowing radionuclides to dissolve in the water film and diffuse through it. Colloids are also assumed to diffuse through this film. However, under low-water conditions, defined as having a RH below 95% and a liquid influx of less than 0.1 L/year, the bulk water is assumed to be unavailable for in-package chemistry calculations and the water films are assumed to be discontinuous and would not allow diffusive transport. At and above the boiling point of water in the repository, the thin film is assumed to evaporate and no transport of radionuclides can take place.

Basis—This assumption and its rationale/basis are described in *In-Package Chemistry Abstraction* (SNL 2007 [DIRS 180506], Section 6.10.9.1[a]) and in *EBS Radionuclide Transport Abstraction* (SNL 2007 [DIRS 177407], Section 5.5).

Supports Total System Performance Assessment Model/Analysis for the SEIS in: Section 6.3.7.2

Assumption—Under low-water conditions, defined as having a RH below 95% and a liquid influx of less than 0.1 L/year, the HLW degradation rate is calculated from the aqueous degradation equations assuming a pH of 10, and the CSNF degradation rate is calculated from the aqueous degradation equations assuming a pH between 6 and 7. These pH ranges are based on limited solubility data under conditions where there is water vapor condensation on HLW and CSNF".

Basis—This assumption and its rationale/basis are described in *In-Package Chemistry Abstraction* (SNL 2007 [DIRS 180506], Sections 5.5[a] and 6.10.9.1[a]).

Supports Total System Performance Assessment Model/Analysis for the SEIS in: Section 6.3.7.2

Assumption—The partial pressure of O_2 in the WPs is a constant value of 0.2 bar and is equated to the partial pressure of O_2 in the emplacement drift environment, which is equal to atmospheric O_2.

Basis—This assumption and its rationale/basis are described in *In-Package Chemistry Abstraction* (SNL 2007 [DIRS 180506], Section 6.3.1.1.

Supports Total System Performance Assessment Model/Analysis for the SEIS in: Section 6.3.7.4.1.3

Assumption—It is assumed that no corrosion products exist in the invert.

Basis—This assumption and its rationale/basis are described in *EBS Radionuclide Transport Abstraction* (SNL 2007 [DIRS 177407], Section 5.6). Assuming that no corrosion products exist in the invert is a bounding assumption that reduces the potential effectiveness of the invert as a transport barrier by ignoring the potential for radionuclide sorption onto steel corrosion products.

Supports Total System Performance Assessment Model/Analysis for the SEIS in: Section 6.3.8.2.4 and 6.3.8.4.2

5.1.5 Unsaturated Zone Transport

Assumption—Radionuclide releases at the location of the repository can be represented stochastically by identifying regions on the basis of the predicted water flux through the medium, and placing particles randomly within this region to represent the release.

Basis—This assumption and its rationale/basis are described in *Particle Tracking Model and Abstraction of Transport Processes* (SNL 2007 [DIRS 181006], Section 5, Assumption 4).

Supports Total System Performance Assessment Model/Analysis for the SEIS in: Section 6.3.9.3

Assumption—For the purposes of computing radionuclide transport, flow through the UZ can be approximated assuming that the system (rock mass and flow conditions) has not been influenced by repository waste heat effects or drift shadow effects. Durable changes to the rock mass hydrologic properties are also assumed to be negligible.

Basis—This assumption and its rationale/basis are described in *Particle Tracking Model and Abstraction of Transport Processes* (SNL 2007 [DIRS 181006], Section 5, Assumption 5).

Supports Total System Performance Assessment Model/Analysis for the SEIS in: Section 6.3.9.4

5.1.6 Saturated Zone Flow and Transport

Assumption—The change in groundwater flow in the SZ from one climatic state to another occurs rapidly and is approximated by a shift from one steady-state flow condition to another steady-state flow condition over one timestep.

Basis—This assumption and its rationale/basis are described in *Saturated Zone Flow and Transport Model Abstraction* (SNL 2007 [DIRS 181650], Section 5, Assumption 5).

Supports Total System Performance Assessment Model/Analysis for the SEIS in: Section 6.3.10.1

Assumption—Per regulatory guidance, it is assumed that the RMEI has a diet and living style representative of the people who now reside in the town of Amargosa Valley, Nevada.

Basis—This assumption is described at NRC Proposed Rule 10 CFR 63.312(b) [DIRS 180319]. Information on the consumption of radionuclides for the RMEI is described and tabulated in *Characteristics of the Receptor for the Biosphere Model* (BSC 2005 [DIRS 172827], Sections 6.4 and 7.1.2.2).

Supports Total System Performance Assessment Model/Analysis for the SEIS in: Sections 6.3.7 and 6.3.11

Assumption—The assumption is made that the average concentration of radionuclides in the groundwater supply of the hypothetical community in which the reasonably RMEI resides is an appropriate estimate of radionuclide concentration for the calculation of radiological dose.

Basis—This assumption is described in *Saturated Zone Flow and Transport Model Abstraction* (SNL 2007 [DIRS 181650], Section 5, Assumption 3

Supports Total System Performance Assessment Model/Analysis for the SEIS in: Sections 6.3.10.2

5.1.7 Biosphere

Assumption—The average concentration of radionuclides in the groundwater supply of the hypothetical community of the RMEI is an appropriate estimate of radionuclide concentration for the calculation of radiological dose.

Basis—This assumption and its rationale/basis are described in *Saturated Zone Flow and Transport Model Abstraction* (SNL 2007 [DIRS 181650], Section 5, Assumption 3).

Supports Total System Performance Assessment Model/Analysis for the SEIS in: Section 6.3.11

5.2 EARLY FAILURE SCENARIO CLASS

Analysis of Mechanisms for Early Waste Package/Drip Shield Failure (BSC 2004 [DIRS 170024]) describes calculations related to the number of early DS and WP failures and summarizes all the assumptions related to those calculations. The assumptions for both DSs and WPs concern flaws related to Alloy 22 and titanium composition, welding, improper heat treatment, improper laser peening, improper handling, surface contamination, and incorrect drip-shield emplacement/interlocking in the repository.

5.2.1 Drip Shield Early Failure Modeling Case

Assumption—The early-failed DSs are assumed to fail at time zero and are independently placed within the repository. In addition, it is assumed that the underlying WP fails at time zero due to localized corrosion.

Basis—The occurrence time for the early-failed DSs is a simplifying assumption used in the TSPA-SEIS in the absence of a model that explicitly accounts for the propagation of DS failures from the flaws, contamination, and improper treatment of the DSs. Furthermore, the as-received and undetected flaws, contamination, and improper treatment of the DSs are due to manufacturing and handling, and precede placement in the repository. Therefore, these assumptions are part of the as-received condition or emplacement of the DSs and are imposed as initial postclosure conditions in the TSPA-SEIS.

Supports Total System Performance Assessment Model/Analysis for the SEIS in: Section 6.4.1

5.2.2 Waste Package Early Failure Modeling Case

Assumption—The early-failed WPs are assumed to fail at time zero and are independently placed within the repository.

Basis—The occurrence time for the early failed WPs is a simplifying assumption used in the TSPA-SEIS that explicitly accounts for the propagation of WP failures from the as-received and undetected flaws, contamination, and improper treatment of the WPs. Furthermore, the flaws, contamination, and improper treatment of the WPs are due to manufacturing and handling, and precede placement in the repository. Therefore, these assumptions are part of the as-received condition of the WPs and are imposed as initial postclosure conditions in the TSPA-SEIS.

Supports Total System Performance Assessment Model/Analysis for the SEIS in: Section 6.4.2

5.3 IGNEOUS SCENARIO CLASS

5.3.1 Igneous Intrusion Modeling Case

Assumption—The permeability of any cooled igneous rock that has invaded emplacement drifts is assumed to be the same as that of the bulk host rock, and does not impede flow.

Basis—Natural analogs indicate that a number of different processes could lower permeabilities in the intrusions immediately in contact with a host rock (Lichtner et al. 1999 [DIRS 121006], pp. 8 and 9; Frankel 1967 [DIRS 168717]). However, the extent or uniformity of any changes to the permeability of the intrusion is not known locally. Therefore, it is assumed that hydraulic properties of the cooled intrusion are the same as those of the host rock. This assumption is necessary for the EBS and UZ flow submodels. This assumption is reasonable, technically defensible, and conservative and does not need further justification.

Supports Total System Performance Assessment Model/Analysis for the SEIS in: Section 6.5.1

Assumption—In the Igneous Intrusion Modeling Case, when any main, drift, turnout or other extension in the repository is simulated to be hit by a dike, then all WPs in the entire repository are considered to fail.

Basis—This assumption is described in *Number of Waste Packages Hit by Igneous Intrusion* (SNL 2007 [DIRS 177432], Section 5.1).

Supports Total System Performance Assessment Model/Analysis for the SEIS in: Sections 6.5.1.1

5.3.2 Volcanic Eruption Modeling Case

Assumption—In the Volcanic Eruption Modeling Case, when a waste emplacement drift is hit by a conduit, then only the number of waste packages that can fit within the profile (footprint) of the conduit are considered to fail.

Basis—This assumption is described in *Number of Waste Packages Hit by Igneous Intrusion* (SNL 2007 [DIRS 177432], Section 5.2).

Supports Total System Performance Assessment Model/Analysis for the SEIS in: Sections 6.5.2.1.1

Assumption—The ASHPLUME code (ASHPLUME_DLL_LA (V. 2.1. STN: 11117-2.1-01 [DIRS 180147]) assumes that volcanic eruptions in the Yucca Mountain repository are violent Strombolian eruptions for the entire duration of the explosive phase. Erupted magma is presumed to be fragmented and dispersed in the convective plume for the entire duration of the eruption. This assumption is conservative in that it maximizes the potential for ash and waste dispersal during Strombolian activity.

Basis—This assumption and its rationale/basis are described in *Atmospheric Dispersal and Deposition of Tephra from a Potential Volcanic Eruption at Yucca Mountain, Nevada* (SNL 2007 [DIRS 177431], Section 5.1.1).

Supports Total System Performance Assessment Model/Analysis for the SEIS in: Section 6.5.2

Assumption—The waste entrained in a volcanic eruption is assumed to be instantaneously fragmented and dispersed in the same manner as the erupted magma.

Basis—For the purpose of estimating waste-particle diameters in the eruptive environment, all waste is assumed to be unaltered CSNF physically disaggregated to a size range that approximately relates to fuel form grain size. If partly or wholly assimilated into the magma melt, the unaltered glass waste forms are likely to have particle diameters comparable to those of the ash particles, which are larger than the values used for spent fuel. The waste particles are transported by combining with ash particles of equal size of larger, and the ash-dispersal model assumes that fuel in the affected WPs is available for entrainment in the ash plume as finely-divided particles with diameters in the range of 1 to 2,000 μm, with a mean of 30 μm. The waste mass is distributed among the ash mass based on relative particle sizes. These assumptions are described in *Atmospheric Dispersal and Deposition of Tephra from a Potential Volcanic Eruption at Yucca Mountain, Nevada* (SNL 2007 [DIRS 177431], Sections 1, 5.1.2, 5.2.4, 5.2.5, and 6.5.2.6).

Supports Total System Performance Assessment Model/Analysis for the SEIS in: Section 6.5.2 and the GoldSim Model File

Assumption—Climatic change is assumed not to significantly affect wind speed and direction. The magnitude of short-term variability in wind speed and direction, which is included in the data that characterize present wind conditions, is assumed to be significantly greater than long-term variability introduced by potential future climatic changes.

Basis—This assumption and its rationale/basis are described in *Atmospheric Dispersal and Deposition of Tephra from a Potential Volcanic Eruption at Yucca Mountain, Nevada* (SNL 2007 [DIRS 177431], Section 5.2.1).

Supports Total System Performance Assessment Model/Analysis for the SEIS in: Section 6.4.2

5.4 SEISMIC SCENARIO CLASS

Assumption—Seismic events occur in a random manner, following a Poisson process, over long periods of time.

Basis—This assumption and its rationale/basis are described in *Seismic Consequence Abstraction* (SNL 2007 [DIRS 176828], Section 5.2).

Supports Total System Performance Assessment Model/Analysis for the SEIS in: Section 6.6.1.3

Assumption—Waste package internals are assumed to degrade as structural elements after the outer corrosion barrier (of a WP) is first damaged by a seismic event. More exactly, the internals degrade as a structural component for the TSPA-SEIS by the time of the next seismic event after the first seismic event that breaches a WP.

Basis—This assumption and its rationale/basis are described in *Seismic Consequence Abstraction* (SNL 2007 [DIRS 176828], Section 5.4).

Supports Total System Performance Assessment Model/Analysis for the SEIS in: Sections 6.6.1.1 and 6.6.1.2

5.5 HUMAN INTRUSION SCENARIO

Assumption—The NRC adopts language from the EPA Proposed Rule 40 CFR 197.26 ([DIRS 177357]) that describes the assumptions related to a stylized human intrusion scenario. The DOE used the following assumptions leading to an estimate of the dose to any RMEI from a human intrusion (NRC Proposed Rule 10 CFR 63.322 [DIRS 180319]):

a. "There is a single human intrusion as a result of exploratory drilling for ground water;

b. The intruders drill a borehole directly through a degraded waste package into the uppermost aquifer underlying the Yucca Mountain repository;

c. The drillers use the common techniques and practices that are currently employed in exploratory drilling for ground water in the region surrounding Yucca Mountain;

d. Careful sealing of the borehole does not occur, instead natural degradation processes gradually modify the borehole;

e. No particulate waste material falls into the borehole;

f. The exposure scenario includes only those radionuclides transported to the saturated zone by water (e.g., water enters the waste package, releases radionuclides, and transports radionuclides by way of the borehole to the saturated zone); and

g. No releases are included which are caused by unlikely natural processes and events."

Basis—These assumptions are described at NRC Proposed Rule 10 CFR 63.322 [DIRS 180319]). Information on the consumption of radionuclides for the RMEI is described and tabulated in *Characteristics of the Receptor for the Biosphere Model* (BSC 2005 [DIRS 172827], Sections 6.4 and 7.1.2.2).

Supports Total System Performance Assessment Model/Analysis for the SEIS in: Section 6.7

INTENTIONALLY LEFT BLANK

6. TSPA-SEIS DESCRIPTION

The Total System Performance Assessment – SEIS Information Package (TSPA-SEIS) of the Yucca Mountain repository system is a systematic probabilistic analysis that synthesizes site characterization data, repository design information, process models, abstractions, and analyses. More specifically, U.S. Nuclear Regulatory Commission (NRC) Proposed Rule 10 CFR 63.2 [DIRS 178394] and [DIRS 180319] defines three activities as part of performance assessment (PA):

Performance assessment means an analysis that:

1. Identifies the features, events, processes (except human intrusion), and sequences of events and processes (except human intrusion) that might affect the Yucca Mountain disposal system and their probabilities of occurring;

2. Examines the effects of those features, events, processes, and sequences of events and processes upon the performance of the Yucca Mountain disposal system; and

3. Estimates the dose incurred by the reasonably maximally exposed individual, including the associated uncertainties, as a result of releases caused by all significant features, events, processes, and sequences of events and processes, weighted by their probability of occurrence.

The first activity determines what representations of possible future states of the repository (i.e., scenario classes) are sufficiently important to warrant quantitative analysis. For the TSPA-SEIS, nominal and event scenario classes are analyzed. The Nominal Scenario Class incorporates all features, events, and processes (FEPs), except those FEPs associated with early failures of the waste packages (WPs) or drip shields (DSs) and disruptive events. The Early Failure Scenario Class addresses FEPs that describe the potential for DS and WP early failure in the absence of disruptive events. The TSPA-SEIS includes two scenario classes that address the possibility that disruptive events may occur at or near the repository and that these events may affect repository performance. In addition, the NRC Proposed Rule at 10 CFR 63.322 [DIRS 180319] requires the U.S. Department of Energy (DOE) to assess a Human Intrusion Scenario and 10 CFR 63.321 [DIRS 178394] provides the performance standard for the Human Intrusion Scenario. Section 6.1.1 summarizes the scenario class development process adopted for the TSPA-SEIS, including the basis for identification and screening of potentially relevant FEPs. Section 6.1.2 summarizes the selection of the scenario classes. The following scenario classes are included in the TSPA-SEIS.

Nominal Scenario Class—The Nominal Scenario Class uses the TSPA-SEIS components to describe all included FEPs that are nominally expected to occur. The Nominal Scenario Class encompasses all processes affecting the integrity of the WPs containing spent nuclear fuel (SNF) and high-level (radioactive) nuclear waste (HLW) in the absence of disruptive events. These processes include WP degradation because of corrosion mechanisms including general corrosion (GC), stress corrosion cracking (SCC), localized corrosion (LC), and microbially influenced corrosion (MIC).

Early Failure Scenario Class—The Early Failure Scenario Class describes performance of the repository system in the event of early failures of the DSs or WPs due to manufacturing or material defects or to pre-emplacement operations including improper heat treatment. Early failure events are addressed by two modeling cases: (1) the Drip Shield Early Failure (EF) Modeling Case that includes an early failure of one or more DSs which results in LC of the WP(s) beneath the failed DS(s) and the subsequent release of radionuclides to the groundwater, and (2) the Waste Package EF Modeling Case that includes an early failure of one or more WPs and the subsequent release of radionuclides to the groundwater.

Igneous Scenario Class—This class considers those FEPs associated with igneous activity. This scenario class includes two modeling cases: (1) the Igneous Intrusion Modeling Case with releases of radionuclides to groundwater, and (2) the Volcanic Eruption Modeling Case with releases of radionuclides to the atmosphere. The Igneous Intrusion Modeling Case assumes that a dike intersects the repository and destroys DSs and WPs in those drifts intruded by magma, exposing the waste forms to percolating water and mobilizing radionuclides. The Volcanic Eruption Modeling Case represents the fraction of igneous intrusions in which a volcanic eruption also occurs.

Seismic Scenario Class—The Seismic Scenario Class describes performance of the repository system in the event of seismic activity capable of disrupting repository emplacement drifts and the engineered barrier system (EBS). This scenario class includes processes captured in the Nominal Scenario Class, as well as damage to DSs and WPs as a function of the magnitude of the seismic event(s). Seismic disruption of the repository is addressed in two modeling cases. The first modeling case represents the DSs and WPs that fail from nominal processes, as well as mechanical damage associated with seismic vibratory ground motion. This modeling case is referred to as the Seismic Ground Motion (GM) Modeling Case. The Seismic GM Modeling Case includes drift degradation and subsequent effects of accumulating rubble. The Seismic GM Modeling Case also includes the effects of SCC of the WPs and diffusion of mobilized radionuclides through WP cracks and WP rupturing with the potential to have both advection and diffusion of mobilized radionuclides through the rupture opening. The second modeling case considers the WPs that are breached because of fault displacement. This modeling case is referred to as the Seismic Fault Displacement (FD) Modeling Case. The Seismic FD Modeling Case includes breaching of WPs and DSs by the displacement along faults, as well as nominal failures of the DSs and WPs. Seismic ground motion damage of the DSs and WPs is excluded from this modeling case. This modeling case includes advection and diffusion of mobilized radionuclides out of the breached WP.

Human Intrusion Scenario—The Human Intrusion Scenario describes performance of the repository system in the event that subsurface exploratory drilling disrupts the repository. Human intrusion disruption of the repository is addressed by a single modeling case.

The second and third PA activities defined by the NRC Proposed Rule 10 CFR 63.2 [DIRS 180319] require the development of a TSPA Model that describes overall system behavior and clearly displays the extent to which uncertainty in the understanding of the repository system affects the description of system behavior. The Yucca Mountain repository system is a combination of integrated processes that are conceptualized and modeled as a collection of coupled model components. For the TSPA-SEIS, eight principal model

components are combined to evaluate repository system performance for Nominal, Early Failure, Igneous, and Seismic Classes and the Human Intrusion Scenario. The model components are:

- Unsaturated Zone (UZ) Flow
- EBS Environment
- WP and DS Degradation
- Waste Form Degradation and Mobilization
- EBS Flow and Transport
- UZ Transport
- Saturated Zone (SZ) Flow and Transport
- Biosphere.

The TSPA-SEIS components and their supporting abstraction models and analyses are illustrated on Figure 6-1. The model components are in the top row of the figure, with submodels and abstractions below the model component level. As shown, model components are comprised of a collection of submodels (e.g., process models, analyses, or abstractions) that together represent a key component of the repository system. Submodels are implemented in the TSPA-SEIS to represent each abstraction, analysis, or process model included in the TSPA-SEIS. Note that submodels have arrows on the left side illustrating links to the parent model component. Figure 6-1 also illustrates specific information that is used to analyze the disruptive event scenario classes. Note that the Nominal, Early Failure, Igneous, (except volcanic eruption), and Seismic Scenario Classes and the Human Intrusion Scenario use many of the same submodels and parameters. Each of the model components included in the TSPA-SEIS quantifies uncertainty in the underlying processes and input parameters, or bounds that uncertainty appropriately by selecting parameters and parameter values that bound potential consequences of the TSPA-SEIS from an overall performance perspective (i.e., that bound the expected dose to the receptor). Input uncertainty in the TSPA-SEIS is explicitly represented by assigning probability distributions to parameters representing epistemic and aleatory uncertainty. Because many of the TSPA-SEIS inputs are uncertain, the TSPA-SEIS uses a probabilistic framework to implement the model components and submodels. The treatment of uncertainty and the probabilistic framework used in implementing the TSPA-SEIS is discussed further in Section 6.1.3.

Section 6 Structure—The primary goals of Section 6 are to describe: (1) how the model components and their submodels, illustrated on Figure 6-1, are integrated in the TSPA-SEIS, and (2) how the TSPA-SEIS is implemented to estimate the dose incurred by the reasonably maximally exposed individual (RMEI) due to radionuclide releases in the Nominal, Early Failure, Igneous, and Seismic Scenario Classes and the Human Intrusion Scenario. The contents of Section 6 are summarized as follows.

Section 6.1 develops the basis for a detailed description of the TSPA-SEIS and its implementation for the Nominal, Early Failure, Igneous, and Seismic Scenario Classes and the Human Intrusion Scenario. The following topics are presented:

- FEP analysis for the TSPA-SEIS and the formation and screening of scenario classes (Section 6.1.1)

- Descriptions of scenario classes and their treatment in the TSPA-SEIS (Section 6.1.2)
- Treatment of uncertainty in the TSPA-SEIS analyses (Section 6.1.3)
- A description of the TSPA-SEIS structure and design (Section 6.1.4)
- TSPA-SEIS file architecture (Section 6.1.5).

Section 6.2 introduces alternative conceptual models (ACMs) for the TSPA-SEIS, including a general discussion of ACMs. Detailed evaluations of the ACMs are included in Sections 6.3, 6.4, 6.5, 6.6, and 6.7.

Section 6.3 provides detailed descriptions of the TSPA-SEIS components and submodels. The model component and submodel descriptions include:

- A discussion of how submodels are connected to other submodels and model components in the TSPA-SEIS.
- A description of the conceptual model on which the submodel is based.
- A description of the submodel abstractions.
- A description of how the abstractions are implemented in the TSPA-SEIS.
- An evaluation of the consistency and reasonable and technically defensible conservatism in assumptions and parameters used in the TSPA-SEIS. Assumptions and parameter values that are different among submodels in the TSPA-SEIS are documented.
- A summary of ACMs that were considered in the development of conceptual model.

The focus of Section 6.3 is on the TSPA-SEIS components and submodels, and their implementation in the Nominal Scenario Class. The majority of these submodels are applied in the same manner to evaluate the consequences of the Early Failure, Igneous, and Seismic Scenario Classes and the Human Intrusion Scenario.

Section 6.3 provides a discussion on the consistency of modeling assumptions for each model component. This section also includes explanations of the differences in model assumptions between different model abstractions, and it discusses their impact on the TSPA-SEIS.

Section 6.3 discusses reasonable and technically defensible conservatisms associated with the TSPA-SEIS for each model component. The list of reasonable and technically defensible conservatisms in each subsection focuses on those aspects of the TSPA-SEIS that result in estimates of performance that either:

- Overestimate the consequences of processes that have potential to degrade subsystem performance

- Underestimate the effects of processes that might result in improved subsystem performance.

The reasonable and technically defensible conservatisms presented in Sections 6.3, 6.4, 6.5, 6.6, and 6.7, in respect to how they impact the TSPA-SEIS at the submodel level, are primarily associated with assumptions from supporting analysis and model reports rather than on the overall TSPA-SEIS performance. These reasonable and technically defensible conservatisms may or may not have a direct impact on the performance of the TSPA-SEIS. Additionally, TSPA-SEIS uncertainties identified in Sections 6.3, 6.4, 6.5, 6.6, and 6.7 will affect the assessment of total system performance and must be taken into account.

Sections 6.4, 6.5, 6.6, and 6.7 describe how the consequences of the Early Failure, Igneous, and Seismic Scenario Classes and the Human Intrusion Scenario, respectively, are evaluated, including modifications to the model components described in Section 6.3. Each scenario class section includes discussions that are specific to each case that outline the differences between the Nominal Scenario Class model components and submodels and those used to model the Early Failure, Igneous and Seismic Scenario Classes and the Human Intrusion Scenario. Sections 6.4, 6.5, 6.6, and 6.7 also include a discussion of the consistency of model assumptions and conservatisms specific to each scenario class.

Model Terminology—A variety of model components and submodels are discussed in Section 6, and it is useful to clarify some terminology. Use of the word model, without any qualification, will be restricted to the TSPA-SEIS itself. A number of elements were identified within the TSPA-SEIS. The elements shown on Figure 1-1, commonly referred to as the TSPA wheel, have been identified by the TSPA-SEIS as particularly important. The items indicated by icons on Figure 1-1 will be referred to as model components. These model components were chosen because they provide a useful framework for discussing and reviewing the TSPA-SEIS and the process level models that support the TSPA-SEIS. All other parts of the TSPA-SEIS will be referred to as submodels. The distinction between the terms model components and submodels are, to a certain extent, arbitrary, but they have been introduced to try to improve the clarity of the discussion within Section 6. Submodels in the TSPA-SEIS are comprised of one or more process models, analyses, or abstractions. Table 6-1 maps the principal model components of the TSPA-SEIS from Figure 6-1 to each submodel discussed in Sections 6.1.4, 6.3, 6.4, 6.5, 6.6, and 6.7. Additionally, the process model, analysis, or abstraction that feeds each submodel is listed in Table 6-1 and discussed in Sections 6.3, 6.4, 6.5, 6.6, and 6.7. The term process model is used throughout Section 6.0 as a generalized term for a mathematical model that represents an event, phenomenon, process, component, evaluated within an analysis and model report, rather than as strictly qualified as such per SCI-PRO-006, *Models*. The process model moniker is used here to identify the detailed computational models that form the basis of the data, analysis, and abstractions implemented with the TSPA-SEIS.

INTENTIONALLY LEFT BLANK

Table 6-1. TSPA-SEIS Breakdown

Figure 6-1		Section 6				Referenced Analyses/Models	
TSPA-SEIS Principal Model Components		Subsection			Submodel for TSPA-SEIS	Abstraction/Process Model(s)/Analysis(es)	Reference
Unsaturated Zone Flow Model Component	Site-Scale UZ Flow	Mountain-Scale UZ Flow	6.3.1		UZ Flow Fields Abstraction	UZ Flow Fields Abstraction	1
						Site-Scale UZ Flow Process Model	
						Active Fracture Model	
						Dual-Permeability UZ Flow Model	
	Infiltration Analysis				Infiltration Submodel	Infiltration Model Abstraction	2
						Infiltration Process Model	2
	Climate Analysis				Climate Submodel	Future Climate Analysis	3
	Drift Seepage	Drift-Scale UZ Flow	6.3.3	6.3.3.1	Drift Seepage Submodel	Drift Seepage Abstraction	4,5
						Drift Seepage Abstraction including Drift Collapse	
						TH Seepage Process Model	
	Drift Wall Condensation			6.3.3.2	Drift Wall Condensation Submodel	In-Drift Natural Convection and Condensation Process Model	7
						Drift Wall Condensation Abstraction	
EBS Environment Model Component	EBS Thermal-Hydrologic Environment	EBS TH Environment	6.3.2		EBS TH Environment Submodel	MSTHM Process Model	6
						MSTHM Abstraction	
	EBS Chemical Environment	EBS Chemical Environment	6.3.4		EBS Chemical Environment Submodel	EBS P & CE Abstraction	8
						IDPS Process Model	15

Table 6-1. TSPA-SEIS Breakdown (Continued)

Figure 6-1		Section 6				Referenced Analyses/Models	
TSPA-SEIS Principal Model Components		Subsection			Submodel for TSPA-SEIS	Abstraction/Process Model(s)/Analysis(es)	Reference
WP and DS Degradation Model Component	WAPDEG	WP and DS Degradation	6.3.5	6.3.5.1	WP and DS Degradation Submodel	WP GC Abstraction	10,11,12
						WP MIC Abstraction	
						WP SCC Abstraction	
						DS GC Abstraction	
	Localized Corrosion on WP Outer Surface			6.3.5.2	LC Initiation Submodel	LC Initiation Analysis	
						LC Penetration Rate Abstraction	
Waste Form Degradation and Mobilization Model Component	Radionuclide Inventory	WF Degradation and Mobilization	6.3.7	6.3.7.1	Radionuclide Inventory Submodel	Initial Radionuclide Inventory Screening Analysis	20,35
						Initial Radionuclide Inventory Abstraction	20,35
	In-Package Chemistry			6.3.7.2	In-Package Chemistry Submodel	In-Package Chemistry Abstraction	21
	Cladding Degradation			6.3.7.3	Cladding Degradation Submodel	Cladding Degradation Abstraction	22
	CSNF, DSNF, HLW Degradation			6.3.7.4	Waste Form Degradation Submodel	CSNF WF Degradation Abstraction	23
						DSNF WF Degradation Abstraction	24
						HLW Glass Degradation Abstraction	25
	Dissolved Radionuclide Concentration Limits			6.3.7.5	Dissolved Concentration Limits Submodel	Dissolved Concentration Limits Abstraction	26
	WF & EBS Colloids			6.3.7.6	Engineered Barrier System Colloids Submodel	WF and In-Drift Colloid Concentration Abstraction	27

Table 6-1. TSPA-SEIS Breakdown (Continued)

Figure 6-1		Section 6			Referenced Analyses/Models	
TSPA-SEIS Principal Model Components		Subsection		Submodel for TSPA-SEIS	Abstraction/Process Model(s)/Analysis(es)	Reference
EBS Flow and Transport Model Component	EBS Flow	EBS Flow	6.3.6	EBS Flow Submodel	EBS Flow Abstraction	13
	EBS Transport	EBS Transport	6.3.8	EBS Transport Submodel	EBS Transport Abstraction	13
					Single Continuum Invert Abstraction	
					Mass of Corrosion Products Abstraction	
					WF Water Volume Abstraction	22,25
				EBS-UZ Interface Submodel	EBS-UZ Interface Abstraction	13
Unsaturated Zone Transport Model Component	UZ Transport (Particle Tracking)	UZ Transport	6.3.9	UZ Transport Submodel	Active Fracture Model Abstraction	14
					Particle Tracking Model Abstraction	
					Dual-Continuum Transport Model Abstraction	
					UZ Transport Abstraction	
SZ Flow and Transport Model Component	3-D SZ Flow and Transport	SZ Transport	6.3.10	SZ Flow and Transport Submodel	3-D SZ Flow and Transport Process Model	17,18
					3-D SZ Flow and Transport Abstraction	16
	1-D SZ Flow and Transport				SZ Convolute Abstraction	
					1-D SZ Flow and Transport Abstraction	
	SZ Recycling					
Biosphere Model Component	Nominal BDCFs	Biosphere	6.3.11	Biosphere Submodel	Biosphere Process Model	19
	Groundwater Protection Conversion Factors				Groundwater Exposure Case Abstraction	
	Disruptive Events BDCFs				Volcanic Ash Exposure Case Abstraction	

Table 6-1. TSPA-SEIS Breakdown (Continued)

Figure 6-1		Section 6				Referenced Analyses/Models	
TSPA-SEIS Principal Model Components		Subsection			Submodel for TSPA-SEIS	Abstraction/Process Model(s)/Analysis(es)	Reference
Events	Early Failure	Early Failure Scenario Class	DS Early Failure	6.4.1	DS Early Failure Submodel	Abstraction of DS Failures from Undetected Defects	28
			WP Early Failure	6.4.2	WP Early Failure Submodel	Abstraction of WP Failures from Undetected Defects	28
	Igneous Activity	Igneous Scenario Class	Igneous Intrusion Modeling Case	6.5.1	Igneous Intrusion Submodel	Ingeous Activity Analysis	29
					Igneous Event Time and Probability Submodel	Annual Frequency Abstraction	
					Igneous Intrusion EBS Damage Submodel	Number of WP Hit by Igneous Intrusion Abstraction	30
					EBS TH Environment Submodel Modifications for Igneous Intrusion	Dike Drift Interactions Analysis	9
					EBS Chemical Environment Submodel Modifications for Igneous Intrusion	Unevaporated Seepage Chemistry Abstraction	
						Basalt Chemistry Abstraction	
					Mean Annual Dose for Igneous Intrusion	Calculation of Expected Dose	Section 6.1.2

Table 6-1. TSPA-SEIS Breakdown (Continued)

Figure 6-1		Section 6				Referenced Analyses/Models	
TSPA-SEIS Principal Model Components		Subsection			Submodel for TSPA-SEIS	Abstraction/Process Model(s)/Analysis(es)	Reference
Events (continued)	Igneous Activity (continued)	Igneous Scenario Class	Volcanic Eruption	6.5.2	Volcanic Eruption Submodel	Eruptive Processes Analysis	31,32
					Volcanic Interaction with the Repository Submodel	Number of WP Hit by Eruptive Conduits Analysis	30
					Atmospheric Transport Submodel	Atmospheric Dispersal and Deposition of Tephra Analysis	32, 33
						ASHPLUME Model Abstraction	
					Volcanic Ash Redistribution Submodel	Redistributed Tephra Abstraction	
					Volcanic Ash Exposure Submodel	Mean Annual Dose for Volcanic Eruption Abstraction	31
	Seismic Activity	Seismic Scenario Class	Ground Motion	6.6.1	GM Damage Submodel	Seismic Damage Abstraction	34
					FD Damage Submodel		
				6.6.2.1	Drift Seepage Submodel Modifications for Seismic Disruption	Drift Seepage Abstraction including Drift Collapse	4,5
				6.6.2.2	EBS TH Environment Submodel Modifications for Seismic Disruption	Collapsed Drift TH Abstraction	6

Table 6-1. TSPA-SEIS Breakdown (Continued)

Figure 6-1		Section 6				Referenced Analyses/Models	
TSPA-SEIS Principal Model Components		Subsection			Submodel for TSPA-SEIS	Abstraction/Process Model(s)/Analysis(es)	Reference
Events (continued)				6.6.2.3	WP and DS General Corrosion Submodel for Seismic Disruption	WP and DS Degradation Submodel	10, 11, 12
				6.6.2.4	WP LC Initiation Submodel for Seismic Disruption	LC Initiation Analysis	10
	Human Intrusion	Human Intrusion Scenario		6.7	Human Intrusion Submodel	10CFR Part 63.322 & 63.321	36

NOTES:

1 *UZ Flow Models and Submodels* (SNL 2007 [DIRS 175177]).
2 *Simulation of Net Infiltration for Present-Day and Potential Future Climates* (SNL 2007 [DIRS 174294]).
3 *Future Climate Analysis* (BSC 2004 [DIRS 170002]).
4 *Abstraction of Drift Seepage* (SNL 2007 [DIRS 181244]).
5 *Seepage Model for PA Including Drift Collapse* (BSC 2004 [DIRS 167652]).
6 *Multiscale Thermohydrologic Model* (SNL 2007 [DIRS 181383]).
7 *In-Drift Natural Convection and Condensation* (SNL 2007 [DIRS 181648]).
8 *Engineered Barrier System: Physical and Chemical Environment* (SNL 2007 [DIRS 177412]).
9 *Dike/Drift Interactions* (SNL 2007 [DIRS 177430]).
10 *General Corrosion and Localized Corrosion of Waste Package Outer Barrier* (SNL 2007 [DIRS 178519]).
11 *Stress Corrosion Cracking of Waste Package Outer Barrier and Drip Shield Materials* (SNL 2007 [DIRS 181953]).
12 *General Corrosion and Localized Corrosion of the Drip Shield* (SNL 2007 [DIRS 180778]).
13 *EBS Radionuclide Transport Abstraction* (SNL 2007 [DIRS 177407]).
14 *Particle Tracking Model and Abstraction of Transport Processes* (SNL 2007 [DIRS 181006]).
15 *In Drift Precipitates/Salts Model* (SNL 2007 [DIRS 177411]).

Table 6-1. TSPA-SEIS Breakdown (Continued)

Figure 6-1	Section 6		Referenced Analyses/Models	
TSPA-SEIS Principal Model Components	Subsection	Submodel for TSPA-SEIS	Abstraction/Process Model(s)/Analysis(es)	Reference

16 *Saturated Zone Flow and Transport Model Abstraction* (SNL 2007 [DIRS 181650]).
17 *Saturated Zone Site-Scale Flow Model* (SNL 2007 [DIRS 177391]).
18 *Site-Scale Saturated Zone Transport* (SNL 2007 [DIRS 177392]).
19 *Biosphere Model Report* (SNL 2007 [DIRS 177399]).
20 *Initial Radionuclides Inventory* (SNL 2007 [DIRS 180472]).
21 *In-Package Chemistry Abstraction* (SNL 2007 [DIRS 180506]).
22 *Cladding Degradation Summary for LA* (SNL 2007 [DIRS 180616]).
23 *CSNF Waste Form Degradation: Summary Abstraction* (BSC 2004 [DIRS 169987]).
24 *DSNF and Other Waste Form Degradation Abstraction* (BSC 2004 [DIRS 172453]).
25 *Defense HLW Glass Degradation Model* (BSC 2004 [DIRS 169988]).
26 *Dissolved Concentration Limits of Radioactive Elements* (SNL 2007 [DIRS 177418]).
27 *Waste Form and In-Drift Colloids-Associated Radionuclide Concentrations: Abstraction and Summary* (SNL 2007 [DIRS 177423]).
28 *Analysis of Mechanisms for Early Waste Package/Drip Shield Failures* (SNL 2007 [DIRS 178765]).
29 *Characterize Framework for Igneous Activity at Yucca Mountain, Nevada* (BSC 2004 [DIRS 169989]).
30 *Number of Waste Packages Hit by Igneous Events* (SNL 2007 [DIRS 177432]).
31 *Characterize Eruptive Processes at Yucca Mountain, Nevada* (SNL 2007 [DIRS 174260]) .
32 *Atmospheric Dispersal and Deposition of Tephra from a Potential Volcanic Eruption at Yucca Mountain, Nevada* (SNL 2007 [DIRS 177431]).
33 *Redistribution of Tephra and Waste by Geomorphic Processes Following a Potential Volcanic Eruption at Yucca Mountain, Nevada* (SNL 2007 [DIRS 179347]).
34 *Seismic Consequence Abstraction* (SNL 2007 [DIRS 176828]).
35 *MOX Spent Nuclear Fuel and LaBS Glass for TSPA-SEIS* (SNL 2007 [DIRS 177422]).
36 NRC Proposed Rule at 10 CFR 63.321 [DIRS 178394] and 63.322 [DIRS 180319].

INTENTIONALLY LEFT BLANK

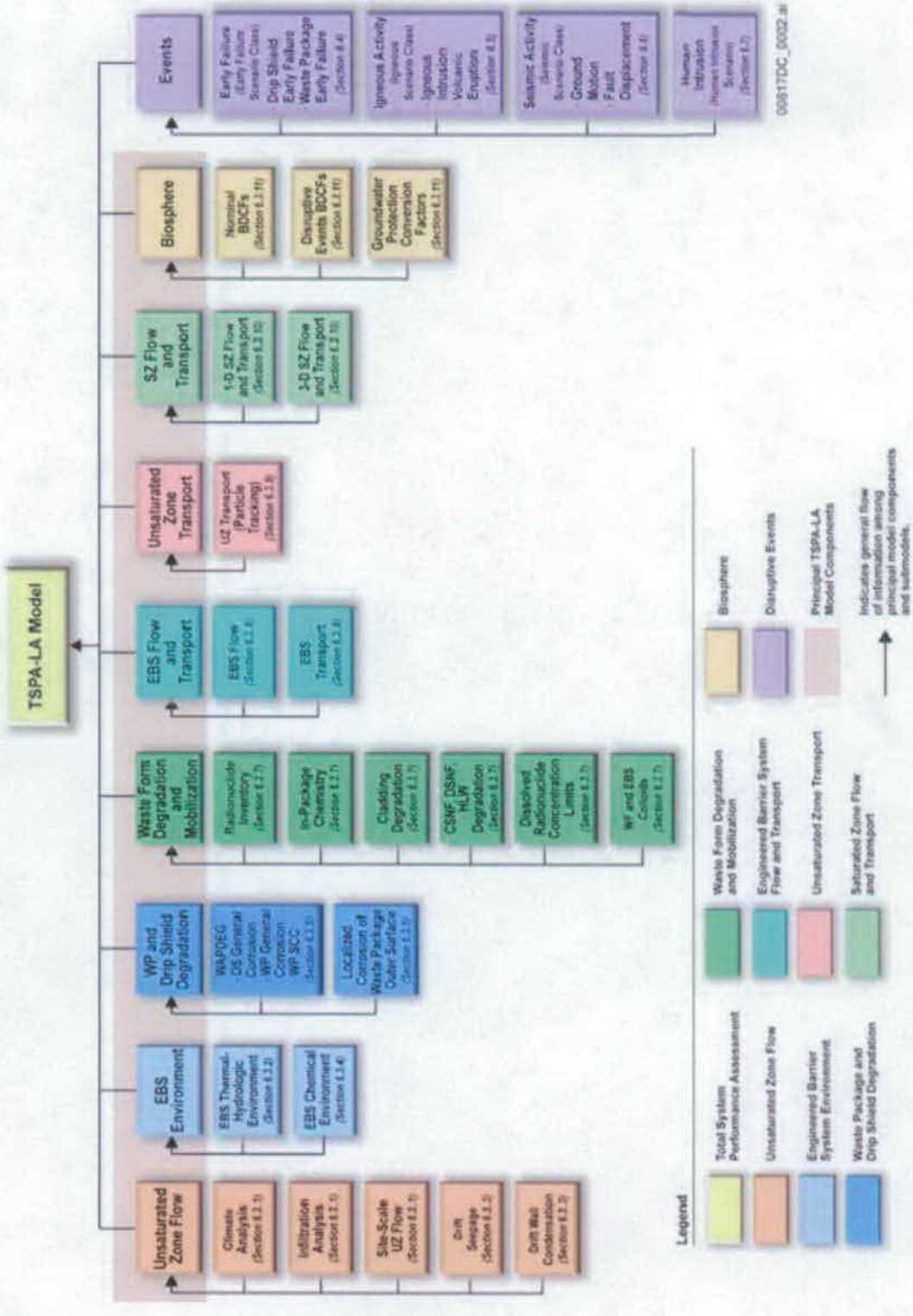

Figure 6-1. TSPA-SEIS Principal Model Components and Submodels

INTENTIONALLY LEFT BLANK

6.1 CONCEPTUAL DESIGN

The TSPA-SEIS evaluates the repository system performance for four scenario classes and for a human intrusion scenario. The TSPA-SEIS is exercised using modeling cases (discussed in detail in Section 6.1.2) that represent the scenario specific conditions over which the repository performance can be assessed. The remainder of Section 6.1 provides a conceptual overview of the FEPs related to the TSPA-SEIS (Section 6.1.1), the scenario classes and modeling cases (Section 6.1.2), a discussion on the treatment of uncertainty in the TSPA-SEIS (Section 6.1.3), the individual model components and submodels that comprise the model scenario classes and modeling cases (Section 6.1.4), and the architecture of the TSPA-SEIS (Section 6.1.5). The model abstraction review process ends with a review of how the abstracted submodels are implemented in the TSPA-SEIS. This section provides overview information to facilitate this review and, in particular, an overview of the integration of model components and submodels that describe processes and conditions in different parts of the Yucca Mountain repository system.

Section 6 provides a text-based description of the TSPA-SEIS. For a complete representation of the conceptual basis and mathematical implementation of the TSPA-SEIS, and for full traceability to the source information used to develop the model, the reader should use the text of Section 6 in conjunction with complementary tools that are provided in this report and in the model files. The following information tools should be used together while reading Section 6:

- Model Components and Submodels, listed in Table 6-1
- Model Implementation Descriptions, mapped in Table 6.1.5-1
- The GoldSim model file
- The TSPA Input Database
- Parameter Entry Forms (PEFs) .

Understanding the conceptual basis for the TSPA-SEIS begins with a review of the FEPs development and screening process, described in Section 6.1.1. Potentially relevant FEPs are identified and evaluated, consistent with available field and laboratory data for the Yucca Mountain site, for inclusion into process models documented in a suite of analysis and model reports.

Table 6-1 provides the roadmap through the conceptual structure of the TSPA-SEIS. The table identifies the process models and associated analyses that support the TSPA-SEIS and gives the principal references. The table also identifies the abstractions that were developed for implementation into the TSPA-SEIS. These elements are mapped to the conceptual structure of the TSPA-SEIS, as defined in Section 6.3. All of this information is mapped to the conceptual structure provided by the TSPA wheel (Figure 1-3), illustrating how the details of the TSPA-SEIS conceptualization relate to the high-level conceptual structure that has formed the basis for analysis and discussion of the Yucca Mountain repository system for many years.

The mathematical implementation of the conceptualization presented in Table 6-1 is discussed in Section 6.3 and documented in the GoldSim model file. Table 6.1.5-1 presents the suite of submodels that were developed to implement the abstractions identified on Table 6-1. Table 6.1.5-1 includes the locations within the GoldSim model file, to view the actual

implementation of the submodels. The model file also includes documentation of the submodel implementation. Decisions made during the implementation of the submodels have resulted in slight differences between the model structure defined in Table 6.1.5-1 and the model structure defined in Section 6.3, and these differences are resolved in Table 6-1. It is important to note that Tables 6-1 and 6.1.5-1 do not attempt to create an inclusive list of all the TSPA-SEIS components, abstractions, and analyses. Collectively, stepping from Figure 6-1 to Table 6-1 to Table 6.1.5-1 and Section 6.3 associates an increase in the detail provided by looking at smaller and smaller logical segments of the model. The basic idea is that the principal model components from Figure 6-1 may be comprised of one or more submodels (listed on Figure 6-1 and in Table 6-1), which may be comprised of one or more abstractions, analyses, or process models (listed in Tables 6-1 and 6.1.5-1). The reader can follow the roadmap, terminating in the model file, which provides the greatest detail of the implementation.

The dose results generated from the GoldSim model file in some cases undergo further processing to calculate the expected dose, conditional on the scenario class event. The overall purpose is to separate the effects of the aleatory and epistemic uncertainty on the total dose results which is discussed in Section 6.1.3. The EXDOC_LA software is used for this purpose and the User Information Document [DIRS 182908] should be consulted.

Parameters connect the model, as implemented in the GoldSim model file, to the field and laboratory measurements that provide the basic data for the TSPA-SEIS. All parameters included in the TSPA-SEIS are documented in the TSPA Input Database, which is a Microsoft Access Database. The parameter database provides the linkage between the description of the parameter, the parameter values used by the model, and the model structure defined in Table 6.1.5-1. Information provided for each parameter includes a brief description, the identification of parameter type (i.e., constant, table, or stochastic) and information on parameter source. The source information includes the source data tracking number (DTN) or the analysis and model report, as well as information on any modifications made to the source information. Traceability to the specific location of source values is provided by the PEFs that are included in the database. The PEFs provide a roadmap to a specific location within a DTN or the analysis and model report where a parameter value can be found.

The database also identifies the submodel where the parameter is implemented within the model file. Many parameters are included in calculations at multiple locations within the model file, but the database identifies at least one location, which is the primary location where the parameter value is brought into the model.

Most of the information from the TSPA Input Database is also captured in the GoldSim model file. At the location where a parameter is implemented in the model file, the information from the database about DTNs or analysis and model report sources and parameter types can be obtained by moving the cursor over the parameter icon.

There are differences in assumptions and parameter sets used in the TSPA-SEIS that have arisen in the development of the abstractions and process models. Most of these differences are due to the use of conservative assumptions in the process model or analysis when uncertainty is difficult to quantify. Assumptions made within the TSPA-SEIS are consistent between the various submodels, assumptions, and parameter values that differ between submodels and are

documented as part of the discussion of each submodel implementation in Section 6.3. To enhance understanding of the complex interactions within the TSPA-SEIS, a discussion of consistency among model components and submodels and identification of conservative assumptions in abstractions, process models, and parameter sets is presented along with each submodel described in Section 6.3.

Using the tools discussed above, in conjunction with review of Section 6.0, all provide the reader with a complete representation of the conceptual basis and mathematical implementation of the TSPA-SEIS, and full traceability to the source information used to develop the model.

INTENTIONALLY LEFT BLANK

6.1.1 Features, Events, and Processes Screening and Scenario Development

This section describes the identification and screening of features, events and processes (FEPs) for the TSPA-SEIS and the development of scenario classes used to estimate repository performance in the TSPA-SEIS.

For the TSPA-SEIS, FEP analysis and scenario development follows a five-step approach (Figure 6.1.1-1):

Step 1. Identify and classify FEPs potentially relevant to the long-term performance of the disposal system.

Step 2. Evaluate the FEPs to identify those FEPs that should be included in the TSPA-SEIS and those that can be excluded from the TSPA.

Step 3. Form appropriate scenario classes from the FEPs that were included in the TSPA. Disruptive events are used to form scenario classes.

Step 4. Construct the calculation of total mean annual dose.

Step 5. Specify the implementation of the scenario classes in the computational modeling for the TSPA-SEIS and document the treatment of FEPs that were included.

FEP analysis, which includes Steps 1 and 2 above, addressed scenario analysis acceptance Criteria 1 and 2, respectively, as outlined in *Yucca Mountain Review Plan, Final Report* (NRC 2003 [DIRS 163274], Section 2.2.1.2.1.3). Scenario development, which includes Steps 3 and 4 above, addressed scenario analysis acceptance Criteria 3 and 4, respectively, as outlined in *Yucca Mountain Review Plan, Final Report* (NRC 2003 [DIRS 163274], Section 2.2.1.2.1.3). Section 6.1.2 outlines the calculation of total mean annual dose using the scenario classes, addressing Step 4 above. Sections 6.1.3 and 6.1.4 describe the implementation of each scenario class in the model components and submodels incorporated into the TSPA-SEIS (Step 5 above).

6.1.1.1 Features, Events, Processes, Scenarios, and Scenario Classes

Features are physical, chemical, thermal, or temporal characteristics of the site or repository system. For the purposes of screening FEPs for the TSPA-SEIS, a feature is defined as an object, structure, or condition that has a potential to affect disposal system performance. Examples of features are the WP and fracture systems or faults.

Processes are phenomena and activities that have gradual, continuous interactions with the system being modeled. For the purposes of screening FEPs for the TSPA-SEIS, a process is defined as a natural or human-caused phenomenon that has a potential to affect disposal system performance and that operates during all or a significant part of the period of performance. Percolation of water into the unsaturated rock layers above the repository is an example of a process.

Events are occurrences that have a specific starting time and, usually, a duration shorter than the time being simulated in a model. Events are also defined as uncertain occurrences that take place within a short time relative to the time frame of a model. For the purposes of screening FEPs for the TSPA-SEIS, an event is defined as a natural or human-caused phenomenon that has a potential to affect disposal system performance and that occurs during an interval that is short compared to the period of performance. An earthquake is an example of an event.

The identification, classification, and screening of a comprehensive list of FEPs potentially relevant to the postclosure performance of the Yucca Mountain repository was an iterative process based on site specific information, design, and regulations. The iterative FEP analysis process was initiated to support the TSPA for the Site Recommendation (TSPA-SR), as described in *The Development of Information Catalogued in REV 00 of the YMP FEP Database* (BSC 2005 [DIRS 154365]), and continued through the TSPA-SEIS FEP analysis.

A scenario is a well defined, connected sequence of FEPs that can be thought of as describing possible future conditions in the repository system. Scenarios can be undisturbed where the performance is the expected or nominal performance of the system, or disturbed if altered by events such as volcanism or seismicity (NRC 2003 [DIRS 163274], Section 3). There is an infinite number of possible future states, and for scenario development to be useful, the process must generate scenarios that can be aggregated into a manageable number of scenario classes representative of the range of futures potentially relevant to the PA of the repository.

A scenario class is a set of related scenarios that share sufficient similarities to usefully aggregate them for the purposes of analysis. The number and breadth of scenario classes depend on the resolution at which scenarios were defined. Coarsely defined scenarios result in fewer broad scenario classes, whereas narrowly defined scenarios result in many scenario classes. The objective of scenario development is to define a limited set of scenario classes that can be quantitatively analyzed while maintaining comprehensive coverage of the range of possible future states of the repository system. The process of scenario development is described by Cranwell et al. (1990 [DIRS 101234], Section 2.4).

The following sections provide summaries of the TSPA-SEIS FEP analysis and scenario development steps.

6.1.1.2 Step 1: Identification and Classification of Features, Events and Processes

In Step 1 of the FEP analysis and scenario development process, FEPs potentially relevant to postclosure performance are identified and classified. The primary objectives of FEP identification and classification are to develop a comprehensive set of FEPs for subsequent screening, to uncover missing FEPs and interactions, and to provide a framework for developing and organizing scenario classes.

An initial list of FEPs relevant to Yucca Mountain was developed from a comprehensive list of FEPs from radioactive waste disposal programs in other countries (BSC 2005 [DIRS 173800], Section 2.1.1). The list was supplemented with additional Yucca Mountain specific FEPs from project literature, technical workshops, and reviews (BSC 2005 [DIRS 173800], Sections 2.1.1). This process is illustrated on Figure 6.1.1-2. This initial FEP list, developed to support TSPA-

SR, contained 328 FEPs (BSC 2002 [DIRS 159684], Table FEPS). This list was revised for TSPA-SEIS in part with an application of a hybrid procedure that included reclassification, refinement, and audits against other recently published international lists. Additional analyses and refinements were conducted during the transition from the TSPA-SR FEP list to the TSPA-SEIS FEP list.

The TSPA-SR FEP classification was derived from a Nuclear Energy Agency classification scheme (NEA 1999 [DIRS 152309], pp. 28 to 34) that was based on a combination of the classification schemes listed in *Development of the Total System Performance Assessment-License Application Features, Events, and Processes* (BSC 2005 [DIRS 173800], Section 2.1.2). The TSPA-SR classification was a layered scheme, with different layers categorized by cause, field of effects, and causative factors, location, scientific discipline, radionuclide transfer agent, and/or radionuclide mobilization. As a check on comprehensiveness, TSPA-SR FEPs were also classified according to technical subject area (i.e., a combination of locations and physical field of effect). The alternate classification did not result in the identification of any additional FEPs. For TSPA-SEIS, yet another classification scheme was applied based on a mapping between Yucca Mountain Project (YMP) specific features (i.e., locations and fields of effect) and processes (i.e., radionuclide mobilization and causative factors). The revised approach improved traceability by relating FEPs directly to YMP specific technical subject areas rather than to generic international groupings.

These FEP identification actions resulted in a comprehensive TSPA-SEIS FEP list containing 375 FEPs.

6.1.1.3 Step 2: Screening of FEPs

In Step 2 of the FEP analysis and scenario development process, the list of FEPs identified and classified in Step 1 was screened to determine which FEPs should be included or excluded from the TSPA-SEIS analysis. A FEP can be excluded based on any one of the following three FEP screening criteria, which derive from NRC Proposed Rule 10 CFR Part 63 [DIRS 178394] and [DIRS 180319] as described below:

- Low Probability (10 CFR 63.342(a) and (b) [DIRS 178394])—Performance assessments shall exclude events that have less than one chance in 10,000 of occurring over 10,000 years. FEPs not meeting this criterion may be excluded (screened out) from the TSPA-SEIS on the basis of low probability. For example, the impact of large meteorites was excluded because of low probability.

- Low Consequence (10 CFR 63.114(e) and (f) [DIRS 178394])—Specific FEPs were evaluated in detail according to whether or not the magnitude and time of radiological exposures or radionuclide releases would be significantly changed by their omission. FEPs not meeting this criterion may be excluded (screened out) from the TSPA-SEIS on the basis of low consequence. For example, erosion and deposition were excluded because of low consequence, even though they are certain to occur.

- By Regulation—FEPs may also be excluded if they are inconsistent with regulations that specify repository system characteristics, concepts, and definitions. The regulations most

commonly used for screening TSPA-SEIS FEPs are those pertaining to the characteristics, concepts, and definitions of the reference biosphere, geologic setting, RMEI, and human intrusion ((NRC 2003 [DIRS 163274], Section 2.2.1.2.1.3, Acceptance Criterion 2).

In addition, according to 10 CFR 63.342(c) (70 FR 53313[DIRS 178394], PAs conducted to show compliance of FEPs with individual protection standards following permanent closure and affected by human intrusion shall project the continued effects of all included FEPs beyond 10,000 years after closure until the period of geologic stability, including seismic and igneous events covered under the probability limits of 10 CFR 63.342(a) (70 FR 53313[DIRS 178394].

The FEP screening process included input from subject matter experts to indicate whether or not each FEP is included in the TSPA-SEIS or was screened out.

6.1.1.4 Step 3: Formation of Scenario Classes

All FEPs screened in during the formal identification and screening for Step 1 and Step 2 are used for TSPA-SEIS scenario development and are incorporated into scenario classes (Sections 6.3, 6.4, 6.5, 6.6, and 6.7). For the purpose of scenario class formation, features and processes generally are present in all possible repository futures. In contrast, events may or may not occur in every future of the repository system. For this reason scenario classes are distinguished by events, while the features and processes are generally applicable across all scenario classes.

The three retained events that have been identified for inclusion in the TSPA-SEIS are:

- Early failure
- Igneous
- Seismic.

These three events lead to the definition of three corresponding scenario classes for the TSPA-SEIS, and one additional scenario class accounting for repository futures in which none of the three events occur:

- Early Failure Scenario Class, A_{EF}: the set of futures each of which includes one or more early failure events (i.e., one or more early failed WPs and/or one or more early-failed DSs).
- Igneous Scenario Class, A_I: the set of futures each of which includes one or more igneous events.
- Seismic Scenario Class, A_S: the set of futures each of which includes one or more seismic events.
- Nominal Scenario Class, A_N: the set of futures each of which includes nominal features and processes (e.g., corrosion processes, such as general corrosion, localized corrosion,

and SCC) but *no* events (i.e., no igneous and no seismic events and no early WP or DS failures).

The first three scenario classes are not mutually exclusive. Because the three types of events occur independently, many potential futures of the repository include events of different types, and such futures are included in more than one of the sets listed above. Section 6.1.2 explains how the four scenario classes listed above are aggregated from a set of mutually exclusive scenario classes and how total dose to the RMEI is correctly calculated using these four scenario classes.

6.1.1.5 Description of Scenario Classes and Modeling Cases

The scenario classes addressed by the TSPA-SEIS are distinguished by the type of event included in each scenario class. For example, the Early Failure Scenario Class accounts for all possible futures in which one or more early failures of DSs or WPs occur, the Igneous Scenario Class accounts for all possible futures in which one or more igneous events occur, and the Seismic Scenario Class accounts for all possible futures in which seismic events occur. In contrast, the Nominal Scenario Class accounts for all possible futures in which no early failures, igneous, or seismic events occur.

Each scenario class is implemented in the TSPA-SEIS by one or more modeling cases. The modeling cases that implement a scenario class are distinguished by different modes and extent of damage to the repository that could result from the occurrence of the events represented by the scenario class. The Early Failure Scenario Class is implemented in two modeling cases, the Waste Package EF Modeling Case and the Drip Shield EF Modeling Case, because early failure of a DS has a different effect on the repository performance than early failure of a WP. Similarly, the Seismic Scenario Class is implemented in two modeling cases, one accounting for damage due to ground motion, and a second accounting for damage due to fault displacement. The Igneous Scenario Class is also comprised of two modeling cases, one for igneous intrusion and one for volcanic eruption.

Each scenario class accounts for FEPs that remain screened in after Step 2. The FEPs addressed by each scenario class, and the modeling cases used for each scenario class, are described below. In general, FEPs that describe a feature, such as the WP, or a process, such as flow in the UZ, are relevant to, and included in, more than one scenario class. In contrast, FEPs that describe an event, such as the occurrence of an igneous intrusion, are only included in the scenario class and modeling case that accounts for the effects of the event on repository performance. Thus, there is not a one-to-one association between FEPs and modeling cases.

A single FEP or related FEPs may be implemented differently in different scenario classes, model components, or portions of a model domain. These differing implementations are not inconsistencies; rather, they are reasonable simplifications that focus the model on things that matter and allow reasonable and technically defensible conservatism where information is controversial or lacking. In cases where an FEP is treated differently in different parts of the model, it is important that the impacts on the overall performance of any simplifications can be shown to be neutral or conservative for the purposes of each model component. For example, flow in fractured basalt is represented realistically for the purposes of an FEP screening

argument (screening out hydrologic effects of the vertical dike on the grounds that flow in the dike will be insignificant), whereas flow through magma-filled drifts is represented conservatively. In another example, a radionuclide solubility model is applied in the WP and invert but is conservatively neglected in the UZ and SZ.

Nominal Scenario Class—The Nominal Scenario Class for the TSPA-SEIS includes all of the FEPs that were screened in according to the FEP screening process described in Section 6.1.1, except for those FEPs that are related to early failures, igneous activity, seismic activity or a human intrusion. This scenario class, therefore, incorporates the important effects and system perturbations caused by climate change and repository heating that is projected to occur after repository closure. In addition, the Nominal Scenario Class considers that the WPs and DSs are subject to the EBS environment and will degrade with time. If the WPs and DSs breach and the waste forms are subsequently exposed to water, radionuclides may be mobilized and eventually be released from the repository. These radionuclides can then be transported by groundwater percolating through the UZ to the SZ and then to the accessible environment by water flowing in the SZ. The TSPA-SEIS includes FEPs associated with the biosphere in order to calculate annual dose to the RMEI. Accordingly, the TSPA-SEIS explicitly includes the following model components (Figure 6.1.2-1):

- UZ Flow
- EBS Environment
- WP and DS Degradation
- Waste Form Degradation and Mobilization
- EBS Flow and Transport
- UZ Transport
- SZ Flow and Transport
- Biosphere.

The FEPs included in these model components are addressed in one modeling case. This modeling case represents those WPs that fail because of corrosion processes (e.g., GC, SCC, or LC). This modeling case is referred to as the Nominal Modeling Case. The Nominal Modeling Case quantifies repository performance in the absence of early failures or disruptive events before 10,000 years. For repository performance 10,000 years after closure, nominal processes are included in the Seismic GM Modeling Case, described below.

Early Failure Scenario Class—The Early Failure Scenario Class describes performance of the repository system in the event of early failures of the DSs or WPs due to manufacturing or material defects or to pre-emplacement operations including improper heat treatment. Early failure events are addressed by two modeling cases: (1) the Waste Package EF Modeling Case that considers the early failure of one or more WPs and the subsequent release of radionuclides to the groundwater; and (2) the Drip Shield EF Modeling Case that considers the early failure of one or more DSs that results in LC of the WPs beneath the failed DSs and the subsequent release of radionuclides to the groundwater.

The Waste Package EF Modeling Case accounts for the consequences of one or more WP failures at the time of repository closure due to manufacturing defects or damage during emplacement. WP early failure compromises the WP, exposing the waste forms to percolating water and mobilizing radionuclides. The released radionuclides may then be transported out of the repository, moved down through the UZ to the SZ, and then be transported through the SZ to the accessible environment. The TSPA-SEIS components needed to calculate total system performance for the Waste Package EF Modeling Case include the following (Figure 6.1.2-2):

- UZ Flow
- EBS Environment
- WP and DS Degradation
- Waste Form Degradation and Mobilization
- EBS Flow and Transport
- UZ Transport
- SZ Flow and Transport
- Biosphere.

The FEPs associated with DS early failure and corrosion failure of WPs are not addressed in the Waste Package EF Modeling Case. Instead, these FEPs are accounted for in the Drip Shield EF and Nominal Modeling Cases.

The Drip Shield EF Modeling Case accounts for the consequences of one or more DS failures at the time of repository closure due to manufacturing defects or damage during emplacement. The WPs beneath the early failed DSs are assumed to be susceptible to LC, which compromises the WPs, exposing the waste forms to percolating water, and mobilizing radionuclides. The released radionuclides may then be transported out of the repository, moved down through the UZ to the SZ, and then be transported through the SZ to the accessible environment. The TSPA-SEIS components needed to calculate total system performance for the Drip Shield EF Modeling Case include the following (Figure 6.1.2-2):

- UZ Flow
- EBS Environment
- WP and DS Degradation
- Waste Form Degradation and Mobilization
- EBS Flow and Transport
- UZ Transport
- SZ Flow and Transport
- Biosphere.

The Drip Shield EF Modeling Case assumes that a WP underneath a failed DS experiences LC.

Igneous Scenario Class—The Igneous Scenario Class describes performance of the repository system in the event of igneous activity that disrupts the repository. Igneous disruption of the repository is addressed by two modeling cases: (1) the Igneous Intrusion Modeling Case that represents the interaction of intrusive magma with the repository and the release of radionuclides

to the groundwater, and (2) the Volcanic Eruption Modeling Case that represents an eruption at the land surface and the release of radionuclides to the atmosphere.

The Igneous Intrusion Modeling Case models a dike intersecting the repository and compromising DSs and WPs in those drifts intruded by magma, exposing the waste forms to percolating water and mobilizing radionuclides. The released radionuclides may then be transported out of the repository, moved down through the UZ to the SZ, and then be transported through the SZ to the accessible environment. The TSPA-SEIS components, needed to calculate total system performance for the Igneous Intrusion Modeling Case, include the following, given that a certain number of WPs are destroyed by the intrusion (Figure 6.1.2-3):

- UZ Flow
- EBS Environment
- WP and DS Degradation
- Waste Form Degradation and Mobilization
- EBS Flow and Transport
- UZ Transport
- SZ Flow and Transport
- Biosphere.

The FEPs associated with corrosion failure of WPs prior to the disruption are included in the Igneous Intrusion Modeling Case. The FEPs associated with corrosion failure of WPs of undisrupted WPs after the disruption occurs are not included in the Igneous Intrusion Modeling Case. Instead, these FEPs are accounted for in the Nominal Modeling Case.

The Volcanic Eruption Modeling Case represents the fraction of igneous intrusions in which a volcanic eruption also occurs. For this modeling case, waste from WPs intersected by eruptive conduits is transported to the land surface, and tephra and entrained waste are discharged into the atmosphere, transported by wind currents, and deposited on the surface. The Volcanic Eruption Modeling Case also evaluates the fluvial and eolian redistribution of contaminated tephra deposited on the land surface. The TSPA-SEIS uses the following processes and model components to calculate repository system performance for the Volcanic Eruption Modeling Case (Figure 6.1.2-4):

- Volcanic interaction with the repository
- Atmospheric transport
- Tephra redistribution
- Biosphere.

Seismic Scenario Class—The Seismic Scenario Class describes performance of the repository system in the event of seismic activity capable of disrupting repository emplacement drifts and damaging the EBS. Radionuclides in damaged WPs may be mobilized and transported out of the repository, transported to the water table by the groundwater percolating through the UZ, and then transported to the accessible environment by water flowing in the SZ. The TSPA-SEIS components needed to calculate total system performance for the Seismic Scenario Class include the following (Figure 6.1.2-5):

- UZ Flow
- EBS Environment
- WP and DS Degradation
- Waste Form Degradation and Mobilization
- EBS Flow and Transport
- UZ Transport
- SZ Flow and Transport
- Biosphere.

Seismic disruption of the repository is addressed in two modeling cases. The first modeling case is the Seismic GM Modeling Case, which represents the consequences of mechanical damage associated with seismic vibratory ground motion. The Seismic GM Modeling Case includes: drift degradation and the effects on the EBS of accumulated rubble, the effects of SCC of the WPs and diffusion of mobilized radionuclides through WP cracks, and the effects of WP rupture with the potential to have both advection and diffusion of mobilized radionuclides through the rupture opening. Because corrosion processes accounted for in the Nominal Scenario Class have the potential to alter the repository's susceptibility to damage during a seismic ground motion event, the Seismic GM Modeling Case includes these nominal processes when calculating consequences after 10,000 years.

The second modeling case is the Seismic FD Modeling Case, which represents advection and diffusion of mobilized radionuclides out of WP breaches caused by a fault displacement. Seismic ground motion damage of the DSs and WPs is excluded from this modeling case.

6.1.1.6 Human Intrusion Scenario

In addition to the four scenario classes described above, the TSPA-SEIS considers a Human Intrusion Scenario as defined in NRC Proposed Rule 10 CFR 63.322 [DIRS 180319]. The Human Intrusion Scenario considers the intrusion of a single water or exploratory well into the repository, through the DS and WP, and into the underlying SZ. Human intrusion is not expected to occur during the first 10,000 years after repository closure (Section 6.3.7). NRC Proposed Rule 10 CFR 63.321 [DIRS 178394] describes the Individual Protection Standard for a Human Intrusion.

The Human Intrusion Scenario in implemented in a single modeling case, the Human Intrusion Modeling Case. This modeling case describes performance of the repository system in the event that subsurface exploratory drilling disrupts the repository. The Human Intrusion Modeling Case assumes that subsurface exploratory drilling activities intersect the repository and destroy a single DS and WP without being recognized by the drillers. After penetrating a thinned DS and WP, the drillers continue to bore a conduit through to the SZ. The drillers penetrate a DS and WP with an opening the size of the drill bit, thereby exposing the waste forms to percolating water and mobilizing radionuclides. The released radionuclides may then be transported out of the repository, move down through the borehole to the SZ, and then be transported through the SZ to the accessible environment. The TSPA-SEIS components needed to calculate total system performance for the Human Intrusion Modeling Case include the following, given that a certain WP is destroyed by the intrusion (Figure 6.1.2-6):

- UZ Flow
- EBS Environment
- WP and DS Degradation
- Waste Form Degradation and Mobilization
- EBS Flow and Transport
- UZ Transport (stylized)
- SZ Flow and Transport
- Biosphere.

The FEPs associated with corrosion failure of WPs prior to the disruption are not included in the Human Intrusion Modeling Case. The FEPs associated with corrosion failure of WPs and of undisrupted WPs after the disruption occurs are also not included in the Human Intrusion Modeling Case.

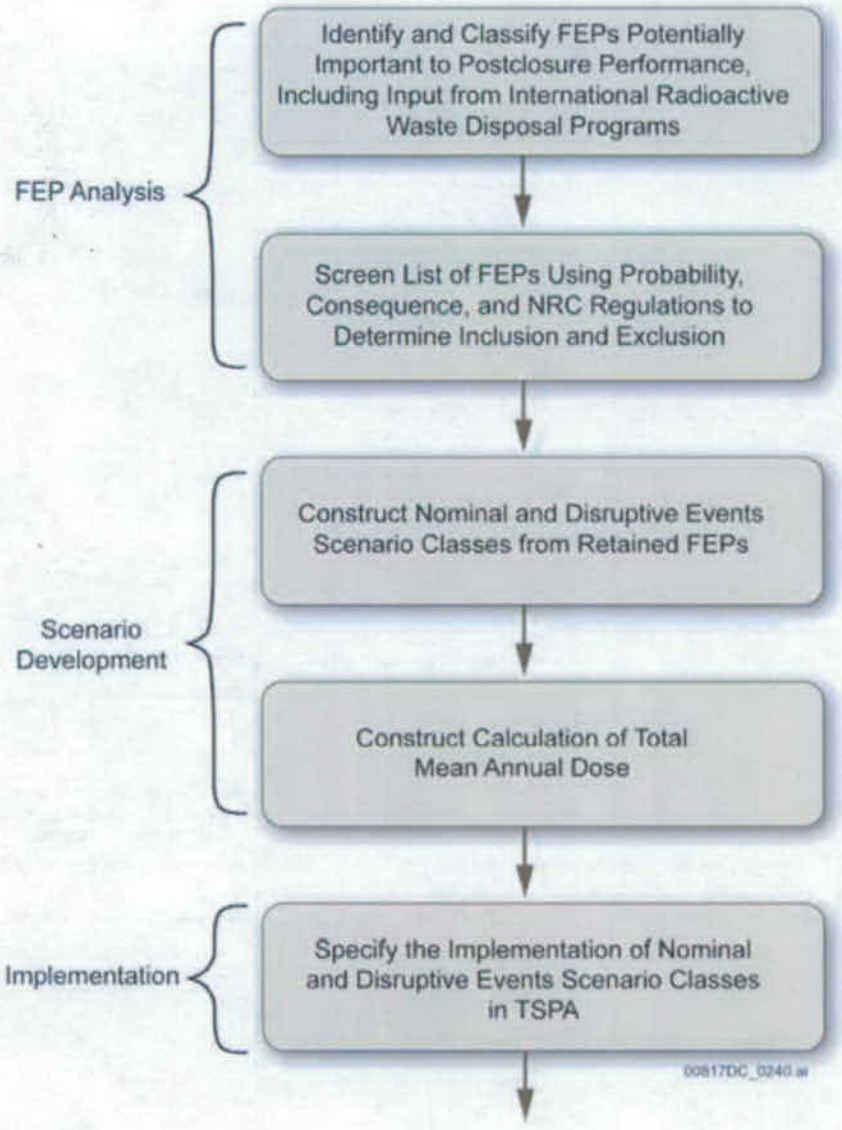

Figure 6.1.1-1. Steps in the Features, Events, and Processes Analysis and Scenario Selection Process

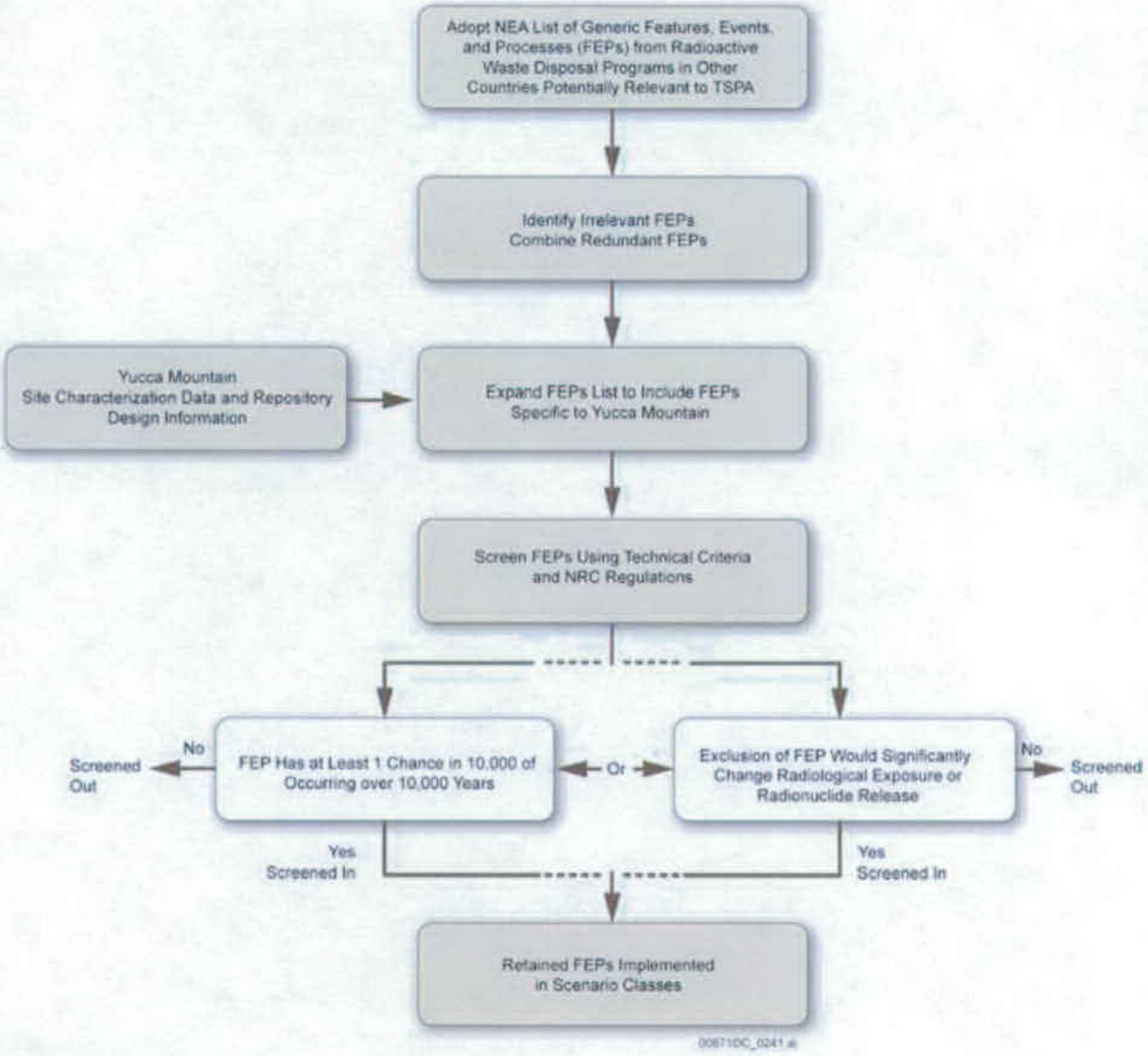

Figure 6.1.1-2. Schematic Illustration of the Features, Events, and Processes Analysis Method

6.1.2 Calculation of Dose for the TSPA-SEIS

The identification and screening of FEPs is discussed in Section 6.1.1. The screening resulted in three retained events that are used to define scenario classes: early failure events, igneous events, and seismic events. Section 6.1.1 describes the scenario classes used to estimate repository performance in the TSPA-SEIS. The scenario classes are the Nominal Scenario Class, Early Failure Scenario Class, Igneous Scenario Class, and Seismic Scenario Class. A separate Human Intrusion Scenario is also described.

This section outlines the calculation of total mean annual dose and total median annual dose using the scenario classes defined in Section 6.1.1. Section 6.1.2.3 describes calculations for each of the individual modeling cases used in the TSPA-SEIS.

6.1.2.1 Description of Uncertainty

The treatment of aleatory and epistemic uncertainty in the TSPA-SEIS is of particular importance to this discussion. In general, aleatory uncertainty derives from inherent uncertainty about future events, and epistemic uncertainty derives from lack of knowledge about quantities, models, or assumptions. Formally, aleatory uncertainty is characterized by a set $A = \{\mathbf{a} : \mathbf{a} = [a_1, a_2, \ldots, a_{nA}]\}$ in which each vector $\mathbf{a} \in A$ represents a possible future of the repository, and each a_j is a specific property of the future $\mathbf{a}$ (e.g., number of WP early failures, time of a seismic event). Each individual element a_i is described by a probability distribution, which conceptually leads to a density function $d_A(\mathbf{a})$ for the set A. In this text it is useful to group the elements a_i of $\mathbf{a}$ into subsets corresponding to the modeling cases (e.g., denote by $\mathbf{a}_{EF}$ the subset of elements that describe early failure events).

Similarly, epistemic uncertainty is characterized by a set $E = \{\mathbf{e} : \mathbf{e} = [e_1, e_2, \ldots, e_{nE}]\}$ where each element e_i of $\mathbf{e}$ is an uncertain parameter (e.g., uncertainty in radionuclide solubility). Associated to each element e_i of $\mathbf{e}$ is a probability distribution, which taken together lead to a density function $d_E(\mathbf{e})$ for the set E. Certain elements of $\mathbf{e}$ are used to characterize distributions for elements of $\mathbf{a}$ and thus are specific to certain modeling cases (e.g., the rate of occurrence for igneous events); other elements characterize uncertainty that applies to all modeling cases (e.g., uncertainty in radionuclide solubility). Where the distinction is important, it is useful to denote by $\mathbf{e}_A$ the subset of elements that influence aleatory uncertainty and to denote by $\mathbf{e}_M$ the elements e_i of $\mathbf{e}$ that are common to all modeling cases. The density function $d_A(\mathbf{a})$ is more correctly expressed as $d_A(\mathbf{a}|\mathbf{e}_A)$ to show the dependence of $\mathbf{a}$ on $\mathbf{e}_A$.

6.1.2.2 Calculation of Total Mean and Median Annual Dose

Total mean annual dose is defined as the expected value of dose to the RMEI, where the expectation is taken over both aleatory and epistemic uncertainty (Section 6.1.3). Total median annual dose is estimated as the median of the distribution of expected dose to the RMEI, where the expectation is taken only over aleatory uncertainty. As specified in the proposed revision to

10 CFR 63.303 ([DIRS 178394]), total mean annual dose is the quantity compared to the regulatory limit specified in 10 CFR 63.321 [DIRS 178394] for the period within 10,000 years after disposal, and total median annual dose is the quantity compared to the regulatory limit specified in the 10 CFR 63.321 [DIRS 178394] for the period after 10,000 years of disposal.

Calculation of total mean annual dose proceeds in a four-step process. First, a set of realizations of epistemic uncertainty are sampled from E consistent with the density function $d_E(\mathbf{e})$. Next, for each scenario class, a set of realizations of aleatory uncertainty, or futures, are selected from the set from A consistent with the density function $d_A(\mathbf{a})$. The contribution to total dose from each scenario class, $D_J(\tau|\mathbf{a},\mathbf{e})$, is computed as a function of time τ for each future $\mathbf{a}$ and each epistemic realization $\mathbf{e}$, where the subscript J in $D_J(\tau|\mathbf{a},\mathbf{e})$ indicates a particular scenario class. Third, for each scenario class and for each epistemic realization $\mathbf{e}$, the expected annual dose $\overline{D}_J(\tau|\mathbf{e})$ is computed where the expectation is taken over aleatory uncertainty. This expectation over aleatory uncertainty accounts for the probabilities that define each scenario class; thus, in the vernacular of previous TSPA analyses, $\overline{D}_J(\tau|\mathbf{e})$ is probability-weighted. Finally, total expected annual dose $\overline{D}(\tau|\mathbf{e})$ is computed for each epistemic realization $\mathbf{e}$ by summing expected annual doses over scenario classes, and total mean annual dose $\overline{\overline{D}}(\tau)$ is calculated as the expectation over epistemic uncertainty.

Total median annual dose $Q_{0.5}\left(\overline{D}(\tau|\mathbf{e})\right)$ is calculated as the median of the distribution of expected dose, where the expectation is taken only over aleatory uncertainty. Formally, at each time τ, the calculation of total expected annual dose produces a distribution $\left\{\overline{D}(\tau|\mathbf{e})\right\}$ of values of total expected annual dose, one value for each epistemic realization $\mathbf{e}$. The TSPA-SEIS estimates the total median annual dose to the RMEI by the median of the distribution $\left\{\overline{D}(\tau|\mathbf{e})\right\}$.

The quantity $\overline{D}(\tau|\mathbf{e})$ is formally described as the total expected annual dose conditional on epistemic uncertainty. For convenience, this text uses the less cumbersome term total expected annual dose to refer to $\overline{D}(\tau|\mathbf{e})$. The quantity $\overline{\overline{D}}(\tau)$ is technically also an expected value. Again, for convenience, and to distinguish this quantity in the text from the total expected annual dose $\overline{D}(\tau|\mathbf{e})$, this text uses the term total mean annual dose to refer to $\overline{\overline{D}}(\tau)$.

For an arbitrary future $\mathbf{a}$ and epistemic realization $\mathbf{e}$, total annual dose, $D(\tau|\mathbf{a},\mathbf{e})$, is approximated as:

$$D(\tau|\mathbf{a},\mathbf{e}) \cong D_N(\tau|\mathbf{a},\mathbf{e}) + D_{EF}(\tau|\mathbf{a},\mathbf{e}) + D_I(\tau|\mathbf{a},\mathbf{e}) + D_S(\tau|\mathbf{a},\mathbf{e}) \qquad \text{(Eq. 6.1.2-1)}$$

where

$D_N(\tau|\mathbf{a},\mathbf{e})$ = Dose at time τ resulting from nominal processes

$D_{EF}(\tau|\mathbf{a},\mathbf{e})$= Additional dose at time τ resulting from any early failures occurring in the future **a**

$D_I(\tau|\mathbf{a},\mathbf{e})$ = Additional dose at time τ resulting from any igneous events occurring in the future **a**

$D_S(\tau|\mathbf{a},\mathbf{e})$ = Additional dose at time τ resulting from any seismic events occurring in the future **a**.

Equation 6.1.2-2 approximates total annual dose as the sum of dose resulting from nominal process and from events. The approximation relies on the simplifying assumption that the dose resulting from a combination of events is the sum of the doses resulting from each separate event; this approximation is justified in Section 6.1.2.3.

Total expected annual dose, $\bar{D}(\tau|\mathbf{e})$, is calculated as the expected value of $D(\tau|\mathbf{a},\mathbf{e})$ where the expectation is over the uncertainty in **a** (aleatory uncertainty). Written simply,

$$\begin{aligned}\bar{D}(\tau|\mathbf{e}) &= \int_A D(\tau|\mathbf{a},\mathbf{e})\,d_A(\mathbf{a}) \\ &= \int_A \left(D_N(\tau|\mathbf{a},\mathbf{e}) + D_{EF}(\tau|\mathbf{a},\mathbf{e}) + D_I(\tau|\mathbf{a},\mathbf{e}) + D_S(\tau|\mathbf{a},\mathbf{e})\right) d_A(\mathbf{a}) \\ &= \int_A D_N(\tau|\mathbf{a},\mathbf{e})\,d_A(\mathbf{a}) + \int_A D_{EF}(\tau|\mathbf{a},\mathbf{e})\,d_A(\mathbf{a}) \\ &\quad + \int_A D_I(\tau|\mathbf{a},\mathbf{e})\,d_A(\mathbf{a}) + \int_A D_S(\tau|\mathbf{a},\mathbf{e})\,d_A(\mathbf{a}) \\ &= \bar{D}_N(\tau|\mathbf{e}) + \bar{D}_{EF}(\tau|\mathbf{e}) + \bar{D}_I(\tau|\mathbf{e}) + \bar{D}_S(\tau|\mathbf{e})\end{aligned} \qquad \text{(Eq. 6.1.2-2)}$$

where the dependence of $d_A(\mathbf{a})$ on **e** is omitted for brevity of notation. The quantity $\bar{D}_N(\tau|\mathbf{e})$ is the expected annual dose resulting from nominal processes. The quantities $\bar{D}_{EF}(\tau|\mathbf{e})$, $\bar{D}_I(\tau|\mathbf{e})$, and $\bar{D}_S(\tau|\mathbf{e})$ are the expected values of the additional annual dose resulting from the occurrence of early failure, igneous and seismic events, respectively.

Total mean annual dose, $\bar{\bar{D}}(\tau)$, is calculated as the expected value of $\bar{D}(\tau|\mathbf{e})$ where the expectation is over the uncertainty in **e** (epistemic uncertainty). $\bar{\bar{D}}(\tau)$ is calculated by:

$$\begin{aligned}\bar{\bar{D}}(\tau) &= \int_E \bar{D}(\tau|\mathbf{e})\,d_E(\mathbf{e}) \\ &\cong \frac{1}{N}\sum_{k=1}^{N} \bar{D}(\tau|\mathbf{e}_k)\end{aligned} \qquad \text{(Eq. 6.1.2-3)}$$

where $\{\mathbf{e}_k\}$ is a Latin hypercube sample (LHS) of the epistemic variables of size N consistent with the distributions defining each of the elements e_i of **e**.

Due to the complexity of $D(\tau|\mathbf{a},\mathbf{e})$, evaluation of the integral in Equation 6.1.2-2 requires that the set of all futures A be divided into subsets, for which the integral can be numerically evaluated. The set A is first divided into eight mutually exclusive, or disjoint, sets of repository futures, defined by the events retained in the TSPA-SEIS (early failure, igneous, and seismic). A sequence of re-arranging terms in the integral, presented below, leads to the calculation of total expected annual dose as the sum of the expected annual dose for each of the four scenario classes $\{A_N, A_{EF}, A_I, A_S\}$ identified in Section 6.1.1.

The three retained events lead directly to the first three disjoint sets of repository futures:

- Early failure scenario set, S_{EF}: the set of futures each of which includes one or more early failure events (i.e., one or more early failed WPs and/or one or more early failed DSs), but no seismic or igneous events, and also includes nominal features and processes.

- Igneous scenario set, S_I: the set of futures each of which includes one or more igneous events, but no seismic or early-failure events, and also includes retained nominal features and processes.

- Seismic scenario set, S_S: the set of futures each of which includes one or more seismic events, but no igneous or early-failure events, and also includes retained nominal features and processes.

The three sets listed above describe only those futures in which a single type of event occurs, thus they are subsets of the scenario classes defined in Section 6.1.1. Because the events occur independently, there are many future states of the repository in which more than one type of event may occur. Therefore, four additional sets are defined to account for futures that include combinations of the three types of events:

- Early failure/Igneous scenario set, S_{EF+I}: the set of futures each of which includes one or more early failure events and one or more igneous events, but no seismic events.

- Early failure/Seismic scenario set, S_{EF+S}: the set of futures each of which includes one or more early failure events and one or more seismic events, but no igneous events.

- Igneous/seismic scenario set, S_{I+S}: the set of futures each of which includes one or more igneous events and one or more seismic events, but no early failure events, and also includes nominal features and processes.

- Igneous/seismic/early failure scenario set, S_{EF+I+S}: the set of futures each of which includes one or more early failure events and one or more seismic events and one or more igneous events, and also includes nominal features and processes.

Each of the four scenario sets listed above can also be defined in terms of intersections of the scenario classes listed in Section 6.1.1. Finally, it is possible that no events occur in the future of the repository. One more set of repository futures, defined as the complement of the union of the sets above, accounts for the futures in which no event occurs:

- Nominal scenario set, S_N: the set of futures each of which includes nominal features and processes (e.g., corrosion processes, such as GC, LC, and SCC) but *no* events (i.e., no igneous and no seismic events and no early WP or DS failures).

The nominal scenario set S_N is identical to the scenario class A_N.

The eight sets of futures defined above partition the set of all futures of the repository into a collection of disjoint sets. The set of all futures is formally a probability space with a probability measure p_A derived from the distributions of the individual elements a_i of $\mathbf{a}$. Hence, a probability can be calculated for each of the eight disjoint sets $\{S_{EF}, S_I, S_S, S_{EF+I}, S_{EF+S}, S_{I+S}, S_{EF+I+S}, S_N\}$. Because the union of the eight sets equals all of A, and the eight sets are disjoint, the probabilities associated with each of the eight sets sum to exactly one.

These eight sets $\{S_{EF}, S_I, S_S, S_{EF+I}, S_{EF+S}, S_{I+S}, S_{EF+I+S}, S_N\}$ form a collection of scenario classes in and of themselves. Since these sets are disjoint and their union covers all futures of the repository, these sets meet the acceptance criteria for scenario classes specified in the *Yucca Mountain Review Plan, Final Report* (NRC 2003 [DIRS 163274]. Total expected annual dose could be calculated separately for these eight scenario classes, and then combined appropriately to estimate repository performance. However, the TSPA-SEIS calculation of total expected annual dose is simplified by aggregating these eight disjoint sets into the scenario classes identified in Section 6.1.1.

Partition the set of futures A into $\{S_{EF}, S_I, S_S, S_{EF+I}, S_{EF+S}, S_{I+S}, S_{EF+I+S}, S_N\}$ as defined above. Next, separate the integral in Equation 6.1.2-2 into a sum of eight integrals over the separate disjoint sets:

$$\begin{aligned}\bar{D}(\tau|\mathbf{e}) &= \int_{A} D(\tau|\mathbf{a},\mathbf{e})\,d_A(\mathbf{a}) \\ &= \int_{S_N} D(\tau|\mathbf{a},\mathbf{e})\,d_A(\mathbf{a}) + \int_{S_{EF}} D(\tau|\mathbf{a},\mathbf{e})\,d_A(\mathbf{a}) \\ &\quad + \int_{S_I} D(\tau|\mathbf{a},\mathbf{e})\,d_A(\mathbf{a}) + \int_{S_S} D(\tau|\mathbf{a},\mathbf{e})\,d_A(\mathbf{a}) \\ &\quad + \int_{S_{EF+I}} D(\tau|\mathbf{a},\mathbf{e})\,d_A(\mathbf{a}) + \int_{S_{EF+S}} D(\tau|\mathbf{a},\mathbf{e})\,d_A(\mathbf{a}) \\ &\quad + \int_{S_{I+S}} D(\tau|\mathbf{a},\mathbf{e})\,d_A(\mathbf{a}) + \int_{S_{EF+I+S}} D(\tau|\mathbf{a},\mathbf{e})\,d_A(\mathbf{a}) \\ &= \int_{\bigcup_J S_J} D(\tau|\mathbf{a},\mathbf{e})\,d_A(\mathbf{a})\end{aligned} \qquad \text{(Eq. 6.1.2-4)}$$

where, for convenience in the presentation, J is an index and the collection $\{S_J\}$ are the eight disjoint sets $\{S_{EF}, S_I, S_S, S_{EF+I}, S_{EF+S}, S_{I+S}, S_{EF+I+S}, S_N\}$.

Next, use Equation 6.1.2-1 in Equation 6.1.2-4 to obtain

$$\begin{aligned}\bar{D}(\tau|\mathbf{e}) &= \int_{\bigcup_J S_J} D(\tau|\mathbf{a},\mathbf{e})\,d_A(\mathbf{a}) \\ &= \int_{\bigcup_J S_J} \left(D_N(\tau|\mathbf{a},\mathbf{e}) + D_{EF}(\tau|\mathbf{a},\mathbf{e}) + D_I(\tau|\mathbf{a},\mathbf{e}) + D_S(\tau|\mathbf{a},\mathbf{e})\right) d_A(\mathbf{a}) \\ &= \int_{\bigcup_J S_J} D_N(\tau|\mathbf{a},\mathbf{e})\,d_A(\mathbf{a}) + \int_{\bigcup_J S_J} D_{EF}(\tau|\mathbf{a},\mathbf{e})\,d_A(\mathbf{a}) \\ &\quad + \int_{\bigcup_J S_J} D_I(\tau|\mathbf{a},\mathbf{e})\,d_A(\mathbf{a}) + \int_{\bigcup_J S_J} D_S(\tau|\mathbf{a},\mathbf{e})\,d_A(\mathbf{a})\end{aligned} \qquad \text{(Eq. 6.1.2-5)}$$

Consider first the integral involving $D_{EF}(\tau|\mathbf{a},\mathbf{e})$. If a future $\mathbf{a}$ does not include any early failure events, there is no additional dose that can result from early failure. Thus, the quantity $D_{EF}(\tau|\mathbf{a},\mathbf{e})$ is zero for any future $\mathbf{a}$ that does not include any early failure events. Using this observation, the term in Equation 6.1.2-5 that involves $D_{EF}(\tau|\mathbf{a},\mathbf{e})$ is expanded as

$$\begin{aligned}\int_{\bigcup_J S_J} D_{EF}(\tau|\mathbf{a},\mathbf{e})\,d_A(\mathbf{a}) &= \sum_J \int_{S_J} D_{EF}(\tau|\mathbf{a},\mathbf{e})\,d_A(\mathbf{a}) \\ &= \int_{S_{EF}} D_{EF}(\tau|\mathbf{a},\mathbf{e})\,d_A(\mathbf{a}) + \int_{S_{EF+I}} D_{EF}(\tau|\mathbf{a},\mathbf{e})\,d_A(\mathbf{a}) \\ &\quad + \int_{S_{EF+S}} D_{EF}(\tau|\mathbf{a},\mathbf{e})\,d_A(\mathbf{a}) + \int_{S_{EF+I+S}} D_{EF}(\tau|\mathbf{a},\mathbf{e})\,d_A(\mathbf{a})\end{aligned} \qquad \text{(Eq. 6.1.2-6)}$$

since the integral of $D_{EF}(\tau|\mathbf{a},\mathbf{e})$ over any of the sets $\{S_I, S_S, S_{I+S}, S_N\}$ is zero. Finally, by using the definition of the Early Failure Scenario Class, A_{EF}, and the eight disjoint scenario sets,

$\{S_{EF}, S_I, S_S, S_{EF+I}, S_{EF+S}, S_{I+S}, S_{EF+I+S}, S_N\}$, write $A_{EF} = S_{EF} \cup S_{EF+I} \cup S_{EF+S} \cup S_{EF+I+S}$. Equation 6.1.2-6 becomes

$$\begin{aligned}
&\int_{S_{EF}} D_{EF}(\tau|\mathbf{a},\mathbf{e}) d_A(\mathbf{a}) + \int_{S_{EF+I}} D_{EF}(\tau|\mathbf{a},\mathbf{e}) d_A(\mathbf{a}) \\
&\quad + \int_{S_{EF+S}} D_{EF}(\tau|\mathbf{a},\mathbf{e}) d_A(\mathbf{a}) + \int_{S_{EF+I+S}} D_{EF}(\tau|\mathbf{a},\mathbf{e}) d_A(\mathbf{a}) \\
&\qquad = \int_{S_{EF} \cup S_{EF+I} \cup S_{EF+S} \cup S_{EF+I+S}} D_{EF}(\tau|\mathbf{a},\mathbf{e}) d_A(\mathbf{a}) \qquad \text{(Eq. 6.1.2-7)} \\
&\qquad = \int_{A_{EF}} D_{EF}(\tau|\mathbf{a},\mathbf{e}) d_A(\mathbf{a}) \\
&\qquad = \bar{D}_{EF}(\tau|\mathbf{e})
\end{aligned}$$

where $\bar{D}_{EF}(\tau|\mathbf{e})$ is the expected additional annual dose due to early failures. Similar sequences of operations lead to the following expressions for the expected additional annual dose due to igneous events, $\bar{D}_I(\tau|\mathbf{e})$, and the expected additional annual dose due to seismic events, $\bar{D}_S(\tau|\mathbf{e})$:

$$\bar{D}_I(\tau|\mathbf{e}) = \int_{A_I} D_I(\tau|\mathbf{a},\mathbf{e}) d_A(\mathbf{a}) \qquad \text{(Eq. 6.1.2-8)}$$

$$\bar{D}_S(\tau|\mathbf{e}) = \int_{A_S} D_S(\tau|\mathbf{a},\mathbf{e}) d_A(\mathbf{a}) \qquad \text{(Eq. 6.1.2-9)}$$

where

$A_I = S_I \cup S_{EF+I} \cup S_{I+S} \cup S_{EF+I+S}$ is the Igneous Scenario Class.

$\bar{D}_I(\tau|\mathbf{e})$ is the expected additional annual dose due to igneous events.

$A_S = S_S \cup S_{EF+S} \cup S_{I+S} \cup S_{EF+I+S}$ is the Seismic Scenario Class.

$\bar{D}_S(\tau|\mathbf{e})$ is the expected additional annual dose due to seismic events.

The final quantity required for calculation of total expected annual dose is $\bar{D}_N(\tau|\mathbf{e})$, the expected annual dose for the Nominal Scenario Class. The Nominal Scenario Class excludes the occurrence of any events, and thus does not depend on any of the aleatory uncertainties that describe a future. Moreover, by definition, $\bar{D}_N(\tau|\mathbf{e})$ is the expected annual dose resulting from nominal corrosion processes, which occur in every future of the repository. Hence, $D_N(\tau|\mathbf{a},\mathbf{e})$ can be simplified as $D_N(\tau|\mathbf{e})$, so

$$\begin{aligned}\bar{D}_N(\tau|\mathbf{e}) &= \int_A D_N(\tau|\mathbf{a},\mathbf{e})\,d_A(\mathbf{a}) \\ &= \int_A D_N(\tau|\mathbf{e})\,d_A(\mathbf{a}) \\ &= D_N(\tau|\mathbf{e})\int_A d_A(\mathbf{a}) \\ &= D_N(\tau|\mathbf{e})\times p_A(A) \\ &= D_N(\tau|\mathbf{e})\end{aligned} \qquad \text{(Eq. 6.1.2-10)}$$

since $p_A(A)=1$. Using these quantities, Equation 6.1.2-5 becomes

$$\begin{aligned}\bar{D}(\tau|\mathbf{e}) &= \int_{\bigcup_j S_j} D_N(\tau|\mathbf{a},\mathbf{e})\,d_A(\mathbf{a}) + \int_{\bigcup_j S_j} D_{EF}(\tau|\mathbf{a},\mathbf{e})\,d_A(\mathbf{a}) \\ &\quad + \int_{\bigcup_j S_j} D_I(\tau|\mathbf{a},\mathbf{e})\,d_A(\mathbf{a}) + \int_{\bigcup_j S_j} D_S(\tau|\mathbf{a},\mathbf{e})\,d_A(\mathbf{a}) \\ &= \bar{D}_N(\tau|\mathbf{e}) + \int_{A_{EF}} D_{EF}(\tau|\mathbf{a},\mathbf{e})\,d_A(\mathbf{a}) \\ &\quad + \int_{A_I} D_I(\tau|\mathbf{a},\mathbf{e})\,d_A(\mathbf{a}) + \int_{A_S} D_S(\tau|\mathbf{a},\mathbf{e})\,d_A(\mathbf{a}) \\ &= \bar{D}_N(\tau|\mathbf{e}) + \bar{D}_{EF}(\tau|\mathbf{e}) + \bar{D}_I(\tau|\mathbf{e}) + \bar{D}_S(\tau|\mathbf{e})\end{aligned} \qquad \text{(Equation 6.1.2-11)}$$

Section 6.1.2.3 describes in further detail the calculation of each term in Equation 6.1.2-11.

6.1.2.3 Screening of Scenario Classes

As outlined in Section 6.1.2.2, the calculation of total annual dose as the sum of annual dose from each scenario class relies on the simplifying assumption that the occurrence of an early failure or other event has no effect on the consequences of a later event. This simplifying assumption allows the TSPA-SEIS to approximate the dose from a future involving a combination of events, such as a seismic event followed by an igneous intrusion, as the sum of the dose from the seismic event and the dose from the igneous event. In general, this method of approximation affects the TSPA-SEIS results in a conservative way, by overestimating the resulting dose. Table 6.1.2-1 summarizes the effect of each combination of events on the calculation of total mean annual dose; these effects are discussed below.

6.1.2.3.1 Nominal Scenario Class with Other Scenario Classes

During the period before 10,000 years, the corrosion processes included in the Nominal Scenario Class have no consequences that affect the consequences of any early failure or disruptive event. Thus, no combinations of the Nominal Scenario Class with other scenario classes are relevant before 10,000 years.

During the period after 10,000 years, the corrosion processes described by the Nominal Scenario Class affect the consequences of seismic ground motion events, so these processes are included in the Seismic GM Modeling Case. As explained in Section 6.1.2.4.1 and Section 6.1.2.4.3, the inclusion of these processes means that dose due to nominal processes is combined with the

additional dose due to seismic ground motion events, and this combined quantity is calculated by the Seismic GM Modeling Case. The corrosion processes are also accounted for in the Igneous Intrusion Modeling Case, but the dose due to corrosion processes before the time of the first intrusion is not included in the results of the Igneous Intrusion Modeling Case. The corrosion processes are included so that the inventory remaining in the WPs at the time of the intrusion is reduced by the radionuclides released due to general corrosion processes prior to the intrusion. Nominal corrosion processes are not included in the Seismic FD, Igneous Eruption, or Early Failure Modeling Cases, which results in over counting of radionuclides released in these modeling cases. However, these modeling cases affect only a small fraction of the WPs (at most 2 percent in the Seismic FD Modeling Case), so the resulting effect on total mean annual dose is minor.

6.1.2.3.2 Early Failure Scenario Class with Other Scenario Classes

In the TSPA-SEIS, early failures are assumed to take place at the time of repository closure. Since an early failure cannot follow any disruptive event, these combinations are not relevant and are not listed in Table 6.1.2-1. In the TSPA-SEIS, if a disruptive event follows an early failure, the inventory released as a consequence of the disruptive event is estimated without subtracting the inventory that may have been released from the WPs affected by early failure. However, on average less than 2.49/11,629=0.02 percent of the WPs are affected by early failure (Section 6.4), so not more than 0.02 percent (on average) of the inventory is counted twice, and the net effect on total mean annual dose of the combination of early failures and disruptive events is negligible.

6.1.2.3.3 Igneous Scenario Class with Other Scenario Classes

The combinations of an igneous intrusion and volcanic eruption with other scenario classes are considered separately.

Igneous Intrusion with Seismic Scenario Class—The TSPA-SEIS assumes that all components of the EBS suffer maximum damage from an igneous intrusion. After the intrusion, the EBS components (DSs and WPs) no longer function as a barrier to advective or diffusive transport of radionuclides. Since the effects of a seismic event (either vibratory ground motion or fault displacement) are damage to components of the EBS, a seismic event following an igneous intrusion should not have any effect on the repository performance.

The TSPA-SEIS overestimates total dose by not excluding the dose resulting from seismic events occurring after an igneous intrusion. However, during 1,000,000 years, the probability of the combination of an igneous intrusion followed by a damaging seismic event is roughly 1.67×10^{-2} , so the over-estimate of dose affects roughly 2 percent of the realizations of the Seismic GM Modeling Case, and the overall effect on total mean annual dose is minor.

Volcanic Eruption with Seismic Scenario Class—The TSPA-SEIS overestimates total dose by not reducing the inventory that could be released by seismic events, by the amount of inventory released by any volcanic eruptions. However, on average an eruptive event affects less that 0.03 percent of the WPs, so not more than 0.03 percent (on average) of the inventory could be

counted twice, and the net effect on total mean annual dose of the combination of volcanic eruptions and seismic events is negligible.

Combinations of Igneous Intrusions with Volcanic Eruptions—The TSPA-SEIS overestimates total dose by not reducing the inventory that could be released by intrusions or eruptions by the amount of inventory released by any preceding igneous event. However, on average an eruptive event affects less that 0.03 percent of the WPs, so the effect on total mean annual dose of an eruptive event preceding other igneous events is negligible. The TSPA-SEIS accounts for multiple igneous intrusion events and for multiple volcanic eruption events in the calculation of total mean annual dose.

6.1.2.3.4 Seismic Scenario Class with Other Scenario Classes

The TSPA-SEIS overestimates total dose by not subtracting the inventory released due to preceding seismic ground motion events from the inventory available at the time of an igneous event. During 1,000,000 years essentially all realizations of the repository will include releases due to seismic ground motion damage; thus, essentially all realizations of the Igneous Modeling Cases overstate releases by the amount of inventory released by seismic events prior to an intrusion. However, on average, the fraction of total inventory released from the EBS in the Seismic GM Modeling Case is expected to be small, and the overall effect on total mean annual dose is expected to be minor.

The inventory released from a fault displacement event is not subtracted from the inventory that could be released by a later disruptive event. In addition, the inventory that could be released from WPs affected by fault displacement is not reduced by releases from any preceding disruptive events. However, a fault displacement affects at most 212/11,629 = 1.8 percent of the WPs, so at most 1.8 percent of the inventory is counted twice, and the net effect on total mean annual dose of the combination of fault displacements, with other disruptive events, is negligible.

6.1.2.4 Calculation of Expected Annual Dose for the Modeling Cases

Equation 6.1.2-11 shows the calculation of total expected annual dose as the sum of expected annual dose for each scenario class. In turn, the expected annual dose for each scenario class is the sum of the expected annual dose for the modeling cases comprising the scenario class. This section summarizes that discussion and gives the equations used to evaluate expected annual dose for each of the modeling cases.

6.1.2.4.1 Nominal Scenario Class

The Nominal Scenario Class includes one modeling case, the Nominal Modeling Case. By definition, $\overline{D}_N(\tau|\mathbf{e})$ is the expected annual dose resulting from nominal corrosion processes, which occur in every future of the repository. Hence, $D_N(\tau|\mathbf{a},\mathbf{e})$ can be simplified as the expected annual dose $D_N(\tau \mid \mathbf{e}_i)$ is calculated by the models described in Section 6.3.

In the estimate for $D_N(\tau \mid \mathbf{e}_i)$, there is no restriction on the sampling to ensure that each realization includes WP failures by corrosion. Therefore, there can be realizations with no WP failures and, therefore, no release and no annual dose.

The expected annual dose for the Nominal Modeling Case is calculated $D_N(\tau \mid \mathbf{e}_i)$ for both 10,000 years and for 1,000,000 years. However, for estimating total expected annual dose for 1,000,000 years, $D_N(\tau \mid \mathbf{e}_i)$ is not used directly in Equation 6.1.2-11. Instead, as described in Section 6.1.2.4.4, the dose due to nominal processes is calculated as part of the Seismic GM Modeling Case.

Conceptually, the location of each WP that fails by nominal corrosion processes are aleatory uncertainties. However, the TSPA-SEIS computes $D_N(\tau \mid \mathbf{e}_i)$ for only one configuration of corrosion failed WPs in each epistemic realization. This treatment greatly reduces the computation burden of the Nominal Modeling Case, and is justified because the Nominal Modeling Case is not significant in the computation of total annual dose. For 10,000 years, few (if any) WPs are expected to fail by nominal corrosion processes. For 1,000,000 years, the majority of WPs are expected to be affected by nominal corrosion, so little variability in the spatial arrangement of these WPs is expected.

6.1.2.4.2 Early Failure Scenario Class

The Early Failure Scenario Class includes two modeling cases: the Waste Package EF Modeling Case, and the Drip Shield EF Modeling Case. For the Early Failure Scenario Class, expected annual dose at time τ is computed as:

$$\overline{D}_{EF}(\tau|\mathbf{e}) = \overline{D}_{EW}(\tau|\mathbf{e}) + \overline{D}_{ED}(\tau|\mathbf{e}) \qquad \text{(Eq. 6.1.2-12)}$$

where $\overline{D}_W(\tau|\mathbf{e}_i)$ is the expected annual dose from early failed WPs, and $\overline{D}_D(\tau|\mathbf{e}_i)$ is the expected annual dose from early failed DSs. Equation 6.1.2-12 is justified because early failure is modeled as occurring independently for each WP and DS.

Waste Package EF Modeling Case—The Waste Package EF Modeling Case estimates the dose resulting from the occurrence of early failure of WPs. The aleatory uncertainties in this modeling case include:

- The number of WP early failures
- The type of each WP having early failure
- The location of each WP having early failure, described in terms of the seepage conditions at each location.

For each realization $\mathbf{e}_i$ of epistemically uncertain parameters, the expected dose $\overline{D}_W(\tau|\mathbf{e}_i)$ is calculated by

$$\overline{D}_W(\tau|\mathbf{e}_i) = \sum_{r=1}^{2}\sum_{s=1}^{5}\sum_{t=0}^{1} pW\, fWT_r\, fBN_s\, pDRP_{rst}\, nWP\, D_W(\tau|[1,r,s,t],\mathbf{e}_i) \quad \text{(Eq. 6.1.2-13)}$$

where

pW is the probability of a single WP having early failure (element of $\mathbf{e}_A$)

fWT_r is the fraction of WPs in the repository of type r (co-disposed [CDSP] or transportation, aging, and dispoal [TAD] canister)

$fDRP_{rs}$ is the fraction of WPs of type r in percolation bin s (Section 6.3.2) that experience dripping conditions (function of elements of $\mathbf{e}_M$)

$$pDRP_{rst} = \begin{cases} 1 - fDRP_{rs} & \text{if } t = 0 \\ fDRP_{rs} & \text{if } t = 1 \end{cases}$$

fBN_s is the fraction of WPs in the repository that are in percolation bin s

nWP is the number of WPs in the repository

$D_D(\tau|[1,r,s,t],\mathbf{e}_i)$ is the dose at time τ that results from early failure of one DS over a WP of type r in percolation bin s with dripping ($t = 1$) or non-dripping conditions ($t = 2$), and is calculated using the GoldSim component of the TSPA-SEIS.

Drip Shield EF Modeling Case—The Drip Shield EF Modeling Case estimates the dose resulting from the occurrence of early failure of DSs. The aleatory uncertainties in this modeling case include:

- The number of DS early failures
- The location of each DS early failure, described in terms of the seepage and conditions at each location
- The type of WP located beneath each DS early failure.

The calculation of expected annual dose for the Drip Shield EF Modeling Case is very similar to Equation 6.1.2-13 for expected annual dose for the Waste Package EF Modeling Case. For each realization $\mathbf{e}_i$ of epistemically uncertain parameters, the expected dose $\overline{D}_D(\tau|\mathbf{e}_i)$ is calculated by

$$\overline{D}_D(\tau|\mathbf{e}_i) = \sum_{r=1}^{2}\sum_{s=1}^{5}\sum_{t=0}^{1} pD\, fWT_r\, pDRP_{rst}\, nWP\, D_D(\tau|[1,r,s,t],\mathbf{e}_i) \quad \text{(Eq. 6.1.2-14)}$$

where

pD is the probability of a single DS having early failure (element of $\mathbf{e}_A$)

fWT_r is the fraction of WPs in the repository of type r (CDSP or TAD canister)

nWP is the number of WPs in the repository

$fDRP_{rs}$ is the fraction of WPs of type r in percolation bin s (Section 6.3.2) that experience dripping conditions (function of elements of $\mathbf{e}_M$)

$$pDRP_{rs} = \begin{cases} 1 - fDRP_{rs} & \text{if } t = 0 \\ fDRP_{rs} & \text{if } t = 1 \end{cases}$$

$D_D(\tau|[1,r,s,t],\mathbf{e}_i)$ is the dose at time τ that results from early failure of one DS over a WP of type r in percolation bin s with dripping ($t = 1$) or non-dripping conditions ($t = 2$), and is calculated using the GoldSim component of the TSPA-SEIS.

6.1.2.4.3 Igneous Scenario Class

The Igneous Scenario Class includes two modeling cases: the Igneous Intrusion Modeling Case, and the Volcanic Eruption Modeling Case. For the Igneous Scenario Class, expected annual dose at time τ is computed as:

$$\overline{D}_I(\tau|\mathbf{e}) = \overline{D}_{II}(\tau|\mathbf{e}) + \overline{D}_{IE}(\tau|\mathbf{e}) \qquad \text{(Eq. 6.1.2-15)}$$

where $\overline{D}_{II}(\tau|\mathbf{e}_i)$ is the expected annual dose from igneous intrusions, and $\overline{D}_{IE}(\tau|\mathbf{e}_i)$ is the expected annual dose from eruptions. Although the occurrence of intrusions and eruptions is not independent, Equation 6.1.2-15 is justified because effects of an intrusion and an eruption are independent.

Igneous Intrusion Modeling Case—The Igneous Intrusion Modeling Case estimates the dose resulting from groundwater transport of radionuclides as a consequence of an igneous intrusion into the repository. The Volcanic Eruption Modeling Case estimates the dose that results from an eruption that occurs during an igneous event. The time of the igneous event is the single aleatory uncertainty in this modeling case. The TSPA-SEIS assumes that an igneous intrusion affects all WPs, and that maximum damage occurs to each WP; thus, the extent of damage is not treated as an aleatory uncertainty.

For each realization $\mathbf{e}_i$ of epistemically uncertain parameters, the expected annual dose $\overline{D}_{II}(\tau|\mathbf{e}_i)$ at time τ is formally calculated by

$$\overline{D}_{II}(\tau|\mathbf{e}_i) = \int_0^{\tau} D_{II}(\tau|[1,t],\mathbf{e}_i)\lambda_{I,i}\,dt \qquad \text{(Eq. 6.1.2-16)}$$

where, $D_{II}(\tau|[1,t],\mathbf{e}_i)$ is the dose conditional on one intrusion occurring at time t, and $\lambda_{I,i}$ is the frequency of igneous events for realization $\mathbf{e}_i$. Equation 6.1.2-16 accounts for the possibility of more than one igneous intrusion occurring in the future of the repository. Because the first intrusion damages the repository to the maximum extent, subsequent intrusions should not contribute additional radionuclides to the expected annual dose. However, on average, only 2 percent of realizations include more than one intrusion, so the over-counting of dose is minor.

Nominal corrosion processes are included in the Igneous Intrusion Modeling Case for calculation of dose to 1,000,000 years. However, Equation 6.1.2-16 does not include the dose from radionuclides released by corrosion processes prior to the intrusion. Rather, nominal corrosion processes are included to more accurately estimate the inventory remaining within the WPs at the time of an intrusion. The dose from radionuclides released prior to the intrusion by corrosion processes is accounted for as part of the Seismic GM Modeling Case, as described in Section 6.1.2.4.3.

The integral in Equation 6.1.2-16 is approximated by employing a quadrature technique to integrate over time t

$$\overline{D}_{II}(\tau|\mathbf{e}_i) = \lambda_{I,i} \sum_{k=0}^{N-1} D_{II}(\tau|[1,t_k],\mathbf{e}_i)/\Delta t_k \qquad \text{(Eq. 6.1.2-17)}$$

where

T is the time period of interest (10,000 or 1,000,000 years)

$[t_0, t_1, \ldots, t_N]$ is a sequence of times of igneous intrusions occurring in $[0,T]$, for which $D_{II}(\tau|[1,t],\mathbf{e}_i)$ has been computed using GoldSim results

$\Delta t_k = t_{k+1} - t_k$

Volcanic Eruption Modeling Case—The Volcanic Eruption Modeling Case estimates the annual dose resulting from eruptions. The aleatory uncertainties in this modeling case include:

- Number of igneous eruptive events
- Time of each eruptive event
- Eruptive power, eruptive velocity, duration, wind speed, and wind direction for each eruptive event
- Number of WPs affected and fraction of WP content that is ejected into the atmosphere.

For each realization $\mathbf{e}_i$ of epistemically uncertain parameters, the expected annual dose $\overline{D}_{IE}(\tau|\mathbf{e}_i)$ at time τ is formally calculated by

$$\overline{D}(\tau|\mathbf{e}_i) = pE\,\lambda_{I,i}\,\overline{N}_{IE}\,\overline{F}\int_{U_{IE}}\left[\int_0^{\tau} D_{IE}(\tau|[1,t,1,\mathbf{u}],\mathbf{e}_i)dt\right]d_U(\mathbf{u})dU \qquad \text{(Eq. 6.1.2-18)}$$

where

pE is the probability that an igneous event includes one or more eruptive conduits that interest waste

$\lambda_{I,i}$ is the frequency of igneous events for realization $\mathbf{e}_i$

$\overline{N}_{IE}$ is the mean number of WPs affected by an eruptive conduit

$\overline{F}$ is the mean fraction of WP content ejected into the atmosphere

U_{IE} is the vector space of all values of eruptive power, eruptive velocity, duration, wind speed, and wind direction

$\mathbf{u}$ is a vector of values sampled from the distributions for eruptive power, eruptive velocity, duration, wind speed, and wind direction

$d_U(\mathbf{u})$ is the probability density function on U_{IE} formed from the individual probability distributions for eruptive power, eruptive velocity, duration, wind speed, and wind direction

$D_{IE}(\tau|[1,t,1,\mathbf{u}],\mathbf{e}_i)$ is the dose calculated by GoldSim conditional on one eruption occurring at time t, which affects one WP, with eruptive power, eruptive velocity, duration, wind speed, and wind direction described by $\mathbf{u}$.

The calculation of expected dose in Equation 6.1.2-18 accounts for the possibility that more than one igneous eruption occurs in the future evolution of the repository. The calculation assumes that each eruption event affects a different set of WPs, thus the consequence of two or more eruption events is the sum of the consequences of each individual event.

Due to the relatively large number of aleatory uncertainties in Equation 6.1.2-18, calculation of expected annual dose employs a Monte Carlo technique. A Latin hypercube sample (LHS) of size nU is generated from U_{IE}, and the quantities $D_{IE}(\tau|[1,t,1,\mathbf{u}],\mathbf{e}_i)$ are computed using GoldSim. The expected dose is calculated using a quadrature technique to integrate over time t

$$\overline{D}(\tau|\mathbf{e}_i) = pE\,\lambda_{I,i}\,\overline{N}_{IE}\,\overline{F}\sum_{k=0}^{N-1}\left[\sum_{l=1}^{nU} D_{IE}(\tau|[1,t_k,1,\mathbf{u}_l],\mathbf{e}_i)/nU\right]\Big/\Delta t_k \qquad \text{(Eq. 6.1.2-19)}$$

where

$\mathbf{u}_l$ are the sampled vectors from U_{IE}

T is the time period of interest (10,000 or 1,000,000 years)

$[t_0, t_2, \ldots, t_N]$ is a sequence of times of igneous eruptions occurring in $[0,T]$, for which $D_{IE}(\tau|[1,t,1,\mathbf{u}],\mathbf{e}_i)$ has been computed using GoldSim results

$\Delta t_k = t_{k+1} - t_k$

6.1.2.4.4 Seismic Scenario Class

The Seismic Scenario Class includes two modeling cases: the Seismic GM Modeling Case, and the Seismic FD Modeling Case. For the Seismic Scenario Class, expected annual dose at time τ for 10,000 years is computed as:

$$\bar{D}_S(\tau|\mathbf{e}) = \bar{D}_{GM}(\tau|\mathbf{e}) + \bar{D}_{FD}(\tau|\mathbf{e}) \qquad \text{(Eq. 6.1.2-20)}$$

where $\bar{D}_{GM}(\tau|\mathbf{e})$ is the expected annual dose from seismic ground motion events, and $\bar{D}_{FD}(\tau|\mathbf{e})$ is the expected annual dose from seismic fault displacement events. Equation 6.1.2-20 is justified because the occurrence of ground motion and fault displacement events is modeled as independent.

For 1,000,000 years, the expected annual dose for the Nominal and the Seismic Scenario Classes are combined, and are computed as:

$$\bar{D}_N(\tau|\mathbf{e}) + \bar{D}_S(\tau|\mathbf{e}) = \bar{D}_{GM}(\tau|\mathbf{e}) + \bar{D}_{FD}(\tau|\mathbf{e}) \qquad \text{(Eq. 6.1.2-21)}$$

Seismic GM Modeling Case—The Seismic GM Modeling Case calculates annual dose from radionuclides released from the EBS due to damage to WPs resulting from vibratory ground motion. In addition, this modeling case accounts for damage to the DS due to vibratory ground motion, and the effects of this damage on radionuclide releases from WPs. The occurrence of seismic events is modeled as a Poisson process with the smallest events of consequence having an annual frequency of 4.287×10^{-4} yr^{-1}. During the first 10,000 years after closure, only a few seismic ground motion events will occur; however, during the 1,000,000 years following closure period, the TSPA-SEIS must account for the effects of a sequence of a few hundred seismic events. In addition, because corrosion processes alter the response of the engineered barrier components to seismic events, corrosion processes are included in the Seismic GM Modeling Case calculation for 1,000,000 years, and the dose from radionuclides release due to corrosion processes is calculated as part of the Seismic GM Modeling Case for 1,000,000 years. Due to these differences, different numerical techniques are used to calculate expected annual dose for 10,000 years and for 1,000,000 years.

The *Seismic Consequence Abstraction* (SNL 2007 [DIRS 176828] outlines a probabilistic model for effects on the EBS due to seismic ground motion events. The abstraction provides different probability models for:

- the occurrence and extent of SCC damage to CDSP WP and TAD canister WPs
- the occurrence and extent of rupture of CDSP WP and TAD canister WPs
- the occurrence and extent of rockfall in the lithophysal and non-lithophysal zones
- the state of the DS and its supporting framework as a function of time.

The abstraction also accounts for the change in susceptibility of each EBS component to damage, and, if damage occurs, the change in the extent of damage, due to GC taking place.

For 10,000 years, the consequences of seismic ground motion events can be approximated by examining only the occurrence of SCC damage to CDSP WPs with the DS intact and without significant rockfall, and without considering the effects of corrosion processes

The aleatory uncertainties in the Seismic GM Modeling Case for 10,000 years include:

- the number of seismic events that cause SCC damage to CDSP WPs
- the time of each damaging seismic event
- the amount of damage caused by each seismic event.

For each realization $\mathbf{e}_i$ of epistemically uncertain parameters, the expected annual dose $\overline{D}_{GM}(\tau|\mathbf{e}_i)$ at time τ for $\tau < 10{,}000\,\text{yr}$ is formally calculated by

$$\overline{D}_{GM}(\tau|\mathbf{e}_i) = \int_0^{\tau}\left(\lambda_1(\mathbf{e}_i)e^{-\lambda_1(\mathbf{e}_i)t}\left(\int_{A_{\min}}^{A_{\max}} D_{GM}(\tau|[1,t,A],\mathbf{e}_i)\,d_{A1}(A|\mathbf{e}_i)\,dA\right)\right)dt + \int_0^{\tau}\left(\lambda_1(\mathbf{e}_i)e^{-\lambda_1(\mathbf{e}_i)t}\left(\int_t^{\tau}\int_{B_{\min}}^{B_{\max}} D_{GM}(\tau|[1,\tilde{t},B],\mathbf{e}_i)\,d_{A2}(B|\mathbf{e}_i)\,\lambda_2(\mathbf{e}_i)\,d\tilde{t}\right)\right)dt \quad \text{(Eq. 6.1.2-22)}$$

where

$\lambda_1(\mathbf{e}_i)$ is the frequency of seismic ground motion events that cause SCC damage to CDSP WPs with intact internals

$\lambda_2(\mathbf{e}_i)$ is the frequency of seismic ground motion events that cause SCC damage to CDSP WPs with degraded internals

$d_{A1}(A|\mathbf{e}_i)$ is the density function that describes the probability of damage area equal to A occurring on CDSP WPs with intact internals, given that a seismic event that causes damage occurs

$d_{A2}(B|\mathbf{e}_i)$ is the density function that describes the probability of damage area equal to B occurring on CDSP WPs with degraded internals, given that a seismic event that causes damage occurs

$D_{GM}\left(\tau\middle|[1,t,A],\mathbf{e}_i\right)$ is the annual dose at time τ resulting from a seismic ground motion event occurring at time t that causes damaged area equal to A.

Two frequencies ($\lambda_1(\mathbf{e}_i)$ and $\lambda_2(\mathbf{e}_i)$) and density functions ($d_{A1}(A|\mathbf{e}_i)$ and $d_{A2}(B|\mathbf{e}_i)$) for damaged area are used in Equation 6.1.2-22 because *Seismic Consequence Abstration* (SNL 2007 [DIRS 176828] specifies different probability models for the occurrence and the extent of damage depending on whether the internals of the WP are intact or degraded. The TSPA-SEIS assumes that WP internals degrade rapidly after the first seismic event that damages the WP outer barrier. The calculation of expected annual dose in Equation 6.1.2-22 accounts for the possibility that more than one damaging event occurs in the future of the repository, using the conservative assumption that the annual dose from a sequence of events causing cumulative damage to WPs is reasonably approximated by the sum of the annual dose resulting from the individual events.

The integral in Equation 6.1.2-22 is approximated by employing quadrature techniques to integrate over time t and damaged areas A and B

$$\bar{D}_{GM}\left(\tau|\mathbf{e}_i\right) \cong \sum_{j=1}^{n} \lambda_1\left(\mathbf{e}_i\right) e^{-\lambda_1(\mathbf{e}_i)t_{j-1}} \left\{ \sum_{l=1}^{n1} D_{GM}\left(\tau\middle|[1,t_j,A_l],\mathbf{e}_i\right) d_{A1}\left(A_l|\mathbf{e}_i\right)\Delta A_l \right\} \Delta t_j$$
$$+ \sum_{j=1}^{n} \lambda_1\left(\mathbf{e}_i\right) e^{-\lambda_1(\mathbf{e}_i)t_{j-1}} \left\{ \sum_{k=j+1}^{n} \left[\sum_{m=1}^{n2} D_{GM}\left(\tau\middle|[1,t_{k-1},B_l],\mathbf{e}_i\right) d_{B1}\left(B_l|\mathbf{e}_i\right)\Delta B_l \right] \lambda_2\left(\mathbf{e}_i\right)\Delta t_k \right\} \Delta t_j$$

(Eq. 6.1.2-23)

where

$[t_0,t_1,\ldots,t_n]$ is a sequence of times of seismic ground motion events for which $D_{GM}\left(\tau\middle|[1,t_k,A],\mathbf{e}_i\right)$ has been computed using GoldSim results, for each of a set of damaged areas $A_1,A_2,\ldots,A_{n1}$.

$\Delta t_k = t_k - t_{k-1}$

For 1,000,000 years, the full *Seismic Consequence Abstraction* (SNL 2007 [DIRS 176828]) is considered, including both the effects of corrosion processes on EBS components, and the dose resulting from corrosion processes. The aleatory uncertainties in the Seismic GM Modeling Case for 1,000,000 years include:

- The number of seismic events
- The time of each seismic event
- The amount of rockfall in the lithophysal zone caused by each seismic event
- The effect of rockfall on the structure and function of DSs at the time of each seismic event

- The occurrence and extent of damage to each type of WP (CDSP and TAD) for each seismic event
- The occurrence and extent of rupture of the outer barrier for each type of WP (CDSP and TAD canister) for each seismic event.

Owing to the complexity of the abstraction and numerous seismic events that could occur in the future of the repository, and the inclusion of corrosion processes that alter the EBS components as corrosion progresses, a Monte Carlo technique is used to calculate expected annual dose. Denote by A_G the set of all sequences of seismic events and corrosion failures that could occur in the future of the repository. A member $\mathbf{a} \in A_G$ is a vector, the elements of which describe the aleatory quantities listed above that define each seismic event, and additional elements that define corrosion failures. For each realization $\mathbf{e}_i$ of epistemically uncertain parameters, the expected annual dose $\overline{D}_{GM}(\tau|\mathbf{e}_i)$ at time τ for $\tau \leq 1{,}000{,}000$ yr is formally calculated by

$$\overline{D}_{GM}(\tau|\mathbf{e}_i) = \sum_{j=1}^{n} D_{N+G}(\tau|\mathbf{a}_{ij}, \mathbf{e}_i)/n \qquad \text{(Eq. 6.1.2-24)}$$

where

$\mathbf{a}_{ij}, j = 1,\ldots,n$ is a random sample from A_G generated in consistency with the distributions that describe each of the elements of a member $\mathbf{a}$ of A_G,

$D_{N+G}(\tau|\mathbf{a}_{ij}, \mathbf{e}_i)$ is the combined dose from seismic events and corrosion failures described by sample element $\mathbf{a}_{ij}$.

The quantity $\overline{D}_{GM}(\tau|\mathbf{e}_i)$ is calculated directly by the GoldSim component of the TSPA-SEIS; results of these calculations are used to compute total expected annual dose. The dose due to nominal corrosion processes, $D_N(\tau|\mathbf{e}_i)$, is computed separately for the purpose of model validation and analysis. For 1,000,000 years, the additional dose due to seismic events only (excluding dose due to nominal corrosion processes) is not calculated separately.

Seismic FD Modeling Case—The Seismic FD Modeling Case calculates annual dose from radionuclides released from the EBS due to damage caused by fault displacements. The aleatory uncertainties in this modeling case include:

- Number of fault displacement events
- Time of each fault displacement event
- Number of WPs of each type (CDSP WP or TAD canister) damaged by each fault displacement event

- The location of each WP damaged by each fault displacement event, described in terms of the seepage conditions at each location
- Area opened in the outer barrier of each WP type by each fault displacement event.

The TSPA-SEIS assumes that each fault displacement event affects a different set of WPs that have not been damaged by prior fault displacement events. When a fault displacement event occurs, the DS above the affected WPs is assumed to be ruptured by the event.

The calculation of expected annual dose for fault displacements does not explicitly treat the aleatory uncertainty for the location of each affected WP. Instead, to save computational resources, expected annual dose is estimated by modeling 100 WPs of each type, placed proportionally into the percolation bins, and within each bin, into dripping or non-dripping locations. Results are calculated for the set of 100 WPs and then scaled to the expected number of packages affected by a fault displacement event.

For each realization $\mathbf{e}_i$ of epistemically uncertain parameters, the expected annual dose $\overline{D}_{FD}(\tau|\mathbf{e}_i)$ at time τ is calculated by

$$\overline{D}_{FD}(\tau|\mathbf{e}_i) = \sum_{r=1}^{2}\left[\overline{N}_r \lambda_{Fr}/100\right]\left[\int_0^{\tau}\left(\int_{A_{\min}}^{A_{\max}} D_{Fr}(\tau|[1,t,100,A_r],\mathbf{e}_i)\, d_{Ar}(A_r)\, dA_r\right) dt\right] \quad \text{(Eq. 6.1.2-25)}$$

where

r indicates each type of WP (CDSP WP or TAD canister)

$\overline{N}_r$ is the expected number of WPs of type r damaged by one fault displacement event

λ_{Fr} is the frequency of fault displacement events that cause damage to WPs of type r

$D_{Fr}(\tau|[1,t,100,A_r],\mathbf{e}_i)$ is the annual dose resulting from a fault displacement occurring at time t which damages 100 WPs of type r, causing an opening with an area equal to A_r on each WP

$d_{Ar}(A_r)$ is the density function describing the probability of a fault displacement creating an opening of area A_r on WPs of type r.

The quantity $D_{Fr}(\tau|[1,t,100,A_r,1],\mathbf{e}_i)$ is calculated directly by the Goldsim component of the TSPA-SEIS. The integrals in Equation 6.1.2-25 are approximated using quadrature techniques similar to those employed in Equation 6.1.2-23.

Human Intrusion Modeling Case—The Human Intrusion Modeling Case estimates repository performance in the event that of a drilling intrusion intersects the repository. Unlike the other modeling cases, the Human Intrusion Modeling Case is not a component of the calculation of total mean annual dose (Section 6.1.2.2). Rather, the results of the Human Intrusion Modeling Case are compared against the regulations specified in 10 CFR 63.321[DIRS 178394].

Calculation of expected annual dose for the Human Intrusion Modeling Case resembles the calculation in the other modeling cases. The aleatory uncertainty in this modeling case is the type of WP intersected and the location of the drilling intrusion. The time of the intrusion is fixed at 200,000 years, and the Human Intrusion Scenario specifies a single drilling intrusion.

The Human Intrusion Scenario uses a Monte Carlo technique to calculate expected dose. For each realization $\mathbf{e}_i$ of epistemically uncertain parameters, the expected annual dose $\bar{D}_{HI}(\tau|\mathbf{e}_i)$ at time τ is calculated by

$$\bar{D}_{HI}(\tau|\mathbf{e}_i) = \sum_{j=1}^{nA} D_{HI}\left(\tau\left|\left[1, r_j, q_j, SR_j\right], \mathbf{e}_i\right.\right) \Big/ nA \qquad \text{(Eq. 6.1.2-26)}$$

where

nA is the number of aleatory realizations

r_j is the type of WP (CDSP WP or TAD canister) intersected in the j^{th} aleatory realization

q_j is the percolation rate in the percolation bin selected in the j^{th} aleatory realization (Section 6.3.2)

SR_j is the SZ source region selected in the j^{th} aleatory realization (Section 6.3.9)

$D_{HI}\left(\tau\left|\left[1, r_j, q_j, SB_j\right], \mathbf{e}_i\right.\right)$ is the annual dose resulting at time τ from a human intrusion that intersects 1 WP of type r_j that experiences percolation rate q_j and intersects the SZ in source region SR_j.

The quantity $D_{HI}\left(\tau\left|\left[1, r_j, q_j, SR_j\right], \mathbf{e}_i\right.\right)$ is calculated directly by the GoldSim component of the TSPA-SEIS.

INTENTIONALLY LEFT BLANK

Table 6.1.2-1. Effect of Combinations of Scenario Classes on Total Mean Annual Dose

	Later Disruptive Event			
Preceding Event	**Igneous Intrusion**	**Igneous Eruption**	**Seismic Ground Motion**	**Seismic Fault Displacement**
Early Failure Waste Package	Very minor (~0.02%) overcounting of inventory. Negligible effect on total mean annual dose.	Overcounting of inventory in WPs affected by the eruption event. Negligible effect on total mean annual dose.	Very minor (~0.02%) overcounting of inventory. Negligible effect on total mean annual dose.	Overcounting of inventory in WPs affected by the fault displacement event. Negligible effect on total mean annual dose.
Early Failure Drip Shield	Very minor (~0.01%) overcounting of inventory. Negligible effect on total mean annual dose.	Overcounting of inventory in WPs affected by the eruption event. Negligible effect on total mean annual dose.	Very minor (~0.01%) overcounting of inventory. Negligible effect on total mean annual dose.	Overcounting of inventory in WPs affected by the fault displacement event. Negligible effect on total mean annual dose.
Igneous Intrusion	Included in calculation of Mean Dose for the Igneous Scenario Class $\overline{\overline{D}}_I(\tau)$.	Conservative overstatement of the consequences of the igneous eruption event. Negligible effect on total mean annual dose.	Conservative overstatement of the consequences of the seismic ground motion event. Minor effect on total mean annual dose.	Conservative overstatement of the consequences of the seismic fault displacement event. Negligible effect on total mean annual dose.
Igneous Eruption	Very minor (~0.03%) overcounting of inventory. Negligible effect on total mean annual dose.	Included in calculation of for the Igneous Scenario Class $\overline{\overline{D}}_I(\tau)$.	Very minor (~0.03%) overcounting of inventory. Negligible effect on total mean annual dose.	Very minor (~0.03%) overcounting of inventory in WPs affected by the fault displacement event. Negligible effect on total mean annual dose.
Seismic Ground Motion	Conservative overcounting of inventory and consequences of an intrusion. Minor effect on total mean annual dose.	Overcounting of inventory in WPs affected by the eruption event. Negligible effect on total mean annual dose.	Included in calculation of mean dose for the Seismic Scenario Class $\overline{\overline{D}}_S(\tau)$.	Overcounting of inventory in WPs affected by the fault displacement event. Negligible effect on total mean annual dose.
Seismic Fault Displacement	Very minor (~1 %) overcounting of inventory. Negligible effect on total mean annual dose.	Overcounting of inventory in WPs affected by the eruption event. Negligible effect on total mean annual dose.	Very minor (~1 %) overcounting of inventory. Negligible effect on total mean annual dose.	Included in calculation of mean dose for the Seismic Scenario Class $\overline{\overline{D}}_S(\tau)$.

INTENTIONALLY LEFT BLANK

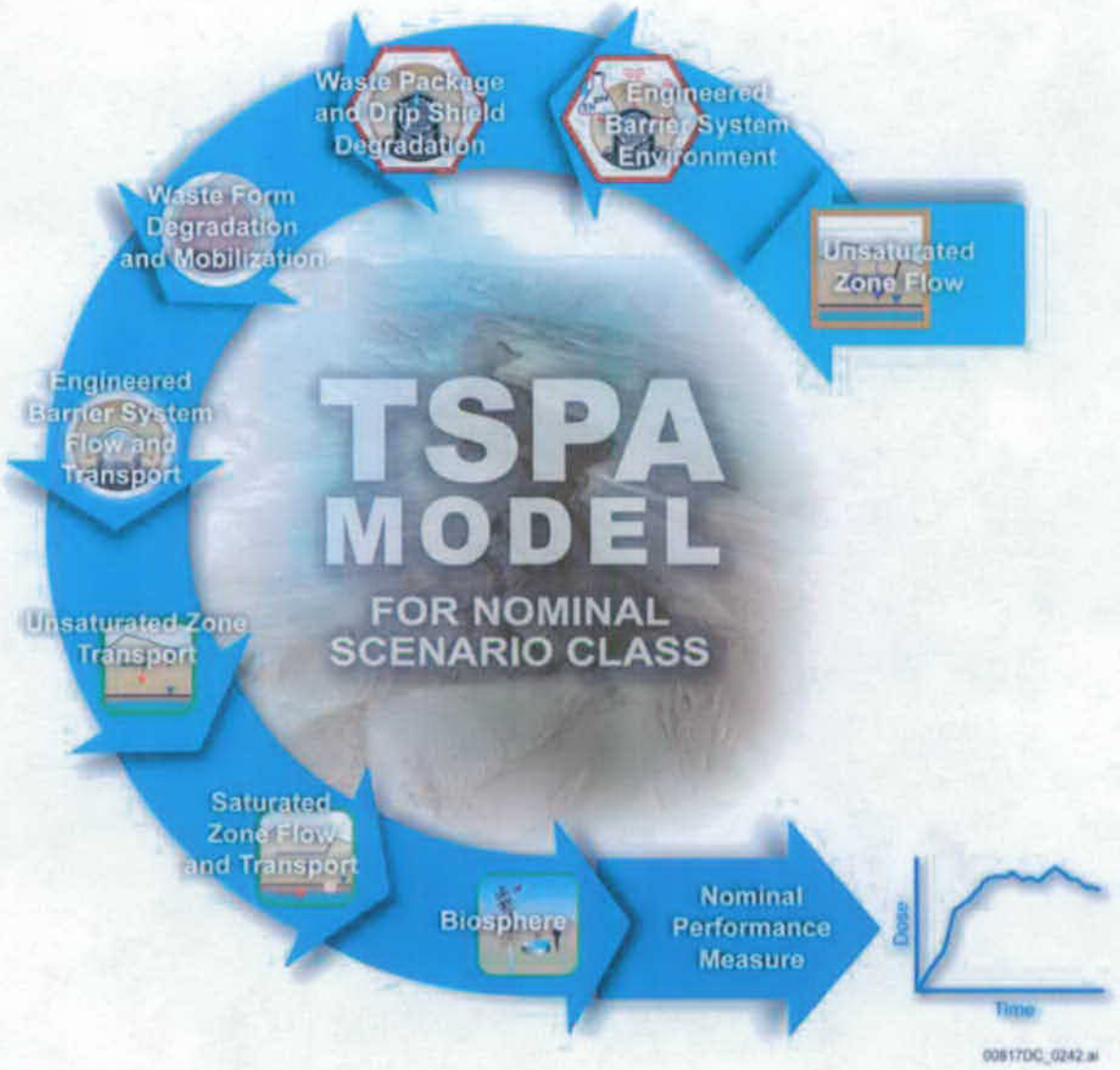

Figure 6.1.2-1. Schematic Representation of the TSPA-SEIS Components for the Nominal Scenario Class

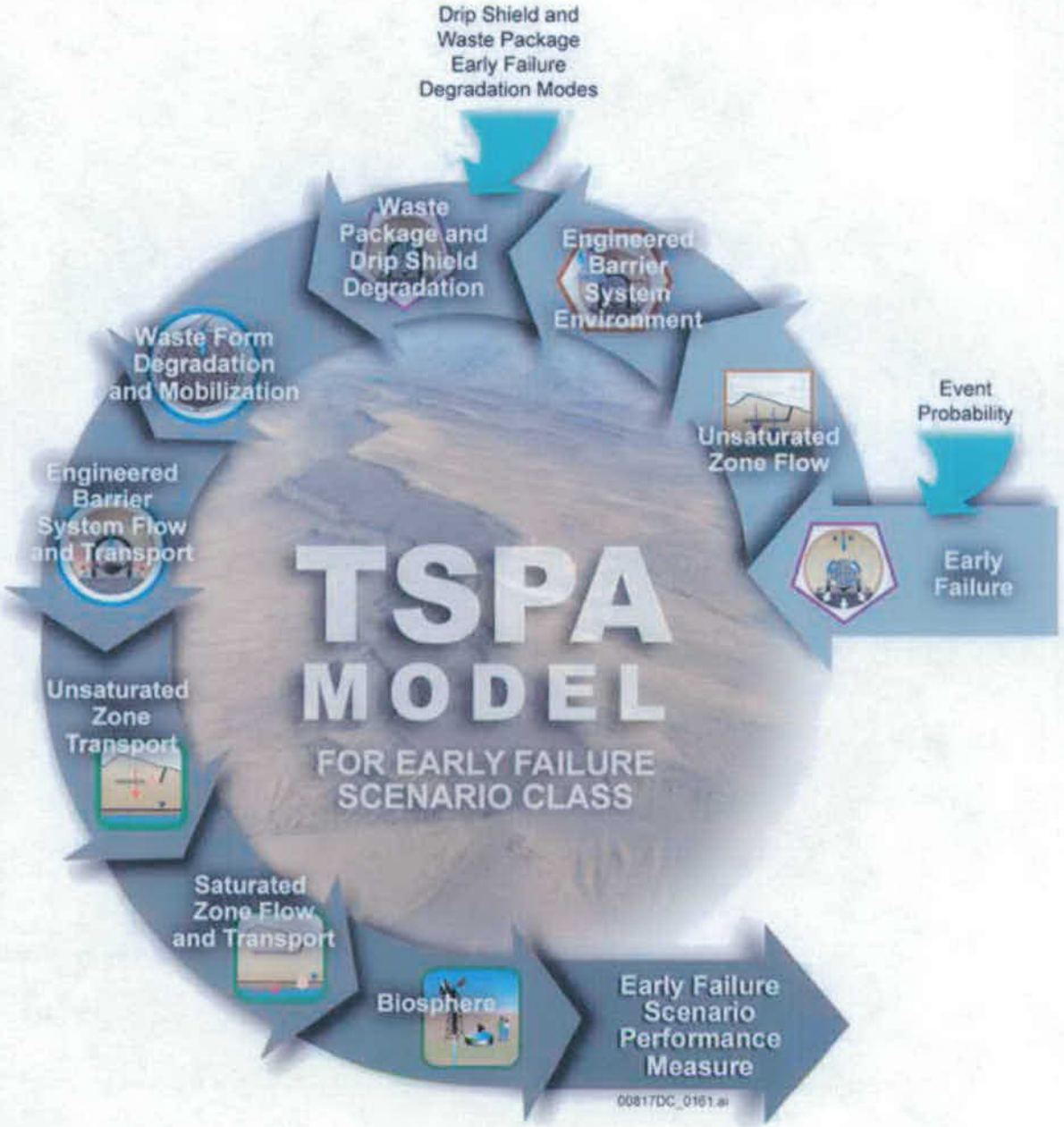

Figure 6.1.2-2. Schematic Representation of the TSPA-SEIS Components for the Early Failure Scenario Class

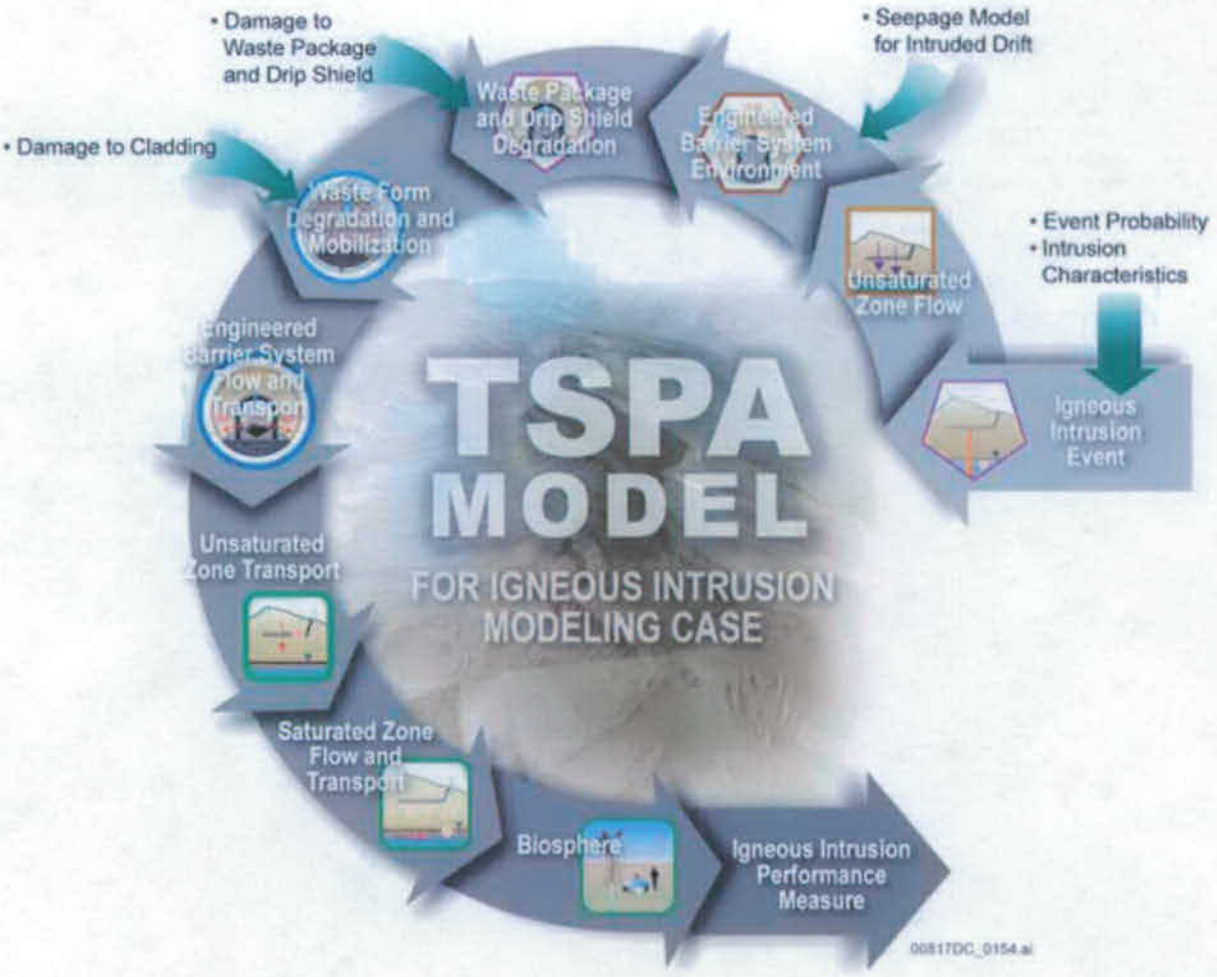

Figure 6.1.2-3. Schematic Representation of the TSPA-SEIS Components for the Igneous Intrusion Modeling Case

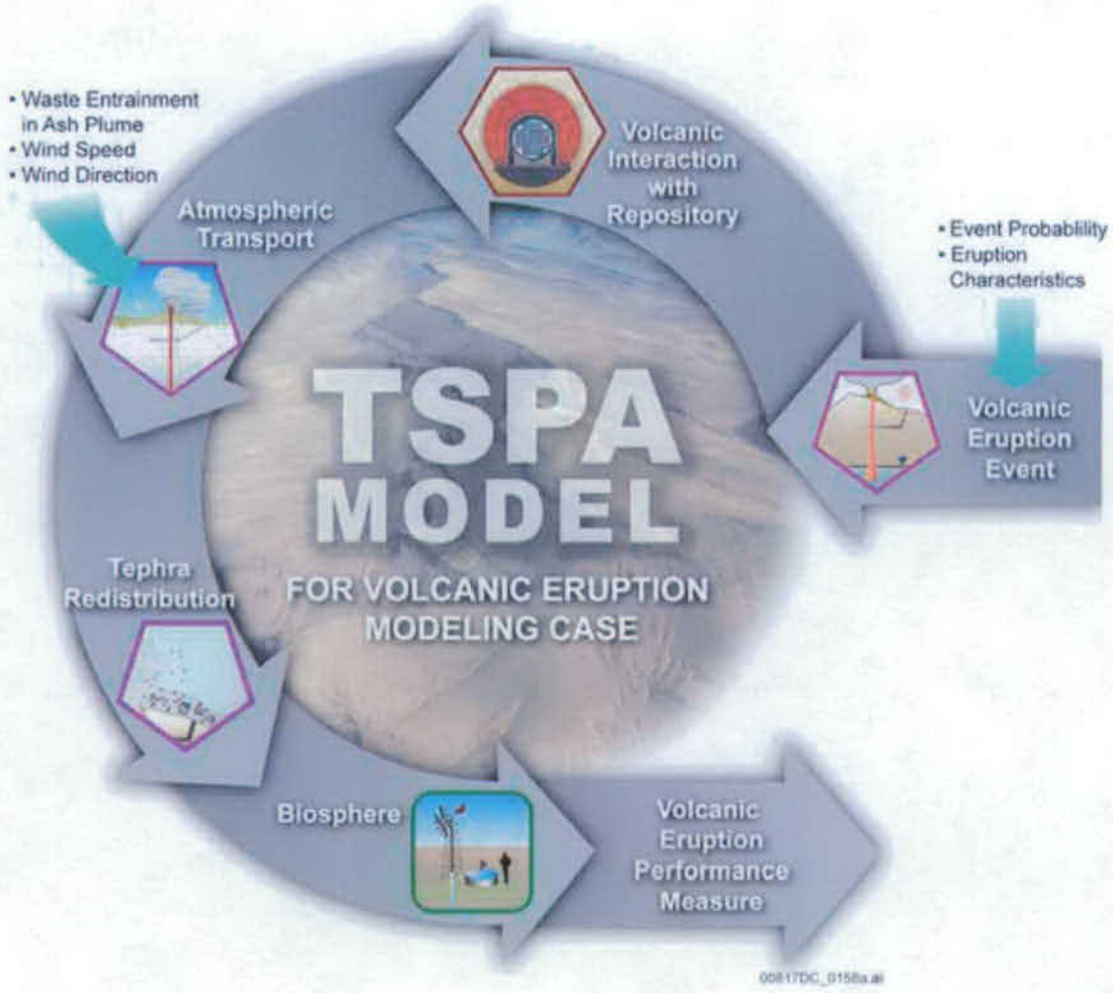

Figure 6.1.2-4. Schematic Representation of the TSPA-SEIS Components for the Volcanic Eruption Modeling Case

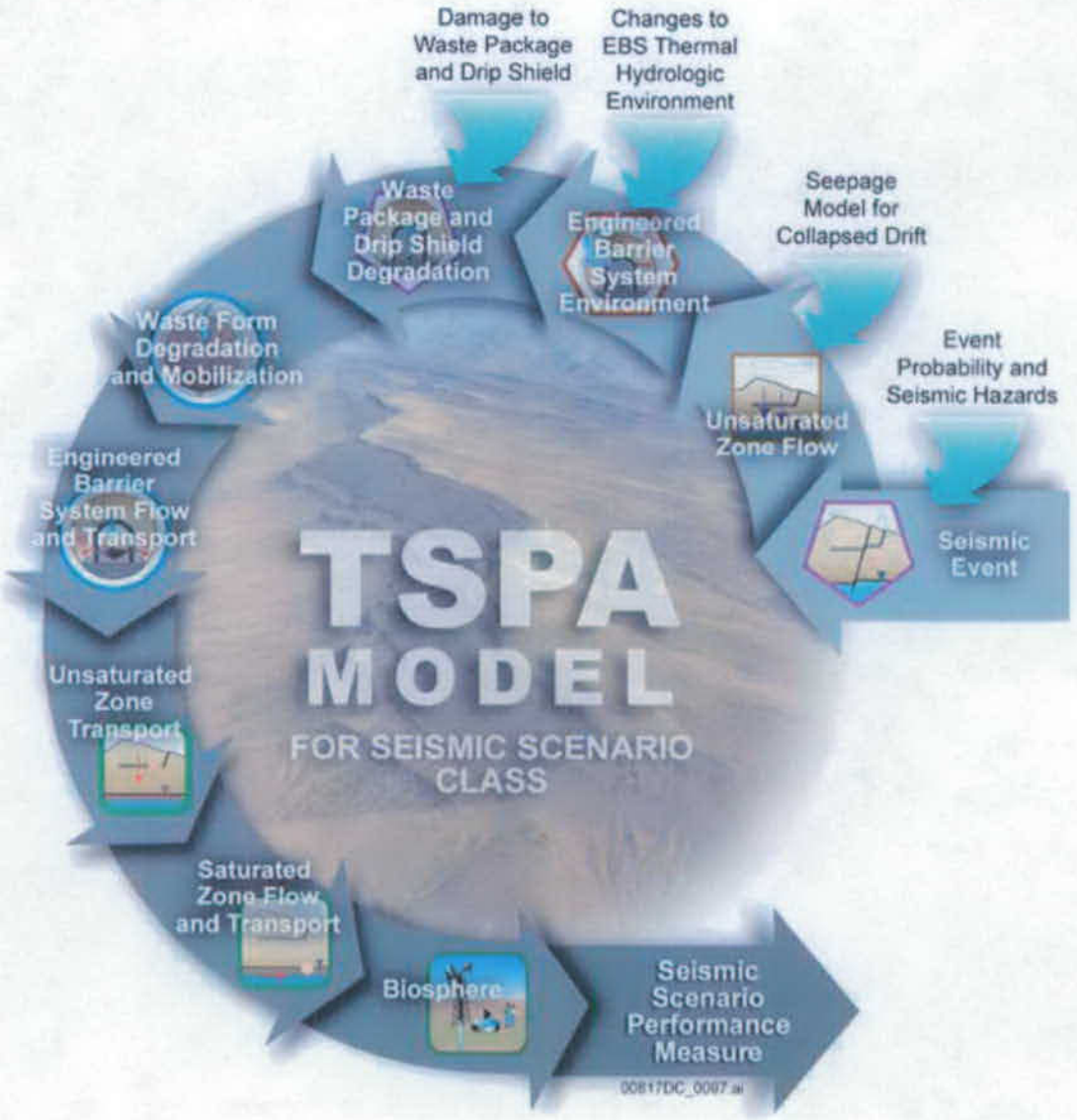

Figure 6.1.2-5. Schematic Representation of the TSPA-SEIS Components for the Seismic Scenario Class

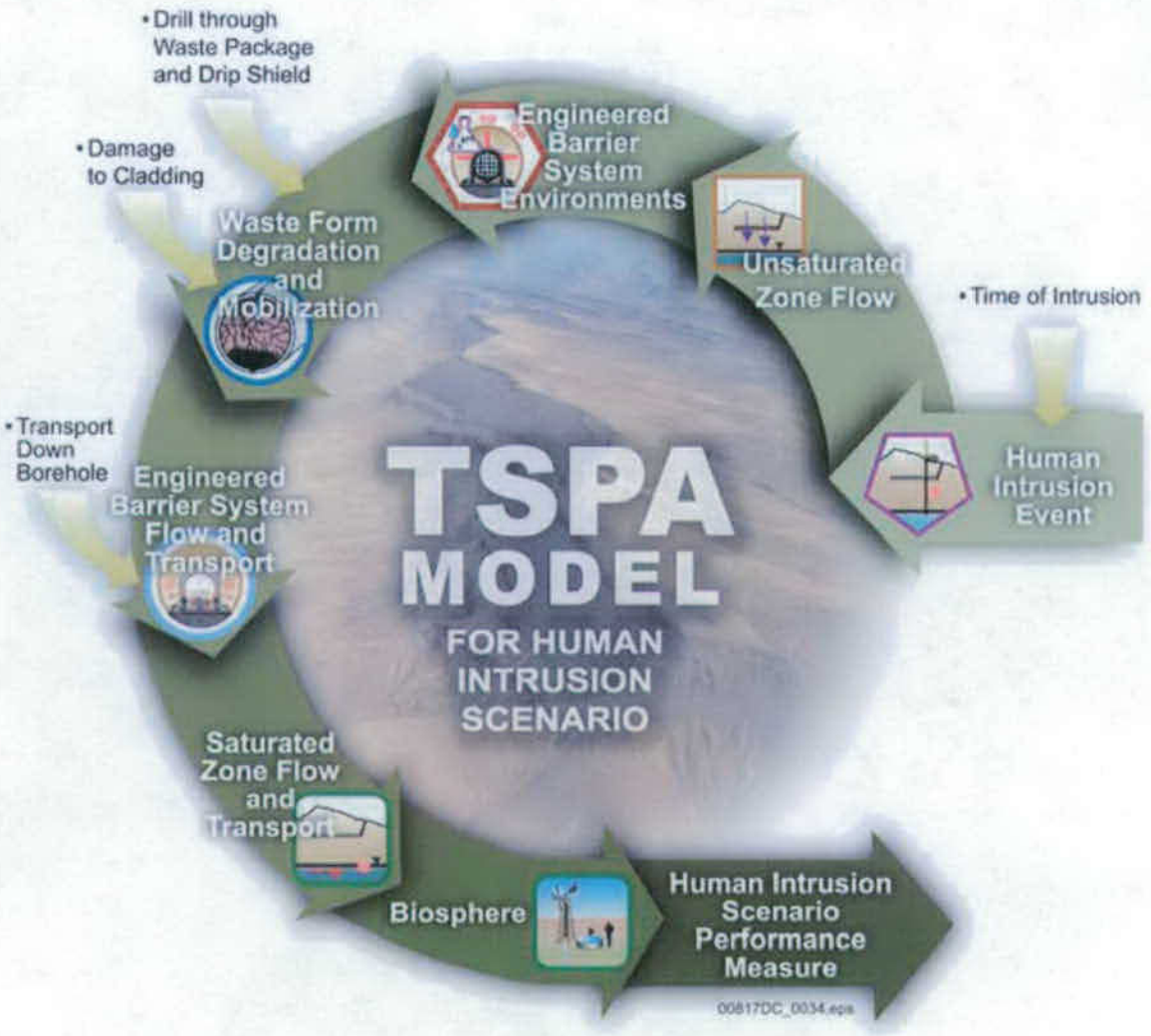

Figure 6.1.2-6. Schematic Representation of the TSPA-SEIS Components for the Human Intrusion Scenario

6.1.3 Treatment of Uncertainty in the TSPA-SEIS

Sources of Uncertainty—Uncertainties are inherent in projections of the geologic and environmental conditions surrounding the Yucca Mountain repository into the future. Assessment of total system performance over this period must take these uncertainties into account. In addition, the discussion of the quantitative estimates of this performance (e.g., estimates of mean annual dose) will include information regarding the impacts of these uncertainties on those estimates (e.g., uncertainty in the estimate of mean annual dose).

The TSPA-SEIS accounts for uncertainty in two categories: aleatory uncertainty and epistemic uncertainty. Aleatory uncertainty arises from inherent uncertainty about the occurrence of future events that may affect the repository and the effect of these events on repository performance. Because aleatory uncertainty cannot be reduced by the acquisition of additional data or knowledge, this kind of uncertainty is also referred to as irreducible uncertainty. Examples of aleatory uncertainty considered in the TSPA-SEIS include the number and location of early failed WPs, time and amplitude of seismic ground motion events, and occurrence of igneous events. Aleatory uncertainties included in the TSPA-SEIS are listed in Table 6.1.3-1.

The second category is referred to here as epistemic uncertainty. Epistemic uncertainty stems from a lack of knowledge about a quantity that is believed to have a fixed (or deterministic) value. Sources of epistemic uncertainties include incomplete data, measurement errors, and estimates based upon expert judgment. Unlike aleatory uncertainty, epistemic uncertainty is potentially reducible with additional data and knowledge. In the TSPA-SEIS, epistemic quantities are generally inputs to specific submodels, with the submodels having been developed to use single values for these quantities. A particular epistemic quantity can be a parameter for a probability distribution or density function (e.g., adsorption coefficients for transport of radionuclides in the UZ), a field of values selected from alternative sets (e.g., the flow field in the UZ), or a factor added to a parameter to represent the uncertainty (e.g., the uncertainty term added to the model for actinide solubilities). Epistemic uncertainties included in the TSPA-SEIS are indicated in Table 6.1.3-2.

Probabilistic Framework for Implementing the TSPA-SEIS—Both aleatory and epistemic uncertainties are quantified using probability distributions. However, in the TSPA-SEIS, the numerical treatment of the two categories of uncertainty is different. Because the aleatory uncertainties vary between modeling cases, treatment of aleatory uncertainties also varies among modeling cases. The subsections of Section 6.1.2 describe the treatment of aleatory uncertainty for each modeling case of the TSPA-SEIS.

In general, epistemic uncertainties are addressed by means of a Monte Carlo technique employing an LHS of the epistemically uncertain quantities. The same LHS is used in each of the modeling cases. This method allows a thorough mapping of the uncertainty in model inputs (parameters) to the corresponding uncertainty in model output (estimates of performance) and also allows results from each modeling case to be combined into an estimate of total mean annual dose. Uncertainty in the model outcome is quantified via multiple model realizations, using LHS to select values for uncertain parameters. The benefits of probabilistic modeling include: (1) obtaining a representative range of possible outcomes (and the likelihood of each

outcome) to quantify predictive uncertainty, and (2) analyzing the relationship between the uncertain inputs and uncertain outputs to provide insight into the effect of the uncertainties.

Propagation of Uncertainty—The Monte Carlo analysis for the TSPA-SEIS involves the following four steps:

- **Select Imprecisely Known Input Parameters to be Sampled**—The TSPA-SEIS includes several thousand parameters, several hundred of which are treated as uncertain. The magnitude of uncertainty, type of probability distribution used to characterize the uncertainty, and guidance on sampling values for the parameters are developed in the individual process models or abstractions or both, as documented in their respective model reports.

- **Construct Probability Distribution Functions for Each Parameter**—The probabilistic framework employed in Monte Carlo simulations requires that the uncertainty in the TSPA-SEIS inputs be quantified using probability distributions. Examples of such representations can be found in the descriptions of various TSPA-SEIS submodels in Section 6.3. These distributions are specified in terms of either empirical distribution functions or coefficients of parametric distributions.

- **Generate a Sample Set by Selecting a Parameter Value from Each Distribution**—The next step in the Monte Carlo process requires the generation of a number of parameter distributions that are sampled in the course of an analysis. The TSPA-SEIS uses LHS, where the range of each parameter is divided into intervals of equal probability, and a value is selected at random within each interval. LHS helps achieve a more complete coverage of the range of values of an uncertain parameter than unstratified sampling.

- **Calculate Outcomes for the Sample Set and Aggregate Results for All Samples**—In this step of the Monte Carlo methodology, the modeling case for the scenario class of interest is evaluated for each of the randomly generated parameter sets. This is an operation consisting of multiple model realizations where the outcome (i.e., annual dose as a function of time) is computed for each sampled parameter set. The aggregation of all results produces distributions of system performance measures for the modeling case. After all of the required model realizations have been completed, the overall uncertainty in the model outcome can be characterized by probability distributions of the system performance measures.

Correlation Methods—The TSPA-SEIS employs several techniques to account for correlations between uncertain input parameters. In some cases, correlations among variables are addressed in the development of the process models and implicitly accounted for in the TSPA-SEIS abstractions. In other cases, correlations among variables are explicitly addressed within the TSPA-SEIS. The GoldSim software provides functionality for correlating pairs of variables when the correlation between each pair is 100 percent. Because GoldSim's stochastic functions only allow correlation between a single pair, Cholesky factorization (Press et al. 1992 [DIRS 103316], Section 2.9) is used to induce the desired rank correlation in sets of three or more random variables while maintaining their marginal distributions. This method is applied to

normally distributed variables by using a linear combination of independent normal variables to produce a multivariate normal vector with the correct correlation structure (Iman and Conover 1982 [DIRS 124158], pp. 313 to 320; Anderson 1984 [DIRS 169668], Section 2.4). By extending this method to nonnormal distributions, the marginal distributions are used in a way such that the rank correlation structure is preserved in the transform.

INTENTIONALLY LEFT BLANK

Table 6.1.3-1. Examples of Aleatory Uncertainties in the TSPA-SEIS

Scenario Class	Aleatory Uncertainties
Nominal (Section 6.3)	None
Early Failure (Section 6.4)	Number of early failed waste packages
	Type and location of each early failed waste package
	Number of early failed drip shields
	Type of waste package under each early failed drip shield
	Location of each early failed drip shield
Igneous (Section 6.5)	Number of igneous events
	Time of each igneous event
	Number of waste packages affected by eruption
	Eruptive power, height, and duration of each eruption
	Wind speed and wind direction during eruption
Seismic (Section 6.6)	Number of seismic events
	Type of each seismic event: ground motion or fault displacement
	Time of each seismic event
	Peak ground velocity of each ground motion seismic event
	Occurrence and extent of damage to each type of waste package caused by ground motion
	Occurrence and extent of rupture of each type of waste package caused by ground motion
	Volume of rockfall caused by ground motion for lithophysal and non-lithophysal zones
	Occurrence and extent of damage to drip shield framework caused by ground motion
	Occurrence and extent of failure of drip shield framework caused by ground motion
	Number of waste packages of each type affected by fault displacement
	Failed area on each type of waste package caused by fault displacement

Table 6.1.3-2. Examples of Epistemic Uncertainties in the TSPA-SEIS

Model Component	Epistemic Uncertainties
Unsaturated Zone Flow	Infiltration Submodel (Section 6.3.1): • Infiltration scenario • Fracture percolation flux Unsaturated Zone Flow Fields Abstraction (Section 6.3.1): • Hydrologic properties • Ratio of porosity to fracture aperture Drift Seepage Submodel (Section 6.3.3.1): • Permeability and capillary strength parameters • Seepage flow rates Drift Wall Condensation Submodel (Section 6.3.3.2): • Correlation parameters for abstraction for fraction of waste package locations with dripping condensation and condensation water flow rate
EBS Environment	EBS Thermal-Hydrologic Environment (Section 6.3.2): • Thermal conductivity of surrounding rock EBS Chemical Environment Submodel (Section 6.3.4): • Ambient waste composition • pCO_2, ionic strength, and pH of in-drift seepage water • Water-rock interaction for seepage water
Waste Package and Drip Shield Degradation	Waste Package and Drip Shield Degradation Submodel (Section 6.3.5.1): • Corrosion rates of Alloy 22 and drip shield components • Temperature and relative humidity at drip shield and waste package • pH, NO_3^-, and Cl^- of crown seepage
Waste Form Degradation and Mobilization	Waste Form Degradation and Mobilization (Section 6.3.7): • Radionuclide inventory for CSNF, DSNF, and HLW • Temperature and relative humidity at waste package • pCO_2, ionic strength, and pH in waste package
EBS Flow and Transport	EBS Flow Submodel (Section 6.3.6): • Representative subregion typical liquid saturation in invert • Representative subregion typical imbibition flux in invert • Liquid flow through waste package and invert • Invert moisture content • Invert transmissivity EBS Transport Submodel (Section 6.3.8): • Corrosion product-specific surface area • Aqueous and reversibly-sorbed colloid-associated radionuclide mass fluxes and concentrations • Waste form colloid-associated radionuclide mass fluxes and concentrations • Irreversibly-sorbed colloid-associated radionuclide mass fluxes and concentrations
Unsaturated Zone Transport	Unsaturated Zone Transport Submodel (Section 6.3.9): • Aqueous and reversibly-sorbed colloid-associated radionuclide concentrations • Irreversibly-sorbed colloid-associated radionuclide concentrations • Radionuclide mass flux at the water table

Table 6.1.3-2. Examples of Epistemic Uncertainties in the TSPA-SEIS (Continued)

Model Component	Epistemic Uncertainties
Saturated Zone Flow and Transport	Saturated Zone Flow and Transport Submodel (Section 6.3.10): • Groundwater specific discharge multiplier • Flowing interval spacing in volcanic units • Colloid retardation in alluvium
Biosphere	Biosphere Submodel (Section 6.3.11): • Biosphere dose conversion factors for groundwater modeling cases • Inhalation biosphere dose conversion factors for Volcanic Eruption Modeling Case
Events	DS Early Failure Submodel (Section 6.4.1): • Probability of early failure for a single drip shield WP Early Failure Submodel (Section 6.4.2) • Probability of early failure for a single waste package Igneous Intrusion Submodel (Section 6.5.1): • Igneous event probability (event frequency) Volcanic Eruption Submodel (Section 6.5.2): • Igneous event probability (event frequency) Seismic GM Damage Submodel (Section 6.6.1.1): • Residual stress threshold for Alloy 22

NOTE: Additional information concerning uncertainty and the distribution of TSPA-SEIS parameters and parameter values can be found in the GoldSim model file.

INTENTIONALLY LEFT BLANK

6.1.4 TSPA-SEIS Structure and Design

This section provides an overview of how model components and submodels are connected within the TSPA-SEIS and how information flows between them. The primary focus of this section is on the description of the TSPA-SEIS for the Nominal Scenario Class. The Nominal Scenario Class reflects the initial starting conditions expected for the proposed repository system and therefore is a natural starting point for presenting the model structure and design. A summary of the TSPA-SEIS structure and information flow for the Early Failure, Igneous, and Seismic Scenario Classes and the Human Intrusion Scenario is presented following the Nominal Scenario Class description.

For all scenario classes, the separation of aleatory and epistemic uncertainty with respect to parameter values was maintained as described in Section 6.1.3. The structure of the model components and submodel reflect this requirement. Connections between the model components and submodels are presented, as well as inputs differentiated between aleatory and epistemic when applicable.

The TSPA-SEIS components and submodels for the following process areas are briefly discussed here and in more detail in Section 6.3:

- Mountain-Scale UZ Flow
- EBS Thermal-Hydrologic (TH) Environment
- Drift-Scale UZ Flow
- EBS Chemical Environment
- WP and DS Degradation
- EBS Flow
- Waste Form Degradation and Mobilization
- EBS Transport
- UZ Transport
- SZ Flow and Transport
- Biosphere.

This list corresponds to model components and submodels previously presented on Figure 6-1 and in Table 6-1. This list is a combination of model components and submodels that represent the order in which these TSPA-SEIS components are discussed in Section 6.3. The intent here is to list the models in the order that information flows within the TSPA-SEIS. Therefore, it is necessary to list the submodels of the EBS Environment and EBS Flow and Transport Model Components separately. For example, as will be described in the next section, the EBS Flow Submodel provides the Waste Form Degradation and Mobilization Model Component with the flow rate of water through a failed WP as a function of time. This information is used by the Waste Form Degradation and Mobilization Model Component to calculate waste form degradation and radionuclide concentrations in WPs. This information in turn is used as input to the EBS Radionuclide Transport Submodel that calculates radionuclide transport through the WP and EBS. Thus, following the flow of information in Section 6.3 requires an expansion of the eight principal model components (and their respective submodels) compared to what is displayed on Figure 6-1. Table 6-1 maps the outline of Section 6.3 to the eight principal model

components depicted on Figure 6-1. The general philosophy used in this document is that the TSPA-SEIS is composed of eight principal model component areas (UZ, SZ, Biosphere, etc.) that represent a part of the natural system or EBS. Each model component area is composed of one or more submodels. A submodel can be either a detailed process model developed, tested, and validated in a supporting document, a simple or detailed abstraction of the process model, an abstraction of the process model results, or direct process model input (e.g., a look-up table or distribution of values). These process models and/or abstractions are defined within the supporting documents. They are developed for use within the TSPA-SEIS to represent the EBS or a natural system process.

Figure 6.1.4-1 schematically depicts the flow of information between the TSPA-SEIS components and submodels for the Nominal Scenario Class. TSPA-SEIS components implemented outside of the GoldSim model file are shown outside of the dashed border on Figure 6.1.4-1. The abstraction information provided by external models is input to the TSPA-SEIS GoldSim model file. Information transferred via internally generated outputs that are used as downstream inputs between model components and submodels within the TSPA-SEIS GoldSim model file are shown within the dashed border on Figure 6.1.4-1. The primary output from each submodel and abstraction is denoted by a numerical index and described in the following sections.

6.1.4.1 Mountain-Scale Unsaturated Zone Flow

Mountain-scale UZ flow in the TSPA-SEIS refers to the percolation of groundwater through the unsaturated rocks between the land surface and the groundwater table and includes the site-scale UZ flow, infiltration changes, and future climates states. The first process model providing key input to the TSPA-SEIS is the Site-Scale UZ Flow Process Model. This process model simulates three-dimensional, dual-permeability, steady-state flow conditions, and generates 16 three-dimensional flow fields for 10th percentile, 30th percentile, 50th percentile, and 90th percentile infiltration boundary-condition scenarios and four different climate states within each infiltration scenario. As given in *Future Climate Analysis* (BSC 2004 [DIRS 170002], Table 6-1) and appended by governing regulations, four climate states are used in the TSPA-SEIS: (1) present-day climate for the first 550 years after repository closure; 600 years after emplacement, (2) monsoon climate for the period 550 to 1,950 years after repository closure, (3) glacial-transition climate for the period 1,950 to 10,000 years after repository closure, and (4) post-10,000-year climate for the period 10,000 to the modeling time frame of 1,000,000 years after repository closure (Section 1, Governing Regulations).

The 16 flow fields and UZ hydrologic properties generated by the Site-Scale UZ Flow Process Model are used by the Multiscale Thermohydrologic Process Model (MSTHM) (SNL 2007 [DIRS 181383]) for the development of EBS environment TH conditions and are accessed directly by the UZ Transport Submodel (SNL 2007 [DIRS 181006], Sections 6 and 8). In both internal and external applications using the flow fields, the four different infiltration scenarios represent epistemic uncertainty in UZ flow conditions. These scenarios are sampled in the TSPA-SEIS once per realization based on the probability-weighting factors, excluding the contingency area, of 0.6191, 0.1568, 0.1645, and 0.0596 for the 10th percentile, 30th percentile, 50th percentile, and 90th percentile infiltration scenarios, respectively. The weighting factors are derived from *UZ Flow Models and Submodels* (SNL 2007 [DIRS 175177], Table 6.8-1). Climate change is

implemented within the TSPA-SEIS UZ calculations by assuming a series of step changes in boundary conditions for UZ flow and utilizing the flow field corresponding to the selected infiltration scenario and climate state. This implementation is based on the assumption that changes in flow fields due to climate state apply instantaneously in the MSTHM Process Model and UZ Transport Model Component (see assumption in Section 5.1.1).

Figure 6.1.4-1 shows that 16 flow fields and UZ hydrologic properties generated by the Site-Scale UZ Flow Process Model are also used by the MSTHM Process Models. These flow fields are used to specify the percolation flux, consisting of liquid flux in fracture and matrix continua at the base of the PTn above the repository horizon, as a boundary condition. In addition, these data are used within the TSPA-SEIS for the simulation of the transport of radionuclides in the UZ Transport Submodel, as shown on Figure 6.1.4-1. The description for Output #1, discussed below, pertains to arrow #1 on Figure 6.1.4-1.

Output 1—For each infiltration scenario and climate state (Section 6.3.1), the following are outputs from the Site-Scale UZ Flow Process Model (SNL 2007 [DIRS 175177], Section 6.6.3).

The following outputs are passed to the MSTHM Process Models (Section 6.3.2):

- The three-dimensional numerical grid
- The percolation flux at the base of PTn units above each subdomain location for each infiltration condition and climate period
- UZ hydrologic properties.

The following outputs are passed to the UZ Transport Submodel (Section 6.3.9):

- The three-dimensional numerical grid representing the model domain
- UZ hydrologic properties for each of the four infiltration scenarios (Section 6.3.1) including:
  - The active fracture parameter for each computational cell in the numerical grid
  - Three three-dimensional steady-state flow fields including:
    - Fracture continuum liquid flux
    - Matrix continuum liquid flux
    - Water table levels
    - Fracture continuum liquid saturation
    - Matrix continuum liquid saturation
    - Liquid flux between matrix and fracture continua.

6.1.4.2 Engineered Barrier System Thermal-Hydrologic Environment

The EBS TH Environment Submodel implements the MSTHM Abstraction in the TSPA-SEIS. The MSTHM Abstraction is provided by the MSTHM Process Model, as shown on Figure 6.1.4-1. The MSTHM Abstraction is described in detail in *Multiscale Thermohydrologic Model* (SNL 2007 [DIRS 181383], Section 6.2[a] and Appendix III[a]). The following paragraphs describe its application for the development of the EBS TH Abstraction and how this abstraction is used in the TSPA-SEIS.

The MSTHM Process Model subdivides the repository footprint into 3,264 equal-area subdomains. Each of the 3,264 MSTHM Process Model subdomains is equally sized in area, 81 m in width by 20 m in length, where the length component is along the waste emplaced drift axis (SNL 2007 [DIRS 181383], Section 6.2.12.1[a]). For each of the four percolation/thermal conductivity scenarios, the MSTHM Process Model calculates time-dependent TH variables, temperature, and relative humidity, for six representative commercial spent nuclear fuel (CSNF) WPs and two representative CDSP WPs, and DS pairs at each subdomain location. In addition, the MSTHM Process Model calculates time-dependent values for average drift-wall temperature, duration of boiling at the drift wall, invert temperature, invert saturation, and invert liquid flux at each of the 3,264 subdomain locations. Before any information is passed to downstream submodels, two sets of analyses are performed. First, the mean infiltration, glacial-transition values of percolation flux at each of the 3,264 MSTHM Process Model subdomain locations are used to group each of the locations into 1 of 5 repository percolation subregions, based on percolation flux at the base of the PTn. The mean infiltration was selected from among the 10th, 30th, 50th, and 90th percentile fields. The second analysis involves determining a single representative CSNF WP and a single representative CDSP WP for each percolation subregion. Representative WPs are selected for each percolation subregion for the purposes of reducing the computational burden of the TSPA-SEIS calculations and adequately representing the spatial variability in repository conditions that control radionuclide release from the repository. The determination of the repository subregions and the selection of the representative WPs are summarized as follows.

The values of percolation flux for each subdomain location were sorted in ascending order to form a cumulative distribution function (CDF) and then grouped together based on the five percolation subregion quantile ranges of 0.0 to 0.05, 0.05 to 0.3, 0.3 to 0.7, 0.7 to 0.95, and 0.95 to 1.0. The MSTHM Process Model subdomain locations and associated TH information corresponding to the percolation values in each of these quantile groups are designated as belonging to repository percolation subregions 1 through 5, respectively. The five repository percolation subregions are shown on Figure 6.1.4-2. The mean infiltration, glacial-transition climate percolation conditions are used to determine the five subregions. The same selected subregions are used for all infiltration conditions and climate states. The grouping of the repository percolation subregions and the number of subdomain locations in each percolation subregion are summarized in Table 6.1.4-1. The MSTHM Abstraction produces two sets of outputs that are indexed by fuel type and percolation subregion. One set contains the comprehensive MSTHM Process Model output (e.g., DS and WP temperature and relative humidity, drift-wall temperature, percolation flux, and fraction of lithophysal unit) for each of eight possible WP/DS combinations at each subdomain location in each percolation subregion for each fuel type. The TH responses (DS and WP temperature and relative humidity, drift-wall

temperature, percolation flux, and fraction of lithophysal unit) are recorded at each subdomain location for six CSNF WPs and two CDSP WPs. The WP and DS Degradation Model Component and the Drift Seepage Submodel use this information. The other set contains the DS and WP temperature and relative humidity; the drift-wall temperature; and the invert temperature, relative humidity, liquid flux, and saturation only for the representative CSNF WP and CDSP WP in each percolation subregion. The data in these two sets are compiled in text files that give parameter values at discrete timesteps. The data in the text files are read into look-up tables at run time to provide time-dependent parameter values to other submodels. The representative CSNF WPs and CDSP WPs in each percolation subregion are selected by compiling the peak WP temperature and duration of boiling at the drift wall for each WP type and percolation subregion. These two values, peak WP temperature and duration of boiling at the drift wall, are sorted from low to high, and a percentile is calculated for each WP type and location. For each WP type and location, the representative WP is the one that is closest to the median for the two parameters of peak WP temperature and drift-wall boiling duration.

After the process described above is completed, temperature and relative humidity for each representative WP and associated DS, average drift-wall temperature, average invert temperature, average invert saturation, and average invert flux are stored in a file set that is directly accessible by the TSPA-SEIS. The data in this file set are accessed by the EBS TH Environment Submodel to provide representative TH responses for each subregion. These TH responses serve as input to the Drift Wall Condensation Submodel, the EBS Chemical Environment Submodel, the EBS Flow Submodel, the Waste Form Degradation and Mobilization Model Component, and the EBS Transport Submodel. For ease of presentation, the WP and DS Degradation Model Component and the Waste Form Degradation and Mobilization Model Component are shown on Figure 6.1.4-1 rather than the individual submodels that comprise these model components (Sections 6.3.5 and 6.3.7, respectively).

Output 2—The following outputs are passed from the MSTHM Process Model through the MSTHM Abstraction to the EBS TH Environment Submodel (Section 6.3.2):

- Definition of the five repository percolation subregions
- Percolation flux at the base of the PTn
- In-drift TH environment (e.g., DS and WP temperature and relative humidity, drift-wall temperature for each fuel type, CSNF, and CDSP WP).

Output 3—The following outputs are passed from the EBS TH Environment Submodel (Section 6.3.2) to the Drift Seepage and Drift Wall Condensation Submodel (Section 6.3.3):

- For each of the five percolation subregions (Section 6.3.2):
  - The percolation flux at the base of the PTn for each infiltration scenario and climate state at each subdomain location (Drift Seepage Submodel)
  - The average percolation flux at the base of the PTn for each infiltration scenario and climate state (Drift Wall Condensation Submodel)

- The drift-wall temperature surrounding each of the eight WPs (two CDSP WPs and six CSNF WPs) at each subdomain location in each percolation subregion (Drift Seepage Submodel)

- Time-dependent temperature for the drift wall for the representative CDSP WP and the representative CSNF WP (Drift Wall Condensation Submodel)

- The fraction of lithophysal unit at each location.

Output 4—The following outputs are passed from the EBS TH Environment Submodel (Section 6.3.2) to the WP and DS Degradation Model Components (Section 6.3.5), which then calculates WP and DS failures, including LC WP failures:

- For each of the five percolation subregions:

  - Time-dependent WP surface temperature on each of the eight WPs (two CDSP WPs and six CSNF WPs) at each subdomain location in each percolation subregion

  - Time-dependent WP surface relative humidity on each of the eight WPs (two CDSP WPs and six CSNF WPs) at each subdomain location in each percolation subregion.

Output 5—The following outputs are passed from the EBS TH Environment Submodel (Section 6.3.2) to the EBS Chemical Environment Submodel (Section 6.3.4):

- For each of the five percolation subregions (Section 6.3.2):

  - Time-dependent temperature for the invert for the representative CDSP WP and the representative CSNF WP

  - Time-dependent relative humidity for the invert for the representative CDSP WP and the representative CSNF WP

  - Time-dependent temperature for the drift wall for the representative CDSP WP and the representative CSNF WP

  - Averaged glacial-transition percolation rate for each infiltration scenario for each percolation subregion.

- For the LC Initiation Analysis (Section 6.3.4.3.2):

  - Time-dependent WP surface temperature on each of the eight WPs (two CDSP WPs and six CSNF WPs) at each subdomain location in each percolation subregion

  - Time-dependent WP surface relative humidity on each of the eight WPs (two CDSP WPs and six CSNF WPs) at each subdomain location in each percolation subregion.

Output 6—The following outputs are passed from the EBS TH Environment Submodel (Section 6.3.2) to the EBS Flow Submodel (Section 6.3.6):

- For each of the five percolation subregions (Section 6.3.2):
  - Time-dependent WP surface temperature for the representative CDSP WP and the representative CSNF WP
  - Time-dependent temperature in the invert for the representative CDSP WP and the representative CSNF WP
  - Time-dependent liquid flux for the representative CDSP WP and the representative CSNF WP.

Output 7—The following outputs are passed from the EBS TH Environment Submodel (Section 6.3.2) to the Waste Form Degradation and Mobilization Model Component (Section 6.3.7):

- For each of the five percolation subregions (Section 6.3.2):
  - Time-dependent WP surface temperature for the representative CDSP WP and the representative CSNF WP
  - Time-dependent WP surface relative humidity for the representative CDSP WP and the representative CSNF WP.

Output 8—The following outputs are passed from the EBS TH Environment Submodel (Section 6.3.2) to the EBS Transport Submodel (Section 6.3.8):

- For each of the five percolation subregions (see Section 6.3.2):
  - Time-dependent WP surface temperature for the representative CDSP WP and the representative CSNF WP
  - Time-dependent WP surface relative humidity for the representative CDSP WP and the representative CSNF WP
  - Time-dependent temperature in the invert for the representative CDSP WP and the representative CSNF WP
  - Time-dependent saturation in the invert for the representative CDSP WP and the representative CSNF WP.

The TH conditions for each representative WP are identical for dripping and non-dripping environments.

6.1.4.3 Drift-Scale Unsaturated Zone Flow

This section describes the implementation of the Drift Seepage and Drift Wall Condensation Submodels. The simulated drift-seepage flux is calculated within the TSPA-SEIS for both ambient and waste-heat-generated thermal periods over a heterogeneous fracture-permeability field for a range of representative percolation flux rates, and for ranges of fracture permeability log(k) and fracture capillary-strength parameter ($1/\alpha$) values (SNL 2007 [DIRS 181244]). The drift-seepage analysis performed external to the TSPA-SEIS provides two response surfaces: (1) mean seepage flux into the drift as a function of long-term percolation flux, k, and $1/\alpha$, and (2) the standard deviation (SD) of seepage flux into the drift as a function of long-term percolation flux, log(k), and $1/\alpha$. Figure 6.1.4-1 shows that drift-scale seepage is modeled externally in the Drift Seepage Submodel (BSC 2004 [DIRS 167652]). For the TSPA-SEIS, the results are then abstracted as described in *Abstraction of Drift Seepage* (SNL 2007 [DIRS 181244]), and imported into the TSPA-SEIS before performing the PA simulations.

Abstraction of Drift Seepage (SNL 2007 [DIRS 181244], Section 6.7.1.1) also provides spatial variability distributions for both k and $1/\alpha$ and the flow focusing factor (f_{ff}) for the percolation flux, as well as uncertainty (epistemic) distributions for $\Delta\log(k)$ and $\Delta 1/\alpha$. The TSPA-SEIS samples these uncertainty distributions once per realization to determine the seepage uncertainty factors $\Delta\log(k)$ and $\Delta 1/\alpha$. The following steps are completed at each of the 3,264 MSTHM Process Model's subdomain locations for each of the six representative CSNF WPs and two representative CDSP WPs. The spatial variability distributions are evaluated for log(k), $1/\alpha$, and f_{ff} at each location. The log(k) and $1/\alpha$ values are adjusted by adding to them the uncertainty factors, $\Delta\log(k)$ and $\Delta 1/\alpha$, sampled from the uncertainty distributions for each realization. The percolation flux at the base of the PTn at each location is provided by the MSTHM Abstraction to the EBS TH Environment Submodel. These percolation flux values are then multiplied by the f_{ff} to yield values of the adjusted percolation flux. The adjusted log(k) and $1/\alpha$ values, along with the adjusted percolation flux at each location, are used to evaluate the response functions for ambient mean seepage and the SD of ambient seepage. These two quantities are used to form a uniform distribution for ambient seepage that ranges between mean seepage -1.7321 SD and mean seepage + 1.7321 SD (SNL 2007 [DIRS 181244], Section 6.5.1.3). This distribution is sampled to yield the ambient seepage for each WP at each location.

The thermal seepage condition at each WP location (e.g., no seepage when the drift-wall temperature is greater than 96°C, otherwise ambient seepage) is then used to appropriately modify the calculated ambient seepage. This process is completed for each of the 3,264 MSTHM Process Model's subdomain locations. This results in a calculated drift-seepage flux for every WP at every subdomain location for the given infiltration scenario and climate state. An average seepage flow rate is calculated for the WPs that have seepage, along with the fraction of WPs that have seepage, for each percolation subregion. The details of the seepage submodel calculations for TSPA-SEIS are discussed in Section 6.3.3.1, and seepage impacts on EBS flow are calculated in Section 6.3.6.

Process modeling has shown that there is a potential for water vapor in the drift atmosphere to condense on cooler portions of the drift walls. Condensation on drift walls and its effects on EBS flow are modeled in the TSPA-SEIS (Sections 6.3.3.2 and 6.3.6). The rate of condensation at a location on the drift wall depends on the availability of water at that location. The rate at

which water is available generally increases with an increase in percolation flux, increasing water transport through the invert, and decreasing axial dispersion within the drifts (SNL 2007 [DIRS 181648], Section 8.3.1.1). The TSPA-SEIS's Drift Wall Condensation Submodel calculates the fraction of DS/WP pairs dripped on by drift-wall condensate and the average rate of condensation in each percolation subregion for each WP type. These quantities are determined from two correlations: (1) a correlation for average condensation rate versus average percolation flux, and (2) a correlation for the fraction of DS and WP pairs dripped on by drift-wall condensate versus average percolation flux. The average percolation flux for each repository percolation subregion is calculated by averaging the percolation fluxes at the base of the PTn at each subdomain location in that subregion using the comprehensive MSTHM Abstraction data (Section 6.3.2). The impact of DS ventilation and axial dispersion uncertainty on condensation are accounted for by selecting between four cases with an equal probability: (1) ventilated DS-low axial dispersion, (2) ventilated DS-high axial dispersion, (3) unventilated DS-low axial dispersion, and (4) unventilated DS-high axial dispersion. For each TSPA-SEIS realization, the drift-wall condensation case is sampled as an epistemic uncertainty, and the average rate of condensation and fraction of DS/WP pairs dripped on by drift-wall condensate at simulation time, t, is calculated for each percolation subregion and WP type. The average rate of condensation dripping from drift walls is combined with drift seepage to increase the dripping flow rate through the EBS.

Three stages are defined for drift-wall condensation. Stage 1 occurs when the temperature of all of the packages in a percolation subregion are above boiling and no condensation occurs. Stage 2 begins when the temperature of the first WP in the percolation subregion drops below boiling. During Stage 2 all CDSP WPs have condensation, but the CSNF WPs, which are hotter, have no condensation. Stage 3 begins when the temperature of the last WP in a percolation subregion drops below boiling. During Stage 3, up until 2,000 years after closure, the regressions for rate and fraction are used to calculate the drift-wall condensation.

Output 9—The following outputs are passed from the Drift Seepage (Section 6.3.3.1) and the Drift Wall Condensation Submodels (Section 6.3.3.2) to the EBS Flow Submodel (Section 6.3.6):

- For each percolation subregion:
  - Time-dependent drift-seepage rate for the DS-representative CDSP WP pairs and DS-CSNF WP pairs
  - The fraction of DS-CDSP WP pairs and DS-CSNF WP pairs in dripping (seepage) environments
  - The average time-dependent condensation rate for the DS-representative CDSP WP pairs and DS-representative CSNF WP pairs
  - The fraction of DS-CDSP WP pairs and DS-CSNF WP pairs in dripping (condensate) environments.

6.1.4.4 Engineered Barrier System Chemical Environment

The time-dependent evolution of the chemical-environment variables, pH and ionic strength, in the invert is determined by the time-dependent composition of water and gas entering the emplacement drift and how these water and gas compositions evolve as the water evaporates under the prevailing TH conditions within the invert. Time histories of seepage water and gas compositions are provided by the EBS P&CE Abstraction (SNL 2007 [DIRS 177412]). Drift-Scale THC Process Model (SNL 2007 [DIRS 177404]) time histories for a single representative location in the repository are applied to all representative WPs and emplacement drifts. Uncertainty (epistemic) and variability in compositions are represented by four different water types. Each water type has an associated time-dependent partial pressure of carbon dioxide (Pco_2). In each realization, one of the four water types is randomly sampled, and this water type is implemented for each representative WP and early-failed WP in each repository percolation subregion. The evolution of the chemistry of the incoming seepage in the invert in terms of pH and ionic strength is modeled within the TSPA-SEIS using response surfaces in the form of look-up tables for these two variables as a function of percolation rate, the amount of water-rock interaction, temperature, relative humidity, and Pco_2. These response surfaces are provided by the EBS P&CE Abstraction (SNL 2007 [DIRS 177412], Section 6.9.2) and are based on calculations that simulate the evaporation/condensation evolution of each of the four seepage water types and gas compositions for a range of representative EBS TH conditions.

The first step in determining values of pH, ionic strength, chloride concentration, and nitrate concentration is determining the in-drift Pco_2. The Pco_2 is a function of the temperature and the water-rock interaction and starting water. Once the Pco_2 is determined, the chemical compositions are found in the look-up tables as a function of water-rock interaction, Pco_2, temperature, and relative humidity. In each realization, one of the four water types is randomly sampled, and this water type is implemented for each representative WP in each repository percolation subregion. Consider a CDSP WP in a non-dripping environment in a repository percolation subregion. For each realization, the TSPA-SEIS determines the pH and ionic strength in the invert for that WP at any point in time during the postclosure period as follows. First, the average invert temperature and average invert relative humidity (both quantities are volume-averaged over the invert) at time, t, are determined from the time histories of temperature and relative humidity that correspond to that representative WP. The appropriate Pco_2 at time, t, is calculated as a function of the water-rock interaction and temperature in the drift. To determine pH and ionic strength in the invert at time, t, the set of chemical composition look-up tables corresponding to the starting water and water-rock interaction are accessed, and the values of temperature, relative humidity, and Pco_2 are used to interpolate between tabulated values to determine the corresponding pH and ionic strength. The pH and ionic strength are adjusted for epistemic uncertainty and variability by sampling uncertainty distributions for each parameter once per realization. This procedure is performed for each percolation subregion.

The EBS Chemical Environment Submodel also provides look-up tables and implementation instructions to determine abstracted values of time-dependent parameters, chloride and nitrate concentrations, and chloride-to-nitrate ratios. These abstracted variables are used to assess the potential for LC on the WP outer surface. However, this application of the EBS Chemical Environment Submodel is implemented in the ancillary LC Initiation Analysis for the TSPA-SEIS, as summarized in the next section and described in detail in Section 6.3.5.2.3.

Output 10—The following outputs are passed from the EBS Chemical Environment Submodel (Section 6.3.4) to the Waste Form Degradation and Mobilization Model Component (Section 6.3.7):

- Outputs from this model component are provided for each percolation subregion and each representative WP, in dripping and non-dripping environments:
  - The time-dependent pH in the invert
  - The time-dependent ionic strength in the invert
  - The time-dependent Pco_2 in the drift.

6.1.4.5 Waste Package and Drip Shield Degradation

Time-dependent WP and DS degradation are implemented within the TSPA-SEIS. For the Nominal Scenario Class, GC is the only degradation mode modeled for DS degradation. GC rates for the inner and outer surfaces of the DSs are represented by two independent CDFs of the GC rate because the environments above and below the DSs are not expected to be similar (SNL 2007 [DIRS 180778], Section 6.5.2, 8.1[a]). These distributions represent epistemic uncertainty in DS GC rates. For each realization, a single GC rate is sampled from each distribution of the GC rate and applied to all DSs. In the Nominal Scenario Class, the DSs are failed as a barrier to flow when the corroded thickness equals or exceeds the initial thickness of the DS plates.

The TSPA-SEIS for the Nominal Scenario Class includes four WP degradation modes: GC, MIC, and SCC, which are modeled using the Waste Package Degradation Model, and LC (SNL 2007 [DIRS 178519], Section 6.4.4).

The Nominal Scenario Class is represented by a single modeling case. This modeling case considers those WPs that fail as a result of corrosion processes (e.g., GC, SCC, and/or LC). The TSPA-SEIS implementation of the WP degradation modes for the Nominal Scenario Class Modeling Case is described as follows.

Nominal Scenario Class Modeling Case: WPs that Degrade by Corrosion—GC rates of the WP outer surface are temperature-dependent and include epistemic uncertainty and variability. The temperature dependence is treated as an epistemic uncertainty and is represented by a CDF that is sampled once per realization. The variation in GC rates under an ambient temperature of 333.15 K is considered to be entirely due to spatial variability (SNL 2007 [DIRS 178519], Section 6.4.3) and is represented by a CDF. This CDF is sampled for every patch on every WP simulated in a percolation subregion. The uncertain temperature dependence for the realization, and each GC rate on a patch, are used to calculate the temperature-dependent GC rate (as a function of time) for every patch on every selected WP in a percolation subregion.

MIC is represented by an enhancement factor applied to the GC rate of the WP outer surface (i.e., GC rate × enhancement factor). The MIC factor is applied to the GC rate when the relative humidity at the WP outer surface is greater than or equal to 90 percent. The MIC factor is uniformly distributed between the values 1 and 2, and this distribution is sampled once per realization and applied to all WPs (SNL 2007 [DIRS 178519], Section 6.4.5).

Another potential failure mode considered for WPs is SCC in the closure lid. Flaws in the closure-lid welds are likely sites for SCC. Two characteristics of weld flaws are treated as epistemic uncertainties: flaw-size distribution and flaw-count distribution. These flaw characteristics are both represented by Gamma distributions, and each is sampled once per realization with the same values used for each lid weld. SCC is determined by stress and stress intensity factor profiles in the closure-lid weld regions, and subsequent crack growth from the flaw sites. The uncertainty in stress and stress intensity profiles is represented by a scaling factor that is sampled independently, once for each realization, from a truncated normal distribution (SNL 2007 [DIRS 181953], Section 6.5.6.2). The uncertainty in crack growth rate is a function of the repassivation slope, n, which is represented by a truncated normal distribution and sampled once per realization.

The results for GC, MIC, and SCC are compiled by the WAPDEG DLL to produce: (1) profiles of the fraction of WPs failed and as a function of time, (2) the number of patch failures per failed WP as a function of time, and (3) the average number of crack penetrations per failed WP as a function of time (Section 6.3.5).

In the TSPA-SEIS Nominal Modeling Case, 10 WAPDEG DLL simulations are run per realization, one for each representative WP type (CSNF and CDSP) in each of the five repository percolation subregions. This process can be described as follows. The EBS TH Environment Submodel provides temperature and relative humidity histories for eight WP and DS pairs (six CSNF WPs and two CDSP WPs) at each of the 3,264 subdomain locations. The process begins by randomly sampling a maximum of 500 DS/WP pairs from all of the pairs for a given fuel type in a percolation subregion. If the percolation subregion contains fewer than 500 DS/WP pairs, then all pairs in the percolation subregion are used. The WAPDEG DLL is part of the TSPA-SEIS, and is run at the start of each EBS calculation. The WAPDEG DLL reads in the temperature and relative humidity histories for each selected DS and WP pair and calculates time-dependent degradation for each pair. This information is used by the WAPDEG DLL to calculate the following output: (1) the cumulative number of WP failures as a function of time, (2) the average number of patches per failed WP as a function of time, and (3) the average number of cracks per failed WP as a function of time.

LC on WPs may occur when a WP is contacted by deleterious brine (SNL 2007 [DIRS 178519], Section 8.1, Figure 8-1). Two mechanisms may cause deleterious brine formation on the WP: seepage from dripping at the emplacement drift crown and dust deliquescence. In the TSPA-SEIS, only crown seepage water chemistry has the potential to fail WPs due to LC (SNL 2007 [DIRS 181267], Section 7.1.5). Only WPs that have DS plate failures coincident with deleterious brine contacting the WP are susceptible to LC failures. LC of the WP is a process that is included in the Nominal Scenario Class.

Output 11—The following outputs are passed from the WP and DS Degradation Model Component (Section 6.3.5) to the EBS Flow Submodel (Section 6.3.6) for the Nominal Modeling Case:

- For each percolation subregion and each WP type (CDSP WPs and CSNF WPs):
  - The time-dependent average number of patch penetrations per failed DS

- The time-dependent average number of patch penetrations per failed WP.

Output 12—The following outputs are passed from the WP and DS Degradation Model Component (Section 6.3.5) to the Waste Form Degradation and Mobilization Model Component (Section 6.3.7):

Nominal Modeling Case:

- For each percolation subregion and each fuel type (CSNF WPs):
  - The time-dependent fraction of WPs failed.

Output 13—The following outputs are passed from the WP and DS Degradation Model Component (Sections 6.3.5.1.1 and 6.3.5.1.3) to the EBS Transport Submodel (Section 6.3.8) for the Nominal Modeling Case:

- For each percolation subregion and each fuel type (CDSP WPs and CSNF WPs):
  - The time-dependent fraction of WPs failed
  - The time-dependent average number of crack penetrations per failed WP
  - The time-dependent average number of patch penetrations per failed WP.

6.1.4.6 Engineered Barrier System Flow

The following discusses the implementation of the EBS Flow Submodel (SNL 2007 [DIRS 177407], Section 6). The EBS Flow Submodel is implemented within the TSPA-SEIS and determines the volumetric flow rate of seepage water (including seepage into the drifts and drift-wall condensation) at different locations as seepage water moves through breached DSs, breached WPs, and the invert. In addition, the EBS Flow Submodel determines the fraction of WPs that are dripped upon, either by drift seepage and/or drift-wall condensation. For each percolation subregion, the TSPA-SEIS includes two dripping environments: (1) the seeping environment, which includes dripping above the WP from drift seepage and may also include drift-wall condensation; and (2) the non-seeping environment, which includes the WPs that are not exposed to drift seepage, but may or may not be exposed to drift-wall condensation. Inputs to the EBS Flow Submodel include the drift-seepage rate and the drift-wall condensation rate and the fraction of WPs exposed to drift-seepage and the drift-wall condensation. Both rates are combined to yield a total dripping rate. The flow rate of water through each breached DS or WP is proportional to the total dripping rate and the average number of patch penetrations on each DS or WP. EBS flow is calculated for WPs of each type located in seeping and non-seeping environments. Flow in the seeping environments combines drift seepage and drift-wall condensation above and below the WP and includes the imbibition flux in the invert. Flow in the non-seeping environments includes drift wall condensation above and below the WP and includes the imbibition flux in the invert. Inputs to the EBS Flow Submodel for each WP type and repository percolation subregion include:

- The average total dripping rates due to seepage and drift-wall condensation

- The fraction of WPs dripped upon due to seepage and drift-wall condensation drift-wall condensation
- The average number of patch penetrations per failed CSNF DS and CDSP DS
- The average number of patch penetrations per failed CSNF WP and CDSP WP.

The EBS Flow Submodel does not use the average number of crack penetrations per failed WP because stress corrosion cracks are too small to allow advective water flow through these cracks.

The EBS Flow Submodel introduces two uncertain (epistemic) flux-splitting parameters to characterize the fraction of flow that enters breaches on DSs and on the WPs. These two parameters are sampled once per realization and are applied to all representative DS and WP pairs located in the dripping environments. Outputs from the EBS Flow Submodel are used by: (1) the Waste Form Degradation and Mobilization Model Component, which uses the flow rate through a failed WP to calculate pH and ionic strength in the WP; and (2) the EBS Transport Submodel, which uses the flow rate through a failed WP and volumetric flow rate through the invert to calculate advective transport of radionuclides through a failed WP and through the invert to the host rock.

Output 14—The following output is passed from the EBS Flow Submodel (Section 6.3.6) to the Waste Form Degradation and Mobilization Model Component (Section 6.3.7):

- For each representative WP group, as applicable, in a seeping and non-seeping environment, in each percolation subregion:
  - The volumetric flow rate of water through the WP as a function of time.

Output 15—The following outputs are passed from the EBS Flow Submodel (Section 6.3.6) to the EBS Transport Submodel (Section 6.3.8):

- These outputs are provided for each representative WP in a seeping and non-seeping environment, in each percolation subregion:
  - The flux through the invert pore space as a function of time
  - The flow rate of water through the WP as a function of time
  - The fraction of WPs in a seeping environment
  - The fraction of WPs in a non-seeping environment.

6.1.4.7 Waste Form Degradation and Mobilization

The Waste Form Degradation and Mobilization Model Component, shown on Figure 6.1.4-1, includes submodels for radionuclide inventory, in-package chemistry, cladding failure, waste form degradation, dissolved concentration limits of radioactive elements, and EBS colloids. In-package chemistry is modeled within the TSPA-SEIS using simplified expressions to define

the bulk chemistry consisting of pH, ionic strength, and total carbonate concentration (ΣCO_3) as a function of time inside a WP. Chemistry outputs are used to set conditions for waste form degradation, colloid stability, and to determine dissolved concentration limits inside the WPs. Within the TSPA-SEIS, no performance credit is taken for zircaloy or stainless steel cladding as a mechanism to prevent radionuclide release or inhibit CSNF waste form degradation (SNL 2007 [DIRS 180616], Section 6.2[a]). Waste form degradation is modeled within the TSPA-SEIS using empirical degradation rate formulas developed for the three different waste form types: CSNF, DOE spent nuclear fuel (DSNF), and HLW. DSNF and HLW glass are combined and disposed in CDSP WPs. Dissolved concentration limits of radionuclides (i.e., solubility limits for radioactive elements in the TSPA-SEIS) are modeled using look-up tables, distributions, or single values. The formation, stability, and concentration of radionuclide-bearing colloids in the WP and EBS, as well as reversible and irreversible sorption of dissolved radionuclides, are modeled using empirical relationships and uncertainty distributions for sorption coefficients.

The three waste form categories (CSNF, DSNF, and HLW glass) are contained and disposed in two types of WPs: CSNF WPs and CDSP WPs. The CDSP WPs will contain both DSNF and HLW glass. The inclusion of mixed oxide SNF and lanthanide borosilicate (LaBS) glass HLW in the TSPA-SEIS is accomplished by adding radionuclide-specific inventories to the GoldSim source term (SNL 2007 [DIRS 180472]). More specifically, the LaBS glass inventory amounts are added to the HLW portion of the initial radionuclide inventory and the mixed oxide SNF is added to the CSNF portion of the initial radionuclide inventory. WPs containing naval SNF WPs are conservatively represented as CSNF WPs containing CSNF inventory (see discussion in Section 6.3.7.1). Each percolation subregion environment represents a group of WPs in that subregion of the same type and in the same environment. The total radionuclide inventory (Section 6.3.7.1) available for degradation and transport is calculated for each percolation subregion by taking into account the number and type of failed WPs. These representative WP groups include:

Nominal Modeling Case:

- CDSP WP in a non-seeping environment
- CDSP WP in a seeping environment that will not have LC damage
- CDSP WP in a seeping environment that will have LC damage
- CSNF WP in a non-seeping environment (includes both CSNF-Zircaloy [CSNF-Z] and CSNF-stainless steel [CSNF-SS] WPs)
- CSNF WP in a seeping environment (includes both CSNF-Z and CSNF-SS WPs) that will not have LC damage
- CSNF WP in a seeping environment that will have LC damage.

The In-Package Chemistry Submodel is implemented using response surfaces and parameter distributions for four different abstraction conditions: CSNF and CDSP WPs that are dripped on,

and CSNF and CDSP WPs that are not dripped on. Due to the contribution of drift-wall condensation, a WP can be dripped on if it is in a seeping or non-seeping environment, but only if its DS has failed. The In-Package Chemistry Submodel is implemented by sampling seepage rate-dependent uncertainty distributions and Pco_2-dependent response surfaces for pH. Ionic strength is determined by sampling uncertainty distributions whose range is a function of the relative humidity within the breached WP for non-dripping conditions and by sampling uncertainty distributions whose range is a function of the seepage rate through a breached WP for dripping conditions. The sampled values of pH and ionic strength represent epistemic uncertainty and are sampled once per realization. The $\sum CO_3$ for each abstraction condition is calculated using a temperature, Pco_2, and pH-dependent equation. This calculated value includes no additional uncertainty. Inputs to the In-Package Chemistry Submodel include volumetric flow rates of seepage into a failed WP as provided by the EBS Flow Submodel, the Pco_2 provided by the EBS Chemical Environment Submodel, and the temperature and relative humidity provided by the EBS TH Environment Submodel.

Outputs from the In-Package Chemistry Submodel are provided for each representative WP and each representative early-failed WP, if available, in dripping and non-dripping environments in each percolation subregion and consist of:

- The pH as a function of time
- The ionic strength as a function of time
- The $\sum CO_3$ as a function of time.

These outputs are used internally in the TSPA-SEIS by the Waste Form Degradation and Mobilization Model Component as inputs to the rate equations for the Waste Form Degradation Submodels, the dissolved concentration limits look-up tables, and EBS colloids stability criteria.

Most of the CSNF is encased in zirconium-alloy cladding, with only 1 percent of CSNF encased in stainless-steel cladding. Both zirconium-alloy cladding and stainless-steel cladding are modeled as being perforated upon emplacement of the WPs in the repository. Perforated rods are modeled as instantly split down the rod length after the WP has failed (SNL 2007 [DIRS 180616], Section 6.2.4[a]).

The following outputs from the Cladding Degradation Submodel are provided for each representative CSNF WP and each early-failed representative CSNF WP group in seeping and non-seeping environments in each percolation subregion:

- The fraction of failed cladding at WP emplacement.

These outputs are used internally in the Waste Form Degradation and Mobilization Model Components to calculate the fraction of CSNF exposed and available for degradation. Waste form degradation is modeled within the TSPA-SEIS using empirical formulas for the degradation rate developed for the three different waste form types: CSNF, DSNF, and HLW.

CSNF is isolated from repository environmental conditions until the WP and CSNF cladding are breached. After the WP and CSNF cladding are breached, the CSNF may be exposed to humid air or dripping water. Upon exposure to moisture, radionuclides can be released by two

mechanisms: (1) instantaneous release of the gap fraction and grain boundary inventory, and (2) matrix dissolution under alkaline or acidic conditions (BSC 2004 [DIRS 169987], Section 6). Four radionuclides are in the instantaneous release inventory: cesium, iodine, technetium, and strontium (BSC 2004 [DIRS 169987], Section 6.3). The fraction of the inventory emplaced in the repository that makes up the initial release inventory for each of these four radionuclides is determined by sampling four triangular distributions representing epistemic uncertainty. These distributions are sampled once per realization. Matrix dissolution is modeled using two rate formulas, one for pH < 6.8 and one for pH ≥ 6.8 (BSC 2004 [DIRS 169987], Section 8.1). Both CSNF degradation rate formulas are a function of specific surface area of exposed fuel, temperature, $\sum CO_3$, Po_2, and in-package pH. A triangular distribution is used to represent epistemic uncertainty in a specific surface area of exposed fuel. This distribution is sampled once per realization. The CSNF degradation rate is calculated using input provided by two submodels: the EBS TH Environment Submodel provides the time-dependent temperature of the CSNF, and the In-Package Chemistry Submodel provides time-dependent pH and total carbonate concentration inside the failed WP. The EBS Transport Submodel calculates the mass and saturated volume for the degraded CSNF rind and a rind thickness. These parameters are used to determine radionuclide concentrations in the fuel rind and to model transport from the CSNF rind into the WP.

The DSNF is modeled as being immediately available for dissolution and mobilization after a WP containing DSNF is breached. Because of this simplification, no rate equation or rate parameters are necessary to implement the DSNF Waste Form Degradation Abstraction for DSNF in the TSPA-SEIS (BSC 2004 [DIRS 172453], Sections 6.2 and 8.1). Each time a CDSP WP fails, the DSNF inventory associated with the failed WP, after accounting for decay and ingrowth, is made immediately available for transport (subject to solubility constraints) in the volume of water associated with the degraded DSNF and WP corrosion products (see Section 6.3.8.2). Once released, radionuclides are available for transport through the WPs to the EBS.

Degradation of HLW glass is initiated if the WP is breached and the relative humidity is greater than or equal to 44 percent (BSC 2004 [DIRS 169988], Section 8.1). The rate of degradation is determined by a rate expression that applies to the amount of glass exposed to humid air or dripping water. The coefficients in the rate equation are dependent on whether or not acidic or alkaline conditions prevail. The rate equation is a function of an effective rate constant, temperature, pH, and the surface area of the HLW glass. The effective rate constant is treated as an epistemic uncertainty, and is represented by two triangular distributions, one for each pH condition (pH < 6.8 and pH ≥ 6.8). These distributions are sampled once per realization. Two values of the HLW glass degradation rate are calculated for any timestep in the realization, and the greater of the two calculated rates is used as the degradation rate (BSC 2004 [DIRS 169988], Section 8.1). The surface area of the glass is calculated as the product of the specific surface area of the glass and the glass exposure factor. The exposure factor is treated as an epistemic uncertainty represented by a triangular distribution. This distribution is sampled once per realization, and the same exposure factor is used for alkaline and acidic conditions (BSC 2004 [DIRS 169988], Section 8.1). The EBS Transport Submodel calculates the mass and saturated volume for the degraded HLW rind and a rind thickness. These parameters are used to determine radionuclide concentrations in the HLW rind and to model transport from the rind into the WP.

Outputs from the Waste Form Degradation Submodel for HLW glass, CSNF, and DSNF degradation are provided for each representative WP and each representative early-failed WP, as applicable in seeping and non-seeping environments, and in each percolation subregion, as follows:

- The degradation rate of HLW glass
- The degradation rate of CSNF fuel
- The instantaneous degradation of DSNF fuel.

These outputs are used internally in the Waste Form Degradation and Mobilization Model Components to determine the concentration of radionuclides in water in the associated degraded fuel rind. The Dissolved Concentration Limits Submodel determines radionuclide concentration limits. The Dissolved Concentration Limits Submodel is used to calculate the solubility of certain radionuclides in the WP and in the invert that are potentially important to dose. The Dissolved Concentration Limits Submodel is implemented in the TSPA-SEIS in the form of: (l) look-up tables for plutonium, neptunium, uranium, thorium, americium, and protactinium, plus one or more epistemic uncertainty terms; (2) constant values over two pH intervals (from 3.0 to 7.75 and 7.75 to 9.75) for radium, with an undefined value for pH values greater than 9.75; or (3) undefined values for technetium, carbon, iodine, cesium, and strontium (SNL 2007 [DIRS 177418], Sections 6 and 8.1). The look-up tables provide radioelement solubility as a function of pH and CO_2 fugacity (fCO_2). Solubilities are evaluated as a function of time to account for the evolution of pH and fCO_2 during the postclosure period. One or more epistemic uncertainty terms are evaluated by sampling their respective distributions once per realization and are added to each tabulated solubility value. These uncertainty terms represent uncertainty in the solubility constants of phases that control the solubility of plutonium, neptunium, uranium, thorium, and americium; uncertainty of the fluoride concentration in water that controls the solubilities of neptunium, uranium, thorium, americium, and protactinium; and uncertainty in the chemical analogy in the case of protactinium. The In-Package Chemistry Submodel and the EBS Chemical Environment Submodel provide the pH, ionic strength, and fCO_2 inputs to the Dissolved Concentration Limits Submodel when the Dissolved Concentration Limits Submodel is implemented in the WPs and in the invert, respectively.

Outputs from the Dissolved Concentration Limits Submodel are provided for each representative WP, as applicable in seeping and non-seeping environments, and for each percolation subregion, as follows:

- The time-dependent solubilities for plutonium, neptunium, uranium, thorium, americium, and protactinium

- The time-dependent value of radium solubility, which can be one of two values depending on pH.

These outputs are used by the EBS Transport Submodel to calculate radionuclide concentration limits that are in the volumes of water associated with the CSNF rind, in the DSNF rind, in the HLW glass rind, in the in-package corrosion products, and in the invert.

The TSPA-SEIS EBS Colloids Submodel calculates the types and concentrations of colloids potentially generated after WP failure. Three types of colloids are considered: (1) waste form degradation colloids, which are generated from degradation of the glass waste form and SNF waste forms; (2) colloids produced from the steel components of the WPs and invert; and (3) colloids present in natural seepage water entering the EBS. Nine radionuclides can potentially sorb on the colloids: plutonium, americium, cesium, protactinium, thorium, tin, radium, uranium, and neptunium. Inputs to the colloid-associated EBS Colloids Submodel include pH and ionic strength in the WP provided by the In-Package Chemistry Submodel, dissolved radionuclide concentrations in the WP and invert from the EBS Transport Submodel, and pH and ionic strength in the invert provided by the EBS Chemical Environment Submodel.

At each timestep in the TSPA-SEIS calculations, the EBS Colloids Submodel uses in-package ionic strength, pH, and dissolved radionuclide concentrations to evaluate the formation and stability of colloids in the WP. Besides reversible sorption, irreversible (kinetic) sorption of plutonium and americium onto iron oxyhydroxide colloids and waste form colloids derived from HLW glass and CSNF is also considered. A competitive sorption model with a sorption capacity is implemented for the reversible sorption onto the three colloid types.

The EBS Chemical Environment Submodel (Section 6.3.4) calculates the ionic strength and pH of the invert water. Based on the values of ionic strength and pH in the invert, the EBS Colloids Submodel determines colloid stabilities and concentrations for the invert conditions and redistributes available radionuclide mass based on the distribution coefficients and the total mass of each type of colloid. These colloids and associated radionuclides are then subject to transport through the invert and into the UZ.

Several epistemic uncertainties, related to colloid stability and colloid-associated radionuclide concentrations, are represented by distributions that are sampled once per TSPA-SEIS realization. These uncertain parameters include the equilibrium sorption distribution coefficients, the specific surface area of corrosion-generated colloids, the groundwater colloid concentration, and the forward rate constant for irreversible (kinetic) sorption.

Output 16—The following outputs are passed from the Waste Form Degradation and Mobilization Model Components (Section 6.3.7) to the EBS Transport Submodel (Section 6.3.8):

- Outputs from the Waste Form Degradation and Mobilization Model Component are provided for each representative WP in seeping and non-seeping environments. For each percolation subregion, they provide:
  - The mass of radionuclides available for transport through the EBS
  - The concentrations limits of radionuclides inside a failed WP and in the invert
  - The concentrations of radionuclides, plutonium and americium, irreversibly attached (embedded in) waste form colloids
  - The concentrations of radionuclides, americium and plutonium, which are irreversibly attached to iron oxyhydroxide colloids

- The concentrations of radionuclides: americium, plutonium, protactinium, cesium, thorium, tin, radium, uranium, and neptunium, which are reversibly attached to colloids.

6.1.4.8 Engineered Barrier System Transport

The EBS Transport Submodel is described in *EBS Radionuclide Transport Abstraction* (SNL 2007 [DIRS 177407], Section 6). EBS transport is modeled directly within the TSPA-SEIS at run time, using a one-dimensional, finite-difference numerical solution algorithm that is embedded in the GoldSim software. Each representative WP group in each repository percolation subregion is modeled. The modeled system uses a linked series of mixing cells that represent the waste form as the source of radionuclides and colloids, corrosion products as a source of iron oxyhydroxide colloids and stationary corrosion products in the WP that sorb radionuclides, and the invert crushed tuff as a sorbing medium. The EBS Transport Submodel describes the transport of both dissolved radionuclides and radionuclides sorbed onto colloids through the TSPA-SEIS mixing cells via diffusion and advection. The invert is treated as if it were a single continuum composed of crushed tuff. The outputs from the EBS Transport Submodel are mass flux of dissolved radionuclides and mass flux of colloid-associated radionuclides into the host-rock fractures and host-rock matrix below the repository. The total mass flux into the UZ host rock and the fraction going into the UZ fracture and matrix continuum is computed based on modeling approximately 18 m of dual continuum below the repository as part of the EBS Transport Submodel. The calculated radionuclide mass flux as a function of time at the EBS-UZ interface is passed directly to the coupled, three-dimensional, dual-permeability, FEHM software that is used for UZ transport.

Several epistemic uncertainties related to transport in WPs and the invert are represented by distributions that are sampled once per realization. In the WPs these include: (1) the water adsorption isotherm parameters, (2) the surface properties such as specific surface area and sorption site density of the stationary corrosion products, (3) the corrosion rate of in-package stainless-steel and carbon-steel components, (4) diffusive path length from a WP to the invert, and (5) the uncertainty in pH from surface complexation calculations. In the invert, these include radionuclide reversible sorption coefficients and an invert diffusion coefficient for radionuclide diffusion.

Implementation of the EBS Radionuclide Transport Submodel requires transport connections between the single-continuum invert and the dual-continuum host rock. For each representative waste-emplacement drift, these connections determine the fraction of radionuclide mass flux transported into the host-rock matrix continuum, and the fraction transported into the host-rock fracture continuum after release from the EBS. The diffusive transport connections are derived by enforcing mass flux continuity between the invert and the host rock, which determines the split of invert diffusive releases between the UZ fracture and matrix continua. However, the split for advective mass flux is imposed. The total advective mass flux leaving the invert is based on the combined fluid flux in the invert (a combination of seepage, condensation, and imbibition flux), but when the advective mass flux is passed to the UZ, it is partitioned such that the advective fraction carried by the imbibition flux is sent to the UZ matrix, while the remainder is sent to the UZ fractures.

The release of radionuclides from the EBS to the UZ is calculated as follows: The radionuclide mass flux, calculated by the EBS Transport Submodel and released from the five repository percolation subregions, enters the FEHM grid nodes that reside within the subregions. The number of FEHM grid nodes receiving released radionuclides depends on the number of WPs that have failed. At each timestep, there are a number of failed WPs from each representative group in each repository percolation subregion. The radionuclide mass flux released from each failed WP in a group is equal to the mass flux from the representative WP group divided by the number of failed WPs in that group. To simulate WPs failing at different locations, the FEHM release nodes in the UZ are randomly selected for each group, without replacement (to prevent a node from being selected more than once), from the available UZ FEHM grid nodes within each percolation subregion. If the number of failed WPs in a group exceeds the number of FEHM grid nodes in a percolation subregion, releases are allocated evenly to all FEHM grid nodes in the percolation subregion. The following time-dependent outputs are calculated for each WP group in each percolation subregion.

Output 17—The following outputs are passed from the EBS Transport Submodel (Section 6.3.8) to the UZ Transport Submodel (Section 6.3.9):

- Outputs from the EBS Transport Submodel are provided for each representative WP and each representative early-failed WP, as applicable, in seeping and non-seeping environments, for each percolation subregion, as follows:
  - The radionuclide mass release rate to the UZ for each WP group.

6.1.4.9 Unsaturated Zone Transport

UZ transport is modeled within the TSPA-SEIS by the UZ Transport Submodel. This submodel implements the three-dimensional, dual-permeability, finite-element software code, FEHM particle tracker. The UZ flow fields for each combination of infiltration scenario and climate change are accessed directly by the UZ Transport Submodel. The FEHM particle tracker transports particles with the same dual-permeability spatial grid as used in the Mountain-Scale UZ Flow Model Component, including the same infiltration and liquid saturation values. When climate changes, the TSPA-SEIS uses the UZ flow fields associated with the new climate for the given infiltration scenario.

As noted in Output 17, Section 6.1.4.8, the mass release rate of dissolved radionuclides and reversibly sorbed radionuclide mass on colloids from the EBS are combined and released to the UZ as a radionuclide mass. This mass is equilibrated within the UZ between the aqueous phase and the groundwater colloids present in the UZ. Americium and plutonium isotopes that are irreversibly sorbed onto colloids are transported separately as fast and slow fractions. The following UZ transport processes are simulated:

- Advective and diffusive transport of dissolved and colloid-associated radionuclides in the fracture and matrix continua
- Sorption of dissolved radionuclides to the matrix continuum

- Retardation of the slow fraction of radionuclides, which are irreversibly sorbed onto colloids in the fracture continuum
- Colloid filtration at interfaces between matrix units
- Colloid size exclusion at fracture-matrix continua interfaces
- Radioactive decay and ingrowth.

For each realization, a set of uncertain material properties for UZ transport is sampled and the values or parameters generated from the sampled values are used in the UZ transport particle tracking analysis. These epistemic uncertainties are represented by distributions and include matrix adsorption coefficients, matrix diffusion coefficients (as generated from sampled values of tortuosities and species-dependent values of free-water diffusion coefficients), fracture apertures (as generated from sampled values of fracture porosity and fracture frequency), active fracture model gamma parameters, colloid equilibrium sorption parameters (as generated from sampled values of sorption coefficients onto colloids and colloid concentrations), and colloid retardation factors for UZ transport. In addition, colloid filtration sizes for rock units are sampled and compared to sampled values of colloid size for each particle during the particle tracking process. This information is accessed by the UZ Transport Submodel during TSPA-SEIS simulations. Note that because UZ transport processes tend to be more sensitive to rock property uncertainties, some UZ rock properties are sampled for the UZ Transport Submodel, whereas they are not sampled for the Site-Scale UZ Flow Process Model. Outputs from the UZ Transport Submodel at each timestep are radionuclide mass release rates from the fractures and matrix to four UZ collector regions at the water table. When the climate changes, the elevation of the water table is instantaneously set to the elevation associated with the new flow field. Any radionuclides in the UZ below the new and higher water table elevation at the time the climate changes are immediately removed from the UZ and provided as inputs to the SZ Flow and Transport Submodel.

Radionuclide releases from the UZ to the SZ are grouped into four UZ collector regions. The total radionuclide mass release rate, for both matrix and fracture continua in each of these four collector regions, is released to a single node that is randomly selected with replacement from the available UZ nodes in each collector region. The location of the random release point in each UZ collector region was selected during the generation of the SZ Convolute Abstraction breakthrough curves for each realization. The location of the UZ release point (Figure 6.3.9-7) used in each realization is, therefore, implicit to the sampled breakthrough curve used in the SZ convolution integral approach. The sum of the fracture and matrix radionuclide mass release rates is released from the four UZ collector regions to four corresponding SZ capture zones (Figure 6.3.10-6) and then fed to the SZ convolution integral model, SZ_Convolute, and to the one-dimensional SZ pipe model at each TSPA-SEIS timestep.

Output 18—The following outputs are passed from the UZ Transport Model Component (Section 6.3.9) to the SZ Flow and Transport Submodel (Section 6.3.10):

- The mass release rate of dissolved radionuclides (or, where applicable, combined dissolved radionuclides and radionuclides reversibly sorbed onto colloids) from each collector region to the SZ
- The mass release rate of radionuclides irreversibly sorbed onto retarded (slow) and unretarded (fast) colloids from each collector region to the SZ
- The cumulative potential mass release of ingrowth products associated with inventory boosting (see Section 6.3.10.3).

6.1.4.10 Saturated Zone Flow and Transport

The SZ Flow and Transport Submodel of the TSPA-SEIS evaluates the transport of radionuclides, from their introduction at the water table below the repository, to the biosphere located at the regulatory boundary 18-km downstream from the repository (66 FR 55732 [DIRS 156671], p. 55753). The groundwater used by the hypothetical farming community is conservatively assumed to contain all radionuclide mass in the SZ that crosses the regulatory boundary. The captured radionuclide mass is homogeneously distributed in 3,000 acre-ft/yr of groundwater (10 CFR 63.312(c) [DIRS 180319]). The TSPA-SEIS SZ Flow and Transport Submodel uses two abstractions to describe SZ flow and transport: (1) a 3-D SZ Flow and Transport Abstraction of individual radionuclides that are important to dose and (2) a 1-D SZ Flow and Transport Abstraction that calculates the transport of second-generation daughter radionuclides (Figure 6.3.10-8).

The 3-D SZ Flow and Transport Abstraction and the 1-D SZ Flow and Transport Abstraction receive inputs from two other sources. The Climate Analysis (BSC 2004 [DIRS 170002]) provides the duration of climate states. The Infiltration Model (SNL 2007 [DIRS 182145]) provides the net infiltration flux (Section 6.3.1) to scale groundwater flux for the future climates considered for the TSPA-SEIS.

Using 12 representative radionuclide groups, the 3-D SZ Flow and Transport Process Model (SNL 2007 [DIRS 181650]) is run outside the TSPA-SEIS. It is used to perform a series of probabilistic transport simulations for a unit mass source rate to obtain unit mass breakthrough curves at the 18-km regulatory boundary, for each of the 12 representative radionuclide groups. For each realization, parameters containing epistemic uncertainty are sampled and used in the three-dimensional and one-dimensional SZ Flow and Transport Models (SNL 2007 [DIRS 181650], Table A-1[a]). Two hundred realizations of the 3-D SZ Flow and Transport Process Model for the 4 source regions provide 9,600 breakthrough curves at the regulatory boundary. The uncertain parameters include: (1) effective porosity in the alluvium; (2) values of the distribution coefficient, K_d, in the tuff and alluvium; (3) parameters used for irreversible and reversible sorption onto colloids; (4) longitudinal dispersivity; (5) transverse dispersivity; (6) point source location; (7) horizontal permeability anisotropy; (8) fraction of the groundwater flow path within the alluvium; and (9) parameters related to matrix diffusion in the tuff (SNL 2007 [DIRS 181650], Table 7.1[a]).

The unit mass breakthrough curves generated by the 3-D SZ Flow and Transport Process Model, in combination with the convolution integral method, are used by the 3-D SZ Flow and Transport Abstraction in the TSPA-SEIS to calculate transport in the SZ to the biosphere. For a given timestep, the convolution integral method takes a point-source radionuclide mass from the bottom of the UZ Transport Submodel. The 3-D SZ Flow and Transport Abstraction combines this source with the appropriate unit mass breakthrough curve for that radionuclide to determine the mass flux of radionuclides across the 18-km boundary. The breakthrough curves reside in files in the GoldSim software run-time directory and are accessed when needed by the SZ_Convolute DLL. The SZ_Convolute method convolves the source term with the SZ_Convolute library of unit breakthrough curves. The horizontal placement of the unit mass point source in each of the four SZ source regions varies randomly from realization to realization, reflecting uncertainty in the location of radionuclide release from WPs and transport pathways in the UZ. Changes in recharge and groundwater flux in the SZ, associated with climate variations, are approximated as step changes from one steady-state flow condition to the next.

For some of the daughter radionuclides that are considered in the TSPA-SEIS, a 1-D SZ Flow and Transport Abstraction is used to account for decay and ingrowth during transport for four decay chains. The 1-D SZ Flow and Transport Abstraction is incorporated directly in the TSPA-SEIS as three one-dimensional pipe segments using GoldSim pipe pathway elements. The simplified 1-D SZ Flow and Transport Abstraction is required because the radionuclide transport methodology used in the 3-D SZ Flow and Transport Abstraction does not calculate ingrowth by radioactive decay. The rates of groundwater flow within individual pipe segments are adjusted to match the flow rates in the 3-D SZ Flow and Transport Abstraction. The flow path length of the first segment is constant. The flow path length of each of the last two segments is a function of two uncertain parameters: the first represents uncertainty in the horizontal permeability anisotropy, and the second represents uncertainty in the northwestern boundary of the alluvium. These two parameters are sampled once per SZ realization. Values of transport parameters in the one-dimensional SZ pipe segments correspond to the values used in the 3-D SZ Flow and Transport Abstraction on a realization-by-realization basis.

Results from the 3-D SZ Flow and Transport Abstraction are combined with the results of the 1-D SZ Flow and Transport Abstraction to produce a radionuclide mass release rate at the regulatory boundary. The TSPA-SEIS coordinates the consistent, random selection of radionuclide breakthrough curves and properties for the one-dimensional transport calculation for each realization.

Output 19—The output passed from the SZ Flow and Transport Submodel (Section 6.3.10) to the Biosphere Submodel (Section 6.3.11) is the mass flux of radionuclides (in 3,000 acre-ft of water) at the 18 km-regulatory boundary (66 FR 55732 [DIRS 156671], p. 55753).

6.1.4.11 Biosphere

The annual dose to the RMEI is modeled using biosphere dose conversion factors (BDCFs) that convert radionuclide concentrations in groundwater, or in volcanic ash to dose. The two exposure cases considered in the TSPA-SEIS are the groundwater exposure case and the volcanic ash exposure case. For the groundwater exposure case, radionuclides enter the

biosphere from wells that extract contaminated groundwater from the SZ aquifer. Human exposure arises from using the contaminated water for domestic and agricultural purposes. Groundwater BDCFs apply to the Nominal Scenario Class, the Early Failure Scenario Class, the Seismic Scenario Class, the Igneous Intrusion Modeling Case of the Igneous Scenario Class, and the Human Intrusion Scenario. In the volcanic ash exposure case, radionuclides are released as contamination in volcanic ash that is dispersed into the atmosphere with possible redistribution by fluvial processes leaving a contaminated layer on surface soil. Human exposure occurs in the accessible environment with the transport of radionuclides from surface soil to other environmental media such as foodstuffs, inhalable contaminated atmospheric particulate matter, and groundshine. Volcanic Ash BDCFs apply to the Volcanic Eruption Modeling Case of the Igneous Scenario Class. The BDCFs are developed outside the TSPA-SEIS, using the Biosphere Process Model (SNL 2007 [DIRS 177399]).

Using the methods developed in *Biosphere Model Report* (SNL 2007 [DIRS 177399]), BDCFs for the groundwater exposure cases and the volcanic ash exposure cases were calculated, using probabilistic analysis, in a series of simulations for each of the primary radionuclides tracked in the TSPA-SEIS. In the case of the Volcanic BDCFs, the results were insensitive to climate change and were provided for only the present-day climate. For the Groundwater BDCFs, climate has an influence on the BDCFs as a result of changes in agricultural practices and swamp cooler usage. For each primary radionuclide, one thousand stochastic BDCFs were developed for each of the three climate states (present-day, monsoon, and glacial transition) anticipated to occur over the next 10,000 years. The present day biosphere, being the warmest and driest, uses the largest volume of contaminated groundwater and generates higher BDCFs than the other climates. To prevent speculation about climate changes over the million year period, TSPA used these conservative, present-day BDCFs for all simulation time periods. In a similar vein, the BDCFs for the Volcanic Eruption Modeling Case were generated stochastically using 1,000 realizations. In the TSPA-SEIS, a discrete distribution whose output is an integer from 1 to 1,000, inclusive, is used to randomly select a particular set of values from these BDCF tables. The selected BDCFs for each radionuclide are then multiplied by the appropriate radionuclide concentrations and summed over all radionuclides to compute annual dose to the RMEI. In the SZ, radionuclide concentrations are calculated from the annual radionuclide mass flux provided by the SZ Flow and Transport Model Component uniformly dispersed in the 3,000 acre-feet of water. For the Volcanic Eruption Modeling Case, the BDCFs are multiplied by the appropriate concentrations, one concentration is that in the resuspendible soil layer, and the other is the concentration appropriate for crop uptake (i.e., averaged over the tillage depth).

In addition to the annual dose calculation, the Biosphere Model Component also includes the calculations of activity concentration in groundwater and beta-photon doses for evaluating compliance with the groundwater protection limits. Three items, including the gross alpha concentration in groundwater, the radium concentration in groundwater, and the annual dose from beta- and photon-emitting radionuclides ingested by daily consumption of two liters of groundwater are evaluated for compliance. These calculations are based on the activity concentration of each primary radionuclide in groundwater, as calculated from radionuclide concentrations that are provided by the SZ Flow and Transport Model Component. They use the conversion factors for calculating the annual beta and photon dose, and the number of alpha particles as per the requirement in 10 CFR 63.331 [DIRS 180319], emitted per decay of the primary radionuclides, as TSPA-SEIS inputs provided by the Biosphere Model Component.

The Biosphere is the last component in the chain of TSPA-SEIS components and, thus, has no output coupling; rather, the Biosphere component outputs are the time evolution of stochastic dose histories and other parameters (alpha activity and organ/whole body doses) required by 10 CFR 63.331 ([DIRS 180319], Table 1) to evaluate repository system performance.

Output 20—The following outputs are passed from the Biosphere Model Component at each time step (Section 6.3.11):

- The annual dose incurred by the RMEI for every radionuclide under consideration for both groundwater exposure and volcanic ash exposure cases
- The gross alpha concentration in groundwater
- The radium concentration in groundwater
- The annual whole body and individual organ doses from beta- and photon-emitting radionuclides by daily consumption of two liters of groundwater.

6.1.4.12 Events

In addition to the analysis of the Nominal Scenario Class described in Sections 6.1.4.1 through 6.1.4.11, the TSPA-SEIS is used to analyze early failure events and other disruptive events. The early failure events analyses consider early failure of WPs and DSs. The early failure events are captured in two separate modeling cases: (1) Waste Package EF Modeling Case, and (2) Drip Shield EF Modeling Case. The disruptive events analyses consider igneous events, including an igneous intrusion into the repository and a volcanic eruption through the repository, seismic events, with either ground motion affecting the repository or fault ruptures intersecting the repository, and a human intrusion. The Igneous Scenario Class includes two modeling cases: (1) Igneous Intrusion Modeling Case, with groundwater transport; and (2) Volcanic Eruption Modeling Case, with atmospheric transport. The Seismic Scenario Class includes two modeling cases: (1) Seismic GM Modeling Case, and (2) Seismic FD Modeling Case. The Human Intrusion Scenario includes one stylized Human Intrusion Modeling Case.

6.1.4.12.1 Early Failure Scenario Class

The two early failure Scenario Class modeling cases, mentioned above and considered for the TSPA-SEIS, are discussed below.

The Waste Package EF Modeling Case considers all WPs that fail early due to manufacturing or material defects, including improper pre-emplacement operations. The implementation of early WP failures in the TSPA-SEIS consists of specifying the number of WPs that fail early in a realization and how these WPs are distributed among the different WP types (Section 6.4). In the TSPA-SEIS early failure WP analysis, two types of WPs are considered: (1) CDSP WPs, and (2) CSNF WPs. The probability density function provides the number of early-failed WPs in a realization, dependent upon sampling an early-failed WP conditional probability distribution. The distribution is conditional on there being at least one early-failed WP. The use of this distribution requires that the resulting dose be weighted by the probability of at least one early failure. The probability of at least one early-failed DS is discussed in more detail in

Section 6.4.1.2, and the probability of at least one early-failed WP is discussed in more detail in Section 6.4.2.2. The number of early-failed WPs is partitioned among the two WP types (CDSP WP, CSNF WP) using sequential conditional binomial distributions. The parameters for the binomial distributions are the number of WPs available for selection and the probabilities of each WP type, where each probability is given by the ratio of the number of WPs of that type to the total number of all WP in the repository. In each realization, a percolation subregion is chosen according to the percolation flux distribution (Section 6.3.2.2.1). A seeping or non-seepping environment is then assigned by comparing a random number to the fraction of WPs in the assigned percolation subregion that are exposed to drift seepage conditions. For each realization for each early-failed WP type, all WPs reside in the same percolation subregion and are exposed to the same seeping or non-seeping environment. LC and GC of the WPs are considered in the Waste Package EF Modeling Case; however, these two mechanisms would not introduce any additional damage to the early-failed WPs. GC of the DS is included in the Waste Package EF Modeling Case. Other than the Waste Package Degradation Model Component, the Waste Package EF Modeling Case invokes the same modeling components and submodels used in the Nominal Scenario Class.

The Drip Shield EF Modeling Case considers all DSs that fail early due to manufacturing or material defects including improper pre-emplacement operations. The implementation of early DS failures in the TSPA-SEIS consists of specifying the number of DSs that fail early in a realization and how these DSs are distributed among the different WP types (Section 6.4). In the TSPA-SEIS's early failure DS analysis, two types of WPs are considered: (1) CDSP WPs and (2) CSNF WPs. The probability density function provides the number of early-failed DSs in a realization dependent upon sampling an early-failed DS conditional probability distribution. The distribution is conditional on there being at least one early-failed DS. In order for WP releases to occur under an early-failed DS, a WP beneath the early-failed DS is modeled as a WP in a seeping environment that fails immediately by LC once seepage contacts the WP. In the absence of LC, the WP under an early-failed DS would not be subject to releases before nominal processes result in WP failures. The combined implementation of placing the early-failed DS in a seeping environment combined with the use of the conditional distribution to invoke an early-failed DS requires that the resulting dose be weighted by the probability of at least one early-failed DS occurring in a seeping environment. The number of early-failed DSs is partitioned among the two WP types (CDSP WP, CSNF WP) using sequential conditional binomial distributions. The parameters for the binomial distributions are the number of DSs available for selection and the probabilities of each WP type, where each probability is given by the ratio of the number of WPs of that type to the total number of all WPs in the repository. In each realization, a percolation subregion is chosen according to the percolation flux distribution (Section 6.3.2.2.1). Instead of randomly chosing a seeping or non-seeping environment, as was done for the early-failed WPs, the early-failed DSs are modeled in a seeping environment. For each realization for each WP type, all early-failed DSs reside in the same percolation subregion and are exposed to a seeping environment. LC of a WP under an early-failed DS is assumed to be instantaneous once seepage contacts the WP. As a result of LC, GC of a WP is considered in the Drip Shield EF Modeling Case; however, this mechanism would not introduce any additional damage to a WP beneath an early-failed DS. GC of the DS is excluded in the Drip Shield EF Modeling Case. Other than the WP and DS Degradation Model Component, the Drip Shield EF Modeling Case invokes the same modeling components and submodels used in the Nominal Scenario Class.

Figure 6.1.4-3 schematically depicts the flow of information between the principal TSPA-SEIS components and submodels for the early failure modeling cases. The flow of information between submodels in these two modeling cases is similar to the Nominal Scenario Class Modeling Case depicted on Figure 6.1.4-1 with some exceptions that are described below and described in detail in Section 6.4.

The WP and DS Degradation Model Component, which combines the LC and GC processes in the Nominal Scenario Class, is replaced with early failure degradation modes for the WPs and/or DSs. As discussed above, LC and GC of WPs provide no additional damage to the early-failed WP, and therefore the WP damage and failure areas calculated by the WP and DS Degradation model component are not applicable in the Waste Package EF Modeling Case. DS degradation by GC is still applicable in the Waste Package EF Modeling Case. As discussed above, GC of DSs provides no additional damage to early-failed DSs, and therefore the DS damage and failure areas calculated by the WP and DS Degradation model component are not applicable in the Drip Shield EF Modeling Case. WP degradation by LC is assumed to occur instantly once a WP beneath an early-failed DS is contacted by seepage water.

6.1.4.12.2 Igneous Scenario Class

The two Igneous Scenario Class modeling cases, mentioned above and considered for the TSPA-SEIS, are discussed below (Section 1.5.3).

The following events occur in the Igneous Intrusion Modeling Case. The Igneous Intrusion Modeling Case considers an igneous event in which a fracture with magma rising in it (dike) intersects the repository drifts. The magma flows into and fills the drifts, cooling in place with no eruption to the surface unless the magma is within an eruptive conduit. The intruding magma engulfs all WPs and DSs in those repository drifts that are intersected by the dike. In response to the heat and corrosive gases, the WPs and fuel cladding fail, exposing the radioactive waste to the magma. After the magma-filled drifts cool to ambient conditions (i.e., temperatures prior to magma emplacement), the water moving into the intruded drifts is altered by the chemistry of the basaltic rock. This affects the mobility (solubility) of the radionuclides in the exposed waste. Radionuclides exposed to water moving into the magma- intruded drifts are transported by the groundwater downward through the UZ to the water table and then out to the accessible environment by flow and transport processes in the SZ.

Figure 6.1.4-4 schematically depicts the flow of information between the principal TSPA-SEIS components and submodels for the Igneous Intrusion Modeling Case. The flow of information between submodels in this modeling case is similar to the Nominal Scenario Class Modeling Case depicted on Figure 6.1.4-1 with some exceptions that are applied after the igneous intrusion occurs. These exceptions are described below and described in detail in Section 6.5.

- The Igneous Intrusion Modeling Case allows for all nominal processes to occur before the igneous intrusion occurs.
- As a result of the igneous intrusion, the Igneous Intrusion Modeling Case fails all WPs and DSs in the repository.

- The Igneous Intrusion Modeling Case does not include drift-wall condensation after the igneous intrusion.

- The TSPA-SEIS uses a seepage flux equal to the local percolation flux and neglects capillary diversion at the drift wall after the igneous intrusion. Therefore, the Drift Seepage Submodel response surfaces for seepage are not implemented after the igneous intrusion. The seepage response surfaces provide the seepage flow rates and seepage fractions applicable for the nominal conditions, which prevail prior to the igneous intrusion.

- For approximately the first 100 years after intrusion, waste form temperatures are perturbed by the hot intruded magma. A temperature abstraction is applied. This abstraction is used to specify waste form and invert temperatures during this period.

In addition to the changes affecting the information flow noted above, the following submodel changes are also implemented:

- In the Igneous Intrusion Modeling Case, the DSs and WPs in intruded drifts provide no further protection; therefore, DS and WP degradation, as calculated by the WP and DS Degradation model component, are no longer applicable in the intruded drifts.

- The TSPA-SEIS exposes waste that is contained in the failed WPs directly to the intruding magma. Radionuclides are then transported through the failed WPs and released to the invert where they are transported to the EBS-UZ interface.

Additional information developed to support the TSPA-SEIS in igneous intrusion groundwater transport includes the following:

- Mean annual frequency of a dike intersecting the repository.

The Volcanic Eruption Modeling Case models: (1) damage to the EBS and the amount of waste erupted to the surface, (2) the atmospheric transport and eventual deposition of the waste-contaminated ash on the land surface (3) redistribution of the contaminated tephra, and (4) the estimate of dose to the RMEI in the Biosphere Model Component. Figure 6.1.4-5 schematically depicts the flow of information for the Volcanic Eruption Modeling Case. The volcanic eruption is modeled using the numerical code ASHPLUME, via the ASHPLUME DLL that is dynamically linked to the TSPA-SEIS Volcanic Eruption Model at run time. The consequences of a volcanic eruption also include the change in dose at the location of the RMEI from the transport of radioactive waste-contaminated ash through sedimentary processes that include both eolian and fluvial transport mechanisms. The Redistributed Tephra Abstraction calculates source term multipliers that are used to account for this effect at the location of the RMEI, for both interstream divide areas and distributary channels. The tephra redistribution calculations for a probability-weighted volcanic event are performed using the FAR DLL.

6.1.4.12.3 Seismic Scenario Class

This Seismic Scenario Class considers seismic disruptions (i.e., fault displacement and ground motion) as additional events that occur during the time period of evaluation. This scenario class includes two modeling cases: (1) a ground motion case for the vibratory ground motion damage to the WPs, and (2) a fault displacement case for the fault displacement damage to the WPs and DSs.

The Seismic Scenario Class describes the performance of the repository system in response to seismic events with a mean annual exceedance frequency in the range of 4.287×10^{-4} to 5.967×10^{-9} per year. This modeling case includes the effects of ground motion and fault displacement on the host rock, DSs, and WPs. The Seismic Scenario Class takes into account changes in seepage flux and TH on the WP surface that might occur as a result of emplacement drift degradation in the lithophysal region due to seismic events. Figure 6.1.4-6 schematically depicts the flow of information between principal TSPA-SEIS submodels for the Seismic Scenario Class. The flow of information between submodels in the Seismic Scenario Class is very similar to the Nominal Scenario Class, as depicted on Figure 6.1.4-1.

The majority of the submodels for the Seismic Scenario Class are the same as those implemented for the Nominal Scenario Class, with two exceptions:

- Ground motion and fault displacement damage to DSs and WPs is calculated as a function of the seismic events, in addition to the damage determined by calculations with the WAPDEG DLL for expected degradation and corrosion processes.

- Drift seepage in the lithophysal and non-lithophysal units is calculated for degraded drifts. Therefore, the Drift Seepage Abstraction, including drift collapse, is implemented. In addition, drift-wall condensation ceases once the drift is fully collapsed.

Additional information that is developed to support the TSPA-SEIS for seismic damage to the DSs and WPs includes an annual frequency of occurrence for seismic events, the hazard curve for mean ground motion at a depth of 300 m beneath the surface of Yucca Mountain, and the mean hazard curves for fault displacement. Multiple seismic events over the modeled duration are included, with the impacts of each event being additive to previous events.

6.1.4.12.4 Human Intrusion Scenario

The Human Intrusion Scenario includes one Human Intrusion Modeling Case. The Human Intrusion Scenario considers the intrusion of a single water or exploratory well into the repository, through a DS and WP, and into the underlying SZ as required by 10 CFR 63.322 (DIRS 180319).

Figure 6.1.4-7 schematically depicts the flow of information between principal TSPA-SEIS submodels needed to calculate total system performance for the Human Intrusion Modeling Case. The flow of information between submodels in the Seismic Scenario Class is very similar to the Nominal Scenario Class, as depicted on Figure 6.1.4-1.

The majority of the submodels for the Human Intrusion Scenario are the same as those implemented for the Nominal Scenario Class (described in Section 6.3), with four exceptions:

- Mechanical damage to WPs, DSs, and cladding
- Drift seepage for the Human Intrusion Scenario
- UZ Transport for the Human Intrusion Scenario
- EBS flow for the Human Intrusion Scenario.

Additional information that is developed to support the TSPA-SEIS for inadvertent Human Intrusion through a DS and a WP includes probability of occurrence for earliest time a WP could be penetrated by drilling.

INTENTIONALLY LEFT BLANK

Table 6.1.4-1. Percolation Subregion Information

Percolation Subregion Number	Percolation Subregion Quantile	Number of Locations in Percolation Subregion
1	0 – 0.05	163
2	0.05 – 0.3	816
3	0.3 – 0.7	1306
4	0.7 – 0.95	816
5	0.95 – 1.0	163

Source: SNL 2007 [DIRS 181383], Section 6.2.12.1[a]

NOTE: The number of locations in each percolation subregion is calculated by multiplying the total number of locations, 3,264 (SNL 2007 [DIRS 181383], Section 6.2.12[a]), by the quantile range. Percolation subregions 1 and 5 are rounded down, while percolation subregion 3 is rounded up.

INTENTIONALLY LEFT BLANK

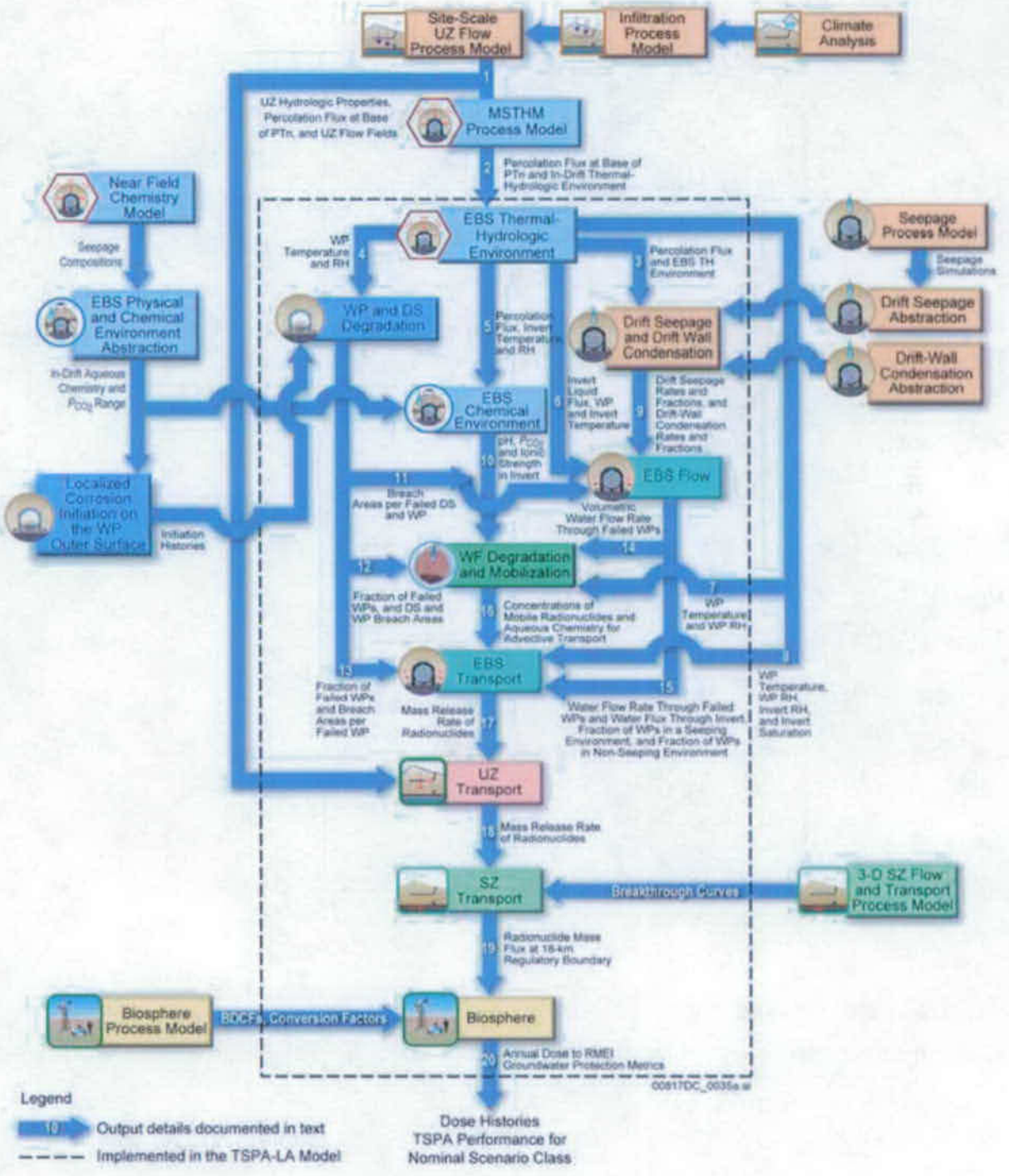

Figure 6.1.4-1. Information Transfer Between the Model Components and Submodels of the TSPA-SEIS Nominal Scenario Class

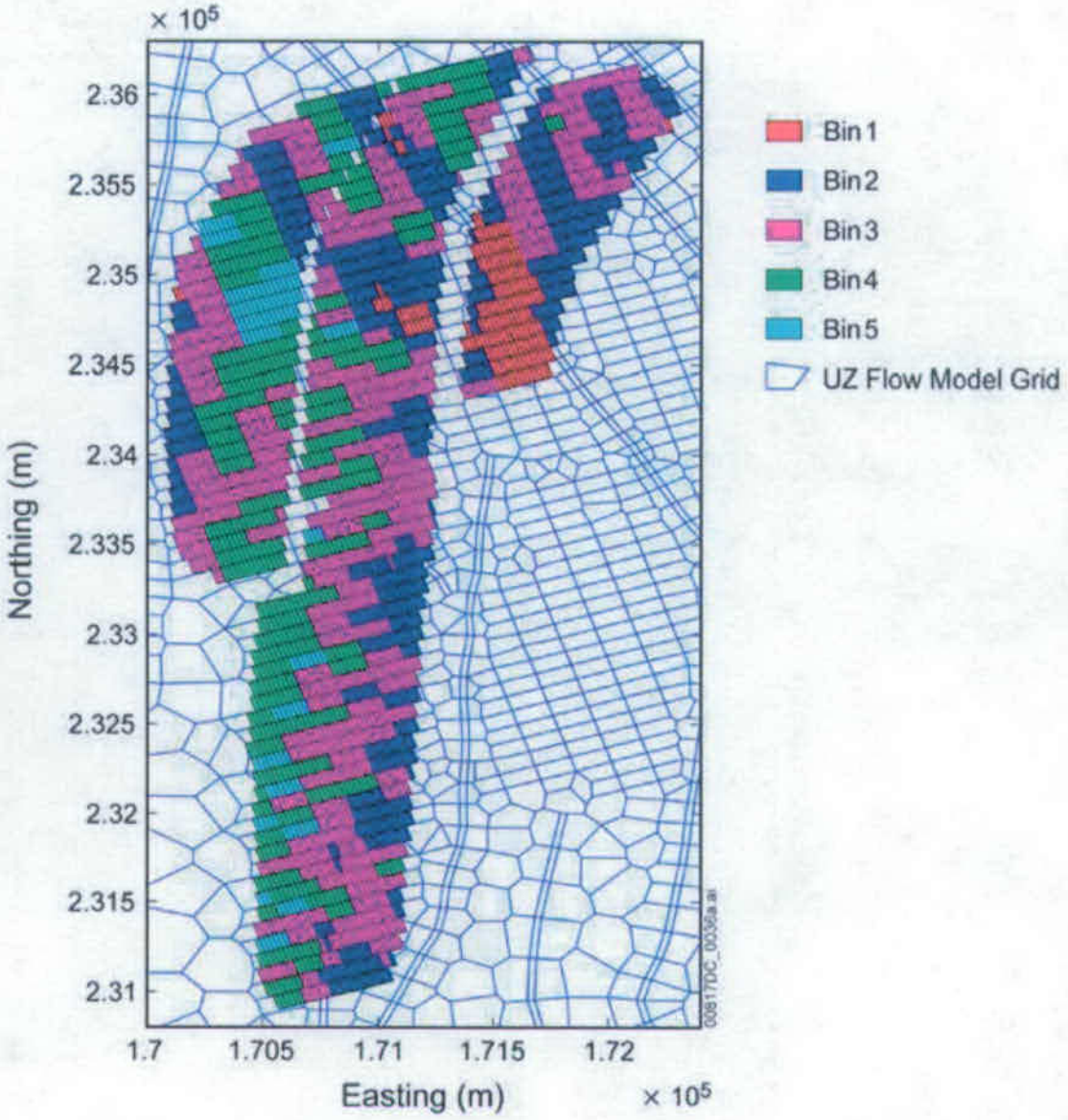

Sources: SNL 2007 [DIRS 181383], Figure VIII-1[a]

Figure 6.1.4-2. Repository Percolation Subregions Used in the TSPA-SEIS (based upon the 10th percentile percolation flux case, glacial-transition climate)

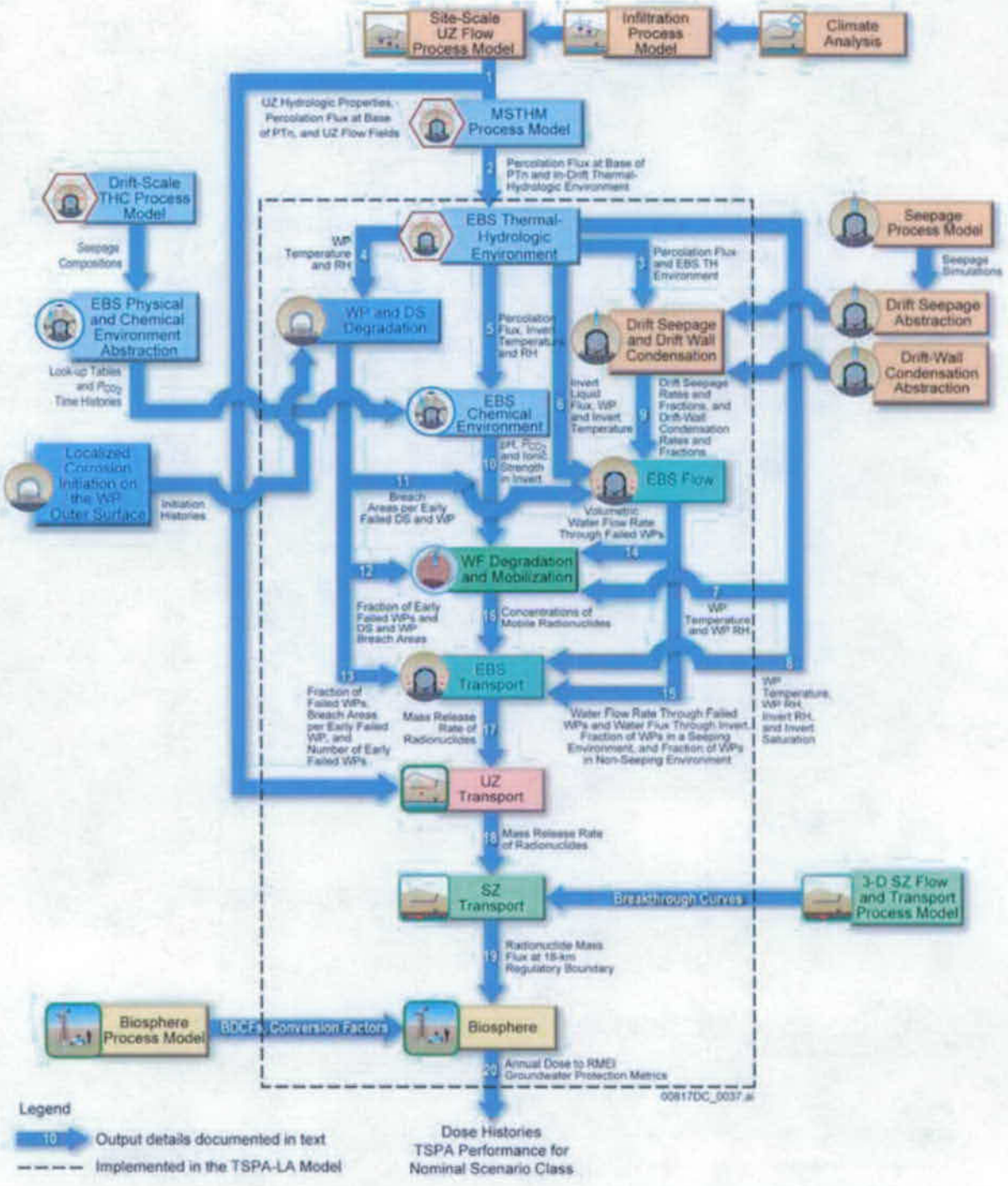

Figure 6.1.4-3. Information Transfer Between the Model Components and Submodels of the TSPA-SEIS Early Failure Scenario Class

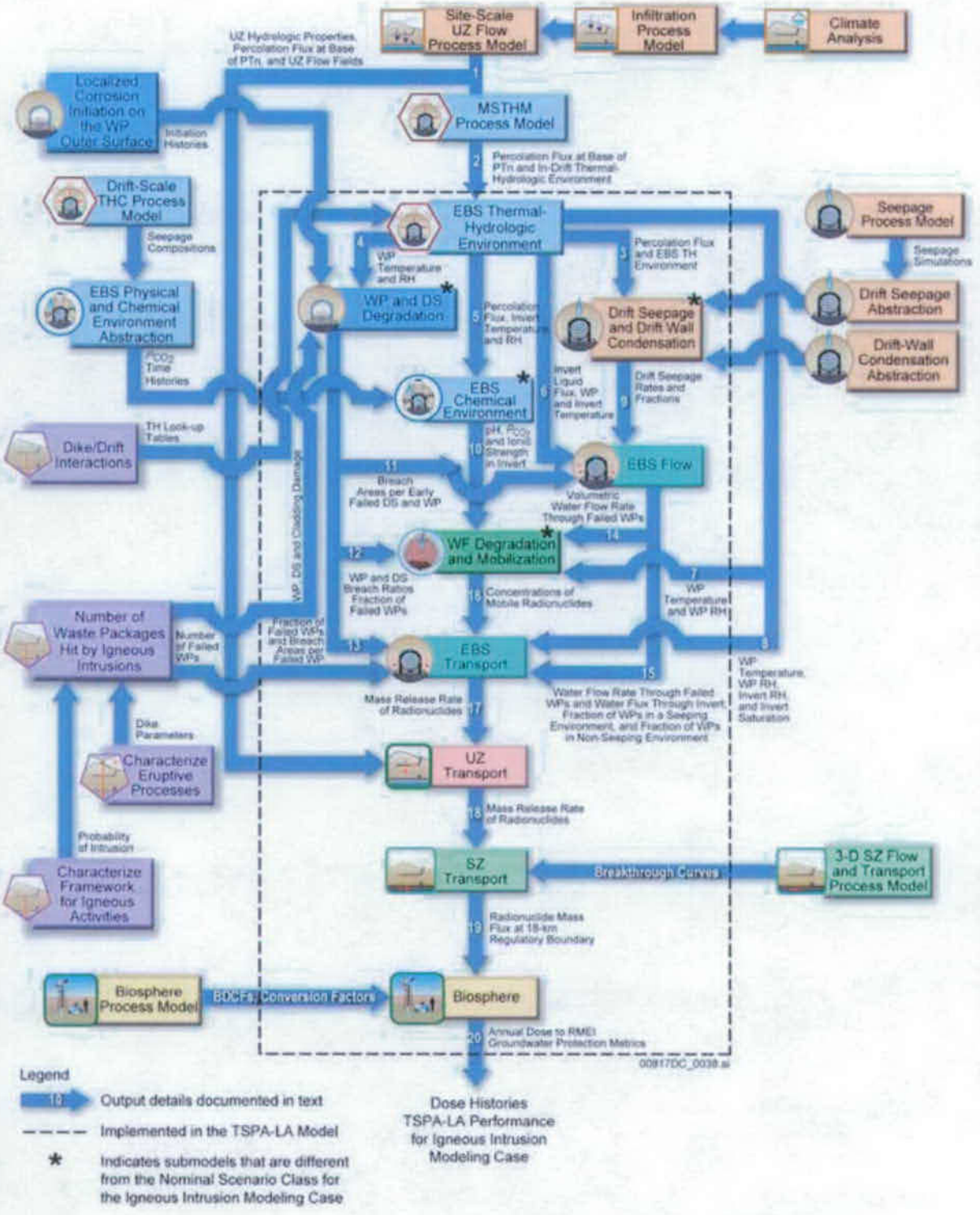

Figure 6.1.4-4. Information Transfer Between the Model Components and Submodels of the TSPA-SEIS Igneous Intrusion Modeling Case

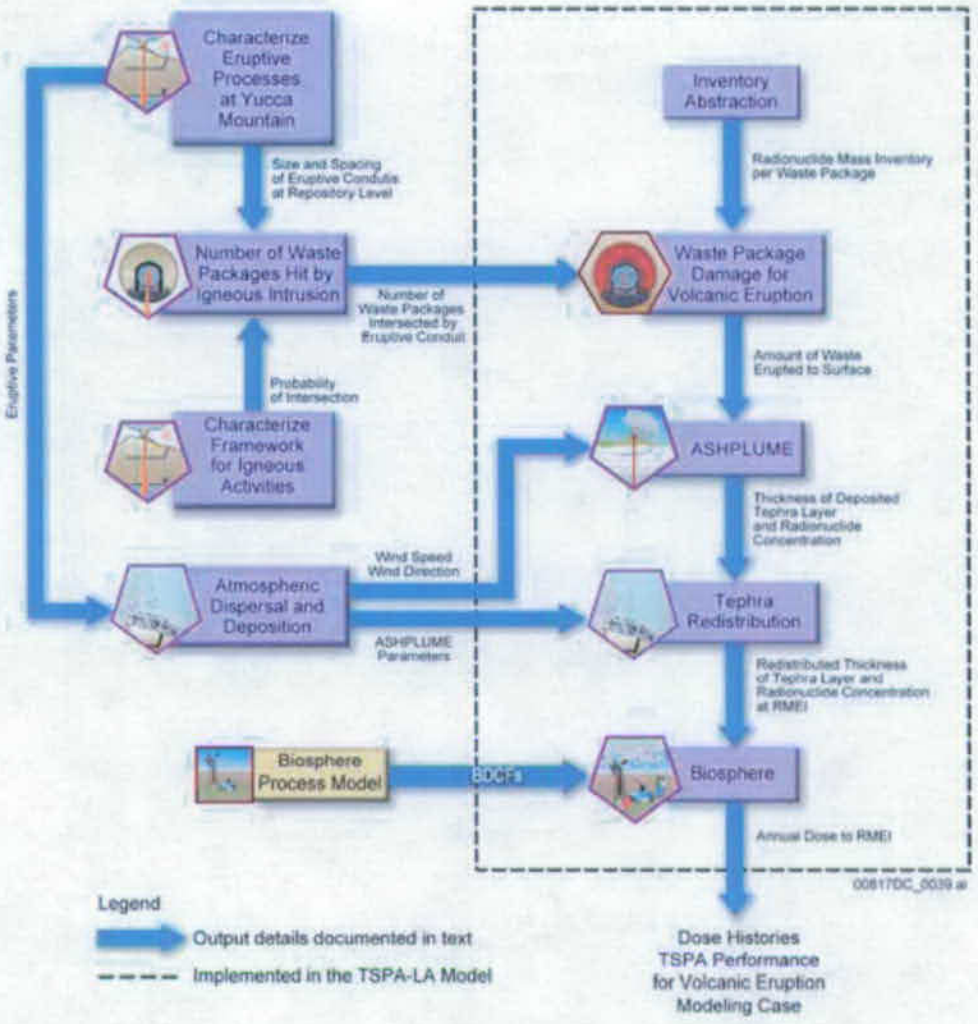

Figure 6.1.4-5. Information Transfer Between the Submodels of the TSPA-SEIS Volcanic Eruption Modeling Case

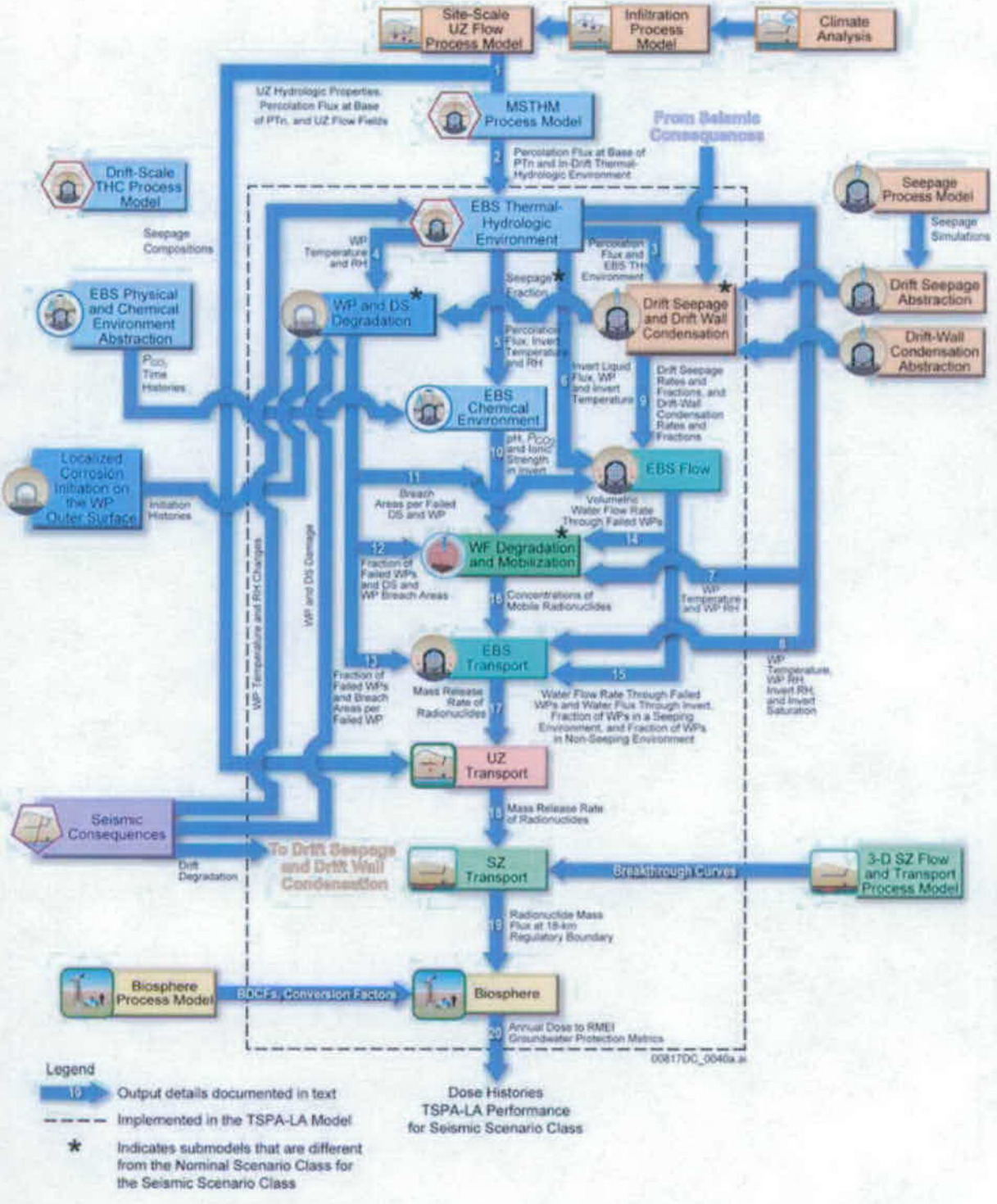

Figure 6.1.4-6. Information Transfer Between the Model Components and Submodels of the TSPA-SEIS Seismic Scenario Class

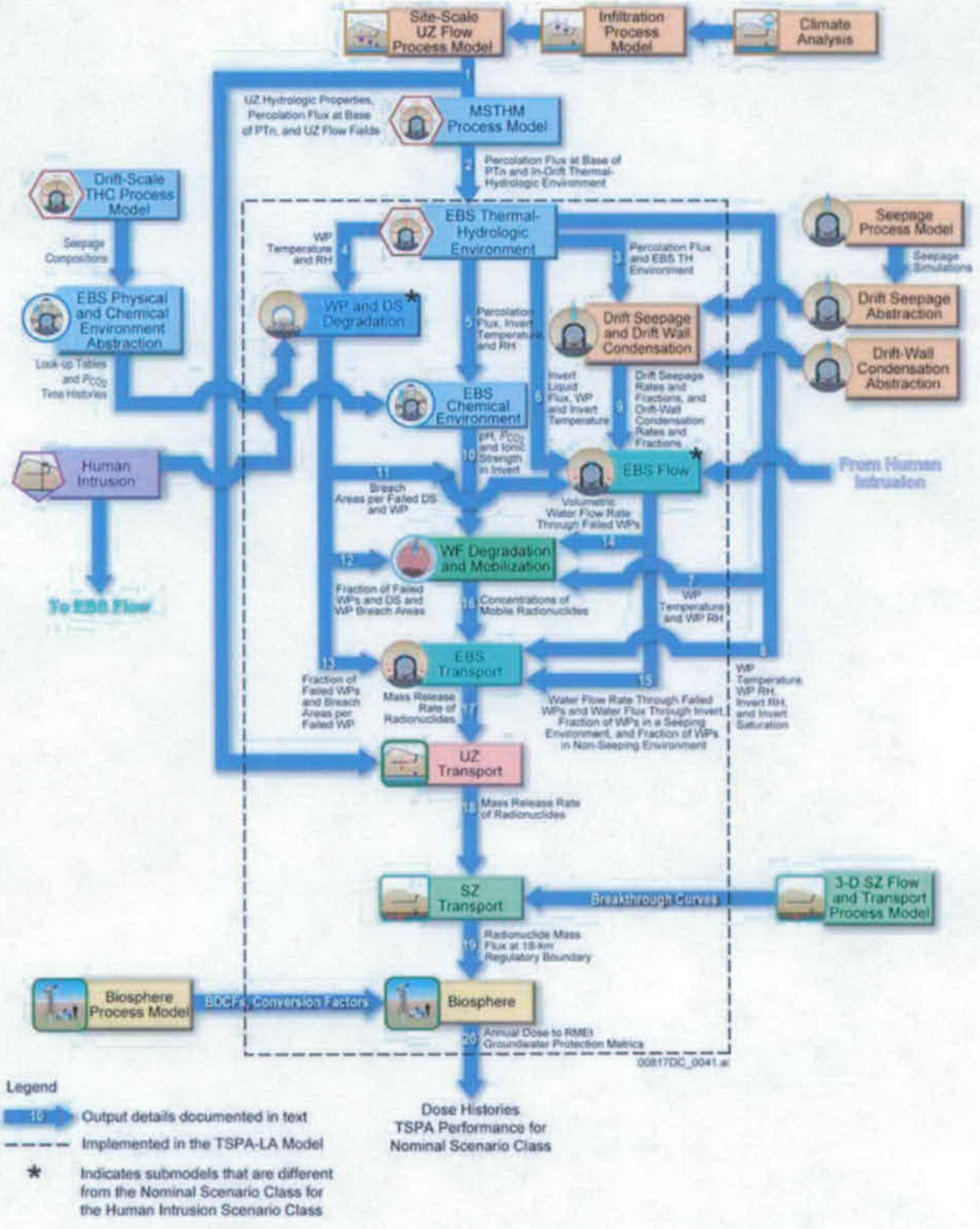

Figure 6.1.4-7. Information Transfer Between the Model Components and Submodels of the TSPA-SEIS Human Intrusion Scenario

INTENTIONALLY LEFT BLANK

6.1.5 TSPA-SEIS File Architecture

The overall information flow discussed above forms the basis for the TSPA-SEIS computational model architecture. GoldSim simulation software serves as the integrating shell that links various submodels and codes that comprise the TSPA-SEIS. For many modeling cases the TSPA-SEIS GoldSim output is further processed with EXDOC_LA V2.0 to determine the expected dose for each modeling case and a total expected dose combining all of the modeling cases.

GoldSim is a stochastic sampling program that integrates all the submodels, codes, and response surfaces together into a coherent structure that allows for consistent sampling of parameter values among the submodels. The GoldSim program is used to conduct multi-realization simulations of the entire repository system. Values of stochastic parameters for each realization are sampled from uncertainty distributions. Thus, each realization of the total system has a unique set of the values of the input parameters. In addition, each realization is considered to be equally likely, unless importance sampling is used to emphasize some realizations (usually to increase the likelihood of sampling an unlikely event or parameter value). Multiple realizations of the TSPA-SEIS yield a probability distribution of dose rate in the biosphere that shows uncertainty in dose rate based on uncertainty in all of the submodels. When an uncertain parameter appears in more than one GoldSim file (e.g., the sampled infiltration scenario is used in both the LC Initiation Analysis model file and the TSPA-SEIS file), replicate sampling in the two GoldSim files can be achieved by copying the distribution from one model file into the other. This feature allows for different model files to share the exact same sampling for common parameters.

GoldSim was used for five work products: (1) the TSPA-SEIS, (2) the LC Initiation Analysis, (3) waste form inventory decay calculation, (4) eruptive phase dose calculation, and (5) TSPA-SEIS post-implementation verification tests. Different qualified versions of GoldSim were used over the two-year period when these work products were under development.

Much of the computational work for the TSPA-SEIS is done a priori using separate software codes whose results are integrated within the GoldSim software as response surfaces, dynamic linked libraries (DLLs), look-up tables, and inputs. For example, the UZ flow fields are computed using the software code Transport of Unsaturated Groundwater and Heat V1.6. This is a three-dimensional, finite-volume numerical simulator, representing the entire UZ model domain for the dual-permeability Site-Scale UZ Flow Process Model. Details of the calculation results using detailed process models are presented in analysis model reports that support the TSPA-SEIS and are described in Section 6.3. Many of the results of these detailed process-level calculations are provided to the TSPA-SEIS as multidimensional tables that are read into GoldSim at run time. Examples of these multidimensional tables include: (1) liquid flux and velocity fields for the UZ as a function of x, y, z, t, and infiltration flux, as well as other uncertain UZ rock property parameters; and (2) temperature and relative humidity as a function of time and location within the repository.

Once the GoldSim runs are completed and the modeling case dose results are exported to text files, additional software is required to calculate the expected dose for a subset of the modeling cases. The GoldSim runs provide the inputs into these additional dose calculations, which are

performed by EXDOC_LA V2.0. The EXDOC_LA V2.0 code calculates the expected dose, conditional on an event happening. The overall purpose is to separate aleatory and epistemic uncertainty. The solution is integrated over the aleatory uncertainty, for fixed values of the epistemic parameters, to calculate an expected value, conditional on one epistemic element. This operation is repeated for each sample element, to obtain a group of expected results. Statistics (i.e., mean and percentiles) are calculated for these results. The treatment of aleatory uncertainty can be thought of as an inner loop in the calculation and the treatment of epistemic uncertainty as an outer loop. Moreover, EXDOC_LA V2.0 calculates the related complementary cumulative density functions (CCDFs) (and associated statistics) for a selected timestep, to allow presentation of both aleatory and epistemic uncertainty on the same graph. In order to produce representative output to be used as input to the EXDOC_LA V2.0 calculations, the TSPA-SEIS in GoldSim is configured with separate sampling of epistemic and aleatory quantities. For computing efficiency, the TSPA-SEIS model is performed with specified aleatory quantities and EXDOC_LA V2.0 is used to calculate the expected dose from these GoldSim runs. As an example, the GoldSim calculations for the Igneous Intrusion Modeling Case are performed for 10 specified event times and EXDOC_LA V2.0 is used to determine the expected dose accounting for event times between these specified values. Thus, GoldSim and EXDOC_LA V2.0 are both required to generate the expected dose.

6.1.5.1 TSPA-SEIS Implementation in GoldSim

The GoldSim V9.60.100 software program is flexible in representing the various component processes in the TSPA-SEIS. The four ways that submodels may be coupled into GoldSim, from most complex to least complex, include the following:

- External function calls to detailed process software codes
- Cell or Pipe Pathway Elements in GoldSim, which are basically equilibrium batch reactors, which when linked in series, provide a description of transport through selected parts of the repository system, such as in EBS transport
- Response surfaces, which take the form of multidimensional tables, representing the results of modeling with detailed process models that are run before running the TSPA-SEIS (e.g., inputs to the EBS TH Environment, such as temperature and relative humidity in the invert)
- Functional or stochastic representations of a submodel directly built into the GoldSim code, such as seismic ground motion damage or BDCFs.

While Sections 6.3.1 to 6.3.9 include a detailed conceptual description of the submodels included in the TSPA-SEIS, each subsection also includes a discussion of TSPA-SEIS implementation of the submodel discussed in that section with a model pathway to the appropriate location in the GoldSim model file allowing a detailed review of the implementation. In addition, the GoldSim model file includes a description of the inputs and calculations being performed within each submodel. A summary of the locations of submodel documentation within the GoldSim model file is provided in Table 6.1.5-1.

6.1.5.2 Controlled Data: TSPA Input Database and Data Control Processes

The TSPA Input Database provides all inputs to the TSPA-SEIS. The input database captures values for fixed and uncertain parameters, coefficients in response surface equations, look-up tables, time series data, stochastic distributions, and external files used by TSPA-SEIS software. To ensure direct inputs to the TSPA-SEIS file are documented, they were also captured on PEFs. Inputs captured by the TSPA Input Database and PEFs consist of three general types. The three types of inputs are:

- Direct inputs from controlled sources used directly in the TSPA-SEIS
- Inputs from controlled sources, but adapted for use in the TSPA-SEIS
- Inputs generated and used by TSPA in the TSPA-SEIS.

Inputs of the first type are acquired by TSPA analysts from the Yucca Mountain Project Technical Data Management System (TDMS) or from the analysis model reports that provide input to the TSPA-SEIS. These inputs are used directly in the TSPA-SEIS without modification. These parameter values are entered in the TSPA Input Database and captured on a PEF.

Inputs of the second type are also acquired by TSPA analysts from the Yucca Mountain Project TDMS or from the analysis model reports that provide input to the TSPA-SEIS. These inputs are used directly in the TSPA-SEIS with minor formatting. In some instances, prior to entering inputs into the TSPA Input Database, input values are modified by a TSPA analyst to be compatible with the form required by TSPA-SEIS software or applicable submodels. Such modifications are simple modifications and may include rounding to a specified number of significant digits, removing duplicate input values in defined look-up tables, sorting input values numerically, or converting inputs to units required by the appropriate TSPA-SEIS submodel or analysis. The changes made by the TSPA analyst are captured on PEFs.

Inputs of the third type are acquired by TSPA analysts from the Yucca Mountain Project TDMS or from the analysis model reports that provide input to the TSPA-SEIS and are processed by TSPA analysts before being captured in the TSPA Input Database and on a PEF. Inputs of the third type include formatting direct inputs through the use of TSPA Department-generated software, manipulating inputs from controlled sources to be consistent with TSPA-SEIS conceptual models, and correlating and sampling of the values of the uncertain parameters used both internally by the TSPA-SEIS and TSPA-SEIS LC Initiation Analysis GoldSim files, and externally by TSPA-SEIS and TSPA-SEIS LC Initiation Analysis DLLs. In addition, TSPA analysts generate input files used external to the TSPA-SEIS and TSPA-SEIS LC Initiation Analysis GoldSim files by other qualified software. Like inputs of the first and second type, the changes made by TSPA are captured on PEFs. In the event that substantial preprocessing is required by the TSPA Department, a TSPA analyst performs the preprocessing calculations, submits the information to the Yucca Mountain Project TDMS, including all pertinent documentation, and retrieves the information from the TDMS or a controlled source for use in the TSPA-SEIS.

Figures 6.1.5-1 to 6.1.5-6 depict a sequence of process steps that take place in order to initialize and run the TSPA-SEIS. The initial figure (Figure 6.1.5-1) provides an illustrated overview of all the various elements that make up the framework required for initializing and running the

TSPA-SEIS. The framework includes project documents and databases (i.e., analysis model reports and TDMS), as well as elements that are specific to the TSPA-SEIS (i.e., controlled files on the TSPA-SEIS file server and in the TSPA Input Database). PEFs are the most important documents for ensuring traceability of information for all inputs, whether from sources supporting TSPA or intermediate inputs produced during the execution of the TSPA-SEIS. A full discussion of PEFs can be found in Section 4.3. The arrows on the figure illustrate the transfer of information or software. Information transfers include input parameter values and files generated as part of a preprocessing step. Figures 6.1.5-2 to 6.1.5-6 describe the succeeding steps in the processing input data to the TSPA-SEIS. For each figure, the elements in use for the step being discussed will be shown in the lighter of the two colors. The dashed lines on the figure indicate cases where the location of files and software are stored in the TSPA Input Database, but the information or software are actually accessed from the TSPA-SEIS file server.

Input parameter values are loaded into the TSPA Input Database (Figure 6.1.5-2). Parameter values that are in files (e.g., UZ flow fields) are placed in a controlled directory on the TSPA-SEIS file server. The locations of those files are stored in the TSPA Input Database, along with the MD5 digital signature identifying the file. The majority of the input parameters are taken from analysis model reports and the TDMS. Inputs are also taken from other sources (e.g., NRC Proposed Rule 10 CFR Part 63 [DIRS 178394] and [DIRS 180319]) or are generated by the TSPA Department. DLLs are obtained from Software Configuration Management and are installed in a controlled directory on the TSPA-SEIS file server. The locations of those DLLs are stored in the TSPA Input Database, along with the MD5 digital signature identifying the DLL. The traceability of the values of the input parameters and DLLs is documented on PEFs. Any modifications to the original source input (e.g., a change in significant figures, unit conversion) are documented as part of the PEF.

The TH information provided by the MSTHM Abstraction is preprocessed by the PREWAP_LA V1.1 code and the resultant preprocessed PREWAP TH files are documented by a PEF (Figure 6.1.5-3). The set of PREWAP TH files are placed in the TDMS and also placed in a controlled directory on the TSPA-SEIS file server and the location of the files is stored in the TSPA Input Database.

Input parameters values are downloaded from the TSPA Input Database to the LC analysis in the GoldSim model file (Figure 6.1.5-4). The file is then run for the same number of realizations as the TSPA-SEIS to generate LC failure histories for each modeling case that includes LC. A database download is performed to transfer input files (e.g., PREWAP TH files) and the DLLs associated with the files to the directory where the LC analysis file runs. The file is run three times, once for the Nominal Modeling Case, once for the Seismic GM Modeling Case, and once for the Seismic FD Modeling Case (Section 6.3.5.2.3). The values of uncertain parameters sampled in the LC Initiation Analysis model file are perfectly correlated to the same distributions sampled within the TSPA-SEIS file. Therefore, each realization of the LC Initiation analysis matches up to the same realization of the TSPA-SEIS GoldSim file. The information for the LC initiation files is extracted from the LC analysis file. A PEF is generated to document the production of the LC initiation files. Then, the LC analysis files are placed in the TDMS and also placed in a controlled directory on the TSPA-SEIS file server. The locations of the files are stored in the TSPA Input Database.

UZ_PARAMS_MULTI_LA_COMPLIANCE files contain samples of the values of uncertain parameters used in the UZ Transport Model Component (Section 6.3.9) and are generated by running the TSPA-SEIS GoldSim model file (Figure 6.1.5-5). Input parameters values are downloaded from the TSPA Input Database to the TSPA-SEIS GoldSim model file. The database download also transfers input files and the DLLs associated with the file to the directory from which the TSPA-SEIS GoldSim model file is run. Because the TSPA-SEIS is run only to sample the values of uncertain UZ parameters needed for the UZ_PARAMS_MULTI_LA_COMPLIANCE file, it can be configured to run for only the first two timesteps. TSPA-SEIS runs are made for the number of epistemic realizations that the TSPA-SEIS is configured to run (i.e., 300 and 1,000 realizations) (Section 6.3.9.3). The values of the UZ uncertain parameters required for a UZ_PARAMS_MULTI_LA_COMPLIANCE file are extracted and put into the UZ_PARAMS_MULTI_LA_COMPLIANCE files. A PEF is generated to document the production of the UZ_PARAMS_MULTI_LA_COMPLIANCE files. Then those files are placed in a controlled directory on the TSPA-SEIS file server. The locations of those files are stored in the TSPA Input Database. Once all the input parameters to the TSPA-SEIS are pre-processed for use by the TSPA-SEIS, the input parameter valuess are downloaded from the TSPA Input Database to the TSPA-SEIS (Figure 6.1.5-6). The database download also transfers input files, and the DLLs associated with the files, to the directory from which the TSPA-SEIS GoldSim model file is run.

Figure 6.1.5-7 illustrates the linkages between the software that supports the execution of the TSPA-SEIS GoldSim model file and the separate GoldSim model file for the Volcanic Eruption Modeling Case. Most of the software consists of DLLs that are called by GoldSim at run time. The software and their functions are described in Section 3. The LC Initiation Analysis is a separate GoldSim model file (Figure 6.1.5-8). This figure illustrates the linkages between the software and the relation of the software to the TSPA-SEIS components discussed in Section 6. The submodels for EBS thermal-hydrology, EBS chemistry, drift seepage, DS degradation, and seismic consequences for the Seismic GM and FD Modeling Cases and the associated DLLs are implemented in both the GoldSim model file and in the GoldSim model file for the LC Initiation Analysis.

6.1.5.3 Implementation File Structure for the TSPA-SEIS

The layout of calculation containers in GoldSim provides a framework for discussing the implementation of the TSPA-SEIS in GoldSim. Understanding the roles of the containers and their contents is essential for navigating through the TSPA-SEIS files. The layout of containers in the GoldSim software generally follows the Section 6.3 discussion of the model components and submodels, but there are differences at the detail level.

The container structure represents the end result of the construction and evolution of the GoldSim model file developed by TSPA analysts. The end result is a complex file structure that meets the requirements of the TSPA-SEIS. This section is designed to provide information that will facilitate investigation of the TSPA-SEIS and the associated GoldSim model file.

GoldSim Submodels—The TSPA-SEIS implemented in GoldSim contains three GoldSim Submodels embedded in one main GoldSim model. Each GoldSim Submodel is a completely separate model within the main model and each has it own simulation settings. A GoldSim

Submodel is a special GoldSim element that performs a complete simulation and passes calculated results to the main model. The three GoldSim Submodels in the TSPA-SEIS are: (1) the Epistemic Parameters GoldSim Submodel, (2) the Aleatory Parameters and Dynamic Calculations GoldSim Submodel, and (3) the EBS GoldSim Submodel. A description of each GoldSim Submodel is presented below. The main model sets the simulation settings for these three embedded models and then calls upon each model to perform its simulation. Once all three embedded models have performed their simulation, the main model receives the results and then performs the calculations for the UZ Transport, SZ Flow and Transport, and Biosphere Model Components using these results.

The Epistemic Parameters GoldSim Submodel is a static model that samples distributions of the values of parameters that characterize epistemic uncertainty. The Epistemic Parameters GoldSim Submodel (GoldSim element name: Epistemic_Params) is located in the Epistemic_Uncertainty container shown on Figure 6.1.5-9 and is one containment level below the Epistemic_Uncertainty container level inside the GoldSim model file. Table 6.1.5-1 provides the GoldSim model file pathway to the Epistemic Parameters GoldSim Submodel. The output of the Epistemic Parameters GoldSim Submodel is a suite of values for all parameters that are characterized by epistemic uncertainty. No additional distributions characterize epistemic uncertainty within the TSPA-SEIS or any of the other two GoldSim submodels. These values may be determined by sampling uncertain distributions or may be determined by the evaluation of time-independent calculations that include values sampled from uncertain distributions. The Epistemic Parameters GoldSim Submodel is a small GoldSim model embedded in a larger model and hence it has its own Monte Carlo simulation settings. Because it has its own Monte Carlo simulation settings, the Epistemic Parameters GoldSim Submodel can perform a unique Latin Hypercube Sampling for all realizations performed by the TSPA-SEIS, or it can repeat sequences of sampled values. Within the suite of modeling cases that are performed, the TSPA-SEIS invokes both sampling options within the Epistemic Parameters GoldSim Submodel. In order of calculation heirarchy, the Epistemic Parameters GoldSim Submodel provides values to both the Aleatory Parameters and Dynamic Calculations GoldSim Submodel and the EBS GoldSim Submodel, as well as to the calculations for the UZ Transport, SZ Flow and Transport, and Biosphere Model Components performed in the main model.

The Aleatory Parameters and Dynamic Calculations GoldSim Submodel is a dynamic model that samples distributions of the values of parameters that characterize aleatory uncertainty and performs additional dynamic calculations utilizing these sampled values. The Aleatory Parameters and Dynamic Calculations GoldSim Submodel (GoldSim element name: Aleatory_Params) is located in the Time_Zero container shown on Figure 6.1.5-9 and is one containment level below the Time_Zero container level inside the GoldSim model file. Table 6.1.5-1 provides the GoldSim model file pathway to the Aleatory Parameters and Dynamic Calculations GoldSim Submodel. The output of the Aleatory Parameters and Dynamic Calculations GoldSim Submodel is a suite of calculated values and time histories for all of the parameters that are characterized by aleatory uncertainty. No additional distributions characterize aleatory uncertainty within the TSPA-SEIS or any of the other two GoldSim submodels. These values may be determined by sampling uncertain distributions or by calculations that include values sampled from uncertain distributions. Because the Aleatory Parameters and Dynamic Calculations GoldSim Submodel is a dynamic model, it has a simulation clock and can perform time-dependent calculations. If a calculation includes an

epistemic quantity, the value of the epistemic quantity is first determined in the Epistemic Parameters GoldSim Submodel and then passed into the the Aleatory Parameters and Dynamic Calculations GoldSim Submodel. The Aleatory Parameters and Dynamic Calculations GoldSim Submodel is a small GoldSim model embedded in a larger model and hence it has its own Monte Carlo simulation settings. Because it has its own Monte Carlo simulation settings, the Aleatory Parameters and Dynamic Calculations GoldSim Submodel can perform a unique Latin Hypercube Sampling for all realizations performed by the TSPA-SEIS, or it can repeat sequences of sampled values. Within the suite of modeling cases that are performed, the TSPA-SEIS invokes both sampling options within the Aleatory Parameters and Dynamic Calculations GoldSim Submodel. The Aleatory Parameters and Dynamic Calculations GoldSim Submodel provides calculated values to the EBS GoldSim Submodel, discussed next, but does not provide values to the Epistemic Parameters GoldSim Submodel and does not directly provide any transport-related values to the UZ Transport, the SZ Flow and Transport, or the Biosphere Model Components performed in the main model. In order of calculation heirarchy, the Aleatory Parameters and Dynamic Calculations GoldSim Submodel receives values from the Epistemic Parameters GoldSim Submodel and provides values to the EBS GoldSim Submodel.

The EBS GoldSim Submodel is also a dynamic model. With the exception of some static calculations that determine the size of the WP groups modeled by the GoldSim source term elements and the fractional failure history of each WP group, this embedded model performs all of the EBS-related calculations that support the UZ Flow, EBS Environment, WP and DS Degradation, Waste Form Degradation and Mobilization, and EBS Flow and Transport Model Components. The EBS GoldSim Submodel (GoldSim element name: EBS_Submodel) is located in the Time_Zero container shown on Figure 6.1.5-9 and is three containment levels below the Time_Zero container level inside the GoldSim model file. Table 6.1.5-1 provides the GoldSim model file pathway to the EBS GoldSim Submodel. The output of the EBS GoldSim Submodel provides the time histories of radionuclide flux from the bottom of the invert into the UZ beneath the repository, taking into account all repository related processes. The EBS GoldSim Submodel does not sample any uncertain distributions. Inputs to the EBS GoldSim Submodel include sampled values of epistemic parameters from the Epistemic GoldSim Submodel and all of the values of the aleatory parameters and associated time history results from the Aleatory Parameters and Dynamic Calculations GoldSim Submodel. In addition, the TSPA-SEIS performs additional calculations between performing the calculations of the Aleatory Parameters and Dynamic Calculations GoldSim Submodel and the EBS GoldSim Submodel. These calculations are static calculations that populate the number of WPs in each GoldSim source term within the EBS GoldSim Submodel and also determine the fraction of WPs that are exposed to drift seepage and the time history of WP failures from general and localized corrosion. These static calculations involve external DLLs that perform the related calculations necessary to model the EBS.

Looping Containers—Unlike the Epistemic GoldSim Submodel and the Aleatory Parameters and Dynamic Calculations GoldSim Submodel, the EBS GoldSim Submodel is placed within looping containers. A looping container is another special GoldSim element that allows the calculations within the container to be repeated in a DO-WHILE loop. The EBS GoldSim Submodel simulation is performed in 15 loops within one realization of the TSPA-SEIS, one loop for each of 15 WP groups. Each of the 15 WP groups is described by a set of average properties for the entire group. Combining groups of WPs that have similar properties results in

average properties that are derived from a subset of WPs that have less variation. For the TSPA-SEIS, the WP properties that define the different WP groups are: (1) the percolation flux rate above the WP location, (2) the occurrence of drift seepage above the WP location, and (3) whether or not drift seepage induced LC damages the WPs at a WP location. Choosing the number of WP groups to model balances computational efficiency against the most important processes that govern releases from the EBS. Using a looping container over each WP group ensures that the calculations that are performed for each WP group are consistent with the calculations performed for the other groups. Therefore, the TSPA-SEIS models the EBS GoldSim Submodel in 15 different loops, each loop models a different WP group. The 15 loops are actually performed in two loops, an outer loop (called EBS_PS_Loop in the GoldSim model file), referred to as the percolation subregion loop, and an inner loop (EBS_PSE_Loop in the GoldSim model file), referred to as the percolation subregion environment loop. The outer loop is performed five times, once for each percolation subregion. These five loops account for spatial variability in the percolation flux above the repository. This discretization is described in detail in Section 6.3.2 of this report. Within each of these five percolation subregion loops, the EBS GoldSim Submodel performs calculations for three additional loops, bringing the total number of loops to 15. These three loops consider two different drift seepage conditions above each WP location and two different damage mechanisms to the WP. The first loop considers all the WPs in a percolation subregion that are not exposed to drift seepage. The fraction of WPs that are exposed to drift seepage is determined by the Drift Seepage Submodel of the UZ Flow Model Component. The second loop models all WPs that are exposed to drift seepage and do not experience LC in the modeled duration. The third loop models all WPs that are exposed to drift seepage and experience LC in the modeled duration. The distinction between seepage locations and non-seepage locations is important because advection and diffusion from a failed WP can result in greater mass release that for diffusion release alone. Advection from the WP can only occur if there is a water source dripping onto a failed WP. The distinction between LC packages and non-LC packages is important when considering the opening area on the WP. The rate of advection and diffusion from a failed WP is proportional to the opening area on the failed WP. In the absence of LC, crack damage from SCC (Section 6.3.5) and/or seismic ground motion (Section 6.6.1) has a different release rate than a WP with LC patch openings that completely penetrate the WP.

High Level Containers—The highest level of the GoldSim model file is a set of containers that define the overall organization of the GoldSim model file (Figure 6.1.5-9). These containers are not all of the same type or size. Global_Model_Input (Figure 6.1.5-9) stores the configuration properties for the TSPA-SEIS and other inputs referenced throughout the TSPA-SEIS. Epistemic_Uncertainty (Figure 6.1.5-9) contains the Epistemic Parameters GoldSim Submodel. Time_Zero (Figure 6.1.5-9) contains both the Aleatory Parameters and Dynamic Calculations GoldSim Submodel and the EBS GoldSim Submodel. This container is a conditional container that performs dynamic calculations prior to advancing the simulation clock controlling the calculations performed for the UZ Transport, SZ Flow and Transport, and Biosphere Model Components in the main model. The calculations for these model components are captured within the TSPA_Model (Figure 6.1.5-9) container. In general, within these high-level containers or the GoldSim Submodels embedded directly beneath them, the model elements that define the input parameters and perform calculations are grouped into nine containers, one for each of the eight principal model components, shown on Figure 6.1.2-1, and one for events. Understanding the containers and their organization is important for navigating through the

GoldSim model file and finding information, but they do not always correspond to the conceptual organization of the TSPA-SEIS discussed elsewhere in this report. For instance, within the Aleatory Parameters and Dynamic Calculations GoldSim Submodel, the Aleatory_Calcs_Seismic container contains information related to the Seismic Scenario Class, discussed in Sections 6.1.4.12.2 and 6.5, but does not contain all of the submodels involved in representing the Seismic Scenario Class. Additional inputs and calculations are defined in the Epistemic Parameters GoldSim Submodel and within the EBS GoldSim Submodel where radionuclide releases from seismic damaged WPs are modeled.

The conceptual TSPA-SEIS discussion focuses on model components and submodels that can be divided, at the highest level, between natural system models and engineered system models. The following discussion will define, at a high level, the implementation of these models in the GoldSim model file.

Submodel Organization—The TSPA-SEIS is a system of scientific models and abstractions sharing numeric information and linked together in the GoldSim software. In general, the TSPA-SEIS is comprised of eight principal model components and an event scenarios component. Each model component is itself a system of dynamic calculations performed by one or more submodels. Within a model component container, the submodels that comprise the model component are organized into separate containers. Each submodel may be a function of the calculated values from other submodels within the same model component or another model component. To enhance transparency, each submodel is further organized into separate containers for inputs, calculations, and outputs. The inputs to a submodel may include parameter definitions and results from other submodels. These two types of inputs are segregated into Model_Input and Model_Feed containers, respectively. The calculations for each submodel are performed in a Model_Calcs container. The outputs of the submodel that are passed to other submodels are captured in a Model_Output container. The elements within the Model_Feeds container of one submodel are linked to the elements within the Model_Output container of another.

Representation of the Natural System above the Repository—The natural system above the repository includes the land surface, the soil and rock near the land surface, and the UZ above the repository. The information pertaining to this part of the repository system is located in three locations in the TSPA-SEIS. Uncertain inputs are captured in the Epistemic_Params_UZ_Flow and Epistemic_Calcs_UZ_Flow containers within the Epistemic Parameters GoldSim Submodel. Additional input parameters and UZ flow calculations are located in the Time_Zero container. Static calculations to obtain the fraction of WPs that are exposed to drift seepage, which is used to determine the number of WPs to model in each WP group, are located in the Static_Calcs_UZ_Flow container. These static calculations are located in the percolation subregion (outer) loop of the EBS calculations. Therefore, the UZ Flow calculations in the Static_Clacs_UZ_Flow container are performed five times, once in each percolation subregion loop. Within each percolation subregion loop, the inputs to the UZ Flow calculations are appropriate for the active percolation subregion and thus the calculated values of the UZ Flow Model Component will vary in each percolation subregion loop. The rest of the calculations that are part of the UZ Flow Model Component are found within the Global_UZ_Flow, Seep_Params and Condensation_Model containers within the EBS GoldSim Submodel. The calculations inside these three containers are performed 15 times, once for each outer loop and inner loop pair

of the EBS GoldSim Submodel. For each loop, implementation using IF...THEN...ELSE functions allows the inputs to the UZ Flow calculations to change to the appropriate values for the active percolation subregion and seeping environment type. However, because WP damage by LC does not affect UZ Flow properties, the calculated values of the UZ Flow Model Component within one percolation subregion loop will be the same in the second and third percolation subregion environment loops. Combining all of this information, the UZ Flow Model Component includes information on climate state, infiltration, seepage into drifts, and drift-wall condensation.

Representation of the Engineered System—The calculations that model the performance of the Engineered_System are located in four locations in the TSPA-SEIS. Uncertain inputs are captured in the Input_Params_Epistemic container within the Epistemic Parameters GoldSim Submodel. Within this container, the input parameters are further organized into containers defined for each EBS Model Component, EBS Environment, WP and DS Degradation, WF Degradation and Mobilization, and EBS Flow and Transport. Within each of these model component containers, the uncertain inputs may be further organized into separate containers for each submodel of the model component. The level of discretization within the Epistemic Parameters GoldSim Submodel increases with increasing complexitey of the model component. Additional input parameters and EBS calculations are located in the Time_Zero container. Dynamic calculations related to the chemical interaction between seepage water and the host rock and the integrity of the DS under nominal conditions are performed in the Aleatory Parameters and Dynamic Calculations GoldSim Submodel. The water-rock interaction calculation is discussed in detail in Section 6.3.4. The nominal corrosion of the DS is discussed in Section 6.3.5. Static calculations that are used to determine the number of WPs to model in each WP group, the WP Parsing Submodel, and localized corrosion and general corrosion failures of the WP are located in the Static_Calcs_PS_Loop container. Two of the four EBS-related model components have calculations within this container, WP and DS Degradation and EBS Flow and Transport. These calculations are located in the percolation subregion (outer) loop of the EBS calculations. Therefore, the EBS calculations in the Static_Calcs_PS_Loop container are performed five times. Each time the inputs to the calculations are appropriate for the active percolation subregion and thus the calculated values will vary in each loop. The rest of the calculations that model the EBS are found within the EBS GoldSim Submdel. The EBS GoldSim Submodel container includes a greater variety of information than any of the other containers. The overall discretization of WP groups and the structure of the container are shown on Figure 6.1.5-10. Some aspects of the implementation of the EBS submodels can be characterized as global and are independent of details such as fuel type or location within the repository. Much of the implementation, however, is dependent on the discretization of the submodel by waste type, percolation flux subregion or bin, and seepage environment.

The first level of discretization is by waste type. The TSPA-SEIS considers two types of WPs: CSNF and CDSP WPs. These WPs represent all of the WP types considered in the TSPA-SEIS. Details of how this representation is developed are found in Section 6.3.2.2.2. Within the TSPA-SEIS, discretization by waste type is handled explicity by implementing different GoldSim elements to perform the fuel type specific calculations.

The second level of discretization is by percolation subregion. The magnitude of infiltration varies spatially across the land surface above the repository footprint and percolation flux varies

spatially at the repository level. This spatial variability is captured in a CDF of percolation flux values that are calculated for 3,264 locations. This CDF provides the basis for the TSPA-SEIS representation by percolation subregions, as described in Section 6.3.2. Percolation subregion locations are shown on Figure 6.1.4-2.

The third level of discretization is by seeping environment (i.e., seepage with or without drift-wall condensate) and LC failure mode. The CSNF and CDSP WPs that are in each percolation subregion are identified as either having seepage above each WP location or not. Those that have seepage are further discretized into two groups, those that experience LC damage and those that do not experience LC damage.

The three levels of discretization result in the 30 environments in the TSPA-SEIS (two fuel types × five percolation flux subregions × three seepage/LC states) that are used to represent all of the WPs in the repository.

Figure 6.1.5-11 illustrates how the repository is conceptualized with the three levels of discretization discussed above. The representation is purposely a schematic to emphasize the conceptually important aspects of the discretization. The left portion of the figure shows the percolation flux subregions, as defined in Section 6.1.4.2, superimposed on the repository footprint. The rest of the figure shows a schematic representation of these subregions (the boxes) and illustrates the discretization by waste type and seeping/LC conditions. The levels of discretization shown on Figure 6.1.5-10 together with the repository conceptualization shown on Figure 6.1.5-11 lead to the implementation found in the GoldSim model file.

The discretization structure determines the type of information that is included in the containers at each level. Containers at the highest level of Global_Inputs_and_Calcs in the EBS GoldSim Submodel, the Global_WP_DS_Deg, Global_EBS_Environ, Global_WF_Deg_Mob, and Global_EBS_F_and_T containers, include global inputs, such as the corrosion rate for Alloy 22, the chemistry inside a failed WP under seeping or non-seeping conditions, and the regression coefficients in the WF degradation rate equations. This is information used for all percolation flux subregion environments.

At the level of discretization by waste type, the CSNF_Packages and CDSP_Packages containers within the EBS GoldSim Submodel, GoldSim containers include information needed to evaluate processes at the EBS-UZ boundary. The parameters defined at this level include those that are used to evaluate water volumes in the fracture and matrix cells of the UZ near the EBS-UZ boundary, and those related to the mass of colloids in the same cells.

The next level of discretization is by percolation subregion environment and refers to the 30 environments defined on Figure 6.1.5-10. As stated earlier, the TSPA-SEIS captures the required EBS calculations for all 15 CSNF environments in one container and for all 15 CDSP environments in another container. These two calculation containers accommodate the 30 environments by using IF...THEN...ELSE functions to vary the calculation inputs to those specific for each of the 30 environments. The detailed source term calculaitons are performed within each of these two percolation subregion environment containers. Parameter values identified here include the temperature and relative humidity of the invert and WP surface, reading WAPDEG V4.07 DLL output to determine crack and patch failures, and chemical

parameters for the WP and invert for dripping and non-dripping conditions, solubilities of radionuclides in the invert and in the WPs, which are values that are determined from look-up tables that are defined elsewhere. At this level, the TSPA-SEIS also calculates the mass flux of radionuclides at the base of the invert.

Once calculated, results of EBS conditions and radionuclide mass flux rates are passed from each loop to TS_PROC.DLL. This is a specialized GoldSim DLL that stores and segregates results for each outer loop of a GoldSim submodel. For results that differ for each inner loop, the DLL can be configured to add or average the results of each inner loop. The model components that comprise the EBS are discussed in additional detail in Sections 6.3.2 through 6.3.8.

Representation of the Natural System Below the Repository—The natural system below the repository includes the UZ, the SZ, and the biosphere. Related model components are shown on Figure 6-1 and are present in the TSPA_Model container at the highest level of the GoldSim model file. Within the TSPA_Model container there are six high level containers. The UZ_Flow container is a repeat implementation of the Climate Submodel of the UZ Flow Model Component. This information is used by the UZ Transport and SZ Flow and Transport Model Components. The Engineered_System container captures the radionuclide mass flux from the bottom of the invert into the UZ beneath the repository and the number of failed WPs. This information is fed directly into the UZ Transport Model Component from within this container. In addition, this container also captures EBS-related results that are useful for model analysis. The calculations for the model components representing the natural system below the repository are captured in the UZ_Transport, SZ_Transport, and Biosphere containers. Each of these containers is briefly discussed below. Finally, all model results that are useful for model analysis are captured within the results container.

Similar to the organization discussed previously, the uncertain parameters that characterize epistemic uncertainty for the UZ Transport, SZ Flow and Transport, and Biosphere Model Components are captured in separate containers within the Epistemic Parameters GoldSim Submodel. Many of the uncertain parameters used in the UZ Transport Model Component are shared by the EBS Flow and Transport Model Component. The uncertain parameters used by both models are sampled within the EBS Flow and Transport Model Component. Additionally, all uncertain parameters used in the UZ Transport Model Component are pre-sampled and written to an external file accessed by the FEHM V2.24 DLL during UZ transport calculations. Because a large number of uncertain parameters are shared between the EBS and UZ transport Submodels, all uncertain parameters used in UZ transport calculations have been co-located with parameters of the EBS Flow and Transport Model Component so that the elements that generate the UZ external file are co-located. Similarly, the epistemic uncertainties in the SZ Flow and Transport Model Component are correlated to input files accessed by the SZ_Convolute V3.10 DLL (STN: 10207-3.10.01-00 [DIRS 181060]). Thus, these parameter values are pre-sampled and stored in look-up tables. The pre-sampled values in the look-up tables share an index value with the external files. The index is randomly sampled in the Epistemic Parameters GoldSim Submodel, ensuring consistency between the calculations performed inside the GoldSim model and those performed by the SZ_Convolute V3.10 DLL. The epistemic uncertainties in the Biosphere Model Component are reflected in BDCFs. The BDCFs for different radionuclides may be highly correlated and are provided to TSPA as look-up tables of correlated values. Each

look-up table shares a common index variable. The index is randomly sampled in the Epistemic Parameters GoldSim Submodel, ensuring that the desired correlation among BDCFs is applied.

The model calculations addressing the performance of the Natural System below the Repository are calculated in the TSPA_Model container of the TSPA-SEIS. Within this container, separate containers exist for the three model components comprising the natural system below the repository. The UZ Transport Model Component receives the radionuclide mass flux from the bottom of the invert. Time histories of releases from the bottom of the invert into the fractures and matrix beneath the repository are captured in the Engineered_System container. Additional EBS outputs are also captured within this container. These results are used by the TSPA analysts to analyze the performance of the EBS.

The UZ_Transport container includes a call to the FEHM V2.24 DLL, as well as input parameters needed by the FEHM V2.24 DLL and outputs from the calculations done by the FEHM V2.24 DLL. 16 flow fields are calculated using TOUGH2 V1.6. These flow fields represent four infiltration scenarios for each of four climate states. These 16 flow fields are used for calculations made in the UZ_Transport container. The UZ_Transport container contains input parameters such as fracture porosity and matrix diffusion coefficients. The FEHM V2.24 DLL calculates radionuclide release rates from the UZ fractures and matrix to the SZ. The UZ Transport Model Component is discussed in additional detail in Section 6.3.9.

The SZ_Transport container includes outputs from the 3-D SZ Flow and Transport Model Component, consisting of radionuclide breakthrough curves that provide the information needed to perform one-dimensional calculations that account for radionuclide decay and the growth of radionuclide daughter products during transport through the SZ. The SZ_Transport container includes parameter values needed for the three-dimensional and one-dimensional calculations, inputs of radionuclide mass from the UZ, the calculations of radionuclide transport through the SZ, and outputs of radionuclide mass to the biosphere. The 3-D SZ Flow and Transport Model Component is performed using the SZ_Convolute V3.10 DLL. The SZ Flow and Transport Model Component is discussed in additional detail in Section 6.3.10.

The Biosphere container includes information needed to calculate dose to the RMEI, due to the radionuclides released from the repository and transported through the UZ and SZ. The Biosphere container includes BDCFs, groundwater protection conversion factors, and radionuclide mass flux inputs from the SZ. The Biosphere Model Component is discussed in additional detail in Section 6.3.11.

Events—Early failures of the WP and DS and other disruptive event scenarios are addressed in the TSPA-SEIS using distinct scenario classes. The implementation of these scenario classes is integrated into the TSPA-SEIS GoldSim model file, along with the implementation of the Nominal Scenario Class. In general, parameters relating to the event scenarios use separate containers to segregate the Nominal Scenario Class calculations from the Early Failure Scenario Class, the Seismic Scenario Class, the Igneous Scenario Class, and the Human Intrusion Scenario. Similar to the calculations supporting the Nominal Scenario Class, much of the information used for the events scenario classes can be found throughout the TSPA-SEIS GoldSim model file in containers used for calculations for the Nominal Scenario Class.

Within the Epistemic Parameters GoldSim Submodel, the Aleatory Parameters and Dynamic Calculations GoldSim Submodel, and the EBS GoldSim Submodel separate containers hold the input parameter definitions and calculations that are applicable in the event scenarios. An events container is placed alongside the other model component containers in each of these locations. Within this container, inputs and calculations are further segregated into containers for each event type. Performing a GoldSim model run for an event scenario is similar to running the Nominal Scenario Class model file. The TSPA-SEIS has been built using GoldSim selector elements to pass submodel outputs from one submodel to another. The default result for these output elements is the sampled or calculated value for the Nominal Scenario Class. When configured to run an event scenario, these submodel output elements use IF...THEN...ELSE functions to replace or augment a Nominal Scenario Class result with the event-specific calculation result (if appropriate).

Modeling early failure event scearios includes the conditions of early failures of the DSs or WPs. The Early Failure Scenario Class is discussed in detail in Section 6.4. The Drip Shield EF and Waste Package EF Modeling Cases model the performance of the repository following an early failure event. Submodels of the WP and DS Degradation Model Component from the Nominal Scenario Class are augmented with additional processes that are applicable for an early failure event. The Drip Shield EF Modeling Case is discussed in greater detail in Section 6.4.1. The Waste Package EF Modeling Case is discussed in greater detail in Section 6.4.2.

Modeling seismic events includes conditions resulting from seismic ground motion activity and fault displacement. The Seismic Scenario Class modeling cases model the performance of the repository following one or more seismic events. Consequences to the drift, DS, and WP from seismic activity are included. Submodels of the UZ Flow, EBS Environment, WP and DS Degradation Model Components from the Nominal Scenario Class are augmented with additional processes that are applicable for the repository following seismic activity. The Seismic GM Modeling Case and the Seismic FD Modeling Case are discussed in detail in Section 6.6.1. The Seismic Scenario-related containers include the parameters needed to characterize a potential seismic event, and the potential consequences to the drift, WPs, and DSs, including levels of ground motion, rockfall potential, and the potential for fault displacment.

The Igneous Scenario-related containers include information for the Igneous Intrusion Modeling Case. The Igneous Intrusion Modeling Case models the performance of the repository following an igneous intrusion. Submodels of the UZ Flow, EBS Environment, WP and DS Degradation, and WF Degradation and Mobilization Model Components from the Nominal Scenario Class are augmented with additional processes that are applicable after the igneous intrusion. The Igneous Intrusion Modeling Case is discussed in greater detail in Section 6.5.1. The Volcanic Eruption Modeling Case is performed in a separate GoldSim model file and is discussed in detail in Section 6.5.2. However, in general, this model file is organized similar to the TSPA-SEIS, but with less complexity because the modeling case excludes a number of the EBS and groundwater-related model components. The information in this model file, includes parameter inputs for ASHPLUME, as well as the call to the ASHPLUME_DLL_LA V2.1, and the calculations for tephra redistribution and the probabilistic weighting of the source term used to detemine dose.

Modeling a human intrusion event includes groundwater drilling operations that intersect the repository resulting in a breach to a DS and a WP, followed by subsequent radionuclide transport down the borehole and into the SZ. Submodels of the UZ Flow, WP and DS Degradation, EBS Flow and Transport, and UZ Transport Model Components from the Nominal Scenario Class are augmented with additional processes that are applicable for a human intrusion event. The Human Intrusion Modeling Case is discussed in greater detail in Section 6.7.1.

INTENTIONALLY LEFT BLANK

Table 6.1.5-1. Location of Implementation Description in the GoldSim TSPA Model File

Submodel	Documentation Location(s)
Epistemic Parameters GoldSim Submodel	\Epistemic_Uncertainty\Epistemic_Params
Aleatory Parameters and Dynamic Calculations GoldSim Submodel	\Time_Zero\Aleatory_Params
EBS GoldSim Submodel	\Time_Zero\EBS_PS_Loop\EBS_PSE_Loop\EBS_Submodel
Natural System below the Repository	\TSPA_Model
Climate	Epistemic: NA Aleatory: NA EBS: \Global_Inputs_and_Calcs\Global_UZ_Flow\Climate Other: \TSPA_Model\UZ_Flow\Climate
Infiltration	Epistemic: \Input_Params_Epistemic\Epistemic_Params_UZ_Flow\Uncertain_Params_Infiltration Aleatory: NA EBS: \Time_Zero\EBS_PS_Loop\Static_Calcs_PS_Loop\Static_Calcs_UZ_Flow\Infiltration \Global_Inputs_and_Calcs\Global_UZ_Flow\Infiltration
Drift Seepage	Epistemic: \Input_Params_Epistemic\Epistemic_Params_UZ_Flow\Input_Params_Seepage_Uncert \Input_Params_Epistemic\Epistemic_Params_UZ_Flow\Uncertain_Params_Seepage Aleatory: NA EBS: \Time_Zero\EBS_PS_Loop\Static_Calcs_PS_Loop\Static_Calcs_UZ_Flow\Drift_Seepage \Global_Inputs_and_Calcs\Global_UZ_Flow\Drift_Seepage
Drift Wall Condensation	Epistemic: \Input_Params_Epistemic\Epistemic_Params_UZ_Flow\Uncertain_Params_DWC Aleatory: NA EBS: \Global_Inputs_and_Calcs\Global_UZ_Flow\Drift_Wall_Condensation
EBS TH Environment	Epistemic: \Input_Params_Epistemic\Epistemic_Params_EBS_Environ\Uncertain_Params_TH Aleatory: NA EBS: \Global_Inputs_and_Calcs\Global_EBS_Environ\EBS_Environment\ThermoHydrology

Table 6.1.5-1. Location of Implementation Description in the GoldSim TSPA Model File (Continued)

Submodel	Documentation Location(s)
WP and DS Degradation	Epistemic: \Input_Params_Epistemic\Epistemic_Params_WP_DS_Deg\ Aleatory: \Model_Calcs_Aleatory\Aleatory_Calcs_WP_DS_Deg EBS: \Time_Zero\EBS_PS_Loop\Static_Calcs_PS_Loop\Static_Calcs_WP_DS_Deg \Global_Inputs_and_Calcs\Global_WP_DS_Deg\Global_IWPD
Localized Corrosion	Epistemic: \Input_Params_Epistemic\Epistemic_Params_WP_DS_Deg\ Aleatory: NA EBS: \Time_Zero\EBS_PS_Loop\Static_Calcs_PS_Loop\Static_Calcs_WP_DS_Deg \Global_Inputs_and_Calcs\Global_WP_DS_Deg\Global_LC
Radionuclide Inventory	Epistemic: \Input_Params_Epistemic\Epistemic_Params_WF_Deg_Mob\Uncertain_Params_RN_Inventory Aleatory: NA EBS: \Global_Inputs_and_Calcs\Global_WF_Deg_Mob\RN_Inventory
In-Package Chemistry	Epistemic: \Input_Params_Epistemic\Epistemic_Params_WF_Deg_Mob\Uncertain_Params_InPkg_Chem Aleatory: NA EBS: \Global_Inputs_and_Calcs\Global_WF_Deg_Mob\In_Package_Chemistry
Waste Form Degradation	Epistemic: \Input_Params_Epistemic\Epistemic_Params_WF_Deg_Mob\Uncertain_Params_CSNF_WF Aleatory: NA EBS: \Global_Inputs_and_Calcs\Global_WF_Deg_Mob\WF_Degradation\CSNF_WF_Dissolution
	Epistemic: \Input_Params_Epistemic\Epistemic_Params_WF_Deg_Mob\Uncertain_Params_HLW_WF Aleatory: NA EBS: \Global_Inputs_and_Calcs\Global_WF_Deg_Mob\WF_Degradation\Input_Params_HLW_WF
	Epistemic: NA Aleatory: NA EBS: \Global_Inputs_and_Calcs\Global_WF_Deg_Mob\WF_Degradation\Input_Params_DSNF_WF

Table 6.1.5-1. Location of Implementation Description in the GoldSim TSPA Model File (Continued)

Submodel	Documentation Location(s)
Cladding Degradation	Epistemic: NA Aleatory: NA EBS: \Global_Inputs_and_Calcs\Global_WF_Deg_Mob\Clad_Degradation
EBS Chemical Environment	Epistemic: \Input_Params_Epistemic\Epistemic_Params_EBS_Environ\Uncertain_Params_EBS_CE Aleatory: \Input_Params_Aleatory\Input_Params_EBS_Environ\Input_Params_EBS_CE EBS: \Global_Inputs_and_Calcs\Global_EBS_Environ\EBS_Environment\EBS_Chemical_Environment
Dissolved Concentration Limits	Epistemic: \Input_Params_Epistemic\Epistemic_Params_WF_Deg_Mob\Uncertain_Params_Solubility Aleatory: NA EBS: \Global_Inputs_and_Calcs\Global_WF_Deg_Mob\Global_Solubility
EBS Colloids	Epistemic: \Input_Params_Epistemic\Epistemic_Params_EBS_F_and_T\Uncertain_Params_Colloids Aleatory: NA EBS: \Global_Inputs_and_Calcs\Global_EBS_F_and_T\Model_Input_EBS_Transport\Input_Params_Colloids
EBS Flow	Epistemic: \Input_Params_Epistemic\Epistemic_Params_EBS_F_and_T\Uncertain_Params_Flux_Split Aleatory: NA EBS: \Time_Zero\EBS_PS_Loop\Static_Calcs_PS_Loop\Static_Calcs_EBS_F_and_T\EBS_Flow \Global_Inputs_and_Calcs\Global_EBS_F_and_T\Model_Feeds_EBS_Flow
EBS Transport	Epistemic: \Input_Params_Epistemic\Epistemic_Params_EBS_F_and_T Aleatory: NA EBS: \Global_Inputs_and_Calcs\Global_EBS_F_and_T\Model_Input_EBS_Transport
EBS-UZ Interface	Epistemic: \Input_Params_Epistemic\Epistemic_Params_EBS_F_and_T\Uncertain_Params_EBS_UZ_Trans Aleatory: NA EBS: \Global_Inputs_and_Calcs\Global_EBS_F_and_T\EBS_UZ_Transport_Inputs

Table 6.1.5-1. Location of Implementation Description in the GoldSim TSPA Model File (Continued)

Submodel	Documentation Location(s)
UZ Transport	Epistemic: \Input_Params_Epistemic\Epistemic_Params_UZ_Transport Aleatory: NA Other: \TSPA_Model\UZ_Transport
SZ Flow and Transport	Epistemic: \Input_Params_Epistemic\Epistemic_Params_SZ_Transport Aleatory: NA Other: \TSPA_Model\SZ_Transport
Biosphere	Epistemic: \Input_Params_Epistemic\Epistemic_Params_Biosphere Aleatory: NA Other: \TSPA_Model\Biosphere
Early Failure Scenario Class	Epistemic: \Input_Params_Epistemic\Epistemic_Params_Events\Epistemic_Parameters_EF Aleatory: \Input_Params_Aleatory\Aleatory_Params_Events\Aleatory_Params_EF EBS: \Time_Zero\EBS_PS_Loop\Static_Calcs_PS_Loop\Static_Calcs_Events\Static_Calcs_EF \Global_Inputs_and_Calcs\Global_Events\Global_EF
Igneous Scenario Class	Epistemic: \Input_Params_Epistemic\Epistemic_Params_Events\Epistemic_Params_Igneous_Intr Aleatory: \Input_Params_Aleatory\Aleatory_Params_Events\Aleatory_Params_Igneous_Intr EBS: \Time_Zero\EBS_PS_Loop\Static_Calcs_PS_Loop\Static_Calcs_Events\Igneous_Intrusion \Global_Inputs_and_Calcs\Global_Events\Igneous_Scenario
	Epistemic: Aleatory: EBS:
Seismic Scenario Class	Epistemic: \Input_Params_Epistemic\Epistemic_Params_Events\Epistemic_Params_Seismic Aleatory: \Input_Params_Aleatory\Aleatory_Params_Events\Input_Params_Seismic_Uncert \Input_Params_Aleatory\Aleatory_Params_Events\Input_Params_Seismic_FD_Uncert EBS: \Time_Zero\EBS_PS_Loop\Static_Calcs_PS_Loop\Static_Calcs_Events\Seismic_Fault_Displacement \Global_Inputs_and_Calcs\Global_Events\Seismic_Scenario

Table 6.1.5-1. Location of Implementation Description in the GoldSim TSPA Model File (Continued)

Submodel	Documentation Location(s)
Human Intrusion Scenario	Epistemic: NA Aleatory: \Input_Params_Aleatory\Aleatory_Params_Events\Aleatory_Params_HI EBS: \Time_Zero\EBS_PS_Loop\Static_Calcs_PS_Loop\Static_Calcs_Events\Human_Intrusion_Events \Global_Inputs_and_Calcs\Global_Events\Human_Intrusion Other: \TSPA_Model\UZ_Transport\UZ_Transport_Calculations\HI_Borehole_Transport

INTENTIONALLY LEFT BLANK

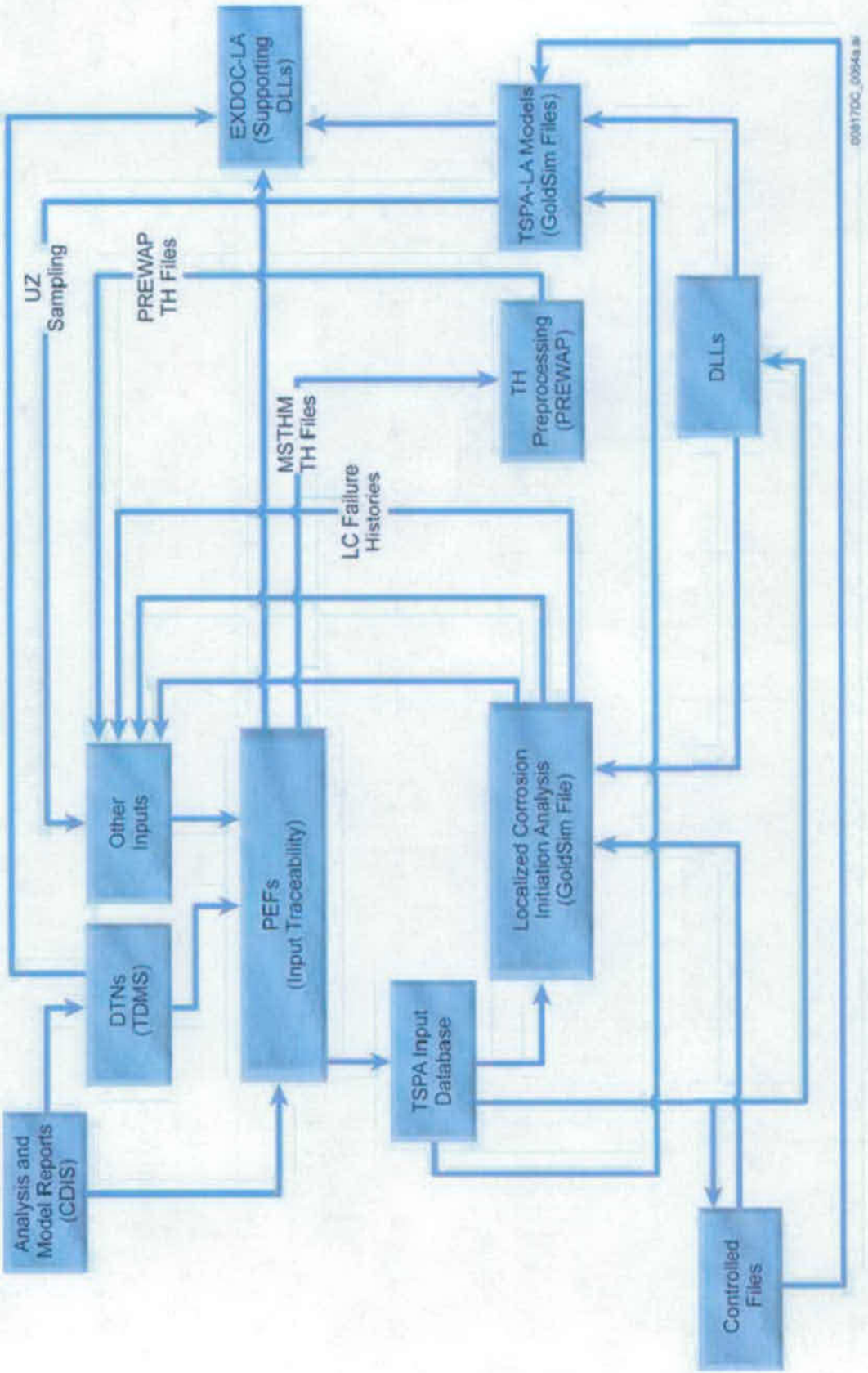

Figure 6.1.5-1. Illustrated Overview of all the Various Elements that Make Up the Framework for Initializing and Running the TSPA-SEIS

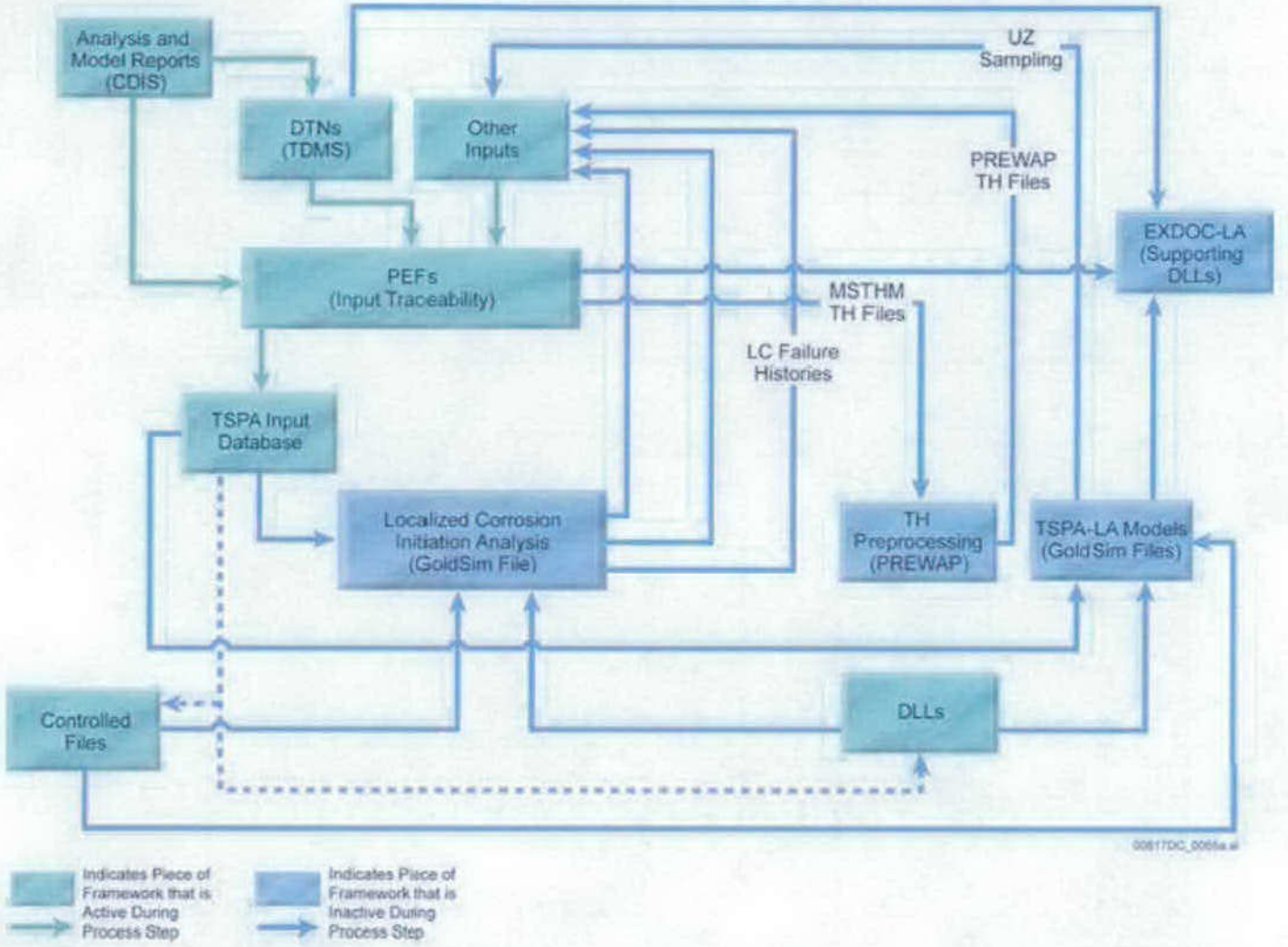

NOTE: Dashed lines indicate cases where location of files and software are stored in the TSPA Input Database, but the information is actually accessed from the TSPA-SEIS file server.

Figure 6.1.5-2. Illustration Depicting Elements Required for Loading of Initial Parameter Values and Dynamically Linked Libraries for the TSPA-SEIS

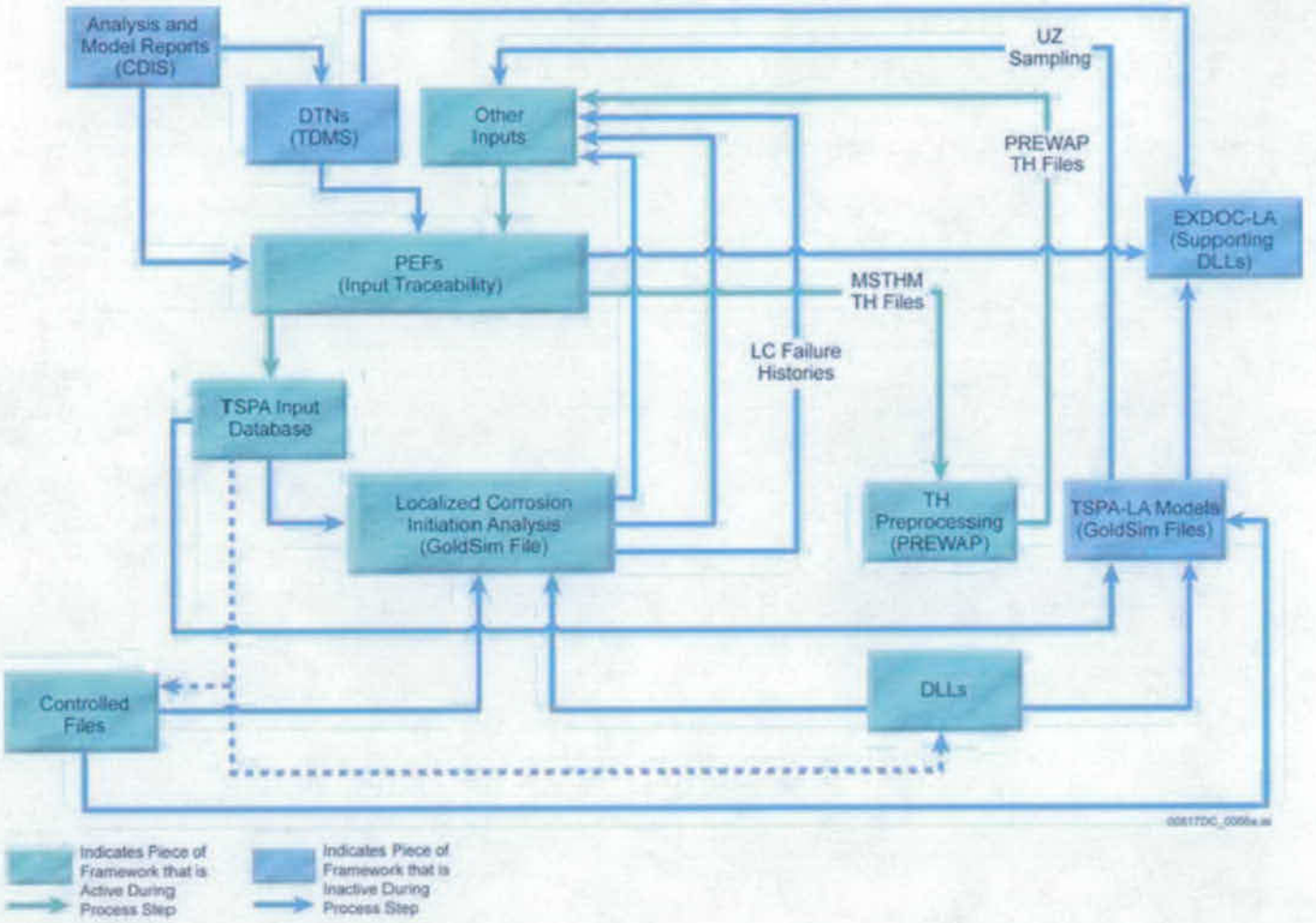

NOTE: Dashed lines indicate cases where location of files and software are stored in the TSPA Input Database, but the information is actually accessed from the TSPA-SEIS file server.

Figure 6.1.5-3. Illustration Depicting Elements Active When Information from the Multiscale Thermohydrologic Model is Preprocessed by PREWAP_LA

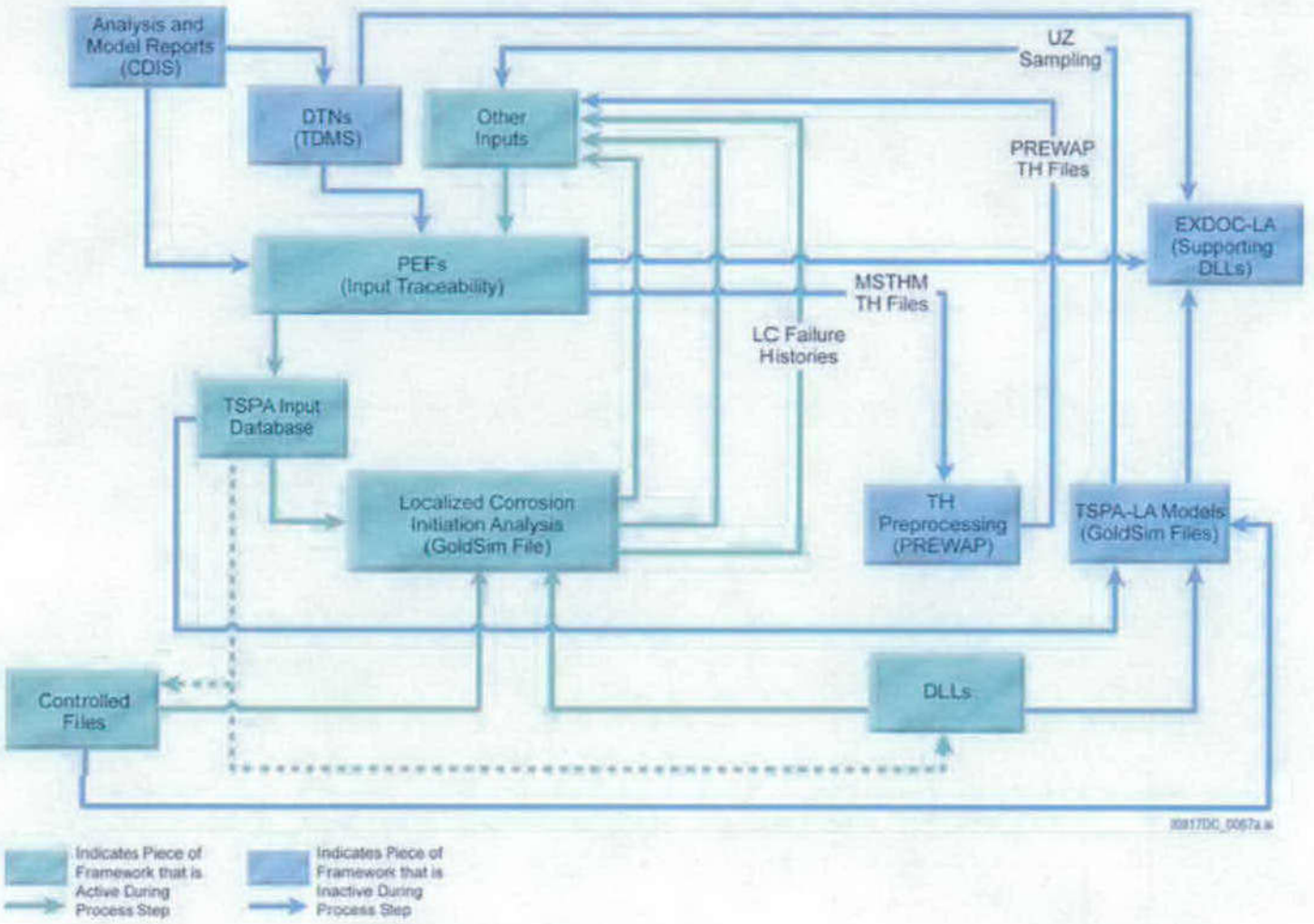

NOTE: Dashed lines indicate cases where location of files and software are stored in the TSPA Input Database, but the information is actually accessed from the TSPA-SEIS file server.

Figure 6.1.5-4. Illustration Depicting Elements Active When Preprocessing for the Localized Corrosion Initiation Analysis

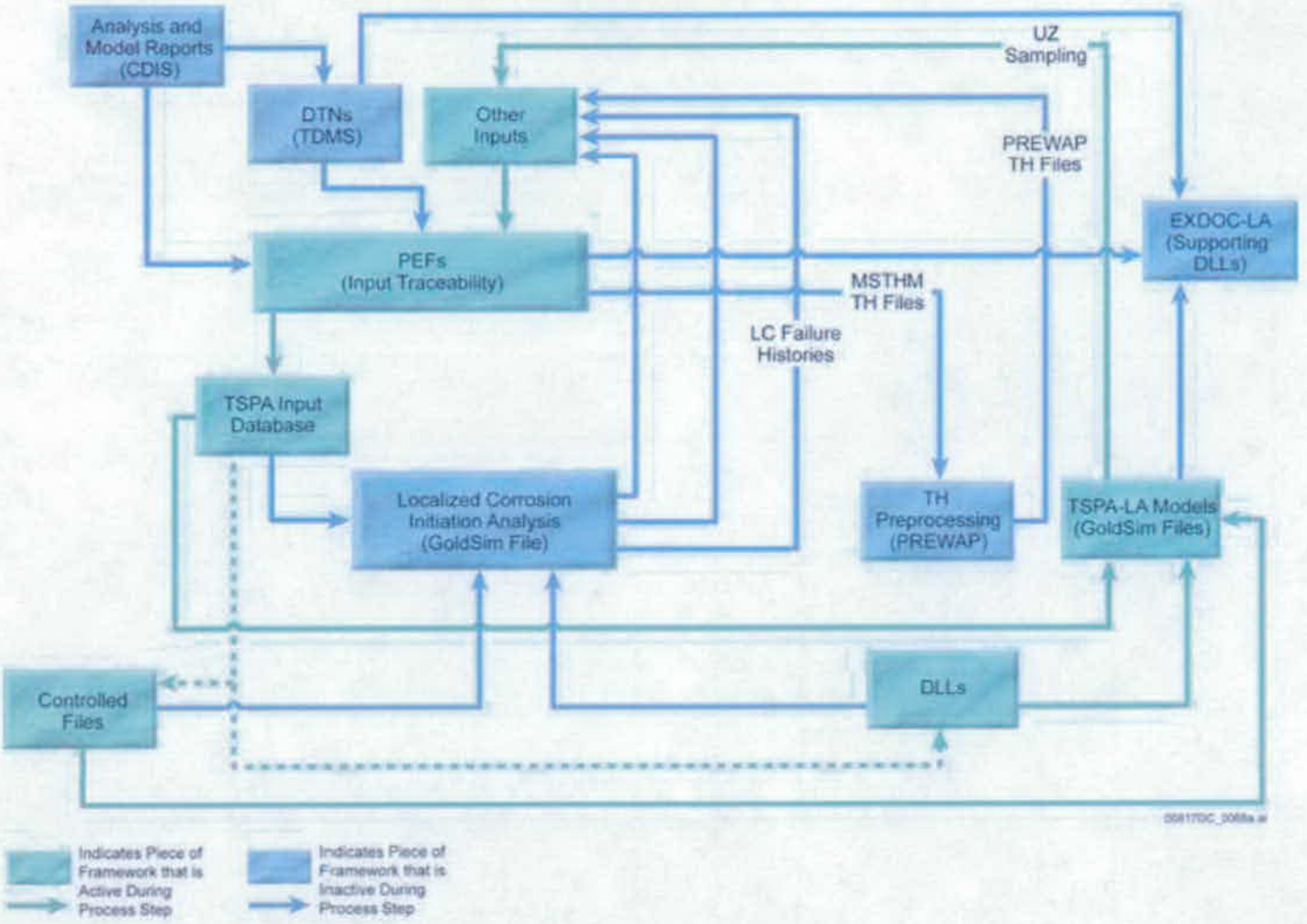

NOTE: Dashed lines indicate cases where location of files and software are stored in the TSPA Input Database, but the information is actually accessed from the TSPA-SEIS file server.

Figure 6.1.5-5. Illustration Depicting Elements Active when Sampling of Uncertain Unsaturated Zone Parameters and Generation of Input Files

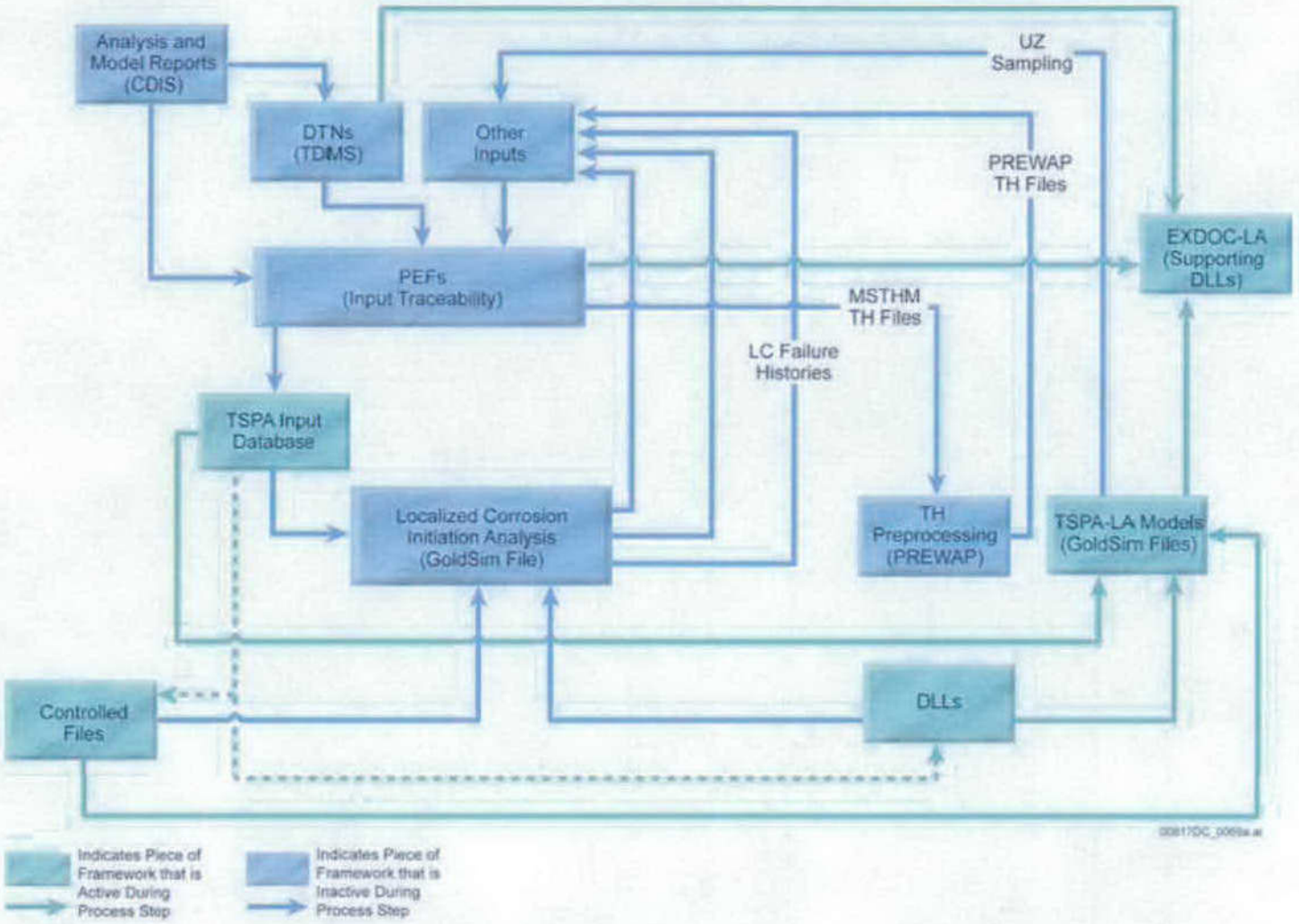

NOTE: Dashed lines indicate cases where location of files and software are stored in the TSPA Input Database, but the information is actually accessed from the TSPA-SEIS file server.

Figure 6.1.5-6. Illustration Depicting Elements Active in the Execution of the TSPA-SEIS GoldSim Model File and the TSPA-SEIS Volcanic Eruption GoldSim Model File

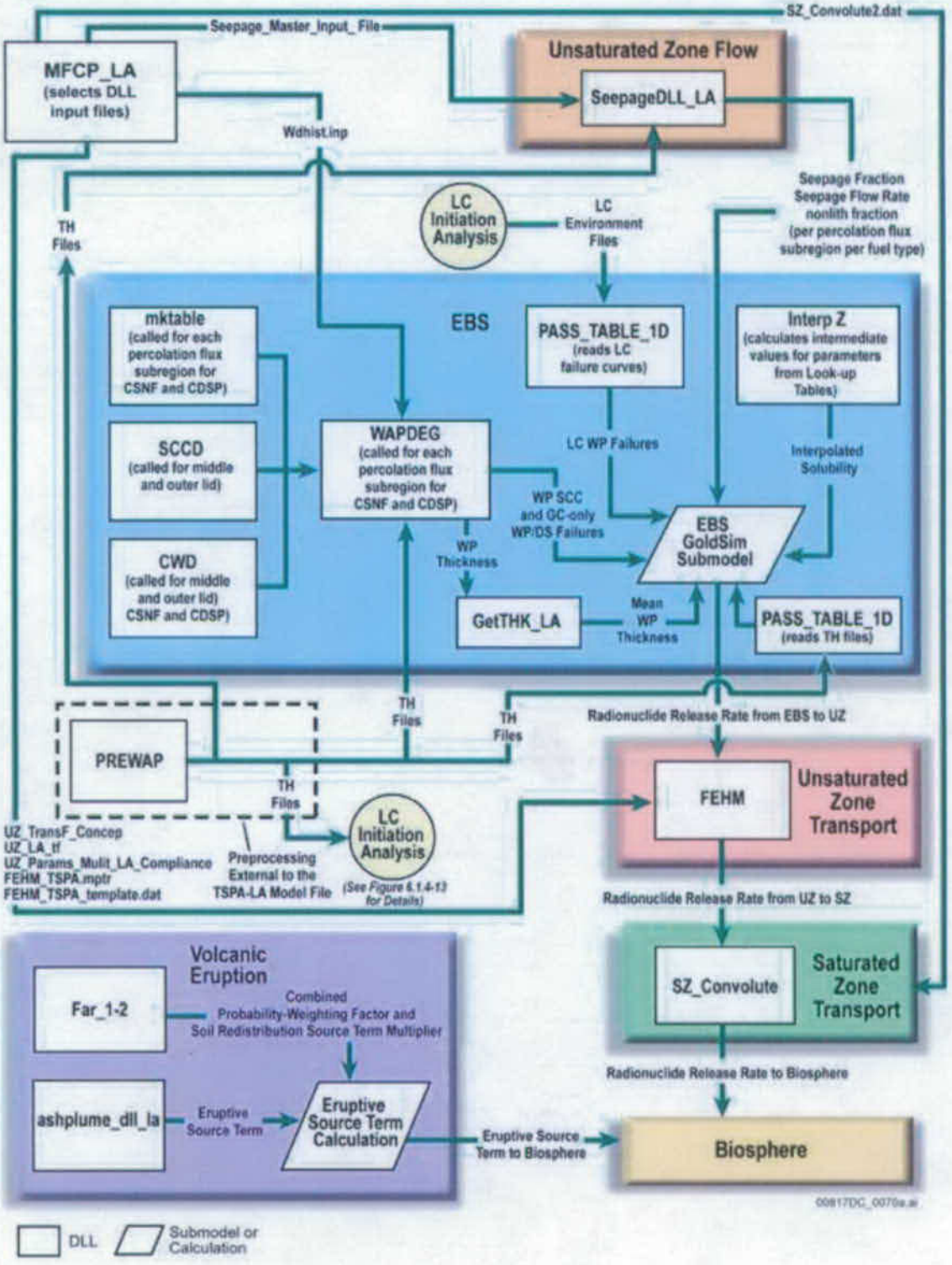

Figure 6.1.5-7. TSPA-SEIS Software Configuration Illustrating Software Run with GoldSim

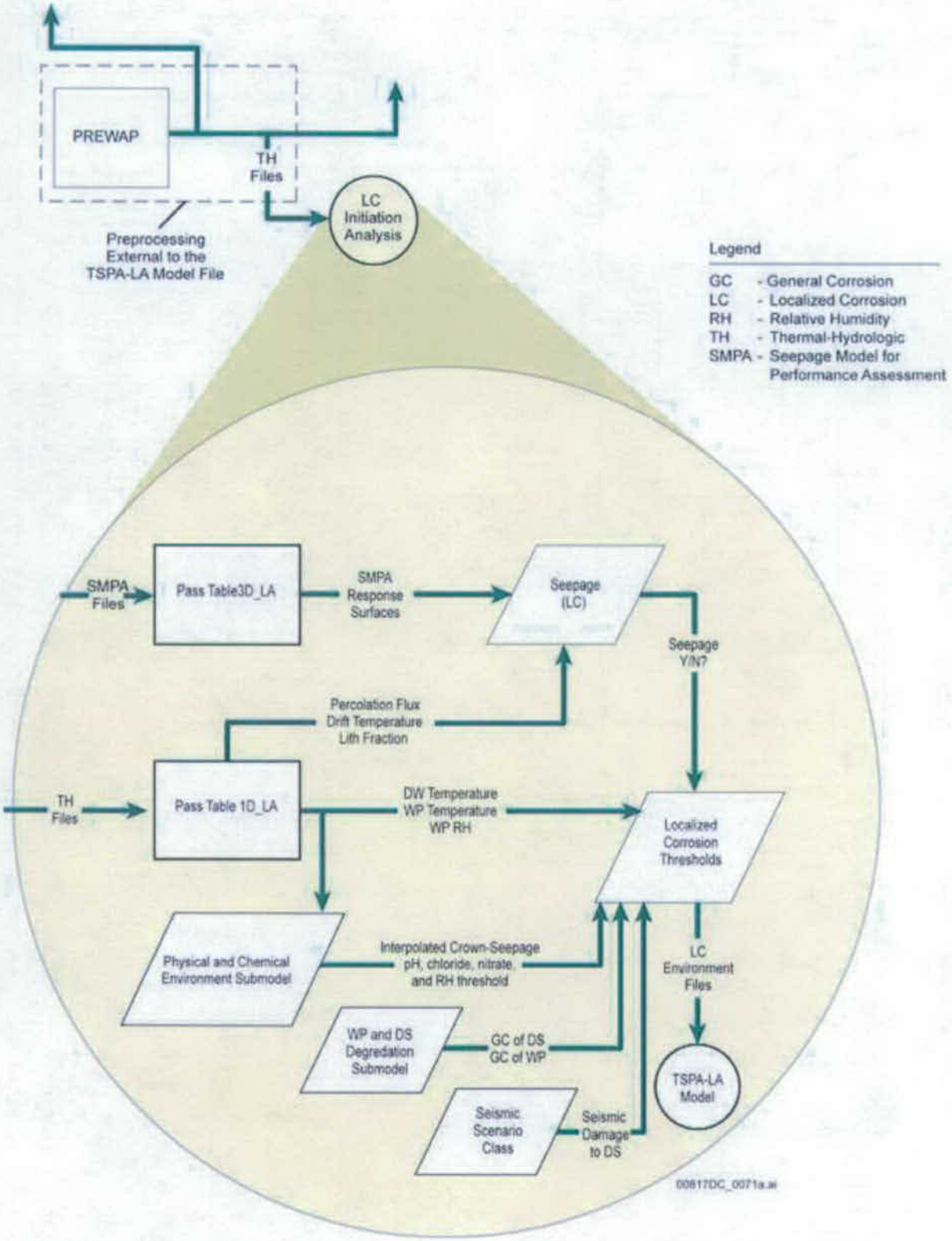

Figure 6.1.5-8. Details of the Software Configuration for the Localized Corrosion Initiation Analysis

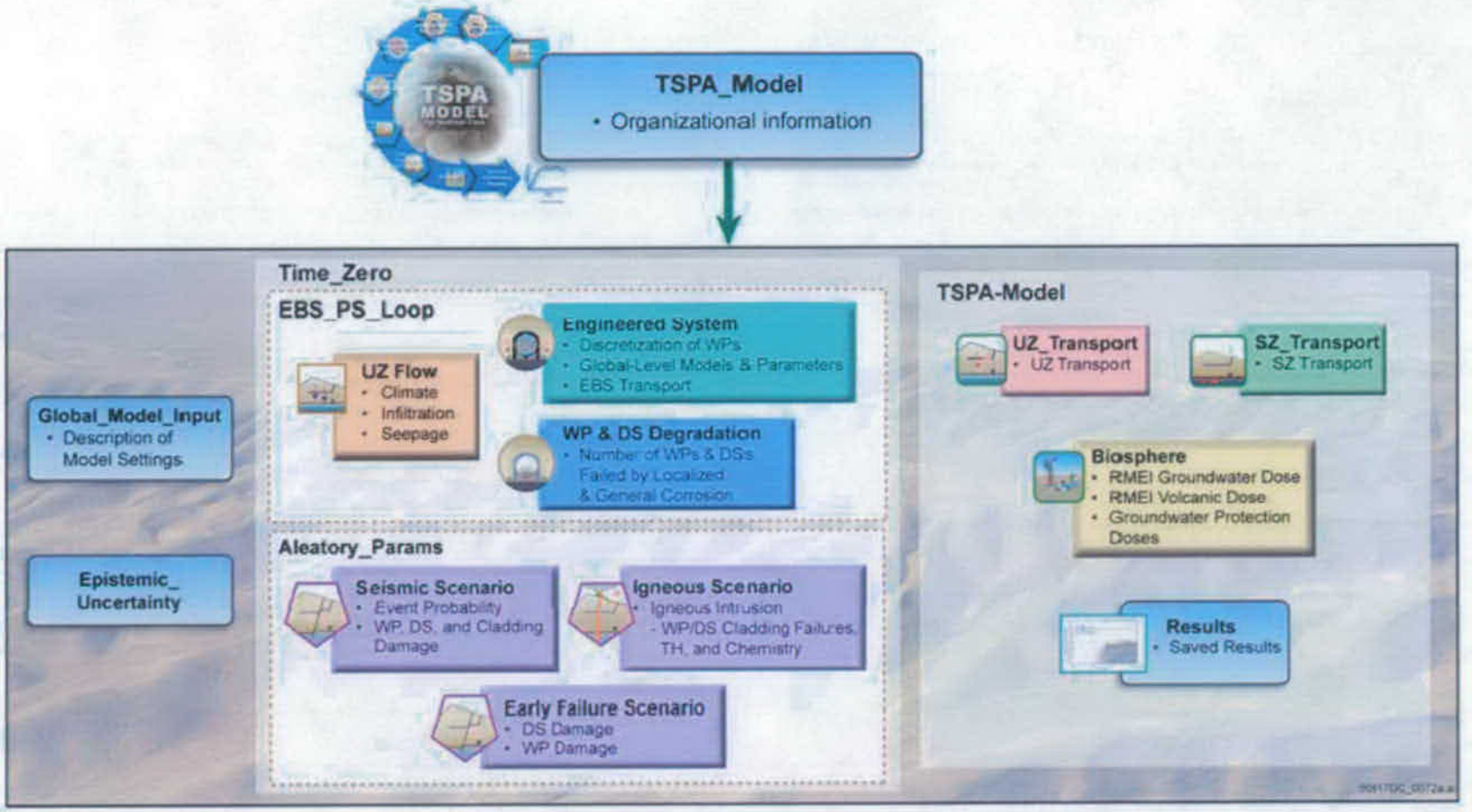

Figure 6.1.5-9. Layout of Calculation Containers that Define the Highest Level of Organization of the TSPA-SEIS File

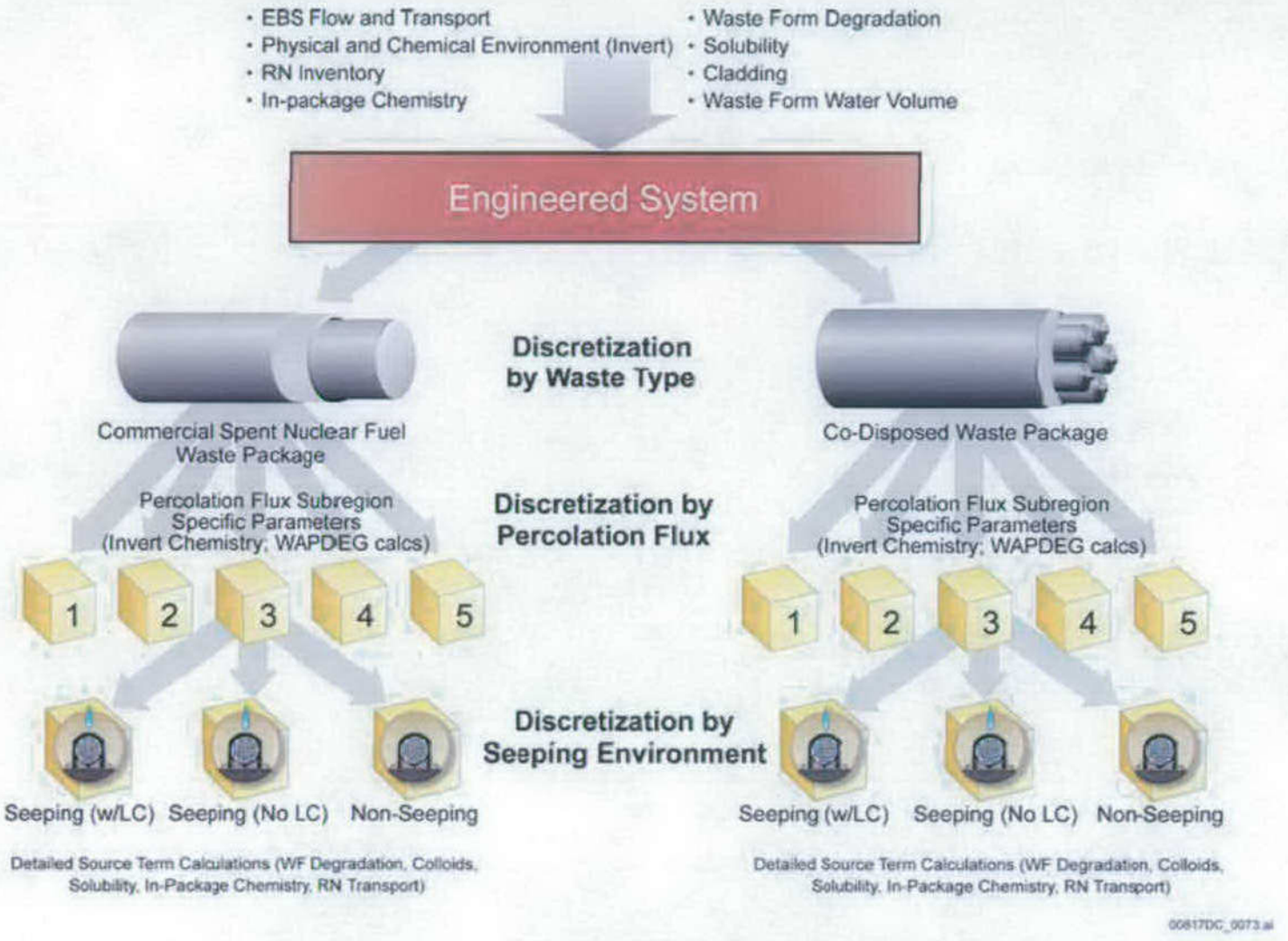

Figure 6.1.5-10. Levels of Discretization of Engineered System Representation in the TSPA-SEIS File

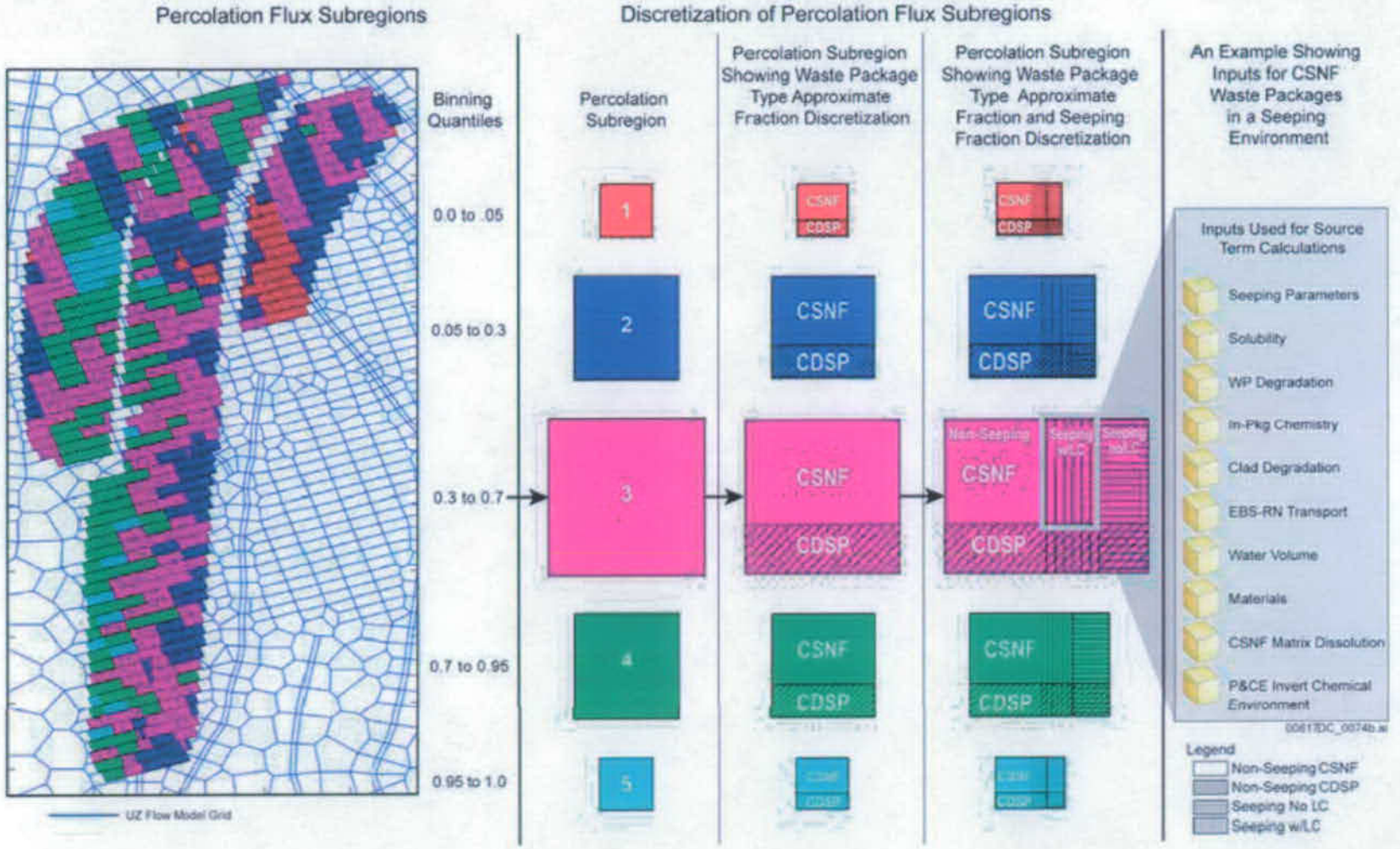

NOTE: The early failure packages are randomly set in one of the five repository percolation subregions at the start of a realization.

Figure 6.1.5-11. Schematic of the Five Repository Percolation Subregions Showing the Implementation of the Levels of Discretization Shown on Figure 6.1.5-10

INTENTIONALLY LEFT BLANK

6.2 ALTERNATIVE CONCEPTUAL MODELS

Alternative conceptual models (ACMs) are a means to specifically acknowledge model form uncertainty. An ACM is a set of working hypotheses and assumptions that provide an acceptable description of a system for the intended purpose. The hypotheses and assumptions must be logically consistent with one another, in agreement with existing information, able to predict system behavior, and able to be tested. In 10 CFR 63.114(c) [DIRS 178394], the NRC specifically requires the DOE to, "Consider alternative conceptual models of features and processes that are consistent with available data and current scientific understanding and evaluate the effects that alternative conceptual models have on the performance of the geologic repository."

A model that is evaluated and chosen to represent a system is called the base-case model. Any remaining models that meet the above criteria are then designated ACMs for the system.

General Consideration of Alternative Conceptual Models

As suggested by the statements in 10 CFR 63.114(c) [DIRS 178394], a conceptual model can be truly alternative only if it meets the following criteria:

- It must differ significantly from the initial (or base-case) conceptual model.
- It must be consistent with available data and current scientific understanding.
- It must be reasonable (i.e., there is a reasonable physical basis for the alternative).

The ACMs in all model components, submodels, and process models that provide inputs to the TSPA-SEIS were considered according to a process that included the identification, screening, and evaluation of potential ACMs as part of the analysis documented in the model reports that feed the TSPA-SEIS. Reasonable and technically defensible conservatism at the subsystem level has been used to select the best ACM to use rather than quantitatively propagate multiple ACMs to the TSPA-SEIS. Generally, additional uncertainty is incorporated into the selected conceptual model if more than one ACM is deemed appropriate for use rather than considering multiple ACMs in the TSPA-SEIS. If an ACM appears to be significant at the subsystem level, an appropriate abstraction is developed for that ACM for consideration within the TSPA-SEIS provides a single- and dual-continuum invert model). The result of the process is documented within the individual analysis and/or model reports. It is important to note that treatment of ACMs within the individual analysis and/or model reports may differ significantly to be consistent with available data and current scientific understanding. For instance, some ACMs may be assessed qualitatively with the conclusion that the ACM is captured by the selected conceptual model abstraction recommended for use in the TSPA-SEIS. Whereas, in another case, a more detailed computational analysis may be needed to assess the ACM, resulting in additional uncertainty or other modification to the selected conceptual model abstraction used in the TSPA-SEIS. ACMs that were identified and evaluated in model components, submodels, process models, and analysis and/or model reports supporting the TSPA-SEIS are summarized in Table 6.2-1 and Sections 6.3, 6.4, 6.5, 6.6, and 6.7. Each model component and submodel discussion includes a summary evaluation of ACMs.

An important reason for considering ACMs at the subsystem level is to help build confidence that plausible changes in modeling assumptions or simplifications will not change conclusions regarding the subsystem and subsequently the total system performance. Consideration and treatment of ACMs used to support the TSPA-SEIS is demonstrated through a stepwise process including subsystem-level impact evaluations and analyses presented in the process level analysis model reports. Important differences demonstrated at the subsystem level are evaluated through TSPA-SEIS sensitivity and regression analyses. Section 6.3 summarizes the general consideration and treatment of ACMs used to support the TSPA-SEIS in each submodel area.

Table 6.2-1. Table of Alternative Conceptual Models

Alternative Conceptual Models	Key Assumptions	Assessment and Basis
Unsaturated Zone Flow Model Component (Section 6.3.1)		
Site Scale UZ Flow Models	The *UZ Flow Models and Submodels report* (SNL 2007 [DIRS 175177]) includes investigation of alternative modeling approaches. Alternative approaches include climate and climate-related changes (Section 6.1.4 and throughout the report), PTn damping effect on transient infiltration pulses (Section 6.9), and water table rise (Section 7.8).	
Drift Seepage: Flow Through Discrete Fractures	ACM that simulates flow through discrete fractures rather than through a stochastic continuum (SNL 2007 [DIRS 181244], Section 6.4).	It was concluded that conceptual model uncertainty is small compared to other sources of uncertainty that are explicitly accounted for by the base case conceptual model, its numerical implementation, and the associated uncertainty estimates that are propagated through the TSPA-SEIS (SNL 2007 [DIRS 181244], Section 6.4).
Drift Seepage: Episodic-Preferential Flow in Superheated Rock	The effectiveness of the vaporization barrier was examined with an ACM representing water flow into a superheated rock environment (SNL 2007 [DIRS 181244], Section 6.4.3.2). In this ACM, the thermally perturbed downward flux from the condensation zone toward the superheated rock zone is conceptualized to form episodic preferential-flow patterns.	It was concluded that results of the ACM are reasonably consistent with the thermal seepage process-model results used for this abstraction (SNL 2007 [DIRS 181244], Section 6.4.3).
Drift-Wall Condensation: Thermal Conductivity/Heat Transfer	In the Thermal Conductivity/Heat Transfer ACM, the air phase is treated as a solid material (SNL 2007 [DIRS 181648], Section 6.1.4).	This ACM is essentially accounted for in the MSTHM Abstraction (SNL 2007 [DIRS 181244]).
Drift-Wall Condensation: CFD Simulation for Drift Condensation Processes	ACM simulates the drift with a CFD code and the surrounding rock with porous media code. The CFD code FLUENT (Software Code: FLUENT. V6.0.12 (Fluent, Inc. [DIRS 164315]) contains limited porous media capabilities that only considers single-phase flow. (SNL 2007 [DIRS 181648], Section 6.1.4).	Conduction-only heat transfer in the surrounding rock and the invert is acceptable, and this ACM is not considered further (SNL 2007 [DIRS 181648], Section 6.1.4).

Table 6.2-1. Table of Alternative Conceptual Models (Continued)

Alternative Conceptual Models	Key Assumptions	Assessment and Basis
EBS Environment Model Component (Section 6.3.2 & 6.3.4)		
Lawrence Berkeley National Laboratory Mountain-Scale UZ Model	An ACM to the MSTHM Process Model is a mountain-scale TH model developed by Lawrence Berkeley National Laboratory (Haukwa et al. 1998 [DIRS 117826]). The Lawrence Berkeley National Laboratory model is a monolithic TH model. The Lawrence Berkeley National Laboratory TH model used: (1) coarser grid discretization at the drift scale than the MSTHM Process Model; (2) a line-averaged approximation of the heat-generation-rate-versus-time table (whereas the MSTHM Process Model represented the WPs as discrete heat sources); and (3) a lumped heat source that filled the entire cross section of the emplacement drift (SNL 2007 [DIRS 181383], Section 6.4)	Given the differences between the MSTHM Process Model and the east-west cross-sectional Lawrence Berkeley National Laboratory mountain-scale model, the agreement between the two models is adequate (SNL 2007 [DIRS 181383], Section 6.4). Moreover, the differences in predicted temperatures between the MSTHM Process Model and the east-west cross-sectional Lawrence Berkeley National Laboratory mountain-scale model are within the range of temperature differences resulting from parametric uncertainty (SNL 2007 [DIRS 181383], Tables 6.3-30 and 6.3-31).
WP & DS Degradation Model Component (Section 6.3.5)		
Parabolic GC Rate Law for DS Degradation (SNL 2007 [DIRS 180778], Section 6.5.6)	Assumes that the increasing oxide layer thickness on diffusion of oxidizing species to the underlying metal will have an inhibiting effect on corrosion.	Model is less conservative than the primary model.
Decreasing GC Rate Law for WP Degradation (SNL 2007 [DIRS 178519], Section 6.4.3.5.1)	GC rates of metals and alloys tend to decrease with time.	The time-dependent GC behavior of the WP was not included in the TSPA-SEIS because the constant (time-independent) rate model (for a given temperature) is more conservative and bounds the GC behavior of the WP outer shell over the repository time period.

Table 6.2-1. Table of Alternative Conceptual Models (Continued)

Alternative Conceptual Models	Key Assumptions	Assessment and Basis
Crevice-Adjusted GC Rate Law for WP Degradation (SNL 2007 [DIRS 178519], Section 6.4.3.5.2)	A crevice-adjusted rate law was developed by assuming that the corrosion rate of the boldly exposed (non-crevice) area of the crevice samples could be represented by the average corrosion rate of the plain weight-loss samples. The corrosion rate for the crevice-area-only (under the crevice former) was calculated by subtracting the effect of the non-crevice area on the crevice samples.	The resulting corrosion rate was found to be much higher than either of the rates derived from the entire crevice samples or the plain weight loss samples. Because the calculated corrosion rates of the crevice area under the crevice former were so much higher than those of the boldly exposed area of the crevice samples, microscopic examinations should have been able to show the differences in the corrosion fronts between the two areas (or at least at the edge of the area under the crevice former). However, examinations by optical microscopy and SEM did not reveal such differences. Since the cause of the higher corrosion rate for the crevice-area-only calculation remained unexplained, it was recommended that this not be included in the WP GC Abstraction.
Critical Temperature-Based Localized Corrosion Initiation Model (SNL 2007 [DIRS 178519], Section 6.4.4.8.1)	The evolution of WP temperature with time, coupled with knowledge of the critical temperature for the initiation of LC, (pitting/crevice corrosion) can be used to determine when LC initiates.	Test conditions at which the required critical temperatures have been measured are not directly relevant to the potential environments on the WP surface. The model does not account for the effects of electrochemical characteristics of the solution contacting the metal.
Coupled Environment Fracture Model for SCC Growth Rate (SNL 2007 [DIRS 181953], Section 6.4.6)	The model, based on charge conservation, incorporates the effects of oxygen concentration, flow rate, and the conductivity of the external environment, as well as accounting for the effect of stress on crack growth.	Model underestimates the crack growth rate, as compared to the slip dissolution/film rupture model, when both models were applied to predict the crack growth rate.
LC Penetration as a Time-Dependent Growth Law (SNL 2007 [DIRS 178519], Section 6.4.4.8.2)	The overall rate of LC is controlled by the rate of surface complexation reactions. Once initiated, the crevice corrosion penetration rate would decrease with increasing depth.	Data needed to apply the model can only be estimated approximately from open literature. The time-independent constant penetration rate model is more conservative.
Passive Film Breakdown Potential for Determination of Critical Potential (SNL 2007 [DIRS 178519], Section 6.4.4.1)	An alternative technique for the determination of critical potential would be to use the passive film breakdown potential (obtained from the forward scan of the cyclic potentiodynamic polarization tests).	This criterion would not account for the (often slow) kinetics of LC initiation and may not be appropriate for modeling the long time periods involved in repository environments. Furthermore, the breakdown potential is likely to be much higher when the passive film has been formed over long time periods, allowing for a decrease in the film defect density.

Table 6.2-1. Table of Alternative Conceptual Models (Continued)

Alternative Conceptual Models	Key Assumptions	Assessment and Basis
Waste Form Degradation and Mobilization Model Component (Section 6.3.7)		
Alternative Conceptual Model I	The WP is compositionally discrete.	The WVC model showed that the resulting chemical effects of individual WP components were comparable to that of their ensembles. See Section 6.5.1 in *In-Package Chemistry Abstraction* (SNL 2007 [DIRS 180506]).
Alternative Conceptual Model II	The composition of seepage entering a WP is likely to vary as a function of changing conditions in the UZ and drift environments.	The SDM model showed that wide compositional ranges in the seepage composition had very little influence on the resulting in-package chemistry. See Section 6.5.2 in *In-Package Chemistry Abstraction* (SNL 2007 [DIRS 180506]).
TSPA-SR Initial Cladding Failures	Addresses various causes of fuel failure (SNL 2007 [DIRS 180616], Table 6-5).	Similar results to the current cladding degradation analysis (SNL 2007 [DIRS 180616], Table 6-5).
Stainless-Steel-Clad Fuel Evenly Distributed	Stainless-steel-clad fuel evenly distributed in all WPs (SNL 2007 [DIRS 180616], Table 6-5).	Even distribution unlikely. Not conservative (SNL 2007 [DIRS 180616], Table 6-5).
Splitting—Dry Oxidation	UO_2 forms U_3O_8 (SNL 2007 [DIRS 180616], Table 6-5).	Unlikely, because it requires low humidity, high temperatures, and produces instant splitting, as in the current cladding degradation analysis (SNL 2007 [DIRS 180616], Table 6-5).
Electrochemical	The anodic Tafel lines can be extrapolated to the corrosion potential. The long-term corrosion behavior of spent nuclear fuel is similar to that of unirradiated UO_2. Differences between the corrosion behavior of spent nuclear fuel and unirradiated UO_2 are due to water radiolysis (BSC 2004 [DIRS 169987]).	Do not incorporate into the TSPA-SEIS; data needed to apply the model can only be estimated. Use for Nominal Scenario Class model validation–particularly for validation of long-term extrapolation (BSC 2004 [DIRS 169987]).
Surface Complexation Model	The overall rate of CSNF corrosion is controlled by the rate of surface complexation reactions. The long-term corrosion behavior of spent nuclear fuel is similar to that of unirradiated UO_2 (BSC 2004 [DIRS 169987]).	Do not incorporate into TSPA-SEIS; data needed to apply the model can only be estimated from open literature. Use for Nominal Scenario Class model validation–particularly for validation of long-term extrapolation (BSC 2004 [DIRS 169987]).
Diffusion-Controlled Release	Release rate of radionuclides determined by solid-state diffusion rates (BSC 2004 [DIRS 169988], Table 6-2).	Not incorporated into TSPA-SEIS. Not supported by data for waste glasses (BSC 2004 [DIRS 169988], Table 6-2).

Table 6.2-1. Table of Alternative Conceptual Models (Continued)

Alternative Conceptual Models	Key Assumptions	Assessment and Basis
Composition-Independent Effective Rate Constant	Intrinsic rate constants vary over a small interval for different compositions and the very low flow rates in the repository compared to those used in the laboratory mean that the affinity term will be low (BSC 2004 [DIRS 169988], Table 6-2).	Not incorporated into TSPA-SEIS. Current approach provides a much more robust range of values for use in the TSPA-SEIS (BSC 2004 [DIRS 169988], Table 6-2).
Plutonium	The theoretical fO_2 model. fO_2 = 0.2 bars (SNL 2007 [DIRS 177418]).	The results of this model differ significantly from experimental measurements (SNL 2007 [DIRS 177418]).
	The empirical Eh model. Eh = 1.04 – 0.0592*pH (SNL 2007 [DIRS 177418]).	The results of this model are lower than experimental results (SNL 2007 [DIRS 177418]).
Neptunium	Neptunium incorporation into uranyl secondary phases. eptunium concentration controlled by solid solution rather than by pure phases (SNL 2007 [DIRS 177418]).	Experimental studies on whether schoepite, the critical secondary uranyl phase, can incorporate sufficient neptunium and immobilize it during spent nuclear fuel corrosion do not provide a solid basis for recommending this model for use in the TSPA-SEIS (SNL 2007 [DIRS 177418]).
Thorium	Solubility control by other thorium phases included in thermodynamic modeling database including ThO_2 (thorianite), $Th_{0.75}PO_4$, $Th(SO_4)_2$, ThF_4, $ThF_4 \cdot 2H_2O$. Solubility of thermodynamically most-stable phase controls concentrations (SNL 2007 [DIRS 177418]).	Solubilities calculated with ThO_2(am) are most consistent with measured thorium solubility in pure water. Other phases may be less soluble only under certain conditions or may be based on questionable data. More soluble ThO_2(am) was chosen for conservatism (SNL 2007 [DIRS 177418]).
Americium	Solubility control by phase with properties between $Am(OH)_3$(am) to $Am(OH)_3$. Initially formed $Am(OH)_3$(am) will invert to more stable $Am(OH)_3$ with time. $Am(OH)_3$ stability decreases with time from self irradiation (SNL 2007 [DIRS 177418]).	$AmOHCO_3$ is formed in americium solubility experiments under Yucca Mountain conditions. Under some conditions, $Am(OH)_3$ may be less soluble, but generally choosing $AmOHCO_3$ is conservative (SNL 2007 [DIRS 177418]).
Protactinium	Solubility is same as that of ThO_2(am). Thorium is also a good analogue to protactinium and was modeled in this report (SNL 2007 [DIRS 177418]).	Solubility of Np_2O_5 was chosen because it is higher than that of ThO_2(am) under conditions modeled, so its choice is conservative (SNL 2007 [DIRS 177418]).
Strontium	Solubility controlled by $SrCO_3$ or $SrSO_4$	No solubility was defined, and inventory release should be in control. This is a conservative approach (SNL 2007 [DIRS 177418]).
Kinectic Sorption	Based on model developed by Painter et al. (2002 [DIRS 174071]) and extended two- and three-site model developed by Wittman et al. 2005 [DIRS 174895].	Additional longer-term data would be required to support this alternative model (SNL 2007 [DIRS 177423]).

Table 6.2-1. Table of Alternative Conceptual Models (Continued)

Alternative Conceptual Models	Key Assumptions	Assessment and Basis
Rate of Colloid Generation (Argonne National Laboratory) (SNL 2007 [DIRS 177423], Table 6-10)	Rate of colloid spallation depends upon the rate of waste degradation. The rate of waste degradation may be defined by the rate of release to the boron content in the alteration fluid (for DHLWG) and technetium (for CSNF).	The ACM is tailored closely to the specific experimental configuration from which the supporting data were acquired. The position of this analysis is that, while promising, the ACM is currently not sufficiently developed for application to more generalized conditions.
Mechanisms of Colloid Generation in CSNF (Pacific Northwest National Laboratory) (SNL 2007 [DIRS 177423], Table 6-10)	Colloid generation at, and mobilization from, the surface of degrading waste is primarily related to flow rate at the waste surface.	The supporting concepts and data from the peer-reviewed literature were developed in the context of deposition and remobilization of existing colloids under conditions of significant groundwater flow. These conditions likely will not apply to conditions anticipated in the repository. Mechanisms of colloid generation at the surface of corroding fuel may be different from mechanisms of mobilization of a discrete deposited colloid.
EBS Flow and Transport Model Component (Sections 6.3.6 & 6.3.8)		
Dual-Continuum Invert Model	Crushed tuff invert ballast is modeled as a dual-continuum material consisting of intergranular pore space and intragranular pore space. All seepage flow into the drift flows through the intergranular pore space and into the UZ fractures. Imbibition from UZ host rock into the invert flows through the intragranular pore space. Diffusion of radionuclides also occurs in both the intergranular and intragranular pore spaces, from the WP corrosion products into UZ fractures and matrix, as well as between the two invert continua (SNL 2007 [DIRS 177407], Section 6.6.4).	Insufficient data to validate diffusion coefficients in individual continua. Insufficient data to confirm whether this is a bounding approach with respect to chemical conditions in the invert for calculating solubility and colloid stability.
Bathtub Flow Model	Seepage water flowing into breached WP accumulates until void volume is filled before water containing dissolved radionuclides flows out. Various cases, such as changing inflow rates and effect of solubility and dissolution rate limits are evaluated (SNL 2007 [DIRS 177407], Section 6.6.1).	For several of the most pertinent cases, the flow-through model is conservative with respect to releases of radionuclides.

Table 6.2-1. Table of Alternative Conceptual Models (Continued)

Alternative Conceptual Models	Key Assumptions	Assessment and Basis
Constrained Water Vapor and Oxygen Diffusion Model	The rate of steel component corrosion inside a WP is compared with the rate of diffusion of water vapor and oxygen through SCCs into a WP. A continuous film of absorbed water cannot form if the consumption rate is higher, which could delay the diffusive releases until all steel is fully corroded (SNL 2007 [DIRS 177407], Section 6.6.2).	Insufficient data to validate.
Dual-Continuum Invert Model	Crushed tuff invert ballast is modeled as a dual-continuum material consisting of intergranular pore space and intragranular pore space. All seepage flow into the drift flows through the intergranular pore space and into the UZ fractures. Imbibition from UZ host rock into the invert flows through the intragranular pore space. Diffusion of radionuclides also occurs in both the intergranular and intragranular pore spaces, from the WP corrosion products into UZ fractures and matrix, as well as between the two invert continua (SNL 2007 [DIRS 177407], Section 6.6.4).	Insufficient data to validate diffusion coefficients in individual continua. Insufficient data to confirm whether this is a bounding approach with respect to chemical conditions in the invert for calculating solubility and colloid stability.
Invert Diffusion Coefficient Model with Lower Limit on Water Content	As the water content of the crushed tuff ballast decreases, the water films that connect pore spaces become disconnected, and the effective diffusion coefficient drops more rapidly than predicted by Archie's law. Below some critical water content, the diffusion coefficient becomes zero, based on models of diffusion in soils (SNL 2007 [DIRS 177407], Section 6.6.5).	Insufficient data to validate diffusive behavior at very low water contents. Nonbounding; does not provide upper bounds on diffusion coefficients.
Reversible Sorption of Radionuclides onto WP Corrosion	Iron oxyhydroxide corrosion products sorb many radionuclide species. Sorption is assumed to be reversible and will not compete with other radionuclides nor compete for irreversible sorption sites (SNL 2007 [DIRS 177407], Section 6.6.6).	Does not account for limitations on total number of sorption sites. Does not account for competition with other radionuclides for sorption sites.
Plutonium Sorption from Stationary Corrosion Products and Colloids	Plutonium sorbs strongly to iron oxyhydroxide corrosion product colloids and stationary corrosion products. Sorption may be considered slowly reversible (and modeled by computing the forward and reverse rate constants for the two-site model) (SNL 2007 [DIRS 177407], Section 6.6.7).	Experiment durations are short (hours to weeks) compared to the repository time scale. The mechanisms of plutonium sorption are not well-enough understood to extrapolate the results outside the experimental design. Plutonium sorption and desorption data are not available for the highest pH ranges expected in the repository environment (SNL 2007 [DIRS 181006], Table 6-30).

Table 6.2-1. Table of Alternative Conceptual Models (Continued)

Alternative Conceptual Models	Key Assumptions	Assessment and Basis
Unsaturated Zone Transport Model Component (Section 6.3.9)		
Discretization of the UZ Matrix (MINC Model)	The matrix is discretized to allow for a more accurate approximation of the concentration gradient at the matrix-fracture interface and within the matrix. Use of the Discrete Fracture Model or Multiple Interacting Continua (MINC) model results in later breakthrough times than generated using the dual-k model. The breakthrough times of the Multiple Interacting Continua model are later than those generated using the Discrete Fracture Model. (SNL 2007 [DIRS 181006], Table 6-30).	The dual-k model is conservative. The MINC model is not used because of its large computational burden (SNL 2007 [DIRS 181006], Table 6-30).
Alternative Finite Difference Numerical Models	An alternate method of approximating radionuclide transport in groundwater based on approximating the governing equations using finite difference equations (SNL 2007 [DIRS 181006], Table 6-30).	Although used for validation of the UZ Abstraction Model, large computational burden limits the utility of models such as T2R3D and EOS9nT (SNL 2007 [DIRS 181006], Table 6-30).
Lateral Flow Diversion In UZ Above the Repository	Lateral flow in the PTn will divert percolating water to the faults and reduce the percolation flux at the repository (SNL 2007 [DIRS 181006], Table 6-30).	The original base case model, which shows more lateral flow occurring within the PTn than the ACM, was chosen due to better predictions of chloride and moisture data. It was also generally more conservative with respect to radionuclide transport. The updated base case model predicts significant diversion and redistribution into faults for the PTn (SNL 2007 [DIRS 181006], Table 6-30).
No Radionuclide Release into Faults	The fault zones are defined as high permeability zones subject to fast advective transport to the the top of the TSw and to the water table (SNL 2007 [DIRS 181006], Table 6-30).	The effects of not allowing direct release of radionuclides into the fault zones, on the overall transport to the water table, are not significant because lateral diversion directs the radionuclides into the fault zones (SNL 2007 [DIRS 181006], Table 6-30).
Inclusion of Drift Shadow Effects	Inclusion of drift shadow effects would approximate the influence of capillary diversion which may cause low fracture saturation below the drift (SNL 2007 [DIRS 181006], Table 6-30).	It is considered conservative to ignore drift shadow effects. Additionally, the increases infiltration associated with later climate states may decrease the effects (SNL 2007 [DIRS 181006], Table 6-30).

Table 6.2-1. Table of Alternative Conceptual Models (Continued)

Alternative Conceptual Models	Key Assumptions	Assessment and Basis
Perched Water Permeability Zones	Perched water may delay and dilute radionuclide concentration and reduce advective transport. Large scale lateral flow of water can also occur in perched water zones which can divert and redistribute flow into faults. Continuous well-connected fractures are used to model transport processes in the particle tracking method and the flow fields from the UZ Flow Submodel account for perched water effects (SNL 2007 [DIRS 181006], Table 6-30).	Perched water may only be present in the northern part of the repository. Treating perched water in a manner such that well connected pathways exist is a conservative treatment (SNL 2007 [DIRS 181006], Table 6-30).
Inclusion of TH, THC, and THM Effects on UZ Flow and Transport	Vaporization due to repository heat will keep the drift dry for several hundred to a few thousand years. THC and THM effects may alter flow and transport properties of the UZ rocks (SNL 2007 [DIRS 181006], Table 6-30).	TH, THC, and THM effects are insignificant after the change to glacial-transition climate (SNL 2007 [DIRS 181006], Table 6-30)..
Saturated Zone Flow and Transport Model Component (Section 6.3.10)		
Minimal Matrix Diffusion	Diffusion of radionuclides into the pore space of the rock matrix in the fractured volcanic units is extremely limited due to highly channelized groundwater flow, fracture coatings, or other factors (SNL 2007 [DIRS 181650], Section 6.4).	This ACM is implicitly included in the SZ Flow and Transport Model Abstraction and the 1-D SZ Flow and Transport Submodel through the range of uncertainty in key input parameters. The uncertain input parameters influencing matrix diffusion include DCVO, FISVO, and FPVO (SNL 2007 [DIRS 181650],Table 6.3.10-1).
Horizontal Anisotropy in Permeability	Alternative interpretations of pump test results in the fractured volcanic units indicate preferential permeability along structural features oriented in the NNE-SSW direction, or in the WNW-ESE direction (SNL 2007 [DIRS 181650], Section 6.4).	This ACM is implicitly included in the 3-D SZ Flow and Transport Model Abstraction and the 1-D SZ Flow and Transport Abstraction through the range of uncertainty in an input parameter. The uncertain input parameter influencing horizontal anisotropy in permeability in the volcanic units near Yucca Mountain is the ratio of N-S to E-W permeability (SNL 2007 [DIRS 181650], HAVO; Table 6.3.10-2). This continuously distributed parameter varies from less than one to greater than one with most of the realizations greater than one.
Biosphere Model Component (Section 6.3.11)		
Radon Release from Soil (Air Submodel)	This ACM considers radon transport in the soil and the atmosphere, which requires more input data. The ERMYN conceptual model does not include these processes and uses a simple release factor.	This ACM is from the Biosphere Model Component based on an analysis (SNL 2007 [DIRS 177399], Section 7.4.3.1) showing that the ACM and the ERMYN model produce comparable results.

Table 6.2-1. Table of Alternative Conceptual Models (Continued)

Alternative Conceptual Models	Key Assumptions	Assessment and Basis
Evaporative Cooler (Air Submodel)	This ACM considers an inhalation dose from aerosols generated from evaporative coolers and is based on calculating radionuclide concentrations in the air due to an increase in humidity. The ERMYN conceptual model uses a submodel based on the amount of water evaporated rather than an increase in humidity.	This ACM is from the Biosphere Model Component based on an analysis (SNL 2007 [DIRS 177399], Section 7.4.3.2) showing that this ACM and the ERMYN model produce equivalent results.
Direct Deposition of Irrigated Water (Plant Submodel)	This ACM considers two processes, one where the deposited radionuclide moves from external plant surfaces into the plant tissues, and then from plant tissues into the edible portion of the crop. Weathering is applied only to contaminants that remain on external plant surfaces. Food processing loss is also considered in the ACM. The ERMYN conceptual model considers the radionuclides in irrigation water to be directly translocated to the edible parts of plants with weathering and accumulation during the growing period but without food preparation loss.	This ACM is from the Biosphere Model Component based on an analysis (SNL 2007 [DIRS 177399], Section 7.4.4.1) showing that this ACM and the ERMYN model produce comparable results.
Direct Deposition of Airborne Particulates (Plant Submodel)	This ACM is based on the crop external contamination. This contamination factor is very similar to a soil-to-plant transfer factor. The ERMYN conceptual model considers the deposited airborne particles on crop leaves acting the same way as the intercepted irrigation water.	This ACM is from the Biosphere Model Component based on an analysis (SNL 2007 [DIRS 177399], Section 7.4.4.3) showing that this ACM and the ERMYN model produce comparable results for reasonable input values.
Animal Product Contamination (Animal Submodel)	Two pathways are considered in this ACM. They are animal inhalation of contaminated air and animal soil ingestion. The ERMYN conceptual model excludes the inhalation of contaminated air, but it includes animal soil ingestion.	This ACM is from the Biosphere Model Component based on an analysis (SNL 2007 [DIRS 177399], Section 7.4.5) showing that soil ingestion is important but that inhalation of contaminated air is not.
14C Special Submodel	This ACM considered root uptake only. The ERMYN conceptual model includes external exposure, inhalation of 14C gas, soil ingestion pathways, and 14C transfer into plants through photosynthesis.	This ACM is from the Biosphere Model Component based on an analysis (SNL 2007 [DIRS 177399], Section 7.4.7) showing that the selected 14C special submodel considers more processes of 14C contamination in plants than this ACM, which results in a higher 14C concentration in plants.
Environment-Specific Inhalation Submodel (Inhalation Submodel)	This ACM uses average values of input parameters for inhalation exposure. The ERMYN conceptual model considers inhalation exposure as a function of the environment because many model parameters, such as mass loading, breathing rate, and exposure time, differ among environments and activities.	This ACM is from the Biosphere Model Component based on an analysis (SNL 2007 [DIRS 177399], Section 7.4.9) showing that the ACM and the ERMYN model produce comparable results. In addition, it is easier to address uncertainty in the input parameters using environment-specific values.

Table 6.2-1. Table of Alternative Conceptual Models (Continued)

Alternative Conceptual Models	Key Assumptions	Assessment and Basis
Igneous Scenario Class (Section 6.5)		
Estimating the Igneous Event Rates in the Probabilistic Volcanic Hazard Analysis	The PVHA model uses the number of identified post-Miocene era volcanic events observable at the surface plus some buried in the Yucca Mountain region. *Characterize Framework for Igneous Activity at Yucca Mountain, Nevada* (BSC 2004 [DIRS 169989], Sections 6.3.1.6 through 6.3.1.7 and Table 6-4) identifies an ACM for the PVHA in which a significant number of buried (i.e., unidentified) volcanic centers would be included in the estimation of the igneous event rates. The basis for the ACM is that aeromagnetic anomalies suggest that a significant number of unidentified volcanic events were unaccounted for in the PVHA, thus underestimating the volcanic hazard.	This ACM was not propagated into the TSPA Model because its effects on the probability of an igneous event could not be quantified without further data collection. A drilling and sampling program is underway to determine if any of these anomalies represent Quaternary buried volcanic centers. In addition, an update to the PVHA is underway to reassess the probability of intersection and the probability of a volcanic center being located on Yucca Mountain.
Estimating the Intersection Annual Probability in the Probabilistic Volcanic Hazard Analysis	*Characterize Framework for Igneous Activity at Yucca Mountain, Nevada* (BSC 2004 [DIRS 169989], Section 6.3.1.8 and Table 6-5) identifies several ACMs for estimating the intersection probability (i.e., the annual probability of a volcanic event intersecting the repository footprint).	The ACM probabilities are captured by the probability used in the PVHA.
Dike Propagation	*Dike/Drift Interactions* (SNL 2007 [DIRS 177430], Section 6.3.8) identifies ACMs for dike propagation that use hydraulic-fracture models.	*Dike/Drift Interactions* (SNL2007 [DIRS 177430], Section 6.3.8) concluded that none of these models were appropriate for the dike propagation in the vicinity of an underground repository as none of the models has a free surface that can model the changing behavior of the dike as the surface is approached.
Effusive Magma Flow Into Drifts	*Dike/Drift Interactions* (SNL 2007 [DIRS 177430], Section 6.4.7.2) identifies ACMs for effusive or pyroclastic flow from a dike into a drift.	Simulation of these flows and their interactions with WPs is computationally intensive and, therefore, not practical for implementation within the TSPA model. Instead, the abstractions included in Waste Packages Hit accounts for the effects of these flows within the TSPA framework.
TH Effects on Zones 1 and 2 Drifts	*Dike/Drift Interactions* (SNL 2007 [DIRS 177430], Section 6.7.2) identifies ACMs for the TH behavior of magma-filled drifts and its effects on neighboring drifts. These ACMs involve an evaluation of additional physics, including latent heat of crystallization, host-rock saturation, and enhanced vapor diffusion, and an alternative model for heat conduction from Zone 1 to Zone 2 emplacement drifts.	Inclusion of the latent heat of crystallization and host-rock saturation in the heat transfer analyses was evaluated and is shown to have a negligible effect on the results, producing elevated temperature histories (i.e., above boiling) no more than two to five years longer than without these ACMs included in the analysis (SNL 2007 [DIRS 177430], Section 6.7.2.1).

Table 6.2-1. Table of Alternative Conceptual Models (Continued)

Alternative Conceptual Models	Key Assumptions	Assessment and Basis
Volcanic Eruption Phase Dose	An ACM for the calculation of the radiation dose received by a receptor that does not leave the region during a volcanic eruption is detailed in Section 6.5.2.4. The eruption phase of a volcanic event refers to the conditions that exist during the volcanic eruption before the deposition of volcanic ash on the ground is completed The result of this calculation is used as the basis for excluding the potential eruption phase dose in the TSPA-SEIS.	Because a high concentration of airborne radioactive particulates is expected during this phase, inhalation of airborne contaminated ash particles is the only pathway considered (SNL 2007 [DIRS 177399], Section 6.15.2). The receptor has the same inhalation characteristics as those for the RMEI discussed in Section 6.3.11.
Seismic Scenario Class (Section 6.6)		
Alternative Modeling Approaches Evaluated for Conceptual and Computational Models of Lithophysal and Nonlithophysal Rock *BSC* 2004 [DIRS 166107], Section 7.4)	A standard approach for solving excavation stability problems is the use of numerical models based on continuum mechanics. Continuum models use constitutive relations to describe the mechanical behavior of a material. The use of a constitutive model requires that the mechanical effects of fractures be lumped into the constitutive relationships.	Continuum models are unable to predict instabilities, such as fracture and rockfall (BSC 2004 [DIRS 166107], Section 7.4.1). The discontinuum approach is more suitable for representing fracture of the rock mass and separation of the intact rock mass into blocks and was therefore adopted for modeling the drift degradation processes that occur after a seismic event (BSC 2004 [DIRS 166107], Section 7.4.2).
Alternative Conceptual Model for Crack Area Density Presented in Section 6.7.4 (SNL 2007 [DIRS 181953])	The alternative model considered a circular geometry circumscribed by a single through-wall crack. The base case model combines two conceptual models based on hexagonal geometry (SNL 2007 [DIRS 181953], Section 6.7.3).	The hexagonal geometry represents a high effective density of individual cracks and the two hexagonal geometry conceptual models are considered conservative representations. The ACM analysis, which uses circular geometry, is considered a limiting realistic case (SNL 2007 [DIRS 81953], Section 6.7.2).

Table 6.2-1. Table of Alternative Conceptual Models (Continued)

Alternative Conceptual Models	Key Assumptions	Assessment and Basis
Alternative Conceptual Models for Conditional Probability Distributions Representing Damaged Areas on WP, Damaged Areas on DS, and Volume of Rockfall from Seismic Event Considered	These alternate distributions included the gamma, normal, log-normal, Weibull and triangular distributions, as presented in Sections 6.5.1.4, 6.5.2.4, 6.6.1.4, 6.6.2.4, 6.7.1.3, 6.7.2.4, 6.9.4, and 6.10.2.8 of *Seismic Consequence Abstraction* (SNL 2007 [DIRS 176828]).	Gamma distributions generally provided simpler and more accurate representations of the statistical observations than normal, log-normal, log-triangular, and Weibull distributions. The exception to the use of gamma distributions is that the fragility analyses (for drip shield plates and framework) have used log-normal representations to simplify manipulation of products and quotients of random variables.
Alternative Damage Abstraction for FD Damage Proposed by Waiting et al. (*IHLRWM* 2003 [DIRS 164449])	The ACM considered the probability-weighted number of waste package failures from fault displacement and the number of fault intersections with emplacement drifts. The ACM was based on the use of historical data for fault displacement in the western United States.	The results provided by the ACM are consistent with the base-case model for both the probability-weighted number of WP failures and the number of fault intersections with the emplacement drifts (SNL 2007 [DIRS 176828], Section 6.11.6).

NOTES: ANL = Argonne National Laboratory; DHLWG = defense high-level waste glass; 1-D = one-dimensional; DCVO = effective diffusion coefficient in volcanic units; FISVO = flowing interval spacing in volcanic units; FPVC = flowing interval porosity; HAVO = ratio of horizontal anisotropy (north-south over east-west) in permeability; ERMYN = Environmental Radiation Model for Yucca Mountain, Nevada; DFM = discrete fracture model; MINC = multiple interacting continua.

INTENTIONALLY LEFT BLANK

6.3 TSPA-SEIS FOR THE NOMINAL SCENARIO CLASS

Section 6.3 presents a description of the Nominal Scenario Class for the TSPA-SEIS Model. Sections 6.3.1 to 6.3.11 describe the conceptual models, the model abstractions, and implementation of these abstractions in the TSPA-SEIS. Each subsection of Section 6.3, namely Sections 6.3.1 to 6.3.11, will be introduced by two figures that have a consistent format and type of content. The first figure in each Section 6.3 subsection will illustrate how the submodels discussed in the subsection relate to other TSPA-SEIS submodels. The second figure in each subsection will illustrate important information about individual submodels. In particular, the figures illustrate the principal feeds, or inputs, to the submodels, the principal outputs from the submodels, highlights of the theoretical foundation and important characteristics of the submodels, and an indication of the sources of confidence, including field and laboratory data and auxiliary modeling in the submodels, and will vary according to the contents of the individual subsections. Further information regarding the areas singled out on these figures can be found in the accompanying text of the individual Section 6.3 subsections and in the supporting analysis and/or model reports that are referenced in the Section 6.3 subsections.

The TSPA-SEIS of the Yucca Mountain repository system is a combination of integrated processes that have been conceptualized and modeled as a collection of coupled model components. For the TSPA-SEIS, eight principal model components are combined to evaluate repository system performance for the Nominal Scenario Class. The model components are:

- Unsaturated Zone (UZ) Flow
- Engineered Barrier System (EBS) Environment
- Waste Package (WP) and Drip Shield (DS) Degradation
- Waste Form Degradation and Mobilization
- EBS Flow and Transport
- UZ Transport
- Saturated Zone (SZ) Flow and Transport
- Biosphere.

Section 6.3 provides detailed descriptions of the TSPA-SEIS submodels that comprise the model components. Table 6-1 can be considered a guide that links the principal TSPA-SEIS components shown on Figure 6-1 to the TSPA-SEIS submodels. Each submodel description in Section 6.3 includes:

- A discussion of how the submodel is connected to other submodels and model components in the TSPA-SEIS.
- A description of the conceptual model on which the submodel is based.
- A description of the submodel abstraction.
- A description of how the abstraction is implemented in the TSPA-SEIS.

- An evaluation of the consistency and conservatism in assumptions and parameters used in the TSPA-SEIS. Assumptions and parameter values that are different among submodels in the TSPA-SEIS are documented in each section.

- A summary of alternative conceptual models (ACMs) that were considered in the development of the conceptual model.

The focus of Section 6.3 is on the TSPA-SEIS components and submodels and their implementation for the Nominal Scenario Class.

6.3.1 Mountain-Scale Unsaturated Zone Flow

UZ flow in the TSPA-SEIS refers to the percolation of groundwater through the unsaturated rocks between the land surface and the groundwater table. The Site-Scale UZ Flow Model (SNL 2007 [DIRS 175177]) provides the flow fields for the UZ Transport Submodel (Section 6.3.9) and the TSPA-SEIS. The flow fields consist of spatial distributions of fluid saturation, pressure (placeholder values not used in the UZ Transport Submodel), and water fluxes in the fracture and matrix continua. Figure 6.3.1-1 illustrates the connections between the Site-Scale UZ Flow Model and the submodels of the TSPA-SEIS. Figure 6.3.1-1 shows that the Infiltration Model (SNL 2007 [DIRS 182145]) and the Climate Analysis, as described in *Future Climate Analysis* (BSC 2004 [DIRS 170002]) and *Data Analysis for Infiltration Modeling: Extracted Weather Station Data Used to Represent Present-Day and Potential Future Climate Conditions in the Vicinity of Yucca Mountain* (SNL 2007 [DIRS 177081]), contribute to the Site-Scale UZ Flow Model. The Infiltration Model was specifically developed to provide input to the Site-Scale UZ Flow Model. The *Future Climate Analysis* (BSC 2004 [DIRS 170002]) provides climate analogues to be used for assessing the future mean annual temperature and precipitation in the region, including Yucca Mountain. Future climate conditions at Yucca Mountain must be predicted to determine the hydrological conditions at and near Yucca Mountain. The *Data Analysis for Infiltration Modeling: Extracted Weather Station Data Used to Represent Present-Day and Potential Future Climate Conditions in the Vicinity of Yucca Mountain* (SNL 2007 [DIRS 177081]) provides climatological data based on present day conditions in the Yucca Mountain vicinity and the climate analogues presented in BSC 2004 [DIRS 170002]. Figure 6.3.1-2 illustrates the outputs provided by the Climate Analysis to the Infiltration Model and to the TSPA-SEIS. The *Future Climate Analysis* (BSC 2004 [DIRS 170002]) provides three climate states for use in the TSPA-SEIS: present-day, monsoon, and glacial-transition. The outputs from the *Future Climate Analysis* include duration (Table 6.3.1-1), and climate analogues for precipitation rates, and air temperatures for each climate state. The *Data Analysis for Infiltration Modeling: Extracted Weather Station Data Used to Represent Present-Day and Potential Future Climate Conditions in the Vicinity of Yucca Mountain* (SNL 2007 [DIRS 177081]) provides climatological data, such as precipitation rates and temperatures, to the infiltration model.

Figure 6.3.1-3 illustrates and describes the main differences among the three climate states used in the TSPA-SEIS. The future climate states (i.e., monsoon and glacial-transition) were based on analogue sites with representative conditions for those periods. Figure 6.3.1-3 lists the analogue sites used to define the conditions for these future climate states. The present-day climate is based on climatic data available for the Yucca Mountain site. The monsoon climate state will have a higher precipitation rate and higher temperature than the present-day climate (BSC 2004 [DIRS 170002], Section 7.1). The glacial-transition climate state will have a higher precipitation rate but lower temperature than the present-day climate (BSC 2004 [DIRS 170002], Section 7.1). A fourth climate state is also implemented as per regulations found in *Implementation of a Dose Standard After 10,000 Years* (70 FR 53313 [DIRS 178394]). The fourth climate state (post-10,000-year climate state) extends the simulations from 10,000 years to 1,000,000 years.

Net infiltration is the penetration of water through the ground surface to a depth where it can no longer be withdrawn by evaporation or transpiration by plants. The Infiltration Model provides net infiltration rates of meteoric water, which are used as inputs for the upper boundary condition

for the Site-Scale UZ Flow Model. Figure 6.3.1-4 schematically shows the connection between the Infiltration Model and the Site-Scale UZ Flow Model, as well as inputs to and outputs from the Infiltration Model. Figure 6.3.1-5 is a schematic illustration showing the variation of precipitation and consequent net infiltration with respect to elevation and landforms at Yucca Mountain. Net infiltration will be influenced by a number of factors (BSC 2004 [DIRS 169734], Section 7.1.3). Precipitation in the Yucca Mountain region is spatially variable and dependent on meteorological conditions, as well as elevation and physiography (BSC 2004 [DIRS 169734], Section 7.1.3.3). There is a correlation between surface elevations and local precipitation. In the higher elevations, there are likely to be thinner surface soils and shallower fractured bedrock. In the lower elevations, especially in washes, the surface tends to be alluvium and the bedrock tends to be at a greater depth. Some of the factors that have an influence on how precipitation becomes net infiltration are the amount and rate of precipitation, evaporation, transpiration, topography, thickness of surface soils, run-on and runoff of surface water, redistribution of moisture, permeability and sorptive capacity of the soils, the amount of vegetation, as well as fractured bedrock characteristics. In addition, these factors may change through time due to long-term climatic and geomorphologic changes.

Figure 6.3.1-6 displays principal input and output interfaces between the Site-Scale UZ Flow Model, the Multiscale Thermohydrologic Model (MSTHM) (Section 6.3.2), and the UZ Transport Submodel (Section 6.3.9). As shown on Figure 6.3.1-6, outputs of the Site-Scale UZ Flow Model are passed to the MSTHM to specify the percolation flux, consisting of liquid flux in both the fracture and matrix continua, at the base of the Paintbrush nonwelded hydrogeologic unit (PTn). The percolation flux at the base of the PTn unit, above the repository horizon, is used as an upper boundary condition, as described in *Multiscale Thermohydrologic Model* (SNL 2007 [DIRS 181383], Section 6.2.6.6). UZ hydrologic properties such as permeability, porosity, residual saturation, van Genuchten parameters, and Active Fracture Model parameters are also passed to the MSTHM (SNL 2007 [DIRS 181383], Table 4.1-1, Sections 6.2.6 and 6.2.6.5). These parameter values are used to generate the EBS thermal-hydrologic (TH) and drift-seepage conditions, as described in *Abstraction of Drift Seepage* (SNL 2007 [DIRS 181244], Section 6.7.1.2), for implementation in the TSPA-SEIS. In addition, flow fields are passed to the UZ Transport Submodel (Section 6.3.9). The UZ flow fields provide input of fracture and matrix liquid flux, and liquid flux between fracture and matrix continua, along with liquid saturation and pressure values.

6.3.1.1 Conceptual Model

The Site-Scale UZ Flow Model uses a dual-permeability conceptual model that captures the effects of fast-flow paths and allows for fracture-matrix coupling. Flow is modeled in both fracture and matrix continua and these continua interact with one another. Both fracture and matrix continua are assigned their own hydrologic properties, such as permeability and porosity. Hydrologic properties are, in general, uniform layer-wise. Generally, fractures are modeled as part of a highly permeable continuum having low porosity, whereas the matrix is modeled as a much less permeable continuum having higher porosity than the fracture continuum. Fracture-matrix interaction is represented with an active fracture model, in which only some fractures are actively conducting water under unsaturated conditions (SNL 2007 [DIRS 175177], Section 6.1.2). Major faults are explicitly included in the Site-Scale UZ Flow Model. When compared to the same hydrologic units outside the fault zone, the fault zone fracture

permeabilities are generally much higher than in the rest of the Site-Scale UZ Flow Model, enabling preferential flow paths in portions of the Site-Scale UZ Flow Model (SNL 2007 [DIRS 179545], Section 6.3.4 and Tables B1 to B4). Within each hydrogeologic unit, fault zones in the Site-Scale UZ Flow Model assume the same hydrologic property set. Either the ground surface at Yucca Mountain, or the tuff-alluvium contact in areas of significant alluvial cover, is taken as the top model boundary and the groundwater table is taken as the bottom model boundary of the Site-Scale UZ Flow Model. For flow simulations, the top boundary is modeled as a Dirichlet-type condition and the water flux is specified as a source term to the fracture grid blocks in the second grid layer from the top. For flow, the water table is used as the bottom boundary (groundwater table) that is assigned a single-valued fixed water pressure, which is equivalent to specifying a constant liquid saturation (SNL 2007 [DIRS 175177], Section 6.1.3). Changes in the groundwater table elevation at the bottom boundary because of climate-related changes in recharge are not included in the Site-Scale UZ Flow Model simulations. The basis for this implementation is that water flow through the unsaturated rock within Yucca Mountain is predominantly downward and dominated by gravity. Therefore, the elevation of the groundwater table has little influence on the fluxes calculated for the UZ flow fields.

To approximate the effects of a rising groundwater table on a radionuclide transport simulated by the finite element heat and mass (FEHM) transfer code, the external monsoon climate, glacial-transition, and post-10,000-year climate flow field files used in the transport model are post-processed. The groundwater tables for the monsoon climate, glacial-transition, and post-10,000-year climate flow fields are set at an elevation of 850 m above mean sea level. The monsoon, glacial-transition, and post-10,000-year climate groundwater table rise represents an increase of 120 m (Section 5.1.1) above the 730 m above mean sea level groundwater table elevation for the present-day climate (SNL 2007 [DIRS 181006], Section 6.4.8). The post-processed monsoon climate, glacial-transition, and post-10,000-year climate flow field files have the UZ flow conditions for each node at or below the new groundwater table level, 850 m above mean sea level, replaced with default saturated hydrological conditions that trigger a response by the FEHM code. In the FEHM code, the groundwater table rise is approximated in the future climate flow fields by assigning to the nodes, located at or below the new groundwater table, a large mass flux that instantly moves all mass below the new groundwater table level to the SZ Transport Submodel. In the monsoon, glacial-transition climate, and post-10,000-year climate flow fields, the vertical length of the radionuclide flow path is effectively reduced by 120 m, as that is the elevation rise of the groundwater table. In the UZ Transport Submodel's FEHM multispecies particle tracking analysis, the particle exit nodes, where the Site-Scale UZ Flow Model defines the bottom of the UZ and the source input bins of the SZ, become the nodes at the elevation of the new groundwater table that have been assigned the large water flux values by FEHM. At the time of the first updating of the flow field (at the time of change to the monsoon climate), all radionuclide particles below the new groundwater table level are instantaneously made available to the SZ. The groundwater table then remains at the 850 m elevation for the rest of the simulation; the monsoon, glacial-transition, and post-10,000-year climates are assumed to both have a groundwater table level of 850 m above mean sea level. Additional information concerning the groundwater table interface between the UZ Transport Submodel and SZ Flow and Transport Submodels, as well as the effects of groundwater table rise on flow and the transport of radionuclides, is discussed in the subsequent sections on UZ Transport (Section 6.3.9) and SZ Flow and Transport (Section 6.3.10).

Figure 6.3.1-7 shows how the distribution of mountain-scale UZ percolation flux changes as it moves downward through the mountain due to the hydrogeologic processes and conditions within the mountain. A detailed discussion of the Site-Scale UZ Flow Model is contained in *UZ Flow Models and Submodels* (SNL 2007 [DIRS 175177]), and a summary of the processes affecting the percolation flux through the mountain is in the following discussions. Figure 6.3.1-8 shows the stratigraphic column present at a central location within the Yucca Mountain site and is useful for this discussion to visualize the thickness and order of the stratigraphic formations as they are discussed. Water flows through the densely fractured Tiva Canyon welded (TCw) unit mainly through the fractures. The high density of interconnected fractures and low matrix permeabilities in the TCw unit (SNL 2007 [DIRS 179545], Tables 6-6 through 6-9 and Section 6.3.2) are considered to give rise to significant water flow in fractures and limited matrix imbibition (water flow from fractures to the matrix). Thus, episodic infiltration pulses are expected to move rapidly through the TCw fracture networks, with little attenuation by the matrix. The relatively high matrix permeabilities and porosities and low fracture densities of the PTn unit (SNL 2007 [DIRS 179545], Tables 6-6 through 6-9 and Section 6.3.2) convert the predominant fracture flow in the TCw to dominant matrix flow within the PTn. The dominance of matrix flow in the PTn and the relatively large storage capacity of the matrix, resulting from its high porosity and low saturation (under the ambient conditions); give the PTn significant capacity to attenuate infiltration pulses. Faults (or geologic structures) may cut through the entire PTn unit at some locations, leading to fast flow paths if the local PTn tuff matrix is not able to convert all of the fault flow into matrix flow. In addition, some lateral diversion of water occurs in the PTn unit owing to the capillary barrier effects (SNL 2007 [DIRS 175177], Sections 6.1.2 and 6.2.2). Unsaturated flow in the Topopah Spring welded (TSw) hydrologic unit occurs primarily through fractures. The TSw hydrologic units are the host-rock units for the entire repository footprint (Figure 6.3.2-4).

The main hydrogeologic units below the repository are the Calico Hills (CHn), the Prow Pass, (, and the Bull Frog (also known as the Crater Flat undifferentiated) units. All of these units have vitric and zeolitic components that differ in their degree of hydrothermal alteration and subsequent hydrologic properties. The zeolitic rocks have low matrix permeability and some fracture permeability. Perched water occurrences are found to be associated with the low-permeability zeolitic portions of the CHn and the densely welded basal vitrophyre unit of the TSw (SNL 2007 [DIRS 175177], Section 6.2.2.2 and BSC 2004 [DIRS 169861], Section 6.2.2.2). Consequently, a relatively small amount of water may flow through the zeolitic units or basal vitrophyre, with most of the water flowing laterally in perched-water bodies and then vertically down along faults. On the other hand, similar to the PTn unit, the vitric units have relatively high matrix porosity and permeability. Therefore, matrix flow dominates in the vitric units. One distinctive feature below the repository is the existence of perched-water zones (SNL 2007 [DIRS 175177], Section 6.2.2.2). The occurrence of perched water suggests that certain portions of the lower TSw (e.g., the basal vitrophyre) and the upper CHn (zeolitic portion) impede vertical flow (SNL 2007 [DIRS 175177], Section 6.2.2.2). These hydrogeologic units of lower permeability act to divert the downward progression of contaminant transport by forcing path changes and increases in lateral flow components (SNL 2007 [DIRS 175177], Section 6.2.2.2).

6.3.1.2 Model Abstraction

The UZ flow fields were abstracted using the three-dimensional Site-Scale UZ Flow Model (SNL 2007 [DIRS 175177], Section 6.6), with input parameters based on calibrations conducted using four sets of parameters of one-dimensional site-scale calibrated properties and two-dimensional site-scale calibrated fault properties documented in *Calibrated Unsaturated Zone Properties* (SNL 2007 [DIRS 179545], Section 6.3). The final calibrated three-dimensional properties for the perched-water conceptual model, which are used to generate the 16 flow fields, are documented in SNL 2007 ([DIRS 175177], Appendix B (Tables B1 – B4)).

Twelve of these UZ flow fields are developed for spatially varying net infiltration maps representing the three simulated climate scenarios, present-day, monsoon, and glacial-transition, and four infiltration cases, resulting in a total of 12 base-case flow field. As noted earlier, a fourth climate state is also implemented as per regulations found in *Implementation of a Dose Standard After 10,000 Years* (70 FR 53313 [DIRS 178394]). The fourth climate state (post-10,000-year climate state) extends the simulations from 10,000 years to 1,000,000 years. The fourth climate state contains four uncertainty cases, the development of which is based on the prescribed percolation flux distribution through the repository footprint given in the proposed rule found in *Implementation of a Dose Standard After 10,000 Years* (70 FR 53313 [DIRS 178394]), as a log-uniform distribution ranging from 13 mm/yr to 64 mm/yr (SNL 2007 [DIRS 175177], Sections 6.1.4 and 6.2.2). The 16 post-10,000-year flow fields are implemented directly in the TSPA-SEIS and used by the UZ Transport Submodel (Section 6.3.9). The UZ Flow Fields Abstraction is briefly described in this section. Water flux rates applied to the top model boundary are varied for three climate states (i.e., present-day, monsoon, and glacial-transition). These utilize studies of modern and future climates in *Future Climate Analysis* (BSC 2004 [DIRS 170002]) and in *Simulation of Net Infiltration for Present-Day and Potential Future Climates* (SNL 2007 [DIRS 182145]). For the Future Climate Abstraction, the 10,000-year simulation period has been divided into three climate regimes: modern (present-day), monsoon, and glacial-transition, as shown in Table 6.3.1-1 and illustrated on Figure 6.3.1-3. Table 6.3.1-1 indicates that the Future Climate Abstraction consists of three periods: the first 600 years, of which 550 years are postclosure, are simulated with the present-day climate; 1,400 subsequent years as a monsoon climate; and a glacial-transition climate for the remainder of the 10,000-year simulation period. The TSPA-SEIS's present-day climate period begins at the beginning of WP emplacement, which is 50 years before closure. The TSPA-SEIS is only used for postclosure performance assessment.

The durations of future climates, as given in *Future Climate Analysis* (BSC 2004 [DIRS 170002], Table 6-1), are 400 to 600 years for the present-day climate, and 900 to 1,400 years for the monsoon climate. The glacial-transition climate duration is then predicted to last the rest of the simulation period. To simplify how the Climate Submodel is implemented in the TSPA-SEIS, only the maximum durations were used (i.e., the present-day climate duration is modeled as 600 years, the monsoon climate duration is 1,400 years, and the glacial-transition climate is used for the rest of the TSPA-SEIS simulation period). This simplification of the future climate uncertainty was reasonable because it has an insignificant effect on repository performance estimates. The minimal effect of climate duration uncertainty on repository performance is expected because the timing of present-day and monsoon climate changes occur relatively early during the simulation period, making the glacial-transition climate period

dominant. A quantitative understanding of how minimal the influence of climate duration uncertainty is can be estimated by comparing the total weighted average infiltration over the UZ model domain for the early and late extremes of climate durations. This approach assumes that radionuclide release through the UZ is roughly correlated with infiltration; this assumption is based on net infiltration being the ultimate source of percolation through the UZ (SNL 2007 [DIRS 175177], Section 6.1.4) and also that advective transport plays a dominant role in radionuclide transport through the UZ (SNL 2007 [DIRS 177396], Section 6.1.2.1) and (SNL 2007 [DIRS 175177], Section 6.1.4).

The Infiltration Submodel includes the four infiltration cases (10^{th}, 30^{th},50^{th}, and 90^{th} percentile infiltration scenarios) for each climate state for the TSPA-SEIS simulations. It is necessary to estimate a set of weighting factors describing the likelihood of each infiltration scenario to occur. The weighting factors are derived using a generalized likelihood uncertainty estimation (GLUE) methodology (Beven and Binley 1992 [DIRS 179079]) described in *UZ Flow Models and Submodels* (SNL 2007 [DIRS 175177], Section 6.8.5). The results of this generalized likelihood uncertainty estimation analysis are displayed in the last column of Table 6.3.1-2. A weighted average infiltration rate for each climate scenario was calculated using the 10th percentile, 30th percentile, 50th percentile, and 90th percentile net infiltration rates (Table 6.3.1-2) weighted by the frequency of occurrence (0.6191, 0.1568, 0.1645, and 0.0596, respectively) of each value. As an example, the present-day weighted average infiltration rate is the summation of the four products of the domain average of the 10th percentile infiltration rate multiplied by the 10th percentile weighting factor, the 30th percentile infiltration rate multiplied by the 30th percentile weighting factor, the 50th percentile infiltration rate multiplied by the 50th percentile weighting factor, and the 90th percentile infiltration rate multiplied by the 90th percentile weighting factor. Then, the weighted average infiltration rate results (6.74 mm/yr for the present-day climate, 13.09 mm/yr for the monsoon climate, and 17.09 mm/yr for the glacial-transition climate) were multiplied by the duration of each climate scenario used in the Site-Scale UZ Flow Model.

Using a 10,000-year simulation period and the maximum duration estimated for each climate state (600 years for the present-day, 1,400 years for the monsoon, and 8,000 years for the glacial-transition climate), a total weighted average infiltration amount of 159,110 mm is estimated from the weighted average infiltration rates. Once again using a 10,000-year simulation period, the weighted average infiltration rates were multiplied by the minimum estimated durations of each climate scenario (400 years for the present-day, 900 years for the monsoon, and 8,700 years for the glacial-transition climate). These minimum estimated climate durations and their weighted average infiltration rates were multiplied and then summed to obtain a total weighted average infiltration amount of 163,182 mm in 10,000 years. The difference in total weighted average infiltration amounts, assuming the full range of uncertainty estimated for the climate state durations, is only about 2.6 percent. Though comparison of total weighted average infiltration amounts is not reflective of all possible transport mechanisms (diffusion, sorption, retardation, and focused flow) comparison of the total weighted average infiltration amounts is indicative of advective radionuclide transport behavior in the UZ because of the relationship between net infiltration and percolation through the UZ (SNL 2007 [DIRS 175177], Section 6.1.4). Because of the dominant duration of the glacial-transition climate and the roughly nine percent difference in total weighted average infiltration amounts when considering the full range of estimated climate state durations, the use of later climate transition times is not likely to have a significant effect on releases or their travel times. Note that in the one-million-year simulations the post-

10,000 part of the simulation is regulatory-based and therefore an equivalent analysis is not performed for the one-million-year runs (70 FR 53313 [DIRS 178394]).

Spatially distributed net infiltration rates (mm/yr) were determined for the present-day, monsoon, and glacial-transition climate states (SNL 2007 [DIRS 182145], Figures 6-5.7.1-2 to 6-5.7.1-5, 6-5.7.2-2 to 6-5.7.2-5, and 6-5.7.3-2 to 6-5.7.3-5). For the present-day, monsoon, and glacial-transition climate states, infiltration uncertainty in UZ flow simulations, four infiltration maps were implemented for each of the climate states. The four infiltration rate scenarios are the 10th percentile, 30th percentile, 50th percentile, and 90th percentile infiltration cases.

For the post-10,000–year period, four uncertain cases were developed by selecting from the 12 available infiltration maps that generated an average infiltration rate (through the repository footprint) that most closely matched target rates based on *Implementation of a Dose Standard After 10,000 Years* (70 FR 53313 [DIRS 178394]). The four selected infiltration maps were the present-day 90th percentile, the glacial-transition 50th percentile, the glacial-transition 90th percentile, and the monsoon 90th percentile. These maps were scaled so that the average water flux rates through the repository footprint matched the target values. Once the infiltration boundary condition was determined, the methods used to generate the post-10,000-year flow fields were the same as used to generate the pre-10,000-year flow fields (SNL 2007 [DIRS 175177], Section 6.1.3).

To represent infiltration uncertainty in UZ flow simulations, four infiltration maps were implemented for each of four climate states. The four infiltration rate scenarios are the 10th percentile, 30th percentile, 50th percentile, and 90th percentile infiltration cases. The four climate states combined with the four infiltration cases result in 16 net infiltration scenarios included in the UZ Flow Field Abstraction. The infiltration scenarios are summarized in Table 6.3.1-2 for average values over the model domain. The Site-Scale UZ Flow Model (SNL 2007 [DIRS 175177], Sections 6.6) is used to generate a set of steady-state flow fields for each infiltration scenario. For each selected infiltration case, the four related climate state flow fields are implemented sequentially in the TSPA-SEIS over the modeled period: present-day, monsoon, glacial-transition, and post-10,000 year for specified durations (Table 6.3.1-1). The use of the 10th percentile, 30th percentile, 50th percentile, and 90th percentile infiltration values is intended to cover the uncertainties associated with the infiltration for each climate (SNL 2007 [DIRS 175177], Section 6.1.4). The first two future climate scenarios, the monsoon and glacial-transition periods, are used to account for possible climate-induced changes in precipitation and net infiltration. The glacial-transition climate has higher net infiltration rates than the present-day. The glacial transition state also has higher net infiltration rates than the monsoon climates for the first three infiltration scenarios but not for the fourth. The third future climate, the post-10,000-year period, uses an additional four uncertainty cases that are developed based on prescribed percolation fluxes through the repository footprint as given in the proposed rule found in *Implementation of a Dose Standard After 10,000 Years* (70 FR 53313 [DIRS 178394]).

Figure 6.3.1-9 shows the surface infiltration map for the 10th percentile infiltration scenario during the glacial-transition climate along with the corresponding estimated vertical percolation flux at the repository horizon level and the groundwater table level. Comparisons of the map of the calculated repository percolation flux with that of the surface infiltration map indicate that the spatial distributions of percolation flux at the repository horizon are significantly different

from the patterns of the net infiltration rate. The surface infiltration rates and distributions are independent of faults. The major differences in the percolation flux distribution at the repository level compared to the surface infiltration patterns are: (1) flow occurs mainly through faults in the very northern part of the model domain, north of the 237,000-m northing coordinate (see Figure 6.3.1-7 for coordinates); (2) flow is diverted into or near faults located in the model domain; and (3) a west to east shift of high infiltration zones away from the Yucca Mountain crest (SNL 2007 [DIRS 175177], Section 6.6.2.1). Overall, percolation at the repository horizon displays a very different pattern than that of the distribution of surface infiltration. One reason for this difference is the substantial amount of large-scale lateral flow within the PTn unit. In addition, there is a flow redistribution in the very northern part of the model domain (beyond the repository block) caused by the repository grid layer horizon laterally intersecting the CHn zeolitic and perched-water zones locally, with major flow diverted to faults. The lateral flow within the PTn unit, and flow focusing into faults in the north have a large influence on percolation flux distribution at the repository horizon (SNL 2007 [DIRS 175177], Section 6.6.2.1). Figure 6.3.1-9 also shows that the distribution of percolation flux at the groundwater table level, when compared to the distribution of net infiltration rates shown at the infiltration boundary, has had the percolation fluxes corresponding to high infiltration rate zones reduced still further from what is shown at the repository horizon level.

6.3.1.3 TSPA-SEIS Implementation

Infiltration Submodel—The four different infiltration cases represent epistemic uncertainty in the net infiltration rates. These scenarios are sampled in the TSPA-SEIS once per realization, based on the probability-weighting factors 61.91 percent, 15.68 percent, 16.45 percent, and 5.96 percent for the 10th percentile, 30th percentile, 50th percentile, and 90th percentile, respectively (Table 6.3.1-2). Because of the once per realization sampling, the infiltration cases are completely correlated across the four climate states modeled during the simulation period (e.g., during a realization in which the 10th percentile infiltration case is sampled, the 10th percentile infiltration scenario of all four climate states will be used to select the appropriate UZ flow fields). This correlation of the infiltration uncertainty across the climate transitions ensures that the full effects of the infiltration uncertainty are not dampened out of the TSPA-SEIS performance results.

Climate Submodel—The durations of the climate states are 600 years (550 years postclosure) for the present-day climate, 1,400 years for the monsoon climate, 8,000 years for the glacial-transition climate, and the remainder of the simulation period is simulated as a post 10-k climate (Table 6.3.1-1). Climate change is specified within the TSPA-SEIS by assuming climate-specific boundary conditions for UZ flow and accessing the flow field that corresponds to the selected infiltration case and climate state of the simulation period.

UZ Flow Fields Abstraction—The 16 base-case UZ flow fields and associated information generated by the Site-Scale UZ Flow Model (Output 1 in Section 6.1.4.1) are reformatted for use by the UZ Transport Submodel to simulate the transport of radionuclides in the UZ (note that information from Output 1 is provided to the MSTHM Model, as described in Section 6.3.2).

In the UZ Transport Submodel (Section 6.3.9), changes in flow fields and boundary conditions due to climate state changes, (i.e., groundwater table rise), are applied instantaneously at the time

the climate changes (SNL 2007 [DIRS 181006], Section 5). An instantaneous change from one steady-state flow field to another is a reasonable approximation, given the uncertainties and the inability to observe climate changes directly (SNL 2007 [DIRS 181006], Section 6.4.8). With a change to wetter conditions in the future, flow velocities will immediately be greater, and the flow path length to the groundwater table will be shorter due to the higher groundwater table. By applying these conditions instantaneously, there will be no model implementation-caused delay imparted to climate transition-induced changes of UZ flow and radionuclide transport conditions (SNL 2007 [DIRS 181006], Section 6.4.8).

Prior to implementation, the reformatted UZ flow fields are placed in a library of files that are read by the UZ Transport Submodel during run time. There are 16 UZ flow field files for use by the UZ Transport Submodel, one for each of the combinations of the four climate states and four possible infiltration scenarios. These files contain fracture and matrix liquid flux values, and liquid flux between fracture and matrix, along with liquid saturation. These files include:

- Three-dimensional, steady-state flow fields defined at each node in the FEHM UZ grid below the repository, which contain the following information used in the particle-tracking model:
  - Fracture continuum liquid flux
  - Matrix continuum liquid flux
  - Fracture continuum liquid saturation values
  - Matrix continuum liquid saturation values
  - Liquid flux between matrix and fracture continua.
- Note that the files also contain dummy pressure values (pressures are not used in the particle tracking model) and large liquid flux values of 10^{10} m^3 to indicate to FEHM which nodes watertable release nodes.

6.3.1.4 Model Component Consistency and Conservatism in Assumptions and Parameters

To enhance understanding of the complex interactions within the TSPA-SEIS, this section presents a discussion of consistency among model components and submodels and identification of conservative assumptions in abstractions, models, and parameter sets supporting the Mountain-Scale UZ Flow Submodel.

6.3.1.4.1 Consistency of Assumptions

Flow Focusing—The Drift Seepage Submodel (Section 6.3.3) (SNL 2007 [DIRS 181244]) accounts for flow-focusing effects, which can locally concentrate liquid flow above the repository drifts, thereby increasing seepage locally. This can, in turn, increase liquid flow locally through WPs and/or invert. This can have the effect of increasing advective transport of radionuclides from WPs and/or invert to the UZ. The small scale focusing phenomenon is not accounted for in the Site-Scale UZ Flow Model in generating the UZ flow fields.

Effect on the TSPA-SEIS—The Drift Seepage Submodel includes the effects of flow focusing in the EBS Environment Model Component and the EBS Transport Submodel of the TSPA-

SEIS. However, flow focusing is not included in the Site-Scale UZ Flow Model because flow focusing is a local effect and is below the resolution of the Site-Scale UZ Flow Model gridblock size that is used to generate the UZ flow fields. In the TSPA-SEIS, the UZ transport is modeled over a distance of several hundred meters below the repository. Thus, for computational efficiency, it is appropriate to evaluate the hydrologic processes at the gridblock scale of the Site-Scale UZ Flow Model. Accordingly, the effects of flow focusing are not distinguishable in the Site-Scale UZ Flow Model.

Effect of Temperature Perturbation on UZ—Although changes in thermal conditions due to decay heat in and around the emplaced WPs are important inputs to the TSPA-SEIS EBS submodels, they are not applied to UZ flow or transport. UZ flow is approximated with the assumption that the rock mass and flow conditions have not been influenced by repository waste heat effects or durable changes to host-rock hydrologic properties (SNL 2007 [DIRS 181006], Section 5).

Effect on the TSPA-SEIS—Possible effects of the repository waste heat are temporary dry out in the near-field UZ and mineral precipitation in UZ fractures and matrix. Both of these effects could reduce the release of radionuclides from the EBS. Model component integration without the inclusion of these effects is acceptable as radionuclide releases occur after the main part of the repository waste heat perturbation takes place, at which time the UZ flow conditions will have returned to flow conditions similar to ambient conditions (SNL 2007 [DIRS 181006], Section 5). Another effect could be the thermal alteration of the zeolites, a durable change that could reduce sorption in the UZ. Neglecting the thermal alteration of zeolites could be non-conservative; however, two- and three-dimensional mountain-scale TH calculations (BSC 2005 [DIRS 174101], Figure 6.2-6c, Section 6.3.1) indicate that temperatures at the base of the TSw will remain below the estimated minimum zeolite alteration temperature of 85°C, as suggested by Smyth (1982 [DIRS 119483], p. 201). Additionally, heating the Topopah Spring basal vitrophyle with available water may cause an alteration of glasses to zeolites, which would increase the sorptive capacity and increase mineral volume, thus decreasing permeability. It is assumed that the range of flow conditions found in the flow fields used in the TSPA-SEIS will encompass possible far-field changes in flow fields associated with repository waste heat-induced changes to the host-rock conditions (SNL 2007 [DIRS 181006], Section 5).

6.3.1.4.2 Identification of Conservatisms in Submodels and Abstractions

Dual-Permeability Conceptual Model—The dual-permeability conceptual model and its dual-continuum grid system are used by the Site-Scale UZ Flow Model rather than a more refined-gridding method for fracture-matrix interaction, such as the Multiple Interacting Continua (MINC) method. Dual-continuum models are needed in order to model the large domain and highly fractured rock at Yucca Mountain (SNL 2007 [DIRS 175177], Section 6.1.2). UZ flow models at the site-scale using a MINC grid are not feasible because the number of model grid elements is too large. The dual-permeability model provides conservative results for flow and tracer transport, as compared with MINC, because fracture-matrix interaction is less with a dual-permeability grid (SNL 2007 [DIRS 181006], Section 7.2.2, and SNL 2007 [DIRS 177396], Section 6.19.1). In addition, the dual-permeability (dual-continuum) representation of fractures as a continuum conservatively assumes complete interconnectivity of the fracture system (i.e., the model does not account for discontinuous fractures) (SNL 2007

[DIRS 177396], Section 6.7.8). The effects of this conservatism tend to increase flow velocity and radionuclide transport rate in the fractures, resulting in shorter radionuclide transport times to the groundwater table.

High-Permeability Fault Pathways—Faults are modeled as high-permeability pathways from the repository to the groundwater table. Uncertainty in fault characteristics has led to the bounding consideration that these faults are high-permeability features that extend from the ground surface to the groundwater table (SNL 2007 [DIRS 175177], Section 5, and SNL 2007 [DIRS 177396], Section 6.7.8). High-permeability fault pathways lead to flow in faults, providing localized high-flow pathways between the ground surface and the repository as well as between the repository and the groundwater table. High-permeability fault pathways, therefore, result in shorter radionuclide transport times to the groundwater table.

6.3.1.5 Alternative Conceptual Model(s) for the Mountain-Scale Unsaturated Zone Flow

Section 6.2 outlines the general consideration and treatment of ACMs used to support the TSPA-SEIS. A brief description of the Mountain-Scale UZ Flow ACM summarized in Table 6.3.1-3 is presented below. Note that the first ACM is based on analyses performed with the original infiltration model and thus references a historical analysis and/or model report (BSC 2004 [DIRS 169861]). The additional ACM is based upon analyses performed with the updated infiltration model or considerations discussed in the present analysis and/or model report (SNL 2007 [DIRS 175177]).

Lateral Flow in the PTn—Uncertainties associated with UZ conceptual flow models were analyzed using two conceptual models of the water flow in the PTn unit (i.e., the base-case UZ Flow Model and an ACM (BSC 2004 [DIRS 169861], Section 6.9). The base-case UZ Flow Model has a hydrogeologic property set for the PTn unit that favors lateral diversion of flow (BSC 2004 [DIRS 169861], Section 6.5.2). The ACM employs a different hydrogeologic property set for the PTn unit that does not favor large-scale lateral diversion (BSC 2004 [DIRS 169861], Section 6.5.2.2). Each of the conceptual models uses three different parameter sets that were calibrated for the lower-bound, mean, and upper-bound infiltration rates that were used in order to address uncertainties in the infiltration. Steady-state UZ flow fields were produced for each of the three infiltration cases (lower-bound, mean, and upper-bound) at each of the three climate states (present-day, monsoon, and glacial-transition). This results in nine base-case and nine alternative three-dimensional UZ flow fields. In general, the nine base-case flow fields show more lateral flow occurring within the PTn than those estimated with the ACM. Additional analyses have been performed to estimate the impact of of the flow model on tracer or radionuclide transport for the nine base-case and nine alternative flow fields. The results of 40 three-dimensional tracer-transport simulations show a wide range of tracer-transport times from the repository to the groundwater table. The results show that the base-case model generally provides slightly more conservative transport time estimates (BSC 2004 [DIRS 169861], Section 6.9.2). Comparative studies of chloride distributions within the UZ, simulated using the base-case and alternative flow fields, indicate consistently that the base-case flow fields provide an overall better match with the observed chloride data (BSC 2004 [DIRS 169861], Section 6.5.2.2).

Transient Infiltration Pulse—The second ACM considered in the UZ is a flow model with a transient pulse infiltration boundary condition. The appropriateness of assuming a steady-state or quasi-steady-state infiltration boundary condition, as opposed to a transient pulse infiltration boundary condition, is a key modeling issue. This assumption relies on the effect of spatial and temporal damping of transient infiltration pulses when flowing through the PTn unit. The PTn consists mainly of non- to patially welded tuffs. The thickness of the PTn ranges from 150 m in the north, to 30 m or less in the south.. The unit can even be missing in certain areas in the south. The PTn is present over the entire repository area where it ranges from 30m to 60 m in the repository area (SNL 2007 [DIRS 175177], Section 6.2.2). In contrast to the units above it (TCw) and below it (TSw), the PTn has high porosity and low fracture intensity, thus having a large capacity for groundwater storage. The effectiveness of the PTn unit to damp episodic flow was examined using episodic infiltration pulses on the top boundary of the model (SNL 2007 [DIRS 175177], Section 6.9). The analyses presented (SNL 2007 [DIRS 175177], Section 6.9) indicate that the steady-state flow approximation used in the UZ flow model is reasonable due to existence of the PTn unit.

Table 6.3.1-1. Durations for Climate States

Climate State	Duration
Present-Day	600 years
Monsoon	1,400 years
Glacial-Transition	Remainder of Simulation Period

Source: DTN: GS000308315121.003 [DIRS 151139]
10 CFR Part 63. Energy: Disposal of High-Level Radioactive Wastes in a Geologic Repository at Yucca Mountain, Nevada [DIRS 180319]

NOTE: The TSPA-SEIS assumes that the present-day climate period begins at first emplacement and that preclosure will be the first 50 years of the present-day climate period.

Table 6.3.1-2. Net Infiltration Rates Averaged over the Unsaturated Zone Model Domain and Probability-Weighting Factors for the Infiltration Scenarios

Infiltration Case	Present-Day Climate (mm/yr)	Monsoon Climate (mm/yr)	Glacial-Transition Climate (mm/yr)	Post-10k Years (mm/yr)	Probability-Weighting Factors (All Climate States)
10th Percentile	3.03	6.74	11.03	16.89	0.6191
30th Percentile	7.96	12.89	20.45	28.99	0.1568
50th Percentile	12.28	15.37	25.99	34.67	0.1645
90th Percentile	26.78	73.26	46.68	48.84	0.0596

Sources: SNL 2007 [DIRS 175177], Tables 6.1-2, 6.1-3, and 6.8-1

Table 6.3.1-3. Alternative Conceptual Models Considered for the Mountain-Scale Unsaturated Zone Flow

Alternative Conceptual Models	Key Assumptions	Screening Assessment and Basis
Lateral Flow in the PTn	Uncertainties associated with UZ conceptual flow models were analyzed using two conceptual models of the water flow in the PTn unit (i.e., the base-case UZ Flow Model and an ACM (BSC 2004 [DIRS 169861], Section 6.9). The base-case UZ Flow Model has a hydrogeologic property set for the PTn unit that favors lateral diversion of flow (BSC 2004 [DIRS 169861], Section 6.5.2). The ACM employs a different hydrogeologic property set for the PTn unit that does not favor large-scale lateral diversion (BSC 2004 [DIRS 169861], Section 6.5.2.2).	Screened out. For the original infiltration model, the base-case UZ Flow Model description of flow in the PTn was selected because it provides better estimates of chloride concentrations and moisture content. Each of the conceptual models used three different parameter sets that were calibrated for the lower-bound, mean, and upper-bound infiltration rates that were used in order to address uncertainties in the infiltration process (DTN: SN0308T0503100.008 [DIRS 165640]).
Transient Infiltration Pulse	The appropriateness of assuming a steady-state or quasi-steady-state infiltration boundary condition was examined by analyzing the effects of using a model with a transient pulse infiltration boundary condition. Effectiveness of the PTn unit to damp episodic flow was examined using episodic infiltration pulses on the top boundary of the model (SNL 2007 [DIRS 175177], Section 6.9).	Screened out. The analyses presented (SNL 2007 [DIRS 175177], Section 6.9) indicate that the steady-state flow approximation used in the UZ flow model is reasonable due to existence of the PTn unit.

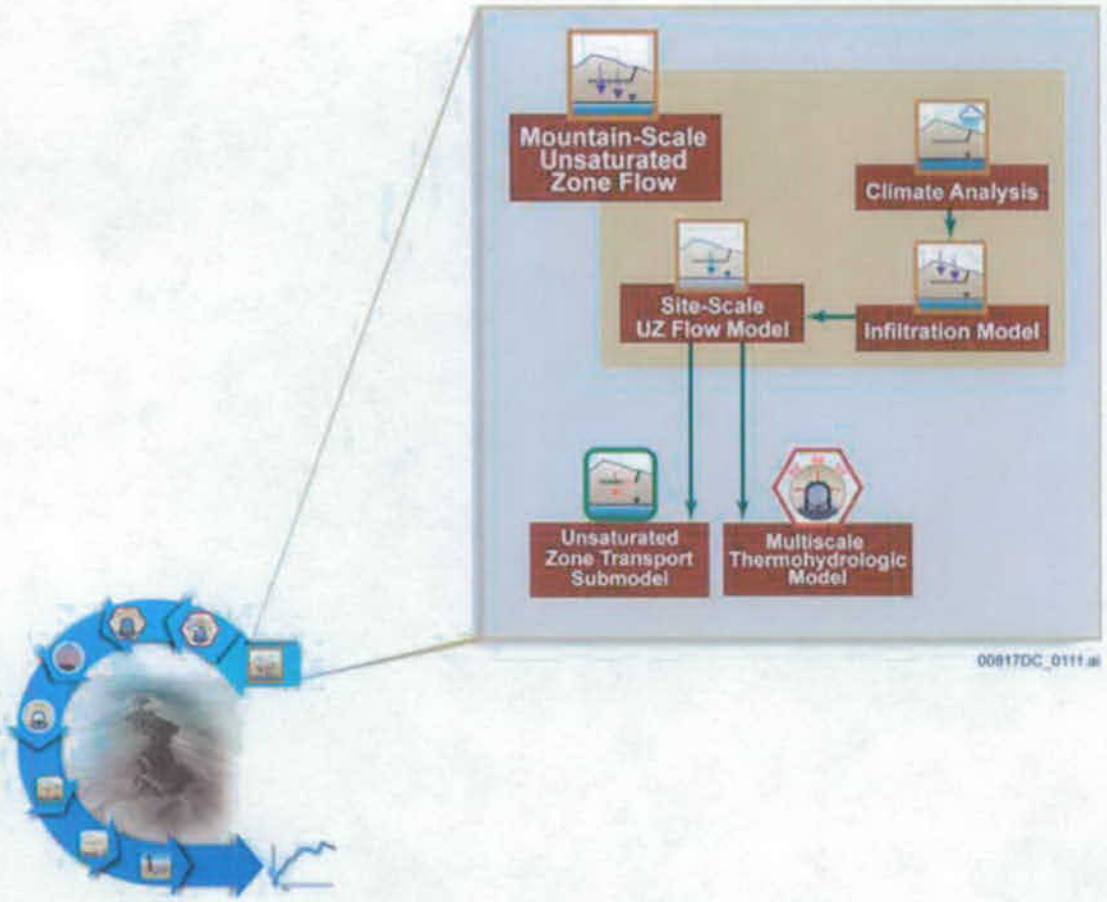

Figure 6.3.1-1. Information Flow Diagram for the Mountain-Scale Unsaturated Zone Flow

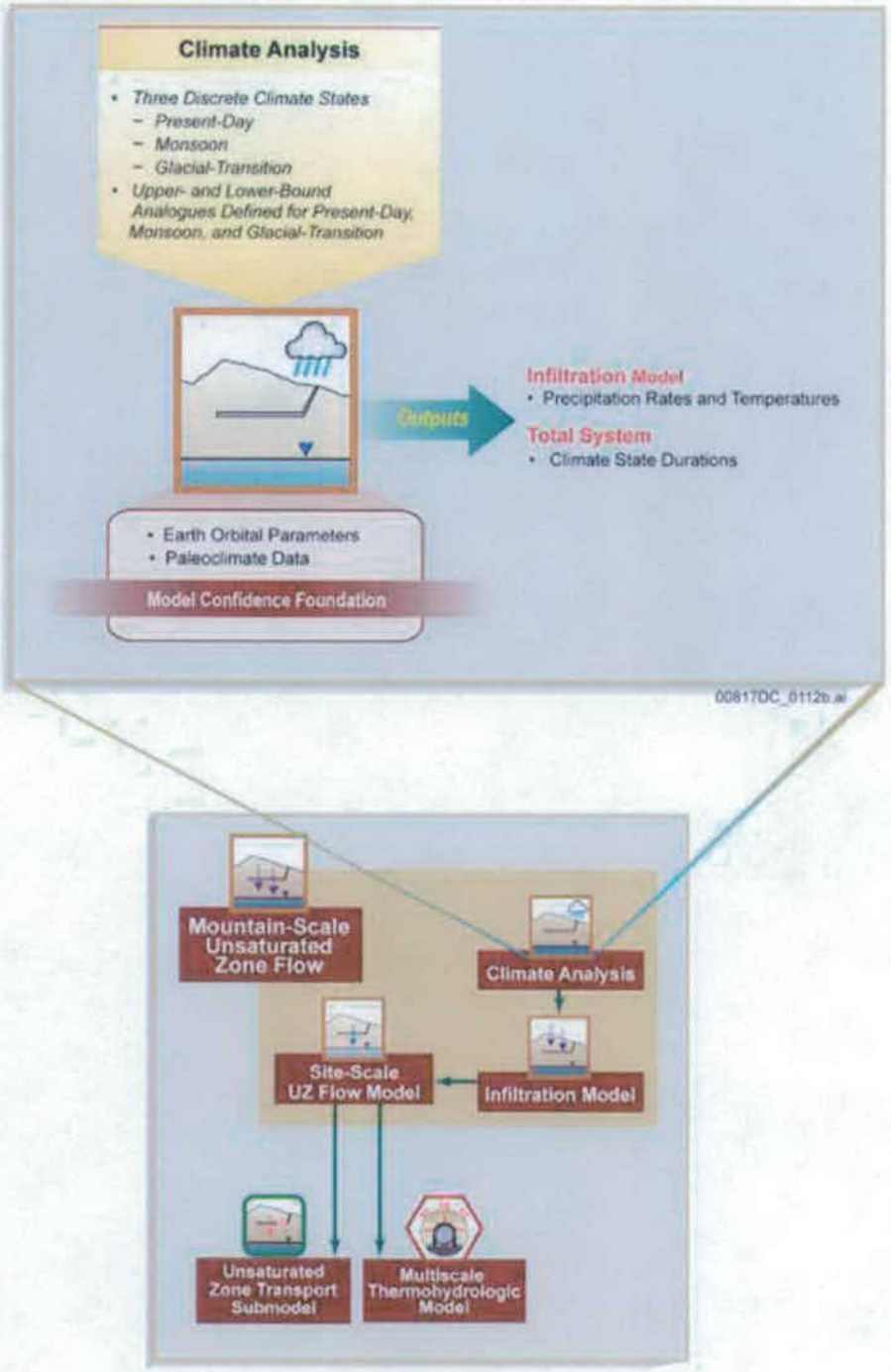

Figure 6.3.1-2. Inputs, Outputs, and Basis for Model Confidence for the Climate Analysis

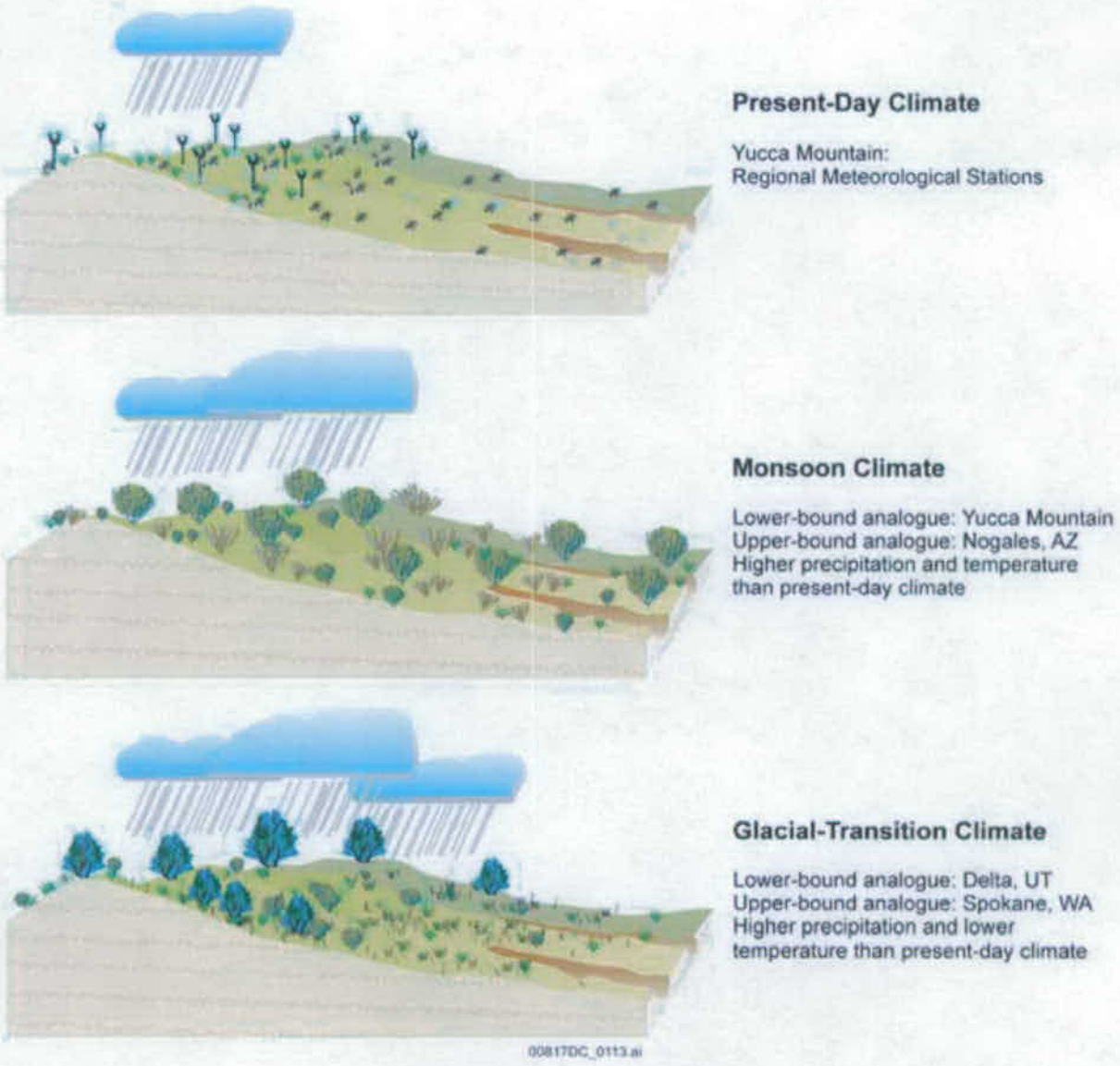

Figure 6.3.1-3. Illustration of the Three Climate States Used in the TSPA-SEIS and the Present-Day Analogues of Those Climates

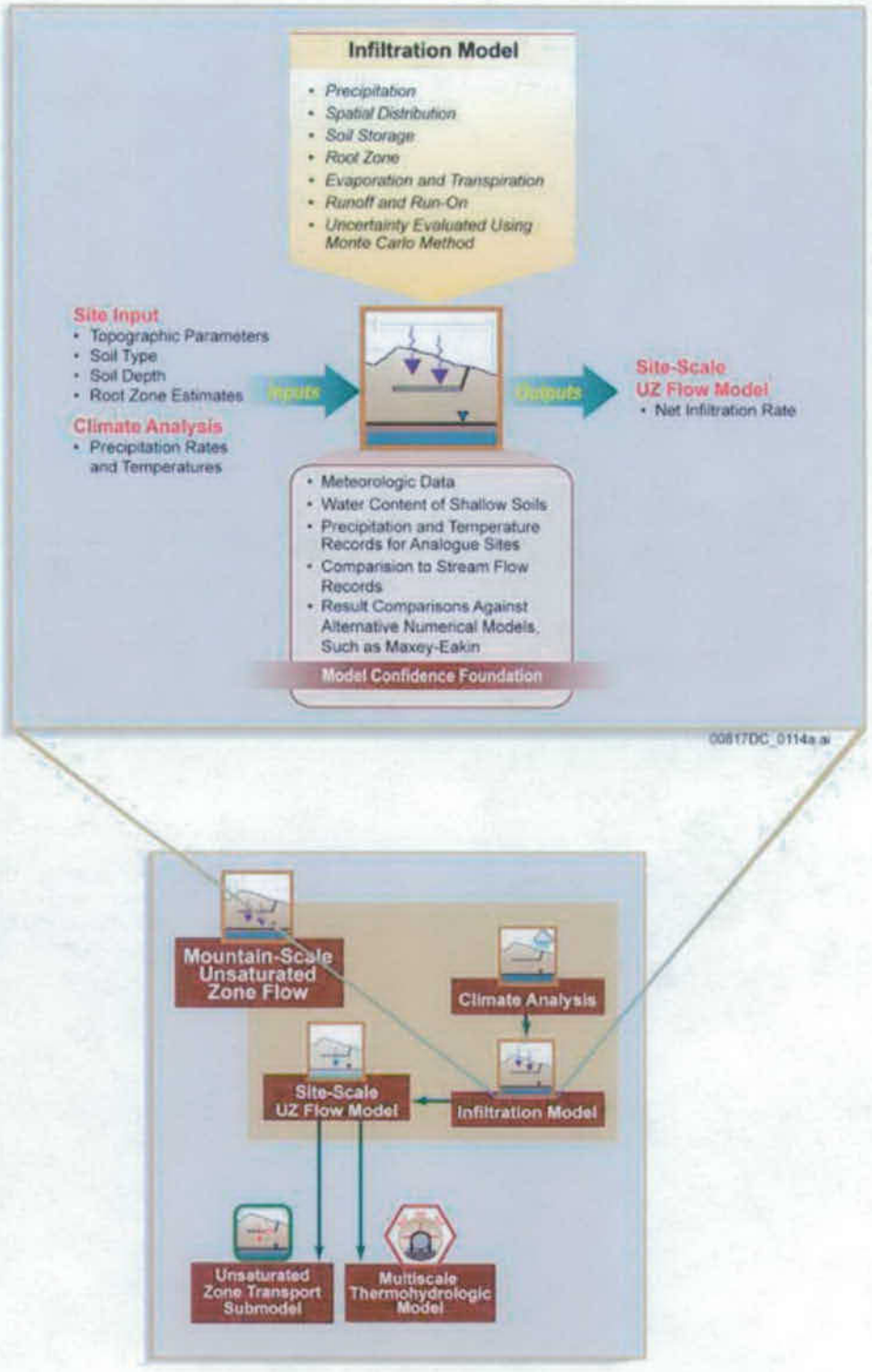

Figure 6.3.1-4. Inputs, Outputs, and Basis for Model Confidence for the Infiltration Model

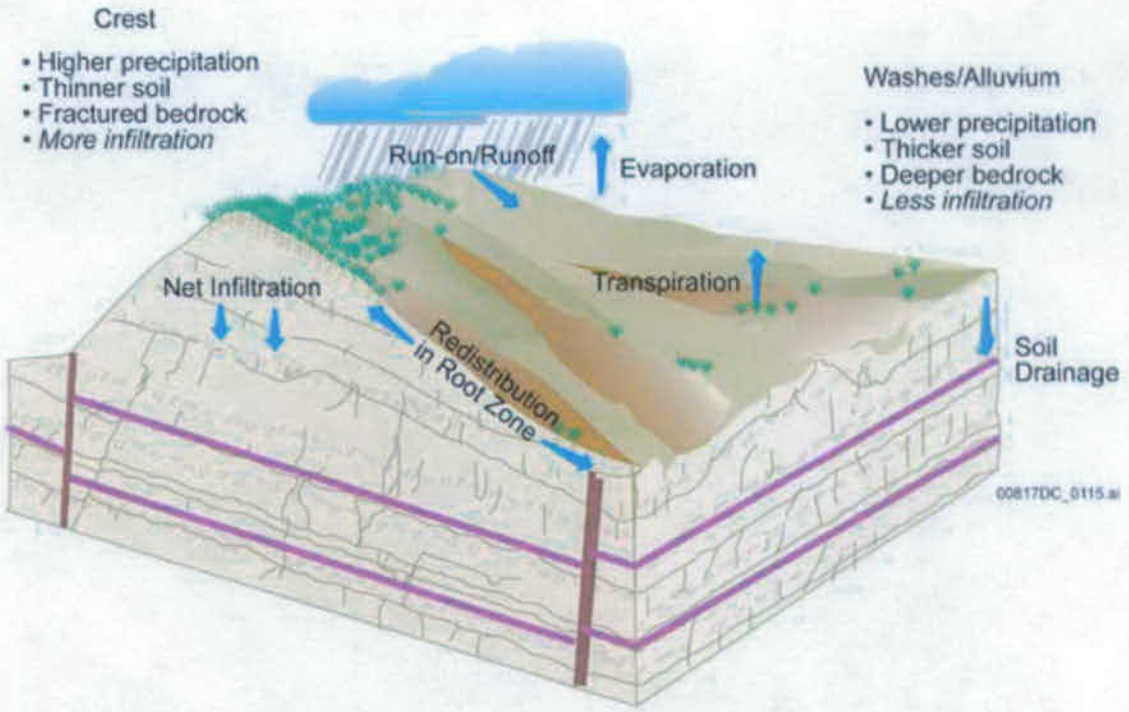

Figure 6.3.1-5. Schematic Illustration Showing the Variation of Precipitation and Consequent Infiltration with Respect to Elevation at Yucca Mountain

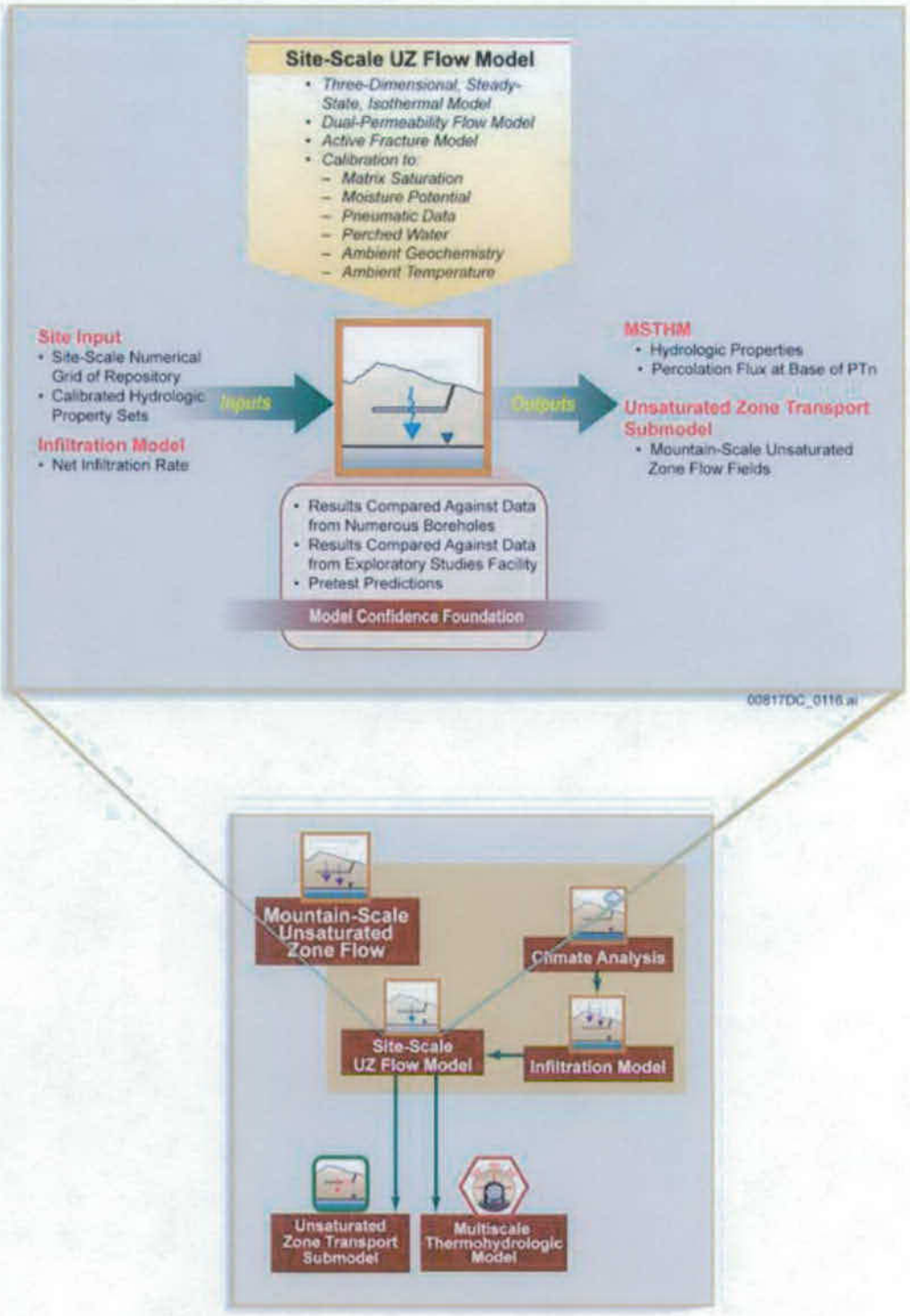

Figure 6.3.1-6. Inputs, Outputs, and Basis for Model Confidence for the Site-Scale Unsaturated Zone Flow Process Model

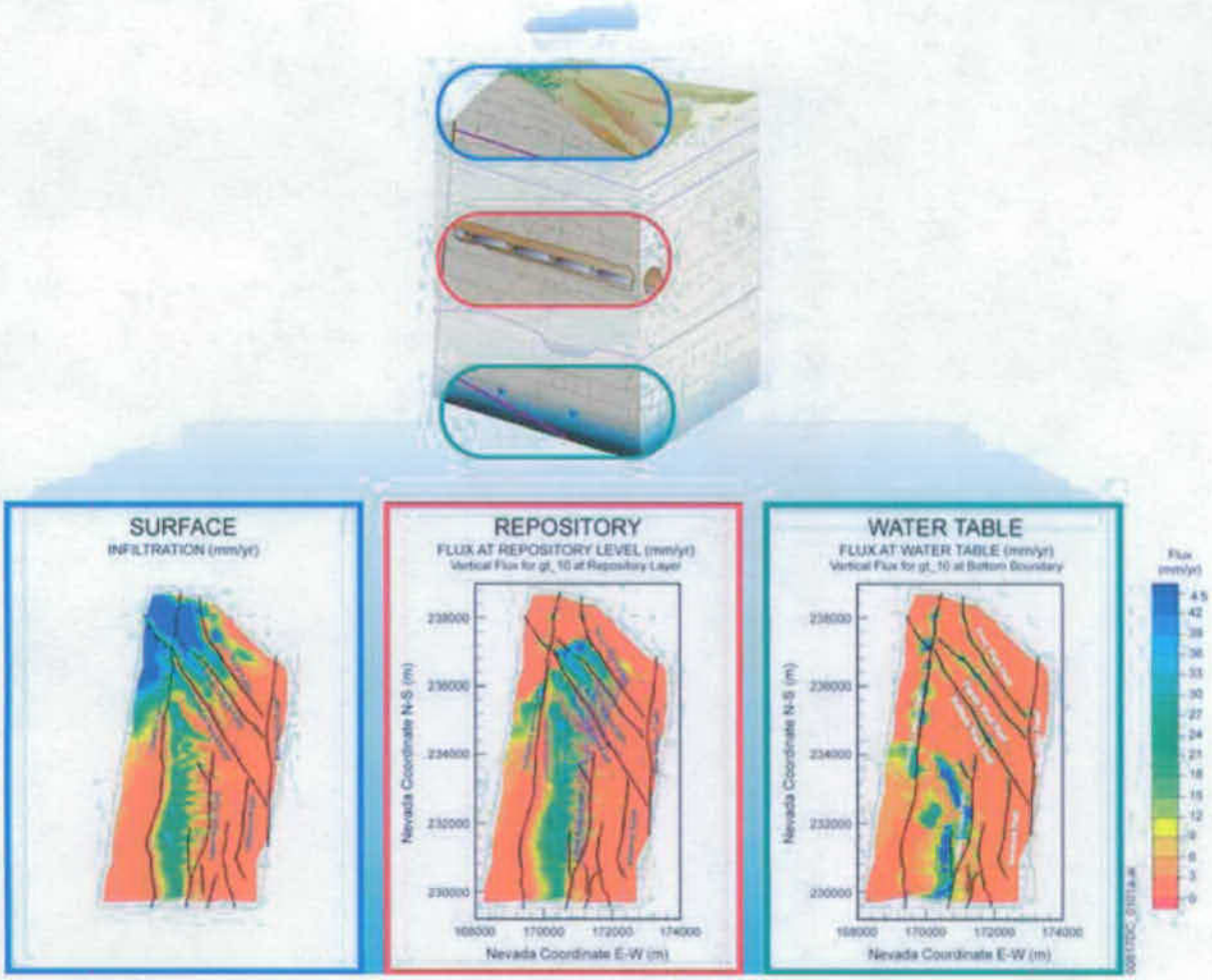

Sources: Modified from SNL 2007 [DIRS 175177], Figures 6.1-4, 6.6-3, and 6.6-7

Figure 6.3.1-7. Infiltration Rate Compared to Percolation Flux at Two Depths for the Tenth Percentile Infiltration Case, Glacial-Transition Period

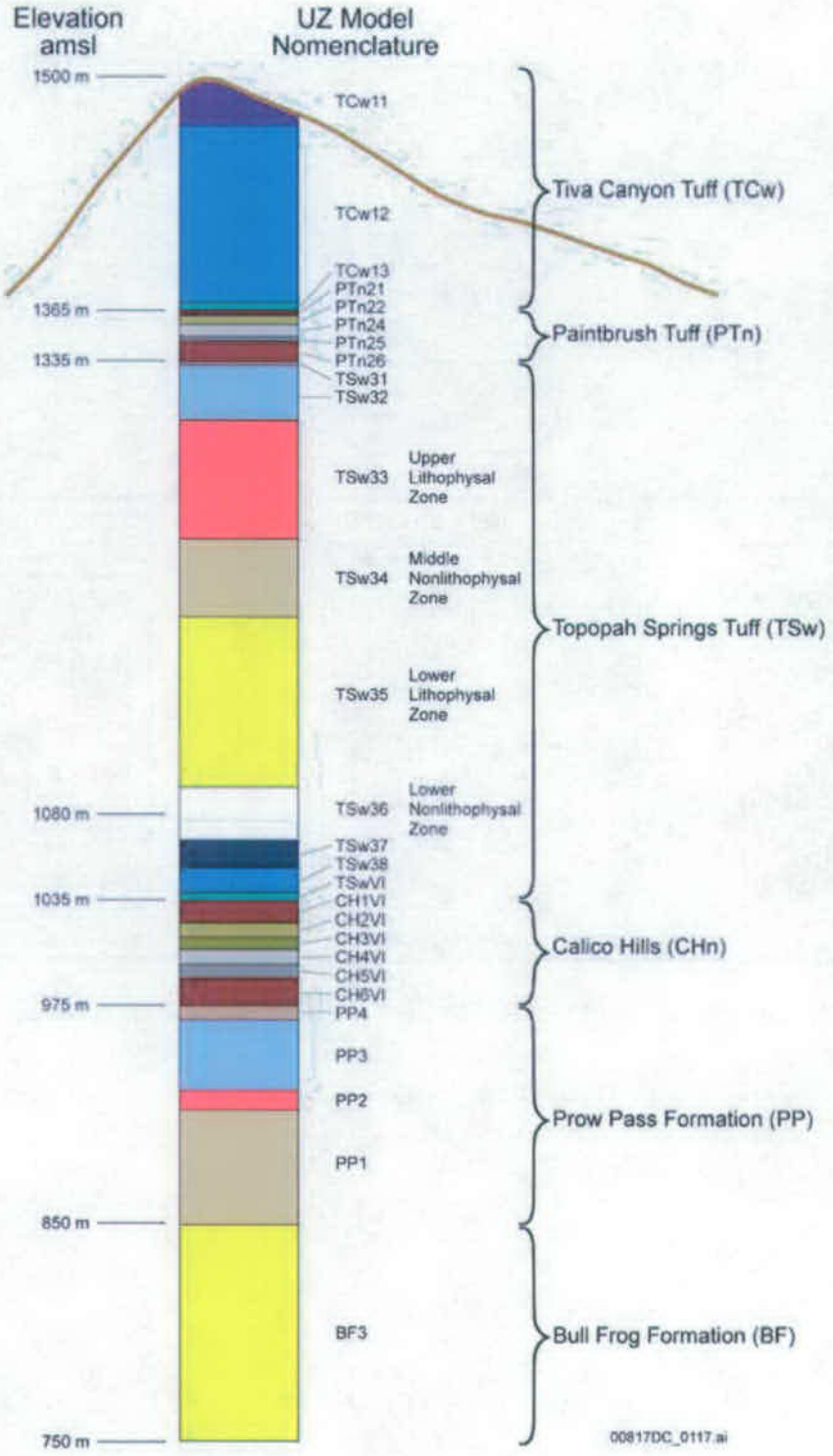

Source: DTN: LB03033DSSFF9I.001 [DIRS 163047], SD-6 Borehole

NOTE: Median elevation of the repository footprint is 1,080 m above mean sea level (amsl).

Figure 6.3.1-8. General Stratigraphy at the Yucca Mountain Site Observed at Borehole SD-6

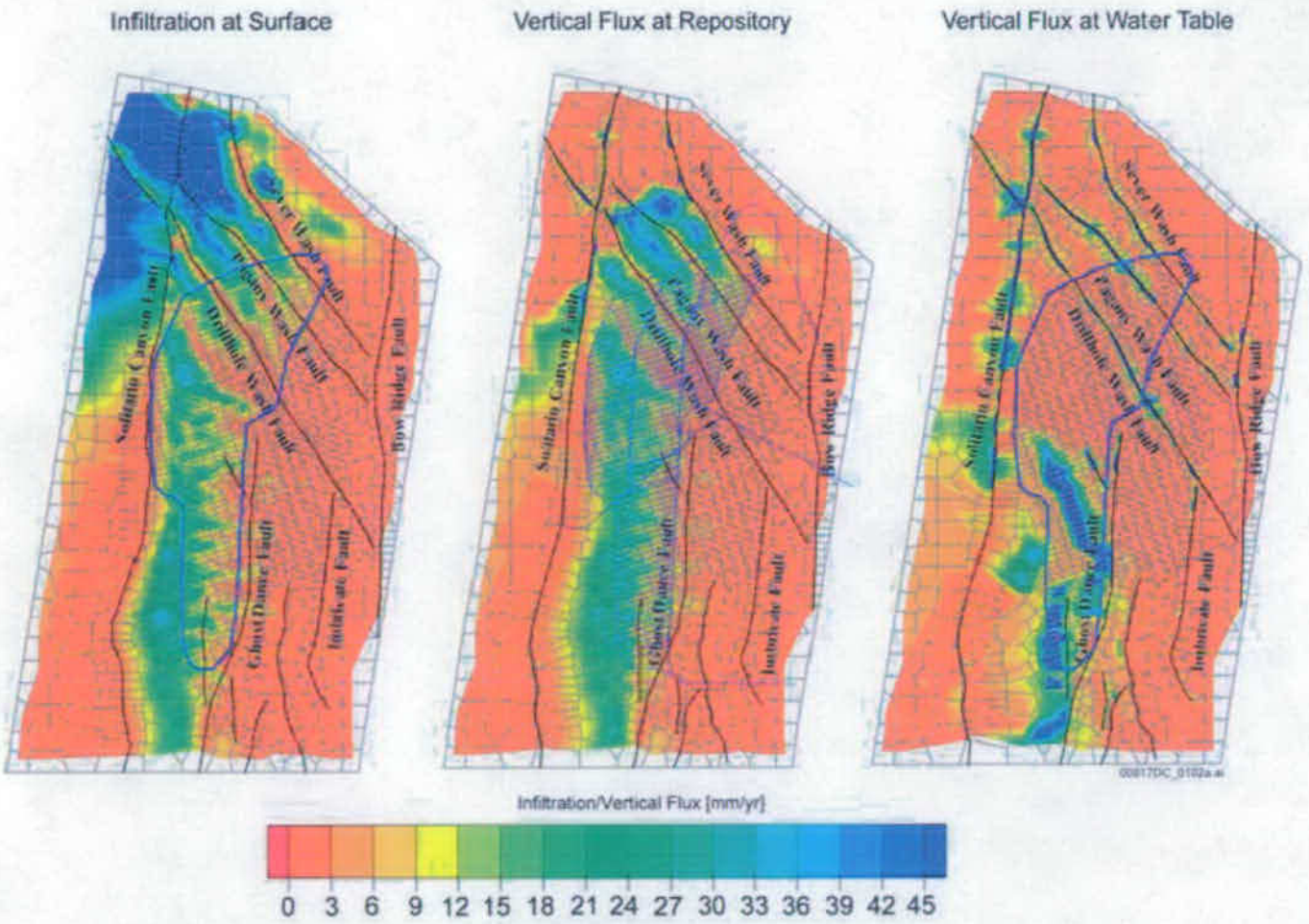

Source: Modified from SNL 2007 [DIRS 175177], Figures 6.1-4, 6.6-3, and 6.6-7

NOTE: The net infiltration boundary and groundwater table are at varying elevations, while the repository horizon is approximated by a constant elevation of 1,080 m.

Figure 6.3.1-9. Comparison of Net Infiltration, Percolation Flux at the Repository Horizon, and Percolation Flux at the Groundwater Table in the Tenth Percentile Infiltration Scenario During the Glacial-Transition Climate State

INTENTIONALLY LEFT BLANK

6.3.2 Engineered Barrier System Thermal-Hydrologic Environment

After permanent closure of the repository, the heat produced by radioactive decay of the waste will influence the thermal and hydrologic conditions in the geologic formations surrounding the repository drifts, the seepage into the repository drifts, local temperature and relative humidity conditions around the WPs, and moisture movement within the drifts. For TSPA-SEIS simulations, the EBS TH Environment Model Component results are computed using results from *Multiscale Thermohydrologic Model* (SNL 2007 [DIRS 181383], Section 1 and Section 1[a]). These MSTHM Process Model results, in the form of the MSTHM Abstraction, are provided as input to the EBS TH Environment Submodel. Figure 6.3.2-1 illustrates the information flow between the Mountain-Scale UZ Flow Submodel (Section 6.3.1), the EBS TH Environment Submodel, and other TSPA-SEIS submodels.

The EBS TH Environment Model Component parameters consist primarily of time-dependent temperature and relative humidity values at various locations within the repository drifts. Other EBS TH Environment Model Component variables include percolation flux above the repository, thermally perturbed liquid saturations, and liquid-flow rates in the invert. Figure 6.3.2-1 shows these TH outputs are used by the Drift Seepage Submodel (Section 6.3.3.1), Drift Wall Condensation Submodel (Section 6.3.3.2), EBS Chemical Environment Submodel (Section 6.3.4), the WP and DS Degradation Model Component (Section 6.3.5), the Waste Form Degradation and Mobilization Model Component (Section 6.3.7), and the EBS Flow and Transport Model Component. The EBS Flow and Transport Model Component is composed of the EBS Flow Submodel (Section 6.3.6) and the EBS Transport Submodel (Section 6.3.8). Figure 6.3.2-2 summarizes the inputs provided to the MSTHM Process Model and the EBS TH Environment Submodel results provided by the MSTHM Abstraction (SNL 2007 [DIRS 181383], Section 8.3[a]). Figure 6.3.2-3 shows the information that the EBS TH Environment Submodel provides to other TSPA-SEIS submodels.

6.3.2.1 Conceptual Model

Nuclear waste emplaced in the Yucca Mountain repository will emit heat from radioactive decay. The MSTHM Process Model is used to model the effects of this decay heat on the evolution of the TH environment in the emplacement drifts. The MSTHM Process Model estimates TH conditions within the emplacement drifts and the surrounding rock as functions of time, WP type, and locations in the repository, as described in *Multiscale Thermohydrologic Model*, (SNL 2007 [DIRS 181383], Section 1). The MSTHM Process Model simulates the evolution of temperature and relative humidity for the components of the EBS. The results are abstracted for the TSPA-SEIS to provide the evolution of temperature and relative humidity on the surfaces of the DSs and WPs, temperature in the invert, temperature on the drift wall, and liquid saturation and liquid flow in the invert.

The heat output from the spent nuclear fuel (SNF) and high-level radioactive waste (HLW) will decline continuously due to the decrease in radioactive decay activity over time. After 50 years of ventilation, the repository enters its postclosure stage where ventilation will cease and the drift-wall rock temperature will be well below boiling but will increase sharply within a few years (SNL 2007 [DIRS 181383], Figure 6.2-4(c)). The maximum postclosure temperature of a WP at any location will be determined by the history of heat output, the resistance to dissipation

of heat in the host rock, heat transfer from the WP to the drift wall, and the relationship to other nearby heat sources. Peak WP temperature considered in the TSPA-SEIS for nominal performance ranges from 107.5°C to 211.0°C (SNL 2007 [DIRS 181383], Table 6.3-49[a]).

Heating of the host rock will produce movement of vapor and liquid water after permanent closure. Much of the heat will be transported away from the drifts by thermal conduction through the rock. A portion of the heat will be transported as latent heat by water that vaporizes near the drift and condenses in cooler rock farther away. Given the projected heat output of the waste and the host-rock characteristics, the near-field host rock, characterized by the drift wall temperature, will be heated to above-boiling temperatures (i.e., greater than 96°C at the repository elevation) for several centuries (SNL 2007 [DIRS 181383], Table 6.3-50[a]). Where temperature exceeds boiling, most of the water will be evaporated from the rock. The duration and extent of dry out will depend on the history of local heat generation, the percolation flux in the host rock, and host-rock properties, notably the thermal conductivity. The variability and uncertainty in host-rock hydrologic properties have an insignificant influence on host-rock dryout (SNL 2007 [DIRS 181383], Section 6.3.9[a]). The maximum lateral extent of the dry-out zone surrounding the emplacement drifts will vary from location to location, ranging from several meters to upward of 11.12 m, but is always expected to be much smaller than the half-drift spacing between emplacement drifts (e.g., 40.5 m) (SNL 2007 [DIRS 181383], Table 6.3-51[a]). Thermal evolution of a particular WP will also depend on its location in the repository layout (i.e., whether it is near the center or the edge of the repository). As the waste heat output decreases with time, the dry-out zone will eventually shrink back to the drift wall, cooling to below-boiling temperatures. The temperatures of the WPs will follow the evolution of the local drift-wall temperature but will be much warmer because of EBS heat transfer mechanisms between the WPs and the local drift wall. This temperature difference will approach zero at later times as the heat output declines.

The influence of heat-generation variability on WP relative humidity variability is similar to the influence on host-rock dry out (SNL 2007 [DIRS 181383], Section 6.3.9, and Section 6.3.13). Because the relative humidity at the drift wall strongly depends on the liquid-phase saturation (as well as on temperature) at the drift wall, the variability of drift-wall relative humidity is similar to that of drift-wall liquid-phase saturation. Relative humidity on a given WP depends on two factors: the drift-wall relative humidity adjacent to the WP, and the temperature difference between the WP and adjacent drift-wall surface. The relative humidity on a given WP is calculated using the relative humidity at the adjacent drift-wall surface and the temperature difference between the WP and the drift-wall surface (SNL 2007 [DIRS 181383], Section 6.1.4[a] and Section 6.2.4[a], Stage 6). WPs with higher heat-generation rates result in a greater relative humidity reduction than those with lower heat-generation rates. The differences in heat-generation rates between the eight different WP types result in differences in relative humidity histories.

6.3.2.2 Model Abstraction

The EBS TH Environment Abstraction is based on two-dimensional, drift-scale, dual-permeability TH models combined with one-, two-, and three-dimensional, thermal-conduction-only models of drift- and mountain-scale. The MSTHM Process Model combines these TH and thermal-conductivity-only models in a methodology that incorporates

thermal interactions between WPs, between WPs and other EBS components, and between the EBS and the surrounding hydrogeologic environment at the repository-scale, as described in *Multiscale Thermohydrologic Model* (SNL 2007 [DIRS 181383], Sections 1 and 6.2). The MSTHM Abstraction results describe heat-related responses within and among the component parts of the emplacement drifts, including the effects of repository-scale heat transfer to the surrounding environment.

The MSTHM Process Model simulates two categories of WPs: a commercial spent nuclear fuel (CSNF) WP, which includes CSNF from pressurized-water reactors (PWRs) and boiling-water reactors (BWRs), and a WP that contains both defense high-level (radioactive) waste (DHLW) and U.S. Department of Energy (DOE) owned SNF (DSNF) (SNL 2007 [DIRS 181383], Table6.2-6[a]). WPs that contain both DHLW and DSNF are referred to as DHLW/DOE SNF WPs in the *Multiscale Thermohydrologic Model* (SNL 2007 [DIRS 181383], Tables 4.1-1[a] and 6.2-6[a]). The TSPA-SEIS, however, refers to these DHLW/DOE SNF WPs as co-disposed (CDSP) WPs. Each waste fuel type has a different rate of heat generation over time. To develop the time histories of heat generated by the waste in the repository, the MSTHM Process Model considers a nominal WP sequence consisting of six CSNF WPs and two CDSP WPs producing results for eight distinct, local heating conditions for each repository subdomain, as described in *Multiscale Thermohydrologic Model* (SNL 2007 [DIRS 181383], Section 6.2.17[a], Table 6.2-6[a]).

The MSTHM Process Model accounts for the following natural and engineered system features:

- Repository-scale variability of percolation flux
- Temporal variability of percolation flux, as influenced by climate change
- Uncertainty in percolation flux addressed by the 10^{th}, 30^{th}, 50^{th}, and 90^{th} percentile infiltration scenarios.
- Uncertainty in thermal properties of the repository host rock using mean, high, and low values of thermal conductivity
- Variation in thermal properties between stratigraphic units in and around the repository
- Repository-scale variability of overburden thickness
- Edge-cooling effect relative to the repository footprint
- Repository design features including WPs, DSs, invert dimensions, invert material properties, drift spacing, WP spacing, and duration of preclosure ventilation
- WP-to-WP variability in heat generation rate
- Time-and distance-dependent heat removal efficiency of preclosure drift ventilation.

The effects of climate change and the resulting infiltration due to precipitation are included by changing the percolation flux boundary condition at the base of the PTn at prescribed times

during the simulations. At the beginning of the preclosure period, the climate is initially set to the present-day climate, which changes to the monsoonal climate after 600 years (of which 550 years are postclosure with present-day climate), followed by 1,400 years of a monsoonal climate, a glacial-transition climate at 2,000 years, and then a post-10,000-year climate (Section 6.3.1.2). A 50-year preclosure period with drift ventilation is included at the beginning of the MSTHM Process Model analyses and is accounted for in the input to the TSPA-SEIS (SNL 2007 [DIRS 181383], Sections 5.2.3 and 6.1.4, Table 4.1-1). However, because the TSPA-SEIS analyzes postclosure performance, the TSPA-SEIS uses the abstraction results starting at the time of closure (at the end of the ventilation period). Climate-induced changes to water table elevation are not included in the TH submodels of the TSPA-SEIS because the elevation of the water table is not expected to have a significant impact on the computed in-drift environments (SNL 2007 [DIRS 181383], Section 5.1.5).

Processes not included in the MSTHM Process Model are:

- Water Vapor mixing or transport within the drifts along the drift axis caused by natural convection. See Section 6.3.3.2 for a description of how in-drift natural convection and condensation is included in the Drift Wall Condensation Submodel.

- The effects of drift degradation or collapse, due to reasons other than a seismic event, on the EBS TH responses are not included in the nominal TH abstractions. The Seismic Scenario Class includes a collapsed drift EBS TH adjustment that is limited to only a few EBS TH parameters, as described in Section 6.6.

- Changes in rock properties because of coupled thermal-hydrologic-chemical or thermal-hydrologic-mechanical processes (SNL 2007 [DIRS 181383], Section 6.2.1[a]). The variability and uncertainty in host-rock hydrologic properties have an insignificant influence on host-rock dryout (SNL 2007 [DIRS 181383], Section 6.3.9[a]). The influence of mechanical and chemical coupling on the TH response is demonstrated to be insignificant compared to parametric uncertainties addressed in the MSTHM Process Model (SNL 2007 [DIRS 181383], Section 8.4.1[a]).

- Changes in the TH properties of water because of dissolved solutes (SNL 2007 [DIRS 181383], Section 6.2.1[a]).

- Flow focusing over distinct sections of emplacement drifts, though a sensitivity study was performed to analyze this exclusion (SNL 2007 [DIRS 181383], Section 6.3.2.1). See Section 6.3.3.1.2 for a description of how flow focusing is included in the Drift Seepage Submodel.

The results computed by the MSTHM Process Model are used directly in the MSTHM Abstraction for the TSPA-SEIS. The abstraction process is described below. Figure 6.3.2-4 shows the distribution of the four primary host-rock units that intersect the repository layout considered in the MSTHM Abstraction. Figures 6.3.2-5 and 6.3.2-6 show examples of the output from the MSTHM Abstraction, as described in *Multiscale Thermohydrologic Model* (SNL 2007 [DIRS 181383], Section 6.3[a]. Figure 6.3.2-4 also shows five representative locations where detailed TH sensitivity analyses were performed. Peak temperatures occur near

the center of the repository and decreases near the edges. This spatial variability in temperature is caused by increased lateral heat loss at the edges of the repository, (i.e., the edge-cooling effect), and a reduction in heat removal efficiency due to ventilation exhaust shafts being located at the center of the repository. The location of the ventilation exhaust shafts at the center of the repository affects the spatial variability of heat in the repository because heat removal efficiency decreases with distance from the ventilation inlet (SNL 2007 [DIRS 181383], Section 6.3.1.1). Figure 6.3.2-5 shows estimated TH conditions for mean host-rock thermal conductivity and the 10th, 30th, 50th, and 90th percentile percolation flux cases, and Figure 6.3.2-6 shows estimated TH conditions for the 50th percentile percolation flux scenario combined with low, mean, and high estimates of host-rock thermal conductivity at the same location. Figures 6.3.2-5 and 6.3.2-6 show that TH conditions depend, to a moderate degree, on both the infiltration scenario and thermal conductivity of the host rock. Spatial variability of percolation flux at the repository horizon and heat transfer processes within and between drifts are two TH factors that are simulated by the MSTHM Process Model.

The MSTHM Process Model accounts for the impact of percolation-flux and host-rock thermal conductivity uncertainty on the TH environment conditions, using simulations conducted for the 10th, 30th, 50th, and 90th percentiles of percolation flux with the mean host-rock thermal conductivity values for the host-rock units. Three additional cases are used in conjunction with the four mean host-rock thermal conductivity cases to capture the impact of host-rock thermal conductivity uncertainty: 10th percentile percolation flux with low- and high-thermal conductivity, and 90th percentile percolation flux with high-thermal conductivity. The TH data sets associated with the remaining five of the 12 possible combinations of percolation flux and host-rock thermal conductivity are provided to the TSPA-SEIS as surrogates from the previously identified seven cases. These five cases use their associated values of percolation flux, but refer to one of the other seven cases for the TH data (SNL 2007 [DIRS 181383], Section 6.3.15[a]). The three thermal conductivities analyzed were assigned probability-weighting factors of 0.29, 0.37, and 0.34 for the low, mean, and high host-rock thermal conductivities, respectively (shown in Table 6.3.2-1 as a discrete distribution). The Infiltration Submodel (Section 6.3.1.2) uses weightings of 0.6191, 0.1568, 0.1645, and 0.0596 for the 10th, 30th, 50th, and 90th percolation flux percentiles, respectively (shown in Table 6.3.1-2). Table 6.3.2-3 describes how the four probability weightings for percolation flux uncertainty and the three probability weightings for host-rock thermal conductivity uncertainty are used to determine the aggregate probability weightings for the 12 MSTHM Process Model data sets provided as input to the TSPA-SEIS. For further discussion of how the 12 combinations of host-rock thermal conductivity uncertainty and infiltration scenario uncertainties are addressed with the provided MSTHM Abstraction results, see *Multiscale Thermohydrologic Model* (SNL 2007 [DIRS 181383], Section 6.3.15[a]).

To characterize the variability in repository TH conditions, the MSTHM Process Model grid subdivides the drifts in the repository footprint into 3,264 equal-area subdomains corresponding to 20-m repository drift segments (SNL 2007 [DIRS 181383], Section 6.2.5.1 and Section 6.2.12[a]). For each of the 12 infiltration/host-rock thermal conductivity cases (Table 6.3.2-3) the MSTHM Abstraction includes the time-dependent TH variables, temperature, and relative humidity, for six different possible CSNF WPs and two different possible CDSP WPs at each of the 3,264 repository subdomains (SNL 2007 [DIRS 181383], Tables 6.2.6[a] and Section 6.2.17[a]). In addition, the MSTHM Abstraction includes time-dependent values for DS temperature and relative humidity; average drift-wall temperature, the duration of boiling at the

drift wall, the average invert temperature, the average invert saturation, and the average invert flux for each of the 3,264 repository subdomains. For the abstraction of the MSTHM Process Model data for downstream model components and submodels, two sets of output parameter analyses and organizations are performed. First, TH values and their associated repository subdomains are grouped into one of five repository percolation subregions based on the magnitude of the percolation flux at the base of the PTn. The second analysis involves determining a single "representative" CSNF WP and a single "representative" CDSP WP for each percolation subregion given the complete set of TH parameters at each of the repository subdomains in that percolation subregion. These output parameter analyses are summarized as follows.

6.3.2.2.1 Determination of Repository Percolation Subregions

The 30th percentile infiltration, glacial-transition climate percolation flux values at the base of the PTn for each of the 3,264 MSTHM Process Model subdomains are used to group each of the subdomains into one of five repository percolation subregions. The percolation flux values for each repository subdomain are sorted in ascending order to form a cumulative distribution function (CDF) and then grouped together based on the five quantiles shown in Table 6.3.2-2. The repository subdomains and their associated TH result abstraction values are then grouped according to the percolation quantile groups and then become designated as belonging to repository percolation subregions one through five. The five repository percolation subregions are shown on Figure 6.3.2-7. Because each of the 3,264 MSTHM Process Model subdomains are equally sized in area, 81 meters in width by 20 meters in length (SNL 2007 [DIRS 181383], Section 6.2.12[a]), the probability of an event (e.g., early failed WP) occurring in any of the five percolation subregions is the same as the quantile distribution used to define the percolation subregions (i.e., 5 percent, 25 percent, 40 percent, 25 percent, and 5 percent). The MSTHM Abstraction inputs to the TSPA-SEIS are provided in two output file sets. Both TH output file sets are indexed by subregion and waste fuel type categories.

The first file set contains WP surface temperature and relative humidity; DS surface temperature and relative humidity; and average drift-wall temperature for each of the eight WP at each repository subdomain within each percolation subregion. Because this data set from the MSTHM Abstraction is so extensive, covering eight different possible TH drift environments at each of the 3,264 repository subdomains, it is referred to as the comprehensive TH response data set. The parameter values provided in the comprehensive TH response data set are indexed by their percolation subregion and the percolation flux at each of the repository subdomains is included. Included with the comprehensive TH response data set at each of the 3,264 repository subdomains is the percolation flux experienced by that location during the simulation period. Also, included with each of the 3,264 repository subdomains are the fraction of each subdomain in lithophysal rock; the fraction of lithophysal unit value specifies whether each repository subdomain is in a lithophysal host-rock unit or not. These repository subdomain-specific TH data values and parameters are input to the WP and DS Degradation Model Component (Section 6.3.5), the Drift Seepage Submodel (Section 6.3.3.1), and the Drift Wall Condensation Submodel (Section 6.3.3.2).

A second MSTHM Abstraction file set for the TSPA-SEIS contains TH response histories for each of the five repository subregions based on a single, representative WP for each fuel type.

The determination of the representative WP for each bin is described in Section 6.3.2.2.2. This data set from the MSTHM Abstraction is referred to as the representative TH response data set (Section 6.3.2.2.2). The TH information from a single representative CSNF WP and a representative CDSP WP for each repository subregion provides the following inputs: WP surface temperature and relative humidity; DS temperature and relative humidity; drift-wall temperature; invert temperature; invert saturation; and invert flux. Table 6.3.2-4 summarizes the variables estimated by the MSTHM Abstraction for the representative TH conditions at each of the five repository percolation subregions in the TSPA-SEIS. Parameter values from the representative TH response data set are used for input to the EBS Flow and Transport Model Component (Sections 6.3.6 and 6.3.8), the Waste Form Degradation and Mobilization Model Component (Section 6.3.7), the EBS Chemical Environment Submodel (Section 6.3.4), and the Drift Wall Condensation Submodel (Section 6.3.3.2).

In summary, Figure 6.3.2-1 shows the flow of MSTHM Abstraction results for the comprehensive and representative TH data sets provided to the TSPA-SEIS, consisting of TH abstractions at each of the 3,264 repository subdomains and TH abstractions at the representative WPs for each subregion. When a submodel or model component of the TSPA-SEIS requires input of TH response conditions associated with the representative CSNF or CDSP WP in a selected repository subregion, then the TH response conditions for that representative CSNF or CDSP WP are used as the TH response conditions for all CSNF or CDSP WPs in that subregion. For example, the time-dependent TH response conditions for the representative CSNF WP in a selected percolation subregion are used as the TH conditions for both the CSNF WPs in the dripping environment and the CSNF WPs in the non-dripping environment of that percolation subregion. The TH inputs to the TSPA-SEIS do not make a distinction between dripping and non-dripping environments because the TH conditions in the emplacement drifts are more strongly influenced by percolation flux and saturation in the host rock surrounding the drifts than by the flow-focusing effects associated with a dripping environment (SNL 2007 [DIRS 181383], Section 6.3.2.1). The influence of percolation flux on TH conditions is included in the MSTHM Process Model methodology. *Multiscale Thermohydrologic Model* (SNL 2007 [DIRS 181383], Section 6.2.1) outlines the MSTHM Process Model approach and the TH processes accounted for by the model.

6.3.2.2.2 Determination of Representative Waste Packages

The representative CSNF and CDSP WPs are selected by compiling the peak WP temperature and the duration of boiling at the drift wall for each WP type in each repository percolation subregion. For each repository percolation subregion, these values are sorted from low to high, and a percentile is assigned to each WP location. For each repository percolation subreagion, two representative WP's are selected, one for each WP type., Each representative WP is the one whose simulated peak WP temperature and drift-wall boiling period is closest to the calculated median value for peak WP temperature and the median boiling period duration in the selected percolation subregion, as described in *Multiscale Thermohydrologic Model* (SNL 2007 [DIRS 181383], Appendix VIII[a]). The two criteria, peak WP temperature and duration of boiling at the drift wall, that were used to select the representative CSNF and CDSP WP TH response curves were chosen because of their correlation to how dry the emplacement drifts will get and how quickly water or water vapor will return. After the process of selecting the representative WPs is completed for each waste fuel type in each percolation subregion, the TH

response parameters of temperature and relative humidity values for each representative WP and associated DS, the average drift-wall temperature, the average invert temperature, the average invert saturation, and the average invert flux at each representative WP location are assembled in a representative TH response data file set. These data are accessed by the EBS TH Environment Submodel and provided as input to the Waste Form Degradation and Mobilization Model Component (Section 6.3.7), the EBS Flow and Transport Model Component (Sections 6.3.6 and 6.3.8), the EBS Chemical Environment Submodel (Section 6.3.4), and the Drift Wall Condensation Submodel (Section 6.3.3.2).

6.3.2.3 TSPA-SEIS Implementation

EBS TH Environment Submodel—Results from the MSTHM Abstraction serve as inputs to TSPA-SEIS components and submodels, as described in Section 6.3.2.2 and as follows. The TH parameters from the MSTHM Abstraction in the EBS TH Environment Submodel are time histories of:

- WP temperature
- DS Temperature
- Drift-wall temperature
- WP relative humidity
- Invert relative humidity
- Invert liquid flux (vertical component)
- Invert saturation.

An additional parameter, relative humidity of the invert, is calculated within the EBS TH Enviroment Submodel as described in the MSTHM Process Model (SNL 2007 [DIRS 181383], Appendix XVI[a]).

Two sets of TH parameter files are provided by the MSTHM Abstraction, a comprehensive set and a representative set (Section 6.3.2.2.1). The comprehensive TH response files have the TH parameter time histories (listed above) for each of the eight possible WPs at each of the 3,264 MSTHM Process Model repository subdomains, and are categorized by percolation subregion and fuel type (Figure 6.3.2-8). Included with the comprehensive TH response data set at each of the 3,264 repository subdomains is the percolation flux experienced by that location during the simulation period. Also, included for each of the 3,264 repository subdomains is a note specifying whether that repository subdomain is in a lithophysal host-rock unit or not. These comprehensive TH data values and parameters are input to the WP and DS Degradation Model Component (Section 6.3.5) and the Drift Seepage Submodel (Section 6.3.3.1). In addition, the comprehensive TH data set is used to calculate other TSPA Model inputs (i.e. thermal measures) including the average percolation flux for the drift used in the Drift Wall Condensation Submodel (Section 6.3.3.2).

The representative TH response file set has the TH parameter time histories for a single representative WP for a given fuel type in each percolation flux subregion. Each of the two sets of TH parameters is provided for the 12 infiltration/host-rock thermal-conductivity uncertainty combinations (Table 6.3.2-3). The TH parameter set containing the representative WPs is implemented into the TSPA-SEIS as a set of two-dimensional tables. Each two-dimensional

table contains the TH parameter time histories for one of the 120 combinations of infiltration/thermal-conductivity uncertainty (twelve each), fuel type (two each), and percolation subregion (five each). The TH parameters from the representative WPs are used as inputs to the Waste Form Degradation and Mobilization Model Component (Section 6.3.7), EBS Flow and Transport Model Component (Sections 6.3.6 and 6.3.8), the EBS Chemical Environment Submodel (Section 6.3.4), and Drift Wall Condensation Submodel (Section 6.3.3.2). The comprehensive TH parameter set that includes each WP for a given fuel type (six CSNF WPs, two CDSP WPs) at each of the MSTHM Process Model repository subdomains (3,264 each) in a given percolation subregion (five each) is implemented as a set of externally carried model input files which are used by the seepage dynamically linked library (DLL), the WP Degradation Model (WAPDEG) DLL, and the Waste Package Localized Corrosion (LC) Initiation Analysis. In addition the representative TH data set is used to calculate the duration of boiling (e.g. time needed of drift cooling to 96°C) for each of the representative WPs which is used in the EBS Chemical Environment Submodel (Section 6.2.4).

6.3.2.4 Model Component Consistency and Conservatism in Assumptions and Parameters

To enhance understanding of the complex interactions within the TSPA-SEIS, a discussion of consistency among model components and submodels, and identification of conservative assumptions in abstractions, process models, and parameter sets supporting the EBS TH Environment Submodel are discussed below.

6.3.2.4.1 Consistency of Assumptions

In-Drift Axial Fluid Flow—The MSTHM Process Model, which provides the basis for the in-drift temperature and relative humidity abstraction of the TSPA-SEIS, does not consider the longitudinal transport of water vapor along the length of the emplacement drifts. Thus, the influence of evaporation, transport, and condensation in the heated and unheated regions of the drifts, which result in a cold-trap effect, is not fully accounted for. On the other hand, the influence of the longitudinal transport of water vapor and associated condensation on the drift walls is approximated in the In-Drift Natural Convection and Condensation Process Model (SNL 2007 [DIRS 181648], Section 6.3). Therefore, there is a conceptual difference between the MSTHM Process Model and the In-Drift Natural Convection and Condensation Process Model.

Effect on the TSPA-SEIS—Although drift-wall condensation effects have been included in the TSPA-SEIS (Section 6.3.3.2), the difference in the modeling assumptions regarding the axial transport of moisture between the MSTHM Process Model and the Drift Wall Condensation Abstraction are possibly contradictory. If longitudinal vapor transport were included in the MSTHM Process Model, condensation in the unheated regions of the repository would affect the longitudinal variation of predicted in-drift temperature and relative humidity, with the effects on relative humidity having the greater potential impact, with vapor transport resulting in drier conditions than those predicted by the MSTHM (SNL 2007 [DIRS 181383], Section 7.8[a]). The thermal effects associated with the evaporation and condensation tend to dampen longitudinal temperature and relative humidity variations because heat would more effectively move from the hotter regions in a drift where the water evaporates, and then move to the cooler regions of the drift where the water vapor condenses. Thus, the WP-to-WP variation in temperature and relative humidity could be affected. However, both analysis/model reports,

Multiscale Thermohydrologic Model (SNL 2007 [DIRS 181383], Section 7.5.3) and *In-Drift Natural Convection and Condensation* (SNL 2007 [DIRS 181648], Section 6.3.7.2.4), indicate that these longitudinal mass/energy transfer processes are shown to have an insignificant effect on the primary MSTHM Model predictions of temperature and relative humidity.

6.3.2.4.2 Identification of Conservatisms in Submodels and Abstractions

Repository Edge Effect—Although the heat loss into the host rock due to the repository edge effect is captured in the MSTHM Process Model via thermal conduction, the thermal convection component of the heat loss into the host rock expected at the edges of the repository is not included (SNL 2007 [DIRS 181383], Section 5.2.1). The bulk permeability of the repository host rock makes thermal conductivity the dominant heat flow mechanism because mass movement, via convection, from the drifts into the host rock is impeded by the limited permeability (SNL 2007 [DIRS 181383], Section 5.2.1).

6.3.2.5 Alternative Conceptual Model(s) for Engineered Barrier System Thermal-Hydrologic Environment

An important reason for considering ACMs is to help build confidence that plausible changes in modeling assumptions or simplifications will not change conclusions regarding subsystem and total system performance. Section 6.2 outlines the general consideration and treatment of ACMs used to support the TSPA-SEIS. Conservatism at the subsystem level has been used to select the best ACM to use rather than quantitatively propagate multiple ACMs to the TSPA-SEIS. Generally, additional uncertainty is incorporated into the selected conceptual model if more than one ACM is deemed appropriate for use rather than considering multiple ACMs in the TSPA-SEIS. If an ACM appears to be significant at the subsystem level, then an appropriate abstraction is developed for that ACM for consideration within the TSPA-SEIS. The result of the process is documented within the individual analysis/model reports. It is important to note that treatment of ACMs within the individual analysis/model reports may differ significantly to be consistent with available data and current scientific understanding. Therefore, a brief description of the EBS TH Environment ACM summarized in Table 6.3.2-5 is presented below.

Lawrence Berkeley National Laboratory Mountain-Scale UZ Model ACM—An ACM to the MSTHM Process Model is a mountain-scale TH model developed by Lawrence Berkeley National Laboratory (Haukwa et al. 1998 [DIRS 117826]). The Lawrence Berkeley National Laboratory model is a monolithic TH model. The Lawrence Berkeley National Laboratory TH model used: (1) coarser grid discretization at the drift scale than the MSTHM Process Model; (2) a line-averaged approximation of the heat-generation-rate-versus-time table (whereas, the MSTHM Process Model represented the WPs as discrete heat sources); and (3) a lumped heat source that filled the entire cross section of the emplacement drift (SNL 2007 [DIRS 181383], Section 6.4).

The temperature predicted by the MSTHM Process Model is the perimeter-averaged drift-wall temperature adjacent to an "average" 21-PWR medium-heat CSNF WP. The MSTHM Process Model discretely represents the decay-heat source from individual WPs. The drift-wall gridblocks over which the drift-wall temperature is averaged extend 0.5 meter into the host rock surrounding the emplacement drifts (SNL 2007 [DIRS 181383], Section 6.4). The temperature

prediction in the east-west cross-sectional Lawrence Berkeley National Laboratory mountain-scale TH model is for a gridblock that occupies the entire cross section of a drift; therefore, it is a lumped representation of the drift temperature (SNL 2007 [DIRS 181383], Section 6.4). Moreover, because the east-west cross-sectional mountain-scale model uses a line-averaged heat source, it axially smears out the differences between "hot" and "cold" WP locations along the drift (SNL 2007 [DIRS 181383], Section 6.4).

During the post-boiling period, the temperatures predicted by both the MSTHM Process Model and the ACM modeling approach are in good agreement (SNL 2007 [DIRS 181383], Section 6.4). During the early-time heat-up period, the coarse (lateral and axial) grid-block spacing in the east-west cross-sectional mountain-scale model does not capture the rapid drift-wall temperature rise that the more finely gridded MSTHM Process Model predicts. Because of the coarse lateral grid block spacing in the east-west model, it smears out the lateral temperature gradient between the drift and the mid-pillar location. Therefore, it tends to overpredict the temperature at the mid-pillar location, thereby preventing condensate from shedding between drifts (SNL 2007 [DIRS 181383], Section 6.4). The fine lateral grid-block spacing in the MSTHM Process Model captures the influence that the lateral temperature gradient has on allowing condensate to shed between drifts. The tendency for the east-west cross-sectional mountain-scale model to under represent condensate shedding results in a more substantial condensate buildup above the repository horizon (SNL 2007 [DIRS 181383], Section 6.4). Also, the line-averaged heat-source approximation smears out differences in temperature between otherwise "hot" and "cold" WP locations, thereby preventing condensate from breaking through "cold" WP locations along the emplacement drifts (SNL 2007 [DIRS 181383], Section 6.4). Altogether, the under prediction of condensate shedding between drifts and condensate breakthrough at "cold" WP locations causes the east-west cross-sectional mountain-scale model to build up more condensate above the repository horizon that leads to episodic heat-pipe behavior.

The MSTHM Process Model and the east-west cross-sectional Lawrence Berkeley National Laboratory mountain-scale model are in agreement (SNL 2007 [DIRS 181383], Section 6.4). Moreover, the differences in predicted temperatures between the MSTHM Process Model and the east-west cross-sectional Lawrence Berkeley National Laboratory mountain-scale model are within the range of temperature differences resulting from parametric uncertainty (SNL 2007 [DIRS 181383], Tables 6.3-30 and 6.3-31).

No ACMS related to the EBS TH Environment Submodel were recommended for inclusion in the TSPA-SEIS.

INTENTIONALLY LEFT BLANK

Table 6.3.2-1. Parameter Distribution for Host-Rock Thermal-Conductivity Uncertainty

Parameter Name in TSPA-SEIS	Description	Distribution
Thermal_Conductivity_Uncert_a	Uncertainty between the three host-rock thermal-conductivity scenarios (low, mean, and high).	Discrete (p, v) [(0.29, 1), (0.37, 2), (0.34, 3)]

Source: *Multiscale Thermohydrologic Model* (SNL 2007 [DIRS 181383], Table 6.3-47[a]).

Table 6.3.2-2. Percolation-Based Probability Subregion Quantile Ranges

Subregion Index	Quantile Range
1	$p < 0.05$
2	$0.05 \leq p < 0.30$
3	$0.30 \leq p < 0.70$
4	$0.70 \leq p < 0.95$
5	$p \geq 0.95$

Source: DTN: MO0505SPAROCKM.000 [DIRS 173893]

Table 6.3.2-3. Probability Weighting for the 12 Percolation Flux and Host-Rock Thermal-Conductivity Combinations

Percolation Flux Case	Probability			
	Host-Rock Thermal-Conductivity			
	All	Low	Mean	High
All	1.0000	0.34	0.37	0.29
10%	0.6191	0.1795	0.2291	0.2105
30%	0.1568	0.0455	0.0580	0.0533
50%	0.1645	0.0477	0.0609	0.0559
90%	0.0596	0.0173	0.0220	0.0203

Source: *Multiscale Thermohydrologic Model* (SNL 2007 [DIRS 181383], Table 6.3-47[a]

Table 6.3.2-4. List of Thermal-Hydrologic Variables Predicted by the MSTHM Process Model and Used in the TSPA-SEIS

Thermal-Hydrologic Variable	Drift-Scale Location
Temperature	Drift wall (perimeter average)
	Drip shield (upper surface)
	Waste package (surface average)
	Invert (average)
Relative humidity	Waste package (surface average)
	Drip Shield (average)
Liquid-phase saturation (intragranular)	Invert (average)
Liquid-phase flux	Invert (average)

Table 6.3.2-5. Alternative Conceptual Model Considered for the Engineered Barrier System Thermal-Hydrologic Environment

Alternative Conceptual Models	Key Assumptions	Screening Assessment and Basis
Lawrence Berkeley National Laboratory Mountain-Scale UZ Model	An ACM to the MSTHM Process Model is a mountain-scale TH model developed by Lawrence Berkeley National Laboratory (Haukwa et al. 1998 [DIRS 117826]). The Lawrence Berkeley National Laboratory model is a monolithic TH model. The Lawrence Berkeley National Laboratory TH model used: (1) coarser grid discretization at the drift scale than the MSTHM Process Model; (2) a line-averaged approximation of the heat-generation-rate-versus-time table (whereas the MSTHM Process Model represented the WPs as discrete heat sources); and (3) a lumped heat source that filled the entire cross section of the emplacement drift (SNL 2007 [DIRS 181383], Section 6.4).	Screened out. Given the differences between the MSTHM Process Model and the east-west cross-sectional Lawrence Berkeley National Laboratory Mountain-Scale Model, the agreement between the two models is adequate (SNL 2007 [DIRS 181383], Section 6.4). Moreover, the differences in predicted temperatures between the MSTHM Process Model and the east-west cross-sectional Lawrence Berkeley National Laboratory Mountain-Scale Model are within the range of temperature differences resulting from parametric uncertainty (SNL 2007 [DIRS 181383], Tables 6.3-30 and 6.3-31).

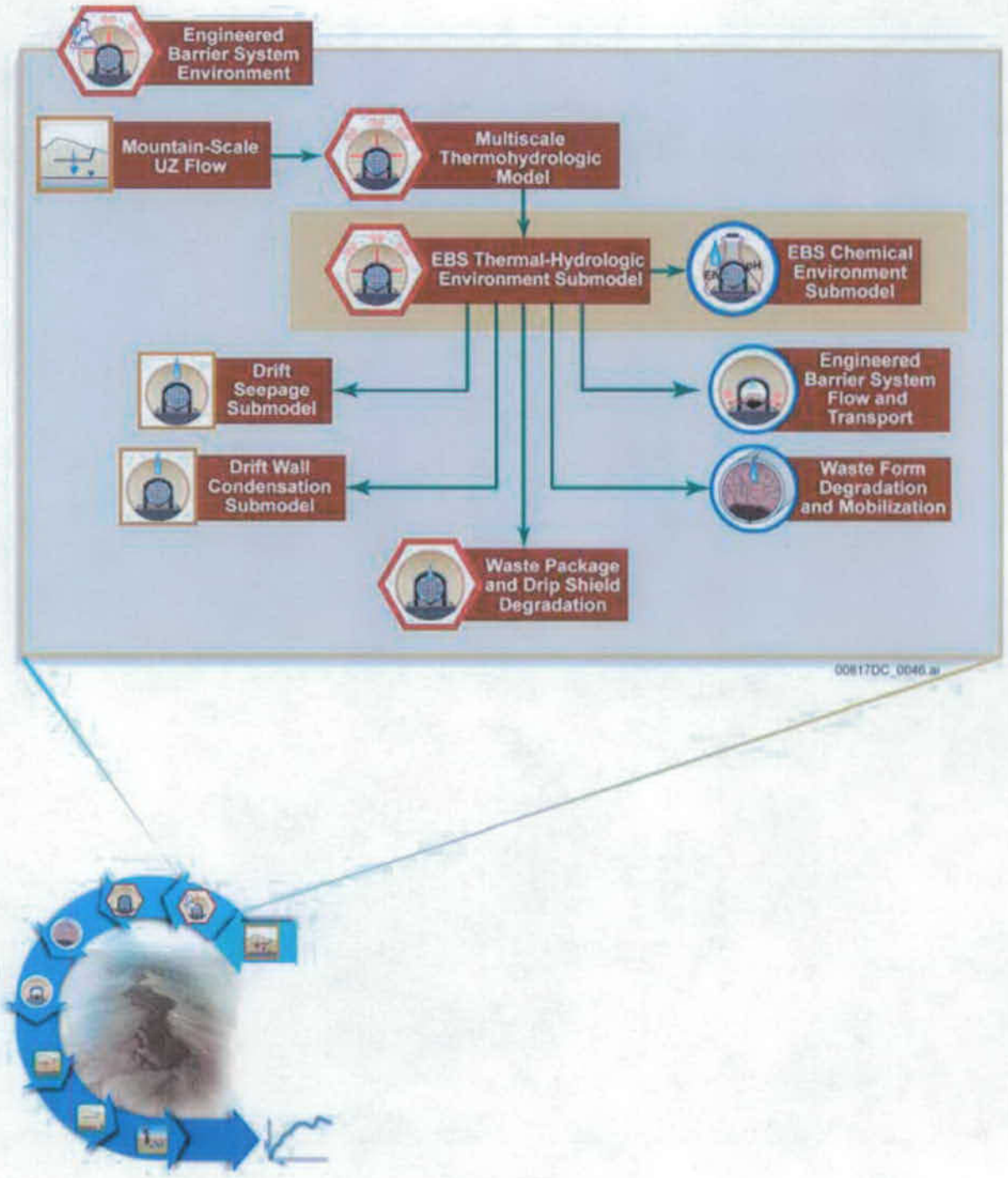

Figure 6.3.2-1. Information Flow Diagram for the EBS Thermal-Hydrologic Environment Submodel

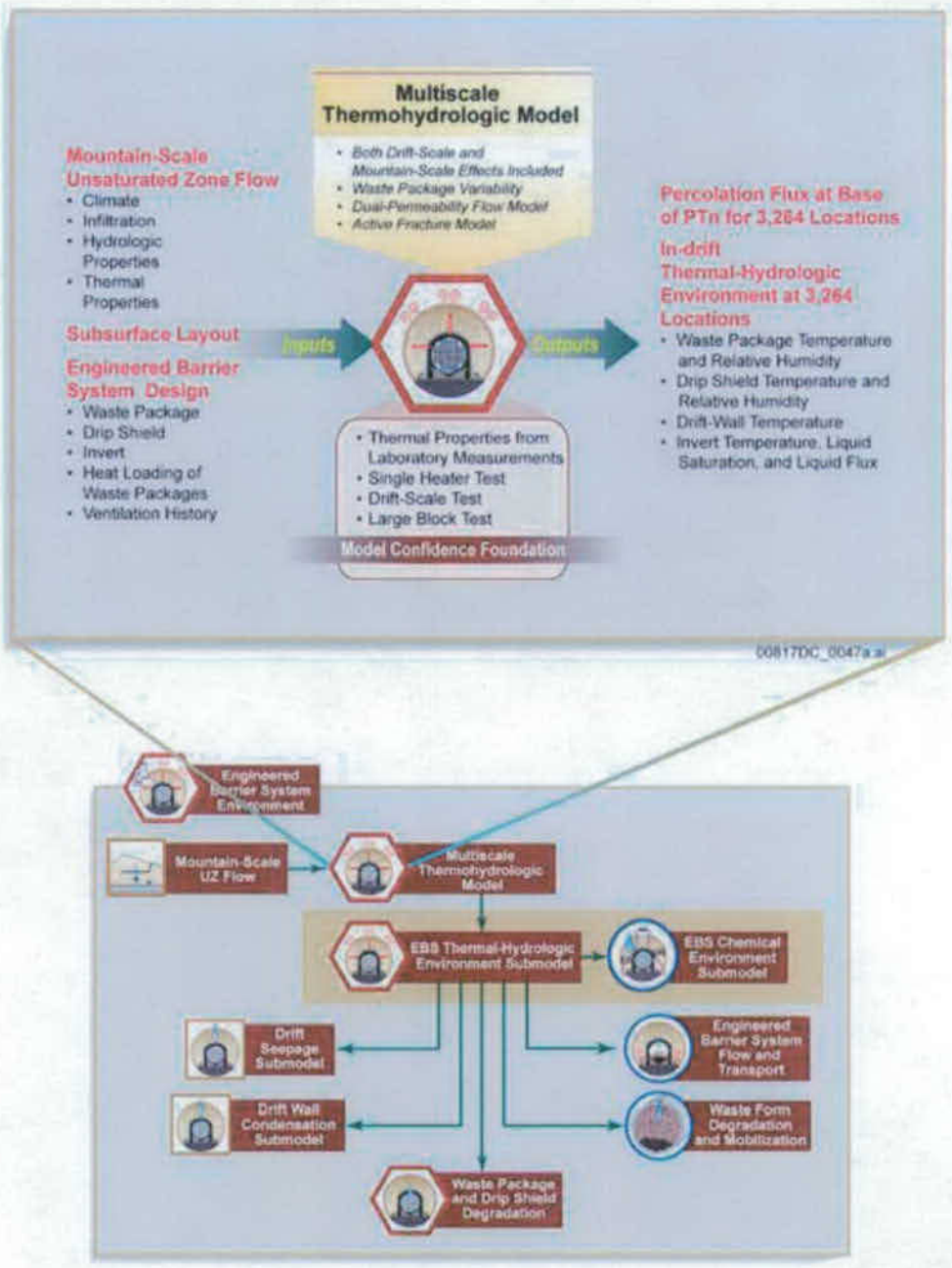

Figure 6.3.2-2. Inputs, Outputs, and Basis for Model Confidence for the Multiscale Thermohydrologic Process Model

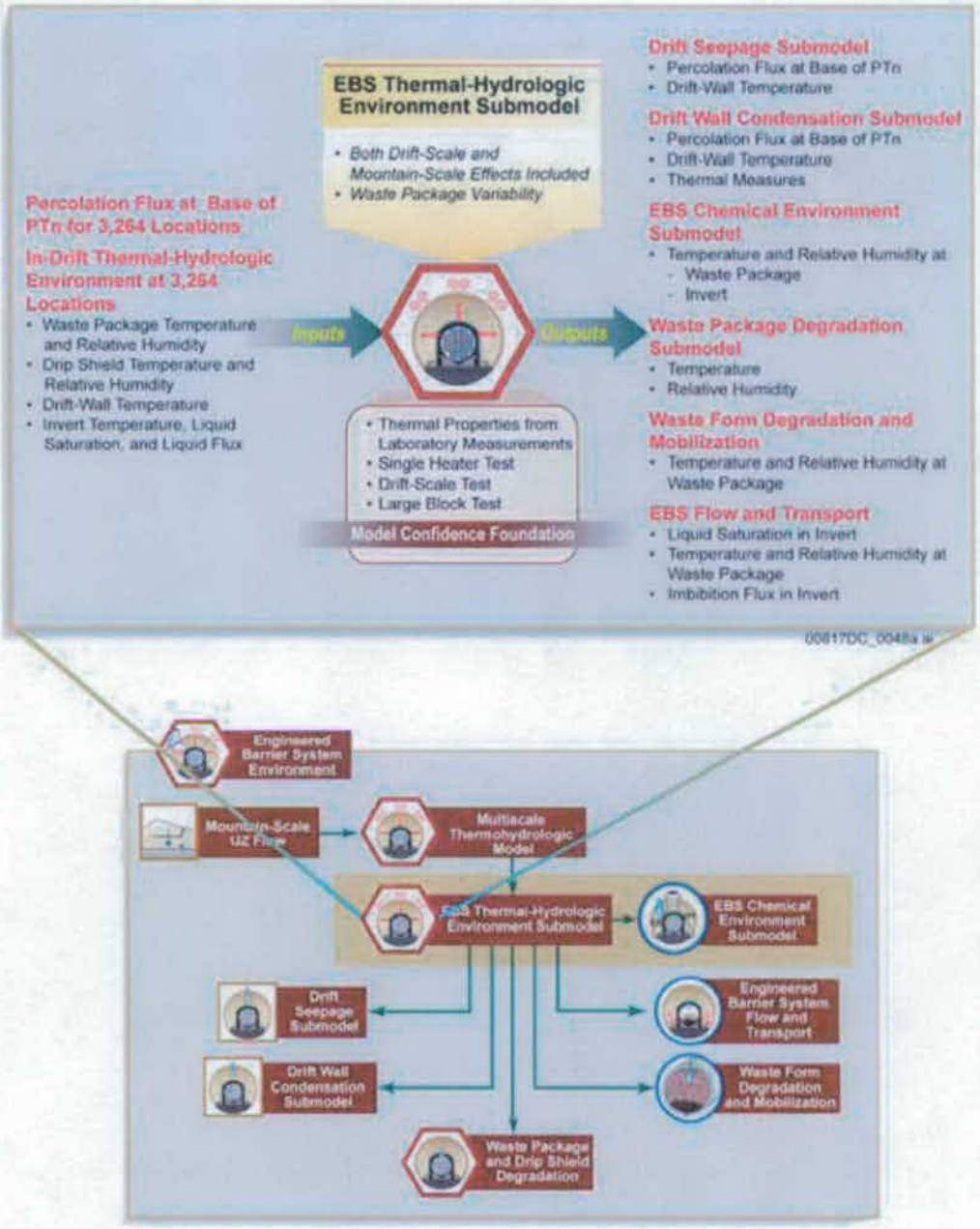

Figure 6.3.2-3. Inputs, Outputs, and Basis for Model Confidence for the EBS Thermal-Hydrologic Environment Submodel

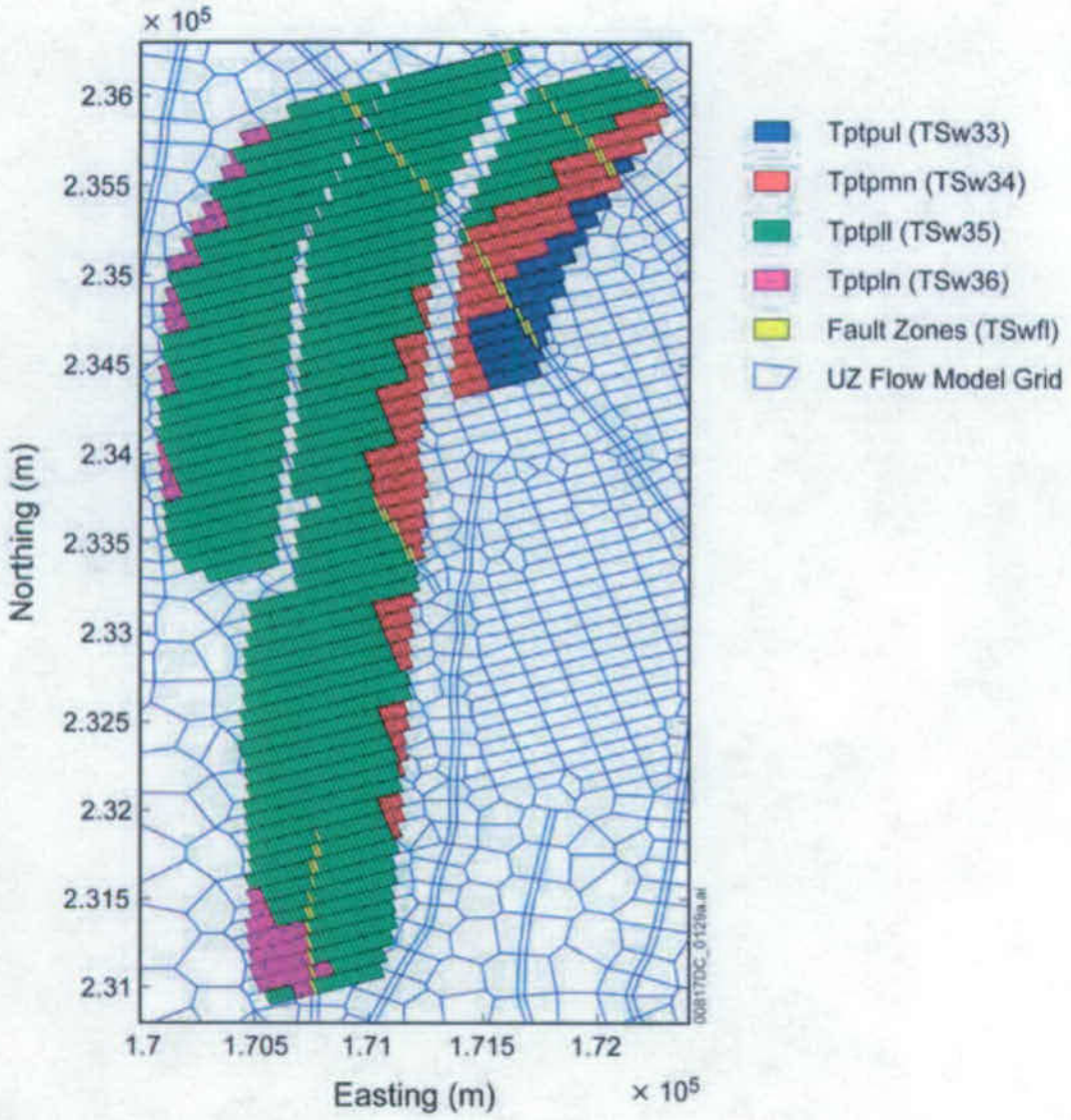

Source: SNL 2007 [DIRS 181383], Figure 6.2-18[a]

NOTES: Also shown are the five representative locations (indicated by circles) that were selected to examine thermal-hydrologic conditions in the four primary host-rock units.

Tptpul = Topopah Spring Tuff crystal-poor upper lithophysal zone; Tptpmn = Topopah Spring Tuff middle nonlithophysal zone; Tptpll = Topopah Spring Tuff crystal-poor lower lithophysal zone; Tptpln = Topopah Spring Tuff lower nonlithophysal zone.

Figure 6.3.2-4. The Distribution of the Four Primary Host-Rock Units is Shown for the Repository Layout Considered in the Multiscale Thermohydrologic Model Calculations for the TSPA-SEIS

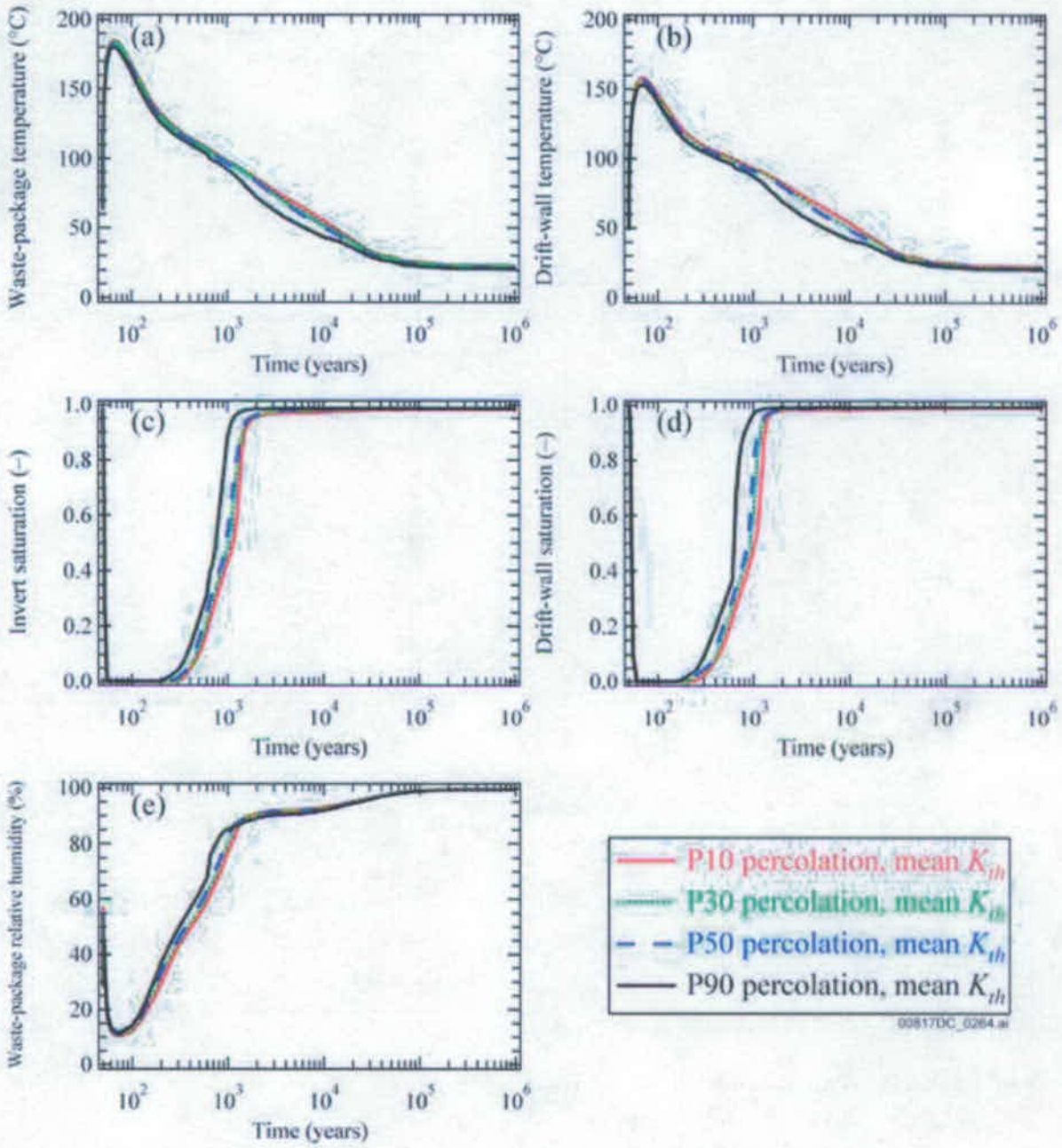

Source: DTNs: LL0703PA011MST.006 [DIRS 179853], LL0703PA012MST.007 [DIRS 179854], LL0703PA013MST.008 [179855], and LL0703PA014MST.009 [DIRS 179856]

NOTE: Plotted thermal-hydrologic variables are: (a) drift-wall temperature; (b) WP temperature; (c) drift-wall liquid-phase saturation; (d) WP relative humidity; and (e) invert liquid-phase saturation.

Figure 6.3.2-5. Thermal-Hydrologic Conditions for the PWR1-2 Waste Package Plotted for Low, Mean, and High Percolation-Flux Cases at a Location Near the Center of the Repository

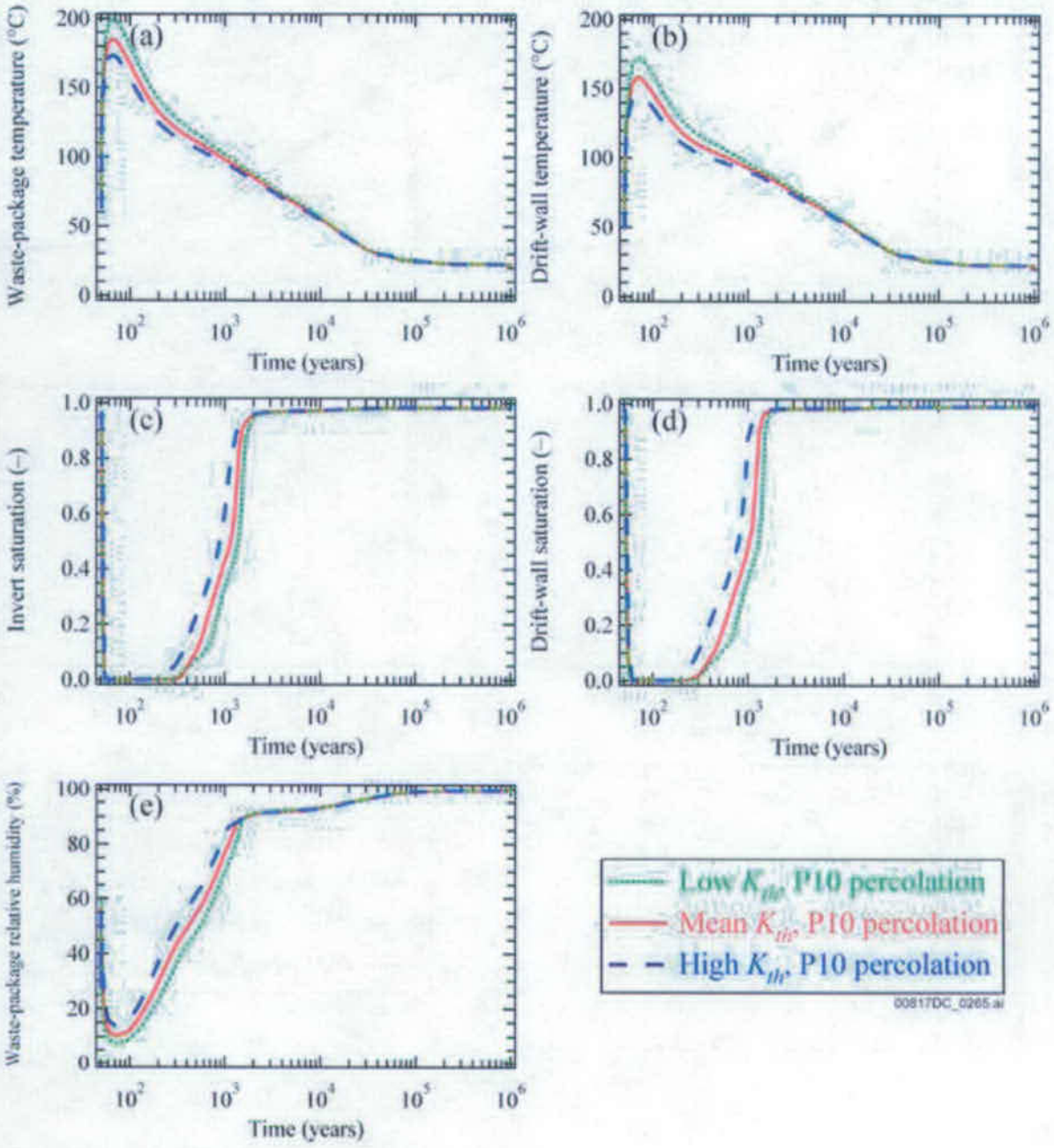

Source: DTNS: LL0703PA011MST.006 [DIRS 179853], IL0703PA015MST.010, [DIRS 179857], and LL0703PA017MST.012 [DIRS 179859]

NOTE: The plotted thermal-hydrologic variables are: (a) drift-wall temperature; (b) WP temperature; (c) drift-wall liquid-phase saturation; (d) WP relative humidity; and (e) invert liquid-phase saturation.

Figure 6.3.2-6. Thermal-Hydrologic Conditions for the PWR1-2 Waste Packages Plotted for Mean Infiltration Case at a Location Near the Center of the Repository

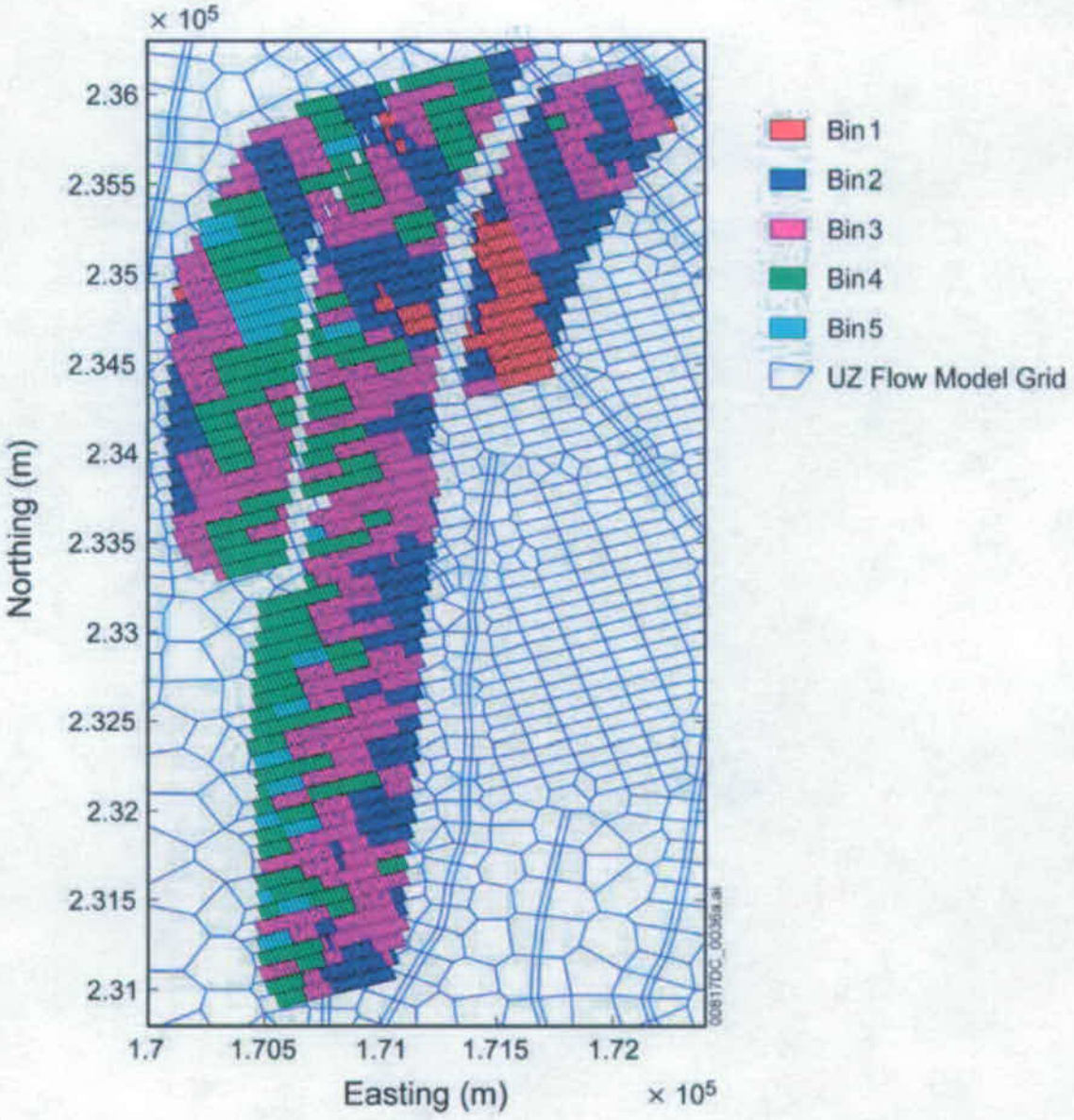

Sources: SNL 2007 [DIRS 181383], Figure VIII-1[a]

NOTE: The contingency area in the southern portion of the repository is not included in the percolation subregions.

Figure 6.3.2-7. Repository Percolation Subregions Used in the TSPA-SEIS (based upon the 30th percentile infiltration case, glacial-transition period)

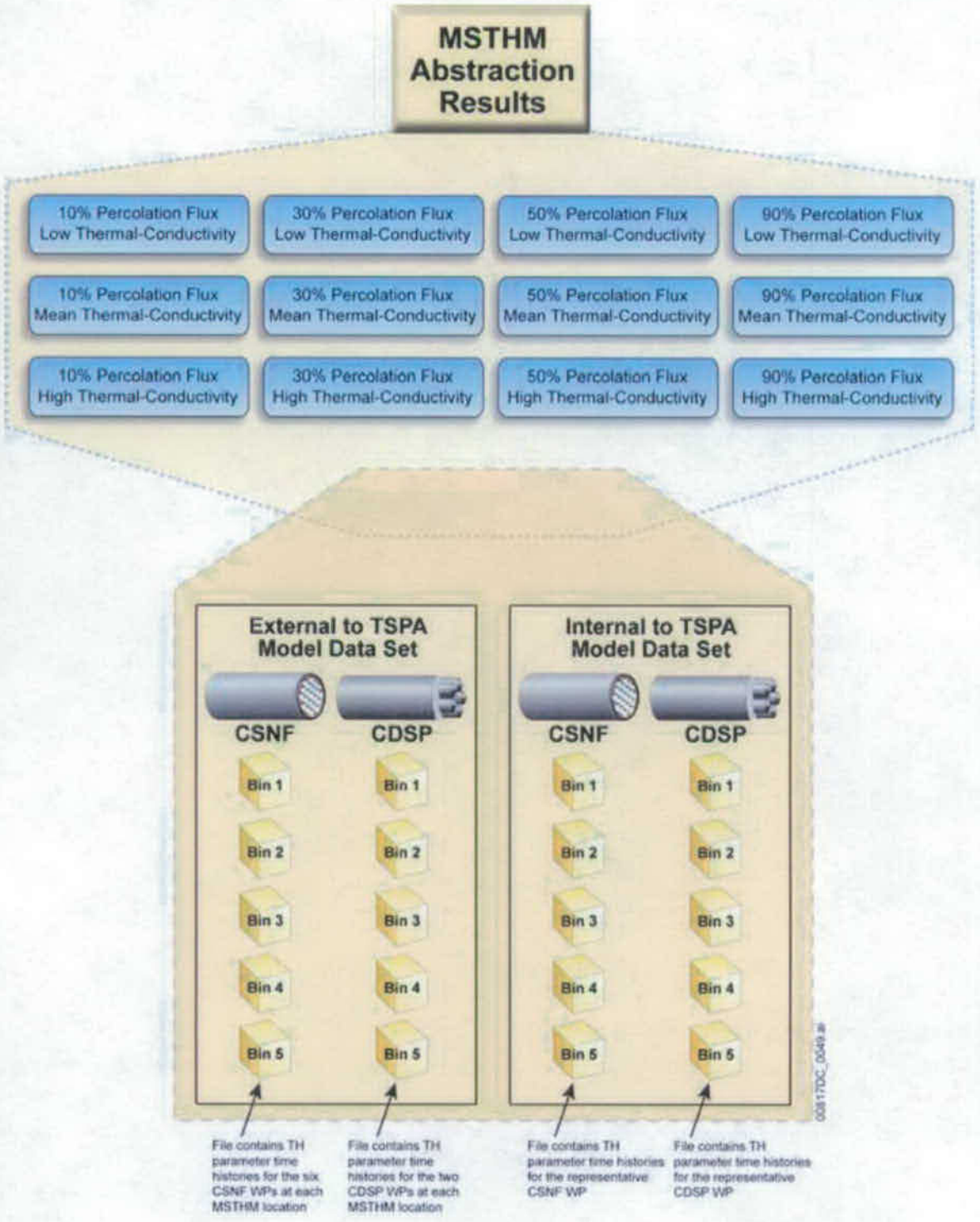

Figure 6.3.2-8. Thermal-Hydrologic Time History Parameter Inputs to the TSPA-SEIS

6.3.3 Drift-Scale Unsaturated Zone Flow

Water contacting DSs and WPs is expected to originate from two sources: (1) seepage of groundwater from the UZ above the repository into the emplacement drifts (SNL 2007 [DIRS 181244], Section 1) and (2) water-vapor condensate dripping from the walls of the drifts (SNL 2007 [DIRS 181648]Sections 6.3, 8.3, 6[a], and 8[a]). Percolation flux at the base of the PTn is used as the source of water for both drift seepage and drift-wall condensation. However, in this analysis no water balance is applied between the percolation flux, drift seepage, and drift-wall condensation. The TSPA-SEIS calculates drift seepage and drift-wall condensation flow rates using the Drift Seepage Submodel (Section 6.3.3.1) and the Drift Wall Condensation Submodel (Section 6.3.3.2), respectively. These two flow rates are combined in the EBS Flow Submodel (Section 6.3.6) to yield a total dripping rate. Section 6.3.3.1 discusses the Drift Seepage Submodel (SNL 2007 [DIRS 181244], Section 6), and Section 6.3.3.2 presents the Drift Wall Condensation Submodel (SNL 2007 [DIRS 181648], Section 6 and Section 6[a]).

6.3.3.1 Drift Seepage

Drift seepage refers to the flow of liquid water from the UZ above the repository into waste emplacement drifts. The Drift Seepage Submodel calculates two quantities: (1) the fraction of WP locations that experience seepage and (2) the average seepage flow rate for WP locations that have seepage (Section 6.3.3.1.3). The calculations are performed for each fuel type in each percolation flux subregion (MSTHM Abstraction, Section 6.3.2.2.1). Figure 6.3.3-1 illustrates the flow of information for the Drift Seepage (SNL 2007 [DIRS 181244], Section 6) and Drift Wall Condensation Submodels (SNL 2007 [DIRS 181648], Section 6)). Figure 6.3.3-2 shows the connections between the Drift Seepage Submodel and the EBS Flow Submodel (Section 6.3.6). Figure 6.3.3-2 shows inputs to and outputs from the Drift Seepage Submodel and indicates the principal features of the Drift Seepage Submodel and the foundation for confidence in the model.

6.3.3.1.1 Conceptual Model

Numerical modeling, natural analogues, and field tests summarized in (SNL 2007 [DIRS 181244], Sections 6.4.1, 6.4.2, 6.4.3, 7.3.1, and 7.3.2) indicate that seepage flux into emplacement drifts will be less than the local percolation flux. This difference results from two main processes: (1) the formation of capillary barriers at drift walls that are active during the thermal and ambient postclosure periods, and (2) the formation of dry-out zones helping to prevent percolation from reaching the repository during the thermal period. The effectiveness of these processes depends on the strength of the capillary pressure in the fractures close to the drift, the host rock's permeability close to the drift, the local percolation flux above the drift, the temperature of the rock near the drift wall, and the shape of the drift opening.

Figure 6.3.3-3 shows TH effects and the dry-out zone in the vicinity of the emplacement drifts due to repository heating. As water approaches a waste emplacement drift, conditions near the drift wall affect the amount of water that eventually seeps into the drifts. For preclosure conditions, the water may first encounter a dry-out zone caused by drift ventilation. During the first several hundreds of years of the postclosure period, the dry-out zone may also develop from an increase in temperature due to decay heat from the emplaced waste, and where temperatures

are high enough, may reach several meters from the drift wall due to boiling of rock water in the drift vicinity. Under boiling conditions, water will not enter the emplacement drifts (BSC 2005 [DIRS 172232], Section 6.1.2). The dry-out zone, indicated by the red shading around the drifts, is shown on Figure 6.3.3-3. The zone around the emplacement drift affected by TH processes is characterized by boiling, vapor transport, condensation, and migration of water back toward the heat source, either by capillary forces or gravity drainage (SNL 2007 [DIRS 181244], Section 6.3.2, p. 6-12). If liquid water approaches the immediate vicinity of the drift wall after the repository cools, a zone of increased saturation is expected to develop as a result of the capillary-barrier effect of the drift opening (Figure 6.3.3-4). Most of this water cannot seep into the drift because of capillary suction, which retains water in the pore space of the rock. If the permeability and capillarity of the fracture network are sufficiently high, some or all of the water is diverted around the drift under partially saturated conditions. Locally, however, the water potential in the formation could become great enough to allow seepage from the formation into the drifts, as described in *Seepage Model for PA Including Drift Collapse,* (BSC 2004 [DIRS 167652], Section 6.2.1).

Emplacement drifts may degrade with time as a result of thermal stress, seismic ground motion, and time-dependent degradation of rock strength. These effects may lead to partial or complete drift collapse, with rock material filling the enlarged drifts and changing their shape and size. Depending upon the intensity of these effects, damage to drifts may be small, with local rockfall at the ceiling of otherwise intact drift openings, or in extreme cases, may result in partial or complete drift collapse, with rubble rock material filling the enlarged drifts. These changes alter the potential for drift seepage (SNL 2007 [DIRS 181244], Sections 6.2[a], 6.3.1 and 6.3.2). Local breakouts in the drift ceiling may also lead to geometry changes that may reduce or prevent flow diversion around the drifts and thus increase the seepage into drifts. The larger size and potentially altered shape of collapsed drifts can also bring about reduction in flow diversion. In addition, the larger footprint of collapsed drifts causes an increase in the percolation flux arriving at the drifts, which increases seepage into the drifts. Further, drift degradation may lead to fracture dilation that would promote flow diversion around the drifts, but at the same time decrease fracture capillary strength and cause less flow diversion around the drifts. Thus, the seepage into a collapsed drift may be different from that into an intact drift.

6.3.3.1.2 TSPA-SEIS Abstraction

As described in Section 6.1.4.3, water seepage into emplacement drift segments on the scale of a WP is a process that is modeled outside of the TSPA-SEIS, and the results are then abstracted (SNL 2007 [DIRS 181244]) for use in the TSPA-SEIS simulations. The abstracted results are based on drift-seepage simulations conducted for both ambient (BSC 2004 [DIRS 167652]) and thermal periods (BSC 2005 [DIRS 172232]).

The Drift Seepage Abstraction calculations differ for collapsed and noncollapsed drifts, as explained below. In the Nominal Scenario Class, partial drift degradation occurs rather than drift collapse. In the Seismic Scenario Class, drift collapse occurs in both lithophysal and nonlithophysal units. For the Seismic Scenario Class, partial collapse is considered in the lithophysal units, by comparing the cumulative rubble volume generated by seismic events to a lower and an upper threshold to determine whether to; (1) use the intact seepage model, (2) interpolate between intact-drift seepage model and collapsed drift seepage model, or (3) use the

collapsed-drift seepage model (SNL 2007 [DIRS 181244], Section 6.2.2[a]). In the nonlithophysal units, once a specified degree of drift collapse has occurred, the intact-drift seepage model is no longer appropriate. The cumulative rubble volume generated by seismic events, is compared to a threshold rubble volume to determine whether; (1) the intact-drift seepage model is used or (2) the percolation fluxes are used (SNL 2007 [DIRS 181244], Sections 6.2.3[a]). Drift collapse is not considered for the Igneous Scenario Class, as the drifts are filled with basalt by the intrusive event. For a detailed understanding of the rationale for the abstraction decisions, refer to (SNL 2007 [DIRS 181244], Sections 6.5.1.5 and 6.5.1.7).

Ambient seepage process model simulations were conducted for a range of representative local percolation fluxes ($q_{perc,ff}$), ranges of local permeability (k) and capillary strength ($1/\alpha$), nondegraded and degraded drift profiles and multiple realizations of the small-scale heterogeneous fracture-permeability field (BSC 2004 [DIRS 167652], Sections 6.3, 6.4, and 6.6). The local percolation fluxes ($q_{perc,ff}$) are derived from the fluxes at the base of the PTn from the MSTHM Abstraction (q_{perc}) (Section 6.3.2) by multiplication with flow-focusing factors (f_{ff}). The flow-focusing factors account for intermediate-resolution (SNL 2007 [DIRS 181244], Section 6.6.5.2) heterogeneity (on the spatial resolution of a few drift diameters) that is not accounted for in the MSTHM Process Model. In addition, it is possible that the initially circular-shaped emplacement drifts degrade with time principally as a result of seismic ground motion. These changes affect the potential for drift seepage (SNL 2007 [DIRS 181244], Sections 6.2[a], 6.3.1 and 6.3.2). The Seepage Model for Performance Assessment simulations (SNL 2007 [DIRS 181244], Section 6.4.2) produce, for both nondegraded and degraded drifts, response surfaces in the form of look-up tables for a seepage rate into a 5.1-m long drift section and a seepage rate standard deviation (SD) that are functions of $q_{perc,ff}$, $\log(k)$, and $1/\alpha$.

Probability distributions were developed to represent the spatial variability in flow-focusing factor (f_{ff}), $\log(k)$, and $1/\alpha$, and the uncertainty in $\log(k)$ and $1/\alpha$ (SNL 2007 [DIRS 181244], Section 6.3[a] and Section 6.7.1.1).

Four different methods were identified to derive statistical parameters that describe spatial variability and uncertainty in $1/\alpha$ with respect to the geologic units present around the drifts (SNL 2007 [DIRS 181244], Sections 6.3[a] and 6.6.2.2). However, as discussed in SNL 2007 [DIRS 181244], Section 6.3[a]), the overall seepage results do not significantly differ between methods (SNL 2007 [DIRS 181244], Section 6.8.2). Therefore, the probability distributions for spatial variability and uncertainty in $1/\alpha$, defined in Table 6.3.3-1, are used. Spatial variability and uncertainty for $\log(k)$ are dependent on the geologic units present around the drifts. The distributions for spatial variability and uncertainty in $\log(k)$ in the nonlithophysal and lithophysal repository units are defined in Table 6.3.3-2. Local percolation flux values in the vicinity of the drifts are determined from percolation fluxes at the base of the PTn. These are provided at each repository subdomain, r, by the MSTHM Abstraction which obtains the information from the Site-Scale UZ Flow Process Model (Figure 6.3.1-1), as described in Section 6.3.2. The percolation fluxes in the UZ are time dependent (represented by four different climate periods), spatially variable (because of nonuniform infiltration and nonuniform flow in the UZ), and uncertain (as represented by four different infiltration cases) as discussed in Section 6.3.1. As discussed in (SNL 2007 [DIRS 181244], Section 6.5.1.1), these percolation fluxes, q_{perc}, are adjusted for intermediate-scale heterogeneity, which is not represented in the distributions of fluxes provided by the MSTHM Abstraction. This adjustment uses a spatial distribution of

flow-focusing factors (f_{ff}). Multiplication of the q_{perc} from the MSTHM Abstraction by the f_{ff} gives the local percolation flux, $q_{perc,ff}$, to be used in the TSPA-SEIS calculations. The spatial variability distribution for the flow-focusing factor is defined as a cumulative probability distribution in the following form (SNL 2007 [DIRS 181244], Section 6.7.1.1).

The equation:

$$Y = -0.3137 f_{ff}^4 + 5.4998 f_{ff}^3 - 35.66 f_{ff}^2 + 102.3 f_{ff} - 11.434 \qquad \text{(Eq. 6.3.3-1)}$$

where Y is the cumulative probability in percent (SNL 2007 [DIRS 181244], Section 6.7.1.1).

The values of local percolation flux ($q_{perc,ff}$), the sampled values of local permeability ($\log(k)$), and capillary strength parameters ($1/\alpha$) are used to interpolate from the look-up tables for the mean seepage rate into a 5.1-m-long drift section and the seepage rate SD. The value of SD is used to account for uncertainty in the estimation of seepage rates.

The estimation uncertainty in the calculated seepage rates is accounted for by a uniform distribution with a mean of zero and a range defined by the seepage rate SD (–1.7321 SD, 1.7321 SD) (SNL 2007 [DIRS 181244], Section 6.7.1.1).

For noncollapsed drifts, the ambient seepage is increased by 20 percent to account for additional uncertainty due to partial drift degradation, such as breakouts in the drift ceiling that do not lead to complete drift collapse. However, for collapsed drifts, this increase is not implemented because this extreme degree of damage and its impact on seepage is represented by the seepage response surface for a collapsed drift, which includes sufficient conservatism (SNL 2007 [DIRS 181244], Section 6.7.2).

Analyses performed with the TH Seepage Process Model for noncollapsed drifts have shown that thermal seepage (seepage that is influenced by heat generated by the WP) will always be less than ambient seepage and that thermal seepage never occurs when there is boiling in the rock close to the emplacement drifts (BSC 2005 [DIRS 172232], Section 6.2.4). The recommended abstraction sets the thermal seepage equal to zero during the period of above-boiling temperatures at the crown of the drift. The threshold temperature that defines when seepage can occur is set to 100°C (SNL 2007 [DIRS 181244], Sections 6.5.2.2 and 6.7.1.2). After the temperature falls below 100°C, thermal seepage is set equal to the estimated ambient seepage.

For collapsed drifts, the thermal seepage abstraction conservatively sets the seepage equal to the estimated ambient seepage at all times in the TSPA period. This is based on the results of analyses that found that with the expanded drift opening, the rock temperature at the crown, is always below 100°C, or nearly so (SNL 2007 [DIRS 181244], Section 6.4.3.4). Thus there is no vaporization barrier in the intact rock to prevent water flow into a rubble-filled drift (SNL 2007 [DIRS 181244], Section 6.5.3).

For the Igneous Intrusion Modeling Case, the abstraction considers setting the seepage percentage to 100 percent, where the seepage rate is equal to the local percolation rate (L/t) at the base of the PTn multiplied by the footprint area (L^2) of the considered drift segment times the sampled flow-focusing factor. This abstraction is the most conservative available for

implementation in the TSPA-SEIS. It is applied from the time at which the igneous event occurs.

6.3.3.1.3 TSPA-SEIS Implementation

The TSPA-SEIS implementation of drift seepage is primarily accomplished through the use of an external DLL. When drift-seepage submodel calculations are required by the TSPA-SEIS, the Seepage DLL (STN: 11076-1.3-00 [DIRS 181058]) is called, and a total of 35 inputs are passed by the TSPA-SEIS to the Seepage DLL (refer to Table 6.3.3-3 for a list of these inputs).

The output of the Seepage DLL is a set of tables of seepage flow rate versus time. Each table corresponds to a WP type and percolation flux subregion (e.g., CSNF subregion 1; see Section 6.3.2.2.1 for a description of how the subregions are defined). The timesteps in the tables are related to the climate periods and to the timesteps used in the MSTHM. These tables are then interpolated to determine the seepage flow rate at each TSPA-SEIS timestep.

In addition to these inputs passed directly from TSPA-SEIS to the Seepage DLL, the Seepage DLL reads a set of PREWAP (STN: 10939-1.1-00 [DIRS 181053]) input files and a set of seepage look-up tables. The PREWAP output files contain the output results from the MSTHM in a format that can be used by both the WP and DS Degradation Submodels (Section 6.3.5) for WP and DS failure calculations and by the Seepage DLL. There are 120 PREWAP files, one for each of the five percolation subregions, two WP types, four infiltration scenarios, and three TH uncertainty cases. The inputs that the Seepage DLL reads from these files are the percolation flux at the base of the PTn at each MSTHM subdomain location, the drift-wall temperature for each WP at that subdomain location, and the fraction of lithophysal rock at that location. Two files contain seepage look-up tables, one for noncollapsed drifts and one for collapsed drifts. These files contain three-dimensional tables of mean seepage rate and seepage rate SD as a function of percolation flux, capillary strength, and fracture permeability.

The Seepage DLL uses these inputs to implement the calculations outlined in *Abstraction of Drift Seepage* (SNL 2007 [DIRS 181244], Section 6.7.1) to obtain the fraction of WPs that is expected to experience seepage and the seepage rate (m^3/yr per WP) onto those WPs that experience seepage. The DLL also adjusts the calculated ambient seepage rates for thermal and drift degradation effects, as necessary, as follows: (1) the ambient seepage rates are increased by 20 percent to account for drift degradation for the noncollapsed drift locations, and (2) seepage is set to zero for noncollapsed drift locations if the drift-wall temperature exceeds 100°C. The results of the Seepage DLL's seepage rate calculations (seepage rate versus time) are passed to the TSPA-SEIS in the form of 10 one-dimensional tables, one table for each WP type in each percolation subregion. The DLL also passes to GoldSim the fraction of WPs that experiences seepage for each percolation subregion and WP type, and the fraction of each percolation subregion that is in nonlithophysal rock. The EBS Flow Submodel (Section 6.3.6) uses the results for seepage rate, the fraction of WPs that experiences seepage, and the fraction of each percolation subregion that is in nonlithophysal rock. The Waste Package LC Submodel uses the results for the fraction of WPs that experiences seepage. The Drift Wall Condensation Submodel (Section 6.3.3.2) and the Seismic Scenario Class (Section 6.6) uses the results for the fraction of each percolation subregion that is in nonlithophysal rock.

The remainder of this section describes the drift-seepage implementation in more detail. Figure 6.3.3-5 illustrates the procedure for the probabilistic calculation of seepage in the TSPA-SEIS. The seepage DLL is applied for each WP (i.e., six CSNF or two CDSP; Section 6.3.2.3) at each of the 3,264 repository subdomains, r, identified by the MSTHM Abstraction comprehensive data set (Engineered Barrier System Thermal-Hydrologic Environment, Section 6.3.2). For each WP at each repository subdomain, r, the calculation of drift seepage involves two main steps: (1) evaluate ambient seepage rate from seepage look-up tables, and (2) adjust ambient seepage rate for thermal and drift degradation effects. As shown on Figure 6.3.3-5, these two steps are implemented for each probabilistic TSPA-SEIS realization and repository location.

Step 1: Ambient Seepage—Step 1 involves three main activities. The first activity deals with random sampling of spatial variability and uncertainty distributions, and the application of spatial variability and uncertainty to arrive at values for the capillary-strength parameter ($1/\alpha$), fracture permeability ($\log(k)$), and local percolation flux ($q_{perc,ff}$). The sampling and calculations are performed as follows:

- The uncertainty distributions specified in Tables 6.3.3-1 and 6.3.3-2 are sampled once per TSPA-SEIS realization, R, to determine $\Delta\log(k)$ and $\Delta 1/\alpha$. The seepage rate uncertainty is sampled from a uniform distribution. At each subdomain, r, the following steps are completed:

- The spatial variability distributions specified in Tables 6.3.3-1 and 6.3.3-2 and Equation 6.3.3-1 are sampled randomly for $\log(k)$, $1/\alpha$, and f_{ff} at the subdomain, r, for each WP (six CSNF and two CDSP WPs).

- The $\log(k)$ and $1/\alpha$ values are adjusted, using the values for $\Delta\log(k)$ and $\Delta 1/\alpha$ that are sampled in each realization, R, to arrive at the values of $\log(k)$ and $1/\alpha$ that account for both spatial variability and uncertainty.

- The mountain-scale percolation flux at each subdomain, r, for each WP (six CSNF and two CDSP WPs) (from the MSTHM Abstraction as obtained from the Site-Scale UZ Flow Process Model), provided by the PREWAP_LA files, is adjusted by multiplying it by f_{ff} to yield a local percolation flux, $q_{perc,ff}$.

It is possible, but unlikely, that the parameter ranges for $1/\alpha$, $\log(k)$, and $q_{perc,ff}$ covered by the seepage look-up tables are exceeded for parameter values sampled from the unbounded distributions of permeability and percolation flux. To avoid sampling values outside the parameter's ranges, the following constraints on $1/\alpha$, $\log(k)$, and $q_{perc,ff}$ (based on the range limits presented in SNL 2007 [DIRS 181244], Section 6.1[a],) are imposed:

- If $1/\alpha$ is larger than 1,000 Pa, set it to 1,000 Pa.
- If local percolation flux is less than 0.01 mm/yr, set it to 0.01 mm/yr.
- If local percolation flux is more than 5,000 mm/yr, set it to 5,000 mm/yr.
- If $\log(k)$ is less than -14, set it to -14.
- If $\log(k)$ is larger than -10, set it to -10.

The second activity in Step 1 is to extract (by linear interpolation between the three independent input parameters) at each subdomain, *r*, the ambient mean seepage rate and SD of ambient seepage rate from the appropriate seepage look-up tables originally from the *Seepage Model for Performance Assessment Including Drift Collapse* (BSC 2004 [DIRS 167652], Section 6.6.1) but extended as noted in *The Abstraction of Drift Seepage* [DIRS 181244], Section 6.1[a]. The TSPA-SEIS selects the appropriate look-up tables, depending on the host geologic unit and the selected Scenario Class. For the Nominal Scenario Class, look-up tables for noncollapsed drifts are selected because extensive roof collapse is not expected. The selection of the appropriate table for the Seismic Scenario Class depends on the character of the host-rock unit (SNL 2007 [DIRS 181244], Sections 6.2.2[a] and 6.2.3[a]). In the lithophysal zone, the appropriate tables correspond to the choice of noncollapsed or collapsed drift look-up tables. In the nonlithophysal zone, the appropriate tables correspond to the choice of the noncollapsed table or percolation rates (100 percent seepage). In the Seismic Scenario Class, multiple implementations of the Seepage DLL are utilized. Separate implementations for collapsed and noncollapsed conditions are used. In addition, separate collapsed condition implementations are utilized for lithophysal and nonlithophysal rock. Composite tables are then generated within GoldSim to account for the change from noncollapsed to collapsed conditions. For lithophysal rock (SNL 2007 [DIRS 181244], Section 6.2.2[a]) if rockfall volumes into the drift are less than or equal to 5 m^3/m of drift length, the intact-drift look-up table is utilized. If rockfall volumes into drifts are greater than 60 m^3/m of drift length, the collapsed-drift look-up table is utilized. If rockfall volumes (per unit drift length) into the drift are between 5 m^3/m and 60 m^3/m, seepage values are linearly interpolated between a Seepage DLL analysis based on the intact-drift look-up table and a Seepage DLL analysis based on the collapsed-drift look-up table. In the nonlithophysal zone (SNL 2007 [DIRS 181244], Section 6.2.3[a]), if rockfall volumes into the drift are less than or equal to 0.5 m^3/m, the intact-drift look-up table is utilized; if not, the percolation rates are utilized. The above criteria based on rockfall volumes are described in *The Abstraction of Drift Seepage* [DIRS 181244], Section 6.1[a]. Note that since both collapsed and noncollapsed seepage analyses are used for the Seismic Scenario Class, the seismic threshold data and seismic event frequencies are now used only as control parameters for controlling the multiple calls to the Seepage DLL (Table 6.3.3-3).

The third activity in Step 1 is to calculate the local seepage rate; that is, the volumetric flow rate. Note that for this calculation, the density of water is assumed to be 960 kg/m^3 for water at 100°C and 1 atm (Incropera and DeWitt 2002 [DIRS 163337], Appendix A.6) for a footprint of 5.1 m × 5.5 m, representing a WP length of 5.1 m (SNL 2007 [DIRS 181244], Sections 6.7.1 and 4.1[a} and *Seepage Model for PA Including Drift Collapse,* (BSC 2004 [DIRS 167652], Section 6.3.1) and a drift diameter of 5.5 m (SNL 2007 [DIRS 181244], Section 6.4.2.1 and *Seepage Model for PA Including Drift Collapse,* (BSC 2004 [DIRS 167652], Section 6.3.1). The results, are the mean seepage values and SDs. The SDs represent the estimation of uncertainty in the seepage results and are different for each sampled set of parameters. The mean seepage rates are, therefore, adjusted by applying a uniform distribution, with a mean of zero and upper and lower bounds, respectively, of +/-1.7321 times the seepage rate SD (SNL 2007 [DIRS 181244], Section 6.5.1.3). The sampled value from this uniform distribution is then added to the mean seepage value to obtain the ambient seepage rate. Note that the WP length of 5.1 m is based upon an average WP length of 5.0 m, which was the rounded length of the 44-BWR and 21-PWR WPs considered in previous designs (SNL 2007 [DIRS 181244], 4.1[a]). The additional 0.1 m represents 0.1-m spacings between packages. The 5.1 m length was the basis for the

model domain length used in the Seepage Model for Performance Assessment seepage simulations and the resultant seepage look-up tables. The addition of the transportation, aging, and disposal (TAD) canisters for CSNF increased the average length of all WPs to about 5.614 m. This longer average length increases the probability that WPs may encounter seepage (SNL 2007 [DIRS 181244], 4.1[a]). The TSPA-SEIS does not account for this updating of the waste package length in its seepage calculations.

Before Step 1 is completed, the results are checked for consistency. If the resulting seepage rates are less than zero, they are set to zero. If the resulting seepage rates correspond to a value higher than the local percolation flux applied to the footprint of 5.1 m × 5.5 m, the seepage rates are set to a rate corresponding to the local percolation flux.

For each TSPA-SEIS realization, *R*, the result from Step 1 of the seepage calculation is an ambient seepage rate for the four climate states in the TSPA-SEIS simulation for each WP (six CSNF and two CDSP WPs) at 3,264 MSTHM Abstraction locations (MSTHM Abstraction comprehensive data set as discussed in Section 6.3.2). Note that temporal changes in percolation flux through the UZ and, therefore, ambient seepage rate occur instantaneously when the climate state changes (Assumption 5.1.1). During a climate state, percolation flux and ambient seepage rate are at steady state.

Step 2: Seepage Adjusted for Thermal Effects and Drift Degradation Uncertainty—The ambient seepage rates calculated in Step 1 are adjusted to account for additional uncertainty due to the effects of some partial degradation (roof breakouts) of noncollapsed drifts and for thermal perturbations where the drift-wall temperature is at or above 100°C (determined for each repository location). The following adjustments are implemented:

- For all collapsed drift cases, uncertainty is already accounted for by using the look-up tables for fully collapsed drifts and taking into consideration uncertainty in the estimation of rubble volumes in the Seismic Submodel. For noncollapsed cases, the ambient seepage rates are increased by 20 percent to account for uncertainty associated with the seepage evaluation for these cases. This uncertainty stems in part from the limited number of simulation cases studied for moderately degraded drifts, but is mainly related to the large estimation differences between the stochastic realizations conducted for those cases (SNL 2007 [DIRS 181244], Section 6.7.1.2).

- Two abstraction approaches for thermal seepage are implemented: (1) for collapsed drifts, thermal seepage is set equal to the adjusted ambient seepage, and (2) for noncollapsed drifts, thermal seepage is set to zero for the period of above-boiling temperature, using a 100°C threshold temperature at the drift wall (SNL 2007 [DIRS 181244], Section 6.7.1.2).

Seepage in the Igneous Intrusion Modeling Case is discussed in Section 6.4.

Step 3: Determination of Seepage Fraction—The seepage fraction is calculated as the ratio of WPs experiencing seepage to all WPs in a percolation subregion by WP type for a given realization. WPs with seepage at any time during the 20,000-year simulation period are counted as WPs in a location with drift seepage (for 20,000-year simulations) and any time during the

1,000,000-year simulation period (for 1,000,000-year simulations). The seepage fraction is calculated using a threshold seepage rate of 0.1 kg/yr per WP. WP locations with less than this threshold rate are counted as locations where seepage does not occur because such small values are considered to be the result of the interpolation procedure (SNL 2007 [DIRS 181244], Section 6.8). WPs with seepage at any time are in a seep environment, and those without seepage are in a non-seep environment.

6.3.3.2 Drift-Wall Condensation

Condensate dripping from drift walls affects TSPA-SEIS calculations by adding additional water to the drift seepage volumetric flow rate (which may be zero in the non-seep environments). This combined flow rate flows through the invert and, in some scenarios, through the DSs, WPs, and the waste forms. The Drift Wall Condensation Submodel calculates a probability of condensation on the drift walls at any location and, if condensation occurs, the rate of condensation. The source of condensation water is evaporated water from the invert and evaporated seepage water from the drift wall. Water vapor is transported axially by convective mixing from hotter drift regions to cooler drift regions where it can then condense. The axial movement of the water vapor, the saturated vapor pressure at the drift wall and in the invert, and temperature differences along the drifts are important factors that drive the occurrence of condensation (SNL 2007 [DIRS 181648], Section 6.3.1.1). The probability of drift-wall condensation occurrence and the condensation rate are abstracted as functions of the percolation flux at the base of the PTn (Section 6.3.3.1.2) and simulation time, as described in *In-Drift Natural Convection and Condensation* (SNL 2007 [DIRS 181648], Section 8.1[a]).

Information flow and connections between the EBS TH Environment Submodel (Section 6.3.2) and the Drift Seepage Submodel (Section 6.3.3.1), Drift Wall Condensation Submodel (Section 6.3.3.2.1), and EBS Flow Submodel (Section 6.3.6) are shown on Figure 6.3.3-1. Figure 6.3.3-6 shows the inputs and outputs to the Drift Wall Condensation Submodel and indicates the principal features of the submodel and the bases for confidence in the submodel.

6.3.3.2.1 Conceptual Model

The Drift Wall Condensation Process Model (SNL 2007 [DIRS 181648], Section 6.3) is used to calculate the occurrence and quantity of water vapor condensation at WP locations along the entire lengths of seven drifts selected to characterize the expected range of axial temperature gradients (see discussion below). The Drift Wall Condensation Process Model includes heat transfer from WPs through EBS components to the drift walls, evaporation of water vapor at the drift walls, radial vapor flux from drift walls, axial water vapor movement along the drift by convection, and condensation on the drift walls where the wall temperature is less than the condensation temperature. Probabilities of condensation at any location are calculated as the ratio of the drift length over which condensation occurs to total drift length.

Temperature at drift locations where water evaporation or condensation may occur is based on heat transfer calculations. Heat transfer between surfaces (WPs and DSs, WPs and inverts, DSs and drift walls, drift walls and inverts, and DSs and inverts) is based on literature references for correlations of natural convection heat and mass transfer for representative geometry. Thermal radiation is calculated from surface-to-surface radiation with appropriate radiation view factors.

Only heat transferred in the radial direction is considered. The effects of axial heat transfer are assumed to be minimal, as described in *In-Drift Natural Convection and Condensation* (SNL 2007 [DIRS 181648], Sections 5.3, 6.3.3.2.6, and Executive Summary).

Evaporative water vapor sources include the drift wall and the invert at each WP location (Figure 6.3.3-7). The local water vapor partial pressure is the saturation pressure at the calculated temperature. The rate at which water evaporates from a surface depends on the local difference between the saturation vapor pressure at the evaporating surface and the local gas-phase partial pressure, using the corresponding mass-transfer correlation. The condensation rate is limited by the available water vapor, which, in turn, is limited by the rate of water transfer to the drift by capillary wicking and percolation through the host rock.

Condensation is modeled with a lumped parameter approach using standard heat and mass transfer processes within the drift. The Drift Wall Condensation Process Model considers the entire length of each of seven drifts. The seven drifts are chosen to represent the range of thermal conditions in the repository (SNL 2007 [DIRS 181648], Section 6.3.5.1). Figure 6.3.3-8 illustrates the locations of the seven drifts. Drift-wall temperature boundary conditions are derived from analytical heat line-source solutions. The amount and location of water vapor depend on the availability of water and the axial transport properties. Axial and radial mass transport equations and radial heat transport equations are solved to estimate the water vapor distribution and condensation on various surfaces along each of the seven selected drifts at six selected times of 1,000; 3,000; 10,000; 30,000; 100,000; and 300,000 years. The selection of the first three analysis times is based on when the wall temperature drops below the saturation temperature (boiling temperature—approximately 96°C at the repository elevation) and the rate at which the waste-form decay heat declines during the first 10,000 years after repository closure. The remaining three analysis times span the remainder of the TSPA modeling period. Note here that the Drift Wall Condensation Model uses 96°C as the boiling temperature of water at the repository elevation and the Seepage Abstraction sets a threshold of 100°C as the temperature for thermal seepage in the TSPA-SEIS (Section 6.3.3.3.1).

The calculated results for the seven drifts at the selected times are used to estimate the location and rate of condensation on the drift walls, under the DSs, and on individual WPs. The TSPA-SEIS uses only the condensation abstraction for condensation on drift walls. Condensation under DSs and on WPs is calculated by the model, but is not significant and is not recommended for inclusion in the TSPA-SEIS (SNL 2007 [DIRS 181648], Section 8.1[a]. The condensation model defines three stages for the occurrence of condensation. Stage 1 is when the drift wall temperature is above the boiling temperature of water at all locations in the drift. No condensation occurs during Stage 1. Stage 2 is for times between when the first location in a drift drops below the boiling temperature and the last location drops below the boiling temperature. A separate part of the Drift Wall Condensation Abstraction (SNL 2007 [DIRS 181648], Section 6.2[a]) describes the Stage 2 condensation occurrence and rate. Stage 3 occurs after all WPs (and thus the drift wall) drop below the boiling temperature. The abstraction for Stage 2 uses a reasonable-bound approach for the occurrence and rate of condensation.

6.3.3.2.2 TSPA-SEIS Abstraction

The Drift Wall Condensation Abstraction (SNL 2007 [DIRS 181648], Section 8.1[a]) calculates a probability of condensation occurrence on the drift walls at a WP location and, if condensation occurs, a rate of condensation for all locations in the drift that are below the boiling temperature. Lower- and upper-bounding cases for axial dispersion coefficients are provided. Lower-bound values for the axial dispersion coefficients are computed without any axial gradients in the process model boundary temperatures, whereas the upper bound on the axial dispersion coefficients is computed using an axial gradient in the boundary temperature (SNL 2007 [DIRS 181648], Section 6.3.7.1). Additionally, high- and low-invert transport cases are computed, but only low-invert cases are recommended for use in the TSPA-SEIS (SNL 2007 [DIRS 181648], Section 6.1.2[a]). The low-invert transport case assumes that the partial pressure at the bottom of the invert surface is the saturation vapor pressure at the drift-wall temperature. The high-invert transport case assumes that the partial pressure at the invert surface underneath the DS is the saturation vapor pressure for the invert surface temperature (SNL 2007 [DIRS 181648], Section 6.3). Finally, ventilated and unventilated (alternatively, mixed and unmixed) DS cases are provided (SNL 2007 [DIRS 181648], Section 8.1[a]). This gives eight possible cases for drift-wall condensation. After further analysis, the high-invert transport case is determined to be unrealistic, so it is not included in the TSPA abstraction (SNL 2007 [DIRS 181648], Section 6.1.2[a]).

The Drift Wall Condensation Abstraction results are determined through 144 different steady-state simulations, with results for each of the seven drifts being produced for each of the 144 runs ((two axial dispersion coefficients) × (two invert transport properties) × (two DS ventilation cases) × (three infiltration cases) × (six simulation times)) (SNL 2007 [DIRS 181648], Section 6.1.1[a] and Section 6.1.2[a]). These results are reduced to four distinct cases because the three different infiltration case results for each of these 48 cases are combined and used to create functional relationships in which condensation flux and condensation fraction are dependent upon percolation flux. That is, the four cases are composed of eight simulations at each of the six output times of 1,000, 3,000, 10,000, 30,000, 100,000, and 300,000 years. The eight simulations include the possible combinations of two values of dispersion coefficient (low and high), two values of invert transport properties (low and high), and two values for DS ventilation (ventilated and unventilated). By performing linear regressions between the probability of condensation on the drift wall and the mean percolation fluxes for the chosen drifts at the given time as $\ln[1-P_w]$ and $\ln(\bar{p})$, and between the condensation rate and the percolation flux, as CW and $\bar{p}$ (time-dependent percolation rate), functional relationships are developed in which condensation flux and condensation fraction are dependent on average percolation flux. These functional relationships are developed for each of the 48 simulation cases. The following mathematical relationship was developed (SNL 2007 [DIRS 181648], Section 8.3.1.1, Equation 8.3.1.1-3) from the linear regression analysis to approximate the probability of condensation on the drift walls:

$$\hat{P}_w = 1 - e^{a\ln(\bar{p})+b} \qquad \text{(Eq. 6.3.3-2)}$$

where the parameters a and b are the slope and y-intercept of the linear regressions. As mentioned previously, the high invert transport case is not included in the abstraction for TSPA.

Also, the analysis showed that condensation only occurs at 1,000 years. There are four non-zero values for a and four non-zero values for b.

Uncertainty in $\hat{P}_w$ is captured using the standard error on the linear regression coefficients. Plus/minus one standard error is used as uncertainty ranges around the slope and intercept parameters. Uncertainty in the slope and intercept parameters are modeled as normally distributed about the computed value for each parameter, with the standard deviation equal to the standard error. The parameter values are sampled independently (SNL 2007 [DIRS 181648], Section 8.3.1.1, Equation 8.3.1.1-4).

The equation:

$$CW = c\bar{p} + d \qquad \text{(Eq. 6.3.3-3)}$$

approximates the rate of condensation on the wall, CW, where the parameters c and d are the slope and y-intercept of the linear regression. There are four non-zero values for c and four non-zero values for d.

Uncertainty in CW is captured using the standard error on the linear regression coefficients. The standard errors are used as uncertainty ranges around the slope and intercept parameters. Uncertainty in the slope and intercept parameters are modeled as normally distributed about the computed value for each parameter, with standard deviation equal to the standard error. The parameter values are sampled independently (SNL 2007 [DIRS 181648], Section 8.3.1.1).

Table 6.3.3-4 shows one of the four tables containing values and standard errors for coefficients a, b, c, and d used in Equations 6.3.3-2 and 6.3.3-3. The R-squared values for each regression are also provided to indicate how well each linear regression model fits the results. Table 6.3.3-5 shows the values for the parameter distributions, which are sampled independently in the TSPA-SEIS for each TSPA-SEIS realization.

For condensation rate correlations at 1,000 years and for high axial dispersion, the correlation models have a larger standard error. The correlation uncertainty is applied by sampling a normal distribution with the standard deviation equal to the standard error (SNL 2007 [DIRS 181648], Section 8.3, Appendix H). Applying the uncertainty to the correlation coefficients produces a range of possible values covering, and in some cases exceeding, the Drift Wall Condensation Abstraction output that was used to develop the correlation model. The TSPA-SEIS uses zero as the lower bound on the condensation rate and condensation probability.

The Drift Wall Condensation Abstraction (SNL 2007 [DIRS 181648]), Section 6.2.2[a]) describes a reasonable-bound approach for the condensation rate during Stage 2. Ultimately, the Stage 2 condensation rate is a single reasonably bounding value with rate in kg/m/yr. Only CDSP WPs have non-zero Stage 2 condensation. Stage 2 begins at a particular WP location when the drift wall cools to the boiling temperature of water. No probability is given for Stage 2 condensation. In other words, the Stage 2 condensation rate is applied to all CDSP WPs during Stage 2.

6.3.3.2.3 TSPA-SEIS Implementation

The TSPA-SEIS implementation of the Drift Wall Condensation Submodel uses the abstracted probability of condensation on the drift wall (Equation 6.3.3-2) and an abstracted rate of condensation (Equation 6.3.3-3) whenever condensation occurs for Stage 3 condensation. The four cases corresponding to the four combinations of the two values for axial dispersion coefficient and two values of DS ventilation are treated as four equally likely cases and are given are sampled with equal frequency in the TSPA-SEIS (SNL 2007 [DIRS 181648], Section 8.1[a]). The CSNF and CDSP WPs are treated equally in terms of drift-wall condensation. The abstraction for the fraction of WPs that experience condensation and the corresponding condensation flow volume apply equally to CSNF and CDSP WPs. In the Drift Wall Condensation Abstraction, the average percolation flux $\overline{p}$, represents the average of the MSTHM Abstraction percolation fluxes along the length of each of the seven simulated drifts. In the TSPA-SEIS, $\overline{q}_{perc}$ represents the average of the percolation flux over a TSPA-SEIS percolation subregion (EBS TH Environment, Section 6.3.2). This average characterizes the percolation flux for that subregion (SNL 2007 [DIRS 181648], Section 8.3.1.1). In the TSPA-SEIS, $\overline{q}_{perc}$ is used for $\overline{p}$ in the Drift Wall Condensation Submodel. The TSPA-SEIS implementation does not include condensation under the DSs (SNL 2007 [DIRS 181648], Section 6.1.2[a]).

Inputs to the Drift Wall Condensation Submodel include slope, intercept, and standard error values for the slope and intercept. These inputs are provided for each combination of the invert transport properties, axial dispersion coefficient, and time. In addition, the average percolation rate is for each percolation subregion. For the Seismic Scenario Class, drift collapse is not expected in the nonlithophysal units, so condensation can only occur on drift walls above DSs in the nonlithophysal units. In contrast, there is no condensation in the lithophysal units after drift collapse (SNL 2007 [DIRS 180655], Section 2.0). Consequently, the fraction of WPs in the nonlithophysal region is used in the implementation of the Drift Wall Condensation Submodel for the Seismic Scenario Class in the TSPA-SEIS.

The Drift Wall Condensation Abstraction provides correlations to calculate the condensation rate as a function of time and percolation rate (SNL 2007 [DIRS 181648], Section 8[a], Appendix A[a], and Appendix B[a]). During Stage 1, before the first WP location in the drift drops below boiling, the condensation rate is zero. The TSPA-SEIS uses a "representative WP" to represent the thermal and flow properties for the percolation subregion. See Section 6.1.5 for a discussion of the percolation subregions. Before the temperature of the representative WP drops below boiling, there is no condensation. The temperature of the representative WP drops below boiling some time during Stage 2, after the first location in the drift drops below boiling,

but before the last location drops below boiling. The Stage 2 condensation rate is used until the time when Stage 3 starts, which is the time when the last location in the drift drops below boiling. For Stage 3, the 1,000-year condensation rate and probability is used up until 2,000 years. After 2,000 years, the 3,000-year rate and probability would be used, but because it is zero, the condensation rate is zero. The condensation rate remains zero for the remainder of the simulation up to 1,000,000 years. The TSPA-SEIS drift-wall condensation implementation also requires a stochastic parameter, Seepage_Condensation_Prob_a, a U[1,0] that is used to determine whether the first failed WP in a percolation subregion is in a location with condensation or not. Seepage_Condensation_Prob_a is an epistemic parameter sampled once per realization. The TSPA-SEIS treats WPs with seepage separately from WPs with no seepage. Drift-wall condensation is added to the seepage flux, or becomes the only advective flux in a non-seep environment. The drift-wall condensation fraction for Stage 3 is independent of the seepage fraction, so some of the WP in both the seep and non-seep environments will potentially have condensation and some will not. Thus, the very first WP to fail in a percolation subregion can potentially have condensation or not. If Seepage_Condensation_Prob_a is less than or equal to the drift-wall condensation fraction, the first failed WP is assumed to be in an environment that can potentially have condensation. After more than one WP has failed in a percolation subregion, the drift-wall condensation flux is multiplied by the drift-wall condensation fraction to give an average condensation rate for the percolation subregion. This technique preserves the mass balance of condensing water and properly treats the percolation subregion as an average of WP. It also properly applies the full condensation flux to a single failed WP in a percolation subregion during Stage 3. During Stage 2, no seepage fraction is applied and every CDSP WP receives the full condensation flux.

The output of the Drift Wall Condensation Submodel is the fraction of WPs exposed to condensation flux and the flux rate as functions of percolation flux for each WP type (SNL 2007 [DIRS 181648], Section 8[a], Appendix A[a], and Appendix B[a]). These outputs are used in the EBS Flow Submodel to determine the average flow rate in the drift above a DS and WP and also below the WP in the invert. The EBS Flow Submodel calculations include effects of both drift seepage and drift-wall condensation.

6.3.3.3 Model Component Consistency and Conservatism in Assumptions and Parameters

To enhance understanding of the complex interactions within the TSPA-SEIS, a discussion of consistency among model components, submodels, and identification of conservative assumptions in abstractions, process models, and parameter sets supporting seepage and drift-wall condensation are discussed below.

6.3.3.3.1 Consistency of Assumptions

In-Drift Evaporation—In-drift evaporation of seepage flow is not included in the Drift Seepage Submodel in any of the scenario classes at temperatures less than 100°C, even though below-boiling evaporation is a process that is modeled in the MSTHM Process Model (Section 6.3.2), Drift Wall Condensation Submodel (Section 6.3.3.2), and the EBS Chemical Environment Submodel (Section 6.3.4).

Effect on TSPA—Not including evaporation of seepage flux (Section 5.1.4) leads to an overestimate in TSPA-SEIS of: (1) the water present at any point in time; (2) the amount of water flux through the invert and/or WP; and, therefore, (3) the radionuclide mass released.

Repository Boiling Temperature—The thermal seepage model conservatively uses 100°C for the boiling temperature of water while the drift wall condensation model uses 96°C, which is the actual boiling temperature at the repository horizon.

Effect on TSPA—The 100°C threshold for thermal seepage means that seepage starts sooner and water is available for transport sooner. This approach is conservative and can lead to earlier doses to the reasonably maximally exposed individual (RMEI).

Water Balance—There is no water balance (liquid or vapor) between the MSTHM, drift seepage, and drift-wall condensation models.

Effect on TSPA—It is assumed for each model that there is sufficient water to support the predicted flow rates. This results in an over-prediction of flow rates, as well as an over-prediction of the number of WPs that are in an advective environment. This results in higher rates of radionuclide transport, which lead to higher doses to the reasonably maximally exposed individual (RMEI). Therefore, this approach is conservative.

6.3.3.3.2 Identification of Conservatisms in Submodels and Abstractions

Ambient Seepage—For drift-wall temperatures less than 100°C, the thermal seepage model implemented into the TSPA-SEIS conservatively uses ambient drift seepage instead of taking credit for thermal effects (SNL 2007 [DIRS 181244], Section 6.7.1.2). Seepage for drift-wall temperatures between 100°C and ambient temperatures would be less than seepage at ambient drift-wall temperature, as shown in *Abstraction of Drift Seepage* (SNL 2007 [DIRS 181244], Figure 6.4-15). In the TSPA-SEIS, rather than the seepage rate, the presence or absence of flowing water in the drift is the dominant factor controlling radionuclide releases when the DSs are intact. Reducing the seepage slightly to account for thermal effects may have a slight impact on the radionuclide release from the EBS for WPs with breached DSs.

6.3.3.4 Alternative Conceptual Model(s) for Drift Seepage and Drift-Wall Condensation

Section 6.2 outlines the general consideration and treatment of ACMs used to support the TSPA-SEIS. A brief description of the ACMs for the Drift Seepage and Drift Wall Condensation Submodels summarized in Table 6.3.3-6 is presented below.

Drift-Seepage ACMs—Two ACMs for drift seepage were considered: (1) flow through discrete fractures and (2) episodic-preferential flow in superheated rock.

The most important ACM for ambient seepage is one that simulates flow through discrete fractures rather than through a stochastic porous continuum. It was concluded that conceptual model uncertainty is small compared to other sources of uncertainty that are explicitly accounted for by the base-case conceptual model, its numerical implementation, and the associated

uncertainty estimates, which are propagated through the TSPA-SEIS (SNL 2007 [DIRS 181244], Section 6.4.1.2).

The effectiveness of the vaporization barrier was examined with an ACM representing episodic-preferential flow into a superheated rock environment (SNL 2007 [DIRS 181244], Section 6.4.3.2). In this ACM, the thermally perturbed downward flux from the condensation zone toward the superheated rock zone is conceptualized to form episodic preferential-flow patterns. The effectiveness of the vaporization barrier was then tested for these extreme conditions where downward flux is fast and large in magnitude compared to average flow. A semi-analytical solution was employed to simulate the complex flow processes of episodic fingerflow in a superheated fracture. With this solution, the maximum penetration distance into the superheated rock was determined for specific episodic flow events and thermal conditions. In addition, the amount of water arriving at the drift crown and the impact of capillary diversion were calculated. It was concluded that the thermal seepage process model results are reasonably consistent with the ACM (SNL 2007 [DIRS 181244], Section 6.4.3.2).

Drift-Wall Condensation ACMs—Two ACMs for drift-wall condensation were considered: (1) a thermal conductivity/heat transfer ACM and (2) a computational fluid dynamics simulation for drift condensation processes ACM.

In the Thermal Conductivity/Heat Transfer ACM, the air phase is treated as a solid material. To account for the higher heat transfer between surfaces due to convection, the effective thermal conductivity of the solid (air) can be increased so that the same amount of heat can transfer from one surface to another for the same temperature difference. This ACM is essentially accounted for in the MSTHM Abstraction (SNL 2007 [DIRS 181244]). This ACM is not considered further because it is implemented in the MSTHM Abstraction (SNL 2007 [DIRS 181648], Section 6.1.4).

Another ACM simulates the drift with a computational fluid dynamics code and the surrounding rock with a porous media code. The computational fluid dynamics code FLUENT (Fluent, Inc. 2003 [DIRS 164315]) contains limited porous media capabilities that only consider single-phase flow. To more rigorously simulate physical processes of the rock, the software would need to be able to simulate partially saturated flow as well as phase change in the porous media. Conduction-only heat transfer in the surrounding rock and the invert is acceptable, and this ACM is not considered further (SNL 2007 [DIRS 181648], Section 6.1.4).

No ACMs were recommended for inclusion in the TSPA-SEIS.

Table 6.3.3-1. Spatial Variability and Uncertainty Distributions for *1/α* for Method A as Defined in the Abstraction of Drift Seepage

1/α (Lithophysal Units)		*1/α* (Nonlithophysal Units)	
Spatial Variability Distribution	**Uncertainty Distribution**	**Spatial Variability Distribution**	**Uncertainty Distribution**
Uniform Distribution with Mean 591 Pa Lower Bound is 402 Pa. Upper Bound is 780 Pa.	Triangular Distribution with Mean 0 Lower Bound is – 105 Pa. Upper Bound is + 105 Pa.	Uniform Distribution with Mean 591 Pa Lower Bound is 402 Pa. Upper Bound is 780 Pa.	Triangular Distribution with Mean 0 Lower Bound is – 105 Pa. Upper Bound is + 105 Pa.

Note: Only one method, Method A, is used in the TSPA-SEIS (SNL 2007 [DIRS 181244], Section 6.3[a])

Table 6.3.3-2. Spatial Variability and Uncertainty Distributions for Fracture Permeability (log (k [m^2]))

Fracture log (k [m^2]) (Lithophysal Units)		Fracture log(k [m^2]) (Nonlithophysal Units)	
Spatial Variability Distribution	**Uncertainty Distribution**	**Spatial Variability Distribution**	**Uncertainty Distribution**
Log Normal Distribution with Mean – 11.5	Triangular Distribution with Mean 0	Log Normal Distribution with Mean – 12.2	Triangular Distribution with Mean 0
Standard Deviation 0.47	Lower Bound is – 0.92.	Standard Deviation 0.34	Lower Bound is – 0.68.
	Upper Bound is + 0.92.		Upper Bound is + 0.68.

Source: (SNL 2007 [DIRS 181244], Section 6.6.3, Figures 6.6-7 and 6.6-8).

Table 6.3.3-3. Inputs Passed by the TSPA-SEIS to the Seepage Dynamically Linked Library

Input #	Input Parameter Name	Description	Value	Source
1	Infiltration_Scenario_a	Provides the infiltration scenario for the current realization to the seepage DLL.	1= 10th percentile 2= 30th percentile 3= 50th percentile 4= 90th percentile	NA, not data
2	Random_Seed_1	The first of two random number seeds provided to the Seepage DLL for its internal random number generator. This allows the sampling sequence in the Seepage DLL to be repeated, consistent with the Latin hypercube sampling on uncertain parameters in the GoldSim model file.	Uniform $(1, 2^{31}-1)$	NA, not data
3	Random_Seed_2	The second of two random number seeds provided to the Seepage DLL for its internal random number generator (see above).	Uniform $(1, 2^{31}-1)$	NA, not data
4	Alpha_Uncert_Lith_a	Sampled value from uncertainty distribution for capillary strength parameter. The distribution minimum, most likely, and maximum are defined by which method is chosen.	Triangular; see Table 6.3.3-1.	[a]Section 6.7.1.1
5	Alpha_Uncert_NonLith_a	Sampled value from uncertainty distribution for capillary strength parameter. The distribution minimum, most likely, and maximum are defined by which method is chosen.	Triangular; see Table 6.3.3-1.	[a]Section 6.7.1.1
6	LogK_Uncert_NonLith_a	Sampled value from Log(k) uncertainty for the nonlithophysal rock units.	Triangular (-0.68, 0, 0.68)	[a]Section 6.7.1.1
7	LogK_Uncert_Lith_a	Sampled value from Log(k) uncertainty for the lithophysal rock units.	Triangular (-0.92, 0, 0.92)	[a]Section 6.7.1.1
8	Density_H2O	Density of seeping water.	960 kg/m^3	[b]This is an assumed input parameter.
9	Drift_Diameter	Drift diameter.	5.5 m	[a]Section 6.7.1.2
10	WP_Length_Seepage	WP length.	5.1 m	[a]Section 6.7.1
11	Seepage_Multiplier	A seepage multiplier for noncollapsed conditions that accounts for additional uncertainty due to drift degradation.	1.2	[a]Section 6.7.1.2
12	LogK_SV_Mean_NonLith	The mean of the log of permeability [log(k)] spatial variability for nonlithophysal rock units.	-12.2	[a]Section 6.7.1.1
13	LogK_SV_SD_NonLith	The standard deviation of the log of permeability [log(k)]) spatial variability for nonlithophysal rock units.	0.34	[a]Section 6.7.1.1
14	LogK_SV_Mean_Lith	The mean of the log of permeability [log(k)] spatial variability for lithophysal rock units.	-11.5	[a]Section 6.7.1.1
15	LogK_SV_SD_Lith	The standard deviation of the log of permeability [log(k)]) spatial variability for lithophysal rock units.	0.47	[a]Section 6.7.1.1

Table 6.3.3-3. The Inputs Passed by the TSPA-SEIS to the Seepage Dynamically Linked Library (Continued)

Input #	Input Parameter Name	Description	Value	Source
16	Alpha_SV_LB_Lith	The lower bound for the $1/\alpha$ spatial variability distributions for lithophysal rock. The value is selected based on which of the four ACMs (i.e., methods) is selected during a particular realization for the distribution.	Table 6.3.3-1.	[a]Section 6.7.1.1
17	Alpha_SV_UB_Lith	The upper bound for the $1/\alpha$ spatial variability distributions for lithophysal rock. The value is selected based on which of the four ACMs (i.e., methods) is selected during a particular realization for the distribution.	See Table 6.3.3-1	[a]Section 6.7.1.1
18	Alpha_SV_LB_NonLith	The lower bound for the $1/\alpha$ spatial variability distributions for nonlithophysal rock. The value is selected based on which of the four ACMs (i.e., methods) is selected during a particular realization for the distribution.	See Table 6.3.3-1	[a]Section 6.7.1.1
19	Alpha_SV_UB_NonLith	The upper bound for the $1/\alpha$ spatial variability distributions for nonlithophysal rock. The value is selected based on which of the four ACMs (i.e., methods) is selected during a particular realization for the distribution.	See Table 6.3.3-1	[a]Section 6.7.1.1
20	DE_Event_Time	Selects the appropriate disruptive event time (igneous or seismic) based on the scenario class for the simulation.	0 yr for both igneous and seismic, 20,000 yr or 1,000,000 yr if nominal case	NA, not data
21	Scenario_Flag_Feed _Seep	Determines which scenario class (e.g., nominal, igneous, or seismic) is being simulated.	1 = nominal 2 = igneous 3 = seismic	NA, not data
22	Seismic_Event_Freq _Seep_Feed	Annual exceedance frequency of the seismic event.	0.5 yr^{-1}	Section 6.3.3.1.3
23	Seismic_Thresh_Lith	Seismic event frequency at or below which collapse occurs for lithophysal rock.	1 yr^{-1} = collapsed condition 0 yr^{-1} = noncollapsed condition	Section 6.3.3.1.3
24	Seismic_Thresh_NonLith	Seismic event frequency at or below which collapse occurs for nonlithophysal rock.	1 yr^{-1} = collapsed condition 0 yr^{-1} = noncollapsed condition	Section 6.3.3.1.3
25	Rock_Str_Reduction_Lith	Placeholder for Lithophysal Rock Strength Reduction Function.	0	NA, not data

Table 6.3.3-3. The Inputs Passed by the TSPA-SEIS to the Seepage Dynamically Linked Library (Continued)

Input #	Input Parameter Name	Description	Value	Source
26	Rock_Str_Reduction_ NonLith	Placeholder for Nonlithophysal Rock Strength Reduction Function.	0	NA, not data
27	DE_Seepage_Model	Selects appropriate disruptive event seepage model flag based on the scenario class for the simulation.	Igneous or Seismic	NA, not data
28	Rock_Str_Thresh_Lith	Loss of rock strength, which will result in drift collapse in lithophysal rock units.	40%	[a]Section 6.4.2.4.1
29	Rock_Str_Thresh_ NonLith	Loss of rock strength, which will result in drift collapse in nonlithophysal rock units.	40%	[a]Section 6.4.2.4.1
30	Print_Flag	Controls the amount of information that is written to output files (e.g., none, seepage output only, all possible output, debug information only).	N/A	NA, not data
31	Thermal_Seep_Temp _Limit	Drift crown temperature above which seepage will not occur.	96°C	[a]Section 6.3.2
32	Flow_Focusing_Flag	Specifies whether to use the flow-focusing factor built into the Seepage DLL or to use a value of 1.0 for flow focusing.	0 = use abstraction, 1 = use 1.0	NA, not data
33	End_Time	Specifies the time to which the Seepage DLL runs (TSPA-SEIS simulation time) and returns seepage time histories.	20,000 yr or 1,000,000 yr	NA, not data
34	Seepage_Uncertainty	Provides a value that is used to sample the seepage distribution in the Seepage DLL.	Uniform (0,1)	[a]Section 6.7.1.1
35	Climate4_FF_Index	Index for post 10-k climate state. Used to allow for flexibility in choosing percolation fluxed for the post 10-k climate state.	1	NA, not presently used

NOTE: [a] (SNL 2007 [DIRS 181244]).
[b] A low density (960 kg/m^3, associated with water at 100°C) is used to maximize the volumetric flow

Table 6.3.3-4. Drift-Wall Condensation: 1,000 Years; High Dispersion Coefficient, Low Invert Transport Properties, Well-Ventilated Drip Shield

	Slope (c)	Y-intercept (d)
Rate (CW)	-1.33E+00	1.08E+02
Standard Error	1.42E+00	1.45E+02
Rate R-Squared	4.67E-01	
	Slope (a)	**Y-intercept (b)**
Probability (P_w)	-2.59E-02	5.71E-02
Standard Error	9.35E-03	2.93E-02
Probability R-Squared	2.87E-01	

Source: DTN: MO0702PALOVERT.000_R2 [DIRS 180377]

NOTE: An example of 1 of the 4 tables that provide values of regression slopes, intercepts, and statistical parameters for $\hat{P}_w$ and CW.

Table 6.3.3-5. Parameter Distributions for Drift Wall Condensation Abstraction

Parameter Name in TSPA-SEIS	Description	Distribution
DWC_Dispersivity_Cond_a	A random variable specifying whether the high dispersivity or low dispersivity modeling case is used (0 = low; 1 = high).	Discrete (p, v) [(0.5, 0), (0.5, 1)]
DWC_Invert_Properties_Cond_a	A random variable specifying whether the high invert transport or low invert transport modeling case is used (0 = low; 1 = high).	Discrete (p, v) [(0.5, 0), (0.5, 1)]
DWC_Ventilated_Cond_a	A random variable specifying whether the ventilated or unventilated drip shield modeling case is used (0 = unventilated; 1 = ventilated).	Discrete (p, v) [(0.5, 0), (0.5, 1)]
Seepage_Condensation_Prob_a[a]	Random variable U[0,1] to determine the seepage/condensation regime for the first failed waste package in a seepage environment.	Uniform (0,1)
DWC_Std_Error_a_a	An uncertainty multiplier for the standard deviation on the slope coefficient for determining probability of condensation from the percolation rate.	Normal: mean = 0, standard deviation = 1
DWC_Std_Error_b_a	An uncertainty multiplier for the standard deviation on the y-intercept coefficient for determining probability of condensation from the percolation rate.	Normal: mean = 0, standard deviation = 1
DWC_Std_Error_c_a	An uncertainty multiplier for the standard deviation on the slope coefficient for determining condensation rate from the percolation rate.	Normal: mean = 0, standard deviation = 1
DWC_Std_Error_d_a	An uncertainty multiplier for the standard deviation on the y-intercept coefficient for determining condensation rate from the percolation rate.	Normal: mean = 0, standard deviation = 1

Source: (SNL 2007 [DIRS 181648]), Table A-3).

[a] Seepage_Condensation_Prob_a is a TSPA parameter developed in this report.

Table 6.3.3-6. Alternative Conceptual Models Considered for the Drift Seepage and Drift-Wall Condensation Submodels

Alternative Conceptual Models	Key Assumptions	Screening Assessment and Basis
Drift Seepage: Flow through discrete fractures	ACM that simulates flow through discrete fractures rather than through a stochastic continuum.	Screened out. It was concluded that conceptual model uncertainty is small compared to other sources of uncertainty that are explicitly accounted for by the base case conceptual model, its numerical implementation, and the associated uncertainty estimates that are propagated through the TSPA-SEIS.
Drift Seepage: Episodic-Preferential Flow in Superheated Rock	The effectiveness of the vaporization barrier was examined with an ACM representing water flow into a superheated rock environment (SNL 2007 [DIRS 181244], Section 6.4.3.2). In this ACM, the thermally perturbed downward flux from the condensation zone toward the superheated rock zone is conceptualized to form episodic preferential-flow patterns.	Screened out. It was concluded that results of the ACM are reasonably consistent with the thermal seepage process-model results used for this abstraction (SNL 2007 [DIRS 181244], Section 6.4.3).
Drift-Wall Condensation: Thermal Conductivity/Heat Transfer	In the Thermal Conductivity/Heat Transfer ACM, the air phase is treated as a solid material (SNL 2007 DIRS [181648], Section 6.1.4).	Screened out. This ACM is essentially accounted for in the MSTHM Abstraction (SNL 2007 [DIRS 181244]).
Drift-Wall Condensation: CFD simulation for drift condensation processes	ACM simulates the drift with a CFD code and the surrounding rock with porous media code. The CFD code FLUENT (Fluent, Inc. [DIRS 164315]) contains limited porous media capabilities that only consider single-phase flow (SNL 2007 DIRS [181648], Section 6.1.4).	Screened out. The CFD code was determined to have insufficient advantages over the selected model (SNL 2007 [DIRS 181648], Section 6.1.4).

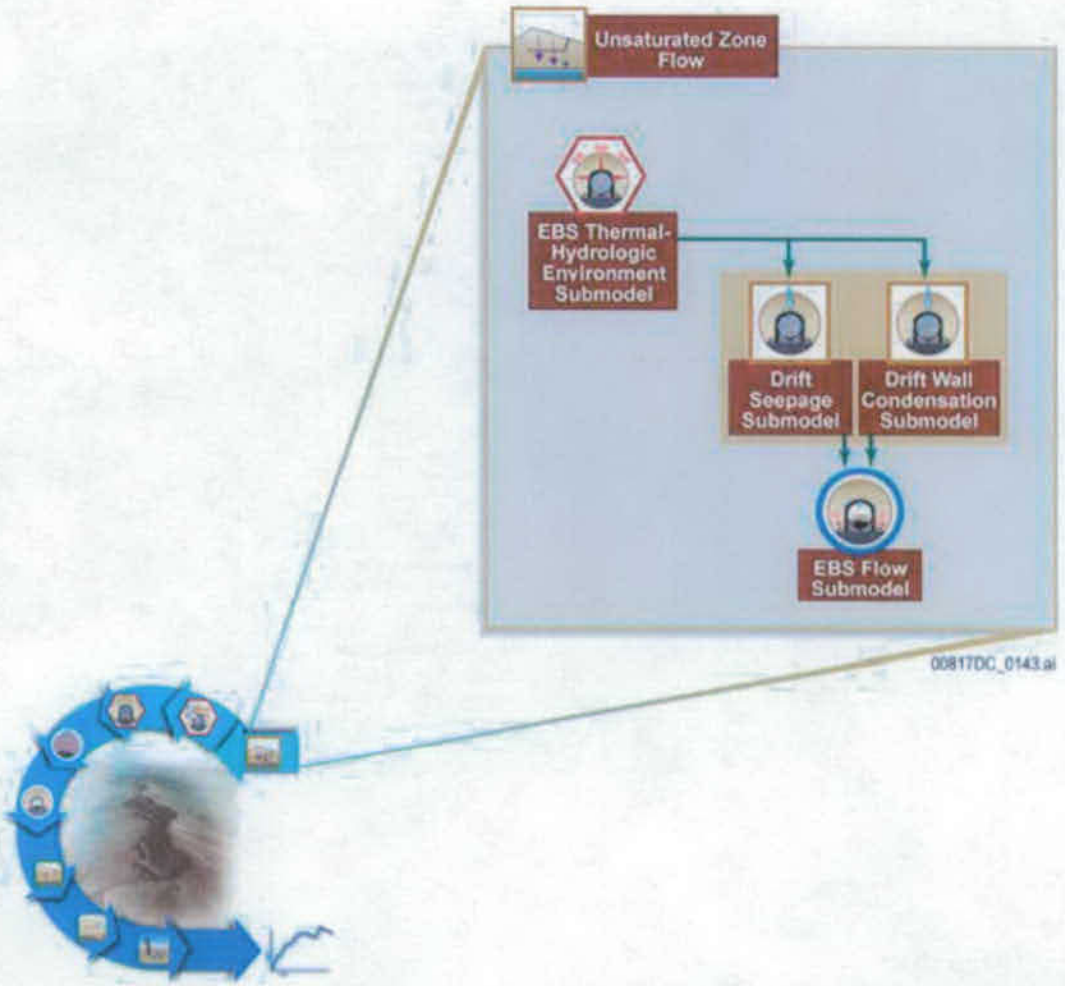

Figure 6.3.3-1. Information Flow Diagram for the Drift Seepage and Drift Wall Condensation Submodels

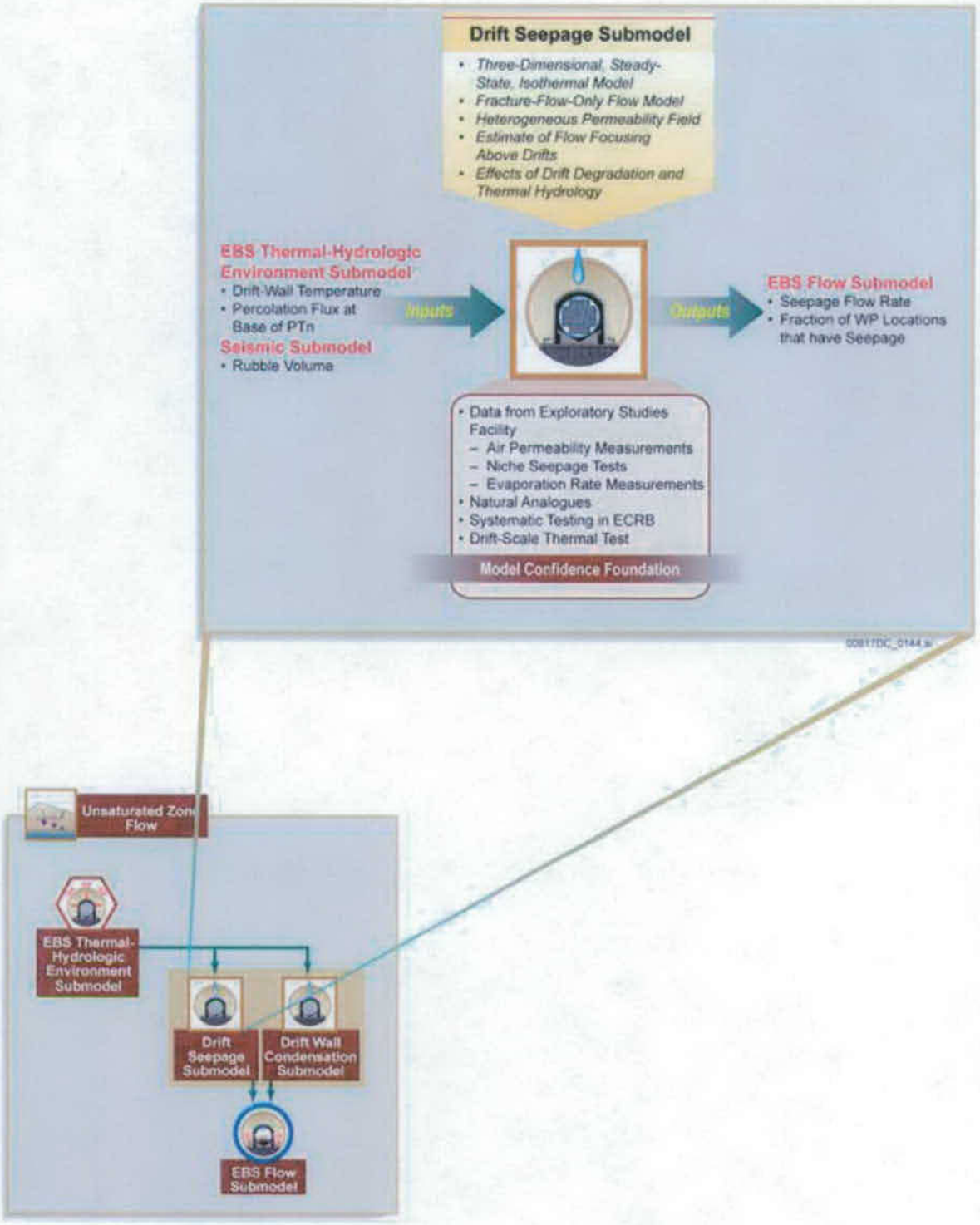

Figure 6.3.3-2. Inputs, Outputs, and Basis for Model Confidence for the Drift Seepage Submodel

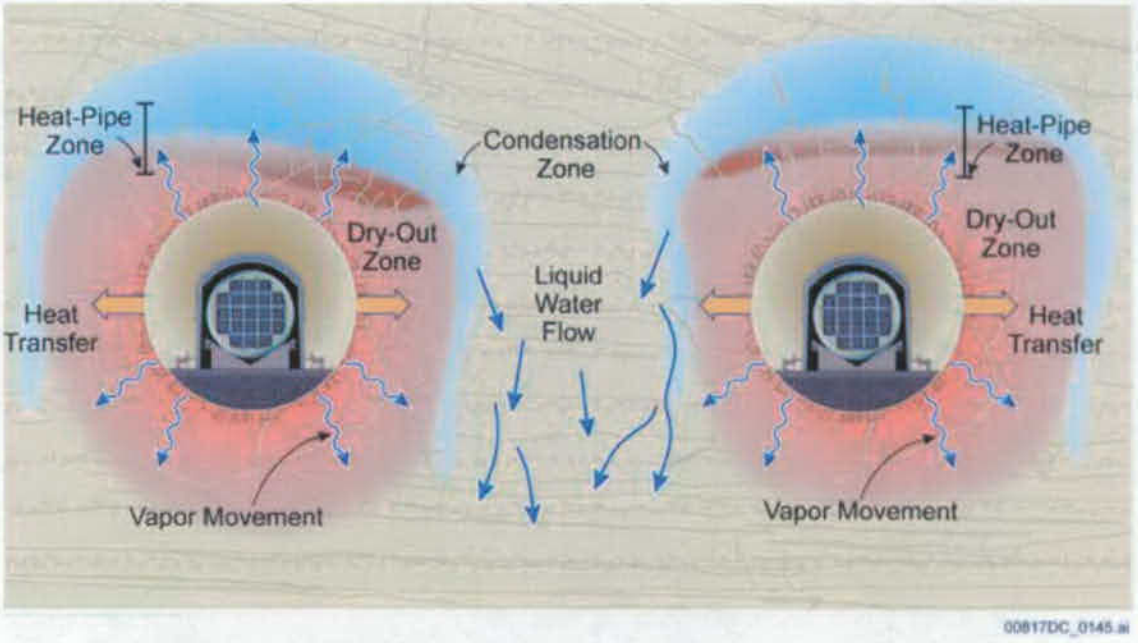

Source: Modified from (BSC 2004 [DIRS 169734], Figure 5-81)

Figure 6.3.3-3. Schematic Illustration (not to scale) of Thermal-Hydrologic Processes in the Vicinity of the Emplacement Drifts Due to Repository Heating

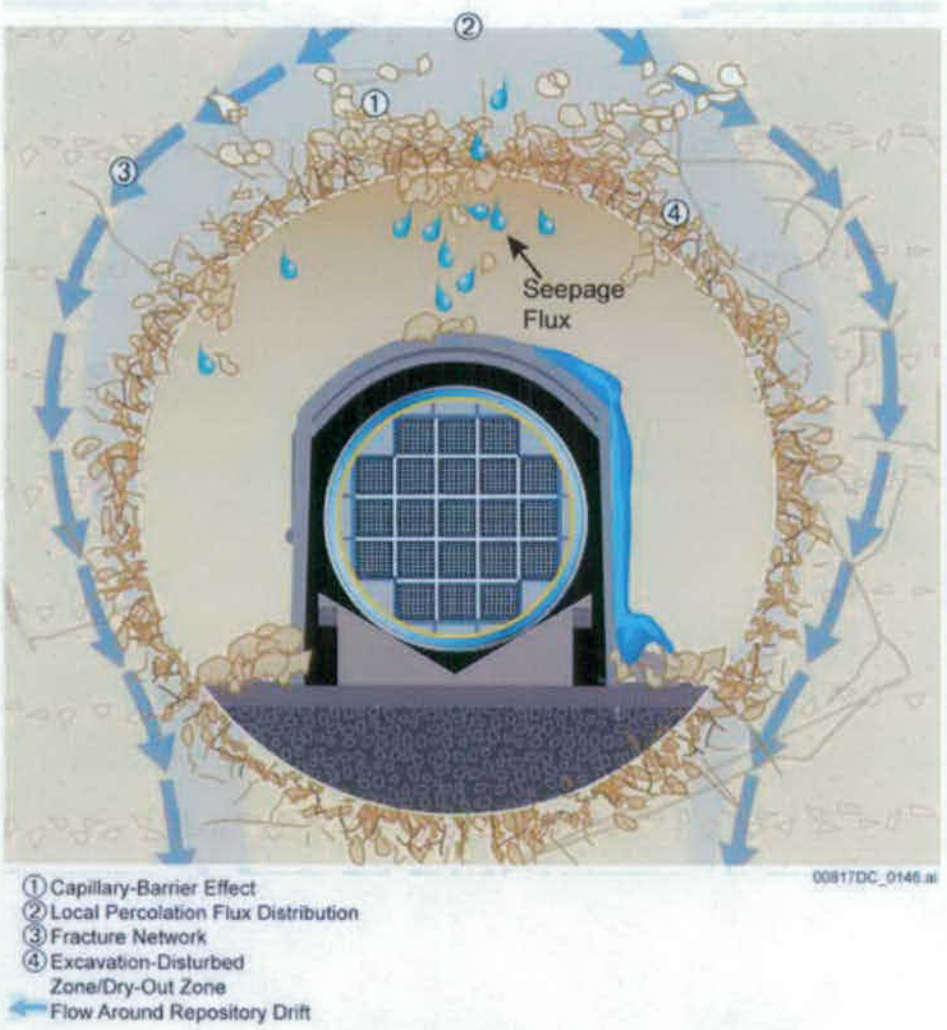

Figure 6.3.3-4. Schematic Illustration of the Processes Affecting Ambient Drift Seepage

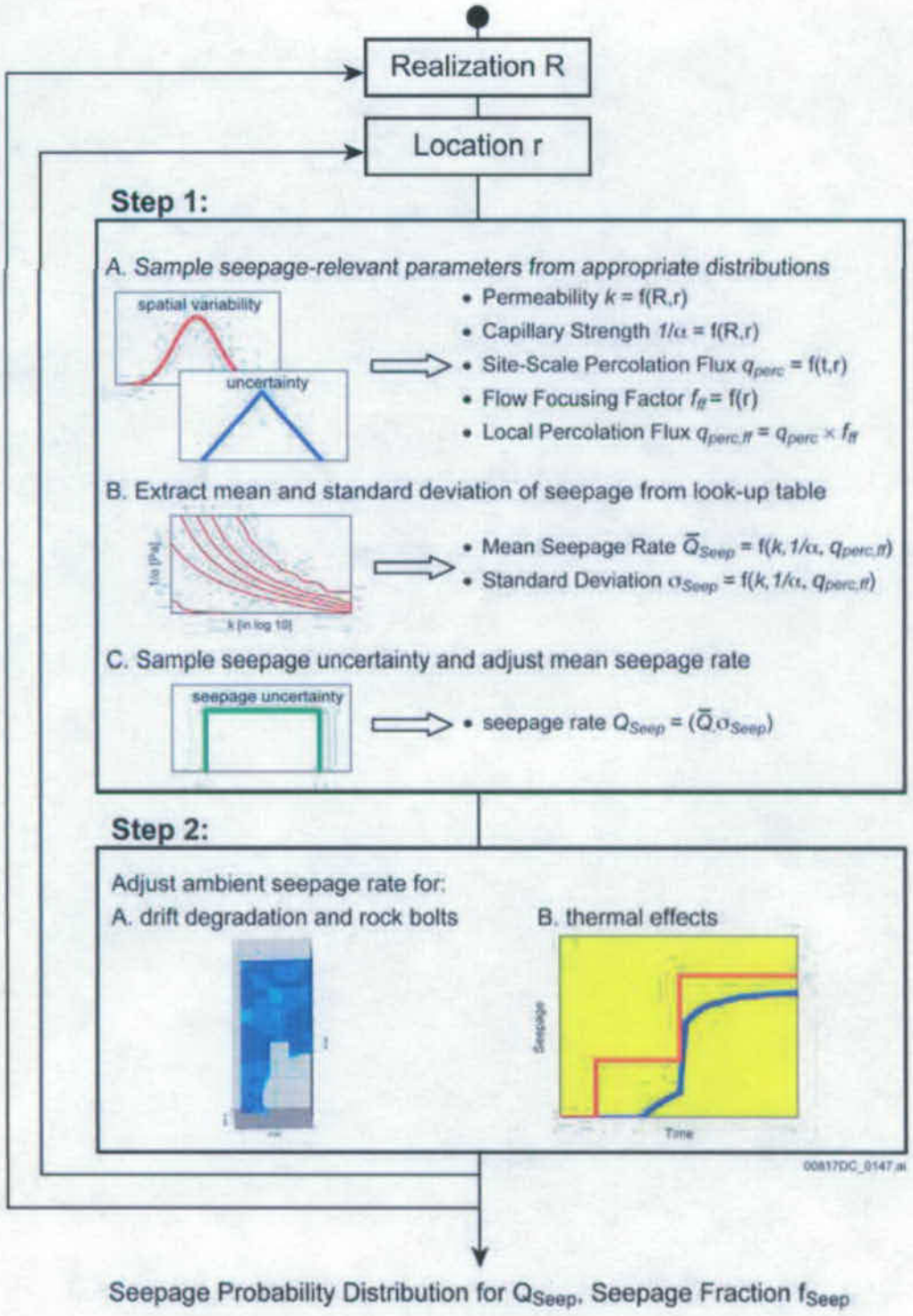

Source: (SNL 2007 [DIRS 181244], Figure 6-1[a])

Figure 6.3.3-5. Procedure for Probabilistic Calculation of Seepage at Selected Timesteps in the TSPA-SEIS

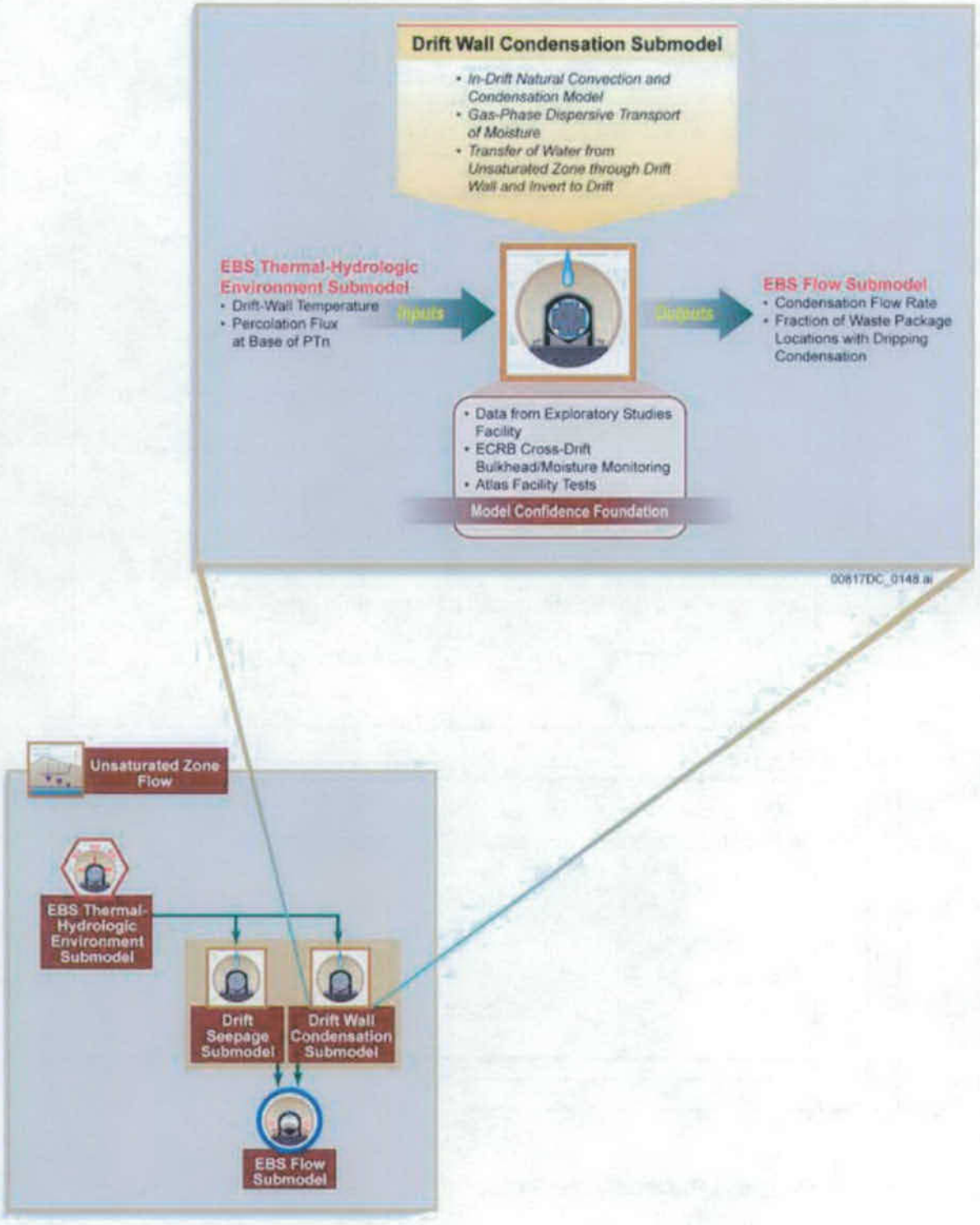

Figure 6.3.3-6. Inputs, Outputs, and Basis for Model Confidence for the Drift Wall Condensation Submodel

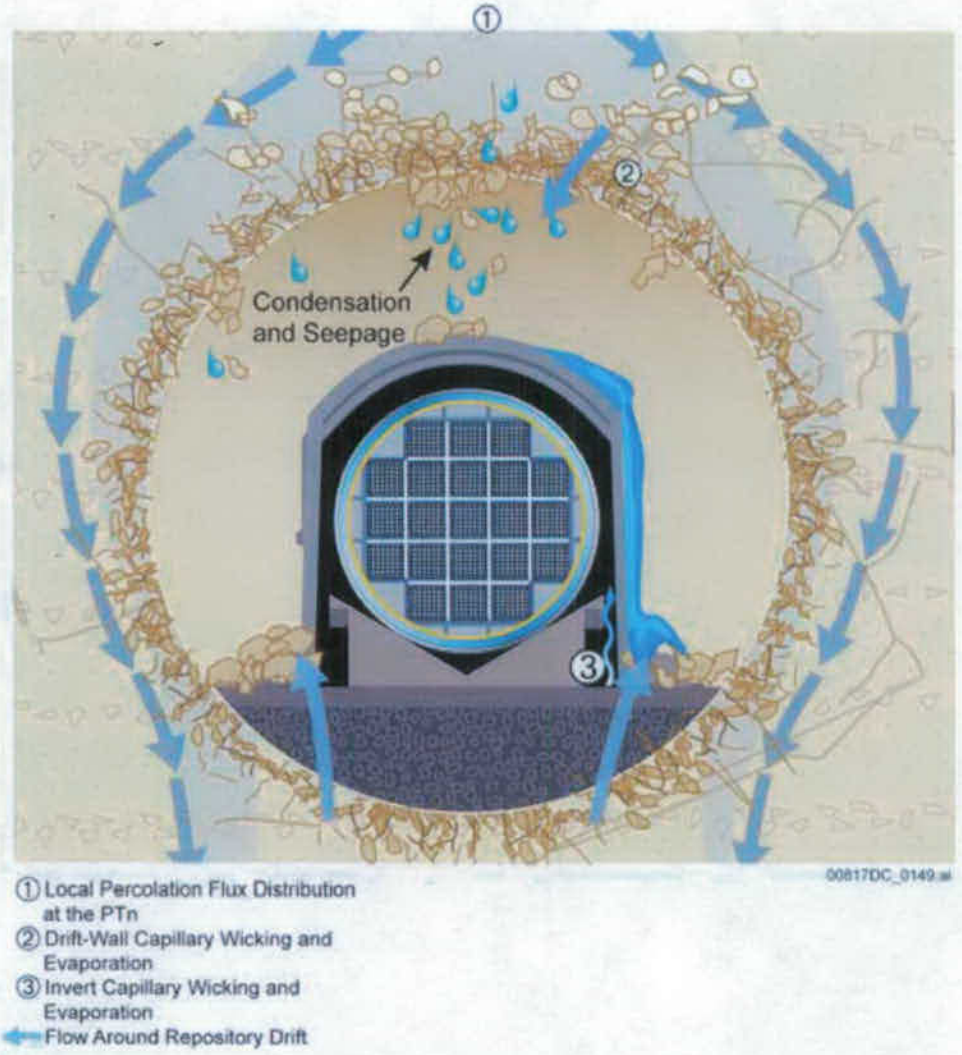

Figure 6.3.3-7. Schematic Illustration of the Processes Affecting Drift-Wall Condensation

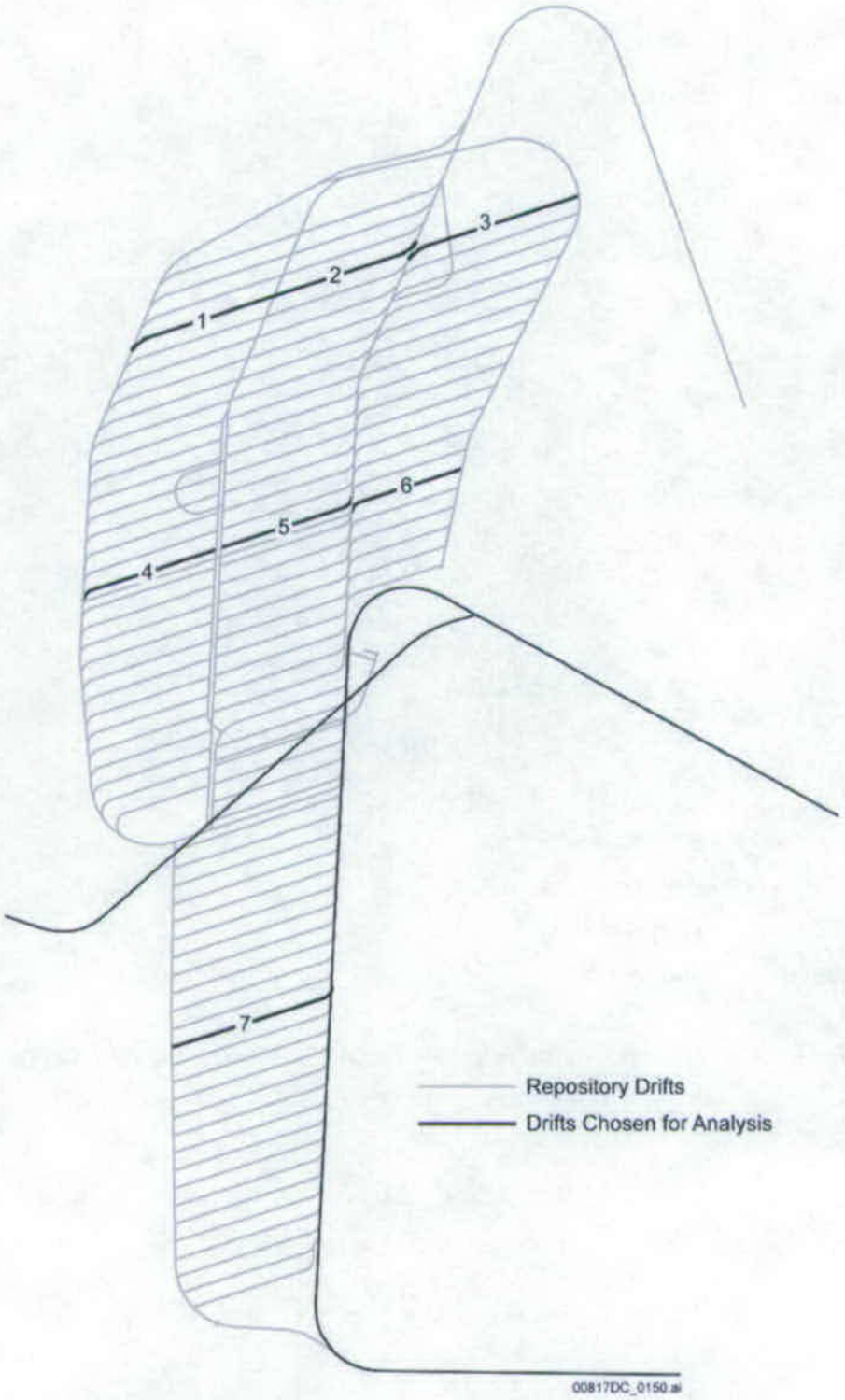

Source: Modified from (SNL 2007 [DIRS 181648], Figure 6-1[a] and 6-2[a]).

Figure 6.3.3-8. Schematic Depicting Approximate Locations of Disposal Drifts Chosen for Condensation Analysis

6.3.4 Engineered Barrier System Chemical Environment

The *Engineered Barrier System: Physical and Chemical Environment* (EBS P&CE) abstractions (SNL 2007 [DIRS 177412]) are implemented in both the TSPA-SEIS and for calculations external to the TSPA-SEIS. The EBS P&CE Abstractions are implemented by the EBS Chemical Environment Submodel. This submodel consists of an algorithm to calculate the time-dependent partial pressure of CO_2 (Pco_2) and look-up tables to determine the values of the time-dependent parameters pH, ionic strength, aqueous chloride concentration [Cl^-], and aqueous nitrate concentration [NO_3^-]. These chemical-environment variables determine whether LC of the WP outer barrier occurs in the TSPA LC Initiation Analysis, and they determine radionuclide mobility in the invert (i.e., radionuclide solubility and colloid stability) in the TSPA-SEIS. Within the TSPA-SEIS, outputs of the EBS Chemical Environment Submodel primarily serve as inputs used to calculate radionuclide solubility (Section 6.3.7.5.3) and colloid stability (Section 6.3.7.6.3) in the invert. Other than the Pco_2 in the drift, the EBS Chemical Environment Submodel does not provide input to in-package chemistry because *In-Package Chemistry Abstraction* (SNL 2007 [DIRS 180506], Section 6.6.2[a]) shows that the chemistry inside a failed WP is insensitive to incoming water composition.

The EBS Chemical Environment Submodel, as implemented in both the TSPA-SEIS and the LC Initiation Analysis, simulates the temporal changes of Pco_2, pH, ionic strength, [Cl^-], and [NO_3^-] using abstractions developed in EBS P&CE (SNL 2007 [DIRS 177412], Section 6.15). The algorithm for Pco_2 calculates the Pco_2 as a function of time and incoming seepage water composition. The response surfaces for pH, ionic strength, [Cl^-], and [NO_3^-] are calculated as functions of incoming seepage water composition, water rock interaction parameter (WRIP), temperature, and Pco_2. The relative humidity is the independent variable in using the response surfaces. The Pco_2 is used as an input to the Dissolved Concentration Limits Submodel (Section 6.3.7.5) and the In-Package Chemistry Submodel (Section 6.3.7.2), as applied to the interior of a failed WP. In addition, Pco_2, pH, and ionic strength are used as inputs to the Dissolved Concentration Limits Submodel (Section 6.3.7.5) and the EBS Colloids Submodel (Section 6.3.7.6), as applied in the invert. The pH, [Cl^-], and [NO_3^-] are used to assess the potential to initiate LC on the WP outer barrier (Section 6.3.5.2). The EBS TH Environment Submodel described in Section 6.3.2 provides the comprehensive time histories of temperature and relative humidity to the EBS Chemical Environment Submodel crown seepage chemistry calculations and provides the representative time histories to the EBS Chemical Environment Submodel invert chemistry calculations. Information flow and connections between the EBS Chemical Environment Submodel and other TSPA-SEIS components and submodels are shown on Figure 6.3.4-1. Figure 6.3.4-2 presents an overview of the important in-drift processes that impact the results, inputs, outputs, and level of confidence in the EBS Chemical Environment Submodel. Figure 6.3.4-3 illustrates the locations of in-drift EBS structures and materials, including WPs, DSs, and the invert.

6.3.4.1 Conceptual Model

The EBS Chemical Environment Submodel quantifies Pco_2 in the drift and invert; pH and ionic strength in the invert water; and pH, $[Cl^-]$, and $[NO_3^-]$ in the crown seepage water. The EBS P&CE (SNL 2007 [DIRS 177412]) applies the same Pco_2 to the drift, the invert, and the inside of the WP. Various physical and chemical processes in the WPs and geochemical processes in the invert depend on the output from the EBS Chemical Environment Submodel. The Pco_2 inside the WPs influences the degradation of the waste forms and the solubility of the radionuclides inside failed WPs. The Pco_2 in the invert influences the solubility of the radionuclides in the invert. Brines that form by evaporative concentration from seepage, which enters the invert by dripping, can influence radionuclide mobility (i.e., radionuclide solubility and colloid stability) in the invert. Acidic or alkaline water in the invert could enhance the solubility of radionuclides. The ionic strength of water in the invert will control the stability of colloidal material transporting sorbed radionuclides and could also influence the solubility of radionuclides in the invert. The pH, $[Cl^-]$, and $[NO_3^-]$ of the crown seepage water dripping onto a WP are parameters used to assess the initiation of LC of the WP outer barrier.

The EBS P&CE (SNL 2007 [DIRS 177412]) performed an analysis of the evolution of the physical and chemical environment in the EBS, including an evaluation of likely changes to the compositions of gas, water, and solids within the emplacement drifts under repository conditions. The following influences were evaluated for their potential to cause compositional changes in water in the EBS:

- The compositions of water and gas that enter the drifts from the host rock
- Changing thermal conditions in the drifts
- The interactions of seepage water and gas with introduced engineered materials
- The compositions of evaporating or condensing waters within the drifts.

The overall conceptual model is simple. As infiltrating water moves downward toward the repository, it moves up a thermal gradient. The thermal gradient extends from the land surface to the repository level, and is assumed to vary linearly with depth. The water interacts with minerals in the rock, maintaining equilibrium with calcite and amorphous silica, present in excess, and dissolving alkali feldspar, while precipitating out one or more secondary phases. The degree of feldspar dissolution is a function of the temperature at any location along the percolation path, and is calculated using a temperature-dependent dissolution rate. The dissolution rate was estimated for ambient conditions from the degree of alteration that the tuff has undergone since it erupted, 12.8 million years ago, and adjusted for temperature using literature data for the activation energy for feldspar dissolution (SNL 2007 [DIRS 177412], Section 6.3.2.1). Little evaporation or degassing occurs as the water moves up the thermal gradient, until it reaches a lower-saturation zone around which steam and gas can readily escape into the drift, where steam is transported axially to cooler zones and condenses. The low saturation zone is the drift and areas in the surrounding rock, including fractures connecting to the drift, which are readily accessed by the in-drift atmosphere. Evaporation occurs at the boundary between the higher saturation area surrounding the drift and the lower saturation area, which will, hereafter, be referred to as the evaporation front. During the boiling period, this boundary corresponds to the boiling zone around the drift. At later times, it corresponds to the drift wall and fractures extending outward from the drift, close enough to be in gas-phase

equilibrium with it. The Pco_2 in the drift is controlled by equilibrium with the water at the evaporation front, with dilution by water vapor, from water that evaporates after entering the drift.

As seepage waters enter drifts their chemical compositions may change due to evaporation, mineral precipitation, or both. Throughout the thermal period (depending on the relative humidity in the drifts), evaporative concentration of seepage can occur in the EBS. Evaporation increases aqueous species concentrations, mineral precipitation, and the concentration of the most soluble components in brines. In accordance with the geochemical divide theory, the composition of the seepage water changes according to the sequence of minerals that precipitate from that solution as a function of initial water composition, thermal conditions, relative humidity, and gas composition where the evaporation occurs (SNL 2007 [DIRS 177412], Section 6.3.3.1).

Figure 6.3.4-4 depicts several representative locations along a vertical flow path from the crown of the drifts to the base of the invert. The chemical compositions of the water and the gas at each of these representative locations could directly affect the degradation rates of the EBS, the quantities and species of mobilized radionuclides, and/or the transport rates of radionuclides and fluids flowing through the drifts into the UZ.

The following describes conditions shown on Figure 6.3.4-4, Locations 1 through 5 (adapted from ((SNL 2007 [DIRS 177407]), Figure 6.6-4) and (SNL 2007 [DIRS 177412], Section 6.5)).

Location 1 (Drift Wall and Air Gap)—Possible seepage water and gas chemistries at Location 1 could be modified by interactions with engineered materials, such as rock bolts and stainless steel sheets and their corrosion products, or directly drip into the drifts and onto surfaces of the DSs (Location 2). Generally, potential seepage water interactions with engineered materials and their corrosion products will not alter the major ion composition in water entering the drifts (SNL 2007 [DIRS 177412], Section 6.8 and Tables 6.8-3 through 6.8-6). Given the limited longevity of the low-alloy steels that comprise some of the ground support and all of the invert materials such as gantry rails, support beams, and other engineered materials, this effect would be on the order of hundreds of years for most materials placed within the drifts (SNL 2007 [DIRS 177412], Section 6.5.2). A sensitivity analysis investigating the potential impacts on water chemistry revealed the impacts are negligible (SNL 2007 [DIRS 177412], Section 6.8). For the longer-lasting materials, such as the 316L stainless steel that comprises the wire mesh ground support component, sensitivity analyses also show that corrosion processes have a negligible effect on the composition of seepage waters (SNL 2007 [DIRS 177412], Section 6.8). Any potential impact of emplaced materials is indirectly considered in the TSPA-SEIS through the output of the EBS P&CE suite of models.

Location 2 (Surface of the DS)—Some portion of the water from Location 1 may be diverted directly to the invert (Location 5) by the DSs, or may undergo evaporative processes, and/or react with debris sitting on the DSs. If the DSs are breached, these fluids could flow onto the surface of the WPs (Location 3) but could only flow into the WPs (Location 4) through an available pathway. Corrosion products associated with the DSs are not expected to adversely affect the compositions of any waters flowing off or through DSs, due to the very slow corrosion rates for titanium and the insoluble nature of titanium oxides (SNL 2007 [DIRS 177412],

Section 6.5.1.1). For the same reasons, the removal or addition of trace elements by sorption or dissolution processes associated with active corrosion of the DSs' titanium alloy is not considered.

Location 3 (Outer Surface of WPs)—Alloy 22, the alloy of the WP outer barrier, like the titanium used for DSs, is also highly corrosion resistant (SNL 2007 [DIRS 177412], Section 6.5.1.2). The processes occurring at Location 2 also apply to Location 3. The potential for LC on the WP outer barrier depends on whether or not seepage-derived water contacting the WPs is capable of initiating LC.

Location 4 (Inside the WP)—This portion of the conceptual process is reported in other modeling reports, such as *In-Package Chemistry Abstraction* (SNL 2007 [DIRS 180506]) and in Section 6.3.7.2 of this report.

Location 5 (Invert)—The chemical environment in the invert affects radionuclide solubility and colloid stability. Both radionuclide solubility and colloid stability could affect the radionuclide mobilization from the source term for transport from the EBS to the UZ. Implementation of the P&CE integrated invert chemistry abstraction model is discussed in SNL 2007 [DIRS 177412], Section 6.13.4, Section 6.15.2, and Table 6.15-1.

6.3.4.2 TSPA Abstraction

Within the TSPA-SEIS, the EBS Chemical Environment Submodel calculates time-dependent P_{CO_2} in the gas phase in the drift above the invert and pH and ionic strength conditions in the invert. Within the LC Initiation Analysis (Section 6.3.5.2), the EBS Chemical Environment Submodel calculates time-dependent P_{CO_2} in the gas phase in the drift above the invert and the pH, $[Cl^-]$, and $[NO_3^-]$ in the crown seepage water. The same time-dependent P_{CO_2} in the gas phase in the drift above the invert is used for the drift P_{CO_2}, the in-package P_{CO_2}, and the invert P_{CO_2}.

The EBS Chemical Environment Submodel is based on the Near Field Chemistry model developed in *Engineered Barrier System: Physical and Chemical Environment* (SNL 2007 [DIRS 177412]). The Near Field Chemistry model provides potential seepage water compositions at the drift wall, the water-rock interaction parameter, and the range of in-drift P_{CO_2}. The evolution of pH, ionic strength, $[Cl^-]$, and $[NO_3^-]$ are also modeled using response surfaces in the form of look-up tables. Each look-up table is a function of initial water type, WRIP, temperature, and P_{CO_2} with relative humidity as the independent variable. The interaction between seepage water and engineered materials is not included in the analysis because the EBS P&CE Abstraction determined that this interaction has a negligible impact on the composition of seepage water and in-drift gas phases (SNL 2007 [DIRS 177412], Sections 6.5, 6.7, and 6.8). The following processes, represented by the EBS Chemical Environment Submodel, are abstracted below:

- Temporal evolution of incoming seepage water composition, where seepage includes dripping from the drift crown
- Changing P_{CO_2} in the drifts and the invert

- Evaporative evolution of seepage water composition from the drift crown and in the invert.

Evolution of Incoming Seepage Composition—The Near Field Chemistry model defines four starting waters as representative of the potential range of the Topopah Spring Tuff pore water compositions (SNL 2007 [DIRS 177412], Sections 6.3.2 and 6.6). As water percolates down through from the surface, it interacts with the rock. The water-rock interactions modify the water composition. The normal compositions due to water-rock interactions are further modified by the repository heating as the water passes through the thermal field in the TSw. Ultimately, this thermally altered water is what enters the drift and controls the chemical conditions in the drift.

The degree of alteration is determined by the amount of water-rock interaction, quantified by the parameter called the water-rock interaction parameter. The water-rock interaction parameter is affected by the percolation rate through the rock and the thermal field through which the water passes. Ambient conditions are characterized as having zero water-rock interaction. Large water-rock interactions can be caused by high temperatures and slow percolation fluxes through the TSw. Lower temperatures and/or fast water movement will cause less water-rock interaction. The model follows a packet of water from the surface as it passes through the time-dependent thermal field to the repository taking into account the climate changes that change the velocity of the water.

The Near Field Chemistry model provides the water-rock interaction parameter as a function of the percolation flux and the thermal measure. The thermal measure is defined as the sum of peak WP temperature (in degrees C) and the duration of boiling (in years). Obviously, this parameter is not really physical because it is in mixed units. However, it does give an estimate of the thermal perturbation near the WP. A large thermal measure, which can cause a large perturbation, can be caused by high temperatures and/or long boiling times. A low thermal measure indicates a cooler WP or one that cools quickly. The percolation rate also can influence the thermal measure of the WP because high percolation tends to cool the repository more quickly. The percolation flux is used as an indicator of how fast the water moves through the thermal field. The thermal measure and glacial transition percolation flux has been extracted from the multi-scale results for the representative WPs used in TSPA-SEIS. Once the thermal measure and percolation flux are specified, the water-rock interaction parameter can be found from the water-rock interaction parameter look-up table.

Uncertainty in input parameters for calculating the water-rock interaction parameter values is propagated through the Near Field Chemistry model as described in the P&CE report (SNL 2007 [DIRS 177412], Section 6.12.2.5). These water-rock interaction parameter values are passed to TSPA as a beta distribution, the mean value of which is extracted from the water-rock interaction parameter lookup table. The maximum value of the beta distribution is specified to be 2.838 times the mean, the minimum is 0.2039 times the mean, and the standard deviation is 0.4251 times the mean. This uncertainty is primarily due to uncertainty in the feldspar dissolution rate. In each realization, the TSPA-SEIS extracts the water-rock interaction parameter value from the lookup table and generates a new distribution at each time step. The TSPA-SEIS implements the uncertainty in water-rock interaction parameter with self-correlation—that is, after sampling the beta distribution for the first time step, it samples at the same probability level for the new

distributions generated at each time step for the entire realization (SNL 2007 [DIRS 177412], Section 6.15.1).The water-rock interaction parameter and the WP temperature form the basis for calculating the P_{CO_2} in the drift. Relevant CO_2 concentrations in the gas phase within the rock are difficult to determine (SNL 2007 [DIRS 177412], Section 6.3.2.5). As water percolates downward through the thermal field and heats up, CO_2 is partitioned into the gas phase. This is offset by the effects of feldspar dissolution, which raises the alkalinity and reduces the degree of partitioning into the gas phase. The relative rates of these two processes are important because the degree to which the gas phase acts as an open system—the amount of CO_2 that would be lost or gained by gas phase advection and mixing—is unknown. Given that matrix saturations are high and fracture porosity is low, it is assumed for the Near Field Chemistry model that gas phase transport is limited, except for the area immediately around the drift, where loss into the drift can occur; therefore, the gas phase composition at any location in the rock column is determined by assuming equilibrium with the aqueous composition, rather than being controlled by gas phase advection and mixing.

P_{CO_2} as a Function of Time—Calculating the P_{CO_2} in the drift is difficult because it is the result of competing processes such as degassing, precipitation, and diffusion and advection of gas in the fractures. Two bounding cases are considered (SNL 2007 [DIRS 177412], Section 6.3.2.8):

- *Minimum CO_2 concentration in the drift.* In this bounding case, gas movement into and out of the drift, and through the mountain, is assumed to occur readily through fractures. The CO_2 concentration in the air fraction entering the drift is equal to the ambient CO_2 concentration in the mountain at the repository level (10^{-3} bars). The contribution of this to the total CO_2 in the drift atmosphere is equal to this concentration times the mole fraction of air in the drift. Assuming ambient CO_2 concentrations and summing the CO_2 entering the drift in air with that released as water evaporates at the dryout front yields a minimum concentration for CO_2 in the drift.

- *Maximum CO_2 concentration in the drift.* Behind the evaporation front, the gas phase is assumed to be in equilibrium with the aqueous phase at the temperature of the evaporation interface, assuming that the water moved up the temperature gradient to the interface without degassing. Treating the drift as a closed system, the in-drift pCO_2 would equal this value, which can be taken as a maximum for the in-drift atmosphere. If the model predicts large amounts of feldspar dissolution, but relatively low temperatures (e.g., for extremely slow percolation flux rates, water percolated through hot rocks, but did not reach the drift wall until it had cooled), then it is possible for the predicted maximum pCO_2 to actually be below 10^{-3} bars. This is because the alkalinity increases as feldspar dissolves, increasing the amount of CO_2 dissolved into the water. If this occurs, it is assumed that the maximum pCO_2 value is 10^{-3} bars.

Thus, combining the lower and upper bounds for the in-drift pCO_2 yields the possible range of CO_2 concentrations in the drift and also in the invert.

Evaporative Evolution of Seepage at the Drift Crown and in the Invert—Equilibrium compositions of aqueous solutions and mineral precipitates that may form from seepage water within the emplacement drifts were calculated using the model developed in Section 6 and summarized in Section 8 of *In-Drift Precipitates/Salts Model* (IDPS) (SNL 2007

[DIRS 177411]), hereafter referred to as the IDPS Process Model. Calculations of water compositions at chemical equilibrium were performed using the geochemical equilibrium code, EQ3/6 Version 8.0 (*Software Code: EQ3/6.* V8.0 (BSC 2003 [DIRS 162228])), and a Pitzer thermodynamic database developed specifically for that purpose (SNL 2007 [DIRS 177412], Table 4.1-1 and Section 6.2.6). The IDPS Process Model simulates the evolution of water in the drifts as it evaporates from its initial composition into concentrated brine. The EBS P&CE applies the IDPS Process Model to each of the four starting waters (SNL 2007 [DIRS 177412] Section 6.6) to produce chemical composition look-up tables (SNL 2007 [DIRS 177412] Section 6.15 and Section 8.2). Within the TSPA-SEIS, the EBS Chemical Environment Submodel evaluates the EBS P&CE Abstraction to determine the chemistry of two drift waters. One type of water is seepage water dripping from the drift crown and the second type of water is the invert water that originated as water dripping from the drift crown. Seepage water dripping from the drift crown may flow onto the DS and, in the event of a failed DS, may subsequently contact the WP surface. Invert water that originated as water dripping from the drift crown may flow directly into the invert or may contact the DS and/or WP before it reaches the invert.

The implementation instructions for evaluating the EBS P&CE, with uncertainties, are given look-up tables in the EBS P&CE (SNL 2007 [DIRS 177412], Sections 6.12 and 6.15). The look-up tables for pH, ionic strength, $[Cl^-]$, and $[NO_3^-]$ are calculated as functions of incoming seepage water composition, water rock interaction parameter (WRIP), temperature, and Pco_2. The relative humidity is the independent variable in using the look-up tables. These chemical composition look-up tables will be referred to as IDPS look-up tables, because they are generated with the IDPS Process Model, and to distinguish them from other look-up tables (such as water-rock interaction paramenter look-up tables illustrated in Table 6.3.4-1) that are generated by the EBS P&CE suite of models (SNL 2007 [DIRS 177412], Section 6.15).

As described below, there are 396 IDPS look-up tables for seepage and invert water composition spanning combinations of Pco_2 and temperature for each of the four starting water types, 11 WRIP levels, and nine combinations of three Pco_2 values and three temperatures. Each table lists values for chemical composition, including pH, ionic strength, $[Cl^-]$, and $[NO_3^-]$ with relative humidity as the independent variable. Each IDPS look-up table is defined for a specific starting water type, temperature, and Pco_2. The tables are defined for Pco_2 values of 10^{-2}, 10^{-3}, and 10^{-4} bar; and temperature values of 30°C, 70°C, and 100°C. There are 99 tables for all possible combinations for each of the four starting waters.

An example of an IDPS look-up table is shown in Table 6.3.4-2.

Model Uncertainties, Variabilities, and Discretization Errors—Model confidence for incoming seepage water, Pco_2, pH, ionic strength, $[Cl^-]$, and $[NO_3^-]$ is discussed in the following paragraphs.

Incoming Seepage Water—The Near Field Chemistry process model (SNL 2007 [DIRS 177412]) provides potential seepage water compositions and the water-rock interaction parameter values for use in the P&CE abstraction models. Uncertainties in the inputs are treated as follows. The four input waters (Groups 1 through 4) were chosen statistically to represent the variability in 34 TSw waters upon evaporation. The uncertainty in the starting water composition is represented by randomally selecting one of the four water types for each

realization. Because representative waters are used, it is also necessary to sample the range of Cl:N in the 34 TSw waters from a discrete CDF to capture the uncertainty associated with these key chemical parameters. Output seepage water compositions are presumed to span the natural variability of the pore water compositions in the repository units (SNL 2007 [DIRS 177412], Section 6.12.3).

Partial Pressure of Carbon Dioxide Gas—The range of uncertainties and variability are included in the abstractions of P_{CO_2} by using minimum and maximum P_{CO_2} bounding cases and then scaling between ambient and the bounding value. These two bounding cases provide the range of P_{CO_2}. The TSPA-SEIS uses a uniform stochastic variable, PCE_Delta_pCO2_a, between -1 and 1, to choose which of the bounding cases to use in each realization (SNL 2007 [DIRS 177412], Section 6.15.1). A negative value of the variable implies using the minimum P_{CO_2} case and a positive value implies the maximum P_{CO_2} case. The actual P_{CO_2} in the drift is calculated by linearly scaling between ambient (0.001 bars) and the minimum or maximum, using the absolute value of PCE_Delta_pCO2_a as the scaling factor. This scaling accounts for the uncertainty in the in-drift P_{CO_2}.

pH, Ionic Strength, [Cl^-], and [NO_3^-]—IDPS uncertainty factors for the Cl, N, Cl:N, and ionic strength of in-drift water are used directly by the P&CE abstraction models. The uncertainty associated with Cl+N is calculated assuming linear combinations of the uncertainties on Cl and N provided by the IDPS Model (SNL 2007 [DIRS 177411], Table 6.12-1). These uncertainties apply between 20°C and 140°C and are defined as triangular distributions with the most likely uncertainty equal to ±0.0 and the maximum and minimum uncertainties shown in Table 6.3.4-3 (SNL 2007 [DIRS 177411], Table 6.12-1).

The IDPS uncertainty for pH was developed by comparison of modeled data with pH values measured in several evaporation and mineral solubility experiments, and the process of measuring pH has significant error. The pH uncertainty value is taken directly from the look-up tables and is adjusted by the uncertainties reported in Table 6.12-2 using a triangular distribution for relative humidity values below 75 percent. Between 100 percent and 75 percent relative humidity, pH uncertainties are sampled from a discrete CDF.

No uncertainty is associated with the ionic strength below 85 percent relative humidity from the look-up tables because the ionic strength is not used by the TSPA-SEIS at these concentrations. Between 85 percent and 100 percent relative humidity the ionic strength is adjusted for uncertainty by applying a triangular distribution and the value in Table 6.12-1 of EBS P&CE (SNL 2007 [DIRS 177412]). The guidance for applying these uncertainty distributions is provided in EBS P&CE (SNL 2007 [DIRS 177412], Section 6.12.3).

6.3.4.3 TSPA-SEIS Implementation

The EBS Chemical Environment Submodel is implemented in the TSPA-SEIS to calculate the chemistry (pH and ionic strength) of the water in the invert (discussed in Section 6.3.4.3.1) and the unevaporated drift crown seepage water in the Igneous Scenario Class (discussed in Section 6.3.4.3.3). The EBS Chemical Environment Submodel is also implemented in the LC Initiation Analysis (Section 6.3.5.2) to calculate the chemistry (pH, [Cl^-], and [NO_3^-]) of the seepage water from the crown of the drift (discussed in Section 6.3.4.3.2). Although performed

in two separate GoldSim files for three different applications, the submodel implementations are similar.

6.3.4.3.1 Invert Chemistry

The EBS Chemical Environment Submodel calculations for the invert are performed in two main levels of the TSPA-SEIS: global and local. Global calculations can be applied to all WPs and local calculations pertain only to those WPs in the local percolation subregion or percolation subregion environment. To reduce redundancy, the EBS Chemical Environment Submodel calculations that can be applied equally to all percolation subregions and both WP types are performed at a higher (global) level. For example, the selection of one of the four starting water compositions is performed at the global level. In the TSPA-SEIS, the selection of one of these four initial water compositions is randomly sampled with equal probability. The probability of selecting any one of the four source waters is 25 percent (SNL 2007 [DIRS 177412], Section 6.15.1). Once selected, the initial water composition determines which total carbon tables and maximum Pco_2 tables are used to calculate the Pco_2. Pco_2 in the drift and in the invert must also match the selected starting water. Therefore, Pco_2 in the drift and Pco_2 in the invert are determined at the global level and the resulting Pco_2 values are applied to the entire repository. The EBS Chemical Environment Submodel calculations for the pH and ionic strength of the invert water require invert temperature and invert relative humidity, which are percolation subregion specific feeds from the EBS TH Environment Submodel (Section 6.3.2), and must be performed separately (locally) within each percolation subregion.

Inputs—Sections 6.9.3 and 6.15 of EBS P&CE (SNL 2007 [DIRS 177412]) provide the guidance for applying the 396 IDPS look-up tables for seepage composition. The IDPS look-up tables are used to determine the pH and ionic strength in the invert as a function of starting water type, water-rock interaction parameter, temperature and Pco_2. In the TSPA-SEIS implementation, the independent variable in each of the IDPS look-up tables is the applicable relative humidity. For the dependent variables, column 1 contains the pH, column 2 contains the ionic strength, column 3 contains $[Cl^-]$, and column 4 contains $[NO_3^-]$. Only the pH and ionic strength values are used in the invert chemistry calculations. The $[Cl^-]$ and $[NO_3^-]$ values are only used in the crown seepage chemistry calculations (Section 6.3.4.3.2). Each set of look-up tables was developed for each temperature combination of 30°C, 70°C, and 100°C; and Pco_2 values of 10^{-2}, 10^{-3}, and 10^{-4} bar; and 11 WRIP levels for a total of 99 look-up tables for each of the 4 starting water types. The PCE_Chemistry_Tables container in the TSPA-SEIS's GoldSim model file provides more information regarding these look-up tables and their applications. The methodology for applying uncertainty to the calculated pH and ionic strength is described in Section 6.12.3 of EBS P&CE (SNL 2007 [DIRS 177412]). Additional calculation details are provided below and in the TSPA-SEIS GoldSim file.

The following describes the determination of the seepage water composition, invert temperature, invert relative humidity, and Pco_2 and their use in selecting the appropriate IDPS look-up tables for chemical composition for the interpolation of the appropriate pH and ionic strength values.

Global Calculations—Global level calculations begin with selecting one of the four initial starting waters, the representative WP and its thermal measure, and then calculating the water-rock interaction parameter for each TSPA percolation subregion (SNL 2007 [DIRS 177412],

Section 6.15). Each TSPA-SEIS realization randomly selects one of the four starting percolating water compositions used for all percolation subregions. All the starting percolating water compositions are equally probable and, therefore, the probability of any given water being selected is 25 percent.

The water-rock interaction parameter is the one time-dependent independent parameter in the EBS Chemical Environment Submodel calculated at the global level. The water-rock interaction parameter describes the evolution of the water and specifies, along with the the temperature and Pco_2, which of the chemical composition look-up tables (0-L) to use for pH, ionic strength, $[Cl^-]$, and $[NO_3^-]$. As described earlier, the water-rock interaction parameter requires sampling from a beta distribution at every time-step. This resampling, as well as the separation of aleatory and epistemic uncertainty, requires that the water-rock interaction parameter for every percolation subregion and WP type be calculated as a time-series at the global level before the main calculation. Then the water-rock interaction parameter is passed to the local level calculations for use along with the the temperature and Pco_2 in selecting the appropriate IDPS look-up table for pH, ionic strength, $[Cl^-]$, and $[NO_3^-]$.

Local Calculations—After the starting water is selected and the water-rock interaction parameter is calculated at the global level, the appropriate Pco_2 for the drift and the invert can be calculated. Pco_2 values are determined at each timestep. The drift Pco_2 is used to calculate radionuclide solubilities in the WPs (Section 6.3.7.5) and total carbonate concentration in the failed WPs (Section 6.3.7.2). The same Pco_2 applies in the invert and is used to calculate radionuclide solubilities in the invert (Section 6.3.7.5) and the pH and ionic strength of the invert water.

The Pco_2 values in the invert are determined at each simulation timestep. The TSPA-SEIS then uses the invert Pco_2 value, the selected starting water composition, and WRIP level (0-L), along with the invert temperature and relative humidity feeds from the EBS TH Environment Submodel (Section 6.3.2), to determine pH and ionic strength in the invert water using the IDPS look-up tables. The EBS TH Environment Submodel (Section 6.3.2) feeds for the representative invert temperature and relative humidity are percolation subregion-specific values, so the remaining calculations in the EBS Chemical Environment Submodel are performed locally (i.e., separately for each percolation subregion or percolation subregion environment).

WPs occupying representative emplacement drift locations, shown on Figure 6.1.4-2, are characterized by representative time histories of TH (temperature and relative humidity) and average drift-seepage rates that are provided by the EBS TH Environment Submodel (Section 6.3.2) and the Drift Seepage Submodel (Section 6.3.3.1), respectively. The EBS Chemical Environment Submodel uses these conditions and Pco_2 to calculate time-dependent pH and ionic strength conditions in the invert for the representative WP location in each percolation subregion.

The determination of pH and ionic strength in the invert water is performed locally within each percolation subregion in the TSPA-SEIS. The actual chemistry used in the invert is determined by the scenario class, the dripping or non-dripping environment, whether the WP and/or DS is intact, whether drift wall condensation occurs, and the seepage flux as specified in Table 6.3.4-4. The EBS TH Environment Submodel (Section 6.3.2) provides the EBS Chemical Environment

Submodel the representative temperature and relative humidity for each percolation subregion at each timestep.

The discussion presented below describes how the IDPS look-up tables are applied in the TSPA-SEIS to determine the chemical parameters in the invert. Although presented as the calculation of invert chemistry in the TSPA-SEIS, the following discussion is meant to be a robust discussion of the EBS Chemical Environment Submodel covering the submodel applications in both the TSPA-SEIS and the LC Initiation Analysis (Section 6.3.5.2). In evaluating the EBS Chemical Environment Submodel for crown seepage chemistry in the LC Initiation Analysis (Section 6.3.5.2), the tables are still applicable and a discussion of these tables is still warranted.

At each timestep, the EBS Chemical Environment Submodel accesses eight of the 396 IDPS look-up tables (see example in Table 6.3.4-2) and uses the current starting water, WRIP level, Pco_2, temperature, and relative humidity to determine the corresponding pH and ionic strength in the invert. The eight most appropriate IDPS look-up tables for the local environment calculations in the invert are determined by eliminating tables that are not appropriate for current invert conditions, as described below. The starting water (1, 2, 3, or 4) reduces the applicability of the 396 IDPS look-up tables to 99. The applicability of the 99 IDPS look-up tables are reduced at each timestep to 18 by choosing only those tables that are associated with the WRIP level at the time-step. The actual chemical conditions are determined by interpolation of values between eight of the 18 IDPS tables. The WRIP level is a decimal number between 0 and 10 that determines which of 11 sets of nine IDPS look-up table to use. These 11 sets of nine IDPS tables can be thought of as arranged in layers. The floor function can be used to calculate the integer below the WRIP level of interest and the ceil function can give the integer above the WRIP level. Thus, the actual WRIP level is somewhere between two layers of IDPS look-up tables. These 18 tables in two layers are further reduced to eight by selecting those tables that represent the eight nearest neighbors to the desired temperature and Pco_2. For example, if the invert temperature is below 70°C, the IDPS look-up tables corresponding to 30°C and 70°C will be used and the 100°C tables can be excluded. Otherwise, the IDPS look-up tables corresponding to 70°C and 100°C will be used and the 30°C tables can be excluded. Similarly, if the invert Pco_2 is below 10^{-3} bar, the IDPS look-up tables corresponding to 10^{-2} bar can be excluded, and if the invert Pco_2 is above 10^{-3} bar, the IDPS look-up tables corresponding to 10^{-4} bar can be excluded. The eight IDPS look-up tables, four in each WRIP level layer, are the resulting look-up tables consistent with the current value of the water-rock interaction parameter, invert temperature, and invert Pco_2.

To select the pH and ionic strength corresponding to the specific invert relative humidity desired from each of the eight IDPS look-up tables, the EBS Chemical Environment Submodel applies linear interpolation in three directions between the eight tables. When selecting pH and ionic strength values for temperature and Pco_2 values that fall between the pre-defined values of the IDPS look-up tables, the parameters are estimated from the eight look-up table results using linear interpolation for temperature and water-rock interaction parameter layer, and log-linear interpolation for Pco_2. Chemistry values are extrapolated for pH and ionic strength if Pco_2 is outside the range of 10^{-4} to 10^{-2} bar. Extrapolation of Pco_2 is valid over the range 10^{-5} to 2×10^{-2} bar (SNL 2007 [DIRS 177412], Section 7.2.2). For temperatures greater than 100°C and less than 30°C, values are taken from the 100°C or 30°C IDPS look-up tables, respectively (SNL 2007 [DIRS 177412], Section 6.15.1). If the relative humidity is greater than

the highest relative humidity value in the IDPS look-up tables, the TSPA-SEIS uses those pH and ionic strength values that are associated with the highest relative humidity in the applicable IDPS look-up table. If relative humidity is lower than the lowest relative humidity value in the IDPS look-up tables, the TSPA-SEIS uses the pH and ionic strength that are associated with the lowest relative humidity in the applicable look-up table (SNL 2007 [DIRS 177412], Section 6.15.1).

After the pH and ionic strength parameters are calculated, these quantities are adjusted for epistemic uncertainty and discretization error in accordance with the specific instructions provided in Section 6.12.3 of EBS P&CE (SNL 2007 [DIRS 177412]). The uncertainty for pH, ionic strength, $[Cl^-]$, $[NO_3^-]$, $[Cl^-]/[NO_3^-]$, is specified as a function of the relative humidity. Except for the pH in the highest relative humidity range, the distributions are triangular distributions. The uncertainty for the pH in the range 75 percent to 100 percent, the uncertainty is a discrete CDF.

Additional detail on the application of uncertainty to the calculated pH and ionic strength in the invert is provided in the PEFs associated with the uncertain parameters. Additional details on the EBS Chemical Environment Submodel calculations, including the application of uncertainty, are provided in the TSPA-SEIS's GoldSim model file.

The EBS Chemical Environment Submodel provides the following outputs for each percolation subregion and each representative WP and early-failed WP group in dripping and non-dripping environments:

- Time-dependent Pco_2 in the invert
- Time-dependent pH in the invert
- Time-dependent ionic strength in the invert.

6.3.4.3.2 Crown Seepage Chemistry

The EBS Chemical Environment Submodel is also used to calculate the time-dependent $[Cl^-]$, $[NO_3^-]$, $[Cl^-]/[NO_3^-]$, and pH of the seepage water contacting the WP surface in the event that a DS fails to divert flow around a WP. These chemical-environment variables are used to calculate LC on the WP outer surface. These determinations are made outside of the main TSPA-SEIS in an analysis developed exclusively for determining the potential for LC occurrence (identified as the LC Initiation Analysis (Section 6.3.5.2)).

The EBS Chemical Environment Submodel is used to calculate pH, $[Cl^-]$, and $[NO_3^-]$ in the crown seepage water in the LC Initiation Analysis. The inputs and calculations discussed in Section 6.3.4.3.1 for the invert chemistry calculations are equally suitable for determinations of the crown seepage chemistry used in the LC Initiation Analysis. However, the feeds for Pco_2, relative humidity, and temperature differ from the invert application. The crown seepage water application of the EBS Chemical Environment Submodel performs the same submodel calculations as the invert calculations using the same 396 chemical composition look-up tables, but it includes different feeds for the applicable Pco_2, temperature, and relative humidity. In the invert application of the EBS Chemical Environment Submodel, the applicable temperature and relative humidity is the representative invert temperature and invert relative humidity from the

EBS TH Environment Submodel (Section 6.3.2). The representative data set is defined in Section 6.3.2.2.1 as the TH response histories for each of the five repository subregions based on a single, representative WP for each fuel type. The LC Initiation Analysis (Section 6.3.5.2) uses the WP surface temperature and relative humidity along with the drift Pco_2 to evaluate conditions on the WP surface from the 396 chemical composition look-up tables.Similar to the seepage model, the LC Initiation Analysis evaluates WPs at each of the 3,264 subdomain locations from the MSTHM Process Model (SNL 2007 [DIRS 181383], Section 6.2.12[a]) as opposed to using representative packages for each subregion. When the chemical composition look-up tables are used, instead of accessing columns 1 and 2 for pH and ionic strength, the crown seepage calculations use the same look-up tables but they extract chemical information from column 1 for pH, column 3 for $[Cl^-]$, and column 4 for $[NO_3^-]$.

Global Calculations—The global calculations for the evaluation of crown seepage chemistry using the EBS Chemical Environment Submodel determine the applicable starting water and the water-rock interaction parameter time history. The implementation is identical to the previous discussion regarding invert calculations and is not being repeated.

Local Calculations—The local calculations of the EBS Chemical Environment Submodel determine the Pco_2 pH, $[Cl^-]$, and $[NO_3^-]$ of the crown seepage water. The extraction of chemical parameters from the 396 IDPS look-up tables is similar to that described for the invert water pH and ionic strength; however, WP surface values for temperature, Pco_2, and relative humidity are fed into the look-up table selections and subsequent calculations.

Section 6.12.3 in EBS P&CE (SNL 2007 [DIRS 177412]) discusses the addition of uncertainty to the EBS Chemical Environment Submodel calculations. The application of uncertainty for pH is analogous to the invert implementation. The treatment of $[Cl^-]$ and $[NO_3^-]$ uncertainty is significantly different from that previously discussed and requires further discussion.

The following steps should be taken to calculate the $[Cl^-]$, $[NO_3^-]$, $[Cl^-+NO_3^-]$ concentrations and $[Cl^-]/[NO_3^-]$ ratios. The EBS P&CE abstraction models (SNL 2007 [DIRS 177412], Section 6.12.3) use the molal concentrations of Cl and N to represent $[Cl^-]$ and $[NO_3^-]$ concentrations.

1. TSPA will choose a P&CE potential seepage water chemistry look-up table from among the 396 look-up tables using a randomly selected group water type (1 through 4); a WRIP value (0, 1, 2,...10); a pCO2 value of either 10^{-2}, 10^{-3}, 10^{-4}, bar; and a Twp = 30°C, 70°C, or 100°C. The Twp, and the independent variable, RHwp, are provided by the MSTHM (SNL 2007 [DIRS 181383], Appendix VIII[a]).

2. TSPA will evaluate for salt separation by comparing the relative humidity used to enter the look-up table selected in Step 1 to the salt separation relative humidity found in the group water salt separation tables. The relative humidity of salt separation is used directly from the salt separation look-up tables for all group waters.

   2.A. In the event of no salt separation:

   a. Take the [Cl+N] concentrations from the look-up tables.

b. Sample the [Cl+N] uncertainty using the appropriate relative humidity range from IDPS uncertainty table by applying a triangular distribution.

c. Calculate ([C+N] + uncertainty) (x) obtained in Steps 2a and 2b.

d. Sample ($[Cl^-]/[NO_3^-]$) (y) from discrete CDFs. Uncertainty due to using a single pore water to represent a group of waters (e.g., the effect of binning potential starting pore waters chemically) is incorporated into the model by sampling the $[Cl^-]/[NO_3^-]$ ratio (represented by Cl:N) for each starting water group from a discrete CDF for the starting water values.

e. Using x ([Cl+N] + uncertainty) and y (Cl:N) sampled from the CDFs to solve for $[Cl^-]$ and $[NO_3^-]$, the calculated values will include uncertainty.

2.B. In the event of salt separation:

a. Once salt separation has occurred, the Cl:N CDFs no longer apply and $[Cl^-]$, $[NO_3^-]$, $[Cl^-]/[NO_3^-]$, and pH are taken directly from the look-up tables selected in Step 1 above. These values are valid at any relative humidity below salt separation.

b. The model assumes that $[Cl^-]$ is proportional to [Cl:N], and thus the uncertainties will also be correlated. Once TSPA samples the uncertainty on $[Cl^-]$ using a triangular distribution with the end-points as shown in the IDPS uncertainty table, an offset of the same sign (either positive or negative) will be applied to the [Cl:N].

c. The look-up tables can continue to be used until the relative humidity rises in the drift, and exceeds the salt separation threshold. At that point, the look-up tables no longer apply and TSPA is instructed to assume that a Cl-rich brine can form. Because the process of salt-brine separation cannot be explicitly modeled, the P&CE report (SNL 2007 [DIRS 177412], Section 6.12.3) abstraction models do not attempt to provide the chemistry for the Cl-rich brines.

The PEFs associated with the uncertain parameters and the TSPA-SEIS's GoldSim file for the LC Initiation Analysis (Section 6.3.5.2) provide additional detail about the application of uncertainty to the calculated $[Cl^-]$, $[NO_3^-]$, $[Cl^-]/[NO_3^-]$, and pH for crown seepage waters, as well as the calculation of those values.

The crown seepage water pH, $[Cl^-]$, and $[NO_3^-]$ are used to assess the potential for LC on the WP outer barrier in the LC Initiation Analysis (Section 6.3.5.2).

6.3.4.4 Model Component Consistency and Conservatism in Assumptions and Parameters

To enhance understanding of the complex interactions within the TSPA-SEIS, a discussion of consistency among model components and submodels, and identification of conservative assumptions in abstractions, process models, and parameter sets supporting the EBS Chemical Environment Submodel is provided below.

6.3.4.4.1 Consistency of Assumptions

Seepage Water Compositions—In-Package Chemistry Abstraction does not use the EBS Chemical Environment crown seepage (EBS P&CE suite of models) as its starting waters (Section 6.3.7.2.1). In the In-Package Chemistry Abstraction, a liquid influx (dripping case or seepage dripping) model where water from the drift, simulated as typical groundwater, enters a WP at a rate determined by the seepage flow through the openings in the breached WP (SNL 2007 [DIRS 180506], Section 6.3).

Partial Pressure of CO_2—The In-Package Chemistry Abstraction uses the in-drift EBS Chemical Environment Submodel (Section 6.3.7.2.1) for Pco_2 in the WP. The in-drift Pco_2 is provided by Near Field Chemistry process model developed in the EBS P&CE Report (SNL 2007 [DIRS 177412]).

6.3.4.4.2 Identification of Conservatisms in Submodels and Abstractions

Mixing In the Invert—Water coming through a breached WP (i.e., reacted with the waste form and corrosion products) would be expected to be mixed in the invert with the waters diverted around the DS and WP and the waters already present in the invert that have equilibrated to the drift relative humidity. The TSPA-SEIS uses the in-package chemistry in the WP and the invert for WP that has advective releases. Mixing of waters would result in different buffer capacities for the EBS Chemical Environment.

pH buffering—The In-Package Chemistry Abstraction (Section 6.3.7.2.1) conceptual model is a batch reactor model that consists of water, oxygen, carbon dioxide, waste forms, and metal alloys. The InPackage Chemistry Abstraction considers the effects of mineral precipitation and WP internal materials as a buffer for the evolution of pH (SNL 2007 [DIRS 180506], Section 6.3). However, both the In-Package Chemistry Abstraction and the P&CE model do not consider the effects of surface complexation reactions as a potential pH buffer due to the presence of EBS components in the drift.

6.3.4.5 Alternative Conceptual Model(s) for Engineered Barrier System Chemical Environment

Section 6.2 outlines the general consideration and treatment of ACMs used to support the TSPA-SEIS. A brief description of an ACM for the EBS Physical and Chemical Environment is described below and in Table 6.3.4-5.

PTn Pore Water ACM—The EBS Physical and Chemical Environment Model uses pore water compositions from the TSw for the ambient conditions for the four starting waters (SNL 2007 [DIRS 177412], Section 6.6). The ACM selects ambient pore water from the overlying unit, the PTn, and then allows this water to seep up the geothermal gradient (from 23 to 96°C) downward through the TSw to the repository horizon (SNL 2007 [DIRS 177412], Section 6.11).

This ACM was not selected for use in the TSPA-SEIS because the analysis showed that use of the TSw pore water adequately captures the behavior of representative PTn pore waters. The use of PTn starting compositions does not significantly impact the key chemical components (pH, Pco_2, Ca, K, Si) of seepage (SNL 2007 [DIRS 177412], Section 6.11).

Closed System Model with Respect to CO_2—The IDPS Model (SNL 2007 [DIRS 177411], Section 6.5), which is a process model providing feeds to the EBS P&CE Model (SNL 2007 [DIRS 177412]) describes an ACM using a closed drift system with respect to CO_2. In a closed system, the volume ratio of air to water is so large that CO_2 degassing from, or dissolution into, seepage water in the drift will negligibly affect the CO_2 fugacity.

This ACM was not selected for use in the IDPS Model directly. However, the EBS P&CE Model incorporates the uncertainty of an open or closed system by using the maximum and minimum Pco_2 values in the abstraction for the TSPA-SEIS (SNL 2007 [DIRS 177412], Section 6.3.2.8 and Section 6.15.1). The minimum value assumes a completely open system and the maximum value assumes a completely closed system. The actual system is something between these two end members.

Table 6.3.4-1. Illustration of the Form of the Mean Water-Rock Interaction Parameter Table

Thermal Measure	Year	Percolation Rate 0.05231146	Percolation Rate 0.495274154
37.7552	50.1	3.77E-09	3.77E-09
37.7552	51	3.77E-08	3.77E-08
37.7552	52	7.55E-08	7.55E-08
37.7552	55	1.89E-07	1.89E-07
37.7552	60	3.79E-07	3.79E-07
37.7552	65	5.71E-07	5.71E-07
37.7552	70	7.64E-07	7.64E-07
37.7552	75	9.61E-07	9.61E-07
37.7552	80	1.16E-06	1.16E-06
37.7552	90	1.58E-06	1.58E-06
37.7552	100	2.01E-06	2.01E-06
37.7552	120	2.96E-06	2.96E-06
37.7552	140	3.98E-06	3.98E-06
37.7552	160	5.09E-06	5.09E-06
37.7552	180	6.27E-06	6.26E-06
37.7552	200	7.51E-06	7.50E-06
37.7552	220	8.80E-06	8.79E-06
37.7552	240	1.01E-05	1.01E-05
37.7552	260	1.15E-05	1.15E-05
37.7552	280	1.29E-05	1.29E-05
37.7552	300	1.44E-05	1.44E-05
37.7552	320	1.59E-05	1.59E-05
37.7552	340	1.74E-05	1.74E-05
37.7552	360	1.89E-05	1.89E-05
37.7552	380	2.05E-05	2.05E-05
37.7552	400	2.21E-05	2.21E-05
37.7552	420	2.37E-05	2.37E-05
37.7552	440	2.54E-05	2.54E-05
37.7552	460	2.70E-05	2.70E-05
37.7552	480	2.87E-05	2.87E-05
37.7552	500	3.04E-05	3.04E-05
37.7552	520	3.21E-05	3.21E-05

Table 6.3.4-1. Illustration of the Form of the Mean Water-Rock Interaction Parameter Table (Continued)

Thermal Measure	Year	Percolation Rate 0.05231146	Percolation Rate 0.495274154
37.7552	540	3.38E-05	3.38E-05
37.7552	560	3.56E-05	3.55E-05
37.7552	580	3.73E-05	3.72E-05
37.7552	600	3.90E-05	3.90E-05

Source: DTN: SN0703PAEBSPCE.006_R2 [DIRS 181571].

Table 6.3.4-2. Illustration of the Form of an In-Drift Precipitated Salts Look-up Table for Each Unique Set of Values of Carbon Dioxide Partial Pressure, Pco_2 and Temperature

Relative Humidity	pH log([H^+])	Ionic Strength molality	[Cl^-] molality	[NO_3^-] molality
0.999995	6.45	6.45	0.000041	0.000006
0.999994	6.64	6.64	0.000065	0.000010
0.999992	6.84	6.84	0.000102	0.000016
0.999989	7.04	7.04	0.000162	0.000026
0.999984	7.23	7.23	0.000256	0.000041
0.999977	7.42	7.42	0.000406	0.000065
0.999966	7.61	7.61	0.000643	0.000103
0.999948	7.79	7.79	0.001017	0.000163
0.999921	7.97	7.97	0.001607	0.000258
0.999898	8.06	8.06	0.002108	0.000340
0.999881	8.09	8.09	0.002368	0.000409
0.999822	8.18	8.18	0.003312	0.000649
0.99982	8.18	8.18	0.003361	0.000661
0.999816	8.18	8.18	0.003412	0.000673
0.999814	8.19	8.19	0.003455	0.000683
0.999813	8.19	8.19	0.003464	0.000686
0.9998111	8.19	8.19	0.003505	0.000696
0.999811	8.19	8.19	0.003515	0.000699
0.999809	8.20	8.20	0.003568	0.000713
0.999807	8.20	8.20	0.003622	0.000727
0.999805	8.21	8.21	0.003680	0.000742
0.999803	8.21	8.21	0.003740	0.000758
0.999801	8.22	8.22	0.003802	0.000774
0.999799	8.23	8.23	0.003868	0.000791
0.999796	8.23	8.23	0.003938	0.000809
0.999794	8.24	8.24	0.004011	0.000828
0.999792	8.25	8.25	0.004087	0.000847
0.999789	8.25	8.25	0.004168	0.000868
0.999786	8.26	8.26	0.004253	0.000889
0.999784	8.27	8.27	0.004329	0.000908
0.99978	8.28	0.004439	0.000935	0.000372
0.999777	8.29	0.004540	0.000960	0.000382
0.999773	8.29	0.004647	0.000986	0.000392
0.99977	8.30	0.004760	0.001014	0.000403
0.999766	8.31	0.004881	0.001044	0.000415

Table 6.3.4-2. Illustration of the Form of an In-Drift Precipitated Salts Look-up Table for Each Unique Set of Values of Carbon Dioxide Partial Pressure, Pco_2 and Temperature (Continued)

Relative Humidity	pH	Ionic Strength	$[Cl^-]$	$[NO_3^-]$
	log($[H^+]$)	molality	molality	molality
0.999762	8.32	0.005010	0.001075	0.000427
0.999757	8.33	0.005147	0.001108	0.000441
0.999753	8.34	0.005294	0.001143	0.000455
0.999748	8.35	0.005451	0.001180	0.000469
0.999742	8.37	0.005620	0.001220	0.000485
0.999737	8.38	0.005801	0.001263	0.000502
0.999731	8.39	0.005997	0.001309	0.000521
0.999724	8.40	0.006208	0.001358	0.000540
0.999717	8.42	0.006437	0.001412	0.000562
0.999709	8.43	0.006685	0.001469	0.000584
0.999701	8.45	0.006956	0.001532	0.000609
0.999692	8.46	0.007252	0.001600	0.000636
0.999682	8.48	0.007577	0.001674	0.000666
0.999671	8.50	0.007935	0.001756	0.000698
0.999659	8.52	0.008332	0.001846	0.000734
0.999646	8.53	0.008772	0.001946	0.000774
0.999631	8.56	0.009265	0.002057	0.000818
0.999614	8.58	0.009820	0.002181	0.000868
0.999595	8.60	0.010449	0.002322	0.000924
0.999574	8.63	0.011166	0.002482	0.000987
0.99955	8.65	0.011993	0.002666	0.001060
0.999522	8.68	0.012956	0.002879	0.001145

Source: This table is an example modified from DTN: SN0701PAEBSPCE.001_R1 [DIRS 180523].

NOTE: The table entries for relative humidity, $[Cl^-]$, $[NO_3^-]$, pH, and ionic strength have been rounded for display purposes and are based upon the seepage evaporation look-up table for Starting Water 1, $Pco_2 = 0.01$ bar, and T = 70°C.

For TSPA-SEIS use, the tabulated values displayed here are not used; the values are taken directly from DTN: SN0701PAEBSPCE.001_R1 [DIRS 180523]. Also, the table in the DTN has more lines than shown here, ending at an RH value of 0.500002.

Table 6.3.4-3. Illustration of Estimated Model Uncertainty Ranges for In-Drift Precipitated Salts Submodel Outputs of pH and Ionic Strength

Parameter	Units	Relative Humidity				
		Range 100% - 85%	Range 85% - 65%	Range 65% - 40%	Range 40% - 20%	Range 20% - 0%
I	log molal	+/- 0.1	0	0	0	0
Cl	log molal	+/- 0.0	+/- 0.1	+/- 0.4	+/- 0.5	+/- 0.7
N	log molal	+/- 0.0	+/- 0.2	+/- 0.4	+/- 0.5	+/- 0.9
$Cl:NO_3$	log mole ratio (unit less)	+/- 0.0	+/- 0.2	+/- 0.5	+/- 0.5	+/- 1.4
Cl+N	log molal	+/- 0.0	+/- 0.22	+/- 0.57	NA	NA
		Range 100% - 75%	Range 75% - 65%	Range 65% - 00%		
pH	pH units	[a]See table	+/- 1	+/-2		

Sources: Modified from DTN: SN0703PAEBSPCE.007_R1 [DIRS 180177].
Ionic strength uncertainty below 85 percent relative humidity is zero (SNL 2007 [DIRS 177412], Table 6.12-1).

NOTE: These uncertainties are defined as triangular distributions.

[a] Table in the pH row refers to a table of pH uncertainty values contained within the DTN.

Table 6.3.4-4. Summary of Chemistry for Seepage and Condensation in the TSPA-SEIS

	Seepage		No Seepage	
	Drift-Wall Condensation	**No Drift-Wall Condensation**	**Drift-Wall Condensation**	**No Drift-Wall Condensation**
Seismic/Nominal				
WP Outer Barrier; DS Intact	Dry air or humidity environment only.	Dry air or humidity environment only.	Dry air or humidity environment only.	Dry air or humidity environment only.
WP Outer Barrier; DS Failed	Use seepage composition equilibrated to T, RH, Pco_2 of WP outer barrier.	Use seepage composition equilibrated to T, RH, Pco_2 of WP outer barrier.	Use seepage composition equilibrated to T, RH, Pco_2 of WP outer barrier.	Dry air or humidity environment only.
IPC; DS Intact (WP Failed)	$[F^-]$=0; use chemistry for non-dripping case.	$[F^-]$=0; use chemistry for non-dripping case.	$[F^-]$=0; use chemistry for non-dripping case.	$[F^-]$=0; use chemistry for non-dripping case.
IPC; DS Failed (WP Failed)	$[F^-] \leq$Fmax; use chemistry for seepage case if $Q_4 \geq 0.1$ L/yr; otherwise non-dripping chemistry.	$[F^-] \leq$Fmax; use chemistry for seepage case if $Q_4 \geq 0.1$ L/yr; otherwise non-dripping chemistry.	F^-=0; use chemistry for seepage case if $Q_4 \geq 0.1$ L/yr; otherwise non-dripping chemistry.	$[F^-]$=0; use chemistry for non-dripping case.
Invert; DS Intact (WP Failed)	Use seepage composition equilibrated to T, RH, Pco_2 of invert.	Use seepage composition equilibrated to T, RH, Pco_2 of invert.	Use seepage composition equilibrated to T, RH, Pco_2 of invert.	Use seepage composition equilibrated to T, RH, Pco_2 of invert.
Invert; DS Failed (WP Failed)	Use In-package chemistry (seepage-based) to represent advective transport.	Use In-package chemistry (seepage-based) to represent advective transport.	Use In-package chemistry (seepage-based) to represent advective transport.	Use seepage composition equilibrated to T, RH, Pco_2 of invert.
Igneous Intrusion				
IPC; DS Failed (WP Failed)		Use basalt water without modification for environment; choose from alternatives in In-package chemistry documentation.		
Invert; DS Failed (WP Failed)		Use In-package chemistry selected above.		

Source: (SNL 2007 [DIRS 177412], Table 6.15-1)

Table 6.3.4-5. Alternative Conceptual Models Considered for EBS Physical and Chemical Environment

Alternative Conceptual Models	Key Assumptions	Assessment and Basis
PTn Pore Water ACM	PTn pore water is used for the starting composition for the water that travels up the geothermal gradient downward through the TSw to the repository horizon (SNL 2007 [DIRS 177412], Section 6.11).	Not recommended for TSPA. Using PTn starting water compositions does not significantly impact the key chemical components (pH, Pco_2, Ca, K, Si) of seepage (SNL 2007 [DIRS 177412], Section 6.11). Using TSw starting waters adequately captures the behavior and uncertainty of the PTn pore water.
Closed System Model with Respect to CO_2	Carbonate exchange with the gas phase via CO_2 degassing or dissolution results in a corresponding increase or decrease of CO_2 in the gas phase (SNL 2007 [DIRS 177411], Section 6.5).	A closed system with respect to CO_2 is not implemented in the IDPS model because the expected volume ratio of air to water in the drift is so large that CO_2 degassing from, or dissolution into, seepage water in the drift will negligibly affect the CO_2 fugacity compared to the uncertainty in the input value for CO_2 fugacity. A closed system might be appropriate in a wetter climate; however, RH would be ~100% and little or no evaporation would occur. To address this issue further, the IDPS model is used to quantify the output uncertainty resulting from the uncertainty in CO_2 fugacity in the P&CE Model (SNL 2007 [DIRS 177412], Section 6.3.2.8 and Section 6.15.1).

INTENTIONALLY LEFT BLANK

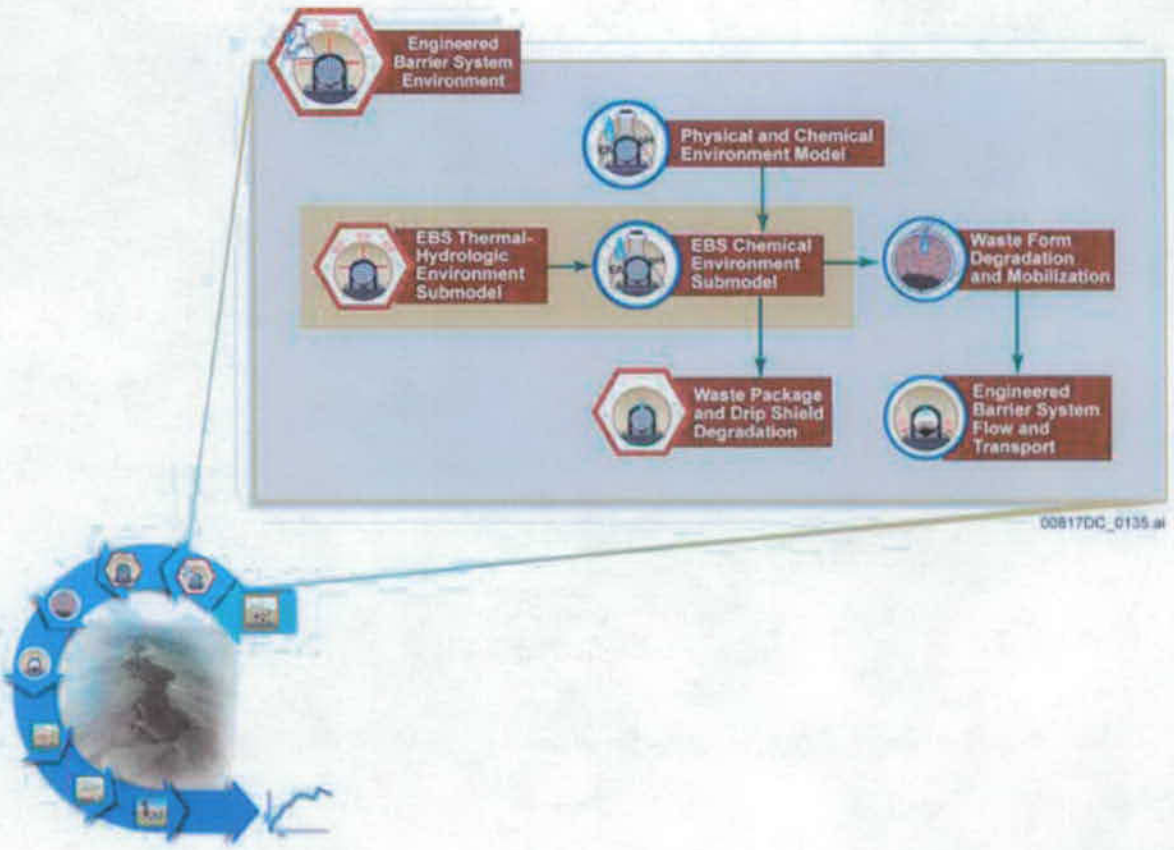

Figure 6.3.4-1. Information Flow Diagram for the EBS Chemical Environment Submodel

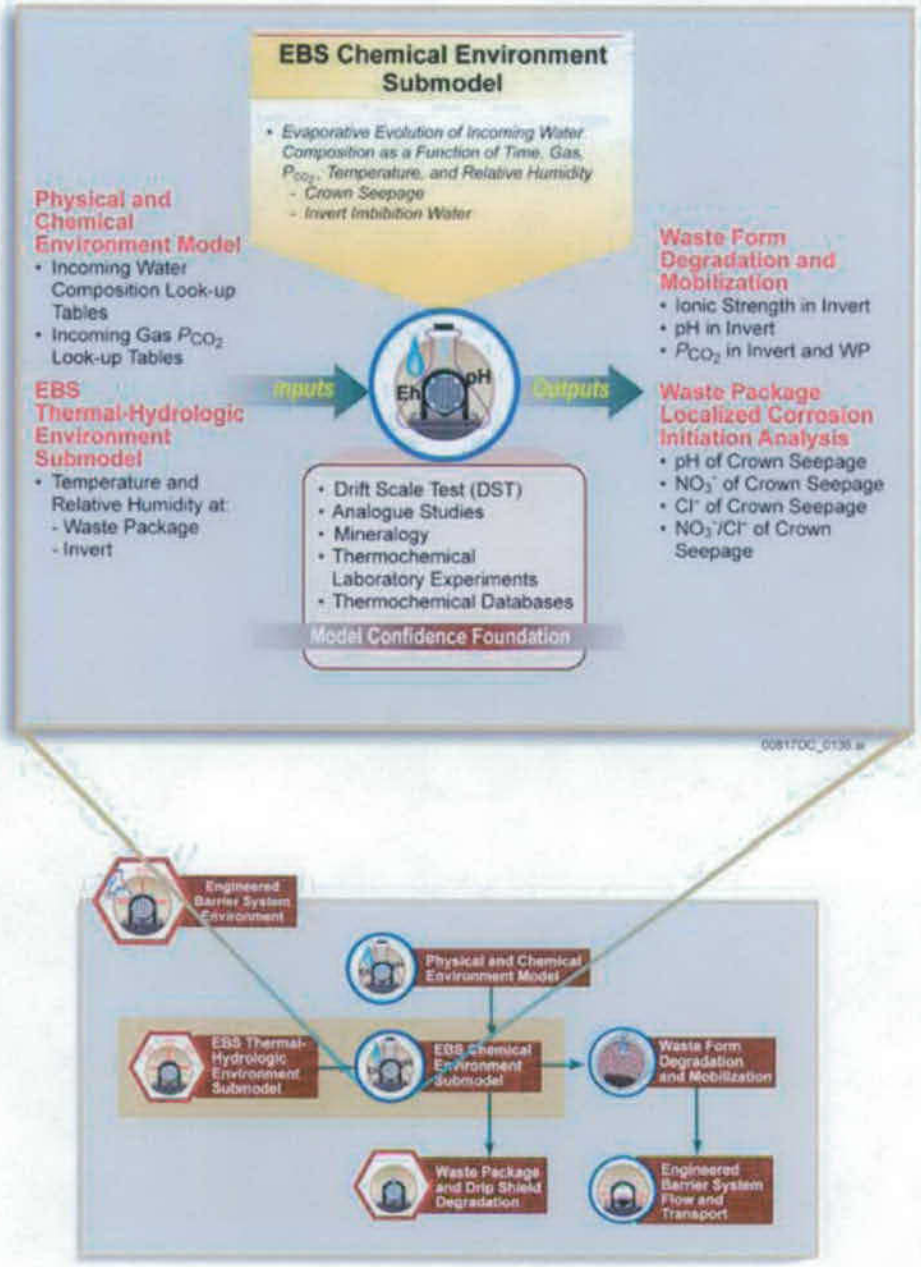

Figure 6.3.4-2. Inputs, Outputs, and Basis for Model Confidence for the EBS Chemical Environment Submodel

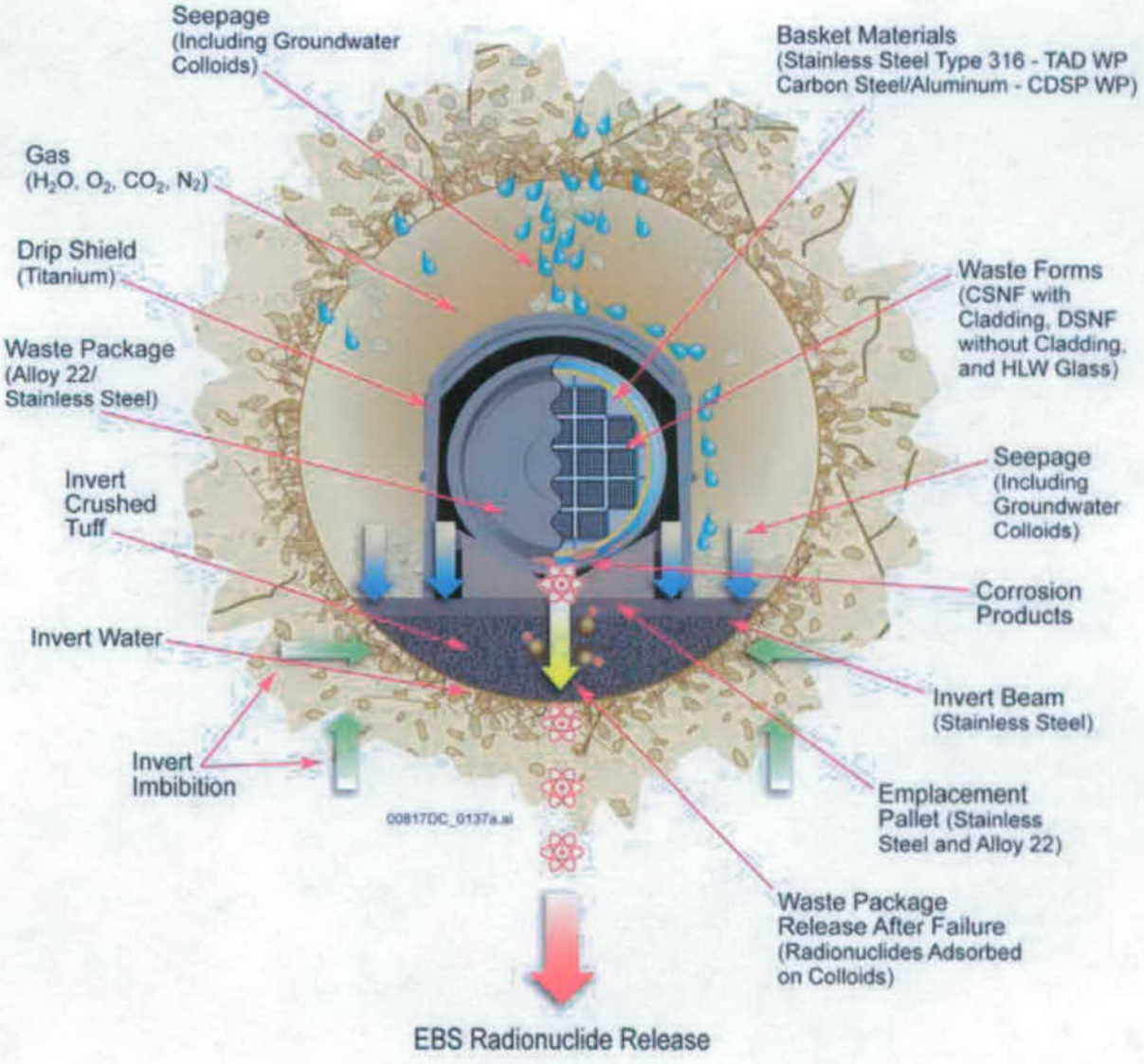

Figure 6.3.4-3. General EBS Design Features and Materials, Water Movement, and Drift Degradation

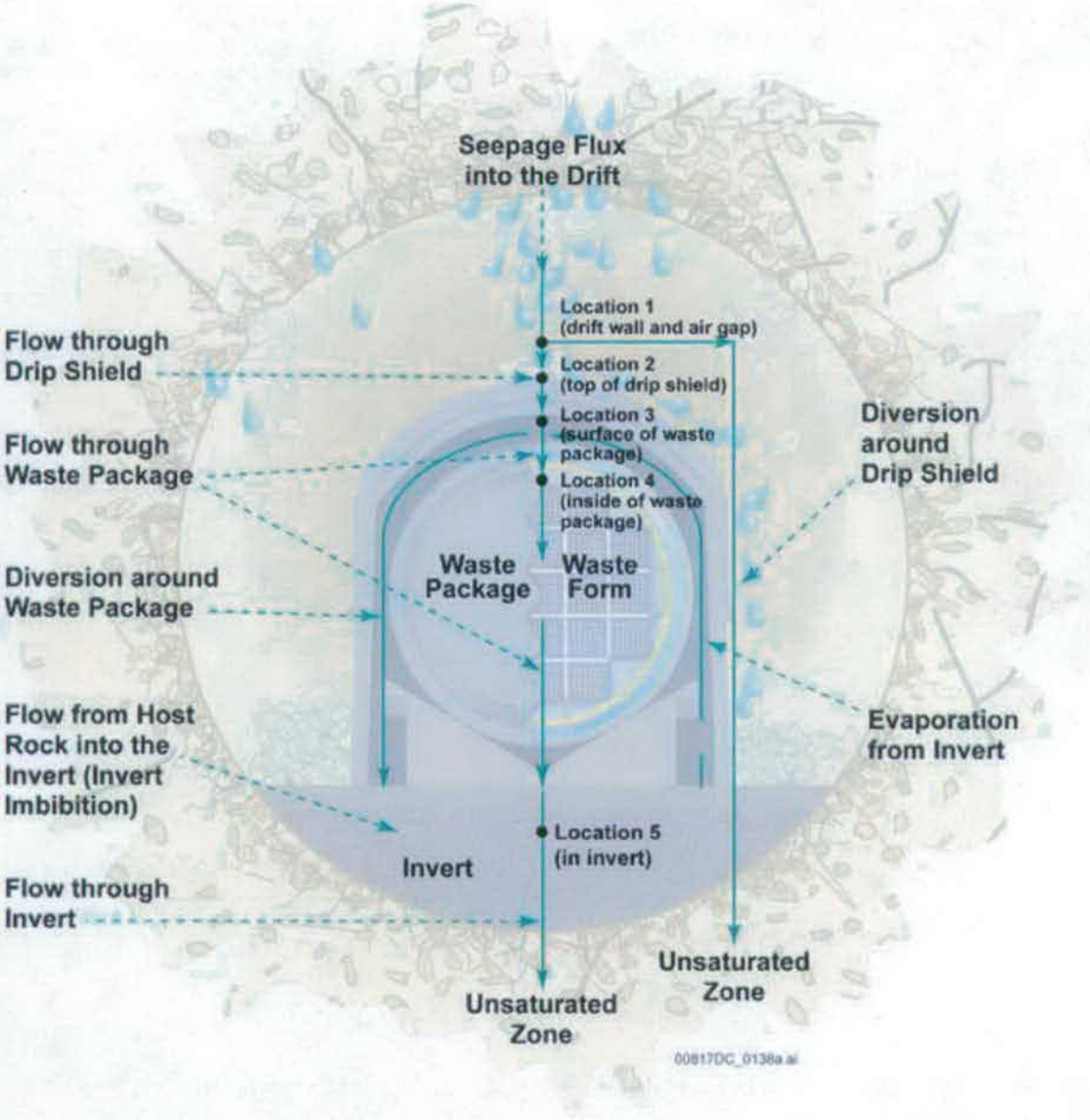

Figure 6.3.4-4. Schematic Diagram of EBS Flow Pathways (arrows) and Critical Locations (labels)

6.3.5 Waste Package and Drip Shield Degradation

The WPs and DSs are important components of the EBS. Figure 6.3.5-1 is a schematic illustration of the design features of the WPs and DSs. The two primary design functions of the DSs are to prevent seepage water from dripping directly on the WPs and to provide protection from rockfall damage to the WPs. The primary design functions of the WPs are to isolate the waste from the repository environment until the WPs fail and, after WP failure, to limit and delay the release of radionuclides to the EBS. The TSPA-SEIS for DS and WP degradation includes five degradation modes: general corrosion, microbially influenced corrosion (MIC), stress corrosion cracking (SCC), localized corrosion, and early failure of WPs and DSs. These degradation modes and their abstraction models are described in *General Corrosion and Localized Corrosion of the Drip Shield* (SNL 2007 [DIRS 180778], Section 6.1[a]); *General Corrosion and Localized Corrosion of Waste Package Outer Barrier* (SNL 2007 [DIRS 178519], Sections 6.4.3, 6.4.4, and 6.4.5); *Stress Corrosion Cracking of Waste Package Outer Barrier and Drip Shield Materials* (SNL 2007 [DIRS 181953], Section 6); and *Analysis of Mechanisms for Early Waste Package/Drip Shield Failure* (SNL 2007 [DIRS 178765], Section 6). The first three WP and DS degradation modes and the early failure degradation modes are modeled within the TSPA-SEIS. The early failure degradation modes are documented in two places. WP early failure resulting from weld flaws is documented in this section, but the remaining WP and DS early failure degradation modes are documented in Section 6.4. The implementation of the localized corrosion degradation mode is summarized in the next paragraph. The relationships between the WP and DS Degradation Model Component and other TSPA-SEIS components and submodels are illustrated on Figure 6.3.5-2. The primary submodel supplying input to the WP and DS Degradation Model Component is the EBS TH Environment Submodel (Section 6.3.2), which provides exposure conditions (i.e., temperature and relative humidity) on WP outer surfaces. Output from the WP and DS Degradation Model Component is provided to the Waste Form Degradation and Mobilization Model Component and the EBS Flow and EBS Transport Submodels in the form of time-dependent tabulations of the fraction of WPs and DSs failed and the average breached area per failed WP and DS. Figure 6.3.5-3 summarizes the issues considered in the formulation of the WP and DS Degradation Model Component and its inputs and outputs.

TSPA-SEIS implementation of localized corrosion is accomplished by exercising several interfaced TSPA-SEIS components and submodels in combination with the Localized Corrosion Initiation Abstraction in a probabilistic framework external to the TSPA-SEIS. A stand-alone analysis is used to compute time-dependent brine chemical composition and corrosion potential on WP outer surfaces. Outputs of the stand-alone analysis are time-dependent tabulations that specify the fraction of WPs that fail due to localized corrosion as a function of time. These WP fractional failure histories are imported into the TSPA-SEIS and used in the determination of WP degradation modes. The TSPA-SEIS implementation of localized corrosion is described in detail in Section 6.3.5.2.3.

The remainder of Section 6.3.5 is summarized as follows: Section 6.3.5.1 describes the WP and DS degradation conceptual models. The inclusion or exclusion of potentially important degradation mechanisms is outlined in Section 6.3.5.1.1. These include general corrosion, MIC, and SCC. Manufacturing and material defects that result in WP early failures are also included. Section 6.3.5.1.2 contains the abstraction models corresponding to these conceptual models.

Section 6.3.5.1.3 describes their implementation in the TSPA-SEIS. Section 6.3.5.2 focuses on the localized corrosion abstraction for the WP outer surface. This section describes how localized corrosion initiation is evaluated on the WP outer surface and how the results of this analysis are incorporated into the TSPA-SEIS. Section 6.3.5.3 discusses differences in assumptions and parameter sets that have arisen in the development of the supporting information for the TSPA-SEIS. Section 6.3.5.4 outlines ACMs used to build confidence in the base-case model and ensure that the base-case model adequately captures the range of conceptual model uncertainty.

6.3.5.1 Waste Package and Drip Shield Degradation

DSs will be installed over the WPs just prior to repository closure. DSs will be made of Titanium Grade 7 plates with Titanium Grade 29 stiffeners and support beams to provide both corrosion resistance and structural strength. The DS plates will be at least 15 mm thick (SNL 2007 [DIRS179354], Table 4-2). As long as they remain substantially intact, the DSs will divert water that seeps into the drift away from the WPs and preclude damage to WPs resulting from rockfall. Because titanium is highly corrosion resistant, initial breaches of the DSs will not occur under nominal conditions until approximately 230,000 years postclosure (Section 6.3.5.1.3). However, a stand alone analysis has shown that DSs can fail as early as 40,000 years when subject to seismic ground motion and the resulting rockfall.

WPs will prevent contact between water and waste as long as they are not breached, and will limit water flow and radionuclide migration even after the WPs are breached. The WPs have a dual-metal design consisting of an inner vessel and a waste package outer barrier. The inner vessel is composed of a 50-mm-thick layer of modified 316-stainless steel. The waste package outer barrier is a 25-mm-thick layer of Alloy 22, a corrosion-resistant nickel-based alloy (SNL 2007 [DIRS179394], Table 4-1). Alloy 22 protects the modified 316 stainless steel inner vessel from corrosion, and the modified 316 stainless steel inner vessel provides additional structural support for the thinner Alloy 22 waste package outer barrier. The potential corrosion performance of the modified 316 stainless steel inner vessel is far less than that of the more corrosion-resistant Alloy 22 WP outer barrier. For this reason, the corrosion performance of the WP inner vessel is conservatively ignored in this report. The WP outer barrier has a single Alloy 22 closure lid. The WP closure lid is welded to the WP outer barrier after the waste form (SNF or HLW glass, or both) is loaded.

6.3.5.1.1 Conceptual Model

The DSs and WPs are expected to be subject to many potential degradation mechanisms during the first 10,000 years after repository closure. Several of these degradation mechanisms were determined as ineffective under repository-relevant exposure conditions. The inclusion or exclusion of potentially important degradation mechanisms in the TSPA-SEIS is summarized in Table 6.3.5-1 and described as follows:

- General corrosion is a relatively uniform thinning of materials that occurs at all times. This degradation process is included in the TSPA-SEIS as a degradation mechanism for both the DSs and WPs. The conceptual models and abstractions are discussed in *General Corrosion and Localized Corrosion of the Drip Shield* (SNL 2007

[DIRS 180778], Section 6.1[a]) and *General Corrosion and Localized Corrosion of Waste Package Outer Barrier* (SNL 2007 [DIRS 178519], Section 6.4.3).

- Localized corrosion (pitting, crevice corrosion) is a phenomenon in which corrosion progresses at discrete sites or in a non-uniform manner.

  – Localized corrosion is excluded from the TSPA-SEIS as a DS degradation mechanism.

  – Localized corrosion is included as a WP degradation mechanism. Crevice corrosion is used to represent localized corrosion for the WP under the exposure conditions expected in the repository environment. This is a conservative and bounding assumption, as the initiation threshold for crevice corrosion in terms of exposure conditions is lower than for pitting corrosion (SNL 2007 [DIRS 178519], Section 6.4.4).

- SCC is a crack propagation process caused by the combined interaction of mechanical stress and corrosion reactions acting on a susceptible material. Possible sources of mechanical stress include weld-induced-residual stresses, plasticity-induced-residual stresses caused by seismic events, and residual stresses produced by rockfall, and sustained rock rubble loading.

  – SCC is included in the TSPA-SEIS as a DS degradation mechanism. After fabrication, the DSs are heat treated for stress relief at 1,100 F +/- 50 degrees F for a minimum of 2 hours (SNL 2007 [DIRS 179354], Table 4-2); therefore, DS weld-induced-residual stresses are not present and do not lead to SCC initiation. Seismic effects are discussed in Section 6.6.1.1 Changes in mechanical properties due to SCC are not included in the Seismic Scenario Class. In the Nominal Scenario Class, the only sources of mechanical stress in the DSs are loading due to rockfall and rock rubble loading. Although SCC of the DS due to rockfall and rock rubble loading may occur, the effective water flow rate through stress corrosion cracks in the DSs is expected to be very low and have a negligible contribution to the radionuclide release rate from the repository. Advective flow through cracks in the DS has been excluded. Therefore, SCC of the DSs has not been implemented in the TSPA-SEIS.

  – SCC is included as a WP degradation mechanism. Because the waste container is fully-annealed prior to being loaded with the waste form, the majority of the waste package will not have appreciable residual tensile stresses upon emplacement and will not be subject to SCC. The outer barrier closure lid weld region cannot be fully annealed and is stress-mitigated (by low plasticity burnishing) to produce a layer of compressive stress (SNL 2007 [DIRS 179394], Section 4.1.2.3; SNL 2007 [DIRS 179567], Section 4.1.1.3) that prevents SCC initiation until general corrosion removes this layer (SNL 2007 [DIRS 181953], Section 8.4.2.1). Because fully annealed WPs will not contain tensile stresses, they will not be subject to SCC. The WP outer surface is protected from rockfall by the presence of the DSs. Therefore, in the Nominal Scenario Class, SCC is considered only for the closure-lid welds. The number and size of weld flaws due to manufacturing defects is calculated in *Analysis*

of Mechanisms for Early Waste Package/Drip Shield Failure (SNL 2007 [DIRS 178765], Section 6.3.1). Distributions for weld flaw number and size are incorporated into the WP SCC Abstraction. Weld flaws are not part of the Waste Package Early Failure (EF) Modeling Case discussed in Section 6.4. Sections 6.4 and 6.5 of *Stress Corrosion Cracking of Waste Package Outer Barrier and Drip Shield Materials* (SNL 2007 [DIRS 181953]) discuss the modeling approach used to assess the degradation of the WP outer barrier due to SCC.

- MIC is caused by the activity of microorganisms. Microorganisms can affect the corrosion of an alloy either by acting directly on the metal or through their metabolic products. MIC is documented in Sections 6.7.2 and 6.4[a] of *General Corrosion and Localized Corrosion of the Drip Shield* (SNL 2007 [DIRS 180778]) and in Section 8.2 of *General Corrosion and Localized Corrosion of Waste Package Outer Barrier* (SNL 2007 [DIRS 178519]).
  - MIC is excluded from the TSPA-SEIS as a DS degradation mechanism.
  - MIC is included as a WP degradation mechanism as a multiplier to the general corrosion rate.
- Thermal aging and phase instability caused by prolonged exposure to elevated temperature environments can lead to microstructural changes of WP and DS materials, which could change their corrosion behavior. This process is excluded from the TSPA-SEIS as a DS degradation mechanism and as a WP degradation mechanism.
- Hydrogen-induced cracking is caused by the migration of atomic hydrogen into the metal and subsequent formation of metal hydrides. This process can cause metals to be more brittle and susceptible to cracking. This process is excluded from the TSPA-SEIS as a DS degradation mechanism and as a WP degradation mechanism.
- Mechanical damage due to dynamic loading conditions can damage WPs and DSs.
- Mechanical damage is excluded as either a DS or WP degradation mechanism in the Nominal Scenario Class.
- Seismic-induced rockfall is included as a degradation mechanism for both DSs and WPs in the Seismic Scenario Class. The Seismic Scenario Class conceptual model and TSPA-SEIS implementation are discussed in Section 6.6.
- Radiolysis can result in the generation of hydrogen peroxide and changes in chemical conditions leading to enhanced corrosion. This process is excluded as a degradation mechanism for both DSs and WPs.

Igneous-induced DS and WP degradation is also included. The impact of igneous events on DS and WP performance is summarized in Section 6.5 of this report.

Seismic-induced DS and WP degradation is described in *Seismic Consequence Abstraction* (SNL 2007 [DIRS 176828]) and summarized in Section 6.6 of this report.

6.3.5.1.2 Abstraction of Waste Package and Drip Shield Degradation

The WP and DS degradation processes included in the TSPA-SEIS are incorporated into the WP and DS Degradation Model Submodel, as documented in this section. The direct output from the WP and DS Degradation Submodel is a set of histories for WP and DS failure and the subsequent number of breaches in failed WPs and DSs, as a function of time. The WP and DS Degradation Submodel includes the DS General Corrosion Abstraction for DS degradation, the WP General Corrosion Abstraction, the WP MIC Abstraction, and the WP SCC Abstraction for WP degradation. The WP and DS Degradation Submodel also includes the abstraction for closure-lid weld flaws due to manufacturing defects. The primary submodel supplying input to the WP and DS Degradation Model Component is the EBS TH Environment Submodel (Section 6.3.2). The EBS TH Environment Submodel provides temperature and relative humidity histories. The WP and DS degradation mechanisms modeled by the WP and DS Degradation Submodel (general corrosion, SCC, and MIC) are not chemistry-dependent. The WP general corrosion rate is a function of the temperature on the WP surface, while DS corrosion rates are independent of temperature.

DS Performance—General corrosion is the only DS degradation mechanism modeled in the WP and DS Degradation Submodel. This process is modeled as being independent of temperature and relative humidity, and is initiated at the time of repository closure. General corrosion is modeled separately for the outer and inner surfaces of the DSs, each with a different general corrosion rate. The major difference between the inner and outer surfaces of the DSs is that the outer surfaces may be exposed to a more complex chemical environment because dust and/or seepage may reside on or contact the outer surfaces of the DSs. The inner surfaces are not expected to be exposed to seepage water.

The general corrosion models for the topside and underside surfaces of the DSs were developed based on corrosion rates determined from the weight-loss measurements of the Titanium Grade 7 coupons after a 2.5-year exposure to at the Long-Term Corrosion Testing Facility (LTCTF) at Lawrence Livermore National Laboratory. The resulting weight-loss data set was divided into three groups with distinctively different rate distributions, namely, Aggressive Condition, Intermediate Condition, and Benign Condition. The data subsets for two bounding conditions (Aggressive Condition and Benign Condition) were used for the model development and analysis (SNL 2007 [DIRS 180778], Section 6.1[a]). The data points termed aggressive were obtained from solutions of simulated concentrated water, considered to be representative of the evolution of groundwater compositions relevant to the repository environment.

The topsides of DSs in seeping environments in the repository are considered to be subject to the potentially aggressive conditions represented by the simulated concentrated water data. A normal probability model was fit to the aggressive condition data. The resulting normal probability model represents the variability in the DS general corrosion rates for the defined aggressive conditions. Because of the small number of data points used for the model fitting, the corrosion model for aggressive condition is considered uncertain. The uncertainty of the normal probability model was developed by assuming that the mean of the normal probability model is

uncertain. The Student's t-distribution was used to characterize the uncertainty in the mean of the fitted normal probability model. The undersides of all DSs are considered to be subject to benign conditions at all times. A Gamma probability model was fit to the benign condition data. The Gamma probability model represents the variability in the DS general corrosion rates for the benign conditions. The uncertainty of the Gamma probability model was developed by assuming the mean of the probability model is uncertain and the variance constant. A normal probability distribution was developed to characterize this uncertainty in the mean of the fitted gamma probability model.

Although there is acknowledged variability in the DS general corrosion processes, it not considered in the TSPA-SEIS implementation. It was not possible to include variability because there was no analysis in *General Corrosion and Localized Corrosion of the Drip Shield* (SNL 2007 [DIRS 180778]) of the relationship between the general corrosion rates at any particular position on a single DS, between the general corrosion rates on different DSs, or the effect of the chemical environment for each realization. Only the uncertain Student's t-distribution for aggressive conditions and the uncertain normal distribution for benign conditions were used to model general corrosion on the topsides and undersides, respectively, of the DSs.

WP Performance—WP performance is modeled in the TSPA-SEIS by the WP and DS Degradation Model Component using two submodels. The first submodel, the WP and DS Degradation Submodel, includes general corrosion, MIC, and SCC. The second submodel, the WP Localized Corrosion Initiation and Propagation Submodel, models the initiation and propagation of localized corrosion.

Two WP configurations are analyzed in the TSPA-SEIS file. The first WP configuration is referred to as the CSNF WP configuration for which the TAD canister configuration parameters are used. The second WP configuration analyzed is the CDSP WP configuration for which the 5 HLW/1 DOE SNF Long WP configuration parameters are used.

The WP surfaces are analyzed as being composed of sub-areas referred to as patches in order to represent spatial variation in degradation processes across the WP surfaces. The general corrosion, MIC, and SCC degradation mechanisms are modeled at the patch level on WPs, as shown on Figure 6.3.5-4, with each patch having, in general, a different general corrosion rate or SCC response. Figure 6.3.5-5 illustrates general corrosion processes for both dripping and non-dripping environments and degradation on the surfaces of both the DSs and the WPs. The patches located in the last annulus shown on the WP on Figure 6.3.5-4 represent the closure-lid weld region, and SCC is modeled only on these closure-lid patches.

The general corrosion model used for the WP is based on weight-loss measurements for samples exposed in the LTCTF (SNL 2007 [DIRS 178519], Section 6.4.3). For the WP outer barrier, samples with the crevice geometry were used to generate the general corrosion rate distribution (applied at 60°C). The crevice geometry samples have nominal dimensions of 2 in. × 2 in. × 1/8 in. and a 0.312-in. diameter hole in the center for sample mounting (SNL 2007 [DIRS 178519], Section 6.4.3). Therefore, the exposed surface area, A, for a crevice geometry sample is calculated as follows:

$$A = 2ab + 2bc + 2ac - \left(\frac{\pi d^2}{2}\right) + \pi dc \qquad \text{(Eq. 6.3.5-1)}$$

where a is the length of the specimen, b is the width of the specimen, c is the thickness of the specimen, and d is the diameter of hole. Using the dimensions above, the exposed surface area for a crevice sample (converted to mm^2) is 5,787 mm^2. The general corrosion analysis performed by the WAPDEG 4.07 software is limited to a maximum of 1,500 patches. Therefore, the TSPA-SEIS analysis uses a patch size of about four times of the crevice coupon area, 23,150 mm^2.

The surface areas of the CSNF and CDSP WPs are taken to be the values used in the EBS Radionuclide Transport Abstraction for the maximum diffusive area of corrosion products, for the path through the outer barrier. The number of patches used for calculation purposes can be derived by dividing the CSNF and CDSP surface areas by the patch area giving 1,430 patches for CSNF WPs and 1,408 patches for CDSP WP. The general corrosion rate distribution applied to the WP outer barrier is modified to reflect this change in scale between the smaller crevice geometry sample size and the patch size.

For modeling purposes, the WP outer barrier is composed of two different regions; the closure-lid weld region and the shell region. The closure-lid weld region is represented as an annulus, one-patch side wide and with the same radius as the WP (Figure 6.3.5-1). Making the reasonable analysis assumption that the patches are square, the length of one side of a patch is then about 152 mm. The fraction of area represented by the closure-lid weld region for CSNF WPs is given by:

$$\frac{\text{Closure–Lid Weld Region Area}}{\text{WP Surface Area}} = \frac{\pi(diameter)(152)mm^2}{\pi(diameter)(5691)mm^2} \approx 0.0267 \qquad \text{(Eq. 6.3.5-2)}$$

or about 38 patches. For CDSP WPs the fraction of area represented by the closure weld region is:

$$\frac{\text{Closure–Lid Weld Region Area}}{\text{WP Surface Area}} = \frac{\pi(diameter)(152)mm^2}{\pi(diameter)(5145)mm^2} \approx 0.0295 \qquad \text{(Eq. 6.3.5-3)}$$

or about 42 patches.

The CSNF and CDSP WP lengths are 5691 mm and 5145 mm, respectively.

Note that the surface area of the closure lids themselves was not considered to be part of the WP surface area. Because the WP surface area is used primarily to determine the fraction of WP surface area subjected to SCC, it is conservative and appropriate to ignore the closure lid surface area in determining the total WP surface area.

Analyses presented in *Stress Corrosion Cracking of Waste Package Outer Barrier and Drip Shield Materials* (SNL 2007 [DIRS 181953], Section 6.6.1), indicate the distance between two neighboring cracks must be greater than the plate thickness for the stress (and stress intensity

factor) profile to be of sufficient magnitude to propagate a crack through-wall. Therefore, for the WP outer barrier outer closure-lid (which is 25-mm-thick) and again making the analysis assumption that the patches are square (side length about 152 mm), about six cracks per patch are able to propagate through-wall.

Modeling degradation mechanisms at the patch level permits a representation of spatial variability in the degradation on the WP surfaces. Every WP in a simulation is assigned different exposure conditions and will, therefore, corrode at a different rate. This variation represents WP-to-WP aleatory uncertainty.

The WP and DS Degradation Submodel also considers general corrosion degradation of the WP inner surfaces, or inside-out corrosion. Inside-out general corrosion can only begin after WP failure. Note that inside-out SCC is not modeled because it would be of negligible consequence to WP performance, either because the WP would have already been breached by the much larger patch penetrations due to general corrosion, or because the patches susceptible to SCC would have already been breached by SCC, thus reducing or eliminating the state of stress.

General Corrosion and MIC—The WP General Corrosion Abstraction for the outer surface of the WP is documented in *General Corrosion and Localized Corrosion of Waste Package Outer Barrier* (SNL 2007 [DIRS 178519], Section 8.2). The Alloy 22 general corrosion rate is considered to be a function of exposure temperature. The temperature-dependent general corrosion rate follows an Arrhenius relationship (SNL 2007 [DIRS 178519], Equation 6-28):

$$R = R_o \exp\left[C_1 \left(\frac{1}{333.15\ \text{K}} - \frac{1}{T} \right) \right] = \exp\left[\ln(R_o) + C_1 \left(\frac{1}{333.15\ \text{K}} - \frac{1}{T} \right) \right] \quad \text{(Eq. 6.3.5-4)}$$

where

T = temperature in Kelvin.

C_1 = a slope term (in Kelvin) determined from short-term polarization resistance measurements for Alloy 22 specimens, tested for a range of sample configurations, metallurgical conditions, and exposure conditions. It is given by a truncated (-3 SD and +2 SD) normal distribution with a mean of 4,905 K and a SD of 1,413 K. The variation in C_1 is due entirely to epistemic uncertainty.

R_o = a rate distribution (in mm/yr) for the WP outer surface at 60°C (333.15 K), developed from weight-loss data obtained from the five-year crevice geometry samples exposed in the Long-Term Corrosion Testing Facility.

Three Weibull distributions were developed from the five-year corrosion rate results, for low, medium, and high uncertainty levels in the general corrosion rate (R_o) (SNL 2007 [DIRS 178519], Section 8.2). The distributions are to be sampled randomly in such a way that the low and high general corrosion rate distributions are each used for 5 percent of realizations and the medium general corrosion rate distribution is used for the remaining 90 percent of realizations.

As noted above, the patch area used to analyze the WPs is four times the area of the crevice geometry sample size used to determine the R_o distribution. Therefore, the general corrosion rates derived from the data analysis are adjusted to account for the effects of this change of scale (Aziz 1956 [DIRS 159379]; Shibata 1996 [DIRS 119589]). The method employed to accomplish this change in scale corresponds to using the highest of four sampled corrosion rates (from the two-parameter Weibull distribution) to analyze general corrosion of the WP patch. The approach is conservative because it is probable that not all four samples from the Weibull distribution will have the highest rate. A more realistic representation of the overall general corrosion rate would be the average of the four sampled corrosion rates. However, this approach would not account for the fact that one fourth of the patch has the maximum of the four sampled corrosion rates. On this basis, the proposed approach is conservative and appropriate for this application. Scaling the corrosion rates shifts the median general corrosion rate to higher values and decreases the probability of sampling lower general corrosion rates. This effect is shown on Figure 6.3.5-6 where the original distributions for R_o are plotted, along with the distributions resulting from a change of scale (or size factor) of four.

The WP outer barrier is assumed to be subject to MIC when the relative humidity at the WP outer barrier surface is above a relative humidity threshold, which is uniformly distributed between 75 and 90 percent (SNL 2007 [DIRS 178519], Section 8.2). The entire variance of this distribution is due to uncertainty. The effect of MIC on general corrosion of the WP outer barrier is represented by a multiplication factor (or MIC factor) to the general corrosion rate in the absence of MIC, such that:

$$CR_{MIC} = CR_{st} \times f_{MIC} \qquad \text{(Eq. 6.3.5-5)}$$

where CR_{st} is the general corrosion rate in the absence of MIC, f_{MIC} is the MIC enhancement factor, and CR_{MIC} is the general corrosion rate in the presence of MIC. The MIC enhancement factor is assumed to be uniformly distributed between 1 and 2, and the entire variance of the distribution is due to path-to-path variability (SNL 2007 [DIRS 178519], Section 8.2).

SCC—All regions of the WPs, except the outer-closure-lid weld region, are solution annealed before the WPs are loaded with waste. Thus, in the absence of seismic activity, they do not develop residual stress or stress-intensity factors high enough for SCC to occur (SNL 2007 [DIRS 181953], Section 6.5.3). The outer barrier closure lid is 25-mm-thick, as shown on Figure 6.3.5-7. The outer barrier closure lid weld region cannot be fully annealed and is stress-mitigated (by low plasticity burnishing) to produce a layer of compressive stress (SNL 2007 [DIRS 179394], Section 4.1.2.3; SNL 2007 [DIRS 179567], Section 4.1.1.3) that prevents SCC initiation until general corrosion removes this layer (SNL 2007 [DIRS 181953], Section 8.4.2.1).SCC can be initiated on a smooth surface (incipient cracks) or at an existing weld flaw (due to manufacturing defects).

The analysis in *Stress Corrosion Cracking of Waste Package Outer Barrier and Drip Shield Materials* (SNL 2007 [DIRS 181953], Section 8) summarizes the abstractions for the SCC initiation and propagation process, the stress and stress intensity thresholds, and the crack growth model based on the slip dissolution film rupture (SDFR) theory.

In *Stress Corrosion Cracking of Waste Package Outer Barrier and Drip Shield Materials* (SNL 2007 [DIRS 181953], Section 8.4.2.2), it is noted that the hoop stress, which promotes radially oriented crack growth, is the dominant component of stress in the WP outer barrier closure-lid weld regions. On this basis, only the hoop stress profiles are considered in the TSPA-SEIS SCC implementation. The hoop stress (σ in MPa) as a function of depth (x in mm) in the closure weld regions of the Alloy 22 WP outer barrier is given by a third order polynomial equation (SNL 2007 [DIRS 181953], Equation 64):

$$\sigma(x,0) = A_0 + A_1 \times x + A_2 \times x^2 + A_3 \times x^3 . \qquad \text{(Eq. 6.3.5-6)}$$

The second argument in the stress function is used to represent angular variation (θ = 0 arbitrarily chosen) around the circumference of the Alloy 22 WP outer closure-lid weld region. The angular variation is included using the following functional form (SNL 2007 [DIRS 181953], Equation 65):

$$\sigma(x,\theta,z) = \left(\sigma(x,0) - \nabla\sigma \times (1-\cos\theta)\right)\left(\frac{\sigma(th,\theta)+z}{\sigma(th,\theta)}\right) \qquad \text{(Eq. 6.3.5-7)}$$

where x is the distance from the weld surface, θ is the angle in degrees from the reference location $\theta = 0$, $\sigma(x,0)$ is the calculated weld residual stress profile at an angle $\theta = 0$, and distance x, th is the lid thickness, $\nabla\sigma$ is the angular variation of the mean stress, and z is the uncertain scaling factor discussed below. Because stress intensity factor (K_I) is a linear function of stress, the variability in stress intensity factor around the circumference can be calculated as (SNL 2007 [DIRS 181953], Equation 66):

$$K_I(x,\theta,z) = K_I(x) \times \left(\frac{\sigma(th,\theta)+z}{\sigma(th,0)}\right) \qquad \text{(Eq. 6.3.5-8)}$$

where th is the thickness of the closure-lid weld, z is the uncertain scaling factor discussed below.and $K_I(x)$ is the stress intensity factor at the zero position. The variation of the stress and stress intensity factor profiles with angle is due to variability.

The uncertainty in the stress and stress intensity factor profiles is introduced through a scaling factor, z. The scaling factor, z, which is sampled from a truncated normal distribution with a mean of zero and an SD of 5 percent of the yield strength, YS, has an upper-bound of 15 percent of the YS and a lower-bound of -15 percent of the YS (SNL 2007 [DIRS 181953], Section 6.5.6.2).

Flaws in the closure-lid welds are possible sites for SCC initiation. Weld flaws are generally larger than other surface defects and are conservatively considered to maintain their depth relative to the advancing general corrosion front (i.e., they are not removed by general corrosion processes). As discussed above, only radially oriented weld flaws are potential sites for SCC initiation. Weld flaws are a result of manufacturing defects (flaws not detected by the inspection processes). The analysis of the nondetection of weld flaws is documented in Section 6.3.1 of *Analysis of Mechanisms for Early Waste Package/Drip Shield Failure* (SNL 2007

[DIRS 178765]). The analysis was performed using the results from the welding of Alloy 22 specimen rings that duplicate closely the outer lid weld of a WP. Sixteen specimen rings were welded, employing procedures, processes, and equipment similar to that expected to be used for the closure of the WP. Nondestructive examinations were performed to accumulate significant information on the weld flaws and included ultrasonic and radiographic testing, which was followed by metallographic examination. This information consisted of weld flaw location, size, and shape. Based on this information, distributions were developed to characterize the size of the flaws in the through-wall extent of the weld, their density (mean number of flaws per volume of weld), and their depth (distance between the outer surface of the weld and the onset of the flaw).

The probability of nondetection, P_{ND}, of weld flaws of length x using an ultrasonic testing inspection technique is given by (SNL 2007 [DIRS 178765], Equation 17):

$$P_{ND}(x) = \varepsilon + \frac{1}{2}(1-\varepsilon)erfc\left(\nu \times \ln\left(\frac{x}{b}\right)\right) \qquad \text{(Eq. 6.3.5-9)}$$

where

x = size of the flaw (in mm)

ε = lower limit of P_{ND}

ν = shape factor

b = characteristic flaw size, in mm, which is the flaw size at the median of the P_{ND} distribution

erfc = complementary error function.

Weld flaw sizes follow an exponential distribution of parameter λ_s normalized to the weld thickness *(th)* (SNL 2007 [DIRS 178765], Equation 8). The flaw size probability density function is:

$$f_s(x) = \frac{\lambda_s \exp(-\lambda_s \cdot x)}{1-\exp(-\lambda_s th)} \qquad \text{(Eq. 6.3.5-10)}$$

The flaw size distribution parameter (representing uncertainty), λ_s, is gamma distributed with shape parameter n_f (the number of weld flaws), and scale parameter, $1/S_f$ (where S_f is the cumulative size of test weld flaws).

The fraction of nondetected defects remaining in the weld (of thickness *th*) after inspection is given by the convolution of the probability of nondetection and the flaw size probability density (SNL 2007 [DIRS 178765], Equation 19):

$$F_{nr}(th) = \int_0^{th} P_{ND}(u) f_s(u) du \,. \qquad \text{(Eq. 6.3.5-11)}$$

The distribution for the number of defects before any inspection or repair is characterized by a flaw count distribution parameter λ_c (SNL 2007 [DIRS 178765], Equation 11). The flaw count distribution parameter (representing epistemic uncertainty), λ_c, is gamma distributed with shape parameter, $(n_f + ½)$, and scale parameter, $1/V_f$, where V_f is the cumulative weld volume in the test welds (SNL 2007 [DIRS 178765], Section 6.3.1.3).

The distribution for the number of defects that remain after inspection can be defined in terms of the quantities derived above. It is Poisson distributed with parameter λ (count per closure weld). For a weld of volume V and thickness th, λ is given by the product (SNL 2007 [DIRS 178765], Equations 23 and 24):

$$\lambda = F_\theta \times F_\psi \times F_{nr}(th) \times (V \times \lambda_c) \qquad \text{(Eq. 6.3.5-12)}$$

where

F_θ = fraction of weld flaws that are radially oriented (SNL 2007 [DIRS 178765], Equation 16) (equal to 0.008)

F_ψ = fraction of embedded weld flaws able to propagate (SNL 2007 [DIRS 181953], Section 6.3.4.2) (equal to 0.25)

$F_{nr}(th)$= fraction of nondetected flaws.

Note that Equation 6.3.5-12 includes two factors that are not explicitly discussed in Section 6.3.1.8 of *Analysis of Mechanisms for Early Waste Package/Drip Shield Failure* (SNL 2007 [DIRS 178765]. The first, F_θ, accounts for the fact that not all weld flaws will be radially oriented, and the second, F_ψ, for the fact that not all embedded weld flaws will propagate.

The detection and repair analysis uses coefficients such that there is a 50 percent probability of detection and repair of a 1/16 inch weld flaw (SNL 2007 [DIRS 178765], Appendix A.5). This treatment is conservative because design uses a repair criterion to repair all flaws 1/16 in. or greater (SNL 2007 [DIRS 179394], Table 4-1).

The slip dissolution-film rupture model describes the propagation of cracks after the stress and stress intensity thresholds are met. The slip dissolution-film rupture model relates SCC initiation and subsequent crack advance to the metal oxidation that occurs when the protective film at the crack tip is ruptured. The slip dissolution model can be applied to assess the breach of the WP due to crack propagation for either manufacturing defects (weld flaws) or inherent defects such as grain boundary junctions, surface asperities or roughnesses (incipient cracks), or both. Inputs to the slip dissolution mechanism include threshold stress, threshold stress-intensity factor, an incipient crack size, and crack-growth-rate parameters.

The threshold stress is defined as the minimum stress at which cracks initiate on a smooth surface. This analysis refers to these as incipient cracks (to distinguish them from weld flaws) and typically form at local surface defects such as grain boundary junctions and surface roughness. Incipient cracks are considered to be 0.05 mm in length at the time of their nucleation (SNL 2007 [DIRS 181953], Section 8.4.2.1). The threshold stress is defined as a uniform distribution between 90 and 105 percent of the yield strength (SNL 2007 [DIRS 181953], Section 8.4.2.1). Incipient cracks nucleate when general corrosion has penetrated to the depth at which the stress profile exceeds the threshold stress. Weld flaws are already nucleated and, thus, do not require a stress threshold to nucleate. However, most weld flaws are embedded within the material and, therefore, not exposed to the environment. As general corrosion proceeds, some initially embedded weld flaws will be exposed to the environment. The distribution for the number of weld flaws capable of propagation by the slip dissolution mechanism was derived in Equation 6.3.5-12.

Stress corrosion crack growth can occur when the stress intensity factor at the tip of the incipient crack or weld flaw exceeds or is equal to a threshold stress intensity factor. The depth of the tip is the sum of the general corrosion depth and the crack or weld flaw depth. The stress intensity factor at this depth is determined from the stress intensity factor profile (Equation 6.3.5-8). The threshold stress intensity factor, K_{ISCC}, is given as a function of the repassivation slope, n and the general corrosion rate, V_{GC}:

$$K_{ISCC} = \left(\frac{V_{GC}}{\overline{A}} \right)^{1/4n} \qquad \text{(Eq. 6.3.5-13)}$$

where $\overline{A}$ is a function of n (repassivation slope) (SNL 2007 [DIRS 181953], Section 8.4.2.3).

Once crack growth initiates the crack(s) grow at a velocity given by (SNL 2007 [DIRS 181953], Section 8.4.2.3):

$$V_t = \overline{A}\left(K_I(x,\theta)\right)^{4n} . \qquad \text{(Eq. 6.3.5-14)}$$

The repassivation slope n should be sampled from a truncated (at ±2 SD) normal distribution with a mean of 1.165 and upper and lower bounds of 1.395 and 0.935, respectively. The variation in the repassivation slope, n, is entirely due to uncertainty.

Figure 6.3.5-8 provides a summary and illustration of the information flow between the DS and WP General Corrosion and SCC Abstractions.

Treatment of Uncertainty—The modeling of WP degradation accounts for aleatory uncertainty (variability) by simulating the performance of several hundred WPs. The effects of spatial and temporal variations in the exposure conditions across the repository are included by explicitly incorporating the relevant exposure condition histories into the TSPA-SEIS. The exposure condition parameters that are considered to vary over the repository are temperature and relative humidity on the WP outer surfaces. In addition, the TSPA-SEIS considers aleatory uncertainty in corrosion processes on a single WP due to variability in corrosion rates. This aleatory uncertainty is represented by dividing the WP outer surface area into sub-areas called patches

and stochastically sampling the degradation model parameter values for each patch. The use of patches explicitly represents the aleatory uncertainty in degradation processes on a single WP at a given time. Every WP in a given simulation is assigned different exposure conditions, thus addressing WP-to-WP aleatory uncertainty.

In the TSPA-SEIS, epistemic uncertainty in WP and DS degradation is analyzed with multiple realizations of the TSPA-SEIS. For each realization, values are sampled for the uncertain degradation parameters shown in Table 6.3.5-3, and these values are passed to the WP and DS Degradation Submodel. Each TSPA-SEIS realization includes a complete model simulation of WP and DS degradation, using explicit values of the uncertain degradation parameters, as described in the following paragraphs.

General corrosion rates for the inner and outer surfaces of the DSs are represented by two distributions, one for aggressive environmental conditions and one for benign environmental conditions. These distributions include both aleatory and epistemic uncertainty in DS general corrosion rates. However, the aleatory uncertainty in general corrosion rate has not been implemented in the TSPA-SEIS (Section 6.3.5.1.3). For each realization, two general corrosion rates are sampled, from the distribution for the uncertain mean of each distribution, and applied to all DSs. All DSs in a given realization fail at the same time.

The general corrosion rate of the WP outer surface is temperature-dependent and includes epistemic and aleatory uncertainty components. Epistemic uncertainty in the general corrosion rate is contained in its temperature-dependent slope term, C_1 (Equation 6.3.5-4). For each realization, a single general corrosion rate slope term is sampled and applied to all WPs, to represent epistemic uncertainty in the general corrosion rate with exposure temperature. The Alloy 22 general corrosion rate (R_o), which is represented by one of three CDFs determined from the five-year crevice geometry samples (Equation 6.3.5-4), has both aleatory and epistemic components. Each individual CDF represents variability (aleatory uncertainty); the choice of which CDF to use for a particular realization represents uncertainty. For every realization, each patch of each WP will have a different sampled value of R_o. In addition, spatial and temporal variability of the exposure temperature in the repository lead to spatial and temporal variability in the general corrosion rates used to model general corrosion of Alloy 22, due to the dependence of the general corrosion rate on temperature. A different exposure history file is assigned to each WP, resulting in a different WP surface temperature at each timestep. The net result is that every patch on each WP will have a different general corrosion rate, determined by the temperature read from the thermal history files at each timestep.

MIC is represented by an enhancement factor applied to the general corrosion rate of the WP outer surface, when the relative humidity threshold is exceeded. The value for the threshold relative humidity above which MIC takes place sampled from a uniform distribution, which represents epistemic uncertainty in the threshold. This distribution is sampled once per realization. The enhancement factor is also sampled from a uniform distribution, which represents variability of the corrosion rate among various areas or patches on the WP outer surface. The MIC enhancement factor is sampled for each WP patch and applied if the threshold relative humidity is exceeded. The variation in the MIC enhancement factor has an additional aleatory component due to the imposition of the relative humidity threshold, since the relative humidity on the WP surface varies from package to package.

The evaluation of weld flaw sizes and numbers of weld flaws includes epistemic and aleatory uncertainty. The variation in weld flaw sizes is expressed as aleatory uncertainty at the WP level, given by a probability density function dependent on an uncertain flaw size parameter that is sampled for each realization (Equation 6.3.5-10). The variation in the number of weld defects is expressed as aleatory uncertainty at the WP level given by a Poisson distribution with an uncertain parameter (count per closure weld) (Equation 6.3.5-12). This parameter is a function of the flaw size and count parameters that are sampled as uncertain for each realization (SNL 2007 [DIRS 178765], Table 7-1). The number and size of the weld flaws are randomly distributed to WP patches subject to SCC degradation. Thus, each SCC patch on every WP will have different initial values for the number and size of the weld flaws.

The evaluation of SCC initiation and propagation for the outer closure lid includes epistemic and aleatory uncertainty. Aleatory uncertainty is represented by the variation of the stress and stress-intensity factor profiles with angle and depth. The epistemic uncertainty in the stress and stress-intensity factor profiles is introduced through a scaling factor, z. The variations in the threshold stress and stress-intensity factor distributions are entirely due to epistemic uncertainty. The thresholds are sampled once per realization. The sampled threshold values are applied to all WP patches. The uncertainty in crack growth rate is a function of the repassivation slope. The variation in the repassivation slope is entirely due to epistemic uncertainty. The repassivation slope is sampled once per realization. The sampled repassivation slope value applies to all WP patches.

6.3.5.1.3 Implementation in the TSPA-SEIS

Overview—The TSPA-SEIS WP and DS Degradation Submodel makes use of several related software packages. The WAPDEG V4.07 software [DIRS 181064] is a DLL that is responsible for simulating the aleatory uncertainty in WP degradation. The GoldSim V9.60.100 software is used to pass values to the WAPDEG V4.07 software and is responsible for treating the epistemic uncertainty in the WAPDEG V4.07 inputs. The GoldSim V9.60.100 software also calls several other DLLs that are used to incorporate uncertainty in various inputs to the WAPDEG V4.07 software. These include the SCCD V2.01 software (STN: 10343-2.01-00 [DIRS 181157], STN: 10343-2.01-01 [DIRS 181054]) for the treatment of uncertainty in stress and stress-intensity factor profiles, and the CWD V2.0 software (STN: 10363-2.0-00 [DIRS 162809], STN: 10363-2.0-01 [DIRS 181037]) for the treatment of uncertainty in the number and size of closure-lid weld manufacturing defects. The MkTable_LA V1.0 software (STN: 11217-1.0-00 [DIRS 181047], STN: 11217-1.0-01 [DIRS 181048]) is used to randomly select a specified number of environment-history tables from the total set of environment-history tables. Each WP within a percolation subregion is assigned a different environment-history table. The environment-history tables are an output of the PREWAP_LA V1.0 software (STN: 10939-1.1-00 [DIRS 181053]), which processes the results from the comprehensive MSTHM Abstraction (Section 6.3.2.3). The PREWAP_LA V1.0 software reads these input files and writes corresponding environment-history output files, containing a subset of the data read from the MSTHM Abstraction files. These output files are created in a format that is compatible with the input files required by the WAPDEG V4.07 software program

In the TSPA-SEIS, some of the parameters for the DS and WP degradation modes are sampled at the global level but the calculations, which use these parameters, are done at the second level of

discretization (Section 6.1.5.3) in the percolation subregions associated with each WP type (CSNF WP or CDSP WP). The number of WPs to be emplaced in the repository is 11,629 (Table 6.3.7-1). The repository is divided into five spatially defined percolation subregions or bins (Section 6.3.2.2.1). Each percolation subregion contains a different number of WPs and is subject to different environmental conditions.

WP and DS Degradation Submodel—GoldSim Interface—The TSPA-SEIS file will typically call the WAPDEG V4.07 software program several times per GoldSim realization. The exact number of calls will depend on the modeling case being run. In the Nominal Modeling Case, 10 WAPDEG simulations are required: one for each CDSP WP and CSNF WP in each of the five repository percolation subregions. The main input to the WAPDEG V4.07 software program is a vector data element of real numbers. The values in the vector data element specify degradation models and degradation model parameters. The WAPDEG V4.07 software program also requires distributions and tables stored in text files that cannot be passed by GoldSim. GoldSim instead passes line numbers that point to entries in a text file (WD4DLL.WAP) containing a list of the file names required by the WAPDEG V4.07 software. The vector data element and the contents of the files identified in the text file are the only inputs to the WAPDEG V4.07 software.

Global Parameters and Calculations—The general corrosion of DSs has been specified with both variability (aleatory uncertainty) and epistemic uncertainty in Section 6.1[a] of *General Corrosion and Localized Corrosion of the Drip Shield* (SNL 2007 [DIRS 180778]). However, the TSPA-SEIS architecture does not support spatial variation between DSs or between patches on individual DSs. Therefore, variability in the corrosion rate is not included in the TSPA-SEIS implementation. Two uncertain mean corrosion rates are sampled independently per realization and are used for the general corrosion calculations for the DS. For this purpose, TSPA uses only the parameters WDDSAggrGC_Mean_a and WDDSBenignGC_Mean_a (Table 6.3.5-3) for the Titanium Grade 7 corrosion rates. In addition, the DS general corrosion rate for aggressive conditions is used on the top side of all DSs, whether or not they encounter seeping conditions. The implementation of two different corrosion rates for the top side of DSs depending on whether or not they are seeped on would impose a significant implementation overhead. The use of the aggressive rate for DSs that are not seeped on has no impact on dose calculations.

The earliest possible DS failure time can be calculated by combining the most severe degradation rates from the aggressive and benign distributions. Using the distributions given in the first two rows of Table 6.3.5-3 and using values at the 0.9999 probability level gives an aggressive rate of 5.764×10^{-5} mm/year and a benign rate of 0.824×10^{-5} mm/year. Combining these gives a rate of 6.588×10^{-5} mm/year, corresponding to a DS failure time of about 230,000 years.

Some of the parameters defining the general corrosion rate for the WP are sampled globally, but the actual calculation of the WP general corrosion rate is done at the percolation subregion level, because the WP general corrosion rate is a function of exposure temperature. The first input to the calculation of the WP general corrosion rate is the slope term for the general corrosion rate, given by a truncated (-3 SD and +2 SD) normal distribution with a mean of 4,905 K and an SD of 1,413 K. This parameter represents epistemic uncertainty and is sampled once per realization. The second parameter is a rate distribution (in mm/yr) for the WP outer surface at 60°C. One of three rate distributions is chosen randomly in such a way that the low and high general corrosion

rate distributions are each used for 5 percent of realizations and the medium general corrosion rate distribution is used for the remaining 90 percent of realizations. This distribution is sampled by the WAPDEG V4.07 software for every patch on each WP. Because the temperature of the WP surface is different for every WP simulated in a given percolation subregion, the result is a different general corrosion rate for every patch on every WP. General corrosion of Alloy 22 is implemented in WAPDEG using the general linear functional form (BSC 2002 [DIRS 162606], Section 4.2.6.5). The WP thickness is taken to be 25 mm, the minimum value specified for design purposes (SNL 2007 [DIRS 179394], Table 4-1).

The relative humidity threshold for MIC is an epistemically uncertain parameter, sampled once per realization. The relative humidity threshold is uniformly distributed between 75 percent and 95 percent. The MIC factor is uniformly distributed between one and two. However, the calculation is done at the percolation subregion level because the initiation of MIC occurs when a threshold relative humidity is exceeded. A unique relative humidity is read, as a function of time, from the environment-history tables generated by the MkTable_LA V1.0 software for each WP surface. The CWD V2.0 software implements the abstraction for the number and size of weld flaws documented above (Equations 6.3.5-9 to 6.3.5-12). The CWD V2.0 software is executed two times per realization: once for the outer-closure lid of the CSNF WPs and once for the outer-closure lid of the CDSP WPs. The CWD V2.0 software computes the cumulative probability of a manufacturing defect based on the probability for the nondetection of weld defects. The inputs to this calculation are weld thickness, weld volume, the defect fraction considered, a detection threshold, a characteristic defect size, a shape factor, a defect count parameter, and a defect-size parameter. The output of each invocation of the CWD V2.0 software consists of two tables, and the probability of occurrence of at least one defect per WP. These output tables contain distributions for the density and size of defect flaws on the outer-closure lid. The CWD outputs are direct inputs to the WAPDEG V4.07 software.

The SCCD V2.01 software implements the abstraction for the stress and stress intensity factor profiles documented above (Equations 6.3.5-6 to 6.3.5-8). The SCCD V2.01 software is executed once per realization for the outer-closure lid. The SCC calculation is the same for both CDSP WPs and CSNF WPs. The SCCD V2.01 software calculates the variation in stress and stress intensity factor versus depth and angle. The inputs to this calculation are four regression coefficients from the model abstraction for stress as a function of depth, the sine of the fracture angle, the number of angles to be calculated, the expected yield strength, the yield-strength scaling factor, the angular amplitude of the stress variation, the uncertainty model, and an uncertain deviation from median yield-strength range. Also required is the stress intensity factor versus depth profile for the zero reference angle. The outputs of the SCCD V2.01 software are stress and stress intensity factor tables, as a function of depth, calculated at a number of angles (equally spaced and in the range 0 to π radians, inclusive). The SCCD V2.01 software outputs are direct inputs to the WAPDEG V4.07 software.

Percolation Subregion Parameters and Calculations—The total number of WPs modeled is 11,629 (8,213 CSNF WPs and 3,416 CDSP WPs). These WPs are partitioned among the five percolation subregions according to the percolation-flux distributions. The resulting partitioning is described in Section 6.3.2.2.1 and shown in Table 6.3.2-2. In the Nominal Modeling Case, the WAPDEG V4.07 software runs twice for each of the five percolation subregions: once for the CSNF WPs in that subregion and once for CDSP WPs. A sensitivity analysis was conducted

with 250, 500, 1,000, and 3,400 DS and WP pairs. Comparison of the mean and 95th percentile WP first failure curves showed that the analysis results were not very sensitive to the number of DS and WP pairs simulated over the range investigated. Therefore, in the TSPA-SEIS file, if the percolation subregion contains fewer than 500 WP/DS pairs, the number of CSNF and CDSP WP and DS pairs simulated by the WAPDEG V4.07 software is equal to the number of pairs in the subregion. If the subregion contains more than 500 WP/DS pairs, then only 500 CSNF and 500 CDSP WP/DS pairs are simulated by the WAPDEG V4.07 software.

The primary submodel supplying input to the WP and DS Degradation Model Component is the EBS TH Environment Submodel (Section 6.3.2). The EBS TH Environment Submodel provides temperature and relative humidity histories for eight WP/DS pairs, composed of six CSNF WPs and two CDSP WPs at each of the 3,264 repository subdomain locations (Section 6.3.2.2). These 3,264 repository subdomain locations are partitioned among the five percolation subregions according to the percolation-flux distributions (Section 6.3.2.2.1). The resulting partitioning is shown in Table 6.3.2-2.

Each WAPDEG simulation requires a unique exposure history for each of the WP/DS pairs being simulated. The MkTable_LA V1.0 software samples these exposure histories from those available for the percolation subregion. The set of exposure histories that is available for sampling is determined by the WP type (CSNF WP or CDSP WP), the percolation subregion, the infiltration scenario, and the thermal conductivity. An external text file, WDHist.inp, contains a list of file names corresponding to exposure histories. The external file, WDHist.inp, is a generic file pointing to one of twelve possible files. These files correspond to combinations of the four possible infiltration scenarios (corresponding to the four climate states) and high, medium, and low thermal conductivity. The choice of which three files to use is controlled by the MFCP_LA V1.0 software (STN: 11071-1.0-00 [DIRS 167884], STN: 11071-1.0-01 [DIRS 181045]) on the basis of the sampled values for infiltration scenario and thermal-conductivity uncertainty.

WAPDEG V4.07 Software Overview—The WAPDEG V4.07 software simulates corrosion degradation of WPs by three penetration modes: patch penetration (due to general corrosion), crack penetration (due to crack tip growth or SCC), and pit penetration (due to pitting corrosion or crevice corrosion) (BSC 2002 [DIRS 162606], Section 3.3). Only the first two of these modes are invoked in the TSPA-SEIS. The WAPDEG V4.07 software structure specifies corrosion-affecting events that affect specific degradation processes. Each event is identified by a unique integer in the WAPDEG input vector. Each event has both event-specific data and generic data. The event-specific data triggers effects that are unique to that event. The data that describes the generic event effects has the same input structure for each event and is read at the end of the event-specific data. There are four possible generic effects of any event. These are to immediately fail the patches affected by the event, and/or to initiate localized corrosion modes, and/or to accelerate a corrosion mode or modes, and/or to reduce thresholds (BSC 2002 [DIRS 162606], Section 3).

General corrosion of Alloy 22 is implemented in the WAPDEG V4.07 software using the general linear functional form (BSC 2002 [DIRS 162606], Section 4.2.6.5). The form used for the TSPA-SEIS implementation of the Alloy 22 corrosion rate is:

$$D = \exp\left(\ln(R_o) + \frac{C_1}{333.15} + \varepsilon\right)\exp\left(-\frac{C_1}{T}\right) t^n \qquad \text{(Eq. 6.3.5-15)}$$

where D is corrosion depth (mm), t is time (yr), and T is exposure temperature (K). The parameter ε is not used in the TSPA-SEIS implementation. It is set to zero. The time exponent, n, has the value 1.0. The effect of MIC on the general corrosion of the WP is analyzed by the use of a MIC event (BSC 2002 [DIRS 162606], Section 4.2.7.10).

In the WAPDEG V4.07 software, the weld flaws are defined by a manufacturing defects event (BSC 2002 [DIRS 162606], Sections 3.3.2.1 and 4.2.7.2). The manufacturing defects event has only one specific effect, to introduce manufacturing defects onto patches. SCC is implemented in WAPDEG by the use of a slip dissolution event (BSC 2002 [DIRS 162606], Sections 3.3.2.1.1 and 4.2.7.5). Incipient cracks are automatically included in the event, but weld flaws must be specifically included via a manufacturing defects event. The slip dissolution event models the rate of crack growth and defines the time of crack penetration. The slip dissolution event implements the abstraction for crack growth presented in Equations 6.3.5-13 and 6.3.5-14.

WP and DS Degradation Submodel Output—There is a one-dimensional table and a two-dimensional table output for each implementation of the WAPDEG V4.07 software. The one-dimensional table contains WP first-failure times versus the fraction of WPs failed. The WP first-failure time is defined as the first penetration by any mechanism (general corrosion or SCC) of the WP. The format of both of these tables is as follows; the first column contains the WP first-failure times in years (sorted in increasing order) and the second column contains the cumulative fraction WPs failed. The two-dimensional table contains 12 columns. The number of rows is controlled by a parameter defined in the TSPA-SEIS and passed to the WAPDEG V4.07 software. The column contents are explained in *User's Manual for WAPDEG 4.07* (BSC 2003 [DIRS 162606], Table 19).

The outputs generated by the WP and DS Model Component and used by the EBS Flow and Transport Model Component (Sections 6.3.6 and 6.3.8) for each percolation subregion and each fuel type (CSNF and CDSP WPs) are:

- The average fraction of WP surface failed by general corrosion (patches), per failed WP, and the average fraction of WP surface failed by cracks, per failed WP, as a function of time
- The fraction of all the WPs and DSs in the subregion that were breached, as a function of time.

Note that the average fraction of WP surfaces failed by general corrosion or by cracks are values that apply to all WPs and DSs in a given percolation subregion and for a given fuel type. These values are calculated by the WAPDEG V4.07 software as an average over failed WPs.

6.3.5.2 Localized Corrosion on the Waste Package Outer Surface

The WP Localized Corrosion Initiation and Propagation Submodel for the WP outer surface is based on the Localized Corrosion Initiation Abstraction developed in *General Corrosion and Localized*

Corrosion of Waste Package Outer Barrier (SNL 2007 [DIRS 178519], Section 8.3.1). The temperature, pH, chloride-ion concentration, and nitrate-ion concentrations in aqueous solutions on the WP outer surface are the primary factors that determine the potential for initiating localized corrosion. These are obtained from the EBS TH Environment Submodel and the EBS Chemical Environment Submodel. Localized corrosion requires the presence of a liquid water film on the WP surface. Two types of aqueous solutions may lead to environmental conditions conducive to localized corrosion initiation on the WP outer surface: (1) dripping crown seepage water that contacts the WP outer surface, and (2) salt deliquescence in dust particles that may reside on the WP outer surface. Localized corrosion resulting from salt deliquescence in dust particles was screened out (*Analysis of Dust Deliquescence for FEP Screening* (SNL 2007 [DIRS 181267])). Also discussed in this section is the localized corrosion growth model, which applies to the WP during the time period when localized corrosion is indicated by the Localized Corrosion Initiation Abstraction.

6.3.5.2.1 Conceptual Model

Initiation of Localized Corrosion (Crevice Corrosion)—The Localized Corrosion Initiation Abstraction stipulates that localized corrosion of the WP outer surface occurs when the open-circuit potential, or corrosion potential (E_{corr}), is equal to or greater than the critical threshold potential ($E_{critical}$); that is, $\Delta E = E_{critical} - E_{corr} \leq 0$ (SNL 2007 [DIRS 178519], Section 8.3.1).

The open-circuit corrosion potential is the potential measured across a metal sample when it is immersed in a liquid. The corrosion potential can change with time, eventually approaching a steady state. Therefore, the long-term steady-state corrosion potential was used for the corrosion potential model of Alloy 22 (SNL 2007 [DIRS 178519], Section 4.1.1.5).

The long-term corrosion potential abstraction for the WP outer surface was developed using a regression model fit to the long-term corrosion potential data as a function of the major exposure-environment variables: temperature, pH, chloride ion concentration, and nitrate ion concentration. Only data with an immersion time of 250 days or higher were used (SNL 2007 [DIRS 178519], Section 6.4.4.5). The WP outer surface is potentially susceptible to crevice corrosion if an acidic chloride-containing solution with relatively lower concentrations of inhibitive ions contacts the WP outer surface while it is at elevated temperature.

The crevice repassivation potential from cyclic potentiodynamic polarization tests was selected as a conservative measure of $E_{critical}$, as described in *General Corrosion and Localized Corrosion of Waste Package Outer Barrier* (SNL 2007 [DIRS 178519], Section 6.4.4.1). The repassivation potential (E_{rcrev}) is the potential at which the reverse scan of a cyclic potentiodynamic polarization curve using a creviced sample crosses the forward scan. The point where the reverse scan intersects the forward scan is called the repassivation point and is indicative of the breakdown of the passive film.

Corrosion Penetration Rate—Because of the relatively high corrosion resistance of Alloy 22, there are limited experimental results regarding localized corrosion under the conditions expected in the repository. The Localized Corrosion Penetration Rate Abstraction for the WP outer surface was based on results that bound the extreme penetration rates found in the literature for Alloy 22. This distribution is considered to be a highly conservative representation of the

localized corrosion rates of Alloy 22 for the exposure conditions anticipated in the repository environment (SNL 2007 [DIRS 178519], Section 8.3.2).

The Localized Corrosion Initiation and Propagation Submodel uses a constant (time-independent) penetration rate after localized corrosion is initiated (SNL 2007 [DIRS 178519], Assumption 5.4). This constant penetration rate is sampled from the epistemic uncertainty distribution for the localized corrosion rate and differs from realization to realization. Although the localized corrosion rate is modeled as time invariant, the crevice corrosion propagation rate would be expected to decrease with increasing depth of the crevices and time under realistic conditions. The use of constant penetration rate versus time is a highly conservative assumption because localized corrosion rates generally decrease with time and this decrease is even more likely under the thin water film environment that is expected to form on the WP outer surface in the postclosure repository period, as described in *General Corrosion and Localized Corrosion of Waste Package Outer Barrier* (SNL 2007 [DIRS 178519], Section 8.3.2) and *Waste Package Degradation Expert Elicitation Project* (CRWMS M&O 1998 [DIRS 100349], Table 3-2).

In the absence of specific information regarding local environments on the WP, the area of the Alloy 22 WP outer barrier that is contacted by seepage is considered to be potentially subject to localized corrosion (SNL 2007 [DIRS 178519], Section 8.3.1).

6.3.5.2.2 Model Abstraction

For the TSPA-SEIS, the Localized Corrosion Initiation Abstraction uses the crevice repassivation potential (E_{rcrev}) as the critical potential. The crevice repassivation potential for crevice corrosion on the WP outer surface is defined in terms of WP surface temperature and chemical conditions as follows:

$$E_{rcrev} = a_o + a_1 T + a_2 \ln\left[Cl^-\right] + a_3 \frac{\left[NO_3^-\right]}{\left[Cl^-\right]} + a_4 T\left[Cl^-\right] + \varepsilon_{rcrev} \qquad \text{(Eq. 6.3.5-16)}$$

where a_o, a_1, a_2, a_3, and a_4 are regression constants, T is the WP outer surface temperature (°C), pH is the negative log of the hydrogen ion activity, $[NO_3^-]$ is the nitrate ion molality (moles/kg water), and $[Cl^-]$ is the chloride ion molality (moles/kg water). The coefficient values and their epistemic uncertainty (±1 SD) are a_o= 190.242 ± 18.373, a_1= -3.008 ± 0.225, a_2= -46.800 ± 3.126, a_3= 535.625 ± 26.140, and a_4= 0.061 ± 0.010. The error term, ε_{rcrev}, is a term representing data variance not explained by the fitting procedure and has a normal distribution with a mean of zero mV versus the saturated silver chloride electrode and an SD of 45.055 mV versus saturated silver chloride. The units of the coefficients should be consistent with E_{rcrev} having units of mV. The covariation of the coefficients (due entirely to epistemic uncertainty) was represented through the use of a covariance matrix derived in *General Corrosion and Localized Corrosion of Waste Package Outer Barrier* (SNL 2007 [DIRS 178519], Section 8.3.1. The Localized Corrosion Initiation Abstraction stipulates that the calculated values of ε_{rcrev} be compared to the ±2 SD prediction intervals of the unconstrained model and truncated at these values if necessary. These coefficients are sampled in the TSPA-SEIS using a Cholesky factorization method to induce correlation..

The long-term steady-state corrosion potential, E_{corr}, for the WP outer surface is expressed as:

$$E_{corr} = c_o + c_1 T + c_2 pH + c_3 \frac{[NO_3^-]}{[Cl^-]} + c_4 T \frac{[NO_3^-]}{[Cl^-]} + c_5 pH \frac{[NO_3^-]}{[Cl^-]} + c_6 pH \ln[Cl^-] + \varepsilon_{corr}$$

(Eq. 6.3.5-17)

where c_o, c_1, c_2, c_3, c_4, c_5, and c_6 are coefficients of the parameters, and the other parameters are as previously defined. The regression coefficients and their epistemic uncertainty (± 1 SD) are: c_0 = 1,051.219 ± 119.774, c_1= -3.024 ± 0.977, c_2= -155.976 ± 11.495, c3 = -1,352.040 ± 252.224, c4 = 10.875 ± 1.890, c5 = 137.856 ± 23.158, and c_6 = -8.498 ± 0.801. The error term, ε_{corr}, is a term representing data variance not explained by the fitting procedure and has a normal distribution with a mean of zero mV versus SSC and an SD of 85.265 mV versus SSC. The units of the coefficients should be consistent with E_{corr} having units of mV.

The covariation of the coefficients (due entirely to epistemic uncertainty) was represented through the use of a covariance matrix. As with the crevice repassivation potential, E_{rcrev}, the epistemic uncertainty of the parameter coefficients of the corrosion potential, E_{corr}, should be limited to ±2 SDs. These coefficients are sampled in the TSPA-SEIS using a Cholesky factorization method to induce correlation.

The WP Localized Corrosion Penetration Rate Abstraction propagates corrosion in the WP outer surface at a constant rate (SNL 2007 [DIRS 178519], Assumption 5.4). The extreme penetration rates found in the literature were used to bound localized corrosion rates for Alloy 22 under expected repository conditions. Based on these published rates, the localized corrosion propagation rates for the WP outer surface were estimated to be log uniformly distributed with a range from 12.7 to 1,270 μm/year .

Localized corrosion initiation requires the presence of liquid brine on the WP outer surface. This brine may be formed by aqueous solutions dripping onto the WP surface. For intact or moderately degraded drifts, there is no seepage water contacting the WP surface if the drift-wall exposure temperature is greater than 100°C (SNL 2007 [DIRS 181244], Section 6.5.3) or if the WP surface temperature is greater than 120°C. The 120°C limit is inferred from examination of peak drift-wall and WP temperatures for the seven modeled uncertainty cases presented in *Multiscale Thermohydrologic Model* (SNL 2000 [DIRS 181383], Table 6.3-49[a]). For collapsed drifts, boiling conditions persist later into the repository lifetime (SNL 2007 [DIRS 181383], Figure 6.3-79[a]). Therefore, the thermal seepage limit for intact or moderately degraded drifts can be considered bounding. Thus, the only relevant chemistries to consider for localized corrosion initiation, for WP surface temperatures greater than 120°C, are those that result from dust deliquescence. However, localized corrosion resulting from salt deliquescence in dust particles was screened out of the TSPA-SEIS, based on geochemical analyses. Therefore, localized corrosion initiation at WP temperatures greater than 120°C need not be considered.

The limits of applicability and the procedures for the implementation of the Localized Corrosion Initiation Abstraction in the TSPA-SEIS are defined in *General Corrosion and Localized Corrosion of Waste Package Outer Barrier* (SNL 2007 [DIRS 178519], Section 8.3.1). The following initiation criteria apply:

- Crown seepage localized corrosion does not occur if the drift-wall temperature is greater than 100°C (WP surface temperature greater than 120°C).

- If it has been determined that localized corrosion can occur and the WP exposure temperature is at least 20°C but does not exceed 120°C, then the empirical correlations for the long-term corrosion potential (E_{corr}) and crevice repassivation potential (E_{rcrev}) are evaluated with the following implementation rules:

  - If the nitrate-to-chloride ion ratio in the environment exceeds one then evaluate Ercrev and Ecorr at a nitrate-to-chloride ion ratio of one. If the molality of chloride ion is less than 0.0005 molal, evaluate the nitrate-to-chloride ion ratio with a chloride ion concentration of 0.0005 molal.

  - If the molality of the chloride ion in the environment exceeds 20 molal, then evaluate E_{rcrev} and E_{corr} at a chloride ion molality of 20 molal. If the chloride ion molality is less than 0.0005 molal, then evaluate E_{rcrev} and E_{corr} at a chloride ion molality of 0.0005 molal.c.

  - If the pH in the environment exceeds 10, then evaluate E_{rcrev} and E_{corr} at a pH of 10. If the pH in the environment is less than 1.9, then initiate localized corrosion.

- If the WP relative humidity is below the threshold at which halite precipitates and the WP is below a failed DS, then when re-wetting occurs the in-package chemistry lookup tables no longer apply and TSPA is instructed to assume that Cl-rich brine can form (SNL 2007 [DIRS 177412], Sections 6.12.3 and 6.15.1.3. Because the process of salt-brine separation cannot be explicitly modeled, the P&CE report (SNL 2007 [DIRS 177412]) abstraction models do not attempt to provide the chemistry for the Cl-rich brines. In this situation it is conservatively assumed that localized corrosion initiates when re-wetting occurs.

- If crown seepage localized corrosion is determined to initiate, then allow localized corrosion to continue to occur at the sampled propagation rate, regardless of changes in the chemical environment.

- The area pf the Alloy 22 WP outer barrier that is contacted by seepage is potentially subject to localized corrosion. (SNL 2007 [DIRS 178519], Section 8.3.1).

6.3.5.2.3 Implementation in the TSPA-SEIS

The Localized Corrosion Initiation Abstraction, described in Sections 6.3.5.2.1 and 6.3.5.2.2, provides input to the localized corrosion implementation in the TSPA-SEIS file by determining if environmental conditions on the WP outer surface will initiate localized corrosion and lead to WP failure. Localized corrosion is included in the Seismic Scenario Class modeling cases

(Section 6.6), and in the Nominal Modeling Case. In the Igneous Scenario Class, the affected WPs and DSs are immediately destroyed at the time of the intrusion event. Only dripping crown seepage water contacting the WP outer surface is considered, in the TSPA-SEIS, to lead to environmental conditions conducive to localized corrosion on the WP outer surface. The Localized Corrosion Initiation and Propagation Submodel contains several interfaced TSPA-SEIS submodels in combination with the Localized Corrosion Initiation Abstraction. This is done in probabilistic analyses external to the main TSPA-SEIS to compute time-dependent chemical conditions of brine formation and the potential for localized corrosion initiation on WP surfaces. Important epistemic and aleatory uncertainties are accounted for, as described below. These analyses are performed for each repository percolation subregion and WP type. The output from this analysis is the fraction of WPs failed due to localized corrosion, as a function of time. The uncertain parameters sampled in the Localized Corrosion Initiation and Propagation Submodel model file are perfectly correlated to the same distributions sampled within the TSPA-SEIS file. Therefore, each realization of the Localized Corrosion Initiation and Propagation Submodel, matches up to the same realization of the TSPA-SEIS GoldSim file. The remainder of this section describes the implementation of the Localized Corrosion Initiation and Propogation Submodel.

Implementation of the Localized Corrosion Initiation and Propagation Submodel

Localized Corrosion Initiation and Propagation Submodel calculations result from the interfacing of several TSPA-SEIS submodels, as illustrated on Figure 6.3.5-9, to determine whether or not environmental conditions on the WP outer surface will initiate localized corrosion and lead to failure. These submodels include:

- EBS Chemical Environment Submodel look-up tables for Pco_2 in the emplacement drifts and abstraction bin history maps for incoming seepage composition history (Section 6.3.4.2). These abstractions are used to define Pco_2 in the emplacement drift as a function of time, and to define the chemical composition of seepage water entering the drifts as a function of time. Pco_2 is an input to the chemical evolution of crown seepage water.

- EBS Chemical Environment Submodel look-up tables for the chemical evolution of crown seepage water on the WP outer surface (Section 6.3.4.3.2) and distributions for the nitrate to chloride ratio (sampled once per realization). The EBS P&CE Abstraction is used to calculate the chloride concentration, nitrate concentration, and pH in crown seepage water as functions of relative humidity. These quantities are then used to evaluate localized corrosion initiation.

- Drift Seepage Submodel (Section 6.3.3.1). The seepage response surfaces for nondegraded and degraded drifts are implemented in the localized corrosion initiation calculations to determine if seepage occurs at a WP location.

- EBS TH Environment Submodel (Section 6.3.2). The EBS MSTHM Abstraction (Section 6.3.2.3) provides time-dependent values for temperature and relative humidity on WP surfaces and drift-wall temperature. The abstraction also provides time-dependent adjusted values that are used to correct temperature and relative

humidity values for the insulating effect of rubble caused by drift degradation induced by seismic ground motion in the lithophysal units. Drift-wall temperatures are used to calculate thermal seepage in the nonlithophysal units. WP temperatures, with adjusted values for rubble, are used to calculate thermal seepage in the lithophysal units.

- Localized Corrosion Initiation Abstraction (Section 6.3.5.2.2). The Localized Corrosion Initiation Abstraction takes input from the various abstractions and submodels to derive the criteria for localized corrosion initiation.

- Seismic Abstraction (Section 6.6). The volume of rubble accumulated in the lithophysal and nonlithophysal zones are inputs to the drift seepage submodel, which in turn feeds the Localized Corrosion Initiation Abstraction. The time of first DS plate failure due to seismic damage is used by the Localized Corrosion Initiation Abstraction to determine the time of initiation of localized corrosion.

- WP and DS Degradation Submodel (Section 6.3.5). The time of first DS failure due to general corrosion is used by the Localized Corrosion Initiation Abstraction to determine the time of initiation of localized corrosion. The general corrosion rate parameters and the MIC factor are used to determine a general corrosion rate, which is added to the localized corrosion rate to determine the WP failure fraction histories.

Figure 6.3.5-9 also illustrates the WP failure fraction histories that are the primary outputs produced by the Localized Corrosion Initiation and Propagation Submodel. Figure 6.3.5-10 illustrates the steps taken to implement localized corrosion initiation in the Localized Corrosion Initiation and Propagation Submodel. The Localized Corrosion Initiation and Propagation Submodel, includes two computational loops for including uncertainty: an outer epistemic uncertainty loop, and an inner aleatory uncertainty loop. In the outer loop, epistemic uncertainties associated with localized corrosion initiation, chemical environment on the WP outer surface, drift seepage, and rubble (natural backfill caused by a strong seismic ground motion event) are sampled using LHS for each localized corrosion realization. These epistemic uncertainties include the following (Table 6.3.5-4).

- Fifteen uncertain parameters from the Localized Corrosion Initiation Abstraction (Section 6.3.5.2.2); 14 coefficients that correspond to the linear regression fitting parameters (a_0, a_1, a_2, a_3, a_4, ε_{rcrev}, c_0, c_1, c_2, c_3, c_4, c_5, c_6, and ε_{corr}) associated with the crevice repassivation potential and the long-term steady-state corrosion potential, respectively; one uncertain parameter that represents the epistemic uncertainty in the localized corrosion propagation rate.

- Six parameters that quantify the evolution of the chemical environment on the WP outer surface; one parameter is used to select crown seepage starting water type (Section 6.3.4.3.1); one uncertain parameter represents uncertainty in partial pressure of CO_2; four parameters represent epistemic uncertainty (Table 6.3.4-3, Section 6.3.4.3.2) in calculated chloride concentration, the nitrate-to-chloride ratio, the combined chloride and nitrate concentration, and pH (each of these four is represented by one of several possible distributions, depending on relative humidity). Five parameters that represent uncertainty in drift-seepage, including the seepage uncertainty scale factor and the

uncertainty in fracture permeability and capillary strength for both the lithophysal and nonlithophysal units (Tables 6.3.3-1 and 6.3.3-2, and Section 6.3.3.1.2).

- One parameter that represents epistemic uncertainty in thermal conductivity of the rubble deposited on the DSs and WPs due to drift degradation in the lithophysal unit (Section 6.6.1.3).

- Two uncertain parameters used to select exposure histories; one that represents epistemic uncertainty in infiltration scenario; one that represents epistemic uncertainty in thermal conductivity of the host rock.

- Two parameters that represent the uncertainty in the maximum rubble volume for the lithophysal and nonlithophysal units.

- Two uncertain parameters that represent the epistemic uncertainty in the Titanium Grade 7 general corrosion rate for aggressive and benign conditions; one uncertain parameter that represents the epistemic uncertainty in the temperature dependence of the Alloy 22 general corrosion rate; one uncertain parameter that represents the relative humidity threshold for the application of the MIC factor.

The MSTHM Abstraction subdivides the repository footprint into 3,264 equal-area subdomains and supplies temperature and relative humidity time histories for six CSNF WPs and two CDSP WP/DS pairs at each subdomain-center location. Time-dependent values for average drift-wall temperature are also supplied at each location. The TH variables and their associated locations are grouped into one of five repository subregions based on percolation flux at the base of the PTn (Section 6.3.2.2.1). Localized corrosion initiation analyses are implemented for each of the 12 cases considered by the MSTHM Abstraction. These 12 cases represent the combinations of epistemic uncertainty in infiltration and host-rock thermal conductivity (Section 6.3.2.2).

After the epistemic parameters are sampled, the percolation subregion, the TH case from the set of 12, and the WP fuel type are selected. Next, for each outer-loop realization, an inner loop over the TH locations in the percolation subregion is executed. For percolation subregions with more than 500 TH locations, this inner loop is constrained to 500 locations randomly sampled from the set of all possible locations (Section 6.3.5.1.3). Aleatory uncertainties are calculated at each WP location in the inner loop. The aleatory uncertainties represent spatial variability in the parameters and they include:

- Two sets of temperature and relative humidity time histories (associated with one of six CSNF WP time histories or one of two CDSP WP time histories): the first set represents values to be used under conditions of no drift collapse (or minor drift collapse); the second set is adjusted for the presence of rubble by adding an increment in temperature and relative humidity (Section.3.2).

- Drift-seepage parameters for flow focusing factor, spatial variability of fracture permeability, and capillary strength (Equation 6.3.3-1, Tables 6.3.3-1 and 6.3.3-2, and Section 6.3.3.1.2.).

The following steps are performed at each WP location within this loop for each percolation subregion and at each timestep:

1. The chemical environment on the WP outer surface due to crown seepage is determined. A calculation is first made to determine if seepage into the drift occurs.

   This calculation is implemented for each WP location, as described in the Drift Seepage Abstraction (Section 6.3.3.1), using the sampled drift-seepage parameters representing epistemic and aleatory uncertainty listed above, the percolation flux, and the drift-wall temperature to account for thermal seepage effects. In addition, if seepage occurs and a WP is located in the lithophysal unit, the adjusted (for the presence of rubble) WP temperature history is used to determine whether or not incoming seepage contacts the WP. If seepage does not contact the WP at the current location and time, localized corrosion initiation due to crown seepage is not evaluated. If drift seepage occurs, the following two evaluations are implemented.

2. The chemical environment on the WP outer surface, in terms of nitrate concentration, chloride concentration, nitrate-to-chloride ratio, and pH due to evolution of crown seepage, is calculated through time, as described in Section 6.3.4.3.2, using temperature and relative humidity time histories for the WP. If the WP is located in the lithophysal unit, the WP temperature and relative humidity values are adjusted for the presence of rubble from drift degradation in the Seismic Scenario Class using the thermal adjustment histories.

3. The values of temperature, relative humidity, pH, chloride concentration, and nitrate concentration are checked against the criteria listed in Section 6.3.5.2.2. If these parameters are outside the ranges specified, the appropriate bounding values are used. Otherwise, localized corrosion is initiated if $\Delta E \leq 0$ on a WP.

4. If localized corrosion initiates, the localized corrosion penetration continues at a constant rate through the regulatory period or until the WP is penetrated. The localized corrosion penetration rate is sampled from a uniform distribution from 0.0127 mm/yr to 1.27 mm/yr. A WP is considered failed by localized corrosion if the WP outer surface thickness is fully penetrated by the combined localized corrosion, general corrosion, and MIC penetration depths.

For each repository subregion and WP type, a corresponding fractional failure history is obtained by adding the failed WPs of that type and dividing by the total number of either CSNF WPs or CDSP WPs in the subregion. This evaluation is carried out for each TH timestep until simulation end time.

The evaluation of penetration time includes general corrosion and MIC enhancement of general corrosion. Because general corrosion is much slower than localized corrosion, a simplified general corrosion abstraction is incorporated into the Localized Corrosion Initiation and Propagation Submodel. This simplified general corrosion abstraction uses the CDF for R_0, which was developed from the average corrosion rate with a scale factor of four and corresponds

to the medium uncertainty level. MIC enhancement of general corrosion is activated only when relative humidity exceeds the MIC threshold.

The primary output from the Localized Corrosion Initiation and Propagation Submodel is the fraction of CSNF WPs and CDSP WPs that fail by localized corrosion due to crown seepage, as a function of time, in each percolation subregion. These fractions are used to define the number of WPs that fail by localized corrosion during the simulation time and their average breach areas as a function of time.

6.3.5.3 Model Component Consistency and Conservatism in Assumptions and Parameters

To enhance understanding of the complex interactions within the TSPA-SEIS, a discussion of consistency among model components and submodels and identification of conservative assumptions in abstractions, process models, and parameter sets supporting the WP and DS Degradation Model Submodel and the Localized Corrosion Initiation and Propagation Submodel are discussed below.

6.3.5.3.1 Consistency of Assumptions

Salt Separation on the WP Surface—The current TSPA-SEIS includes a relative humidity threshold switch to account for a potential salt separation process during seepage water evaporation (Section 6.3.5.2.2). In principle, water evaporation on the Alloy 22 WP surface will first cause the precipitation of halite (NaCl) and then the remaining water will flow away from early precipitated salts, leaving the solids behind rich in Cl^-. In this case, the chemistry look-up tables no longer apply form (SNL 2007 [DIRS 177412], Sections 6.12.3 and 6.15.1.3). For implementation purposes, the TSPA-SEIS assumes that localized corrosion always initiates upon re-wetting of the salt film. The implementation for the WP Localized Corrosion Initiation and Propagation Submodel represents potential differences between several submodels: Drift Seepage, EBS Flow, EBS Chemical Environment, and the localized corrosion aspect of WP degradation. The EBS Chemical Environment Submodel assumes well-mixed equilibrium conditions for chemistry in the drift (Section 5.1.2). Therefore, salt separation is not included in that submodel. In addition, evaporation and flow on a small scale of the possible salt separation phenomenon is overwhelmed by uncertainties at the larger scale of the Drift Seepage Submodel or the EBS Flow Submodel. Evaporation is integral, however, to the equilibrium chemistry response surfaces that are the output of the EBS Chemical Environment Submodel. In order to handle this difference, a conservative assumption is implemented in the TSPA-SEIS, using the NaCl deliquescence relative humidity threshold (Section 6.3.5.2.2; note that concentrated salt solutions are referred to as brines in Section 6.3.5.2.2).

Effect on TSPA—Based on a water volume argument, this separation is unlikely to occur, and if it were to occur, it would be limited in spatial extent. The approach taken in the TSPA-SEIS results in a greater likelihood that those conditions conducive to localized corrosion might exist over the entire surface of the WP and is, therefore, conservative. The TSPA-SEIS assumes that there will always be a sufficient volume of brine available for WP degradation regardless of the types of the resulting brines (Section 6.3.5.2.2). In actual repository environments, however, brines formed from evaporation are expected to be limited in volume. For example, obtaining a saturated NaCl brine requires the water to concentrate by more than 1,000 times. That is, 1 L of

seepage water will result in less than 1 mL of NaCl solution. The assumption of sufficient brine volume may lead to a conservative overestimation of the potential for initiating localized corrosion, if the brine volumes are too small to cause a continuous water film over the WP surface.

6.3.5.3.2 Identification of Conservatisms in Submodels and Abstractions

Threshold Relative Humidity for General Corrosion Initiation on WPs—There is no threshold relative humidity for initiation of general corrosion of the WPs. A relative humidity threshold for the initiation of general corrosion clearly exists (ASM International 1987 [DIRS 133378], p. 82). However, there is insufficient information/data to quantify the general corrosion initiation threshold relative humidity for varying water chemistry conditions (SNL 2007 [DIRS 178519], Assumption 5.1). The assumption that no relative humidity threshold for the initiation of corrosion processes exists is conservative because use of a relative humidity threshold would delay the corrosion initiation start time.

Representation of the Critical Threshold Potential—The critical threshold potential ($E_{critical}$) is conservatively represented by the crevice repassivation potential (E_{rcrev}). The crevice repassivation potential (E_{rcrev}) determined from cyclic potentiodynamic polarization tests was selected as a conservative measure for the critical threshold potential ($E_{critical}$). Other less conservative choices for $E_{critical}$ are possible (e.g., the breakdown potential or potentials based on current density thresholds) (SNL 2007 [DIRS 178519], Section 6.4.4.1). The chemical exposure conditions in creviced regions can be more severe than those in noncreviced regions (SNL 2007 [DIRS 178519], Section 1.2). This leads to the measurement of lower repassivation (critical) potentials in creviced versus noncreviced regions.

Stainless Steel Inner Vessel—No corrosion credit is taken for the use of a stainless-steel inner vessel. The 50 mm inner vessel will provide structural support to the thinner outer barrier, and the outer barrier will protect the inner vessel from significant corrosion degradation while it remains intact. The inner vessel could provide some delay of radionuclide release before it fails and also could retard the release rate of radionuclides from the WP (SNL 2007 [DIRS 178519], Section 6.3.3).

General Corrosion Rate of WP Outer Surface—The general corrosion rate of the WP outer surface at a given temperature is time-independent. General corrosion rates of the WP outer surface decrease with time (SNL 2007 [DIRS 178519], Section 6.4.3.5.1). However, there is insufficient information/data to quantify the time dependence. This conservatism is expected to result in the overestimation of WP general corrosion rate (SNL 2007 [DIRS 178519], Figure 7-1).

General Corrosion Rate Distribution for WP Outer Surface—Two coupon (specimen) types are used for general corrosion weight-loss measurements. These are identified as weight-loss coupons and crevice coupons. The general corrosion rate distribution for the WP outer surface is based on the weight-loss of crevice coupons (specimens). The creviced specimens exhibited generally higher general corrosion rates than the noncreviced specimens. This is attributed to the difference in the surface-polishing treatments between the two groups of specimens (SNL 2007

[DIRS 178519], Section 6.4.3.2). This conservatism is expected to overestimate the general corrosion rates on the WP outer surface.

General Corrosion Rate Distribution Adjustment for Patch Size—The general corrosion rate distribution is conservatively adjusted for patch size. The patch size used in the TSPA-SEIS is a factor of four larger than the size of the crevice samples in the experiments that generated the data from which the general corrosion rate was derived. The adjustment method is to effectively use the highest of four sampled values for the patch general corrosion rate (Section 6.3.5.1.2). The approach is conservative because it is probable that not all four samples from the Weibull distribution will have the highest rate.

Crevice Corrosion—The dominant form of localized corrosion is assumed to be crevice corrosion as opposed to pitting corrosion, which occurs on boldly exposed surfaces. Additionally, crevice corrosion is applied to the entire WP surface, though it is unlikely that crevice attack would occur over the entire surface area (SNL 2007 [DIRS 178519], Assumption 5.3). The initiation threshold for crevice corrosion, in terms of exposure conditions, is lower than that for pitting corrosion (SNL 2007 [DIRS 178519], Section 6.4.4). This conservatism is expected to result in the overestimation of the number of WPs that experience localized corrosion.

Effects Of Inhibitive Anions—No credit is taken in the Localized Corrosion Initiation Abstraction for the effects of inhibitive anions other than nitrate. Nitrate ions inhibit localized corrosion initiation. Carbonate and sulfate ions may also have an inhibitive effect on localized corrosion. However, there is insufficient information and/or data to quantify the effect of other inhibitive anions on localized corrosion initiation (SNL 2007 [DIRS 178519], Section 8.3.1). Results for solutions with significant amounts of other potentially inhibitive ions are conservative (SNL 2007 [DIRS 178519], Section 8.3.1).

Localized Corrosion Rate of WP Outer Surface—The localized corrosion propagation rate for the WP outer surface is assumed to propagate at a (time-independent) constant rate (SNL 2007 [DIRS 178519], Assumption 5.4). The localized corrosion propagation rate is known to decrease with increasing time (SNL 2007 [DIRS 178519], Section 6.4.4.8.2); however, there is insufficient information and/or data to quantify the time dependence. This conservatism is expected to result in the overestimation of the number of WPs that fail due to localized corrosion.

Effect of Changing Chemical Environment on Localized Corrosion Propagation—After localized corrosion is initiated, it continues to propagate regardless of any changes in the bulk chemical exposure environment. This is a conservative modeling assumption because no detailed chemistry evolution model of the crevice solution is available (SNL 2007 [DIRS 178519], Section 8.3.1). This conservatism is expected to result in the overestimation of the number of WPs that fail due to localized corrosion.

6.3.5.4 Alternative Conceptual Model(s) for Waste Package and Drip Shield Degradation

An important reason for considering ACMs is to help build confidence that plausible changes in modeling assumptions or simplifications will not change conclusions regarding subsystem and

total system performance. Section 6.2.1 outlines the general consideration and treatment of ACMs used to support the TSPA-SEIS. Conservatism at the subsystem level was used to select the best ACM to use rather than quantitatively propagate multiple ACMs to the TSPA-SEIS. Generally, additional uncertainty is incorporated into the selected conceptual model if more than one ACM is deemed appropriate for use rather than considering multiple ACMs in the TSPA-SEIS. If an ACM appears to be significant at the subsystem level, then an appropriate abstraction is developed for that ACM for consideration within the TSPA-SEIS. The result of the process is documented within the individual analysis model reports. It is important to note that treatment of ACMs within the individual analysis model reports may differ significantly to be consistent with available data and current scientific understanding. Therefore, a brief description of the WP and DS Degradation Submodel ACMs and the Localized Corrosion Initiation Submodel ACMs are presented below and summarized in Table 6.3.5-2.

Parabolic General Corrosion Rate Law for DS—The parabolic general corrosion rate law for DS degradation (SNL 2007 [DIRS 180778], Section 6.5.6) assumes that the increasing oxide layer thickness on the diffusion of oxidizing species to the underlying metal will have an inhibiting effect on corrosion. This model is less conservative than the primary model and was not recommended for inclusion in the evaluation of DS degradation for the TSPA-SEIS.

Decreasing Rate Law for WP—The corrosion rates of metals and alloys tend to decrease with time (SNL 2007 [DIRS 178519], Section 6.4.3.5.1). The time-dependent general corrosion behavior of the WP was not included in the TSPA-SEIS because the constant (time-independent) rate model (for a given temperature) is more conservative and bounds the general corrosion behavior of the WP outer surface over the repository time period.

General Corrosion Rate Law Based on Weight-Loss Samples Only—The ACM discussion for a general corrosion rate law for WP degradation based on plain weight-loss samples (rather than crevice samples) and is found in the analysis model report (SNL 2007 [DIRS 178519], Section 6.4.3.5.2). The weight-loss data was fit to a Weibull distribution using maximum likelihood estimators (i.e., using the same methods applied to the crevice sample data). A comparison of the general corrosion rate distribution resulting from fitting the 5-year exposed weight-loss sample to the Weibull distributions based on the crevice sample data shows that this conceptual model is less conservative relative to the base case general corrosion model (SNL 2007 [DIRS 178519], Figures 6-28 and 6-23).

Critical Temperature-Based Localized Corrosion Initiation—The evolution of the WP temperature with time, coupled with the knowledge of the critical temperature for the initiation of localized corrosion (pitting/crevice corrosion), can be used to determine when localized corrosion initiates (SNL 2007 [DIRS 178519], Section 6.4.4.8.1). However, the test conditions at which the required critical temperatures were measured are not directly relevant to the potential environments on the WP surface. In addition, the critical temperature-based model does not account for the effects of electrochemical characteristics of the solution contacting the metal. Therefore, the critical temperature-based model is not considered in the TSPA.

Coupled Environmental Fracture Model—The coupled environment fracture model for stress corrosion crack growth rate was evaluated as an ACM for SCC (SNL 2007 [DIRS 181953], Section 6.4.6). The model, based on charge conservation, incorporates the effects of oxygen

concentration, flow rate, and the conductivity of the external environment, as well as accounting for the effect of stress on crack growth. The model underestimated the crack growth rate, as compared to the slip dissolution-film rupture (SDFM) model, when both models were applied to predict the crack growth rate.

Time-Dependent Localized Corrosion Rate—An ACM for localized corrosion penetration is a time-dependent growth law of the form (SNL 2007 [DIRS 178519], Section 6.4.4.8.2):

$$D = k \times t^n \qquad \text{(Eq. 6.3.5-18)}$$

where D is the depth of penetration, t is time, and k is a growth constant. However, insufficient penetration rate data are available, especially for relatively new materials such as Alloy 22, to determine the values of k and n for the exposure conditions relevant to the repository. This ACM was not recommended for incorporation into the TSPA-SEIS because the data needed to apply the model can only be estimated approximately from open literature. The time-independent constant penetration rate model used in the TSPA-SEIS is more conservative.

Passive Film Breakdown Potential for the Determination of Critical Potential—An alternative technique for the determination of critical potential could be to use the passive film breakdown potential obtained from the forward scan of cyclic potentiodynamic polarization tests (SNL 2007 [DIRS 178519], Section 6.4.4.1). This technique would not account for the (often slow) kinetics of localized corrosion initiation and may not be appropriate for modeling the long time periods involved in repository environments. Furthermore, the breakdown potential is likely to be much higher when the passive film has been formed over long time periods, allowing for a decrease in the film defect density.

WP Surface Area Subjected to Localized Corrosion—No information is available regarding local environments on the WP; therefore, the area affected by localized corrosion due to seepage is based on the fraction of the WP surface exposed to seepage. TSPA has conservatively taken the area affected by localized corrosion to be the area wetted by seepage. Therefore, the entire surface area can potentially undergo localized corrosion. A distribution for the minimum area affected by localized corrosion was developed (minimum of 0.05 percent and maximum of the percent of area wetted by seepage) (SNL 2007 [DIRS 178519], Section 6.4.4.8.3). The ACM has not been implemented in the TSPA-SEIS. Sensitivity analyses have shown that dose results are insensitive to the magnitude of the failed area on the WP once the failed area has reached about 5 percent of the WP surface area.

No ACMs were recommended for inclusion in the TSPA-SEIS.

Table 6.3.5-1. Drip Shield and Waste Package Degradation Mechanisms and Their Disposition for Implementation in the TSPA-SEIS

Failure Mechanism	Drip Shield Postclosure Assessment		Waste Package Postclosure Assessment	
	Included in TSPA-SEIS	Screened Out[a]	Included in TSPA-SEIS	Screened Out[a]
General Corrosion	X		X	
Localized Corrosion		X	X	
Stress Corrosion Cracking		X[b]	X	
Microbially Influenced Corrosion		X	X	
Weld Flaws due to Manufacturing Defects		X	X	
Aging and Phase Instability		X		X
Hydrogen Induced Cracking		X		X
Mechanical Impacts		X[c]		X[c]
Radiolysis		X		X

NOTE: [a] Excluded FEPs.

[b] Included FEP, but has not been implemented since advective flow through DS cracks has been excluded.

[c] Screened out for the Nominal Scenario Class; included for both modeling cases of the Seismic Scenario Class.

Table 6.3.5-2. Alternative Conceptual Models Considered for Drip Shield and Waste Package Degradation

Alternative Conceptual Models	Key Assumptions	Screening Assessment and Basis
Parabolic GC rate law for DS degradation (SNL 2007 [DIRS 180778] ,Section 6.5.6)	Assumes that the increasing oxide layer thickness on diffusion of oxidizing species to the underlying metal will have an inhibiting effect on corrosion.	Model is less conservative than the primary model.
Decreasing GC rate law for WP degradation (SNL 2007 [DIRS 178519], Section 6.4.3.5.1)	GC rates of metals and alloys tend to decrease with time.	The time-dependent GC behavior of the WP was not included in the TSPA-SEIS because the constant (time-independent) rate model (for a given temperature) is more conservative and bounds the general corrosion behavior of the WP outer surface over the repository time period.
GC Rate Based on Weight-Loss Samples Only (SNL 2007 [DIRS 178519], Section 6.4.3.5.2)	A GC rate law for WP degradation based on plain weight-loss samples (rather than crevice samples) was developed. The weight-loss data were fit to a Weibull distribution using maximum likelihood estimators (i.e., using the same methods applied to the crevice sample data).	A comparison of the general corrosion rate distribution resulting from fitting the 5-yr exposed weight-loss samples to the Weibull distribution based on the crevice sample data shows that this conceptual model is less conservative relative to the base case general corrosion model (SNL 2007 [DIRS 178519], Figures 6-28 and 6-23).

Table 6.3.5-2. Alternative Conceptual Models Considered for Drip Shield and Waste Package Degradation (Continued)

Alternative Conceptual Models	Key Assumptions	Screening Assessment and Basis
Critical Temperature-Based Localized Corrosion Initiation Model (SNL 2007 [DIRS 178519], Section 6.4.4.8.1)	The evolution of WP temperature with time, coupled with knowledge of the critical temperature for the initiation of LC (pitting/crevice corrosion), can be used to determine when LC initiates.	Test conditions at which the required critical temperatures were measured are not directly relevant to the potential environments on the WP surface. The model does not account for the effects of electrochemical characteristics of the solution contacting the metal. The model is not used in the TSPA-SEIS.
Coupled environment fracture model for stress corrosion crack growth rate (SNL 2007 [DIRS 181953], Section 6.4.6)	The model, based on charge conservation, incorporates the effects of oxygen concentration, flow rate, and the conductivity of the external environment, as well as accounting for the effect of stress on crack growth.	Model underestimates the crack growth rate, as compared to the slip dissolution/film rupture model, when both models were applied to predict the crack growth rate.
Localized corrosion penetration as a time-dependent growth law (SNL 2007 [DIRS 178519], Sections 6.4.4.8.2 and 7.2.5)	Once initiated, the localized corrosion penetration rate decreases with increasing time.	Data needed to apply the model can only be estimated approximately from open literature. The time-independent constant penetration rate model is more conservative.
Passive film breakdown potential for determination of critical potential (SNL 2007 [DIRS 178519], Section 6.4.4.1)	An alternative technique for the determination of critical potential would be to use the passive film breakdown potential (obtained from the forward scan of the cyclic potentiodynamic polarization tests).	This technique would not account for the (often slow) kinetics of LC initiation and may not be appropriate for modeling the long time periods involved in repository environments. Furthermore, the breakdown potential is likely to be much higher when the passive film forms over long time periods allowing for a decrease in the film defect density.
No information is available regarding local environments on the WP; therefore, the area affected by LC due to seepage is based on the fraction of the WP surface exposed to seepage. TSPA has conservatively taken the area affected by LC to be the area wetted by seepage. Therefore, the entire surface area can potentially undergo LC.	A distribution for the minimum area affected by LC was developed (minimum of 0.05 percent and maximum of the percent of area wetted by seepage) (SNL 2007 [DIRS 178519], Section 6.4.4.8.3).	The ACM has not been implemented in the TSPA-SEIS. Sensitivity analyses have shown that dose results are insensitive to the magnitude of the failed area on the WP once the failed area has reached about 5% of the WP surface area.

Table 6.3.5-3. Uncertain Inputs to the TSPA-SEIS for Generalized Corrosion of the Drip Shield and Waste Package and Stress Corrosion Cracking of the Waste Package

Parameter Name	Mathematical Model Symbol	Description	Units	Distribution Specification	Remarks
WDDSBenignGC_Mean_a	None	DS-underside general corrosion rate (epistemic uncertainty)	nm/yr	Normal Mean = 5.15 SD = 0.831	DTN: SN0704PADSGCMT.001_R2, file: TSPA Implementation_DS GC Models.pdf [DIRS 182122]
WDDSAggrGC_Mean_a	None	DS-topside general corrosion rate (epistemic uncertainty)	nm/yr	Student's-t Mean = 46.1 SD = 1.19 Degrees of Freedom: 5	DTN: SN0704PADSGCMT.001_R2, file: TSPA Implementation_DS GC Models.pdf [DIRS 182122]
WDlnR_ESC_L_cdf WDlnR_ESC_M_cdf WDlnR_ESC_H_cdf	ln R_o	Natural logarithm of general corrosion rate: 60°C: WP (aleatory uncertainty)	none	Three CDFs corresponding to low, medium, and high levels of uncertainty in GC_shape and GC_scale parameters (fourth and fifth rows of this table)	Developed by TSPA from GC_scale and GC_shape parameters DTN: MO0707WPDRIPSD.000
GC_shape	None	Shape parameter for Weibull distribution (WP GC)	none	1.380 (low): 5% realizations 1.476 (medium): 90% realizations 1.578 (high): 5% realizations Different values are uncertainty. Overall distribution is spatial variability.	DTN: MO0703PAGENCOR.001_R4, file: BaseCase GC CDFs.xls [DIRS 182029]
GC_scale	None	Scale parameter for Weibull distribution (WP GC)	none	6.628 (low): 5% realizations 8.134 (medium): 90% realizations 9.774 (high): 5% realizations Different values are uncertainty. Overall distribution is spatial variability.	DTN: MO0703PAGENCOR.001_R4, file: BaseCase GC CDFs.xls [DIRS 182029]

Table 6.3.5-3. Uncertain Inputs to the TSPA-SEIS for Generalized Corrosion of the Drip Shield and Waste Package and Stress Corrosion Cracking of the Waste Package (Continued)

Parameter Name	Mathematical Model Symbol	Description	Units	Distribution Specification	Remarks
C1_GenCorr_A22_a	C1	Temperature dependence-slope term of WP GC rate (epistemic uncertainty)	K	Normal (truncated at +2 SD and -3 SD) Mean = 4,905 SD = 1,413	DTN: MO0703PAGENCOR.001_R4, file: BaseCase GC CDFs.xls [DIRS 182029]
Defect_Size_a	λ_s	Flaw size distribution parameter (epistemic uncertainty)	mm^{-1}	Gamma Mean = n_f / S_f SD = sqrt (n_f)/S_f	DTN: MO0701PASHIELD.000_R2, file: Tables for DTN Readme.doc [DIRS 180508]
Defect_Count_a	λ_c	Flaw count distribution parameter (epistemic uncertainty)	flaws/ mm^3	Gamma Mean = (n_f + ½)/V_f SD = sqrt (n_f + ½)/V_f	DTN: MO0701PASHIELD.000_R2, file: Tables for DTN Readme.doc [DIRS 180508]
Z_OL_a	z	Uncertainty variation in the yield strength of the outer WP closure lid (epistemic uncertainty).	None	Normal (truncated at ±3 SD) Mean = 0 SD = 1	DTN: MO0702PASTRESS.002_R2, file: Model Output DTN.doc, Table 8-15 [DIRS 180514]
n_SCC_a	n	Stress corrosion cracking growth rate exponent (repassivation rate) (epistemic uncertainty)	None	Normal (truncated at ±2 SD) Mean = 1.165 SD = 0.115	DTN: MO0702PASTRESS.002_R2, file: Model Output DTN.doc, Table 8-15 [DIRS 180514]

Table 6.3.5-3. Uncertain Inputs to the TSPA-SEIS for Generalized Corrosion of the Drip Shield and Waste Package and Stress Corrosion Cracking of the Waste Package (Continued)

Parameter Name	Mathematical Model Symbol	Description	Units	Distribution Specification	Remarks
Stress_Thresh_SCC_a		Stress threshold for SCC nucleation (epistemic uncertainty)	MPa	Uniform distribution from 315.9 to 368.55.	DTN: MO0702PASTRESS.002_R2, file: Model Output DTN.doc, Table 8-15 [DIRS 180514] This parameter combines the definition for Stress_Thresh_A22 with Yield_Strength_A22 defined the first row of Table 8-15.
MIC_A22_a	f_{MIC}	MIC general corrosion enhancement factor (aleatory uncertainty)	None	Uniform Lower bound = 1 Upper bound = 2	DTN: MO0703PAGENCOR.001_R4, file: MIC Summary.pdf [DIRS 182029]
MIC_RHThresh_a	None	Relative humidity threshold for MIC (epistemic uncertainty)	None	Uniform distribution between 75% to 90%	DTN: MO0703PAGENCOR.001_R4, file: MIC Summary.pdf [DIRS 182029]

Table 6.3.5-4. Uncertain Inputs to Localized Corrosion Initiation Stand-Alone Model

Parameter Name	Model Symbol	Description	Units	Distribution Specification	Remarks
Two_StDev_a0_a	None	Stochastic used to develop the coefficients in crevice repassivation potential functional form (epistemic uncertainty)	NA	Normal Distribution Mean = 0 SD = 1	
Two_StDev_a1_a					
Two_StDev_a2_a					
Two_StDev_a3_a					
Two_StDev_a4_a					
LC_eps_rcrev_a	None	Error term of crevice repassivation potential (epistemic uncertainty)	mV SSC	Normal distribution with a mean of zero and a standard deviation of 45.055	DTN: MO0703PAGENCOR.001_R4, file: Mathcad – Ercrev_Ecorr3.pdf, p. 5 [DIRS 182029]
Two_StDev_c0_a	None	Stochastic used to develop the coefficients in corrosion potential functional form (epistemic uncertainty)	NA	Normal Distribution Mean = 0 SD = 1	
Two_StDev_c1_a					
Two_StDev_c2_a					
Two_StDev_c3_a					
Two_StDev_c4_a					
Two_StDev_c5_a					
Two_StDev_c6_a					
LC_eps_corr_a	None	Error term of long-term corrosion potential model (epistemic uncertainty)	mV SSC	Normal distribution with a mean of zero and a standard deviation of 85.265	DTN: MO0703PAGENCOR.001_R4, file: Mathcad – Ercrev_Ecorr3.pdf, p. 8[DIRS 182029]
LC_rate_a		Localized corrosion penetration rate (epistemic uncertainty)	mm/yr	Log uniform 0 percentile = 0.0127 50th percentile = 0.127 100th percentile = 1.27	DTN: MO0703PAGENCOR.001_R4, file: LC_Propagation.pdf [DIRS 182029]
Seepage_Water_Type_a	N/A	Seepage water type (epistemic uncertainty).	None	Discrete Uniform [0.25,1][0.25,2][0.25,3] [0.25,4]	SNL 2007 [DIRS 177412], Section 6.15.1.

Table 6.3.5-4. Uncertain Inputs to Localized Corrosion Initiation Stand-Alone Model (Continued)

TSPA_LA Parameter Name	Model Symbol	Description	Units	Distribution Specification	Remarks
PCE_Delta_PCO2_a	N/A	Uncertainty in the partial pressure of CO_2 (epistemic uncertainty)	NA	Uniform distribution from -1 to 1.	DTN: SNL 2007 [DIRS 177412], Section 6.15.1
PCE_Cl_MU_RH_0_20_a	N/A	Uncertainty in chloride concentration (epistemic uncertainty)	NA	Triangular Distribution Minimum: -0.7 Most Likely: 0.0 Maximum: 0.7	DTN: SN0703PAEBSPCE.007_R1, file: PCE_IDPS_uncertainties.xls [DIRS 180177]
PCE_Cl_MU_RH_20_40_a	N/A	Uncertainty in chloride concentration (epistemic uncertainty)	NA	Triangular Distribution Minimum: -0.5 Most Likely: 0.0 Maximum: 0.5	DTN: SN0703PAEBSPCE.007_R1, file: PCE_IDPS_uncertainties.xls [DIRS 180177]
PCE_Cl_MU_RH_40_65_a	N/A	Uncertainty in chloride concentration (epistemic uncertainty)	NA	Triangular Distribution Minimum: -0.4 Most Likely: 0.0 Maximum: 0.4	DTN: SN0703PAEBSPCE.007_R1, file: PCE_IDPS_uncertainties.xls [DIRS 180177]
PCE_Cl_MU_RH_65_85_a	N/A	Uncertainty in chloride concentration (epistemic uncertainty)	NA	Triangular Distribution Minimum: -0.1 Most Likely: 0.0 Maximum: 0.1	DTN: SN0703PAEBSPCE.007_R1, file: PCE_IDPS_uncertainties.xls [DIRS 180177]
PCE_Cl_MU_RH_85_100_a	N/A	Uncertainty in chloride concentration (epistemic uncertainty)	NA	Triangular Distribution Minimum: -0.0 Most Likely: 0.0 Maximum: 0.0	DTN: SN0703PAEBSPCE.007_R1, file: PCE_IDPS_uncertainties.xls [DIRS 180177]
PCE_Cl_N_MU_RH_40_65_a	N/A	Uncertainty in combined chloride and nitrate concentration (epistemic uncertainty)		Triangular Distribution Minimum: -0.57 Most Likely: 0.0 Maximum: 0.57	DTN: SN0703PAEBSPCE.007_R1, file: PCE_IDPS_uncertainties.xls [DIRS 180177]

Table 6.3.5-4. Uncertain Inputs to Localized Corrosion Initiation Stand-Alone Model (Continued)

TSPA_LA Parameter Name	Model Symbol	Description	Units	Distribution Specification	Remarks
PCE_Cl_N_MU_RH_65_85_a	N/A	Uncertainty in combined chloride and nitrate concentration (epistemic uncertainty)	NA	Triangular Distribution Minimum: -0.22 Most Likely: 0.0 Maximum: 0.22	DTN: SN0703PAEBSPCE.007_R1, file: PCE_IDPS_uncertainties.xls [DIRS 180177]
PCE_Cl_N_MU_RH_85_100_a	N/A	Uncertainty in combined chloride and nitrate concentration (epistemic uncertainty)	NA	Triangular Distribution Minimum: -0.0 Most Likely: 0.0 Maximum: 0.0	DTN: SN0703PAEBSPCE.007_R1, file: PCE_IDPS_uncertainties.xls [DIRS 180177]
PCE_Cl_NO3_MU_RH_0_20_a	N/A	Uncertainty in nitrate-to-chloride ratio (epistemic uncertainty)		Triangular Distribution Minimum: -1.4 Most Likely: 0.0 Maximum: 1.4	DTN: SN0703PAEBSPCE.007_R1, file: PCE_IDPS_uncertainties.xls [DIRS 180177]
PCE_Cl_NO3_MU_RH_20_65_a	N/A	Uncertainty in nitrate-to-chloride ratio (epistemic uncertainty)	NA	Triangular Distribution Minimum: -0.5 Most Likely: 0.0 Maximum: 0.5	DTN: SN0703PAEBSPCE.007_R1, file: PCE_IDPS_uncertainties.xls [DIRS 180177]
PCE_Cl_NO3_MU_RH_65_85_a	N/A	Uncertainty in nitrate-to-chloride ratio (epistemic uncertainty)	N/A	Triangular Distribution Minimum: -0.2 Most Likely: 0.0 Maximum: 0.2	DTN: SN0703PAEBSPCE.007_R1, file: PCE_IDPS_uncertainties.xls [DIRS 180177]
PCE_Cl_NO3_MU_RH_85_100_a	N/A	Uncertainty in nitrate-to-chloride ratio (epistemic uncertainty)	NA	Triangular Distribution Minimum: -0.0 Most Likely: 0.0 Maximum: 0.0	DTN: SN0703PAEBSPCE.007_R1, file: PCE_IDPS_uncertainties.xls [DIRS 180177]
PCE_pH_Uncert_RH_0_65_a	N/A	Uncertainty in pH (epistemic uncertainty).	NA	Triangular Distribution Minimum: -2.0 Most Likely: 0.0 Maximum: 2.0	DTN: SN0703PAEBSPCE.007_R1, file: PCE_IDPS_uncertainties.xls [DIRS 180177]

Table 6.3.5-4. Uncertain Inputs to Localized Corrosion Initiation Stand-Alone Model (Continued)

TSPA_LA Parameter Name	Model Symbol	Description	Units	Distribution Specification	Remarks
PCE_pH_Uncert_RH_65_75_a	N/A	Uncertainty in pH (epistemic uncertainty)	NA	Triangular Distribution Minimum: -1.0 Most Likely: 0.0 Maximum: 1.0	DTN: SN0703PAEBSPCE.007_R1, file: PCE_IDPS_uncertainties.xls [DIRS 180177]
PCE_pH_Uncert_RH_75_100_a	N/A	Uncertainty in pH (epistemic uncertainty)	NA	Discrete Distribution	DTN: SN0703PAEBSPCE.007_R1, file: PCE_IDPS_uncertainties.xls [DIRS 180177]
Seepage_Uncertainty_a	N/A	Epistemic uncertainty in seepage scale factor	None	Uniform (0,1) Note that the sampled value form the distribution is multiplied by 1.7321 in the SEEPAGEDLL_LA V1.3 software (STN: 11076-1.3-00)	DTN: LB0407AMRU0120.001_R0, file:Summary_seepage_abstraction.doc [DIRS 173280]
Alpha_Uncert_Lith_a	$1/\alpha$	Epistemic uncertainty in capillary strength in lithophysal units	Pa	Triangular Mode = 0 Min = −105 Max = 105	DTN: LB0407AMRU0120.001_R0, file:Summary_seepage_abstraction.doc [DIRS 173280]
Alpha_Uncert_NonLith_a	$1/\alpha$	Epistemic uncertainty in capillary strength in non-lithophysal units	Pa	Triangular Mode = 0 Min. = −105 Max. = 105	DTN: LB0407AMRU0120.001_R0, file:Summary_seepage_abstraction.doc [DIRS 173280]
LogK_Uncert_Lith_a	*log k*	Epistemic uncertainty in fracture permeability in lithophysal units	None	Triangular Mode = 0 Min. = −0.92 Max. = 0.92	DTN: LB0407AMRU0120.001_R0, file:Summary_seepage_abstraction.doc [DIRS 173280]

Table 6.3.5-4. Uncertain Inputs to Localized Corrosion Initiation Stand-Alone Model (Continued)

TSPA_LA Parameter Name	Model Symbol	Description	Units	Distribution Specification	Remarks
LogK_Uncert_NonLith_a	*log k*	Epistemic uncertainty in fracture permeability in non-lithophysal units	None	Triangular Mode = 0 Min. = −0.68 Max. = 0.68	DTN: LB0407AMRU0120.001_R0, file:Summary_seepage_abstraction.doc [DIRS 173280]
dt_dRh_uncertainty	*N/A*	Epistemic uncertainty in the thermal conductivity of the rubble resulting from a seismic event	None	Discrete [0.5,1][0.5,2]	DTN: MO0505SPAROCKM.000_R0 [DIRS 173893]
Infiltration_Scenario_a	*N/A*	Uncertainty in infiltration scenario (10th, 30th, 50th, and 90th percentile) (epistemic uncertainty)	None	Discrete [0.6191,1][0.1568,2][0.1645, 3][0.0596,4]	DTN: LB0701PAWFINFM.001_R0, file: factors.doc [DIRS 179283]
Thermal_Conductivity_Uncert_a	*N/A*	Uncertainty in thermal conductivity (low, medium, or high) (epistemic uncertainty)	None	Discrete (p. v) [0.29,1], [0.37,2], [0.34,3]	SNL 2007 [DIRS 181383], Table 6.3-47[a]
Vol_Rubble_Max_Lith_a	$V_{rubble\_\max}^{Lith}$	Volume of lithophysal rock that must fall to fill the drift	m^3/m	Uniform (30,120)	DTN: MO0703PASEISDA.002_R4, Table 1-16 [DIRS 183156]
Vol_Rubble_Max_NonLith_a	$V_{rubble\_\max}^{NonLith}$	Volume of nonlithophysal rock that must fall to fill the drift	m^3/m	Uniform (30,120)	DTN: MO0703PASEISDA.002_R4, Table 1-16 [DIRS 183156]
WDDSBenignGC_Mean_a		DS-underside GC rate (epistemic uncertainty)	nm/yr	Normal Mean=5.15 SD=0.831	DTN: SN0704PADSGCMT.001_R2, file: TSPA Implementation_DS GC Models.pdf [DIRS 182122]
WDDSAggrGC_Mean_a		DS-topside GC rate (epistemic uncertainty)	nm/yr	Normal Mean=46.1 SD=1.19	DTN: SN0704PADSGCMT.001_R2, file: TSPA Implementation_DS GC Models.pdf [DIRS 182122]

Table 6.3.5-4. Uncertain Inputs to Localized Corrosion Initiation Stand-Alone Model (Continued)

TSPA_LA Parameter Name	Model Symbol	Description	Units	Distribution Specification	Remarks
C1_GenCorr_A22_a	C_1	Temperature dependent-slope term for GC rate (epistemic uncertainty)	K	Normal (truncated at -3 SD and +2 SD) Mean = 4,905 SD = 1,413	DTN: MO0703PAGENCOR.001_R4, file: BaseCase GC CDFs.xls [DIRS 182029]
MIC_A22_a		MIC general corrosion enhancement factor (aleatory uncertainty)		Uniform(1,2)	DTN: MO0703PAGENCOR.001_R4, file: MIC Summary.pdf [DIRS 182029]
MIC_RHThresh_a		Relative humidity threshold for MIC (epistemic uncertainty)		Uniform(75%,90%)	DTN: MO0703PAGENCOR.001_R4, file: MIC Summary.pdf [DIRS 182029]
lnR0_a	ln R_o	Rate used to calculate the first GC penetration (aleatory uncertainty)	nm/yr	Weibull scale = 8.134 nm/yr shape = 1.476 Scaled by the average coupon rate with a size factor of 4	Developed by TSPA from GC_scale and GC_Shape parameters in DTN: MO0702PAGENCOR.001, file: BaseCase GC CDFs.xls [DIRS 182029] Output DTN: MO0707WPDRIPSD.000

INTENTIONALLY LEFT BLANK

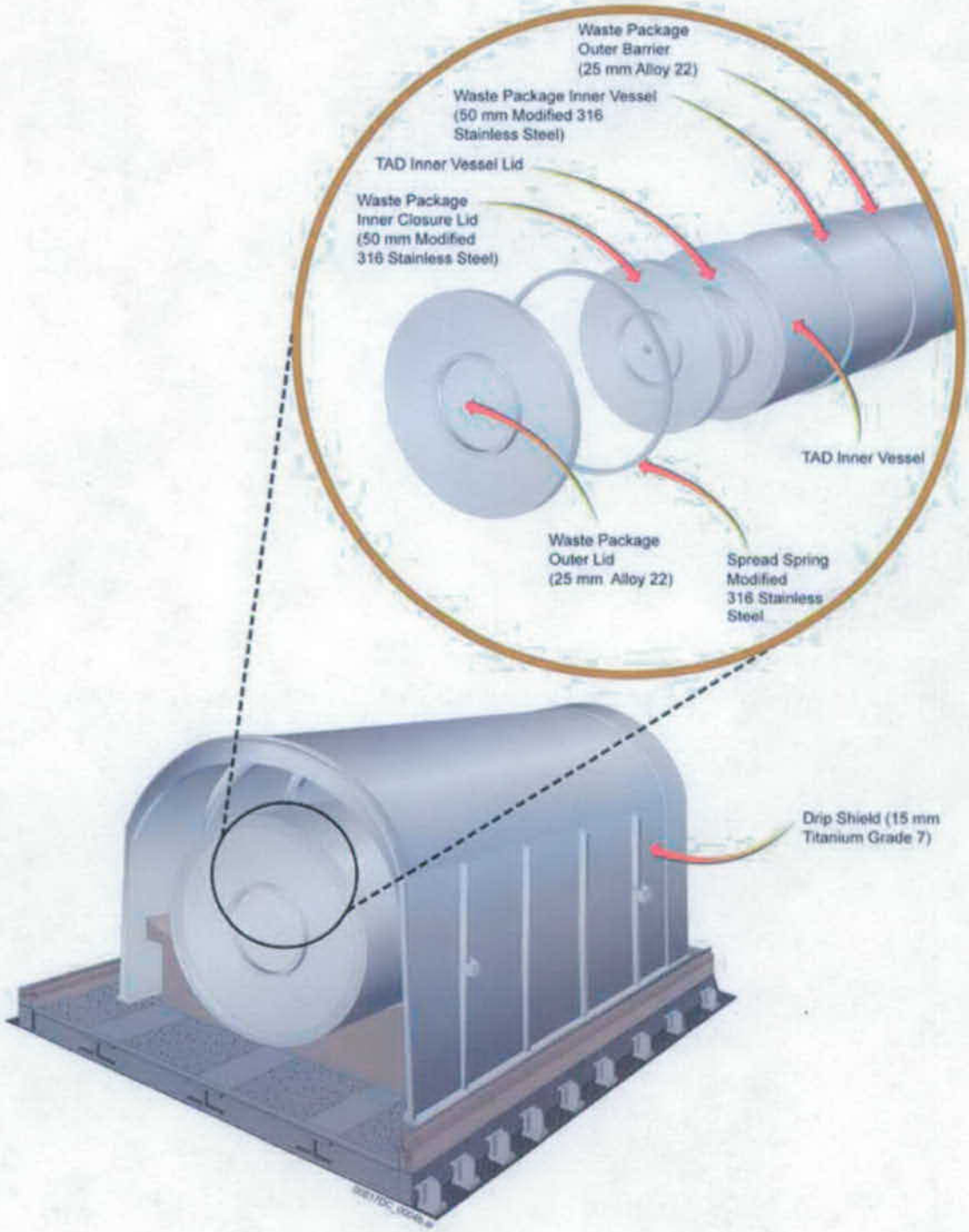

Sources: SNL 2007 [DIRS 179394] and [DIRS 179354]

Figure 6.3.5-1. Schematic Design of the Drip Shield and Waste Package

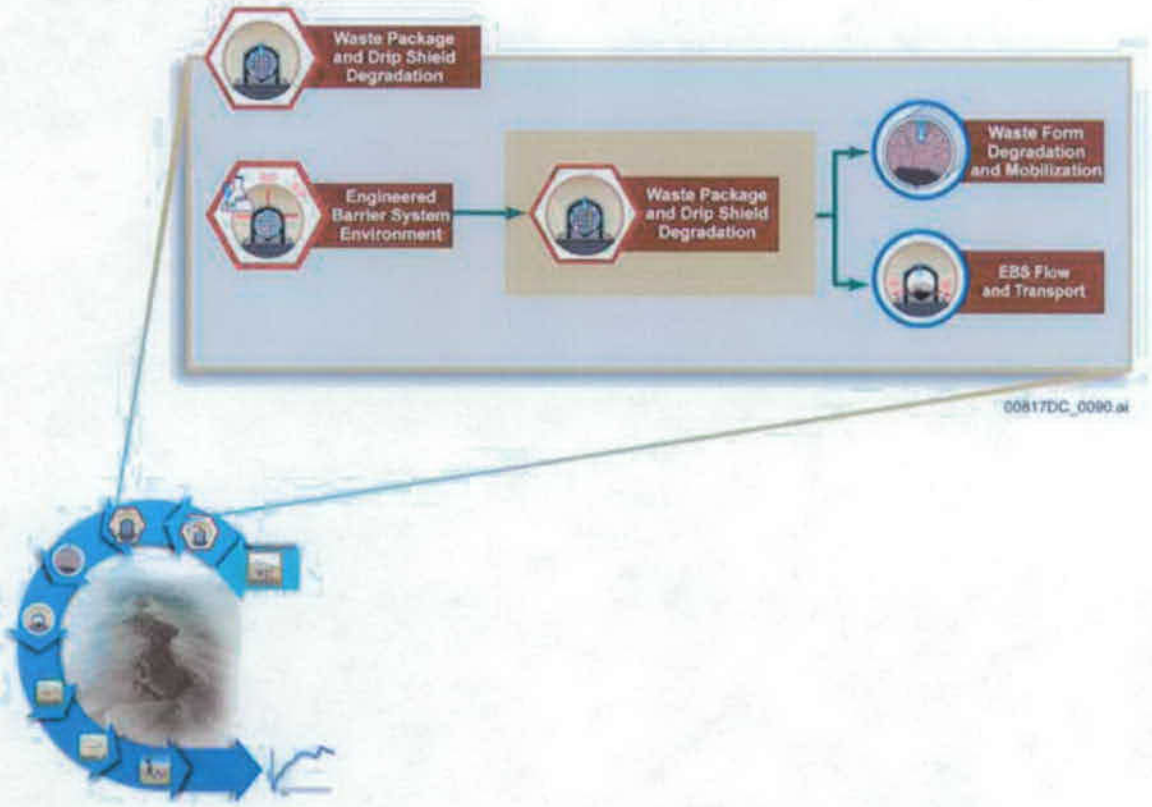

Figure 6.3.5-2. Information Flow Diagram for Waste Package and Drip Shield Degradation

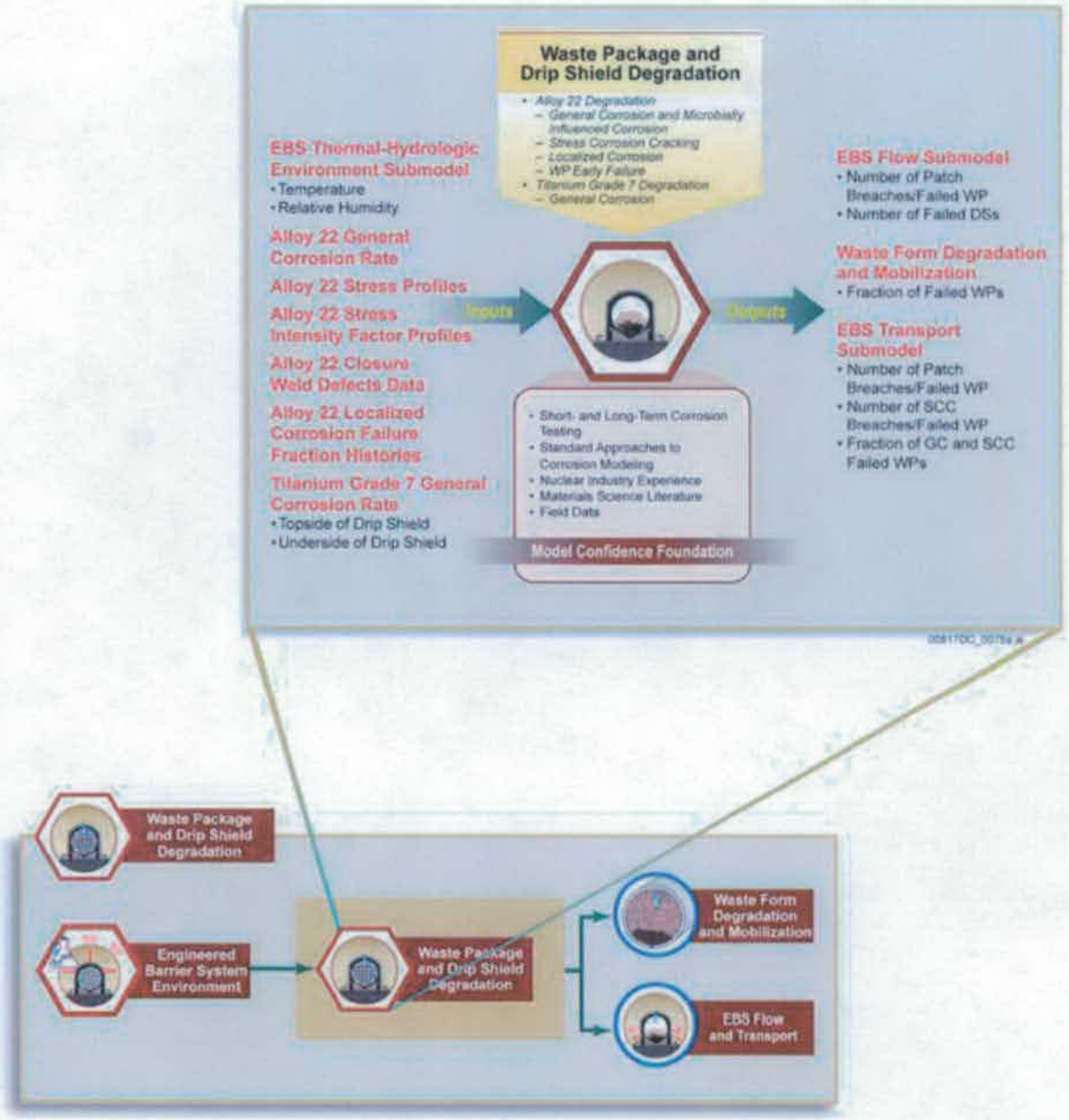

Figure 6.3.5-3. Inputs, Outputs, and Basis for Model Confidence for the Waste Package and Drip Shield Degradation Submodel

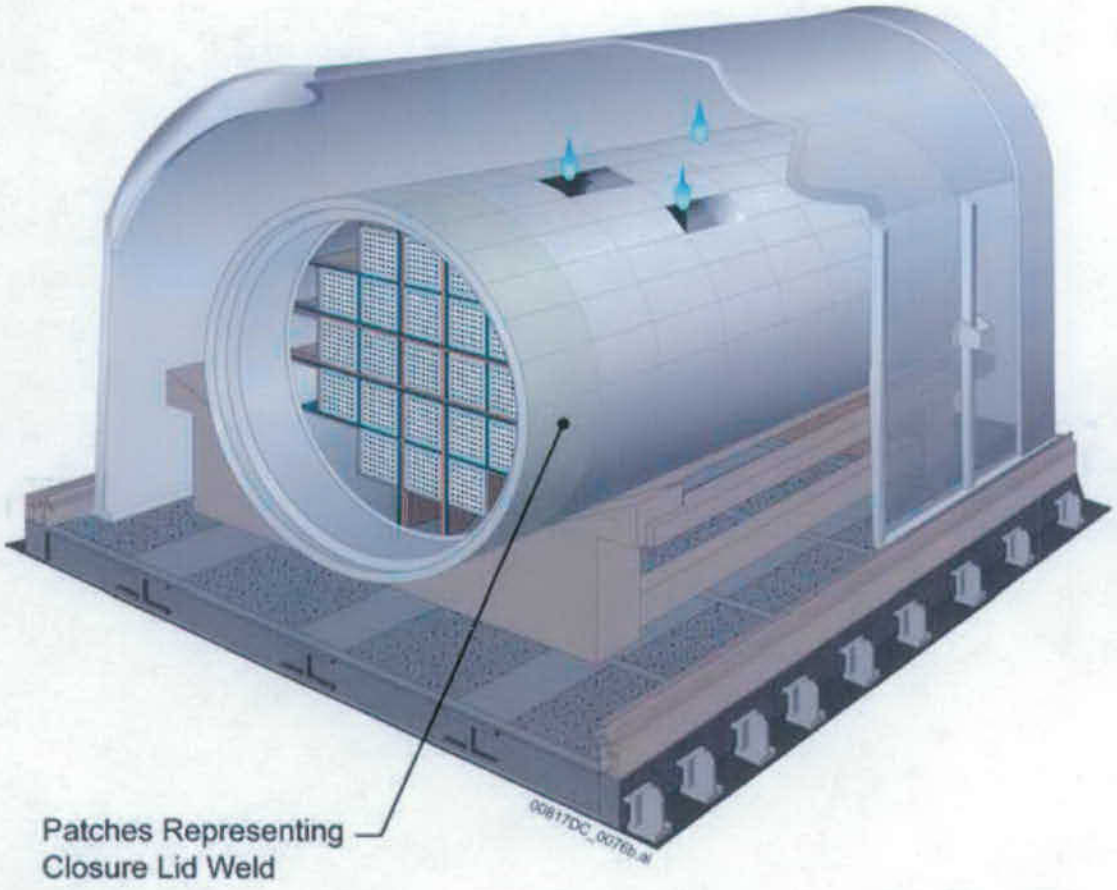

NOTE: Figure is for illustration purposes only and is not representative of repository postclosure performance.

Figure 6.3.5-4. Schematic of Waste Package Implementation in the Waste Package Degradation Model Showing a Waste Package in a Dripping Environment After a Drip Shield Failure and Patches Degrading from General Corrosion on the Surface of the Waste Package

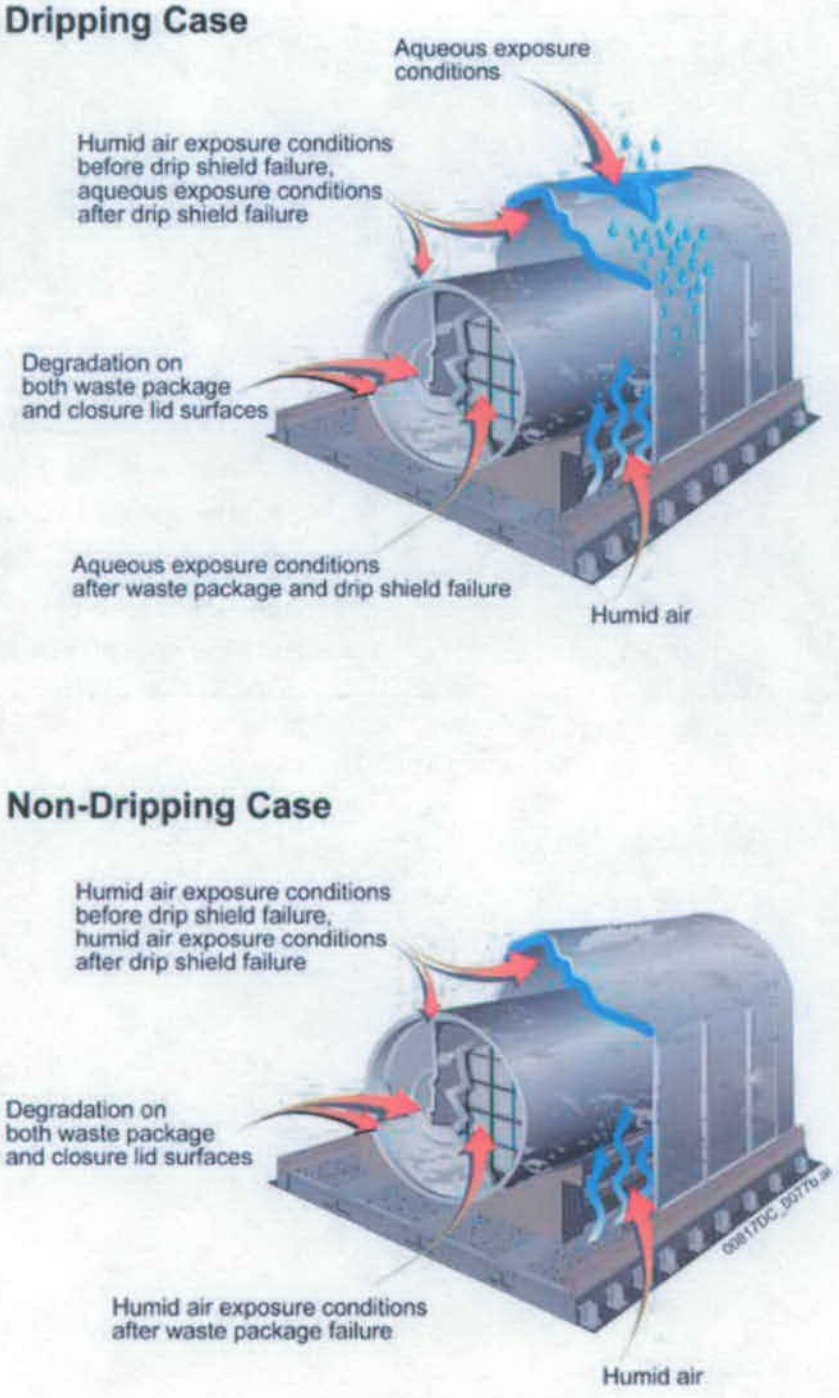

Figure 6.3.5-5. Exposure Conditions and Degradation Processes for the Drip Shield and Waste Package

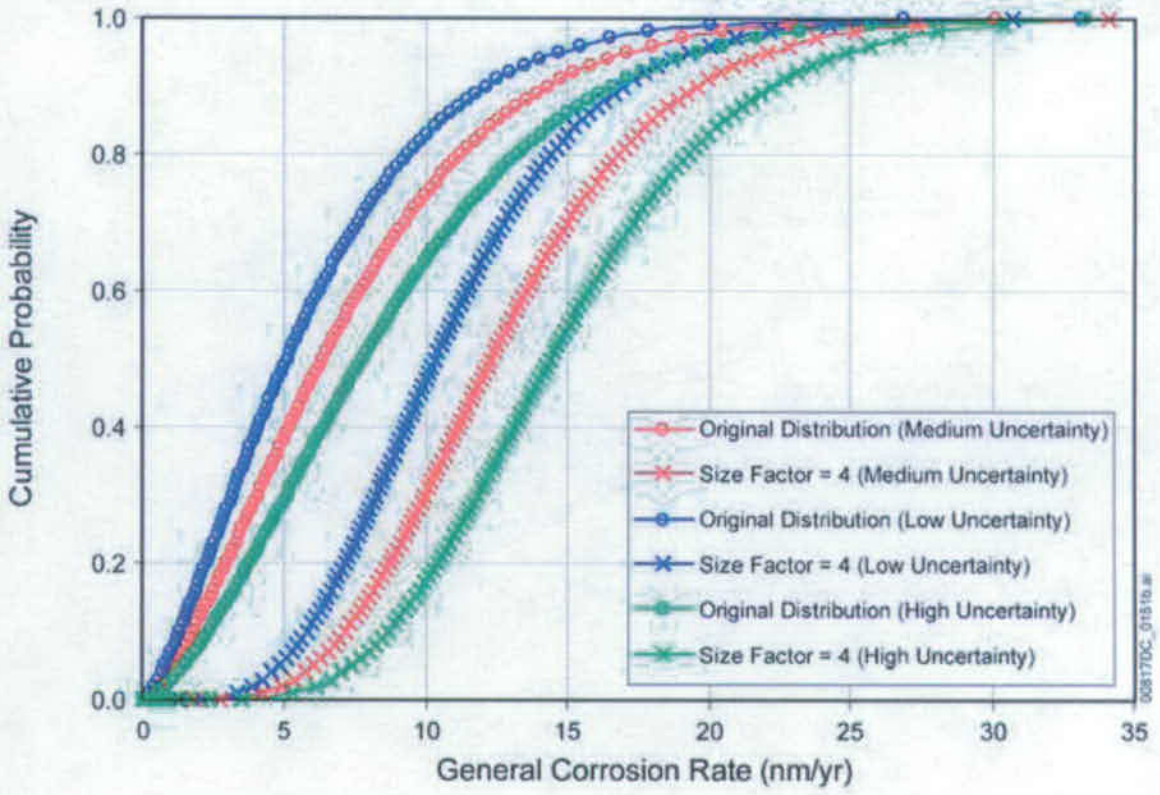

Source: Output DTN: MO0707WPDRIPSD.000

Figure 6.3.5-6. Effect of Scaling the General Corrosion Distribution by a Size Factor of Four

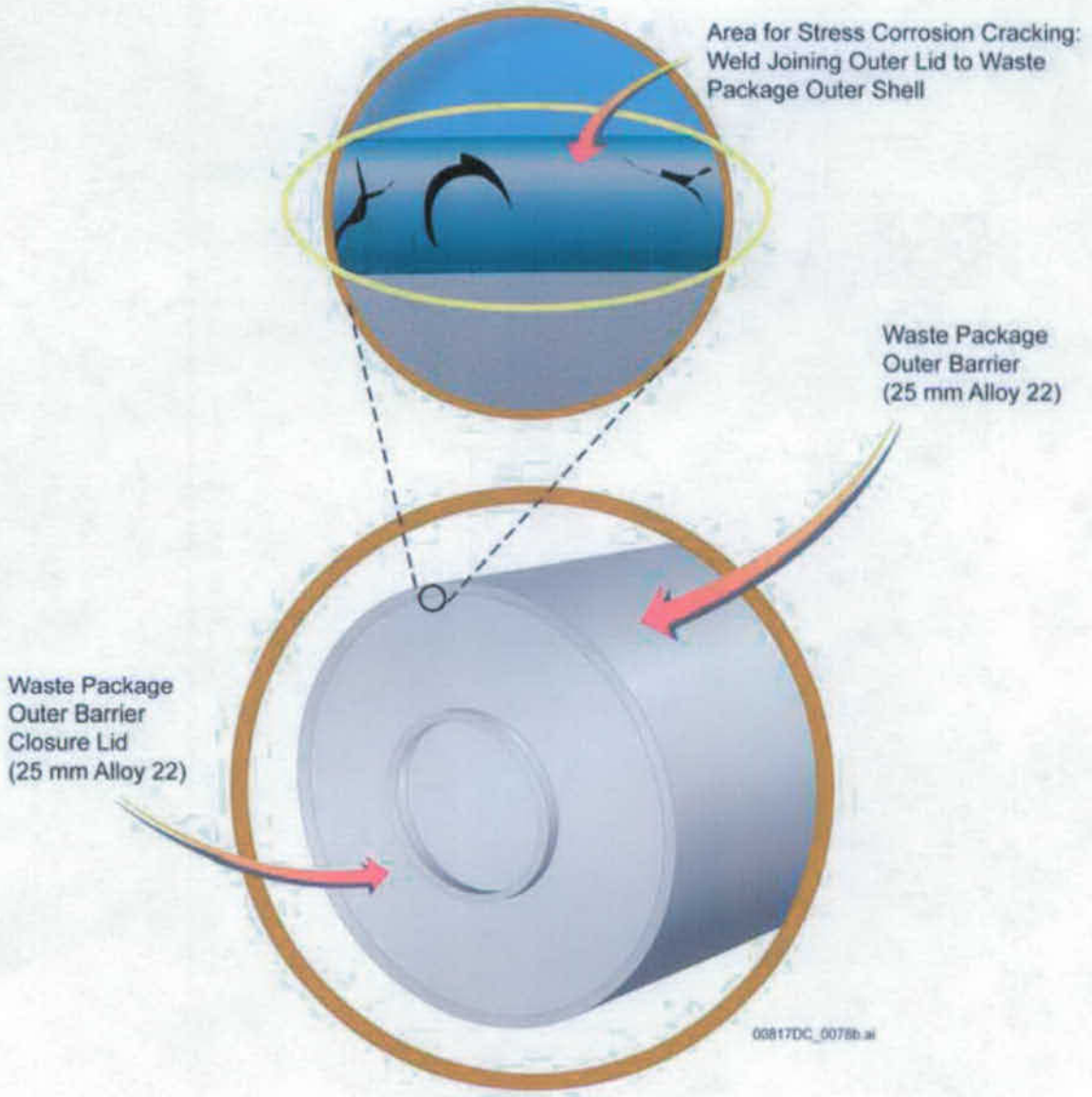

Figure 6.3.5-7. Schematic of Waste Package Closure Lid Design

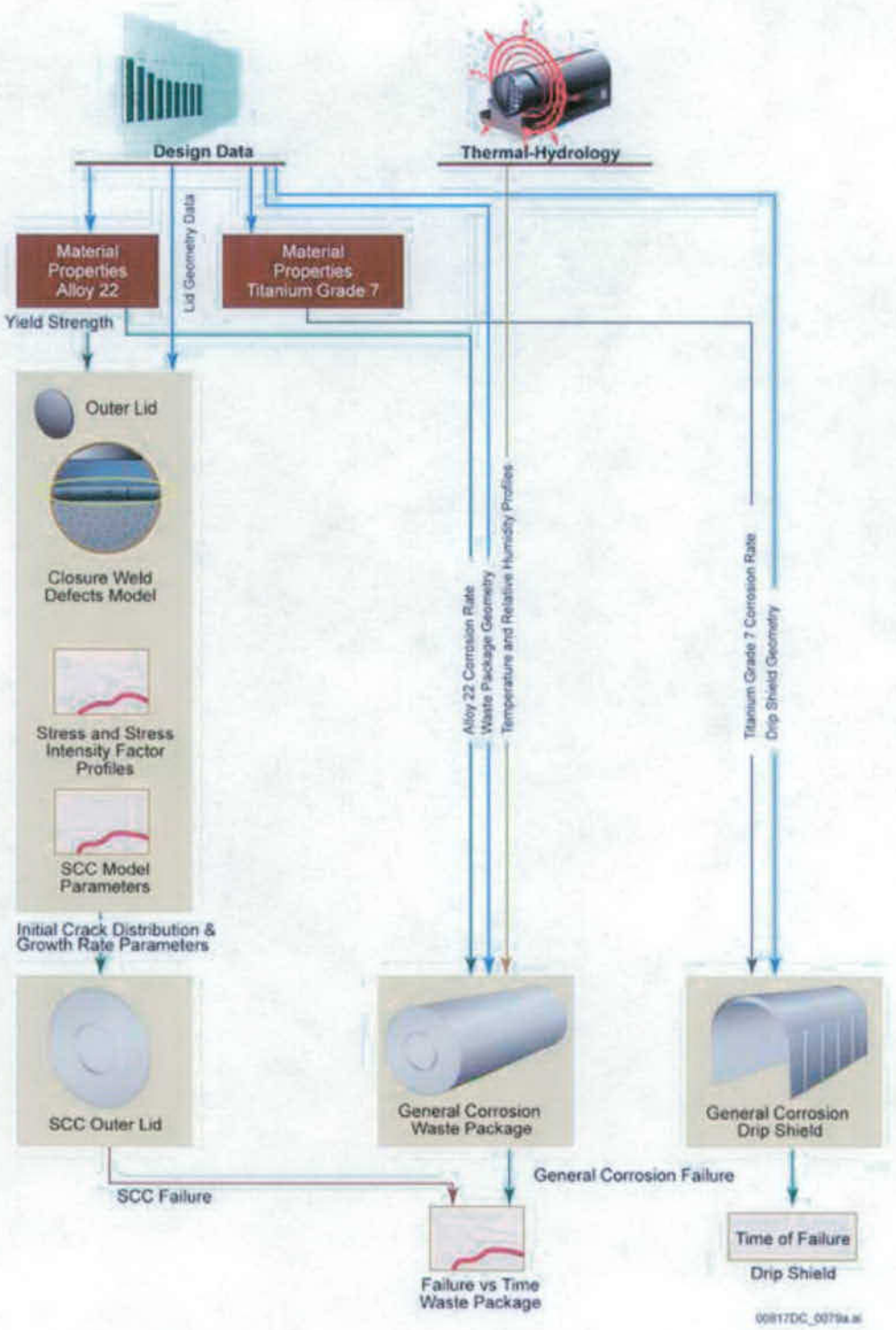

Figure 6.3.5-8. Process and Data Flow for the Waste Package and Drip Shield Degradation Model Component

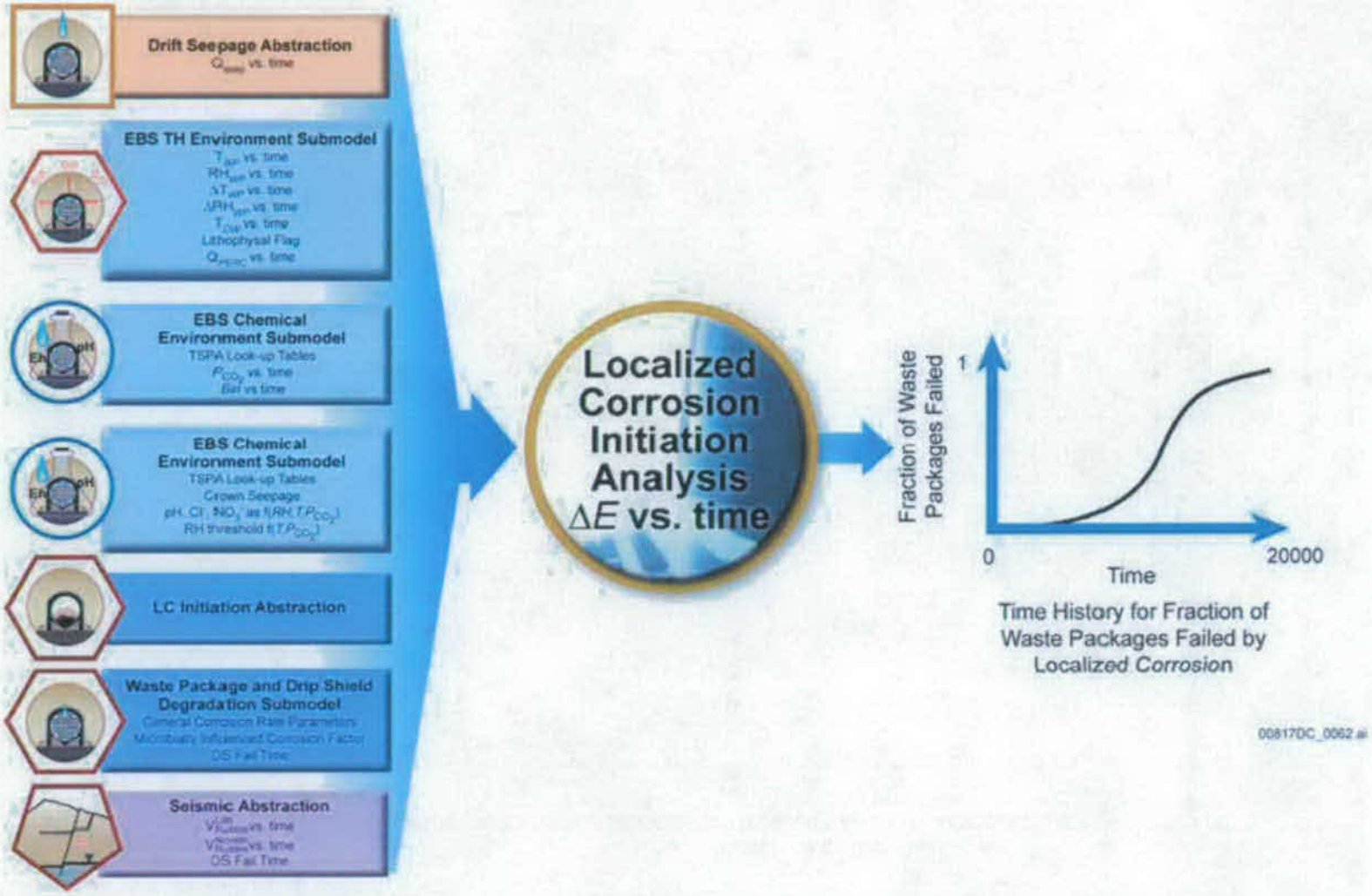

Figure 6.3.5-9. Integration of Submodels for Localized Corrosion Initiation Analysis

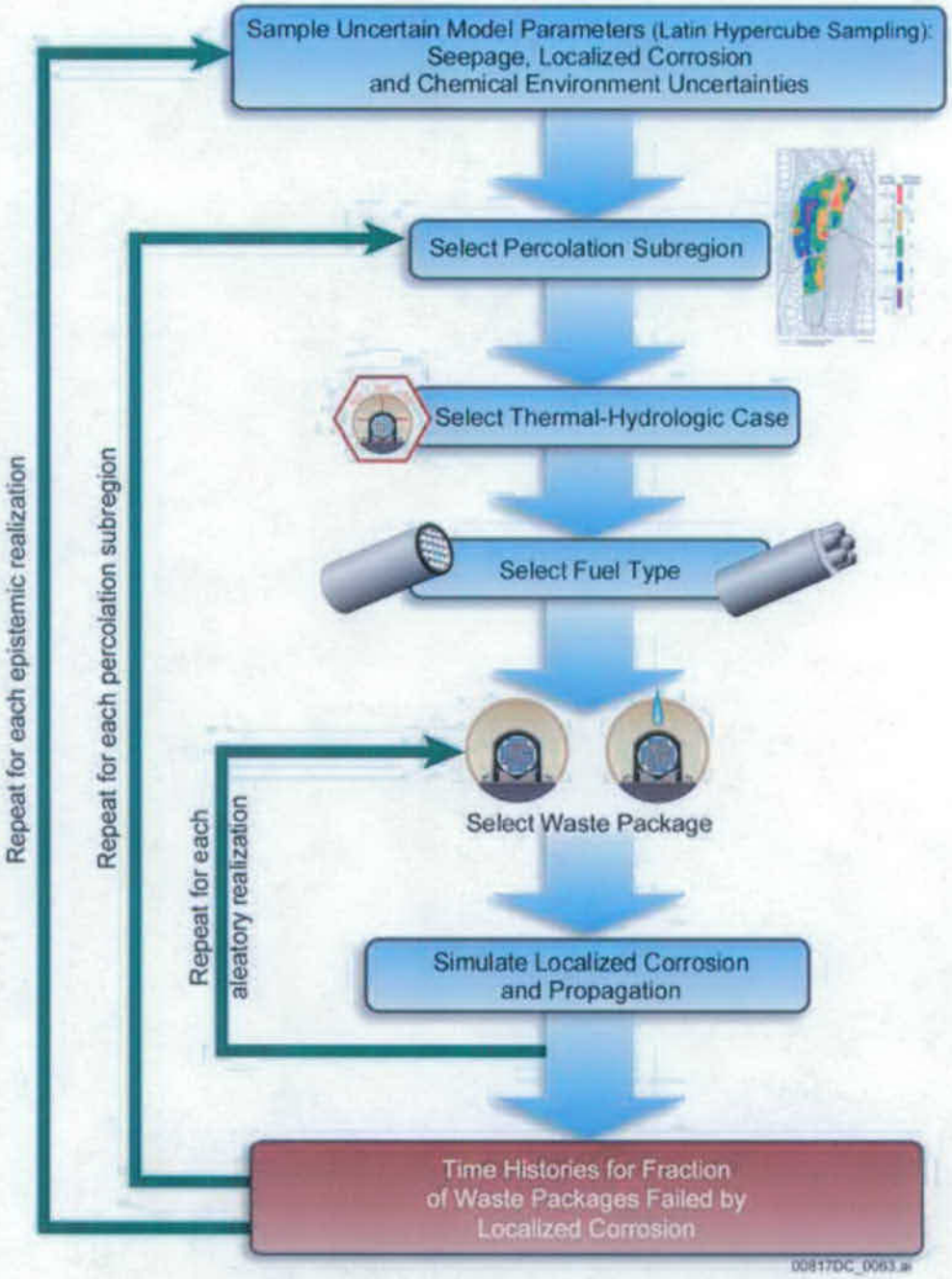

Figure 6.3.5-10. Computational Organization of Localized Corrosion Initiation Analysis for Crown Seepage

6.3.6 Engineered Barrier System Flow

The EBS Flow Submodel implemented in the TSPA-SEIS is described in *EBS Radionuclide Transport Abstraction* (SNL 2007 [DIRS 177407]). The EBS Flow Submodel defines the pathways for water flow in the EBS and specifies how the volumetric flow rate is computed for each pathway. Pathway flow rates are used as inputs to the TSPA-SEIS EBS Transport Submodel. The primary water inputs are the drift-seepage flow rate (SNL 2007 [DIRS 181244], Section 8.2[a]) and the drift wall condensation flow rate (SNL 2007 [DIRS 181648], Sections 8.1[a] and 8.2[a]). Drift seepage and drift wall condensation are further described in Section 6.3.3.1 and 6.3.3.2, respectively. These two flow rates are combined in the EBS Flow Submodel to yield a total dripping flow rate. The type, number, and timing of breaches in the WPs and DSs are also inputs to the EBS Flow Submodel and are provided by the WP and DS Degradation Model Component (Section 6.3.5). An additional source of inflow to the EBS is imbibition into the invert crushed tuff from the surrounding UZ rock matrix (SNL 2007 [DIRS 177407], Section 6.3.1.1). The EBS TH Environment Submodel provides this input and calls it the liquid flow in the invert. Information flow between the EBS Flow Submodel and other TSPA-SEIS components and submodels is shown on Figure 6.3.6-1. Figure 6.3.6-2 presents an overview of the inputs, outputs, and foundation for confidence in the EBS Flow Submodel as implemented in the TSPA-SEIS.

6.3.6.1 Conceptual Model

Water is the principle medium for transport of radionuclides through the EBS (SNL 2007 [DIRS 177407], Section 6.1.1). Water, whether present as thin films or bulk stationary or flowing liquid is necessary for radionuclides to be transported out of the WPs and through the invert to the UZ. Water flow through the EBS will be dependent on a series of processes in the repository. After the WPs are emplaced, radioactive decay of the waste will heat the drifts and locally perturb the normal percolation of water through the mountain. As the drifts cool, some of the water percolating through the mountain may drip into the drifts and subsequently contact some of the DSs. In addition, water that evaporates within the emplacement drifts may condense in cooler regions of the emplacement drifts and drip on DSs in these regions. Over time, the DSs, WPs, and other components of the EBS may degrade, allowing water as dripping or as liquid films to contact the waste forms, resulting in the mobilization and transport of radionuclides through the EBS to the UZ.

The design configuration of the EBS is shown on Figure 6.3.6-3. The drifts will be 5.5 m in diameter (SNL 2007 [DIRS 179354], Section 4.1.1 and Table 4-1). The lower portion of the drifts, commonly referred to as the invert, will be filled with crushed tuff (SNL 2007 [DIRS 179354], Table 4-1). The WPs will be placed on emplacement pallets set on the invert. Titanium DSs will be placed over the WPs and set on the invert.

The primary water input to the EBS will be the total flow rate from two sources: (1) seepage volumetric flow rate into the drifts provided by the Drift Seepage Submodel (Section 6.3.3.1) and, (2) condensation volumetric flow rate on the drift walls provided by the Drift Wall Condensation Submodel (Section 6.3.3.2). A secondary source of inflow to the EBS is imbibition into the invert from the surrounding UZ rock matrix. These sources can flow through

the EBS along eight pathways, shown on Figure 6.3.6-4 and listed below (SNL 2007 [DIRS 177407], Sections 6.3.2 and 6.3.3).

1. **Seepage and DWC**—This is the dripping water flow from the crown (roof) of the drift. Drift seepage and any condensation that may occur on the wall of the drift on the section above the DS are included in the term dripping.

2. **Flow through the DSs**—The flow rate through the DSs is dependent on whether the DS is present. DS failure occurs due to GC (SNL 2007 [DIRS 180778]), which is modeled as occurring uniformly on the DS surface.

3. **Diversion around the DSs**—The dripping flow through the invert that bypasses the WP due to an intact DS.

4. **Flow through the WPs**—Three general types of openings can exist in the WPs due to corrosion. These are: (1) stress corrosion cracks resulting from residual stress or seismic ground motion; (2) breaches resulting from GC and (3) breaches resulting from LC. The flow rate through the WPs is based on the presence of breaches due to GC patches and LC. LC is further discussed in Section 6.3.5. Stress corrosion cracks may occur, but advection of liquid water through stress corrosion cracks in the WPs is excluded. Flow through the WPs is based on the presence of continuous flow paths through the patches that penetrate the WPs. In addition, vertical flow of dripping into the WPs, through the waste form, and out of the WPs is modeled as not affected by the location of patches on the surface of the WPs. Evaporation from the WP is ignored, as discussed further in Section 6.3.6.4.1.

    a. Advective flow of water through stress corrosion cracks in the WPs is neglected for the following reasons: (1) capillary behavior allows water to reside indefinitely within the crack without flow; (2) surface tension opposes hydraulic pressure that may be present at the outlet; and (3) stress corrosion cracks are tight, rough, and tortuous, which limits the transient response to dripping water.

5. **Diversion around the WPs**—The portion of the dripping water that does not flow into the WPs bypasses the waste forms and flows directly to the invert.

6. **Flow into the Invert**—All water flow from the WPs is modeled as flowing into the invert. All flow from the WPs flows to the invert, independent of breach location on the WPs. In addition, the dripping water that is diverted around the WPs and DSs flows into the invert. The presence of the emplacement pallets is ignored in the abstraction of EBS flow, and the WPs are modeled as being in intimate contact with the invert (SNL 2007 [DIRS 177407], Section 6.3.1.1). Thus, the flow leaving the WPs flows directly into the invert, with no resistance offered by the pallets.

7. **Imbibition Flow to the Invert**—Water can be imbibed from the host-rock matrix into the invert. The EBS TH Environment Submodel provides the rate of water imbibition into the invert from the host rock, which it calls the liquid flow in the invert.

8. **Flow from the Invert to the UZ**—The flow from the invert to the UZ is split so that a portion goes into the UZ fractures and a portion goes into the UZ matrix. The portion of the advective flow from the invert equal to the total dripping flow (F_1) flows directly into the UZ fractures. The portion of the advective flow from the invert equal to the imbibition flow to the invert (F_7) flows into the UZ matrix.

These pathways are time-dependent in the sense that total dripping flow, DS failures, and WP breaches will vary with time and percolation subregions. These pathways are further described in Section 6.3.6.2.

6.3.6.2 Abstraction

Figure 6.3.6-4 and Table 6.3.6-2 show that the flow through the EBS can be described by quantifying the flow rates at various flow pathways within the TSPA-SEIS. The EBS flow calculations are repeated in every percolation subregion for each WP type (CSNF WPs and CDSP WPs). Using F to indicate the flow rate at the numbered points on Figure 6.3.6-4, observe that

F_1 = seepage from the drift crown and drift-wall condensation dripping onto the DS (i.e., dripping flow)

F_2 = flow through the DS

F_3 = dripping flow diverted around the DS to the invert

F_4 = flow through the WP

F_5 = dripping flow diverted around the WP to the invert

F_6 = flow into the invert from flow through the WPs and dripping flow diverted around WP and DS

F_7 = imbibition flow between the host rock and the invert

F_8 = flow from the invert to the UZ.

The flow rates within the EBS are calculated based on steady state flow conditions. The primary input to the EBS Flow Submodel is the total dripping flow, F_1, and imbibition from host rock to the invert, F_7. Drift seepage and any condensation that may occur on the wall of the drift are included in this total quantity of dripping water, F_1. Effects of evaporation are ignored in order to maximize drift seepage, drift wall condensation and, consequently, advective releases of radionuclides. The calculation for various flow pathways in the EBS is described as follows:

The dripping flow diverted around the DS is

$$F_3 = F_1 - F_2 \qquad \text{(Eq. 6.3.6-1)}$$

The dripping flow diverted around the WP is

$$F_5 = F_2 - F_4 \quad \text{(Eq. 6.3.6-2)}$$

The flow entering the invert due to seepage and condensation is

$$F_6 = F_1 = F_3 + F_4 + F_5 \quad \text{(Eq. 6.3.6-3)}$$

The flow exiting the invert is

$$F_8 = F_6 + F_7 = F_1 + F_7 \quad \text{(Eq. 6.3.6-4)}$$

The result of flow splitting of the dripping flow at the DS, F_2, and at the WP, F_4, determines all flow within the EBS. The flow through the DSs is a result of the DS flow splitting logic presented in *EBS Radionuclide Transport Abstraction* (SNL 2007 [DIRS 177407], Section 6.3.2.4) as

$$F_2 = \min\left[F_1 \frac{N_{pDS}\, l_{DS}}{L_{DS}} f'_{DS}, F_1\right] \quad \text{(Eq. 6.3.6-5)}$$

where

F_1 = seepage + condensation

N_{pDS} = number of DS GC patches (Note that in the TSPA-SEIS, when the DS fails by GC, the entire DS is modeled as having failed at once, and $N_{pDS} = 1$.)

l_{DS} = axial half-length of DS GC patch

L_{DS} = axial length of DS

f'_{DS} = uncertainty factor (Table 6.3.6-1).

Flow through the WPs is a result of the WP flow splitting logic presented in *EBS Radionuclide Transport Abstraction* (SNL 2007 [DIRS 177407], Section 6.3.3.2), and is described as follows:

$$F_4 = \min\left[F_2 \frac{N_{pWP}\, l_{WP}}{L_{WP}} f'_{WP}, F_2\right] \quad \text{(Eq. 6.3.6-6)}$$

where

F_2 = flow through a DS

N_{pWP} = number of GC patches on failed WP

l_{WP} = axial half-length of GC patch on failed WP

L_{WP} = axial length of WP

f'_{WP} = WP uncertainty factor (Table 6.3.6-1).

The number of GC patches on a failed WP, N_{pWP}, is the time-dependent parameter that controls the fraction of impinging flow that can enter and flow through the WPs. It can vary from zero to the maximum number of patches depending on the modeling case. N_{pWP} increases with time due to GC in the Seismic Ground Motion (GM) and Nominal Modeling Cases. It is set to the maximum value in the Igneous Intrusion, Waste Package EF, and Drip Shield EF Modeling Cases. In the Seismic Fault Displacement (FD) Modeling Case, it is based on the number of patches equivalent to the WP damaged area caused by faulting. N_{pWP} is set to a value corresponding to a single drill hole in the Human Intrusion case. Because the flow splitting model described by Equation 6.3.6-6 is based on the fractional opening length along the crown of the WP, rather than the fractional opening area over the entire WP, the flow splitting fraction reaches 1 (i.e., all the impinging flow can enter a WP) well before N_{pWP} reaches its maximum. For the mean value of the WP flux uncertainty term, f'_{WP}, equal to 1.2, only about 62 GC patches are required on a CSNF WP to allow 100 percent of the impinging flow to enter a WP. This is about 4 percent of the area of the WP (excluding the lids). The EBS Flow Submodel in the TSPA-SEIS is summarized in Table 6.3.6-2.

Uncertainty in the EBS Flow Submodel—The EBS Flow Submodel uses one uncertain (epistemic) flow splitting parameter to characterize the fraction of flow that enters breaches in the DSs and one uncertain (epistemic) flow splitting parameter to characterize the fraction of flow that enters breaches in the WPs. Each parameter is sampled once per realization and applied to all representative WP locations in a dripping environment. Table 6.3.6-1 provides the distribution type and ranges for these two parameters.

6.3.6.3 TSPA-SEIS Implementation

The EBS flow calculation consists of two parts in the TSPA-SEIS. The first part of the EBS flow calculation combines the drift seepage and drift-wall condensation flows to determine the total dripping rate onto the DS and into the invert. The second part calculates the flow through the failed WPs and DSs using the flow splitting logic presented in Equation 6.3.6-5 and Equation 6.3.6-6.

Dripping Flow Calculations—The EBS Flow Submodel calculates the dripping flow into the drift. The EBS Flow Submodel receives feeds (inputs) (Figure 6.3.6-2) from the Drift Seepage Submodel and the Drift Wall Condensation Submodel. The seepage fraction and seepage rate from the Drift Seepage Submodel is passed to the EBS Flow Model. The seepage fraction determines the number of WPs placed in seep and non-seep environments in each percolation subregion. A single element in the model then adds the seepage rate and the drift-wall condensation rate to produce the total dripping rate onto the DS and into the invert for WPs in a seep environment. For a non-seep environment, only the drift-wall condensation rate is used.

Flow Splitting Calculations—The flow splitting calculations determine the volumetric flow rate of water at different locations within the EBS as water moves through breached DSs, breached WPs, and the invert as shown on Figure 6.3.6-4. The volumetric flow rate of water through each breached DS or WP is proportional to the damage fraction on each DS or WP represented by N_{pDS} and N_{pWP} in Equations 6.3.6-5 and 6.3.6-6, respectively. The EBS Flow Submodel introduces two uncertain (epistemic) flow splitting parameters to characterize the fraction of flow that enters breaches on the DSs and WPs. These two parameters are sampled once per realization and applied to all representative DSs and WPs.

Inputs to the EBS Flow Submodel for each WP type and repository subregion include:

- Seepage and condensation rates from the Drift Seepage and Drift Wall Condensation Submodels (Section 6.3.3)
- Damage fraction per failed DS from the WP and DS Degradation Model Component (Section 6.3.5)
- Damage fraction per failed DS from Early DS Failure Abstraction (Drip Shield EF Modeling Case only) (Section 6.4)
- Damage fraction per failed DS from the Seismic Consequences Abstraction (Seismic Scenario Class only) (Section 6.6)
- Damage fraction per failed WP from the WP and DS Degradation Model Component (Nominal Scenario Class only) (Section 6.3.5)
- Damage fraction per failed WP from the Seismic Consequences Abstraction (Seismic Scenario Class only) (Section 6.6).

The EBS Flow Submodel does not use the average number of crack penetrations per failed WP because stress corrosion cracks are too small to allow water flow through these cracks.

The flow splitting model for water flow through a damaged DS is computed by multiplying the dripping flow falling on the DS by the ratio of patch opening length on the DS to the total length of the DS. Similarly, the flow entering each WP is computed by multiplying the flow falling on the WP (i.e., the flow of water through the DS) by the ratio of patch opening length on the WP to the total length of the WP. Both calculations are multiplied by a separate uncertainty factor to account for the variation in location of the patches with respect to the drip location (Table 6.3.6-1). However, the DS corrosion model does not include spatial variation between DSs or between patches on individual DSs (Section 6.3.5.1.3). Therefore, for the TSPA-SEIS, all the DS patches fail when DS failure occurs. Additionally, when N_{pDS} is equal to the maximum number of DS patches, the DS flow splitting algorithm is not used and $F_2 = F_1$ (Eq. 6.3.6-5).

Outputs from the EBS Flow Submodel are used by: (1) the Waste Form Degradation and Mobilization Model Component (volumetric flow rate through a failed WP) to calculate pH and ionic strength in the WP, and (2) the EBS Transport Submodel (volumetric flow rate through a

failed WP and volumetric flow rate through the invert) to calculate advective transport of radionuclides through a failed WP and the invert to the host rock.

6.3.6.4 Consistency and Conservatism in Assumptions and Parameters

To enhance understanding of the complex interactions within the TSPA-SEIS, a discussion of consistency among model components and submodels and identification of conservative assumptions in abstractions, process models, and parameter sets supporting the EBS Flow Submodel are discussed below.

6.3.6.4.1 Consistency of Assumptions

Effects of Evaporation on EBS Flow—Less water may be available for transport if evaporation on the DSs or WPs were taken into account. Generally, the heat output from the WPs will cause the DSs to be hotter than the drift wall from which water is dripping. Some water that drips onto the DSs may be evaporated, thereby reducing the flow of water through the DSs. A reduction in the quantity of water flow through the DSs reduces the potential for advective transfer and subsequent release and transport of radionuclides from the WPs (SNL 2007 [DIRS 177407], Section 5.2).

Heat generated by the waste forms also has the potential to evaporate water within the WPs. In this situation, water cannot collect inside the WPs and cannot support the advective transport of radionuclides. However, complexities in the internal geometry of the WPs, particularly the response of any water pooled at the bottom of the WPs and the presence of small conduits for water vapor to escape through stress corrosion cracks, make it difficult to assess evaporation quantitatively. The potential for evaporation in the WPs is ignored in the TSPA-SEIS (SNL 2007 [DIRS 177407], Section 6.3.3.2).

Effect on the TSPA-SEIS—As further discussed in Section 6.3.8, neglecting the evaporation of water on the DSs and WPs means there is more water available for dissolution and advection of radionuclides. Also, neglecting evaporation leads to higher saturation and more diffusion of radionuclides.

6.3.6.4.2 Identification of Conservatisms in Submodels and Abstractions

No DS Shadow in the Invert—For dripping locations, water will tend to shed around the DSs and not flow through the region of the invert directly under the DSs. However, because of limited information regarding the flow paths and mixing of waters, this effect is not accounted for (SNL 2007 [DIRS 177407], Section 6.5.2.6). For model scenarios without DS failures, a DS shadow would prevent advective transport for some distance beneath the WP, certainly within the invert and for some distance in the UZ fractures and matrix. However, the TSPA-SEIS assumes advection within the invert in the dripping locations. The effect of this assumption is to increase the release of radionuclides from the invert and increase the diffusive concentration gradient from the waste form to the invert and UZ, thereby conservatively increasing the diffusive mass flux.

All Dripping into Drifts is Assumed to Fall on the DSs—All dripping into drifts is assumed to fall on the DSs, not just dripping above the DSs. The approach taken is to simplify the model

since uncertainty in dripping locations is difficult to quantify and seepage into a circular opening is more likely to occur near the crown (SNL 2007 [DIRS 177407], Section 5.1). While all dripping into the drift is assumed to fall on the DSs, the DS flow splitting uncertainty term in Equation 6.3.6-5 is applied. While this uncertainty term may reduce the flow through the DSs to account for the spatial variability of the location of DS patch openings, it does not account for spatial distribution of dripping. The conservative treatment tends to increase the dripping flow contacting the DSs, resulting in an increase in the dripping flow passing through a failed DS and an increase in the dripping flow diverted around the DSs (e.g., passing through the invert) within the dripping locations.

All the Dripping Penetrating a DS Falls on the Crown of the WP—A conservative approach is taken to simplify the modeling approach because uncertainty in dripping locations is difficult to quantify (SNL 2007 [DIRS 177407], Section 5.1). Any increase in the advective flow through the WPs as a result of assuming the entire flow penetrating the DSs falls on the WPs would be negligible with the result of a slight increase in the dripping flow through the breached WPs.

6.3.6.5 Alternative Conceptual Model(s) for Engineered Barrier System Flow

Section 6.2 outlines the general consideration and treatment of ACMs used to support the TSPA-SEIS. Brief descriptions of the EBS Flow Submodel ACMs are summarized in Table 6.3.6-3.

Bathtub Flow Model ACM—This ACM assumes that dripping water collects within the WP before being released to the EBS (SNL 2007 [DIRS 177407], Section 6.6.1). The bathtub effect would be most important during the period when only a few patches or cracks have penetrated the DSs and WPs. In this situation, there may be penetrations through the top of the WP while the bottom surface remains intact, leading to retention of liquid. At later times, the presence of multiple penetrations makes a flow-through geometry the more likely configuration. The response of the bathtub geometry was evaluated for a primary case, with constant boundary conditions and material properties, and for three secondary cases. The three secondary cases considered a step change in inflow rate, such as would occur from a climatic change, a step change in water chemistry, or a step change in flow geometry, as would occur if a patch suddenly appeared beneath the waterline. All cases included consideration of two limiting conditions on radionuclide releases: dissolution rate limited and solubility limited.

This ACM was not used for the TSPA-SEIS EBS Transport Model because for most of the pertinent cases, the base-case flow-through model is bounding with respect to the release of radionuclides.

Dual-Continuum Invert Model ACM—The dual-continuum invert model is an alternative conceptual EBS transport model in which crushed tuff invert ballast is modeled as a dual-continuum material consisting of intergranular pore space and intragranular pore space (SNL 2007 [DIRS 177407], Sections 6.6.3 and 6.6.4.2). All water dripping into the drift is modeled as flowing through the intergranular pore space and UZ fractures. Imbibition from UZ host rock into the invert is modeled as flowing through the intragranular pore space and into the UZ matrix under gravity. Diffusion of radionuclides also occurs in both the intergranular and intragranular pore spaces, from the WP corrosion products into UZ fractures and matrix, as well as between the two invert continua.

This ACM was not used for the TSPA-SEIS EBS Transport Model due to insufficient data to validate diffusion coefficients in individual continua and insufficient data to confirm whether this is a bounding approach with respect to chemical behavior in the invert (SNL 2007 [DIRS 177407], Section 6.6.3.5). However, the dual-continuum invert model ACM was included in the GoldSim model file to be used for sensitivity analyses and to validate the single-continuum model for EBS transport in the TSPA-SEIS.

INTENTIONALLY LEFT BLANK

Table 6.3.6-1. Drip Shield and Waste Package Flow Splitting Parameters

TSPA-SEIS Name	Mathematical Symbol	Description	Units	Distribution Type	Distribution Specification
DS_Flux_Uncertainty_a	f'_{DS}	DS flow splitting uncertainty factor	None	Uniform	Min = 0 Max = 0.85
WP_Flux_Uncertainty_a	f'_{WP}	WP flow splitting uncertainty factor	None	Uniform	Min = 0 Max = 2.41

Sources: SNL 2007 [DIRS 177407], Table 8.2-4 and DTN: SN0703PAEBSRTA.001_R3 [DIRS 183217].

Table 6.3.6-2. The EBS Flow Abstraction within the TSPA-SEIS

Flow Pathway	Flow Parameters	Notes
1. Total dripping flow (seepage + wall condensation), F_1	Total dripping flow is a function of seepage flow and drift-wall condensation flow.	Drift Seepage Submodel (Section 6.3.3.1) provides time- and location-dependent values of seepage flow. Drift Wall Condensation Submodel (Section 6.3.3.2) provides time and location-dependent values of drift-wall condensation flow.
2. Flow through the DS, F_2	N_{pDS} is the number of DS GC patches l_{DS} is the axial half-length of patches due to GC of titanium. L_{DS} is the axial length of the DS. f'_{DS} is the sampled uncertain parameter, DS_Flux_Uncertainty_a.	WP and DS Degradation Model Component (Section 6.3.5) provides the number of GC patches and stress corrosion cracks on the DS. No flow through stress corrosion cracks due to plugging (SNL 2007 [DIRS 181953], Sections 6.8.6 and 8.1.6).
3. Diversion around DS, F_3	$F_3 = F_1 - F_2$.	Continuity of liquid flow.
4. Flow into the WP, F_4	N_{pWP} is the number of WP GC patches l_{WP} is the axial half-length of all patches due to GC of Alloy 22 (UNS N06022). L_{WP} is the axial length of the WP. f'_{WP} is the sampled uncertain parameter, WP_Flux_Uncertainty_a.	WP and DS Degradation Model Component (Section 6.3.5) provides the number of GC patches on the WP. No flow through stress corrosion cracks. Steady-state flow through WP (outflow = inflow in steady state; that is bounding for release).
5. Diversion around the WP, F_5	$F_5 = F_2 - F_4$.	Continuity of liquid flow.
6. Flow to the invert, F_6	$F_6 = F_5 + F_4 + F_3$ $= F_1$.	Note that only F_4 can transport radionuclides into the invert.
7. Imbibition flow from the host rock matrix into the invert, F_7	F_7 is an input to the EBS Flow Submodel.	EBS TH Environment Submodel (Section 6.3.2) provides the imbibition flow.
8. Flow from the invert into the UZ, F_8	$F_8 = F_6 + F_7$ $= F_1 + F_7$.	Total dripping flow portion ($F_1 = F_6$) of advective flow from the invert flows into the UZ fractures; imbibition flow (F_7) flows into the UZ matrix.

Source: Developed from (SNL 2007 [DIRS 177407], Table 8.1-1).

NOTE: See Figure 6.3.6-4.

Table 6.3.6-3. Alternative Conceptual Models Considered for the EBS Flow

Alternative Conceptual Models	Key Assumptions	Assessment and Basis
Dual-continuum invert model	Crushed tuff invert ballast is modeled as a dual-continuum material consisting of intergranular and intragranular pore spaces. All seepage flow into the drift flows through the intergranular pore space and into the UZ fractures. Imbibition from UZ host rock into the invert flows through the intragranular pore space. Diffusion of radionuclides also occurs in both the intergranular and intragranular pore spaces, from the WP corrosion products into UZ fractures and matrix, as well as between the two invert continua (SNL 2007 [DIRS 177407], Section 6.6.4).	Insufficient data to validate diffusion coefficients in individual continua. Insufficient data to confirm whether this is a bounding approach with respect to chemical conditions in the invert for calculating solubility and colloid stability.
Bathtub flow model (alternative to flow-through model)	Seepage water flowing into breached WP accumulates until void volume is filled before water containing dissolved radionuclides flows out. Various cases, such as changing inflow rates and effect of solubility and dissolution rate limits are evaluated (SNL 2007 [DIRS 177407], Section 6.6.1).	For several of the most pertinent cases, the flow-through model is conservative with respect to releases of radionuclides.

Source: Developed from (SNL 2007 [DIRS 177407], Table 6.4-1).

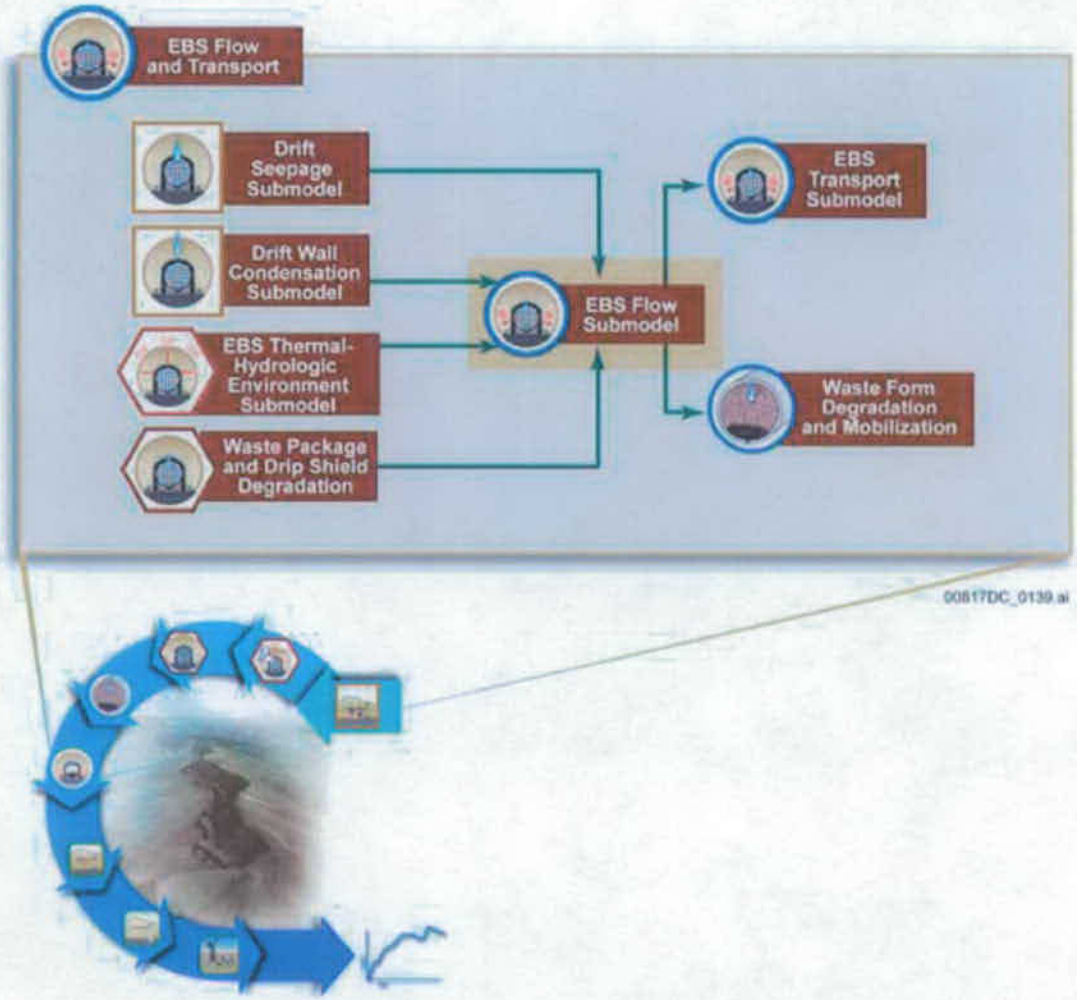

Figure 6.3.6-1. Information Flow Diagram for the EBS Flow Submodel

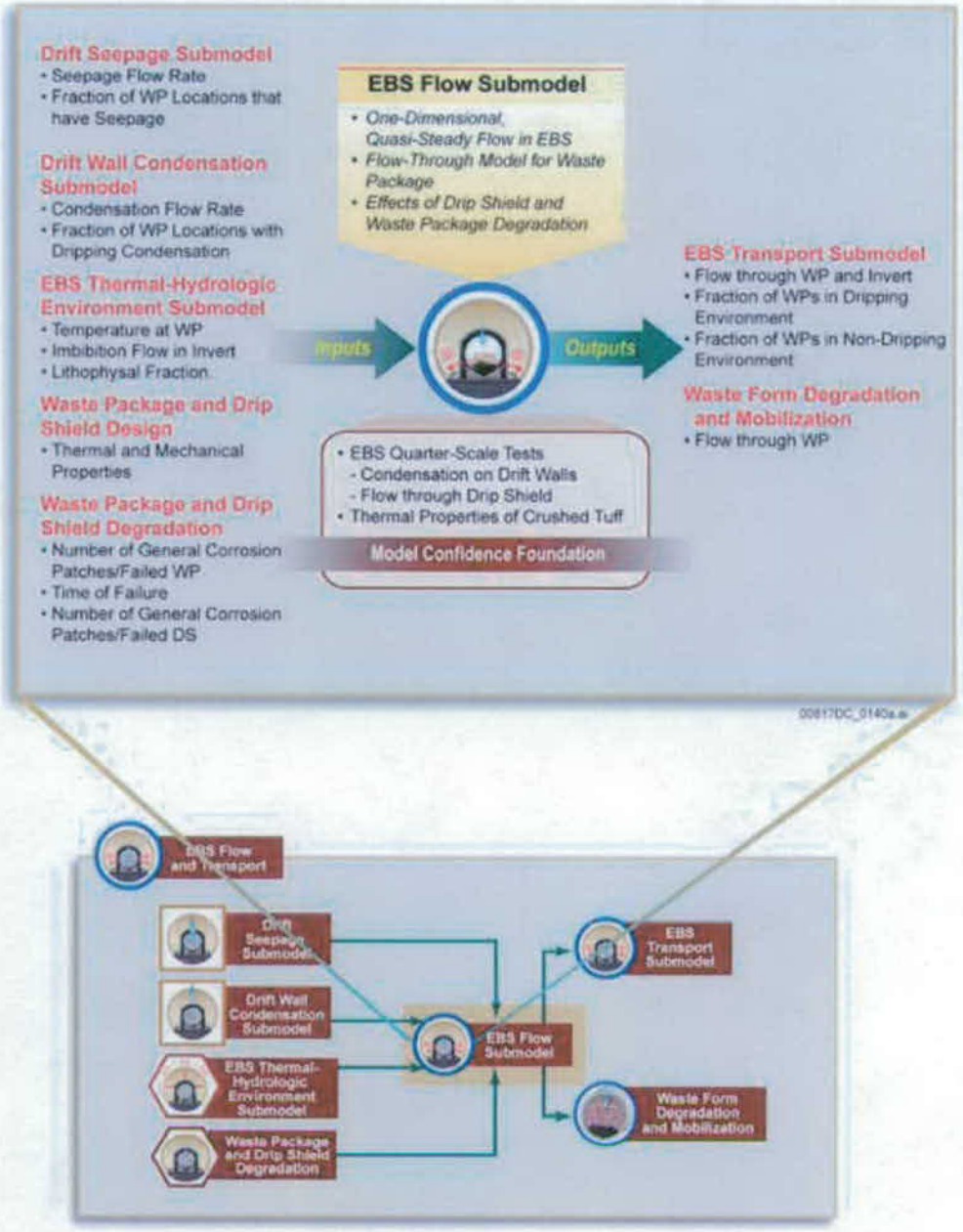

Figure 6.3.6-2. Inputs, Outputs, and Basis for Model Confidence for the EBS Flow Submodel

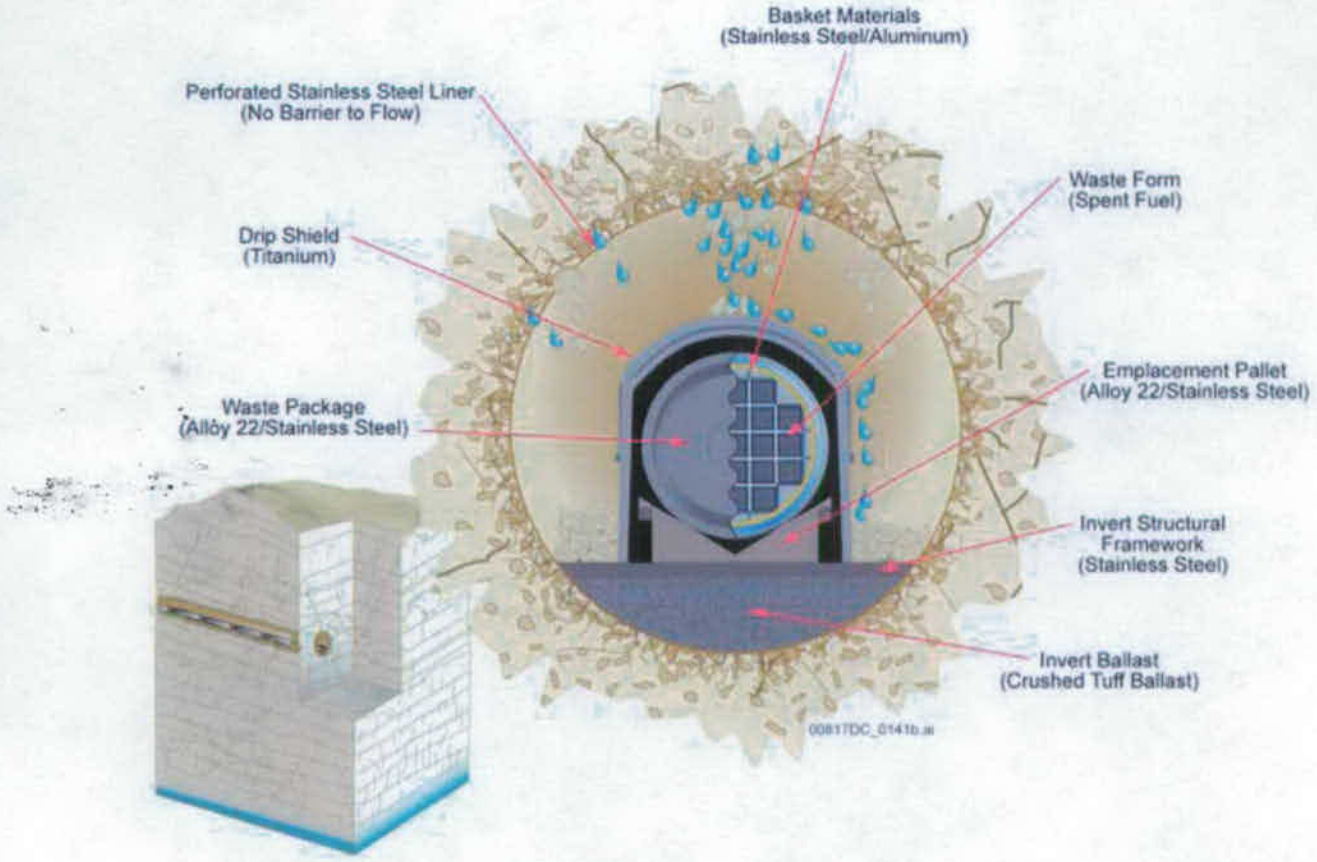

Figure 6.3.6-3. Cross Section of Typical Emplacement Drift

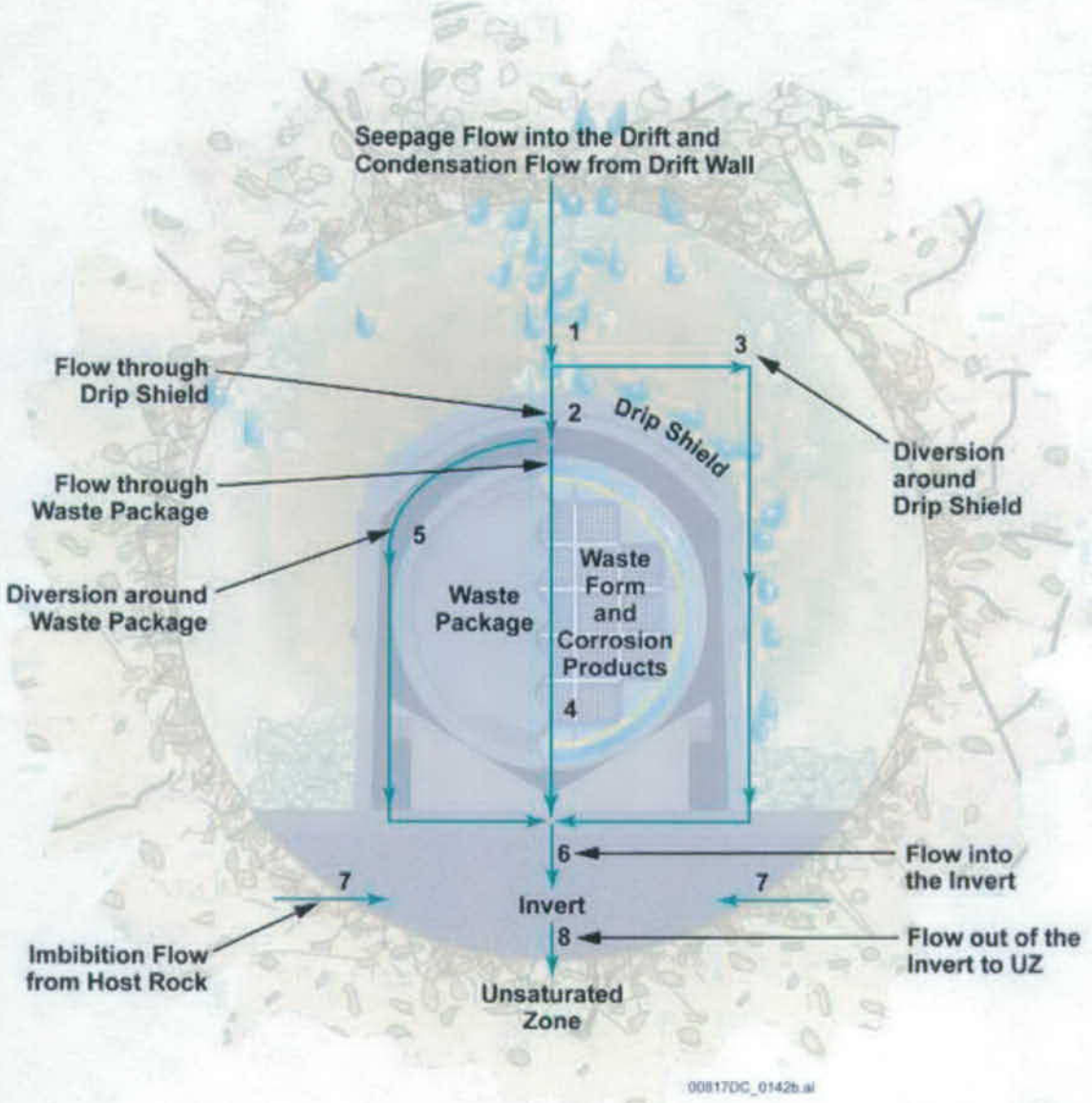

Figure 6.3.6-4. Schematic Diagram of Water Flow Pathways in the EBS

6.3.7 Waste Form Degradation and Mobilization

The Waste Form Degradation and Mobilization Model Component consists of five submodels: (1) Initial Radionuclide Inventory Submodel, which defines the radionuclide inventory and radionuclides of importance for the TSPA-SEIS; (2) In-Package Chemistry Submodel, which evaluates in-package chemical conditions; (3) Waste Form Degradation Rate Submodel, which calculates the degradation rates of CSNF, DSNF, and HLW waste forms; (4) Solubility (or Dissolved Concentration Limits) Submodel, which calculates solubilities (i.e., dissolved concentration limits) of radioactive elements in a failed WP and in the invert; and (5) EBS Colloids Submodel, which calculates colloidal concentrations of radionuclides in a failed WP and in the invert. Solubilities and colloidal concentration of radionuclides serve as inputs to the EBS Transport Submodel (Section 6.3.8), which calculates radionuclide transport within the WPs from the waste form to the EBS and through the EBS to the UZ below the repository.

The TSPA-SEIS Waste Form Degradation and Mobilization Model Component receives inputs from the following analyses and/or model reports:

- *Initial Radionuclide Inventories* (SNL 2007 [DIRS 180472]) and *Radionuclide Screening* (SNL 2007 [DIRS 177424]).
- In-Package Chemistry Abstraction (SNL 2007 [DIRS 180506]).
- CSNF Waste Form Degradation: Summary Abstraction (BSC 2004 [DIRS 169987]), DSNF and Other Waste Form Degradation Abstraction (BSC 2004 [DIRS 172453]), and Defense HLW Glass Degradation Model (BSC 2004 [DIRS 169988]).
- Dissolved Concentration Limits of Elements with Radioactive Isotopes (SNL 2007 [DIRS 177418]).
- Waste Form and In-Drift Colloids-Associated Radionuclide Concentrations: Abstraction and Summary (SNL 2007 [DIRS 177423]).

The three categories of waste form (CSNF, DSNF, and HLW glass) are contained and disposed in two types of WPs: CSNF WPs and CDSP WPs. The CDSP WPs will contain both DSNF and HLW glass. As was done in the TSPA for the Site Recommendation, WPs containing naval SNF waste forms are conservatively represented as containing CSNF.

Key inputs to the submodels for the Waste Form Degradation and Mobilization Model Component include: (1) a set of initial materials within the WP and the materials' major elemental compositions and physical and chemical properties; (2) time-dependent water flux into a failed WP provided by the EBS Flow Submodel (Section 6.3.6); (3) temperature and relative humidity in the WP provided by the EBS TH Environment Submodel (Section 6.3.2); and (4) partial pressure of CO_2 in the gas phase (P_{CO_2}) or negative log of partial pressure of CO_2 (pCO_2) provided by the EBS Chemical Environment Submodel (Section 6.3.4).

Many of the abstractions that support the submodels in the Waste Form Degradation and Mobilization Model Component are implemented to describe single representative CSNF and CDSP WPs. The determination of what comprises a representative WP is discussed in Section 6.3.2.2.2. The EBS Transport Submodel is implemented in the TSPA-SEIS at the scale of a single WP (Section 6.3.8). The pertinent EBS Transport Submodel properties (including the Waste Form Degradation and Mobilization Model Component) for a single representative WP are scaled to the total number of WPs that have failed in each percolation subregion. These properties include the mass of available inventory, pore water volumes, mass of solid materials, advective flow rates, and diffusion areas. See the GoldSim user's guide for source-term element details.

The five submodels discussed in this section deal with processes that govern the mobility of radionuclides inside a failed WP. This section presents the principles and submodel implementation for radionuclide availability in a failed WP but does not discuss the specifics regarding transport in the EBS. This discussion is reserved for Section 6.3.8, which explains radionuclide transport as available inventory moves from the waste form into the waste form alteration products, then into the WP corrosion products, then out of the WP opening into the invert.

In general, the radionuclide inventory of each WP may be immediately available for transport upon WP failure or bound in a matrix that must first degrade before the inventory is available for transport inside the WP (Section 6.3.7.1). As discussed in Section 6.3.7.3, no credit is taken for CSNF and DSNF cladding for the TSPA-SEIS model. After WP failure, the waste form begins to degrade at the calculated rate (Section 6.3.7.4). As the waste form degrades, waste form alteration products are formed (Section 6.3.7.4). The available inventory, both from the degraded waste form and that which was immediately available upon WP failure, is released into the pore water of the alteration product. The available inventory is dissolved in this pore water solution up to its solubility (Section 6.3.7.5). As the waste form degrades, waste form colloids are also formed, and these colloids may facilitate the release of the radionuclides from the breached WPs to the environment. Colloid formation and stability in the EBS are discussed in Section 6.3.7.6. Although the processes described below are closely related to the release of radionuclides from a failed WP into the environment, the topics covered in this section pertain to the availability of the radionuclides for transport. The transport of available radionuclides, by diffusion and advection, is covered in detail in Section 6.3.8.

The chemistry inside a failed WP is calculated by the In-Package Submodel using the abstracted relationships, and then the outputs are fed to other submodels that govern radionuclide availability (Waste Form Degradation Submodel (Section 6.3.7.4), Dissolved Concentration Limits Submodel (Section 6.3.7.5), and EBS Colloids Submodel (Section 6.3.7.6)).

The interaction between the five submodels in the Waste Form Degradation and Mobilization Model Component is common but is limited to the form of the abstractions presented. For example, the waste form degradation rate for a failed CSNF WP was an input to the In-Package Chemistry Process Model. However, the final abstraction, as presented for the TSPA-SEIS, was independent of the waste form degradation rate. This model abstraction is intended to span the range of waste form degradation rates anticipated in the TSPA-SEIS. Therefore, the In-Package Chemistry Submodel (Section 6.3.7.2) does not receive input from the CSNF Waste Form

Degradation Submodel (Section 6.3.7.4.1). The abstracted rate model from the degradation of the CSNF is a function of the pH inside a failed WP. Therefore, in the TSPA-SEIS, the In-Package Chemistry Submodel feeds the pH to the CSNF Waste Form Degradation Submodel (Section 6.3.7.4.1). Other submodel interactions are discussed in greater detail in the subsections below.

The five submodels discussed below are presented sequentially in the sections that follow, but in general, they are evaluated in every timestep of the TSPA-SEIS. Two of the five Waste Form Degradation and Mobilization Model Component Submodels described below may receive feeds from other model components, but they do not receive feeds from the other three submodels in the Waste Form Degradation and Mobilization Model Component. These two submodels are presented first and are the Radionuclide Inventory Submodel (Section 6.3.7.1) and the In-Package Chemistry Submodel (Section 6.3.7.2). The next three submodels discussed are the Waste Form Degradation Submodel (Section 6.3.7.4), the Dissolved Concentration Limits Submodel (Section 6.3.7.5), and the EBS Colloids Submodel (Section 6.3.7.6). These submodels are functions of other submodels of the Waste Form Degradation and Mobilization Model Components, as well as other model components in the TSPA-SEIS. For example, the Waste Form Degradation Submodel, including the calculations of the mass and volume of the alteration products as the waste forms degrade, are functions of the EBS TH Environment Submodel (Section 6.3.2) and the In-Package Chemistry Submodel (Section 6.3.7.2), and receive input feeds directly from these submodels at each TSPA-SEIS timestep. For the purposes of the rate model calculations, the TSPA-SEIS first computes the feed values at each timestep and then evaluates the degradation rate expression for those feed conditions. The simulation software maintains an element hierarchy for evaluating calculations that are dependent on other model calculations at the same simulation time.

Figures 6.3.7-1 and 6.3.7-2 are schematic illustrations showing the submodels of the Waste Form Degradation and Mobilization Model Component, the inputs and outputs of the model component, and the basis for confidence in the model component.

6.3.7.1 Radionuclide Inventory

The *Initial Radionuclide Inventory* analysis (SNL 2007 [DIRS 180472]), hereafter referred to as the Initial Radionuclide Inventory Abstraction for the TSPA-SEIS, considers four categories of wastes for disposal in the repository: DOE-owned HLW glass (including HLW glass from the Savannah River Site, Idaho National Laboratory, and Hanford, as well as commercial HLW glass from the West Valley Demonstration Project), CSNF, DSNF, and naval SNF. The radionuclides of importance to the TSPA-SEIS dose calculations were assessed in the Initial Radionuclide Inventory Screening Analysis in *Radionuclide Screening* (SNL 2007 [DIRS 177424]). Figure 6.3.7-3 shows how the waste types are to be placed in CSNF and CDSP WPs. The Initial Radionuclide Inventory Abstraction and Initial Radionuclide Inventory Screening Analysis together define the source terms for the CSNF and CDSP WPs in terms of both the quantity of WPs and the radionuclide inventory per WP. These two analyses indicate that 32 radionuclides are used to represent the inventory in the TSPA-SEIS. Note that ^{210}Pb, which is specified to be included in the inventory by the Initial Radionuclide Inventory Screening Analysis, is assumed to be in secular equilibrium with ^{226}Ra and is not explicitly modeled in the TSPA-SEIS. The TSPA-SEIS does account for the dose effects of ^{210}Pb by combining its biosphere dose conversion

factor with its parent, ^{226}Ra. Because the TSPA-SEIS accounts for the degradation and failure of individual WPs, the inventories of these 31 radionuclides are provided on a grams-per-WP basis.

6.3.7.1.1 Conceptual Model

The number of WPs projected to be emplaced in the repository is 11,629 (Table 6.3.7-1). Eight WP configurations were designed to accommodate the four waste forms (Table 6.3.7-1). The CSNF configurations contain the commercial fuel assemblies from PWRs and BWRs. The CDSP WP configurations hold both DSNF and HLW in various-sized canisters within the WP. Naval fuel will be packaged in either short- or long-canister configurations. Even though the naval fuel is not considered a commercial fuel in the TSPA-SEIS, the 417 naval SNF WPs are treated as if they were CSNF WPs (SNL 2007 [DIRS 180472]), Table 7-3[a]). The naval SNF is represented by an equivalent amount of CSNF. This modeling approximation is justified because the fuel degradation characteristics more closely resemble CSNF than DSNF, there is no HLW in a naval fuel WP, and surrogate analyses indicate CSNF releases bound the naval fuel releases. The mixed oxide fuel (MOX) (Section 6.3.7.1.2.2) inventory is included as CSNF inventory in the TSPA-SEIS for release purposes. In contrast to the naval SNF that is treated as additional packages, the MOX inventory is averaged over the total number of CSNF WPs and then added to the per package CSNF inventory. For release purposes, the lanthanide borosilicate (LaBS) inventory (Section 6.3.7.1.2.2) is included as HLW inventory in the TSPA-SEIS. The LaBS inventory is averaged over the total number of CDSP WPs and then added to the HLW glass per package inventory.

The Initial Radionuclide Inventory Screening Analysis explicitly considered both 10,000-year and 1,000,000-year modeling periods for the repository at Yucca Mountain. Four scenario classes are considered: (1) Nominal Scenario Class, (2) Igneous Scenario Class, (3) Seismic Scenario Class, and (4) Human Intrusion Scenario. The radionuclide screening for each scenario class is based on the premise that the products of activity inventories and screening factors indicate the relative importance of each radionuclide with respect to the radiation dose that a person near the repository might receive (SNL 2007 [DIRS 177424], Section 6.2.1). The Initial Radionuclide Inventory Screening Analysis takes into account such factors as radionuclide decay rates, soil accumulation, uptake by plants, and exposure to contaminated groundwater. This screening analysis also accounts for differences in WPs and waste forms, radionuclide sorption, and radionuclide solubility. Results of the screening analysis are provided in Table 6.3.7-2. This table lists 32 radionuclides that may contribute the majority of the dose for the different scenario classes (Section 6.1.2) implemented in the TSPA-SEIS.

The radionuclide inventory for the CSNF and CDSP WPs, including uncertainty, is provided by the Initial Radionuclide Inventory Abstraction (SNL 2007 [DIRS 180472]) and is a direct input to the TSPA-SEIS. The CSNF, CDSP, and DSNF radionuclide inventories are provided on a grams-per-WP basis. The radionuclide inventories provided by the Initial Radionuclide Inventory Abstraction are calculated at year 2067 for CSNF WPs and year 2030 for HLW and DSNF. Table 6.3.7-3 shows the expected average inventory in grams per WP for 31 radionuclides at year 2067 for CSNF and year 2030 for DSNF and CDSP. The TSPA-SEIS simulation begins at post-closure and therefore requires an inventory calculated at the time of repository closure, currently estimated to be the year 2,117. Section 6.3.7.1.2.1 describes the radionuclide inventory decay and ingrowth calculations performed for 50 years and 87 years for

CSNF and CDSP/DSNF, respectively. The additional inventory decay is necessary to account for the preclosure period prior to the start time for the TSPA-SEIS simulations. Table 6.3.7-4a shows the per-package inventories aged to year 2117 and used as input to the TSPA-SEIS. In addition to the initial inventories presented in the Initial Radionuclide Inventory Abstraction discussed above, the TSPA-SEIS also includes MOX SNF and LaBS glass HLW. The contributions of MOX and LaBS glass HLW inventory are discussed in Section 6.3.7.1.2.2. Table 6.3.7-4b shows the per package inventories aged to year 2117 for MOX and LaBS glass HLW. Table 6.3.7-5 shows the specific activity for each radionuclide as well as the curies per package inventories for each WP type in the TSPA-SEIS.

6.3.7.1.2 TSPA-SEIS Abstraction

The Initial Radionuclide Inventory Abstraction specifies the initial quantity (grams/WP) of radionuclides for the CSNF, DSNF, and HLW WPs (Table 6.3.7-3). The initial inventories in each WP are decayed as a function of time. The decay chains and radionuclide half-lives are provided on Figure 6.3.7-4, where the radionuclides used for dose calculations are indicated. The following radionuclides are not members of chains: ^{14}C ($t_{1/2}$ = 5,720 yr) and fission products ^{36}Cl ($t_{1/2} = 3.01 \times 10^5$ yr), ^{135}Cs ($t_{1/2} = 2.30 \times 10^6$ yr), ^{137}Cs ($t_{1/2}$ = 30.1 yr), ^{129}I ($t_{1/2} = 15.7 \times 10^6$ yr), ^{79}Se ($t_{1/2} = 2.90 \times 10^5$ yr), ^{126}Sn ($t_{1/2} = 2.30 \times 10^5$ yr), ^{90}Sr ($t_{1/2}$ = 28.8 yr), and ^{99}Tc ($t_{1/2} = 2.13 \times 10^5$ yr), and are not produced by decay of other radionuclides in the waste forms, therefore, they are not included on Figure 6.3.7-4.

Table 6.3.7-6 summarizes the treatment of each radionuclide within the EBS Transport Submodel (Section 6.3.8), the UZ Transport Submodel (Section 6.3.9), the SZ Transport Submodel (Section 6.3.10), and the Biosphere Submodel (Section 6.3.11) for the groundwater release modeling cases. Table 6.3.7-2, Column 3, lists the radionuclides transported in the atmosphere for the Volcanic Eruption Modeling Case. Among the 32 important radionuclides listed in Table 6.3.7-6, 27 are tracked and transported by the EBS Transport, the UZ Transport, and the SZ Transport Submodels. The five radionuclides that are not tracked and transported by the EBS, UZ, and SZ Submodels are ^{245}Cm, ^{241}Pu, ^{227}Ac, ^{228}Ra, and ^{210}Pb. In the Biosphere Submodel, doses from ^{227}Ac, ^{228}Ra, and 210Pb are calculated by assuming they are in secular equilibrium with ^{231}Pa, ^{232}Th, and ^{226}Ra, respectively. Doses from ^{245}Cm and ^{241}Pu are not calculated in the Biosphere Submodel because they are only important for their decay effects on the inventory of ^{241}Am and ^{237}Np, as stated in Table 7-1 of the *Radionuclide Screening* (SNL 2007 [DIRS 177424]). The different transport mechanisms for each radionuclide listed in Table 6.3.7-6 are based upon: (1) the solubility of the radionuclide element within the WP; (2) the subsequent transportability beyond the EBS (based largely on the radionuclide's potential to remain in solution or sorb onto colloids, rather than being sorbed onto the host rock along the transport path from the WP to the biosphere); and (3) the persistence of the radionuclide during the transport period from the WP to the biosphere based on its half-life.

There are a number of sources contributing to the uncertainty in radionuclide inventories. Three sources of uncertainty are common in all waste types. The first is due to the computational method and nuclear characteristics used in predicting future radionuclide inventories (e.g., isotopic neutron cross section or decay half-life). The second source of uncertainty is the completeness of the records that are kept for the SNF and HLW materials (e.g., burn-up history or HLW batch compositions). The third source, and most difficult to quantify, is the uncertainty

about future decisions that will influence the creation, packaging, or shipment of waste. These decisions influence the selection of waste types destined for emplacement into the repository directed by the Nuclear Waste Policy Act of 1982, as amended (42 U.S.C. 10101-10133, 1988 [DIRS 131951]) and implemented under NRC Proposed Rule 10 CFR Part 63 [DIRS 178394] and [DIRS 180319]. Record keeping is important because, given that the wastes are heterogeneous, the selection process can significantly change the average waste characteristics.

For CSNF, an uncertainty multiplier with a uniform distribution between 0.85 and 1.4 was chosen for the TSPA-SEIS (SNL 2007 [DIRS 180472], Table 7-2). The sampled multiplier is applied to the nominal CSNF values, provided in Table 6.3.7-3, for all radionuclides except ^{238}U. For DSNF, an uncertainty multiplier is defined to capture the uncertainty for all radionuclides except ^{238}U. The inventory of ^{238}U has much less relative uncertainty than the other radionuclides because it is present in the initial fuel and generally changes little during reactor operation. The DSNF multiplier is defined as a triangular distribution, with a minimum of 0.45, a most likely value of 0.62, and a maximum value of 2.9. This multiplier is applied to the nominal values for DSNF grams per WP in Table 6.3.7-3 for all radionuclides except ^{238}U. For HLW, a triangular distribution is chosen for the HLW uncertainty multiplier, and this multiplier is applied to the nominal HLW inventories shown in Table 6.3.7-3 for all radionuclides, including ^{238}U. The uncertainty multiplier for HLW has a triangular distribution, with a minimum of 0.7, a most likely value of 1, and a maximum value of 1.5. Table 6.3.7-7 summarizes the uncertainty multipliers for each waste type.

6.3.7.1.2.1 Preclosure Radionuclide Decay and Ingrowth

The initial radionuclide inventory is provided as input to the TSPA-SEIS. There are three categories of waste provided in this per-package format: CSNF, HLW glass, and DSNF. Because the sum total of all waste received at the repository in each fuel type category is used to provide the per-package average source term used in the TSPA-SEIS, the inventory has an age associated with the expected year of the last WP emplacement. Based on previous schedules and repository designs, the CSNF inventory was expected to take 24 years to emplace in the repository, with waste emplacement beginning in the year 2010; the year when the last CSNF WP would have gone into the repository was 2033. The initial radionuclide inventory input to the TSPA-SEIS is provided as it would appear in the year 2033. The HLW and DSNF inventories are each provided to the TSPA-SEIS as they would appear in the year 2030. Table 6.3.7-3 shows the expected average inventory in grams per package for the 31 radionuclides used in the TSPA-SEIS, categorized by waste type, for 2030 and 2033. The current estimate is for emplacement in 2067. The CSNF waste stream is still being produced; therefore, the inventory abstraction assumes that CSNF waste, similar to what would have been emplaced in the year 2033, will be emplaced in 2067.

Because the TSPA-SEIS begins each simulation at repository closure, currently estimated in the year 2117, there will be 50 (CSNF) or 87 (HLW and DSNF) years of radionuclide inventory decay and ingrowth before the inventory is first used by the TSPA-SEIS. In order to synchronize the radionuclide inventory age with the starting point of the TSPA-SEIS, an external calculation was performed to update the radionuclide inventory before entering them into the TSPA-SEIS.

GoldSim Version 9.60 (SP1) was used to perform the radionuclide aging calculation using the species element and the radionuclide half-lives from the TSPA-SEIS. Figure 6.3.7-4 shows the four radionuclide chains modeled in the TSPA-SEIS (note that ^{14}C and the fission products tracked in the TSPA-SEIS are not shown on this figure). Three inventory elements were created, one for each fuel type category, and the radionuclide inventory provided by the Initial Radionuclide Inventory Abstraction. A GoldSim source element for each fuel type performs the calculation, and a collector cell gathers the aged inventory at the closure year.

The updated CSNF inventory was extracted from a 50-year simulation, and the updated HLW and DSNF inventories were extracted from a 87-year simulation. Table 6.3.7-4a shows the inventories provided by the Initial Radionuclide Inventory Abstraction and the updated inventories, which account for the decay and ingrowth experienced during the preclosure period.

Table 6.3.7-4a shows that the majority of included radionuclides experience little to no decay or ingrowth, with the few exceptions of ^{241}Am, ^{137}Cs, ^{237}Np, ^{238}Pu, ^{241}Pu, ^{90}Sr, and ^{234}U. The fission products ^{137}Cs and ^{90}Sr have half-lives of 30.1 years and 28.8 years, respectively, and have decay but no ingrowth because they do not have parent radionuclides. The inventory changes observed with ^{241}Am, ^{237}Np, and ^{241}Pu are related because they are part of the same decay chain (Figure 6.3.7-4). The half-life of ^{241}Pu is 14.4 years and the half-life of ^{241}Am is 432.7 years. The inventory changes observed with ^{238}Pu and ^{234}U occur because of the relatively short ^{238}Pu half-life of 87.7 years, and the fact that the ^{238}Pu inventory decays into the ^{234}U inventory. The inventory changes observed with ^{227}Ac, more than doubling the initial inventory, occur because of the large initial inventories of ^{235}U and ^{231}Pa, compared to the much smaller initial inventories of ^{227}Ac.

6.3.7.1.2.2 Mixed Oxide Spent Nuclear Fuel and Lanthanide Borosilicate Glass Inclusion

The inclusion of MOX SNF and LaBS glass HLW in the TSPA-SEIS is accomplished by adding radionuclide-specific inventories to the initial inventories. More specifically, the LaBS glass inventory is added to the HLW portion of the initial radionuclide inventory and is then subject to the same uncertainty sampling applied to the HLW radionuclide inventory. In addition, the MOX SNF is added to the CSNF portion of the initial radionuclide inventory and is also subject to the uncertainty sampling applied to that inventory. The MOX and LaBS inventories are described in the analysis *MOX Spent Nuclear Fuel and LaBS Glass for TSPA-LA* (SNL 2007 [DIRS 177422]).

Because the ages of the MOX and LaBS waste forms are provided at times that are before the closure of the repository, their inventories were decayed, as described in Section 6.3.7.1.2.1, before addition to the TSPA-SEIS. The MOX inventory is provided at the year 2035, so decay and ingrowth are performed for 82 years before entry into the TSPA-SEIS. The LaBS inventory was provided at the year 2003, so decay and ingrowth is performed for 114 years before entry into the TSPA-SEIS. Table 6.3.7-4b shows the additional radionuclide inventories due to MOX and LaBS waste that are used as input to the TSPA-SEIS; only the inventory that was aged to closure (i.e., after 82 and 114 years, respectively) is used in the TSPA-SEIS.

6.3.7.1.3 TSPA-SEIS Implementation

The initial mass of each radionuclide, provided by the Initial Radionuclide Inventory Abstraction in grams per WP and supplemented by the MOX and LaBS glass inventory, is adjusted to reflect the inventory distribution at repository closure and then is used to initialize source terms during each TSPA-SEIS realization (Table 6.3.7-5). The initial masses are then adjusted to account for uncertainty by applying the multipliers shown in Table 6.3.7-7. That is, at the beginning of each realization, the uncertainty multiplier for each waste form is sampled, and the inventories are adjusted by multiplying the uncertainty multiplier by the masses present at repository closure. The inventory is adjusted for radionuclide decay and ingrowth at each timestep by the simulation software using the first order decay rates shown on Figure 6.3.7-4. The CSNF WPs that are modeled in the TSPA-SEIS use the CSNF inventory values only, while the CDSP WPs contain both the DSNF and HLW inventories. The TSPA-SEIS calculates the specific activities for each radionuclide using the appropriate half-lives.

Additional details regarding the placement of CSNF inventories into a GoldSim source element are provided in the discussion of the CSNF Waste Form Degradation Submodel (Section 6.3.7.4.1.3). The CSNF inventory discussion is presented in Section 6.3.7.4.1.3 because the TSPA-SEIS implementation specifically addresses inventory allocation based on the state of the CSNF waste form. Additional details regarding the placement of DSNF and HLW glass inventories into a GoldSim source element are provided in the discussion of the DSNF and HLW glass Waste Form Degradation Submodels (Sections 6.3.7.4.2.3 and 6.3.7.4.3.3). These inventory discussions are presented in Sections 6.3.7.4.2.3 and 6.3.7.4.3.3 because the TSPA-SEIS implementation specifically addresses inventory allocation based on the state of the DSNF waste form and HLW glass waste form.

6.3.7.2 In-Package Chemistry

The abstractions for determining the chemical parameters inside a failed WP are described in *In-Package Chemistry Abstraction* (SNL 2007 [DIRS 180506]), hereafter referred to as the In-Package Chemistry Abstraction. As to be discussed in Section 6.3.7.2.1, in the TSPA-SEIS, CSNF WPs are discretized into two domains (Cell 1 and Cell 2) and CDSP WPs are discretized into three domains (Cell 1A, Cell 1B, and Cell 2). The In-Package Chemistry Abstraction discussed inthis section deals only with CSNF Cell 1, CDSP Cell 1A, and CDSP Cell 1B (they are collectively called waste form cells, as waste forms are located in those domains). Within the TSPA-SEIS, the In-Package Chemistry Submodel implements the In-Package Chemistry Abstraction to simulate the evolution of the water chemistry inside a failed WP as a function of the relative humidity provided by the EBS TH Environment Submodel (Section 6.3.2), P_{CO_2} provided by the EBS Chemical Environment Submodel (Section 6.3.4), and the water inflow rate provided by the EBS Flow Submodel (Section 6.3.6). Primary outputs from the In-Package Chemistry Submodel that are directly used in the TSPA-SEIS include pH, ionic strength, and total carbonate concentration (ΣCO_3) inside a failed WP.

The water chemistry determined by the In-Package Chemistry Submodel is used by four other Waste Form Degradation and Mobilization submodels. Specifically, the waste form matrix degradation rate for CSNF requires pH and ΣCO_3; the waste form matrix degradation rate for HLW requires pH; the dissolved concentration limits of radioactive elements require pH and

ionic strength; and the stability of colloids requires pH and ionic strength. It is through the influences on other Waste Form Degradation and Mobilization Submodels that the In-Package Chemistry Submodel affects radionuclide availability for transport. Figure 6.3.7-5 is a schematic illustration of the inputs and outputs to and from the In-Package Chemistry Submodel.

6.3.7.2.1 Conceptual Model

The In-Package Chemistry Abstraction calculates the chemistry of water that has reacted with the WP components, including waste forms and basket materials, inside a failed WP. The In-Package Chemistry Submodel implements the abstraction in the TSPA-SEIS. The In-Package Chemistry Abstraction evaluates two different water ingress conceptual models:

- A vapor influx (non-dripping) model where the condensation of vapor onto the WP internals is simulated as pure water, and the resulting solution is in equilibrium with the relative humidity conditions in the drift (SNL 2007 [DIRS 180506], Section 6.3[a]).

- A liquid influx (dripping case or seepage dripping) model where water from the drift, simulated as typical groundwater or drift wall condensate, enters a WP at a rate determined by the liquidinflux ratethrough the openings in the breached WP (SNL 2007 [DIRS 180506], Section 6.3[a]).

Two types of WPs are considered by the In-Package Chemistry Abstraction: CSNF WPs and the CDSP WPs. Furthermore, CSNF WPs are discretized into two domains:

- CSNF Cell 1 (CSNF Waste Form Domain). This cell contains all materials within and including the baskets inside the CSNF WP, excluding the guides. This includes the fuel basket assembly of neutron moderator material and thermal shunts, fuel basket tubes, and CSNF assemblies.

- CSNF Cell 2 (CSNF WP Corrosion Products Domain). This cell contains the TAD canister, and guide assembly.

Similarly, the CDSP WPs are also discretized into three domains:

- CDSP Cell 1A (or 2DHLW Cell). This cell comprises two containers of DHLW glass and their canisters, as designed for the 2 multicanister overpack (MCO)/2DHLW WP.

- CDSP Cell 1B (or 2MCO Cell). This cell comprises two containers of N reactor fuel and their canisters, as designed for the 2MCO/2DHLW WP.

- CDSP Cell 2 (CDSP WP Corrosion Products Domain). This cell contains the divider plate, outer brackets, support tube, and inner vessel.

The In-Package Chemistry Abstraction discussed in this section deals only with CSNF Cell 1, CDSP Cell 1A, and CDSP Cell 1B. The chemistry of Cell 2 of CSNF and CDSP WPs are discussed in Section 6.3.8.

The In-Package Chemistry process model considers the 2MCO/2DHLW waste packages, although the mist numerous CDSP waste packages are the 5DHLW/1DSNF Long. The reasons and justifications for doing that are given in the Section 6.6.6[a] of *In-Package Chemistry Abstraction* (SNL 2007 [DIRS 180506]).

The In-Package Chemistry Abstraction conceptual model is discussed in Section 6.3[a] of *In-Package Chemistry Abstraction* (SNL 2007 [DIRS 180506]), and is briefly described in the paragraphs below.

The In-Package Chemistry Abstraction conceptual model is a batch reactor model that consists of water, oxygen, carbon dioxide, waste forms, and metal alloys. The batch reactor system is in equilibrium with atmospheric conditions, and the reactants degrade in the presence of water according to a rate determined by the physical properties and the exposed surface area of each reactant. For each solid reactant, a degradation rate is selected based on experimental measurements, and the surface area available to react is calculated based on the dimensions of the WP internals. During reaction progress, waste forms and metal alloys are consumed, secondary mineral phases and metal (hydr) oxide corrosion products precipitate from solution, and water changes in its composition and mass due to these reactions.

Inputs for the In-Package Chemistry Abstraction models include thermodynamic properties, parameters such as waste form reaction rates and incoming water compositions, gas phase Pco_2, and compositions and degradation rates of WP components (SNL 2007 [DIRS 180506], Sections 6.3[a]).

Physical-chemical processes considered by the In-Package Chemistry Abstraction model include kinetic dissolution of waste forms and WP internal components, equilibrium precipitation and dissolution of secondary minerals and metal corrosion products, equilibrium oxidation and reduction reactions among gases, secondary minerals, and aqueous species, incoming water compositions, and thermal effects on aqueous phase chemistry (SNL 2007 [DIRS 180506], Section 6.3[a]).

Additional sensitivity cases were run to evaluate the system response to changes in the basecase model. These sensitivity cases evaluated different quantities of water inside the failed WP, different seepage compositions, the oxidation state of chromium, different temperatures, Pco_2 and Po_2, different water fluxes into the failed WP, different WP and waste form configurations and inventories, different corrosion rates of the WP internals, different predominant iron minerals (goethite versus hematite), and different degradation rates of the waste forms inside the failed WP (SNL 2007 [DIRS 180506], Sections 6.6[a]). These sensitivity studies were used to develop an uncertainty range around the basecase model results.

6.3.7.2.2 Model Abstraction

The In-Package Chemistry Abstractions are derived from the output of the In-Package Chemistry Process Models (SNL 2007 [DIRS 180506]) and provide either parameter distributions or response surfaces for the TSPA-SEIS. Both the vapor influx model and the liquid influx model have separate process and abstraction models, which allow the TSPA-SEIS to implement non-dripping and dripping conditions. In *In-Package Chemistry Abstraction* (SNL 2007

[DIRS 180506]), the process model output is discussed in Section 6.5[a] and the abstraction model output, combining the basecase results presented in Section 6.5[a] with the sensitivity studies presented in Section 6.6[a], is discussed in Section 6.10[a]. In this section, the in-package ionic strength and pH abstractions are presented for CSNF Cell 1, CDSP Cell 1A, and CDSP Cell 1B under liquid influx and vapor influx conditions. There are total 12 abstractions (six for ionic strength and another 6 for pH) for the three types of cells under two different water influx conditions. The ΣCO_3 abstraction is developed from equilibrium mass action equations and is presented as a single equation for both liquid influx and vapor influx conditions for CSNF Cell 1 only because HLW glass and DSNF degradation rate calculations do not require this parameter.

The geochemical modeling codes, EQ3NR (Software Code: EQ3/6 V7.2b (CRWMS M&O 1999 [DIRS 153964])) and EQ6 (STN: 10075-7.2bLV-02 [DIRS 159731]), were used to simulate the in-package chemical environment (SNL 2007 [DIRS 180506], Section 1[a]). The output from the In-Package Chemistry Process Model includes concentrations of chemical components and their aqueous complexes that constitute the WP, waste form, seepage, and gas composition in solution in the waste form cells. The In-Package Chemistry Abstraction simplifies the outputs into a form compatible with implementation in the TSPA-SEIS, as to be discussed below.

The abstractions of in-package chemistry are applicable over an oxygen fugacity range from 10^{-17} to $10^{-0.7}$ bars (which is considered oxidizing conditions), a Pco_2 range of 10^{-4} to $10^{-1.5}$ bars, a temperature range from 25°C to 100°C, a relative humidity for vapor influx equal or higher than 95 percent, and a water volumetric flux (hereafter referred to as "flux") for liquid influx equal or higher than 0.1 L/yr (SNL 2007 [DIRS 180506], Section 8.1[a], Table 8-1[a]). Spatially, the applicability of the In-Package Chemistry Abstraction is limited to the waste form cells (i.e., Cell 1 of CSNF WPs, Cell 1a and Cell 1b of CDSP WPs).

The abstraction for the In-Package Chemistry Submodel consists of five parts:

Part I. Determination of whether In-Package Chemistry needs to be calculated

Part II. Determination of which abstraction to be used

Part III. Calculation of ionic strength

Part IV. Calculation of pH

Step V. Calculation of the total concentration of aqueous carbonate (for CSNF Cell 1 only).

These parts are discussed in detail below and summarized in Table 6.3.7-8.

Part I. Determine if In-Package Chemistry needs to be calculated—Whenever the water inflow rate is less than 0.1 L/yr and relative humidity is lower than 95 percent, no in-package chemistry calculation is conducted. The reason is, as stated in *In-Package Chemistry Abstraction* (SNL 2007 [DIRS 180506], Section 6.10.9.1[a]), a relative humidity of 95 percent is the minimum threshold value required to predict a meaningful pH and ionic strength from the vapor influx model. "Given the ultimately small volume of water film being considered at these

relative humidty conditions (RH < 95 percent), virtually all of the waste form materials degraded under these conditions will be precipitated in place and not be available for transport. The small mass of radionuclides that remains dissolved in this minuscule water volume would also not be available for transport because the water film is not expected to be interconnected under these conditions" (SNL 2007 [DIRS 180506], Section 6.10.9.1[a]). In other words, under such conditions, the in-package chemistry becomes undefined, and the in-package chemistry submodel is turned off. The solubilities for all radionuclides, including colloidal species, are set to zero so that no transport is allowed.

However, degradation of waste forms is not considered as ceased below the 95 percent relative humidity threshold because the non-interconnected water film does not prevent waste form from degrading. There are no measurements or methods to calculate waste form degradation rates under vapor flux conditions below 95 percent relative humidity. The *In-Package Chemistry Abstraction* (SNL 2007 [DIRS 180506], Section 6.10.9.1[a]) gives the following estimated values for the HLW glass and CSNF waste forms:

1. For HLW glass, its degradation rate under such conditions is assumed to be equal to the degradation rate at pH of 10 under aqueous corrosion conditions, as is done in the TSPA for temperatures greater than 100°C (Assumption 5.5[a]).

2. For CSNF waste form, its degradation rate under such conditions is assumed to be equal to the degradation rate between pH of 6 and 7 under aqueous corrosion conditions. In the TSPA-SEIS, the pH value that is only used to calculate the CSNF degradation rate is uniformly sampled between 6 and 7.

Part II. Determine which abstraction to be used—Whenever the relative humidity is greater than 95 percent or the water inflow rate is greater or equal to 0.1 L/yr, the in-package chemistry submodel is activated, and a decision is to be made to select one of the two abstractions (the vapor influx versus the liquid influx) to generate outputs for ionic strength and pH. The choice depends on the relative humidity, the water flux rate, and the abstraction that predicts lower ionic strength, as shown in Table 6.3.7-8.

As indicated in Table 6.3.7-8, ionic strength is calculated using the vapor influx abstraction whenever the liquid influx rate is less than 0.1 L/yr (and the relative humidity is equal or greater than 95 percent). At or above 0.1 L/yr, ionic strength is calculated using the liquid influx abstraction. There is an exception that if the vapor influx abstraction predicts a lower ionic strength than that predicted by the liquid influx abstraction, then the vapor influx result should be used. In other words, the vapor influx abstraction is used to set a reasonable upper limit for ionic strength. Its justification is provided in *In-Package Chemistry Abstraction* (SNL 2007 [DIRS 180506], Section 6.10.9.1[a]).

Part III. Calculate Ionic Strength—Ionic strength abstractions for the vapor influx case are given as functions of relative humidity with uncertainty added. The mean value is a piecewise linear function of relative humidity (RH):

$$I = a + b * RH \qquad \text{(Eq. 6.3.7-1)}$$

The intercept (a) and the slope (b) in the above equation have different values under different relative humidities. Table 6.3.7-9 gives those values for CSNF Cell 1, CDSP Cell 1A, and CDSP Cell 1B. The uncertainty range is between the mean value times the lower uncertainty factor (fmin) and the mean value times the upper uncertainty factor (fmax) (i.e., I×fmin, I×fmax). A triangular distribution is assigned for the uncertainty range, with the mean value as the most likely value. The uncertainty factors are also shown in Table 6.3.7-9.

Ionic strength abstractions for the liquid influx case are presented in the logarithm space and are functions of water inflow rate through the breached WPs and time since the representative WP breached. The mean values of logarithm of ionic strength are presented as two-dimensional look-up tables, which are given in Tables 6.3.7-10 through 6.3.7-12 for CSNF Cell 1, CDSP Cell 1A, and CDSP Cell 1B, respectively.

Uncertainties are also included in the logarithm of ionic strength abstractions for the liquid influx case and are presented as a deviation from the mean value. Triangular distributions are assigned to the logarithm of ionic strength for the liquid influx case. That is, the minimum, most likely, and the maximum values are mean-deviation, mean, and mean+deviation, respectively. The deviations are also functions of water inflow rate through the breached WPs and time since breached, presented as two-dimensional look-up tables, which are given in Tables 6.3.7-13 through 6.3.7-15.

Part IV. Calculate pH—When the water influx rate is greater or equal to 0.1 L/yr, the liquid influx pH abstraction will be used to determine in-package pH ranges. The maximum and minimum pHs are functions of pCO_2 (the negative logarithm of P_{CO2}) and log ionic strength as shown in Tables 6.3.7-16 through 6.3.7-21 for those three different cells under the liquid influx conditions.

When the water influx rate is less than 0.1 L/yr, the vapor influx pH abstraction will be used to determine in-package pH ranges. The maximum and minimum pHs are functions of $pCO_2$and log ionic strength, as shown in Tables 6.3.7-22 through 6.3.7-27 for those three different cells under the vapor influx conditions.

For a given pCO_2, the pHs have a uniform distribution between the minimum and maximum pH values defined in the look-up tables in *In-Package Chemistry Abstraction* (SNL 2007 [DIRS 180506], Section 6.10.9.1[a]).

Part V Total Carbonate Concentration Abstraction—ΣCO_3 is used in the degradation rate law for the CSNF waste form. An expression for ΣCO_3 (mol/kg) as a function of temperature, pH, and Pco_2 is based on equilibrium mass action expressions, as discussed in *In-Package Chemistry Abstraction* (SNL 2007 [DIRS 180506], Section 6.10.5). The ΣCO_3 abstraction is:

$$\sum CO_3 = Pco_2\left(10^{K_1} + 10^{pH+K_1+K_2} + 10^{2pH+K_1+K_2+K_3}\right) \qquad \text{(Eq. 6.3.7-2)}$$

where Pco_2 is the carbon dioxide partial pressure in the gas phase. The in-drift Pco_2 (in units of bars) is provided by the EBS Chemical Environment Submodel (Section 6.3.4).

The K_i values in Equation 6.3.7-2 are temperature dependent. Table 6.3.7-28 provides the temperature-dependent K values. The ΣCO_3 abstraction is valid for temperatures ranging from 0°C to 100°C (SNL 2007 [DIRS 180506], Section 6.10.5).

The In-Package Chemistry Abstraction (SNL 2007 [DIRS 180506], Section 1[a]) lists several other limitations of the model, including: (1) limited availability of data on thin film chemistry; (2) limited availability of long-term metal alloy corrosion information such as the identities of the long-term corrosion products and the evolution of the surface area of the metal waste package components as a function of time; (3) simplifications used to define the important processes in the waste form cells; (4) an assumption involving the pH under low water conditions and (5) the approach used to simulate the effects of evaporation.

6.3.7.2.3 TSPA-SEIS Implementation

The abstracted results from the In-Package Chemistry Abstraction are implemented in the TSPA-SEIS to quantify the temporal evolution of values of the aqueous chemistry variables pH, ionic strength, and ΣCO_3. In the TSPA-SEIS, the In-Package Chemistry Submodel is implemented for four different abstraction conditions representing CSNF and CDSP WPs that have water flow through them and CSNF and CDSP WPs that do not have water flow through them. A WP can have water flow through it only if it is in a dripping environment and its DS has failed and the WP failure is not a crack (e.g., cracks cannot support liquid influx (Section 6.3.6.1)). If WPs in a dripping environment are not dripped upon because the DSs remain intact, or the only failure is a crack, the In-Package Chemistry Submodel for non-dripping conditions (i.e., no water flow through the WPs) is evaluated for the WPs.

For the In-Package Chemistry submodel, the time reference is to the elapsed time that a WP has been failed. Because the TSPA-SEIS models groups of failed WPs with each member of a group having the same in-package chemical compositions, it is possible that WPs within a group are failed for different periods of time. To account for this, the TSPA-SEIS calculates an average WP failure time for each group of WPs and uses this average time to evaluate the time dependence for the In-Package Chemistry Submodel. The algorithm for determining the average failed duration in a group of failed WPs is determined by weighting the elapsed duration of failure for the WPs failed in the previous timestep (including the current timestep length) with the new failures in this timestep:

$$\bar{t} = \frac{(N_{WPFailed}^{New} \times \frac{1}{2} TimeStepLength) + (N_{WPFailed}^{Prev} \times (\bar{t}^{prev} + TimeStepLength))}{N_{WPFailed}^{New} + N_{WPFailed}^{Prev}} \qquad \text{(Eq. 6.3.7-3)}$$

where

$\bar{t}$ = the average failure time

$N_{WPFailed}^{New}$ = the number of new failures in the current timestep

$N_{WPFailed}^{Prev}$ = the number of failures in the previous timestep

$\bar{t}^{prev}$ = the previous value of the average failure time

TimeStepLength = the timestep length.

Note that this implementation assigns one-half of a timestep length for newly failed WPs (i.e., on average, the new failures occur halfway through the current timestep). In the TSPA-SEIS, for the purposes of evaluating in-package chemistry, the average WP failure time for the current timestep is set to zero years if the WP temperature exceeds the boiling point of water (i.e., dry conditions prevail in the WP).

The In-Package Chemistry Submodel is implemented by accessing abstractions corresponding to the WP type and dripping condition. These abstractions include distributions representing epistemic uncertainties. For pH, uniform distributions are specified for a given pCO2, and for ionic strength, triangular distributions are specified for a given relative humidity for the vapor influx case or log-triangular distributions are specified for a given time and a given water inflow rate for the liquid influx case. Since pCO2, relative humidity, and water inflow rate all are time-dependent variables in the TSPA-SEIS, the recommended distributions for pH and ionic strength are also time dependent. In other words, the recommended distributions change with time and depend on the outputs of other submodels. Therefore, the pH and ionic strength values for each realization cannot be predetermined by simple sampling prior to the beginning of the realization. To properly account for this time-dependent nature of the In-Package Chemistry Abstraction, dynamic sampling techniques have been implemented in the TSPA-SEIS.

The dynamic sampling technique samples a distribution representing the CDF percentile defined by the specified distributions (for pH it is uniform, for ionic strength it is either triangular or log triangular) for each realization. This percentile remains constant for each realization for the whole duration of the simulation. The distributions are then determined at each time step after the values of the time-varying variables become known. After that, this percentile is applied to the distributions to obtain a pH or an ionic strength values for the current timestep.

For example, for realization *i*, the sampled percentile for pH is 85 percent. At time *t*, the value of pCO2 is 2 and ionic strength is 1 for the CSNF Cell 1 of the liquid influx case. According to Tables 6.3.7-16 and 6.3.7-19, the maximum and minimum of pH are 7.19 and 4.99, respectively. Thus, the pH value at the current timestep is $4.99 + 0.85 \times [7.19-4.99] = 6.86$. The ionic strength values at each timestep are obtained dynamically by a similar scheme, it is a little bit more complicated than pH because it has a triangular or a log-triangular distribution.

The ΣCO_3 is calculated at each timestep using Equation 6.3.7-2 and the relationships provided in Table 6.3.7-28. The variables in the calculation include: (1) the calculated pH from the In-Package Chemistry Submodel (discussed above), (2) the WP temperature provided by the EBS TH Environment Submodel (Section 6.3.2), and (3) the P_{CO_2} provided by the EBS Chemical Environment Submodel (Section 6.3.4).

At each timestep, the outputs from the In-Package Chemistry Submodel are provided to four other Waste Form Degradation and Mobilization submodels. The pH and ΣCO_3 are provided to calculate the waste form matrix degradation rate for CSNF and the pH is also provided to

calculate the degradation of HLW. The pH and ionic strength are provided to calculate solubility limits of radionuclides and to calculate the stability of colloids.

The outputs from the In-Package Chemistry Submodel are provided for each representative CSNF and CDSP cell (Section 6.1.4.7) in dripping and non-dripping environments in each percolation subregion. These outputs are:

- pH as a function of time
- Ionic strength as a function of time
  - ΣCO3 as a function of time.

6.3.7.3 Cladding Degradation

Most CSNF is encased in zirconium-alloy cladding, and a small percentage is encased in stainless steel cladding. In the TSPA-SEIS model, no cladding credit is taken for CSNF (SNL 2007 [DIRS 180616]). In other words, the cladding of all CSNF is assumed to be failed upon arrival at the repository (Section 5.1.3). In addition, the TSPA-SEIS does not take credit for DSNF cladding either (Sections 5.1.3 and 6.3.7.7.2).

Naval SNF, as discussed in Section 6.3.7.1.1, is conservatively treated as CSNF in the TSPA-SEIS. The dose resulting from an equivalent amount of Zircaloy-clad CSNF is higher than the dose from the source-term simulation for naval SNF, thus representing naval SNF as Zircaloy-clad CSNF is conservative. Removing the CSNF cladding credit from the TSPA-SEIS calculations will not alter that conclusion.

6.3.7.3.1 Conceptual Model

The cladding of all CSNF and DSNF is assumed to be failed upon arrival at the repository (Section 5.1.3).

6.3.7.3.2 TSPA-SEIS Implementation

The TSPA-SEIS contains only two cladding related parameters: a cladding failure parameter and a cladding splitting parameter. In the TSPA-SEIS model no credit is taken for CSNF cladding, therefore, it is assumed that the initial fraction of failed cladding (Initial_Rod_Failures) and the fraction of fuel available for corrosion (Fuel_Split_Fraction) is one.

6.3.7.4 Waste Form Degradation

The CSNF Waste Form Degradation Abstraction for the TSPA-SEIS is described in *CSNF Waste Form Degradation: Summary Abstraction* (BSC 2004 [DIRS 169987]). The DSNF Waste Form Degradation Abstraction for the TSPA-SEIS is described in *DSNF and Other Waste Form Degradation Abstraction* (BSC 2004 [DIRS 172453]). The HLW Glass Degradation Abstraction for the TSPA-SEIS is described in *Defense HLW Glass Degradation Model* (BSC 2004 [DIRS 169988]). The abstraction models for the waste form matrix estimate the rates at which the CSNF and HLW waste forms degrade as a function of chemical conditions in failed WPs. For DSNF waste forms, an instant degradation rate is implemented, as to be discussed in detail in Section 6.3.7.4.2.

In the TSPA-SEIS, radionuclide inventory added to a GoldSim source element and bound by a matrix (i.e., UO_2 or borosilicate glass) is not available for transport from a failed WP until the binding matrix degrades. The waste form degradation rates, calculated using the submodels discussed below, are applied by GoldSim source elements. Within each source element, the per-package inventory subject to waste form degradation prior to release from the source element is specified by defining an inventory and then specifying that the inventory is "bound in matrix" in the GoldSim source element. The source element requires a fractional degradation rate, and in the TSPA-SEIS, the applicable rate is the output of the Waste Form Degradation submodels, discussed below. Additional details on the use of GoldSim source elements are provided in Section 6.3.8 and in *User's Guide, GoldSim Probabilistic Simulation Environment* Version 9.60 (GoldSim Technology Group 2007 [DIRS 181727]). The source element applies the degradation rate to the bound inventory, releasing the inventory into the cell network where it then becomes available for transport. Transport of available inventory added to the cell network is discussed in Section 6.3.8.2.1.

Section 6.3.7.4.1 discusses the availability of CSNF inventory from the CSNF source elements in the TSPA-SEIS. Section 6.3.7.4.2 discusses the availability of DSNF inventory in the TSPA-SEIS. Section 6.3.7.4.3 discusses the availability of HLW glass inventory in the CDSP WP source elements of the TSPA-SEIS.

6.3.7.4.1 Commercial Spent Nuclear Fuel Waste Form Degradation

In the TSPA-SEIS, the CSNF Waste Form Degradation Submodel implements the CSNF Waste Form Degradation Abstraction described in *CSNF Waste Form Degradation: Summary Abstraction* (BSC 2004 [DIRS 169987]). Internal inputs to the CSNF Waste Form Degradation Submodel include representative WP temperature provided by the EBS TH Environment Submodel (Section 6.3.2) and pH and ΣCO_3 provided by the In-Package Chemistry Submodel (Section 6.3.7.2). In addition to the temperature, pH, and total carbonate concentration inputs, the CSNF Waste Form Degradation Submodel is also dependent on the partial pressure of oxygen in the failed WP. The output of the CSNF Waste Form Degradation Submodel is the CSNF fractional degradation rate.

6.3.7.4.1.1 Conceptual Model

CSNF pellets and radionuclides in fuel rods with failed cladding will be isolated from the external repository environment until the CSNF WPs are breached. After a CSNF WP is breached, the CSNF may be exposed to dripping water or humid air. Upon exposure to moisture, radionuclides may be released by: (1) instantaneous release of the gap and grain boundary inventories of cesium, iodine, technetium, and strontium; (2) dissolution of the fuel matrix inventory under alkaline and acidic conditions; and (3) instantaneous release of carbon in the WP hardware, external to the cladding. The gap and grain boundary inventory denotes the fission gasses and more mobile radionuclides such as cesium, iodine, and technetium that migrated out of the fuel matrix during reactor operations and accumulated between the fuel pellets and cladding and the fuel matrix grain boundaries. In the TSPA-SEIS, because radionuclides in the gap and grain boundary may be released rapidly, CSNF fuel rods are modeled as two heterogeneous fractions: the matrix inventory and the combined gap and grain boundary inventory. The radionuclide inventory in the fuel matrix is referred to as the bound inventory.

The inventory in the gap and grain boundary regions is referred to as the unbound inventory and is modeled as being available for instantaneous release from fuel rods. Additionally, a third CSNF inventory, the carbon inventory in the WP hardware region, is modeled as being available for instantaneous release from the failed WP, regardless of the integrity of the cladding.

The scope of the CSNF Waste Form Degradation Submodel does not address processes that control the extent to which the radionuclides available for dissolution are mobilized as dissolved and colloidal species. Those features, events, and processes (FEPs) are addressed as follows: Dissolved Concentration Limits Submodel, Section 6.3.7.5; EBS Colloids Submodel, Section 6.3.7.6; and EBS Transport Submodel, Section 6.3.8. Figure 6.3.7-7 illustrates the dependence of CSNF fuel degradation on the In-Package Chemistry Submodel (Section 6.3.7.2) and temperature. Figure 6.3.7-8 provides a schematic drawing of the CSNF fuel rods and CSNF waste form degradation processes.

6.3.7.4.1.2 TSPA-SEIS Abstraction

The CSNF Waste Form Degradation Abstraction developed in *CSNF Waste Form Degradation: Summary Abstraction* (BSC 2004 [DIRS 169987]) provides two abstractions: the instantaneous release fraction of CSNF inventory and the mathematical model for the rate of degradation for the CSNF matrix.

The instantaneous release fraction is computed as the fraction of cesium, iodine, technetium, and strontium in the total inventory in CSNF fuel that is instantly available for release once cladding is degraded, as discussed in Sections 6.3.1 and 6.3.2 of *CSNF Waste Form Degradation: Summary Abstraction* (BSC 2004 [DIRS 169987]). The fraction of CSNF inventory that makes up this instantaneous release inventory is specified by four triangular distributions, as defined in Table 6.3.7-29.

CSNF Waste Form Degradation: Summary Abstraction (BSC 2004 [DIRS 169987]) provides the discussion and mathematical forms for alkaline conditions (Section 6.4.1.2), for acidic conditions (Section 6.4.1.3), and for calculating the specific or absolute dissolution rate. The specific or absolute dissolution rate is a function of four independent variables, which vary spatially in the repository: WP temperature in degrees Kelvin, aqueous pH, ΣCO_3, and oxygen fugacity according to the rate law:

$$\log_{10}(F) = \log_{10}(A) + a_0 + a_1 \times IT + a_2 \times pCO_3 + a_3 \times pO_2 + a_4 \times pH \qquad \text{(Eq. 6.3.7-4)}$$

where dependent variable

$\log_{10}(F)$ = log base 10 of the fractional dissolution rate of the CSNF in unit of [1/d] (d stands for days)

and independent variables

IT = inverse temperature of the WP [K^{-1}] (i.e., IT = 1/T)

pCO_3 = negative base 10 log of ΣCO_3 [molar] (i.e., $pCO_3 = -\log_{10}([HCO_3^-]+[CO_3^{2-}])$)

pO_2 = negative base 10 log of the oxygen partial pressure (atmospheres)

pH = in-package pH

and parameters

$\log(A)$ = log base 10 of the fuel specific surface area (m^2/mg)

a_0, a_1, a_2, a_3, a_4 are regression parameters for the dissolution rate per unit area.

Under dripping conditions, the pH inside a failed WP is a function of the liquid flow rate through the failed WPs (Section 6.3.7.2). The flow rate through the failed WPs depends on the damage state of the WP outer shell and the dripping rate (Section 6.3.6), which may vary in the different percolation subregion environments in the TSPA-SEIS. Therefore, pH and pCO_3 are spatially dependent outputs of the In-Package Chemistry Submodel (Section 6.3.7.2) and in the TSPA-SEIS are calculated within each percolation subregion environment. The partial pressure of O_2 in the WP is a constant value of 0.2 bar and is equated to the partial pressure of O_2 in the drift environment, which is equal to atmospheric O_2 (See Section 5.1.3). The representative temperature of the WPs is a spatially dependent output of the EBS TH Environment Submodel (Section 6.3.2), and in the TSPA-SEIS it is calculated for each percolation subregion.

The dissolution rate is modeled for an alkaline state with a pH $\geq$ 6.8 and an acidic state with a pH < 6.8. The equation used for the alkaline state does not include pH dependence ($a_4 = 0$) and is:

$$\log_{10}(F) = \log_{10}(A) + a_0 + a_1 \times IT + a_2 \times pCO_3 + a_3 \times pO_2 \qquad \text{(Eq. 6.3.7-5)}$$

The distribution for the log base 10 of the specific surface area and values for the coefficients are presented in Table 6.3.7-30.

The equation used for the acidic state is

$$\log_{10}(F) = \log_{10}(A) + a_0 + a_1 \times IT + a_3 \times pO_2 + a_4 \times pH \qquad \text{(Eq. 6.3.7-6)}$$

For the acidic state, the dissolution rate does not depend on the ΣCO_3 ($a_2 = 0$). The distribution for the log of specific surface area and the coefficient values is shown in Table 6.3.7-31.

6.3.7.4.1.3 TSPA-SEIS Implementation

After a WP is breached, the entire CSNF has failed cladding and is exposed to moisture. Radionuclides are then released by: (1) instantaneous release of the gap fraction inventory and (2) matrix dissolution under alkaline or acidic conditions. Cesium, iodine, technetium, and strontium are in the instantaneous release inventory. The fraction of emplaced inventory that makes up the instantaneous release inventory for cesium, iodine, technetium, and strontium is determined by sampling four triangular distributions representing epistemic uncertainty. These distributions are sampled once per realization. The instantaneous release inventory, the product of the instantaneous release fraction, and the per-package inventory (accounting for decay and

ingrowth) are treated as unbound inventory within the inner barrier function of the GoldSim source element (GoldSim Technology Group 2007 [DIRS 181727]).

Similarly, the ^{14}C hardware inventory, the product of the hardware inventory fraction, and the per-package inventory (accounting for decay and ingrowth), are treated as unbound inventory between the inner and outer barrier functions of the GoldSim source element. The hardware inventory fraction originates from neutron activation of stainless-steel hardware outside the fuel rods and is specified to be 18 percent of the ^{14}C inventory in a CSNF WP (SNL 2007 [DIRS 180472], Section 6.7 and Table 7-1[a]).

The TSPA-SEIS considers three CSNF inventories in each CSNF WP of a GoldSim source element (e.g., group of WPs). The first inventory in the CSNF WP is the ^{14}C hardware inventory. At the global level, the hardware inventory is calculated as the fraction of the per-package inventory that is associated with the WP hardware and the per-package inventory, discussed in Section 6.3.7.1. This inventory is calculated at the global level but is added to each GoldSim source element within each percolation subregion environment. Within the GoldSim source element, this inventory is immediately released when the WP fails.

The second inventory in the CSNF source term is the instantaneous release inventory. At the global level, the instantaneous release inventory is calculated as the fraction of the per-package inventory that is in the gap and grain boundaries (BSC 2004 [DIRS 169987], Sections 6.3.1 and 6.3.2) and the per-package inventory, discussed in Section 6.3.7.1. The gap and grain boundary inventory fractions are presented in Table 6.3.7-29. If a radionuclide in the CSNF WP is not included in Table 6.3.7-29, the radionuclides' instantaneous release inventory is zero grams per WP. This inventory is calculated at the global level but is added to each GoldSim source element within each percolation subregion environment. Within the GoldSim source element, this inventory is immediately released when the WP fails.

The third inventory in the CSNF source term is the inventory bound in the CSNF matrix. At the global level, the bound inventory is calculated as the total per package inventory minus the other hardware and instantaneous release inventories. This inventory is calculated at the global level but is added to each GoldSim source element within each percolation subregion environment. Within the GoldSim source element, this inventory is bound in a matrix and is only available for transport after the matrix is degraded. In the CSNF WP, the matrix degrades at the calculated degradation rate, discussed in Section 6.3.7.4.1.2. Within an intact CSNF WP, the waste form does not degrade. In a failed CSNF WP, the waste form is allowed to degrade and make radionuclides available for transport.

The fractional degradation rate is calculated using the rate formulas (Equations 6.3.7-5 and 6.3.7-6 described in Section 6.3.7.4.1.2) for conditions with a pH greater than or equal to 6.8 and for conditions with a pH less than 6.8. Degradation rates under both alkaline and acidic conditions are a function of the specific surface areas of exposed fuel, the representative WP temperature provided at each TSPA-SEIS timestep by the EBS TH Environment Submodel (Section 6.3.2), ΣCO_3 provided at each TSPA-SEIS timestep by the In-Package Chemistry Submodel (Section 6.3.7.2), the in-package pH provided by the In-Package Chemistry Submodel (Section 6.3.7.2), and the partial pressure of oxygen inside the failed WP. A triangular distribution is used to represent epistemic uncertainty in a specific surface area of exposed fuel

(Tables 6.3.7-30 and 6.3.7-31). This distribution is sampled once per realization and the sampled value is applied in all of the percolation subregion environment degradation rate calculations. The values for the uncertain coefficients in the rate expressions are correlated. These coefficients are sampled in the TSPA-SEIS using a Cholesky factorization method to induce correlation, as described in Section 6.1.2.

At temperatures greater than 100°C, the In-Package Chemistry Submodel (Section 6.3.7.2) pH and ΣCO_3 are not valid, nor is the CSNF degradation rate equation. Within the TSPA-SEIS, when a breached CSNF WP is exposed to temperatures exceeding 100°C, the calculated CSNF degradation rate is replaced with a rate that instantaneously degrades the exposed waste form. A rate of 1×10^6 per year (i.e., 0.032 per second) is used in the TSPA-SEIS to implement this recommendation because it results in complete CSNF degradation within one year.

The calculated fractional degradation rate is input to the GoldSim source element located in each percolation subregion environment. The GoldSim source element applies the fractional degradation rate to degrade the CSNF waste form inside within a failed WP. The fraction of failed cladding rods is assumedto be one and discussed in Section 6.3.7.3. The fraction of failed WPs is discussed in Section 6.3.5. After the waste form is degraded, the GoldSim source element releases the mass associated with the degraded fuel into the volume occupied by the waste form alteration products, the schoepite rind, and the inventory becomes available for transport. In addition, the GoldSim source element releases the hardware inventory and the instantaneous release inventory into this same volume. For modeling purposes, a default volume is applied before waste form degradation is initiated. Section 6.3.8.2.1 provides the discussion for calculating the volume of rind formed as the CSNF waste form degrades and the subsequent transport of the available inventory to other areas of the failed WP.

A supplemental calculation is provided in the TSPA-SEIS to evaluate the average fraction of the CSNF that is degraded inside each failed WP. This supplemental calculation is provided as an analysis tool for evaluating the performance of the waste form and also provides a desirable result used to determine the volume of rind formed in the waste form (Section 6.3.8.2.1). This calculation is the average fraction of the CSNF waste form that is degraded in the failed CSNF WPs. Equation 6.3.7-7 is the evaluation of F_{cor} in the TSPA-SEIS:

$$F_{cor}(t) = \frac{M_i^{released}(t)}{M_i(t=0)} = 1 - \frac{M_i^{retained}(t)}{M_i(t=0)} \qquad \text{(Eq. 6.3.7-7)}$$

where

$M_i^{released}$ = the cumulative mass of radionuclide "i" released from the degraded waste form in the failed CSNF WPs

$M_i^{retained}$ = the total mass of radionuclide "i" retained by an undegraded waste form in the failed CSNF WPs

and

$M_i(t=0)$ = the initial inventory (in grams) of radionuclide "i" associated with the failed CSNF WPs.

This calculation uses the knowledge of the internal functions and properties of a GoldSim source element (GoldSim Technology Group 2007 [DIRS 181727]) to evaluate the degradation state of the CSNF matrix inside each failed CSNF WP. The GoldSim source element internally tracks the value of $M_i^{released}$ used in the evaluation of Equation 6.3.7-7. $M_i^{retained}$ can be computed by performing a mass balance on the failed WPs, using the released inventory, $M_i^{released}$, and the initial inventory for the failed WPs, accounting for decay and ingrowth as necessary. As discussed below, the species considered in the TSPA-SEIS calculation of F_{cor} is a non-radioactive species that does not participate in the transport and dose calculations, and is added as supplemental inventory to each CSNF WP specifically to calculate F_{cor}.

The TSPA-SEIS includes 10 grams of an additional species "Col" per CSNF WP. In the TSPA-SEIS "Col" is an unreacting species that is added as a fully bound species in the CSNF waste form. "Col" does not participate in radionuclide decay chains or contribute to the total dose. As a noncompeting species in the transport calculations ("Col" does not influence the solubility of other elements), "Col" can be used as a "tracer" to evaluate the waste form performance. Within each GoldSim source element, the amount of inventory accounting for decay and ingrowth, and number of WPs (both failed and not failed), are internally tracked. In addition, the cumulative amount of each bound and unbound radionuclide, both retained by and released from the waste form, is also tracked. By performing a mass balance on the amount of "Col" remaining in the waste form, the average fraction of the CSNF waste form that has degraded can be evaluated at each timestep. Within each percolation subregion environment, the total amount of "Col" associated with the GoldSim source element for that percolation subregion environment is the product of the "Col" inventory per WP and the number of WPs. The total amount of "Col" retained by each GoldSim source element is an output of the GoldSim source element and is internally tracked by GoldSim. However, the internally tracked value includes both failed and not failed WPs and is not the value discussed in Equation 6.3.7-7, unless all of the WPs in the source term are failed. The total amount of "Col" released by the failed WPs associated with each GoldSim source element, $M_i^{released}$ in Equation 6.3.7-7, is also an output of the GoldSim source element and is internally tracked by GoldSim, but it can also be computed by subtracting the amount retained from the total inventory of "Col." The total amount of "Col" released by the GoldSim source element, divided by the number of failed WPs associated with the GoldSim source element, is the average amount of "Col" released from each of the failed WPs. This result divided by the initial per-package inventory for those failed WPs yields the average fraction of "Col" released from each failed WP represented by the source element. With the knowledge that the GoldSim source element congruently releases each bound species as the waste form degrades (i.e., if 10 percent of species X is released in one timestep, then 10 percent of all other bound species are also released in that timestep), the average fraction of the waste form degraded in each WP can be equated to the average fraction of "Col" that is released from each failed WP. This result is used to determine the volume of fuel that is degraded in the CSNF water volume calculations (Sections 6.3.8.2.1) and assess the performance of the CSNF waste form and WP.

6.3.7.4.2 U.S. Department of Energy Spent Nuclear Fuel Waste Form Degradation

The DSNF Waste Form Degradation Abstraction for the TSPA-SEIS is described in *DSNF and Other Waste Form Degradation Abstraction* (BSC 2004 [DIRS 172453]). The DSNF Waste Form Degradation Submodel implements this abstraction and does not require inputs from other TSPA-SEIS submodels. The output of the DSNF Waste Form Degradation Submodel is the instantaneous release of the DSNF inventory from a breached CDSP WP.

6.3.7.4.2.1 Conceptual Model

Several hundred distinct types of DSNF may eventually be emplaced in the Yucca Mountain repository. It is not practical to attempt to determine the impact of each individual fuel type on dose. Instead, the DSNF Waste Form Degradation Abstraction categorized the DSNF in 11 groups (BSC 2004 [DIRS 172453], Sections 1.2, 6.1, and Table 6-2) to represent the entire DSNF inventory for the TSPA-SEIS. These DSNF groups are:

- Group 1 – Naval SNF
- Group 2 – Plutonium/uranium alloy (Fermi 1 SNF)
- Group 3 – Plutonium/uranium carbide (Fast Flux Test Facility -Test Fuel Assembly SNF)
- Group 4 – Mixed oxide and plutonium oxide (Fast Flux Test Facility -Demonstration Fuel Assembly / Fast Flux Test Facility -Test Demonstration Fuel Assembly SNF)
- Group 5 – Thorium/uranium carbide (Fort St. Vrain SNF)
- Group 6 – Thorium/uranium oxide (Shippingport light water breeder reactor SNF)
- Group 7 – Uranium metal (N-Reactor SNF)
- Group 8 – Uranium oxide (Three Mile Island-2 core debris)
- Group 9 – Aluminum-based SNF (Foreign Research Reactor SNF)
- Group 10 – Other (Miscellaneous Fuel)
- Group 11 – Uranium-zirconium hydride (Training Research Isotopes–General Atomics SNF).

For the TSPA-SEIS, an upper-limit degradation model is used for all the DSNF other than naval SNF. In this upper-limit degradation model, the DSNF inventory is immediately available for mobilization, subject to solubility constraints, after the outer surface of the CDSP WP is breached. The release rate of radionuclides from exposed naval SNF is less than that from exposed CSNF. To provide a conservative simplification, the TSPA-SEIS represents naval SNF

with an equivalent amount of CSNF, as discussed in Section 6.3.7.1 and in *Initial Radionuclide Inventories* (SNL 2007 [DIRS 180472], Section 6.2). Thus, naval SNF will not be discussed below as a specific type of DSNF. Figure 6.3.7-9 is a schematic illustration of DSNF waste form degradation within the CDSP WP as part of the model for waste form degradation.

6.3.7.4.2.2 TSPA-SEIS Abstraction

The DSNF Waste Form Degradation Submodel releases the entire per package DSNF inventory for solubilization and mobilization from the CDSP WPs when the WPs are breached. Because of this simplification, the DSNF inventory is treated as unbound inventory in the TSPA-SEIS, and no TSPA parameters are necessary to implement a degradation rate calculation in the TSPA-SEIS.

The volume of water associated with the degraded DSNF is a product of the DSNF rind porosity, rind saturation, and rind volume. Within the representative CDSP WP, the volume occupied by DSNF is 1.0 m^3/WP (BSC 2004 [DIRS 172453], Section 8.1, Table 8-1). The porosity of the powdered form of the corrosion product occupying the volume of the DSNF is 0.20 and is fully saturated (SNL 2007 [DIRS 177407], Table 8.2-1).

6.3.7.4.2.3 TSPA-SEIS Implementation

In the TSPA-SEIS, the DSNF degradation rate is based on an instantaneous release of the radionuclide inventory and does not use any input parameters or rate equations. In addition, the DSNF inventory is not placed into a GoldSim source element with the HLW glass inventory. Instead, each time a CDSP WP fails, the DSNF inventory associated with the failed WP (accounting for decay and ingrowth) is placed into the volume of water associated with the volume occupied by the DSNF. Once released, radionuclides are available for transport to the WP corrosion products and through to the EBS, subject to solubility constraints.

In the TSPA-SEIS, the initial DSNF inventory, with the uncertainty described in Section 6.3.7.1 accounted for, changes through time as a result of radionuclide decay. The DSNF inventory for a single package is fed into a GoldSim source element at the global level of the TSPA-SEIS. This source element has been specified such that it is not allowed to fail and is, therefore, not a DSNF source for radionuclide releases. This implementation is a calculation to account for radionuclide decay. For each representative inventory (i.e., CSNF, DSNF, or HLW glass), a GoldSim source element internally tracks all of the radionuclide decay calculations for the specified decay chains. By utilizing a source element with the DSNF inventory, the TSPA-SEIS simplifies the implementation of the radionuclide decay and ingrowth calculations for DSNF inventory and is consistent with the decay rates specified for the HLW glass and CSNF inventories. Each time a CDSP WP fails, this DSNF source element is queried for the DSNF inventory, adjusted for decay and ingrowth, and the TSPA-SEIS subsequently adds a discrete amount of mass, equivalent to the current amount of "unexposed" mass in the DSNF source element, into the CDSP WP EBS cell network (Section 6.3.8) for each failed CDSP WP.

The volume of water associated with the fully saturated DSNF corrosion product is a product of the DSNF rind porosity, rind saturation, and DSNF volume.

6.3.7.4.3 High-Level Radioactive Waste Glass Waste Form Degradation

The HLW Glass Waste Form Degradation Submodel for the TSPA-SEIS is described in the HLW Glass Degradation Abstraction (BSC 2004 [DIRS 169988]). Internal inputs to the HLW Glass Degradation Submodel of the TSPA-SEIS include representative WP temperature and relative humidity provided by the EBS TH Environment Submodel (Section 6.3.2), and pH provided by the In-Package Chemistry Submodel (Section 6.3.7.2). The output from the HLW Glass Waste Form Degradation Submodel is the HLW radionuclide fractional degradation rate and the average fraction of the HLW glass that is degraded in each failed WP.

6.3.7.4.3.1 Conceptual Model

The HLW Glass Degradation Abstraction provides a rate equation that describes the degradation rate of HLW glass when the HLW glass is contacted by water or humid air. The radionuclide release rate is calculated as the product of the surface area of HLW glass contacted by water, the degradation rate of the HLW glass, and the mass fractions of the radionuclides in the HLW glass. Degradation of the HLW glass does not occur in the TSPA-SEIS when the relative humidity is less than 44 percent. Mathematical expressions and parameter values for the HLW glass surface area and degradation rate are described in the following section. The mass fractions of radionuclides in the HLW glass are obtained from the Initial Radionuclide Inventory Abstraction described in Section 6.3.7.1. The HLW Glass Degradation Abstraction also provides functional relationships for the volume of water in the HLW glass degradation products (the rind) and the rind thickness. These parameters are used to model in-package radionuclide transport (Section 6.3.8.2.2) and calculate the diffusive release of radionuclides from the HLW rind. Although the HLW Glass Degradation Abstraction provides the conceptual model for both the glass degradation rate and the subsequent mass and volume of the rind formed from the degradation process, the discussion of the conceptual model for rind formation is deferred to Section 6.3.8.2.2. The rind layer affects the transport of the radionuclides after they become available. The discussions presented in Section 6.3.7 pertain to radionuclide availability, and the discussions presented in Section 6.3.8 pertain to the transport of available radionuclides.

6.3.7.4.3.2 TSPA-SEIS Abstraction

The HLW glass fractional degradation rate is the main quantity calculated in the TSPA-SEIS by the HLW Glass Waste Form Degradation Submodel.

Glass Degradation and Radionuclide Release—The same rate expression is used to calculate the degradation rate of HLW glass exposed to humid air, exposed to dripping water, or immersed in water, as discussed in Section 8.1 of *Defense HLW Glass Degradation Model* (BSC 2004 [DIRS 169988]). The resulting simplified HLW glass dissolution rate expression for the TSPA-SEIS is:

$$rate_G = k_E 10^{\eta \bullet pH} \exp(-E_a / RT) \qquad \text{(Eq. 6.3.7-8)}$$

where

$rate_G$ = absolute HLW glass dissolution rate ($g/m^2/d$)

k_E = affinity term ($g/m^2/d$)

η = pH dependence coefficient (dimensionless)

E_a = effective activation energy (kJ/mol)

R = universal gas constant (8.14E-03 kJ/mol/K)

T = temperature (K).

The rate equation requires the specification of three parameter values: k_E, η, and E_a, and the two model variables, temperature and pH. HLW glass degradation does not occur if relative humidity is less than 44 percent (BSC 2004 [DIRS 169988], Section 8.1). If the relative humidity is greater than or equal to 44 percent, the same rate expression is used to calculate the degradation rate when HLW glass is exposed to humid air or dripping water, or is immersed in water. However, separate sets of parameter values are used for degradation in acidic and alkaline solutions. Values for η, E_a, and distributions for k_E for acidic and alkaline solutions are provided in Table 6.3.7-33. In accordance with the guidance provided in Section 8.1 of *Defense HLW Glass Degradation Model* (BSC 2004 [DIRS 169988]), the degradation rate that is applied in the TSPA-SEIS is the greater of the acidic and alkaline condition degradation rates, regardless of modeled pH. At temperatures greater than 100°C, the In-Package Chemistry Submodel (Section 6.3.7.2) pH calculation is not valid. Therefore, the abstracted rate model, Equation 6.3.7-8, cannot be applied when the representative WP temperature is greater than 100°C. Within the TSPA-SEIS, when a breached CDSP WP is exposed to temperature exceeding 100°C, the abstracted HLW degradation rate model becomes independent of the pH. The developed rate equation is equivalent in form to Equation 6.3.7-8, replacing the pH term with a constant value (= 10) (BSC 2004 [DIRS 169988], Section 8.1). In addition, the alkaline side model coefficients are used to evaluate the modified rate equation. Furthermore, as stated in Section 8.1 of *Defense HLW Glass Degradation Model* (BSC 2004 [DIRS 169988]), glass degradation does not occur when relative humidity is below 44 percent (equivalent to a temperature of 125°C). Under such conditions, the degradation rate of HLW glass is set to zero.

The HLW glass mass dissolution rate, presented in *Defense HLW Glass Degradation Model* (BSC 2004 [DIRS 169988], Section 8.1) is the specific rate, $rate_G$, multiplied by the surface area available for dissolution over a timestep. The surface area that remains as the HLW glass degrades is the product of the specific surface area, the exposure factor, and the mass of HLW glass that remains. The expression used to calculate the HLW glass surface area (m^2) as HLW glass dissolves in a timestep is:

$$S = f_{\text{exposure}} S_{sp} (M_0 - \Sigma M_t) \qquad \text{(Eq. 6.3.7-9)}$$

where

S_{sp} = the geometric specific surface area available for reaction (m^2/kg)

$f_{exposure}$ = the exposure factor (accounting for the higher effective surface area of the glass log resulting from cracking of the HLW glass after it is poured into the canister)

M_0 = the initial mass of HLW glass (kg)

$\sum M_t$ = the total mass of HLW glass degraded in all previous timesteps (kg).

The mass of HLW glass degraded in a timestep is calculated as the product of the HLW glass degradation rate for that realization and the duration of the timestep. Table 6.3.7-32 provides the value for the specific surface area. The initial mass of HLW glass is 2,710 kg.

The expression used to calculate the surface area for the next timestep is:

$$S = 2.70 \times 10^{-3} f_{\text{exposure}} (2710 - \Sigma M_t) \qquad \text{(Eq. 6.3.7-10)}$$

The exposure factor is an uncertain parameter with sampling shown in Table 6.3.7-32. The initial timestep is conducted with $\sum M_t = 0$. The value of $\sum M_t$ is revised after each timestep by adding the mass of HLW glass degraded over the current TSPA-SEIS timestep, as shown below:

$$M_t = rate_G \times \Delta t \times S \qquad \text{(Eq. 6.3.7-11)}$$

The release rate of radionuclides due to HLW glass degradation is the product of the HLW glass mass dissolution rate and the mass fraction of a radionuclide in the HLW glass:

$$R_{RN} = S \times rate_G \times I_{RN} \qquad \text{(Eq. 6.3.7-12)}$$

where

R_{RN} = radionuclide release rate (Ci/d)

I_{RN} = mass fraction of a radionuclide in the HLW glass (Ci/g).

The radionuclide release rate determines the rate of radionuclide release from degraded HLW glass to the volume of water in the rind of altered HLW glass.

6.3.7.4.3.3 TSPA-SEIS Implementation

The HLW glass source term within each percolation subregion environment of the TSPA-SEIS contains two HLW glass inventories: a bound inventory and an unbound inventory. In the TSPA-SEIS, the HLW glass inventory is fully bound in the glass; therefore, the unbound inventory becomes zero grams for each radionuclide in the glass inventory (Section 6.3.7.1).

The unbound inventory is included in the TSPA-SEIS to facilitate the development of sensitivity runs. Both inventories are added to each GoldSim source term, but the package inventory is bound in the glass matrix. At the global level, the bound inventory is calculated as the total per-package inventory, including uncertainty, and the unbound inventory is set to zero grams. These inventories are calculated at the global level but are added to each GoldSim source element within each percolation subregion environment. Within the GoldSim source element, the bound inventory is bound in a matrix and is only available for transport after the matrix is degraded. In the CDSP WP, the HLW glass matrix degrades at the calculated degradation rate, discussed in Section 6.3.7.4.3.2. Within an intact CDSP WP, the waste form does not degrade. In a failed CDSP WP, the waste form degrades at the calculated rate, and radionuclides become available for transport.

Degradation of HLW glass starts when the CDSP WPs are breached and if relative humidity is greater than or equal to 44 percent. The rate of degradation used in the TSPA-SEIS is the fractional form of the dissolution rate. This degradation rate is the product of the absolute glass dissolution rate (Section 6.3.7.4.3.2), the specific surface area of the glass, and the waste form exposure factor. The coefficients in the rate equation are dependent on pH conditions: one set for acidic conditions and one set for alkaline conditions (Table 6.3.7-32).. The rate expression is simultaneously evaluated with both acidic and alkaline condition coefficients with the current inputs, regardless of the applied pH, and the greater of the two calculated rates is applied to degrade the HLW glass. At temperatures greater than 100°C and less than 125°C, the rate expression is evaluated using the alkaline-side coefficients, with the pH term taking on a constant alkaline value (=10). The rate equation is a function of an affinity term, temperature, pH, and HLW glass surface area. The affinity term is treated as an epistemic uncertainty and is represented by two triangular distributions (k_{E_acid}, $k_{E\_alkaline}$) used for acidic and alkaline conditions. These distributions are sampled once per realization. The exposure factor, $f_{exposure}$, is treated as an epistemic uncertainty represented by a triangular distribution. This distribution is sampled once per realization, and the same exposure factor is used for alkaline and acidic conditions.

The calculated fractional degradation rate is input to the GoldSim source element located in each percolation subregion environment. The GoldSim source element applies the fractional degradation rate to degrade the HLW glass waste form inside a failed CDSP WP. The fraction of failed WPs is discussed in Section 6.3.5. After the glass degrades, the GoldSim source element releases the mass associated with the degraded waste form into the volume occupied by the waste form alteration products, the rind, and the inventory becomes available for transport. Section 6.3.8.2.2 provides the discussion for calculating the volume of rind formed as the HLW glass waste form degrades and the subsequent transport of the available inventory to other areas of the failed WP.

A supplemental calculation is provided in the TSPA-SEIS to evaluate the average fraction of the HLW glass waste form that is degraded inside each failed WP. This supplemental calculation is provided as an analysis tool for evaluating the performance of the waste form and also provides a desirable result used to determine the volume of rind formed in the waste form (Section 6.3.8.2.2). This calculation is the average fraction of the HLW glass waste form that is degraded in the failed CDSP WPs, and for the purposes of the CDSP rind volume calculation, is called variable F_{cor} to be consistent with the CSNF discussion. Equation 6.3.7-7, and the

supplemental discussion provided in Section 6.3.7.4.1.3, is the evaluation of F_{cor} in the TSPA-SEIS and is applicable to both CSNF and CDSP WPs. Within the TSPA-SEIS, the calculation of F_{cor} is the same for both CSNF and CDSP source terms, so the discussion is not repeated.

Although presented in Section 6.3.7.4.3.2, Equations 6.3.7-9 through 6.3.7-12 are not directly incorporated into the TSPA-SEIS. These equations adjust the specific degradation rate to compensate for differences in the amount of glass degraded as a function of time. Using a fractional degradation rate, the type required by GoldSim source elements, the TSPA-SEIS does not need to compensate for depleting the glass as degradation processes occur. Similarly, because the TSPA-SEIS calculates the fraction of the HLW glass that is degraded, F_{cor} for analysis purposes, this result is used to determine the rind volume (Section 6.3.8.2.2) and assess the performance of the HLW glass waste form.

6.3.7.5 Dissolved Concentration Limits

The Dissolved Concentration Limits Abstraction for the TSPA-SEIS is described in *Dissolved Concentration Limits of Elements with Radioactive Isotopes* (SNL 2007 [DIRS 177418]). Within the TSPA-SEIS, the Dissolved Concentrations Limits (i.e., solubility) Submodel implements the Dissolved Concentrations Limits Abstraction to calculate solubilities for 8 elements, including plutonium (Pu), neptunium (Np), uranium (U), thorium (Th), americium(Am), protactinium (Pa), tin (Sn), and radium (Ra). As pointed out in Table 6.3.7-33, for technetium (Tc), carbon (C), iodine(I), cesium (Cs), strontium (Sr), selenium (Se), and chlorine (Cl), no solubility-controlling solids are expected to form under the repository conditions, therefore, their solubilities are not evaluated. As stated in Table 6.3.7-6, actinium (Ac) and curium (Cm) are not transported within the TSPA-SEIS. Thus, their solubilities are not needed and are not evaluated in the solubility abstraction. The output of the Dissolved Concentration Limits Submodel is used in the TSPA-SEIS to constrain the dissolved concentrations of radioactive elements in the WPs and in the invert.

6.3.7.5.1 Conceptual Model

The Dissolved Concentration Limits Abstraction is based on calculations using geochemical modeling tools and thermodynamic databases. Inputs to the Dissolved Concentration Limits Abstraction include solution chemistry, thermodynamic properties, and associated uncertainties of pertaining species (SNL 2007 [DIRS 177418], Table 4-1). Laboratory and field observations and measurements were used in the selection of solubility controlling phases and model validation. The Dissolved Concentration Limits Abstraction details the treatment of solubilities for 8 elements that are included in the TSPA-SEIS. The resulting outputs from the Dissolved Concentration Limits Abstraction are, with exceptions, functions of pH and fco_2 and can be applied for a wide range of environmental conditions in both the WPs and the invert. Figure 6.3.7-10 is a schematic illustration showing the relations of the Dissolved Concentration Limits (Solubility) Submodel with the other submodels of the Waste Form Degradation and Mobilization Model Component.

The selection of solubility controlling phase(s) has a direct impact on the outcome of the Dissolved Concentration Limits Abstraction calculations. Based on the laboratory and field observations, or conservative assumptions, solubility-controlling phases for the 8 elements

considered in the TSPA-SEIS were carefully selected, as summarized in Table 6.3.7-33. The justification for using each solid phase is discussed in *Dissolved Concentration Limits of Elements with Radioactive Isotopes* (SNL 2007 [DIRS 177418], Section 6).

The environmental conditions expected in the repository are considered for the solubility calculations. Ligands that can form aqueous complexes with radioactive elements and are common in Yucca Mountain waters, such as OH^-, CO_3^{2-}, F^-, HPO_4^{2-}, Cl^-, SO_4^{2-}, and NO_3^-, are included in solubility calculations in *Dissolved Concentration Limits of Radioactive Elements* (SNL 2007 [DIRS 177418], Section 6). The sensitivity analysis shows that, among the environmental conditions considered by the Dissolved Concentration Limits Abstraction, pH and fCO_2 have the primary impact on actinide solubilities. Therefore, those two variables are chosen as the independent variables for solubility calculations. Solubility limits were calculated for a wide range of pH and fCO_2 values. Other environmental variables that have a significant impact on actinide solubilities are accounted for by assigning them as a charge balance species in the Dissolved Concentration Limits Abstraction calculations (e.g., SO_4^{2-}) or through an added uncertainty term to the Dissolved Concentration Limits Submodel (e.g., F^-).

Four types of uncertainties -(1) uncertainties in the K values of solubility controlling solids and aqueous species, (2) uncertainties of activity coefficients, (3) uncertainties in water chemistry, and (4) uncertainties in temperature - have been evaluated in *Dissolved Concentration Limits of Elements with Radioactive Isotopes* (SNL 2007 [DIRS 177418] Section 6.3.3.). In the outputs of the Dissolved Concentration Limits Abstraction, the first two types of uncertainties are combined together by the mean-square-root approach and are collectively called thermodynamic uncertainties. The third type of uncertainty is presented as the uncertainty associated with fluoride concentrations. The last type of uncertainty (i.e., uncertainty in temperature) was treated using a bounding approach. In other words, the solubility calculations are conducted at a temperature of 25°C and are applied for all temperatures greater than 25°C (up to 100°C). The use of solubility values calculated at 25°C for higher temperatures is bounding because there is evidence showing that the solubility of actinides decreases with increased temperature, which is called retrograde solubility in *Dissolved Concentration Limits of Elements with Radioactive Isotopes* (SNL 2007 [DIRS 177418], Section 6.3.3.3).

6.3.7.5.2 TSPA-SEIS Abstraction

Outputs from the Dissolved Concentration Limits Abstraction can be divided into three groups: (1) elements whose solubility is a function of pH and $\log fCO_2$; (2) radium solubility that is a function of pH only; and (3) elements for which no solubility limits are defined (SNL 2007 [DIRS 177418], Section 8.1).

The first group includes americium, neptunium, plutonium, protactinium, thorium, tin, and uranium. The abstracted solubility models for these elements are in the form of look-up tables with pH and $\log fCO_2$ as the independent variables. Two uncertainty terms accounting for uncertainties associated with thermodynamic properties and variations in water chemistry are also included for this group of elements. The exception to this treatment is protactinium, where the thermodynamic uncertainty is replaced by uncertainty in the choice of an analogue element. For tin, the uncertainty term associated with variations in fluoride concentrations is not given because the calculated tin solubility is not sensitive to fluoride concentrations (SNL 2007

[DIRS 177418], Section 6.19). For radium, solubility values are given as a step function of pH, uncertainties were not included.

The remaining elements (technetium, carbon, iodine, cesium, chlorine, selenium, and strontium) are considered highly soluble and no solubility-controlling solids are expected to form under repository conditions. Thus, their solubilities are not given. Consequently, their release is controlled by the dissolution rate of the waste form and waste inventories. Each of these three groups is discussed below.

pH and log fco_2 Dependent Solubility—The pH and log fco_2 dependent solubility for americium, neptunium, plutonium, protactinium, thorium, tin, and uranium can be summarized by the following relationship (SNL 2007 [DIRS 177418], Section 8.1):

$$[\text{Pu, Np, U, Am, Th, and Sn}] = 10^{s} \bullet 10^{\varepsilon_1} + \varepsilon_2 \bullet N \qquad \text{(Eq. 6.3.7-13a)}$$

and

$$[\text{Pa}] = 10^{s} \bullet 10^{\varepsilon_1} + \varepsilon_2 \qquad \text{(Eq. 6.3.7-13b)}$$

where

$[E]$ = the logarithm of the predicted solubility for a given element, E

$S(pH, \log f_{CO_2})$ = the logarithm of the base solubility value from a look-up table for that element, E, which is a function of pH and log f_{CO2}

ε_1 = a term accounting for uncertainty in thermodynamic properties for americium, neptunium, plutonium, thorium, and tin (for protactinium, uncertainty is accounted for using the analogue phase Np_2O_5)

ε_2 = the uncertainty term associated with variations in fluoride concentration. This uncertainty term is perfectly correlated among the Pu, Np, U, Th, Am, and Pa solubility models during sampling. This term has a right-sided triangular distribution with the minimum (indicated by "a"), most probable values (indicated by "b") equal to one another (i.e., a = b) and the maximum value (indicated by "c") corresponding to the maximum uncertainty.

$N(pH)$ = multiplication factor used to make the second uncertainty term a function of pH, with the exception of protactinium for which no multiplication factor is used.

While the calculation of uranium solubility uses Equation 6.3.7-13, its implementation is more complex and is discussed separately below. For the other elements listed above, the Dissolved Concentration Limits Abstraction provides a two-dimensional look-up table giving a calculated value of solubility as a function pH and log fco_2. The look-up tables for americium, neptunium (Np_2O_5 and NpO_2), plutonium, protactinium, thorium, and tin can be found in Tables 6.3.7-34 through 6.3.7-40, respectively. A base solubility value, $S(pH, \log fco_2)$, for each element is obtained for a given pH and log fco_2 value by linear interpolation of the nearest pH and log fco_2

values in the table. After the base solubility value is determined, the uncertainty terms are added to it in the manner shown in Equation 6.3.7-13.

In general, two types of uncertainty terms are included to describe the pH and log fco_2 dependent solubility. The first term, ε_1, is used to account for uncertainty in the thermodynamic properties used to calculate the solubility look-up tables. These uncertainties are represented by truncated normal distributions with mean values of 0.0 and SDs specific to each element (Tables 6.3.7-41 through 6.3.7-47). The solubility calculations were conducted using the B-dot equation, which is only rigorously applicable up to ionic strength values of 1 molal. In order to extend the applicable range of the solubility model to 3 molal, extra uncertainty is added to the ε_1 uncertainty term (SNL 2007 [DIRS 177418], Section 8.1). For solutions with an ionic strength between 1 molal and 3 molal, a modified SD is used for the ε_1 uncertainty term. This modification requires that 0.3 be added to the 1 molal SD using the root-mean-square method (SNL 2007 [DIRS 177418], Section 6.3.3.4, Equation 6.3-7). The resulting SDs are also shown in Tables 6.3.7-41 through 6.3.7-47. The ε_1 normal distributions are truncated at the 2σ level for all elements except protactinium (SNL 2007 [DIRS 177418], Section 8.2). The exception to the above discussion of ε_1 is protactinium. For protactinium, ε_1 represents uncertainty in the choice of analogue used to determine the base protactinium solubility, which has a uniform distribution over the range of [-4.42, -0.05] (SNL 2007, [DIRS 177418], Table 6.11-4).

The second uncertainty term, $\varepsilon_2 \bullet N$, is used to account for variations in the base solubility value due to variable fluoride concentration in the fluid. Because the vapor influx mode does not contribute fluoride to the fluid, this uncertainty term is zero for vapor influx mode (SNL 2007 [DIRS 177418], Section 8.1). For the liquid influx mode, this uncertainty term depends on the WP types and ionic strength. Thus, three groups of abstractions for this term were given. Group 1 is for CSNF WPs when ionic strength is less that 0.2 molal, and for CDSP WPs when ionic strength is less than 0.004 molal. Group 2 is for CSNF WPs when ionic strength is greater or equal to 0.2 molal, and for invert under CSNF WPs. Group 3 is for CDSP WPs when ionic strength is greater than or equal to 0.004 molal and for invert under CDSP WPs (SNL 2007 [DIRS 177418], Section 6.19.4.2.2 and Table 6.3-3).

The uncertainty parameters ε_2 are in the form of triangular distributions with minimum and most likely values of zero and maximum values specified for each element (SNL 2007 [DIRS 177418], Section 8.1). These parameters are perfectly correlated with each other during sampling (i.e., with a correlation coefficient of 1.0) (SNL 2007 [DIRS 177418], Section 8.1).

Because the impact of fluoride concentration on the actinide solubilities varies strongly with pH, as described in *Dissolved Concentration Limits of Elements with Radioactive Isotopes* (SNL 2007 [DIRS 177418], Section 6), the second part of the uncertainty term associated with fluoride concentrations, the multiplication factor N that is a function of pH, is introduced to present the pH dependency. The multiplication factor, N(pH), is an element-specific parameter that varies from zero to one as a function of pH. It is calculated by normalizing the differences in solubility values between the elevated F^- cases and the base case for each element by the maximum observed difference in solubility values (for example, Tables 6.6-4 and 6.6-6 in *Dissolved Concentration Limits of Elements with Radioactive Isotopes* (SNL 2007

[DIRS 177418]). This modification requires that the ε_2 uncertainty terms for each element be fixed at the values sampled for each realization. The sampled value of ε_2 is then multiplied by N(pH) at each timestep to produce a modified ε_2^i. Tables 6.3.7-48 through 6.3.7-52 give the multiplication factors for americium, Np_2O_5, NpO_2, plutonium, and thorium. For protactinium, no multiplication factor is used in conjunction with ε_2^i.

Neptunium Solubility—Neptunium solubility is calculated using Equation 6.3.7-13 and the uncertainty terms discussed above. However, two different solubility models are presented for neptunium in *Dissolved Concentration Limits of Elements with Radioactive Isotopes* (SNL 2007 [DIRS 177418], Section 6.6). These two models are based on different solubility-controlling solid phases, Np_2O_5 and NpO_2. The NpO_2 solubility model is used within WPs when reductants (CSNF fuels or stainless steels) remain. After reductants within WPs are consumed, Np_2O_5 will be applied. For the invert, the Np_2O_5 solubility model is always applied (SNL 2007 [DIRS 177418], Section 6.6).

Uranium Solubility—There are two methods used to calculate uranium solubility based on different chemistries of in-package fluids (SNL 2007 [DIRS 177418], Section 6.7). In the first method, the amount of silica and alkaline elements in the fluid are far less than the amount of available uranium, which precludes the abiquitous formation of uranyl silicates (e.g., Na-boltwoodite) and their use as solubility controlling phases. In the second method, the amount of silica and alkaline elements are comparable to the amount of available uranium and uranyl silicates can readily precipitate. These two methods apply as follows:

Method 1. CSNF WPs that are breached in the Nominal or Seismic Scenario Classes

Method 2. CDSP WPs breached under all scenario classes, CSNF WPs breached in the course of the igneous intrusion, and for all evaluations in the invert.

Using the first method, uranium solubility is controlled by schoepite under all pH and fco_2 conditions. This method is used because the source of the degrading water in a CSNF WP in the Nominal, Early Failure, or Seismic Scenario Classes is water vapor entering the WPs, which has low or no initial dissolved Na or silica (SNL 2007 [DIRS 177418], Section 6.7.3). A single look-up table is used for calculating the base solubility value, $S(pH, \log fco_2)$ (Table 6.3.7-53). The uncertainty terms are handled using the same method discussed above with a multiplication factor for ε_2^i. Values of the uncertainty terms and $N^i(pH)$ for the CSNF WPs (Nominal, Early Failure, and Seismic Scenario Classes) are given in Tables 6.3.7-54 and 6.3.7-55. There are two sets of ε_2 and N(pH): one for low ionic strength conditions (< 0.2 molal) and the other for high ionic strength conditions (greater than or equal to 0.2 molal).

Using the second method, uranium solubility is controlled by schoepite, Na-Boltwoodite, or $Na_4UO_2(CO_3)_3$, depending on the pH and fco_2. In this environment, silica is available to the degrading waste from the CDSP glass, surrounding igneous material, and invert construction material, so Na-boltwoodite is included as a uranium solubility-controlling phase (SNL 2007 [DIRS 177418], Section 6.7.3). As a result, two additional base solubility look-up tables are defined. The solubility limits in Table 6.3.7-56 represent schoepite solubility and extend over lower pH values, where this mineral is the least soluble of the three mineral phases considered.

Table 6.3.7-57 represents solubilities of Na-Boltwoodite and $Na_4UO_2(CO_3)_3$ and covers the higher pH ranges. Uncertainties in thermodynamic properties lead to a range of pH and log fco_2 values in which either schoepite or Na-Boltwoodite could control the uranium solubility. The shading in Table 6.3.7-56 and the upper shaded area in Table 6.3.7-57 indicate these ranges. For environmental conditions within these ranges, the uranium solubility should be sampled from a uniform distribution with bounds based on the values in Tables 6.3.7-56 and 6.3.7-57. After the base solubility value is determined from one or both of the look-up tables, uncertainties are added as discussed above. Values for the uncertainties are shown in Table 6.3.7-58. The exception is that six sets of ε_2 and different N(pH) tables are now defined, as there are two sets for each of the three groups discussed previously, each set is for one solubility look-up table (SNL 2007 [DIRS 177418], Section 6.7.5). Table 6.3.7-59 gives the values of multiplication factors for this solubility model.

Radium Solubility—Radium solubility is presented as a simple step function of pH. For pH values from 3.0 to 7.75, the logarithm of radium solubility is fixed at –1.16 mg/L; and at pH values between 7.75 and 9.75, it is fixed at 1.68 mg/L (log value) (SNL 2007 [DIRS 177418], Table 6.12-1). At pH values greater than 9.75, radium solubility is undefined, and its concentration is controlled by release from the waste form.

Undefined Solubility—Under repository environmental conditions, no solubility-controlling solids are expected to form for carbon, cesium, chlorine, iodine, selenium, and technetium (SNL 2007 [DIRS 177418], Section 8.1); therefore, no solubilities are defined for these elements. Although strontium (Sr) may precipitate in carbonates and sulfates under repository conditions, for the purpose of simplicity, its solubility is assumed also to be undefined. In the TSPA-SEIS, the release of these elements is controlled by the waste inventory and dissolution rates of the waste forms.

Although actinium is not transported in the TSPA-SEIS (Table 6.3.7-60), it is included as a species in the TSPA-SEIS. This is because certain impact analyses consider the transport of actinium in the EBS. For this reason, it is necessary to specify an actinium solubility value in the TSPA-SEIS. However, no thermodynamic data exist for calculating actinium solubility (SNL 2007 [DIRS 177418], Section 6.10). Thus, in the TSPA-SEIS, no solubility is calculated for actinium.

Restrictions on the Dissolved Concentration Limits Abstraction—The solubility models developed for this abstraction are valid for a wide range of environmental conditions and can be applied both inside and outside the WPs. However, these models are subject to the following restrictions (SNL 2007 [DIRS 177418], Table 8-3):

1. The valid temperature range for the solubility models is from 25°C to 100°C.

2. The solubility models are also restricted to pH values between 3.0 and 11.0, and log fco_2 values from –1.5 to –5.0 bar.

3. The solubility models are restricted to ionic strength less than or equal to 3 molal.

Treatments of Solubility Model Out-Of-Bounds—Under certain circumstances, the solubility of one or more elements cannot be calculated. This is called Out-of-Bounds solubility model According to the cause, out-of-bounds can be categorized into three types.

Type I Out-of-Bounds: As shown on Figure 6.3.7-11, Type I out-of-bounds occur when the given pH-f_{CO2} conditions fall into the gray areas where the solubility look-up table has 3 valid values (A, B, and C) but with one flagged as invalid (i.e., 500) at "D". Since GoldSim two-dimensional look-up tables use rectangular interpolation scheme, a meaningful solubility cannot be calculated using the standard interpolation scheme by the two-dimensional look-up table element. However, in general, solubility can be calculated using EQ3 for these conditions. This type of out-of-bounds is caused by the limited resolutions of solubility look-up tables. A triangular interpolation scheme that produces valid results for the gray shaded areas has been implemented for the uranium solubility models at CSNF Cell 1 to obtain solubility values when this type of out-of-bounds occurs.

Type II Out-of-Bounds: Type II out-of-bounds occurs when the given pH-fco_2 conditions are outside the valid ranges of the solubility look-up table and they cannot be removed by a triangular interpolation scheme. The unshaded area of the rectangle ABCD on Figure 6.3.7-11 indicates the area where Type II out-of-bounds (in the Pu solubility model) could occur. However, since the pH-fco_2 conditions given by the In-Package Chemistry Submodel may be narrower than the whole unshaded area, the ranges of pH-fco_2 conditions where Type II out-of-bounds can actually occur can be narrower than as shown on the figure. For the uranium solubility model at CSNF Cell 1, Type II out-of-bounds occurs only for a very narrow range. A base uranium solubility of 1,000 mg/l is assigned for this narrow range (SNL 2007 [DIRS 177418], Table 8-1). This value is justifiable, because the maximum uranium solubility calculated by EQ3 calculations for conditions very close to where Type II out-of-bounds occurs is 500 mg/l. Type II out-of-bounds can also occur for the uranium solubility model at CDSP Cell 1a. Uranium concentrations are capped at 71,400 mg/L (SNL 2007 [DIRS 177418], Table 8-1).

Type III Out-of-Bounds: Type III out-of-bounds occur when ionic strength is greater than 3 molal, and the concentrations of actinides are then capped at the values shown in Tables 6.3.7-60 and 6.3.7-61, for CSNF Cell 1 and CDSP Cell 1b, respectively (SNL 2007 [DIRS 177418], Tables 6.22-2 and 6.22-3).

An empirical approach that addresses Type III out-of-bounds in the plutonium solubility model has been developed and documented below.

The approach relies on the evaluation of the solubility-limited dissolved concentrations model for Pu (including uncertainties for ionic strength above 1 molal (SNL 2007 [DIRS 177418], Table 6.5-1), against a data set for measured PuO_2(am) solubility at high ionic strengths (Rai et al., 2001 [DIRS 168392]). This evaluation is a direct comparison (Figure 6.3.7-12) of the look-up table model values to the data sets collected in 0.4 and 4 Molar $NaClO_4$ and NaCl solutions (i.e., 0.408 and 4.92 molal $NaClO_4$, respectively), and 0.4 and 4 Molar NaCl solutions (i.e., 0.403 and 4.36 molal NaCl, respectively).

Examination of Figure 6.3.7-12 indicates that the measured concentrations of plutonium in perchlorate (an oxyanion) solutions decrease at higher ionic strengths and are closely represented

by the solubility-limited dissolved concentrations model for plutonium. The measured concentrations of plutonium in NaCl (salt) solutions increase at higher ionic strength and can be seen to exceed the 2-sigma upper uncertainty band shown on Figure 6.3.7-12 for the model results. It is noted here that the data shown in the plot (Rai et al., 2001 [DIRS 168392]) are for the longest equilibration times reported by the authors. Because the observed increase for the 4.36 m NaCl solutions is seen for the longer equilibration times, this increase is attributed by Rai et al. (2001 [DIRS 168392]) as probably reflecting alpha radiolysis of the electrolyte to NaOCl with concurrent increase in the solution redox state. However, the measured data for plutonium in the 0.403 m NaCl solutions show a slight decrease over approximately the same time. In a spectroscopic study of actinide solubilities in highly concentrated chloride solutions (Runde et al., 1997 [DIRS 182190]), it was shown that at increased chloride concentrations, chloride complexes were forming for plutonium (and other actinides), and it was concluded that the higher dissolved actinide concentrations were attributable to this process. Regardless of which of these two possibilities occurred in the experimental work, they are both relevant to potential increased solubility-limited concentrations of plutonium in concentrated chloride solutions above 3 molal, and therefore the data from Rai et al. (2001 [DIRS 168392]) can be used in an empirical approach to define a high ionic strength cap value that is for plutonium in about 4.3 molal chloride solutions. Given the behavior in perchlorate solutions, such a cap value would be bounding for concentrated solutions that are dominated by oxyanions because either mechanism discussed above involved the chloride in the electrolyte directly to account for the increased solubility at higher ionic strength.

Based on the values shown on Figure 6.3.7-12, the solubility cap can be generated to cover the pH range from 4 to 10 and provides an upper bounding value for the dissolved concentration of plutonium that is applicable in concentrated chloride solutions up to ionic strengths of about 4.3 molal. This empirically derived concentration cap is 100 mg/L based on the data set and would be applicable without any further uncertainty treatment because of its bounding nature. For the TSPA-SEIS, this application (TSPA parameter name: Pu_TSPA_DS_Cap) would take place above the 3.0 molal ionic strength limit of the plutonium model. Given the data sets from Rai et al. (2001 [DIRS 168392]), the applicable pH range is from 4 to 10 (the higher end considers the trend of the 4.36 molal NaCl data set, as well as the higher pH behavior of the other data). When pH condition is outside this applicable range, then, the Type III Pu Cap described previously in Tables 6.3.7-60 and 6.3.7-61 is invoked.

6.3.7.5.3 TSPA-SEIS Implementation

The Dissolved Concentration Limits Abstraction is implemented in the TSPA-SEIS to calculate elemental solubility values for both the in-package (CDSP WP and CSNF WP) and invert environments. The Dissolved Concentration Limits Submodel is implemented at two locations in the TSPA-SEIS. The stochastic elements describing the uncertainty distributions are defined in the Epistemic_Params submodel. Solubility values are calculated within the EBS_Submodel container, which sits inside the percolation subregion loop.

In the Epistemic_Params Submodel, the stochastic elements describing solubility-related uncertainties are sampled once for each realization. These sampled values are then passed to the EBS_Submodel.

Within the EBS_Submodel, the environmental parameters, pH, log fco_2, and ionic strength pertaining to the current percolation subregion are provided to the Dissolved Concentration Limits Submodel by the In-Package Chemistry and EBS Chemical Environment Submodels (Sections 6.3.7.2 and 6.3.4, respectively). These parameter values are then used to obtain a local base solubility value from the look-up tables.

The sampled values of the uncertainty parameters are then added to the local base solubility according to Equation 6.3.7-13 to obtain the final solubility values at each timestep and for each realization. The same value sampled for a given uncertainty parameter is used in all percolation subregions at all times for a particular realization.

The Dissolved Concentration Limits Submodel provides elemental solubilities. The GoldSim software automatically partitions the elemental solubility among the isotopes of an element according to the isotopic ratios so that the sum of the concentrations of all the element's isotopes will not exceed its solubility.

The GoldSim software requires that all the element's isotopes have the same solubility value. If isotopes of the same element are assigned different solubility values, GoldSim will force all of the isotopes to have the solubility values of the first isotope in the species list. When this is done, a warning message is generated in the GoldSim run log for every timestep and each isotope that had its solubility redefined. In the TSPA-SEIS, solubility values are calculated in units of mg/L. In its internal calculations, GoldSim converts all units to the International System of Units, which for solubility is mol/L. Therefore, each isotope of an element will have a slightly different solubility value after the conversion to the International System of Units. This results in as many as 100,000 warning messages being written to the GoldSim run log. In order to suppress these messages, a slight modification is made to the calculated solubility values in the TSPA-SEIS.

The calculated solubility value for an element is converted from mg/L to mol/L by dividing it by the molecular weight of the lightest isotope for that element. For each isotope of an element, this mole-based solubility value is then reconverted to mg/L based on the molecular weight of the isotope in this calculation. As a result, all isotopes of an element will have equivalent solubility values in terms of mol/L but will have slightly differing values in terms of mg/L. This modification introduces a slight discrepancy between calculated solubility values and the estimated concentrations at which the solubility limit is reached in the TSPA-SEIS. Calculated element concentrations can be as much as 0.6 percent higher than the calculated solubility value.

6.3.7.6 Engineered Barrier System Colloids

The Waste Form and In-Drift Colloid Concentration Abstraction for the TSPA-SEIS is described in *Total System Performance Assessment Data Input Package for Waste Form and In-Drift Colloids* (SNL 2007 [DIRS 180679]) and *Waste Form and In-Drift Colloids-Associated Radionuclide Concentrations: Abstraction and Summary* (SNL 2007 [DIRS 177423]). Within the TSPA-SEIS, the EBS Colloids Submodel implements the Waste Form and In-Drift Colloid Concentration Abstraction to address the formation, stability, and concentration of radionuclide-bearing colloids in the waste form and WP, as well as sorption of dissolved radionuclides. Colloids are fine particles ranging in size from 1 nm to 1 μm in maximum dimension that have the potential to

remain in suspension. Colloids are of concern because radionuclides attached to colloids may move faster and farther than dissolved radionuclides; however, colloids may only significantly facilitate radionuclide transport when their suspensions are stable and when they carry significant amounts of radionuclides.

The processes included in the EBS Colloids Submodel are described in this section. Some processes that slow or limit colloid migration were not incorporated into the model, including colloid filtration, colloid sorption at the air-water interface, microbial effects, and the effects of elevated temperature (SNL 2007 [DIRS 177423], Sections 5 and 6.3.1).

6.3.7.6.1 Conceptual Model

Colloids—Three types of colloids were considered in the Waste Form and In-Drift Colloid Concentration Abstraction and are accounted for in the EBS Colloids Submodel implemented in the TSPA-SEIS: (1) Waste form degradation colloids: (a) colloids generated from degradation of the glass waste forms, (b) residue colloids generated from degradation of the CSNF waste forms, and (c) uranium mineral colloids generated from degradation of the SNF waste forms; (2) colloids produced from the steel components of the WPs; and (3) colloids present in natural seepage water entering the EBS.

1. Waste Form Degradation Colloids—(a) Glass Waste Form Colloids—Experimental work at Argonne National Laboratory has shown that quantities of colloids containing plutonium are generated from glass waste during the degradation process. These colloids are a mixture of clays, zeolites, and oxides but are predominantly clays. For further description of these colloids, see *Waste Form and In-Drift Colloids-Associated Radionuclide Concentrations: Abstraction and Summary* (SNL 2007 [DIRS 177423], Section 6.3.3). (b) Residue CSNF Waste Form Colloids—A layer of plutonium and Zr-rich oxides forms at the reaction front of degrading CSNF waste forms, particles of which may become suspended (SNL 2007 [DIRS 177423], Section 6.3.4). (c) Uranium Mineral SNF Waste Form Colloids—Colloidal-sized particles of uranium minerals such as uranophane have been observed in solutions in contact with degrading CSNF. Degrading uranium metal DSNF has been shown to release colloid-sized particles of UO_2.(SNL 2007 [DIRS 177423], Sections 6.3.5 and 6.3.6)

2. Corrosion Product Colloids—The occurrence of iron oxyhydroxide colloids from the corrosion of the WP materials is included in the Waste Form and In-Drift Colloid Concentration Abstraction described in *Waste Form and In-Drift Colloids-Associated Radionuclide Concentrations: Abstraction and Summary* (SNL 2007 [DIRS 177423], Section 6.3.8). Iron oxyhydroxides derived from the corrosion of steel components in the repository will occur in two forms: (1) large-sized corrosion products consisting of immobile materials and large particles and (2) colloid-sized particles that could potentially transport sorbed radionuclides.

3. Seepage Water Colloids—Colloid concentrations in SZ groundwater were used in the Waste Form and In-Drift Colloid Concentration Abstraction to estimate the colloid concentrations in seepage water that could enter a failed WP. There is a wide range in natural groundwater colloid concentrations in the Yucca Mountain vicinity over a

relatively narrow range of groundwater ionic strength. The Yucca Mountain colloid concentration data were collected from nine different sources.

Colloid Stability—The stability of a colloidal suspension is controlled by electrostatic and chemical processes at colloid surfaces and by the attractive and repulsive forces between colloids. The attractive force is inversely proportional to both the distance between the colloids and colloid size. That is, the closer the colloids are to each other and the smaller they are, the higher the strength of the attractive force, and the more likely the colloid suspensions are to become unstable and coagulate. Higher ionic strength and higher temperature lead to weaker repulsive forces between colloids, causing colloidal suspensions to become unstable and the colloids to coagulate.

Another factor in colloid stability is pH. Colloids become unstable and flocculate near a pH value (zero point of charge) that is characteristic for a particular colloid mineralogy because of reduced repulsive forces between the colloids. The result is an ionic strength threshold that is dependent on pH, above which, the colloid suspensions are unstable. Examples of the pH dependent ionic strength thresholds are shown on Figure 6.3.7-13 for the idealized minerals that represent the colloid types: montmorillonite for glass degradation and local groundwater clay colloids, ZrO_2 for CSNF degradation colloids with irreversibly attached radionuclides, meta-autunite ($Ca(UO_2)_2(PO_4)_2 \cdot 6\text{-}8H_2O$) for SNF degradation colloids with reversibly attached radionuclides, and hematite (Fe_2O_3) for steel degradation colloids (SNL 2007 [DIRS 177423], Section 6.3).

Radionuclide Attachment—Radionuclides may be attached to colloids in many ways. In some cases the attachment is reversible, such as simple ion exchange. This attachment is well described by a simple K_d sorption model. In other cases attachment may be fast but detachment very slow, as in co-precipitation where the radionuclide becomes embedded in the host colloid. This type of attachment is more complex to model and is referred to here as irreversible or kinetic attachment. Attachment to the types of colloids is approximated as follows:

1. Waste form degradation colloids

   a. glass degradation colloids – reversible and irreversible
   b. CSNF degradation rind colloids – irreversible
   c. SNF uranium mineral colloids – reversible

2. Steel degradation colloids – kinetic (*Engineered Barrier System Radionuclide Transport Abstraction* (SNL 2007 [DIRS 177407], Section 6.5.1.2).

3. Groundwater colloids – reversible.

Nine elements are modeled as reversibly sorbed to colloids using a linear isotherm model (K_d): plutonium, americium, cesium, protactinium, thorium, tin, radium, uranium, and neptunium. This list represents the isotopes most likely to exhibit dose-significant colloidal transport (SNL 2007 [DIRS 177423], Section 6.3.12.1). The two elements most likely to impact total dose from transport of irreversibly attached colloids were modeled: plutonium and americium.

6.3.7.6.2 TSPA-SEIS Abstraction

The TSPA-SEIS EBS Colloids Submodel addresses the formation and stability of three types of colloids in the waste forms and WPs and calculates colloid concentrations and reversible sorption of nine radionuclides to colloids. The EBS Colloids Submodel also calculates irreversible attachment of plutonium and americium to HLW and CSNF waste form colloids and iron oxyhydroxide colloids. These features are summarized in Section 6.3.7.6.1 and described in detail in *Waste Form and In-Drift Colloids-Associated Radionuclide Concentrations: Abstraction and Summary* (SNL 2007 [DIRS 177423]).

This section describes the abstraction of these processes for use in the TSPA-SEIS.

Colloid Stability—The following equations and pH bounds describe quantitatively the schematic ionic strength threshold model results in Figure 6.3.7-13 . The pH bounds and equation coefficients are provided in Tables 6.3.7-62 through 6.3.7-66.

Groundwater and Glass Degradation Colloids:

$$I_{threshold} = (-0.008 \times pH^2) + (0.12 \times pH) - 0.03 \quad \text{(Eq. 6.3.7-14)}$$

If $pH_{wp,inv}$ is greater than 9, then the $I_{threshold}$ value calculated at pH 9 is used, and if $pH_{wp,inv}$ is less than 1.5, then colloids are assumed to be unstable.

CSNF Residue (ZrO_2) Colloids:

Between pH 7 and 9.3, the irreversible CSNF colloids are unstable irrespective of the ionic strength.

When the pH is between 4 and 7, the following relationship is used:

$$I_{threshold} = (0.0089 \times pH^3) - (0.1466 \times pH^2) + (0.7462 \times pH) - 1.092 \quad \text{(Eq. 6.3.7-15)}$$

When the pH is greater than 9.3, equation 2-7b is used:

$$I_{threshold} = (0.087362 \times pH^3) - (2.4078 \times pH^2) + (22.126 \times pH) - 67.791 \quad \text{(Eq. 6.3.7-16)}$$

If the pH is less than 4.0, the $I_{threshold}$ value that was calculated at pH 4.0 is used, and if the pH is greater than 10.6, the $I_{threshold}$ value calculated at pH 10.6 is used.

SNF Uranium Mineral Colloids:

$$I_{threshold} = -(0.008 \times pH^2) + (0.14 \times pH) - 0.4 \quad \text{(Eq. 6.3.7-17)}$$

If the pH is less than 4.0, the $I_{threshold} = 0$; if the pH is greater than 9, the $I_{threshold}$ value calculated at pH 9 is used.

Waste Package Degradation Products Colloids:

When the pH is between 4.5 and 8.4, the following relationship is used:

$$I_{threshold} = -0.013 \times pH + 0.11 \quad \text{(Eq. 6.3.7-18)}$$

In contrast, when the pH is between 9.4 and 10.4, the following equation is used:

$$I_{threshold} = (0.0017 \times pH^2) - (0.0327 \times pH) + 0.158 \quad \text{(Eq. 6.3.7-19)}$$

If the pH is less than 4.5, the $I_{threshold}$ value calculated at pH 4.5 is used; and if the pH is greater than 10.4, the $I_{threshold}$ value calculated at pH 10.4 is used.

Reversible Attachment—Reversible sorption is modeled using the simple linear sorption isotherm model implemented in GoldSim with a cap on the amount of sorption given by a sorption capacity model (SNL 2007 [DIRS 177423] Section 6.3.12.3). This simplified competitive reversible sorption capacity model begins with the assumption that the available sorption sites can be partitioned linearly amongst the radionuclides based on their sampled K_d values and their concentrations in solution. This model is necessarily a recursive model as implemented in GoldSim; i.e., there will be a one timestep delay, as shown below, in the sorption capacity calculation. The following is a conceptualization for this option as implemented in the GoldSim model:

By partitioning the total molar density of sorption sites, $\overline{c}_{\max_T}$, into an allowable molar density of sorption sites for each species, $\overline{c}^n_{\max_i}$, according to the following equation, the model assumes that all sites are available for reversible sorption:

$$\overline{c}^{n-1}_{\max_i} = \overline{c}_{\max_T} \left(\frac{\overline{K}_{d,i} \frac{c_i^{n-1}}{M_{W_i}}}{\sum_j \overline{K}_{d,j} \frac{c_j^{n-1}}{M_{W_j}}} \right) \quad \text{(Eq. 6.3.7-20a)}$$

where:

$\overline{K}_{d,i}$ = sampled K_d for the ith species (different for each realization), [=] m^3 solution per kg smectite or uranophane colloids

$\overline{c}^n_{\max_i}$ = molar density of sites for the ith species at the $(n-1)$th time-step, [=] kg-moles sorbed of ith species per kg colloid mass

$\overline{c}_{\max_T}$ = molar density of sites, [=] kg-moles of sites per kg colloid mass

c_i^{n-1} = aqueous concentration of the ith species at the $(n-1)$th time-step, [=] kg ith species per m^3 solution

M_{W_i} = molecular weight of ith species, [=] kg of ith species per kg-mole.

Next, each side of Equation 6.3.7-20a is divided by $\frac{c_i^{n-1}}{M_{w_i}}$:

$$\frac{\overline{c}_{\max_i}^{n-1}}{c_i^{n-1}/M_{W_i}} = \overline{c}_{\max_T}\left(\frac{\overline{K}_{d,i}}{\sum_j \overline{K}_{d,j}\frac{c_j^{n-1}}{M_{W_j}}}\right) \quad \text{(Eq. 6.3.7-20b)}$$

The left-hand side of the equation is defined to be the maximum allowable partition coefficient, $K_{d,i}^{\max,n}$, for the *i*th species at the *n*th timestep:

$$K_{d,i}^{\max,n} \equiv \frac{\overline{c}_{\max_i}^{n-1}}{c_i^{n-1}/M_{W_i}} = \overline{c}_{\max_T}\left(\frac{\overline{K}_{d,i}}{\sum_j \overline{K}_{d,j}\frac{c_j^{n-1}}{M_{W_j}}}\right) \quad \text{(Eq. 6.3.7-20c)}$$

At the *n*th timestep, the partition coefficient, $K_{d,i}^n$, that is used for the *i*th species is given by the following (i.e., it is the minimum of the competitive K_d computed in Equation 6.3.7-20c and the sampled K_d):

$$K_{d,i}^n = \min\left(\overline{K}_{d,i}, K_{d,i}^{\max,n}\right) \quad \text{(Eq. 6.3.7-20d)}$$

The reversible sorption model is parameterized by the K_d for each element on each colloid type and by the specific surface area and sorption site density of each colloid type.

Irreversible Attachment—Irreversible/kinetic attachment is modeled for steel, glass, and CSNF corrosion-product colloids for plutonium and americium. The kinetic attachment to steel corrosion products is described in *Engineered Barrier System Radionuclide Transport Abstraction* (SNL 2007 [DIRS 177407], Section 6.5.1.2). The irreversible attachment of plutonium and americium to glass and CSNF corrosion products is described here.

The values measured in glass and CSNF degradation experiments are the concentration of plutonium attached to colloid-sized particles and the total colloid concentration. From these measurements, the ranges of ratio of the concentration of plutonium to concentration of colloid (CPu_Per_CSNF_Embed_Col_a and CPu_Per_WF_Embed_Col_a) were developed in Tables 6.3.7-63 and 6.3.7-62. Depending on the ionic strength and pH, the concentration of Pu on colloids in the source cell is set to the sampled value for the concentration when colloids are stable or the minimum concentration for when the colloids are unstable (Pu_Col_WF_Embed_Sampled_a; CPu_Col_CSNF_Sampled_a; CPu_Col_Glass_Embed_Min; and CPu_Col_CSNF_Min in Tables 6.3.7-62 and 6.3.7-63). The concentration of the colloids within each computational cell of the EBS is then calculated by dividing the sampled

concentration of Pu associated with colloids in suspension divided by the ratio of the concentration of plutonium to concentration of colloid.

See *Engineered Barrier System Radionuclide Transport Abstraction* (SNL 2007 [DIRS 177407]) for a discussion of the implementation of irreversible colloid transport model.

6.3.7.6.3 TSPA-SEIS Implementation

All the elements of the EBS Colloids Submodel described in Sections 6.3.7.6.1 and 6.3.7.6.2 are combined in the TSPA-SEIS. The TSPA-SEIS takes the fluid characteristics, pH, and ionic strength and the concentrations of dissolved radionuclides and calculates the mass concentrations of each colloid type. It calculates reversible attachment of nine elements onto four colloid subtypes and irreversible attachment of two elements onto three colloid subtypes.

Figure 6.3.7-14 provides an overview of the implementation of the EBS Colloids Submodel in the TSPA-SEIS for the WP environment. All uncertain parameters are sampled once for each realization. At each timestep and for each representative WP in each percolation subregion environment in the TSPA-SEIS calculations, the EBS Colloids Submodel uses in-package ionic strength, pH, and dissolved radionuclide concentrations to calculate the formation and stability of colloids and the attachment of radionuclides to stationary corrosion products and to the waste form, iron oxyhydroxide, and seepage water colloids.

The colloid and radionuclide concentration values in the WPs, along with the ionic strength and pH of the solution and dissolved radionuclide concentrations in the solution, serve as source terms for the invert. The EBS Chemical Environment Submodel (Section 6.3.4) calculates the ionic strength and pH of the invert water. Based on the values of ionic strength and pH in the invert, the EBS Colloids Submodel determines colloid stabilities and concentrations for the invert conditions and redistributes the reversibly sorbed radionuclides and dissolved radionuclides based on the distribution coefficients and the total mass of each type of colloid. These colloids and associated radionuclides are then subject to transport through the invert and into the UZ.

The stability of colloids is calculated using the values of ionic strength and pH, with separate relationships for each colloid type. At each timestep and for each representative WP in each percolation subregion environment, the values of ionic strength and pH of the solutions in the WPs are used as input to determine colloid stability. For all types of colloids, a low, nonzero colloid concentration limit is used under unstable conditions.

The EBS Colloids Submodel in the TSPA-SEIS calculates the reversible sorption of each of the nine modeled radionuclides onto the smectite (waste form and groundwater colloids), uranium mineral colloids, and iron oxyhydroxide colloids. The EBS Colloids Submodel also calculates the irreversible sorption of plutonium and americium onto glass, CSNF, and steel corrosion products. Within the WPs, the sorption partition distribution coefficients (K_d values) are sampled for each of the radionuclides for smectite (waste form and groundwater colloids), uranium mineral, and iron oxyhydroxide colloids to determine their sorbed concentrations and applied at all times to all representative WPs in all percolation subregion environments. For iron

oxyhydroxide colloids, irreversible sorption of plutonium and americium is modeled in the EBS Transport Submodel (Section 6.3.8.3).

6.3.7.7 Model Component Consistency and Conservatism in Assumptions and Parameters

To enhance understanding of the complex interactions within the TSPA-SEIS, a discussion of consistency among model components and submodels and identification of conservative assumptions in abstractions, process models, and parameter sets supporting the Waste Form Degradation and Mobilization Submodel are discussed below.

6.3.7.7.1 Consistency of Assumptions

Waste Form Temperature versus WP Surface Temperature—In the absence of waste form temperatures, the TSPA-SEIS treats waste form temperature as if it were the same as the WP surface temperature. It is expected that waste form temperatures would be higher than WP surface temperatures, and the effect of hotter temperatures is not included in the waste form submodels.

Effect on TSPA—The submodels of the TSPA-SEIS that are directly dependent on the waste form temperature are the In-Package Chemistry Submodel for CSNF WPs (Section 6.3.7.2), the CSNF Waste Form Degradation Rate Submodel (Section 6.3.7.4.1), the HLW Glass Degradation Submodel (Section 6.3.7.4.3), and the EBS Transport Submodel (Section 6.3.8). The influences are discussed below. Both the CSNF Waste Form Degradation Submodel (Section 6.3.7.4.1) and HLW Glass Degradation Submodel (Section 6.3.7.4.3) are direct functions of temperature, with the rate increasing as temperatures increase. The temperature dependence for the In-Package Chemistry Submodel (Section 6.3.7.2) is in the total carbonate abstraction, which only impacts the CSNF Waste Form Degradation Submodel (Section 6.3.7.4.1) calculations. The temperature dependence in the EBS Transport Submodel (Section 6.3.8) pertains to the presence of water inside the waste form. At temperatures greater than 100°C, the TSPA-SEIS assumes that water in the WP evaporates and the system is dry and does not support radionuclide transport.

For all waste forms, the transport of the radionuclides released by any failure mechanism is driven by the amount of water available to entrain and transport the radionuclides past the WP boundary. In the TSPA-SEIS, water will not accumulate in the WP if the temperature is greater than 100°C. Because the waste form temperature is greater than the WP surface temperature, any transport calculations using the lower WP surface temperature would be conservative because water would be accumulating at higher temperatures than physically possible in the waste form.

HLW Glass Degradation Rate Coefficient—The HLW glass degradation rate coefficient (k_E) in the glass degradation rate equation is uncertain, and the distribution of values for k_E is skewed to the low end to reflect the greater likelihood that glass will be degraded by contact with water vapor (which gives the lowest measured rates) rather than by immersion (which gives the highest measured rates) (BSC 2004 [DIRS 169988], Section 6.5.3). The probability distribution function of k_E was constructed in such a way as to correspond to the quantity of water in a WP, but it is sampled randomly in the TSPA-SEIS without any correlation to the quantity of water contacting the waste (Section 6.3.7.4.3.3). Thus, for a CDSP WP experiencing high seepage rates, the

calculated glass degradation rate will not necessarily reflect the effects of that high seepage rate because uncertainty in the glass degradation rate as a function of the quantity of water contacting the waste was not propagated consistently between the EBS Flow Submodel (Section 6.3.6) and the HLW Glass Degradation Submodel (Section 6.3.7.4.3).

The effect of applying an HLW glass degradation rate coefficient that is skewed to result in lower degradation rates is not significant compared to the overall uncertainty propagated through the TSPA-SEIS, because the HLW glass degradation rate has little effect on dose.

In-Package Chemistry and the Instantaneous Degradation of CSNF—The In-Package Chemistry Abstraction (SNL 2007 [DIRS 180506]) does not consider the instantaneous degradation of CSNF in the process model and subsequent abstraction. However, within the TSPA-SEIS, the chemistry inside the failed CSNF WP following the instantaneous degradation of the CSNF is determined using the abstractions developed in *In-Package Chemistry Abstraction* (SNL 2007 [DIRS 180506]). Instantaneous degradation of the CSNF occurs in the Waste Package EF Modeling Case and in the Seismic GM and Seismic FD Modeling Cases when the seismic event damages CSNF WPs, and the CSNF is exposed to WP temperatures exceeding 100°C.

Effect on the TSPA—The instantaneous degradation of the CSNF waste form is the recommended waste form treatment when the waste form in a failed CSNF WP is exposed to temperatures exceeding 100°C (Section 6.3.7.4.1.3). The in-package chemistry process models presented in the In-Package Chemistry Abstraction (SNL 2007 [DIRS 180506]) considered very fast degradation rates but did not consider the instantaneous degradation of the CSNF.

Because the in-package pH conditions are controlled by the buffering capacity of the degradation products of CSNF (SNL 2007 [DIRS 180506], Section 6.3.4.1[a]), the instantaneous degradation of CSNF means that the maximum pH buffering capacity will be achieved after the CSNF experiences instantaneous degradation. Therefore, the pH conditions within CSNF WPs after instantaneous degradation of CSNF will be well constrained.

Therefore, it is concluded that following the instantaneous degradation of CSNF inside a failed WP, the implemented pH abstraction is sufficient to cover this condition, although the consequence had not explicitly been included in the abstraction process.

Similarly, the ionic strength abstraction is sufficient to cover the condition following the instantaneous degradation of CSNF inside a failed WP, although the consequence had not been explicitly included in the abstraction processes.

6.3.7.7.2 Identification of Conservatisms in Submodels and Abstractions

Secondary Phases of Uranium—The TSPA-SEIS does not consider the incorporation of any elements into secondary phases of uranium. Neptunium would likely be incorporated into secondary phases; however, additional quantitative information required to develop a reliable predictive numerical model is not currently available. Using a neptunium-bearing uranyl compound instead of a pure neptunium phase as the solubility-controlling solid would lead to

lower solubilities. The details of this conservatism are discussed in *Dissolved Concentration Limits of Elements with Radioactive Isotopes* (SNL 2007 [DIRS 177418], Section 6.6.4).

Controlling Solid for Radium—Pure $RaSO_4$ is used as the controlling solid for radium instead of solid solutions. Field studies have shown that radium concentrations in some natural waters are orders of magnitude below levels corresponding to $RaSO_4$ saturation. Radium concentrations likely correspond to the solubilities of radium in solid solutions in more common sulfate solids such as $SrSO_4$ or $BaSO_4$ (SNL 2007 [DIRS 177418], Section 6.12). This results in the overestimation of aqueous radium concentrations.

Solubility versus Temperature—The solubility of radioactive elements at 25°C is used for all temperatures. Actinide solubility values tend to decrease with increasing temperature; however, this conservatism simplifies the model approach (SNL 2007 [DIRS 177418], Sections 6.3.3.3 and 6.4.2.2). This conservatism may result in the overestimation of aqueous radioactive element concentrations.

CSNF Radionuclide Release Rate—In developing the models for the rate of fractional radionuclide release from the CSNF matrix, it is assumed that the fractional degradation rate of the CSNF matrix conservatively bounds the rate of the fractional release of radionuclides located in the fuel matrix. The fission product and actinide elements embedded in the fuel matrix are made available for mobilization and behave (dissolve) as individual elements as the fuel matrix degrades. The fission-product technetium is known to be partly in the form of noble five-metal alloy particles. The properties of the five-metal alloy particles are likely to control the technetium release rate at a level much lower than the CSNF matrix degradation rate. Assuming that technetium release from the CSNF matrix is limited only by the matrix degradation rate, is therefore conservative, as demonstrated in *CSNF Waste Form Degradation* (BSC 2004 [DIRS 169987], Section 5.1).

Specific Surface Area of Corroding CSNF—In assessing the effective specific surface area of corroding CSNF in fuel rods following breaching of the cladding, it is conservatively assumed that the configuration of the fuel is represented by fuel pellet fragments and short fuel rod segments. There is insufficient information to discriminate between the scenarios proposed for the progression of the degradation of fuel rods after the cladding is breached. Thus, the conservative assumption is made that the degradation progresses rapidly, leaving the fuel in the form of fuel pellet fragments or short rod segments (BSC 2004 [DIRS 169987], Sections 5.2 and 6.2.2.1). This is a conservative assumption imposed by the cited source.

All CSNF Cladding Failed at Arrival—The TSPA-SEIS model assumes all CSNF cladding failed at arrival.

Failed Cladding—After cladding failure, no credit is taken for the failed cladding limiting the amount of water or moist air that can contact the fuel pellets. The failed cladding still limits the interaction of the fuel pellets and the environment; however, no credit is taken for this in the TSPA-SEIS. In the TSPA-SEIS, after cladding failure, the fuel pellets corrode as if they were bare fuel pellets (SNL 2007 [DIRS 180616], Section 6.1.4). Credit is taken for the reduction in the release rate of the radionuclides through the failed cladding. The diffusion of radionuclides

across the split opening is modeled in *Cladding Degradation Summary for LA* (SNL 2007 [DIRS 180616], Section 6.2.4).

DSNF Cladding—No credit is taken for DSNF cladding. This simplified modeling approach is used because there is no technical basis for giving credit for DSNF cladding, and the recommended DSNF release model is an upper limit model invoking the complete release of DSNF upon exposure to groundwater (BSC 2004 [DIRS 172453], Section 8.1). Furthermore, a significant fraction of the Uranium Metal SNF (DSNF Group 7), the representative DSNF used in the TSPA-SEIS, is visibly damaged and much of the rest could have small pinholes/cracks in the cladding (BSC 2004 [DIRS 172453], Sections 6.1.7 and 6.1.12).

This conservatism is not applied to naval SNF. Unlike some DSNF, naval SNF is completely characterized, and the degradation of naval SNF was modeled using the same environmental conditions used for the degradation of CSNF.

Degradation Of Metallic Uranium N-Reactor Fuel—A constant degradation rate is used that conservatively bounds degradation of metallic uranium present in N-Reactor fuel; upon WP breach, degradation of DSNF occurs in one timestep of TSPA. Little quality assurance data exists on DSNF fuel, so a conservative approach is used to bound uncertainty in the characteristics of the DSNF fuel (BSC 2004 [DIRS 172453], Section 8.1).

HLW Inventory—The number of canisters of HLW glass is overestimated by about four percent because of the assumption to emplace full CDSP WPs in the repository (SNL 2007 [DIRS 180472], Assumption 5.10[a]). The calculation indicates that the DSNF waste fills a certain number of WPs with one canister of DSNF per package. However, emplacing five HLW canisters in all of these packages requires approximately twice as many HLW canisters than are actually predicted to be sent to the repository given the HLW allocation of two-thirds of 10 percent of 70,000 metric tons of heavy metal (SNL 2007 [DIRS 180472], Assumption 5.10[a]).

Total Number of Waste Packages—The number of CSNF and CDSP WPs is overestimated by about four percent because TSPA assumes that all of the 108 drifts (including contingency drifts) in the repository design will be filled with WPs (SNL 2007 [DIRS 180472], Assumption 5.14[a]). This additional four percent of both types of WPs is in addition to the four percent extra HLW previously discussed. Filling all the drifts with WPs results in the "qualification" of all 108 drifts for emplacement, but increases the total metric tons of heavy metal in the footprint to 76,223 (including the extra HLW discussed above). The inclusion of more than 70,000 metric tons of heavy metal in the TSPA-SEIS is conservative for dose (SNL 2007 [DIRS 180472], Assumption 5.14[a]).

Degradation of CSNF Waste Greater Than 100°C—If the breached CSNF WP temperature exceeds 100°C, CSNF will undergo "dry air oxidation" (BSC 2004 [DIRS 169987], Section 6.2.2.2). The major effect of dry air oxidation is the very large increase in the specific area of CSNF. As a result, the fractional dissolution rate increases accordingly. Therefore, it is assumed that the degradation of the CSNF waste form would be instantaneous (BSC 2004 [DIRS 169987], Section 8.1). This treatment is conservative when considering that the estimation for the increase in specific surface area of CSNF undergoing dry air oxidation has a large uncertainty.

6.3.7.8 Alternative Conceptual Model(s) for Waste Form Degradation and Mobilization

Section 6.2 outlines the general consideration and treatment of ACMs used to support the TSPA-SEIS. A brief description of the Waste Form Degradation and Mobilization Submodel ACMs that are summarized in Tables 6.3.7-67 through 6.3.7-72 are presented below.

In-Package Chemistry ACMs—Three ACMs were considered as alternatives to the In-Package Chemistry Abstraction (SNL 2007 [DIRS 180506], Section 6.4). The first ACM was a one-dimensional column composed of *n* cells, where the reactants in each cell represent the WP components in a vertical cross section of a WP (SNL 2007 [DIRS 180506], Section 6.4.1). This model would eliminate the constraint of the solid-centered flow through mode of a well-mixed batch reactor used in the EQ6 (*Software Code: EQ6.* 7.2bLV (BSC 2002 [DIRS 159731]) calculations in the In-Package Chemistry Abstraction and provide a water stream with a variable composition along its flow path. This ACM was excluded from the In-Package Chemistry Abstraction on the basis that, in comparisons between the vapor influx model and the spatially heterogeneous model, the vapor influx model is much simpler and yielded comparable results (SNL 2007 [DIRS 180506], Section 6.4.1). Inclusion of this ACM in the TSPA-SEIS would not likely have an effect on dose because the implemented abstraction yields comparable results.

The second ACM considered variable-composition seepage entering a failed WP as a function of time, changing with time-varying changes in the physical and chemical environment in the drifts and the EBS (SNL 2007 [DIRS 180506], Section 6.4.2). Section 6.5.2 of *In-Package Chemistry Abstraction* (SNL 2007 [DIRS 180506]) demonstrates that the EQ6 STN: 10075–7.2bLV-02 (BSC 2002 [DIRS 159731]) calculations were largely insensitive to initial seepage water compositions because the WP materials have a stronger influence on the resulting chemistry. Inclusion of this ACM in the TSPA-SEIS would not likely have an effect because the implemented abstraction yields comparable results.

A third ACM considers the alternate methodologies for determining the vapor flux rate through the stress corrosion cracks in a failed WP (SNL 2007 [DIRS 180506], Section 6.4.3). In this ACM, Fick's Law and Stefan Tube Diffusion Calculations are used to develop a relationship between the vapor flux rate through SCC and relative humidity. Calculated results demonstrate that the abstracted relationship presented for the TSPA-SEIS is appropriate, and no change to dose is expected if this ACM were included in the TSPA-SEIS.

The first two ACMs and the associated screening arguments for in-package chemistry are summarized in Table 6.3.7-67. The third ACM was excluded because the abstracted relationship for the vapor flux rate into a stress corrosion cracked-failed WP provided for the TSPA-SEIS is simpler and spans the expected range by this ACM.

Cladding Degradation ACMs—The ACMs considered for cladding degradation are summarized in Table 6.3.7-68. The summary shows that most of the ACMs are not suitable for use in the TSPA-SEIS because they are deemed not realistic (Table 6.3.7-68).

CSNF Waste Form Degradation ACMs—Two ACMs for CSNF waste form degradation were considered in the abstraction to TSPA: (1) an electrochemical model based on modeling the rates of redox reactions involved in fuel oxidation and dissolution and (2) a surface complexation

model based on a three-step bicarbonate-promoted oxidative dissolution mechanism (BSC 2004 [DIRS 169987], Section 6.4.2).

Using estimates for the unknown parameters in the developed ACMs, an analysis was performed comparing the basecase abstraction with the ACMs. The degradation rates from the electrochemical model were three times greater than the basecase model implemented in the TSPA-SEIS (BSC 2004 [DIRS 169987], Section 7.2). However, it was later concluded that this model was overly conservative because it does not consider slower surface complexation, dissolution, and/or mass transfer limitations. Inclusion of this ACM in the TSPA-SEIS would only have an impact on the TSPA-SEIS dose in the Seismic Scenario when WP failures occur after the WP temperature is less than 100°C. In the Waste Package EF and Igneous Intrusion Modeling Cases, the WP temperature exceeds 100°C after the WP is failed and instantly degrades the CSNF waste form. Using estimates for the unknown parameters, the surface complexation ACM analysis yielded a CSNF degradation rate that was 40 percent lower than the basecase model implemented in the TSPA-SEIS. In the TSPA-SEIS, the inclusion of this ACM would only have a dose impact in the Seismic Scenario when WP failures occur after the WP temperature is less than 100°C. The expected result is a slower degradation rate for the CSNF. Both of these ACMs were screened out of the CSNF Waste Form Degradation Abstraction, and the basis for this assessment is summarized in Table 6.3.7-69.

DSNF Waste Form Degradation ACM—An ACM for DSNF waste form degradation was based on the best-estimates dissolution models presented in *DSNF and Other Waste Form Degradation Abstraction* (BSC 2004 [DIRS 172453], Section 6.3). The application of this ACM would require that the dissolution rate expression be multiplied by the "actual" effective surface area of the SNF. This ACM was screened out of the DSNF Waste Form Degradation Submodel (Section 6.3.7.4.2) because insufficient qualified data on the corrosion rates and the surface areas of the fuel in each group are available. In addition, the upper-limit degradation model that is implemented as a surrogate for all the DSNF, other than naval SNF, is a bounding model with respect to the degradation rate.

HLW Glass Degradation ACM—The HLW Glass Degradation Abstraction (BSC 2004 [DIRS 169988], Section 6.4), screened ACMs to simplify the basecase mechanistic model for HLW glass degradation to a form that could be used in the TSPA-SEIS. The screening eliminated parts of the mechanistic model that were deemed unnecessary for describing HLW glass degradation over the range of anticipated physical and chemical conditions in the repository. Most nuclear waste HLW glass degradation models were developed to predict a changing dissolution rate over long times. In contrast, the HLW Glass Degradation Abstraction was developed to provide a constant HLW glass degradation rate under a specific set of exposure conditions that could change for every realization in the simulation because time is not a parameter in the HLW Glass Degradation Abstraction. Instead, the exposure conditions, consisting of the amount of water contacting the HLW glass, the solution pH, and the waste form and in-package temperature, change with time.

ACMs for HLW glass degradation under near-saturation conditions are based on: (1) solid-state diffusion-controlled release; and (2) the composition-independent effective rate constant, which was screened out of the HLW Glass Degradation Abstraction for the TSPA-SEIS analysis. The first ACM was screened out as being unconvincing. Using estimates for unknown fitting

parameters, a negligible impact on the calculated rates using this ACM was observed (BSC 2004 [DIRS 169988], Section 6.4.1).

The second ACM considered the effects of different compositions on the intrinsic dissolution rate and affinity term, which in the basecase model implemented in the TSPA-SEIS, have been combined into a single effective rate constant. An analysis of available literature data reveals that combining the two terms into one effective parameter has little effect on the overall reaction rate and that the basecase implementation is more robust for use in the TSPA-SEIS.

The screening arguments are described in detail in *Defense HLW Glass Degradation Model* (BSC 2004 [DIRS 169988], Section 6.4) and are summarized in Table 6.3.7-71. In addition, the *Defense HLW Glass Degradation Model* (BSC 2004 [DIRS 169988], Section 7) indicates that the basecase HLW Glass Degradation Abstraction is validated for HLW borosilicate glass waste forms. Thus, the HLW Glass Degradation Abstraction is applicable to both commercial HLW and DOE-owned HLW glass waste forms.

Dissolved Concentration Limits ACMs—Several ACMs were considered in developing the submodels for the solubility limits of radioactive elements for the TSPA-SEIS (SNL 2007 [DIRS 177418]), and these are summarized in Table 6.3.7-71. Two ACMs are considered for plutonium solubility: (1) the Theoretical fO_2 Model; and (2) the Empirical Eh Model. In the Theoretical fO_2 Model, calculations are carried out with the solution redox condition controlled by theoretical equilibrium between the solution and the atmosphere (with fO_2 equal to 0.2 bars). This ACM is screened out because the results differ significantly from experimental measurements. The Empirical Eh Model uses an empirical (instead of theoretical) equation to set the redox conditions. This ACM is not used because the plutonium solubility results for this model are lower than the experimental values. For the remaining elements (neptunium, thorium, americium, protactinium, and strontium), the ACMs involved the use of other solubility-controlling solids. These ACMs are screened out because either there is not enough thermodynamic data available to justify their use or a more soluble solid was chosen for conservatism (Table 6.3.7-71).

EBS Colloids ACMs—Three conceptual models were considered as alternatives to the current TSPA-SEIS EBS Colloids Submodel (SNL 2007 [DIRS 177423], Section 6.4). These ACMs are listed in Table 6.3.7-72, along with the principal bases and screening criteria. The first ACM considers two-site and three-site sorption kinetic models as an alternative to the assumption of irreversible sorption used in the basecase model. The kinetic model represents a useful tool for examining sorption data and examining the evidence for slow reversible sorption of plutonium on colloids. The model clearly demonstrates that the data from Lu et al. (2000 [DIRS 166315]) can be fit with reversible components, suggesting that irreversible sorption is conservative. The kinetic model has not been adopted because it is immature and the base model is conservative and bounding. A second ACM considers the rate of colloid generation as a function of the waste form degradation rate. In this ACM, the rate of colloid spallation would depend upon the rate of waste degradation. The rate of HLW glass degradation may be defined by the rate of boron release to the alteration fluid, and likewise, the rate of technetium release could be correlated to the degradation rate of CSNF. However, this ACM is currently not sufficiently developed for application to more generalized conditions. A third ACM considers colloid generation as primarily a function of the rate of advective water flow penetrating the degrading waste forms.

This ACM addresses the possibility that colloids can form from both DSNF and CSNF, but their release from the waste weathering rind is governed by the energy of flowing water. The supporting concepts for this ACM were developed in the context of deposition and remobilization of existing colloids under conditions of significant groundwater flow. These conditions likely will not apply to conditions anticipated in the repository.

INTENTIONALLY LEFT BLANK

Table 6.3.7-1 Waste Package Configurations

Waste Package Type	Number of Waste Packages	Spent Nuclear Fuel Unit	Max # of Units per Package	# of Glass Canisters per Package	Glass Unit	Shorthand
CSNF	4,586	PWR assembly	21	0		21P-TAD
CSNF	173	PWR assembly	12	0		12-Long-TAD
CSNF	3,037	BWR assembly	44	0		44B-TAD
CDSP WP	1,940	Short canister	1	5	Short	CDSP-Short
CDSP WP	1,257	Long canister	1	5	Long	CDSP-Long
CDSP WP	219	MCO	2	2	Long	CDSP-MCO
Naval	323	Canister	1	0		SNF-Long
Naval	94	Canister	1	0		SNF-Short
Total CDSP	3,416					
Total in CSNF+Naval	8,213					
Grand Total	11,629					

Sources: DTN: MO0702PASTREAM.001_R0 (SNL 2007 [DIRS 179925]), Item 6 of worksheet "COMMERCIAL," Item 4 of worksheet "NON-COMMERCIAL," and rows 49 and 59 of worksheet "UNIT CELL" *in spreadsheet DTN-Inventory-Rev00.xls.*

NOTE: MCO = multicanister overpack, TAD = transportation, aging, and disposal (canister)

Table 6.3.7-2. Radionuclides Included in TSPA-SEIS

Radionuclide	Screened-in for Groundwater Modeling Cases: Nominal, Human Intrusion, Igneous Intrusion, and Seismic	Volcanic Eruption Modeling Case
^{227}Ac	^{227}Ac	^{227}Ac
^{241}Am	^{241}Am	^{241}Am
^{243}Am	^{243}Am	^{243}Am
^{14}C	^{14}C	NA
^{36}Cl	^{36}Cl	NA
^{245}Cm	Added to ensure that the effect of its decay on the inventory of ^{241}Am are included	
^{135}Cs	^{135}Cs	NA
^{137}Cs	^{137}Cs	^{137}Cs
^{129}I	^{129}I	^{129}I
^{237}Np	^{237}Np	^{237}Np
^{231}Pa	^{231}Pa	^{231}Pa
^{210}Pb	Assumed to be in secular equilibrium with ^{226}Ra. Not explicitly modeled, but dose effects included with ^{226}Ra.	
^{238}Pu	^{238}Pu	^{238}Pu
^{239}Pu	^{239}Pu	^{239}Pu
^{240}Pu	^{240}Pu	^{240}Pu
^{241}Pu	Added to ensure that the effect of its decay on the inventory of ^{241}Am and ^{237}Np are included	
^{242}Pu	^{242}Pu	^{242}Pu
^{226}Ra	^{226}Ra	^{226}Ra
^{228}Ra	^{228}Ra	^{228}Ra
^{79}Se	^{79}Se	NA
^{126}Sn	^{126}Sn	^{126}Sn
^{90}Sr	^{90}Sr	^{90}Sr
^{99}Tc	^{99}Tc	^{99}Tc
^{229}Th	^{229}Th	^{229}Th
^{230}Th	^{230}Th	^{230}Th
^{232}Th	^{232}Th	^{232}Th
^{232}U	^{232}U	NA
^{233}U	^{233}U	^{233}U
^{234}U	^{234}U	^{234}U
^{235}U	^{235}U	NA
^{236}U	^{236}U	NA
^{238}U	^{238}U	^{238}U
Count	29	22

Sources: Developed from Table 7-1 in *Radionuclide Screening* (SNL 2007 [DIRS 177424]) and DTN: MO0701RLTSCRNA.000_R0 (SNL 2007 [DIRS 179334]).

NOTE: The count in the last row does not include ^{245}Cm and ^{241}Pu.

NA = not applicable.

Table 6.3.7-3 Nominal Grams of Radionuclides per Waste Package for Each Type of Waste

Year of Projection: CSNF = Year 2067, DSNF = Year 2030, and HLW = Year 2030 Total Number of Waste Packages is 11,629 (8,213 CSNF and 3,416 CDSP WP)			
	Grams per Waste Package		
Radionuclide	CSNF	DSNF	HLW
^{227}Ac	2.47E-06	1.22E-03	1.91E-04
^{241}Am	8.18E+03	2.18E+02	3.75E+01
^{243}Am	1.24E+03	6.73E+00	5.75E-01
^{14}C [a]	1.35E+00	1.81E+00	0.00E+00[b]
^{36}Cl	3.23E+00	4.23E+00	0.00E+00[b]
^{245}Cm	1.75E+01	9.25E-02	5.43E-02
^{135}Cs	4.36E+03	9.74E+01	1.27E+02
^{137}Cs	5.90E+03	9.72E+01	3.02E+02
^{129}I	1.73E+03	3.56E+01	7.27E+01
^{237}Np	4.57E+03	8.14E+01	9.95E+01
^{231}Pa	9.17E-03	2.14E+00	1.53E+00
^{238}Pu	1.52E+03	1.25E+01	3.91E+01
^{239}Pu	4.32E+04	2.21E+03	5.58E+02
^{240}Pu	2.05E+04	4.35E+02	4.61E+01
^{241}Pu	2.66E+03	2.92E+01	1.22E+00
^{242}Pu	5.28E+03	3.02E+01	3.89E+00
^{226}Ra	0.00E+00 [b]	4.57E-05	2.42E-05
^{228}Ra	0.00E+00 [b]	1.51E-05	6.00E-06
^{79}Se	4.19E+01	6.82E+00	7.01E+00
^{126}Sn	4.63E+02	9.40E+00	1.70E+01
^{90}Sr	2.49E+03	5.22E+01	1.74E+02
^{99}Tc	7.55E+03	1.58E+02	1.01E+03
^{229}Th	0.00E+00 [b]	3.24E-01	3.30E-03
^{230}Th	1.52E-01	1.18E-01	8.12E-04
^{232}Th	0.00E+00 [b]	2.17E+04	2.98E+04
^{232}U	1.02E-02	1.28E+00	4.08E-04
^{233}U	5.76E-02	5.38E+02	1.94E+01
^{234}U	1.75E+03	4.73E+02	2.33E+01
^{235}U	6.26E+04	2.51E+04	1.41E+03
^{236}U	3.84E+04	1.25E+03	5.99E+01
^{238}U	7.82E+06	6.84E+05	2.37E+05

Source: DTN: MO0702PASTREAM.001_R0 (SNL 2007 [DIRS 179925]),'worksheet "RN INVENTORY" *in spreadsheet DTN-Inventory-Rev00.xls*..

NOTE: ^{210}Pb is not listed in this table because it is considered to be in secular equilibrium with ^{226}Ra.

[a] 18 percent of ^{14}C for CSNF resides in the hardware outside of the cladding (DTN: SN0310T0505503.004_R0 [DIRS 168761]).

[b] Grams listed as 0.00E+00 is the value presented in the data input source.

Table 6.3.7-4a. Radionuclide Inventory Per Waste Package Showing the Amount of Decay and Ingrowth Experienced During the Preclosure Period

Grams Per Waste Package Inventory, g/pkg						
Radionuclide	CSNF at 2067[a]	CSNF after 50 Years[b]	DSNF at 2030[a]	DSNF after 87 Years[b]	HLW at 2030[a]	HLW after 87 Years[b]
^{227}Ac	2.47E-06	6.27E-06	1.22E-03	1.39E-03	1.91E-04	9.47E-04
^{241}Am	8.18E+03	9.84E+03	2.18E+02	2.15E+02	3.75E+01	3.37E+01
^{243}Am	1.24E+03	1.23E+03	6.73E+00	6.68E+00	5.75E-01	5.70E-01
^{14}C	1.35E+00	1.34E+00	1.81E+00	1.79E+00	0.00E+00	0.00E+00
^{36}Cl	3.23E+00	3.23E+00	4.23E+00	4.23E+00	0.00E+00	0.00E+00
^{245}Cm	1.75E+01	1.74E+01	9.25E-02	9.18E-02	5.43E-02	5.39E-02
^{135}Cs	4.36E+03	4.36E+03	9.74E+01	9.74E+01	1.27E+02	1.27E+02
^{137}Cs	5.90E+03	1.86E+03	9.72E+01	1.31E+01	3.02E+02	4.07E+01
^{129}I	1.73E+03	1.73E+03	3.56E+01	3.56E+01	7.27E+01	7.27E+01
^{237}Np	4.57E+03	5.32E+03	8.14E+01	1.12E+02	9.95E+01	1.04E+02
^{231}Pa	9.17E-03	1.22E-02	2.14E+00	2.14E+00	1.53E+00	1.53E+00
^{238}Pu	1.52E+03	1.02E+03	1.25E+01	6.28E+00	3.91E+01	1.96E+01
^{239}Pu	4.32E+04	4.31E+04	2.21E+03	2.20E+03	5.58E+02	5.57E+02
^{240}Pu	2.05E+04	2.04E+04	4.35E+02	4.31E+02	4.61E+01	4.57E+01
^{241}Pu	2.66E+03	2.40E+02	2.92E+01	4.49E-01	1.22E+00	1.89E-02
^{242}Pu	5.28E+03	5.28E+03	3.02E+01	3.02E+01	3.89E+00	3.89E+00
^{226}Ra	0.00E+00	1.29E-04	4.57E-05	1.80E-04	2.42E-05	2.68E-05
^{228}Ra	0.00E+00	8 1.90E-11	1.51E-05	8.77E-06	6.00E-06	1.20E-05
^{79}Se	4.19E+01	4.19E+01	6.82E+00	6.82E+00	7.01E+00	7.01E+00
^{126}Sn	4.63E+02	4.63E+02	9.40E+00	9.40E+00	1.70E+01	1.70E+01
^{90}Sr	2.49E+03	7.46E+02	5.22E+01	6.43E+00	1.74E+02	2.14E+01
^{99}Tc	7.55E+03	7.55E+03	1.58E+02	1.58E+02	1.01E+03	1.01E+03
^{229}Th	0.00E+00	2.07E-05	3.24E-01	5.22E-01	3.30E-03	1.05E-02
^{230}Th	1.52E-01	4.32E-01	1.18E-01	2.33E-01	8.12E-04	9.02E-03
^{232}Th	0.00E+00	5.63E-02	2.17E+04	2.17E+04	2.98E+04	2.98E+04
^{232}U	1.02E-02	6.20E-03	1.28E+00	5.39E-01	4.08E-04	1.72E-04
^{233}U	5.76E-02	1.37E-01	5.38E+02	5.38E+02	1.94E+01	1.94E+01
^{234}U	1.75E+03	2.24E+03	4.73E+02	4.79E+02	2.33E+01	4.24E+01
^{235}U	6.26E+04	6.27E+04	2.51E+04	2.51E+04	1.41E+03	1.41E+03
^{236}U	3.84E+04	3.85E+04	1.25E+03	1.25E+03	5.99E+01	6.03E+01
^{238}U	7.82E+06	7.82E+06	6.84E+05	6.84E+05	2.37E+05	2.37E+05

[a] DTN: MO0702PASTREAM.001_R0 [DIRS 179925].

[b] DTN: TBD

Table 6.3.7-4b. Supplemental Radionuclide Inventory Per Waste Package due to Mixed Oxide Fuel and Lanthanide Borosilicate Waste Showing the Amount of Decay and Ingrowth Experienced During the Preclosure Period

Grams Per Waste Package MOX and LaBS Specific Additional Inventory, g/pkg				
Radionuclide	MOX at 2035[a]	MOX after 82 Years[b]	LaBS at 2003[a]	LaBS after 114 Years[b]
^{227}Ac	1.11E-10	4.29E-09	0.00E+00	1.40E-08
^{241}Am	1.90E+01	3.89E+02	2.78E+01	3.40E+01
^{243}Am	4.82E+01	4.78E+01	0.00E+00	0.00E+00
^{14}C	2.52E-02	2.50E-02	0.00E+00	0.00E+00
^{36}Cl	2.42E-07	2.42E-07	0.00E+00	0.00E+00
^{245}Cm	1.36E+00	1.35E+00	0.00E+00	0.00E+00
^{135}Cs	7.00E+01	7.00E+01	0.00E+00	0.00E+00
^{137}Cs	1.64E+02	2.48E+01	0.00E+00	0.00E+00
^{129}I	3.02E+01	3.02E+01	0.00E+00	0.00E+00
^{237}Np	1.44E+01	5.55E+01	4.77E-01	6.76E+00
^{231}Pa	3.99E-06	8.43E-06	0.00E+00	2.94E-05
^{238}Pu	1.46E+01	7.63E+00	3.43E+00	1.39E+00
^{239}Pu	1.00E+03	9.98E+02	3.48E+03	3.47E+03
^{240}Pu	7.09E+02	7.03E+02	3.10E+02	3.06E+02
^{241}Pu	4.20E+02	8.21E+00	1.26E+01	5.33E-02
^{242}Pu	1.79E+02	1.79E+02	6.09E+00	6.09E+00
^{226}Ra	8.79E-11	3.03E-07	0.00E+00	8.15E-07
^{228}Ra	5.89E-17	2.18E-14	0.00E+00	6.31E-09
^{79}Se	5.30E-01	5.30E-01	0.00E+00	0.00E+00
^{126}Sn	1.13E+01	1.13E+01	0.00E+00	0.00E+00
^{90}Sr	3.57E+01	4.96E+00	0.00E+00	0.00E+00
^{99}Tc	9.75E+01	9.75E+01	0.00E+00	0.00E+00
^{229}Th	2.68E-09	1.24E-07	0.00E+00	2.25E-08
^{230}Th	4.29E-06	1.07E-03	0.00E+00	1.71E-03
^{232}Th	1.15E-06	6.06E-05	1.56E+01	1.56E+01
^{232}U	9.85E-06	4.36E-06	0.00E+00	0.00E+00
^{233}U	2.28E-05	8.58E-04	0.00E+00	1.31E-04
^{234}U	8.91E-01	7.75E+00	4.24E+00	6.24E+00
^{235}U	5.48E+01	5.71E+01	2.61E+02	2.72E+02
^{236}U	2.18E+01	2.78E+01	0.00E+00	3.66E+00
^{238}U	7.99E+04	7.99E+04	8.58E+02	8.58E+02

[a] DTN: MO0702PASTREAM.001_R0 [DIRS 179925].

[b] DTN: TBD.

Table 6.3.7-5. Initial Radionuclide Inventories and Initial Radionuclide Activities Per Waste Package Type in the TSPA-SEIS

Per Waste Package Inventory and Activity at Closure, 2117							
Radionuclide	Specific Activity[a] Ci/g	CSNF w/MOX added[b], g/pkg	CSNF w/MOX added, Ci/pkg	DSNF[b], g/pkg	DSNF, Ci/pkg	HLW w/LaBS added[b], g/pkg	HLW w/LaBS added, Ci/pkg
^{227}Ac	7.22E+01	6.27E-06	4.53E-04	1.39E-03	1.00E-01	9.47E-04	6.84E-02
^{241}Am	3.43E+00	1.02E+04	3.51E+04	2.15E+02	7.37E+02	6.77E+01	2.32E+02
^{243}Am	2.00E-01	1.28E+03	2.56E+02	6.68E+00	1.34E+00	5.70E-01	1.14E-01
^{14}C	4.46E+00	1.37E+00	6.09E+00	1.79E+00	7.98E+00	0.00E+00	0.00E+00
^{36}Cl	3.30E-02	3.23E+00	1.07E-01	4.23E+00	1.40E-01	0.00E+00	0.00E+00
^{245}Cm	1.72E-01	1.88E+01	3.23E+00	9.18E-02	1.58E-02	5.39E-02	9.27E-03
^{135}Cs	1.15E-03	4.43E+03	5.09E+00	9.74E+01	1.12E-01	1.27E+02	1.46E-01
^{137}Cs	8.67E+01	1.88E+03	1.63E+05	1.31E+01	1.14E+03	4.07E+01	3.53E+03
^{129}I	1.77E-04	1.76E+03	3.12E-01	3.56E+01	6.30E-03	7.27E+01	1.29E-02
^{237}Np	7.05E-04	5.38E+03	3.79E+00	1.12E+02	7.90E-02	1.11E+02	7.81E-02
^{231}Pa	4.72E-02	1.22E-02	5.76E-04	2.14E+00	1.01E-01	1.53E+00	7.22E-02
^{238}Pu	1.71E+01	1.03E+03	1.76E+04	6.28E+00	1.07E+02	2.10E+01	3.59E+02
^{239}Pu	6.21E-02	4.41E+04	2.74E+03	2.20E+03	1.37E+02	4.03E+03	2.50E+02
^{240}Pu	2.27E-01	2.11E+04	4.79E+03	4.31E+02	9.78E+01	3.52E+02	7.98E+01
^{241}Pu	1.03E+02	2.48E+02	2.56E+04	4.49E-01	4.62E+01	7.22E-02	7.44E+00
^{242}Pu	3.94E-03	5.46E+03	2.15E+01	3.02E+01	1.19E-01	9.98E+00	3.93E-02
^{226}Ra	09.89E-01	1.29E-04	1.28E-04	1.80E-04	1.78E-04	2.76E-05	2.73E-05
^{228}Ra	2.72E+02	1.90E-11	5.17E-09	8.77E-06	2.39E-03	1.20E-05	3.27E-03
^{79}Se	1.53E-02	4.24E+01	6.49E-01	6.82E+00	1.04E-01	7.01E+00	1.07E-01
^{126}Sn	1.13E-02	4.74E+02	5.36E+00	9.40E+00	1.06E-01	1.70E+01	1.92E-01
^{90}Sr	1.38E+02	7.51E+02	1.04E+05	6.43E+00	8.87E+02	2.14E+01	2.95E+03
^{99}Tc	1.70E-02	7.65E+03	1.30E+02	1.58E+02	2.69E+00	1.01E+03	1.72E+01
^{229}Th	2.14E-01	2.08E-05	4.46E-06	5.22E-01	1.12E-01	1.05E-02	2.25E-03
^{230}Th	2.06E-02	4.33E-01	8.92E-03	2.33E-01	4.80E-03	1.07E-02	2.21E-04
^{232}Th	1.10E-07	5.64E-02	6.20E-09	2.17E+04	2.39E-03	2.98E+04	3.28E-03
^{232}U	2.21E+01	06.20E-03	1.37E-01	5.39E-01	1.19E+01	1.72E-04	3.80E-03
^{233}U	9.65E-03	01.38E-01	1.33E-03	5.38E+02	5.19E+00	1.94E+01	1.87E-01
^{234}U	6.21E-03	2.25E+03	1.40E+01	4.79E+02	2.97E+00	4.86E+01	3.02E-01
^{235}U	2.16E-06	6.28E+04	1.36E-01	2.51E+04	5.42E-02	1.68E+03	3.63E-03
^{236}U	6.47E-05	3.85E+04	2.49E+00	1.25E+03	8.09E-02	6.40E+01	4.14E-03
^{238}U	3.36E-07	7.90E+06	2.65E+00	6.84E+05	2.30E-01	2.38E+05	7.99E-02

[a] DTN: MO0702PASTREAM.001_R0 [DIRS 179925].

[b] Output DTN: MO0707EMPDECAY.000_R0

Table 6.3.7-6. Disposition of Radionuclides for Groundwater Release Modeling Cases: Nominal, Igneous Intrusion, and Seismic

Radionuclide (see Table 6.3.7-2)	Disposition in WF, EBS, and UZ TSPA-SEIS Components (see Section 6.3.7)	Disposition in 3-D UZ FEHM Submodel[a] (see Section 6.3.9)	Disposition in SZ Submodels (3-D SZ_Convolute and 1-D Pipe)[b] (see Section 6.3.10)	Disposition in Biosphere (see Section 6.3.11)
^{227}Ac	Not transported	Not transported	Not transported	Dose from 1-D[9], assuming secular equilibrium with ^{231}Pa
^{241}Am	Transport embedded colloid $^{241}Am_{emb}$ (decay to ^{237}Np) Transport irreversible FeO colloid $^{241}Am_{FeO}$ (decay to ^{237}Np) Transport reversible colloid and solute (decay to ^{237}Np)	Transport slow irreversible colloid $^{241}Am_{irs}$ (decay to ^{237}Np) Transport fast irreversible colloid $^{241}Am_{irf}$ (decay to ^{237}Np) Transport reversible colloid and solute (decay to ^{237}Np)	3-D transport of americium/plutonium slow irreversible colloid [SZ BTC 6] 3-D transport of americium/plutonium fast irreversible colloid [SZ BTC 10] 3-D transport of americium/thorium/protactinium reversible colloid [SZ BTC 2]	Dose from 3-D
^{243}Am	Transport embedded colloid $^{243}Am_{emb}$ (decay to $^{239}Pu_{emb}$) Transport irreversible FeO colloid $^{243}Am_{FeO}$ (decay to $^{239}Pu_{FeO}$) Transport reversible colloid and solute (decay to ^{239}Pu)	Transport slow irreversible colloid $^{243}Am_{irs}$ (decay to $^{239}Pu_{irs}$) Transport fast irreversible colloid $^{243}Am_{irf}$ (decay to $^{239}Pu_{irf}$) Transport reversible colloid and solute (decay to ^{239}Pu)	3-D transport of americium/plutonium slow irreversible colloid [SZ BTC 6] 3-D transport of americium/plutonium fast irreversible colloid [SZ BTC 10] 3-D transport of americium/thorium/protactinium	Dose from 3-D
^{14}C	Transport solute	Transport solute	3-D transport of nonsorbing solute [SZ BTC 1]	Dose from 3-D
^{36}Cl	Transport solute	Transport solute	3-D transport of nonsorbing solute [SZ BTC 1]	Dose from 3-D
^{245}Cm	Not transported (decay to ^{241}Pu)	Not transported	Not transported	Dose not computed[e]
^{135}Cs	Transport reversible colloid and solute	Transport reversible colloid and solute	3-D transport of cesium colloid [SZ BTC3]	Dose from 3-D
^{137}Cs	Transport reversible colloid and solute	Transport reversible colloid and solute	3-D transport of cesium colloid [SZ BTC 3]	Dose from 3-D
^{129}I	Transport solute	Transport solute	3-D transport of nonsorbing solute [SZ BTC 1]	Dose from 3-D

Table 6.3.7-6. Disposition of Radionuclides for Groundwater Release Modeling Cases: Nominal, Igneous Intrusion, and Seismic (Continued)

Radionuclide (see Table 6.3.7-2)	Disposition in WF, EBS, and UZ TSPA-SEIS Components (see Section 6.3.7)	Disposition in 3-D UZ FEHM Submodel[a] (see Section 6.3.9)	Disposition in SZ Submodels (3-D SZ_Convolute and 1-D Pipe)[b] (see Section 6.3.10)	Disposition in Biosphere (see Section 6.3.11)
^{237}Np	Transport solute (decay to ^{233}U)	Transport solute (decay to ^{233}U)	3-D transport of neptunium solute [SZ BTC 5], boosted[c] by $^{241}Am_{irs}$, $^{241}Am_{irf}$, and $^{241}Am_{rev/sol}$	Dose from 3-D
^{231}Pa	Transport reversible colloid and solute (decay to ^{227}Ac)	Transport reversible colloid and solute (simple decay)	1-D transport reversible colloid and solute (decay to ^{227}Ac) [SZ BTC 2]	Dose from 1-D
^{210}Pb[f]	Not explicitly included	Not explicitly included	Not explicitly included	Dose included with ^{226}Ra BDCF[f]
^{238}Pu	Transport embedded colloid $^{238}Pu_{emb}$ (decay to ^{234}U) Transport irreversible FeO colloid $^{238}Pu_{FeO}$ (decay to ^{234}U) Transport reversible colloid and solute (decay to ^{234}U)	Transport slow irreversible colloid $^{238}Pu_{irs}$ (decay to ^{234}U) Transport fast irreversible colloid $^{238}Pu_{irf}$ (decay to ^{234}U) Transport reversible colloid and solute (decay to ^{234}U)	3-D transport of americium/plutonium slow irreversible colloid [SZ BTC 6] 3-D transport of americium/plutonium fast irreversible colloid [SZ BTC 10] 3-D transport of plutonium reversible colloid [SZ-BTC 4]	Dose from 3-D
^{239}Pu	Transport embedded colloid $^{239}Pu_{emb}$ (decay to ^{235}U) Transport irreversible FeO colloid $^{239}Pu_{FeO}$ (decay to ^{235}U) Transport reversible colloid and solute (decay to ^{235}U)	Transport slow irreversible colloid $^{239}Pu_{irs}$ (decay to ^{235}U) Transport fast irreversible colloid $^{239}Pu_{irf}$ (decay to ^{235}U) Transport reversible colloid and solute (decay to ^{235}U)	3-D transport of americium/plutonium slow irreversible colloid [SZ BTC 6], boosted[c] by $^{243}Am_{irs}$ 3-D transport of americium/plutonium fast irreversible colloid [SZ BTC 10], boosted[c] by $^{243}Am_{irf}$ 3-D transport of plutonium reversible colloid [SZ BTC 4], boosted[c] by $^{243}Am_{rev/sol}$	Dose from 3-D
^{240}Pu	Transport embedded colloid Pu_{emb} (decay to ^{236}U) Transport irreversible FeO colloid $^{240}Pu_{FeO}$ (decay to ^{236}U) Transport reversible colloid and solute (decay to ^{236}U)	Transport slow irreversible colloid $^{240}Pu_{irs}$ (decay to ^{236}U) Transport fast irreversible colloid $^{240}Pu_{irf}$ (decay to ^{236}U) Transport reversible colloid and solute (decay to ^{236}U)	3-D transport of americium/plutonium slow irreversible colloid [SZ BTC 6] 3-D transport of americium/plutonium fast irreversible colloid [SZ BTC 10] 3-D transport of plutonium reversible colloid [SZ BTC 4]	Dose from 3-D
^{241}Pu	Not transported (decay to ^{241}Am)	Not transported	Not transported	Dose not computed[e]

Table 6.3.7-6. Disposition of Radionuclides for Groundwater Release Modeling Cases: Nominal, Igneous Intrusion, and Seismic (Continued)

Radionuclide (see Table 6.3.7-2)	Disposition in WF, EBS, and UZ TSPA-SEIS Components (see Section 6.3.7)	Disposition in 3-D UZ FEHM Submodel[a] (see Section 6.3.9)	Disposition in SZ Submodels (3-D SZ_Convolute and 1-D Pipe)[b] (see Section 6.3.10)	Disposition in Biosphere (see Section 6.3.11)
^{242}Pu	Transport embedded colloid $^{242}Pu_{emb}$ (decay to ^{238}U) Transport irreversible FeO colloid $^{242}Pu_{FeO}$ (decay to ^{238}U) Transport reversible colloid and solute (decay to ^{238}U)	Transport slow irreversible colloid $^{242}Pu_{irs}$ (decay to ^{238}U) Transport fast irreversible colloid $^{242}Pu_{irf}$ (decay to ^{238}U) Transport reversible colloid and solute (decay to ^{238}U)	3-D transport[d] of americium/plutonium slow irreversible colloid [SZ BTC 6] 3-D transport[d] of americium/plutonium fast irreversible colloid [SZ BTC 10] 3-D transport[d] of plutonium reversible colloid [SZ BTC 4]	Dose from 3-D[g]
^{226}Ra	Transport solute (simple decay)	Transport solute (simple decay)	1-D transport of solute (simple decay) [SZ BTC 7]	Dose from 1-D[g]; concentration from 1-D[f]
^{228}Ra	Not transported	Not transported	Not transported	Dose from 1-D[g]; concentration from 1-D, both assuming secular equilibrium with ^{232}Th
^{79}Se	Transport solute	Transport solute	3-D transport of nonsorbing solute [SZ BTC 11]	Dose from 3-D
^{126}Sn	Transport solute	Transport solute	3-D transport of nonsorbing solute [SZ BTC 12]	Dose from 3-D
^{90}Sr	Transport solute	Transport solute	3-D transport of strontium solute [SZ BTC 8]	Dose from 3-D
^{99}Tc	Transport solute	Transport solute	3-D transport of nonsorbing solute [SZ BTC 1]	Dose from 3-D
^{229}Th	Transport reversible colloid and solute (simple decay)	Transport reversible colloid and solute (simple decay)	1-D transport of reversible colloid and solute (simple decay) [SZ BTC 2]	Dose from 1-D
^{230}Th	Transport reversible colloid and solute (decay to ^{226}Ra)	Transport reversible colloid and solute (decay to ^{226}Ra)	1-D transport of reversible colloid and solute (decay to ^{226}Ra) [SZ BTC 2]	Dose from 1-D[g]; concentration from 1-D
^{232}Th	Transport reversible colloid and solute (decay to ^{228}Ra)	Transport reversible colloid and solute (simple decay)	1-D transport of reversible colloid and solute (decay to ^{228}Ra) [SZ BTC 2]	Dose from 1-D[g]; concentration from 1-D
^{232}U	Transport solute	Transport solute	3-D transport of ^{232}U solute [SZ BTC 9]	Dose from 3-D
^{233}U	Transport solute (decay to ^{229}Th)	Transport solute (decay to ^{229}Th)	1-D transport of solute (decay to thorium) [SZ BTC 9]	Dose from 1-D

Table 6.3.7-6. Disposition of Radionuclides for Groundwater Release Modeling Cases: Nominal, Igneous Intrusion, and Seismic (Continued)

Radionuclide (see Table 6.3.7-2)	Disposition in WF, EBS, and UZ TSPA-SEIS Components (see Section 6.3.7)	Disposition in 3-D UZ FEHM Submodel[a] (see Section 6.3.9)	Disposition in SZ Submodels (3-D SZ_Convolute and 1-D Pipe)[b] (see Section 6.3.10)	Disposition in Biosphere (see Section 6.3.11)
^{234}U	Transport solute (decay to ^{230}Th)	Transport solute (decay to ^{230}Th)	3-D transport of ^{234}U solute [SZ BTC 9], boosted[c] by ^{238}U, $^{238}Pu_{irs}$, $^{238}Pu_{irf}$, and $^{238}Pu_{rev/sol}$	Dose from 3-D
^{235}U	Transport solute (decay to ^{231}Pa)	Transport solute (decay to ^{231}Pa)	1-D transport of solute (decay to ^{231}Pa) [SZ BTC 9]	Dose from 1-D[g]
^{236}U	Transport solute (decay to ^{232}Th)	Transport solute (decay to ^{232}Th)	3-D transport[d] of ^{236}U solute [SZ BTC 9], boosted[c] by $^{240}Pu_{irs}$, $^{240}Pu_{irf}$, and $^{240}Pu_{rev/sol}$	Dose from 3-D
^{238}U	Transport solute (decay to ^{234}U)	Transport solute (decay to ^{234}U)	3-D transport of ^{238}U solute [SZ BTC 9], boosted[c] by $^{242}Pu_{irs}$, $^{242}Pu_{irf}$, and $^{242}Pu_{rev/sol}$	Dose from 3-D

NOTE: [a] Plutonium and americium isotopes are transported irreversibly on two different colloid types (minerals) in the EBS: FeO_x colloids (e.g., see $^{239}Pu_{FeO}$ in the above table) and waste form colloids (e.g., see $^{239}Pu_{emb}$ in the above table). However, at the EBS-UZ interface, the plutonium or americium mass associated with these two types of colloids is combined (effectively losing or ignoring the mineral specificity) and then resplit into slow-Transport and fast-Transport irreversible colloids in the natural system (e.g., see $^{239}Pu_{irs}$ and $^{239}Pu_{irf}$ in the above table). Thus, the specific radionuclides in GoldSim designated "Ic" and "If" are used differently in the EBS versus the natural system—in the EBS "Ic" stands for plutonium and americium mass transported in "embedded" colloids (i.e., the plutonium and americium mass is embedded in the mineral matrix of these colloid particles), and "If" stands for plutonium and americium mass sorbed irreversibly onto FeOx colloids, whereas in the UZ (see Section 6.3.9) and SZ (see Section 6.3.10), "Ic" stands for plutonium and americium mass transported irreversibly on slow colloids, and "If" stands for plutonium or americium mass transported irreversibly on fast colloids.

[b] Saturated Zone Breakthrough Curve and the associated number refers to the "Radionuclide Group Number" listed in the first column of Table 6.3.10-3 (see Section 6.3.10).

[c] Boosting of a daughter (e.g., ^{239}Pu) means that the injected mass of the daughter over any timestep at the UZ-SZ interface is increased by the maximum decay (over the remaining simulation time) of the designated parent (e.g., ^{243}Am).

[d] This nuclide could have been deleted from the 3-D SZ model (see Section 6.3.10), because only the 1-D SZ transport results are used for the ingrowth of its daughter.

[e] ^{245}Cm and ^{241}Pu were recommended for inclusion in *Radionuclide Screening* (SNL 2007 [DIRS 177424], Section 6.6.2 and Table 7-1) only to ensure that the effect of their decay on the inventories of ^{241}Am and ^{237}Np are included in the model. They are not recommended for transport or dose consequences.

[f] Though ^{210}Pb is not tracked, it is assumed to be in secular equilibrium with ^{226}Ra; that is, the BDCF used for ^{226}Ra is the summation of the BDCFs provided for ^{226}Ra and ^{210}Pb.

[g] Doses only calculated for million-year simulations (SNL 2007 [DIRS 177424], Table 7-1).

WF = waste form; SZ BTC = Saturated Zone Breakthrough Curve.

Table 6.3.7-7. Uncertainty Multipliers for Grams per Waste Package of Radionuclides for Each Waste Type

TSPA Parameter Name	CSNF	DSNF	HLW
	CSNF_Mass_Uncert_a	DSNF_Mass_Uncert_a	HLW_Mass_Uncert_a
Isotopes	All except ^{238}U	All except ^{238}U	All
Distribution	Uniform	Triangular	Triangular
Minimum	0.85	0.45	0.70
Most Likely	N/A	0.62	1
Maximum	1.4	2.9	1.5

Sources: DTN: SN0310T0505503.004_R0 [DIRS 168761]
Initial Radionuclide Inventories (SNL 2007 [DIRS 180472], Table 7-2).

Table 6.3.7-8. Summary of In-Package Chemistry Abstraction (Vapor or Liquid Influx)

	RH			
	<95%		≥95%	
Q (L/yr)	< 0.1	≥0.1	< 0.1	≥0.1
I (V) < I(L)	In-Package Chemistry Submodel Off	I(L) pH(L)	I (V) pH(V)	I (V), pH(L)
I (V) ≥ I(L)				I (L), pH(L)

Source: Modified from *In-Package Chemistry Abstraction* (SNL 2007 [DIRS 180506]) Table 6-23[a].

NOTE: Q is the water inflow rate; I(V) and I(L) are ionic strength given by the vapor influx abstraction and that given by the liquid influx abstraction, respectively; pH(V) and pH(L) are pH given by the vapor influx abstraction and that given by the liquid influx abstraction, respectively.

Table 6.3.7-9. In-Package Ionic Strength Abstraction for Vapor Influx Case

Cell	RH Range	A	B	Lower Uncertainty Factor (fmin)	Upper Uncertainty Factor (fmax)
CSNF Cell 1	95%–98.3%	45.846	-45.525	0.5	1.5
	98.3%–99.9%	64.0629	-64.0602		
	99.9%–100%	66.4312	-66.4308		
CDSP Cell 1A	95%–97.2%	42.992	-42.654	0.5	1.5
	97.2%–100%	54.7803	-54.7776		
CDSP Cell 1B	95%–98.33%	42.992	-42.654	0.5	1.5
	98.33%–100%	62.4136	-62.4112		

Source: DTN: SN0702PAIPC1CA.001_R2 [DIRS 180451], *Abstr CSNF No Drip Ion Str.xls*, *Abstr 2DHLW No Drip Ion Str.xls*, and *Abstr 2MCO No Drip Ion Str.xls*.

Table 6.3.7-10. In-Package Ionic Strength Abstraction for CSNF Cell 1 of Liquid Influx Case (log I (molal))

Log Time Since WP Breach (year)	Log Liquid Influx Rate (L/yr)					
	3	2	1	0	-0.3	-1
-1.75	-2.451	-2.433	-2.452	-2.454	-2.454	-2.455
-1.25	-2.501	-2.494	-2.501	-2.502	-2.502	-2.502
-0.75	-2.503	-2.506	-2.503	-2.502	-2.502	-2.502
-0.25	-2.466	-2.477	-2.456	-2.453	-2.453	-2.453
0.25	-2.390	-2.365	-2.320	-2.339	-2.311	-2.247
0.75	-2.317	-2.107	-2.004	-2.032	-1.982	-1.866
1.25	-2.306	-1.803	-1.608	-1.586	-1.585	-1.582
1.75	-2.305	-1.586	-1.178	-1.163	-1.160	-1.154
2.25	-2.305	-1.530	-0.786	-0.686	-0.677	-0.657
2.75	-2.305	-1.945	-1.106	-0.371	-0.320	-0.202
3.25	-2.305	-2.091	-1.634	-0.411	-0.178	0.366
3.75	-2.305	-2.091	-1.929	-0.987	-0.426	0.881
4.25	-2.305	-2.091	-2.095	-2.072	-1.540	-0.299
4.75	-2.305	-2.091	-2.095	-2.134	-2.131	-2.124
5.25	-2.305	-2.091	-2.095	-2.134	-2.134	-2.134
5.75	-2.305	-2.091	-2.095	-2.134	-2.134	-2.134
6.00	-2.305	-2.091	-2.095	-2.134	-2.134	-2.134

Source: DTN: SN0702PAIPC1CA.001_R2 [DIRS 180451], *Abstr CSNF Seepage Ion Str 2.xls.*

Table 6.3.7-11. In-Package Ionic Strength Abstraction for CDSP Cell 1A of Liquid Influx Case (log I (molal))

Log Time Since WP Breach (year)	Log Liquid Influx Rate (L/yr)				
	3	2	1	0	-1
-1.75	-2.391	-2.391	-2.391	-2.391	-2.391
-1.25	-2.391	-2.391	-2.391	-2.391	-2.391
-0.75	-2.391	-2.391	-2.391	-2.390	-2.390
-0.25	-2.391	-2.389	-2.389	-2.388	-2.388
0.25	-2.391	-2.386	-2.384	-2.380	-2.381
0.75	-2.391	-2.384	-2.369	-2.358	-2.360
1.25	-2.391	-2.384	-2.342	-2.296	-2.298
1.75	-2.391	-2.384	-2.319	-2.179	-2.162
2.25	-2.391	-2.384	-2.315	-2.021	-1.878
2.75	-2.391	-2.384	-2.315	-1.928	-1.551
3.25	-2.391	-2.384	-2.315	-1.917	-1.239
3.75	-2.391	-2.384	-2.315	-1.917	-1.088
4.25	-2.391	-2.384	-2.315	-1.917	-1.070
4.75	-2.391	-2.384	-2.315	-1.917	-1.070
5.25	-2.391	-2.384	-2.315	-1.917	-1.070
5.75	-2.391	-2.384	-2.315	-1.917	-1.070
6.00	-2.391	-2.384	-2.315	-1.917	-1.070

Source: DTN: SN0702PAIPC1CA.001_R2 [DIRS 180451], *Abstr 2DHLW Seepage Ion Str 2.xls*.

Table 6.3.7-12. In-Package Ionic Strength Abstraction for CDSP Cell 1B of Liquid Influx Case (log I (molal))

Log Time Since WP Breach (year)	Log Liquid Influx Rate (L/yr)					
	3	2	1	0	-0.5	-1
-1.75	-2.511	-2.512	-2.514	-2.514	-2.493	-2.472
-1.25	-2.505	-2.509	-2.515	-2.515	-2.515	-2.515
-0.75	-2.489	-2.495	-2.514	-2.516	-2.516	-2.517
-0.25	-2.462	-2.448	-2.508	-2.514	-2.514	-2.515
0.25	-2.448	-2.315	-2.493	-2.512	-2.513	-2.515
0.75	-2.447	-2.087	-2.446	-2.506	-2.510	-2.515
1.25	-2.491	-1.912	-2.309	-2.486	-2.501	-2.515
1.75	-2.514	-2.477	-2.019	-2.444	-2.491	-2.538
2.25	-2.514	-2.512	-1.702	-2.208	-2.286	-2.364
2.75	-2.514	-2.513	-2.467	-1.374	-1.688	-2.003
3.25	-2.514	-2.513	-2.505	-1.242	-1.088	-0.935
3.75	-2.514	-2.513	-2.505	-2.144	-0.690	0.763
4.25	-2.514	-2.513	-2.505	-2.157	-1.663	-1.169
4.75	-2.514	-2.513	-2.505	-2.157	-1.675	-1.194
5.25	-2.514	-2.513	-2.505	-2.157	-1.675	-1.192
5.75	-2.514	-2.513	-2.505	-2.157	-1.675	-1.192
6.00	-2.514	-2.513	-2.505	-2.157	-1.675	-1.675

Source: DTN: SN0702PAIPC1CA.001_R2 [DIRS 180451], *Abstr 2MCO Seepage Ion Str 2.xls.*

Table 6.3.7-13. In-Package Ionic Strength Deviation for CSNF Cell 1 of Liquid Influx Case (log I (molal))

Log Time Since WP Breach (year)	Log Liquid Influx Rate (L/yr)					
	3	2	1	0	-0.3	-1
-1.75	1.00	1.00	1.00	1.00	1.00	1.00
-1.25	1.00	1.00	1.00	1.00	1.00	1.00
-0.75	1.00	1.00	1.00	1.00	1.00	1.00
-0.25	1.00	1.00	1.00	1.00	1.00	1.00
0.25	1.00	1.00	1.00	1.00	1.00	1.05
0.75	1.00	1.00	1.00	1.00	1.00	1.08
1.25	1.00	1.00	1.00	1.00	1.00	1.00
1.75	1.00	1.00	1.00	1.00	1.00	1.00
2.25	1.00	1.00	1.00	1.00	1.00	1.01
2.75	1.00	1.00	1.00	1.00	1.00	1.08
3.25	1.00	1.00	1.00	1.00	1.00	1.39
3.75	1.00	1.00	1.00	1.00	1.00	1.93
4.25	1.00	1.00	1.00	1.00	1.00	1.89
4.75	1.00	1.00	1.00	1.00	1.00	1.01
5.25	1.00	1.00	1.00	1.00	1.00	1.00
5.75	1.00	1.00	1.00	1.00	1.00	1.00
6.00	1.00	1.00	1.00	1.00	1.00	1.00

Source: DTN: SN0702PAIPC1CA.001_R2 [DIRS 180451], *Abstr CSNF Seepage Ion Str 2.xls.*

Table 6.3.7-14. In-Package Ionic Strength Deviation for CDSP Cell 1A of Liquid Influx Case (log I (molal))

Log Time Since WP Breach (year)	Log Liquid Influx Rate (L/yr)				
	3	2	1	0	-1
-1.75	1.0	1.0	1.0	1.0	1.0
-1.25	1.0	1.0	1.0	1.0	1.0
-0.75	1.0	1.0	1.0	1.0	1.0
-0.25	1.0	1.0	1.0	1.0	1.0
0.25	1.0	1.0	1.0	1.0	1.0
0.75	1.0	1.0	1.0	1.0	1.0
1.25	1.0	1.0	1.0	1.0	1.0
1.75	1.0	1.0	1.0	1.0	1.0
2.25	1.0	1.0	1.0	1.0	1.0
2.75	1.0	1.0	1.0	1.0	1.0
3.25	1.0	1.0	1.0	1.0	1.0
3.75	1.0	1.0	1.0	1.0	1.0
4.25	1.0	1.0	1.0	1.0	1.0
4.75	1.0	1.0	1.0	1.0	1.0
5.25	1.0	1.0	1.0	1.0	1.0
5.75	1.0	1.0	1.0	1.0	1.0
6.00	1.0	1.0	1.0	1.0	1.0

Source: DTN: SN0702PAIPC1CA.001_R2 [DIRS 180451], *Abstr 2DHLW Seepage Ion Str 2.xls.*

Table 6.3.7-15. In-Package Ionic Strength Deviation for CDSP Cell 1B of Liquid Influx Case (log I (molal))

Log Time Since WP Breach (year)	Log Liquid Influx Rate (L/yr)					
	3	2	1	0	-0.5	-1
-1.75	1.00	1.00	1.00	1.00	1.00	1.02
-1.25	1.00	1.00	1.00	1.00	1.00	1.00
-0.75	1.00	1.00	1.00	1.00	1.00	1.00
-0.25	1.00	1.00	1.00	1.00	1.00	1.00
0.25	1.00	1.00	1.00	1.00	1.00	1.00
0.75	1.00	1.00	1.00	1.00	1.00	1.00
1.25	1.00	1.00	1.00	1.00	1.00	1.01
1.75	1.00	1.00	1.00	1.00	1.00	1.05
2.25	1.00	1.00	1.00	1.00	1.00	1.08
2.75	1.00	1.00	1.00	1.00	1.00	1.31
3.25	1.00	1.00	1.00	1.00	1.00	1.15
3.75	1.00	1.00	1.00	1.00	1.00	2.45
4.25	1.00	1.00	1.00	1.00	1.00	1.49
4.75	1.00	1.00	1.00	1.00	1.00	1.48
5.25	1.00	1.00	1.00	1.00	1.00	1.48
5.75	1.00	1.00	1.00	1.00	1.00	1.48
6.00	1.00	1.00	1.00	1.00	1.00	1.24

Source: DTN: SN0702PAIPC1CA.001_R2 [DIRS 180451], *Abstr 2MCO Seepage Ion Str 2.xls.*

Table 6.3.7-16. Maximum pH for CSNF Cell 1 of Liquid Influx

pCO2 (bar)	Log Ionic Strength (molal)						
	-1.411	-0.162	-0.135	-0.059	0	0.5	1
4	9.07	8.90	8.90	8.90	8.90	8.90	8.90
3	8.32	8.14	8.13	8.13	8.13	8.13	8.13
2	7.55	7.22	7.21	7.19	7.19	7.19	7.19
1.5	7.17	6.82	6.81	6.79	6.79	6.79	6.79

Source: DTN: SN0702PAIPC1CA.001_R2 [DIRS 180451], *Abstr CSNF Seepage pH.xls.*

Table 6.3.7-17. Maximum pH for CDSP Cell 1A of Liquid Influx

pCO2 (bar)	Log Ionic Strength (molal)									
	-2.283	-1.516	-1.486	-1.418	-0.474	-0.406	-0.369	0	0.5	1
4	9.37	9.81	9.83	9.87	10.23	10.25	10.27	10.41	10.60	10.79
3	8.46	9.09	9.13	9.17	9.67	9.71	9.73	9.92	10.19	10.45
2	7.48	8.21	8.23	8.29	9.02	9.07	9.10	9.38	9.77	10.16
1.5	7.02	7.84	7.87	7.92	8.73	8.79	8.82	9.14	9.56	9.99

Source: DTN: SN0702PAIPC1CA.001_R2 [DIRS 180451], *Abstr 2DHLW Seepage pH.xls.*

Table 6.3.7-18. Maximum pH for CDSP Cell 1B of Liquid Influx

pCO2 (bar)	Log Ionic Strength (molal)									
	-2.409	-1.192	-1.166	-1.150	-0.128	-0.106	-0.014	0	0.5	1
4	8.99	9.06	9.06	9.06	8.89	8.89	8.89	8.89	8.89	8.89
3	8.15	8.30	8.31	8.31	8.12	8.11	8.11	8.11	8.11	8.11
2	7.21	7.55	7.54	7.53	7.21	7.20	7.17	7.17	7.17	7.17
1.5	6.78	7.17	7.16	7.15	6.81	6.80	6.77	6.77	6.77	6.77

Source: DTN: SN0702PAIPC1CA.001_R2 [DIRS 180451], *Abstr 2MCO Seepage pH.xls.*

Table 6.3.7-19. Minimum pH for CSNF Cell 1 of Liquid Influx

pCO2 (bar)	Log Ionic Strength (molal)				
	-1.531	-0.349	0	0.5	1
4	5.51	5.11	4.99	4.82	4.65
3	5.51	5.11	4.99	4.82	4.65
2	5.51	5.11	4.99	4.82	4.65
1.5	5.51	5.11	4.99	4.82	4.65

Source: DTN: SN0702PAIPC1CA.001_R2 [DIRS 180451], *Abstr CSNF Seepage pH.xls.*

Table 6.3.7-20. Minimum pH for CDSP Cell 1A of Liquid Influx

pCO2 (bar)	Log Ionic Strength (molal)					
	-2.259	-1.416	-0.422	0	0.5	1
4	5.88	5.54	5.20	5.04	4.87	4.68
3	5.87	5.54	5.20	5.04	4.87	4.69
2	5.87	5.54	5.20	5.04	4.87	4.69
1.5	5.87	5.54	5.20	5.04	4.87	4.69

Source: DTN: SN0702PAIPC1CA.001_R2 [DIRS 180451], *Abstr 2DHLW Seepage pH.xls.*

Table 6.3.7-21. Minimum pH for CDSP Cell 1B of Liquid Influx

pCO2 (bar)	Log Ionic Strength (molal)					
	-2.448	-1.399	-0.396	0	0.5	1
4	6.02	5.59	5.23	5.07	4.89	4.69
3	6.01	5.59	5.23	5.07	4.89	4.70
2	5.97	5.59	5.23	5.08	4.90	4.72
1.5	5.96	5.59	5.23	5.09	4.91	4.73

Source: DTN: SN0702PAIPC1CA.001_R2 [DIRS 180451], *Abstr 2MCO Seepage pH.xls.*

Table 6.3.7-22. Maximum pH for CSNF Cell 1 of Vapor Influx

pCO2 (bar)	Log Ionic Strength (molal)						
	-1.198	-0.164	-0.138	-0.066	0	0.5	1
4	9.06	8.90	8.90	8.90	8.90	8.90	8.90
3	8.31	8.12	8.12	8.12	8.12	8.12	8.12
2	7.54	7.22	7.21	7.19	7.19	7.19	7.19
1.5	7.17	6.82	6.81	6.79	6.79	6.79	6.79

Source: DTN: SN0702PAIPC1CA.001_R2 [DIRS 180451], *Abstr CSNF No Drip pH.xls.*

Table 6.3.7-23. Maximum pH for CDSP Cell 1A of Vapor Influx

pCO2 (bar)	Log Ionic Strength (molal)									
	-2.287	-1.517	-1.486	-1.419	-0.474	-0.406	-0.369	0	0.5	1.5
4	9.37	9.81	9.83	9.87	10.23	10.26	10.27	10.41	10.60	10.98
3	8.46	9.09	9.13	9.17	9.67	9.71	9.73	9.92	10.19	10.72
2	7.47	8.21	8.23	8.29	9.02	9.07	9.10	9.38	9.77	10.54
1.5	7.02	7.84	7.87	7.92	8.73	8.79	8.82	9.14	9.56	10.42

Source: DTN: SN0702PAIPC1CA.001_R2 [DIRS 180451], *Abstr 2DHLW No Drip pH.xls.*

Table 6.3.7-24. Maximum pH for CDSP Cell 1B of Vapor Influx

pCO2 (bar)	Log Ionic Strength (molal)									
	-2.127	-1.193	-1.166	-1.150	-0.129	-0.107	-0.015	0	0.5	1
4	9.04	9.06	9.06	9.06	8.89	8.89	8.89	8.89	8.89	8.89
3	8.25	8.31	8.31	8.31	8.12	8.11	8.11	8.11	8.11	8.11
2	7.38	7.55	7.54	7.53	7.21	7.20	7.17	7.17	7.17	7.17
1.5	6.94	7.17	7.15	7.15	6.75	6.74	6.70	6.70	6.70	6.70

Source: DTN: SN0702PAIPC1CA.001_R2 [DIRS 180451], *Abstr 2MCO No Drip pH.xls.*

Table 6.3.7-25. Minimum pH for CSNF Cell 1 of Vapor Influx

pCO2 (bar)	Log Ionic Strength (molal)				
	-1.344	-0.350	0	0.5	1
4	5.44	5.11	4.99	4.82	4.65
3	5.44	5.11	4.99	4.82	4.65
2	5.44	5.11	4.99	4.82	4.65
1.5	5.44	5.11	4.99	4.82	4.65

Source: DTN: SN0702PAIPC1CA.001_R2 [DIRS 180451], *Abstr CSNF No Drip pH.xls.*

Table 6.3.7-26. Minimum pH for CDSP Cell 1A of Vapor Influx

pCO2 (bar)	Log Ionic Strength (molal					
	-2.318	-1.372	-0.365	0	0.5	1.5
4	5.84	5.46	5.12	4.98	4.81	4.45
3	5.84	5.46	5.12	4.98	4.81	4.45
2	5.83	5.46	5.12	4.98	4.81	4.45
1.5	5.83	5.46	5.12	4.98	4.81	4.45

Source: DTN: SN0702PAIPC1CA.001_R2 [DIRS 180451], *Abstr 2DHLW No Drip pH.xls.*

Table 6.3.7-27. Minimum pH for CDSP Cell 1B of Vapor Influx

pCO2 (bar)	Log Ionic Strength (molal)					
	-2.456	-1.351	-0.352	0	0.5	1
4	5.91	5.46	5.13	4.98	4.82	4.63
3	5.91	5.46	5.13	4.98	4.82	4.63
2	5.90	5.46	5.13	4.98	4.82	4.63
1.5	5.90	5.46	5.13	4.99	4.82	4.63

Source: DTN: SN0702PAIPC1CA.001_R2 [DIRS 180451], *Abstr 2MCO No Drip pH.xls.*

Table 6.3.7-28. Log K Temperature Interpolation Functions for Use in the Total Carbonate Concentration Abstraction

Log K Function of Temperature (°C)
$\mathrm{Log}(K_1) = 7.0 \times 10^{-5} T^2 - 0.0159T - 1.1023$
$\mathrm{Log}(K_2) = 5.0 \times 10^{-7} T^3 - 0.0002T^2 + 0.0132T - 6.5804$
$\mathrm{Log}(K_3) = -8.0 \times 10^{-5} T^2 + 0.0128T - 10.618$

Source: DTN: SN0702PAIPC1CA.001_R2 [DIRS 180451], worksheet *Total Carbonate Validation" in Total Carbonate and Eh Abstractions.xls* .

Table 6.3.7-29. Initial Release Fraction Percentage Distributions

Parameter Name	Model Abstraction Symbol	Description	Units	Distribution Type	Distribution Specification
Initial_Release_Frac_Cs_a	NA	Cesium release fraction %	None	Triangular	Min = 0.39 Max = 11.06 Most likely = 3.63
Initial_Release_Frac_I_a	NA	Iodine release fraction %	None	Triangular	Min = 2.04 Max = 26.75 Most likely = 11.24
Initial_Release_Frac_Tc_a	NA	Technetium release fraction %	None	Triangular	Min = 0.01 Max = 0.26 Most likely = 0.10
Initial_Release_Frac_Sr_a	NA	Strontium release fraction %	None	Triangular	Min = 0.02 Max = 0.25 Most likely = 0.09

Source: DTN: MO0404ANLSF001.001_R0 [DIRS 169007].

Table 6.3.7-30. Linear Regression Model Alkaline Case (pH ≥ 6.8)

Parameter Name	Model Abstraction Symbol	Description	Units	Distribution Type	Distribution Specification
Log_Specific_SA_CSNF_a	$Log_{10}(A)$	Log of fuel specific surface area	None	Triangular	Min = –7.3 Max = –5.4 Most likely = –6.7
DR_CSNF_Alk_a0_mean	a_0	Constant coefficient in dissolution rate model	None	Regression analysis	μ = 4.705 Standard error: 0.601
DR_CSNF_Alk_a1_mean	a_1	Coefficient of inverse temperature in dissolution rate model	None	Regression analysis	μ = –1093.826 Standard error: 186.829
DR_CSNF_Alk_a2_mean	a_2	Coefficient of $log_{10}TCC$ in dissolution rate model	None	Regression analysis	μ = –0.102 Standard error: 0.0471
DR_CSNF_Alk_a3_mean	a_3	Coefficient of pO_2 in dissolution rate model	None	Regression analysis	μ = –0.338 Standard error: 0.0506

Source: DTN: MO0404ANLSF001.001_R0 [DIRS 169007].

NOTE: Parameter a_4 = 0 under alkaline conditions.

Table 6.3.7-31. Linear Regression Model for Acid Case (pH < 6.8)

Parameter Name	Model Abstraction Symbol	Description	Units	Distribution Type	Distribution Specification
Log_Specific_SA_CSNF_a	$Log_{10}(A)$	Log of fuel specific surface area	None	Triangular	Min = –7.3 Max = –5.4 Most likely = –6.7
DR_CSNF_Acid_a0_mean	a_0	Constant coefficient in dissolution rate model	None	Regression analysis	μ = 6.60 Standard error: 0.446
DR_CSNF_Acid_a1_mean	a_1	Coefficient of inverse temperature in dissolution rate model	None	None	μ = –1093.826 Standard error: 186.829
DR_CSNF_Acid_a3_mean	a_3	Coefficient of pO_2 in dissolution rate model	None	None	μ = –0.338 Standard error: 0.0506
DR_CSNF_Acid_a4_mean	a_4	Coefficient of pH in dissolution rate model	None	Regression analysis	μ = –0.340 Standard error: 0.110

Source: DTN: MO0404ANLSF001.001_R0 [DIRS 169007].

NOTE: Parameter a_2 = 0 under acidic conditions.

Table 6.3.7-32. Dissolution Rate Parameters for High-Level Radioactive Waste Glass

Parameter Name	Model Abstraction Symbol	Description	Units	Distribution Type/Uncertainty Type	Distribution Specification
Specific_Surface_Area_Glass	S_{sp}	Specific surface area for glass	m^2/kg	Single Value	2.70×10^{-3}
Rind_Porosity_CDSP	ϕ	Porosity of rind (alteration layer)	%	Single Value	17
HLW_Diss_Eta_Acidic	η_{acidic}	Dimensionless pH dependence coefficient acidic condition	None	Single Value	–0.49
HLW_Diss_Ea_Acidic	E_{a_acidic}	Effective activation energy acidic condition	kJ/mol	Single Value	31
HLW_Diss_kE_Acidic_a	k_{E_acid}	Affinity term in HLW dissolution rate acid condition	$g/m^2/d$	Triangular/ Epistemic	Min = 8.41×10^3 Max = 1.15×10^7 Most likely = 8.41×10^3
HLW_Diss_Eta_Alkaline	$\eta_{alkaline}$	Dimensionless pH dependence coefficient alkaline condition	None	Single Value	0.49
HLW_Diss_Ea_Alkaline	$E_{a\_alkaline}$	Effective activation energy alkaline condition	kJ/mol	Single Value	69
HLW_Diss_kE_Alkaline_a	$k_{E\_alkaline}$	Affinity term in HLW dissolution rate alkaline condition	$g/m^2/d$	Triangular/ Epistemic	Min = 2.82×10^1 Max = 3.47×10^4 Most likely = 2.82×10^1
Exposure_Factor_a	$f_{exposure}$	Glass exposure factor	None	Triangular/ Epistemic[a]	Min = 4 Max = 17 Most likely = 4
Glass_Log_Length_CDSP		Weighted average length of HLW glass	m	Single Value	3.9

Source: DTN: MO0502ANLGAMR1.016_R0 [DIRS 172830].

[a] The DTN lists this parameter as an aleatory uncertain parameter, but it is treated as an epistemic uncertain parameter in the TSPA-SEIS.

Table 6.3.7-33. Solubility-Controlling Solid Phases Used in the Dissolved Concentration Limits Model Abstraction

Radionuclide	Solubility-Controlling Solid	Comments
Americium	$AmOHCO_3$	None.
Carbon	NA	No solubility-controlling solid is expected to form under repository conditions.
Cesium	NA	No solubility-controlling solid is expected to form under repository conditions.
Chlorine	NA	No solubility-controlling solid is expected to form under repository conditions.
Iodine	NA	No solubility-controlling solid is expected to form under repository conditions.
Neptunium	NpO_2 Np_2O_5 $NaNpO_2CO_3$	NpO_2 used within WPs while reductants remain. Np_2O_5 used within WPs after reductants are consumed and for Invert. $NaNpO_2CO_3$ used for high pH values.
Protactinium	No thermodynamic data available for Pa phases	Used calculated Np_2O_5 solubility values as analogue for Pa.
Plutonium	PuO_2 (hydrous, aged)	None.
Radium	$RaSO_4$	None.
Selenium	NA	No solubility-controlling solid is expected to form under repository conditions.
Strontium	NA	No solubility-controlling solid is expected to form under repository conditions.
Technetium	NA	No solubility-controlling solid is expected to form under repository conditions.
Thorium	ThO_2 (amorphous)	None.
Tin	SnO2(amorphous)	None
Uranium	Schoepite	Schoepite used for CSNF WPs in the Nominal and Seismic Scenario Classes.
Uranium	Schoepite Na-Boltwoodite $Na_4UO_2(CO_3)_3$	Schoepite used for lower pH values. Na-Boltwoodite used for higher pH values. $Na_4UO_2(CO_3)_3$ used only at high pH and log fco_2 values. This set of solubility-controlling solids is used for CSNF WPs in the Igneous Scenario Class, CDSP WPs in all scenarios and in all invert locations.

Source: *Dissolved Concentration Limits of Elements with Radioactive Isotopes* (SNL 2007 [DIRS 177418]).

Table 6.3.7-34. Base Americium Solubility Look-Up Table (log[Am], mg/L)

	log fco_2 (bars)							
pH	**-1.50**	**-2.00**	**-2.50**	**-3.00**	**-3.50**	**-4.00**	**-4.50**	**-5.00**
5.50	2.40E+00	3.27E+00	500	500	500	500	500	500
5.75	1.53E+00	2.10E+00	2.80E+00	500	500	500	500	500
6.00	7.99E-01	1.30E+00	1.83E+00	2.43E+00	3.30E+00	500	500	500
6.25	1.60E-01	5.93E-01	1.07E+00	1.58E+00	2.14E+00	2.84E+00	500	500
6.50	–3.33E-01	–2.76E-02	3.88E-01	8.60E-01	1.36E+00	1.89E+00	2.50E+00	3.37E+00
6.75	–6.62E-01	–5.20E-01	–2.16E-01	1.98E-01	6.69E-01	1.16E+00	1.68E+00	2.25E+00
7.00	–9.13E-01	–8.85E-01	–7.05E-01	–3.84E-01	3.99E-02	5.14E-01	1.01E+00	1.52E+00
7.25	–1.11E+00	–1.16E+00	–1.08E+00	–8.65E-01	–5.11E-01	–6.96E-02	4.11E-01	9.07E-01
7.50	–1.20E+00	–1.36E+00	–1.38E+00	–1.25E+00	–9.73E-01	–5.76E-01	–1.14E-01	3.74E-01
7.75	–1.12E+00	–1.46E+00	–1.60E+00	–1.56E+00	–1.35E+00	–1.01E+00	–5.65E-01	–8.59E-02
8.00	–7.46E-01	–1.39E+00	–1.71E+00	–1.80E+00	–1.67E+00	–1.37E+00	–9.51E-01	–4.80E-01
8.25	–3.64E-02	–1.07E+00	–1.66E+00	–1.93E+00	–1.93E+00	–1.68E+00	–1.29E+00	–8.22E-01
8.50	8.95E-01	–4.41E-01	–1.38E+00	–1.90E+00	–2.10E+00	–1.95E+00	–1.58E+00	–1.13E+00
8.75	1.93E+00	4.47E-01	–8.11E-01	–1.66E+00	–2.12E+00	–2.16E+00	–1.86E+00	–1.41E+00
9.00	500	1.48E+00	3.02E-02	–1.15E+00	–1.92E+00	–2.26E+00	–2.09E+00	–1.68E+00
9.25	500	2.63E+00	1.06E+00	–3.53E-01	–1.46E+00	–2.14E+00	–2.27E+00	–1.93E+00
9.50	500	500	2.24E+00	6.65E-01	–7.01E-01	–1.74E+00	–2.28E+00	–2.15E+00
9.75	500	500	500	1.88E+00	3.08E-01	–1.02E+00	–1.98E+00	–2.28E+00
10.00	500	500	500	500	1.56E+00	–1.70E-02	–1.31E+00	–2.15E+00
10.25	500	500	500	500	500	1.25E+00	–3.16E-01	–1.57E+00
10.50	500	500	500	500	500	500	9.70E-01	–5.94E-01
10.75	500	500	500	500	500	500	500	7.01E-01

Source: DTN: MO0702PADISCON.001_R0 [DIRS 179358], Table 8.

NOTE: This look-up table is implemented in the TSPA-SEIS as parameter Sol_Am_LUT. Entries reported as "500" in the table indicate conditions for which a valid solubility value does not exist.

Table 6.3.7-35. Base Neptunium (Np_2O_5) Solubility Look-Up Table (log[Np], mg/L)

	log fco_2 (bars)							
pH	**-1.5**	**-2.0**	**-2.5**	**-3.0**	**-3.5**	**-4.0**	**-4.5**	**-5.0**
3.00	4.38E+00	4.38E+00	4.38E+00	4.38E+00	4.38E+00	4.38E+00	4.38E+00	4.38E+00
3.25	4.10E+00	4.10E+00	4.10E+00	4.10E+00	4.10E+00	4.10E+00	4.10E+00	4.10E+00
3.50	3.82E+00	3.82E+00	3.82E+00	3.82E+00	3.82E+00	3.82E+00	3.82E+00	3.82E+00
3.75	3.55E+00	3.55E+00	3.55E+00	3.55E+00	3.55E+00	3.55E+00	3.55E+00	3.55E+00
4.00	3.29E+00	3.29E+00	3.29E+00	3.29E+00	3.29E+00	3.29E+00	3.29E+00	3.29E+00
4.25	3.03E+00	3.03E+00	3.03E+00	3.03E+00	3.03E+00	3.03E+00	3.03E+00	3.03E+00
4.50	2.77E+00	2.77E+00	2.77E+00	2.77E+00	2.77E+00	2.77E+00	2.77E+00	2.77E+00
4.75	2.52E+00	2.52E+00	2.52E+00	2.52E+00	2.52E+00	2.52E+00	2.52E+00	2.52E+00
5.00	2.26E+00	2.26E+00	2.26E+00	2.26E+00	2.26E+00	2.26E+00	2.26E+00	2.26E+00
5.25	2.01E+00	2.01E+00	2.01E+00	2.01E+00	2.01E+00	2.01E+00	2.01E+00	2.01E+00
5.50	1.76E+00	1.76E+00	1.76E+00	1.76E+00	1.76E+00	1.76E+00	1.76E+00	1.76E+00
5.75	1.51E+00	1.51E+00	1.51E+00	1.51E+00	1.51E+00	1.51E+00	1.51E+00	1.51E+00
6.00	1.26E+00	1.26E+00	1.26E+00	1.26E+00	1.26E+00	1.26E+00	1.26E+00	1.26E+00
6.25	1.01E+00	1.01E+00	1.01E+00	1.01E+00	1.01E+00	1.01E+00	1.01E+00	1.01E+00
6.50	7.66E-01	7.62E-01	7.61E-01	7.60E-01	7.60E-01	7.60E-01	7.60E-01	7.60E-01
6.75	5.35E-01	5.17E-01	5.12E-01	5.11E-01	5.10E-01	5.10E-01	5.10E-01	5.10E-01
7.00	3.46E-01	2.84E-01	2.68E-01	2.63E-01	2.61E-01	2.60E-01	2.60E-01	2.60E-01
7.25	2.41E-01	8.83E-02	3.52E-02	1.83E-02	1.28E-02	1.11E-02	1.05E-02	1.03E-02
7.50	2.76E-01	–1.94E-02	–1.63E-01	–2.14E-01	–2.31E-01	–2.37E-01	–2.39E-01	–2.39E-01
7.75	4.56E-01	8.77E-03	–2.77E-01	–4.12E-01	–4.64E-01	–4.81E-01	–4.87E-01	–4.89E-01
8.00	5.33E-01	1.71E-01	–2.53E-01	–5.29E-01	–6.61E-01	–7.13E-01	–7.31E-01	–7.37E-01
8.25	5.98E-01	4.49E-01	–9.89E-02	–5.11E-01	–7.78E-01	–9.11E-01	–9.63E-01	–9.81E-01
8.50	1.42E+00	1.00E+00	1.47E-01	–3.62E-01	–7.64E-01	–1.03E+00	–1.16E+00	–1.21E+00
8.75	500	1.06E+00	5.38E-01	–1.30E-01	–6.20E-01	–1.01E+00	–1.28E+00	–1.41E+00
9.00	500	500	7.93E-01	1.89E-01	–3.95E-01	–8.75E-01	–1.26E+00	–1.53E+00
9.25	500	500	500	8.19E-01	–1.08E-01	–6.54E-01	–1.12E+00	–1.51E+00
9.50	500	500	500	1.36E+00	3.72E-01	–3.81E-01	–9.10E-01	–1.37E+00
9.75	500	500	500	500	1.12E+00	2.16E-02	–6.44E-01	–1.16E+00
10.00	500	500	500	500	500	9.56E-01	–2.78E-01	–9.00E-01
10.25	500	500	500	500	500	1.96E+00	5.24E-01	–5.52E-01
10.50	500	500	500	500	500	500	1.76E+00	1.72E-01

Source: DTN: MO0702PADISCON.001_R0 [DIRS 179358], Table 3.

NOTE: This look-up table is implemented in the TSPA-SEIS as parameter Sol_Np2O5_LUT. Entries reported as "500" in the table indicate conditions for which a valid solubility value does not exist.

Table 6.3.7-36. Base Neptunium (NpO_2) Solubility Look-Up Table (log[Np], mg/L)

	log fco_2 (bars)							
pH	**-1.5**	**-2.0**	**-2.5**	**-3.0**	**-3.5**	**-4.0**	**-4.5**	**-5.0**
3.00	3.09E+00	3.09E+00	3.09E+00	3.09E+00	3.09E+00	3.09E+00	3.09E+00	3.09E+00
3.25	2.82E+00	2.82E+00	2.82E+00	2.82E+00	2.82E+00	2.82E+00	2.82E+00	2.82E+00
3.50	2.56E+00	2.56E+00	2.56E+00	2.56E+00	2.56E+00	2.56E+00	2.56E+00	2.56E+00
3.75	2.30E+00	2.30E+00	2.30E+00	2.30E+00	2.30E+00	2.30E+00	2.30E+00	2.30E+00
4.00	2.05E+00	2.05E+00	2.05E+00	2.05E+00	2.05E+00	2.05E+00	2.05E+00	2.05E+00
4.25	1.80E+00	1.80E+00	1.80E+00	1.80E+00	1.80E+00	1.80E+00	1.80E+00	1.80E+00
4.50	1.55E+00	1.55E+00	1.55E+00	1.55E+00	1.55E+00	1.55E+00	1.55E+00	1.55E+00
4.75	1.29E+00	1.29E+00	1.29E+00	1.29E+00	1.29E+00	1.29E+00	1.29E+00	1.29E+00
5.00	1.04E+00	1.04E+00	1.04E+00	1.04E+00	1.04E+00	1.04E+00	1.04E+00	1.04E+00
5.25	7.94E-01	7.94E-01	7.94E-01	7.94E-01	7.94E-01	7.94E-01	7.94E-01	7.94E-01
5.50	5.44E-01	5.44E-01	5.44E-01	5.44E-01	5.44E-01	5.44E-01	5.44E-01	5.44E-01
5.75	2.93E-01	2.94E-01	2.94E-01	2.94E-01	2.94E-01	2.94E-01	2.94E-01	2.94E-01
6.00	4.37E-02	4.36E-02	4.36E-02	4.36E-02	4.36E-02	4.36E-02	4.36E-02	4.36E-02
6.25	–2.05E-01	–2.06E-01	–2.06E-01	–2.06E-01	–2.06E-01	–2.06E-01	–2.06E-01	–2.06E-01
6.50	–4.48E-01	–4.54E-01	–4.56E-01	–4.56E-01	–4.56E-01	–4.56E-01	–4.56E-01	–4.56E-01
6.75	–6.65E-01	–6.98E-01	–7.04E-01	–7.06E-01	–7.06E-01	–7.06E-01	–7.06E-01	–7.06E-01
7.00	–8.00E-01	–9.24E-01	–9.48E-01	–9.54E-01	–9.56E-01	–9.56E-01	–9.56E-01	–9.56E-01
7.25	–7.26E-01	–1.09E+00	–1.18E+00	–1.20E+00	–1.20E+00	–1.21E+00	–1.21E+00	–1.21E+00
7.50	–3.77E-01	–1.09E+00	-1.36E+00	–1.43E+00	–1.45E+00	–1.45E+00	–1.46E+00	–1.46E+00
7.75	2.05E-01	–8.33E-01	–1.41E+00	–1.62E+00	–1.68E+00	–1.70E+00	–1.70E+00	–1.71E+00
8.00	2.70E-01	–3.51E-01	–1.23E+00	–1.70E+00	–1.87E+00	–1.93E+00	–1.95E+00	–1.95E+00
8.25	5.98E-01	3.96E-01	–8.43E-01	–1.59E+00	–1.97E+00	–2.12E+00	–2.18E+00	–2.20E+00
8.50	1.42E+00	4.41E-01	–2.14E-01	–1.27E+00	–1.90E+00	–2.23E+00	–2.37E+00	–2.43E+00
8.75	500	1.06E+00	4.57E-01	–7.55E-01	–1.65E+00	–2.18E+00	–2.48E+00	–2.63E+00
9.00	500	500	7.93E-01	9.62E-02	–1.22E+00	–1.98E+00	–2.45E+00	–2.74E+00
9.25	500	500	500	1.33E+00	–5.02E-01	–1.63E+00	–2.27E+00	–2.71E+00
9.50	500	500	500	1.36E+00	6.43E-01	–1.03E+00	–1.98E+00	–2.55E+00
9.75	500	500	500	500	1.12E+00	2.13E-02	–1.48E+00	–2.29E+00
10.00	500	500	500	500	500	9.54E-01	–5.42E-01	–1.88E+00
10.25	500	500	500	500	500	1.96E+00	8.53E-01	–1.05E+00
10.50	500	500	500	500	500	500	1.76E+00	3.90E-01
10.75	500	500	500	500	500	500	500	1.61E+00

Source: DTN: MO0702PADISCON.001_R0 [DIRS 179358], Table 2.

NOTE: This look-up table is implemented in the TSPA-SEIS as parameter Sol_NpO2_LUT. Entries reported as "500" in the table indicate conditions for which a valid solubility value does not exist.

Table 6.3.7-37. Base-Case Plutonium Solubility Look-Up Table (log[Pu], mg/L)

	log fco_2 (bars)							
pH	**-1.50**	**-2.00**	**-2.50**	**-3.00**	**-3.50**	**-4.00**	**-4.50**	**-5.00**
2.00	4.53E+00	4.53E+00	4.53E+00	4.53E+00	4.53E+00	4.53E+00	4.53E+00	4.53E+00
2.25	3.84E+00	3.84E+00	3.84E+00	3.84E+00	3.84E+00	3.84E+00	3.84E+00	3.84E+00
2.50	3.19E+00	3.19E+00	3.19E+00	3.19E+00	3.19E+00	3.19E+00	3.19E+00	3.19E+00
2.75	2.62E+00	2.62E+00	2.62E+00	2.62E+00	2.62E+00	2.62E+00	2.62E+00	2.62E+00
3.00	2.14E+00	2.14E+00	2.14E+00	2.14E+00	2.14E+00	2.14E+00	2.14E+00	2.14E+00
3.25	1.74E+00	1.74E+00	1.74E+00	1.74E+00	1.74E+00	1.74E+00	1.74E+00	1.74E+00
3.50	1.38E+00	1.38E+00	1.38E+00	1.38E+00	1.38E+00	1.38E+00	1.38E+00	1.38E+00
3.75	1.04E+00	1.03E+00	1.03E+00	1.03E+00	1.03E+00	1.03E+00	1.03E+00	1.03E+00
4.00	7.22E-01	7.12E-01	7.09E-01	7.08E-01	7.07E-01	7.07E-01	7.07E-01	7.07E-01
4.25	4.32E-01	4.12E-01	4.06E-01	4.04E-01	4.03E-01	4.03E-01	4.03E-01	4.03E-01
4.50	1.72E-01	1.35E-01	1.23E-01	1.19E-01	1.18E-01	1.17E-01	1.17E-01	1.17E-01
4.75	−5.78E-02	−1.22E-01	−1.45E-01	−1.52E-01	−1.54E-01	−1.55E-01	−1.55E-01	−1.55E-01
5.00	−2.54E-01	−3.60E-01	−3.99E-01	−4.12E-01	−4.17E-01	−4.18E-01	−4.19E-01	−4.19E-01
5.25	−4.13E-01	−5.75E-01	−6.42E-01	−6.65E-01	−6.73E-01	−6.75E-01	−6.76E-01	−6.76E-01
5.50	−5.33E-01	−7.62E-01	−8.70E-01	−9.11E-01	−9.25E-01	−9.29E-01	−9.30E-01	−9.31E-01
5.75	−6.17E-01	−9.17E-01	−1.08E+00	−1.15E+00	−1.17E+00	−1.18E+00	−1.18E+00	−1.18E+00
6.00	−6.73E-01	−1.03E+00	−1.27E+00	−1.37E+00	−1.41E+00	−1.43E+00	−1.43E+00	−1.43E+00
6.25	−7.07E-01	−1.12E+00	−1.42E+00	−1.58E+00	−1.65E+00	−1.67E+00	−1.68E+00	−1.69E+00
6.50	−7.28E-01	−1.17E+00	−1.54E+00	−1.77E+00	−1.88E+00	−1.92E+00	−1.93E+00	−1.93E+00
6.75	−7.39E-01	−1.21E+00	−1.62E+00	−1.92E+00	−2.08E+00	−2.15E+00	−2.18E+00	−2.18E+00
7.00	−7.44E-01	−1.23E+00	−1.67E+00	−2.04E+00	−2.27E+00	−2.38E+00	−2.42E+00	−2.43E+00
7.25	−7.44E-01	−1.24E+00	−1.70E+00	−2.12E+00	−2.42E+00	−2.58E+00	−2.65E+00	−2.67E+00
7.50	−7.32E-01	−1.24E+00	−1.72E+00	−2.17E+00	−2.53E+00	−2.76E+00	−2.87E+00	−2.91E+00
7.75	−6.64E-01	−1.23E+00	−1.72E+00	−2.20E+00	−2.61E+00	−2.91E+00	−3.08E+00	−3.15E+00
8.00	−2.26E-01	−1.17E+00	−1.71E+00	−2.20E+00	−2.65E+00	−3.02E+00	−3.25E+00	−3.37E+00
8.25	9.33E-01	−8.71E-01	−1.66E+00	−2.19E+00	−2.67E+00	−3.08E+00	−3.39E+00	−3.56E+00
8.50	2.39E+00	1.11E-01	−1.44E+00	−2.14E+00	−2.65E+00	−3.11E+00	−3.48E+00	−3.73E+00
8.75	500	1.50E+00	−6.37E-01	−1.96E+00	−2.59E+00	−3.09E+00	−3.51E+00	−3.84E+00
9.00	500	3.20E+00	6.73E-01	−1.31E+00	−2.43E+00	−3.01E+00	−3.49E+00	−3.88E+00
9.25	500	500	2.25E+00	−8.16E-02	−1.90E+00	−2.85E+00	−3.40E+00	−3.84E+00
9.50	500	500	500	1.46E+00	−7.69E-01	−2.41E+00	−3.22E+00	−3.74E+00
9.75	500	500	500	3.65E+00	7.62E-01	−1.39E+00	−2.86E+00	−3.56E+00
10.00	500	500	500	500	2.74E+00	1.24E-01	−1.96E+00	−3.24E+00

Table 6.3.7-37. Base-Case Plutonium Solubility Look-Up Table (log[Pu], mg/L)(Continued)

	log fco_2 (bars)							
pH	**-1.50**	**-2.00**	**-2.50**	**-3.00**	**-3.50**	**-4.00**	**-4.50**	**-5.00**
10.25	500	500	500	500	500	2.10E+00	–4.65E-01	–2.47E+00
10.50	500	500	500	500	500	500	1.52E+00	–1.02E+00
10.75	500	500	500	500	500	500	500	9.86E-01

Source: DTN: MO0702PADISCON.001_R0 [DIRS 179358], Table 1.

NOTE: This look-up table is implemented in the TSPA-SEIS as parameter Sol_Pu_LUT. Entries reported as "500" in the table indicate conditions for which a valid solubility value does not exist.

Table 6.3.7-38. Base Protactinium Solubility Look-Up Table (log[Pa], mg/L)

	log fco_2 (bars)							
pH	**-1.50**	**-2.00**	**-2.50**	**-3.00**	**-3.50**	**-4.00**	**-4.50**	**-5.00**
3.00	4.38E+00	4.38E+00	4.38E+00	4.38E+00	4.38E+00	4.38E+00	4.38E+00	4.38E+00
3.25	4.10E+00	4.10E+00	4.10E+00	4.10E+00	4.10E+00	4.10E+00	4.10E+00	4.10E+00
3.50	3.82E+00	3.82E+00	3.82E+00	3.82E+00	3.82E+00	3.82E+00	3.82E+00	3.82E+00
3.75	3.55E+00	3.55E+00	3.55E+00	3.55E+00	3.55E+00	3.55E+00	3.55E+00	3.55E+00
4.00	3.29E+00	3.29E+00	3.29E+00	3.29E+00	3.29E+00	3.29E+00	3.29E+00	3.29E+00
4.25	3.03E+00	3.03E+00	3.03E+00	3.03E+00	3.03E+00	3.03E+00	3.03E+00	3.03E+00
4.50	2.77E+00	2.77E+00	2.77E+00	2.77E+00	2.77E+00	2.77E+00	2.77E+00	2.77E+00
4.75	2.52E+00	2.52E+00	2.52E+00	2.52E+00	2.52E+00	2.52E+00	2.52E+00	2.52E+00
5.00	2.26E+00	2.26E+00	2.26E+00	2.26E+00	2.26E+00	2.26E+00	2.26E+00	2.26E+00
5.25	2.01E+00	2.01E+00	2.01E+00	2.01E+00	2.01E+00	2.01E+00	2.01E+00	2.01E+00
5.50	1.76E+00	1.76E+00	1.76E+00	1.76E+00	1.76E+00	1.76E+00	1.76E+00	1.76E+00
5.75	1.51E+00	1.51E+00	1.51E+00	1.51E+00	1.51E+00	1.51E+00	1.51E+00	1.51E+00
6.00	1.26E+00	1.26E+00	1.26E+00	1.26E+00	1.26E+00	1.26E+00	1.26E+00	1.26E+00
6.25	1.01E+00	1.01E+00	1.01E+00	1.01E+00	1.01E+00	1.01E+00	1.01E+00	1.01E+00
6.50	7.66E-01	7.62E-01	7.61E-01	7.60E-01	7.60E-01	7.60E-01	7.60E-01	7.60E-01
6.75	5.35E-01	5.17E-01	5.12E-01	5.11E-01	5.10E-01	5.10E-01	5.10E-01	5.10E-01
7.00	3.46E-01	2.84E-01	2.68E-01	2.63E-01	2.61E-01	2.60E-01	2.60E-01	2.60E-01
7.25	2.41E-01	8.83E-02	3.52E-02	1.83E-02	1.28E-02	1.11E-02	1.05E-02	1.03E-02
7.50	2.76E-01	−1.94E-02	−1.63E-01	−2.14E-01	−2.31E-01	−2.37E-01	−2.39E-01	−2.39E-01
7.75	4.56E-01	8.77E-03	−2.77E-01	−4.12E-01	−4.64E-01	−4.81E-01	−4.87E-01	−4.89E-01
8.00	5.33E-01	1.71E-01	−2.53E-01	−5.29E-01	−6.61E-01	−7.13E-01	−7.31E-01	−7.37E-01
8.25	5.98E-01	4.49E-01	−9.89E-02	−5.11E-01	−7.78E-01	−9.11E-01	−9.63E-01	−9.81E-01
8.50	1.42E+00	1.00E+00	1.47E-01	−3.62E-01	−7.64E-01	−1.03E+00	−1.16E+00	−1.21E+00
8.75	500	1.06E+00	5.38E-01	−1.30E-01	−6.20E-01	−1.01E+00	−1.28E+00	−1.41E+00
9.00	500	500	7.93E-01	1.89E-01	−3.95E-01	−8.75E-01	−1.26E+00	−1.53E+00
9.25	500	500	500	8.19E-01	−1.08E-01	−6.54E-01	−1.12E+00	−1.51E+00
9.50	500	500	500	1.36E+00	3.72E-01	−3.81E-01	−9.10E-01	−1.37E+00
9.75	500	500	500	500	1.12E+00	2.16E-02	−6.44E-01	−1.16E+00
10.00	500	500	500	500	500	9.56E-01	−2.78E-01	−9.00E-01
10.25	500	500	500	500	500	1.96E+00	5.24E-01	−5.52E-01
10.50	500	500	500	500	500	500	1.76E+00	1.72E-01

Source: DTN: MO0702PADISCON.001_R0 [DIRS 179358], Table 9.

NOTE: This look-up table is implemented in the TSPA-SEIS as parameter Sol_Pa_LUT. Entries reported as "500" in the table indicate conditions for which a valid solubility value does not exist.

Table 6.3.7-39. Base Thorium Solubility Look-Up Table (log[Th], mg/L)

	log fco_2 (bars)							
pH	**-1.50**	**-2.00**	**-2.50**	**-3.00**	**-3.50**	**-4.00**	**-4.50**	**-5.00**
3.25	3.84E+00	3.84E+00	3.84E+00	3.84E+00	3.84E+00	3.84E+00	3.84E+00	3.84E+00
3.50	2.54E+00	2.54E+00	2.54E+00	2.54E+00	2.54E+00	2.54E+00	2.54E+00	2.54E+00
3.75	1.61E+00	1.61E+00	1.62E+00	1.62E+00	1.62E+00	1.62E+00	1.62E+00	1.62E+00
4.00	1.14E+00	1.14E+00	1.14E+00	1.14E+00	1.14E+00	1.14E+00	1.14E+00	1.14E+00
4.25	9.41E-01	9.41E-01	9.41E-01	9.41E-01	9.41E-01	9.41E-01	9.41E-01	9.41E-01
4.50	7.42E-01	7.42E-01	7.42E-01	7.42E-01	7.42E-01	7.42E-01	7.42E-01	7.42E-01
4.75	3.82E-01	3.82E-01	3.82E-01	3.82E-01	3.82E-01	3.82E-01	3.82E-01	3.82E-01
5.00	–2.92E-01	–2.94E-01	–2.95E-01	–2.95E-01	–2.95E-01	–2.95E-01	–2.95E-01	–2.95E-01
5.25	–1.17E+00	–1.20E+00	–1.21E+00	–1.21E+00	–1.22E+00	–1.22E+00	–1.22E+00	–1.22E+00
5.50	–1.75E+00	–1.99E+00	–2.10E+00	–2.14E+00	–2.16E+00	–2.16E+00	–2.16E+00	–2.16E+00
5.75	–1.69E+00	–2.13E+00	–2.50E+00	–2.73E+00	–2.84E+00	–2.88E+00	–2.89E+00	–2.90E+00
6.00	–1.46E+00	–1.94E+00	–2.39E+00	–2.75E+00	–2.99E+00	–3.10E+00	–3.14E+00	–3.16E+00
6.25	–1.22E+00	–1.70E+00	–2.17E+00	–2.60E+00	–2.91E+00	–3.09E+00	–3.17E+00	–3.20E+00
6.50	–9.69E-01	–1.46E+00	–1.94E+00	–2.40E+00	–2.77E+00	–3.02E+00	–3.15E+00	–3.19E+00
6.75	–7.16E-01	–1.22E+00	–1.70E+00	–2.18E+00	–2.60E+00	–2.92E+00	–3.10E+00	–3.18E+00
7.00	–4.60E-01	–9.69E-01	–1.46E+00	–1.94E+00	–2.40E+00	–2.78E+00	–3.03E+00	–3.15E+00
7.25	–2.02E-01	–7.16E-01	–1.22E+00	–1.70E+00	–2.18E+00	–2.60E+00	–2.92E+00	–3.10E+00
7.50	5.88E-02	–4.60E-01	–9.69E-01	–1.46E+00	–1.94E+00	–2.40E+00	–2.78E+00	–3.03E+00
7.75	3.22E-01	–2.02E-01	–7.15E-01	–1.22E+00	–1.70E+00	–2.18E+00	–2.60E+00	–2.92E+00
8.00	5.90E-01	5.91E-02	–4.60E-01	–9.69E-01	–1.46E+00	–1.94E+00	–2.40E+00	–2.78E+00
8.25	1.04E+00	3.23E-01	–2.01E-01	–7.15E-01	–1.22E+00	–1.70E+00	–2.18E+00	–2.60E+00
8.50	500	5.96E-01	6.01E-02	–4.59E-01	–9.68E-01	–1.46E+00	–1.94E+00	–2.40E+00
8.75	500	1.41E+00	3.25E-01	–2.00E-01	–7.14E-01	–1.22E+00	–1.70E+00	–2.18E+00
9.00	500	500	6.29E-01	6.31E-02	–4.57E-01	–9.67E-01	–1.47E+00	–1.94E+00
9.25	500	500	2.62E+00	3.33E-01	–1.96E-01	–7.12E-01	–1.22E+00	–1.70E+00
9.50	500	500	500	9.49E-01	7.17E-02	–4.53E-01	–9.65E-01	–1.47E+00
9.75	500	500	500	500	3.81E-01	–1.86E-01	–7.07E-01	–1.21E+00
10.00	500	500	500	500	500	9.60E-02	–4.41E-01	–9.58E-01
10.25	500	500	500	500	500	1.67E+00	–1.61E-01	–6.93E-01
10.50	500	500	500	500	500	500	6.41E-01	–4.13E-01
10.75	500	500	500	500	500	500	500	4.71E-03

Source: DTN: MO0702PADISCON.001_R0 [DIRS 179358], Table 7.

NOTE: This look-up table is implemented in the TSPA-SEIS as parameter Sol_Pa_LUT. Entries reported as "500" in the table indicate conditions for which a valid solubility value does not exist.

Table 6.3.7-40. Base Tin Solubility Look-Up Table (log[Sn], mg/L)

pH	log fCO2 (bars)							
	-1.5	-2.0	-2.5	-3.0	-3.5	-4.0	-4.5	-5.0
2.00	-2.38E+00	-2.38E+00	-2.38E+00	-2.38E+00	-2.38E+00	-2.38E+00	-2.38E+00	-2.38E+00
2.25	-2.38E+00	-2.38E+00	-2.38E+00	-2.38E+00	-2.38E+00	-2.38E+00	-2.38E+00	-2.38E+00
2.50	-2.39E+00	-2.39E+00	-2.39E+00	-2.39E+00	-2.39E+00	-2.39E+00	-2.39E+00	-2.39E+00
2.75	-2.39E+00	-2.39E+00	-2.39E+00	-2.39E+00	-2.39E+00	-2.39E+00	-2.39E+00	-2.39E+00
3.00	-2.39E+00	-2.39E+00	-2.39E+00	-2.39E+00	-2.39E+00	-2.39E+00	-2.39E+00	-2.39E+00
3.25	-2.39E+00	-2.39E+00	-2.39E+00	-2.39E+00	-2.39E+00	-2.39E+00	-2.39E+00	-2.39E+00
3.50	-2.39E+00	-2.39E+00	-2.39E+00	-2.39E+00	-2.39E+00	-2.39E+00	-2.39E+00	-2.39E+00
3.75	-2.39E+00	-2.39E+00	-2.39E+00	-2.39E+00	-2.39E+00	-2.39E+00	-2.39E+00	-2.39E+00
4.00	-2.39E+00	-2.39E+00	-2.39E+00	-2.39E+00	-2.39E+00	-2.39E+00	-2.39E+00	-2.39E+00
4.25	-2.39E+00	-2.39E+00	-2.39E+00	-2.39E+00	-2.39E+00	-2.39E+00	-2.39E+00	-2.39E+00
4.50	-2.39E+00	-2.39E+00	-2.39E+00	-2.39E+00	-2.39E+00	-2.39E+00	-2.39E+00	-2.39E+00
4.75	-2.39E+00	-2.39E+00	-2.39E+00	-2.39E+00	-2.39E+00	-2.39E+00	-2.39E+00	-2.39E+00
5.00	-2.38E+00	-2.38E+00	-2.38E+00	-2.38E+00	-2.38E+00	-2.38E+00	-2.38E+00	-2.38E+00
5.25	-2.38E+00	-2.38E+00	-2.38E+00	-2.38E+00	-2.38E+00	-2.38E+00	-2.38E+00	-2.38E+00
5.50	-2.38E+00	-2.38E+00	-2.38E+00	-2.38E+00	-2.38E+00	-2.38E+00	-2.38E+00	-2.38E+00
5.75	-2.38E+00	-2.38E+00	-2.38E+00	-2.38E+00	-2.38E+00	-2.38E+00	-2.38E+00	-2.38E+00
6.00	-2.37E+00	-2.37E+00	-2.37E+00	-2.37E+00	-2.37E+00	-2.37E+00	-2.37E+00	-2.37E+00
6.25	-2.37E+00	-2.37E+00	-2.37E+00	-2.37E+00	-2.37E+00	-2.37E+00	-2.37E+00	-2.37E+00
6.50	-2.35E+00	-2.35E+00	-2.35E+00	-2.35E+00	-2.35E+00	-2.35E+00	-2.35E+00	-2.35E+00
6.75	-2.33E+00	-2.33E+00	-2.33E+00	-2.33E+00	-2.33E+00	-2.33E+00	-2.33E+00	-2.33E+00
7.00	-2.29E+00	-2.29E+00	-2.29E+00	-2.29E+00	-2.29E+00	-2.29E+00	-2.29E+00	-2.29E+00
7.25	-2.22E+00	-2.22E+00	-2.22E+00	-2.22E+00	-2.22E+00	-2.22E+00	-2.22E+00	-2.22E+00
7.50	-2.12E+00	-2.12E+00	-2.13E+00	-2.13E+00	-2.13E+00	-2.13E+00	-2.13E+00	-2.13E+00
7.75	-1.98E+00	-1.99E+00	-1.99E+00	-1.99E+00	-2.00E+00	-2.00E+00	-2.00E+00	-2.00E+00
8.00	-1.81E+00	-1.82E+00	-1.83E+00	-1.83E+00	-1.83E+00	-1.83E+00	-1.83E+00	-1.83E+00
8.25	-1.60E+00	-1.62E+00	-1.63E+00	-1.63E+00	-1.63E+00	-1.64E+00	-1.64E+00	-1.64E+00
8.50	-1.37E+00	-1.39E+00	-1.41E+00	-1.41E+00	-1.42E+00	-1.42E+00	-1.42E+00	-1.42E+00
8.75	-1.12E+00	-1.14E+00	-1.16E+00	-1.18E+00	-1.18E+00	-1.19E+00	-1.19E+00	-1.19E+00
9.00	500	-8.70E-01	-9.03E-01	-9.26E-01	-9.36E-01	-9.40E-01	-9.42E-01	-9.42E-01
9.25	500	-5.82E-01	-6.18E-01	-6.55E-01	-6.76E-01	-6.84E-01	-6.87E-01	-6.88E-01
9.50	500	500	-2.98E-01	-3.55E-01	-3.94E-01	-4.13E-01	-4.20E-01	-4.22E-01
9.75	500	500	500	2.60E-03	-7.35E-02	-1.16E-01	-1.34E-01	-1.40E-01
10.00	500	500	500	500	3.29E-01	2.28E-01	1.85E-01	1.67E-01

Table 6.3.7-40. Base Tin Solubility Look-Up Table (log[Sn], mg/L) (Continued)

pH	log fCO2 (bars)							
	-1.5	-2.0	-2.5	-3.0	-3.5	-4.0	-4.5	-5.0
10.25	500	500	500	500	500	6.89E-01	5.71E-01	5.17E-01
10.50	500	500	500	500	500	500	1.08E+00	9.45E-01
10.75	500	500	500	500	500	500	500	1.51E+00

Source: DTN: MO0702PADISCON.001_R0 [DIRS 179358], Table 16.

NOTE: This look-up table is implemented in the TSPA-SEIS as parameter Sol_Sn_LUT. Entries reported as "500" in the table indicate conditions for which a valid solubility value does not exist.

Table 6.3.7-41. Uncertainty in Americium Solubility Model

TSPA-SEIS Name	Model Abstraction Symbol	Description	Units	Distribution Type	Distribution Specification
Am_Eps_1_low_a	ε_1	Uncertainties in log K below 1 molal ionic strength	None	Truncated normal	$\mu = 0$ $\sigma = 1.0$ $2\sigma = \pm 2.0$
Am_Eps_1_high_a	ε_1	Uncertainties in log K at 1 to 3 molal ionic strength	None	Truncated normal	$\mu = 0$ $\sigma = 1.04$ $2\sigma = \pm 2.08$
Am_Eps_2_Glass_Low_a	$\varepsilon_2^{\text{CSNF-low}}$ $\varepsilon_2^{\text{CDSP-Glass}}$ $\varepsilon_2^{\text{CDSP-F-low}}$	Fluoride Uncertainty, CSNF waste packages when I < 0.2m. CDSP packages, Cell 1b when I < 0.004m and Cell 1a.	None	Triangular	Min = 0 Max = 4.42 Most likely = 0
Am_Eps_2_CSNF_High_a	$\varepsilon_2^{\text{CSNF-high}}$ $\varepsilon_2^{\text{CSNF-invert}}$	Fluoride Uncertainty, CSNF waste packages when I ≥ 0.2m and invert below CSNF waste packages	None	Triangular	Min = 0 Max = 109.03 Most likely = 0
Am_Eps_2_CDSP_High_a	$\varepsilon_2^{\text{CDSP-F-high}}$ $\varepsilon_2^{\text{CDSP-invert}}$	Fluoride Uncertainty, CDSP waste packages when I ≥ 0.004m and invert below CDSP waste packages	None	Triangular	Min = 0 Max = 688.6 Most likely = 0

Source: DTN: MO0702PADISCON.001_R0 [DIRS 179358], Table 19, DTN: MO0702PAFLUORI.000_R1 [DIRS 181219], Table 13.

Table 6.3.7-42. Uncertainty in Neptunium (Np_2O_5) Solubility Model

TSPA-SEIS Name	Model Abstraction Symbol	Description	Units	Distribution Type	Distribution Specification
Np2O5_Eps_1_low_a	ε_1	Uncertainties in log K below 1 molal ionic strength	None	Truncated normal	$\mu = 0$ $\sigma = 0.8$ $2\sigma = \pm 1.6$
Np2O5_Eps_1_high_a	ε_1	Uncertainties in log K at 1 to 3 molal ionic strength	None	Truncated normal	$\mu = 0$ $\sigma = 0.85$ $2\sigma = \pm 1.7$
Np2O5_Eps_2_ Glass_Low CSNF_High_a	$\varepsilon_2^{\text{CSNF-low}}$ $\varepsilon_2^{\text{CDSP-Glass}}$ $\varepsilon_2^{\text{CDSP-F-low}}$	Fluoride Uncertainty, CSNF waste packages when I < 0.2m. CDSP packages, Cell 1b when I < 0.004m and Cell 1a.	None	Triangular	Min = 0 Max = 11 Most likely = 0
Np2O5_Eps_2_CSNF_High_a	$\varepsilon_2^{\text{CSNF-high}}$ $\varepsilon_2^{\text{CSNF-invert}}$	Fluoride Uncertainty, CSNF waste packages when I ≥ 0.2m and invert below CSNF waste packages	None	Triangular	Min = 0 Max = 197 Most likely = 0
Np2O5_Eps_2_CDSP_High_a	$\varepsilon_2^{\text{CDSP-F-high}}$ $\varepsilon_2^{\text{CDSP-invert}}$	Fluoride Uncertainty, CDSP waste packages when I ≥ 0.004m and invert below CDSP waste packages	None	Triangular	Min = 0 Max = 853 Most likely = 0

Source: DTN: MO0702PADISCON.001_R0 [DIRS 179358], Table 19, DTN: MO0702PAFLUORI.000_R1 [DIRS 181219], Table 5.

Table 6.3.7-43. Uncertainty in Neptunium (NpO_2) Solubility Model

TSPA-SEIS Name	Model Abstraction Symbol	Description	Units	Distribution Type	Distribution Specification
NpO2_Eps_1_low_a	ε_1	Uncertainties in log K below 1 molal ionic strength	None	Truncated normal	$\mu = 0$ $\sigma = 0.6$ $2\sigma = \pm 1.2$
NpO2_Eps_1_high_a	ε_1	Uncertainties in log K at 1 to 3 molal ionic strength	None	Truncated normal	$\mu = 0$ $\sigma = 0.67$ $2\sigma = \pm 1.34$
NpO2_Eps_2_Glass_Low_a	$\varepsilon_2^{CSNF\text{-}low}$ $\varepsilon_2^{CDSP\text{-}Glass}$ $\varepsilon_2^{CDSP\text{-}F\text{-}low}$	Fluoride Uncertainty, CSNF waste packages when I < 0.2m. CDSP packages, Cell 1b when I < 0.004m and Cell 1a.	None	Triangular	Min = 0 Max = 14.1 Most likely =0
NpO2_Eps_2_CSNF_High_a	$\varepsilon_2^{CSNF\text{-}high}$ $\varepsilon_2^{CSNF\text{-}invert}$	Fluoride Uncertainty, CSNF waste packages when I ≥ 0.2m and invert below CSNF waste packages	None	Triangular	Min = 0 Max = 255.8 Most likely =0
NpO2_Eps_2_CDSP_High_a	$\varepsilon_2^{CDSP\text{-}F\text{-}high}$ $\varepsilon_2^{CDSP\text{-}invert}$	Fluoride Uncertainty, CDSP waste packages when I ≥ 0.004m and invert below CDSP waste packages	None	Triangular	Min = 0 Max = 1093.5 Most likely =0

Source: DTN: MO0702PADISCON.001_R0 [DIRS 179358], Table 19, DTN: MO0702PAFLUORI.000_R1 [DIRS 181219], Table 3.

Table 6.3.7-44. Uncertainty in Plutonium Solubility Model

TSPA-SEIS Name	Model Abstraction Symbol	Description	Units	Distribution Type	Distribution Specification
Pu_Eps_1_low_a	ε_1	Uncertainties in log K below 1 molal ionic strength	None	Truncated normal	$\mu = 0$ $\sigma = 0.7$ $2\sigma = 1.4$
Pu_Eps_1_high_a	ε_1	Uncertainties in log K at 1 to 3 molal ionic strength	None	Truncated normal	$\mu = 0$ $\sigma = 0.76$ $2\sigma = 1.52$
Pu_Eps_2_Glass_Low_a	$\varepsilon_2^{CSNF\text{-}low}$ $\varepsilon_2^{CDSP\text{-}Glass}$ $\varepsilon_2^{CDSP\text{-}F\text{-}low}$	Fluoride Uncertainty, CSNF waste packages when I < 0.2m. CDSP packages, Cell 1b when I < 0.004m and Cell 1a.	None	Triangular	Min = 0 Max = 79 Most likely = 0
Pu_Eps_2_CSNF_High_a	$\varepsilon_2^{CSNF\text{-}high}$ $\varepsilon_2^{CSNF\text{-}invert}$	Fluoride Uncertainty, CSNF waste packages when I ≥ 0.2m and invert below CSNF waste packages	None	Triangular	Min = 0 Max = 1374 Most likely = 0
Pu_Eps_2_CDSP_High_a	$\varepsilon_2^{CDSP\text{-}F\text{-}high}$ $\varepsilon_2^{CDSP\text{-}invert}$	Fluoride Uncertainty, CDSP waste packages when I ≥ 0.004m and invert below CDSP waste packages	None	Triangular	Min = 0 Max = 5460 Most likely = 0

Source: DTN: MO0702PADISCON.001_R0 [DIRS 179358], Table 19,DTN: MO0702PAFLUORI.000_R1 [DIRS 181219], Table 1.

Table 6.3.7-45. Uncertainty in Protactinium Solubility Model

TSPA-SEIS Name	Model Abstraction Symbol	Description	Units	Distribution Type	Distribution Specification
Pa_Eps_1_a	ε_1	Uncertainties in analogue	None	Uniform	Min = –4.42 Max = –0.05
Pa_Eps_2_Glass_Low_a	$\varepsilon_2^{CSNF\text{-}low}$ $\varepsilon_2^{CDSP\text{-}Glass}$ $\varepsilon_2^{CDSP\text{-}F\text{-}low}$	Fluoride Uncertainty, CSNF waste packages when I < 0.2m. CDSP packages, Cell 1b when I < 0.004m and Cell 1a.	None	Triangular	Min = 0 Max = 11 Most likely = 0
Pa_Eps_2_CSNF_High_a	$\varepsilon_2^{CSNF\text{-}high}$ $\varepsilon_2^{CSNF\text{-}invert}$	Fluoride Uncertainty, CSNF waste packages when I ≥ 0.2m and invert below CSNF waste packages	None	Triangular	Min = 0 Max = 197 Most likely = 0
Pa_Eps_2_CDSP_High_a	$\varepsilon_2^{CDSP\text{-}F\text{-}high}$ $\varepsilon_2^{CDSP\text{-}invert}$	Fluoride Uncertainty, CDSP waste packages when I ≥ 0.004m and invert below CDSP waste packages	None	Triangular	Min = 0 Max =853 Most likely = 0

Source: DTN: MO0702PADISCON.001_R0 [DIRS 179358], Table 19, DTN: MO0702PAFLUORI.000_R1 [DIRS 181219], Table 15.

Table 6.3.7-46. Uncertainty in Thorium Solubility Model

TSPA-SEIS Name	Model Abstraction Symbol	Description	Units	Distribution Type	Distribution Specification
Th_Eps_1_low_a	ε_1	Uncertainties in log K below 1 molal ionic strength	None	Truncated normal	$\mu = 0$ $\sigma = 0.7$ $2\sigma = \pm 1.4$
Th_Eps_1_high_a	ε_1	Uncertainties in log K at 1 to 3 molal ionic strength	None	Truncated normal	$\mu = 0$ $\sigma = 0.76$ $2\sigma = \pm 1.52$
Th_Eps_2_Glass_Low_a	$\varepsilon_2^{\text{CSNF-low}}$ $\varepsilon_2^{\text{CDSP-Glass}}$ $\varepsilon_2^{\text{CDSP-F-low}}$	Fluoride Uncertainty, CSNF waste packages when I < 0.2m. CDSP packages, Cell 1b when I < 0.004m and Cell 1a.	None	Triangular	Min = 0 Max = 626.2 Most likely = 0
Th_Eps_2_CSNF_High_a	$\varepsilon_2^{\text{CSNF-high}}$ $\varepsilon_2^{\text{CSNF-invert}}$	Fluoride Uncertainty, CSNF waste packages when I ≥ 0.2m and invert below CSNF waste packages	None	Triangular	Min = 0 Max = 7848.3 Most likely = 0
Th_Eps_2_CDSP_High_a	$\varepsilon_2^{\text{CDSP-F-high}}$ $\varepsilon_2^{\text{CDSP-invert}}$	Fluoride Uncertainty, CDSP waste packages when I ≥ 0.004m and invert below CDSP waste packages	None	Triangular	Min = 0 Max = 23723.3 Most likely = 0

Source: DTN: MO0702PADISCON.001_R0 [DIRS 179358], Table 19, DTN: MO0702PAFLUORI.000_R1 [DIRS 181219], Table 11.

Table 6.3.7-47. Uncertainty in Tin Solubility Model

TSPA-SEIS Name	Model Abstraction Symbol	Description	Units	Distribution Type	Distribution Specification
Sn_Eps_1_low_a	ε_1	Uncertainties in log K below 1 molal ionic strength	None	Truncated normal	$\mu = 0$ $\sigma = 0.45$ $2\sigma = 0.90$
Sn_Eps_1_high_a	ε_1	Uncertainties in log K at 1 to 3 molal ionic strength	None	Truncated normal	$\mu = 0$ $\sigma = 0.54$ $2\sigma = 1.08$

Source: DTN: MO0702PADISCON.001_R0 [DIRS 179358], Table 19.

Table 6.3.7-48. Multiplication Factor, N(pH), Used to Modify Fluoride Concentration Uncertainty Terms (ε_2) for Americium

pH	Multiplication Factor for Fluoride Uncertainty		
	Glass, CSNF low, and CDSP low	CSNF high and CSNF invert	CDSP high and CDSP invert
6.00	1.00E+00	1.00E+00	1.00E+00
6.25	8.91E-02	1.45E-01	3.20E-01
6.50	1.30E-02	2.92E-02	7.24E-02
6.75	2.13E-03	5.61E-03	1.36E-02
7.00	3.44E-04	1.04E-03	2.47E-03
7.25	4.98E-05	1.98E-04	4.50E-04
7.50	3.39E-06	4.08E-05	8.39E-05
7.75	0.00E-00	1.04E-05	1.68E-05
8.00	0.00E-00	4.41E-06	4.13E-06
8.25	3.62E-06	2.41E-06	1.52E-06
8.50	3.39E-06	2.34E-06	1.36E-06
8.75	8.82E-06	6.00E-06	3.67E-06
9.00	3.69E-05	2.59E-05	1.65E-05
9.25	1.92E-04	1.36E-04	8.82E-05
9.50	1.13E-03	8.02E-04	5.23E-04
9.75	7.24E-03	5.10E-03	3.33E-03

Source: DTN: MO0702PAFLUORI.000_R1 [DIRS 181219], Table 14.

NOTE: These multiplication factors are implemented in the TSPA-SEIS as parameters Am_Eps_2_Glass_Low, Am_Eps_2_CSNF_High, Am_Eps_2_CDSP_High.

Table 6.3.7-49. Multiplication Factor, N(pH), Used to Modify Fluoride Concentration Uncertainty Terms (ε_2) for Neptunium (Np_2O_5)

pH	Multiplication Factor for Fluoride Uncertainty		
	Glass, CSNF low, and CDSP low	CSNF high and CSNF invert	CDSP high and CDSP invert
3.00	1.00E+00	1.00E+00	1.00E+00
3.25	7.27E-01	7.36E-01	7.63E-01
3.50	4.91E-01	5.09E-01	5.47E-01
3.75	3.18E-01	3.30E-01	3.60E-01
4.00	1.91E-01	2.01E-01	2.17E-01
4.25	1.09E-01	1.17E-01	1.41E-01
4.50	6.64E-02	6.66E-02	9.31E-02
4.75	3.82E-02	3.74E-02	5.70E-02
5.00	2.09E-02	2.08E-02	3.36E-02
5.25	1.18E-02	1.16E-02	1.94E-02
5.50	6.64E-03	6.51E-03	1.11E-02
5.75	3.73E-03	3.68E-03	6.28E-03
6.00	2.09E-03	2.15E-03	3.55E-03
6.25	1.18E-03	1.24E-03	2.00E-03
6.50	6.64E-04	7.13E-04	1.13E-03
6.75	3.73E-04	4.12E-04	6.37E-04
7.00	2.09E-04	2.41E-04	3.60E-04
7.25	1.18E-04	1.44E-04	2.04E-04
7.50	6.45E-05	8.96E-05	1.17E-04
7.75	3.45E-05	6.01E-05	6.97E-05
8.00	1.55E-05	4.81E-05	4.52E-05
8.25	4.64E-05	4.15E-05	3.37E-05
8.50	4.09E-05	3.80E-05	3.11E-05
8.75	5.45E-05	5.13E-05	4.43E-05
9.00	1.55E-04	1.55E-04	1.47E-04
9.25	1.34E-03	1.32E-03	1.29E-03

Source: DTN: MO0702PAFLUORI.000_R1 [DIRS 181219], Table 6.

NOTE: These multiplication factors are implemented in the TSPA-SEIS as parameters Np2O5_Eps_2_Glass_Low_N, Np2O5_CSNF_High_N, Np2O5_CDSP_High_N .

Table 6.3.7-50. Multiplication Factor, N(pH), Used to Modify Fluoride Concentration Uncertainty Terms (ε_2) for Neptunium (NpO_2)

pH	Multiplication Factor for Fluoride Uncertainty		
	Glass, CSNF low, and CDSP low	CSNF high and CSNF invert	CDSP high and CDSP invert
3.00	1.00E+00	1.00E+00	1.00E+00
3.25	5.77E-01	6.74E-01	7.77E-01
3.50	2.86E-01	4.12E-01	5.75E-01
3.75	1.23E-01	2.16E-01	3.77E-01
4.00	4.96E-02	9.57E-02	2.04E-01
4.25	1.92E-02	3.78E-02	9.00E-02
4.50	7.66E-03	1.42E-02	3.50E-02
4.75	3.26E-03	5.53E-03	1.31E-02
5.00	1.49E-03	2.26E-03	4.98E-03
5.25	7.09E-04	9.96E-04	2.01E-03
5.50	3.62E-04	4.71E-04	8.74E-04
5.75	1.91E-04	2.37E-04	4.10E-04
6.00	1.06E-04	1.24E-04	2.04E-04
6.25	5.74E-05	6.74E-05	1.07E-04
6.50	3.12E-05	3.74E-05	5.74E-05
6.75	1.84E-05	2.11E-05	3.15E-05
7.00	9.93E-06	1.22E-05	1.75E-05
7.25	5.53E-06	7.21E-06	9.88E-06
7.50	3.05E-06	4.45E-06	5.68E-06
7.75	1.49E-06	3.01E-06	3.46E-06
8.00	4.26E-07	2.82E-06	2.61E-06
8.25	4.40E-06	3.92E-06	3.22E-06
8.50	1.00E-05	9.27E-06	8.17E-06
8.75	4.75E-05	4.55E-05	4.40E-05
9.00	4.18E-04	4.07E-04	4.07E-04
9.25	5.53E-03	5.47E-03	5.48E-03

Source: DTN: MO0702PAFLUORI.000_R1 [DIRS 181219], Table 4.

NOTE: These multiplication factors are implemented in the TSPA-SEIS as parameters NpO2_Glass_low_N, NpO2_CSNF_High_N, NpO2_CDSP_High_N.

Table 6.3.7-51. Multiplication Factor, N(pH), Used to Modify Fluoride Concentration Uncertainty Terms (ε_2) for Plutonium

pH	Multiplication Factor for Fluoride Uncertainty		
	Glass, CSNF low, and CDSP low	CSNF high and CSNF invert	CDSP high and CDSP invert
2.00	1.00E+00	1.00E+00	1.00E+00
2.25	7.67E-01	7.58E-01	7.42E-01
2.50	5.08E-01	4.98E-01	4.83E-01
2.75	3.50E-01	3.42E-01	3.33E-01
3.00	2.41E-01	2.40E-01	2.44E-01
3.25	1.48E-01	1.60E-01	1.81E-01
3.50	7.51E-02	9.41E-02	1.27E-01
3.75	3.18E-02	4.69E-02	7.81E-02
4.00	1.18E-02	1.96E-02	3.95E-02
4.25	4.06E-03	7.20E-03	1.64E-02
4.50	1.34E-03	2.45E-03	5.90E-03
4.75	4.32E-04	8.03E-04	1.98E-03
5.00	1.37E-04	2.58E-04	6.44E-04
5.25	4.32E-05	8.19E-05	2.07E-04
5.50	1.34E-05	2.58E-05	6.61E-05
5.75	4.08E-06	8.04E-06	2.12E-05
6.00	1.19E-06	2.47E-06	6.81E-06
6.25	3.29E-07	7.39E-07	2.22E-06
6.50	6.33E-08	2.12E-07	7.38E-07
6.75	0.00E+00	5.60E-08	2.54E-07
7.00	0.00E+00	1.34E-08	9.23E-08
7.25	0.00E+00	3.20E-09	3.64E-08
7.50	0.00E+00	2.04E-09	1.62E-08
7.75	0.00E+00	3.35E-09	9.16E-09
8.00	0.00E+00	7.71E-09	8.44E-09
8.25	1.90E-08	1.68E-08	1.43E-08
8.50	4.94E-08	4.79E-08	4.62E-08
8.75	2.91E-07	2.90E-07	3.07E-07
9.00	2.85E-06	2.91E-06	3.15E-06
9.25	3.85E-05	3.94E-05	4.24E-05
9.50	7.34E-04	7.44E-04	7.90E-04
9.75	6.33E-02	6.43E-02	6.90E-02

Source: DTN: MO0702PAFLUORI.000_R1 [DIRS 181219], Table 2.

NOTE: These multiplication factors are implemented in the TSPA-SEIS as parameters Pu_Glass_low_N, Pu_CSNF_High_N, Pu_CDSP_High_N.

Table 6.3.7-52. Multiplication Factor, N(pH), Used to Modify Fluoride Concentration Uncertainty Terms (ε_2) for Thorium

pH	Multiplication Factor for Fluoride Uncertainty		
	Glass, CSNF low, and CDSP low	CSNF high and CSNF invert	CDSP high and CDSP invert
3.25	1.00E+00	1.00E+00	1.00E+00
3.50	7.51E-02	1.01E-01	1.48E-01
3.75	2.70E-02	3.53E-02	4.75E-02
4.00	2.08E-02	2.74E-02	3.60E-02
4.25	1.76E-02	2.41E-02	3.19E-02
4.50	1.45E-02	2.15E-02	2.91E-02
4.75	1.05E-02	1.90E-02	2.67E-02
5.00	4.73E-03	1.59E-02	2.44E-02
5.25	8.99E-04	1.19E-02	2.17E-02
5.50	1.02E-04	6.88E-03	1.82E-02
5.75	1.04E-05	2.26E-03	1.32E-02
6.00	1.04E-06	3.40E-04	6.85E-03
6.25	1.03E-07	3.62E-05	1.77E-03
6.50	7.98E-09	3.65E-06	2.26E-04
6.75	0.00E-00	3.62E-07	2.34E-05
7.00	0.00E-00	3.25E-08	2.36E-06
7.25	0.00E-00	0.00E-00	2.63E-07
7.50	0.00E-00	4.33E-09	7.86E-08
7.75	0.00E-00	4.00E-08	1.08E-07
8.00	0.00E-00	1.73E-07	2.14E-07
8.25	2.87E-07	3.57E-07	3.72E-07
8.50	3.83E-07	5.08E-07	5.61E-07
8.75	5.11E-07	6.79E-07	7.91E-07
9.00	4.79E-07	8.28E-07	1.02E-06
9.25	7.98E-07	1.07E-06	1.42E-06
9.50	3.61E-05	5.21E-05	7.81E-05

Source: DTN: MO0702PAFLUORI.000_R1 [DIRS 181219], Table 12.

NOTE: These multiplication factors are implemented in the TSPA-SEIS as parameters Th_Glass_low_N, Th_CSNF_High_N, Th_CDSP_High_N.

Table 6.3.7-53. Uranium Solubility Look-Up Table (log[U], mg/L) for CSNF WPs Breached under Nominal Conditions or by Seismic Activity

pH	log fCO_2 (bars)							
	-1.5	-2.0	-2.5	-3.0	-3.5	-4.0	-4.5	-5.0
3.50	4.41E+00	4.41E+00	4.41E+00	4.41E+00	4.41E+00	4.41E+00	4.41E+00	4.41E+00
3.75	3.55E+00	3.55E+00	3.55E+00	3.55E+00	3.55E+00	3.55E+00	3.55E+00	3.55E+00
4.00	2.87E+00	2.87E+00	2.87E+00	2.87E+00	2.87E+00	2.87E+00	2.87E+00	2.87E+00
4.25	2.33E+00	2.33E+00	2.33E+00	2.33E+00	2.33E+00	2.33E+00	2.33E+00	2.33E+00
4.50	1.93E+00	1.92E+00	1.92E+00	1.92E+00	1.92E+00	1.92E+00	1.92E+00	1.92E+00
4.75	1.62E+00	1.60E+00	1.60E+00	1.59E+00	1.59E+00	1.59E+00	1.59E+00	1.59E+00
5.00	1.35E+00	1.32E+00	1.31E+00	1.31E+00	1.30E+00	1.30E+00	1.30E+00	1.30E+00
5.25	1.10E+00	1.03E+00	1.00E+00	9.95E-01	9.93E-01	9.92E-01	9.92E-01	9.91E-01
5.50	9.31E-01	7.65E-01	6.97E-01	6.74E-01	6.66E-01	6.63E-01	6.63E-01	6.62E-01
5.75	9.05E-01	6.19E-01	4.67E-01	4.07E-01	3.86E-01	3.79E-01	3.77E-01	3.76E-01
6.00	1.03E+00	6.26E-01	3.76E-01	2.51E-01	2.03E-01	1.87E-01	1.82E-01	1.80E-01
6.25	1.25E+00	7.58E-01	4.13E-01	2.07E-01	1.17E-01	8.36E-02	7.27E-02	6.92E-02
6.50	1.52E+00	9.60E-01	5.30E-01	2.48E-01	9.90E-02	3.93E-02	1.87E-02	1.19E-02
6.75	1.86E+00	1.21E+00	7.12E-01	3.53E-01	1.32E-01	3.21E-02	-4.74E-03	-1.71E-02
7.00	2.33E+00	1.51E+00	9.38E-01	5.01E-01	2.11E-01	5.47E-02	-8.42E-03	-3.04E-02
7.25	500	1.89E+00	1.20E+00	6.98E-01	3.34E-01	1.09E-01	6.00E-03	-3.21E-02
7.50	500	2.54E+00	1.52E+00	9.32E-01	4.92E-01	2.00E-01	4.29E-02	-2.10E-02
7.55	500	2.90E+00	1.60E+00	9.95E-01	5.39E-01	2.24E-01	5.35E-02	-1.69E-02
7.75	500	500	1.98E+00	1.21E+00	6.96E-01	3.26E-01	1.09E-01	7.58E-03
7.90	500	500	2.51E+00	1.42E+00	8.48E-01	4.32E-01	1.66E-01	3.59E-02
8.00	500	500	500	1.58E+00	9.38E-01	4.97E-01	2.12E-01	6.04E-02
8.25	500	500	500	2.27E+00	1.24E+00	7.07E-01	3.47E-01	1.45E-01
8.30	500	500	500	2.58E+00	1.33E+00	7.66E-01	3.88E-01	1.66E-01
8.50	500	500	500	500	1.73E+00	9.65E-01	5.26E-01	2.59E-01
8.65	500	500	500	500	2.31E+00	1.19E+00	6.64E-01	3.56E-01
8.75	500	500	500	500	500	1.34E+00	7.47E-01	4.16E-01
9.00	500	500	500	500	500	2.11E+00	1.04E+00	6.11E-01
9.07	500	500	500	500	500	2.67E+00	1.18E+00	6.84E-01
9.25	500	500	500	500	500	500	1.58E+00	8.56E-01
9.50	500	500	500	500	500	500	500	1.24E+00
9.75	500	500	500	500	500	500	500	2.08E+00

Source: DTN: MO0702PADISCON.001_R0 [DIRS 179358], Table 4.

NOTE: This look-up table is implemented in the TSPA-SEIS as parameter Sol_U_LUT_Schoepite_CSNF. Entries reported as "500" in the table indicate conditions for which a valid solubility value does not exist.

Table 6.3.7-54. Uncertainty in Log K Values for Base-Case Uranium Solubility Model (CSNF WP Nominal and Seismic Scenario Classes)

TSPA-SEIS Name	Model Abstraction Symbol	Description	Units	Distribution Type	Distribution Specification
U_Eps_1_low_Nominal_a	ε_1	Uncertainties in log K (schoepite) below 1 molal ionic strength	None	Truncated normal	$\mu = 0$ $\sigma = 0.5$ $2\sigma = \pm 1.0$
U_Eps_1_high_Nominal_a	ε_1	Uncertainties in log K (schoepite) at 1 to 3 molal ionic strength	None	Truncated normal	$\mu = 0$ $\sigma = 0.6$ $2\sigma = \pm 1.2$
U_Eps_2_CSNF_Low_Nomina_a	$\varepsilon_2^{\text{CSNF-low}}$	Fluoride Uncertainty, CSNF waste packages when I < 0.2m.	None	Triangular	Min = 0 Max = 78 Most likely = 0
U_Eps_2_CSNF_High_Nominal_a	$\varepsilon_2^{\text{CSNF-high}}$ $\varepsilon_2^{\text{CSNF-invert}}$	Fluoride Uncertainty, CSNF waste packages when I ≥ 0.2m	None	Triangular	Min = 0 Max = 1361 Most likely = 0

Source: DTN: MO0702PADISCON.001_R0 [DIRS 179358], Table 19;
DTN: MO0702PAFLUORI.000_R1 [DIRS 181219], Table 7.

Table 6.3.7-55. Multiplication Factor, N(pH), Used to Modify Fluoride Concentration Uncertainty Terms (ε_2) for Uranium (CSNF WP, Nominal and Seismic Scenario Classes)

pH	Multiplication Factor for Fluoride Uncertainty	
	CSNF low	CSNF high
3.50	1.00E+00	1.00E+00
3.75	7.24E-01	7.03E-01
4.00	5.17E-01	4.85E-01
4.25	4.18E-01	3.73E-01
4.50	3.48E-01	2.99E-01
4.75	2.70E-01	2.41E-01
5.00	1.85E-01	1.92E-01
5.25	1.06E-01	1.45E-01
5.50	4.86E-02	9.86E-02
5.75	1.83E-02	5.67E-02
6.00	6.17E-03	2.63E-02
6.25	1.99E-03	1.01E-02
6.50	6.31E-04	3.42E-03
6.75	1.94E-04	1.11E-03
7.00	5.00E-05	3.49E-04
7.25	0.00E-00	1.07E-04
7.50	0.00E-00	4.64E-05
7.75	0.00E-00	1.67E-04
8.00	0.00E-00	2.01E-03
8.25	2.44E-02	2.51E-02

Source: DTN: MO0702PAFLUORI.000_R1 [DIRS 181219], Table 8.

NOTE: This multiplication factor is implemented in the TSPA-SEIS as parameters U_CSNF_Low_Nominal_N and U_CSNF_High_Nominal_N.

Table 6.3.7-56. Schoepite Controlled Uranium Solubility Look-Up Table (log[U], mg/L) for CDSP WPs Breached Under any Scenario, CSNF WPs Breached in by an Igneous Intrusion, and in the Invert (all locations and scenarios)

	log fco_2 (bars)							
pH	-1.50	-2.00	-2.50	-3.00	-3.50	-4.00	-4.50	-5.00
3.50	4.41E+00	4.41E+00	4.41E+00	4.41E+00	4.41E+00	4.41E+00	4.41E+00	4.41E+00
3.75	3.55E+00	3.55E+00	3.55E+00	3.55E+00	3.55E+00	3.55E+00	3.55E+00	3.55E+00
4.00	2.86E+00	2.86E+00	2.86E+00	2.86E+00	2.86E+00	2.86E+00	2.86E+00	2.86E+00
4.25	2.33E+00	2.33E+00	2.33E+00	2.33E+00	2.33E+00	2.33E+00	2.33E+00	2.33E+00
4.50	1.92E+00	1.91E+00	1.91E+00	1.91E+00	1.91E+00	1.91E+00	1.91E+00	1.91E+00
4.75	1.61E+00	1.59E+00	1.59E+00	1.59E+00	1.59E+00	1.59E+00	1.59E+00	1.59E+00
5.00	1.34E+00	1.31E+00	1.30E+00	1.30E+00	1.30E+00	1.30E+00	1.30E+00	1.30E+00
5.25	1.10E+00	1.02E+00	9.94E-01	9.85E-01	9.83E-01	9.82E-01	9.81E-01	9.81E-01
5.50	9.24E-01	7.55E-01	6.86E-01	6.62E-01	6.54E-01	6.51E-01	6.51E-01	6.50E-01
5.75	9.10E-01	6.11E-01	4.57E-01	3.94E-01	3.73E-01	3.66E-01	3.64E-01	3.63E-01
6.00	1.04E+00	6.30E-01	3.68E-01	2.41E-01	1.92E-01	1.75E-01	1.70E-01	1.68E-01
6.25	1.25E+00	7.66E-01	4.09E-01	2.01E-01	1.09E-01	7.55E-02	6.43E-02	6.08E-02
6.50	1.52E+00	9.70E-01	5.37E-01	2.45E-01	9.45E-02	3.42E-02	1.33E-02	6.55E-03
6.75	1.86E+00	1.22E+00	7.22E-01	3.52E-01	1.30E-01	2.93E-02	-7.88E-03	-2.03E-02
7.00	2.33E+00	1.51E+00	9.48E-01	5.09E-01	2.10E-01	5.32E-02	-1.02E-02	-3.22E-02
7.25		1.89E+00	1.21E+00	7.08E-01	3.34E-01	1.08E-01	5.05E-03	-3.31E-02
7.50		2.54E+00	1.53E+00	9.44E-01	5.01E-01	2.00E-01	4.24E-02	-2.16E-02
7.75			1.98E+00	1.22E+00	7.07E-01	3.33E-01	1.09E-01	7.28E-03
8.00				1.57E+00	9.51E-01	5.06E-01	2.12E-01	6.02E-02

Source: DTN: MO0702PADISCON.001_R0 [DIRS 179358], Table 5.

NOTE: This look-up table is implemented in the TSPA-SEIS as parameter Sol_U_LUT_Schoepite. This solubility corresponds to schoepite saturation. The shaded area indicates the region where it is uncertain if uranium solubility is controlled by schoepite or Na-Boltwoodite.

Table 6.3.7-57. Na-Boltwoodite and $Na_4UO_2(CO_3)_3$ Controlled Uranium Solubility Look-Up Table (log[U], mg/L) for CDSP WPs Breached under Any Scenario, CSNF WPs Breached by an Igneous Intrusion, and in the Invert (all locations and scenarios)

	log fco_2 (bars)							
pH	-1.50	-2.00	-2.50	-3.00	-3.50	-4.00	-4.50	-5.00
6.50	2.56E+00							
6.75	2.16E+00	2.00E+00	1.51E+00	1.07E+00	7.46E-01	5.56E-01	4.73E-01	4.43E-01
7.00	1.94E+00	1.82E+00	1.28E+00	8.21E-01	4.79E-01	2.77E-01	1.88E-01	1.56E-01
7.25	2.14E+00	1.51E+00	1.09E+00	5.88E-01	2.28E-01	2.04E-02	-7.08E-02	-1.04E-01
7.50	2.79E+00	1.55E+00	1.03E+00	3.97E-01	-9.31E-03	-2.29E-01	-3.23E-01	-3.56E-01
7.75	4.78E+00	1.98E+00	1.03E+00	3.18E-01	-2.14E-01	-4.68E-01	-5.67E-01	-6.01E-01
8.00	4.78E+00	2.76E+00	1.34E+00	4.67E-01	-3.27E-01	-6.84E-01	-8.00E-01	-8.35E-01
8.25	4.78E+00	4.78E+00	1.92E+00	7.59E-01	-2.27E-01	-8.41E-01	-1.01E+00	-1.05E+00
8.50	4.78E+00	4.78E+00	2.75E+00	1.25E+00	1.67E-01	-8.36E-01	-1.19E+00	-1.25E+00
8.75	4.78E+00	4.78E+00	4.77E+00	1.89E+00	6.32E-01	-5.27E-01	-1.27E+00	-1.41E+00
9.00	4.78E+00	4.78E+00	4.77E+00	2.75E+00	1.20E+00	3.81E-02	-1.13E+00	-1.51E+00
9.25	4.78E+00	4.78E+00	4.77E+00	4.76E+00	1.88E+00	5.47E-01	-6.60E-01	-1.51E+00
9.50	4.78E+00	4.78E+00	4.77E+00	4.76E+00	2.78E+00	1.15E+00	-9.89E-02	-1.26E+00
9.75	4.78E+00	4.78E+00	4.77E+00	4.76E+00	4.73E+00	1.89E+00	4.56E-01	-7.58E-01
10.00	4.78E+00	4.78E+00	4.77E+00	4.76E+00	4.73E+00	2.92E+00	1.13E+00	-2.57E-01
10.25	500	500	500	500	500	500	2.02E+00	3.92E-01

Source: DTN: MO0702PADISCON.001_R0 [DIRS 179358] Table 6.

NOTE: This look-up table is implemented in the TSPA-SEIS as parameter Sol_U_LUT_Boltwoodite. The upper shaded area indicates the region where it is uncertain if uranium solubility is controlled by schoepite or Na-Boltwoodite saturation. The lower shaded area is where solubility is controlled by $Na_4UO_2(CO_3)_3$. Entries reported as "500" indicate conditions for which a valid solubility value does not exist.

Table 6.3.7-58. Uncertainty in Uranium Solubility Model in CDSP WPs Breached Under Any Scenario, CSNF WPs Breached by an Igneous Intrusion, and in the Invert (all locations and scenarios)

TSPA-SEIS Name	Model Abstraction Symbol	Description	Units	Distribution Type	Distribution Specification
U_Eps_1_low_other_a	ε_1	Uncertainties in solubility (schoepite and Na-Boltwoodite) below 1 molal ionic strength; to be used in the colorless and shaded regions in Table 6.3.7-37 and upper shaded region in Table 6.3.7-38	None	Truncated normal	$\mu = 0$ $\sigma = 0.5$ $2\sigma = \pm 1.0$
U_Eps_1_high_other_a	ε_1	Uncertainties in solubility (schoepite and Na-Boltwoodite) at 1 to 3 molal ionic strength; uncertainties in log K ($Na_4UO_2(CO_3)_3$) below 3 molal ionic strength (blue regions in Table 6.3.7-38)	None	Truncated normal	$\mu = 0$ $\sigma = 0.6$ $2\sigma = \pm 1.2$
U_Eps_2_Schoepite_Glass_Low_a	$\varepsilon_2^{\text{CSNF-low}}$ $\varepsilon_2^{\text{CDSP-Glass}}$ $\varepsilon_2^{\text{CDSP-F-low}}$	Fluoride uncertainty, CSNF waste packages when I < 0.2m. CDSP packages, Cell 1b when I < 0.004m and Cell 1a.	None	Triangular	Min = 0 Max = 78 Most likely = 0
U_Eps_2_Schoepite_CSNF_High_a	$\varepsilon_2^{\text{CSNF-high}}$ $\varepsilon_2^{\text{CSNF-invert}}$	Fluoride uncertainty, CSNF waste packages when I ≥ 0.2m and invert below CSNF waste packages	None	Triangular	Min = 0 Max = 1361 Most likely = 0
U_Eps_2_Schoepite_CDSP_High_a	$\varepsilon_2^{\text{CDSP-F-high}}$ $\varepsilon_2^{\text{CDSP-invert}}$	Fluoride uncertainty, CDSP waste packages when I ≥ 0.004m and invert below CDSP waste packages	None	Triangular	Min = 0 Max = 5385 Most likely = 0
U_Eps_2_Boltwoodite_Glass_Lo_a	$\varepsilon_2^{\text{CSNF-high}}$ $\varepsilon_2^{\text{CSNF-invert}}$	Fluoride uncertainty, CSNF waste packages when I < 0.2m. CDSP packages, Cell 1b when I < 0.004m and Cell 1a.	None	Triangular	Min = 0 Max = 6.13 Most likely = 0
U_Eps_2_Boltwoodite_CSNF_Hig_a	$\varepsilon_2^{\text{CSNF-high}}$ $\varepsilon_2^{\text{CSNF-invert}}$	Fluoride uncertainty, CSNF waste packages when I ≥ 0.2m and invert below CSNF waste packages	None	Triangular	Min = 0 Max = 57.01 Most likely = 0
U_Eps_2_Boltwoodite_CDSP_Hig_a	$\varepsilon_2^{\text{CDSP-F-high}}$ $\varepsilon_2^{\text{CDSP-invert}}$	Fluoride uncertainty, CDSP waste packages when I ≥ 0.004m and invert below CDSP waste packages	None	Triangular	Min = 0 Max = 272.3 Most likely = 0
Schoepite_Boltwoodite_Interp_a	N/A	Used in the TSPA-SEIS to determine the fractional value that is used to interpolate between schoepite and Na-Boltwoodite look-up tables	None	Uniform	Min. = 0 Max = 1

Source: DTN: MO0702PADISCON.001_R0 [DIRS 179358], Table 19, MO0702PAFLUORI.000_R1 [DIRS 181219], Table 9.

NOTE: The parameter Schoepite_Boltwoodite_Interp_a was developed by TSPA based on information given in notes to Table 6 of DTN: MO0702PADISCON.001_R0 [DIRS 179358].

Table 6.3.7-59. Multiplication Factor, N(pH), Used to Modify Fluoride Concentration Uncertainty Terms (ε_2) for Uranium in CDSP WPs Breached under Any Scenario, CSNF Waste Packages Breached by an Igneous Intrusion and in the Invert (all locations and scenarios)

Glass, CSNF low, and CDSP low			CSNF high and CSNF invert			CDSP high and CDSP invert		
pH	**Schoepite**	**Boltwoodite-Na**	**pH**	**Schoepite**	**Boltwoodite-Na**	**pH**	**Schoepite**	**Boltwoodite-Na**
3.50	1.00E+00		**3.50**	1.00E+00		**3.50**	1.00E+00	
3.75	7.24E-01		**3.75**	7.03E-01		**3.75**	6.68E-01	
4.00	5.17E-01		**4.00**	4.85E-01		**4.00**	4.44E-01	
4.25	4.18E-01		**4.25**	3.73E-01		**4.25**	3.34E-01	
4.50	3.48E-01		**4.50**	2.99E-01		**4.50**	2.73E-01	
4.75	2.70E-01		**4.75**	2.41E-01		**4.75**	2.31E-01	
5.00	1.85E-01		**5.00**	1.92E-01		**5.00**	1.98E-01	
5.25	1.06E-01		**5.25**	1.45E-01		**5.25**	1.68E-01	
5.50	4.86E-02		**5.50**	9.86E-02		**5.50**	1.36E-01	
5.75	1.83E-02		**5.75**	5.67E-02		**5.75**	1.03E-01	
6.00	6.17E-03		**6.00**	2.63E-02		**6.00**	6.91E-02	
6.25	1.99E-03		**6.25**	1.01E-02		**6.25**	3.93E-02	
6.50	6.32E-04	6.36E-02	**6.50**	3.42E-03	3.62E-01	**6.50**	1.81E-02	1.00E+00
6.75	1.95E-04	1.89E-02	**6.75**	1.11E-03	7.86E-02	**6.75**	6.90E-03	3.30E-01
7.00	4.87E-05	7.98E-03	**7.00**	3.48E-04	1.79E-02	**7.00**	2.36E-03	7.49E-02
7.25	0.00E-00	4.36E-03	**7.25**	1.07E-04	5.52E-03	**7.25**	7.96E-04	1.55E-02
7.50	0.00E-00	3.13E-03	**7.50**	4.58E-05	2.88E-03	**7.50**	3.34E-04	4.08E-03
7.75	0.00E-00	3.82E-03	**7.75**	1.64E-04	3.25E-03	**7.75**	4.02E-04	2.75E-03
8.00	0.00E-00	9.87E-03	**8.00**	1.98E-03	8.60E-03	**8.00**	2.13E-03	6.92E-03
8.25	2.44E-02	4.89E-02	**8.25**	2.50E-02	2.56E-02	**8.25**	2.90E-02	1.93E-02
8.50		9.10E-02	**8.50**		6.80E-02	**8.50**		5.55E-02
8.75		2.40E-01	**8.75**		2.17E-01	**8.75**		1.82E-01
9.00		1.00E+00	**9.00**		1.00E+00	**9.00**		8.43E-01

Source: DTN: MO0702PAFLUORI.001_R1 [DIRS 181219], Table 10.

NOTE: These multiplication factors are implemented in the TSPA-SEIS as parameters: U_Schoepite_Glass_low_N, U_Schoepite_CSNF_High_N, U_Schoepite_CDSP_High_N, U_Boltwoodite_Glass_low_N, U_Boltwoodite_CSNF_High_N, and U_Boltwoodite_CDSP_High_N.

Table 6.3.7-60. Actinide Caps (mg/L) Between an Ionic Strength of 3 and 10 Molal for CSNF Packages

Controlling solid	Element	IS = 3	IS = 7	IS= 10
PuO_2 (hyd,aged)	Pu	39487	92135	131622
NpO_2	Np	981	2289	3270
Np_2O_5	Np	1417	3306	4723
Schoepite	U	29698	69294	98992
ThO_2 (am)	Th	1400	3266	4666
$AmOHCO_3$	Am	1285	2999	4285
Np_2O_5 (by analog)	Pa	1417	3306	4723

NOTE: IS = ionic strength in units of molal

Source: DTN: MO0704PASOLCAP.000_R0 [DIRS 180389], Table 2.

NOTE: These caps are implemented in the TSPA-SEIS as parameters: CSNF_Pu_TypeIII_Cap, CSNF_NpO2_TypeIII_Cap, CSNF_Np2O5_TypeIII_Cap, CSNF_U_Scheopite_TypeIII_Cap, CSNF_Th_TypeIII_Cap, CSNF_Am_TypeIII_Cap, CSNF_Pa_TypeIII_Cap

Table 6.3.7-61. Actinide Caps (mg/L) Between an Ionic Strength of 3 and 10 Molal for CDSP Packages, Cell 1b

Controlling solid	Element	IS = 3	IS = 7	IS= 10
PuO_2 (hyd,aged)	Pu	39487	92135	131622
NpO_2	Np	981	2289	3270
Np_2O_5	Np	1417	3306	4723
Schoepite*	U	29698	69294	98992
Na-Boltwoodite*	U	33636	61967	88524
ThO_2 (am)	Th	1400	3266	4666
$AmOHCO_3$	Am	1285	2999	4285
Np_2O_5 (by analog)	Pa	1417	3306	4723

Source: DTN: MO0704PASOLCAP.000_R0 [DIRS 180389], Table 2.

NOTE: These caps are implemented in the TSPA-SEIS as parameters: CDSP_Pu_TypeIII_Cap, CDSP_NpO2_TypeIII_Cap, CDSP_Np2O5_TypeIII_Cap, CDSP_U_Scheopite_TypeIII_Cap, CDSP_U_Boltwoodite_TypeIII_Cap, CDSP_Th_TypeIII_Cap, CDSP_Am_TypeIII_Cap, CDSP_Pa_TypeIII_Cap.

When sampling between the schoepite and boltwoodite LUTs, use the schoepite values.

IS = ionic strength (molal).

Table 6.3.7-62. Parameters for TSPA-SEIS Glass Waste Form Colloid Abstraction

Parameter Name	Model Abstraction Symbol	Description	Units	Distribution Type	Distribution Specification
DTN: MO0701PAGLASWF.000					
CPu_Col_Wf_Embed_Sampled_a	$C_{RNcoll,DHLWG,}$	Concentration of irreversibly attached plutonium, associated with DHLWG colloids	mol/L	Uniform	1.E-11 to 1.E-8
CPu_Col_Glass_Embed_Min	$C_{RNcoll,DHLWG,}$	Lowest observed or expected concentration of irreversibly attached plutonium associated with DHLWG colloids	mol/L	Deterministic	1.E-13
CPu_Per_WF_Embed_Col_a	$C_{coll,DHLWG,sample}$	Concentration of irreversibly attached plutonium per concentration of colloids	(mol/L) /(mg/L)	Triangular Distribution	min 5×10^{-9} Mode 2×10^{-8} Max 2.5×10^{-8}
Smectite_ZPC	—	Smectite zero point of charge, pH below which the smectite does not sorb	No units	Deterministic	1.5
Smectite_pH_hi	—	High pH for smectite ionic strength threshold fit	No units	Deterministic	9
Coeff_pH_Sq_Smectite	—	Coefficient of pH squared term for fit of ionic strength threshold for smectite colloid stability	No units	Deterministic	-0.008
Coeff_pH_Smectite	—	Coefficient of pH term for fit of ionic strength threshold for smectite colloid stability	No units	Deterministic	0.12
Coeff_inter_Smectite	—	Intercept term for fit of ionic strength threshold for smectite colloid stability	No units	Deterministic	0.03
Specific _SA_Smectite_Col_a	SA, Smectite, coll	Specific surface area for DHLWG (smectite) colloid	M2/g	Uniform	10 to 100

Table 6.3.7-62. Parameters for TSPA-SEIS Glass Waste Form Colloid Abstraction (Continued)

Parameter Name	Model Abstraction Symbol	Description	Units	Distribution Type	Distribution Specification	
Smectite_Site_Density	NS, Smectite, coll	Site density for DHLWG (smectite) colloid	Sites/ nm^2	Deterministic	2.3	
DTN: MO0701PASORPTN.000						
Kd_Pu_Rev_Smectite_a	$K_{d,Pu,coll,wf}$	Distribution coefficient for reversible sorption of plutonium to smectite colloids	mL/g	Cumulative Distribution Function	Prob Level	Value
					0	1×10^3
					0.45	5×10^3
					0.80	1×10^4
					0.95	5×10^4
					1	1×10^5
Kd_Am_Rev_Smectite_a Kd_Th_Rev_Smectite_a Kd_Pa_Rev_Smectite_a	$K_{d,Am,coll,wf}$ $K_{d,Th,coll,wf}$ $K_{d,Pa,coll,wf}$	Distribution coefficient for reversible sorption of americium, thorium, and protactinium to smectite colloids	mL/g	Cumulative Distribution Function	Prob Level	Value
					0	1×10^4
					0.07	5×10^4
					0.17	1×10^5
					0.4	5×10^5
					0.6	1×10^6
					0.92	5×10^6
					1	1×10^7
Kd_Cs_Rev_Smectite_a	$K_{d,Cs,coll,wf}$	Distribution coefficient for reversible sorption of cesium to smectite colloids	mL/g	Cumulative Distribution Function	Prob Level	Value
					0	5×10^1
					0.05	1×10^2
					0.4	5×10^2
					0.7	1×10^3
					1	5×10^3
DTN: MO0701PAKDSUNP.000						
Kd_Np_Rev_Smectite_a	$K_{d,Np,coll,Smect}$	Distribution coefficient for reversible sorption of neptunium to smectite colloids	mL/g	Log Uniform	1×10^1 to 5×10^2	
Kd_U_Rev_Smectite_a	$K_{d,U,coll,Smectit}$	Distribution coefficient for reversible sorption of tin to smectite colloids	mL/g	Log Uniform	5×10^2 to 5×10^4	

Table 6.3.7-62. Parameters for TSPA-SEIS Glass Waste Form Colloid Abstraction (Continued)

Parameter Name	Model Abstraction Symbol	Description	Units	Distribution Type	Distribution Specification
Kd_Sn_Rev_Smectite_a	$K_{d,Sn,coll,Smecti}$	Distribution coefficient for reversible sorption of uranium to smectite colloids	mL/g	Log Uniform	1×10^5 to 1×10^6
Kd_Ra_Rev_Smectite_a	$K_{d,Ra,coll,Smecti}$	Distribution coefficient for reversible sorption of radium to smectite colloids	mL/g	Log Uniform	1×10^2 to 5×10^3

Sources: DTN: MO0701PAGLASWF.000_R1 [DIRS 180393]; DTN: MO0701PASORPTN.000_R1 [DIRS 180391]; DTN: MO0701PAKDSUNP.000_R1 [DIRS 180392].

Table 6.3.7-63. Parameters for TSPA-SEIS CSNF Waste Form Irreversible Colloid Abstraction

Parameter Name	Model Abstraction Symbol	Description	Units	Distribution Type	Distribution Specification	
CPu_Col_CSNF_Sampled_a	$C_{RNcoll,SNF,embed,}$	Concentration of irreversibly attached radionuclide element RN (plutonium, americium) associated with SNF colloids	mol/L	Cumulative Distribution Function	Prob Level	Value
					0	1×10^{-10}
					0.05	5×10^{-10}
					0.1	1×10^{-9}
					0.15	5×10^{-9}
					0.2	1×10^{-8}
					0.3	5×10^{-8}
					0.5	1×10^{-7}
					0.7	5×10^{-7}
					0.9	1×10^{-6}
					1	5×10^{-6}
CPu_Col_CSNF_Min	$C_{RNcoll,SNF,\min}$	Lowest observed or expected concentration of irreversibly attached plutonium associated with DHLWG colloids	Mol/L	Deterministic	1.E-13	
CPu_Per_CSNF_Embed_Col_a	$C_{coll,SNF,uniform}$	Concentration of Irreversibly attached plutonium per concentration of CSNF colloids	(mol/L) /(mg/L)	Uniform Distribution	Min 5×10^{-7} Max 1×10^{-6}	
CSNF_pH_lo	—	Lower limit of pH range for CSNF colloid stability data	No units	Deterministic	4	
CSNF_ZPC_lo	—	Lower limit of pH range for zero point of charge for CSNF colloid stability data	No units	Deterministic	7	
CSNF_ZPC_hi	—	Upper limit of pH range for zero point of charge for CSNF colloid stability data	No units	Deterministic	9.3	
CSNF_pH_hi	—	Upper limit of pH range for CSNF colloid stability data	No units	Deterministic	10.6	
Coeff_pH_Cube_lo_CSNF	—	Coefficient of pH cubed term for fit of ionic strength threshold for CSNF colloid stability at low pH	No units	Deterministic	0.0089	

Table 6.3.7-63. Parameters for TSPA-SEIS CSNF Waste Form Irreversible Colloid Abstraction (Continued)

Parameter Name	Model Abstraction Symbol	Description	Units	Distribution Type	Distribution Specification
Coeff_pH_Sq_lo_CSNF	—	Coefficient of pH squared term for fit of ionic strength threshold for CSNF colloid stability at low pH	No units	Deterministic	−0.1466
Coeff_pH_lo_CSNF	—	Coefficient of pH term for fit of ionic strength threshold for CSNF colloid stability at low pH	No units	Deterministic	0.7462
Coeff_inter_pH_lo_CSNF	—	Coefficient of intercept term for fit of ionic strength threshold for CSNF colloid stability at low pH	No units	Deterministic	−1.092
Coeff_pH_Cube_hi_CSNF	—	Coefficient of pH cubed term for fit of ionic strength threshold for CSNF colloid stability at high pH	No units	Deterministic	0.087362
Coeff_pH_Sq_hi_CSNF	—	Coefficient of pH squared term for fit of ionic strength threshold for CSNF colloid stability at high pH	No units	Deterministic	−2.4078
Coeff_pH_hi_CSNF	—	Coefficient of pH term for fit of ionic strength threshold for CSNF colloid stability at high pH	No units	Deterministic	22.126
Coeff_inter_pH_hi_CSNF	—	Coefficient of intercept term for fit of ionic strength threshold for CSNF colloid stability at high pH	No units	Deterministic	−67.791

Source: DTN: MO0701PACSNF.000_R1 [DIRS 180439].

Table 6.3.7-64. Parameters for TSPA-SEIS SNF Waste Form Reversible Colloid Abstraction

Parameter Name	Model Abstraction Symbol	Description	Units	Distribution Type	Distribution Specification	
Conc_Col_U_Sampled_a	$m_{coll,Uranophane}$	Expected mass of uranophane colloids per unit volume or mass of water	mg/L	Cumulative Distribution Function	Prob Level	Value
					0	1×10^{-3}
					0.5	1×10^{-1}
					0.75	1×10^{0}
					0.90	1×10^{1}
					0.98	5×10^{1}
					1	2×10^{2}
Conc_Col_U_Min	$m_{coll,Uranophane}$	Lowest observed or expected mass of uranophane colloids per unit volume or mass of water	mg/L	Deterministic	1×10^{-6}	
U_pH_lo	—	Lower limit of pH range for U colloid stability data	No units	Deterministic	4	
U_pH_hi	—	Upper limit of pH range for U colloid stability data	No units	Deterministic	9	
Coeff_pH_Sq_U	—	Coefficient of pH squared term for fit of ionic strength threshold for U colloid stability	No units	Deterministic	−0.008	
Coeff_pH_U	—	Coefficient of pH term for fit of ionic strength threshold for U colloid stability	No units	Deterministic	0.14	
Coeff_inter_U	—	Coefficient of intercept term for fit of ionic strength threshold for U colloid stability	No units	Deterministic	0.4	
Kd_Pu_Rev_U_Col_a	Kd,Pucoll,uranophane	Distribution coefficient for reversible sorption of plutonium onto uranophane colloids	mL/g	Log Uniform	5×10^{0} to 1×10^{4}	
Kd_Am_Rev_U_Col _a	Kd,Amcoll,uranophane	Distribution coefficient for reversible sorption of americium onto uranophane colloids	mL/g	Log Uniform	5×10^{0} to 1×10^{4}	
Kd_Th_Rev_U_Col _a	Kd,Thcoll,uranophane	Distribution coefficient for reversible sorption of thorium onto uranophane colloids	mL/g	Log Uniform	5×10^{0} to 1×10^{4}	

Table 6.3.7-64. Parameters for TSPA-SEIS SNF Waste Form Reversible Colloid Abstraction (Continued)

Parameter Name	Model Abstraction Symbol	Description	Units	Distribution Type	Distribution Specification
Kd_Pa_Rev_U_Col _a	Kd,Pacoll,uranophane	Distribution coefficient for reversible sorption of Pa onto uranophane colloids	mL/g	Log Uniform	5×10^0 to 1×10^4
Kd_Cs_Rev_U_Col _a	Kd,Cscoll,uranophane	Distribution coefficient for reversible sorption of cesium onto uranophane colloids	mL/g	Log Uniform	1×10^1 to 1×10^3
Kd_Np_Rev_U_Col _a	Kd,Npcoll,uranophane	Distribution coefficient for reversible sorption of neptunium onto uranophane colloids	mL/g	Log Uniform	1×10^1 to 5×10^2
Kd_Ra_Rev_U_Col _a	Kd,Racoll,uranophane	Distribution coefficient for reversible sorption of radium onto uranophane colloids	mL/g	Log Uniform	1×10^1 to 1×10^3
Kd_Sn_Rev_U_Col _a	Kd,Sncoll,uranophane	Distribution coefficient for reversible sorption of tin onto uranophane colloids	mL/g	Log Uniform	1×10^0 to 1×10^2
Specific_SA_U_Col	$S_{A,\ uranophane,\ coll}$	Specific surface area for uranophane	m^2/g	Deterministic	30
U_Site_Density	$N_{S,uranophane,\ coll}$	Site density for uranophane particle colloid	Sites/ nm^2	Deterministic	2

Source: DTN: MO0701PACSNF.000_R1 [DIRS 180439].

Table 6.3.7-65 Parameters for TSPA-SEIS Iron Oxyhydroxide Colloid Abstraction

Parameter Name	Model Abstraction Symbol	Description	Units	Distribution Type	Distribution Specification
Conc_Col_FeOx_Min	$m_{coll,FeOx,\min}$	Minimum concentration of FeOx colloids	mg/L	Deterministic	1×10^{-6}
Conc_Col_FeOx_CS_Sampled_a		Sampled FeOX colloid concentration when carbon steel is degrading	mg/L	Log Normal	Mean = 03.69 Standard deviation = 2.79
Conc_Col_FeOx_SS_Sampled_a	$m_{coll,FeOx,sampled}$	Sampled FeOX colloid concentration for locations containing degraded stainless steel	mg/L	Cumulative Distribution Function	Prob Level / Value 0 / 1×10^{-3} 0.6 / 1×10^{-1} 0.90 / 1×10^{0} 0.95 / 1×10^{1} 1 / 3×10^{1}
FeOx_pH_lo		Low pH for FeOx colloid ionic strength threshold fit	No units	Deterministic	4.5
FeOx_ZPC_lo		Low end of zero point of charge range	No units	Deterministic	8.4
FeOx_ZPC_hi		Low end of zero point of charge range	No units	Deterministic	9.4
FeOx_pH_hi	—	Low pH for FeOx colloid ionic strength threshold fit	No units	Deterministic	10.4
Coeff_pH_lo_FeOx	—	Coefficient of pH term for fit of ionic strength threshold for FeOx colloid stability at low pH	No units	Deterministic	−0.013
Coeff_Inter_pH_lo_FeOx	—	Intercept term for fit of ionic strength threshold for FeOx colloid stability at low pH	No units	Deterministic	0.11
Coeff_pH_sq_hi_FeOx	—	Coefficient of pH squared term for fit of ionic strength threshold for FeOx colloid stability at high pH	No units	Deterministic	0.0017
Coeff_pH_hi_FeOx	—	Coefficient of pH term for fit of ionic strength threshold for FeOx colloid stability at high pH	No units	Deterministic	−0.0327
Coeff_inter_pH_hi_FeOx	—	Intercept term for fit of ionic strength threshold for FeOx colloid stability at high pH	No units	Deterministic	0.158

Table 6.3.7-65. Parameters for TSPA-SEIS Iron Oxyhydroxide Colloid Abstraction (Continued)

Parameter Name	Model Abstraction Symbol	Description	Units	Distribution Type	Distribution Specification
Min_Default_Fwd_Rate_Const	k	Minimum value for the log uniform default forward rate constant	m^3/m^2, yr	Log uniform	0.002
Max_Default_Fwd_Rate_Const	k	Maximum value for the log uniform default forward rate constant	m^3/m^2, yr	Log uniform	0.05
Target_Flux_Out_Ratio_a	F_{RN}	Target-flux out ratio: ratio of radionuclide mass associated with colloids (reversible and irreversible) to radionuclide mass associated with colloids and dissolved radionuclide mass	No units	Uniform	Min = 0.9 Max = 0.99

Source: DTN: MO0701PAIRONCO.000 [DIRS 180440].

Table 6.3.7-66 Parameters for TSPA-SEIS Groundwater Colloid Abstraction

Parameter Name	Model Abstraction Symbol	Description	Units	Distribution Type	Distribution Specification	
M_Col_GW_Minimum	$m_{coll,gw,\min}$	Minimum GW colloid concentration	mg/L	Deterministic	1×10^{-6}	
M_Col_GW_Sampled_a	$m_{coll,gw,sampled}$	Sampled GW colloid concentration	mg/L	Cumulative Distribution Function	Prob Level	Value
					0	0.001
					0.5	0.1
					0.75	1
					0.9	10
					0.98	50
					1	200
Kd_Pu_Rev_Smectite_a Kd_Am_Rev_Smectite_a Kd_Th_Rev_Smectite_a Kd_Pa_Rev_Smectite_a Kd_Cs_Rev_Smectite_a Kd_Np_Rev_Smectite_a Kd_U_Rev_Smectite_a Kd_Sn_Rev_Smectite_a Kd_Ra_Rev_Smectite_a	see Table 6.3.7-63	see Table 6.3.7-63	mL/g	see Table 6.3.7-63	see Table 6.3.7-63	
Smectite_ZPC Smectite_ph_hi Coeff_pH_Sq_Smectite Coeff_pH_Smectite Coeff_Inter_Smectite		See Table 6.3.7-63	No units	Deterministic	See Table 6.3.7-63	

Source: DTN: MO0701PAGROUND.000 [DIRS 179310].

Table 6.3.7-67 Alternative Conceptual Models Considered for In-Package Chemistry

Alternative Conceptual Model	Key Assumptions	Screening Assessment and Basis
Alternative Conceptual Model I	The WP is compositionally discrete.	The WVC model showed that the resulting chemical effects of individual WP components were comparable to that of their ensembles. See Section 6.5.1 in *In-Package Chemistry Abstraction* (SNL 2007 [DIRS 180506]).
Alternative Conceptual Model II	The composition of seepage entering a WP is likely to vary as a function of changing conditions in the UZ and drift environments.	The SDM showed that wide compositional ranges in the seepage composition had very little influence on the resulting in-package chemistry. See Section 6.5.2 in *In-Package Chemistry Abstraction* (SNL 2007 [DIRS 180506]).

Source: *In-Package Chemistry Abstraction* (SNL 2007 [DIRS 180506], Table 6-14).

Table 6.3.7-68 Alternative Scientific Approaches Considered in Cladding Degradation

Alternative Conceptual Model	Key Assumptions	Screening Assessment and Basis
TSPA-SR Initial Cladding Failures	Addresses various causes of fuel failure.	Similar results to the current cladding degradation analysis.
Stainless-Steel-Clad Fuel Evenly Distributed	Stainless-steel-clad fuel evenly distributed in all WPs.	Even distribution unlikely. Not conservative.
Splitting – Dry Oxidation	UO_2 forms U_3O_8.	Unlikely, because it requires low humidity and high temperatures and produces instant splitting, as in the current cladding degradation analysis.

Source: *Cladding Degradation Summary for LA* (SNL 2007 [DIRS 180616], Table 6-5).

Table 6.3.7-69. Alternative Conceptual Models Considered for CSNF Waste Form Degradation

Alternative Conceptual Model	Key Assumptions	Screening Assessment and Basis
Electrochemical	The anodic Tafel lines can be extrapolated to the corrosion potential. The long-term corrosion behavior of commercial spent nuclear fuel is similar to that of unirradiated UO_2. Differences between the corrosion behavior of commercial spent nuclear fuel and unirradiated UO_2 are due to water radiolysis.	Do not incorporate into the TSPA-SEIS; data needed to apply the model can only be estimated. Use for Nominal Scenario Class model validation–particularly for validation of long-term extrapolation.
Surface Complexation Model	The overall rate of CSNF corrosion is controlled by the rate of surface complexation reactions. The long-term corrosion behavior of commercial spent nuclear fuel is similar to that of unirradiated UO_2.	Do not incorporate into TSPA-SEIS; data needed to apply the model can only be estimated from open literature. Use for Nominal Scenario Class model validation–particularly for validation of long-term extrapolation.

Source: Table 6-13 in *CSNF Waste Form Degradation: Summary Abstraction* (BSC 2004 [DIRS 169987]).

Table 6.3.7-70. Alternative Conceptual Models Considered for High-Level Radioactive Waste Glass Degradation

Alternative Conceptual Model	Key Concepts	Screening Assessment and Basis
Diffusion-Controlled Release	Release rate of radionuclides determined by solid-state diffusion rates.	Not incorporated into TSPA-SEIS. Not supported by data for waste glasses.
Composition-Independent Effective Rate Constant	Intrinsic rate constants vary over a small interval for different compositions and the very low flow rates in the repository compared to those used in the laboratory mean that the affinity term will be low.	Not incorporated into TSPA-SEIS. Current approach provides a much more robust range of values for use in the TSPA-SEIS.

Source: *Defense HLW Glass Degradation Model* (BSC 2004 [DIRS 169988], Table 6-2).

Table 6.3.7-71 Alternative Conceptual Models Considered for Dissolved Concentration Limits

Element	Alternative Conceptual Model	Model Basis	Screening Assessment and Basis
Plutonium	The theoretical fO_2 model	fO_2 = 0.2 bars.	The results of this model differ significantly from experimental measurements.
	The empirical Eh model	Eh = 1.04 – 0.0592*pH.	The results of this model are lower than experimental results.
Neptunium	Neptunium incorporation into uranyl secondary phases	Neptunium concentration controlled by solid solution rather than by pure phases.	Experimental studies on whether secondary uranyl phase can incorporate neptunium and immobilize it during spent nuclear fuel corrosion do not provide a solid basis for recommending this model to be used in the TSPA-SEIS.
Thorium	Solubility control by other thorium phases including ThO_2 (thorianite), $Th_{0.75}PO_4$, $Th(SO_4)_2$, ThF_4, $ThF_4 \cdot 2H_2O$	Solubility of thermodynamically most-stable phase controls concentrations	Solubilities calculated with ThO_2(am) are consistent with measured thorium solubility in pure water. Other phases may be less soluble only under certain conditions or may be based on questionable data.
Americium	Solubility control by phase with properties between $Am(OH)_3$(am) to $Am(OH)_3$	Initially formed $Am(OH)_3$(am) will invert to more stable $Am(OH)_3$ with time. $Am(OH)_3$ stability decreases with time from self irradiation.	$AmOHCO_3$ is formed in americium solubility experiments under Yucca Mountain conditions. Under some conditions, $Am(OH)_3$ may be less soluble, but choosing $AmOHCO_3$ is, generally, conservative.
Protactinium	Solubility is same as that of ThO_2(am)	Thorium is also a good analogue to protactinium and was modeled in this report.	Solubility of Np_2O_5 was chosen because it is higher than that of ThO_2(am) under conditions modeled, so its choice is conservative.
Ra	Solid solution (Ra, Ba, Sr, Ca)SO_4	N/A	Chemistry of in-package and invert waters are not so far outside the normal range of natural waters to cause different radium solubilities.
Tc	Tc incorporation into epsilon or "5 metal" phases during CSNF corrosion	Tc in the epsilon particles may not be released when the fuel matrix corrodes.	Studies on fuel corrosion indicate the formation of Epsilon particles ("5 metal particles"). Tc in these particles may not be released when the fuel corrodes. Sparse data on this phenomenon, however, do not provide a solid basis for recommending this as a Tc model. Therefore, no solubility was defined, and inventory release should be in control.
Strontium	Solubility controlled by SrCO3 or SrSO4	NA	No solubility was defined, and inventory release should be in control. This is a conservative approach.
Sn	Solubility controlled by very insoluble crystalline phase cassiterite (SnO2)	Solubility of thermodynamically most-stable phase controls concentrations	Solubilities calculated with SnO_2(am) are consistent with measured Sn solubility in pure water. Other phases may form only under certain conditions.

Source: Modified from Table 6.23-1 in *Dissolved Concentration Limits of Radioactive Elements* (SNL 2007 [DIRS 177418]).

Table 6.3.7-72. Alternative Conceptual Models Considered for Colloids

Alternative Conceptual Model	Basis for Model	Screening Assessment
Kinectic Sorption	This model provides a method for predicting sorption behavior beyond laboratory time scales. Allows interpretation of data from different time scales. Based on the model developed by Painter et al. (2002 [DIRS 174071]) and extended two- and three-site model developed by Wittman et al. (2005 [DIRS 174895]).	This ACM is screened out for the following reasons: – Slow kinetic sorption rates are difficult to determine in laboratory tests that have been run for less than 150 days. – The lack of sufficient sorption data on colloids for sufficient time periods causes uncertainty in the extrapolation beyond the experimental times.
Rate of Colloid Generation	Method for using markers for waste form corrosion for estimating colloid production.	This ACM is screened out for the following reasons: – The model may overestimate colloid formation by not accounting for significant retention of actinides to the immobilized phase as has been observed in waste form corrosion experiments. – The model does not include colloids from CSNF and DSNF.
Mechanisms of Colloid Generation	Mobile colloid generation will require large perturbations to the system that may not occur within the waste package. Furthermore, attachment of particles to air-water interfaces may limit mobile colloid generation.	This ACM is screened out for the following reasons: – Data for Yucca Mountain related conditions are unavailable. – The process of attachment to air-water interfaces will depend on the degree of particle hydrophobicity. Smectite clays and iron oxyhydroxides in general will not attach to air-water interfaces but various oxides and U(VI) oxides phases may. – For flow rates similar to those anticipated in the repository waste package environment, there is no literature evidence to indicate mobile colloid generation.

Source: *Waste Form and In-Drift Colloids-Associated Radionuclide Concentrations: Abstraction and Summary* (SNL 2007 [DIRS 177423], Table 6-19).

NOTE: DHLWG = defense high-level waste glass.

INTENTIONALLY LEFT BLANK

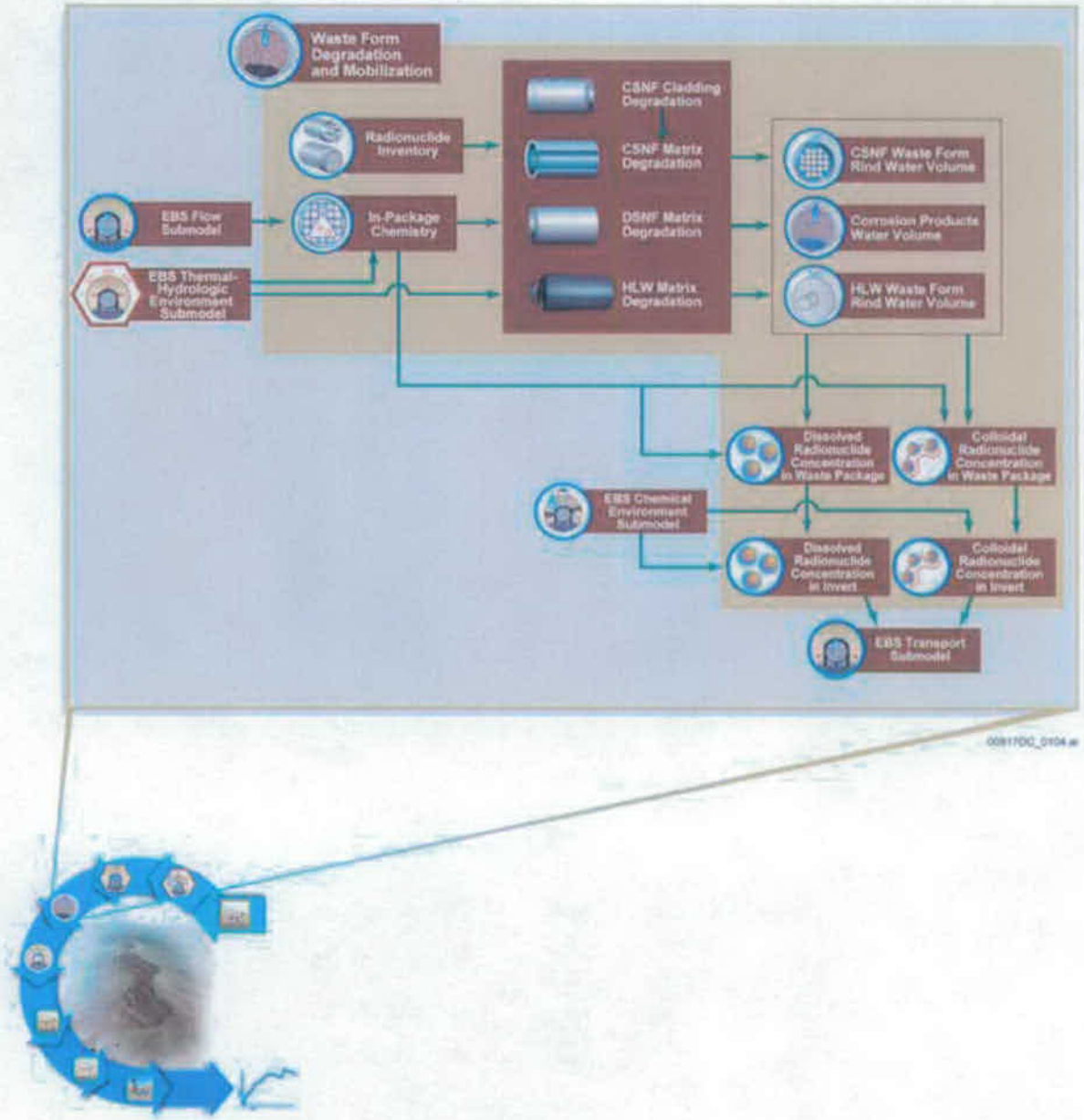

Figure 6.3.7-1. Information Flow Diagram for Waste Form Degradation and Mobilization

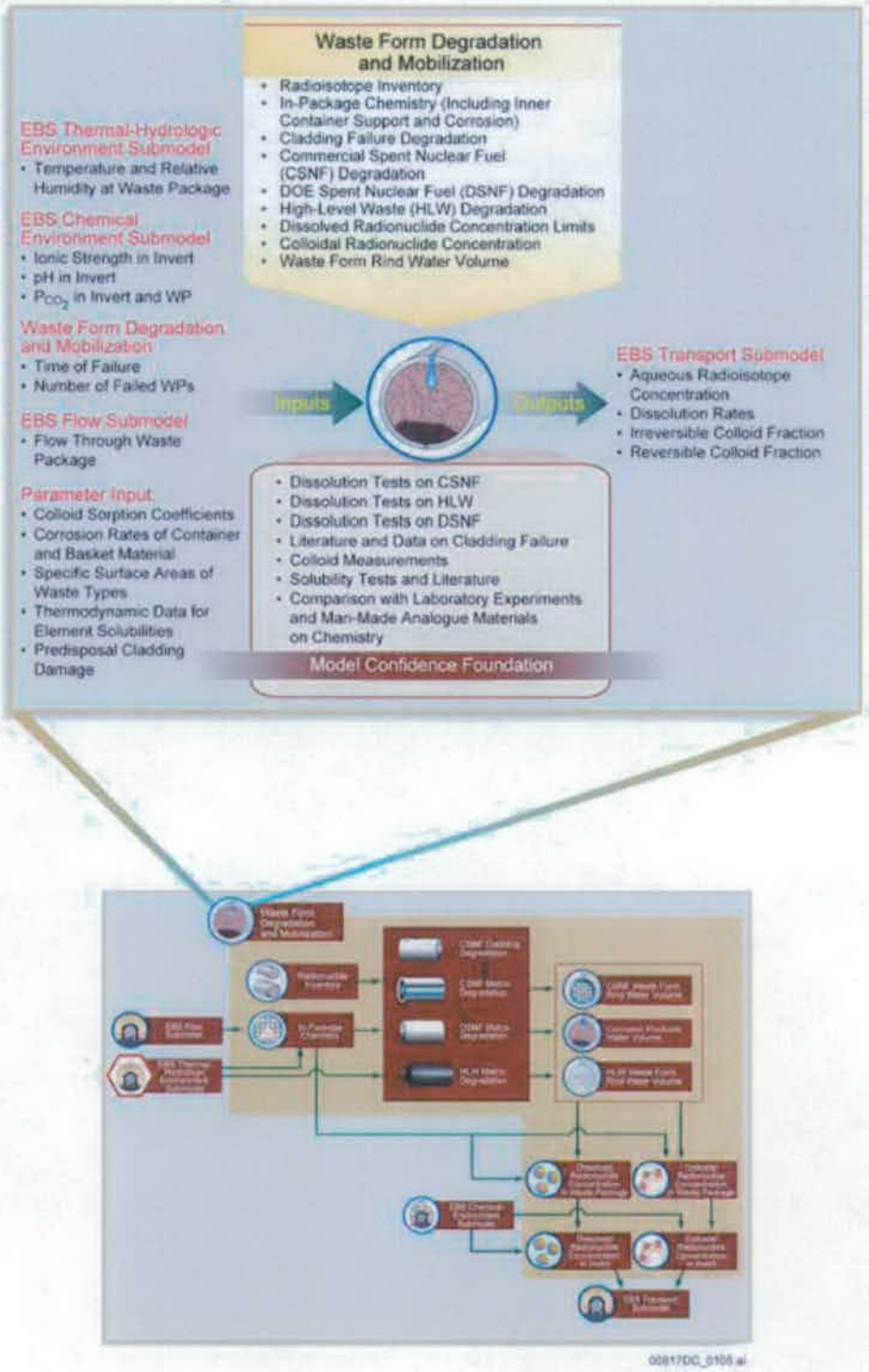

Figure 6.3.7-2. Inputs, Outputs, and Basis for Model Confidence for Waste Form Degradation and Mobilization

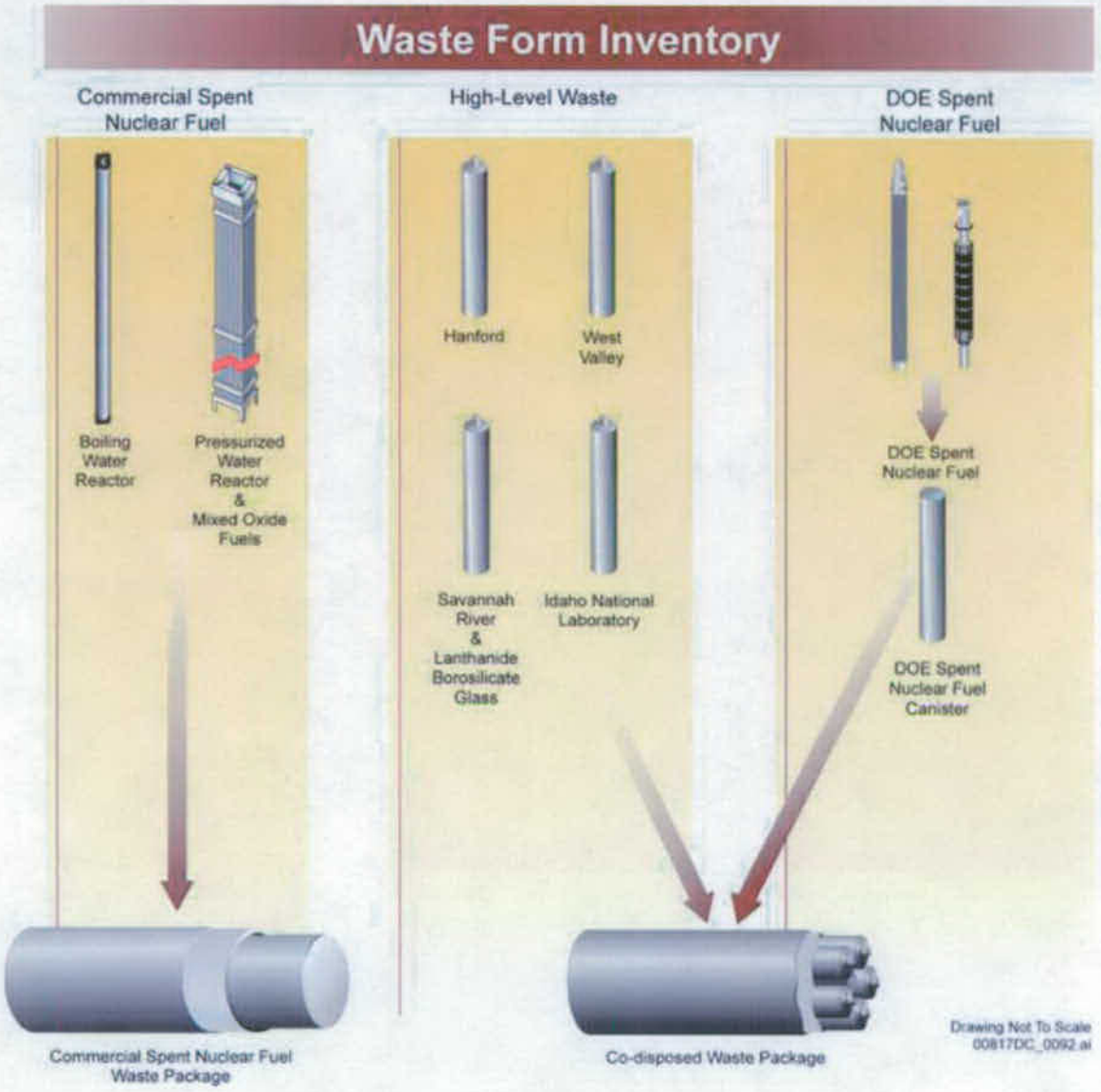

Source: Modified (SNL 2007 [DIRS 180472], Figure 6-1).

NOTE: For modeling purposes, the naval fuels are treated as CSNF.

Figure 6.3.7-3. Three Waste Types Grouped into Two Representative Waste Packages: CSNF and CDSP WPs

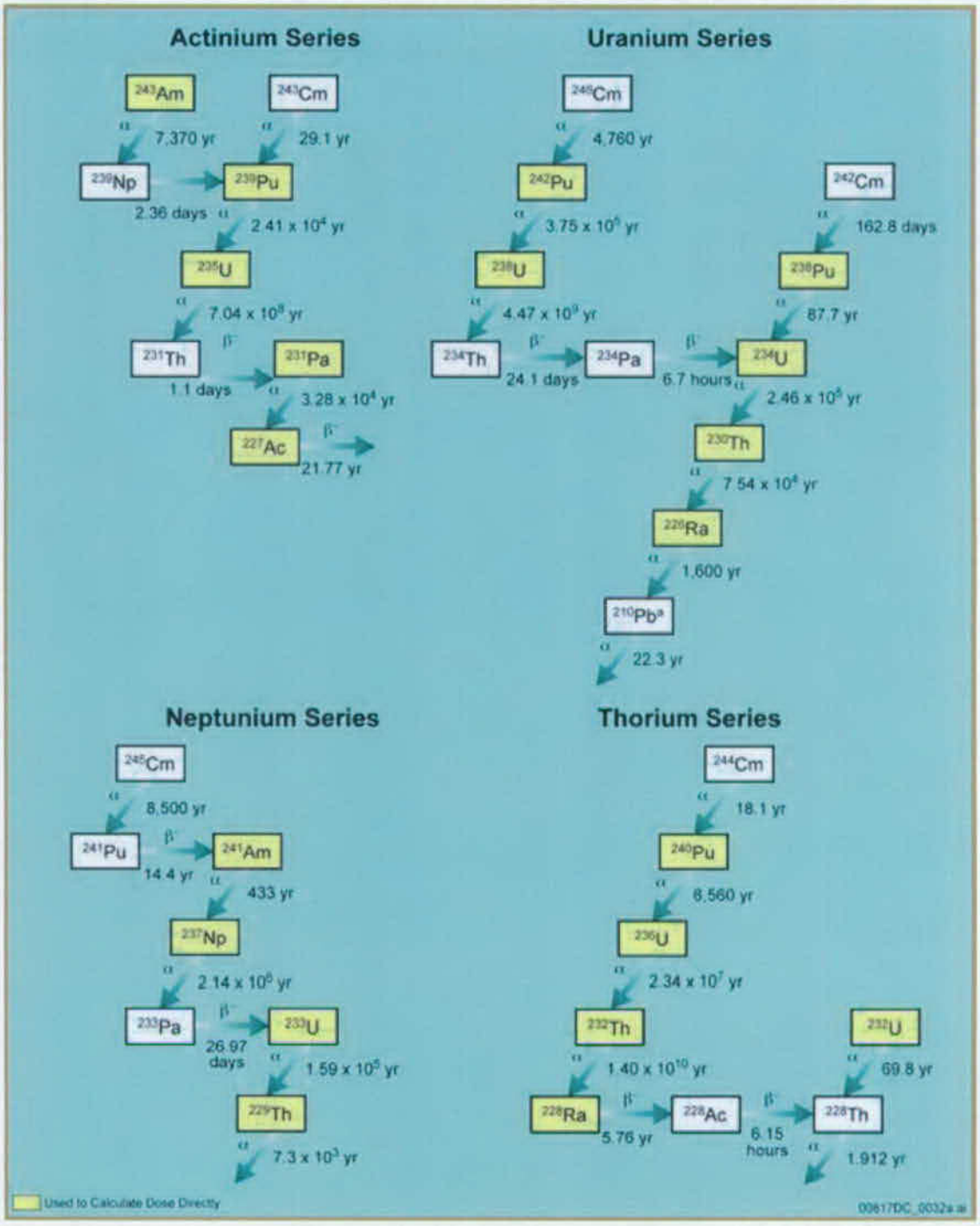

Source: Modified from Rechard 1993 [DIRS 147343], Volume 2 Appendices and DTN: MO0702PASTREAM.001_R0 [DIRS 179925].

NOTE: Value listed under each radionuclide is the decay half-life for the radionuclide.

[a]A series of short-lived daughters is between ^{226}Ra and ^{210}Pb. Also, ^{210}Pb is not used to calculate dose directly, but its biosphere dose conversion factor is included with that of ^{226}Ra.

Figure 6.3.7-4. Decay Chains of the Actinide Elements

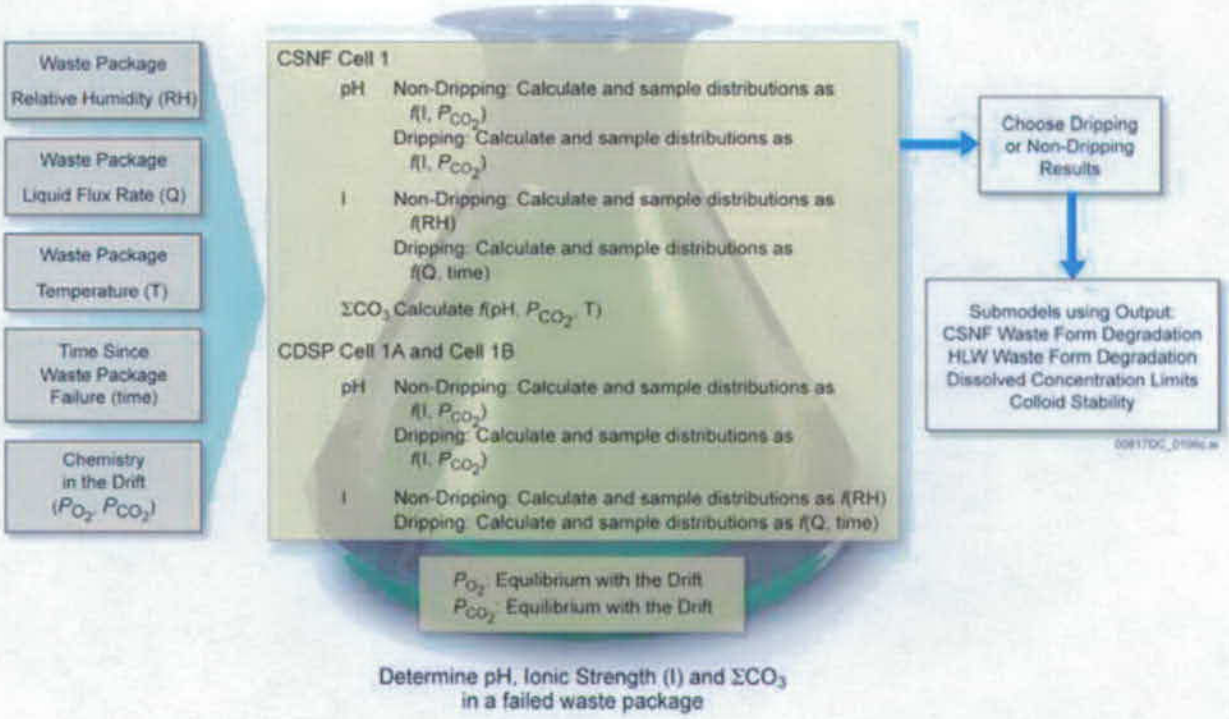

Figure 6.3.7-5. Implementation of the In-Package Chemistry Submodel

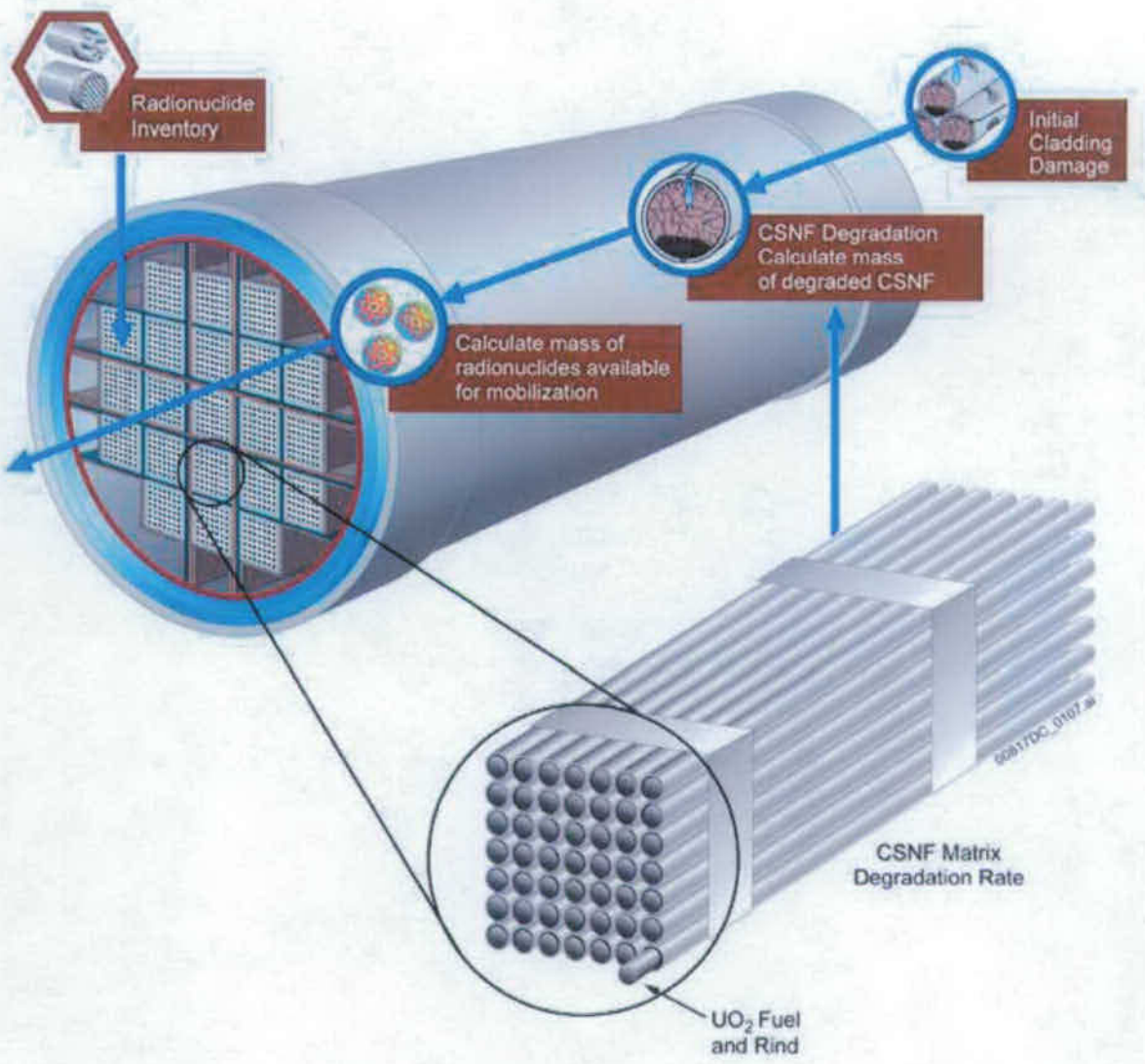

Figure 6.3.7-6. Implementation of the CSNF Cladding Degradation Submodel

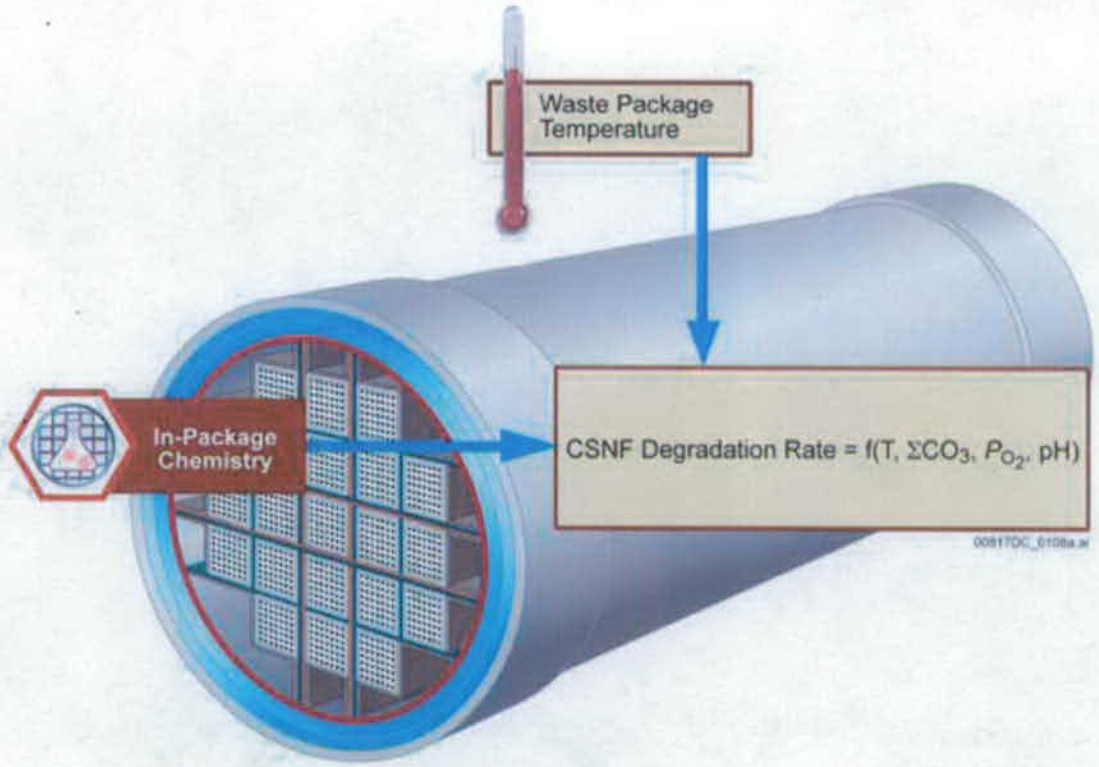

Figure 6.3.7-7. Implementation of the CSNF Matrix Degradation Submodel

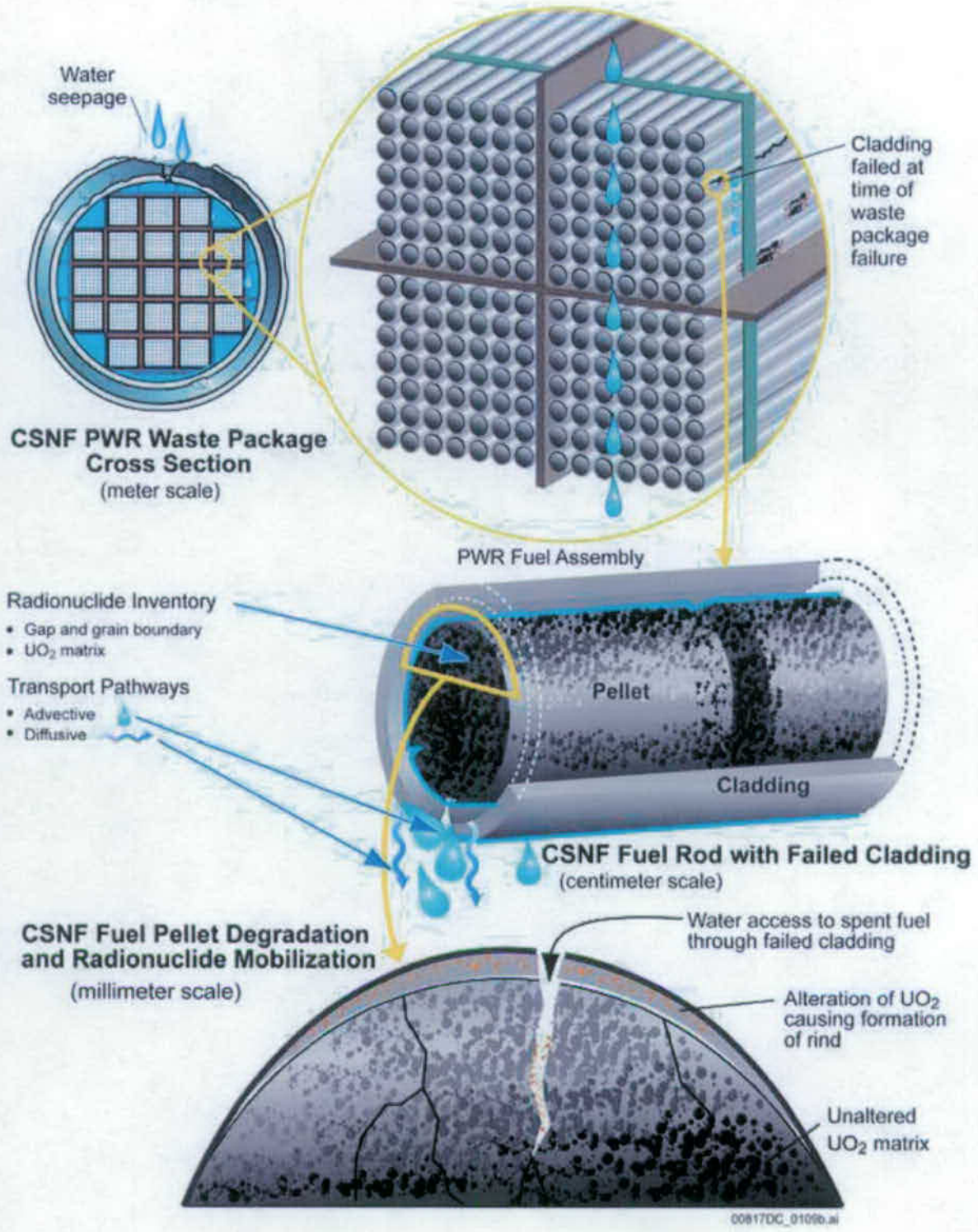

Figure 6.3.7-8. Schematic of CSNF Fuel Waste Form Degradation Mechanisms at Various Scales

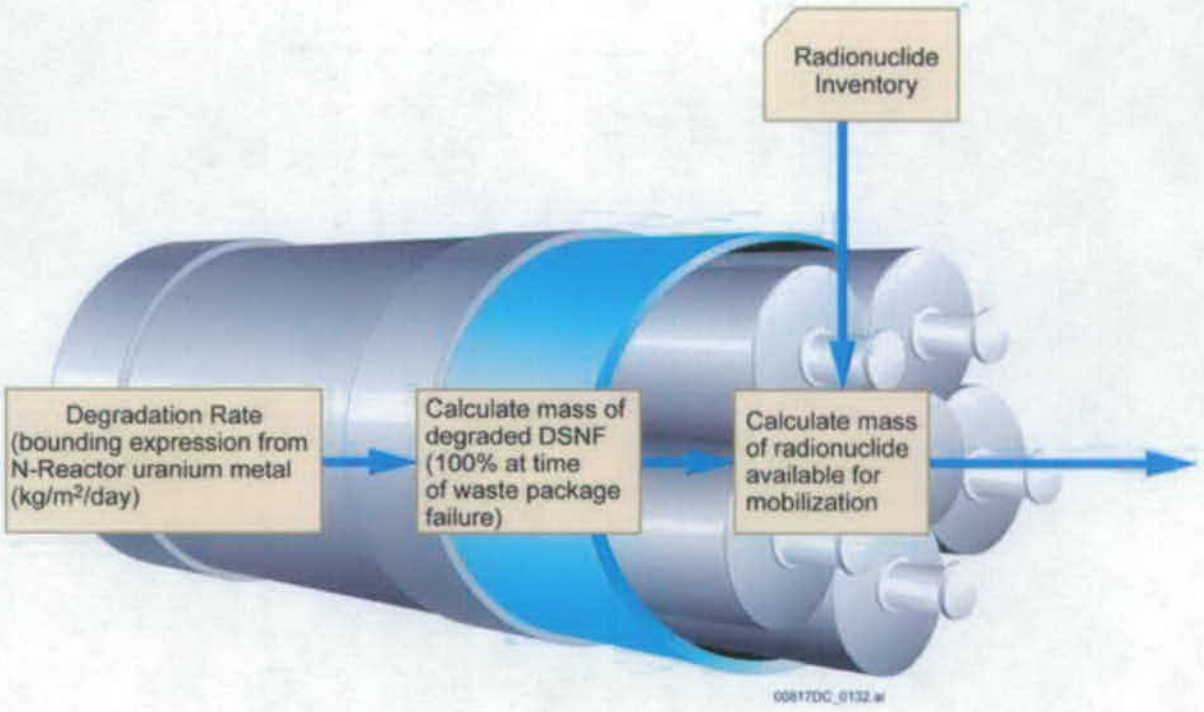

Figure 6.3.7-9. Implementation of the DSNF Degradation Submodel

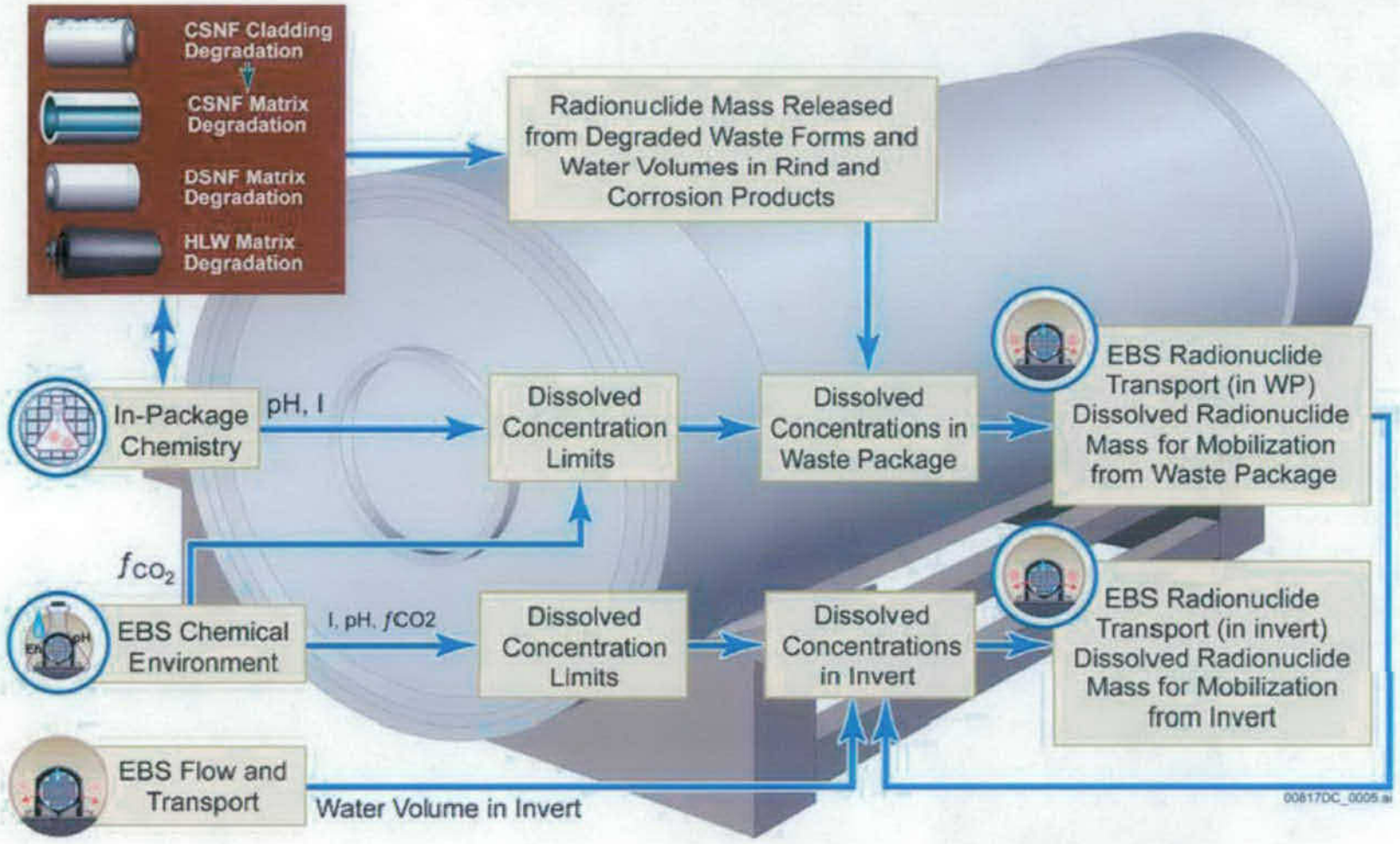

Figure 6.3.7-10. Connections between the Dissolved Concentrations Limits Submodel and Other TSPA-LA Submodels

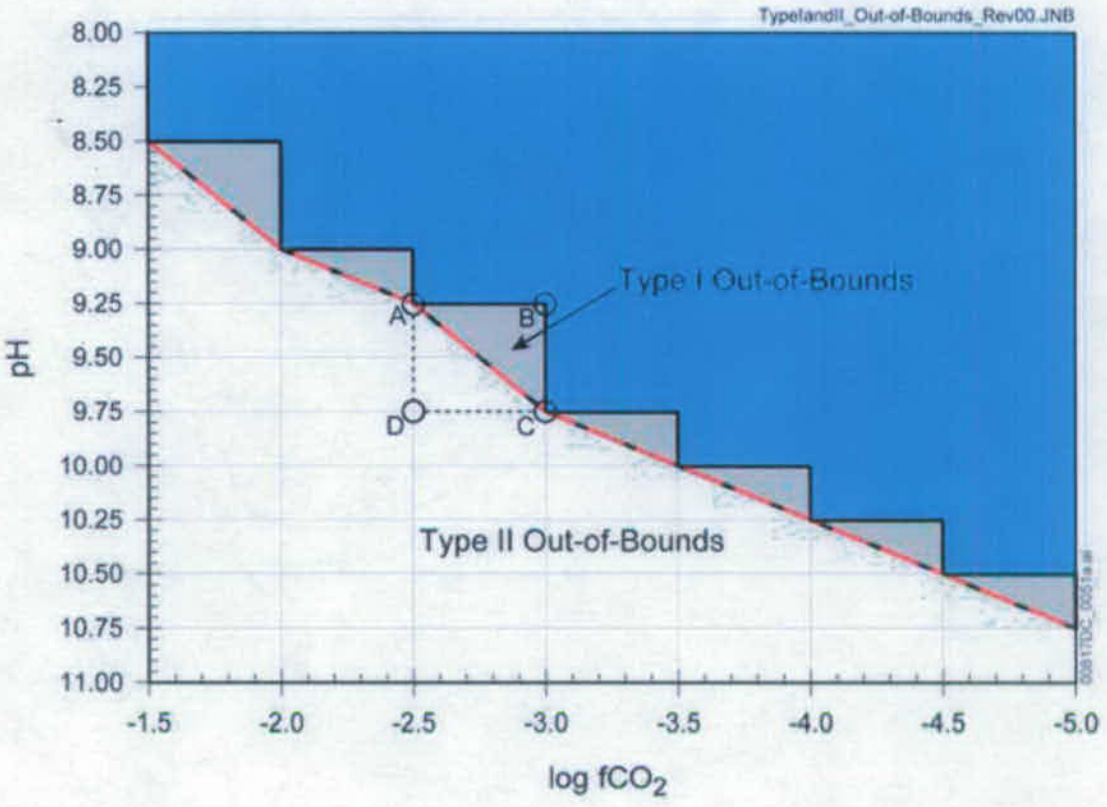

NOTE: Type I out-of-bounds can be removed by implementing a triangular interpolation scheme and a dynamic sampling approach for pH.

Figure 6.3.7-11. Illustration of Type I and Type II Out-of-Bound Conditions Using the Plutonium Solubility Model as an Example

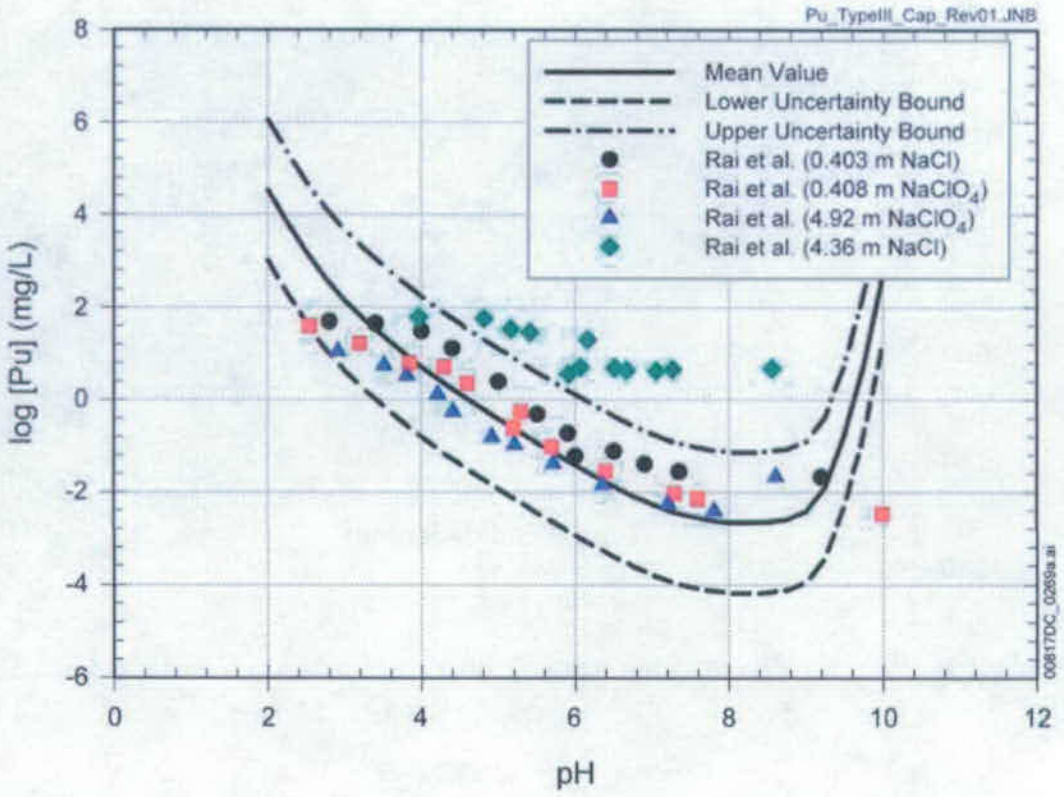

Sources: (SNL 2007 [DIRS 177418], Table 6.5-1) and (Rai et al. 2001 [DIRS 168392], Tables A.1 and A.2).

Figure 6.3.7-12. Comparison of the Solubility-Limited Dissolved Concentration Model for Plutonium

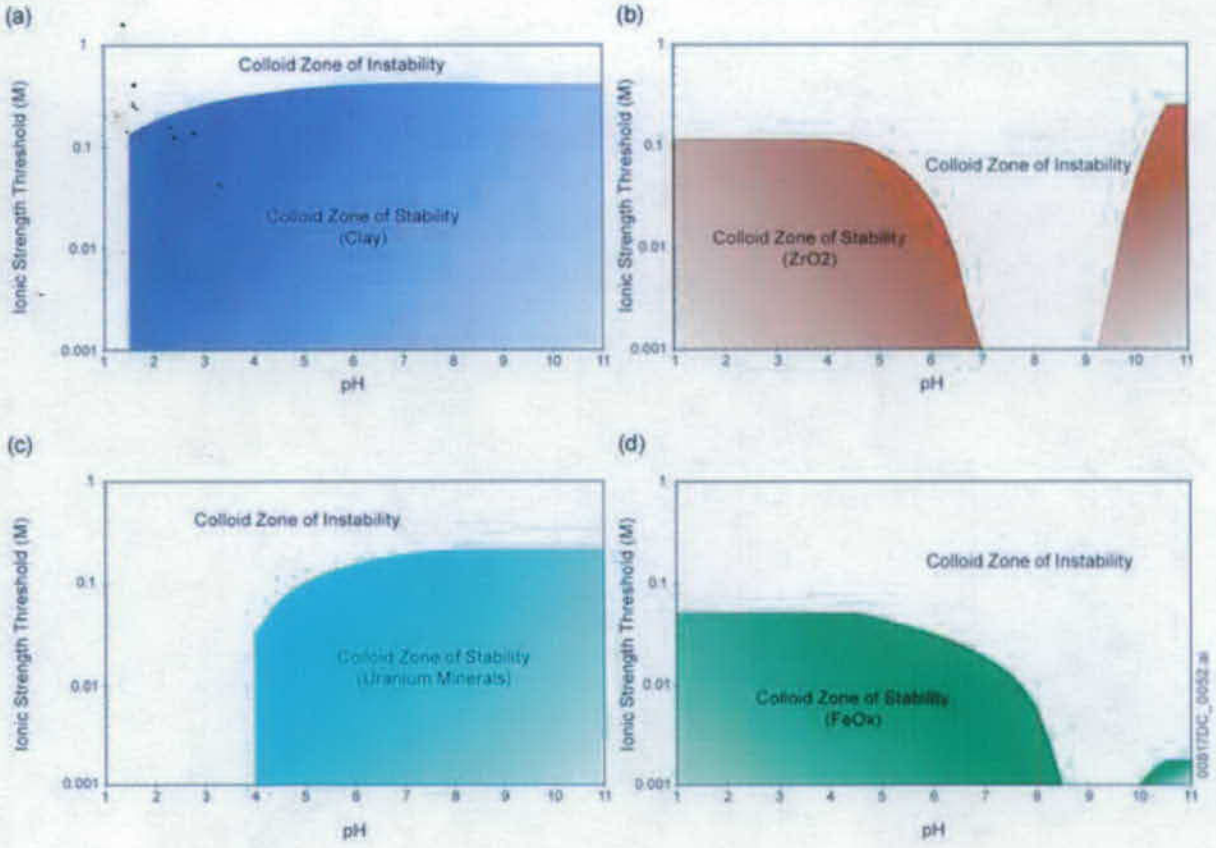

Source: Modified from (SNL 2007 [DIRS 177423], Figures 6-9, 6-12, 6-14, and 6-5).

Figure 6.3.7-13. Schematic Representation of Colloid Suspension Stability as a Function of pH and Ionic Strength for (a) Groundwater and Glass Degradation Colloids (montmorillonite), (b) CSNF Residue Colloids (ZrO_2), (c) Uranium Mineral Colloids (meta-autunite), and (d) Steel Degradation Colloids (hematite)

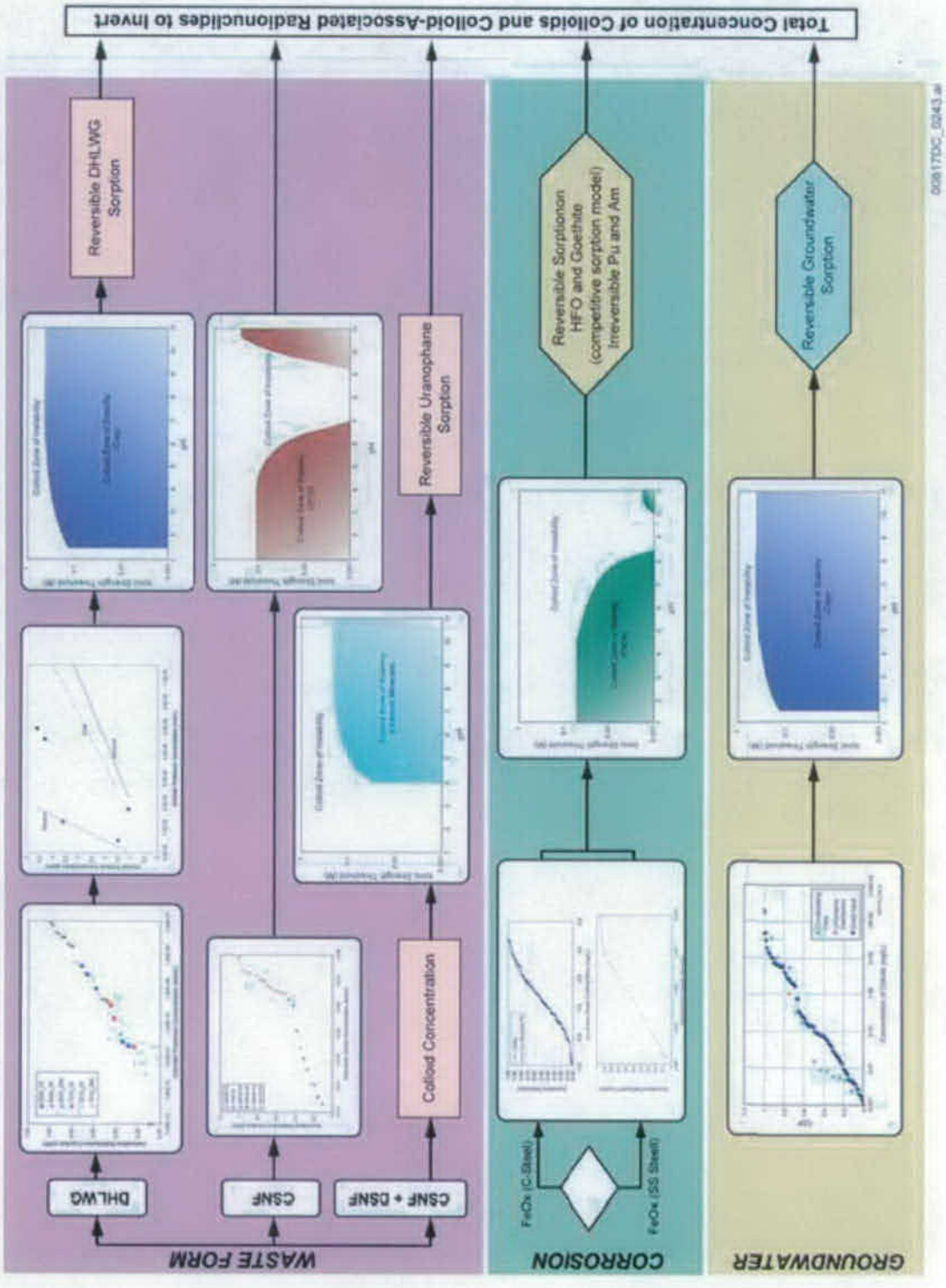

Source: Modified from (SNL 2007 [DIRS 177423], Figure 6-17).

Figure 6.3.7-14. Logic Diagram for Computing the Concentration and Stability of All Colloids in the Waste Package

6.3.8 Engineered Barrier System Transport

The EBS Transport Submodel calculates the time-dependent mass flux of radionuclides from failed WPs through the EBS to the UZ Transport Submodel. The EBS Transport Submodel implemented in the TSPA-SEIS is described in (SNL 2007 [DIRS 177407]). The EBS Transport Submodel considers the transport of radionuclides through the EBS after the radionuclides are mobilized. The mass of radionuclides available for transport through the EBS is provided by the Waste Form Degradation Submodel for the various waste forms (Section 6.3.7.4). Additional inputs and boundary conditions for the EBS Transport Submodel are provided by the EBS Flow Submodel (Section 6.3.6), the EBS TH Environment Submodel (Section 6.3.2), the Dissolved Concentration Limits Submodel (Section 6.3.7.5), and the EBS Colloids Submodel (Section 6.3.7.6). Information flow between the EBS Transport Submodel and other TSPA-SEIS components and submodels is shown on Figure 6.3.8-1. Figure 6.3.8-2 presents an overview of the inputs, outputs, and foundation for confidence in the EBS Transport Submodel as implemented in the TSPA-SEIS. In summary, the inputs include:

- Water flow through failed WPs and the underlying invert provided by the EBS Flow Submodel (Section 6.3.6)
- Temperature, relative humidity, saturation in the invert, and imbibition flux from the host rock exiting the invert under gravity provided by the EBS TH Environment Submodel (Section 6.3.2)
- The waste form dissolution rates provided by the Waste Form Degradation Submodel for the various waste forms (Section 6.3.7.4)
- Solubility limits provided by the Dissolved Concentration Limits Submodel (Section 6.3.7.5)
- Colloidal concentrations and sorption coefficients required to define the mobilized concentration of colloid-associated radionuclides provided by the EBS Colloids Submodel (Section 6.3.7.6).

The EBS Transport Submodel and many of the above supporting submodels that provide feeds were abstracted to describe single representative CSNF and CDSP WPs for each percolation subregion. The determination of what comprises a representative WP is discussed in Section 6.3.2.2.2. The EBS Transport Submodel is implemented in the TSPA-SEIS in terms of a single WP. The pertinent EBS Transport Submodel properties (including the Waste Form Degradation and Mobilization Model Components) for a single representative WP are integrated over the total number of WPs that have failed in each percolation subregion. These properties include the mass of available inventory, pore water volumes, mass of solid materials, advective flow rates, and diffusion areas.

6.3.8.1 Conceptual Model

The EBS consists of the DS, the WP on an emplacement pallet, and an invert constructed with steel supports and filled with crushed tuff between the steel framework. The conceptual model

of radionuclide transport through the EBS (Figure 6.3.8-3) discretizes the system into three primary domains: (1) the waste form domain; (2) the WP corrosion products domain; and (3) the invert domain composed of crushed tuff. An additional domain, the EBS-UZ Interface, is included beneath the invert domain to establish a boundary condition for calculating the diffusive flux from the invert to the UZ and to compute the mass flux fraction going into the UZ fracture and matrix continua. The waste form and corrosion products domains are more specifically described below by the WP type (CSNF or CDSP) (SNL 2007 [DIRS 177407], Section 6.5.2.5):

Commercial spent nuclear fuel (CSNF) WP	
CSNF waste form domain	Waste form (CSNF rods), basket tubes (Stainless Steel Type 316), absorber plates (Borated Stainless Steel Type 304B4)
Corrosion products domain	TAD canister (Stainless Steel Type 316), guide assembly (Stainless Steel Type 316), inner vessel (Stainless Steel Type 316)
Co-disposed (CDSP) WP	
High-level (radioactive) waste (HLW) glass waste form subdomain	HLW glass, HLW glass canisters (Stainless Steel Type 316)
DOE spent nuclear fuel (DSNF) waste form subdomain	DSNF (SNF and Stainless Steel Type 304), DSNF canister (Carbon Steel Type A 516, Borated Stainless Steel Type 304 , and Stainless Steel Type 316)
Corrosion products domain	Divider plate (Carbon Steel Type A 516), inner brackets (Carbon Steel Type A 516), outer brackets (Carbon Steel Type A 516), support tube (Carbon Steel Type A 516), inner vessel (Stainless Steel Type 316)

In the EBS Transport Submodel, the transport along the surface of emplacement pallet is conservatively ignored and the WPs are modeled as being in intimate contact with the invert (SNL 2007 [DIRS 177407], Sections 5.6 and 6.3.1.1). Thus, the mass flux leaving the WPs flows directly into the invert, with no resistance offered by the pallets. A schematic representation and discretization of various domains for the CSNF WP is shown on Figure 6.3.8-4. The implementation details are described in Section 6.3.8.3.

Radionuclide transport through each domain occurs by advection and diffusion. After the WP fails (breached by either general or localized corrosion, seismic damage, igneous intrusion or early failure mechanisms), a portion of the water that may flow through the DS could enter the WP, mobilizing radionuclides from the degraded waste form, and transporting these radionuclides into the UZ. Diffusion is the primary transport mechanism when the water flux into the WP is negligibly small or zero. Advective transport becomes important when there is appreciable flow through the WP. When stress corrosion cracks are the only penetrations through the DS and WP, no advective transport can occur through them (SNL 2007 [DIRS 177407], Section 6.3.3.1.2.1, Table 8.1-2). Advective transport can only occur when

there are corrosion patch failures or when the DS and WP are damaged by igneous intrusion or ruptured by a seismic event. Species-dependent free-water diffusion coefficients are applied that are corrected for tortuosity and temperature. The diffusion coefficient for the colloids is separately computed based on the sampled size of the colloids (SNL 2007 [DIRS 177407], Section 6.3.4.4).

Conceptually, the waste form domain represents that portion of the fuel that has degraded to rind (alteration product), along with the associated corrosion products from degradation of the steel that are present in the domain. Within the waste form domain, a number of processes occur. The waste form degradation processes include dissolution of SNF and HLW glass (Section 6.3.7.4), rapid degradation of DSNF, and formation of waste form colloids from the alteration of HLW glass and SNF (Section 6.3.7.6). Radionuclides may be reversibly sorbed or "embedded" irreversibly in the waste form colloids. The amount of each radionuclide mobilized from a waste form is limited by the solubility of the radionuclide in water (Section 6.3.7.5) and the amount of the radionuclide associated with suspended colloids (Section 6.3.7.6). Colloids may be important to the total system performance because they can increase the mass release of radionuclides from the WP. Both dissolved and colloid-associated radionuclide mass are transported by advection and/or diffusion to the WP corrosion products domain.

The CDSP WP has two fuel types (HLW and DSNF) and thus the CDSP waste form domain is divided into two subdomains, one for the HLW and the other for DSNF. This is required because a CDSP WP consists of five cylindrical canisters containing HLW glass logs surrounding a central canister of DSNF. After the WP is breached, the HLW glass degrades at a specified rate to a clay-like alteration product. However, the DSNF degrades almost instantaneously to oxides and hydrated oxides of uranium. In addition to the ongoing fuel degradation, the steel support framework inside the inner vessel of the WP will corrode gradually, allowing the HLW glass logs to collapse slowly within the inner vessel, such that the general cylindrical shape of the glass logs is retained. On the other hand, because DSNF degrades almost instantaneously, and with no credit taken for the canister, it is expected that DSNF will not retain its cylindrical geometry, and may settle to the bottom of the interior of the inner vessel. With this assumption of the internal configuration of a degraded CDSP WP, two separate waste form subdomains are conceptualized, one for HLW and the other for DSNF. The transport characteristics are expected to be different in each waste form subdomain. Because the EBS Transport Submodel is a one-dimensional model, the two waste form subdomains are modeled sequentially, such that the HLW domain is upstream of the DSNF domain. The mass released from the degradation of HLW glass moves to the DSNF domain by advection and/or diffusion and then is transported to the corrosion products domain. Because of the one-dimensional assumption, each waste form subdomain and the corrosion products domain have the same seepage flux.

Conceptually, the corrosion products domain is composed of corroded internal components of the WP, predominantly from the inner vessel and TAD canister. The internal components of a breached WP will degrade slowly over tens of thousands of years, forming corrosion products (assumed to be iron oxyhydroxides) that can sorb and delay the release of radionuclides from the WP (SNL 2007 [DIRS 177407], Sections 6.3.4.2 and 6.5.1.2). Degradation of the internal WP components results in two types of materials: (1) stationary iron oxyhydroxide corrosion products that are assumed to remain in the WP and (2) iron oxyhydroxide colloids that are

mobile and can move out of the WP. The primary interactions with the corrosion products are equilibrium and kinetic sorption of dissolved radionuclide species onto the stationary corrosion products and iron oxyhydroxide colloids. The sorption parameters are developed from a mechanistic surface-complexation-based competitive sorption model that is applicable over the range of pH and P_{CO_2} expected in the repository over the simulation timescales. Dissolved species also undergo reversible sorption onto groundwater (seepage-water) colloids and waste form colloids that are passing through the corrosion products domain. Radionuclides are transported by advection and diffusion from the corrosion products domain to the invert domain.

In the invert domain of the EBS Transport Submodel, radionuclide transport occurs by both advection and diffusion and the mass flux of radionuclides (in both the dissolved state and associated with colloids) is passed to the UZ. Reversible sorption of radionuclides on the crushed tuff is also considered. The EBS-UZ Interface domain is conceptualized to apply an effective semi-infinite zero-concentration boundary condition for computing the diffusive flux from the invert to the UZ. It is also used to calculate the mass fraction going into the UZ fracture and matrix continua.

In all of the EBS domains, there are additional parameters that influence the release of radionuclide mass from each domain. For example, the water volume, porosity, water saturation, cross-sectional area for diffusion, diffusive path length, temperature, relative humidity, and chemistry affect the rate of advective and diffusive transport of radionuclides through the EBS domains. The concentration of dissolved species may also be solubility limited, which could result in precipitation of radionuclide mass if the solubility limit is reached. Radionuclide transport is assumed not to occur when the temperatures are greater than 100°C (the boiling point of water) due to a lack of bulk water and a continuous film of water. However, below this temperature, a continuous thin film of adsorbed water is assumed to behave as bulk liquid in order to allow radionuclides to dissolve and diffuse through it (SNL 2007 [DIRS 177407], Section 5.5).

6.3.8.2 Abstraction

The EBS Transport Submodel calculates the time-dependent rate of radionuclide releases from the EBS to the UZ. The mass of each radionuclide at any particular location is dependent on the transport characteristics of the radionuclide, the quantity of the radionuclide remaining at its source, the extent of radioactive decay or ingrowth associated with a particular radionuclide, and the diffusive area and diffusive length in a given domain. The continuum mass balance equations for the EBS Transport Submodel are described and developed in (SNL 2007 [DIRS 177407], Section 6.5.1.2). These equations represent one-dimensional mass balance for:

- Transport of dissolved radionuclide species and radionuclide species that are reversibly sorbed onto three types of colloids: iron oxyhydroxide, waste form, and groundwater
- Transport of kinetically (and irreversibly) sorbed radionuclide species on iron oxyhydroxide colloids

- Kinetic sorption of radionuclide species onto stationary corrosion products in the WP
- Transport of embedded (irreversibly sorbed) radionuclide species in waste form colloids
- Decay and ingrowth for a given radionuclide.

Implementation of the three-domain EBS Abstraction requires that the following properties be specified for each domain: the domain water volume, volumetric flow rate, water saturation, porosity, diffusive area, diffusive path length, and diffusion coefficient. Note that species-dependent free water diffusion coefficients are used in each domain that are corrected for tortuosity and temperature. The preceding properties may vary among the dripping and non-dripping environments for each fuel type and WP (CSNF and CDSP WPs), the invert, and the EBS-UZ Interface. The advective or diffusive transport pathways and transport processes included in the EBS Transport Submodel of the TSPA-SEIS are summarized in Table 6.3.8-1. The parameters that define the transport of radionuclides through the waste form and the corrosion products domains, as discussed in the following sections, are summarized in Table 6.3.8-2. Table 6.3.8-3 and Table 6.3.8-4 summarize various sampled parameters used in the EBS Transport Submodel, with the ranges and distributions for each parameter provided. Table 6.3.8-5 provides the UZ fracture and matrix saturation and flux inputs for the four glacial transition climates (gt10, gt30, gt50, and gt90) and four post-10,000-year climates (pk10, pk30, pk50, and pk90) used in the EBS-UZ Interface model in each of the five percolation subregions (PS1, PS2, PS3, PS4, and PS5). Table 6.3.8-6 summarizes the parameters used in the rind volume calculation from the degradation of CSNF. The general modeling approach and properties used to calculate radionuclide transport in each of the domains are detailed in the following sections.

6.3.8.2.1 Commercial Spent Nuclear Fuel Waste Form Domain

The CSNF waste form domain represents material inside the TAD canister, which includes, fuel rods, basket tubes, and absorbed plates that may degrade once the WP is breached (Figure 6.3.8-5).

Transport out of the waste form domain can occur by advection, when there is liquid flow through the WPs, and by diffusion, through continuous thin water films assumed to be present in the WPs when temperatures are less than 100°C. Diffusion can occur in both dripping and non-dripping environments. In addition to being transported in the dissolved state, radionuclides in the CSNF waste form domain can be transported via waste form colloids and groundwater colloids. Two different waste form colloids are generated by the degradation and alteration of CSNF and have different stability fields and concentrations. One is modeled to only include "embedded" plutonium and americium, which are considered as intrinsic parts of the colloids and, thus, not in equilibrium with the aqueous system. These embedded radionuclides are modeled as irreversibly attached to the host colloids. The second waste form colloid type is modeled to undergo only reversible sorption similar to groundwater colloids.

Solving the mass transport equations requires that the following properties be defined at the beginning of the timestep: (1) the volume of water in the domain; (2) the diffusive area of the domain; (3) the diffusive length of the domain; (4) diffusion coefficients; and (5) advective flow rates.

CSNF Waste Form Water Volume—The cladding degradation abstraction (SNL 2007 [DIRS 180616], Section 6.2.4) estimates the rind water volume for both dripping and non-dripping cases. The volume of water in the rind as a function of time is given by:

$$V_w(t) = \phi_{CSNF} S_{CSNF} V_{rr}(t) N_f(t) \qquad \text{(Eq. 6.3.8-1)}$$

where

$V_w(t)$ = time-dependent volume of water in rind (m^3)

ϕ_{CSNF} = porosity of the CSNF rind material (schoepite)

S_{CSNF} = saturation of the CSNF rind material (schoepite)

$V_{rr}(t)$ = time-dependent volume of rind in a fuel rod (m^3)

$N_f(t)$ = number of failed rods as a function of time.

The porosity of the waste form rind is an epistemic uncertain parameter, sampled from a uniform distribution between 0.05 and 0.3 (Table 6.3.8-6). The time-dependent number of failed fuel rods, $N_f(t)$, is not needed as all the rods are assumed to be failed, as there is no credit taken for the cladding in the base case calculations (see Section 6.3.7.3).

The volume of rind in a rod, $V_{rr}(t)$, is (SNL 2007 [DIRS 180616], Table 6-4, Equation 6-7):

$$V_{rr}(t) = \frac{V_{init} F_{cor}(t) V_{rm}}{N_f(t)} \qquad \text{(Eq. 6.3.8-2)}$$

where

V_{init} = initial volume of fuel in a WP (m^3)

$F_{cor}(t)$ = time-dependent fraction of total corroded waste form inventory

V_{rm} = rind volume multiplier.

The initial volume of fuel in a CSNF WP is calculated as the product of the number of fuel rods in a CSNF WP and the volume of a single undegraded fuel rod (SNL 2007 [DIRS 180616], Table 6-4, Equation 6-4). The time-dependent fraction of total corroded (degraded) waste form inventory, F_{cor}, is calculated within the TSPA-SEIS using Equation 6.3.7-7 (Section 6.3.7.4.1.3).

For the purposes of modeling the rind formation, the CSNF matrix and schoepite inside a failed cladding rod are abstracted as concentric cylinders, with the fuel matrix modeled as a receding inner cylinder and with the schoepite modeled as an expanding outer cylinder, constrained by a

split cladding rod (Figure 6.3.8-5). The rind volume multiplier, V_{rm}, accounts for the increase in volume associated with rind development due to density change between fuel matrix (UO_2) and schoepite. This multiplier is proportional to the differences in density and molecular weight of the intact fuel and schoepite (SNL 2007 [DIRS 180616], Table 6-4, Equation 6-3):

$$V_{rm} = \left(\frac{MW_{sch}}{MW_{UO2}}\right)\frac{\rho_{UO2}}{(1-\phi_{sch})\rho_{sch}} \qquad \text{(Eq. 6.3.8-3)}$$

where

MW_{sch} = molecular weight of schoepite (g/mol)

MW_{UO2} = molecular weight of UO_2 (g/mol)

ρ_{UO2} = density of UO_2 (g/cm^3)

ρ_{sch} = density of schoepite (g/cm^3).

The parameters used in the TSPA-SEIS abstraction for CSNF rind volume are given in Table 6.3.8-6. The total bulk volume of the CSNF domain is the sum of the rind volume and the volume of basket tube and absorber plate steel corrosion products, which also increase over time:

$$V_{CSNF}(t) = V_{rind,CSNF}(t) + V_{CP,CSNF}(t). \qquad \text{(Eq. 6.3.8-4)}$$

The rind volume in a CSNF WP ($V_{rind,CSNF}$) is calculated by multiplying the volume of rind in a rod (V_{rr}) by the number of failed rods. The bulk volume of CSNF domain corrosion products is (SNL 2007 [DIRS 177407], Equation 6.5.2.2.2.1-4):

$$V_{CP,CSNF}(t) = \left(\frac{1}{1-\phi_{CP}}\right)\sum_{CPm}\left[\frac{\left[m_{CPm,CS,CSNF}(t) + m_{CPm,SS,CSNF}(t)\right]}{\rho_{CPm}}\right]. \qquad \text{(Eq. 6.3.8-5)}$$

where ϕ_{CP} is the steel corrosion products porosity (a constant value of 0.4), $m_{CPm,CS,CSNF}$ is the mass of corrosion products from degradation of carbon steel (zero for CSNF), $m_{CPm,SS,CSNF}$ is the mass of corrosion products from degradation of stainless steel, ρ_{CPm} is the grain density of corrosion products, and subscript 'm' refers to the metal type (iron or nickel or chromium) in the steel from which the type of corrosion products is formed (goethite, ferrihydrite, NiO, Cr_2O_3).

The pore volume in the CSNF waste form domain is the sum of CSNF rind pore volume and steel corrosion products pore volume:

$$V_{\phi,CSNF}(t) = \phi_{CSNF} V_{rind,CSNF}(t) + \phi_{CP} V_{CP,CSNF}(t), \qquad \text{(Eq. 6.3.8-6)}$$

where the CSNF rind porosity, ϕ_{CSNF}, is a sampled parameter.

The effective porosity of the CSNF waste form domain, which is needed for computing the diffusion coefficient using Archie's law, is time dependent because the pore volume and bulk volume of the domain are time dependent:

$$\phi_{CSNF}(t) = \frac{V_{\phi,CSNF}(t)}{V_{CSNF}(t)}. \quad \text{(Eq. 6.3.8-7)}$$

The water volume in the CSNF waste form domain is the sum of CSNF rind water volume and steel corrosion products water volume:

$$V_{w,CSNF}(t) = \phi_{CSNF} S_{w,rind,CSNF} V_{rind,CSNF}(t) + \phi_{CP} S_{w,CP,CSNF} V_{CP,CSNF}(t). \quad \text{(Eq. 6.3.8-8)}$$

The saturation of the rind and corrosion products is determined separately, when there is no flow through the WP, using separate water vapor adsorption isotherms that are functions of relative humidity and specific surface areas, among other parameters. The calculations are described in Section 6.5.2.2 of the *EBS Radionuclide Transport Abstraction*, (SNL 2007 [DIRS 177407]). Since the adsorption isotherm functions are unbounded as relative humidity (*RH*) approaches 1.0, the saturation is limited to a value of 1.0. Under flowing conditions through the WP, complete saturation of the pore space is assumed. The effective water saturation for the CSNF waste form domain is given by:

$$S_{w,CSNF}(RH) = \min\left[\frac{V_{w,CSNF}(RH,t)}{V_{\phi,CSNF}(t)}, 1.0\right]. \quad \text{(Eq. 6.3.8-9)}$$

CSNF Waste Form Diffusive Area and Length—The area through which radionuclides may diffuse after being released from fuel rods depends on the state of the waste form. No credit is taken for the fuel rod cladding, so once a WP is breached, all of the SNF is modeled as exposed to the environment inside the WP. As a result, the diffusive area for the waste form domain is based on the radial geometry inside the WP that is bounded by the TAD canister. Since the diffusive area increases with increasing distance from the origin point in the radial geometry, the area of the CSNF waste form domain is taken at half the radius of the TAD canister (Figure 6.3.8-5) and set at a constant value of 12.5 m^2 (Table 6.3.8-2). The diffusive path length is set to be the inside radius of the TAD canister (= 0.819 m) (Table 6.3.8-2). In calculating the diffusive conductance across the interface between the CSNF waste form domain and the downstream corrosion products domain the harmonic average of the diffusive areas and diffusive lengths of the two domains is considered. The radial transport is modeled in the Cartesian coordinates in a one-dimensional model by specifying the diffusive areas and lengths consistent with the radial geometry.

Calculation of Diffusion Coefficients in the CSNF Waste Form Domain—Diffusion coefficients for dissolved radionuclides in the CSNF waste form domain are calculated using Archie's law. This approach implicitly includes the effects of porosity, saturation, and tortuosity in calculating an effective diffusion coefficient for a porous medium. For the CSNF waste form domain, Archie's law is expressed as (SNL 2007 [DIRS 177407], Equation 6.3.4.3.5-2):

$$\phi_{CSNF} S_{w,CSNF} D_{WF} = D_{wi} \phi_{CSNF}^{1.3} S_{w,CSNF}^{2} \qquad \text{(Eq. 6.3.8-10a)}$$

where

D_{WF} = effective diffusion coefficient that includes the effect of tortuosity in a porous medium (cm^2/s)

D_{wi} = species dependent free water diffusion coefficient (cm^2/s)

ϕ_{CSNF} = porosity of domain

$S_{w,CSNF}$ = liquid saturation of the domain (fraction).

After the effective diffusion coefficient has been calculated using Equation 6.3.8-10a, it is modified to account for temperature effects. The diffusion coefficient at a given temperature is given as (SNL 2007 [DIRS 177407], Equation 6.3.4.1.2-4)

$$D_T = D_{T_0} \frac{T}{T_0} 10^{\left[\frac{1.3272(293.15-T_0)-0.001053(T_0-293.15)^2}{T_0-168.15}\right]-\left[\frac{1.3272(293.15-T)-0.001053(T-293.15)^2}{T-168.15}\right]} \qquad \text{(Eq. 6.3.8-10b)}$$

where

D_T = effective diffusion coefficient at temperature T (cm^2/s)

D_{T_0} = diffusion coefficient at temperature T_0 (as calculated by Equation 6.3.8-10a) (cm^2/s)

T = invert temperature (K)

T_0 = reference temperature (298.15 K).

Advective Transport in the CSNF Waste Form Domain—Advective transport out of the waste form domain and into the corrosion products domain can only occur when there is liquid flow through the WPs. The EBS Flow Submodel determines the flux through the WP (flow pathway 4 on Figure 6.3.6-4) based on the flux through the DS, the damage fraction on a WP, and a WP flux-splitting logic (Section 6.3.6). Advective flux to the WPs is only possible when the DSs are breached. Details regarding the calculation of the flow through the WP are given in the EBS Flow Submodel (Section 6.3.6.2). If the only breaches in a WP are stress corrosion cracks, advective transport through the WP does not occur, but diffusion of radionuclides out of the WP could still take place.

6.3.8.2.2 Co-Disposed Waste Form Domain

As conceptualized in Section 6.3.8.1, the CDSP waste form domain is divided into two subdomains, one for the HLW glass and another for the DSNF. The two waste form subdomains are modeled sequentially, such that the HLW subdomain is upstream of the DSNF subdomain as described in Section 6.3.8.1. The mass released from the degradation of HLW glass moves to the DSNF domain by advection and/or diffusion and is then transported to the corrosion products domain. Radionuclide concentrations are subject to the solubility constraints defined by the Dissolved Concentration Limits Submodel (Section 6.3.7.5).

In addition to being transported in the dissolved state, radionuclides in the HLW subdomain can be transported via waste form colloids. These colloids are generated by the degradation and alteration of HLW glass and include "embedded" plutonium and americium, which are considered as intrinsic parts of the colloids and, thus, not in equilibrium with the aqueous system. These embedded radionuclides are modeled as irreversibly attached to the host colloids. Reversible sorption onto waste form colloids is also considered for various radionuclides. Details of the waste form colloid generation, stability, and sorption capability are given in Section 6.3.7.6.2.

Transport out of the CDSP waste form subdomains can occur by advection, when there is liquid flow through the WPs, and by diffusion, through continuous thin water films assumed to be present in the WPs. Diffusion can occur in both dripping and non-dripping environments. Solving the mass transport equation requires that the following properties be defined: (1) the volume of water in the degraded fuel; (2) the diffusive areas of the domains; (3) the diffusive length of the domains; (4) diffusion coefficients; (5) sorbent mass; and (6) advective flow rates. The diffusive areas through various subdomains are shown on Figure 6.3.8-6.

HLW Waste Form Water Volume—The HLW glass degradation abstraction (BSC 2004 [DIRS 169988]), estimates the rind water volume for both dripping and non-dripping cases. The rind volume in the altered rind is provided by the expression (BSC 2004 [DIRS 169988], Section D.1, Equation D-3b):

$$V_{rind,HLWG}(t) = \frac{1}{\rho_G}\sum M_t \qquad \text{(Eq. 6.3.8-11)}$$

where

$V_{rind,HLWG}$ = bulk rind volume (m^3)

ρ_G = the bulk HLW glass density (kg/m^3)

$\sum M_t$ = total mass of degraded HLW glass up to time t (kg).

Because the properties of the HLW glass and the clay making up the rind layer are similar, Equation 6.3.8-11 assumes that a degraded volume of glass generates an equal volume of clay as the rind layer (BSC 2004 [DIRS 169988], Section D.2). Therefore, the glass density (2,700 kg/m^3) is the same for the unreacted glass and the clay alteration products. The total mass of glass degraded over a timestep of size Δt is provided by the HLW Glass Waste Form Degradation Submodel (Section 6.3.7.4.3).

The total bulk volume of the HLW subdomain is the sum of the rind bulk volume and the bulk volume of corrosion products from degradation of steel canisters encasing the fuel, which also increase over time:

$$V_{HLWG}(t) = V_{rind,HLWG}(t) + V_{CP,HLWG}(t). \quad \text{(Eq. 6.3.8-12)}$$

The bulk volume of CSNF domain corrosion products is (SNL 2007 [DIRS 177407], Section 6.5.2.2):

$$V_{CP,HLWG}(t) = \left(\frac{1}{1-\phi_{CP}}\right)\sum_{CPm}\left[\frac{\left[m_{CPm,CS,HLWG}(t) + m_{CPm,SS,HLWG}(t)\right]}{\rho_{CPm}}\right]. \quad \text{(Eq. 6.3.8-13)}$$

where ϕ_{CP} is the steel corrosion products porosity (a constant value of 0.4), $m_{CPm,CS,HLWG}$ is the mass of corrosion products from degradation of carbon steel, $m_{CPm,SS,HLWG}$ is the mass of corrosion products from degradation of stainless steel, ρ_{CPm} is the grain density of corrosion products, and subscript 'm' refers to the type of corrosion products formed (goethite, ferrihydrite, NiO, Cr_2O_3).

The pore volume in the HLW waste form domain is the sum of HLW rind pore volume and steel corrosion products pore volume:

$$V_{\phi,HLWG}(t) = \phi_{rind} V_{rind,HLWG}(t) + \phi_{CP} V_{CP,HLWG}(t), \quad \text{(Eq. 6.3.8-14)}$$

where ϕ_{rind} is the rind porosity given by a constant value of 0.17 (BSC 2004 [DIRS 169988], Table 8-1).

The effective porosity of the HLW waste form domain, which is needed for computing the diffusion coefficient using Archie's law, is time dependent because the pore volume and bulk volume of the domain are time dependent:

$$\phi_{HLWG}(t) = \frac{V_{\phi,HLWG}(t)}{V_{HLWG}(t)}. \quad \text{(Eq. 6.3.8-15)}$$

The water volume in the HLW waste form domain is the sum of HLW rind water volume and steel corrosion products water volume:

$$V_{w,HLWG}(t) = \phi_{rind} S_{w,rind,HLWG} V_{rind,HLWG}(t) + \phi_{CP} S_{w,CP,HLWG} V_{CP,HLWG}(t) \quad \text{(Eq. 6.3.8-16)}$$

The saturation of the rind and corrosion products is determined separately, when there is no flow through the WP, using separate water vapor adsorption isotherms that are functions of relative humidity and specific surface areas, among other parameters. The calculations are described in Section 6.5.2.2 of the *EBS Radionuclide Transport Abstraction*, (SNL 2007 [DIRS 177407]). Since the adsorption isotherm functions are unbounded as the relative humidity approaches one, the saturation is limited to a value of one. Under flowing conditions through the WP, complete saturation of the pore space is assumed.

The effective water saturation for the HLW waste form domain is given by:

$$S_{w,HLWG}(RH) = \min\left[\frac{V_{w,HLWG}(RH,t)}{V_{\phi,HLWG}(t)}, 1.0\right]. \qquad \text{(Eq. 6.3.8-17)}$$

DSNF Waste Form Water Volume—The water volume of the DSNF waste form is computed by multiplying the initial volume of DSNF in a CDSP WP, which is equal to 1 m^3 (BSC 2004 [DIRS 172453], Section 8.1), by its porosity and saturation. The porosity of DSNF rind is assumed to be 0.2, as degraded DSNF is conceptualized to be a porous medium (SNL 2007 [DIRS 177407], Section 6.5.2.1.2). The total bulk volume of the DSNF waste form subdomain is the sum of the rind volume and the volume of corrosion products from degradation of associated steel (Section 6.3.8.1), which also increases with time. The equations used for calculating the bulk volume, pore volume, effective porosity, water volume, and effective saturation are the same as those shown for CSNF.

HLW Waste Form Diffusive Area and Length—Consistent with the treatment for the CSNF waste form domain, radionuclides will tend to diffuse radially outward from the HLWG waste form subdomain. Since the diffusive area increases with increasing distance from the origin point in the radial geometry, the area of the HLW waste form domain is taken at half the radius of the inner vessel cavity (Figure 6.3.8-6) and set at a constant value of 13.7 m^2 (Table 6.3.8-2). The diffusive path length is set to be the inside radius of inner vessel of a CDSP WP (= 0.941 m) (Table 6.3.8-2). In calculating the diffusive conductance across the interface between the HLW waste form subdomain, and the downstream DSNF waste form subdomain the harmonic average of the diffusive areas and diffusive lengths of the two domains is used.

DSNF Waste Form Diffusive Area and Length—DSNF is modeled as degrading instantaneously upon WP breach. Since the carbon steel support tube, divider plates, and brackets that support the HLWG canisters surrounding the DSNF also degrade rapidly (compared to the degradation rates of HLWG and stainless steel inner vessel), the DSNF is not expected to retain its initial cylindrical shape, but rather will settle to the bottom of the interior of the inner vessel. In the 1-D EBS Transport Model, this implies that the DSNF diffusive area is the same as for the HLWG waste form subdomain (= 13.7 m^2) (Table 6.3.8-2). The effective diffusive path length is calculated by dividing the initial volume of DSNF 1 m^3 by the diffusive area leading to a total diffusive length of 0.0730 m (Table 6.3.8-2).

Calculation of Diffusion Coefficients in the CDSP Waste Form Domain—The effective diffusion coefficient for dissolved radionuclides in the HLW and DSNF subdomain is computed using Archie's law (Equation 6.3.8-10a and b). Both subdomains are considered to be fully

saturated when there is flow through the WP. The diffusion coefficient for the colloids is separately computed based on the sampled size of the colloids (SNL 2007 [DIRS 177407], Section 6.3.4.4).

Advective Transport in the CDSP Waste Form Domain—The HLW and DSNF waste form subdomains are modeled sequentially, such that the HLW subdomain is upstream of the DSNF subdomain. Because of the one-dimensional model geometry, the DSNF waste form subdomain sees the same water flux as the HLW waste form subdomain. The advective transport out of the HLW waste form subdomain and into the DSNF waste form subdomain can only occur when there is liquid flow through the WPs. The EBS Flow Submodel determines the flux through the WP (Section 6.3.6).

6.3.8.2.3 Corrosion Products Domain

The corrosion products domain represents that portion of the internal components of a WP that has degraded after the WP is breached (see Section 6.3.8.1 for the steel components included in this domain). Degradation of the internal WP components results in two types of materials: (1) stationary iron oxyhydroxide corrosion products that are assumed to remain in the WP and (2) iron oxyhydroxide colloids that are mobile and can move out of the WP. Although only iron oxyhydroxide colloids are generated in this domain, waste form colloids (generated from HLW degradation) and groundwater colloids (from seepage waters) can also be present.

A surface complexation-based competitive sorption model is developed for modeling sorption of dominant actinides in the inventory (uranium, neptunium, plutonium, americium, and thorium) to the iron oxyhydroxide surfaces. It is a mechanistic model based on a single-site diffuse-layer surface complexation model that couples the pH in the corrosion products domain with the type of surface complexes formed under varying chemical conditions and sorption site densities. The model is applicable to a wide range of concentrations and accounts for competition among various actinides for the finite number of sorption sites. The stationary corrosion products and iron oxyhydroxide colloids are considered to be a mixture of goethite and ferrihydrite, the proportion of which is treated as uncertain. The details of the model development are described in *EBS Radionuclide Transport Abstraction* (SNL 2007 [DIRS 177407], Section 6.5.2.4).

The mass of corrosion products in a breached WP varies over time, from zero when the WP is first breached to a maximum amount (SNL 2007 [DIRS 177407], Table 6.3-8) when all of the steel in the domain is corroded. The mass, at any given time, is computed by linearly interpolating over the lifetime of each of the two major types of steel comprising the internal components of a WP—carbon steel and stainless steel. The equations used to calculate the time-dependent mass of corrosion products, present in the corrosion products domain, are developed in *EBS Radionuclide Transport Abstraction* (SNL 2007 [DIRS 177407], Section 6.5.2.2.1). Note that only the mass of corrosion products contributed by goethite and ferrihydrite is used in competitive sorption calculations of radionuclides, while for water vapor adsorption calculations the entire mass of corrosion products is used, including nickel oxides and chromium oxides. The corrosion products mass from degradation of steel shield plug in the TAD canister is not considered in TSPA as the mass is localized at one end of the WP and will not appreciably affect transport throughout the rest of the WP. A minimum initial mass of 10 kg of

stationary corrosion products is assumed, as it is required to initiate the water volume and sorption calculations after the WP failure.

Corrosion Products Domain Within a CSNF WP—Both advective and diffusive transport can occur from the corrosion products domain to the invert domain. Solving the mass transport equations requires that the following properties be defined: (1) mass of corrosion products; (2) volume of water in the corrosion products; (3) diffusive area of the domain; (4) diffusive length of the domain; and (5) advective flow rate.

CSNF Corrosion Products Water Volume—The volume of water in the CSNF corrosion products domain is calculated as the product of the pore volume and water saturation of the corrosion product mass. The pore volume of the corrosion products is calculated by the expression (SNL 2007 [DIRS 177407], Section 6.5.2.2.1)

$$V_{\phi,CP}(t) = \left(\frac{\phi_{CP}}{1-\phi_{CP}}\right)\sum_{CPm}\left[\frac{\left[m_{CPm,CS}(t) + m_{CPm,SS}(t)\right]}{\rho_{CPm}}\right] \qquad \text{(Eq. 6.3.8-18)}$$

where, ϕ_{CP} is the steel corrosion products porosity (a constant value of 0.4), $m_{CPm,CS}$ is the mass of corrosion products from degradation of carbon steel, $m_{CPm,SS}$ is the mass of corrosion products from degradation of stainless steel, ρ_{CPm} is the grain density of corrosion products, and subscript '*m*' refers to the type of corrosion products formed (goethite, ferrihydrite, NiO, and Cr_2O_3).

When there is flow through the WP, the water saturation is assigned a value of 1.0 (SNL 2007 [DIRS 177407], Section 6.5.2.2). In conditions when there is no flow through the WP, the only water present is adsorbed water and the water saturation in the domain for each type of corrosion product (goethite, ferrihydrite, NiO, and Cr_2O_3) is computed separately as given by (SNL 2007 [DIRS 177407], Section 6.5.2.2.1):

$$S_{w,CPm}(RH) = \min\left[t_f \rho_{CPm} \bar{s}_{CPm}\left(\frac{1-\phi_{CP}}{\phi_{CP}}\right)\theta_{CP}(RH), 1.0\right] \qquad \text{(Eq. 6.3.8-19)}$$

where

$S_{w,CPm}$ = effective water saturation of corrosion products (fraction)

$\bar{s}_{CPm}$ = specific surface area of corrosion products (m^2/kg)

ρ_{CPm} = corrosion products grain density (kg/m^3)

θ_{CP} = number of monolayers of water adsorbed on the surface of corrosion products; a function of relative humidity

t_f = thickness of a monolayer of water (m)

RH = relative humidity (fraction).

A single adsorption isotherm is used for all corrosion products, so a single relative humidity-dependent value of $\theta_{CP}(RH)$ is used for all corrosion products in this domain. The water volume for the entire domain is calculated as:

$$V_{w,CP}(RH,t) = \sum_m V_{\phi,CPm}(t) S_{w,CPm}(RH) \qquad \text{(Eq. 6.3.8-20)}$$

The water saturation for the entire domain is calculated as:

$$S_{we,CP}(RH) = \min\left[\frac{V_{w,CP}(RH,t)}{V_{\phi,CP}(t)}, 1.0\right] \qquad \text{(Eq. 6.3.8-21)}$$

CSNF Corrosion Products Diffusive Area and Length—Since the WP outer barrier undergoes variable damage specified by the scenario classes and modeling cases, the corrosion products domain is divided into two regions: (a) the region that only includes the outer barrier and (b) the region that includes the TAD canister and inner vessel but excludes the outer barrier. The diffusive area for the path excluding the outer barrier is given by the surface area of a cylinder halfway between the inside surface of the TAD canister and the outside surface of the inner vessel (= 29.9 m^2) (Table 6.3.8-2), while the diffusive path length is given by the distance from the inside of the TAD canister to the outside of the inner vessel (= 0.0914 m) (Table 6.3.8-2). The diffusive area for the path through the outer barrier of the WP is taken to be the smaller of either: (a) the WP breached area (scenario class dependent) or (b) the surface area of a cylinder at the midpoint between the inner vessel outer surface and the outer surface of the CSNF WP outer barrier (= 33.1 m^2) (Table 6.3.8-2). The diffusive path length through the outer barrier is the radial distance from the outside of the inner vessel to the outside of the outer barrier (= 0.0302 m) (Table 6.3.8-2).

Calculation of Diffusion Coefficients in the CSNF Corrosion Products Domain—The diffusion coefficient of the corrosion products is computed using Archie's law (Equation 6.3.8-10a,b), with the porosity of the corrosion products (0.4) and an assigned water saturation as discussed earlier.

Advective Transport in the CSNF Corrosion Products Domain—Advective transport through the CSNF corrosion products domain can only occur when there is liquid flow through the WPs. The EBS Flow Submodel determines the flux through the WP (Section 6.3.6).

Corrosion Products Domain Within a CDSP WP—The CDSP corrosion products domain consists of corroded internal WP components (see Section 6.3.8.1 for the steel components included in this domain). Both advective and diffusive transport can occur in the corrosion products domain. Solving the mass transport equations requires that the following properties be defined for each domain: (1) mass of corrosion products; (2) volume of water in the corrosion products; (3) diffusive area of the corrosion products domain; (4) diffusive length; and (5) advective flow rates.

The discussion presented for the corrosion products domain within a CSNF WP is applicable to CDSP WP except for parameter values such as mass of steel, diffusive lengths, and diffusive

areas. Since the WP outer barrier undergoes variable damage specified by the scenario classes and modeling cases, the corrosion products domain, just like for CSNF, is divided into the region that only includes the outer barrier and the one that is inside the WP but excludes the outer barrier. The diffusive area for the path excluding the outer barrier is given by the surface area of a cylinder halfway between the inside surface and the outside surface of the inner vessel (= 29.7 m^2) and diffusive path length is given by the thickness of the inner vessel (= 0.0508 m). The diffusive area for the path through the outer barrier of the WP is taken to be the smaller of either (a) the WP breached area (scenario class dependent) or (b) the surface area of a cylinder at the midpoint between the inner vessel outer surface and the outer surface of the CDSP WP outer barrier (= 32.6 m^2). The diffusive path length through the outer barrier is the radial distance from the outside of the inner vessel to the outside of the outer barrier (= 0.0301 m).

6.3.8.2.4 Invert Domain

The invert domain is conceptualized as a single continuum rather than as a dual continuum for modeling radionuclide transport. Both advective and diffusive transport can occur from the invert domain to the UZ. Sorption of radionuclides may occur on the crushed tuff in the invert and is modeled by the linear sorption isotherm approach using the distribution coefficient (K_d). The ranges and distributions of radionuclide sorption coefficients for sorption on crushed tuff in the invert are the same as those for devitrified tuff implemented in the UZ Transport Submodel (Table 6.3.9-2). [Note: Since K_d for Se is set to zero for the TSw unit in the UZ Transport Submodel, the K_d for Se in the invert is also set to zero as most of the repository host rock is composed of TSw unit.] Solving the mass transport equations requires that the following properties be defined: (1) the volume of water in the invert; (2) the diffusive area of the invert domain; (3) the diffusive length; and (4) advective flow rates.

Invert Domain Water Volume—The water volume of the invert domain is calculated as the product of the bulk volume and the water content of the invert (SNL 2007 [DIRS 177407], Section 6.5.2.3). The total bulk invert volume is equal to the cross-section area of the invert times the length of a WP (CDSP or CSNF). The water content of the invert cell is calculated according to the following relationship (SNL 2007 [DIRS 177407], Equation 6.5.2.3-11):

$$\theta_{inv} = \theta_{inter} + (1 - \phi_{inter})\theta_{intra} \qquad \text{(Eq. 6.3.8-22)}$$

where

θ_{inv} = invert water content

θ_{inter} = water content of the intergranular invert

ϕ_{inter} = porosity of the intergranular invert

θ_{intra} = water content of the intragranular invert.

Because the crushed tuff invert has both intergranular and intragranular porosity, the bulk water content of the invert is calculated by combining the water contents of both pore types as shown in Equation 6.3.8-22. The intragranular water content is calculated by multiplying the

intragranular water saturation with the intragranular porosity. The intragranular water saturation is provided by the MSTHM Abstraction from the EBS TH Environment Submodel (Section 6.3.2). The intergranular water saturation is calculated based on the seepage flux per cross-sectional area of the drift over the length of a WP (BSC 2004 [DIRS 167652], Section 6.3.1) by using the van Genuchten moisture retention relationship for the crushed tuff, as described in the *EBS Radionuclide Transport Abstraction* (SNL 2007 [DIRS 177407], Section 6.5.2.3). The porosity of the intragranular continuum is 0.111, the porosity for the intergranular continuum is 0.224, and the residual water content of the intergranular continuum is 0.00224. The bulk density of the invert material is estimated to be 1.27 g/cm^3.

Invert Diffusive Length—The true geometry of the invert is that of a segment of a circle where the top of the invert is flat and the bottom is formed by the arc of the drift. However, for the purposes of modeling flow and diffusion through the invert, the invert is regarded as having a rectangular cross section with the top being the actual top surface of the invert (Figure 6.3.8-7). The bulk volume of the invert is conserved by calculating an average thickness of the invert using the following equation (SNL 2007 [DIRS 177407], Equation 6.5.2.3-5):

$$\bar{t}_I = \frac{A_I}{w_I} = 0.934 \text{ m} \qquad \text{(Eq. 6.3.8-23)}$$

where

$\bar{t}_I$ = average invert thickness (m)

A_I = actual invert vertical cross-sectional area (4.39 m^2) (SNL 2007 [DIRS 177407], Section 6.5.2.3)

w_I = actual width of invert top surface (4.70 m) (SNL 2007 [DIRS 177407], Section 6.5.2.3).

The diffusive path length from the WP outer barrier to the mid-point of the invert is a sampled value between 0.3 m and 1.24 m to represent uncertainty in the location of the breach on the WP and the average thickness from the invert (Table 6.3.8-4). The diffusive length from the mid-point of the invert to the interface with the host rock (part of EBS-UZ Interface domain) is taken to be half of the average invert thickness.

Invert Diffusive Area—The diffusive area implemented for the invert cell is the plan area of the rectangular invert. It is equal to the width of the invert top surface times the length of a WP (CDSP or CSNF).

Calculation of Diffusion Coefficients in the Invert Domain—The diffusion coefficient for dissolved radionuclides in the invert is computed using the following formulation of Archie's law (SNL 2007 [DIRS 177407], Equation 6.3.4.1.1-22):

$$\phi_{inv} S_w D = D_{wi} \theta_{inv}^{1.863} 10^{ND(\mu=0.033,\sigma=0.218)} \qquad \text{(Eq. 6.3.8-24)}$$

where

D = invert diffusion coefficient (cm^2/s)

D_{wi} = species dependent free water diffusion coefficient (cm^2/s)

S_w = invert water saturation

ϕ_{inv} = bulk invert porosity

ND = truncated normal distribution (±3 SDs from the mean)

μ = mean

σ = SD.

After the invert diffusion coefficient has been calculated using Equation 6.3.8-24, it is modified to account for temperature effects. The diffusion coefficient at a given temperature is given by (SNL 2007 [DIRS 177407], Equation 6.3.4.1.2-4)

$$D_T = D_{T_0} \frac{T}{T_0} 10^{\left[\frac{1.3272(293.15-T_0)-0.001053(T_0-293.15)^2}{T_0-168.15}\right]-\left[\frac{1.3272(293.15-T)-0.001053(T-293.15)^2}{T-168.15}\right]} \quad \text{(Eq. 6.3.8-25)}$$

where

D_T = invert diffusion coefficient at temperature T (cm^2/s)

D_{T_0} = invert diffusion coefficient at temperature T_0 (as calculated by Equation 6.3.8-24) (cm^2/s)

T = invert temperature (K)

T_0 = reference temperature (298.15 K).

Advective Transport in the Invert Domain—There are two sources of advective water flux into the invert domain. The first is the advective flux that comes from the overlying corrosion products domain. This flux is defined by Flow Pathway F_6 (flux into the invert) of the EBS Flow Submodel (Section 6.3.6.2). The other advective flux source is due to possible imbibition from the host rock that enters the invert and flows out under gravity. This imbibition flux is defined by Flow Pathway F_7 (Section 6.3.6.2 and Figure 6.3.6-4). The EBS TH Environment Submodel (Section 6.3.2) provides the rate of water imbibition from the host rock that enters the invert and flows out under gravity.

EBS-UZ Interface Domain—The EBS-UZ Interface domain is included beneath the invert domain to establish a boundary condition for calculating the diffusive flux from the invert to the UZ and to compute the radionuclide mass flux fraction going into each of the UZ fracture and matrix continua. The EBS Transport Abstraction applies a semi-infinite zero-concentration boundary condition near the base of the drift (SNL 2007 [DIRS 177407], Section 6.5.2.6). This boundary condition is approximated by applying an effective zero-concentration boundary in the

UZ at approximately three drift diameters below the invert-UZ boundary. In the EBS-UZ Interface domain, the near-field UZ is modeled as a dual continuum consisting of overlapping UZ-matrix and UZ-fracture continua. This approach is consistent with the dual-permeability modeling approach used by the UZ Transport Submodel, as described in (SNL 2007 [DIRS 181006], Section 1). The ranges and distributions of radionuclide sorption coefficients for sorption on the UZ matrix are the same as those for devitrified tuff implemented in the UZ Transport Submodel (Table 6.3.9-2). [Note: Since K_d for Se is set to zero for the TSw unit in the UZ Transport Submodel, the K_d for Se in the UZ matrix of the EBS-UZ Interface domain is also set to zero as most rock near the drift is composed of TSw unit.] Advective fluid flux defined by Flow Pathway F_6 (combined seepage and condensation) is passed to the UZ fracture from the invert, while the advective flux due to imbibition from the host rock, defined by Flow Pathway F_7, is passed from the invert to the UZ matrix. Details of the implementation of the EBS-UZ Interface boundary condition are given in Section 6.3.8.3.

The radionuclide mass flux fractions going into the near-field UZ-matrix and UZ-fracture continua is calculated from the EBS-UZ Interface domain for each radionuclide species and passed to the UZ model along with the mass flux from the invert. The mass flux fraction varies as a function of time and may differ for each radionuclide species based on its transport characteristics. A detailed description of how the mass fractions are calculated is given in the next section.

6.3.8.3 TSPA-SEIS Implementation

The transport of radionuclides through the EBS is modeled in the TSPA-SEIS by spatially discretizing the EBS components into transport domains, as described in Section 6.3.8.1. In each domain, the four EBS transport one-dimensional continuum-form mass balance equations described at the beginning of Section 6.3.8.2 are approximated and solved using a finite-difference approach. The implementation and numerical solution of the EBS Transport Submodel's equations are performed using the GoldSim software cell pathway capability. The number of cell pathways in the finite-difference network and the discretization of the cells are chosen in such a way as to capture the physical and chemical properties of the EBS components with respect to radionuclide transport. The cell pathway acts as a batch reactor, where radionuclide mass is modeled as instantaneously and completely mixed and partitioned among all media, fluid or solid, within the cell. Both advective and diffusive transport mechanisms can be explicitly represented using the cell pathways. When multiple cells are linked together via advective and diffusive connections, the performance of the cell network is mathematically described using a coupled system of differential equations, and is mathematically equivalent to a finite-difference network. The GoldSim software numerically solves the coupled system of equations to compute the radionuclide mass present in each cell and the mass fluxes between cells as a function of time. Both initial and boundary conditions for a cell can be defined explicitly, and systems of varying geometry can be modeled.

This finite-difference approach used to solve the mass balance equations requires the discretization of the time derivative (or mass accumulation term) and the advective and diffusive terms for both dissolved and colloidal transport. The spatially dependent derivative terms, which include advective and diffusive transport, are discretized using implicit difference approximations. Using an implicit difference approximation, if the solution is known at

timestep, n, and is to be computed at the next timestep, n+1, the advective/diffusive flux difference approximations use the concentrations at timestep n+1. Further, the source terms, such as radionuclide decay/ingrowth and reactions due to reversible sorption, are also represented implicitly. Therefore, the difference equations are fully implicit in the unknown cell concentrations. The difference equations have variable coefficients (e.g., water content), which can be both time and space dependent. These coefficients are evaluated at the start of the timestep. The resulting system of difference equations is a linear algebraic system in the unknown cell concentrations. A complete description of the discretized transport equations is provided by (SNL 2007 [DIRS 177407], Section 6.5.2.5). Another consideration is the computational time requirement. An implicit solution technique is used because it provides an unconditionally stable solution (i.e., a solution is obtainable for any size timestep). In addition, the GoldSim equation-solver software tests solution accuracy by applying several mass balance and convergence tests based on a GoldSim model file precision setting of high, medium, or low. All simulations for TSPA-SEIS are run using the high-precision setting. If a solution in a given cell pathway fails to meet the mass balance and convergence criteria in the user-specified timestep, the software will dynamically reduce the computational timestep until the required precision is obtained.

Figure 6.3.8-4 shows a schematic representation of the GoldSim cell pathway network used to implement the EBS Transport Submodel for CSNF WPs. For the waste form domain, a single waste form cell (Cell 1) is used to represent the entire volume of the degraded waste form and the associated mass transport processes. Similarly, for CDSP WPs (figure not shown), two cell pathways representing each waste form subdomain are used: one for HLW fuel (Cell 1a) and another for DSNF fuel (Cell 1b). The mass transport processes in the corrosion products domain are modeled by the corrosion product cell (Cell 2), where sorption reactions are modeled. Similarly, the processes in the invert domain are modeled by the invert cell (Invert Cell). The EBS-UZ domain is modeled by an array of near-field UZ cells (UZ Fracture Cell and UZ Matrix Cell). The interface cell, namely, Invert-UZ Interface cell, shown on Figure 6.3.8-4, is used for computing the concentrations at the interface boundaries for maintaining diffusive flux continuity between a single continuum domain and a dual continuum domain, as described in (SNL 2007 [DIRS 177407], Section 6.5.2.5).

Within the GoldSim cell network, diffusive and advective flux connections are defined for each cell. The advective and diffusive flux connections between the various cells in the EBS Transport Submodel are indicated on Figure 6.3.8-4. The flow through various cells is based on the continuity equations and conservation of mass, as described in (SNL 2007 [DIRS 177407], Section 6.3.1.1). Each computational cell is provided with parameters describing water volumes, diffusive properties, and advective and diffusive flux links to other cells. Between any two cells, the diffusive flux can be bidirectional, depending on the concentration gradient, while the advective flux is unidirectional. The output of a cell is given in terms of the advective and diffusive mass fluxes for each radionuclide species and its concentration at the cell center. The mass transport equations in a cell network are solved on a per package basis and then scaled by GoldSim to the number of failed WPs.

Implementation of the EBS Transport Submodel for the TSPA-SEIS uses the output of the Waste Form Degradation Submodel (Section 6.3.7.4), the EBS Flow Submodel (Section 6.3.6), the EBS TH Environment Submodel (Section 6.3.2), the Dissolved Concentration Limits Submodel

(Section 6.3.7.5), and the EBS Colloids Submodel (Section 6.3.7.6). An overview of the computational model for the TSPA-SEIS, as implemented using the GoldSim software, is provided below.

Waste Form Cells—The waste form cell receives radionuclide mass from a specialized GoldSim Source element, which models the WP failure, degradation of the waste form, and release of the radionuclide inventory for possible transport through the EBS. The Source element provides the specified flux boundary condition for solving the mass transport equations. There is no advective or diffusive transport of dissolved radionuclides or radionuclides sorbed onto colloids when the temperature is greater than the boiling point of water in the TSPA-SEIS (Section 5.1.4). This is achieved by setting the radionuclide solubilities to zero at temperatures greater than 100°C (the boiling point of water).

CSNF Waste Form—The setup of a waste form cell for CSNF WPs and its relationship to other cells for modeling transport through the WP are illustrated on Figure 6.3.8-5. Both advective and diffusive transport can occur from the waste form cell (Cell 1) to the corrosion products cell (Cell 2). Radionuclides are transported from this cell to the downstream cell in the dissolved state and reversibly sorbed on waste form and groundwater colloids. Plutonium and americium can also be transported as irreversibly sorbed on the specified waste form colloids. Solving the mass transport equation requires that the following properties be defined: (1) the volume of water in the rind; (2) the diffusive area; (3) the diffusive length; and (4) advective flow rates.

CDSP Waste Form—The implementation of the waste form cells for CDSP WPs differs from the approach used for CSNF WPs, in that degraded fuel is represented by two cell pathways. The setup of the waste form cell pathways for both CDSP WP fuel types and their relationship to actual waste forms are illustrated on Figure 6.3.8-6. One cell pathway (Cell 1a) represents the degraded HLW glass logs, while the other cell pathway is for the degraded DSNF waste form (waste form Cell 1b). Solving the mass transport equations for these cells requires that the similar properties be defined as for the CSNF waste form.

Although presented in Section 6.3.8.2.2, Equation 6.3.8-11 is not directly implemented into the TSPA-SEIS. The TSPA-SEIS calculates the fraction of the HLW glass that is degraded at each timestep (Section 6.3.7.4.3.3) and the result is used to determine the rind volume at each timestep. For the CDSP WP rind volume, the TSPA-SEIS implements a modification to the relationship provided in Equation 6.3.8-11, which utilizes the fraction of mass degraded instead of the total mass degraded:

$$V_{rind,HLWG}(t) = \phi_{rind} V_{total} F_{cor} \qquad \text{(Eq. 6.3.8-26)}$$

where

$V_{rind,HLWG}(t)$ = the time-dependent rind volume (m^3)

ϕ_{rind} = rind porosity

V_{total} = the initial total volume of HLW glass in a CDSP WP (m^3)

F_{cor} = fraction of mass degraded into rind.

The fraction of mass degraded is calculated by Equation 6.3.7-8.

In addition to being transported in the dissolved state, radionuclides in the CDSP WP waste form cell can be transported via waste form colloids and groundwater colloids. The waste form colloids form from the degradation of HLW glass and can reversibly sorb radionuclide. They also include embedded plutonium and americium, which are considered as intrinsic parts of the colloids and, thus, not in equilibrium with the aqueous system. These embedded radionuclides are modeled as attached irreversibly to the host colloids. Details of the waste form colloid generation, stability, and sorption capability are given in Section 6.3.7.6.2. Waste form colloids are also produced in the DSNF waste form subdomain (WF Cell 1b). The waste form colloids generated from the HLW waste form subdomain, as well as groundwater colloids from the seepage water, pass through the DSNF waste form cell.

Corrosion Products Cell—Conceptually, the corrosion products cell (Cell 2) is the part of the corrosion products domain (described in Section 6.3.8.1) that represents the degraded steel components of the WP, which is modeled as iron oxyhydroxides. However, it does not include the corrosion products from the degradation of the outer barrier, which is treated as a separate cell (see discussion below). The corrosion products cell includes both stationary corrosion products and iron oxyhydroxide colloids; which both participate in equilibrium and kinetic sorption of radionuclide mass. A surface complexation-based competitive sorption model is used to calculate sorption of uranium, neptunium, plutonium, thorium, and americium onto stationary corrosion products and iron oxyhydroxide colloids as a function of available sorption sites, P_{CO_2}, and dissolved concentration of the radionuclides. For a detailed discussion of this mechanistic model, see (SNL 2007 [DIRS 177407], Section 6.3.4.2.3 and Section 6.5.2.4). A multiple regression model for computing the sorbed mass is developed based on the dissolved concentration of the radionuclides computed at the end of the previous timestep. The effective K_d value, which is needed by the GoldSim solver, is calculated by dividing the sorbed mass by the dissolved concentration. The computed effective K_d value is directly used in the transport equation for uranium, neptunium, and thorium, which are modeled to undergo equilibrium sorption. Plutonium and americium are modeled to undergo kinetic sorption-desorption reactions where the desorption rate is calculated by dividing the forward reaction rate by the K_d for plutonium and americium (from the surface complexation based regression equation).

Table 6.3.8-3 summarizes the distributions used to determine the available sites for competitive sorption on the stationary corrosion products and iron oxyhydroxide colloids. The pH in the cell is also computed based on the results of surface complexation modeling by the following equation (SNL 2007 [DIRS 177407], Equation 6.5.2.4-6):

$$pH = 4.5342 + 0.6132(pCO2) - 0.3805\log_{10}[U] - 0.0254(\log_{10}[U])^2 + E \qquad \text{(Eq. 6.3.8-27)}$$

where, pCO_2 is the negative log of the in-drift CO_2 partial pressure (bars), [U] is the dissolved concentration of U in mol L^{-1}, and E is the error term (pH_Cell_2_Regression_Error) defined by a normal distribution with mean of zero and SD of 0.32 truncated at ± 2 SDs.

As with the waste form cells, there is no advective or diffusive transport of dissolved radionuclides or radionuclides sorbed onto colloids in the corrosion products cell when the WP temperature is greater than 100°C in the TSPA-SEIS. This is achieved by setting the radionuclide solubilities to zero at temperatures greater than 100°C.

Outer Barrier Cell—An additional cell pathway is added at the base of the corrosion products domain to represent transport through the outer barrier. The WP outer barrier is composed of Alloy 22 (UNS N06022) and undergoes general corrosion at a different rate than the stainless steel inside the WP and the corrosion products formed from the degradation of Alloy 22 are different from those formed from the degradation of stainless steel. The breach area of the outer barrier varies by the individual scenario class modeling cases and exerts strong control on the advective and diffusive releases out of the WP: (1) for the Nominal Scenario Class, the outer barrier degradation from general corrosion and stress corrosion is determined by WAPDEG code (Section 6.3.5.1.3); (2) for the Seismic Scenario Class, the outer barrier damage from the ground motion and fault displacement is variable and determined probabilistically by the seismic damage abstraction (Section 6.6); (3) for the Igneous Intrusion Modeling Case the entire surface area of the outer barrier is assumed to be breached at the time of the igneous event (Section 6.5); (4) for the Waste Package EF and Drip Shield EF Modeling Cases the entire surface of the outer barrier is assumed to be breached at the start of simulation (Section 6.4); and (5) for the Human Intrusion Modeling Case, the breach area is considered to be the same as the cross-sectional area of the borehole (Section 6.7.3). No radionuclide sorption is modeled in the outer barrier cell even though the tortuosity computed for Cell 2 is applied to the outer barrier cell.

Invert Cells—In the TSPA-SEIS, the invert domain is represented by the invert cell pathway. For radionuclide transport, the invert is modeled as a single-continuum porous medium composed of crushed tuff (SNL 2007 [DIRS 177407], Section 6.5.2.3). The invert cell receives advective and diffusive mass flux from the outer barrier cell. The setup of the invert cell pathway is illustrated on Figure 6.3.8-7. Both advective and diffusive mass transport can occur from the invert cell to the near-field UZ cells.

Invert-UZ Interface Cell—This cell pathway is added between the invert cell and EBS-UZ Interface cells to model diffusive transport between a single-continuum invert (represented by one cell) and the dual-continuum UZ (represented by two cells). The diffusive flux needs to be bifurcated correctly between the two UZ continua while preserving the flux continuity condition at the interface. This is achieved by introducing the Invert-UZ Interface cell, which is conceptualized as a very thin slice of the invert cell (Figure 6.3.8-4). The purpose of this interface cell is to provide an approximate concentration boundary at the interface for diffusive flux calculation. All the properties of the interface cell are the same as the invert cell, except for the diffusive length, mass, and volume, which are computed by multiplying the equivalent invert cell properties by a scale factor of 10^{-6}. The diffusive area is the same as that of the overlying invert cell. For more details, see (SNL 2007 [DIRS 177407], Section 6.5.2.5).

EBS-UZ Interface Cells—The TSPA-SEIS uses an array of cells to model part of the near-field UZ below the invert. Modeling the near-field UZ serves to establish a far-field zero-concentration boundary for computing the flux from the invert to the UZ. The dual-continuum approach for modeling the near-field UZ is implemented by creating an overlapping continua of UZ matrix and fracture cells. Figure 6.3.8-8 illustrates how the conceptual model of the near-field UZ domain is implemented into the EBS Transport Submodel. The invert interface cell is connected with the UZ matrix and fracture cells directly below it in the UZ cell array.

The overlapping matrix and fracture continua are represented by a two-dimensional vertical array of cells oriented parallel to a cross section of a drift and located immediately beneath a drift. The entire cell array, consisting of three sets of two columns or vertical zones, with each zone containing both a fracture cell and a matrix cell, is shown on Figure 6.3.8-9. The invert is directly connected with the middle zone of UZ matrix/fracture cells. Each zone is four layers deep in the vertical direction. Thus, the array consists of 12 pairs of matrix and fracture cells within the UZ (Figure 6.3.8-9). Laterally, each zone is one drift diameter wide, with the middle zone centered beneath the drift, so that each layer of the array extends one drift diameter on either side of the drift. In the longitudinal direction of a drift, the length of the array is equal to the length of the WP being modeled.

As described in (SNL 2007 [DIRS 177407], Section 6.5.2.6), the thickness of the first (top) layer of cells is 1.0274 m, or 10 percent greater than the 0.934 m average invert thickness beneath a WP. The thickness of the second layer is double that of the first layer, or 2.05481 m. The third and fourth layers are given a thickness of 5 m and 10 m, respectively (Figure 6.3.8-9). Grid sizes are more refined near the base of the invert to accurately capture the higher concentration gradient in the region. A "collector cell" is placed beneath the fourth layer and is given a very large, numerically infinite water volume (10^{10} m^3) to simulate an effective zero-concentration boundary. This collector cell acts as a sink for all the mass flux from the UZ cells.

A description of the mass flux between the invert and UZ fracture and matrix cells is provided in (SNL 2007 [DIRS 177407], Section 6.5.2.6). Each fracture cell interacts, via a diffusive connection only, with the matrix cell of the same zone (Figure 6.3.8-9). The fracture cell also interacts vertically via a diffusive connection with the fracture cell of overlying and underlying layers. The matrix cell interacts via a diffusive connection laterally with adjacent matrix cells in the same layer and vertically with the matrix cells of overlying and underlying layers. Radionuclides diffuse based on the concentration gradient between cells. Advection occurs vertically downward only, from the fracture cell of one layer to the fracture cell of the underlying layer and from the matrix cell of one layer to the matrix cell of the underlying layer in the same zone. Lateral advection is not considered. Figure 6.3.8-9 illustrates the diffusive and advective flux connections between the various cells in the network.

The pore volume of each continuum is computed by multiplying the bulk volume for each discretized zone (based on the geometry) by either the fracture continuum porosity or the matrix continuum porosity. Similarly, the water volume is calculated by multiplying the pore volume of each continuum by its respective saturation. Reversible sorption of radionuclides to the matrix is modeled by using the K_d values for the devitrified tuff sampled by the UZ Transport Submodel

(Table 6.3.9-2). The mass of the UZ matrix is computed by multiplying the matrix volume (bulk volume × (1- fracture porosity)) of the cell by the dry bulk density of the UZ matrix.

Advective fluid flux due to seepage flows from the invert into the top middle UZ fracture cell, while the advective flux due to imbibition from the host rock, which enters the invert and flows under gravity, goes from the invert into the top middle UZ matrix cell. This partitioning of fracture and matrix advective flux is based on the actual source of the two components. That is, seepage comes from the host-rock fractures and imbibition from the host-rock matrix. An additional component of flow from the invert to the UZ is flux due to condensation on the drift walls. The condensation flux is treated in the same manner as seepage flux and is combined with the seepage flux. In the dripping environment, the advective flux flowing through the UZ fracture cells in the middle zone is the larger of the advective flux out of the invert or the steady-state UZ fracture flux. The advective flux in the two outer zones is the steady-state UZ flux in each continuum at the repository horizon.

Diffusive mass flux from the invert can go into both fracture and matrix UZ continua based on the concentration gradient and effective diffusion coefficient. All three types of colloids in the TSPA-SEIS are transported from the invert to the UZ cells. Groundwater colloids are present in all four layers. Because the UZ Transport Submodel only models groundwater colloids (with reversibly sorbed radionuclide mass), in order to be consistent, the iron oxyhydroxide and waste form colloids with reversibly sorbed radionuclides are modeled as present in only the first two layers of the middle column, making the groundwater colloids the only types of colloids available for far-field transport. Americium and plutonium mass that is irreversibly sorbed on iron oxyhydroxide colloids or embedded in waste form colloids is transported from the invert to the UZ cells, as long as these colloids are stable in the invert. If the chemical conditions in the invert are such that the iron oxyhydroxide or waste form colloids become unstable, they are not transported from the invert to the UZ. However, if the colloids are stable in the invert then they also remain stable in the UZ and SZ. Solubility constraints are not imposed on any species in the UZ cells. Additional details regarding the hydrologic parameters used in the EBS-UZ interface cells are provided in the *EBS Radionuclide Transport Abstraction* (SNL 2007 [DIRS 177407], Section 6.5.2.6).

EBS Transport Submodel Outputs—The output from the EBS Transport Submodel consists of the total radionuclide mass flux out of the single-continuum invert. The mass flux from the single-continuum invert to the dual-continuum UZ, computed by the EBS-UZ Interface cells, is passed to the UZ Transport Submodel for TSPA-SEIS calculations. It is used as the mass flux boundary condition for the UZ Transport Submodel, as described in Section 6.3.9. Three different types of mass fluxes are passed to the UZ Transport Submodel. The first type of mass flux is applicable for all radionuclides transported in the TSPA-SEIS. This flux includes all of the radionuclide mass that exists in the dissolved state or is reversibly sorbed onto the three different colloid types: groundwater, waste form, and iron oxyhydroxide. After it is input into the UZ Transport Submodel, this mass is repartitioned onto the groundwater colloids in the UZ based on the sampled colloid concentration and sorption coefficients defined for the UZ Transport Submodel (Section 6.3.9.2). Radionuclides that are irreversibly sorbed onto waste form and iron oxyhydroxide colloids form the basis for the next two mass flux types. These masses are defined in the EBS Transport Submodel as distinct species ("Ic" species for mass irreversibly sorbed onto waste form colloids and "If" species for mass irreversibly sorbed onto

iron oxyhydroxide species). After exiting the EBS, and before being passed to the UZ Transport Submodel, the "Ic" and "If" masses are added together for each irreversibly sorbed radionuclide. The total irreversibly sorbed mass, for a given radionuclide, is then repartitioned onto a fast and a slow colloid fraction through the UZ and SZ. The fraction of colloids that travel unretarded through the UZ and SZ are called the fast fraction, while the remaining colloids that undergo some degree of retardation are called the slow fraction. A value of 0.00168 is used in the TSPA to represent the fast fraction of colloids (BSC 2004 [DIRS 170006], Section 6.6 and Table 6-4). The partitioning of irreversible mass associated with the fast fraction is calculated by multiplying the total irreversibly sorbed mass for a radionuclide by 0.00168, while that for the slow fraction is done by multiplying total irreversibly sorbed mass by (1–0.00168). The mass associated with the fast fraction is assigned to the "If" species, while the mass associated with the slow fraction is assigned to the "Ic" species in the UZ and SZ transport submodels. In effect, for the EBS Transport calculations, the terms "Ic" and "If" represent irreversibly sorbed mass on the waste form colloids and iron oxyhydroxide colloids, respectively, but for the UZ and SZ transport (and for the dose calculations) the "Ic" means irreversibly sorbed mass traveling on the slow colloid fraction while the "If" means irreversibly sorbed mass traveling on the fast colloid fraction.

In addition to the total mass flux, the relative fraction of the mass going into each of the fracture and matrix cells at the EBS-UZ boundary is required by the UZ Transport Submodel. This fracture-matrix partitioning of mass is calculated on the basis of the mass fraction going into the fracture continuum, as compared to the total going into the fracture and matrix continua, from the invert. This partitioning is time-dependent and captures the temporal processes active in the EBS, such as varying radionuclide concentrations in the WP and invert and changing water flow through various components of the EBS. Furthermore, this partitioning is computed by solving the mass transport equations for the EBS and part of the UZ as a coupled system with appropriate boundary conditions.

Modification of Diffusive Lengths in GoldSim—When two cells with different diffusive areas are connected, an adjustment is required in the GoldSim setup to properly compute the diffusive conductance. Figure 6.3.8-10 is a simplified depiction of a cell-to-cell connection in which two cells have different diffusive areas. Such differences in diffusive area between connected cells occur due to varying domain dimensions, for example, the diffusive area at the node of the waste form cell (Cell 1) is different from the diffusive area at the node of the corrosion products cell (Cell 2).

The diffusive conductance (C_{12}) from the node in Cell 1 to the node in Cell 2 controls the diffusive mass flux to Cell 2. This conductance is properly calculated as the harmonic sum of two diffusive conductance links (SNL 2007 [DIRS 177407], Section 6.5.2.5, simplified from Equation 6.5.2.5-7):

$$C_{12} = \frac{1}{\frac{(L_1/2)}{D_1 A_1} + \frac{(L_2/2)}{D_2 A_2}} \qquad \text{(Eq. 6.3.8-28)}$$

where

L_1 = diffusive length of Cell 1 (m)

D_1 = effective diffusion coefficient of Cell 1 (includes effects of porosity, saturation, and tortuosity) (m^2/s)

A_1 = diffusive area of Cell 1 (m^2)

L_2 = diffusive length of Cell 2 (m)

D_2 = effective diffusion coefficient of Cell 2 (includes effects of porosity, saturation, and tortuosity) (m^2/s)

A_2 = diffusive area of Cell 2 (m^2).

That is, each conductance link is properly defined using the effective diffusion coefficient, length, and area of that link. However, in the GoldSim cell pathway only a single diffusive area can be defined, which is the area of the upstream cell (in this case A_1). In order to conform to the GoldSim formulation, the assigned diffusive area is set equal to a unit area of 1.0 m^2 (the numerator in the following equation) and the cell areas are implicitly included in the diffusive length terms by dividing the diffusive lengths by their respective areas, as shown below:

$$C_{12} = \frac{1}{\frac{(L_1/2)/A_1}{D_1} + \frac{(L_2/2)/A_2}{D_2}} \qquad \text{(Eq. 6.3.8-29)}$$

In the TSPA-SEIS, the approach illustrated by Equation 6.3.8-29 is applied to all diffusive connections between cells in the EBS Transport Submodel. Within each GoldSim cell pathway the diffusive areas are set equal to 1.0 m^2 and the calculated diffusive half-length is divided by the appropriate diffusive area to compute an effective diffusive half-length. This modification results in the proper diffusive conductance being calculated in the solution of the EBS Transport mass balance equations.

6.3.8.4 Model Component Consistency and Conservatism in Assumptions and Parameters

To enhance understanding of the complex interactions within the TSPA-SEIS, a discussion of consistency among model components and submodels, and identification of conservative assumptions in abstractions, process models, and parameter sets supporting the EBS Transport Submodel are discussed below.

6.3.8.4.1 Consistency of Assumptions

Water Balance in the TSPA-SEIS Within the EBS—The conceptual, mathematical, and abstraction models for estimating how much water can enter, accumulate, and move through various EBS components are discussed in Sections 6.3.6 and 6.3.8.2. The water balance discussion can be divided into two categories, one related to water flow and the other to water volumes.

There are two potential inconsistencies with respect to water flow through various EBS components in the TSPA-SEIS: (1) the reduction in water flow due to evaporation is conservatively ignored; and (2) the condensation flux calculations are performed separate from the MSTHM calculations that are used to define the temperature and relative humidity conditions in the EBS.

Water volume calculations in TSPA-SEIS are primarily based on phenomenological laws for fluid retention in porous media. For example, the saturation and water volume in the invert is calculated based on the soil-moisture retention relationships of crushed tuff; the saturation of the corrosion products and waste form rind, under no flow conditions, are computed as a function of relative humidity based on adsorption isotherm. While most calculations for the saturations (and water volumes) are based on phenomenological laws, some assumptions had to be made for other components to model them in a reasonable, and technically defensible manner. These include the assumption of complete saturation of corrosion products and waste form rind under water-flowing conditions. In addition, some inconsistencies in water volumes exist among process-level models mainly due to the limitation of the models used in the calculations. For example, a minimum water volume was required for in-package chemistry calculations so as to keep the ionic strengths less than 4 molal, the effective limit of the B-dot equation used in the EQ3/6 based model. This water volume is independent of the relative humidity and temperature histories as predicted in the MSTHM and is likely larger than is realistic at low relative humidity conditions.

Effect on the TSPA—The water balance related issues are significant primarily in the integrated suite of EBS submodels, rather than in the natural system models, because of the direct effect of water volume and flux on the radionuclide source term. Within the EBS, water balance issues are primarily related to the diffusion-dominated modeling cases, where the limited water availability may control the degree of liquid saturation inside the WP and, therefore, the radionuclide transport rates through the WP. In the advection-dominated modeling cases, the water balance related issues are not very important, because sufficient water flows through the WP to result in rapid turnover rate with respect to pore volume in the WP and thus the assumption of complete saturation is a reasonable one.

Although water balance issues in the EBS are less applicable to advection-dominated modeling cases, a summary of the treatment of liquid advection in the EBS is appropriate here. In particular, water balance in the EBS for advection dominated scenarios is imposed through various process model abstractions. The percolation flux, which is a direct input from the spatially variable three-dimensional UZ flow-fields, is used as the boundary condition for seepage flux calculation at the drift-scale. Some of the water flows through the drift while the rest is diverted between the drifts (through the pillars) and does not influence radionuclide transport. The total amount of water is conserved. The fraction of percolation flux that enters the drift as seepage then goes through its own water balance, as discussed in Section 6.3.6 and as shown on Figure 6.3.6-4, based on the fractions that can flow through the breaches in the DS and WP. The fraction of water flowing through the WP determines the mass rate of radionuclides released into the invert and natural system. Finally, in advection-dominated scenarios, the water chemistry in the invert is assumed to be dominated by the in-package chemistry and the only effect in the invert related to water balance is an increase in velocity through remixing with DS diverted flux.

There are a couple of minor inconsistencies with respect to water balance in the EBS for advection-dominated scenarios. Both are related to coupling of the thermal processes to the flow processes, with the first being the effect of evaporation and the second being the effect of condensation. First, consider evaporative effects. If DS failure occurs, water can drip from the drift wall and fall directly onto the WP. Water initially dripping onto a WP will evaporate. Eventually, the water flux onto the WP will exceed evaporation flux and water will enter and flow through the breached WP. Depending on the rate of dripping and the thermal output of the WP, the rate of evaporation for most WPs may not be exceeded by seepage for hundreds to thousands of years. The TSPA-SEIS assumes that when WP surface temperature is at or greater than 100°C, the bulk water is not available in the WP for radionuclide transport (Section 5.1.4). After WP surface temperature drops to less than 100°C, any liquid water flux falling on the breached WP (except when the breach is only from SCC) could immediately enter a WP (subject to the flux-splitting model calculations) to initiate radionuclide transport. The delay of water entry and the reduction of water flux entering and exiting the WP due to evaporation are ignored. Second, consider condensation within the drifts. The inclusion of condensation flux is based on a model not coupled to seepage flux. However, because the condensation flux is much lower than the seepage flux and because it only occurs for at most the first 2,000 years after closure, its effect on overall performance (radionuclide releases by advection) is small.

For diffusion-dominated modeling cases, where seepage cannot enter the WP, the water balance in the EBS is imposed through various process model abstractions for invert flow and saturation (from MSTHM), and through both process model abstractions and assumptions for the in-package saturation. The following assumptions are made in the TSPA-SEIS with respect to the water balance inside the WP: (1) sufficient condensate water is available for waste form degradation; and (2) sufficient water vapor is present to establish a continuous film of liquid water on metal surfaces under no flow conditions when relative humidity greater than 95 percent. The in-package chemistry and saturation of the waste form rind and corrosion products is calculated based on relative humidity.

The overall effect of the previous assumptions regarding the complete saturation inside the WP under flowing conditions is a conservative over-estimation of the release of radionuclides and the timing of the release. To illustrate this, consider the assumption of specifying a liquid saturation inside a failed WP that effectively ignores the drying-out effects of evaporation inside the WP. This results in an earlier time at which water enters a WP after a WP is breached (via the liquid and/or gas phases), and over predicts the rate at which water is available for waste alteration and radionuclide transport.

The highest temperature is always inside the WP, where heat due to radioactive decay is generated, especially in the first hundreds to thousands of years. This temperature will lead to elevated vapor pressures within the WP that tends to prevent water vapor from diffusing into a breached WP. Only at later times, upon cooling, will water vapor migrate into a breached WP and sorb or condense onto solid surfaces when the water vapor pressure within the WP becomes equal to the local saturation vapor pressure. Again, these processes may not occur for hundreds to thousands of years, depending on the thermal output of the WP. The TSPA-SEIS assumes no time delay for the entry of water vapor into a breached WP for initiating waste form degradation and steel corrosion. However, under no flow conditions, continuous film of water is not assumed

to be available for radionuclide transport until the WP relative humidity is greater than 95 percent (Section 5.1.4).

6.3.8.4.2 Identification of Conservatisms in Submodels and Abstractions

All Seepage Falls on DSs—All seepage into the drifts is assumed to fall on the DSs, not just seepage above the DSs. This conservative approach is taken to simplify the modeling approach and because the uncertainty in the seepage locations is difficult to quantify (SNL 2007 [DIRS 177407], Section 5.1). This approach will increase the seepage flux contacting the DS and thereby increase the radionuclide release in the scenarios where there is advective flux in the waste form cell.

Seepage on the WP—All the seepage penetrating a DS falls on the crown of the WP. This conservative approach is taken to simplify the modeling approach and because the uncertainty in the seepage locations is difficult to quantify (SNL 2007 [DIRS 177407], Section 5.1). This conservatism will increase the flux through the breached DSs and WPs and thereby increase the radionuclide release in the scenarios where there is advective flux in the waste form cell.

No Evaporation of the Seepage Water from the Surfaces of the DSs—A reduction in the quantity of water flux through the DS reduces the potential for advective transfer and subsequent release and transport of radionuclides from the WPs (SNL 2007 [DIRS 177407], Section 5.2). Ignoring evaporation from the DS surface tends to increase the seepage flux falling on the WPs.

No Evaporation of the Seepage Water from the WPs—Transport within the WP is not possible if evaporation eliminates liquid fluxes and effective water saturation (SNL 2007 [DIRS 177407], Section 5.3). Ignoring evaporation on the WP surface tends to increase the potential for advective and diffusive transport of radionuclides.

Emplacement Pallets—The presence of emplacement pallets for WPs is conservatively ignored to allow water and radionuclides to pass directly from the WP to the invert without increasing the transport distance (SNL 2007 [DIRS 177407], Section 6.3.1.1). This conservatism leads to a shortened advective flow path and increases the concentration gradient for diffusion.

Consumption of Water—There is no consumption of water by chemical reactions. The consumption of water by the corrosion of iron inside a WP and by hygroscopic salts deposited on the DS and WP surfaces would reduce the amount of water for dissolution and transport of radionuclides (SNL 2007 [DIRS 177407], Section 5.4). The assumption that there is no consumption of water is a bounding assumption, which increases the amount of water available for advective transport.

Thin Water Films—It is conservatively assumed that continuous thin water films exist on the internal components of the breached WPs and on the breached areas at temperatures less than the boiling point of water. Multiple water layers are needed in order for radionuclides to dissolve in and diffuse. Ignoring the thickness of the water film will overestimate the release of radionuclides. Assuming the presence of continuous water film allows radionuclides to diffuse from the degraded waste form to the outside of the breached WP (SNL 2007 [DIRS 177407],

Section 5.5). Diffusive transport occurs continuously after the WP is breached and the waste form is degraded, irrespective of the path length.

One-Dimensional Advective and Diffusive Transport Through the EBS—A one-dimensional vertical advective and diffusive transport from the WPs to the invert occurs irrespective of the breach location on the WP surface (SNL 2007 [DIRS 177407], Section 6.3.1.2) even though breaches in the WP are expected to occur randomly over the WP surface area. In other words, assuming diffusion can occur through all breaches, regardless of location, maximizes the diffusive area thereby giving a conservative estimate of releases from the WP.

Invert Corrosion Products—No corrosion products exist in the invert. By assuming that there are no corrosion products in the invert, there will be no sorption or delay of radionuclides by corrosion products (SNL 2007 [DIRS 177407], Section 5.6). Not taking credit for the sorption of radionuclides onto the corrosion products will tend to increase the mass flux of radionuclides through the invert.

No DS Shadow in the Invert—Water will tend to divert around the DS and not flow through the region of the invert directly under the DS. However, because of the limited information regarding the flow paths and mixing of waters, this effect is not accounted for (SNL 2007 [DIRS 177407], Sections 6.3.3.4 and 6.5). The flux diverted by the DSs to the invert is assumed to mix with the water carrying the radionuclides from the WPs to the invert, which tends to increase the advective transport.

No Physical Filtration or Gravitational Settling of Colloids—Stable colloids once formed do not undergo physical filtration or gravitation settling in the CSNF and CDSP WPs and in the invert (SNL 2007 [DIRS 177407], Section 5.7). By assuming that there is no physical filtration or gravitational settling of colloids, the model will tend to overestimate the colloid mass flux and the colloid-facilitated radionuclide transport in the EBS.

Colloid Retardation—Colloid retardation due to sorption at the air-water interface and interaction with microbes and organic components is not modeled. Not including colloid retardation tends to increase the colloid mass flux and the colloid-facilitated radionuclide transport in the EBS (SNL 2007 [DIRS 177423], Section 5.9).

6.3.8.5 Alternative Conceptual Model(s) for Engineered Barrier System Transport

Section 6.2 outlines the general consideration and treatment of ACMs used to support the TSPA-SEIS. A brief description of the EBS Transport Submodel ACMs summarized in Table 6.3.8-7 is presented below.

Bathtub Flow Model ACM—This ACM assumes that seepage collects within the WP before being released to the EBS (SNL 2007 [DIRS 177407], Section 6.6.1). The "bathtub" effect would be most important during the period when only a few patches or cracks have penetrated the DS and WP. In this situation, there may be penetrations through the top of the WP while the bottom surface remains intact, leading to retention of liquid. At later times, the presence of multiple penetrations makes a "flow-through" geometry the more likely configuration. The response of the bathtub geometry was evaluated for a primary case, with constant boundary conditions and material properties, and for three secondary cases. The three secondary cases

considered a step change in inflow rate, such as would occur from a climatic change, a step change in water chemistry, or a step change in flow geometry, as would occur if a patch suddenly appeared beneath the waterline. All cases included consideration of two limiting conditions on radionuclide releases: dissolution rate limited and solubility limited.

This ACM was not used for the TSPA-SEIS EBS Transport Model because, for most of the pertinent cases, the basecase flow-through model is bounding with respect to the release of radionuclides.

Constrained Water Vapor and Oxygen Diffusion through SCC ACM—This ACM compares the rate of water vapor and oxygen diffusion through stress corrosion cracks with the rate of corrosion of steel components inside a WP (SNL 2007 [DIRS 177407], Section 6.6.2). If the consumption rate is greater than the diffusion rate then a film of adsorbed water cannot form, which could delay diffusive releases until all steel is fully corroded. The water vapor concentration inside a WP is assumed to be zero to maximize the concentration gradient. Alternative cases consider the effects of stress corrosion cracks that are assumed to be: (1) fully open; and (2) filled with corrosion products but still permeable. This ACM could potentially delay releases for hundreds to thousands of years. However, the assumption that no water is physically adsorbed until all steel is corroded is questionable, because adsorption is typically a fast process. On the other hand, if water consumption by corrosion keeps the relative humidity inside the WP low, the effective water saturation will be so low that the bulk liquid phase behavior allowing dissolution and diffusion of dissolved radionuclides will not exist until the corrosion is complete.

This ACM was not used for the TSPA-SEIS EBS Transport Submodel because it is potentially nonconservative and there are insufficient data to validate this ACM.

Dual-Continuum Invert Model ACM—The dual-continuum invert model is an alternative conceptual EBS Transport Model in which crushed tuff invert ballast is modeled as a dual-continuum material consisting of intergranular pore space and intragranular pore space (SNL 2007 [DIRS 177407], Section 6.6.3). All seepage into the drift flows through the intergranular pore space and into the UZ fractures. Imbibition from the UZ host rock into the invert flows through the intragranular pore space and into the UZ matrix under gravity. Diffusion of radionuclides also occurs in both the intergranular and intragranular pore spaces, from the WP corrosion products into UZ fractures and matrix, as well as between the two invert continua.

This ACM was not used for the TSPA-SEIS EBS Transport Model. It was screened out due to insufficient data to validate diffusion coefficients in individual continua and insufficient data to confirm whether this is a bounding approach with respect to chemical behavior in the invert. However, the dual-continuum invert model ACM was included in the GoldSim model file to be used for sensitivity analyses and to validate the single-continuum model for EBS transport in the TSPA-SEIS.

Alternative Invert Diffusion Coefficient ACM—The invert diffusion coefficient model with a lower limit on water content is an alternative conceptual EBS Transport Model in which, as the water content of the crushed tuff decreases, the water films that connect pore spaces become

disconnected, and the effective diffusion coefficient drops more rapidly than predicted by Archie's law (SNL 2007 [DIRS 177407], Section 6.6.4). Below some critical water content, the diffusion coefficient becomes zero, based on models of diffusion in soils.

This ACM was not used for the TSPA-SEIS EBS Transport Model because there is insufficient data to validate diffusive behavior at very low water contents.

Reversible Sorption of Radionuclides onto WP Corrosion Products ACM—In this ACM, an empirical approach based on sampling a partition coefficient (K_d value) for reversible sorption of radionuclides onto stationary corrosion products is considered (SNL 2007 [DIRS 177407], Section 6.6.5). Iron oxyhydroxides are generated through corrosion of mild steel and stainless steels within the WP. The iron oxyhydroxides are known to be excellent sorbers (as indicated by their high K_d values) of many radionuclide species. In this ACM, sorption is modeled as being completely reversible for all radionuclides and represented by linear adsorption isotherms in the form of K_d values. The K_d values allow retardation factors to be computed for transport through the EBS.

This ACM was not used for the TSPA-SEIS EBS Transport Submodel because it does not account for limitations on the total number of sorption sites. Also, this ACM does not account for competition with other radionuclides.

Plutonium Sorption from Stationary Corrosion Products and Colloids ACM—This ACM accounts for the slow desorption of plutonium observed in experiments investigating sorption and desorption of plutonium from iron oxyhydroxide (SNL 2007 [DIRS 177407], Section 6.6.6). Postulated mechanisms of plutonium sorption are described and the experimentally observed desorption is interpreted in the context of these mechanisms. K_d values are calculated for application to plutonium transport in the EBS.

This ACM is not incorporated into the basecase EBS Transport Submodel because the fitting parameters are specific to the experiment design and cannot be extrapolated to other transport conditions as would be expected in the TSPA model. Furthermore, the developed parameters do not take into account the competition with other radionuclides.

INTENTIONALLY LEFT BLANK

Table 6.3.8-1. Summary of EBS Transport Abstraction

Transport Pathway	Transport Modes	Transport Parameters and Data Sources
1. Waste form and corrosion products domains	Waste form domain: Diffusion and advection (when possible) through the waste form rind. Corrosion products domain: Diffusion through SCC (no advective transport through stress corrosion cracks). Diffusion and advection through corrosion patches.	No lateral or longitudinal dispersion. Colloidal particles will transport radionuclides. Diffusive area for stress corrosion cracks is obtained. Diffusion coefficient (all radionuclides): • Species-dependent free-water diffusion coefficients given in DTN: LB0702PAUZMTDF.001_R1 [DIRS 180776], file *Readme.doc*, Table 8 • Modified for temperature, porosity, and saturation • Colloid diffusion coefficient computed as a function of waste form and corrosion product temperatures and sampled colloid particle diameter (SNL 2007 [DIRS 177407], Section 6.3.4.4). Competitive sorption of radionuclides onto corrosion products; time-dependent mass of corrosion products available for sorption is calculated based on corrosion rates of carbon and stainless steels. The breach area of the WP outer barrier for radionuclide transport is dependent on the scenario class modeled.
2. Invert domain	Diffusion and advection from corrosion products domain into the invert domain.	Liquid flux for advection (sum of drift seepage flux, drift condensation flux, and invert imbibition flux). Diffusion coefficient (all radionuclides): • Species-dependent free-water diffusion coefficients given in DTN: LB0702PAUZMTDF.001_R1 [DIRS 180776], file *Readme.doc*, Table 8. • Modified for temperature, porosity, and saturation • Colloid diffusion coefficient computed as a function of invert temperature and sampled colloid particle diameter. The diffusive area for radionuclide transport is the width of the invert times the waste package length. Transport of radionuclides is retarded by sorption onto crushed tuff in invert.
3. Invert-UZ interface domain	Advection from the invert to UZ fractures and matrix. Diffusion from the invert to UZ fractures and matrix.	The invert diffusion calculation uses radionuclide concentrations in the WP corrosion products domain as the boundary condition at the top of the invert and a series of UZ computational cells below the invert that provide a gradient to a zero radionuclide concentration at some distance from the bottom of the invert. For additional details, see SNL 2007 [DIRS 177407], Section 6.5.2.6.

Sources: Modified from DTN: SN0703PAEBSRTA.001_R3 [DIRS 183217] from *EBS Radionuclide Transport Abstraction* (SNL 2007 [DIRS 177407], Table 8.1-2).

Table 6.3.8-2. Parameters for EBS Transport Abstraction

Waste Type	Transport Properties	Seeping Case	Non-Seeping Case
Waste Form Domains			
CSNF	Domain bulk volume, pore volume, and water volume	Waste Form Domain consists of degradation products in fuel rods (SNF rind), fuel basket tubes (steel corrosion products), absorber plates (steel corrosion products): • SNF rind volume (V_{rind}, function of time) and porosity (ϕ_{rind}) provided by *Cladding Degradation Summary for LA* (SNL 2007 [DIRS 180616], Tables 6-3 and 6-4) • Steel corrosion products (CP) mass from Equation 8-4, pore volume ($V_{\phi,CP}$) from Equation 8-7, bulk volume from Equation 8-8 of *EBS Radionuclide Transport Abstraction* (SNL 2007 [DIRS 177407]) • Total pore volume of CSNF Waste Form Domain, $V_{\phi,CSNF}$, given by Equation 8-13 of *EBS Radionuclide Transport Abstraction* (SNL 2007 [DIRS 177407]) • S_w = water saturation in domain = 1.0 • Domain water volume = total pore volume.	• Domain characteristics (rind volume, corrosion products mass and volume, total pore volume) same as for Seeping Case • $S_{w,rind}$ function of relative humidity and sampled density and specific surface area of rind (SNL 2007 [DIRS 177407] Equation 8-12) • Rind water volume: $V_{w,rind} = S_{w,rind}\,\phi_{rind}\,V_{rind}$ • $S_{w,CP}$ function of relative humidity, density, and sampled specific surface area of corrosion products (SNL 2007 [DIRS 177407], Equation 8-5) • Corrosion products water volume: $V_{w,CP} = S_{w,CP}\,V_{\phi,CP}$ • Domain water volume = $V_{w,CSNF} = V_{w,rind} + V_{w,CP}$.
	Advection and Diffusion	Advective flow = volumetric flow rate through the waste package Diffusive area of Waste Form Domain: • Set equal to surface area of a cylinder at half the radius of the TAD canister excluding ends (= 12.5 m^2) Diffusive path length: • Set equal to TAD inside radius (= 0.819 m) Diffusion coefficient in Waste Form Domain, D_{WF}: • $\phi S_w D_{WF} = \phi^{1.3} S_w^2 D_{wi}$ • ϕ = effective porosity of CSNF Waste Form Domain given by Equation 8-14 of *EBS Radionuclide Transport Abstraction* (SNL 2007 [DIRS 177407]) • S_w = water saturation in domain = 1.0 • D_{wi} = species dependent free water diffusion coefficient. (D_{WF} is an effective value that implicitly includes the effect of tortuosity in a porous medium).	• No advective flux • Diffusive area same as for Seeping Case • Diffusive path length same as for Seeping Case Diffusion coefficient in Waste Form Domain, D_{WF}: • $\phi S_w D_{WF} = \phi^{1.3} S_w^2 D_{wi}$ • Effective porosity ϕ of CSNF Waste Form Domain given by Equation 8-14 of *EBS Radionuclide Transport Abstraction* (SNL 2007 [DIRS 177407]), same as for Seeping Case • Water saturation in Waste Form Domain is based on water vapor adsorption isotherms: $S_w = \min[(V_{w,CSNF}/V_{\phi,CSNF}), 1.0]$ • D_{wi} = species dependent free water diffusion coefficient • Modified for temperature. (D_{WF} is an effective value that implicitly includes the effect of tortuosity in a porous medium).

Table 6.3.8-2. Parameters for EBS Transport Abstraction (Continued)

Waste Type	Transport Properties	Seeping Case	Non-Seeping Case
Waste Form Domains			
CDSP	Domain bulk volume, pore volume, and water volume	Waste Form Domain is divided into two subdomains: HLWG and DSNF Subdomains HLWG Subdomain: • Consists of degradation products of five stainless steel canisters and HLW glass contained therein • Volume of HLWG degradation rind provided as function of time by *Defense HLW Glass Degradation Model* (BSC 2004 [DIRS 169988], Section 8.1, Eq. 54) • Porosity of HLWG rind provided by *Defense HLW Glass Degradation Model* (BSC 2004 [DIRS 169988], Table 8-1) • Steel corrosion products (CP) mass from Equation 8-4, pore volume ($V_{\phi,CP}$) from Equation 8-7, bulk volume from Equation 8-8 of *EBS Radionuclide Transport Abstraction* (SNL 2007 [DIRS 177407]) • Total pore volume of HLWG Waste Form Subdomain, $V_{\phi,HLWG}$, given by Equation 8-13 of *EBS Radionuclide Transport Abstraction* (SNL 2007 [DIRS 177407]) • S_w = water saturation in HLWG Waste Form Subdomain = 1.0. DSNF Subdomain: • Consists of degradation products of standard stainless steel DSNF canister containing degraded DSNF (rind) • Volume of DSNF rind, V_{DSNF} = 1.0 m^3 (BSC 2004 [DIRS 172453], Section 8.1) • Porosity of DSNF rind, ϕ_{DSNF} = 0.2 • Steel corrosion products (CP) mass from Equation 8-4 , pore volume ($V_{\phi,CP}$) from Equation 8-7, bulk volume from Equation 8-8 of *EBS Radionuclide Transport Abstraction* (SNL 2007 [DIRS 177407]) • Total pore volume of DSNF Waste Form Subdomain, $V_{\phi,DSNF}$, given by Equation 8-13 of *EBS Radionuclide Transport Abstraction* (SNL 2007 [DIRS 177407]) • S_w = water saturation in DSNF = 1.0.	HLWG Subdomain: Diffusion coefficient in HLWG Waste Form Subdomain, D_{WF}: • $\phi S_w D_{WF} = \phi^{1.3} S_w^2 D_{wi}$ • Effective porosity ϕ of HLWG Waste Form Subdomain given by Equation 8-14 of *EBS Radionuclide Transport Abstraction* (SNL 2007 [DIRS 177407]), same as for Seeping Case • Water saturation in HLWG Waste Form Subdomain is based on water vapor adsorption isotherm: S_w = min[($V_{w,HLWG}/V_{\phi,HLWG}$),1.0] • Modified for temperature • D_{wi} = species dependent free water diffusion coefficient. DSNF Subdomain: Diffusion coefficient in DSNF Waste Form Subdomain, D_{WF}: • $\phi S_w D_{WF} = \phi^{1.3} S_w^2 D_{wi}$ • Effective porosity ϕ of DSNF Waste Form Subdomain given by Equation 8-14 of *EBS Radionuclide Transport Abstraction* (SNL 2007 [DIRS 177407]), same as for Seeping Case • Water saturation in DSNF Waste Form Subdomain is based on water vapor adsorption isotherm: S_w = min[($V_{w,DSNF}/V_{\phi,DSNF}$),1.0] • Modified for temperature • D_{wi} = species dependent free water diffusion coefficient. (D_{WF} is an effective value that implicitly includes the effect of tortuosity in a porous medium).

Table 6.3.8-2. Parameters for EBS Transport Abstraction (Continued)

Waste Type	Transport Properties	Seeping Case	Non-Seeping Case
Waste Form Domains			
CDSP (continued)	Advection and Diffusion	Advective flow = volumetric flow rate through the waste package. HLWG Subdomain: Diffusive area: • Diffusive area equal to surface area of cylinder with radius equal to half the radius of inner vessel cavity of five DHLW/DOE SNF Long waste package, excluding ends (= 13.7 m^2) Diffusive path length: • Set equal to the radius of inner vessel of 5 DHLW/DOE SNF Long waste package (= 0.941 m) Diffusion coefficient in HLWG Waste Form Subdomain, D_{WF}: • $\phi S_w D_{WF} = \phi^{1.3} S_w^2 D_{wi}$ • ϕ = effective porosity of HLWG Waste Form Subdomain given by Equation 8-14 of *EBS Radionuclide Transport Abstraction* (SNL 2007 [DIRS 177407]) • S_w = water saturation = 1.0 • D_{wi} = species dependent free water diffusion coefficient. (D_{WF} is an effective value that implicitly includes the effect of tortuosity in a porous medium).	• No advective flux • Diffusive area same as for Seeping Case • Diffusive path length same as for Seeping Case
		DSNF Subdomain: Diffusive area: • Diffusive area set equal to the geometric surface area of HLWG subdomain (= 13.7 m^2) Diffusive path length: • The effective diffusive path length is calculated by dividing the initial volume of DSNF (1 m^3) by the diffusive area leading to total diffusive length of 0.0730 m. Diffusion coefficient in Waste Form Subdomain, D_{WF}: • $\phi S_w D_{WF} = \phi^{1.3} S_w^2 D_{wi}$ • ϕ = effective porosity of DSNF Waste Form Subdomain given by Equation 8-14 of *EBS Radionuclide Transport Abstraction* (SNL 2007 [DIRS 177407]) • S_w = water saturation = 1.0 • D_{wi} = species dependent free water diffusion coefficient	• No advective flux • Diffusive area same as for Seeping Case • Diffusive path length same as for Seeping Case

Table 6.3.8-2. Parameters for EBS Transport Abstraction (Continued)

Waste Type	Transport Properties	Seeping Case	Non-Seeping Case
Corrosion Products Domain			
CSNF	Bulk volume and water volume	Pore volume of Corrosion Products Domain, $V_{\phi CP}$: • Mass of corrosion products, m_{CP}, is function of time, Equation 8-4 of *EBS Radionuclide Transport Abstraction* (SNL 2007 [DIRS 177407]) • Porosity $\phi_{CP} = 0.4$ • $V_{\phi CP}$ from Equation 8-7 of *EBS Radionuclide Transport Abstraction* (SNL 2007 [DIRS 177407]).	• Same as Seeping Case.
		Volume of water: • S_w = water saturation in corrosion products = 1.0 • Water volume: $V_{w,CP} = S_w V_{\phi CP}$	Volume of water: • $S_{we,CP}$ = effective water saturation in Corrosion Products Domain from Equation 8-11 of *EBS Radionuclide Transport Abstraction* (SNL 2007 [DIRS 177407]) • Water volume = $S_{we,CP} V_{\phi CP}$
	Advection and Diffusion	Advective flow = volumetric flow rate through the waste package	• No advective flux.
		Diffusive area: • Diffusive area, for the path excluding the outer barrier, is the surface area of a cylinder halfway between the inside surface of the TAD canister and the outside surface of the inner vessel (= 29.9 m^2) • Diffusive area for the path through the outer barrier of the waste package is taken to be the minimum of total area of all waste package breaches (scenario class dependent) and surface area of CSNF waste package (= 33.1 m^2).	• Same as Seeping Case.
		Diffusive path length: • Diffusive path excluding the outer barrier is given by the combined thickness of TAD canister and inner vessel, constant parameter (= 0.0914 m) • Diffusive path through the outer barrier is the radial distance from the outside of the inner vessel to the outside of the outer barrier (= 0.0302 m)	• Same as Seeping Case.

Table 6.3.8-2. Parameters for EBS Transport Abstraction (Continued)

Waste Type	Transport Properties	Seeping Case	Non-Seeping Case
		Diffusion coefficient in Corrosion Products Domain, D_{CP}: • $\phi_{CP} S_w D_{CP} = \phi_{CP}^{1.3} S_w^2 D_{wi}$ • ϕ_{CP} = porosity of corrosion products = 0.4 • S_w = water saturation in corrosion products = 1.0 • D_{wi} = species dependent free water diffusion coefficient. (D_{CP} is an effective value that implicitly includes the effect of tortuosity in a porous medium).	Diffusion coefficient in Corrosion Products Domain, D_{CP}: • $\phi_{CP} S_{we,CP} D_{CP} = \phi_{CP}^{1.3} S_{we,CP}^2 D_{wi}$ • $S_{we,CP}$ = effective water saturation in corrosion products, Equation 8-11 of *EBS Radionuclide Transport Abstraction* (SNL 2007 [DIRS 177407]) • ϕ_{CP} = porosity of corrosion products = 0.4 • Modified for temperature • D_{wi} = species dependent free water diffusion coefficient. (D_{CP} is an effective value that implicitly includes the effect of tortuosity in a porous medium).
Corrosion Products Domain			
CDSP	Bulk volume and water volume	Pore volume of Corrosion Products Domain, $V_{\phi,CP}$: • Same as for CSNF Seeping Case • ϕ_{CP} = porosity of corrosion products = 0.4	• Same as Seeping Case
		Volume of water: • S_w = water saturation in corrosion products = 1.0 • Water volume = $S_w V_{\phi,CP}$	• $S_{we,CP}$ = effective water saturation in corrosion products, Equation 8-11 of *EBS Radionuclide Transport Abstraction* (SNL 2007 [DIRS 177407]) • Water volume = $S_{we,CP} V_{\phi,CP}$

Table 6.3.8-2. Parameters for EBS Transport Abstraction (Continued)

Waste Type	Transport Properties	Seeping Case	Non-Seeping Case
	Advection and Diffusion	Advective flow = volumetric flow rate through the waste package Diffusive area: • Diffusive area, for the path excluding the outer barrier, is given by the surface area of a cylinder halfway between the inside surface and the outside surface of the inner vessel (= 29.7 m^2) • Diffusive area for the path through the outer barrier of the waste package is taken to be the minimum of total area of all waste package breaches (scenario class dependent) and surface area of CDSP waste package given by the constant parameter (= 32.6 m^2). Diffusive path length: • Diffusive path excluding the outer barrier is given by the thickness of the inner vessel, constant parameter (= 0.0508 m) • Diffusive path through the outer barrier is the radial distance from the outside of the inner vessel to the outside of the outer barrier (= 0.0301 m). Diffusion coefficient in Corrosion Products Domain, D_{CP}: • $\phi_{CP}S_wD_{CP} = \phi_{CP}^{1.3}S_w^2D_{wi}$ • ϕ_{CP} = porosity of corrosion products = 0.4 • S_w = water saturation = 1.0 • D_{wi} = species dependent free water diffusion coefficient. (D_{CP} is an effective value that implicitly includes the effect of tortuosity in a porous medium).	• No advective flux • Diffusive area same as for Seeping Case • Diffusive path length same as for Seeping Case. Diffusion coefficient in Corrosion Products Domain, D_{CP}: • $\phi_{CP}S_{we,CP}D_{CP} = \phi_{CP}^{1.3}S_{we,CP}^2D_{wi}$ • $S_{we,CP}$ = effective water saturation in corrosion products, Equation 8-11 of *EBS Radionuclide Transport Abstraction* (SNL 2007 [DIRS 177407]) • ϕ_{CP} = porosity of corrosion products = 0.4 • D_{wi} = species dependent free water diffusion coefficient. (D_{CP} is an effective value that implicitly includes the effect of tortuosity in a porous medium).

Sources: Modified from DTN: SN0703PAEBSRTA.001_R3 [DIRS 183217] from *EBS Radionuclide Transport Abstraction* (SNL 2007 [DIRS 177407], Table 8.2-1).

Table 6.3.8-3. Sampled Parameter Ranges and Distributions Used for Kinetic Sorption on Stationary Corrosion Products

Input Name	Input Description	Range	Distribution
Goethite_Site_Density_a	Goethite site density; discrete distribution	Density (sites nm^{-2})	Probability Level
		1.02	0.01786
		1.21	0.01786
		1.32	0.03571
		1.46	0.01786
		1.50	0.01786
		1.66	0.01786
		1.68	0.03571
		1.70	0.01786
		1.80	0.01786
		1.87	0.01786
		1.93	0.01786
		1.95	0.01786
		1.97	0.01786
		2.20	0.01786
		2.30	0.07143
		2.31	0.01786
		2.32	0.01786
		2.55	0.01786
		2.60	0.03571
		2.70	0.01786
		2.89	0.01786
		2.90	0.03571
		3.00	0.01786
		3.12	0.01786
		3.13	0.01786
		3.30	0.03571
		3.40	0.01786
		4.00	0.01786
		4.20	0.01786
		4.60	0.01786
		4.84	0.01786
		4.90	0.01786

Table 6.3.8-3. Sampled Parameter Ranges and Distributions Used for Kinetic Sorption on Stationary Corrosion Products (Continued)

Input Name	Input Description	Range	Distribution
Goethite_Site_Density_a (continued)	Goethite site density; discrete distribution (continued)	5.00	0.01786
		5.53	0.01786
		6.15	0.01786
		6.30	0.01786
		6.31	0.03571
		6.60	0.01786
		7.00	0.05357
		7.20	0.01786
		7.40	0.01786
		8.00	0.01786
		8.16	0.01786
		8.38	0.01786
		8.59	0.01778
HFO_Site_Density_a	HFO site density; discrete distribution	Density (sites nm^{-2})	Probability Level
		0.56	0.05263
		1.13	0.10526
		1.47	0.05263
		1.58	0.05263
		1.69	0.10526
		1.81	0.05263
		2.03	0.10526
		2.26	0.26316
		2.60	0.05263
		2.71	0.05263
		4.00	0.05263
		5.65	0.05265

Sources: Modified from DTN: SN0703PAEBSRTA.001_R3 [DIRS 183217] from *EBS Radionuclide Transport Abstraction* (SNL 2007 [DIRS 177407], Table 8.2-2).

Table 6.3.8-4. Sampled Model Inputs Used in the EBS Radionuclide Transport Abstraction

Input Name	Input Description	Range	Distribution
Invert_Diff_Coeff_Uncert_a	Invert diffusion coefficient uncertainty	Range: $10^{\mu \pm 3\sigma}$ (dimensionless) Mean: $\mu = 0.033$; Std. Dev. $\sigma = 0.218$	10^{ND}
SS_Corrosion_Rate_a	Stainless steel corrosion rate	0.01 – 0.51 μm yr-1 Mean = 0.267 μm yr-1 Std. Dev. = 0.209 μm yr-1	Truncated Lognormal
CS_Corrosion_Rate_a	Carbon steel corrosion rate	25 – 135 μm yr^{-1} Mean = 78.5 μm yr^{-1} Std. Dev. = 25.0 μm yr^{-1}	Truncated Lognormal
DS_Flux_Uncertainty_a	Drip shield flux-splitting uncertainty factor	0 – 0.85 (dimensionless)	Uniform
WP_Flux_Uncertainty_a	Waste package flux-splitting uncertainty factor	0 – 2.41 (dimensionless)	Uniform
Diameter_Colloid_a	Diameter of colloid particle	50 – 300 nm	Uniform
Goethite_SA_a	Specific surface area of goethite (FeOOH)	14.7 – 110 $m^2 g^{-1}$ Mean = 51.42 $m^2 g^{-1}$ Std. Dev. = 30.09 $m^2 g^{-1}$	Log-Normal (Truncated)
HFO_SA_a	Specific surface area of HFO	68 – 600 $m^2 g^{-1}$ Mean = 275.6 $m^2 g^{-1}$ Std. Dev. = 113.4 $m^2 g^{-1}$	Log-Normal (Truncated)
NiO_SA_a	Specific surface area of NiO	1 – 30 $m^2 g^{-1}$	Uniform
Cr2O3_SA_a	Specific surface area of Cr_2O_3	1 – 20 $m^2 g^{-1}$	Uniform
Relative_Abundance_Goethite_a	Mass fraction of iron oxides (goethite and HFO) that is goethite	0.45 – 0.80 (fraction)	Uniform
FHH_Isotherm_k_CP_a	FHH adsorption isotherm parameter *k* for corrosion products	1.048 – 1.370 (dimensionless)	Uniform
FHH_Isotherm_s_CP_a	FHH adsorption isotherm parameter *s* for corrosion products	1.525 – 1.852 (dimensionless)	Uniform
CSNF_Rind_SA_a	Specific surface area of CSNF rind	0.5 – 60 $m^2 g^{-1}$	Uniform
Density_CSNF_Rind_a	Density of CSNF rind	5,600 – 11,500 kg m^{-3}	Uniform
Porosity_Rind_CSNF_a	Porosity of CSNF rind	0.05 – 0.3 (fraction)	Uniform
FHH_Isotherm_k_CSNF_Rind_a	FHH adsorption isotherm parameter *k* for CSNF rind	1.606 – 8.215 (dimensionless)	Uniform
FHH_Isotherm_s_CSNF_Rind_a	FHH adsorption isotherm parameter *s* for CSNF rind	1.656 – 3.038 (dimensionless)	Uniform
HLWG_Rind_SA_a	Specific surface area of HLWG rind	10 – 38 $m^2 g^{-1}$	Uniform
Diameter_Colloid_a	Colloid particle diameter	50 – 300 nm	Uniform
Gamma_AFM_a	Active fracture model gamma parameter DTN: LA0701PANS02BR.003_R2 [DIRS 180497]	0.2 – 0.6	Uniform

Table 6.3.8-4. Sampled Model Inputs Used in the EBS Radionuclide Transport Abstraction (Continued)

Input Name	Input Description	Range	Distribution
EBS_UZ_Flux_Sat_PS1 EBS_UZ_Flux_Sat_PS2 EBS_UZ_Flux_Sat_PS3 EBS_UZ_Flux_Sat_PS4 EBS_UZ_Flux_Sat_PS5	Unsaturated zone fracture saturation DTN: LA0701PANS02BR.003_R2 [DIRS 180497] This includes the average fracture and matrix percolation fluxes and saturations for both glacial transition and post-10,000-year periods. There are total of five percolation subregions.	Average values for the five percolation subregions based on the average of repository nodes in each percolation subregion.	2-D Table; see Table 6.3.8-5
Diff_Path_Length_Invert_Top_a	Diffusive path length from waste package outer corrosion barrier to mid-point of invert.	0.30 – 1.24 m	Uniform

Sources: Modified from DTN: SN0703PAEBSRTA.001_R3 [DIRS 183217] from *EBS Radionuclide Transport Abstraction* (SNL 2007 [DIRS 177407], Table 8.2-4).

NOTES: ND = Truncated normal distribution
$E(x)$ = Expected value
$\sigma(x)$ = Standard deviation
CDF = cumulative distribution function.

Table 6.3.8-5. Unsaturated Zone Saturation and Flux Inputs Used in the EBS Radionuclide Transport Abstraction

Parameter: EBS_UZ_Flux_Sat_PS1				
	Fracture Saturation	**Matrix Saturation**	**Fracture Flux**	**Matrix Flux**
gt10	1.29E-02	9.14E-01	3.44E-01	3.32E-01
gt30	1.65E-02	9.34E-01	1.82E+00	4.81E-01
gt50	1.41E-02	9.00E-01	1.94E+00	4.25E-01
gt90	1.43E-02	8.85E-01	4.77E+00	5.86E-01
pk10	1.57E-02	9.66E-01	1.55E+00	7.14E-01
pk30	1.65E-02	9.32E-01	1.99E+00	4.66E-01
pk50	1.52E-02	9.23E-01	3.55E+00	5.39E-01
pk90	1.52E-02	9.02E-01	7.10E+00	7.01E-01
Parameter: EBS_UZ_Flux_Sat_PS2				
	Fracture Saturation	**Matrix Saturation**	**Fracture Flux**	**Matrix Flux**
gt10	1.69E-02	9.75E-01	2.81E+00	5.12E-01
gt30	2.17E-02	9.83E-01	1.11E+01	6.21E-01
gt50	1.61E-02	9.68E-01	1.21E+01	6.45E-01
gt90	1.82E-02	9.39E-01	3.29E+01	7.77E-01
pk10	2.23E-02	9.87E-01	1.27E+01	7.23E-01
pk30	2.25E-02	9.84E-01	1.35E+01	6.55E-01
pk50	1.79E-02	9.73E-01	2.41E+01	7.37E-01
pk90	1.87E-02	9.41E-01	3.81E+01	8.16E-01
Parameter: EBS_UZ_Flux_Sat_PS3				
	Fracture Saturation	**Matrix Saturation**	**Fracture Flux**	**Matrix Flux**
gt10	2.06E-02	9.86E-01	9.10E+00	6.69E-01
gt30	2.50E-02	9.88E-01	2.43E+01	7.64E-01
gt50	1.86E-02	9.75E-01	3.28E+01	7.92E-01
gt90	2.09E-02	9.31E-01	6.96E+01	9.21E-01
pk10	2.51E-02	9.88E-01	2.18E+01	7.28E-01
pk30	2.76E-02	9.89E-01	3.67E+01	7.89E-01
pk50	2.03E-02	9.76E-01	5.15E+01	8.11E-01
pk90	2.06E-02	9.30E-01	6.34E+01	8.99E-01
Parameter: EBS_UZ_Flux_Sat_PS4				
	Fracture Saturation	**Matrix Saturation**	**Fracture Flux**	**Matrix Flux**
gt10	2.36E-02	9.87E-01	1.92E+01	7.25E-01
gt30	2.72E-02	9.88E-01	3.72E+01	7.99E-01
gt50	1.95E-02	9.70E-01	5.36E+01	8.14E-01
gt90	2.14E-02	9.14E-01	9.32E+01	9.77E-01
pk10	2.53E-02	9.87E-01	2.62E+01	7.34E-01
pk30	3.07E-02	9.88E-01	6.00E+01	8.12E-01
pk50	2.04E-02	9.70E-01	6.93E+01	8.24E-01
pk90	2.06E-02	9.11E-01	7.62E+01	9.20E-01

Table 6.3.8-5. Unsaturated Zone Saturation and Flux Inputs Used in the EBS Radionuclide Transport Abstraction (Continued)

Parameter: EBS_UZ_Flux_Sat_PS5				
	Fracture Saturation	**Matrix Saturation**	**Fracture Flux**	**Matrix Flux**
gt10	2.52E-02	9.88E-01	2.81E+01	7.34E-01
gt30	2.82E-02	9.89E-01	4.51E+01	8.04E-01
gt50	1.95E-02	9.73E-01	6.68E+01	8.15E-01
gt90	2.16E-02	9.30E-01	1.09E+02	1.02E+00
pk10	2.55E-02	9.88E-01	2.95E+01	7.36E-01
pk30	3.21E-02	9.90E-01	7.48E+01	8.20E-01
pk50	2.03E-02	9.74E-01	8.11E+01	8.18E-01
pk90	2.05E-02	9.26E-01	8.49E+01	9.42E-01

NOTE: Flux values are given in mm/yr but are entered as dimensionless in database. The units are added later in the model.

Sources: Modified from DTN: SN0703PAEBSRTA.001_R3 [DIRS 183217] from *EBS Radionuclide Transport Abstraction* (SNL 2007 [DIRS 177407], Table 8.2-5).

Table 6.3.8-6. Summary of CSNF Rind Volume Calculation Parameters for TSPA-SEIS

TSPA-LA Parameter Name	Model Abstraction Symbol	Description	Units	Distribution Type	Distribution Specification
Initial_Rod_Failures_a	NA	Initial fraction of failed cladding, as received	None	Constant	100%
Fuel_Split_Fraction	NA	Fraction of fuel available for corrosion at any timestep	None	Deterministic	1.0
Density_UO2	ρ_{UO_2}	Density of UO_2	g/cm^3	Deterministic	10.97
Density_Schoepite	ρ_{sch}	Density of schoepite	g/cm^3	Deterministic	4.83
MW_UO2	MW_{UO_2}	Molecular weight of UO_2	g/mole	Deterministic	270
MW_Schoepite	MW_{sch}	Molecular weight of schoepite	g/mole	Deterministic	322.1
Rind_Porosity_CSNF_a	ϕ_{sch}	Porosity in rind	None	Uniform	Min = 0.05 Max = 0.3
Rod_Length_CSNF	L_r	Active fuel rod length	cm	Deterministic	366
Num_Rods_WP_CSNF	N_r	Number of rods per WP	None	Deterministic	5,544
Pellet_Diameter_CSNF	D_{init}	Initial pellet diameter	cm	Deterministic	0.819

Source: SNL 2007 [DIRS 180616] Tables 7-1[a] & 7-2[a]

Table 6.3.8-7. Alternative Conceptual Models Considered for EBS Transport

Alternative Conceptual Models	Key Assumptions	Assessment and Basis
Bathtub flow model	Seepage water flowing into breached waste package accumulates until void volume is filled before water containing dissolved radionuclides flows out. Various cases, such as changing inflow rates and effect of solubility and dissolution rate limits, are evaluated (SNL 2007 [DIRS 177407], Section 6.6.1).	For several of the most pertinent cases, the flow-through model is bounding with respect to releases of radionuclides.
Constrained water vapor and oxygen diffusion model	The rate of steel component corrosion inside a WP is compared with the rate of diffusion of water vapor and oxygen through stress corrosion cracks into a WP. A continuous film of adsorbed water cannot form if the consumption rate is higher, which could delay the diffusive releases until all steel is fully corroded (SNL 2007 [DIRS 177407], Section 6.6.2).	Insufficient data to validate.
Dual-continuum invert model	Crushed tuff invert ballast is modeled as a dual-continuum material consisting of intergranular pore space and intragranular pore space. All seepage flow into the drift flows through the intergranular pore space and into the UZ fractures. Imbibition from UZ host rock into the invert flows through the intragranular pore space. Diffusion of radionuclides also occurs in both the intergranular and intragranular pore spaces, from the WP corrosion products into UZ fractures and matrix, as well as between the two invert continua (SNL 2007 [DIRS 177407], Section 6.6.3).	Insufficient data to validate diffusion coefficients in individual continua. Insufficient data to confirm whether this is a bounding approach with respect to chemical conditions in the invert for calculating solubility and colloid stability.
Invert diffusion coefficient model with lower limit on water content	As the water content of the crushed tuff ballast decreases, the water films that connect pore spaces become disconnected, and the effective diffusion coefficient drops more rapidly than predicted by Archie's law. Below some critical water content, the diffusion coefficient becomes zero, based on models of diffusion in soils (SNL 2007 [DIRS 177407], Section 6.6.4).	Insufficient data to validate diffusive behavior at very low water contents.
Reversible sorption of radionuclides onto WP corrosion products (empirical K_d sorption model)	Iron oxyhydroxide corrosion products sorb many radionuclide species. Sorption is assumed to be reversible and will not compete with other radionuclides nor compete for irreversible sorption sites (SNL 2007 [DIRS 177407], Section 6.6.5).	Does not account for limitations on total number of sorption sites. Does not account for competition with other radionuclides for sorption sites.
Plutonium sorption from stationary corrosion products and colloids	Plutonium sorbs strongly to iron oxyhydroxide corrosion product colloids and stationary corrosion products. Sorption may be considered "slowly reversible" (and modeled by computing the forward and reverse rate constants for the two-site model) (SNL 2007 [DIRS 177407], Section 6.6.6).	Experiment durations are short (hours to weeks) compared to the repository time scale. The mechanisms of plutonium sorption are not understood well enough to extrapolate the results outside the experiment design. Plutonium sorption and desorption data are not available for the highest pH ranges expected in the repository environment.

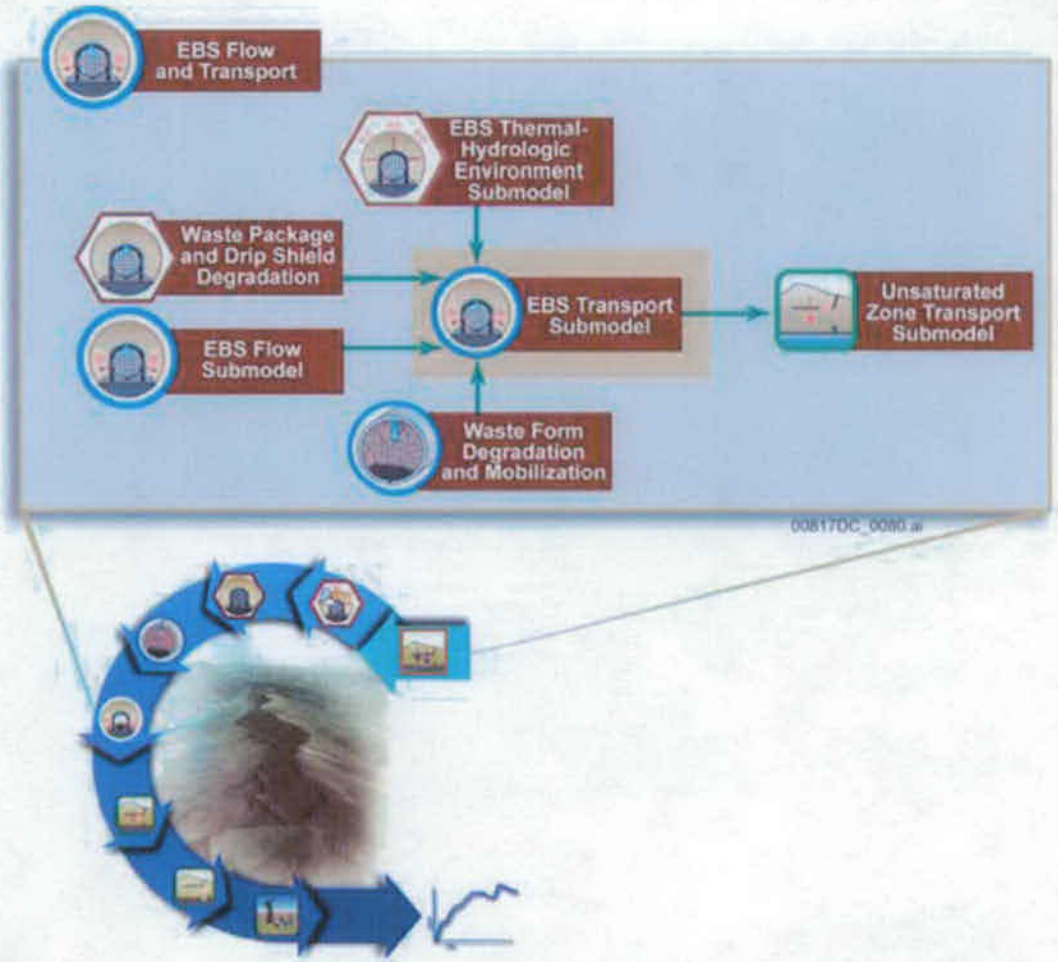

Figure 6.3.8-1. Information Flow Diagram for the EBS Transport Submodel

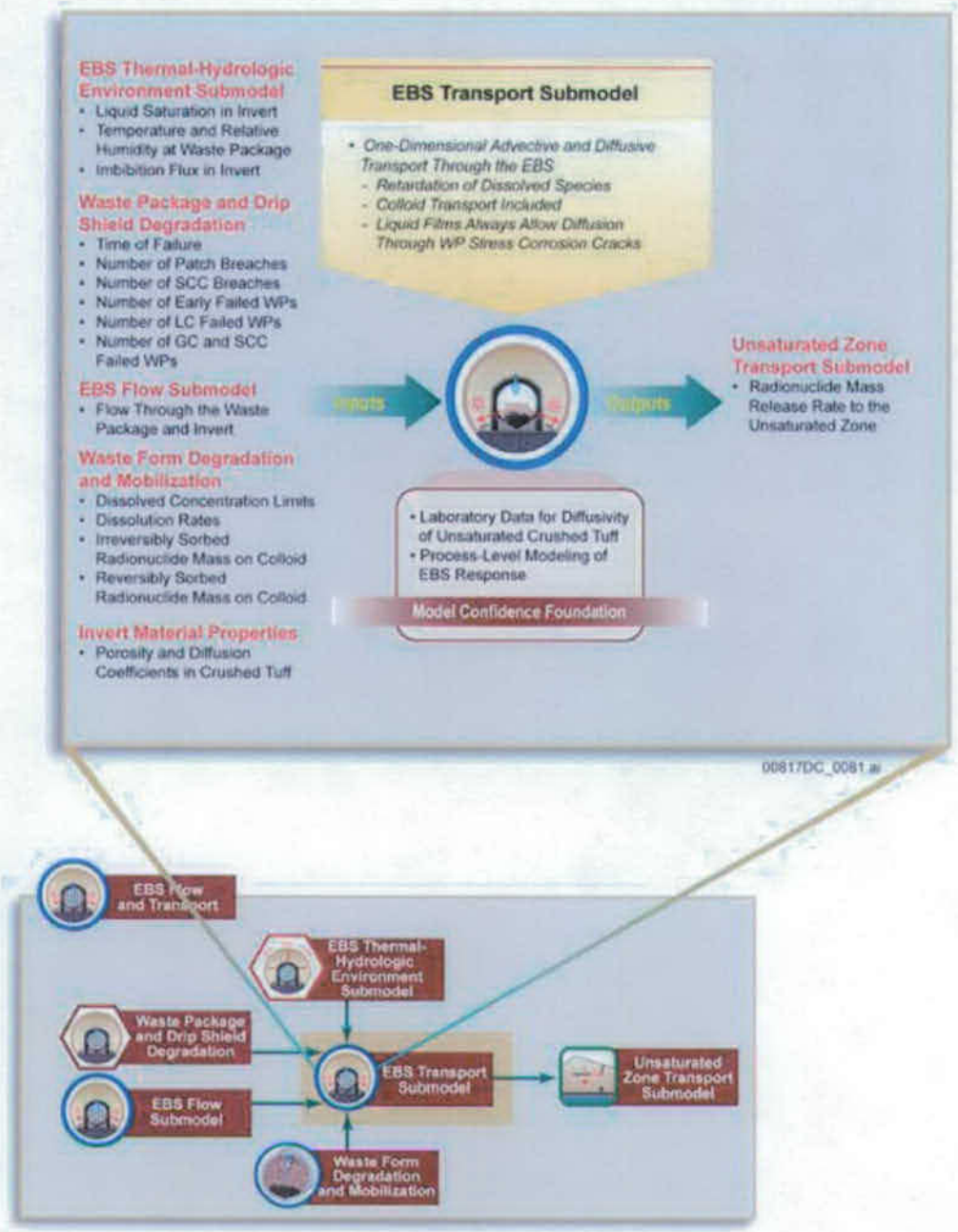

Figure 6.3.8-2. Inputs, Outputs, and Basis for Model Confidence for the EBS Transport Submodel

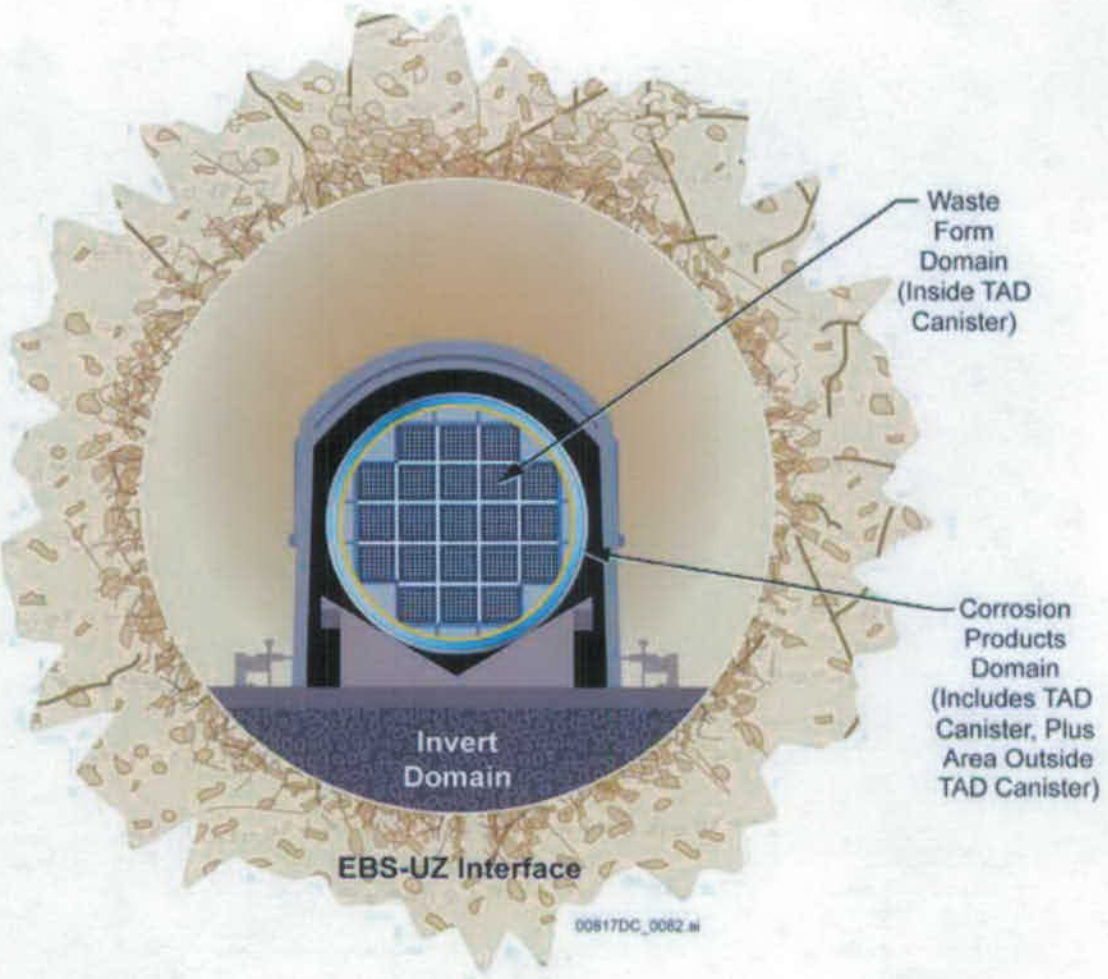

Figure 6.3.8-3. Cross Section of Idealized Drift Showing EBS Transport Submodel Domains for a CSNF Waste Package

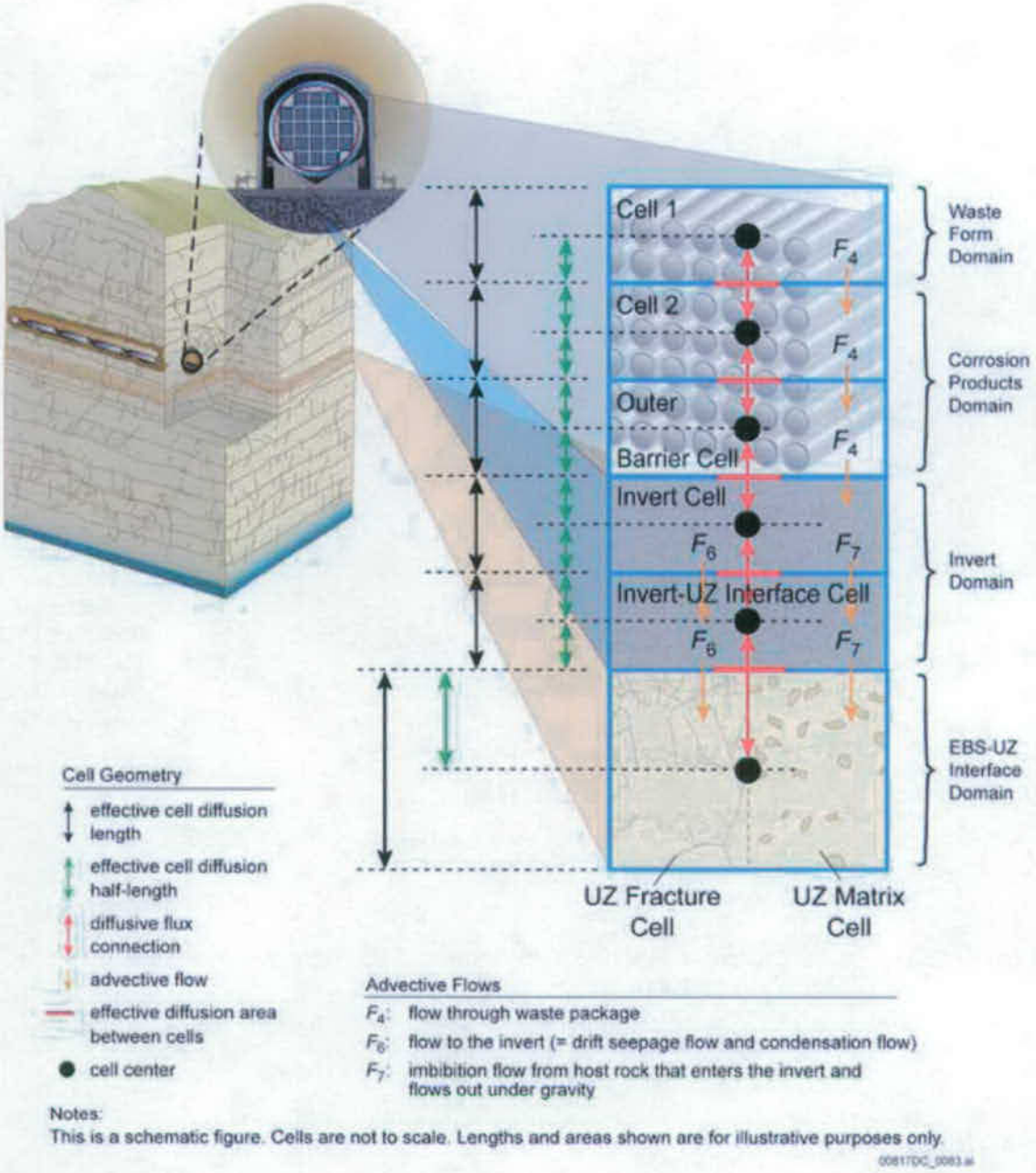

Figure 6.3.8-4. Schematic Representation of CSNF Waste Package Showing its Relationship to the Cell Pathway Network Used to Implement the EBS Transport Submodel

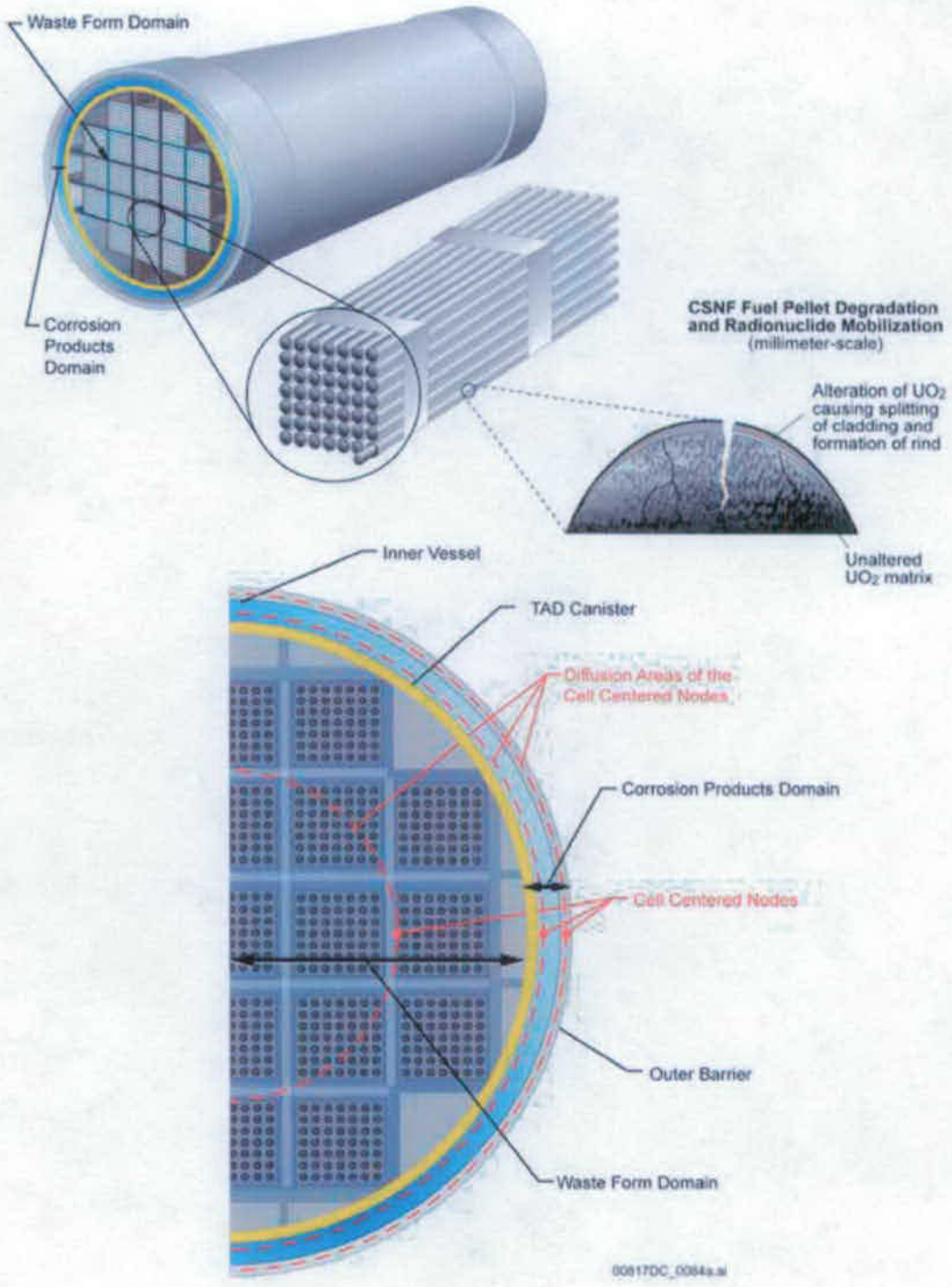

Figure 6.3.8-5. Setup of Cell Pathways for a CSNF Waste Package Used in the EBS Transport Submodel

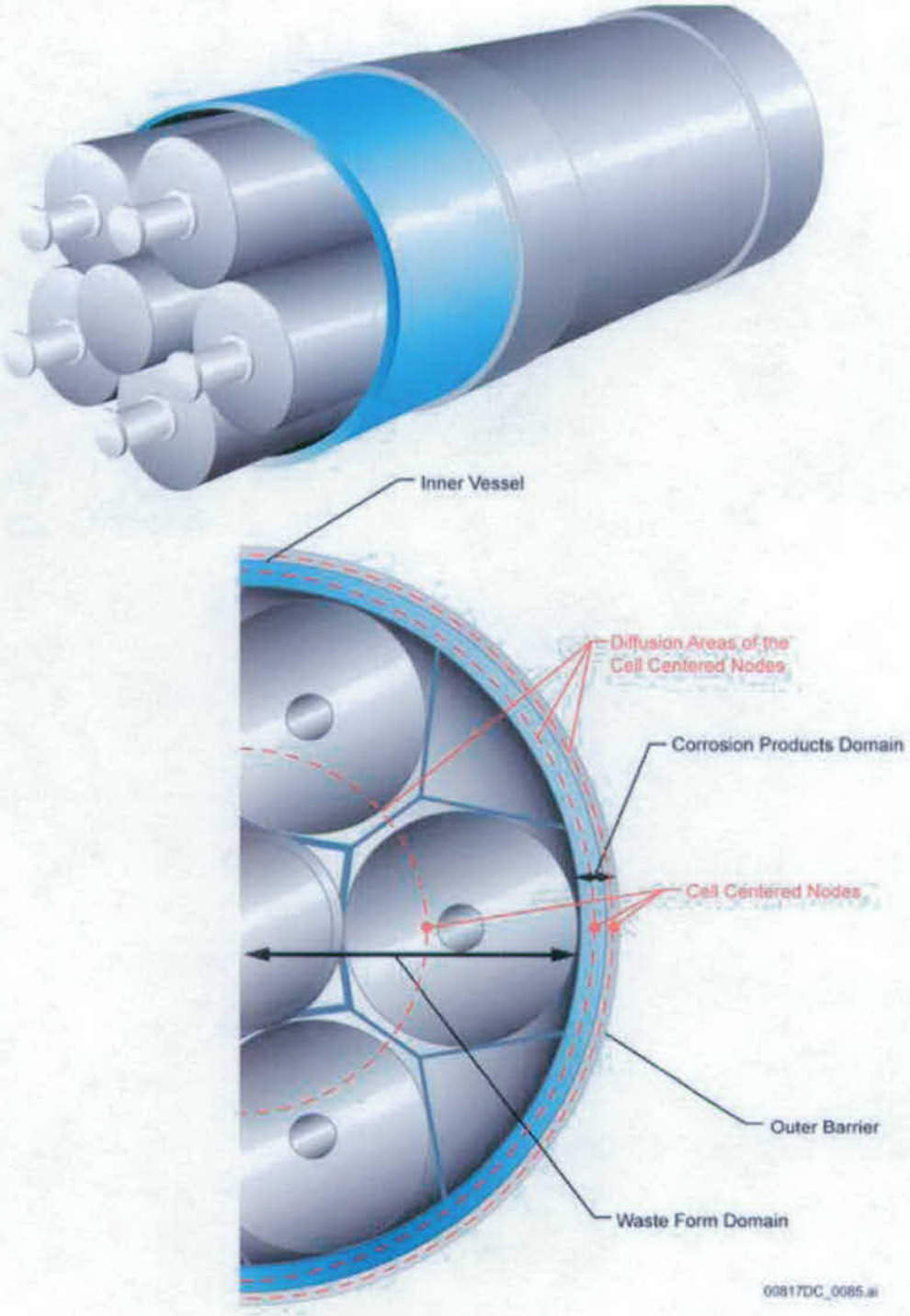

Figure 6.3.8-6. Setup of Cell Pathways for a CDSP Waste Package Used in the EBS Transport Submodel

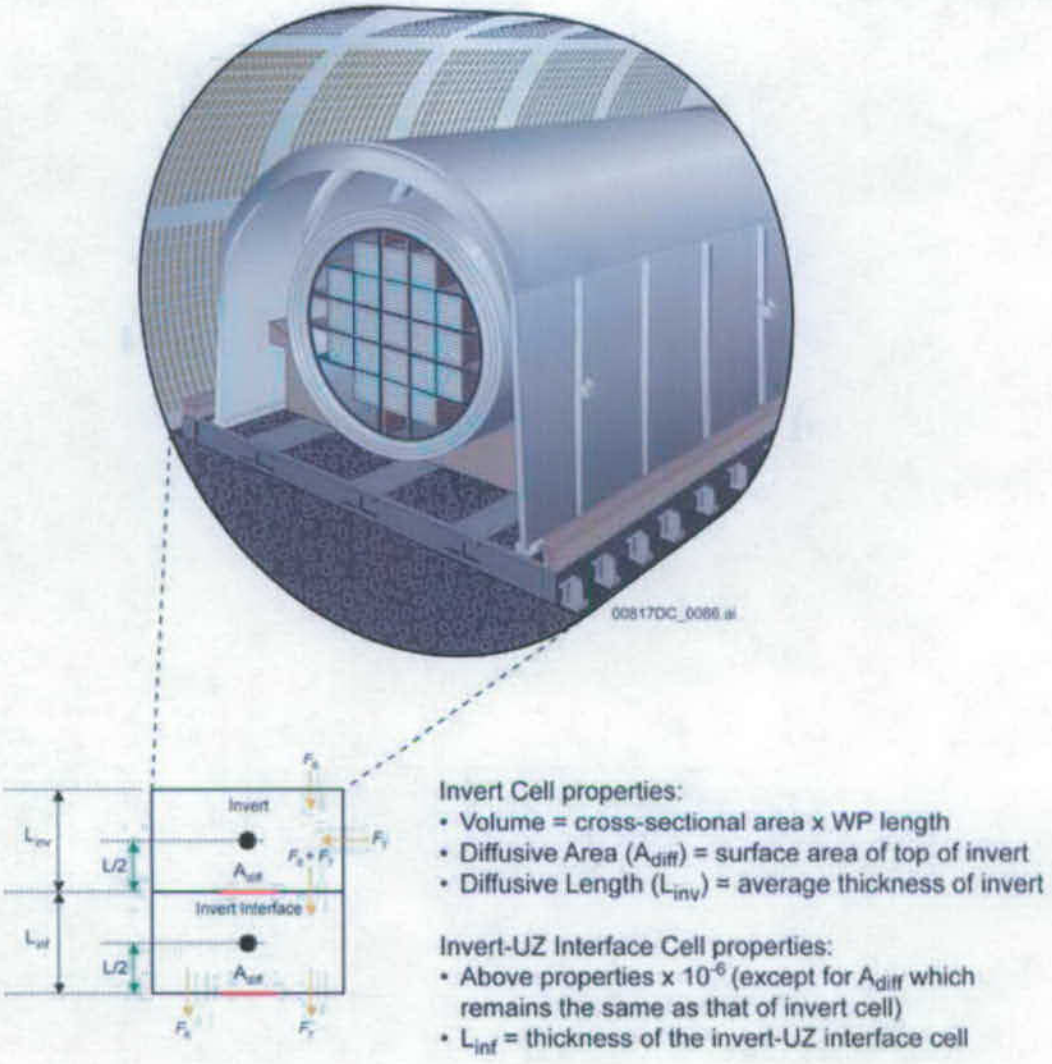

NOTE: The flow pathways (F_6 and F_7) are discussed in Section 6.3.6.1 and Figure 6.3.6-4.

Figure 6.3.8-7. Setup of Invert Cell Pathways Used in the EBS Transport Submodel and their Relationship to the Actual Invert Geometry

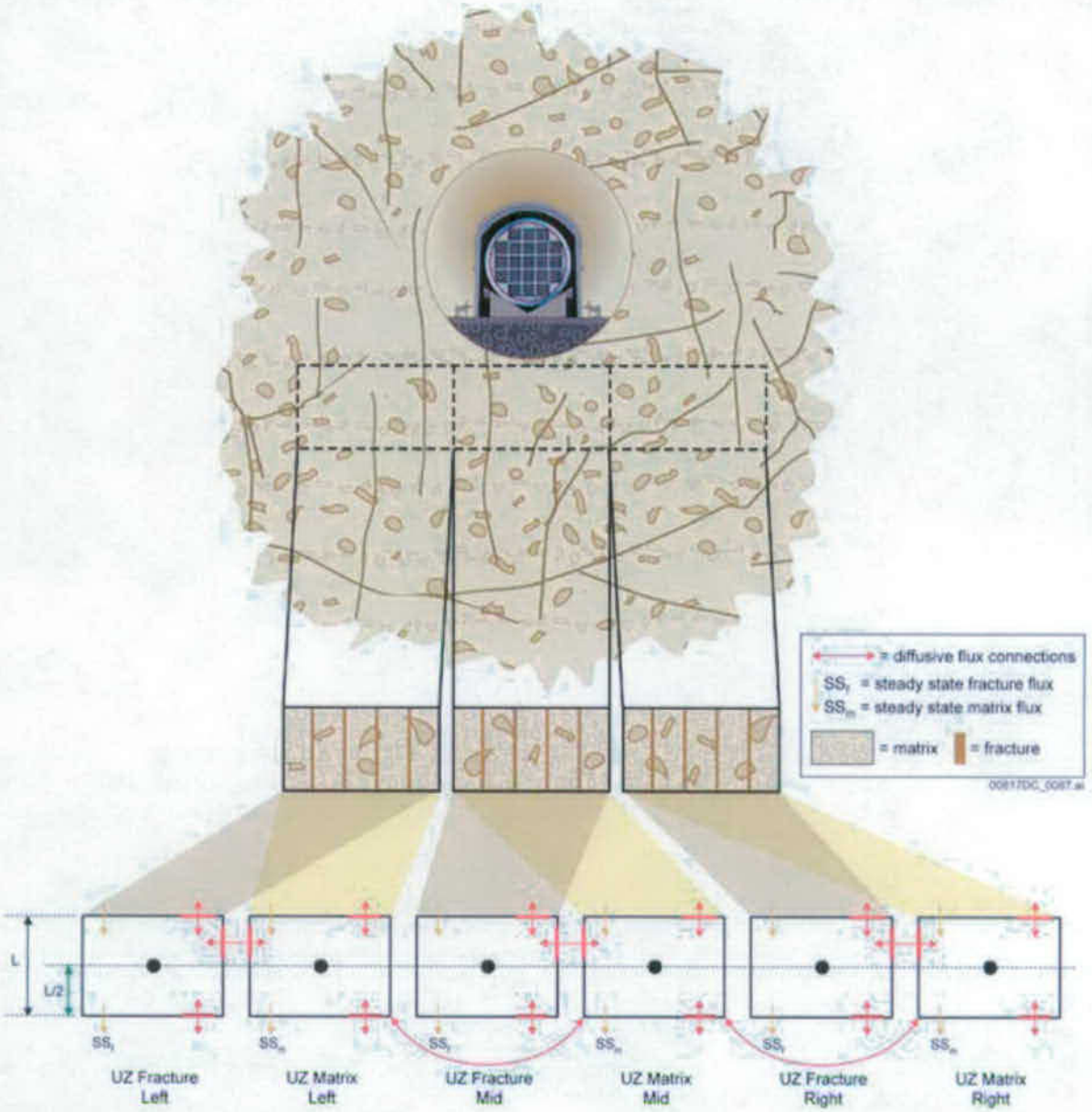

EBS-UZ Cell Properties:

- Bulk Volume = Drift Diameter × Cell Height × Waste Package Length
- Pore Volume (Matrix) = Bulk Volume × Matrix Porosity × (1-Fracture Fraction)
- Pore Volume (Fracture) = Bulk Volume × Fracture Fraction
- Diffusive length and area are based on geometry

Figure 6.3.8-8. Setup of Dual-Continuum EBS-UZ Interface Cell Pathway Network and its Relationship to the Near-Field Unsaturated Zone

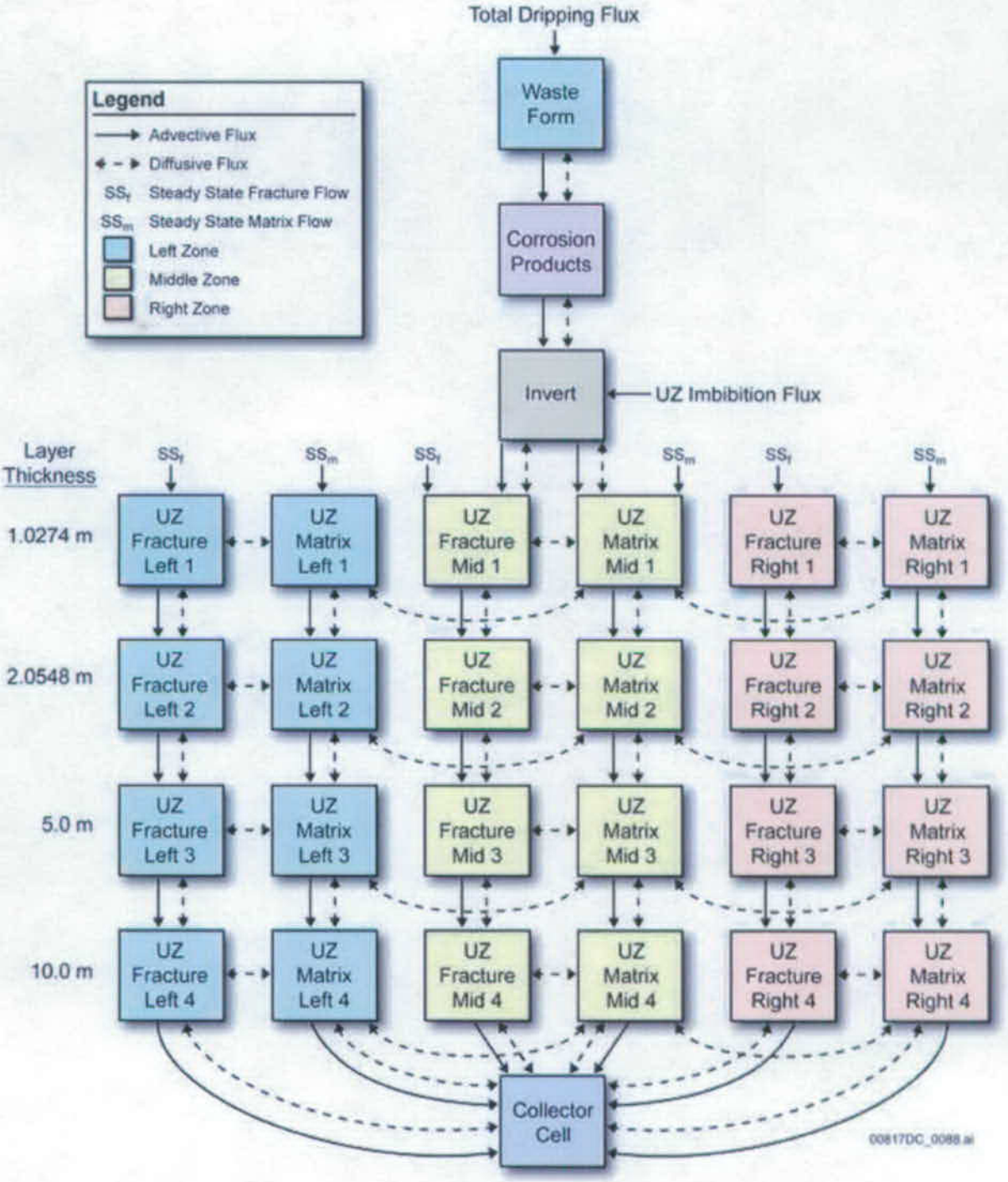

Source: (SNL 2007 [DIRS 177407], Figure 6.5-4)

Figure 6.3.8-9. Schematic Representation of the Computational Grid for the EBS-UZ Interface Model

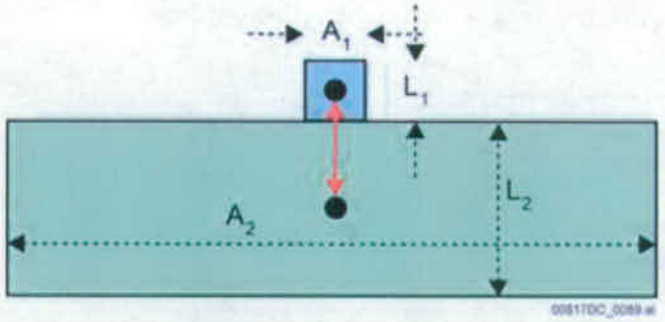

Figure 6.3.8-10. Simple Model Setup Using Cell Pathways with Different Diffusive Areas

6.3.9 Unsaturated Zone Transport

The UZ Radionuclide Transport Submodel of the TSPA-SEIS calculates the transport of radionuclides from the EBS of the Yucca Mountain repository, through the UZ to the SZ. UZ transport will depend on the flow fields from the *UZ Flow Models and Submodels* (SNL 2007 [DIRS 175177]), and on the rates of radionuclide mass releases from the waste emplacement drifts, as well as uncertainties associated with transport parameters. The UZ Transport Submodel provides, as output, the rate and spatial distribution of radionuclide releases to the SZ Flow and Transport Model Component. Information flow between the UZ Transport Submodel and other TSPA-SEIS components and submodels, is shown on Figure 6.3.9-1. Figure 6.3.9-2 shows the connections between the UZ Transport Submodels and indicates elements of the foundation for confidence in the UZ Transport Submodel, the characteristics of radionuclide transport in the UZ, and the inputs and outputs associated with the UZ Transport Submodel.

Note that for the UZ Transport Submodel, the basic parameters used in the model are input from the FEHM DLL's (FEHM V2.24-01, STN: 10086-2.24-01-00 [DIRS 179419]) external input files. These basic FEHM DLL input parameters and their sources are described in this section. Input variable names presented in the tables of this section are of two origins. For deterministic values of parameters, the names provided in the tables are consistent with the input variable names defined in the FEHM user guide (LANL 2003 [DIRS 167579]; DOE 2007 [DIRS 181096]). For stochastic input parameters, found in FEHM external files, the variable names reference the GoldSim elements that are used to generate the sampled values. These sampled values are downloaded from a supplemental GoldSim TSPA-SEIS simulation, performed at any stage in the model development or utilization, when any parameter stochastic distribution changes. The sampled values are downloaded from GoldSim into the FEHM stochastic parameter external files. Using the updated FEHM stochastic parameter external files, simulations are then performed using these files until there is any change in any stochastic parameter. Also, note that all references to FEHM in this section (Section 6.3.9) refer to FEHM Version 2.24-01 [DIRS 179419], which is the version of FEHM used in the TSPA-SEIS Model and it will not be repeated every time FEHM is mentioned.

6.3.9.1 Conceptual Model

Transport of dissolved and colloid-bound radionuclides through the UZ below the repository will occur in both the fractures and the rock matrix, as shown on the conceptual drawing of UZ transport processes on Figure 6.3.9-3. Flow pathways will be determined by the hydrogeologic characteristics of the rock units, the presence or absence of faults, and whether or not there is perched water present along individual flow pathways. These characteristics will control the extent of downward versus lateral flow, advective transport between the fractures and matrix, matrix diffusion, and the partitioning of flow between the fractures and rock matrix. Fractures and faults can provide fast flow paths. Additionally, diffusion into the rock matrix and/or sorption onto the rock/mineral surfaces are important retardation processes for radionuclide transport (BSC 2004 [DIRS 170035], Sections 6.2.2 and 6.2.3).

Five basic processes will affect the transport of radionuclides:

- **Advection**—Advection is the movement of dissolved or colloidal-bound radionuclides in conjunction with the bulk flow of water containing radionuclides. Advection tends to enhance radionuclide transport.

- **Diffusion**—Diffusion of radionuclides from fluid flowing in fractures into rock-matrix pores will be a potential retardation mechanism because matrix transport is typically slower than fracture transport. Conversely, diffusion from the matrix to the fractures would tend to decrease transport times. Figure 6.3.9-4 is a conceptual drawing of diffusion into and out of matrix pores.

- **Sorption**—Sorption onto the rock/mineral surfaces will slow or retard the transport of certain dissolved radionuclides through the UZ. Sorption also results in radionuclide attachment to colloids, which can enhance radionuclide transport.

- **Hydrodynamic Dispersion**—Hydrodynamic dispersion, which is the spreading of a plume of dissolved constituents, such as radionuclides released from the repository as they are transported, is caused by localized variations in the flow field. Hydrodynamic dispersion tends to dilute and smear sharp concentration gradients and reduce the concentration at the leading edge of a breakthrough curve of radionuclides at the water table. Figure 6.3.9-5 is a conceptual drawing illustrating hydrodynamic dispersion in relationship to the rocks surrounding the repository. The UZ Transport Submodel only considers longitudinal hydrodynamic dispersion and does not consider transverse dispersion (SNL 2007 [DIRS 181006], Section 5.0, Assumption 3).

- **Radioactive Decay and Ingrowth**—Radioactive decay reduces the concentration of radionuclides in a predictable way, but it also produces decay products that typically have sorption characteristics different from those of the source radionuclides.

Colloid transport in the UZ is primarily in the fractures because colloids are limited in their capacity to diffuse into rock matrix as reflected in the low estimated values for diffusion coefficients (SNL 2007 [DIRS 177396], Section 6.18.2). Colloid transport into the rock matrix is also limited by size exclusion. Colloids can also be transported between the fractures and rock matrix and through the rock matrix by advection as long as the colloids are smaller than the matrix pores. In the UZ Transport Submodel, diffusion of colloids between the fractures and rock matrix is assumed to be negligible, while advective transport between the fractures and rock matrix is modeled explicitly. Figure 6.3.9-6 is a conceptual drawing showing some of the elements related to colloid-facilitated transport. Two principal types of colloid attachment can exist: reversible attachment where the radionuclides are temporarily attached to the surface of colloids and irreversible attachment where the radionuclides are permanently imbedded in the colloid structure. Advection of colloids through fractures is expected to dominate colloid transport in welded and zeolitic tuffs because permeability in the welded and zeolitic tuff matrix is much lower than that in the fractures. The rock matrix pores are typically smaller than the fracture apertures and the colloids themselves in many instances. Colloid filtration can occur in

the matrix during transport from one hydrogeologic unit to another. That is, when the size of the colloids is larger than the matrix pores, in the downgradient unit, the colloids are stopped at the unit interface. This filtration effect results in permanent immobilization of radionuclides irreversibly attached to the colloids but not of radionuclides reversibly attached to colloids. In the latter instance, the radionuclides could desorb from the colloids and continue to migrate. For this reason only irreversible colloids are filtered at unit interfaces in the TSPA-SEIS. In addition, colloid exclusion from the matrix can occur when there is a component of flow from the fractures into the matrix and some colloids that would otherwise migrate from the fracture continuum to the matrix continuum are excluded due to their size relative to the matrix pore size. Filtration of colloids during transport within fractures is implicitly considered in the colloidal retardation parameter.

A change to wetter climates may also impact the transport of radionuclides through the UZ by increasing net infiltration at the ground surface and, subsequently, the percolation flux through the UZ. Along with increased transport rates through the UZ, wetter climates would also lead to an increase in water table elevation. A higher water table shortens transport distances from the EBS to the water table. In the TSPA-SEIS, a rise in the water table is accompanied by an instantaneous release, to the SZ, of the radionuclides that are presently in the geologic units impacted by the water table rise.

6.3.9.2 TSPA-SEIS Abstraction

Consistent with the Mountain-Scale UZ Flow Submodel, the UZ Transport Submodel is a dual-continuum model. In the UZ Transport Submodel, fracture and matrix transport are coupled and calculated using the FEHM [DIRS 179419] residence-time transfer-function particle-tracking technique, as described in *Particle Tracking Model and Abstraction of Transport Processes* (SNL 2007 [DIRS 181006], Section 6.4). This technique is a cell-based approach in which particles move from cell to cell in the FEHM numerical grid. Particle movement from cell to cell is computed probabilistically based on flow balance, dispersivity, and matrix diffusion. The fracture matrix interactions are evaluated using transfer functions when diffusive transport between fracture and matrix (i.e., dual-permeability or discrete fracture models) is simulated. The transfer functions used in the TSPA-SEIS are a set of breakthrough curves defined using dual-permeability numerical solutions of the transport equations for parallel flow in a fracture and adjacent rock matrix and diffusion normal to the flow direction (SNL 2007 [DIRS 181006], Appendix C). After a particle enters a cell, the adjacent cell it will travel to next (or whether it will switch media in the same cell) is probabilistically determined using random sampling based on the water flow balance. Note that only outflows from cells are included in the calculations; particles are not moved to a cell if water flows from that cell to the current cell. For the dissolved species and reversible colloids simulated in the TSPA-SEIS, the transfer functions are used to randomly decide if a particle will change medium (go from fracture to matrix or from matrix to fracture) and to determine the cell residence times for each particle. For the irreversible colloids, which are not subject to matrix diffusion, the residence times for each particle are a function of the the cell pore volumes, the flux out of the cells, and the colloid retardations (for the retarded or Ic species only). To simulate the effects of longitudinal dispersivity in dissolved species, reversible colloids, and irreversible colloids, the residence times are updated with a random factor based on the Peclet number between cells, where the Peclet number is a function of the dispersivity and the distance between cells.

The dual-continuum UZ Transport Submodel includes a numerical grid of fracture cells representing the fracture continuum and a grid of matrix cells representing the matrix continuum, with each fracture cell connected to a corresponding matrix cell. Twenty-seven radionuclides are transported through the UZ. The radionuclide half-lives and decay products used in the TSPA-SEIS are listed in Table 6.3.9-1. The following processes are simulated in the TSPA-SEIS:

- Advective transport of dissolved and colloidal-bound radionuclides in the fracture and matrix continua, and between continua
- Longitudinal dispersion
- Sorption of dissolved radionuclides to the matrix continuum
- Exchange of mass between fracture and matrix continua via molecular diffusion
- Retardation of irreversible and reversible colloids in the fracture continuum
- Colloid filtration at interfaces between rock-matrix units
- Colloid size exclusion at fracture-matrix continua interfaces
- Radioactive decay and ingrowth
- Climate change and its effect on fluid flow rates in the UZ
- Climate change and associated rise in water-table elevation and its effect on radionuclide release to the SZ.

Uncertainty is included in the UZ Transport Submodel by defining statistical distributions for a number of input parameters. Thus, each realization of the total system has a unique set of input parameters. In addition, each realization is considered to be equally likely. Some of the uncertainty in UZ transport results from uncertainties passed to the UZ Transport Submodel from other submodels. For example, there may be uncertainty in infiltration and UZ flow from the Site-Scale UZ Flow Process Model; uncertainty in the number of failed WPs from the WP and DS Degradation Model Component; and uncertainty in numerous EBS parameters and processes used to define the radionuclide source term received from the EBS Transport Submodel. These uncertainties from upstream submodels are passed to the UZ Transport Submodel either implicitly through the passing of the radionuclide fluxes and ratios of fluxes applied to the fractures versus total fluxes (fluxes applied to fractures and rock matrix) from GoldSim to FEHM, or explicitly through the passing of data, such as the number of WPs failed in each percolation subregion (source bin) or indices denoting which infiltration rate scenario should be applied (10th percentile, 30th percentile, 50th percentile , or 90th percentile rate scenario). For the sampled infiltration rate scenario a set (10th percentile, 30th percentile, 50th percentile, or 90th percentile) of four flow fields made up of present day, monsoonal, glacial-transition, and post-10,000 year flow fields is read in by the FEHM DLL for that realization. The uncertainty distributions sampled to derive parameters for the FEHM DLL are summarized in Tables 6.3.9-2 through 6.3.9-12. The uncertainty distribution for the infiltration scenarios is presented in

Table 6.3.1-2. Note that some of the parameters derived for the UZ Transport Submodel, such as matrix sorption and matrix diffusion coefficients, are also used in the EBS Submodel for sections of cell networks representing the UZ directly below the repository.

In the TSPA-SEIS, radionuclide sorption on the rock matrix is approximated using a linear, equilibrium sorption model characterized by a single parameter, the sorption coefficient K_d. A set of three probability distributions for the K_ds used in the model, have been developed, for each radioelement. Each set of K_ds describes the radioelement's sorptive behavior in each of three major rock types (vitric, devitrified, and zeolitic tuffs) in the UZ (SNL 2007 [DIRS 177396], Appendices A[a] and B[a] for selenium and tin, and Appendices A and B for all other species). These effective sorption coefficients are a function of many factors, including mineralogy, groundwater aqueous chemistry, and heterogeneity at scales smaller than those considered in the numerical model. Furthermore, in developing the sorption coefficients, the kinetics of sorption reactions and nonlinear sorption effects that would lead to lower K_ds were considered. The above factors were considered when establishing the parameter uncertainty distributions for the K_d values. In addition, sorption coefficients may be affected by temperature. With elevated temperatures, the sorption coefficient generally increases for cationic species, thereby causing longer transport times (SNL 2007 [DIRS 177396], Section 6.1.2.9). The linear equilibrium sorption coefficients used in the TSPA-SEIS, do not account for elevated temperatures and, therefore, are conservative with respect to transport times for cationic species through the UZ (SNL 2007 [DIRS 177396], Section 6.1.5.2). The parameter distributions used in the UZ Transport Submodel for matrix sorption coefficients are provided in Table 6.3.9-2.

For the TSPA-SEIS, unsaturated matrix diffusion coefficients are generated as the product of the matrix tortuosities for specified rock groups and the free-water diffusion coefficients for the elements considered. The tortuosities are based on a correlation between matrix diffusion, porosity, and saturated permeability developed from diffusion data in saturated samples by Reimus et al. (2007 [DIRS 179246]). To adapt the relationship for the UZ, porosity is replaced by water content, and saturated permeability is replaced by effective permeability. The methodology used in the derivation of the distributions for tortuosities is described in *Particle Tracking Model and Abstraction of Transport Processes* (SNL 2007 [DIRS 181006], Section 6.5.5[a] and Appendix A[a]). The derivation of the constant values for element specific free-water matrix diffusion coefficients is also described in *Particle Tracking Model and Abstraction of Transport Processes* (SNL 2007 [DIRS 181006], Section 6.5.5[a] and Appendix A[a]).

The equation describing the correlation between matrix diffusion, porosity (or water content for the UZ), and saturated permeability (or effective permeability for the UZ) used for calculating the matrix diffusion coefficient, as presented by Reimus et al. (2007 [DIRS 179246]), is

$$\log\left(D_m / D^*\right) = 1.42 + 1.91\theta_m + 0.19\log\left(k_m\right) \qquad \text{(Eq. 6.3.9-1)}$$

where

D_m/D^* = the matrix tortuosity

D_m = the matrix diffusion coefficient in m^2/s

D^* = the free water diffusion coefficient in m^2/s

θ_m = the matrix water content

k_m = the effective permeability to water in m^2.

Note that Equation 6.3.9-1 is an adaptation of the original equation for the UZ with water content replacing matrix porosity and effective permeability replacing permeability. The element-specific values for free-water diffusion coefficients are presented in Table 6.3.9-3. The $\log_{10}$ values of the mean tortuosities for the three rock groups that are assembled based on similar attributes are presented in Table 6.3.9-4. The SDs of the $\log_{10}$ tortuosities, based on the standard error of the regression curves defined by Equation 6.3.9-1 are also presented in Table 6.3.9-4 (see also SNL 2007 [DIRS 181006], Table 6.5.5-1[a] and Section 6.5.5.4 [a]). The uncertainty is implemented in the TSPA-SEIS for each rock group by selecting a standard normal random number and adding the product of the standard normal random number and SD (in $\log_{10}$ space) to the $\log_{10}$ value of the mean tortuosity, taking the antilog of the value to derive the tortuosity for the present realization and multiplying each element-specific free-water diffusion coefficient by the tortuosity to derive 15 element-specific effective diffusion coefficients (SNL 2007 [DIRS 179301], Section 3.2.1).

As previously noted, for TSPA-SEIS simulations, the diffusion of colloids from the fracture to the matrix is not simulated. This treatment is considered conservative with respect to colloid transport times to the SZ (SNL 2007 [DIRS 181006], Section 6.5.5).

In the UZ Transport Submodel, the fracture dispersivity is set to 10 m. According to the feed analysis model report (SNL 2007 [DIRS 181006], Section 4.1.2[a] and Section 6.5.2), the value of 10 m represents a conservative value chosen from the lower end of the field studies. A higher dispersivity tends to spread the plume and reduce the peak concentrations. In addition, in comparison with the effects of matrix diffusion and the large-scale heterogeneities in the UZ, dispersivity effects are expected to have a small influence on the breakthrough curves (SNL 2007 [DIRS 181006], Section 6.5.2). Note that FEHM's multi-species particle tracking model limits the peclet number between adjacent nodes to ≥ 1, where the peclet number is the ratio of path length to dispersivity (SNL 2007 [DIRS 181006], Section 6.4.2). This means that for nodal distances ≤ 10.0, the dispersivity will be set equal to the path length. For most of the TSPA-SEIS, the dispersivity will be 10 m, but just below the repository, for some of the links between cells, the dispersivities may be as low as 5 m.

Part of the conceptual model upon which the UZ Transport Submodel is based, is the Active Fracture Model of Liu et al. 1998 [DIRS 105729]. The active fracture model takes into consideration the fact that due to the nonlinearities associated with unsaturated flow, only a portion of fractures in the UZ fracture network are subject to water flow and the others are bypassed. The Active Fracture Model assumes that since only a portion of the fractures in a network have water flowing through them there is an effect on the fracture spacing, the fracture/matrix interface area, and the number of active fractures in a grid block. In the TSPA-SEIS, the spacing between flowing fractures is calculated as a function of the geometric fracture spacing, fracture saturation, fracture residual saturation, and the active fracture model parameter (γ) (Liu et al. 1998 [DIRS 105729]). In the TSPA-SEIS, a constant fracture residual saturation of 0.01 is used for all layers (SNL 2007 [DIRS 181006], Section 6.5.6).

In addition to adjusting the spacing between flowing fractures, the active fracture conceptualization calls for an adjustment to the interface area across which matrix diffusion occurs. The interface adjustment accounts for the reduction of the wetted area within an individual fracture and for the reduction in area caused by the smaller number of active fractures. This adjustment to the interface area is a reduction by a factor of the effective saturation (SNL 2007 [DIRS 181006], Appendix C, Section C-5). Note that the interface area between the fracture and matrix is reduced by this factor of the effective saturation even when all fractures are considered active ($\gamma = 0$). The area reduction associated with the active fracture model is a conservative representation for situations in which radionuclide mass is introduced into the fracture continuum. An underestimation of the diffusive area would slow the movement of mass applied to the rock matrix and increase the rate of movement of mass through the fractures. For mass applied to the rock matrix, there would be a decrease in mass diffusing out of the matrix slowing its movement through the system. As implemented, the active fracture conceptualization is consistent with the assumptions of the fracture-matrix interaction, as validated in *Particle Tracking Model and Abstraction of Transport Processes* (SNL 2007 [DIRS 181006], Section 7.2.3.3). Note that the UZ Transport Submodel uses different active fracture model parameter values than the UZ Flow Field Abstraction. In the UZ Flow Model, the active fracture model parameter values are calibrated. To be rigorous, the AFM parameters should be consistent between the flow and transport model because the AFM parameters affect both flow and transport processes (SNL 2007 [DIRS 181006], Section 6.6.4). However, since process flow model studies (SNL, 2007 DIRS 175177]) have shown that the AFM parameter values have little influence on the fluid saturations and steady-state fracture to fracture and matrix to matrix flow, the use of the base case flow fields is justified (SNL 2007 [DIRS 181006], Section 6.6.4). Sensitivity studies presented in SNL 2007 ([DIRS 181006], Section 6.6.4, Figures 33–35), show the sensitivity of transport to the variance in the AFM gamma indicating that consideration of uncertainty is important for the transport process. Uncertainty in the active fracture parameter gamma is applied to the TSPA-SEIS by sampling the parameter uniformly over a range between 0.2 and 0.6 as noted in Table 6.3.9-5 (SNL 2007 [DIRS 181006], Section 6.5.6[a]). This range of gamma values spans the values considered appropriate for tsw32-tsw38, based on ^{14}C data (SNL 2007 [DIRS 181006], Section 6.5.6[a]) and the values based on the flow model calibration.

Fracture spacing and aperture values are used to estimate the effect of matrix diffusion on radionuclide transport. In the TSPA-SEIS, the fracture spacing is the inverse of fracture frequency. Fracture apertures are calculated from randomly sampled fracture porosity and frequency values using the following relationship (SNL 2007 [DIRS 181006], Section 6.5.7, Equation 6-26):

$$2b = \phi_f / f \qquad \text{(Eq. 6.3.9-2)}$$

where

$2b$ = the fracture aperture (m).

ϕ_f = the fracture porosity (dimensionless).

f = the fracture frequency (m^{-1}).

The distributions used by the TSPA-SEIS for fracture porosity values (ϕ_f) and fracture frequency values (f, unit 1/m) are presented in Tables 6.3.9-6 and 6.3.9-7, respectively. Note that there is a large amount of uncertainty in the estimates of fracture porosity (BSC 2004 [DIRS 170038], Section 6.1.3). This uncertainty stems from two areas: (1) the nature of the air permeability testing and (2) using estimates from one-dimensional and two-dimensional simulation results and not from three-dimensional tests.

Retardation of dissolved radionuclides associated with sorption onto fracture surfaces is not simulated in the TSPA-SEIS (SNL 2007 [DIRS 181006], Section 6.5.8). Therefore, in the TSPA-SEIS, fracture retardation factors are set to 1.0, indicating that there is no sorption onto fracture surfaces, which is a conservative approximation.

Colloid sizes and matrix pore sizes are used in FEHM to determine filtration of irreversible colloids at interfaces between rock matrix units. At the start of each FEHM simulation, each potential particle is assigned a size based on sampling from a colloid size distribution. The uncertainty in colloid size is represented by a CDF, shown in Table 6.3.9-8 (see also SNL 2007 [DIRS 181006], Section 6.5.11). During particle tracking, the size of each particle is compared to a randomly sampled value from a CDF for colloid transport at a matrix interface, which reflects the distribution of pore sizes of the matrix rock unit(s) (see also SNL 2007 [DIRS 181006], Section 6.5.9). If the particle size is larger than the sampled pore size, then the colloid does not enter the underlying rock matrix unit and is removed from the simulation or permanently filtered out. Table 6.3.9-9 lists the cumulative probability distributions for colloid transport at matrix interfaces for UZ transport in the various UZ rock units.

For the case in which colloids travel from fractures to the matrix via advection, an exclusion process may occur based on the matrix pore size. This colloid-exclusion process is implemented for irreversible colloids in the TSPA-SEIS through the use of an exclusion factor, f_c, based on the percentage of pores that are greater than the expected colloid size of 100 nm (SNL 2007 [DIRS 181006], Section 6.5.10). Each colloid particle has a chance of being excluded from entering the matrix based on a probability, equal to the fraction of matrix pores that are smaller than the expected colloid size. The colloid exclusion factors used in the TSPA-SEIS are presented in Table 6.3.9-10.

The sorption of radionuclides onto colloids may be either a reversible or an irreversible process. When the sorption process is irreversible, a very large number (10^{20}) is assigned to the colloid equilibrium sorption coefficient, K_c (SNL 2007 [DIRS 181006], Section 6.5.12). For reversible radionuclide sorption on the colloids, the K_c values are calculated by multiplying a radionuclide's sorption coefficient for a species onto a colloid, K_d, by the colloid concentrations in the water. Table 6.3.9-8 provides the CDF for colloid concentration (SNL 2007 [DIRS 181006], Section 6.5.12[a]).

Uncertainties associated with colloid sorption coefficients for various radionuclides are represented by a set of CDFs, as shown in Table 6.3.9-11. These colloid sorption coefficients are consistent with those used in the EBS Transport Submodel (SNL 2007 [DIRS 177423], Table 6-15). Note that only the CDFs for smectite colloids are presented in Table 6.3.9-11. The use of smectite colloids in the UZ is consistent with the guidance presented in *Waste Form and In-Drift Colloids-Associated Radionuclide Concentrations: Abstraction and Summary* (SNL 2007 [DIRS 177423], Section 6.5.3).

A colloid retardation factor, R_{coll}, is used in the TSPA-SEIS to simulate the impact of reversible filtration of both the reversible and irreversible colloids in fractures. Because there is no information regarding colloid retardation factors in the UZ, the TSPA-SEIS uses the SZ output, which is deemed appropriate for use in the UZ (SNL 2007 [DIRS 181006], Section 6.5.13). Table 6.3.9-12 shows the CDF for colloid retardation factors used in the UZ Submodel. The CDF for colloid retardation factors, presented in Table 6.3.9-12, is consistent with the CDF for the colloidal retardation factor in volcanic units for the SZ, as presented in Table 6.3.10-2. There is also a fraction of colloids escaping retardation due to physical and chemical processes. In the TSPA-SEIS, this fraction is defined as a function of the residence time of the colloid. In this relationship, progressively fewer colloids migrate unretarded with time. Based on a combined UZ/SZ travel time of 100 years, the model uses a value of 0.00168 for the fraction of colloids migrating unretarded, as recommended in *Particle Tracking Model and Abstraction of Transport Processes* (SNL 2007 [DIRS 181006], Section 6.5.13). Colloids traveling unretarded are given a retardation factor of 1.0.

6.3.9.3 TSPA-SEIS Implementation

The TSPA-SEIS implementation of UZ transport calculations is primarily achieved through the use of the FEHM DLL. The UZ Transport Submodel is directly coupled (i.e., dynamically linked) with the TSPA-SEIS using an external pathway element within the GoldSim software to link with the UZ transport code, FEHM. The FEHM external pathway element is used to call the FEHM DLL, pass it a set of inputs, define the set of inflows from the EBS that the DLL will receive, and define the outflow cells to which the FEHM results will be sent.

The FEHM DLL receives inputs at run time both directly from GoldSim and from a set of external files. At run time, GoldSim passes direct inputs to FEHM, such as the flow field index (used to select the desired UZ flow field abstraction based on climate state and infiltration scenario), the number of radionuclides, and the number of repository zones (i.e., percolation subregions). In addition, for each realization, a randomly selected initial random seed is passed from GoldSim to FEHM for use in FEHM's particle migration logic. Similarly, a second random seed is passed to FEHM for use in the logic that locates the release points associated with each failed WP. GoldSim also passes inputs from the EBS, such as the combined EBS releases for both WP types (from each of the five percolation subregions), the ratio of the EBS release applied to fractures to the total EBS release (which is used to apportion the released radionuclides between fracture and matrix nodes), and the total number of failed CSNF WPs and CDSP WPs in each repository subregion. The FEHM DLL receives new sets of inputs from GoldSim every realization and for time-dependent inputs every timestep in each realization.

FEHM must also read in a set of external files that provides many inputs including the control parameters, deterministic transport parameters, and values for all the stochastic transport parameters. Data provided from the external input files include: (1) the numerical grid structure; (2) rock properties, such as porosity and bulk density; (3) solute transport parameters, such as fracture apertures, matrix diffusion coefficients, matrix K_d values, colloid distribution parameters, colloid retardation factors, Active Fracture Model gammas; and (4) the UZ flow fields. One line of input comprised of fracture apertures, active fracture model gamma, matrix diffusion coefficients, matrix K_d values, colloid distribution parameters, and colloid retardation factors is read from an external file for each realization. Each TSPA-SEIS realization also uses one set of UZ flow fields; there are sets for 10th percentile infiltration, 30th percentile infiltration, 50th percentile infiltration, and 90th percentile infiltration, scenarios (Sections 6.1.4.1 and 6.3.1). Each set has four flow fields: one each for present-day, monsoon, glacial-transition, and post-10,000-year climates (Section 6.3.1). When a climate change occurs, a new flow field is read in and the particles instantly travel with the updated water fluxes. In addition, when transition occurs from present-day to monsoon climate with a raised water table, mass associated with all particles located between the previous water table, and the new water table is released to the SZ Submodel during the timestep when the flow field change takes place.

The set of uncertain transport properties, consisting of matrix sorption coefficients, matrix diffusion coefficients, fracture apertures, active fracture model gammas, colloid sorption coefficients, and colloid retardation factors (as presented in SNL 2007 [DIRS 181006], Sections 6.5.4, Section 6.5.5[a], Section 6.5.6[a], Section 6.5.7, Section 6.5.9, Section 6.5.10, Section 6.5.11, and Section 6.5.12[a]), is statistically sampled or generated from a set of statistically sampled parameters using GoldSim. During a supplemental simulation, the TSPA-SEIS is used to generate a set of external files containing these sampled parameters for FEHM. The set contains files sampled for 300 and 1,000 realizations. The TSPA-SEIS can then be run for simulations of 300 or 1,000 realizations. These files are used until there is a change in a parameter distribution or sampling seed, in which case a new set of files is generated. To use these files, the multiple species particle-tracking files contain placeholder indices identifying which of the variables in the external FEHM stochastic sample file belongs at the locations of the placeholder indices. Additionally, to ensure compatibility between the UZ and EBS Transport Submodels, matrix K_d values generated by the sampling elements in the TSPA-SEIS GoldSim Model, are fed from these elements to the EBS for use in cell-networks representing the UZ immediately under the repository.

The matrix K_d values as generated in the process described above, take their distributions from Radionuclide Transport Models Under Ambient Conditions (SNL 2007 [DIRS 177396], Table 6-1[a]). The K_d values are also correlated based on the similarities in the chemical dependencies of the sorption coefficients for the various radionuclides as discussed in Radionuclide Transport Models Under Ambient Conditions (SNL 2007 [DIRS 177396], Appendix B[a]). Starting with the correlation matrix defined by the similarities in the chemical dependencies of the sorption coefficients for the various radionuclide, a subset containing only a single representative (basis) species for each subset of 100 percent correlated species is developed. Such a subset or non-singular correlation matrix is presented in *Radionuclide Transport Models under Ambient Conditions* (SNL 2007 [DIRS 177396], Appendix B[a], Table B-2[a]). Note that in the TSPA-SEIS analysis, the correlation matrix presented in *Radionuclide Transport Models under Ambient Conditions* (SNL 2007 [DIRS 177396], Appendix B[a], Table B-2[a]), is redefined as two

separate non-singular correlation matrices. The use of two matrices is based on the non-correlation of uranium and selenium to any of the other species. Therefore the TSPA-SEIS utilizes a 10 by 10 non-singular correlation matrix for all species except uranium and selenium, and a 2 by 2 non-singular correlation matrix for uranium and selenium. The method used in the TSPA-SEIS to induce correlations is the Cholesky factorization method (SNL 2007 [DIRS 177396], Appendix B[a]).

The basic correlation procedure used is as follows. The m (rows) by m (columns) matrix, C, is the target rank correlation to be imposed. Note that, in the TSPA-SEIS two C matrices, one 10 by 10 and one 2 by 2 are evaluated. For each non-singular correlation matrix and associated species, which is 100 percent correlated with any of the basis species, the procedure used in the TSPA-SEIS is as follows:

Compute by Cholesky factorization (Press et al. 1992 [DIRS 103316], Section 2.9), the m by m lower triangular matrix, **P**, such that $\mathbf{PP}^{\mathrm{T}} = \mathbf{C}$ (Tables 6.3.9-13 and 6.3.9-14, respectively)

Create **z**, a vector of length, *m*, consisting of independent standard normal values

Compute the vector, **x**, of length, *m*, such that $\mathbf{x} = \mathbf{Pz}$. Note $\mathbf{x} \sim \mathrm{N}(0,\mathbf{C})$

Compute the result sample vector, **u**, such that $\mathbf{u}_i = \mathbf{F}_i^{-1}(\mathbf{\Phi}(x_i))$ for the *m* different variables, $i = 1,\ldots, m,$. where $\mathbf{F}_i(x)$ are the marginal CDFs for each of the *m* variables and $\mathbf{\Phi}(x)$ is the standard normal CDF.

The resultant vector, **u**, has a rank correlation structure that approximates **C**. The sample vector **w** for the species not chosen as basis species can then be generated as $\mathbf{w}_{ij} = \mathbf{F}_i^{-1}(\mathbf{\Phi}(x_j))$ where j is the index denoting the basis species with which the species i is 100 percent correlated. Within FEHM, the matrix K_d values are used in conjunction with bulk density, matrix porosity, and matrix saturation values to derive the retardation coefficient used to determine the effective transport rate for sorbing species. The retardation coefficient, *R*, can be defined as

$$R = 1 + \frac{\rho_{bulk} K_d}{\phi_{matrix} S_{matrix}} \qquad \text{(Eq. 6.3.9-3)}$$

where

ρ_{bulk} = the bulk density (g/ml)

K_d = the rock matrix sorption coefficient (ml/g)

ϕ_{matrix} = the rock matrix porosity (-)

S_{matrix} = the rock matrix saturation (-).

The values of bulk density and matrix porosity used in the TSPA-SEIS are presented in *Particle Tracking Model and Abstraction of Transport Processes* (SNL 2007 [DIRS 181006], Section 6.5.3[a]). The rock matrix saturations, used by FEHM to derive the matrix retardation coefficients, are read from the appropriate input flow-field files (based on the sampled

infiltration scenario) and are updated during the simulation to account for present-day, monsoon, glacial-transition, and post-10,000-year climates.

Radionuclide mobilization and transport through the EBS are calculated during each TSPA-SEIS simulation, and the radionuclide mass flux at the EBS boundary at each timestep is provided as the boundary condition for UZ transport (Section 6.3.8). The UZ Transport Submodel then provides radionuclide mass fluxes at the water table, for each timestep, as the boundary condition for SZ transport (Section 6.3.10). The elevation of the water table changes instantaneously when a climate change occurs. Any change in the water table level redefines the release points for mass leaving the UZ. In addition, as previously noted, any radionuclides between the old water table and the updated water table at the time the water table elevation changes are immediately removed from the UZ Transport Submodel and are provided as input to the SZ Flow and Transport Model Component (SNL 2007 [DIRS 181006], Section 6.4.8).

Releases from the EBS are computed for each environmental group: dripping and non-dripping CSNF WPs, dripping and non-dripping CDSP WPs, and each selected early-failed WP group, including CSNF-Zircaloy, CSNF-stainless steel, and CDSP WPs, in each repository percolation subregion. As described in Section 6.3.8, of the EBS Transport Submodel, radionuclide releases from the EBS enter both the fracture and matrix continua of the UZ Transport Submodel. Radionuclide releases from each of the five repository percolation subregions are modeled using a random release model that accounts for early failed WPs and temporally and spatially variable radionuclide releases (SNL 2007 [DIRS 181006], Section 6.4.7). This random release model avoids spreading out radionuclide releases artificially, by taking into account the number of WPs that have failed within each of the five subregions. If only one WP has failed in a subregion, the releases for that subregion are put into a single numerical grid node that is randomly sampled from the nodes in that subregion. If two WPs have failed, releases are put into two randomly selected nodes. This process continues for additional WPs until the number of failed WPs is equal to the number of nodes in the subregion. The nodes are randomly selected without replacement. After the number of failed WPs exceeds the number of nodes in a subregion, later releases are evenly spread over all nodes in the subregion, and additional WP failures cause no change to the release locations (SNL 2007 [DIRS 181006], Section 6.4.7).

The repository-release nodes comprising each of the five repository percolation subregions were chosen based on the cumulative probability of percolation for the 12 flow fields (three different climate periods: present-day, monsoon and glacial-transition; each climate period is categorized with 4 infiltration scenarios: 10 percent, 30 percent, 50 percent and 90 percent). A 4-step binning process was applied to each of the twelve flow fields, resulting in a list of repository release nodes divided into 5 percolation subregions (bins) that share common infiltration ranges, based on the cumulative probability intervals for these bins (SNL 2007 [DIRS 181006], Section 6.5.15[a]). The cumulative probability intervals for these five bins of percolation rates sorted in ascending order are 0.0-0.05, 0.05-0.30, 0.30-0.70, 0.70-0.95, and 0.95-1.00 (SNL 2007 [DIRS 181006], Section 6.5.15). An analysis, of the degree of similarity or difference of the results of the binning process depending on which flow field is considered, was performed. The results indicated that the bins for the 12 flow fields are quite similar to one another. As noted in SNL 2007 [DIRS 181006], Section 6.5.15[a], if a bin is identified for a particular node in the glacial-transition, 10th percentile flow field, it is very often identified as the same bin for the other flow fields. When they are different, they almost always differ by only one bin, that is, a 3

in GT10 becomes a 4 in another flow field, or a 2 becomes a 1. Based upon this result it was considered acceptable to use bins from one flow field to approximate all infiltration scenarios and climate states. Furthermore, if the post-10,000 year flow fields are similar to the ones developed so far, the bins should remain similar for these as well. Figure 6.3.9-7 shows the locations of the FEHM repository release nodes, colored by percolation bin for the glacial-transition, 10th-percentile flow field.

The fraction of irreversible colloids traveling through the UZ unretarded is determined before releasing colloids from the EBS. After they are released into the UZ, the fraction of unretarded colloids remains unchanged. Based on a conservative estimate for transport time in the natural system (UZ and SZ), of 100 years (SNL 2007 [DIRS 181006], Section 6.5.13 and Table 6-23), the fraction of unretarded colloids leaving the EBS is estimated to be 0.00168. This value is used in all TSPA-SEIS realizations, and is referred to as the "fast fraction" in the implementation of the EBS Colloids Transport Submodel. Since the transport time through the UZ and SZ of the fast fraction of colloids is uncertain, and the fast fraction model is also uncertain, a conservative approach is taken for implementing the fast fraction of colloids (BSC 2004 [DIRS 170006], Section 6.6). The approach is conservative because it is highly unlikely that any TSPA-SEIS realization will have a combined UZ-SZ transport time of less than 100 years (BSC 2004 [DIRS 170006], Section 6.6).

To account for arrival locations and reduce artificial spreading in releases to the SZ, all nodes at or below the water table of the UZ Transport Submodel are grouped into four source regions, as shown on Figure 6.3.10-6. Radionuclide mass reaching the water table in one location may have a different SZ travel path and transport time than mass arriving at some other location. To reduce the effects of artificial dilution at the interfaces between TSPA-SEIS submodels, the total radionuclide mass flow rate in each of these four source regions is focused at a random point within each of the four source regions in the SZ Flow and Transport Model Component.

The random release point or points in each of the four UZ Transport Submodel (Figure 6.3.10-6) outflow regions is a function of sampling during each realization. The four UZ outflow regions are named 701, 702, 703, and 704 in FEHM, corresponding to the SZ source inflow regions 1, 2, 3, and 4, respectively (SNL 2007 [DIRS 181006], Section 6.5.16).

The four FEHM UZ outflow regions (Figure 6.3.10-6) are as follows (SNL 2007 [DIRS 181006], Section 6.5.16):

- Outflow Region 701 contains all nodes with a Universal Transverse Mercator (UTM) grid easting coordinate less than 548500 m (Nevada State Plane [NSP]: 171189.79 m) and a UTM northing coordinate greater than 4078630 m (NSP: 233459.87 m).

- Outflow Region 702 contains all nodes with a UTM easting coordinate greater than 548500 m (NSP: 171189.79 m) and a UTM northing coordinate greater than 4078630 m (NSP: 233459.87 m).

- Outflow Region 703 contains all nodes with a UTM easting coordinate less than 548500 m (NSP: 171189.79 m) and a UTM northing coordinate less than 4078630 m (NSP: 233459.87 m).

- Outflow Region 704 contains all nodes with a UTM easting coordinate greater than 548500 m (NSP: 171189.79 m) and a UTM northing coordinate less than 4078630 m (NSP: 233459.87 m).

The radionuclide mass release from FEHM is applied to four UZ outflow capture zones modeled using four GoldSim mixing cells. The mass outflows of the four cells are then fed to the SZ convolution integral model, SZ_Convolute (SZ_Convolute V3.10, STN: 10207-3.10-10 [DIRS 181060]), at each TSPA-SEIS timestep. The release rates are also integrated over time using GoldSim integrator elements for use as input to the alternative SZ one-dimensional pipe element model (SNL 2007 [DIRS 181650], Section 6.5.1.2).

6.3.9.4 Model Component Consistency and Conservatism in Assumptions and Parameters

To enhance understanding of the complex interactions within the TSPA-SEIS, a discussion of consistency among model components, and submodels, and identification of conservative assumptions in abstractions, process models, and parameter sets supporting the UZ Transport Submodel are presented below.

6.3.9.4.1 Consistency of Assumptions

UZ and SZ Solubilities—Mineral precipitation is not considered in the 3-D UZ Transport Submodel (Table 6-1 and Section 6.3.9) or the 3-D SZ Flow and Transport Submodel (Table 6-1 and Section 6.3.10). Thus, all of the dissolved mass of various moderate- to low-solubility radionuclides (e.g., neptunium and plutonium, respectively), is transported through the UZ and SZ without considering any chemical effects that might cause precipitation of these elements. This implementation is different from the EBS implementation where solubility constraints are imposed (Section 6.3.7.5.2).

Effect on TSPA-SEIS Results—Transporting these elements through the natural system without solubility constraints is conservative; the occurrence of precipitation would lessen the quantity of mass migrating downgradient.

UZ Transport Properties—The UZ Transport Submodel uses different material properties than the UZ Flow Fields Abstraction. In the UZ Transport Submodel, fracture frequency and fracture porosity, which are used to derive fracture apertures, are sampled for every realization for nine different rock groups (SNL 2007 [DIRS 181006], Table 6-13). However, in developing the 16 different UZ flow fields that are used in the UZ transport calculations, fracture frequency and fracture porosity were held constant. The active fracture model gamma values are calibrated values in the UZ Flow Submodel calculations. Although calibrated, the flow model is relatively insensitive to this parameter. To the contrary, during transport modeling when subject to matrix diffusion the gamma parameter represents a parameter to which the system is sensitive. For this reason, the gamma parameter is sampled from a distribution that is based both on the flow model calibrated values and field test-based values. Thus, fracture frequency, fracture porosity, and

active fracture model gamma values used to derive UZ transport processes may differ between the UZ Transport Submodel and the UZ Flow Fields Abstraction (Section 6.3.1).

Effect on TSPA-SEIS Results—The intended purpose of the two submodels warrants the different treatment of material properties. The UZ Flow Fields Abstraction (Section 6.3.1) is used to define the steady-state flow fields within the model domain, while the UZ Transport Submodel is used for computing the radionuclide mass flux for the given flow field. In the UZ Flow Fields Abstraction, the 16 steady-state UZ flow fields are generated based on the calibrated set of hydrologic parameters that lead to an acceptable match with the field observations of the matrix liquid saturation, water potential, and perched-water elevation. The calibrated set of parameters, such as fracture frequency, porosity, active fracture model gamma values, etc., are, by definition, held constant for a given rock group in a steady-state flow field simulation. On the other hand, the UZ Transport Submodel is a transient model that uses the steady-state flow fields for dynamic mass transport calculations based on the transient mass flux from the EBS Transport Submodel (Section 6.3.8). Because fracture parameters, such as frequency and porosity, are used to calculate the fracture aperture effect on matrix diffusion, the uncertainty in matrix diffusion is propagated by sampling the fracture parameters for different rock groups. Similarly, when including the diffusive transport uncertainty in the matrix cells, active fracture model gamma values are varied by sampling. These and other transport parameters, along with their uncertainties, as used in the UZ Transport Submodel, are discussed and justified in Sections 6.5 and 6.5[a]of *Particle Tracking Model and Abstraction of Transport Processes* (SNL 2007 [DIRS 181006]). Therefore, even though the material properties may be different among respective submodels, separate sampling is necessary to adequately propagate uncertainty in mass transport under steady-state flow conditions.

UZ Failed WP Location Assignment—The footprints of the five percolation subregions are defined by ranges of percolation rates at the repository horizon (Figure 6.3.9-7). Each percolation subregion is associated with a set of UZ Transport Model nodes found directly beneath the repository. For each WP that fails within each zone, one of the nodes is chosen by random sampling to determine the release location. A new node is chosen for each failed WP within the zone until all nodes are chosen. If any more WPs in the zone fail or have failed, the mass release for that WP is distributed among all the source nodes in that zone. In addition, for each particle assigned to a specific WP, random sampling determines whether the particle is initialized in the fractures or the rock matrix. A particle is initialized in the fracture continuum if the sampled number is less than or equal to the fraction of mass assigned to the fractures versus the total mass release (fractures and rock matrix), as determined by the EBS Transport Submodel. If the sampled number is greater than the aforementioned fraction, the particle is initialized in the rock matrix. The particle assignment process is described in Sections 6.4.7 and 6.5.15 of *Particle Tracking Model and Abstraction of Transport Processes* (SNL 2007 [DIRS 181006]).

Effect on TSPA-SEIS Results—Random selection of the EBS mass release locations in the UZ Transport Submodel allow for the consideration of the aleatory uncertainty associated with the WPs that fail, and its effects on radionuclide transport to the SZ.

UZ Mass Release to the SZ—The particles leaving the UZ at the SZ are assigned to one of four UZ-SZ release zones that are defined by four quadrants (NE, NW, SE, SW) at the water table

below the repository (Figure 6.3.10-6). For a specific zone and water-table configuration, when a particle reaches a node that is considered an exit node, it becomes inactive in the UZ model, and its assigned mass is added to the SZ model. Although the mass is assigned to one of four SZ source zones, the breakthrough curves used in the SZ-Convolute algorithm are based on specific release locations within each zone. The release zone assignment process is described in Section 6.5.16 of *Particle Tracking Model and Abstraction of Transport Processes* (SNL 2007 [DIRS 181006]).

Effect on TSPA-SEIS Results—Release of all mass to four randomly selected locations during a single realization will focus the mass release. A point source of radionuclides is appropriate for release from a single WP or for considering the influence of groundwater flow focusing along a fault or single fracture. A more diffuse release of radionuclides at the water table may be more physically appropriate for later times when more numerous WPs are leaking and flow focusing does not occur. The use of a point source will overestimate the concentration of the radionuclides near the source (SNL 2007 [DIRS 181650], Section 6.5.2.13) but is of little consequence 18 km downgradient.

6.3.9.4.2 Identification of Conservatisms in Submodels and Abstractions

Climate Change—Climate changes can be considered in an approximate way by imparting an instantaneous jump from one steady-state flow field to another with a corresponding instantaneous rise in the water table (SNL 2007 [DIRS 181006], Section 6.4.8). This approximation is considered conservative because it instantaneously shortens the time it takes for mass to reach the SZ. The method instantaneously increases the flow velocities due to the change in climate and shortens the pathway to the SZ due to the rising of the water table. In addition, all mass between the original water table and the updated water table is immediately applied to the SZ (SNL 2007 [DIRS 181006], Section 5, Assumption 6). This conservatism is a logical approach, given the uncertainties associated with temporal delays in reaching the more rapid transport conditions and the inability to observe the process directly (SNL 2007 [DIRS 181006], Section 5, Assumption 6).

This conservatism tends to shorten radionuclide transport times (SNL 2007 [DIRS 181006], Section 6.4.8).

Fixed Groundwater Table Rise—Groundwater table rise is fixed at 120 m higher than the present-day groundwater table elevation for all future climates (SNL 2007 [DIRS 181006], Section 6.4.8). This groundwater table rise to 850 m above mean sea level was selected as the nominal groundwater table elevation under future climates and is consistent with studies documented in *Saturated Zone Site-Scale Flow Model* (SNL 2007 [DIRS 177391], Section 6.6.4.1). A higher groundwater table elevation reduces UZ transport path length and, therefore, results in shorter radionuclide transport times to the groundwater table. The use of a 120 m rise is consistent with estimates suggesting that site data are consistent with past water table elevations of up to 120 m above present day elevations (Forester, et al. [DIRS 109425, p.56]; and SNL 2007 [DIRS 181006], Section 6.4.8). The 120-m rise in the groundwater table is assumed to occur immediately following the change from present-day to monsoon climate, instantly reducing the flow path of radionuclides in the UZ by 120 m. However, there could be a significant period of groundwater table adjustment associated with transition to a wetter climate.

After the groundwater table is raised to 850 m above sea level, it is assumed to remain at that level for the duration of the simulation period; there is no change to the groundwater table elevation assumed between the monsoon and glacial-transition climates.

Sorption on Fractures—Sorption of radionuclides on fracture surfaces is neglected in the UZ Transport Submodel because sufficient data are not available to consider the process (SNL 2007 [DIRS 181006], Section 6.5.8). This assumption eliminates retardation of radionuclides within the fractures and results in shorter radionuclide transport times (SNL 2007 [DIRS 181006], Section 6.5.8).

Unretarded Colloid Fraction—Unretarded fraction of irreversible colloids used in the UZ model is based on a 100-year transport time. Travel time is uncertain through both the UZ and SZ, but it is unlikely that any TSPA realization will have a combined UZ-SZ travel time of less than 100 years (BSC 2004 [DIRS 170006], Section 6.6).

This assumption results in an increase in the unretarded colloidal fraction, increasing the mass that reaches the SZ rapidly (BSC 2004 [DIRS 170006], Section 6.6); and (SNL 2007 [DIRS 181006], Section 6.5.13).

Isothermal Transport Conditions in the UZ—UZ transport occurs at isothermal 25°C conditions. Increased temperature would result in increased diffusion from the fractures into the matrix (SNL 2007 [DIRS 177396], Section 6.1.2.9). However, to simplify the modeling approach, higher temperatures from decay heat and the geothermal gradient are conservatively ignored. Additionally, increased temperature leads to increased sorption of catatonic species and decreased sorption of anionic species (SNL 2007 [DIRS 177396], Section 6.1.2.9). Conclusions of the K_d temperature dependence study presented in SNL 2007 [DIRS 177396], Section I, indicate that for various radionuclides a small positive increase in K_d with temperature is seen. Therefore neglecting temperature dependence as suggested in SNL 2007 [DIRS 177396], would be conservative.

This assumption results in a reduction of matrix diffusion at early times, shortening radionuclide transport times (SNL 2007 [DIRS 177396], Section 6.1.2.9).

No Solubility Limits—No solubility limits are applied to radionuclide concentrations in the UZ. The potential influence of precipitation on dissolved radionuclides migrating through the UZ is disregarded regardless of the chemical conditions.

This assumption results in shorter radionuclide travel times and higher contributions to dose, because the radionuclides cannot leave the system by precipitation.

No Drift Shadow Effects—No drift shadow effects from flow diversion around the waste emplacement drift are included in the UZ Transport Model Component. Capillary diversion, even under ambient conditions, may result in low fracture saturation below the drift. Reductions in fracture saturations below the drift would delay diffusive radionuclide transport from the EBS.

Ignoring drift shadow effects is a conservative assumption that will result in faster transport times in the UZ (SNL 2007 [DIRS 181006], Section 6.7).

Effects of Perched Water Zones—Effects of perched water low permeability zones are implicit to the UZ flow fields used in the UZ Transport Submodel. Although perched water indicates areas of lower permeability, which can delay and dilute radionuclide concentration, resulting in a reduced advective transport of radionuclides from the UZ, another impact of the perched (and zeolitic) zone in the TSPA-SEIS is to create a lateral diversion of water into the faults and downward to the water table (SNL 2007 [DIRS 175177], Section 8.6).

The lateral diversion of water around perched zones and into faults may result in faster transport times to the UZ.

6.3.9.5 Alternative Conceptual Model(s) for Unsaturated Zone Transport

Section 6.2 outlines the general consideration and treatment of ACMs used to support the TSPA-SEIS. A brief description of the UZ Transport Submodel ACMs is summarized in Table 6.3.9-15 below. A detailed discussion of these ACMs can be found in Section 6.7 of *Particle Tracking Model and Abstraction of Transport Processes* (SNL 2007 [DIRS 181006]).

Discretization of the UZ Matrix (MINC Model)—Discrete Fracture Models and Multiple Interacting Continua (MINC) models of UZ fracture/matrix interaction represent ACMs. A set of transfer functions obtained using a Discrete Fracture Model with fine discretization in the matrix has been developed to allow FEHM's multi-species particle-tracking model to capture sharp concentration gradients. In this Discrete Fracture Model abstraction of the fracture/matrix interaction, the more accurate depiction of the concentration gradients between the fracture and the matrix represents an ACM, which is also more consistent with a MINC formulation (SNL 2007 [DIRS 181006], Section 7.2.2 and Section 7.2.2[a]). Note that the FEHM multi-species particle-tracking model using the Discrete Fracture Model transfer functions still uses the dual-permeability (dual-k) flow fields, while the MINC formulation, as described in *Particle Tracking Model and Abstraction of Transport Processes* (SNL 2007 [DIRS 181006]), differs in the flow regimes. Simulations performed using Discrete Fracture Model and MINC models are shown to result in later breakthrough times than the Dual-k Model (SNL 2007 [DIRS 181006], Section 7.2.2 and Section 7.2.2[a]). A comparison of Discrete Fracture Model and MINC model results showed that the MINC model predicts even later breakthrough times than the Discrete Fracture Model abstraction model (SNL 2007 [DIRS 181006], Section 7.2.2 and Section 7.2.2[a]). Presently, a Multiple Interacting Continua formulation is not directly used in TSPA because of its large computational burden.

To evaluate the impact on the dose calculations associated with the use of the Discrete Fracture Model ACM, the sensitivity of the model simulations to the choice of matrix diffusion models was examined in a simulation using the Discrete Fracture Model transfer functions described in *Particle Tracking Model and Abstraction of Transport Processes* (SNL 2007 [DIRS 181006], Section 6.8.2[a]). The ACM impact evaluation is described in Section 7.2.3.2[a] of *Particle Tracking Model and Abstraction of Transport Processes* (SNL 2007 [DIRS 181006]).

Alternate Finite Difference Numerical Models—The UZ Transport Submodel used FEHM particle tracking. Alternate finite difference numerical models include EOS9nT, T2R3D, and DCPT particle tracking. Two of these models provide a basis for modeling coupled flow and transport of single (T2R3D) or multiple radionuclides (EOS9nT). They were used primarily to

provide validated models of UZ transport processes that form the basis for the abstraction models used in the TSPA-SEIS. The computationally intensive nature of these models limits the finite difference ACMs use for multiple realizations that can provide uncertainty estimates. The FEHM Particle Tracking Transport Abstraction Model can reproduce the results predicted by dual-k models by using transfer functions developed using a dual-k formulation (SNL 2007 [DIRS 181006], Sections 7.2.2[a] and 7.2.3.1[a]).

Lateral Flow Diversion in UZ above the Repository—Lateral flow in the PTn will divert percolating water to the faults and reduce the percolation flux at the repository. The original base case model, which shows more lateral flow occurring within the PTn than the ACM, was chosen due to better predictions of chloride and moisture data (SNL 2007 [DIRS 175177], Section 6.9.2). It was also generally more conservative with respect to radionuclide transport (SNL 2007 [DIRS 175177], Section 6.9.2). The updated base case model predicts significant diversion and redistribution into faults for the PTn (SNL 2007 [DIRS 175177], Section 8.6).

No Radionuclide Release into Faults—The fault zones are defined as high permeability zones subject to fast advective transport to the top of the TSw and to the water table. The effects of not allowing direct release of radionuclides into the fault zones, on the overall transport to the water table, are not significant because lateral diversion directs the radionuclides into the fault zones (SNL 2007 [DIRS 177396], Section 6.20.2).

Inclusion of Drift Shadow Effects—Inclusion of drift shadow effects would approximate the influence of capillary diversion which may cause low fracture saturation below the drift. It is considered conservative to ignore drift shadow effects (SNL 2007 [DIRS 181006], Section 6.7). Additionally, the increases infiltration associated with later climate states may decrease the effects (SNL 2007 [DIRS 181006], Section 6.7).

Perched Water Permeability Zones—Perched water may delay and dilute radionuclide concentration and reduce advective transport (SNL 2007 [DIRS 181006], Section 6.7). Large scale lateral flow of water can also occur in perched water zones which can divert and redistribute flow into faults (SNL 2007 [DIRS 175177], Section 8.6). Continuous well-connected fractures are used to model transport processes in the particle tracking method and the flow fields from the UZ Flow Submodel account for perched water effects.

Inclusion of TH, THC, And THM Effects On UZ Flow And Transport—Vaporization due to repository heat will keep the drift dry for several hundred to a few thousand years. THC and THM effects may alter flow and transport properties of the UZ rocks. TH, THC and THM effects are insignificant after the change to glacial-transition climate (SNL 2007 [DIRS 181006], Section 6.7).

The Standard Fracture Model—The TSPA-SEIS utilizes the active fracture model (Liu et al. 1998 [DIRS 105729]), which takes into consideration flow focusing and the associated reduction in fracture/matrix interaction. The active fracture model, with its reduced effective area of diffusion between fracture and matrix, is used in the TSPA-SEIS because of its more conservative nature and its ability to explain travel times associated with ^{14}C test data (SNL 2007 [DIRS 181006], Section5, Assumption 1) and (BSC 2004 [DIRS 170035], Section 7.4.1). An alternative fracture model would use the standard methodology, which does not consider a

reduced diffusive area. Using the standard methodology would enhance diffusion between the fracture and matrix. Because the active fracture model is more conservative and has better reflected field test results, the standard methodology was not recommended for inclusion in the TSPA-SEIS.

No ACMs were recommended for inclusion in the TSPA-SEIS.

Table 6.3.9-1. Radionuclide Half-Life and Daughter Products Used in the TSPA-SEIS

No.	Species	Half Life (years)	Daughter Index
1	C14	5.715e3	—
2	Cs135 (rev)	2.3e6	—
3	Cs137 (rev)	3.007e1	—
4	I129	1.57e7	—
5	Sr90	2.878e1	—
6	Tc99	2.13e5	—
7	Am243 (rev)	7.37e3	10
8	IcAm243	7.37e3	11
9	IfAm243	7.37e3	12
10	Pu239 (rev)	2.410e4	13
11	IcPu239	2.410e4	13
12	IfPu239	2.410e4	13
13	U235	7.04e8	14
14	Pa231 (rev)	3.28e4	—
15	Am241 (rev)	4.327e2	18
16	IcAm241	4.327e2	18
17	IfAm241	4.327e2	18
18	Np237	2.14e6	19
19	U233	1.592e5	20
20	Th229 (rev)	7.3e3	—
21	Pu240 (rev)	6.56e3	24
22	IcPu240	6.56e3	24
23	IfPu240	6.56e3	24
24	U236	2.342e7	25
25	Th232 (rev)	1.40e10	—
26	U232	6.98e1	—
27	Pu242 (rev)	3.75e5	33
28	IcPu242	3.75e5	33
29	IfPu242	3.75e5	33
30	Pu238 (rev)	8.77e1	34
31	IcPu238	8.77e1	34
32	IfPu238	8.77e1	34
33	U238	4.47e9	34
34	U234	2.46e5	35
35	Th230 (rev)	7.54e4	36

Table 6.3.9-1. Radionuclide Half-Life and Daughter Products Used in the TSPA-SEIS (Continued)

No.	Species	Half Life (years)	Daughter Index
36	Ra226	1.599e3	—
37	Cl36	3.01e5	—
38	Se79	2.95e5	—
39	Sn126 (rev)	2.50e5	—

Sources: SNL 2007 [DIRS181006], Table 6-25 [a].

Reference for Half-Lives: Parrington et al., 1996 [DIRS 103896], for all radionuclides except Se79, which comes from Singh 2002 [DIRS 164741].

NOTE: Numbers presented in scientific notation format, e.g. 1.57e7 = 1.57×10^7.

Table 6.3.9-2. Matrix Sorption Coefficient Distributions for Unsaturated Zone Units in the Unsaturated Zone Transport Submodel

Parameter Name in TSPA-SEIS	Description	Distribution Type	Coefficients Describing Distribution (K_d: ml/g)
KdU_Zeo_a	K_d of Uranium in Zeolitic Tuff	Cumulative	(K_d value, probability) (0, 0) (0.5, 0.5) (30, 1.0)
KdU_Devit_a	K_d of Uranium in Devitrified Tuff	Cumulative	(K_d value, probability) (0, 0) (0.2, 0.5) (4, 1.0)
KdU_Vit_a	K_d of Uranium in Vitric Tuff	Cumulative	(K_d value, probability) (0, 0) (0.2, 0.5) (3, 1.0)
KdNp_Zeo_a	K_d of Neptunium in Zeolitic Tuff	Cumulative	(K_d value, probability) (0, 0) (0.5, 0.5) (6, 1.0)
KdNp_Devit_a	K_d of Neptunium in Devitrified Tuff	Cumulative	(K_d value, probability) (0, 0) (0.5, 0.5) (6, 1.0)
KdNp_Vit_a	K_d of Neptunium in Vitric Tuff	Cumulative	(K_d value, probability) (0, 0) (1.0, 0.5) (3, 1.0)
KdPu_Zeo_a	K_d of Plutonium in Zeolitic Tuff	Cumulative	(K_d value, probability) (10, 0) (100, 0.5) (200, 1.0)
KdPu_Devit_a	K_d of Plutonium in Devitrified Tuff	Cumulative	(K_d value, probability) (10, 0) (70, 0.5) (200, 1.0)
KdPu_Vit_a	K_d of Plutonium in Vitric Tuff	Cumulative	(K_d value, probability) (10, 0) (100, 0.5) (200, 1.0)
KdAm_Zeo_a	K_d of Americium in Zeolitic Tuff	Truncated Normal	Range = 1,000 – 10,000; μ = 5,500, σ = 1,500
KdAm_Devit_a	K_d of Americium in Devitrified Tuff	Truncated Normal	Range = 1,000 – 10,000; μ = 5,500, σ = 1,500
KdAm_Vit_a	K_d of Americium in Vitric Tuff	Cumulative	(K_d value, probability) (100, 0) (400, 0.5) (1,000, 1.0)
KdPa_Zeo_a	K_d of Protactinium in Zeolitic Tuff	Truncated Normal	Range = 1,000 – 10,000; μ = 5,500, σ = 1,500
KdPa_Devit_a	K_d of Protactinium in Devitrified Tuff	Truncated Normal	Range = 1,000 – 10,000; μ = 5,500, σ = 1,500
KdPa_Vit_a	K_d of Protactinium in Vitric Tuff	Truncated Normal	Range = 1,000 – 10,000; μ = 5,500, σ = 1,500
KdCs_Zeo_a	K_d of Cesium in Zeolitic Tuff	Cumulative	(K_d value, probability) (425, 0) (5,000, 0.5) (20,000, 1.0)
KdCs_Devit_a	K_d of Cesium in Devitrified Tuff	Uniform	Minimum = 1 Maximum = 15
KdCs_Vit_a	K_d of Cesium in Vitric Tuff	Cumulative	(K_d value, probability) (0, 0) (2, 0.5) (100, 1.0)
KdSr_Zeo_a	K_d of Strontium in Zeolitic Tuff	Uniform	Minimum = 50 Maximum = 2,000
KdSr_Devit_a	K_d of Strontium in Devitrified Tuff	Uniform	Minimum = 10 Maximum = 70
KdSr_Vit_a	K_d of Strontium in Vitric Tuff	Uniform	Minimum = 0 Maximum = 50
KdRa_Zeo_a	K_d of Radium in Zeolitic Tuff	Uniform	Minimum = 1,000 Maximum = 5,000
KdRa_Devit_a	K_d of Radium in Devitrified Tuff	Uniform	Minimum = 100 Maximum = 1,000
KdRa_Vit_a	K_d of Radium in Vitric Tuff	Uniform	Minimum = 50 Maximum = 600
KdTh_Zeo_a	K_d of Thorium in Zeolitic Tuff	Uniform	Minimum = 1,000 Maximum = 30,000
KdTh_Devit_a	K_d of Thorium in Devitrified Tuff	Uniform	Minimum = 1,000 Maximum = 10,000

Table 6.3.9-2. Matrix Sorption Coefficient Distributions for Unsaturated Zone Units in the Unsaturated Zone Transport Submodel (Continued)

Parameter Name in TSPA-SEIS	Description	Distribution Type	Coefficients Describing Distribution (K_d: ml/g)
KdTh_Vit_a	K_d of Thorium in Vitric Tuff	Uniform	Minimum = 1,000 Maximum = 10,000
KdSe_Zeo_a	K_d of Selenium in Zeolitic Tuff	Truncated Log-Normal	Mean = 14.3 Standard deviation = 7.9 Minimum = 1.0 Maximum = 35.0
KdSe_Devit_a	K_d of Selenium in Devitrified Tuff	Truncated Log-Normal	Mean = 14.0 Standard deviation = 11.2 Minimum = 1.0 Maximum = 50.0
KdSe_Vit_a	K_d of Selenium in Vitric Tuff	Truncated Log-Normal	Mean = 8.6 Standard deviation = 7.9 Minimum = 0.0 Maximum = 25.0
KdSn_Zeo_a	K_d of Tin in Zeolitic Tuff	Log-Uniform	Minimum = 100.0 Maximum = 5000.0
KdSn_Devit_a	K_d of Tin in Devitrified Tuff	Log-Uniform	Minimum = 100.0 Maximum = 100000.0
KdSn_Vit_a	K_d of Tin in Vitric Tuff	Log-Uniform	Minimum = 100.0 Maximum = 5000.0

Sources: DTN: LA0408AM831341.001 [DIRS 171584]
DTN: LB0701PAKDSESN.001_R0 [DIRS 179299], Readme.pdf, Table 3-1.

NOTES: Se is set to zero for rock in the TSw
The parameter names given here are those from the TSPA-SEIS.

Table 6.3.9-3. Species Dependent Free Water Diffusivities Used to Calculate the Effective Matrix Diffusion Coefficients for Unsaturated Zone Transport

Parameter Name in TSPA-SEIS	Description	Distribution Type	Coefficients Describing Distribution
Am_Dfw	Americium free water diffusivity (m^2/s)	Constant	9.49E-10
C_Dfw	Americium free water diffusivity (m^2/s)	Constant	1.18E-09
Cl_Dfw	Chlorine free water diffusivity (m^2/s)	Constant	2.03E-09
Cs_Dfw	Cesium free water diffusivity (m^2/s)	Constant	2.06E-09
I_Dfw	Iodine free water diffusivity (m^2/s)	Constant	2.05E-09
Np_Dfw	Neptunium free water diffusivity (m^2/s)	Constant	6.18E-10
Pa_Dfw	Protactium free water diffusivity (m^2/s)	Constant	6.04E-10
Pu_Dfw	Plutonium free water diffusivity (m^2/s)	Constant	1.30E-09
Ra_Dfw	Radium free water diffusivity (m^2/s)	Constant	8.89E-10
Se_Dfw	Selenium free water diffusivity (m^2/s)	Constant	1.04E-09
Sn_Dfw	Tin free water diffusivity (m^2/s)	Constant	1.55E-09
Sr_Dfw	Strontium free water diffusivity (m^2/s)	Constant	7.91E-10
Tc_Dfw	Technicium free water diffusivity (m^2/s)	Constant	1.95E-09
Th_Dfw	Thorium free water diffusivity (m^2/s)	Constant	5.97E-10
U_Dfw	Uranium free water diffusivity (m^2/s)	Constant	6.64E-10

Source: DTN: LB0702PAUZMTDF.001_R1 [DIRS 180776], *Free-Water Diffusion Coefficients.xls*

Table 6.3.9-4. Parameter Distributions for Tortuosities Used to Calculate the Effective Matrix Diffusion Coefficients for Unsaturated Zone Transport

Parameter Name in TSPA-SEIS	Description	Parameters (in Log10) Describing Distribution
UZDC_Mean_RG1	Log mean tortuosity for rock units: ch1z, ch6v, pp3, pp2, bf2/tr2	-1.15
UZDC_SD_RG1	Log standard deviation of tortuosity for rock units: ch1z, ch6v, pp3, pp2, bf2/tr2	0.29
UZDC_Mean_RG2	Log mean tortuosity for rock units: tsw33, tsw39z, tsw39v, ch1v, ch[2-5]z, ch[2-5]v, ch6z, pp4, bf3/tr3, pcM1z, pcM[2,5]z, pcM6z, M	-1.57
UZDC_SD_RG2	Log standard deviation of tortuosity for rock units: tsw33, tsw39z, tsw39v, ch1v, ch[2-5]z, ch[2-5]v, ch6z, pp4, bf3/tr3, pcM1z, pcM2,5]z, pcM6z, pcM4p	0.29
UZDC_Mean_RG3	Log mean tortuosity for rock units: tsw34, tsw35, tsw3[6,7], tsw38, pp1, pcM38, pcM39	-1.84
UZDC_SD_RG3	Log standard deviation of tortuosity for rock units: : tsw34, tsw35, tsw3[6,7], tsw38, pp1, pcM38, pcM39	0.29

Source: DTN: LB0702PAUZMTDF.001_R1 [DIRS 180776], ReadMe.pdf, Table2-5.

NOTE: See also SNL 2007 [DIRS 181006], Tables 6.5.5-1 and Section 6.5.5.4.

NOTE: The Log10 values are rounded off to two decimal places which could give slightly differenct mean values than the antilogs

Table 6.3.9-5. Fracture γ Parameter Distribution for all Rock in the Unsaturated Zone Transport

Parameter Name in TSPA-SEIS	Description	Distribution Type	Lower-Bound Infiltration	Upper-Bound Infiltration
GAMMA_AFM	Fracture γ for all rock units	Uniform	0.2	0.6

Source: DTN: LA0701PANS02BR.003_R2 [DIRS 180497], Readme.doc

Table 6.3.9-6. Parameter Distributions for Fracture Porosity for Unsaturated Zone Transport

Parameter Name in TSPA-SEIS	Description	Distribution Type	Coefficients Describing Distribution
Por_group1_a	Porosity for chnFf rock unit	Beta	Mean = 1.0E-03 Standard deviation = 3.09E-04 Minimum = 0 Maximum = 1
Por_group2_a	Porosity for tswFf rock unit	Beta	Mean = 2.5E-02 Standard deviation = 7.25E-03 Minimum = 0 Maximum = 1
Por_group3_a	Porosity for rock units: ch[2, 5]Fz/ pcF[2,5]z, ch[3,4]Fz, pp4Fz/pcf4p, pp1Fz, bf2Fz, tr2Fz	Beta	Mean = 3.7E-04 Standard deviation = 1.09E-04 Minimum = 0 Maximum = 1
Por_group4_a	Porosity for rock units: pp3Fd, pp2Fd, bf3Fd, tr3Fd	Beta	Mean = 9.7E-04 Standard deviation = 2.85E-04 Minimum = 0 Maximum = 1
Por_group5_a	Porosity for rock units: ch1Fz/pcF1z, ch6Fz/pcF6z	Beta	Mean = 1.6E-04 Standard deviation = 4.71E-05 Minimum = 0 Maximum = 1
Por_group6_a	Porosity for rock units: ch[1,2,3,4,5,6]Fv	Beta	Mean = 6.9E-04 Standard deviation = 2.03E-04 Minimum = 0 Maximum = 1
Por_group7_a	Porosity for rock units: tswFv, tswFz/pcF39 (tswF9)	Beta	Mean = 4.3E-03 Standard deviation = 1.26E-03 Minimum = 0 Maximum = 1
Por_group8_a	Porosity for rock units: tswF[4,5], tswF[6,7], tswF8/pcF38	Beta	Mean = 1.05E-02 Standard deviation = 3.10E-03 Minimum = 0 Maximum = 1
Por_group9_a	Porosity for tswF3 rock unit	Beta	Mean = 5.8E-03 Standard deviation = 1.71E-03 Minimum = 0 Maximum = 1

Source: DTN: LA0701PANS02BR.003_R2 [DIRS 180497], Table 1.doc.

Table 6.3.9-7. Parameter Distributions for Fracture Frequency for Unsaturated Zone Transport

Parameter Name in TSPA-SEIS	Description	Distribution Type	Coefficients Describing Distribution
ff_group1_a	Fracture frequency [1/m] for chnFf rock unit	Log normal	Mean ln *f* = -2.33E00 Standard deviation ln *f* = 7.24E-01
ff_group2_a	Fracture frequency [1/m] for tswFf rock unit	Log normal	Mean ln *f* = 2.96E-01 Standard deviation ln *f* = 7.24E-01
ff_group3_a	Fracture frequency [1/m] for rock units: ch[2, 5]Fz/ pcF[2,5]z, ch[3,4]Fz, pp4Fz/pcf4p, pp1Fz, bf2Fz, tr2Fz	Log normal	Mean ln *f* = -2.23E00 Standard deviation ln *f* = 7.24E-01
ff_group4_a	Fracture frequency [1/m] for rock units: pp3Fd, pp2Fd, bf3Fd, tr3Fd	Log normal	Mean ln *f* = -1.87E00 Standard deviation ln *f* = 7.24E-01
ff_group5_a	Fracture frequency [1/m] for rock units: ch1Fz/pcF1z, ch6Fz/pcF6z	Log normal	Mean ln *f* = -3.48E00 Standard deviation ln *f* = 7.24E-01
ff_group6_a	Fracture frequency [1/m] for rock units: ch[1,2,3,4,5,6]Fv	Log normal	Mean ln *f* = -2.38E00 Standard deviation ln *f* = 7.24E-01
ff_group7_a	Fracture frequency [1/m] for rock units:tswFv, tswFz/pcF39 (tswF9)	Log normal	Mean ln *f* = -3.03E-01 Standard deviation log *f* = 7.24E-01
ff_group8_a	Fracture frequency [1/m] for rock units: tswf[4,5], tswf[6,7], tswF8/pcF38	Log normal	Mean ln *f* = 1.12E00 Standard deviation ln *f* = 7.24E-01
ff_group9_a	Fracture frequency [1/m] for tswF3 rock unit	Log normal	Mean ln *f* = -6.92E-01 Standard deviation ln *f* = 9.81E-01

Source: DTN: LA0701PANS02BR.003_R2 [DIRS 180497], Table 1.doc.

Table 6.3.9-8. Colloid Size and Concentration Distributions for Unsaturated Zone Transport

Parameter Name in TSPA-SEIS	Description	Distribution Type	Coefficients Describing Distribution
PART_SIZE[a, b]	Colloid size [nm] distribution data for use in simulating colloid filtration effect at matrix interface	Cumulative	(Colloid size, probability): (450, 1.0) (200, 0.8) (100, 0.6) (50, 0.4) (6, 0.2) (1, 0)
Colloidal_Concentration_uz_a[c]	Colloid concentration [mg/L] when ionic strength is less than 0.05	Cumulative	(Colloid concentration, probability): (200, 1.0) (50, 0.98) (10, 0.9) (1.0, 0.75) (0.1, 0.5), (0.001, 0.0)

[a] This parameter has no formal name in the TSPA-SEIS because it is implemented directly in the FEHM UZ Particle Tracking Submodel.
[b] Source: DTN: LA0701PANS02BR.003_R2 [DIRS 180497], Table 4.doc .
[c] Source: DTN: LA0701PANS02BR.003_R2 [DIRS 180497], Table 7.doc .

Table 6.3.9-9. Cumulative Probability Distributions for Colloid Transport at Matrix Interfaces for Unsaturated Zone Transport

Parameter Name in TSPA-SEIS[a]	Description	Distribution Type	Coefficients Describing Distribution
ITFCPORSIZE	Effective pore size [nm] for rock units: TMN/TSW4	Cumulative	(Effective pore size, probability): (2,000, 1.0) (1,000, 0.92) (450, 0.87) (200, 0.81) (100, 0.71) (50, 0.55) (6, 0.31)
ITFCPORSIZE	Effective pore size [nm] for rock units: TLL/TSW5	Cumulative	(Effective pore size, probability): (2,000, 1.0) (1,000, 0.8) (450, 0.79) (200, 0.70) (100, 0.61) (50, 0.51) (6, 0.19)
ITFCPORSIZE	Effective pore size [nm] for rock units: TM2/TSW6	Cumulative	(Effective pore size, probability): (2,000, 1.0) (1,000, 0.94) (450, 0.9) (200, 0.82) (100, 0.65) (50, 0.51) (6, 0.21)
ITFCPORSIZE	Effective pore size [nm] for rock units: TM1/TSW7	Cumulative	(Effective pore size, probability): (2,000, 1.0) (1,000, 0.99) (450, 0.99) (200, 0.99) (100, 0.93) (50, 0.68) (6, 0.36)
ITFCPORSIZE	Effective pore size [nm] for rock units: PV3/TSW8	Cumulative	(Effective pore size, probability): (2,000, 1.0) (1,000, 0.98) (450, 0.96) (200, 0.94) (100, 0.90) (50, 0.89) (6, 0.68)
ITFCPORSIZE	Effective pore size [nm] for rock units: PV2/TSW9	Cumulative	(Effective pore size, probability): (2,000, 1.0) (1,000, 0.72) (450, 0.57) (200, 0.47) (100, 0.39) (50, 0.35) (6, 0.22)
ITFCPORSIZE	Effective pore size [nm] for rock units: BT1a/CH1	Cumulative	(Effective pore size, probability): (2,000, 1.0) (1,000, 0.91) (450, 0.89) (200, 0.87) (100, 0.85) (50, 0.83) (6, 0.53)
ITFCPORSIZE	Effective pore size [nm] for rock units: CHV	Cumulative	(Effective pore size, probability): (2,000, 1.0) (1,000, 0.58) (450, 0.49) (200, 0.43) (100, 0.39) (50, 0.36) (6, 0.07)
ITFCPORSIZE	Effective pore size [nm] for rock units: CHZ	Cumulative	(Effective pore size, probability): (2,000, 1.0) (1,000, 0.79) (450, 0.76) (200, 0.73) (100, 0.68) (50, 0.56) (6, 0.3)
ITFCPORSIZE	Effective pore size [nm] for rock units: BT/CH6	Cumulative	(Effective pore size, probability): (2,000, 1.0) (1,000, 0.95) (450, 0.94) (200, 0.92) (100, 0.92) (50, 0.85) (6, 0.40)
ITFCPORSIZE	Effective pore size [nm] for rock units: PP1	Cumulative	(Effective pore size, probability): (2,000, 1.0) (1,000, 0.79) (450, 0.68) (200, 0.63) (100, 0.57) (50, 0.48) (6, 0.21)
ITFCPORSIZE	Effective pore size [nm] for rock units: PP2	Cumulative	(Effective pore size, probability): (2,000, 1.0) (1,000, 0.91) (450, 0.86) (200, 0.81) (100, 0.65) (50, 0.53) (6, 0.22)
ITFCPORSIZE	Effective pore size [nm] for rock units: PP3	Cumulative	(Effective pore size, probability): (2,000, 1.0) (1,000, 0.49) (450, 0.34) (200, 0.26) (100, 0.21) (50, 0.16) (6, 0.07)
ITFCPORSIZE	Effective pore size [nm] for rock units: PP4	Cumulative	(Effective pore size, probability): (2,000, 1.0) (1,000, 0.99) (450, 0.99) (200, 0.98) (100, 0.98) (50, 0.96) (6, 0.32)
ITFCPORSIZE	Effective pore size [nm] for rock units: BF2	Cumulative	(Effective pore size, probability): (2,000, 1.0) (1,000, 0.98) (450, 0.97) (200, 0.96) (100, 0.96) (50, 0.83) (6, 0.25)
ITFCPORSIZE	Effective pore size [nm] for rock units: BF3	Cumulative	(Effective pore size, probability): (2,000, 1.0) (1,000, 0.97) (450, 0.94) (200, 0.83) (100, 0.74) (50, 0.66) (6, 0.14)

Source: DTN: LA0701PANS02BR.003_R2 [DIRS 180497], Table 2.doc.

[a] These parameters are listed with one name in the TSPA-SEIS because they are implemented directly in the FEHM UZ Particle Tracking Submodel.

Table 6.3.9-10. Colloid Size Exclusion Factor Used in the Compliance Model

HGU (Group Numbers)	UZ Model Units (entry layer)	Size Exclusion Factor
TMN / TSW4	tswF4	0.29
TLL / TSW5	tswF5	0.39
TM2 / TSW6	tswF6	0.35
TM1 / TSW7	tswF7	0.07
PV3 / TSW8	tswF8/pcF38	0.10
PV2 / TSW9	tswFz, tswFv (tswF9) / pcF39	0.61
BT1a / CH1	ch1Fv, ch1Fz/pcF1z	0.15
CHV	ch[2,3,4,5]Fv	0.61
CHZ	ch[3,4]Fz, ch[2,5,6]Fz/pcF[2,5,6]z	0.27
BT / CH6	ch6Fv	0.08
PP4	pp4Fz/pcF4p	0.02
PP3	pp3Fd	0.79
PP2	pp2Fd	0.35
PP1	pp1Fz	0.43
BF3	bf3Fd, tr3Fd	0.26
BF2	bf2Fz, tr2Fz	0.04
	tswFf	0.29
	chnFf	0.27

Source: DTN: LA0701PANS02BR.003_R2 [DIRS 180497], Table 3.doc.

FEHM = finite element heat and mass (model)

HGU = Hydrogeologic Units or layers (SNL 2007 [DIRS 175177], Section 6.1); Correlation of HGU units and list of all UZ Model layers (FEHM zones) (SNL 2007 [DIRS 181006], Table 6-3).

Table 6.3.9-11. Radionuclide Sorption Coefficients onto Colloids for Unsaturated Zone Transport (revised groundwater colloid mass concentration parameters for TSPA-SEIS)

Parameter Name in TSPA-SEIS	Description	Distribution Type	K_d Value Intervals	K_d Value Interval Probability of Occurrence
Colloidal_Kd_Pu_uz_a	K_d [mL/g] of Plutonium on Smectite Colloid	Cumulative	1×10^3 to 5×10^3	0.45
			5×10^3 to 1×10^4	0.8
			1×10^4 to 5×10^4	0.95
			5×10^4 to 1×10^5	1.00
Colloidal_Kd_Am_uz_a	K_d [mL/g] of Americium on Smectite Colloid	Cumulative	1×10^4 to 5×10^4	0.07
			5×10^4 to 1×10^5	0.17
			1×10^5 to 5×10^5	0.40
			5×10^5 to 1×10^6	0.60
			1×10^6 to 5×10^6	0.92
			5×10^6 to 1×10^7	1.00
Colloidal_Kd_Th_uz_a	K_d [mL/g] of Thorium on Smectite Colloid	Cumulative	1×10^4 to 5×10^4	0.07
			5×10^4 to 1×10^5	0.17
			1×10^5 to 5×10^5	0.40
			5×10^5 to 1×10^6	0.60
			1×10^6 to 5×10^6	0.92
			5×10^6 to 1×10^7	1.00
Colloidal_Kd_Pa_uz_a	K_d [mL/g] of Protactinium on Smectite Colloid	Cumulative	1×10^4 to 5×10^4	0.07
			5×10^4 to 1×10^5	0.17
			1×10^5 to 5×10^5	0.40
			5×10^5 to 1×10^6	0.60
			1×10^6 to 5×10^6	0.92
			5×10^6 to 1×10^7	1.00
Colloidal_Kd_Cs_uz_a	K_d [mL/g] of Cesium on Smectite Colloid	Cumulative	5×10^1 to 1×10^2	0.05
			1×10^2 to 5×10^2	0.40
			5×10^2 to 1×10^3	0.70
			1×10^3 to 5×10^3	1.00
Colloidal_Kd_Sn_uz_a	K_d [mL/g] of Tin on Smectite Colloid	Log Uniform	1×10^5 to 1×10^6	N/A

Source: SNL 2007 [DIRS 181006].

Table 6.3.9-12. Colloid Retardation Factors (Colloidal_Retard_Factor_dist) for Unsaturated Zone Transport

Colloid Retardation Factor	Cumulative Probability	Input Description
6.00	0	The colloid retardation factor is used by FEHM in simulating the effects of colloid retardation in fractured rock on colloid-facilitated radionuclide transport.
6.00[a]	0.15	
10.23	0.25	
26.00	0.5	
59.98	0.8	
799.83[b]	1	

Source: DTN: LA0701PANS02BR.003_R2 [DIRS 180497], Table 5.doc.

[a] The value used in the TSPA-SEIS is 6.00000001. This change was implemented to coincide with the GoldSim requirement that cumulative probability functions are defined by monotonically increasing values.

[b] The source DTN: LA0303HV831352.002 (for the feed DTN [DIRS 180497]) presents the colloid retardation factor as 799.83 for a cumulative probability of 1.00 rather than rounded to 800 as presented in Table 5 ([DIRS 180497]).

Table 6.3.9-13. Lower Triangular Matrix for all Species Except Uranium and Selenium as Generated from the Correlation (Covariance) Matrix by Cholesky Factorization Using MathCad

	Am_ devit	Cs_ devit	Cs_ zeo	Np_ devit	Pa_ devit	Pu_ devit	Ra_ zeo	Sn_ devit	Sr_ devit	Th_ devit
Am_devit	1	0	0	0	0	0	0	0	0	0
Cs_devit	0	1	0	0	0	0	0	0	0	0
Cs_zeo	0	0.1	0.995	0	0	0	0	0	0	0
Np_devit	0.25	0	0	0.968	0	0	0	0	0	0
Pa_devit	0.75	0	0	-0.194	0.632	0	0	0	0	0
Pu_devit	0.1	0	0.754	0.077	-0.095	0.638	0	0	0	0
Ra_zeo	0	0.1	0.492	0	0	0.202	0.841	0	0	0
Sn_devit	0.75	0	0	-0.09	0.269	0.09	-0.022	0.59	0	0
Sr_devit	0	0.25	0.075	0.516	0.158	-0.128	0.076	0.029	0.786	0
Th_devit	0	0	0	0.516	0.158	-0.039	0.009414	0.013	0.576	0.612

Source: DTN: MO0707UZKDCORR.000 [DIRS 183003], radio_020807a.xmcd.

Table 6.3.9-14. Lower Triangular Matrix for Uranium and Selenium as Generated from the Correlation (Covariance) Matrix by Cholesky Factorization Using MathCad

	Se_devit	U_devit
Se_devit	1	0
U_devit	0.75	0.661

Source: DTN: MO0707UZKDCORR.000 [DIRS 183003], radio_020807a_SE_U.xmcd.

Table 6.3.9-15. Alternative Conceptual Models Considered for the Unsaturated Zone Transport Model

Alternative Conceptual Model	Key Assumptions	Screening Assessment and Basis
Discretization of the UZ Matrix (MINC Model)	The matrix is discretized to allow for a more accurate approximation of the concentration gradient at the matrix-fracture interface and within the matrix. Use of the Discrete Fracture Model or Multiple Interacting Continua (MINC) Model results in later breakthrough times than generated using the dual-k model. The breakthrough times of the Multiple Interacting Continua Model are later than those generated using the Discrete Fracture Model.	The dual-k model is conservative. The Multiple Interacting Continua Model is not used because of its large computational burden.
Alternative Finite Difference Numerical Models	An alternate method of approximating radionuclide transport in groundwater based upon approximating the governing equations using finite difference equations.	Although used for validation of the UZ Abstraction, large computational burden limits the utility of models such as T2R3D and EOS9nT.
Lateral Flow Diversion In UZ Above The Repository	Lateral flow in the PTn will divert percolating water to the faults and reduce the percolation flux at the repository.	The original base case model, which shows more lateral flow occurring within the PTn than the ACM, was chosen due to better predictions of chloride and moisture data (SNL 2007 [DIRS 175177], Section 6.9.2). It was also generally more conservative with respect to radionuclide transport. The updated base case model predicts significant diversion and redistribution into faults for the PTn (SNL 2007 [DIRS 177396], Section 6.20.2).
No Radionuclide Release Into Faults	The fault zones are defined as high permeability zones subject to fast advective transport to the the top of the TSw and to the water table.	The effects of not allowing direct release of radionuclides into the fault zones, on the overall transport to the water table, are not significant because lateral diversion directs the radionuclides into the fault zones (SNL 2007 [DIRS 177396], Section 6.20.2).

Table 6.3.9-15. Alternative Conceptual Models Considered for the Unsaturated Zone Transport Model (Continued)

Alternative Conceptual Model	Key Assumptions	Screening Assessment and Basis
Inclusion of Drift Shadow Effects	Inclusion of drift shadow effects would approximate the influence of capillary diversion which may cause low fracture saturation below the drift.	It is considered conservative to ignore drift shadow effects. Additionally, the increased infiltration associated with later climate states may decrease the effects.
Perched Water Permeability Zones	Perched water may delay and dilute radionuclide concentration and reduce advective transport. Large scale lateral flow of water can also occur in perched water zones which can divert and redistribute flow into faults. Continuous well-connected fractures are used to model transport processes in the particle tracking method and the flow fields from the UZ Flow Submodel account for perched water effects.	Perched water may only be present in the northern part of the repository. Treating perched water in a manner such that well connected pathways exist is a conservative treatment.
Inclusion Of TH, THC, And THM Effects On UZ Flow And Transport	Vaporization due to repository heat will keep the drift dry for several hundred to a few thousand years. THC and THM effects may alter flow and transport properties of the UZ rocks.	TH, THC and THM effects are insignificant after the change to glacial-transition climate.

Source: SNL 2007 [DIRS 181006], Table 6-30). Additional sources are noted within the text.

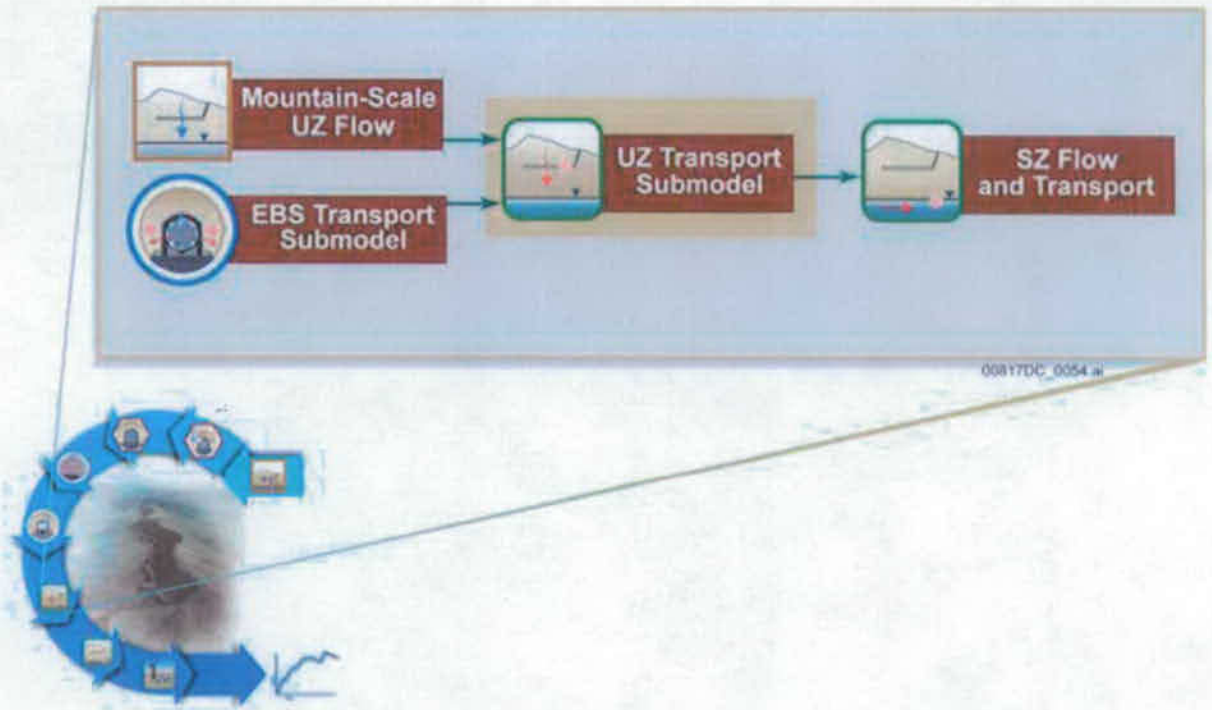

Figure 6.3.9-1. Information Flow Diagram for Unsaturated Zone Transport

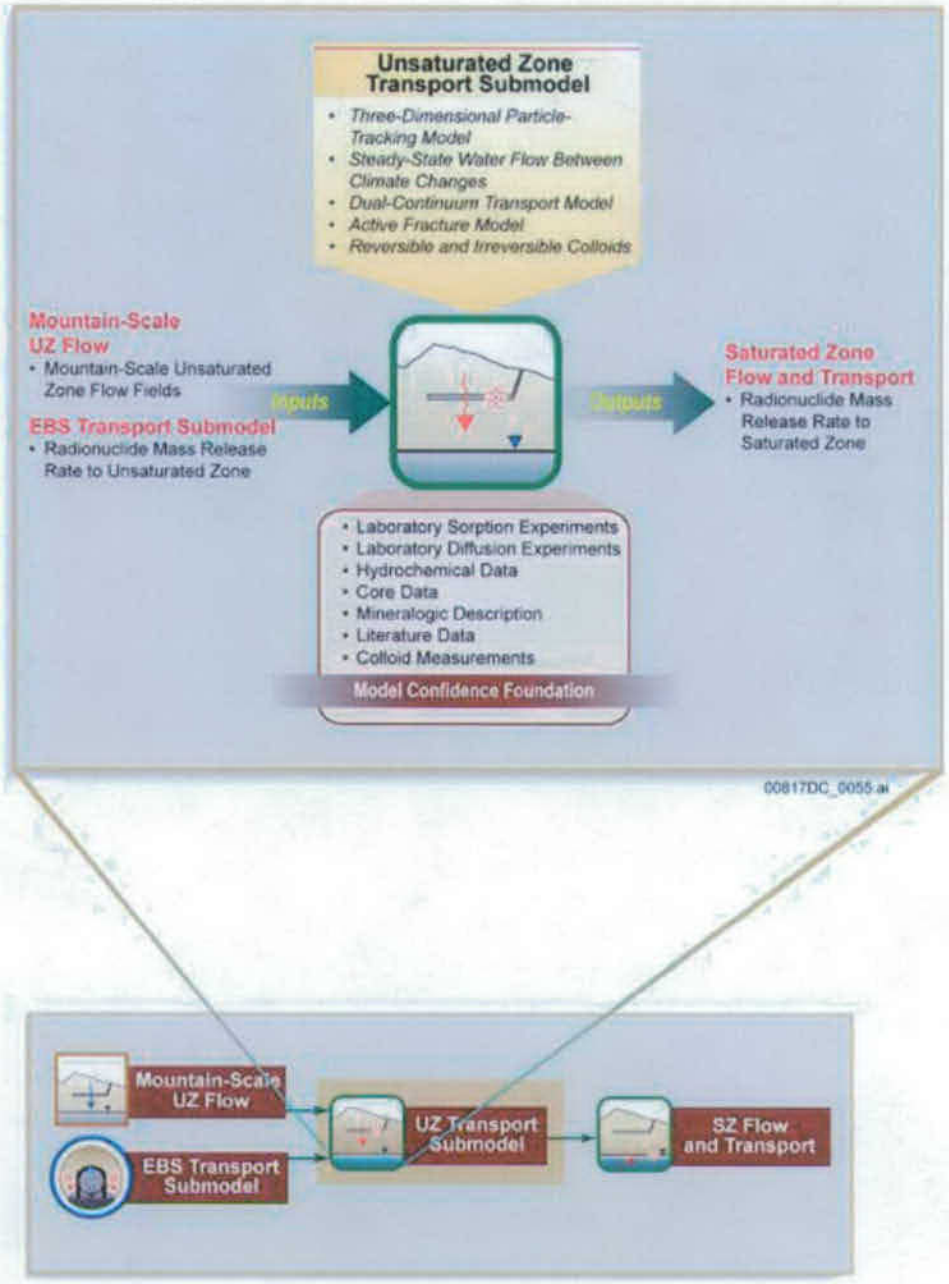

Figure 6.3.9-2. Inputs, Outputs, and Basis for Model Confidence for the Unsaturated Zone Transport Submodel

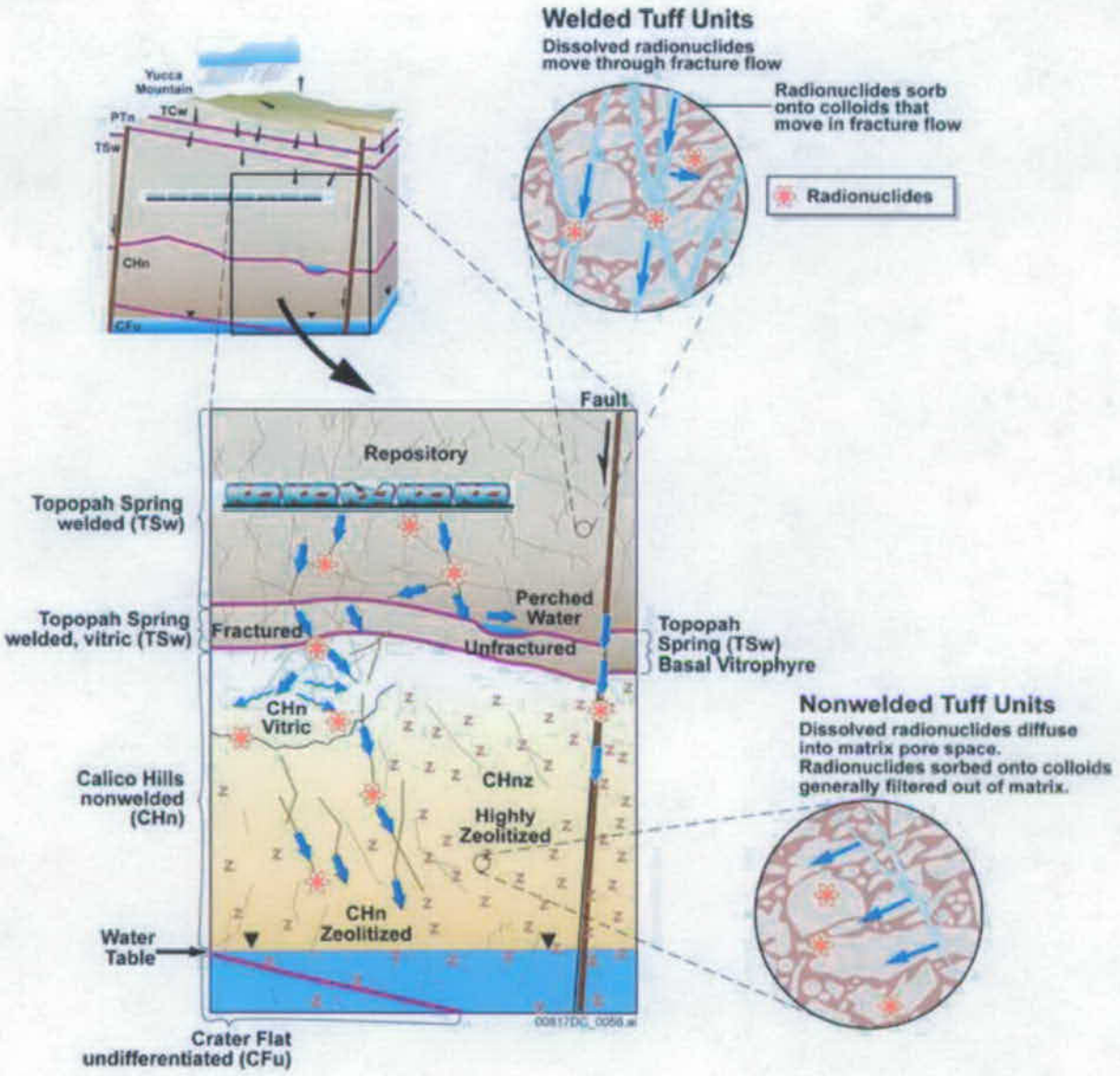

Figure 6.3.9-3. Conceptualization of Unsaturated Zone Transport Processes

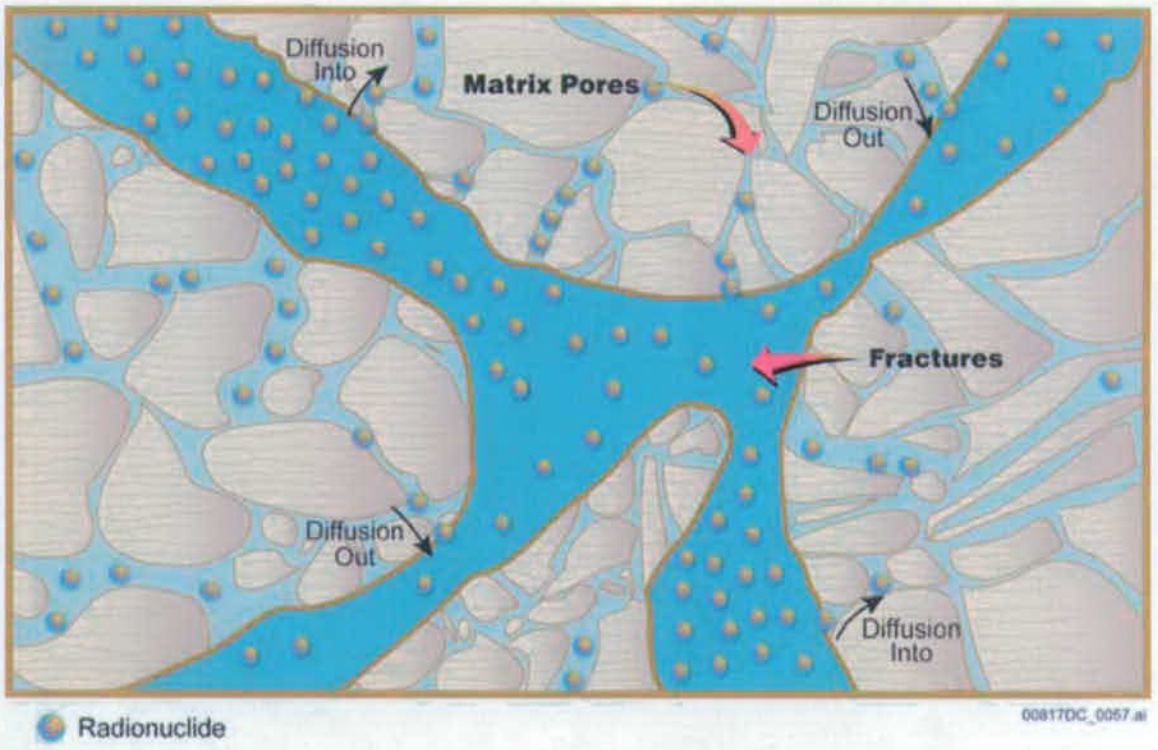

Figure 6.3.9-4. Illustration of Radionuclide Diffusion Into and Out of Matrix Pores

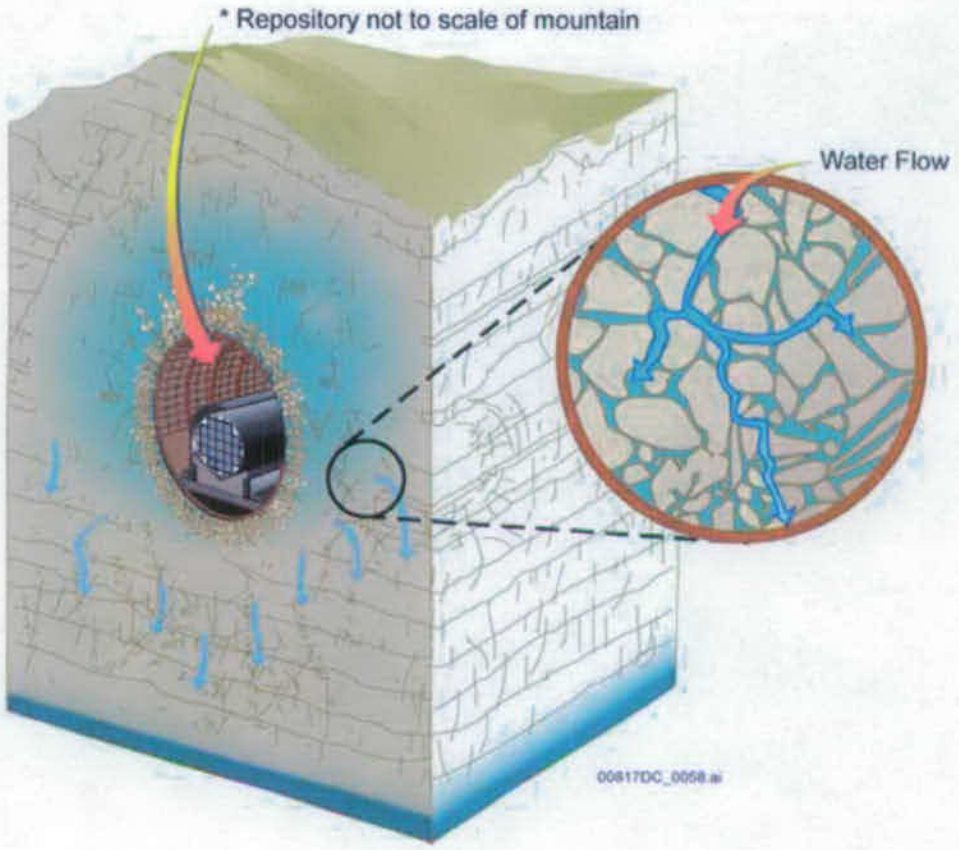

Figure 6.3.9-5. Illustration of Hydrodynamic Dispersion

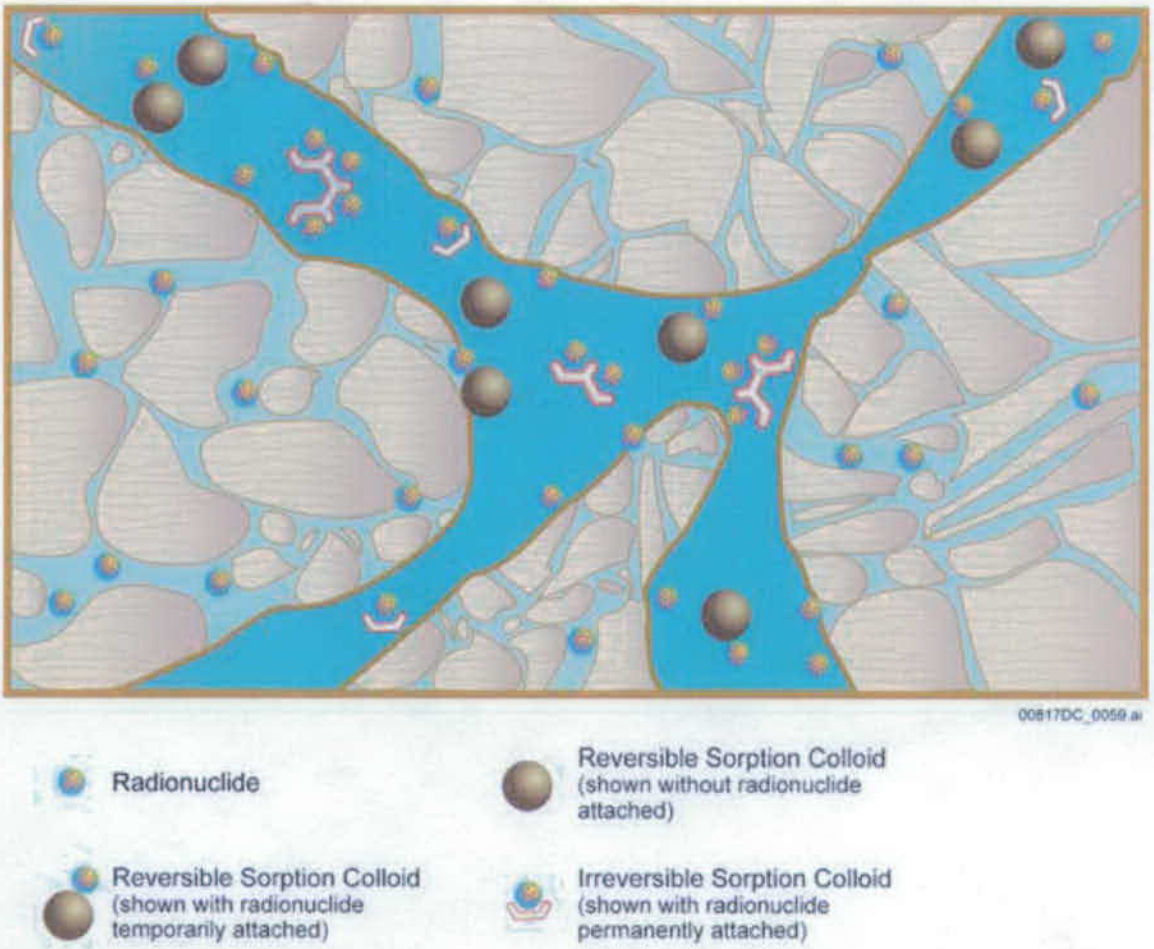

Figure 6.3.9-6. Illustration of Colloid-Facilitated Transport Processes

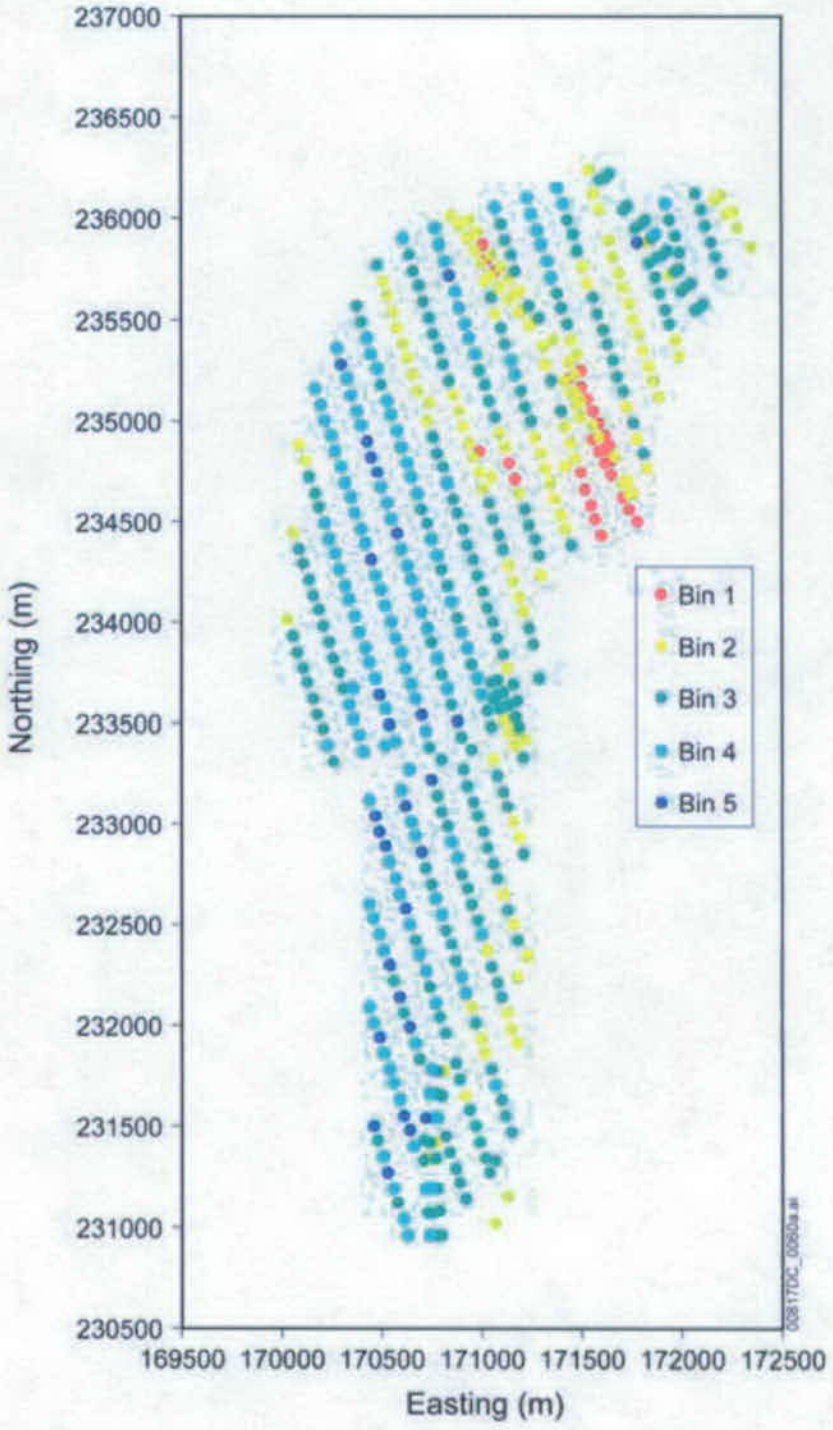

Sources: DTN: LA0702PANS02BR.001 ([DIRS 180322], *fehm_repo_nodes_PD10%.xls*)

Figure 6.3.9-7. Location of Repository Release Nodes for Five Percolation Subregions

INTENTIONALLY LEFT BLANK

6.3.10 Saturated Zone Flow and Transport Model Component

The SZ Flow and Transport Model Component of the TSPA-SEIS (Table 6-1 and Figure 6-1) is used to evaluate the transport of radionuclides from their introduction, at the water table, to the accessible environment that is approximately 18 km downgradient from the repository. Figure 6.3.10-1 shows the relationship between the SZ Flow and Transport Model Component and other model components and submodels of the TSPA-SEIS. The UZ Transport Submodel provides the magnitude and distribution of radionuclide mass release rates to the SZ. Figure 6.3.10-2 summarizes the principal inputs and outputs, model features, and the foundations for confidence in the SZ Flow and Transport Model Component. The SZ Flow and Transport Model Component is linked to the Biosphere Model Component through the simulated time histories of radionuclide concentrations in groundwater at the boundary to the accessible environment. In the TSPA-SEIS analyses for different scenario classes and groundwater protection per 10 CFR 63.331 [DIRS 180319], radionuclide concentrations are calculated by including the mass of all radionuclides that reaches the accessible environment in any given annual period into 3,000 acre-feet of water, as specified in 10 CFR 63.312(c) [DIRS 180319].

6.3.10.1 Conceptual Model

Figure 6.3.10-3 provides a conceptual illustration of SZ flow and transport between Yucca Mountain and the biosphere, showing the relevant processes and geologic media in the SZ. The conceptual model of SZ flow includes southerly groundwater flow from recharge areas at higher elevations north of Yucca Mountain, through the Tertiary age volcanic rocks, and into the alluvium and other valley-fill deposits. For the SZ flow and transport abstraction used in the TSPA-SEIS (SNL 2007 [DIRS 181650]), groundwater flow between the repository and the biosphere is modeled using three-dimensional steady-state flow conditions. A continuum representation is used for the fracture network in the volcanic rocks beneath the repository; and the alluvium and valley-fill deposits are modeled as porous media. The model of the SZ flow system includes higher groundwater flux during potential wetter and cooler monsoon and glacial-transition climate states that are likely to occur within the 10,000-year and 1 million-year modeling time periods.

Several processes are involved in the transport of radionuclides through the SZ. Advection in groundwater, dispersion, matrix diffusion in fractured media, sorption of radionuclides, colloid-facilitated transport, radioactive decay, and radioactive ingrowth are explicitly included in the TSPA-SEIS simulations. The processes are represented in the TSPA-SEIS as follows:

- **Advective transport**—This process occurs only within the fracture network of the volcanic hydrogeologic units due to the very high contrast in permeability between the fractures and the rock matrix, but is widely distributed within the alluvium, except in low-permeability materials. This mode of transport is the primary mechanism for the transport of radionuclides from the SZ to the accessible environment.

- **Dispersion of radionuclide mass**—This process, which includes hydrodynamic dispersion and molecular diffusion, occurs in both the fractured volcanic units and

in the alluvium, with longitudinal dispersion typically much greater than transverse dispersion.

- **Matrix diffusion in fractured volcanic units**—This process determines the transfer of dissolved radionuclide mass from the flowing groundwater within fractures to the relatively stagnant groundwater contained in the pores of the rock matrix. The mass transfer, which could be in either direction, is a function of the concentration of the radionuclide in the fractures and matrix. The process of matrix diffusion of colloids is considered to be small and thus is not accounted for. The diffusion of colloids from fractures into the rock matrix is not included in the TSPA-SEIS.

- **Radionuclide sorption**—Sorption in fractured media occurs in the rock matrix only. In the alluvium, sorption occurs only in the effective porosity of the alluvium.

- **Colloid-facilitated transport**—This process can occur by two modes: (1) when radionuclides are reversibly sorbed onto colloids and (2) when radionuclides are irreversibly sorbed onto colloids. A large fraction of the colloids with irreversibly sorbed radionuclides undergoes reversible filtration during transport. Figure 6.3.10-4 illustrates the mechanisms involved in colloid-facilitated transport. Reversible filtration of irreversible colloids is represented by a retardation factor in the SZ Flow and Transport Model Component.

- **Radioactive decay and ingrowth**—Radioactive decay occurs for all radionuclides. Radionuclide ingrowth is represented for the daughter radionuclides in four principal decay chains.

Two ACMs regarding groundwater flow and radionuclide transport in the SZ were considered in the development of the SZ Flow and Transport Model Component. These ACMs are discussed in Section 6.3.10.5.

6.3.10.2 TSPA-SEIS Abstraction

Two abstractions of the SZ Flow and Transport Model Component were implemented for the TSPA-SEIS:

- The 3-D SZ Flow and Transport Abstraction Model was developed outside of the TSPA-SEIS to calculate the flow and transport through the SZ to the accessible environment for individual radionuclides important to dose. The output from the 3-D SZ Flow and Transport Abstraction Model is developed in the form of unit-source radionuclide breakthrough curves. Within the TSPA-SEIS, a convolution integral technique combines these radionuclide breakthrough curves with the time-varying radionuclide sources from the UZ to quantify radionuclide transport to the accessible environment. The convolution technique inherently assumes the system being simulated exhibits a linear response to the input function, and a steady-state flow condition in the SZ. This approach was validated for the

3-D SZ Flow and Transport Abstraction, as documented in *Saturated Zone Flow and Transport Model Abstraction* (SNL 2007 [DIRS 181650], Section 7.1.1[a]).

- The 1-D SZ Flow and Transport Abstraction is implemented directly in the TSPA-SEIS to calculate the radioactive decay, ingrowth, and transport for four decay chains. Although the decay products from these chains are not significant contributors to total dose, regulations for groundwater protection (contained in 10 CFR 63.331 [DIRS 180319]) require explicit analysis of their concentrations in the water supply of the critical group.

A brief summary of these two submodels is presented below.

3-D SZ Flow and Transport Abstraction—The three-dimensional SZ flow and transport process modeling, described in *Saturated Zone Site-Scale Flow Model* (SNL 2007 [DIRS 177391]) and *Site-Scale Saturated Zone Transport* (SNL 2007 [DIRS 177392]) forms the technical bases for the 3-D SZ Flow and Transport Abstraction, as implemented in the TSPA-SEIS. Figure 6.3.10-5 is a regional map showing the area of the SZ flow system, the direction of SZ flow, and an outline of the 3-D SZ Flow and Transport Process Model domain. The 3-D SZ Flow and Transport Abstraction is based on the 3-D SZ Flow and Transport Abstraction Model that uses a control-volume, finite-element method to model groundwater flow, and a particle-tracking method to model SZ radionuclide transport. These methods, as implemented in FEHM V2.24-01 (FEHM V2.24-01, STN: 10086-2.24-01-00 [DIRS 179419]), simulate groundwater flow in fractured and porous media, as well as advection along groundwater streamlines, dispersion, retardation due to sorption, matrix diffusion and colloid-facilitated transport. The groundwater flow boundary conditions for the 3-D SZ Flow and Transport Abstraction Model are specified heads at the lateral boundaries, a no-flow condition on the lower model boundary, and specified groundwater flux for recharge at the upper model boundary. These boundary conditions are described in detail in *Saturated Zone Site-Scale Flow Model* (SNL [DIRS 177391], Sections 6.3.1.6 and 6.3.1.7).

The specified flux for recharge at the upper model boundary is scaled in proportion to an uncertainty in groundwater specific discharge that is represented by an uncertainty distribution (SNL 2007 [DIRS 179412], Table 3-1). This parameter (groundwater specific discharge scaling factor) is a multiplier that is applied to all values of permeability, and values of specified recharge fluxes, in the 3-D SZ Flow and Transport Abstraction Model to effectively scale the simulated specific discharge in the model. Scaling the recharge flux and the values of permeability in proportion to the uncertainty in groundwater specific discharge maintains the calibration of the 3-D SZ Flow and Transport Abstraction Model with regard to water-level measurements (SNL 2007 [DIRS 181650], Section 6.5[a]).

The sources of radionuclides entering the SZ are specified as point sources within each of the four source regions beneath the repository, as described in Section 6.3.9 (UZ Radionuclide Transport). Figure 6.3.10-6 shows the repository outline and the four SZ source regions used in the TSPA-SEIS. The horizontal location of the point source in each of the four source regions varies randomly from simulation to simulation. Source Regions 1, 3, and part of Source Region 2 are primarily located directly below the repository to capture radionuclides transported vertically downward in the UZ Transport Submodel. Portions of Source Regions 2 and 4 are

located to the east of the repository to capture radionuclides transported by the lateral diversion of groundwater to the east along dipping volcanic strata in the UZ. In addition, the northern part of Source Region 2 underlies a northeasterly extension of the repository. The random locations of the radionuclide source terms for each realization, are defined by eight stochastic parameters (input names listed in the first column, last row of Table 6.3.10-2) that determine the areal model coordinates for the source locations within Source Regions 1 to 4, respectively. These parameter values are drawn from independent, uniform distributions from 0.0 to 1.0, and result in randomly located point sources within each of the four source regions for each realization of the SZ Flow and Transport Submodel.

In addition to the transport of radionuclides as solutes in groundwater, radionuclides may also be sorbed onto colloids and travel through the SZ to the accessible environment (BSC 2004 [DIRS 170006], Section 6.3). The radionuclides may be reversibly or irreversibly sorbed onto colloids. A retardation factor is established for radionuclides that are irreversibly sorbed onto colloids. Implied in the use of a retardation factor to describe colloid transport is that colloid filtration and detachment rates are fast relative to groundwater transport times through the system (BSC 2004 [DIRS 170006], Section 7.1). In addition, a small fraction of colloids, also called the "fast fraction," is transported unretarded through the SZ, based on groundwater transport times (BSC 2004 [DIRS 170006], Section 6.6). Radionuclides that are reversibly sorbed onto colloids are in equilibrium with the aqueous phase and the geologic medium. In this mode of transport, the effective retardation of these radionuclides during transport in the SZ depends on the sorption of radionuclides to colloids, the concentration of colloids in the groundwater, and the sorption coefficient of the radionuclide onto the geologic medium. Because the effective sorptive capacity of the porous medium is reduced when groundwater colloids carry a significant fraction of radionuclide mass in the system, an adjusted sorption coefficient is calculated for the alluvium and undifferentiated valley fill hydrologic units (SNL 2007 [DIRS 181650], Section 6.5.1.1, Equation 6-5). For transport in fractured media, the effective diffusion coefficient into the rock matrix is reduced due to the affinity of radionuclides for sorption onto colloids in the fractures (SNL 2007 [DIRS 181650], Section 6.5.1.1, Equation 6-9).

As discussed in Section 6.3.7.1.2, 27 of the 31 important radionuclides are tracked and transported by the SZ transport submodel. The 4 radionuclides that are not tracked and transported are ^{245}Cm, ^{241}Pu, ^{227}Ac and ^{228}Ra. Details on the 4 radionuclides can be found in Section 6.3.7.1.2. The radionuclides tracked by the SZ Flow and Transport Model Component are divided into 12 groups, based on their transport characteristics. These 12 groups and their modes of transport are summarized in Table 6.3.10-1. The first group contains the nonsorbing radionuclides technetium, iodine, carbon, and chlorine; they are grouped together in the TSPA-SEIS because their solute migration is identical. Carbon is considered nonsorbing and is transported without chemical reactions or ionic exchange with the host rocks, thus providing a conservative bound on transport in the absence of a detailed model for reactive transport. The second group contains americium, thorium, and protactinium, representing colloid-facilitated transport of the radionuclides reversibly sorbed onto colloids. The third group contains cesium, representing colloid-facilitated transport of the radionuclide reversibly sorbed onto colloids. The fourth group contains plutonium, representing colloid-facilitated transport of the radionuclide reversibly sorbed onto colloids. The fifth group contains neptunium, being transported as a solute. The sixth group contains plutonium and americium, representing colloid-facilitated

transport of the radionuclides irreversibly sorbed onto colloids. The seventh, eighth, and ninth groups contain radium, strontium, and uranium, respectively, all transported as a solute. The tenth group contains plutonium and americium, representing the fast fraction of colloid-facilitated transport of the radionuclides irreversibly sorbed onto colloids. The eleventh group contains selenium, transported as a solute. Lastly, the twelfth group contains tin, representing colloid-facilitated transport of the radionuclide reversibly attached to colloids.

The 3-D SZ Flow and Transport Abstraction breakthrough curves are calculated outside of the TSPA-SEIS, as shown on Figure 6.1.4-1. The epistemic uncertain parameters shown in Table 6.3.10-2 are sampled 200 times to produce 200 sets of input parameters to the 3-D SZ Flow and Transport Abstraction Model. The 3-D SZ Flow and Transport Abstraction Model then uses these 200 input parameter sets to perform a series of probabilistic transport simulations for a unit mass flux source. The simulated transport particle paths from the *Site-Scale Saturated Zone Transport* Model (SNL 2007 [DIRS 177392]) are illustrated on Figure 6.3.10-7. The output of these simulations is a set of 200 breakthrough curves for each of the four source regions and 12 radionuclide groups. The resulting 9,600 breakthrough curves describe the (unit-source) mass of radionuclides that cross the 18-km boundary as a function of time. These breakthrough curves, the SZ_Convolute DLL, and control files for SZ_Convolute are the principal parts of the 3-D SZ Flow and Transport Abstraction. The convolution integral method employed in SZ_Convolute exhibits a linear response to the input function. In the case of solute transport in the SZ, this approach implies, for example, that a doubling of the input mass flux results in a doubling of the output mass flux. This approach is valid for the SZ Flow and Transport Submodel because the underlying transport processes (e.g., advection and sorption) are described by linear partial differential equations with respect to solute mass (SNL 2007 [DIRS 177392], Section 6.4.2.1, Equation 1 and Section 6.4.2.5, Equation 42).

The processes of colloid filtration and sorption are both represented as equilibrium retardation processes. Simple retardation affects the timing of the release of radionuclides from the SZ, but still constitutes a linear relationship between mass input and mass output for the SZ. Future monsoonal and glacial-transition climate states with potentially wetter and cooler climate conditions would increase groundwater recharge, which in turn would increase the specific discharge. When climate change occurs, the convolution technique accounts for the change in specific discharge explicitly (*Design Document for: SZ_Convolute Version 3.0*, 10207-DD-3.0-00 (DOE 2003 [DIRS 167588], Section 3.1). The climate state groundwater flow scaling factors presented in Table 6.3.10-3 (i.e., parameters Flow_Rate_Fact_Vclim_CS1, Flow_Rate_Fact_Vclim_CS2 and Flow_Rate_Fact_Vclim_CS3) are based on mean case conditions and do not include uncertainty in groundwater flux estimates within a given climate state. The uncertainty is captured by the stochastic parameter groundwater specific discharge multiplier (GWSPD) (Table 6.3.10-2). The uncertainty in groundwater specific discharge multiplier is applied to all of the climate states. It is assumed that the instantaneous change from one climate steady-state flow condition to another steady-state condition in the SZ can be described as a linear function (SNL 2007 [DIRS 181650], Section 6.5, p. 6-18). For post-10,000-year (climate state 4) calculations the scaling factor Flow_Rate_Fact_Vclim_CS3, which represents the glacial transition climate conditions, is applicable.

1-D SZ Flow and Transport Abstraction—Because the ingrowth of radionuclides is not explicitly included in the 3-D SZ Flow and Transport Abstraction, a 1-D SZ Flow and Transport Abstraction is used to account for the decay and ingrowth of radionuclide daughter products for the four decay chains shown on Figure 6.3.10-8. The representation of the radionuclide decay chains is simplified in a manner that overestimates the concentration of daughter radionuclides by calculating the secular equilibrium between the final daughter products and their parents in two decay chains (SNL 2007 [DIRS 181650], Section 6.5.1.2). ^{227}Ac is in secular equilibrium with ^{231}Pa in the actinium chain at the downstream end of the one-dimensional SZ flow pathway, and ^{228}Ra is in secular equilibrium with ^{232}Th in the thorium series.

A conceptualization of the 1-D SZ Flow and Transport Abstraction is shown on Figure 6.3.10-9. The 1-D SZ Flow and Transport Abstraction is implemented directly in the TSPA-SEIS as a series of one-dimensional GoldSim model elements (called pipes). The one-dimensional pipes are able to simulate advection, longitudinal dispersion, retardation, decay and ingrowth, and matrix diffusion. Thus, the same radionuclide transport processes that are simulated in the 3-D SZ Flow and Transport Abstraction are included in the one-dimensional pipes, with the exception of transverse dispersion, which cannot be included in a one-dimensional model. The 1-D SZ Flow and Transport Abstraction includes the same uncertain input parameters as the 3-D SZ Flow and Transport Abstraction, shown in Table 6.3.10-2. The two abstractions are coupled so that, for a given realization, the same set of sampled input parameters is used. In addition, the 1-D SZ abstraction uses the constant parameters given in Table 6.3.10-3. Flow rates in the one-dimensional pipe segments are modified for the transitions in climate state, using the same climate state scaling factors listed in Table 6.3.10-3 that are used to modify the flow rates in the 3-D SZ Flow and Transport Abstraction. However, note that limitations in the Laplace transform solution implemented in the pipe module of GoldSim preclude a change to the migration velocity of radionuclides that have entered the pipe segments.

Radionuclide mass already within a given pipe segment of the 1-D SZ Flow and Transport Abstraction does not increase in velocity in response to increased specific discharge resulting from climate change. Radionuclide mass introduced after the change in specific discharge is transported at the proper, correspondingly faster rate. Therefore, a potential discrepancy exists between the rate at which the radionuclides are transported using the 3-D SZ Flow and Transport Abstraction Model and the 1-D SZ Flow and Transport Abstraction. The impacts of this limitation to calculations in the TSPA-SEIS are not large due to the following considerations. First, the 1-D SZ Flow and Transport Abstraction results are used only for the daughter products of the decay chains in the TSPA-SEIS calculations. Second, this limitation applies only to radionuclide mass that enters a given pipe segment prior to 2,000 years, after which glacial-transition climatic conditions continue unchanged. The radionuclide mass that enters the 1-D SZ Flow and Transport Abstraction prior to 600 years, at the time of change from present to monsoon conditions, would experience this limitation to the largest extent because it would be subject to two climate changes. Section 6.3.10.3 describes the implementation of this process in greater detail.

In the 1-D SZ Flow and Transport Abstraction, the flow path from the repository to the accessible environment is subdivided into three concentric zones centered on the repository that are nominally: (1) 0 km to 5 km from the repository; (2) 5 km to 13 km from the repository; and (3) 13 km to 18 km from the repository. The actual flow path length (Table 6.3.10-4) of each

pipe segment in zones 2 and 3 varies as a function of: (1) the northwestern boundary of the alluvial uncertainty zone (FPLANW in Table 6.3.10-2); (2) the value of horizontal anisotropy (HAVO in Table 6.3.10-2); and (3) the source region from which the radionuclide source originates beneath the repository. The value of the parameter defining the location of the northwestern boundary of the alluvial uncertainty zone varies from zero to one, and is used to establish the location of the contact between tuff and alluvium below the water table. The length of the first pipe segment is fixed at 5 km for all realizations. The second pipe segment represents that portion of the flow path from a 5-km distance to contact between the volcanic aquifer and the alluvial aquifer in the SZ. The third pipe segment represents the portion of the flow path from the contact between the volcanic units and the alluvium out to the accessible environment. The lengths of the second and third pipe segments are estimated from the particle-tracking results of the 3-D SZ Flow and Transport Abstraction Model, as summarized in Table 6.3.10-4. It is important to note that the total length of the three pipe segments for a given source region can be greater than 18 km due to the effects of the horizontal anisotropy on the simulated flow paths (Figure 6.3.10-10). Estimated pipe segment lengths are shown for differing values of the horizontal anisotropy and for the four source regions. Each entry in the table contains a range of values in pipe length, where the minimum value shown for the second pipe (5- to 13-km zone) is used when the parameter defining the location of the northwestern boundary of the alluvial uncertainty zone is equal to 1.0, and the maximum value is used when the northwestern boundary parameter is equal to 0.0. By contrast, the minimum value of length for the third (13- to 18-km zone) pipe segment is used when the parameter defining the location of the northwestern boundary of the alluvial uncertainty zone is equal to 0.0, and the maximum value corresponds to a northwestern boundary parameter equal to 1.0. In other words, the maximum length of the flow path in the alluvial aquifer corresponds to the maximum northwesterly extent of the alluvial uncertainty zone, and the minimum length of the flow path in the alluvial aquifer corresponds to the minimum northwesterly extent of the alluvial uncertainty zone. The values in Table 6.3.10-4 are input into the SZ One-Dimensional Transport Model as a look-up table.

The average specific discharge along each pipe segment of the 1-D SZ Flow and Transport Abstraction varies as a function of the horizontal anisotropy. The resulting values of average specific discharge, as used in the 1-D SZ Flow and Transport Abstraction, are shown in Table 6.3.10-5. Figure 6.3.10-10 shows the simulated flow paths from Source Region 1 for the different values of horizontal anisotropy listed in Table 6.3.10-5.

The values of specific discharge are also scaled linearly, using the groundwater specific discharge multiplier (Table 6.3.10-2) to represent the uncertainty in specific discharge. The values of specific discharge within the three pipe segments are calculated within the 1-D SZ Flow and Transport Abstraction by interpolating between the values of horizontal anisotropy, shown in Table 6.3.10-5, and through scaling by the value of the groundwater specific discharge multiplier (Table 6.3.10-2). The volumetric flow rate is the same for all segments in the 1-D SZ Flow and Transport Abstraction, and variations in specific discharge along the flow path are incorporated into the model by varying the cross-sectional areas of the pipe segments.

A summary of alpha concentration results in Amargosa Valley groundwater is given in Table 6.3.10-6. The best estimate for the mean gross alpha concentration in groundwater is 0.50 pCi/L with a 95 percent confidence that the concentration will not exceed 0.71 pCi/L. In the absence of data on the combined concentrations of ^{226}Ra and ^{228}Ra, it should be conservatively

assumed for these radionuclides that they are responsible for all gross alpha activity. For ^{226}Ra and ^{228}Ra, the mean concentration is 0.50 pCi/L with a 95 percent confidence that the concentration will not exceed 0.71 pCi/L. Details can be found in *Saturated Zone Flow and Transport Model Abstraction* (SNL 2007 [DIRS 181650], Section 6.8.6). These parameters are used in the biosphere model component of the TSPA-SEIS (Section 6.3.11).

6.3.10.3 TSPA-SEIS Implementation

Figure 6.3.10-11 presents a flow chart that shows the implementation of the SZ Flow and Transport Submodel.

The 3-D SZ Flow and Transport Submodel calculations are performed by an external DLL, SZ_Convolute V3.10.01, which is directly coupled to the TSPA-SEIS. At the beginning of each realization, an integer variable (SZ index) with a range of 1 to 200 is randomly sampled in the TSPA-SEIS and is used to select the radionuclide breakthrough curve to be used for that realization. The same breakthrough curve is selected for each radionuclide group based on the sampled SZ index value. This maintains consistency among the different radionuclide groups because the breakthrough curves for each value of the SZ index were produced using the same set of input parameters. For each timestep, the SZ_Convolute DLL takes the radionuclide source mass from the nodes at the water table of the UZ Transport Submodel (Section 6.3.9.1) and combines it with the selected breakthrough curve for that radionuclide and source region.

Because the 3-D SZ Flow and Transport Abstraction does not account for ingrowth of daughter products in the chain decay, adjustments are necessary to properly account for these radionuclides (Figure 6.3.10-8). The TSPA-SEIS adjustments increase the inventory of the first-generation daughters (namely: ^{239}Pu, ^{237}Np, ^{236}U, ^{238}U, and ^{234}U) before they are released into the 3-D SZ Flow and Transport Abstraction. This adjustment is performed using a method termed "inventory boosting" in the TSPA-SEIS's GoldSim model file. For each timestep, the inventory of each of these first-generation daughters is increased or "boosted" by the amount that their respective parent radionuclides would decay during the remaining simulation time.

The 1-D SZ Flow and Transport Abstraction is used to account for the ingrowth of the second-generation daughters: ^{235}U, ^{231}Pa, ^{227}Ac, ^{233}U, ^{229}Th, ^{232}Th, ^{228}Ra, ^{230}Th, and ^{226}Ra. The 1-D SZ Flow and Transport Abstraction is incorporated directly into the TSPA-SEIS as four sets of three pipe elements (one set for each SZ source region). The radionuclide mass input to the 1-D SZ Flow and Transport Abstraction also comes from the UZ Transport Submodel. The same integer value used by the 3-D SZ Flow and Transport Abstraction to select a set of breakthrough curves is used in the 1-D SZ Flow and Transport Abstraction to choose additional input parameter values from look-up tables in the TSPA-SEIS. This method ensures consistency between the 1-D and 3-D SZ Flow and Transport Abstractions on a realization-by-realization basis.

Even though they are accounted for in the 3-D SZ Flow and Transport Abstraction, the parents of the second-generation daughters are also transported in the 1-D SZ Flow and Transport Abstraction. The parents are included in the 1-D SZ Flow and Transport Abstraction to account for the ingrowth of the second-generation daughters. The first-generation daughter products are

not boosted for the 1-D SZ Flow and Transport Abstraction because the GoldSim software correctly calculates the decay and ingrowth of radionuclides.

The radionuclide mass for all species is tracked in both the 1-D and 3-D SZ Flow and Transport Abstractions. However, the radionuclide mass exiting each submodel is then screened, such that only the mass for second-generation daughter species is taken from the 1-D SZ Flow and Transport Abstraction. All the other radionuclide results are taken from the 3-D SZ Flow and Transport Abstraction.

Radionuclides are released from the SZ to the accessible environment approximately 18 km from the repository. The 18-km regulatory boundary ([DIRS 180319], III Comments and Responses, 3.5, p. 55750) represents the location where a RMEI resides (based on 10 CFR 63.332 [DIRS 180319]). All of the radionuclide mass that crosses this regulatory boundary in the SZ is assumed to be homogeneously distributed in a 3,000 acre-ft volume per annum (10 CFR 63.332(3) [DIRS 180319]). The resulting release of radionuclide mass to the biosphere is then used to calculate dose to the RMEI (Section 6.3.11).

6.3.10.4 Model Component Consistency and Conservatism in Assumptions and Parameters

To enhance understanding of the complex interactions within the TSPA-SEIS, a discussion of consistency among model components and submodels and identification of conservative assumptions in abstractions, process models, and parameter sets supporting SZ flow and transport are discussed below.

6.3.10.4.1 Consistency of Assumptions

SZ Release Location–The 3-D SZ Flow and Transport Abstraction, which is used to transport all parent radionuclides and first-generation daughters, is based on three-dimensional simulations that use a random release location beneath the repository for each of the four SZ source regions (Section 6.3.10.2). However, the 1-D SZ Flow and Transport Abstraction, used for most granddaughters, is based on a central release location for each of the four source regions. This can result in different transport behavior for isotopes of the same chemical element in a given realization. For example, ^{234}U (a daughter of ^{238}Pu, but a granddaughter of ^{242}Pu) is transported with the three-dimensional model, whereas ^{233}U is transported with the one-dimensional model. Thus, for certain realizations, where the three-dimensional random-release model produces a significantly different transport pathway than the one-dimensional central-location model, the transport times through the SZ for the two radionuclides can be different by thousands of years, even though they would be expected to behave similarly because they have similar transport properties.

Effect on TSPA—The effect of this difference is minimal, because the central release location used in the 1-D SZ Flow and Transport Abstraction is representative of the average behaviour taken over multiple realizations.

6.3.10.4.2 Identification of Conservatisms in Submodels and Abstractions

Radionuclide Mass Release from the UZ Matrix to the SZ—The transfer of radionuclide mass reaching the water table from the matrix of the UZ directly to the fractures of the SZ tends

to maximize the simulated concentrations of radionuclides at the outlet to the accessible environment. This approximation results in less dispersion of the radionuclide transport times through the SZ and, thus, to less attenuation of peaks in radionuclide discharge. This conservatism is used because it simplifies the modeling approach ((SNL 2007 [DIRS 181650], Sections 6.3.3 and 6.5.2.13).

Instantaneous Change in SZ Groundwater Flow at Climate State Changes—The increase in groundwater flux will be gradual during the transition period going from drier conditions to wetter conditions. However, in the TSPA-SEIS, groundwater flux is assumed to increase instantaneously at climate state changes. This conservatism is applied because it simplifies the modeling approach (SNL 2007 [DIRS 181650], Section 6.5, p. 6-18). This approach tends to overestimate the rate of radionuclide transport in the SZ.

Colloids are Retarded by Filtration—The conceptual model of filtration for colloids with irreversibly sorbed radionuclides assumes that colloids are retarded by filtration. Permanent removal of colloids by mechanical filtration in the SZ is not considered in the TSPA-SEIS, although it is likely to occur (SNL 2007 [DIRS 181650], Sections 6.3.1, 6.3.2, 6.5.1[a], and 6.5.2.11). The exclusion of permanent colloid filtration tends to overestimate the quantity of colloids that are transported through the SZ. In the compliance model (SNL 2007 [DIRS 181650], Section 6.5.2.11), transport of retarded irreversible colloids in both the volcanic units and the alluvium is calculated using single retardation factors (one for the volcanic units and another for the alluvium). Analysis of experimental data shows that use of a single retardation factor does not fit experimental observations.

No Solubility Limits or Enhanced Sorption Applied to Radionuclide Concentrations in the SZ—No solubility limits are applied to radionuclide concentrations in the SZ. Dissolved radionuclide concentrations in the far field are assumed to be the same as in the near field regardless of the chemical conditions. The application of solubility limits in the SZ is screened out. In addition, significantly greater sorption could occur for some redox-sensitive radionuclides if chemically reducing conditions occur locally in the SZ. Changes due to redox conditions in the SZ could have a potential impact on solubility, sorption, and radionuclide transport through the SZ. Enhanced sorption due to the presence of reducing zones in the SZ could increase retardation, resulting in longer travel times in the SZ.

Implementation of Ingrowth of radionuclides in the SZ Model—Ingrowth of radionuclides is not explicitly included in the SZ transport model component of the TSPA-SEIS for some radionuclides. A simplified approach, "inventory boosting", accounts for this process for some of the radionuclides that have parent radionuclides as described in *Saturated Zone Flow and Transport Model Abstraction* SNL 2007 ([DIRS 181650], Sections 6.3.1). The TSPA-SEIS 1-D SZ transport model adds the pre-decayed daughter products to transported inventory in the SZ and also transports the full inventory of the parents by applying "inventory boosting". The parent radionuclides of these boosted decay products are not diminished, resulting in an overestimation of the mass of radionuclides transported in the SZ.

6.3.10.5 Alternative Conceptual Model(s) for Saturated Zone Flow and Transport

Section 6.2 outlines the general consideration and treatment of ACMs used to support the TSPA-SEIS. A brief description of the SZ flow and transport ACMs summarized in Table 6.3.10-7 is presented below.

Minimal Matrix Diffusion ACM—Diffusion of radionuclides into the pore space of the rock matrix in the fractured volcanic units is potentially extremely limited due to highly channelized groundwater flow, fracture coatings, or other factors. The uncertain input parameters influencing matrix diffusion in the SZ Flow and Transport Submodel include effective diffusion coefficient, flowing interval spacing, and flowing interval porosity. Minimal matrix diffusion in the SZ Flow and Transport Submodel would tend to increase the rate of radionuclide transport. However, this ACM is implicitly included in the 3-D SZ Flow and Transport Abstraction and in the 1-D SZ Flow and Transport Abstraction through the range of uncertainty in the key input parameters mentioned above (SNL 2007 [DIRS 181650], Section 6.4).

This ACM was shown to be captured within the range of uncertainty already in the SZ Flow and Transport Submodel and, therefore, is not recommended for inclusion in the TSPA-SEIS.

Horizontal Anisotropy in Permeability ACM—Alternative interpretations of pump test results in the fractured volcanic units indicate preferential permeability along structural features oriented in the NNE-SSW direction or in the WNW-ESE direction. This ACM is implicitly included in the 3-D SZ Flow and Transport Abstraction and in the 1-D SZ Flow and Transport Abstraction through the range of uncertainty in the input parameter HAVO. The uncertain input parameter influencing horizontal anisotropy in permeability in the volcanic units near Yucca Mountain is the ratio of N-S to E-W permeability (SNL 2007 [DIRS 181650], Section 6.5.2.10). This continuously distributed parameter varies from less than one to greater than one with most of the realizations greater than one.

This ACM was also shown to be captured within the range of uncertainty already in the SZ Flow and Transport Submodel and, therefore, is not recommended for inclusion in the TSPA-SEIS.

INTENTIONALLY LEFT BLANK

Table 6.3.10-1. Radionuclides Transported in the Saturated Zone Flow and Transport Submodel

Radionuclide Group Number	Transport Mode	Radionuclides
1	Solute	Carbon, Technetium, Iodine, Chlorine
2	Colloid-facilitated (Reversible)	Americium, Thorium, Protactinium
3	Colloid-facilitated (Reversible)	Cesium
4	Colloid-facilitated (Reversible)	Plutonium
5	Solute	Neptunium
6	Colloid-facilitated (Irreversible)	Plutonium, Americium
7	Solute	Radium
8	Solute	Strontium
9	Solute	Uranium
10	Colloid-facilitated (Fast fraction of Irreversible)	Plutonium, Americium
11	Solute	Selenium
12	Colloid-facilitated (Reversible)	Tin

Source: *Saturated Zone Flow and Transport Model Abstraction* (SNL 2007 [DIRS 181650], Table 6-9[a]).

Table 6.3.10-2. Uncertain Model Inputs Used in the 3-D Saturated Zone Flow and Transport Process Model and 1-D Saturated Zone Flow and Transport Abstraction

Input Name	Input Description	Value or Distribution	Units	Type of Uncertainty
Kd_Np_Vo	Neptunium sorption coefficient in volcanic units	CDF: Probability / Value 0.0 / 0.0 0.05 / 0.99 0.90 / 1.83 1.0 / 6.0	mL/g	Epistemic
Kd_Np_Al	Neptunium sorption coefficient in alluvium	CDF: Probability / Value 0.0 / 1.8 0.05 / 4.0 0.95 / 8.7 1.0 / 13.0	mL/g	Epistemic
Kd_Sr_Vo	Strontium sorption coefficient in volcanic units	Uniform: Minimum 20.0 Maximum 400.0	mL/g	Epistemic
Kd_Sr_Al	Strontium sorption coefficient in alluvium	Uniform: Minimum 20.0 Maximum 400.0	mL/g	Epistemic
Kd_U_Vo	Uranium sorption coefficient in volcanic units	CDF: Probability / Value 0.0 / 0.0 0.05 / 5.39 0.95 / 8.16 1.0 / 20.0	mL/g	Epistemic
Kd_U_Al	Uranium sorption coefficient in alluvium	CDF: Probability / Value 0.0 / 1.7 0.05 / 2.9 0.95 / 6.3 1.0 / 8.9	mL/g	Epistemic
Kd_Ra_Vo	Radium sorption coefficient in volcanic units	Uniform: Minimum 100.0 Maximum 1,000.0	mL/g	Epistemic
Kd_Ra_Al	Radium sorption coefficient in alluvium	Uniform: Minimum 100.0 Maximum 1,000.0	mL/g	Epistemic
Kd_Pu_Vo	Plutonium sorption coefficient in volcanic units	CDF: Probability / Value 0.0 / 10.0 0.25 / 89.9 0.95 / 129.87 1.0 / 300.0	mL/g	Epistemic
Kd_Pu_Al	Plutonium sorption coefficient in alluvium	Beta: Mean 100 Standard Deviation 15 Minimum 50 Maximum 300	mL/g	Epistemic

Table 6.3.10-2. Uncertain Model Inputs Used in the 3-D Saturated Zone Flow and Transport Process Model and 1-D Saturated Zone Flow and Transport Abstraction (Continued)

Input Name	Input Description	Value or Distribution	Units	Type of Uncertainty
Kd_Am_Vo	Americium sorption coefficient in volcanic units	Truncated Normal: Mean 5,500 Standard Deviation 1,500 Minimum 1,000 Maximum 10,000	mL/g	Epistemic
Kd_Am_Al	Americium sorption coefficient in alluvium	Truncated Normal: Mean 5,500 Standard Deviation 1,500 Minimum 1,000 Maximum 10,000	mL/g	Epistemic
Kd_Cs_Vo	Cesium sorption coefficient in volcanic units	CDF: Probability Value 0.0 100.0 0.05 3,000.59 1.0 6,782.92	mL/g	Epistemic
Kd_Cs_Al	Cesium sorption coefficient in alluvium	Truncated Normal: Mean 728 Standard Deviation 464 Minimum 100 Maximum 1,000	mL/g	Epistemic
Kd_Se_Vo	Selenium sorption coefficient in volcanic units	Truncated Log_Normal: Mean 14.0. Standard Deviation 11.2 Minimum 1.0 Maximum 50.0	mL/g	Epistemic
Kd_Se_Al	Selenium sorption coefficient in alluvium	Truncated Log_Normal: Mean 14.0. Standard Deviation 11.2 Minimum 1.0 Maximum 50.0	mL/g	Epistemic
Kd_Sn_Vo	Tin sorption coefficient in volcanic units	Log-Uniform: Minimum 1.e2 Maximum 1.e5	mL/g	Epistemic
Kd_Sn_Al	Tin sorption coefficient in alluvium	Log-Uniform: Minimum 1.e2 Maximum 1.e5	mL/g	Epistemic
Correlation matrix for K_d sampling in the SZ	Correlation coefficient values among radionuclides and between volcanic units and alluvium	DTN: LA0702AM150304.001 [DIRS 182480]	NA	Matrix of Single Values

Table 6.3.10-2. Uncertain Model Inputs Used in the 3-D Saturated Zone Flow and Transport Process Model and 1-D Saturated Zone Flow and Transport Abstraction (Continued)

Input Name	Input Description	Value or Distribution	Units	Type of Uncertainty
FISVO	Flowing interval spacing in volcanic units	CDF: Probability / Value 0.0 / 1.860 0.01 / 2.925 0.20 / 12.036 0.50 / 25.773 0.80 / 39.965 0.90 / 45.797 0.92 / 47.207 0.94 / 49.115 0.96 / 51.710 0.98 / 55.249 0.99 / 58.439 1.0 / 80.0	M	Epistemic
CORAL	Colloid retardation factor in alluvium	CDF: (Log_{10}-transformed) Probability / Value 0.0 / 0.903 0.331 / 0.904 0.50 / 1.531 1.0 / 3.715	NA	Epistemic
CORVO	Colloid retardation factor in volcanic units	CDF: (Log_{10}-transformed) Probability / Value 0.0 / 0.778 0.15 / 0.779 0.25 / 1.010 0.50 / 1.415 0.80 / 1.778 1.0 / 2.903	NA	Epistemic
HAVO	Ratio of horizontal anisotropy (north-south over east–west) in permeability	CDF: Probability / Value 0.0 / 0.05 0.0042 / 0.2 0.0168 / 0.4 0.0379 / 0.6 0.0674 / 0.8 0.10 / 1.0 0.60 / 5.0 0.744 / 8.0 0.856 / 11.0 0.936 / 14.0 0.984 / 17.0 1.0 / 20.0	NA	Epistemic
LDISP	Longitudinal dispersivity	Truncated Normal: (Log_{10}-transformed) Mean 2.0 Standard Deviation 0.75	m	Epistemic

Table 6.3.10-2. Uncertain Model Inputs Used in the 3-D Saturated Zone Flow and Transport Process Model and 1-D Saturated Zone Flow and Transport Abstraction (Continued)

Input Name	Input Description	Value or Distribution	Units	Type of Uncertainty
Kd_Pu_Col	Plutonium sorption coefficient onto colloids	CDF: Probability / Value 0.0 / 1.e3 0.45 / 5.e3 0.80 / 1.e4 0.95 / 5.e4 1.0 / 1.e5	mL/g	Epistemic
Kd_Am_Col	Americium sorption coefficient onto colloids	CDF: Probability / Value 0.0 / 1×10^4 0.07 / 5×10^4 0.17 / 1×10^5 0.40 / 5×10^5 0.60 / 1×10^6 0.92 / 5×10^6 1.0 / 1×10^7	mL/g	Epistemic
Kd_Cs_Col	Cesium sorption coefficient onto colloids	CDF: Probability / Value 0.0 / 5.e1 0.05 / 1.e2 0.40 / 5.e2 0.70 / 1.e3 1.0 / 5.e3	mL/g	Epistemic
Kd_Sn_Col	Tin sorption coefficient onto colloids	Log-Uniform: Minimum 1.e5 Maximum 1.e6	mL/g	Epistemic
Conc_Col	Groundwater concentration of colloids	CDF: (Log_{10}-transformed) Probability / Value 0.0 / -9.0 0.50 / -7.0 0.75 / -6.0 0.90 / -5.0 0.98 / -4.3 1.0 / -3.6	g/mL	Epistemic
FPLANW	Northwestern boundary of alluvial uncertainty zone	Uniform: Minimum 0.0 Maximum 1.0	NA	Epistemic
NVF26	Effective porosity in shallow alluvium	Truncated Normal: Mean 0.18 Standard Deviation 0.051 Minimum 0.00 Maximum 0.30	NA	Epistemic
NVF11	Effective porosity in undifferentiated valley fill	Truncated Normal: Mean 0.18 Standard Deviation 0.051 Minimum 0.00 Maximum 0.30	NA	Epistemic

Table 6.3.10-2. Uncertain Model Inputs Used in the 3-D Saturated Zone Flow and Transport Process Model and 1-D Saturated Zone Flow and Transport Abstraction (Continued)

Input Name	Input Description	Value or Distribution	Units	Type of Uncertainty
FPVO	Fracture porosity in volcanic units	CDF: (Log_{10}-transformed) Probability / Value 0.0 / –5.0 0.05 / –4.0 0.50 / –3.0 0.80 / –2.0 1.0 / –1.0	NA	Epistemic
DCVO	Effective diffusion coefficient in volcanic units	CDF: (Log_{10}-transformed) Probability / Value 0.0 / –11.3 0.08 / –10.7 0.50 / –10.3 0.83 / –9.9 1.0 / –9.3	m^2/s	Epistemic
GWSPD	Groundwater specific discharge multiplier	CDF: (Log_{10}-transformed) Probability / Value 0.0 / -0.951 0.05 / -0.506 0.10 / -0.394 0.25 / -0.208 0.5 / 0.000 0.75 / 0.208 0.90 / 0.394 0.95 / 0.506 1.0 / 0.951	NA	Epistemic
Alluvium_Density	Bulk density of alluvium	Normal: Mean 1,910 Standard Deviation 78	kg/m^3	Epistemic
SRC1X SRC1Y SRC2X SRC2Y SRC3X SRC3Y SRC4X SRC4Y	Source regions beneath the repository	Uniform: Minimum 0.0 Maximum 1.0	NA	Epistemic and Aleatory

Sources: Modified from *Saturated Zone Flow and Transport Model Abstraction* (SNL 2007 [DIRS 181650], Tables 6-7[a] and 6-8). The following updated or new parameters are from Table 6-7[a]: GWSPD, FISVO, FPLANW, Kd_Pu_Col, Kd_Cs_Col, Kd_Sn_Col, Kd_Sn_Vo, Kd_Sn_Al, Kd_Se_Vo, Kd_Sn_Al, and Correlation matrix for K_d sampling in the SZ. Parameters NVF26 and NVF11 are new names for Parameters NVF19 and NVF7 in Table 6-8. Only the names changed. The rest of the parameters are from Table 6-8.

NOTES: Only those parameters in the source that are uncertain were included in this table;
NA = not applicable; Log_{10}-transformed values are given in Log_{10}. They are transformed to actual values when used.

Table 6.3.10-3. Constant TSPA Parameters for SZ One-dimensional Transport Model

Parameter Name	Input Description	Input Value	Units
Coating Porosity	Porosity of the fracture coating	0.01	NA
Coating Thickness	Fracture coating thickness	0.00001	m
Flow_Rate_fact_Vclim_CS1	SZ_1D, Discharge flowrate multiplier for climate state 1 (present day)	1	NA
Flow_Rate_fact_Vclim_CS2	SZ_1D, Discharge flowrate multiplier for climate state 2 (monsoonal)	1.9	NA
Flow_Rate_fact_Vclim_CS3	SZ_1D, Discharge flowrate multiplier for climate state 3 (glacial)	3.9	NA
Pipe_Length_Pipe_a	Pipe length for pipe segment a	5,000	m
Volcanic_Fracture_Perimeter	Volcanic fracture perimeter for the determination of fracture surface area.	2	m
Alluvium_Porosity	Effective porosity of the alluvium	0.30	NA
Volcanic_Matrix_Porosity	Porosity of the volcanic matrix	0.22	NA
Volcanic_Density	Bulk density of the volcanic matrix material	1,880	kg/m^3
Fracture_Porosity	Average fracture porosity of the volcanic units	0.001	NA

Source: DTN: SN0702PASZFTMA.002 [DIRS 179494].

Table 6.3.10-4. Flow Path Lengths of Pipe Segments

Horizontal Anisotropy	Minimum and Maximum Flow Path Lengths of Pipe Segments (km)							
	Source Region 1		Source Region 2		Source Region 3		Source Region 4	
	5 - 13 km	13 - 18 km	5 - 13 km	13 - 18 km	5 - 13 km	13 - 18 km	5 - 13 km	13 - 18 km
0.05	15.9 - 16.4	7.7 – 8.2	15.2 - 15.5	7.7 - 8.0	13.6 - 14.4	6.9 - 7.7	14.1 - 15.0	6.7 - 7.6
1.00	11.3 - 12.3	6.7 - 7.7	10.3 - 11.0	7.2 - 7.9	7.7 - 8.6	6.5 - 7.4	7.3 - 8.3	6.8 - 7.8
5.00	11.3 - 12.3	6.7 - 7.7	10.0 - 10.6	7.3 - 7.9	7.7 - 8.6	6.5 - 7.4	7.3 - 8.3	6.8 - 7.8
20.00	11.3 - 12.3	6.7 - 7.7	10.0 - 10.7	7.2 - 7.9	7.7 - 8.6	6.5 - 7.4	7.3 - 8.3	6.8 - 7.8

Source: DTN: SN0702PASZFTMA.002 [DIRS 179494].

Table 6.3.10-5. Average Specific Discharge in Flow Path Segments

Horizontal Anisotropy	Average Specific Discharge (m/yr)		
	0 - 5 km	5 - 13 km	13 - 18 km
0.05	0.354	0.408	2.56
1.00	0.459	0.486	0.769
5.00	0.409	0.544	5.98
20.00	0.555	0.500	5.93

Source: DTN: SN0702PASZFTMA.002 [DIRS 179494].

Table 6.3.10-6. Summary of Alpha Concentration Results in Amargosa Valley Groundwater

Input	Expected Value (mean) pCi/L	Upper (95%) Limit pCi/L
Gross Alpha Concentration	0.50	0.71
Combined Concentration of 226Ra and 228Ra	0.50	0.71

Source: DTN: SN0702PASZFTMA.002 [DIRS 179494].

Table 6.3.10-7. Alternative Conceptual Models Considered for Saturated Zone Flow and Radionuclide Transport

Alternative Conceptual Model	Key Assumptions	Screening Assessment and Basis
Minimal Matrix Diffusion	Diffusion of radionuclides into the pore space of the rock matrix in the fractured volcanic units is extremely limited due to highly channelized groundwater flow, fracture coatings, or other factors.	This ACM is implicitly included in the 3-D SZ Flow and Transport Abstraction, and in the 1-D SZ Flow and Transport Abstraction, through the range of uncertainty in key input parameters. The uncertain input parameters influencing matrix diffusion include DCVO, FISVO, and FPVO (Table 6.3.10-2).
Horizontal Anisotropy in Permeability	Alternative interpretations of pump test results in the fractured volcanic units indicate preferential permeability along structural features oriented in the NNE-SSW direction, or in the WNW-ESE direction.	This ACM is implicitly included in the 3-D SZ Flow and Transport Model Abstraction, and in the 1-D SZ Flow and Transport Abstraction, through the range of uncertainty in an input parameter. The uncertain input parameter influencing horizontal anisotropy in permeability in the volcanic units near Yucca Mountain is the ratio of N-S to E-W permeability (HAVO; Table 6.3.10-2). This continuously distributed parameter varies from less than one to greater than one, with most of the realizations greater than one.

Source: *Saturated Zone Flow and Transport Model Abstraction* (SNL 2007 [DIRS 181650], Section 6.4).

NOTES: 1-D = one-dimensional; DCVO = effective diffusion coefficient in volcanic units; FISVO = flowing interval spacing in volcanic units; FPVC = flowing interval porosity; HAVO = ratio of horizontal anisotropy (north-south over east-west) in permeability.

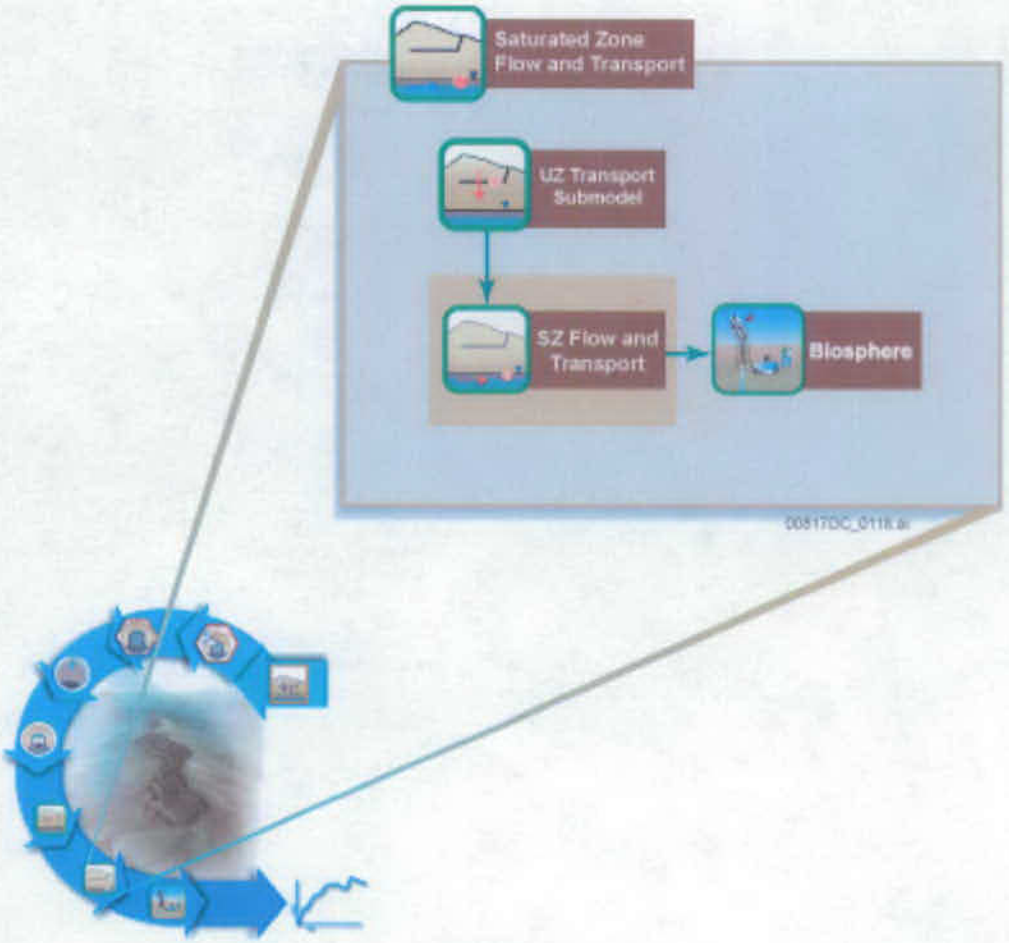

Figure 6.3.10-1. Information Flow Diagram for Saturated Zone Flow and Transport

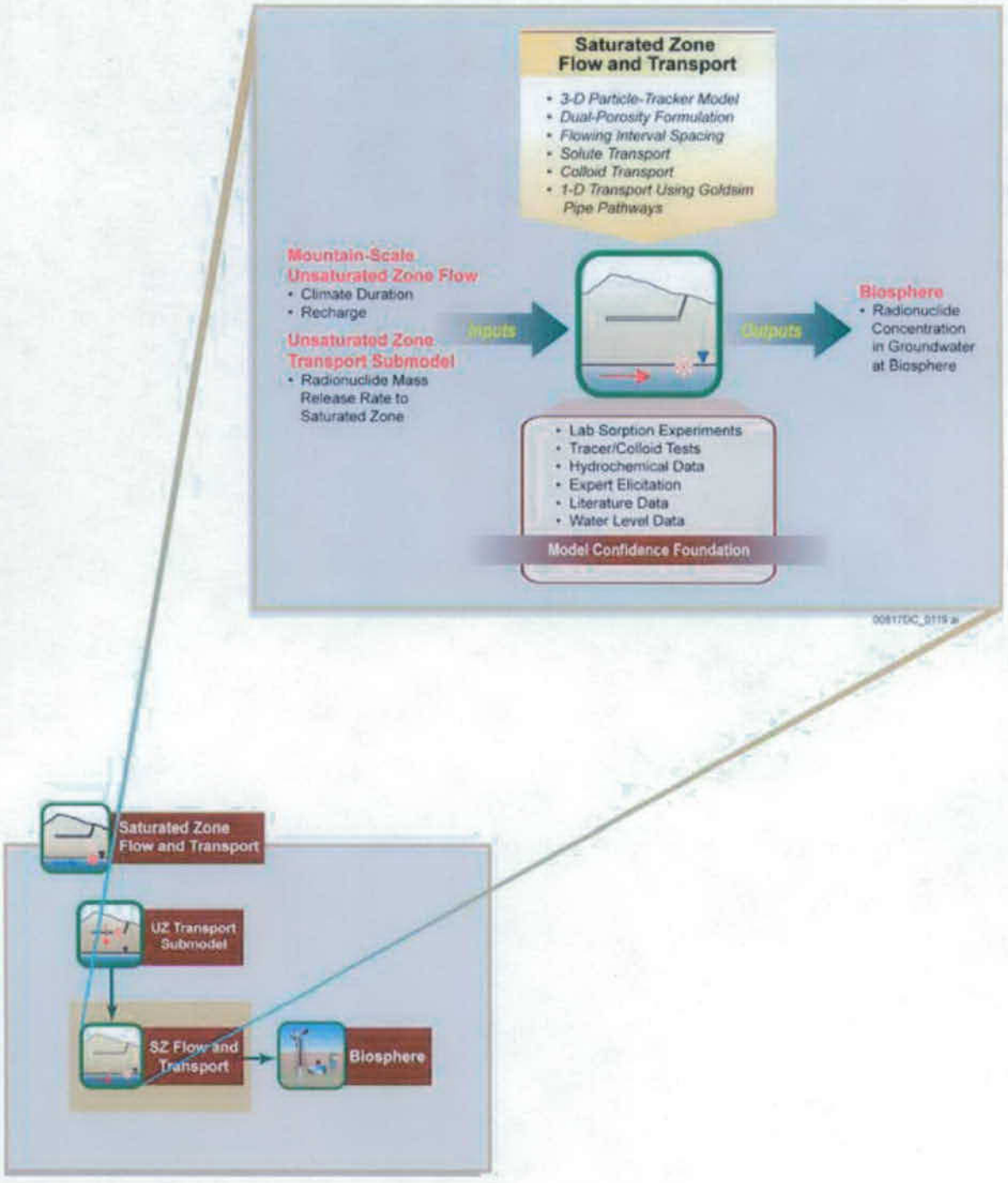

Figure 6.3.10-2. Inputs, Outputs, and Basis for Model Confidence for the Saturated Zone Flow and Transport Model Component

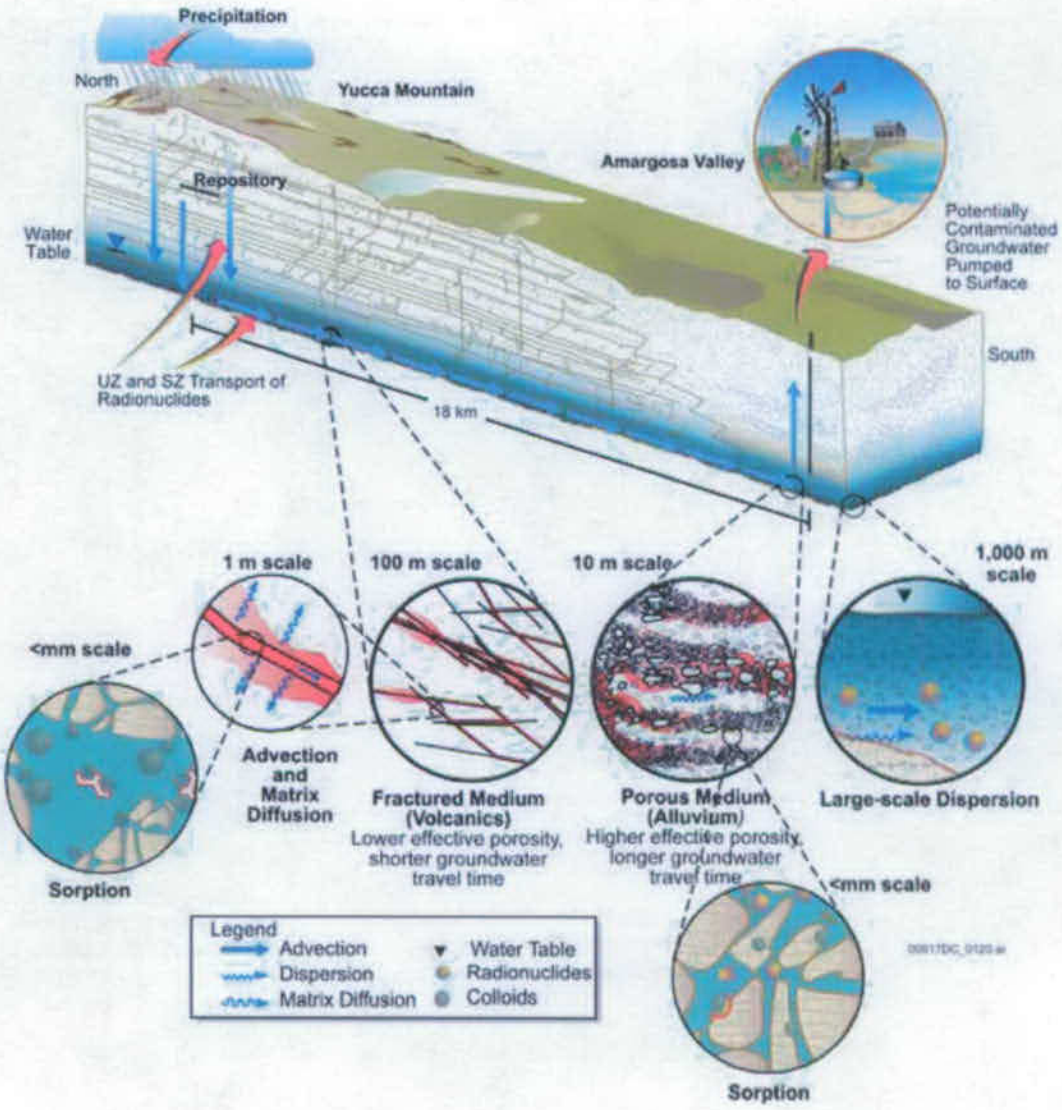

Figure 6.3.10-3. Conceptualization of Features and Processes Important to Saturated Zone Transport

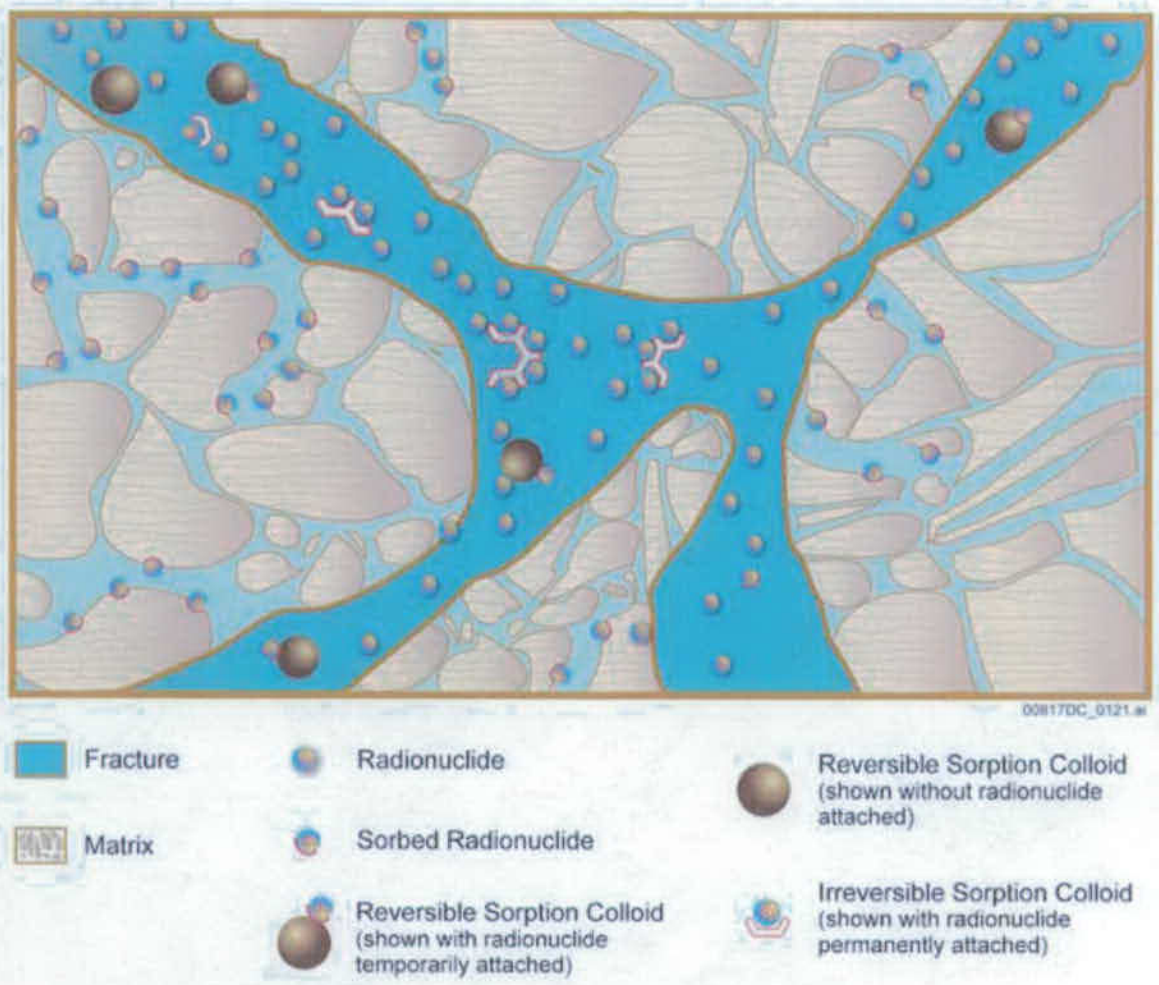

Figure 6.3.10-4. Illustration of Colloid-Facilitated Transport Processes

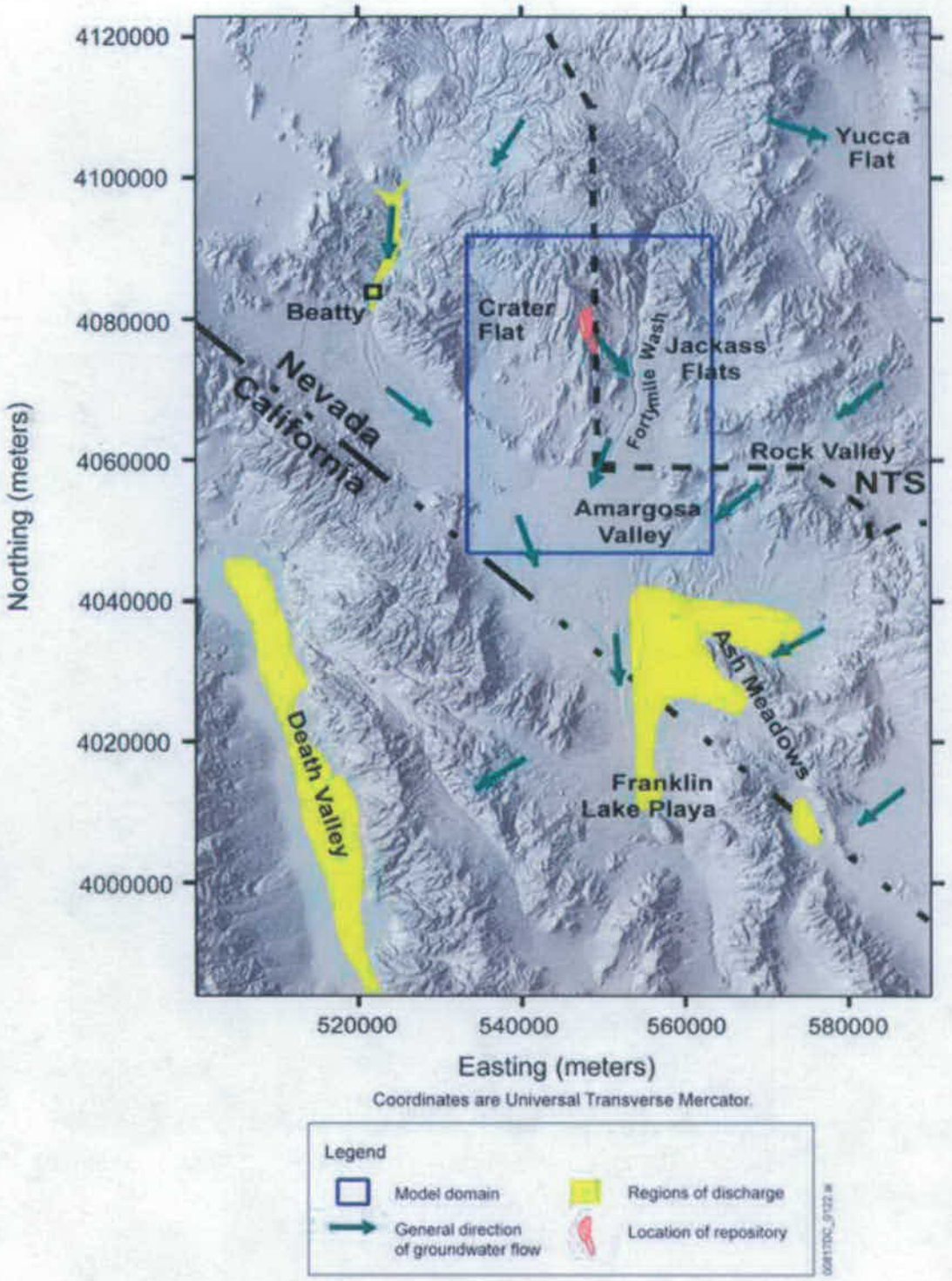

Source: Compiled from *Yucca Mountain Site Description* (BSC 2004 [DIRS 169734], Figures 8-2, 8-5, and 8-6)

Figure 6.3.10-5. Regional Map of the Saturated Zone Flow System, Showing Direction of Flow and Outline of the 3-D Saturated Zone Site-Scale Flow Model Domain

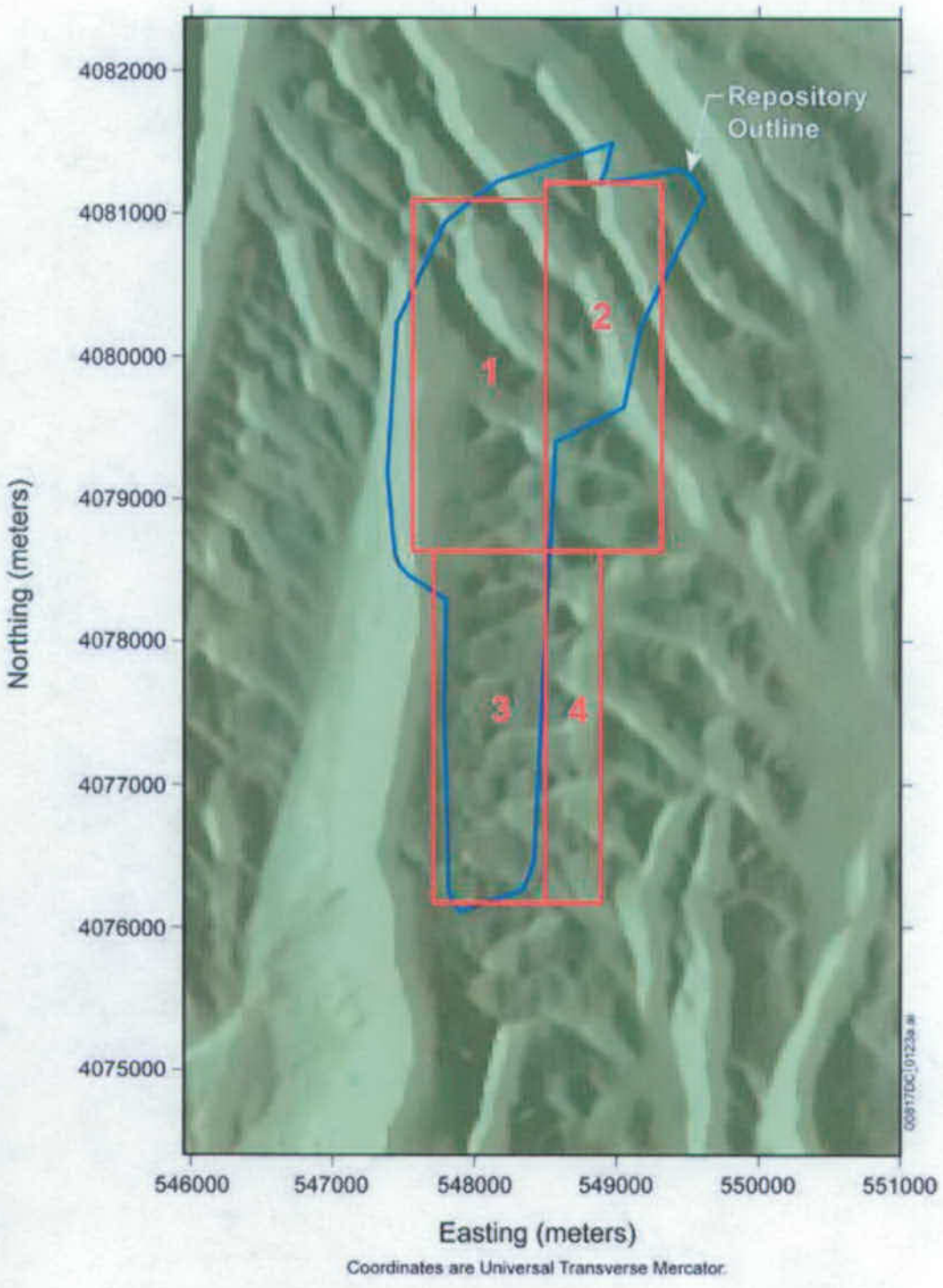

Source: Modified from (SNL 2007 [DIRS 181650], Figure 6-27).

NOTE: The solid blue line shows repository outline and the solid red lines show the four source regions.

Figure 6.3.10-6. Source Regions for Radionuclide Release in the Saturated Zone Flow and Transport Abstraction Model

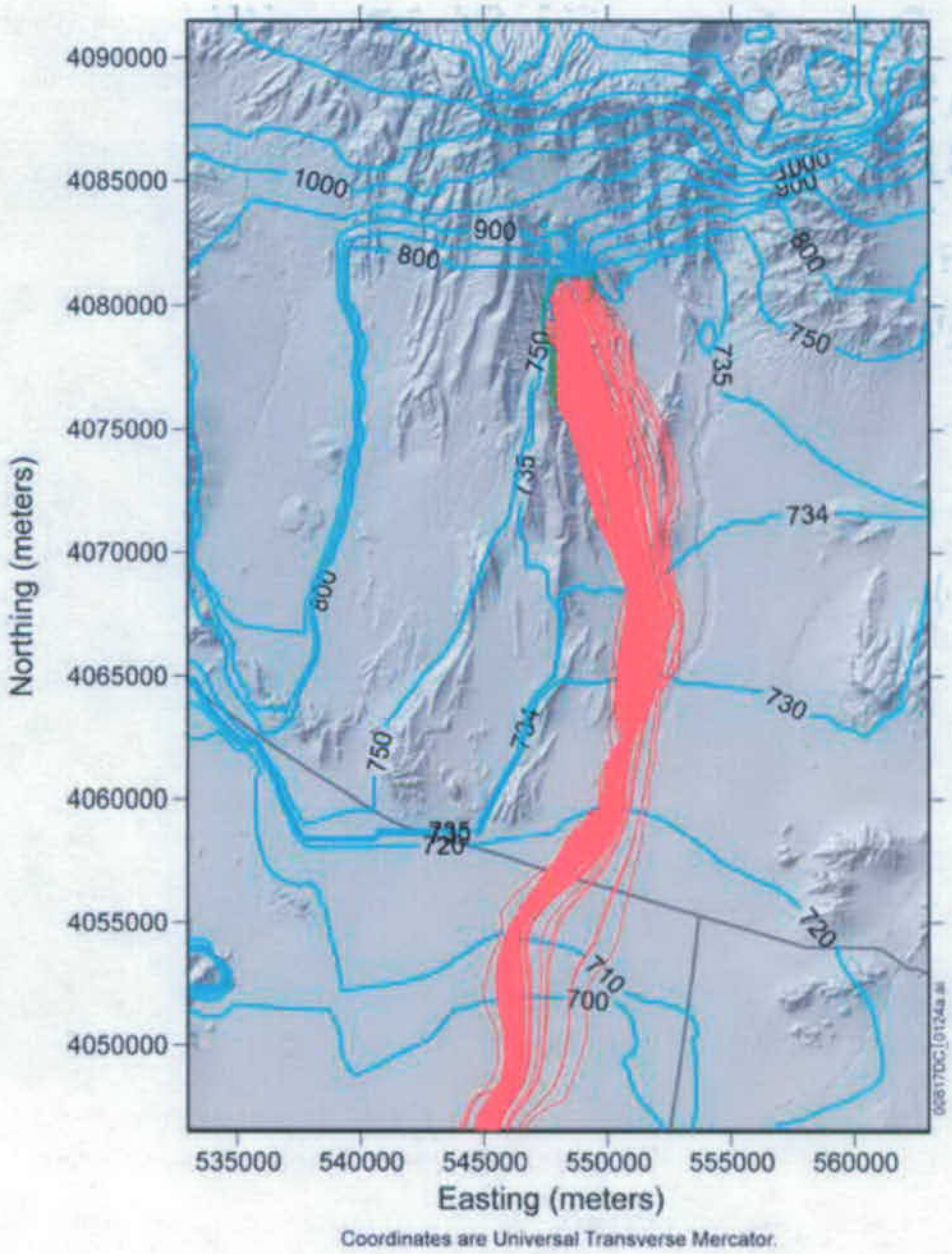

Source: Modified from (SNL 2007 [DIRS 177391], Figure 6-43).

NOTE: Blue lines refer to simulated head contours at the water table in meters; red lines refer to simulated particle paths; direction of flow is from the repository to the accessible environment (bottom of figure).

Figure 6.3.10-7. Map of the 3-D Saturated Zone Model Domain, Showing Simulated Particle Paths

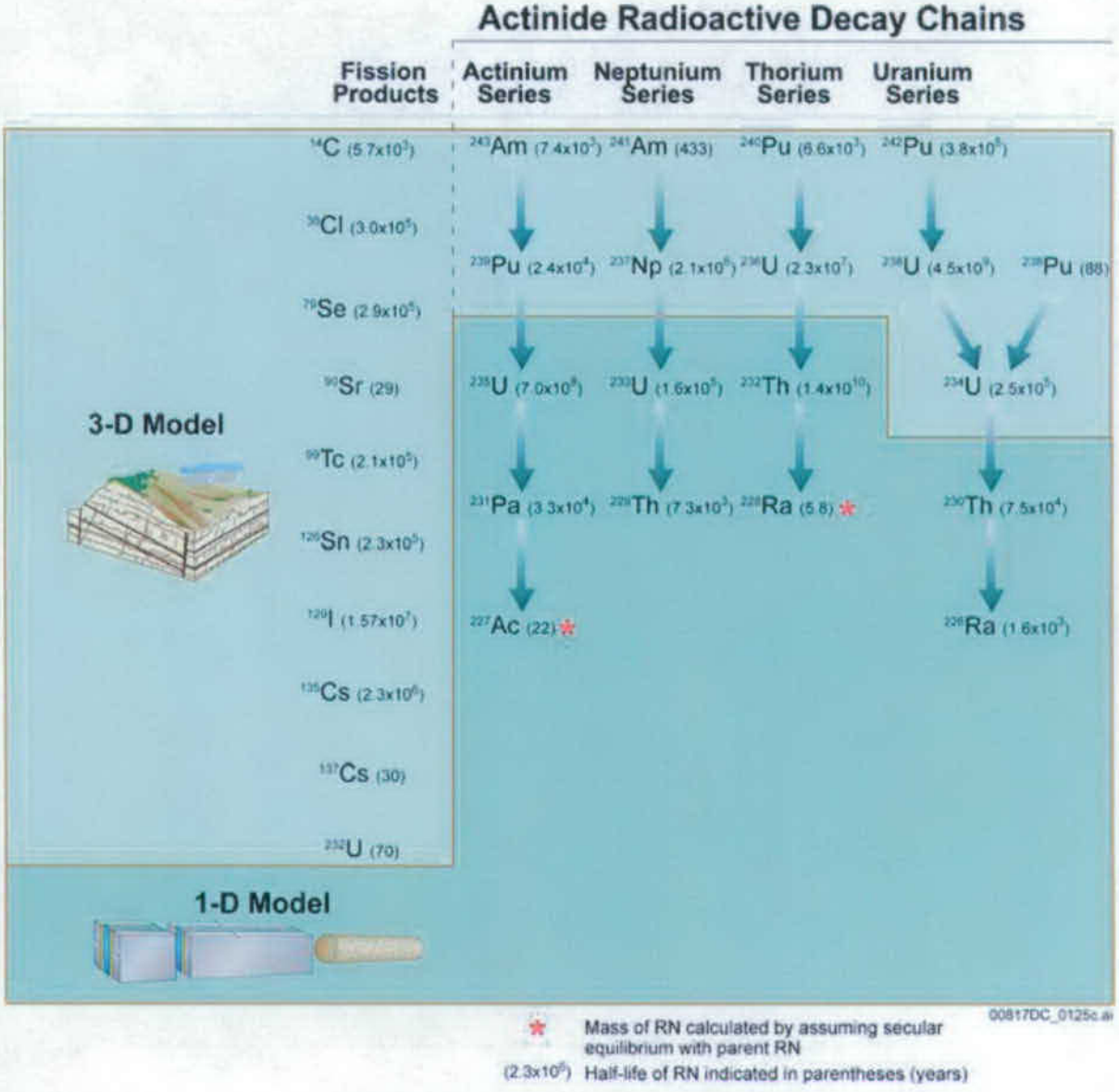

Note: Half-life values are based on DTN: MO0702PASTREAM.001 [DIRS 179925]. The Saturated Zone 3D Abstraction uses slightly different half-life values for ^{79}Se and ^{126}Sn [DIRS 103896 and 164741].

Figure 6.3.10-8. Radionuclide Decay Chains Considered in Saturated Zone Transport Calculations

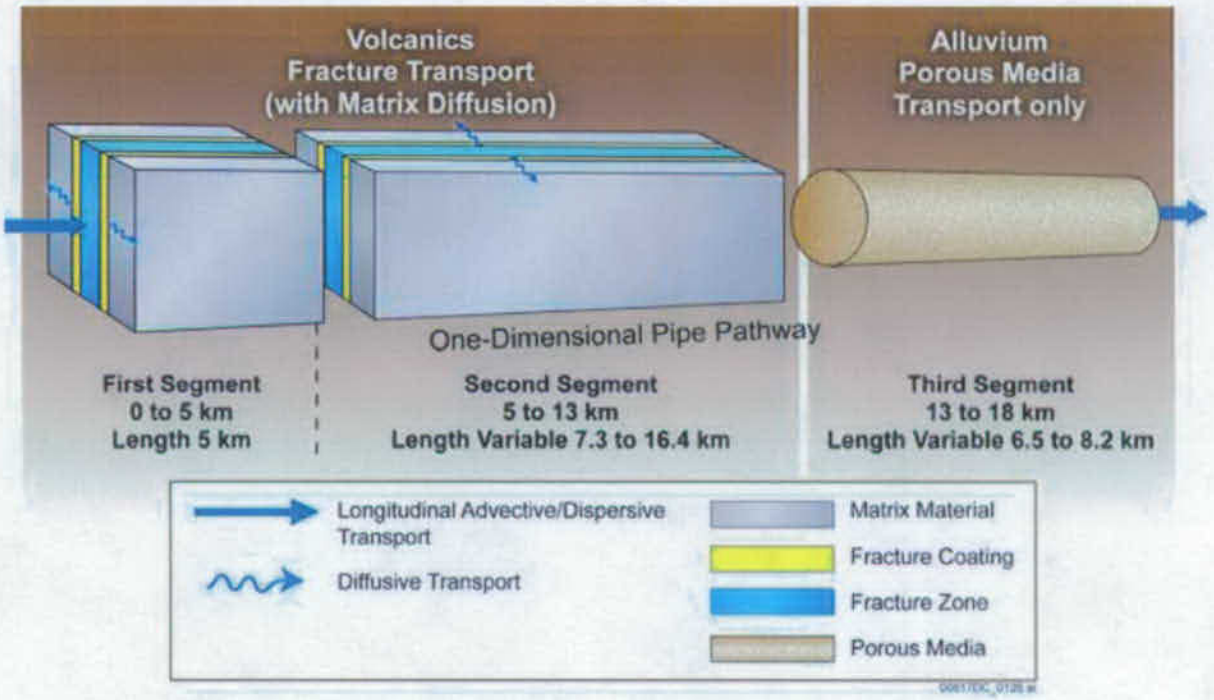

Figure 6.3.10-9. Conceptualization of the 1-D Saturated Zone Flow and Transport Abstraction

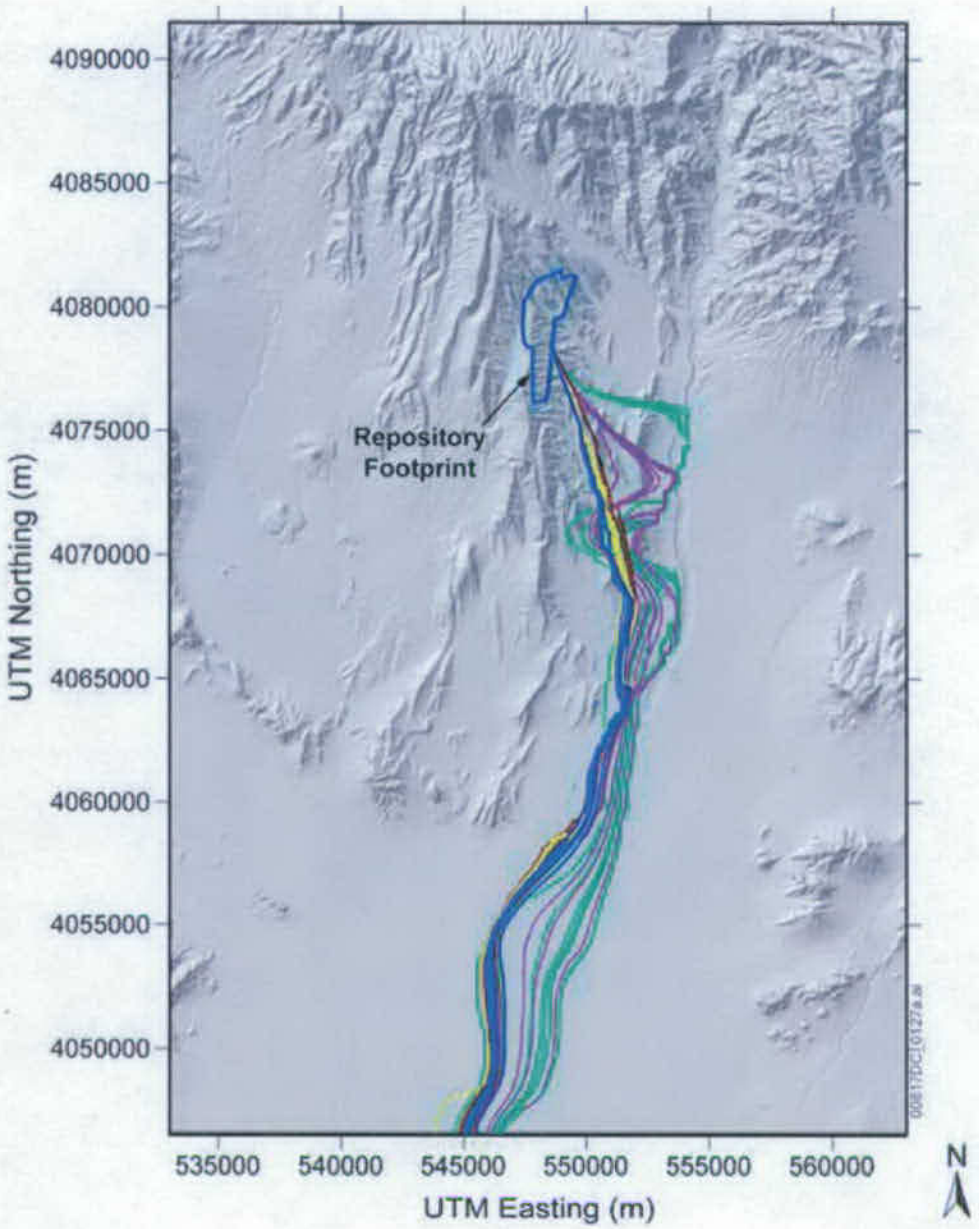

Source: Modified from (SNL 2007 [DIRS 181650], Figure 6-1 [a]).

NOTE: Green, purple, blue, yellow, and red lines show simulated particle paths for particles released from Source Region 1 for horizontal anisotropy values of 0.05, 0.20, 1.0, 5.0, and 20.0, respectively.

Figure 6.3.10-10. Simulated Particle Paths for Different Values of Horizontal Anisotropy in Permeability

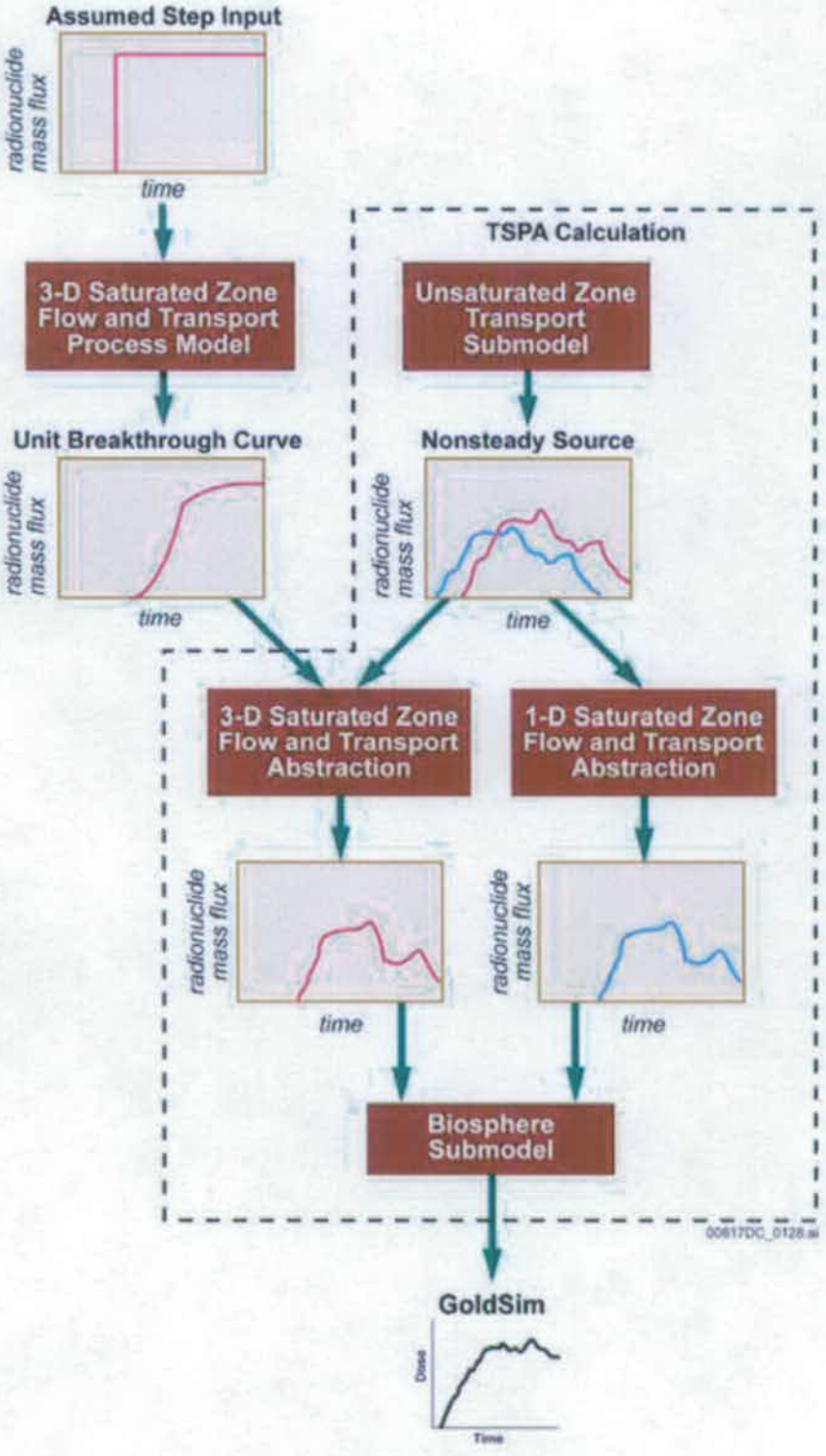

Figure 6.3.10-11. Flow Chart of the Implementation of the Saturated Zone Flow and Transport Submodel in the TSPA-SEIS

INTENTIONALLY LEFT BLANK

6.3.11 Biosphere

The Biosphere Model Component of the TSPA-SEIS estimates the annual radiation dose to the RMEI that is expected to result if radionuclides are released to the accessible environment from the repository after closure. For the set of scenario classes considered in the TSPA-SEIS, there are two possible radionuclide release pathways from the repository to the accessible environment: one through groundwater and one through the atmosphere with volcanic ejections (tephra). These two radionuclide release pathways result in the two exposure scenarios developed in the biosphere. To eliminate possible confusion with the TSPA scenario classes, these two exposure scenarios, which are developed in the biosphere documents, are called the exposure cases in this TSPA-SEIS document. The groundwater exposure case applies to those TSPA-SEIS modeling cases that consider the groundwater transport of radionuclides from the repository at Yucca Mountain to the accessible environment. These modeling cases are included in the Nominal Scenario Class, the Early Failure Scenario Class, the Seismic Scenario Class, the Igneous Intrusion Modeling Case of the Igneous Scenario Class, and the Human Intrusion Scenario. The volcanic ash exposure case applies to the Volcanic Eruption Modeling Case of the Igneous Scenario Class, which considers a volcanic release of radionuclides from the repository at Yucca Mountain.

The Biosphere Process Model documented in *Biosphere Model Report* (SNL 2007 [DIRS 177399]), is implemented external to the TSPA-SEIS and is used to develop the capabilities for calculating annual radiation dose to the RMEI using the TSPA-SEIS. The analyses and abstractions of the two exposure cases in the Biosphere Process Model and reported in *Biosphere Model Report* (SNL 2007 [DIRS 177399]) resulted in the two following data sets giving biosphere dose conversion factors (BDCFs) for the groundwater and volcanic exposure cases as inputs to the TSPA-SEIS:

- Groundwater Biosphere Dose Conversion Factors
- Volcanic Biosphere Dose Conversion Factors.

An additional set of data was developed to estimate the inhalation dose to the RMEI accrued during a tephra deposition.

These BDCFs are used in the Biosphere Model Component of the TSPA-SEIS to calculate the annual dose to the RMEI, required to assess compliance with the post-closure individual protection standard at 10 CFR 63.311 [DIRS 178394]. In addition to the BDCFs, the data used in TSPA-SEIS to demonstrate compliance with the groundwater protection standards (at 10 CFR 63.331 [DIRS 180319] titled *Groundwater Protection Standards Conversion Factors* (DTN: MO0702PAGWPROS.001 [DIRS 179328] are included for two calculations: the estimation of annual dose (whole body and individual organs) from beta and photon emitting radionuclides from consuming two liters of well water daily, and the contribution to the gross alpha activity concentration in groundwater, as defined in 10 CFR 63.331 [DIRS 180319], Table 1), from radionuclides released from the repository.

Figure 6.3.11-1 uses the example of the groundwater exposure case to show the relationships between the Biosphere Model Component, the SZ Flow and Transport Model Component, and the calculation of annual dose for evaluation of compliance with the individual protection

standard and with the groundwater protection standards. Figure 6.3.11-2 summarizes the TSPA-SEIS Biosphere Model Component, its inputs and outputs, and the technical basis for confidence in the Biosphere Model Component. The inputs for the Biosphere Model Component, the two BDCF sets for the groundwater and volcanic cases, and the groundwater protection standards data set are used in the TSPA-SEIS GoldSim model. The inhalation dose factors for the period during the volcanic eruption are used outside the TSPA-SEIS and this use is documented in Section 6.5.2.4.

6.3.11.1 Conceptual Models

The two exposure cases considered in the TSPA-SEIS are illustrated on Figures 6.3.11-3 and 6.3.11-4. For the groundwater exposure case, radionuclides enter the biosphere from one or more wells that extract contaminated groundwater from an aquifer. Human exposure arises from using the contaminated water for domestic and agricultural purposes. Groundwater BDCFs apply to all modeling cases except the Volcanic Eruption Modeling case of the Igneous Scenario Class. In the volcanic ash exposure case, human exposure arises from contaminated tephra deposited on surface soil and the subsequent radionuclide transport from surface soil to other environmental media (e.g., air and plants). Volcanic ash BDCFs apply only to the Volcanic Eruption Modeling Case of the Igneous Scenario Class.

The radionuclides of interest for the Biosphere Process Model, also referred to as the primary radionuclides as tracked in the TSPA-SEIS, depend on the exposure case, and are developed in *Radionuclide Screening,* (SNL 2007 [DIRS 177424]). The treatment of radionuclide transport in the Biosphere Process Model is the same for most radionuclides in both exposure cases. However, two radionuclides, ^{14}C and ^{222}Rn (a short-lived decay product of ^{226}Ra), are modeled differently because of the large amount of stable carbon (^{12}C) in the environment, and the gaseous release from soils of ^{222}Rn and $^{14}CO_2$.

To facilitate modeling for dose calculations the reference biosphere is developed in the *Biosphere Model Report* (SNL 2007 [DIRS 177399], Section 6.1.1). The reference biosphere has to represent the environment inhabited by the RMEI along with associated human exposure pathways and parameters (10 CFR 63.102(i) [DIRS 180319]). Required characteristics of the reference biosphere are the following:

- Features, events, and processes that describe the reference biosphere must be consistent with present knowledge of the conditions in the region surrounding the Yucca Mountain site (10 CFR 63.305(a) [DIRS 180319]).

- DOE should not project changes in society, the biosphere (other than climate), human biology, or increases or decreases of human knowledge or technology. In all analyses done to demonstrate compliance with this part, DOE must assume that all of those factors remain constant as they are at the time of submission of the license application (10 CFR 63.305(b) [DIRS 180319]).

- DOE must vary factors related to the geology, hydrology, and climate at NRC Proposed Rule 10 CFR 63.305(c), [DIRS 178394], and based upon cautious, but reasonable assumptions consistent with present knowledge of factors that could

affect the Yucca Mountain repository system during the period of geologic stability 10 CFR 63.302 [DIRS 178394] and consistent with the requirements for performance assessments specified at 10 CFR 63.342 [DIRS 178394].

- Biosphere pathways must be consistent with arid or semi-arid conditions (10 CFR 63.305(d) [DIRS 178394]).

The RMEI is a hypothetical person who meets the following criteria (10 CFR 63.312 [DIRS 180319]):

a. Lives in the accessible environment above the highest concentration of radionuclides in the plume of contamination.

b. Has a diet and living style representative of the people who now reside in the Town of the Amargosa Valley, Nevada, based on surveys that determine current diets and living styles, and for whom the mean values of these factors are used in the assessments conducted for the Individual Protection Standard at 10 CFR 63.311 [DIRS 178394] and the Individual Protection Standard for Human Intrusion at 10 CFR 63.321 [DIRS 178394].

c. Uses well water with average concentrations of radionuclides based on annual water demand of 3,000 acre-feet.

d. Drinks two liters of water per day from wells drilled into the groundwater from a point above the highest concentration of radionuclides in the plume of contamination.

e. Is an adult with metabolic and physiological considerations consistent with present knowledge of adults.

To meet the requirement at 10 CFR 63.312(b) [DIRS 180319], the dietary and living style characteristics of the RMEI were determined based on surveys of people living in the Amargosa Valley, combined with the 2000 census data (Bureau of the Census 2002 [DIRS 159728]) as well as regional and national information on behavioral patterns and food intake (USDA 2000 [DIRS 154158]), EPA 1997 [DIRS 116135], and ICRP 1994 [DIRS 153705]). Characteristics of the RMEI were developed, using these data, in a separate analysis (BSC 2005 [DIRS 172827]).

Groundwater Exposure Case—In the groundwater exposure case, radionuclides are introduced into the biosphere with groundwater pumped from wells for agricultural and domestic purposes. Once in the biosphere, the radionuclides migrate through various environmental components. During this migration, some of the radionuclides give rise to a dose to the RMEI through one of three exposure pathways: inhalation, ingestion, or external exposure. Each of the exposure pathways is modeled using the diet, living style, and other characteristics of the RMEI. The biosphere model for the groundwater exposure case considered five environmental components (or submodels): soil, air, plant, animal, and fish. The radionuclides in each of these components can result in exposure to the RMEI. Figure 6.3.11-5 illustrates the relationships among the biosphere submodels indicating the migration of radionuclides in the biosphere between the various biosphere submodels starting with the introduction of contaminated groundwater into the

biosphere and resulting in a dose to the RMEI. On Figure 6.3.11-5, arrows point in the direction of radionuclide transfer between biosphere components in the Biosphere Submodel. For example, groundwater is used for human drinking water (to ingestion submodel), animal drinking water (to animal submodel), irrigation water (to soil and plant uptake submodels), fish pond water (to fish submodel), and evaporative cooler water (to air submodel).

The submodels described above are the same for all primary radionuclides with the sole exception of ^{14}C. Special submodels are used to calculate ^{14}C concentrations in the surface soil, air, crops, and animal products because the transfer mechanisms for this radionuclide are different from the others in the model by virtue of the presence of the stable carbon (^{12}C) in the biosphere. The transfer of ^{14}C between submodels follows that for other radionuclides as shown on Figure 6.3.11-5.

The following environmental transport processes are explicitly included in the Biosphere Process Model (SNL 2007 [DIRS 177399], Section 6.3.1.3)

- Radionuclide accumulation in surface soil layers as a result of continuous long-term cultivation using contaminated water
- Resuspension of contaminated soil
- Radionuclide deposition on crop surfaces by dry processes (resuspension of contaminated soil and subsequent adhesion of soil particles onto vegetation surfaces)
- Radionuclide deposition on crop surfaces by interception of contaminated irrigation water
- Removal of surface contamination by weathering processes
- Translocation and retention of contaminants from the deposition site to the edible tissues of vegetation
- Radionuclide uptake from soil by plants through the roots
- Release of radionuclides in gaseous phases, ^{222}Rn and $^{14}CO_2$, from the soil into the air with subsequent inhalation
- Photosynthesis by crops of $^{14}CO_2$ from the atmosphere
- Radionuclide intake by animals through consumption of contaminated feed, water, and soil, followed by transfer to animal products
- Radionuclide transfer from water to air through use of evaporative coolers
- Radionuclide transfer from water to fish.

Exposure to radionuclides in the environment arises when the RMEI's diet and living style give rise to intake of, and external exposure to, radionuclides in environmental media. The Biosphere Process Model then calculates the annual dose from ingestion, inhalation, and external exposure pathways resulting from those intakes and exposures. Table 6.3.11-1 provides a summary of human-exposure pathways for the groundwater exposure case considered in the Biosphere Process Model, including the contributing submodels of the environmental media and the examples of typical activities that may potentially lead to radiation exposure (SNL 2007 [DIRS 177399], Sections 6.3.1.1).

The TSPA-SEIS only considers the release and transport of the primary radionuclides. To avoid underestimating annual dose to the RMEI, the Biosphere Process Model accounts for the decay products of the primary radionuclides after they are introduced into the biosphere. The short-lived decay products with half-lives of less than 180 days are considered to be in secular equilibrium with the parent radionuclide, and their radiation dose contributions are included in the BDCF for the primary radionuclide or a long-lived decay product of the primary radionuclide (SNL 2007 [DIRS 177399] Sections 6.3.1.4 and 6.3.5). The Biosphere Process Model also accounts for the build-up of the primary radionuclides in soil as well as the decay and ingrowth of long-lived decay products in the soil as a result of long-term irrigation (from 25 years up to one thousand years) (SNL 2007 [DIRS 177399] Sections 6.4.1.1 and 6.4.1.2). In this case, the BDCF contributions of the long-lived decay products created in the soil are added to that of the parent primary radionuclides (SNL 2007 [DIRS 177399], Section 6.4.1.2 and Table 6.4-3). The output of the Biosphere Process Model for the groundwater exposure case is the *Groundwater Biosphere Dose Conversion Factors.* This provides the groundwater case BDCFs for all primary radionuclides and the following combination of radionuclides where the effect of longer term decay products are included with the BDCF of the initial primary radionuclide (^{226}Ra and ^{212}Pb), (^{232}Th, ^{228}Ra, and ^{228}Th), and (^{232}U and ^{228}Th). This summation approach allows a realistic assessment of dose to be made if TSPA does not directly consider (i.e., track) all radionuclides.

To support climate change modeling for the TSPA-SEIS, BDCFs for the groundwater exposure case were initially developed for the three climate states (SNL 2007 [DIRS 177399], Sections 6.1.1.2 and 6.11.1.2.2) but were further analyzed for consistency with the regulatory requirements. Future climate forecasts (BSC 2004 [DIRS 170002], Section 6.1) indicate that the climate at Yucca Mountain is reasonably expected to evolve to the cooler, wetter conditions of a glacial transition climate within the first 10,000 years after disposal. Monsoon and glacial-transition (intermediate) climate states are predicted to last until 38,000 years A.P. (after present) (Sharpe 2003 [DIRS 161591], page 57). Over the period of geologic stability, it is expected that there will be more than one climate cycle. 10 CFR 63.305(c) [DIRS 178394] requires that the DOE vary factors related to climate based on cautious, but reasonable assumptions. At the same time, changes in society, the biosphere (other than climate), human biology, or increases or decreases of human knowledge or technology should not be projected (10 CFR 63.305(b) [DIRS 180319]). The climate change in the Biosphere Process Model was thus evaluated and addressed from the perspective of natural processes and from the perspective of the factors that are related to human activity.

In the Biosphere Process Model (SNL 2007 [DIRS 177399], Sections 6.11.1.2), the effect of climate change on the BDCFs for the groundwater exposure scenario was evaluated from the perspective of the factors that are related to the human society, which 10 CFR 63.305(b) [DIRS

180319], directs DOE not to vary in its performance assessments, and those factors that are independent of human activities, which 10 CFR 63.305(c) [DIRS 178394] directs DOE to vary over the period of geologic stability. The climate-related factors that have the largest effect on the BDCFs depend on human activities and the BDCFs are relatively insensitive to the effects of climate changes in the other factors. Furthermore, the BDCFs for the future climate, which is predicted to be cooler and wetter than the present-day climate, are lower than the corresponding present-day climate BDCFs and would result in lower doses to the RMEI. Therefore, using the present-day climate BDCFs represents a conservative choice, meets the requirements at 10 CFR 63.305(a) and (b) [DIRS 180319], and is appropriate for the assessment of doses to the RMEI for the entire period of the geologic stability (SNL 2007 [DIRS 177399], Sections 6.11.1.2). Thus for all TSPA-SEIS dose calculations the BDCFs for the present day climate are used.

Volcanic Ash Exposure Case—The biosphere conceptual model for the ash exposure case uses a similar reference biosphere and human receptor as the groundwater exposure case. The major difference between the exposure cases is that in this case the radionuclide source consists of contaminated tephra deposited on the ground surface and mixed with soil, rather than the multiple uses of contaminated groundwater. Figure 6.3.11-6 illustrates the relationships among the biosphere submodels indicating the migration of radionuclides in the reference biosphere between the various biosphere submodels starting with the introduction of contaminated tephra into the reference biosphere and resulting in a dose to the RMEI. On Figure 6.3.11-6, arrows point in the direction of radionuclide transfer between components in the Biosphere Submodel.

The following environmental transport processes are explicitly included in the Biosphere Process Model for the ash exposure case (SNL 2007 [DIRS 177399], Section 6.3.2.1 and 6.3.2.6):

- Resuspension of contaminated soil and tephra from soils both undisturbed and from activities that disturb the soil surface
- Dry deposition of radionuclides on crop surfaces, including resuspension of contaminated soil and subsequent adhesion of soil particles on crop surfaces
- Removal of surface contamination by weathering processes
- Translocation and retention of contaminants from the site of deposition to the edible portions of crops
- Radionuclide uptake by crops through the roots
- Radionuclide intake by animals through consuming contaminated feed and soil, and subsequent transfer to animal products
- Release of radon (^{222}Rn) from the soil.

Because the groundwater is contamination free in the volcanic ash exposure case, fewer exposure pathways are considered, as shown in Table 6.3.11-2, than for the groundwater exposure case. As described in *Biosphere Model Report,* (SNL 2007 [DIRS 177399], Section 6.3.2.1), the

volcanic ash exposure case does not include a contribution to annual dose from ingestion of drinking water, ingestion of locally produced fish, and inhalation of indoor aerosols generated by evaporative coolers. In addition, the dose contribution from ^{14}C in solid or gaseous forms is not considered because ^{14}C was assessed to be a negligible contributor to dose in the volcanic ash exposure case in *Radionuclide Screening,* (SNL 2007 [DIRS 177424], Tables 6-7 and 6-8). The consideration of short-lived non-primary radionuclide decay products in the volcanic ash exposure case is the same as discussed above for the groundwater exposure case, i.e., their contributions to dose are included in the BDCFs of the parent radionuclide.

The analysis of BDCFs for the volcanic ash exposure case (SNL 2007 [DIRS 177399], Section 6.12.1.2) indicates that the results of the Biosphere Process Model for the volcanic ash exposure case are relatively insensitive to climate change (BDCF changes over climate are less than 1 percent). Therefore, one set of BDCFs, applies to all climate states considered in the TSPA-SEIS.

6.3.11.2 TSPA-SEIS Abstraction

The objectives of the Biosphere Process Model and analyses are to develop the capabilities and associated data sets to allow TSPA to evaluate compliance with the postclosure individual protection standard at 10 CFR 63.311 [DIRS 178394], the groundwater protection standards at 10 CFR 63.331 [DIRS 180319] and the individual protection standard for human intrusion (10 CFR 63.321 [DIRS 178394]). In the case of the individual protection standard this information is identified in *Biosphere Model Report* (SNL 2007 [DIRS 177399], Section 8.1.1). The mathematical abstraction and the required BDCFs for the two exposure cases needed to calculate annual dose to the RMEI from radionuclide concentrations in groundwater or soil at the accessible environment are presented in *Groundwater Biosphere Dose Conversion Factors*; and *Volcanic Biosphere Dose Conversion Factors*. In addition, dose factors to calculate inhalation exposure during the volcanic eruption from predictions of atmospheric concentrations of radionuclides are provided in *Inhalation Dose Factors.* The dose factors are used outside of the TSPA model to calculate inhalation dose during a volcanic eruption (Section 6.5.2.4).

The data required to demonstrate compliance with the groundwater protection standards are given in the *Biosphere Model Report* (SNL 2007 [DIRS 177399] Section 8.1.1) presents the data that allows TSPA to use radionuclide concentration in groundwater to evaluate the whole body and individual organ doses from consumption of two liters of water per day, and to calculate alpha particle activity in groundwater as per 10 CFR 63.331 [DIRS 180319]. These data are provided in *Groundwater Protection Standards Conversion Factors* DTN: MO0702PAGWPROS.001 [DIRS 179328].

To incorporate uncertainty into the TSPA-SEIS input, BDCFs were calculated in a manner to propagate the uncertainties of the biosphere input parameters. This was accomplished by conducting a series of 1,000 stochastic model realizations. Uncertain input parameters to the Biosphere Process Model were sampled using Latin hypercube sampling for consistency with the sampling technique used for the TSPA-SEIS as discussed in this report. The resulting set of BDCFs incorporates the uncertainty from those input parameters. The sampling was structured such that for a given iteration the sampled value for each non-radionuclide specific parameter was the same for every radionuclide. This approach ensured that the correlation between BDCFs

arising from the commonality of receptor and environmental characteristics was retained. The full set of BDCFs consists of a BDCF for each primary radionuclide for each Biosphere Process Model realization. As listed in Table 6.3.7-2, there are 31 radionuclides for the groundwater exposure case and 27 radionuclides for the volcanic ash exposure case. Table 6.3.11-3 lists the TSPA-SEIS parameters used to represent groundwater BDCF uncertainty in the TSPA-SEIS. In addition to the BDCFs for the primary radionuclides, the BDCF data set also contains composite values for cases where one primary radionuclide with a relatively short half-life is combined with the BDCF for the much longer-lived parent that is also a primary radionuclide; this approach allows TSPA the option to only track the parent without systematic underestimation of dose.

Summaries of the parameters and their distributions used to develop BDCFs for the groundwater and volcanic eruption cases are provided in *Biosphere Model Report* (SNL 2007 [DIRS 177399], Tables 6.6-2 and 6.6-3).

Calculation of Annual Dose to the RMEI for the Groundwater Exposure Case—The TSPA-SEIS calculates the total annual dose to the RMEI at a given time using the set of BDCFs and radionuclide concentrations in the groundwater used by the RMEI. The total annual dose is the sum of the annual doses from all radionuclides tracked in the TSPA-SEIS as is given in *Biosphere Model Report* (SNL 2007 [DIRS 177399], Sections 6.4.10.4 and 6.11.3):

$$D_{total}(t) = \sum_i BDCF_i \times Cw_i(t) \qquad \text{(Eq. 6.3.11-1)}$$

where

$D_{total}(t)$ = time-dependent total annual dose from groundwater to the RMEI resulting from the release of radionuclides from the repository. This includes contributions from all radionuclides considered in the TSPA-SEIS (Sv/yr).

$BDCF_i$ = groundwater biosphere dose conversion factor for radionuclide i (Sv/yr per Bq/m^3).

$Cw_i(t)$ = time-dependent activity concentration of radionuclide i in groundwater at the RMEI location (Bq/m^3).

Calculation of Alpha Activity Concentration in Groundwater—The methods and the conversion factor values described in *Biosphere Model Report* (SNL 2007 [DIRS 177399], Section 6.15.1.1) are used to calculate the gross alpha activity concentration in groundwater for evaluation of compliance with the groundwater protection standards at 10 CFR 63.331 [DIRS 180319]. Natural background activity concentrations are added to calculated values for comparison with the limit for combined ^{226}Ra and ^{228}Ra activity concentration in groundwater, and with the limit for gross alpha activity concentration. The alpha particle activity concentration in the groundwater is calculated in the TSPA-SEIS using the number of alpha particles per decay of each primary radionuclide and using the following equation (SNL 2007 [DIRS 177399], Equation 6.15-1, Table 6.15-3):

$$C_\alpha(t) = \sum_i Cw_i(t)\, N\alpha_i \qquad \text{(Eq. 6.3.11-2)}$$

where $Cw_i(t)$ (Bq/m^3 or pCi/L) is defined above and

$C_\alpha(t)$ = the time-dependent total alpha particle activity concentration in groundwater (Bq/m^3 or pCi/L)

$N\alpha_i$ = number of alpha particles emitted per one decay of a primary radionuclide *i*.

Contributions from radon and uranium are excluded when calculating $N\alpha_i$, as directed in 10 CFR 63.331 [DIRS 180319].

Calculation of Beta-Photon Dose from Drinking Two Liters of Water per Day—The beta-photon doses to the whole body and individual organs are calculated using conversion factors from *Biosphere Model Report* (SNL 2007 [DIRS 177399], Table 6.15-6); and the following equation (SNL 2007 [DIRS 177399], Equation 6.15-4):

$$D(t) = \sum_i Cw_i(t)\, CF_i \qquad \text{(Eq. 6.3.11-3)}$$

where $Cw_i(t)$ (Bq/m^3) is defined above and

$D(t)$ = time-dependent total annual dose for an individual organ or for the whole body from beta-gamma emitters in the groundwater from daily consumption of 2 liters of water (Sv/yr)

CF_i = conversion factor for calculating beta-photon annual dose for an individual organ or for the whole body from radionuclide *i* from daily consumption of 2 liters of water (Sv/yr per Bq/m^3).

The conversion factors are provided for the following organs (23) and for the whole body:

Adrenals	Muscle
Bone Surface	Ovaries
Brain	Pancreas
Breast	Red Bone Marrow
Stomach Wall	Skin
Small Intestine Wall	Spleen
Upper Large Intestine Wall	Testes
Lower Large Intestine Wall	Thymus
Kidneys	Thyroid
Liver	Uterus
Extrathoracic Airways	Urinary Bladder Wall
Lung	Whole Body

Calculation of Annual Dose to the RMEI for the Volcanic Ash Exposure Case—The TSPA-SEIS calculates the total annual dose for the volcanic ash exposure case using the following equations (SNL 2007 [DIRS 177399], Section 6.12.3 and Equation 6.12-1):

$$D_{total}(t,T) = \sum_i D_{all\ pathway,i}(t,T)$$

and

$$D_{all\ pathway,i}(t,T) = BDCF_{ext,ing,Rn,i}\ Cs_i(t) + \left(BDCF_{inh,v,i} f(t-T) + BDCF_{inh,p,i}\right) Cs_{mc,i}(t)$$

(Eq. 6.3.11-4)

where

$D_{total}(t,T)$ = total annual dose from all radionuclides at time t-T after a volcanic release of radionuclides from the repository at time t after repository closure (Sv/yr)

$D_{all\ pathway,i}(t,T)$ = all-pathway annual dose for primary radionuclide i at time t-T after a volcanic release of radionuclides from the repository at time t after repository closure (Sv/yr)

$BDCF_{ext,ing,Rn,i}$ = BDCF component for external exposure, ingestion, and inhalation of radon decay products for primary radionuclide i (Sv/yr per Bq/m^2)

$Cs_i(t)$ = areal radionuclide concentration in a specified depth of surface soil at time t (yr) after the repository closure (Bq/m^2) calculated in TSPA-SEIS

$BDCF_{inh,v,i}$ = BDCF component representing average early-time increase in inhalation exposure in the first year after a volcanic eruption; used in calculation of short-term inhalation exposure at post-eruption level of mass loading in excess of nominal mass loading for primary radionuclide i (Sv/yr per Bq/kg)

$BDCF_{inh,p,i}$ = BDCF component for long-term inhalation at nominal level of mass loading for primary radionuclide i (Sv/yr per Bq/kg)

$f(t-T)$ = decay function describing reduction of the annual average mass loading with time at time t-T following a volcanic

$Cs_{mc,i}(t)$ = activity concentration of radionuclide i per unit mass of soil in the resuspendable layer of surface soil (critical thickness) at time t (yr) after the repository closure (Bq/kg).

The time function, $f(t)$, accounts for the reduction of mass loading in the years immediately following a volcanic eruption. The mass loading decreases exponentially with time as (SNL 2007 [DIRS 177399], Equation 6.12-3):

$$f(t-T) = e^{-\lambda(t-T)} \qquad \text{(Eq. 6.3.11-5)}$$

where

λ = mass loading decrease rate (a constant) (1/yr)

$t\text{-}T$ = time after a volcanic eruption at T (years); $t\text{-}T = 0$ is the first year after a volcanic eruption.

The mass loading decrease rate is provided by the Biosphere Process Model as an input parameter implemented in the TSPA-SEIS.

Both source terms used in the calculation of doses (Equation 6.3.11-4), i.e., the areal radionuclide concentration in surface soil, $Cs_i(t)$, and the mass radionuclide concentration in the resuspendable soil layer, $Cs_{mc,i}(t)$, are calculated in the TSPA by weighting the appropriate radionuclide concentrations by the respective expected areas of the distributary channels and the interchannel divides at the location of the RMEI. The radioactive waste mass concentrations in the resuspendable layer of soil, $Cs_{mc,i}(t)$, and in the surface soil, $Csi(t)$, are determined from the results of the ASHPLUME and FAR models as discussed in Section 6.5.2.2.

These models produce the results in terms of waste volumetric concentration. The waste volumetric concentration can be converted to waste mass concentration in the soil by dividing it by the density of the resuspendable layer, ρ_c. In the interchannel divides, the density of the resuspendable layer, ρ_c, can be calculated from the known tephra thickness, d_a, and density, ρ_a, and surface soil density, ρ_s, (SNL 2007 [DIRS 177399], Equation 6.12-2) as:

$$\rho_c = \frac{d_a\,\rho_a + (d_c - d_a)\,\rho_s}{d_c} \qquad \text{when } d_a < d_c \text{ and}$$

$$\rho_c = \rho_a \qquad \text{when } d_a \geq d_c \qquad \text{(Eq. 6.3.11-6)}$$

where

ρ_c = bulk density of resuspendable layer of surface soil, including tephra (kg/m^3)

d_c = thickness of resuspendable soil layer, i.e., the critical thickness (m)

d_a = thickness of initial tephra layer (m)

ρ_a = bulk density of tephra (kg/m^3)

ρ_s = bulk density of the original surface soil (i.e., without tephra) (kg/m^3)

The TSPA model keeps track of the radionuclide activity concentration per unit mass of waste and apportions the correct activity of each radionuclide to the known waste concentration in the surface soil.

The sampling results of bulk density and tillage depth of the surface soil for individual biosphere model realizations are in part of the modeling. In the channels, where the tephra is mixed with soil and diluted, the density of resuspendable layer, ρ_c, can be approximated by the density of soil, ρ_s (SNL 2007 [DIRS 177399], Section 6.12.3).

Calculation of Inhalation Dose Accrued During the Volcanic Eruption—To calculate the inhalation dose to the RMEI during the eruption phase of a volcanic event (usually lasting less

than a year), dose factors for the inhalation exposure pathway are used instead of the all pathway BDCFs. The daily dose from inhaling a specific radionuclide during the tephra fall from a volcanic eruption was calculated external to the TSPA-SEIS. The total daily inhalation dose, D_{inh}, from concentrations of primary radionuclides in the air was calculated as (SNL 2007 [DIRS 177399], Section 6.15.2.2, Equation 6.15-9):

$$D_{inh} = \sum_i D_{inh,i} = \sum_i DF_i \times Ca_{i,outdoor} \quad \text{(Eq. 6.3.11-7)}$$

where

$D_{inh,i}$ = daily inhalation dose (i.e., committed dose from one day's inhalation intake) for a primary radionuclide i (Sv/d)

DF_i = inhalation dose factor for a primary radionuclide i (Sv/d per Bq/m^3)

$Ca_{i,outdoor}$ = one day average activity concentration of a primary radionuclide i in outdoor air (Bq/m^3).

The inhalation of airborne radionuclides in tephra once they are deposited on the ground and subsequently resuspended is included in the BDCFs. The calculation results show that the probability-weighted annual dose from inhalation of airborne radionuclides in tephra during the deposition phase is lower by several orders of magnitude than the probability-weighted annual dose caused by tephra deposited on the ground. Therefore, the contribution of an eruptive phase dose is neglected in the TSPA-SEIS. See Section 6.5.2.4 for details of this calculation and comparison with the TSPA-SEIS results.

6.3.11.3 TSPA-SEIS Implementation

The Biosphere Process Model provides stochastic BDCFs for the calculation of the annual dose to the RMEI. In addition, deterministic conversion factors for beta and photon dose from drinking two liters of water per day, and the number of alpha particles emitted per decay of primary radionuclides, are provided as inputs to the TSPA-SEIS. The BDCFs are transferred into the TSPA-SEIS in the form of one-dimensional tables, one for each radionuclide, that consist of 1,000 rows, which represent individual model realizations. The conversion factors used to calculate beta-photon dose are in a two-dimensional look-up table consisting of 19 columns representing each of the relevant, i.e., beta-photon emitting, primary radionuclides and three additional columns for the combination of long- and short-lived radionuclide combinations. The table has 24 rows that correspond to individual organs and the whole body. In the case of alpha activity calculations, a look-up table is provided that gives the total number of alpha particles attributable to one radioactive decay of each of the (16) primary radionuclides that include alpha emitters in their short-lived decay chains.

The annual dose to the RMEI is calculated in the TSPA-SEIS Biosphere Model Component using the BDCFs that convert radionuclide concentrations in groundwater or soil-tephra mixture to an annual all-pathway dose (based on Equations 6.3.11-1 and 6.3.11-4). A discrete distribution that represents the epistemic model uncertainty, whose output is an equally probable

integer from 1 to 1,000 inclusive, is used to randomly select a particular sequence of realizations from the BDCF tables. For the groundwater exposure case, one set of BDCFs, the set corresponding to the present-day climate, is used throughout the modeling time period of the TSPA-SEIS (Section 6.3.11.1). The selected BDCFs are then multiplied by the radionuclide concentrations provided by the SZ Flow and Transport Model Component (or by concentrations in tephra as calculated by FAR) to compute the annual dose (Equations 6.3.11-1 and 6.3.11-4). Probability weighting of dose is calculated in the Biosphere Model Component for the Nominal Early Failure (Section 6.4) and Igneous Intrusion Modeling Cases (Section 6.5.1), and the Seismic Scenario Class (Section 6.6). The probability weighting for the Volcanic Eruption Modeling Case is handled in the source term calculation (Section 6.5.2).

The calculations for the groundwater protection standards are based on the activity concentration of each primary radionuclide in groundwater, as calculated from radionuclide concentrations provided by the SZ Flow and Transport Model Component. The alpha particle activity concentration in water and the beta-photon dose from drinking two liters of water per day are then calculated using Equations 6.3.11-2 and 6.3.11-3, respectively. Equations 6.3.11-5 and 6.3.11-6 are implemented in the Volcanic Ash Exposure Submodel under the Volcanic Eruption Modeling Case (Section 6.5.2.2). As noted previously, the inhalation dose during a volcanic eruption period (Equation 6.3.11-7) was not implemented in the TSPA-SEIS because, as a result of external evaluation, it was determined that the contribution from this pathway to the probability-weighted annual dose was insignificant.

6.3.11.4 Model Component Consistency and Conservatism in Assumptions and Parameters

To enhance understanding of the complex interactions within the TSPA-SEIS, a discussion of consistency among model components and submodels and identification of conservative assumptions in abstractions, process models, and parameter sets supporting the biosphere are discussed as follows.

6.3.11.4.1 Consistency of Assumptions

It is important to ensure that the parameters and assumptions in each model component or submodel of the TSPA-SEIS are consistent. The first discussion concerns tephra particle sizes during eruptive atmospheric transport and when they are used for the inhalation dose calculation. The second applies to the groundwater release case and concerns the elemental partition coefficients used for transport calculations in the UZ and SZ and those employed in the Biosphere Submodel (soil submodel).

Volcanic Tephra Particle Size—In the Biosphere Process Model, the reference biosphere describes the environment around the location of the RMEI (10 CFR 63.312 [DIRS 180319]), which is located about 18 km south of the repository ([DIRS 180319], III Public Comments and Responses, 3.5, p. 55750), as specified in the definition of the *Controlled Area* found at 10 CFR 63.302 [DIRS 180319]. The size of resuspended particles used to calculate the inhalation component of the dose to the RMEI is smaller than the particle size in the ASHPLUME code used to predict atmospheric transport (advection and diffusion) and surface deposition (gravitational settling) of the tephra from a volcanic eruption. After the eruption, fluvial

processes redistribute the tephra from the immediate vicinity of the eruption down Fortymile Wash to the location of the RMEI. This Tephra Redistribution Submodel (Section 6.5.2.1.3) does not explicitly consider mechanical processes that generate smaller tephra particles nor is any account taken of subsequent weathering processes. However, the redistribution model does account for the diffusion of radionuclides into the adjacent soil or soil-tephra mixture. This diffusion process is calibrated from measured ^{137}Cs profiles on channels and inter-channel divides of the upper Fortymile Wash alluvial fan. This diffusion process models the migration of the contaminants in the tephra to the local soil thereby providing a source of resuspendable and inhalable contaminated particles. The inhalation dose is calculated in the Biosphere Process Model by using inhalation dose coefficients for 1-μm particles, while the ASHPLUME code predictions concern particles greater than 15 to 30 μm. This is because of ASHPLUME's inability to accurately represent the transport of tephra particles of mean diameter less than approximately 15 μm (Jarzemba et al. 1997 [DIRS 100987], Section 2.1; and SNL 2007 [DIRS 177431], Section 1.3.1). Because the typical mean diameter of tephra particles after an eruption is generally much larger than 15 μm, the model is applicable for calculating the distribution of the majority of the mass of potential tephra and radionuclide releases from a possible future eruption at Yucca Mountain (SNL 2007 [DIRS 177431], Section 1.3.1). However, it does not address well the particles in the respirable (less than 4 μm) and thoracic (less than 10 μm) size range, which are more important for the evaluation of inhalation doses (BSC 2005 [DIRS 172827], Section 6.5.5.1). This apparent difference in the particle size distribution of tephra deposited at the location of the RMEI and the particle size distribution used to calculate inhalation dose to the RMEI becomes less significant with time as tephra particles weather and radionuclides diffuse and attach to small soil particles. The processes that cause redistribution of the contaminated tephra after the volcanic eruption, as well as other natural processes and human activities at the location of the RMEI, may change the initial particle size distribution of deposited tephra.

Effect of Volcanic Tephra Particle Size on TSPA—A study was completed in *Characteristics of the Receptor for the Biosphere Model* (BSC 2005 [DIRS 172827], Section 6.5.5.2) regarding the effect of differences in tephra particle size on predicted consequences. It was concluded that "...the application of dose coefficients for particles with activity median aerodynamic diameter of 1 μm will not underestimate the doses from inhalation of resuspended material and that these dose coefficients are adequate for use in the biosphere model."

Elemental Partition Coefficients—Values of the partition coefficients for the soluble species considered in the TSPA-SEIS play a significant role in quantifying the details of their transport. Both components of the natural barrier beneath the repository (UZ and SZ) make use of partition coefficients measured in the appropriate geologic units (for UZ see BSC 2004 [DIRS 170035], Section 6.2.3 where partition coefficients are refered to as distribution coefficients and for SZ see SNL 2007 [DIRS 181650] Section 6.5.1.2 where the equivalent term sorption coefficient is used). The biosphere soil submodel also requires partition coefficients to ascertain radionuclide build-up in soil to establish plant uptake as well as resuspension of activity into the atmosphere for inhalation. The partition coefficients used by the biosphere were developed independently from those used in the natural barriers and were based on published results and analyses

appropriate for the surface soil types present in the Amargosa Valley farming area (*Soil-Related Input Parameters for the Biosphere Model* [DIRS 179993], Section 6.3).

Effect of Elemental Partition Coefficients on TSPA—The soil layers considered in the Biosphere Submodel are derived from the local underlying parent material that formed the alluvium of the SZ and may initially have had like values for the partition coefficient as the unconsolidated parent material. However, the slow and lengthy soil formation process that generates the top soil results in physical and chemical (weathering) changes to the material as well as incorporation of organic matter. These changes include a large increase in the specific surface area (area per unit mass) available to adsorb suitable elements. Thus it is to be expected that partition coefficients for soils are different (larger) that those applicable to the parent materials. By using the reported range of values for a particular soil type (fractional combinations of clay, sand and silt) found in Amargosa Valley, the Biosphere Submodel provides TSPA-SEIS the capability to estimate dose while incorporating the reported uncertainty without the concern of underestimating the dose.

6.3.11.4.2 Identification of Conservatisms in Submodels and Abstractions

Dose Coefficients for Internal Exposure—The dose coefficients for internal exposure (inhalation and ingestion), used to calculate the BDCFs are the most conservative of the values provided in the source reference (EPA 2002 [DIRS 175544]) for a given radionuclide. Different dose coefficient choices correspond to different gastrointestinal absorption fractions for ingestion and in the case of inhalation differing transfer fractions from the lung to blood stream for different chemical compounds of a given radionuclide. The conservative values were used because of uncertainty in the final chemical/physical form of the radionuclides supplied to the biosphere from groundwater and the uncertainty in the subsequent evolution of the chemical/physical form in the biosphere (SNL 2007 [DIRS 177399], Sections 6.4.8.5 and 6.4.9.6). This conservatism results in either a realistic estimate of dose or an overestimation of dose.

Dose Coefficients for External Exposure to Contaminated Soil—For calculating the external dose from exposure to contaminated soil for the groundwater case, the dose coefficients for an infinite depth of contamination were used. This approach allowed the time evolution of soil build-up to be considered only in the tillage depth while accounting for the external exposure to radionuclides that could have been leached from the surface soil into the deep soil. Use of these dose coefficients is reasonable yet conservative as dose coefficients for an infinite depth and those for a 15-cm depth (note that tillage depths extend up to 30 cm) differ by less than 10 percent for most primary radionuclides (EPA 2002 [DIRS 175544]). Only for radionuclides with strong gamma emissions, such as ^{226}Ra and ^{137}Cs, do dose coefficients exhibit a larger difference for these two depths. The use of dose coefficients for an infinite depth cannot underestimate dose.

Roots in Surface Soil—All crop roots are considered to be in the surface soil layer i.e., the soil layer extending down to the tilling depth. For many crops, the root systems can extend to below the tillage depth. This approach effectively assumes (conservatively) that all roots, the source of radionuclide uptake for plants, are exposed to a radionuclide concentration as calculated for the tillage region.

Resuspended Volcanic Ash—Radionuclide concentrations in the air were calculated separately for cultivated and uncultivated lands. The concentration of radionuclides in cultivated (i.e., tilled) soil was used to calculate concentrations of radionuclides in crops and animal products. The concentration of radionuclides in uncultivated soil was used to calculate inhalation and external exposure to the RMEI. This was done because for most of the land area the soil in the reference biosphere would not be cultivated. Using radionuclide mass concentrations of uncultivated soil to calculate inhalation and external exposure is a conservative approach because the concentrations in uncultivated soil would be higher than in cultivated soil where tilling causes additional dilution. Because uncultivated lands would not be disturbed by agricultural activities, tephra would not mix quickly with surface soil and tephra would remain on or near the soil surface where it is available for resuspension (SNL 2007 [DIRS 177399], Section 6.3.2.6). This conservatism results in the overestimation of dose.

External Exposure from Tephra on the Ground Surface—Unlike the groundwater exposure scenario, where soil contamination could be deep, tephra and associated radionuclides could be distributed on or near the soil surface and the source for external exposure could be a thin layer of uncultivated soil on the ground surface. Thus external exposure was evaluated using the dose coefficients for exposure to contaminated ground surface (EPA 2002 [DIRS 175544]) rather than volumetric concentrations. This modeling approximation was reasonable because there is considerably more uncultivated land than cultivated land in Amargosa Valley (BSC 2004 [DIRS 177101], Section 6.2), and the mixing of tephra on uncultivated lands would be limited. The effects of radiation attenuation in the soil and tephra were conservatively minimized (SNL 2007 [DIRS 177399], Section 6.3.2.4). This conservative assumption results in the overestimation of dose in cases where radionuclides are distributed throughout the soil where their radiations are attenuated by the soil layer between the point of emission and the RMEI. For radionuclides with a significant dose contribution from external exposure, such as ^{137}Cs and ^{126}Sn this conservatism could overestimate annual dose predictions.

6.3.11.5 Alternative Conceptual Model(s) for Biosphere

Section 6.2 outlines the general consideration and treatment of ACMs used to support the TSPA-SEIS. Brief descriptions of the biosphere ACMs as discussed in *Biosphere Model Report* (SNL 2007 [DIRS 177399], Section 6.3.3) and summarized in Table 6.3.11-4 are presented below.

ACM for Radon Release from Soil—The conceptual model for radon used in the Biosphere Process Model is based on a radon release factor from radium-contaminated soil. The ACM relies on modeling radon transport in the soil and the atmosphere (Yu et al. 2001 [DIRS 159465], Appendix C). A numerical comparison between the selected model and the ACM shows that the resulting ^{222}Rn concentrations in air are comparable (SNL 2007 [DIRS 177399], Section 7.4.3.1). The method used in the Biosphere Process Model was selected because it required fewer parameters. The more complex ACM did not produce results different enough to warrant its implementation (SNL 2007 [DIRS 177399], Section 7.3.2.2).

ACM for Evaporative Cooler—The conceptual model for evaporative coolers used in the Biosphere Process Model was based on the mechanical operation of evaporative coolers and considered the generation of aerosols as air is forced through a wet, porous surface. An ACM would be to calculate radionuclide concentrations based on differences in absolute humidity

between indoor and outdoor air caused by the operation of evaporative coolers. An evaluation of these two methods showed that they produced results of air activity concentrations that were deemed to be acceptably equivalent (SNL 2007 [DIRS 177399], Section 7.4.3.2).

ACM for Direct Deposition of Irrigation Water on Plant Surfaces—The Biosphere Process Model considers a fraction of radionuclides in irrigation water to be directly translocated into edible plant parts with accumulation and weathering occurring during the growing period. An ACM developed in BIOMASS ERB2A (BIOMASS 2003 [DIRS 168563]) considers this process in two sequential steps: (1) movement of deposited radionuclides from external plant surfaces into the plant tissues and (2) movement of radionuclides from plant tissues into edible parts of the crop. This ACM applies weathering to contaminants that remain on external plant surfaces and also considers food-processing losses (BIOMASS 2003 [DIRS 168563], Section C3). The two models were evaluated using the same input values or using default data from BIOMASS ERB2A (BIOMASS 2003 [DIRS 168563]). The ACM and the selected model produced comparable results with reasonable input values (SNL 2007 [DIRS 177399], Section 7.4.4.1). The ACM was not chosen because it requires parameters that are not commonly used in environmental transport modeling and are, thus, difficult to quantify. In addition, the ACM was developed for a temperate climate and implies infrequent irrigation episodes, which may be inappropriate for the arid or semiarid conditions at Yucca Mountain (SNL 2007 [DIRS 177399], Section 7.3.3.2).

ACM for Direct Deposition of Airborne Particulates on Plant Surfaces—In the Biosphere Process Model, resuspended soil deposited on crop leaves is treated in the same manner as intercepted irrigation water. The ACM takes a different approach, based on a contamination factor for the external contamination of crops, which is similar to a soil-to-plant transfer factor. Differences between the selected model and the ACM were evaluated using the same input values when the parameters are comparable, or by using default data from the published ACM. The evaluation showed that the approach used in the Biosphere Process Model and that used in the ACM produce comparable results for reasonable input values (SNL 2007 [DIRS 177399], Section 7.4.4.3).

ACM for Animal Product Contamination—The Biosphere Process Model considers animal contamination resulting from the ingestion of contaminated water, soil, and feed. The GENII Model (Napier et al. 1988 [DIRS 157927]; Leigh et al. 1993 [DIRS 100464]) only includes the consumption of water and feed; however, GENII Version 2 (Napier et al. 2006 [DIRS 177331]) includes soil ingestion and the BIOMASS ERB2A model (BIOMASS 2003 [DIRS 168563]) includes an additional pathway: inhalation of contaminated air by animals. These animal transport pathways are compared to determine their relative importance (SNL 2007 [DIRS 177399], Section 7.4.5). For this comparison, "meat" (i.e., beef, mutton, pork, deer, rabbit, etc.) was used as an example animal product with ^{239}Pu as the test radionuclide. Soil ingestion is an important contributor to the total activity concentration in meat and, therefore, is included in the Biosphere Process Model. The inhalation of contaminated dust contributes little to concentrations in meat and, therefore, is not included.

ACM for ^{14}C Special Submodel—The methods used in the Biosphere Process Model to calculate ^{14}C concentrations in environmental media were different from those used for the other primary radionuclides. Concentrations of ^{14}C in crops were based on experimental results of the

release of $^{14}CO_2$ gas from soil (Sheppard et al. 1991 [DIRS 159545]; Yu et al. 2001 [DIRS 159465], Section L.3). The Biosphere Process Model included two transport pathways of ^{14}C to plants: direct root uptake and intake of $^{14}CO_2$ gas by plants during photosynthesis. Six RMEI exposure pathways were considered: external exposure to and ingestion of ^{14}C in soil, inhalation of $^{14}CO_2$ gas and airborne particulate matter containing ^{14}C, and ingestion of ^{14}C in crops and animal products. An ACM (Napier et al. 1988 [DIRS 157927], p. 4.89) used different methods to calculate ^{14}C concentrations. That model considered uptake into plants only from roots and used a very low removal rate of carbon from soil because the model did not account for gaseous release of $^{14}CO_2$. The method used by the biosphere model was chosen because it more realistically considered uptake of $^{14}CO_2$ gas into plants, resulting in higher plant concentrations (SNL 2007 [DIRS 177399], Sections 6.3.3, 7.3.6, and 7.4.7). An additional alternative model for calculating concentrations of ^{14}C in plant and animal products has also been proposed (BIOMASS 2000 [DIRS 154522], Appendix A) but was not considered because the default parameter values necessary to run the model have not been developed by the authors of the model (SNL 2007 [DIRS 177399], Section 7.3.6 and Table 7.3-21).

ACM for Environment-Specific Inhalation Submodel—In the Biosphere Process Model, inhalation exposure was treated as a function of environment and human activity because many of the input parameters (mass loading, breathing rate, exposure time, and enhancement factors) would be influenced by human activities. Similar models, called microenvironmental models, were used to assess exposure to particulate matter and other contaminants (Duan 1982 [DIRS 162466]; Mage 1985 [DIRS 162465]; and Klepeis 1999 [DIRS 160094]). An alternative but simpler method that is commonly used in risk assessments is to use one or two environments that are representative of the entire range of people, conditions, and times being modeled. These methods produce the same results if average values used in the biosphere model for each environment are used for the alternative method. The method used in the Biosphere Process Model better incorporates variation and uncertainty in each of the input parameters and provides more transparency for the expected RMEI exposure changes between the groundwater (localized contamination) and volcanic release cases (widespread contamination) (SNL 2007 [DIRS 177399], Sections 6.3.3, 7.3.7, 7.3.8, and 7.4.9).

All seven ACMs are numerically compared with those selected in the Biosphere Process Model. The results indicate that most of the ACMs are numerically similar to those selected, and some ACMs are not chosen because those selected match better conceptually with site-specific conditions. Therefore, none of the ACMs were used in the calculations of BDCFs that support the TSPA-SEIS.

No ACMs were recommended for inclusion in the TSPA-SEIS.

Table 6.3.11-1. Pathways for the Groundwater Exposure Case

Environmental Medium	Exposure Mode	Exposure Pathways	Examples
Water	Ingestion	Water intake	Drinking water and water-based beverages.
Soil	Ingestion	Inadvertent soil ingestion	Recreational activities, occupational activities, gardening, and consumption of fresh fruits and vegetables with attached soil.
Soil	External	External radiation exposure	Activities on or near contaminated soils.
Air	Inhalation	Breathing resuspended particles, gases (^{222}Rn and progeny, plus $^{14}CO_2$), and aerosols from evaporative coolers	Outdoor activities, including soil-disturbing activities related to work and recreation; domestic activities including sleeping.
Plants	Ingestion	Consumption of locally produced crops: vegetables, fruit, and grains	Eating contaminated crops.
Animals	Ingestion	Consumption of locally produced animal products: meat, poultry, milk, and eggs	Eating contaminated animal products.
Fish	Ingestion	Consumption of locally produced freshwater fish	Eating contaminated fish.

Source: Modified from Table 6.3-1 in *Biosphere Model Report* (SNL 2007 [DIRS 177399])

Table 6.3.11-2. Pathways for the Volcanic Ash Exposure Case

Environmental Medium	Exposure Mode	Exposure Pathways	Examples
Soil	Ingestion	Inadvertent soil ingestion	Recreational activities, occupational activities, gardening, and consumption of fresh fruit and vegetables with attached soil.
Soil	External	External radiation exposure	Activities on or near contaminated soils.
Air	Inhalation	Breathing resuspended particles; ^{222}Rn and progeny	Outdoor activities, including soil-disturbing activities related to work and recreation; domestic activities, including sleeping.
Plants	Ingestion	Consumption of locally produced crops: vegetables, fruit, and grains	Eating contaminated crops.
Animals	Ingestion	Consumption of locally produced animal products: meat, poultry, milk, and eggs	Eating contaminated animal products.

Source: Modified from Table 6.3-3 in *Biosphere Model Report* (SNL 2007 [DIRS 177399])

Table 6.3.11-3. Groundwater BDCF Uncertainty Representation in the TSPA-SEIS, GoldSim Model File for the Present-Day Climate

Parameter Name[a,b]	Description
GW_BDCF_MIC_Ac227	^{227}Ac - Modern Interglacial Climate BDCF
GW_BDCF_MIC_Am241	^{241}Am - Modern Interglacial Climate BDCF
GW_BDCF_MIC_Am243	^{243}Am - Modern Interglacial Climate BDCF
GW_BDCF_MIC_C14	^{14}C - Modern Interglacial Climate BDCF
GW_BDCF_MIC_Cl36	^{36}Cl - Modern Interglacial Climate BDCF
GW_BDCF_MIC_Cs135	^{135}Cs - Modern Interglacial Climate BDCF
GW_BDCF_MIC_Cs137	^{137}Cs - Modern Interglacial Climate BDCF
GW_BDCF_MIC_I129	^{129}I - Modern Interglacial Climate BDCF
GW_BDCF_MIC_Np237	^{237}Np - Modern Interglacial Climate BDCF
GW_BDCF_MIC_Pa231	^{231}Pa - Modern Interglacial Climate BDCF
GW_BDCF_MIC_Pb210	^{210}Pb - Modern Interglacial Climate BDCF
GW_BDCF_MIC_Pu238	^{238}Pu - Modern Interglacial Climate BDCF
GW_BDCF_MIC_Pu239	^{239}Pu - Modern Interglacial Climate BDCF
GW_BDCF_MIC_Pu240	^{240}Pu - Modern Interglacial Climate BDCF
GW_BDCF_MIC_Pu242	^{242}Pu - Modern Interglacial Climate BDCF
GW_BDCF_MIC_Ra226	^{226}Ra - Modern Interglacial Climate BDCF
GW_BDCF_MIC_Ra226_Pb210[c]	^{226}Ra & ^{210}Pb - Modern Interglacial Climate BDCF
GW_BDCF_MIC_Ra228	^{228}Ra - Modern Interglacial Climate BDCF
GW_BDCF_MIC_Se79	^{79}Se - Modern Interglacial Climate BDCF
GW_BDCF_MIC_Sn126	^{126}Sn - Modern Interglacial Climate BDCF
GW_BDCF_MIC_Sr90	^{90}Sr - Modern Interglacial Climate BDCF
GW_BDCF_MIC_Tc99	^{99}Tc - Modern Interglacial Climate BDCF
GW_BDCF_MIC_Th228	^{228}Th - Modern Interglacial Climate BDCF
GW_BDCF_MIC_Th229	^{229}Th - Modern Interglacial Climate BDCF
GW_BDCF_MIC_Th230	^{230}Th - Modern Interglacial Climate BDCF
GW_BDCF_MIC_Th232	^{232}Th - Modern Interglacial Climate BDCF
GW_BDCF_MIC_Th232_Ra228_Th_228[c]	^{232}Th & ^{228}Ra & ^{228}Th - Modern Interglacial Climate BDCF
GW_BDCF_MIC_U232	^{232}U - Modern Interglacial Climate BDCF
GW_BDCF_MIC_U232_Th228	^{232}U & ^{228}Th - Modern Interglacial Climate BDCF
GW_BDCF_MIC_U233	^{233}U - Modern Interglacial Climate BDCF
GW_BDCF_MIC_U234	^{234}U - Modern Interglacial Climate BDCF

Table 6.3.11-3. Groundwater BDCF Uncertainty Representation in the TSPA-SEIS, GoldSim Model File for the Present-Day Climate (Continued)

Parameter Name[a,b]	Description
GW_BDCF_MIC_U235	^{235}U - Modern Interglacial Climate BDCF
GW_BDCF_MIC_U236	^{236}U - Modern Interglacial Climate BDCF
GW_BDCF_MIC_U238	^{238}U - Modern Interglacial Climate BDCF

[a] There are three one-dimensional tables, one for each of the three climate states (MIC = modern interglacial climate, MC = monsoonal climate, and GTC = glacial-transitional climate) modeled for each radionuclide; only the MIC is shown here. Using ^{227}Ac as an example, the TSPA-SEIS contains the following one-dimensional BDCF tables for the groundwater exposure scenarios: GW_BDCF_MIC_Ac227, GW_BDCF_MC_Ac227, and GW_BDCF_GTC_Ac227.

[b] To incorporate uncertainty into the model input, the Biosphere model component ran a series of 1,000 model realizations to define a set of BDCFs for each radionuclide modeled. The resulting probability distribution represents uncertainty in the BDCFs. This set of BDCFs is given in a one-dimensional table for each radionuclide.

[c] These composite BDCF data defined to provide the opportunity to only consider the release and transport of the long-lived parent radionuclide while retaining the dose consequences of the short-lived progeny.

Table 6.3.11-4. Alternative Conceptual Models Considered for the Biosphere

Alternative Conceptual Model	Overview	Screening Assessment and Basis
Radon release from soil (Air Submodel)	This ACM considers radon transport in the soil and the atmosphere, which requires more input data. The ERMYN conceptual model does not include these processes and uses a simple release factor.	This ACM is screened from the Biosphere Model Component based on an analysis showing that the ACM and the ERMYN Model produce comparable results (SNL 2007 [DIRS 177399], Section 7.4.3.1).
Evaporative cooler (Air Submodel)	This ACM considers an inhalation dose from aerosols generated from evaporative coolers and is based on calculating radionuclide concentrations in the air due to an increase in humidity. The ERMYN conceptual model uses a submodel based on the amount of water evaporated rather than an increase in humidity.	This ACM is screened from the Biosphere Model Component based on an analysis showing that this ACM and the ERMYN Model produce equivalent results (SNL 2007 [DIRS 177399], Section 7.4.3.2).
Direct deposition of irrigated water (Plant Submodel)	This ACM considers two processes, one where the deposited radionuclide moves from external plant surfaces into the plant tissues, and then from plant tissues into the edible portion of the crop. Weathering is applied only to contaminants that remain on external plant surfaces. Food processing loss is also considered in the ACM. The ERMYN conceptual model considers the radionuclides in irrigation water to be directly translocated to the edible parts of plants with weathering and accumulation during the growing period, but without food preparation loss.	This ACM is screened from the Biosphere Model Component based on an analysis showing that this ACM and the ERMYN Model produce comparable results (SNL 2007 [DIRS 177399], Section 7.4.4.1).
Direct deposition of airborne particulates on crops (Plant Submodel)	This ACM is based on the crop external contamination. This contamination factor is very similar to a soil-to-plant transfer factor. The ERMYN conceptual model considers the deposited airborne particles on crop leaves acting the same way as the intercepted irrigation water.	This ACM is screened from the Biosphere Model Component based on an analysis showing that this ACM and the ERMYN Model produce comparable results for reasonable input values (SNL 2007 [DIRS 177399], Section 7.4.4.3).
Animal product contamination (Animal Submodel)	This ACM considers animal inhalation of contaminated air. The ERMYN conceptual model excludes the inhalation of contaminated air as a negligible pathway.	This ACM is screened from the Biosphere Model Component based on an analysis showing that inhalation of contaminated air is not an important contributor to the animal product contamination (SNL 2007 [DIRS 177399], Section 7.4.5).
^{14}C Special Submodel (^{14}C Special Submodel)	This ACM considers root uptake as the only mechanism of ^{14}C transfer to crops. ERMYN also includes ^{14}C uptake from air during photosynthesis. In addition to ingestion, ERMYN also includes other pathways that result in human exposure to ^{14}C: external exposure, inhalation of ^{14}C as gas and in soil, as well as soil ingestion.	This ACM is screened from the Biosphere Model Component based on an analysis showing that the selected ^{14}C special submodel considers more processes of ^{14}C transfer to plants than this ACM, which results in a higher ^{14}C concentration in plants (SNL 2007 [DIRS 177399], Section 7.4.7).
Environment-Specific Inhalation Submodel (Inhalation Submodel)	This ACM uses average values of input parameters for inhalation exposure. The ERMYN conceptual model considers inhalation exposure as a function of the environment because many model parameters, such as mass loading, breathing rate, and exposure time, differ among environments and activities.	This ACM is screened from the Biosphere Model Component based on an analysis showing that the ACM and the ERMYN model produce comparable results (SNL 2007 [DIRS 177399], Section 7.4.9). In addition, it is easier to address uncertainty in the input parameters using environment-specific values.

Source: Table 6.3-5 in *Biosphere Model Report* (SNL 2007 [DIRS 177399])

NOTE: ERMYN = Environmental Radiation Model for Yucca Mountain, Nevada.

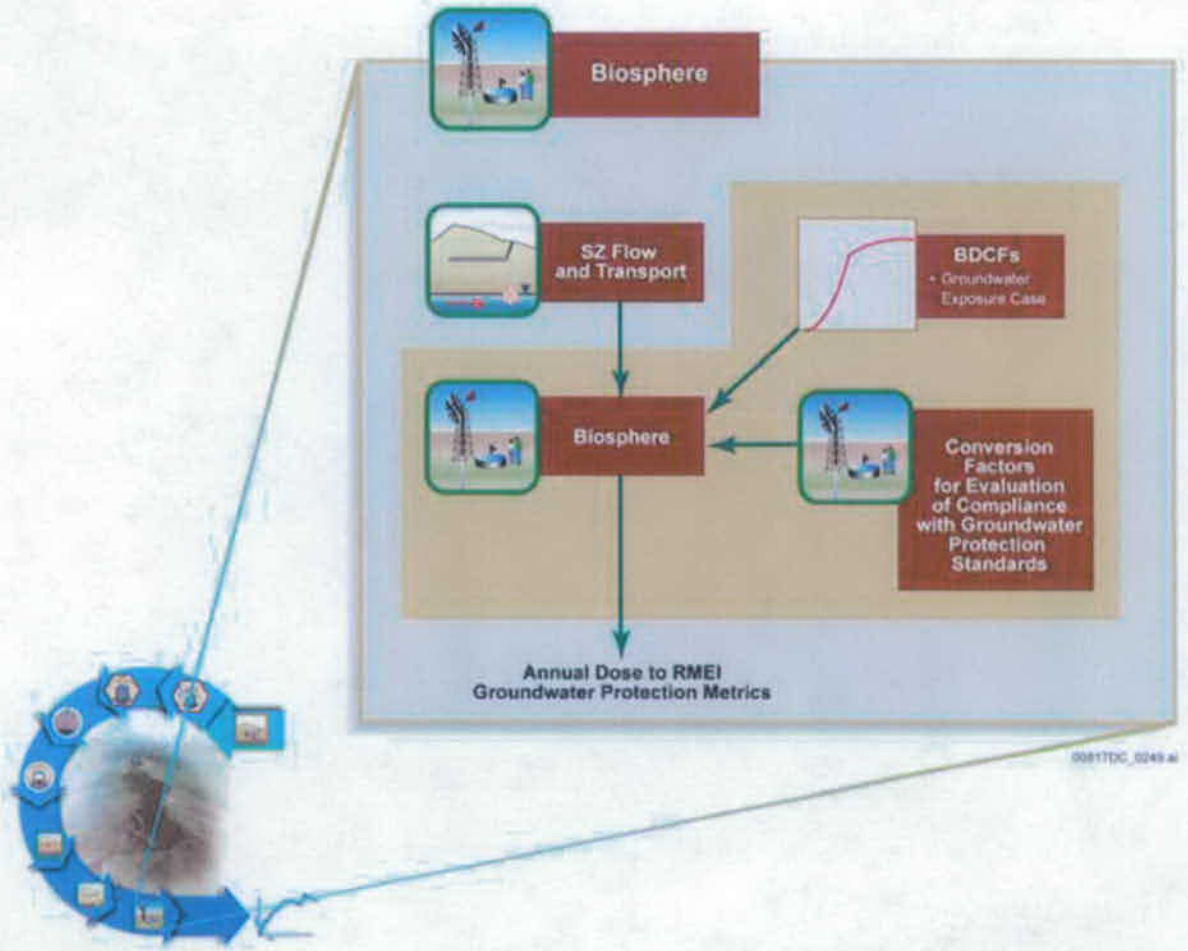

Figure 6.3.11-1. Information Flow Diagram for the Biosphere Model Component of the TSPA-SEIS

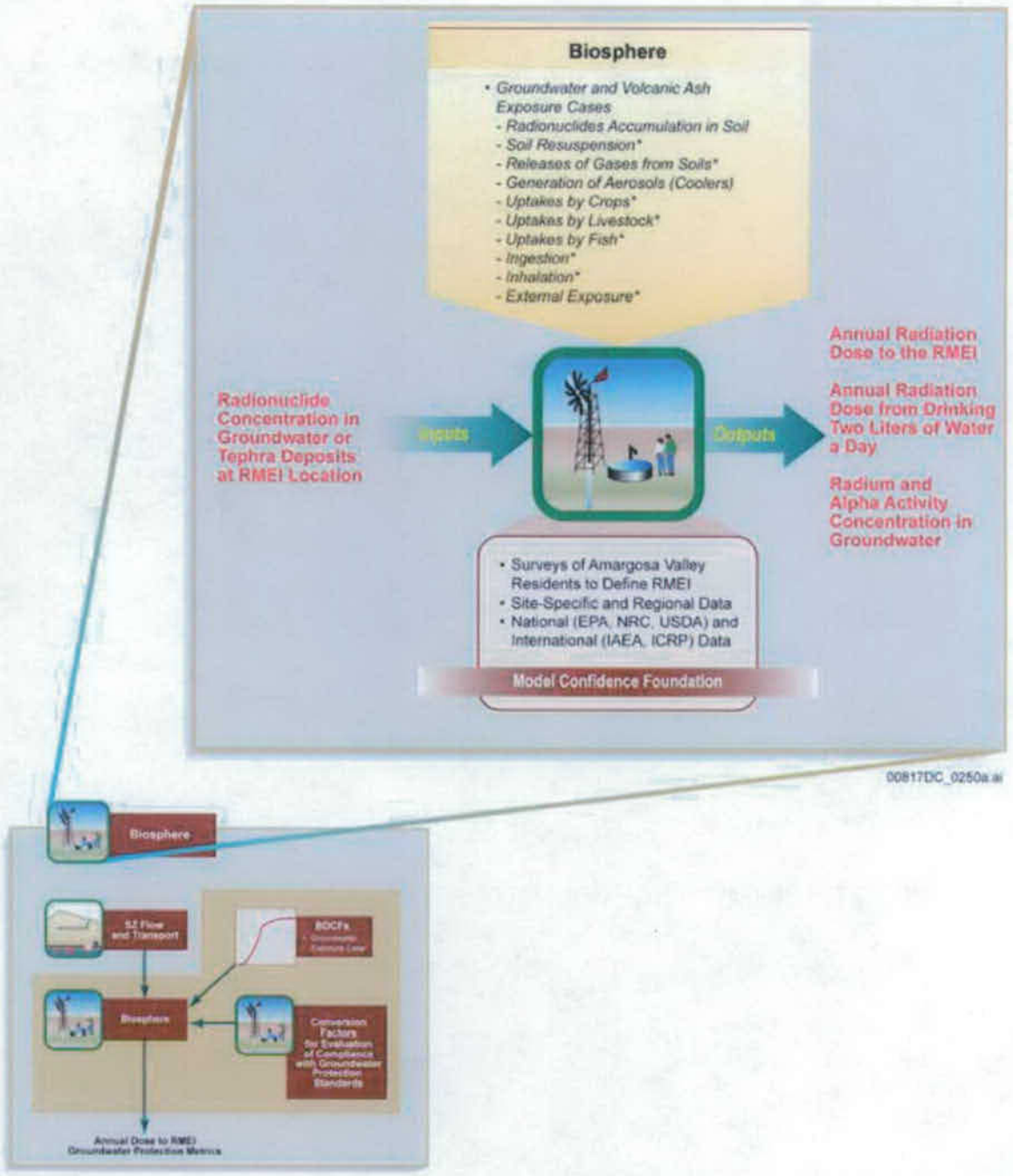

NOTE: The asterisk in the figure denotes that the volcanic ash exposure case only includes four environmental transport pathways. ICRP = International Commission on Radiological Protection.

Figure 6.3.11-2. Inputs, Outputs, and Basis for Model Confidence for the Biosphere Model Component of the TSPA-SEIS

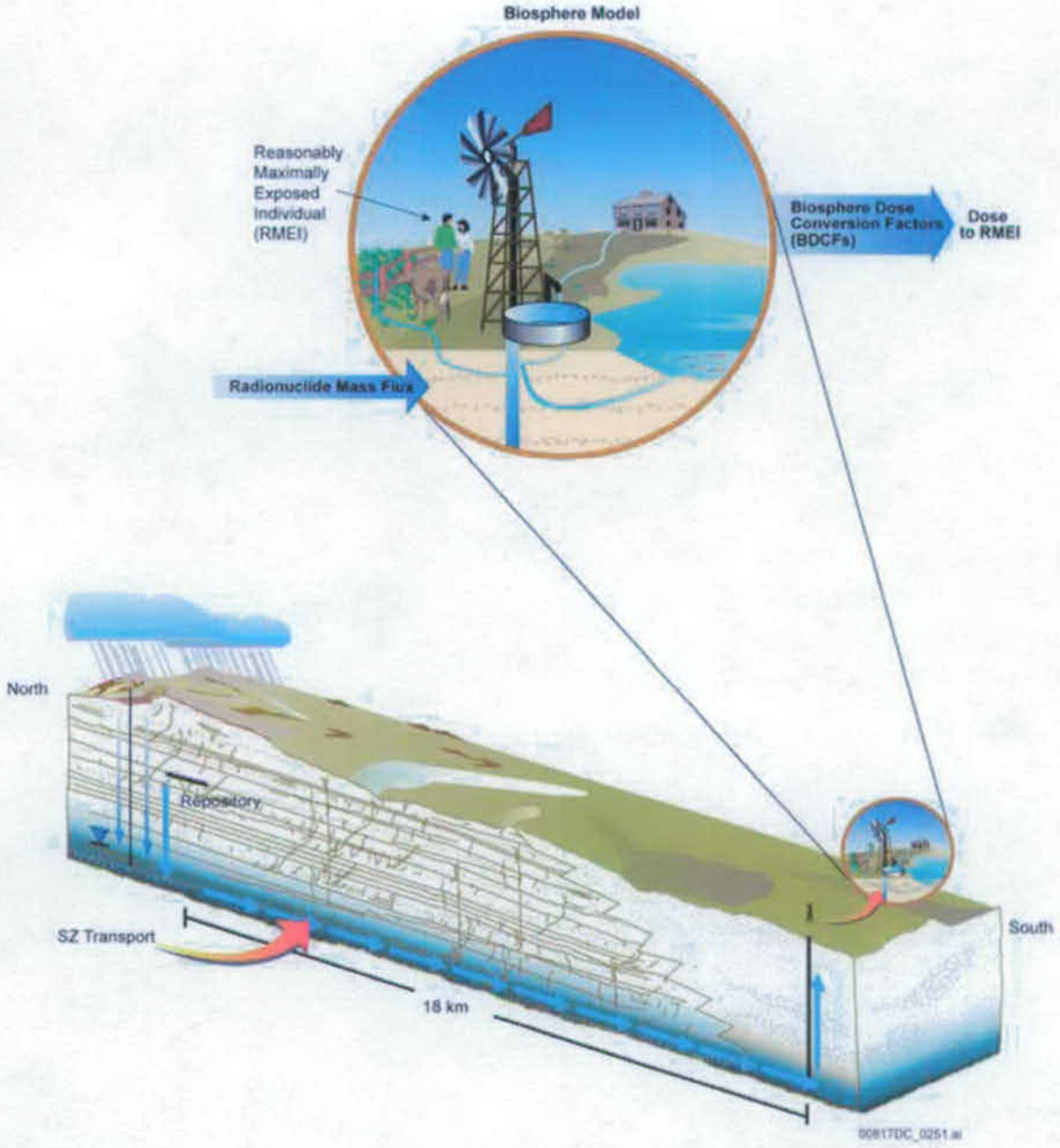

Figure 6.3.11-3. Overview of the Biosphere Groundwater Exposure Case Showing Groundwater Transport of Radionuclides and Exposure to the Reasonably Maximally Exposed Individual

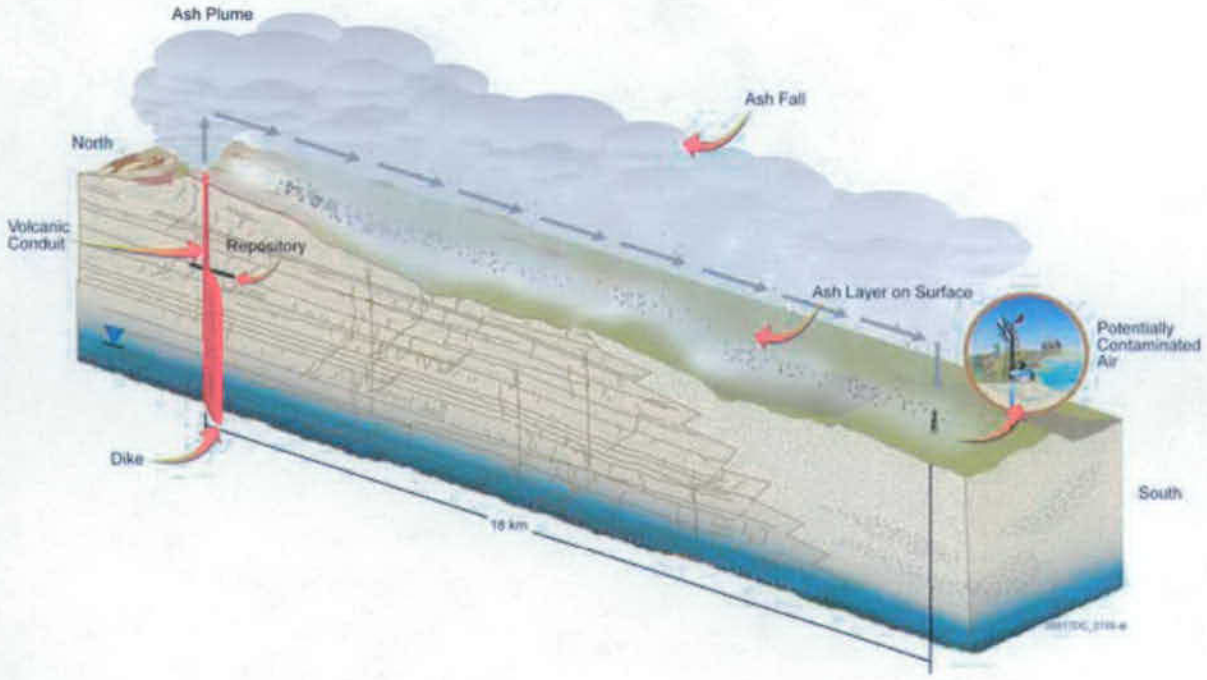

Figure 6.3.11-4. Schematic Representation of the Transport of Radioactive Waste in the Volcanic Ash Exposure Case

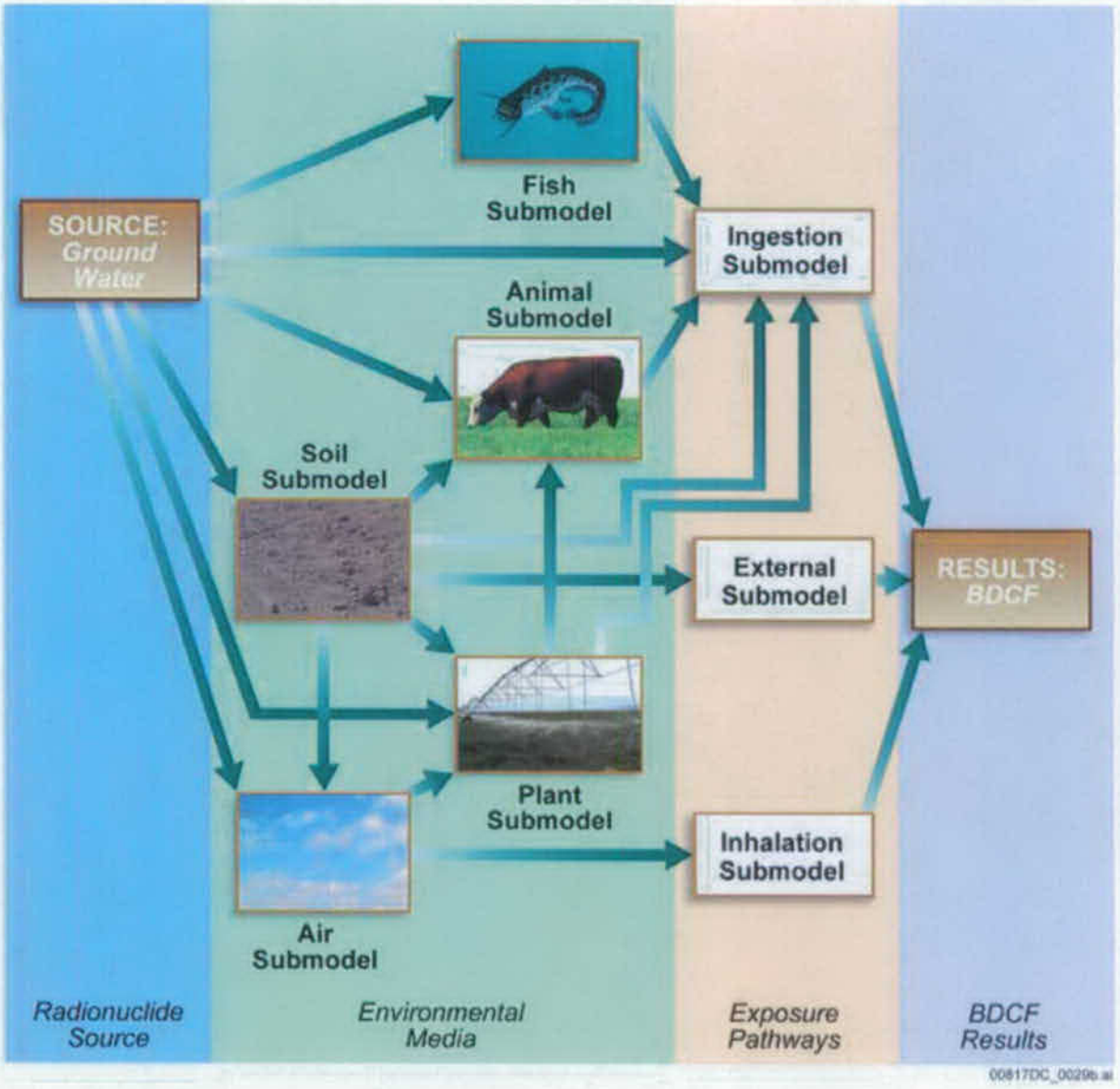

Source: Modified from (SNL 2007 [DIRS 177399], Figure 6.3-2).

Figure 6.3.11-5. Relationship among Biosphere Submodels for the Groundwater Exposure Case

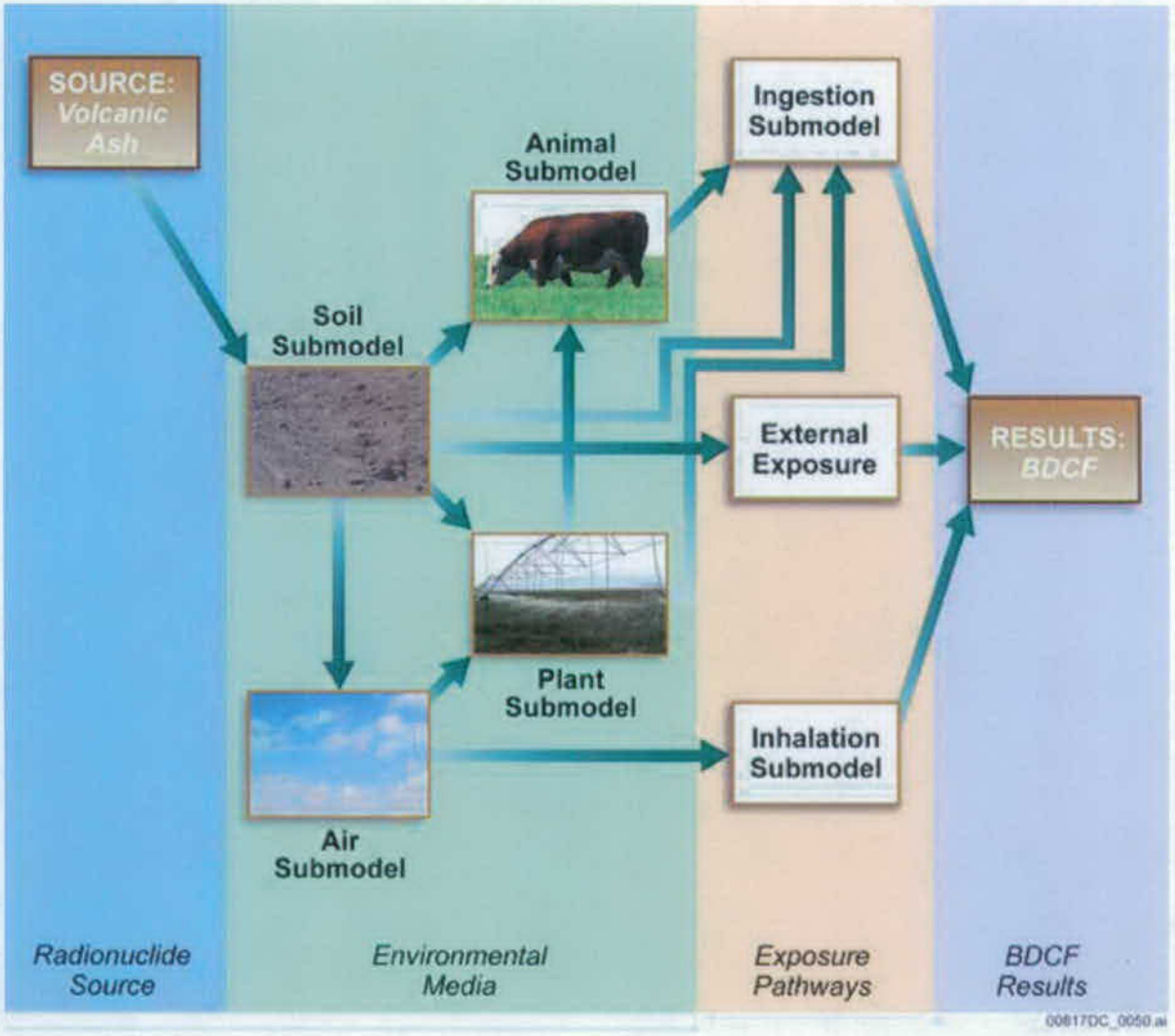

Source: (SNL 2007 [DIRS 177399], Figure 6.3-4)

Figure 6.3.11-6. Relationship among Biosphere Submodels for the Volcanic Ash Exposure Case

6.4 TSPA-SEIS FOR THE EARLY FAILURE SCENARIO CLASS

The Early Failure Scenario Class describes future performance of the repository system in the event of early failure of waste packages (WPs) and drip shields (DSs). An early failure is defined as the through wall penetration of a WP or DS due to manufacturing or handling-induced defects at a time earlier than would be predicted by mechanistic degradation models for a defect-free WP or DS. The conceptual models and abstractions for probability of WP and DS early failure are documented in *Analysis of Mechanisms for Early Waste Package/Drip Shield Failure* (SNL 2007 [DIRS 178765], Sections 6.1 through 6.5).

The Early Failure Scenario Class contains two modeling cases: the Drip Shield EF Modeling Case and Waste Package EF Modeling Case. In the Drip Shield EF Modeling Case, complete failure of the DS is assumed to occur. A WP under an early-failed DS is assumed to experience localized corrosion as soon as seepage contacts the WP, since the area of the Alloy 22 WP outer barrier that is contacted by seepage is potentially subject to localized corrosion (Section 6.3.5.2.3). In the Waste Package EF Modeling Case, an early-failed WP is considered breached from the beginning of the simulation, and its entire surface area is considered degraded. General corrosion of the DSs due to nominal corrosion processes (Section 6.3.5.1.2) is included in the Waste Package EF Modeling Case.

The two modeling cases in the Early Failure Scenario Class have the same framework as the Nominal Scenario Class Modeling Case. The two modeling cases invoke the same modeling components and submodels as are invoked in the Nominal Scenario Class. That is, the framework includes the TSPA-SEIS components to evaluate the mobilization of radionuclides exposed to seeping water, release from the EBS, transport in the unsaturated zone (UZ) down to the saturated zone (SZ), and transport in the SZ to the location of the reasonably maximally exposed individual (RMEI). In the WP and DS Degradation Model Component, the Nominal Scenario Class WP and DS degradation modes are replaced with the early failure DS and early failure WP degradation modes. The relationships between the TSPA-SEIS components and submodels for the Early Failure Scenario Class are illustrated on Figure 6.4-1. Figure 6.4-2 shows the information flow within the TSPA-SEIS associated with the Early Failure Scenario Class. Figure 6.4-3 indicates the major inputs and outputs of the model components and submodels of the Early Failure Scenario Class, features included in the TSPA-SEIS, and foundation for confidence in the TSPA-SEIS.

The statistical distribution of annual dose is estimated in a Monte Carlo approach in which a set of realizations of repository system characteristics is used to represent the range of uncertainty and variability in the parameters of the TSPA-SEIS components. The mean annual dose is estimated as described in Equation 6.1.2-13 for the Waste Package EF Modeling Case and Equation 6.1.2-14 for the Drip Shield EF Modeling Case.

Section 6.4 can be summarized as follows: Section 6.4.1 describes the conceptual and abstraction models for the Drip Shield EF Modeling Case. Section 6.4.1.1 outlines the DS early failure conceptual model. Section 6.4.1.2 contains the abstraction model corresponding to this conceptual model. Section 6.4.1.3 describes the implementation in the TSPA-SEIS. Section 6.4.2 describes the conceptual and abstraction models for the Waste Package EF Modeling Case. Sections 6.4.2.1, 6.4.2.2, and 6.4.2.3 describe the WP early failure conceptual

model, corresponding abstraction model, and implementation in the TSPA-SEIS. Section 6.4.3 discusses the treatment of uncertainty. Section 6.4.4 discusses consistency of assumptions between TSPA submodels and model components. It also discusses conservatisms in model abstractions.

6.4.1 Drip Shield Early Failure Modeling Case

6.4.1.1 Drip Shield Early Failure Modeling Case Conceptual Model

Thirteen potential mechanisms that could cause manufacturing defects in welded metallic containers were identified in Section 6.1.6 of *Analysis of Mechanisms for Early Waste Package/Drip Shield Failure* (SNL 2007 [DIRS 178765]). Of these thirteen flaws or processes, four were identified as potentially significant for mechanisms leading to early DS failure. Four processes were retained for further analysis:

- Improper heat treatment
- Base metal selection flaws
- Improper weld filler material
- Emplacement errors.

For the applicable DS defects, the probability of occurrence and consequences for postclosure performance was assessed. The four processes were analyzed using an event tree/fault tree approach (SNL 2007 [DIRS 178765], Section 6.4). The probabilities of occurrence for the four DS early failure mechanisms were combined to yield a probability distribution for the rate of occurrence of undetected defects in DSs. The occurrence of an undetected defect is assumed to result in complete failure of the DS as a barrier to seepage at the time of repository closure (SNL 2007 [DIRS 178765], Section 6.5.2); hence, the probability distribution for the rate of occurrence of undetected defects is equivalent to a probability distribution for the rate of DS early failures. The occurrence of undetected defects is assumed to be independent between DSs; hence, DS early failure is also independent between DSs.

6.4.1.2 Abstraction of Drip Shield Early Failure

The uncertain rate of DS early failures was abstracted to a log-normal distribution (SNL 2007 [DIRS 178765], Table 7-1). Because DS early failure is independent between DSs, the number of DS early failures can be represented by a Poisson distribution, for any particular value of the rate of DS early failures, λ. The Poisson distribution for the number of DS early failures was developed by integrating the Poisson probability density function for each rate of early failure with the probability density function for the rate of early failure, $f(\lambda)$, given by the log-normal distribution. The integral was numerically evaluated over its domain from zero to a truncated upper-bound λ_m, and set at the 0.999999 quantile value for the given log-normal distribution. The log-normal probability density function $f(\lambda)$ was also adjusted to its truncated upper-bound representation so that the probability density function integrates to one over the specified range. The integral is shown in Equation 6.4-1, where $f(\lambda)$ and $F(\lambda)$ are the probability density function and cumulative distribution function (CDF) of the log-normal distribution, N is

the population of DSs considered, $n = 0,1,2,3,\ldots$ is the count of early failures, and $p(n)$ is the probability of n DS early failures.

$$p(n) = \int_0^{\lambda_m} (\lambda N)^n \times \frac{e^{(-\lambda N)}}{n!} \times \frac{f(\lambda)}{F(\lambda_m)} \times d\lambda \qquad \text{(Eq. 6.4-1).}$$

Table 6.4-1 shows the results of evaluating Equation 6.4-1. The probability of no DS early failures is 0.9834. The probability of only one DS early failure is 0.0155, and the probability of two or more DS early failures is 0.0011. The expected number of DS early failures is given by the sum

$$\sum_{n=1}^{n_m} p(n).n = 0.018 \qquad \text{(Eq. 6.4-2)}$$

where n_m is the number of terms in the distribution for the number of DS early failures, chosen so that including more terms in the summation is not significant.

Analyses in *Analysis of Mechanisms for Early Waste Package/Drip Shield Failure* (SNL 2007 [DIRS 178765], Table 7-1) predicted rates for the introduction of defects into DS fabrication but did not predict the impact on repository performance. The report acknowledged that failure of the DS will only occur after degradation processes take place, which may happen hundreds or even thousands of years after emplacement. However, a realistic estimate of the time at which components with defects will fail was considered difficult to develop. Therefore, the report recommended the assumption of complete failure of the DS, with respect to its seepage diversion function, at the time of repository closure for implementation in the TSPA-SEIS (SNL 2007 [DIRS 178765], Section 6.5.2). This assumption will overestimate the potential for radionuclide release early in the life of the repository.

6.4.1.3 Implementation of Drip Shield Early Failure in the TSPA-SEIS

The rate of DS early failure is sampled from a log-normal distribution with a median of 4.30×10^{-7} and an error factor of 14 (Table 6.4-2). These inputs need to be adjusted to conform to the input requirements of GoldSim for log-normal distributions, which require either the geometric mean and geometric standard deviation (SD) or the true mean and true standard deviation as parameters. First, note that the median is equal to the geometric mean for log-normal distributions (Evans et al. 1993 [DIRS 112115], Chapter 25). Second, the shape parameter, σ_l, is related to the error factor by:

$$\sigma_l = \frac{\ln(errorfactor)}{1.645} = \ln\left(errorfactor^{1/1.645}\right). \qquad \text{(Eq. 6.4-3)}$$

The shape parameter is the SD of the log transformed variates (Evans et al. 1993 [DIRS 112115], Chapter 25). Therefore, the geometric SD of the log-normal distribution is given by Equation 6.4-4 (GoldSim Technology Group 2007 [DIRS 181727], Appendix B, p. 668):

$$\sigma_g = \exp(\sigma_l) = errorfactor^{1/1.645}. \quad \text{(Eq. 6.4-4)}$$

For the DS early failure implementation, the DSs are associated with the two WP fuel type groups (CSNF and CDSP). The TSPA-SEIS makes the simplifying assumption that each DS early failure affects a single WP. The length of a DS is approximately 228 in. (SNL 2007 [DIRS 179354], Table 4-2); the length of a WP varies between 146 and 230 inches (SNL 2007 [DIRS 179567], Table 4-5; SNL 2007 [DIRS 179394], Table 4-3). Thus, the assumption that a DS early failure affects one WP is reasonable.

The TSPA-SEIS models a DS early failure by removing the DS as a barrier to seepage at the time of repository closure and allowing the full volume of seepage to contact the WP (Section 6.4.1.2).

The TSPA-SEIS conservatively assumes that a WP underneath an early failed DS experiences localized corrosion, which completely compromises the outer barrier of the WP at the time of repository closure, allowing both the advective and diffusive transport of radionuclides. Analysis of the Localized Corrosion Initiation Abstraction shows that localized corrosion initiation conditions can be present in the repository for the first few hundred years in a minority of epistemic realizations. Rather than incurring significant computational expense to account for the epistemic uncertainty and the temporal and spatial variation in the initiation of localized corrosion, this simplifying assumption of immediate initiation of localized corrosion is made. Similarly, the TSPA-SEIS assumes that localized corrosion rapidly compromises the entire outer barrier of the affected WP, rather than modeling the progression and extent of localized corrosion, to simplify the calculation of expected dose.

DS early failures that occur in locations but that do not experience seepage are assumed to contribute negligibly to the expected dose. In a location without seepage, localized corrosion does not occur because the WP surface is not wetted. Since localized corrosion does not occur, and the Drip Shield EF Modeling Case does not address other events (i.e., seismic events) that could compromise the WP integrity, there are no mechanisms in the Drip Shield EF Modeling Case that would lead to releases from a WP in a location without seepage. Therefore, the assumption of negligible dose impact is justified.

The GoldSim component of the TSPA-SEIS computes the dose resulting from a single DS early failure occurring in each of the 5 percolation subregions (Section 6.3.2.2.1), in a seeping environment, and affecting each type of WP (CSNF or CDSP), for a total of 10 dose histories for each epistemic realization. The GoldSim results are used in Equation 6.1.2-14 with the sampled rate of DS early failure, the distribution of the numbers of WPs of each type, and the seepage fraction for each percolation bin, to calculate the expected dose for each epistemic realization. The mean and median dose is estimated from the ensemble of expected dose results at each point in time.

6.4.2 Waste Package Early Failure Modeling Case

6.4.2.1 Waste Package Early Failure Modeling Case Conceptual Model

Thirteen potential mechanisms that could result in early-failed WPs were identified in Section 6.1.6 of *Analysis of Mechanisms for Early Waste Package/Drip Shield Failure* (SNL 2007 [DIRS 178765]). Of these thirteen flaws or processes, seven were identified as potentially significant for the WP outer corrosion barrier (OCB). The seven processes retained for further analyses were (SNL 2007 [DIRS 178765], Section 6.3):

- Weld flaws
- Improper heat treatment of OCB
- Improper heat treatment of OCB lid
- Improper stress relief of OCB lid (low plasticity burnishing)
- WP mishandling damage
- Improper base metal selection
- Improper weld filler material.

The processes were assessed for probability of occurrence and consequences for postclosure performance of the WPs.

A more detailed analysis was done for WP weld flaws (SNL 2007 [DIRS 178765], Section 6.3.1) than for the other six processes. This analysis resulted in distributions for the size and number of undetected weld flaws. The characteristics of weld flaws that remain in the WP closure welds can be calculated from these distributions by knowing the per-WP closure weld volume and weld thickness. The TSPA-SEIS utilizes these results, with the critical flaw orientation probability and an applicable depth factor to model where undetected flaws might remain and might result in SCC that could penetrate the WP closure weld. The implementation of the weld flaw analysis requires inputs that are supplied by the TSPA-SEIS file (Section 6.3.5.1.2). Therefore, the implementation of the weld flaw analysis is not part of the Waste Package EF Modeling Case but is part of the Nominal Modeling Case WP and DS degradation analysis (Section 6.3.5.1.2).

The remaining six processes were analyzed using an event tree/fault tree approach (SNL 2007 [DIRS 178765], Section 6.3). Improper base metal selection was rejected as a potential mechanism (SNL 2007 [DIRS 178765], Section 6.3.2), based on the probability of selecting improper base metal material in the fabrication of the OCB of the WP and the probability that the error is not detected.

Results from the event tree analyses of WP event sequences for the remaining five processes were collected into event tree end states and probability distributions for the presence of undetected defects were developed by running 90,000 realizations for these end states (SNL 2007 [DIRS 178765], Section 6.5.1). The occurrence of an undetected defect is assumed to result in early failure of the WP; hence, the probability distribution for the rate of occurrence of undetected defects is equivalent to a probability distribution for the rate of WP early failures. The occurrence of undetected defects is assumed to be independent between WPs; hence, WP early failure is also independent between WPs. No distinction is made between the different types of WP (i.e. DSNF-Short, DSNF-Long, etc.)

6.4.2.2 Abstraction of Waste Package Early Failure

The uncertain rate of WP early failures was abstracted to a log-normal distribution (SNL 2007 [DIRS 178765], Table 7-1). Because WP early failure is independent between WPs, the number of WP early failures can be represented by a Poisson distribution. The distribution for the number of early failure WPs was developed in an analagous manner to the development described in Section 6.4.1.2 for early failure DSs. Table 6.4-1 shows the results of evaluating Equation 6.4-1 for WP early failures. The probability of no WP early failures is 0.558. The probability of only one WP early failure is 0.224, the probability of exactly two WP early failures is 0.096, and the probability of three or more WP early failures is 0.123. The expected number of early-failed WPs is 1.09, evaluated using Equation 6.4-2, and the probability of WP early failures.

Analyses in *Analysis of Mechanisms for Early Waste Package/Drip Shield Failure* (SNL 2007 [DIRS 178765], Table 7-1) predicted rates for the introduction of defects into WP fabrication but did not predict the impact on the WP performance. The report acknowledged that failure of the WP will only occur after degradation processes take place, which may happen hundreds or even thousands of years after emplacement. However, a realistic estimate of the time at which components with defects will fail was considered difficult to develop. Therefore, the report recommended, for implementation in the TSPA-SEIS Model, the assumption of complete failure of the WP, with respect to radionuclide containment, at the time of repository closure (SNL 2007 [DIRS 178765], Section 6.5.2). This assumption will overestimate the potential for radionuclide release early in the life of the repository.

6.4.2.3 Implementation of Waste Package Early Failure in the TSPA-SEIS

The rate of WP early failure is sampled from a log-normal distribution with a median of 4.14×10^{-5} and an error factor of 8.17 (Table 6.4-2). These inputs are adjusted as described in Section 6.4.1.3 to conform to the input requirements of GoldSim.

For WP early failure implementation, the WPs are divided into two fuel type groups denoted by CSNF early-failed WPs and CDSP early-failed WPs. The GoldSim component of the TSPA-SEIS computes the dose resulting from early failure of a single WP of each type, occurring in each of the 5 percolation subregions (Section 6.3.2.2.1), with and without seepage in each percolation subregion, for a total of 20 dose histories for each epistemic realization. The GoldSim results are used in Equation 6.1.2-13 with the sampled rate of WP early failure, the distribution of the numbers of WPs of each type, and the seepage fraction for each percolation bin, to calculate the expected dose for each epistemic realization. The mean and median dose is estimated from the ensemble of expected dose results at each point in time.

The WAPDEG V4.07 software is used to cause each early-failed WP to fail at the beginning of the simulation (i.e., at the end of the first time step). A simplified WAPDEG V4.07 input vector is used for this purpose. The input vector contains a single corrosion-affecting event that uses the power law functional form (BSC 2002 [DIRS 162606], Section 4.2.6.6) to impose an arbitrarily chosen large corrosion rate that causes breach of all WPs in the first time step. In addition, all WPs completely fail at the end of the first time step. The use of the WAPDEG software allows a relative humidity threshold to be imposed for the initiation of WP failure.

General corrosion of DSs over early-failed WPs occurs according to the nominal corrosion processes discussed in Section 6.3.5.1.2.

6.4.3 Treatment of Uncertainty

The TSPA-SEIS includes input parameter uncertainty in the Early Failure Scenario Class. See Table 6.4-2 for a list of uncertain parameters specific to the Early Failure Scenario Class. The Early Failure Scenario Class also includes other uncertain parameters associated with the model components and submodels shown on Figure 6.4-1 and described in Section 6.3. The treatment of aleatory uncertainty in the Early Failure Scenario Class is described in Section 6.1.2.4.2.

6.4.4 Model Component Consistency and Conservatisms in Assumptions and Parameters

To enhance understanding of the complex interactions within the TSPA-SEIS, a discussion of consistency among model components and submodels and identification of conservative assumptions in abstractions, process models, and parameter sets supporting the DS Early Failure Submodel and the WP Early Failure Submodel are discussed below.

6.4.4.1 Consistency of Assumptions

The Early Failure Scenario Class does not include potential inconsistencies between model components or submodels since its effect on the TSPA-SEIS is limited to replacing the Nominal Scenario Class conceptual models for DS and WP degradation with the early failure conceptual models. These models are simpler, in the sense that failure mechanisms are not treated in detail and failure is assumed to occur at the beginning of the simulation. No inconsistencies have been identified between the DS and WP Early Failure Submodels and other Submodels of the TSPA-SEIS.

6.4.4.2 Identification of Conservatisms in Submodels and Abstractions

Consequences of Defects—Section 6.5.2 of *Analysis of Mechanisms for Early Waste Package/Drip Shield Failure* (SNL 2007 [DIRS 178765]) notes that even if a WP or DS is affected by a type of defect that may lead to its early failure, it does not mean that this WP or DS is due to fail at emplacement in the repository. Failure of the WP will only occur after degradation processes take place, which may happen hundreds or even thousands of years after emplacement. Even if a WP or DS were to fail soon after emplacement because of a defect, its radionuclide inventory might not necessarily be available for transport. This is because most through-wall penetrations, especially cracks from SCC, are usually tight, highly tortuous, and limited in length. A realistic estimate of when components with defects will fail would be difficult to develop and justify given the nature of the problem:

- Physical failure of highly corrosion resistant metallic structures with very small loads under nominal conditions
- The time frames involved—centuries to millennia or longer
- The lack of experience with such engineered systems in standard industrial or engineering practice.

Because of such considerations, an approach to the assumption of complete failure of the components with respect to radionuclide containment or seepage diversion function at the time of repository closure was recommended for implementation in the TSPA-SEIS. This approach will overestimate the potential for radionuclide release early in the life of the repository.

Table 6.4-1. Early Failure Unconditional Probability Values

n (Number of Early Failures)	p(n), Waste Packages	p(n), Drip Shields
0	0.5580	0.9834
1	0.2237	0.0155
2	0.0955	0.0009
≥ 3	0.1228	0.0002

Source: DTN: MO0707WPDRIPSD.000 [DIRS 183005]

Table 6.4-2. Uncertain Inputs Used in the Early Failure Scenario Class

TSPA Parameter Name	Description	Units	Distribution	Remarks
UNC_WP_EF	Parameters for probability distribution for undetected defects in WPs. For TSPA purposes, this distribution is the probability that a WP will experience early failure after emplacement.	per WP	Log-normal distribution with a median of 4.14×10^{-5} and an error factor of 8.17. (epistemic uncertainty)	DTN: MO0701PASHIELD.000_R2, file: Tables for DTN Readme.doc [DIRS 180508]
UNC_DS_EF	Parameters for probability distribution for undetected defects in DSs. For TSPA purposes, this distribution is the probability that a DS will experience early failure after emplacement.	per WP	Log-normal distribution with a median of 4.30×10^{-7} and an error factor of 14. (epistemic uncertainty)	DTN: MO0701PASHIELD.000_R2, file: Tables for DTN Readme.doc [DIRS 180508]

INTENTIONALLY LEFT BLANK

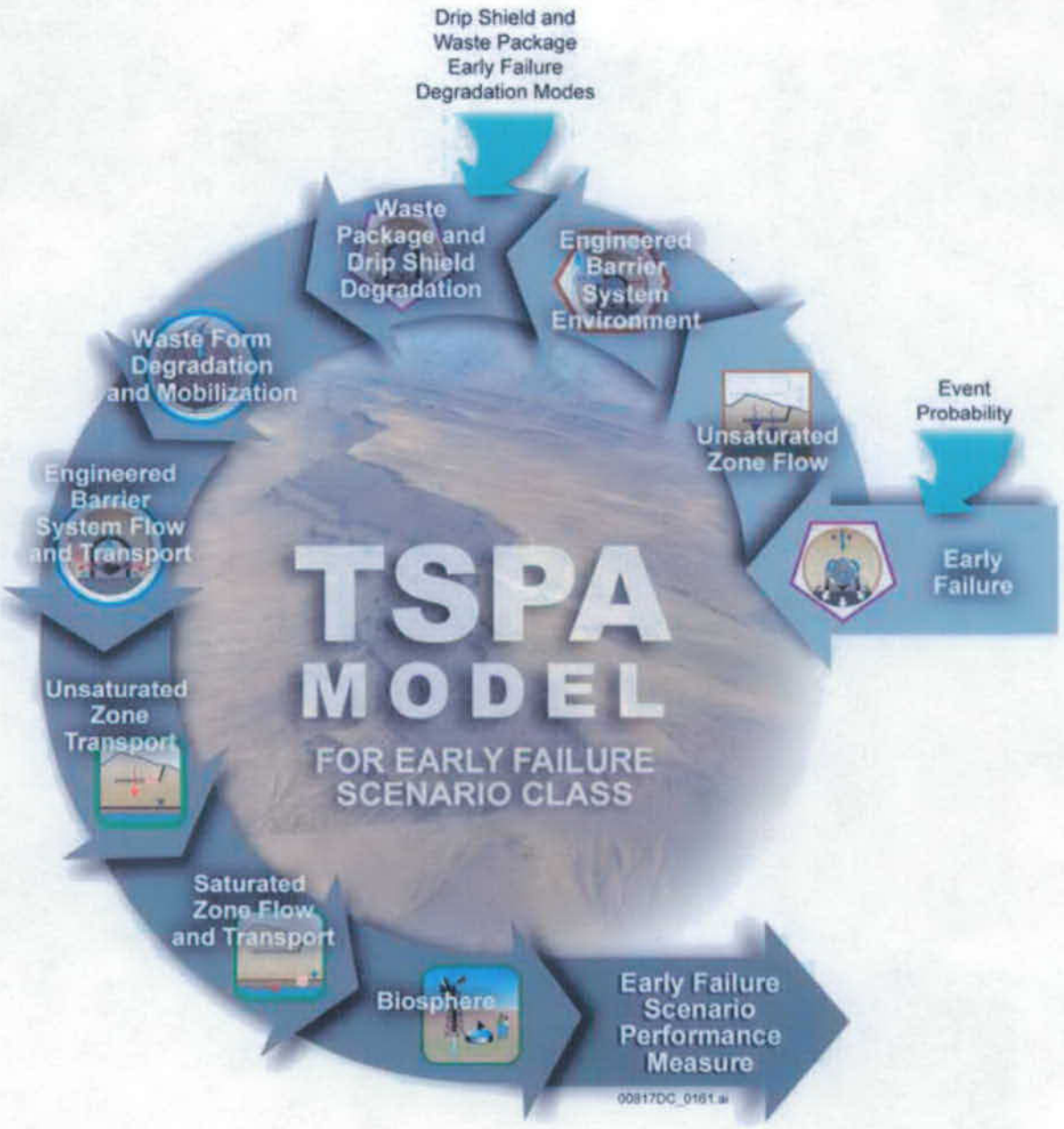

Figure 6.4-1. Schematic Representation of the TSPA-SEIS Components for the Early Failure Scenario Class

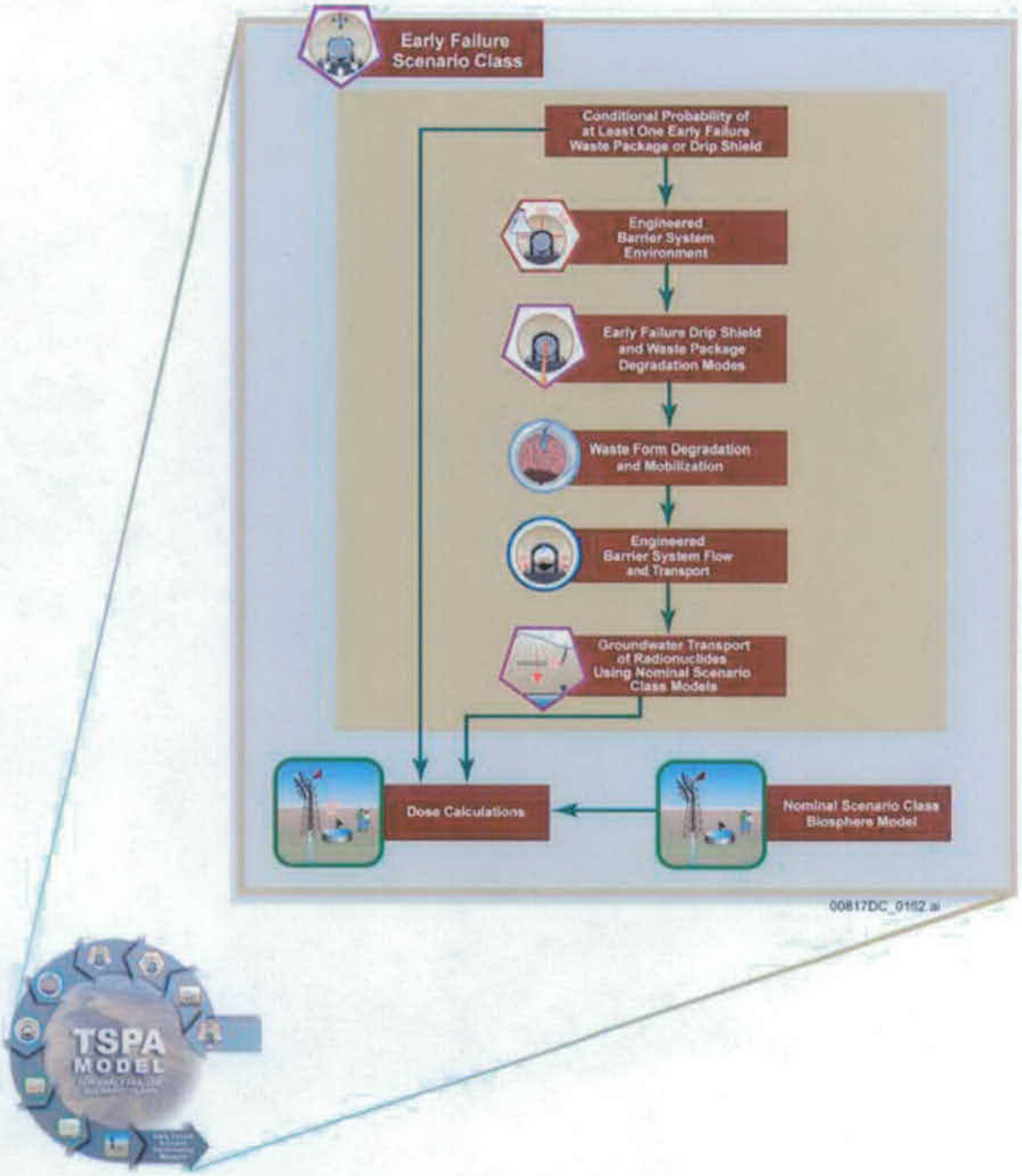

Figure 6.4-2. Information Flow Diagram for the Early Failure Scenario Class in the TSPA-SEIS

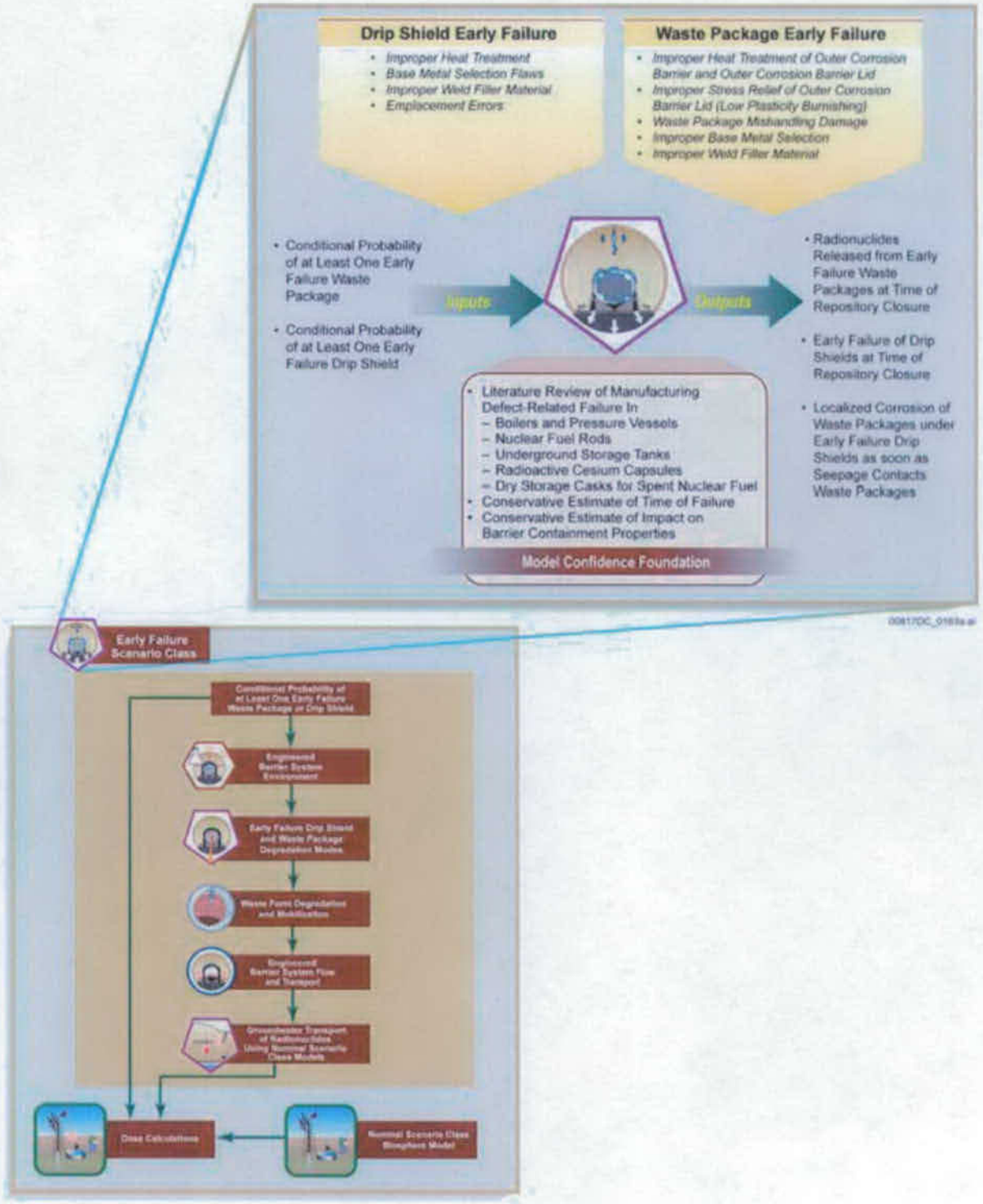

Figure 6.4-3. Inputs, Outputs, and Basis for Model Confidence for the Early Failure Scenario Class

INTENTIONALLY LEFT BLANK

6.5 TSPA-SEIS FOR THE IGNEOUS SCENARIO CLASS

Igneous activity can lead to disruptive events that can affect the long-term performance of the Yucca Mountain repository. Yucca Mountain is in a region that has had volcanic activity in the geologic past, and, although there is a very low probability of recurrence of igneous activity affecting the repository, the mean probability is greater than 1 in 10,000 in 10,000 years (BSC 2004 [DIRS 169989], Table 7-1). Accordingly, igneous activity is examined with the TSPA-SEIS because it is not excluded under the probability criterion at 10 CFR 63.642(a) [DIRS 178394]). The framework for this examination is the Igneous Scenario Class. The Igneous Scenario Class includes all screened-in features, events, and processes (FEPs) related to igneous activity. Analysis of igneous activity in the Yucca Mountain region has led to a focus on post-Miocene activity as a basis for the TSPA-SEIS (BSC 2004 [DIRS 169989], Section 6.1.1.1). Figure 6.5-1 is a Yucca Mountain region map that shows the locations and ages of post-Miocene (less than 5.3 million years) igneous activity, represented by multiple volcanic centers.

A probabilistic volcanic hazard analysis (PVHA) was performed to assess the volcanic hazard at Yucca Mountain. For the PVHA, an expert panel was convened in the year 1995 to review pertinent data relating to volcanism at Yucca Mountain and, based on these data, to quantify both the annual probability and associated uncertainty of a volcanic event intersecting a proposed repository sited at Yucca Mountain (BSC 2004 [DIRS 169989], Section 6.1). Work is currently in progress to update the PVHA expert elicitation to take into account new information available since 1996 (SNL 2007, Section 1.2.1 [DIRS 182219]). Results of the PVHA update are not anticipated to be ready for use in the SEIS, however, and the information provided in the 1995 review will provide a suitable basis for the TSPA-SEIS consistent with information available at this time. An alternative set of parameter values based on the PVHA update will be provided to the TSPA for evaluation when available.

Disruption of the repository in the Igneous Scenario Class is addressed by two modeling cases: the Igneous Intrusion Modeling Case and the Volcanic Eruption Modeling Case. Figure 6.5-2 shows the theoretical relationship between an igneous intrusion and volcanic eruption at Yucca Mountain. Information about natural volcanic systems and parameters used to model their behavior is provided in *Characterize Eruptive Processes at Yucca Mountain, Nevada* (SNL 2007 [DIRS 174260]. In both modeling cases, Magma propagates upward through the Earth's crust in fluid-driven cracks (dikes). The Igneous Intrusion Modeling Case considers only the intersection of repository drifts by one or more dikes. The Igneous Eruption Modeling Case considers an eruptive conduit that forms when a portion of the erupting dike begins to widen, creating a conduit to focus magma flow to the surface.

In the Igneous Intrusion Modeling Case, magma from dikes engulfs all DSs and WPs in the intersected repository drifts, rendering them incapable of protecting their contents. llThe CDSP WP and CSNF WP inner and outer barriers, the cladding in the case of CSNF, and the waste form itself are instantly degraded, with the exception being the HLW glass waste form that undergoes the same degradation processes as described in the Nominal Modeling Case.The magnitude of radionuclide transport to the UZ is controlled by the amount of seepage and the radionuclide solubilities. The radionuclides may be transported by groundwater downward through the UZ to the water table, then to the accessible environment by the water that flows in the SZ.

In the Volcanic Eruption Modeling Case, magma erupts into the atmosphere. The eruptive conduit(s) intersects the repository and damages the WPs located within the conduit cross-sectional area. The rising magma entrains radionuclide waste particles and a portion of the erupting stream becomes a bouyant, convecting column that is ejected into the atmosphere. The associated tephra plume is transported downwind and the particles in the plume are dispersed and eventually deposited on the land surface. The contaminated soil, including tephra, is then subject to redistribution by sedimentary processes. The conceptual and mathematical model of contaminated tephra transport implemented by the TSPA-SEIS is described in *Atmospheric Dispersal and Deposition of Tephra from a Potential Volcanic Eruption at Yucca Mountain, Nevada* (SNL 2007 [177431]). The conceptual and mathematical model of redistribution processes implemented by the TSPA-SEIS is described in *Redistribution of Tephra and Waste by Geomorphic Processes Following a Potential Volcanic Eruption at Yucca Mountain, Nevada* (SNL 2007 [DIRS 179347]).

Both of these modeling cases is represented separately in the TSPA-SEIS analyses. Section 6.5.1 discusses the Igneous Intrusion Modeling Case and Section 6.5.2 discusses the Volcanic Eruption Modeling Case.

6.5.1 Igneous Intrusion Modeling Case

The implementation of the Igneous Intrusion Modeling Case includes the definition of submodels for the processes affecting release of radionuclides associated with igneous intrusion, and the implementation of submodels in the integrated TSPA-SEIS for the calculation of mean annual dose. The following sections address these two different aspects of the implementation.

6.5.1.1 TSPA-SEIS Submodels for the Igneous Intrusion Modeling Case

The Igneous Intrusion Modeling Case considers an igneous event in which a dike intersects the repository drifts, and magma flows into and fills the drifts. In this modeling case, the magma remains in the subsurface with no eruption out of the ground surface. The flow characteristics of the intruding magma, cause it to fill every drift within the repository. Hence, all WPs, DSs, and fuel cladding are damaged so that they no longer have waste isolation capability. Magma intrusion, however, does not damage the invert. Because an intruded drift will fill with magma within 15 to 25 minutes (depending on the size of the aperture) (SNL 2007 [DIRS 177430], Sections 6.3.3.5.6), the igneous event is treated as an instantaneous event in the TSPA-SEIS. The magma then cools and solidifies in the emplacement drifts. Radionuclides dissolved in water moving through the basalt may be transported by the groundwater downward through the invert and into the UZ to the water table, and then to the accessible environment by flow and transport processes in the SZ, just as is simulated by the Nominal Modeling Case

The TSPA-SEIS selects parameter values from the appropriate distributions for each of the model components and submodels for each realization of the Igneous Intrusion Modeling Case. The amount of seepage water, the chemistry of the seepage water, and the temperature of the waste form specific to this modeling case are used to simulate degradation of the HLW glass and subsequent radionuclide mobilization. The radionuclides in the CSNF and U.S. Department of Energy spent nuclear fuel (DSNF) are considered immediately available for dissolution and transport. Using these inputs, the fate of the radionuclides mobilized by the igneous intrusion is

evaluated using the Nominal Scenario Class TSPA-SEIS components and submodels for flow and transport of the released radionuclides in the invert of the EBS, UZ, and SZ. The TSPA-SEIS components needed to estimate mean annual dose in the Igneous Intrusion Modeling Case are shown on Figure 6.5-3. Modifications to the Nominal Scenario Class are indicated by the bulleted items on the figure.

- The probability of an igneous event is the annual frequency, expressed as a cumulative distribution function (CDF), of an intersection of the repository by a volcanic dike. The CDF is calculated in *Characterize Framework for Igneous Activity at Yucca Mountain, Nevada* (BSC 2004 [DIRS 169989], Section 6.5 and Table 7-10. The annual frequency of an igneous event ranges from approximately 7.4×10^{-10} to 5.5×10^{-8} for the 5th and 95th percentiles, respectively, with a mean annual frequency of 1.7×10^{-8}. This mean annual frequency, which is independent of the characteristics of the event (i.e. size, duration, power) is applied to both the Igneous Intrusion and Volcanic Eruption Modeling Cases to determine mean annual dose.

- The TSPA-SEIS for the Igneous Intrusion Modeling Case for 20,000 years and 1,000,000 years, considers a single igneous intrusion event per realization that occurs at some uniformly sampled time between the first and last timesteps, or between 10 years, and 20,000 years or 1,000,000 years.

- Because nominal processes do not progress sufficiently in 20,000 years to result in the release of any radionuclides, the Igneous Intrusion Modeling Case for 20,000 years does not evaluate any pre-intrusion degradation of the WPs, DSs, or CSNF cladding in emplacement drifts. Degradation of these EBS components is accounted for in the Nominal Scenario Class for 20,000 years (Section 6.1.3). However, for the 1,000,000-year Igneous Intrusion Modeling Case, the nominal processes of degradation of the WPs, DSs, and CSNF cladding do occur up until the time of the igneous intrusion. The inclusion of nominal processes before the igneous intrusion, prevents over counting of any radionuclides released by nominal processes prior to the igneous intrusion.

- The intruded drifts have a seepage flux equal to the local percolation flux (SNL 2007 [DIRS 181244], Section 6.7.1.1) (i.e., capillary effects at the drift wall are neglected). The volumetric seepage rate is, therefore, obtained by applying the percolation flux at the base of the Paintbrush nonwelded hydrologic unit (PTn), provided by the EBS Thermal-Hydrologic (TH) Environment Submodel for the appropriate percolation flux subregion, to the projected area of the emplacement drift. In particular, the volumetric seepage rate for a single WP is set equal to that obtained by applying the flux at the base of the PTn to the 5.1-m-long by 5.5-m-wide drift segment representing one WP footprint.

- The DSs and WPs provide no hindrance to flow because they were damaged at the time of the igneous intrusion. Likewise, the basalt that has filled the drift is considered to be fractured so as to not hinder the flow of seepage (SNL 2007 [DIRS 177430], Section 8.1.2).

- No credit is taken for the CSNF cladding because it is considered entirely degraded at the time of the igneous intrusion (SNL 2007 [DIRS 177430], Section 8.1.2).

- The chemistry of the water contacting the waste (i.e. the freely suspended radionuclides within the basalt) is determined using the chemical environment submodel processes of the Nominal Modeling Case. Chemical reactions between the basalt and the incoming seepage have a range of pH and ionic strength of 6.05 to 8.12, and 0.000290 moles/kg to 0.0959 moles/kg, respectively (SNL 2007 [DIRS 177430], Section 6.7.7). These ranges are bound by the EBS chemical environment submodel, and therefore the effects of basalt/seepage water interactions are indirectly accounted for.

Figure 6.5-4 shows information flow within the TSPA-SEIS for the Igneous Intrusion Modeling Case. Figure 6.5-5 indicates major inputs and outputs for each TSPA-SEIS realization, and describes the basis for confidence in the TSPA-SEIS analysis. Figures 6.5-3 and 6.5-4 indicate that the TSPA-SEIS framework for the Igneous Intrusion Modeling Case is similar to that of the Nominal Scenario Class. The principal model components and submodels used in the Igneous Intrusion Modeling Case are the same as those included in the Nominal Scenario Class. They are described in Sections 6.3.1 to 6.3.11. However, Sections 6.5.1.1.1 and 6.5.1.1.2 describe some model components and submodels that are modified to account for igneous intrusion. The following describes other changes to the Nominal Scenario Class that apply to the Igneous Intrusion Modeling Case.

6.5.1.1.1 Igneous Intrusion Engineered Barrier System Damage Submodel

Conceptual Model—The Igneous Intrusion Modeling Case describes the consequences of magma that intrudes into repository emplacement drifts, damages CSNF WPs and CDSP WPs in the intruded drifts, and solidifies. Since the flow characteristics of the magma cause it to intrude into every drift within the repository, every WP (and CSNF cladding) and DS is rendered incapable of protecting its contents. Conceptually, the CDSP and CSNF WP inner and outer barriers, the cladding in the case of CSNF, and the waste form itself are instantly degraded, leaving radionuclides available for transport through normal dissolution processes when seepage re-enters the drift. While the entire inventory is available for transport following an igneous intrusion, with the exception of the inventory associated with the HLW glass which undergoes the same degradation processes as described in the Nominal Modeling Case, the magnitude of radionuclide transport to the UZ is controlled by the amount of seepage and the radionuclide solubilities. WP and DS degradation processes associated with normal conditions are considered in the Igneous Intrusion Modeling Case for 1,000,000 years up until the time of the event, but are not considered in the Igneous Intrusion Modeling Case for 20,000 years.

The geologic feature associated with an igneous intrusion entering the repository is a dike. Dikes are subvertical to subhorizontal, elongated, tabular bodies of magma that can extend for many kilometers from a magma source. In the Yucca Mountain region, and for the Igneous Intrusion Modeling Case, the dikes are generally vertically oriented (SNL 2007 [DIRS 177432], Section 6.3.1). A grouping of more than one dike related to the same source of magma is a dike swarm. It is possible for one or more dikes in a swarm to intersect the repository and damage WPs. Figure 6.5-6 is a schematic diagram of the intersection of an igneous dike and a repository drift containing WPs.

TSPA-SEIS Abstraction—The TSPA-SEIS analysis of the Igneous Intrusion Modeling Case considers the assessment of the consequences of an igneous intrusion intersecting the repository. *Number of Waste Packages Hit by Igneous Intrusion* (SNL 2007 [DIRS 177432]) describes the analysis conducted to estimate the number of WPs that would be damaged by an igneous intrusion.

6.5.1.1.2 Engineered Barrier System Environment Submodels in the Igneous Intrusion Modeling Case

The EBS TH Environment Submodel for the Igneous Intrusion Modeling Case differs from that used for the Nominal Scenario Class Modeling Case (Sections 6.3.2), in that it accounts for the temperature increase within and around the drift due to the intrusion of magma that fills the drift.

Conceptual Model—The heat from magma intruding into repository emplacement drifts will affect the EBS TH environment. Temperatures of the WPs, DSs, and the invert, spike to a maximum temperature at the time of the intrusion, and then cool back to ambient conditions (i.e. pre-igneous intrusion) over a 100-year time period. The associated temperature increases are described in *Dike/Drift Interactions* (SNL 2007 [DIRS 177430], Section 6.4.6 and Table 6-13). The in-drift relative humidity, invert liquid saturation, and invert liquid flux are similarly affected. The EBS chemical environment conditions are simulated just as they are for the Nominal Modeling Case since the ranges of pH and ionic strength of seepage water that has interacted with basalt, is bounded by the ranges used by the Nominal Modeling Case (SNL 2007 [DIRS 177430], Section 6.7.6). EBS flow and transport processes are also simulated just as they are for the Nominal Modeling Case. Relevant EBS chemical, and flow and transport processes are turned "off" while boiling conditions exist within the drift.

TSPA-SEIS Abstraction—The EBS TH Environment Submodel (Sections 6.3.2) for the Igneous Intrusion Modeling Case accounts for the temperature of the intrusive body and its effect on the EBS temperatures at the time of intrusion. This temperature is derived as described in *Dike/Drift Interactions* (SNL 2007 [DIRS 177430], Section 6.4. The Igneous Intrusion Modeling Case uses an initial temperature of the intrusive body of 1,150°C, and uses a cylindrical one-dimensional, transient heat conduction model to describe the cooling of the intrusive body and the surrounding rock mass. The effects of latent heat were considered and were found to have no impact on the results provided to the TSPA in form of Table 6.5-1 (SNL 2007 [DIRS 177430], Section 7.3.2.1.1.2). Temperatures return to ambient conditions (i.e., temperatures just before the event occurred) in approximately 100 years. Temperatures resulting from this abstraction are shown in Table 6.5-1. The five main columns of the table, labeled "For an Intrusion into a Repository at 25, 50, 100, 150, or 200°C," represent different 100-year temperature history shifts on the WP and drift wall depending on the temperatures of the WP and the drift wall at the time of the event.

The relative humidity within the intruded drifts is modeled as equal to zero when the magma temperature is at or greater than 100°C. Water saturation in the waste form and in corrosion product cells is set to zero for temperatures greater than 100°C, and set to one for temperatures less than 100°C.

The EBS Chemical Environment Submodel (Section 6.3.4) for the Igneous Intrusion Modeling Case uses the ranges of pH and ionic strength, and solubilities associated with the Nominal Modeling Case.

6.5.1.2 Mean Annual Dose Submodel for the Igneous Intrusion Modeling Case (Integration of Submodels)

The TSPA-SEIS calculates the mean annual dose for the Igneous Intrusion Modeling Case using a three-step process. First, an LHS of uncertain TSPA-SEIS parameters is generated. Each element of the LHS is a vector, specifying a value for each uncertain parameter. For each element in the LHS, a number of annual dose histories are computed using GoldSim. Each annual dose history is associated with a single igneous intrusion occurring at a specified time. For the 20,000 year intrusion case, the LHS sample size is 300 with event times at 10, 100, 600, 1000, 2000, 4000, 6000, 10,000, 14,000, and 18,000 years. For the 1,000,000 year intrusion case, the LHS sample size is 300 with event times at 250, 600, 1000, 4000, 10,000, 40,000, 100,000, 200,000, 400,000, and 800,000 years. The seepage water chemistry and temperature of the waste form specific to the Igneous Intrusion Modeling Case are used to calculate waste form degradation and radionuclide mobilization. Using these inputs, the fate of the mobilized radionuclides is evaluated using the Nominal Scenario Class submodels for radionuclide transport in the EBS, UZ, and SZ.

Second, for each element in the LHS, the expected annual dose history is calculated by Equation 6.1.2-16, using the annual dose histories computed for that realization. The integral in Equation 6.1.2-16 accounts for the uncertainty in the time of an igneous intrusion, and for the uncertainty in the frequency of igneous events, and is evaluated numerically by EXDOC (Section 6.1.5). The frequency of igneous events is sampled from the probability distribution described by Table 6.5-2. Finally, the mean annual dose history is calculated as the average of the expected annual dose histories from the set of realizations. Therefore, the analysis performed in the TSPA-SEIS for the Igneous Intrusion Modeling Case relies on: (1) inputs to assess consequences of an igneous intrusion within the repository and (2) inputs associated with the probability of the intrusive event.

6.5.1.3 Implementation in the TSPA-SEIS

Several inputs and feeds to the Igneous Intrusion Modeling Case originate from other TSPA-SEISs and are used in Igneous Intrusion Modeling Case calculations. Feeds from other model components and submodels to the Igneous Intrusion Modeling Case include the number of CSNF WPs and CDSP WPs in the intruded drifts and the log of the carbon dioxide fugacity. The Igneous Intrusion Modeling Case inputs are: (1) time-dependent temperature look-up tables and (2) parameters for the timing and probability of an igneous intrusion. Igneous Intrusion Modeling Case inputs are described in more detail in the following paragraphs.

For the temperature perturbation associated with an igneous intrusion, a two-dimensional look-up table based on Table 6.5-1 is implemented, which defines the shift in WP temperature for times up to 100 years after magma intrusion into the drift(s). A similar two-dimensional look-up table is implemented for drift-wall and invert temperatures as magma enters the drift(s). Temperature values are interpolated from the tables based on: (1) the temperatures of the WP,

drift wall, and invert when the igneous intrusion occurs and (2) the elapsed time since the igneous intrusive event occurred (SNL 2007 [DIRS 177430], Table 8-2), where $T_{r=0m}$ and $T_{r=3m}$ refer to the temperatures at a radius of 0 m (i.e., centerline of the WP) and 3 m (i.e., drift wall and invert) from the drift center, respectively.

Inputs also include: (1) the mean annual frequency of a dike intersecting the repository (BSC 2004 [DIRS 169989]), Section 6.5.3); and (2) the minimum and maximum times during the simulation at which the igneous intrusion can occur.

6.5.1.4 Evaluation of Implementation Provisions for the TSPA-SEIS

There are differences in assumptions and parameter sets used in the TSPA-SEIS that have arisen in the development of the abstractions and process models. Most of these differences are due to the use of conservative assumptions in the process model or analysis when uncertainty is difficult to quantify. Understanding and evaluating potential impacts from these assumptions with respect to the mean annual dose is conducted through a series of processes including Uncertainty Characterization Reviews, Corroboration of Results with Auxiliary Analyses, and Validity and Defensibility of Performance Demonstration. To enhance understanding of the complex interactions within the TSPA-SEIS, a discussion of consistency among model components and submodels and identification of conservative assumptions in abstractions, process models, and parameter sets supporting the Igneous Intrusion Modeling Case are discussed below.

6.5.1.4.1 Model Component Integration

6.5.1.4.2 Identification of Conservatisms in Submodels and Abstractions

WPs and DSs are Completely Damaged—In the Igneous Intrusion Modeling Case, all WPs and DSs located in magma-intruded drifts are assumed to be sufficiently damaged that they provide no hindrance to flow, or protection of their radionuclide inventories to dissolution processes. In addition, no credit is taken for entombment of the waste by the solidified magma. Rather, when in-drift conditions are favorable for the re-entry of seepage, the mobilization of the CDSP and CSNF inventories is controlled only by the radionuclide solubilities. Because there will be no backfill in the drifts, there are no credible mechanisms to block or mitigate the resulting effects from a dike intrusion into a drift or the effects of the magma on the WPs and DSs (SNL 2007 [DIRS 177432], Section 5.1).

In addition, since the waste form is conservatively assumed to be entirely degraded during an igneous intrusion, any contribution to its degradation that could have occurred by seepage through fracturing of the basalt is already accounted for. This conservative assumption increases the release of radionuclides from the EBS above the release that would occur if some credit were taken for WPs, DSs, and the solidified magma, all of which would provide some hindrance to flow, through the waste form.

Drift Seepage Equal to Percolation after Intrusion—In the Igneous Intrusion Modeling Case, the seepage is set equal to 100 percent of the local percolation flux at the base of the PTn (Section 6.3.3) for magma-intruded drifts. The intruded basalt in the drift is assumed to provide no resistance to water flow. Because all of the WPs and DSs are failed, the entire seepage flux

enters the WP and is available for advective transport of radionuclides from the EBS (SNL 2007 [DIRS 181244], Section 6.7.1.1).

This is a conservative abstraction for implementation in the TSPA-SEIS that results in an increase in the release of radionuclides from the EBS over that which would occur if some credit were taken for the cooled magma diverting some of the seepage away from the waste form.

Drift and Dike Interactions—Several conservative assumptions are made for the dike and drift interactions as follows:

1. The filling of the drifts with magma does not consider the presence of the EBS component (e.g., DSs), rubble filled drift, or other features that could impede the flow of magma and therefore contact fewer WPs than the total inventory (SNL 2007 [DIRS 177430], Section 5.2).

2. WPs engulfed by magma are instantaneously destroyed and provide no further protection of their contents (SNL 2007 [DIRS 177430], Section 8.1.2).

3. Upon cooling, the basalt is highly fractured and does not provide any hindrance to seepage. The thermal properties of the basalt-filled drift are assumed to be the same as the surrounding host rock (SNL 2007 [DIRS 177430], Section 5.3.1).

These conservative assumptions result in an overestimation of the amount and mobilization of radionuclide inventory for transport through the EBS, UZ and SZ, and hence contribute to higher than expected doses.

6.5.1.5 Alternative Conceptual Model(s) for Igneous Intrusion Modeling Case

An important reason for considering alternative conceptual models (ACMs) is to help build confidence that plausible changes in modeling assumptions or simplifications will not change conclusions regarding subsystem and total system performance. Section 6.2 outlines the general consideration and treatment of ACMs used to support the TSPA-SEIS. Conservatism at the subsystem level has been used to select the best ACM to use rather than quantitatively propagate multiple ACMs to the TSPA-SEIS. Generally, additional uncertainty is incorporated into the selected conceptual model if more than one ACM is deemed appropriate for use rather than considering multiple ACMs in the TSPA-SEIS. If an ACM appears to be significant at the subsystem level, then an appropriate abstraction is developed for that ACM for consideration within the TSPA-SEIS. The result of the process is documented within the individual analysis model reports. It is important to note that treatment of ACMs within the individual analysis model reports may differ significantly to be consistent with available data and current scientific understanding. Therefore, the Igneous Intrusion Modeling Case ACMs are summarized below.

ACM for Estimating the Igneous Event Rates in the Probabilistic Volcanic Hazard Analysis—The PVHA model uses the number of identified post-Miocene era volcanic events observable at the surface plus some buried in the Yucca Mountain region. *Characterize Framework for Igneous Activity at Yucca Mountain, Nevada* (BSC 2004 [DIRS 169989], Sections 6.3.1.6 through 6.3.1.7 and Table 6-4) identifies an ACM for the PVHA in which a significant number of buried (i.e., unidentified) volcanic centers would be included in the estimation of

the igneous event rates. The basis for the ACM is that aeromagnetic anomalies suggest that a significant number of unidentified volcanic events were unaccounted for in the PVHA, thus underestimating the volcanic hazard. However, this ACM was not considered because its effects on the probability of an igneous event could not be quantified without further data collection. A drilling and sampling program is underway to determine if any of these anomalies represent Quaternary buried volcanic centers. In addition, an update to the PVHA is underway to reassess the probability of intersection and the probability of a volcanic center being located on Yucca Mountain. Total mean annual dose from the Igneous Scenario Class can reasonably be expected to vary linearly with frequency.

ACMs for Estimating the Intersection Annual Probability in the Probabilistic Volcanic Hazard Analysis—*Characterize Framework for Igneous Activity at Yucca Mountain, Nevada* (BSC 2004 [DIRS 169989], Section 6.3.1.8 and Table 6-5) identifies several ACMs for estimating the intersection probability (i.e., the annual probability of a volcanic event intersecting the repository footprint). The ACM probabilities are captured by the probability used in the PVHA, which indicates that any impacts on the TSPA-SEIS from using one of these ACMs would be negligible.

ACMs for Dike Propagation—*Dike/Drift Interactions* (SNL 2007 [DIRS 177430], Section 6.3.3.5), identifies ACMs for dike propagation that use hydraulic-fracture models. The *Dike/Drift Interactions* report (SNL 2007 [DIRS 177430], Section 6.3.8) concluded that none of these models were appropriate for the dike propagation in the vicinity of an underground repository, as none of the models has a free surface that can model the changing behavior of the dike as the surface is approached. Thus, the ACMs were used for validation comparisons only and were not appropriate for use in the TSPA-SEIS.

ACMs for Effusive Magma Flow Into Drifts—*Dike/Drift Interactions* (SNL 2007 [DIRS 177430], Section 6.3.3.5) identifies ACMs for effusive or pyroclastic flow from a dike into a drift. Simulation of these flows and their interactions with WPs is computationally intensive and, therefore, not practical for implementation within the TSPA model. Instead, the abstractions included in *Number of Waste Packages Hit by Igneous Intrusion* (SNL 2007 [DIRS 177432]), accounts for the effects of these flows within the TSPA framework.

ACMs for TH Effects on Magma Filled and Neighboring Non-Magma Filled Drifts Drifts—*Dike/Drift Interaction* (SNL 2007 [DIRS 177430], Section 6.4.7) identifies ACMs for the TH behavior of magma-filled drifts and its effects on neighboring drifts when an igneous intrusion into the repository affects a limited number of drifts rather than all the drifts.. These ACMs involve an evaluation of additional physics, including latent heat of crystallization, host-rock saturation, and enhanced vapor diffusion, and an alternative model for heat conduction around affected emplacement drifts. Inclusion of the latent heat of crystallization and host-rock saturation in the heat transfer analyses was evaluated and is shown to have a negligible effect on the results, producing elevated temperature histories (i.e., above boiling) no more than two to five years longer than without these ACMs included in the analysis (SNL 2007 [DIRS 177430], Section 6.4.7).

With respect to the TH implementation of igneous intrusion in the TSPA-SEIS, these ACMs do not produce elevated temperature histories (i.e., above boiling) significantly longer than those already in use. Hence, the impact to the TSPA-SEIS of using any of these TH ACMs is negligible.

No ACMs were recommended for inclusion in the TSPA-SEIS.

6.5.2 Volcanic Eruption Modeling Case

The Volcanic Eruption Modeling Case in the TSPA-SEIS considers the possibility of a volcanic eruptive conduit intersecting the repository footprint resulting in the dispersal of waste-contaminated tephra in the atmosphere with eventual deposition on the ground surface. This modeling case evaluates only the post-eruption consequences due to waste deposited at the location of the reasonably maximally exposed individual (RMEI) directly or redistributed from upstream in the Fortymile Wash watershed. It does not include an evaluation of annual dose received during the active volcanic eruption phase when the waste is transported and dispersed in the atmosphere. The active eruption phase is evaluated separately in Section 6.5.2.4 to show that the mean annual dose during the active eruption phase is small compared to the mean annual dose during the post-eruption time period.

Implementation of the Volcanic Eruption Modeling Case for the TSPA-SEIS includes the determination of both the probability of the event and its consequences. The probability of an eruptive event is determined by two factors. The first is the probability of an eruption penetrating the repository sampled from the probability distribution for the annual frequency of an intersection of the repository by a dike, as provided in *Characterize Framework for Igneous Activity at Yucca Mountain, Nevada* (BSC 2004 [DIRS 169989], Table 6-8, Section 6.5.3.1; and shown in Table 6.5-2. The second factor is the probability of an eruption, given that a dike intersection of the repository occurs; this value is 0.28. The annual frequency of an eruption through the repository is estimated by multiplying the two probability factors described above.

The Volcanic Eruption Modeling Case in the TSPA-SEIS includes submodels for the processes affecting the release, transport, and redistribution of radionuclides associated with the volcanic eruption, and implements the submodels for the calculation of mean annual dose. The following sections (Sections 6.5.2.1 to 6.5.2.2) address these submodels and their implementation for the Volcanic Eruption Modeling Case. In addition, the model evaluation, model conservatism, and ACMs are discussed in Sections 6.5.2.3 and 6.5.2.4.

6.5.2.1 TSPA-SEIS Submodels for the Volcanic Eruption Modeling Case

The submodels for evaluating the consequences of the Volcanic Eruption Modeling Case are shown on Figure 6.5-7, which does not contain as many model components and submodels as the Igneous Intrusion Modeling Case (Figure 6.5-3). Figure 6.5-8 illustrates the flow of information in the TSPA-SEIS Volcanic Eruption Modeling Case and the relationship between the submodels for the Volcanic Eruption Modeling Case. Figure 6.5-9 indicates the major inputs and outputs of the Volcanic Eruption Modeling Case, the features included in the TSPA-SEIS, and the foundation for confidence in the Volcanic Eruption Modeling Case.

Four submodels are considered in the Volcanic Eruption Modeling Case. Volcanic Interaction with the Repository Submodel (Section 6.5.2.1.1) describes the number of WPs that may be destroyed by, and entrained in, a volcanic eruption and the amount of waste available for atmospheric transport. The Atmospheric Transport Submodel (Section 6.5.2.1.2) describes the atmospheric transport of this erupted tephra/waste mixture and eventual deposition on the land surface. The Tephra Redistribution Submodel (Section 6.5.2.1.3) describes the redistribution of the contaminated tephra to the location of the RMEI. The Volcanic Ash Exposure Submodel (Section 6.5.2.1.4) uses the volcanic ash biosphere dose conversion factors (BDCFs) to estimate mean annual dose to the RMEI, which was previously presented in the Biosphere Model Component (Section 6.3.11.2). The following subsections describe these four components of the Volcanic Eruption Modeling Case.

6.5.2.1.1 Volcanic Interaction with the Repository Submodel

Conceptual Model—Eruptive events involving the intersection of an eruptive conduit with the repository could result in the atmospheric release of volcanic tephra and mobilized waste from the repository and subsequent deposition on the ground surface. Figure 6.5-10 is a schematic diagram of the intersection of an igneous dike and eruptive conduit with the repository. The quantity of waste erupted into the atmosphere in any one event is conceptualized in the Volcanic Eruption Modeling Case as depending on the distribution of WPs in the emplacement drifts, the number and size of eruptive conduits intersecting the drifts, the degree of damage to those WPs, the amount of waste from the WPs that is entrained into the erupting material, and the fraction of magma that is erupted into the ash cloud. The size and number of dikes associated with an eruptive event considered credible for the Yucca Mountain region are described in *Characterize Eruptive Processes at Yucca Mountain, Nevada* (SNL 2007 [DIRS 174260], Table 7-1). The conduit diameter is given as a normal distribution with a mean diameter of 15 m. The distribution for the number of eruptive centers within the repository footprint is presented in *Characterize Framework for Igneous Activity at Yucca Mountain, Nevada* (BSC 2004 [DIRS 169989], Figure 6-21). The number of WPs intersected by magmatic conduits is a function of conduit area, the number of conduits, and the conduit location within the repository. Only WPs located partially or entirely within a magmatic conduit are assumed to be destroyed, making all of the waste in these WPs available for entrainment in the erupting pyroclastic material. The potential for WPs located outside the conduit diameter to be mobilized by magma and moved toward the conduit is analyzed in *Dike/Drift Interactions* (SNL 2007 [DIRS 177430], Section 6.4.8.3.2). The analysis concludes that WP movement outside of a conduit profile is not expected considering expected magma velocities, pressures, and viscosities, as well as WP dimensions and densities. Estimates of the number of WPs that might be intersected during an eruptive sequence are based on a probability distribution.

TSPA-SEIS Abstraction—The mass of waste incorporated in the tephra plume from an eruptive event depends on the waste inventory, the number of WPs intersected, and the fraction of waste-containing magma that is erupted as a tephra plume instead of lava flows and scoria cone. The CDF for the number of WPs intersected by conduits is shown in Table 6.5-3. Figure 6.5-11 graphically illustrates the CDF and probability for the number of WPs that could be potentially affected by an eruptive conduit(s) from igneous activity culminating in a volcanic eruption within the repository footprint (SNL 2007 [DIRS 177432], Section 7.1). As seen on the figure, the Waste Packages Hit analysis indicates that there is approximately a 70 percent probability

that no WPs will be hit by a volcanic eruption intersecting the repository. The small conduit diameters relative to drift spacing mean that 70 percent of the conduits intersecting the repository footprint would intersect between drifts and therefore not impact any WPs. In the 30 percent of cases in which one or more packages are hit, the most likely number hit is four and the maximum number hit is seven.

The Volcanic Eruption Modeling Case includes the mass of waste in both the CSNF WPs and CDSP WPs that are hit, and the proportions of each kind of waste released from the repository to the erupting volcanic magma. The mass of waste hit is multiplied by the magma partitioning factor to account for the partitioning of magma into surface lava flows, scoria cone, and tephra plume (SNL 2007 [DIRS 177431], Section 6.5.2.9). The magma partitioning factor is specified as a uniform distribution from 0.1 to 0.5 and represents the fraction of magma that is erupted into the tephra plume to be considered in the Volcanic Eruption Modeling Case. Waste potentially deposited with surface lava flows and scoria cone is excluded from the TSPA-SEIS analysis on the basis of low consequence at the RMEI location.

6.5.2.1.2 Atmospheric Transport Submodel

Conceptual Model—The conceptual model for the Atmospheric Transport Submodel is a vertical column of heated tephra and waste particles, resulting in a buoyant plume that reaches neutral buoyancy at some level in the atmosphere. The plume is then transported downwind and, because of dispersive processes, spreads out laterally as it is transported. Solids fall from the plume as it travels depending on the wind speed, particle density, and settling velocity. The pyroclastic material ejected into the atmosphere from a volcanic eruption eventually falls to the ground surface and forms a contaminated tephra sheet of varying thickness extending and thinning, generally, downwind from the volcanic vent (SNL 2007 [DIRS 177431], Section 6.3).

Figure 6.5-12 is a schematic illustration of a volcanic eruption intersecting the repository at Yucca Mountain. The figure shows the transport of radioactive waste in the tephra plume from the repository to the location of the RMEI under the condition of a southerly directed wind.

TSPA-SEIS Abstraction—Atmospheric transport and deposition of erupted waste is evaluated using the ASHPLUME code (ASHPLUME_DLL_LA V2.1, STN: 11117-2.1-00 [DIRS 181035]) described in *Atmospheric Dispersal and Deposition of Tephra from a Potential Volcanic Eruption at Yucca Mountain, Nevada* (SNL 2007 [DIRS 177431], Section 6.5). The ASHPLUME code is implemented directly in the TSPA-SEIS Volcanic Eruption Model, using the ASHPLUME computer code as a dynamically linked library (DLL).

The ASHPLUME code simulates a violent Strombolian eruption with entrainment of radioactive waste in the erupted plume as waste particles attached to the pyroclastic fragments in the plume. The waste-contaminated tephra particles ejected into the atmosphere form a contaminated deposit on the land surface. The parameter "incorporation ratio" is a cutoff ratio for the minimum size of a tephra particle that can carry a waste particle of a given size. Expressed as the Log_{10} of the ratio, an incorporation ratio of 0 is used in the TSPA implementation, meaning the maximum waste particle size is equal to the tephra particle size. The mathematical formulation of this incorporation ratio and the approach to determining the mass fraction of waste that is incorporated in an eruption is discussed in *Atmospheric Dispersal and Deposition of*

Tephra from a Potential Volcanic Eruption at Yucca Mountain, Nevada (SNL 2007 [DIRS 177431], Section 6.5.2.6). The wind speed and direction that result in atmospheric transport of the erupted material are represented in the ASHPLUME code in terms of CDFs. These CDFs are specified for 1-km height increments between 0 km and 13 km above the mountain. Wind speed and direction for a given model realization are selected from the height bin appropriate to the eruption column height for that realization. Once selected, the wind speed and direction are assumed to be constant throughout the eruption duration in the ASHPLUME model. The impact of this simplification is considered to be negligible based on the analysis in SNL (2007 [DIRS 177431], Section 7.6). The ASHPLUME mathematical model for atmospheric dispersion and deposition of the particles in the plume is based on the theoretical model by Suzuki in "A Theoretical Model for Dispersion of Tephra" (Suzuki 1983 [DIRS 100489], pp. 95 to 113). The movement of air mass in the atmosphere is random within the scale of eddy motions in wind currents. Therefore, the dispersion of the tephra-containing waste particles in the atmosphere is also random. Particles disperse in the atmosphere in both vertical and horizontal directions. The scale of horizontal turbulence is much greater than the scale of vertical turbulence. Therefore, particle diffusion is considered to be two-dimensional in the horizontal "x-y" plane. Particle movement in the vertical "z" direction is accounted for by the particle settling velocity. The ASHPLUME mathematical model and its solution are described in *Atmospheric Dispersal and Deposition of Tephra from a Potential Volcanic Eruption at Yucca Mountain, Nevada* (SNL 2007 [DIRS 177431], Section 6.5). The Atmospheric Transport Submodel predicts the ground-level concentrations (areal density, g/cm^2) of tephra and waste directly deposited at the location of the RMEI and the spatial distribution of tephra and waste in the Fortymile Wash watershed for a simulated volcanic event. The tephra concentration in the Fortymile Wash watershed is converted into volcanic ash thickness by the Tephra Redistribution Submodel and potentially redistributed to the RMEI location along with incorporated waste.

The uncertain ASHPLUME code input parameters that may significantly affect the outcome of TSPA-SEIS calculations are expressed as probability distributions to be used in the TSPA-SEIS. Table 6.5-4 shows key ASHPLUME code input parameters, and indicates those that are represented by probability distributions and those that use fixed values.

6.5.2.1.3 Tephra Redistribution Submodel

Conceptual Model—Waste-contaminated tephra deposited on the ground surface in Fortymile Wash by the Atmospheric Transport Submodel could potentially be redistributed to the RMEI location due to hillslope and fluvial processes. Therefore, the waste concentration used in the Biosphere Submodel to determine dose consists of contributions from both waste-contaminated tephra at the RMEI location deposited directly when atmospheric conditions move the eruptive plume toward that location, and any waste-contaminated tephra redistributed from upstream that may have been deposited in the Fortymile Wash Watershed. Three major processes are considered in the tephra redistribution conceptual model: (1) mobilization from hillslopes; (2) mixing and dilution with uncontaminated sediments during channel transport; and (3) diffusion into the soil column at the RMEI location. A detailed description of the tephra redistribution conceptual model can be found in *Redistribution of Tephra and Waste by Geomorphic Processes Following a Potential Volcanic Eruption at Yucca Mountain, Nevada* (SNL 2007 [DIRS 179347], Section 6.2).

The conceptual tephra redistribution model divides the Fortymile Wash drainage area into two domains: the drainage basin and the alluvial fan. The drainage basin includes the vent location and the tephra and waste deposited on the landscape in the event of a volcanic eruption through the repository (Figure 6.5-13). The RMEI location is considered to be on the Fortymile Wash alluvial fan south of the fan apex. The drainage basin and the alluvial fan are divided at the fan apex. The location of the RMEI is specified in the same area for the igneous eruption case as for all other modeling cases so that estimates of the dose are calculated at a consistent location for the nominal, intrusive, and eruptive modeling cases. This means that model realizations with wind blowing away from this location and away from the Fortymile Wash do not contribute to dose calculations.

The tephra redistribution model uses a spatially distributed analysis of hillslopes and channels in the drainage basin upstream of the fan apex to provide an estimate of the mass of tephra and waste that could be transported from the upper drainage basin to the RMEI location by hillslope and fluvial processes. The model mobilizes and transports tephra and waste deposited on the landscape toward the RMEI location if it falls on steep slopes or on active channels. Before the mobilized tephra and waste are deposited at the RMEI location, they are transported through the alluvial channel system where mixing with uncontaminated channel sediments leads to dilution. Mixing occurs during flood events as sediment and tephra are entrained from the bed, mixed by turbulent flow, and redeposited on the bed. The depth to which tephra and channel sediment are mixed is the scour depth. The ratio of the tephra thickness to the scour depth at the fan apex, just upstream from the RMEI location, is used as the fraction of channel-bed material composed of tephra when the redistributed tephra and waste reach the RMEI location.

The tephra and waste transported from the upper drainage basin, and primary tephra and waste deposited at the RMEI location, provide the initial conditions for redistribution of radionuclides into the soil column at the RMEI location. The Tephra Redistribution Submodel considers the migration of radionuclides within the soil as a diffusion process due to suspension and redeposition of fine particles by infiltration, and physical mixing of soil particles by freeze-thaw cycles and bioturbation. The diffusion coefficients used in the model were calibrated using measured ^{137}Cs profiles on channels and inter-channel divides of the upper Fortymile Wash alluvial fan and therefore incorporate all of the potential diffusion processes (SNL 2007 [DIRS 179347], Sections 6.3.3 and 6.5.9). The time-dependent concentration resulting from the diffusion process is used by the Volcanic Ash Exposure Submodel to calculate dose to the RMEI.

TSPA-SEIS Abstraction—The Tephra Redistribution Submodel is implemented in the TSPA-SEIS Volcanic Eruption Model using the computer code FAR V1.2 (STN: 11190-1.2-00 [DIRS 182225]). The FAR V1.2 code is implemented as a DLL and is incorporated directly within the TSPA-SEIS Volcanic Eruption Model. The mathematical description of the FAR V1.2 code is provided in SNL (2007 [DIRS 179347] Section 6.3).

Gridded values of tephra and waste concentration computed by the ASHPLUME code are passed to the FAR code for redistribution calculations. FAR V1.2 maps the tephra and waste concentration to a 30-m resolution digital elevation model (DEM) grid covering the Fortymile Wash drainage basin. The calculation of time-dependent waste concentration at the RMEI location proceeds in six steps (SNL 2007 [DIRS 179347], Section 6.3.3).

Step 1: Because ASHPLUME calculations are carried out on a relatively coarse polar grid, a bilinear interpolation is performed on the ASHPLUME generated grid values of tephra and waste concentration to rectify the concentration values to the much higher resolution DEM grid.

Step 2: The DEM file is processed to fill any artificial "holes" in topography due to imperfections in the DEM data. The file is scanned recursively to slightly raise any "pits" or "flats" where the downstream direction is not well defined.

Step 3: A set of spatial analyses are performed on the input DEM to determine slopes, contributing area, and scour depths for the drainage basin. The waste-contaminated tephra is mobilized from slopes greater than a specified critical slope.

Step 4: The mobilized tephra is routed through the channel system to model the dilution effect. Routing of mobilized tephra and uncontaminated channel-bed sediments is performed using a bifurcation routing algorithm. The resulting grid of tephra thickness routed through each DEM pixel is divided by the grid of scour depth routed through each pixel to yield a dilution factor at each channel grid cell in the basin. The dilution factor at the apex of the alluvial fan (one particular cell in the grid) is used in subsequent steps.

Step 5: Initial concentrations of waste in channels and on interchannel divides at the RMEI location are determined. This step represents the transfer of waste from the upper drainage basin to the RMEI location on the alluvial fan. In channels, the mass of waste is the sum of the direct deposition of waste and waste transported from the upper basin by fluvial processes. On interchannel divides, the concentration of waste is determined solely from direct deposition of waste-contaminated tephra.

Step 6: Time-dependent diffusion of radionuclides within a finite depth of permeable soil is calculated using the initial concentrations determined in **Step 5**. Inputs to this step include the permeable depths on divides, L_d, and in channels, L_c, and diffusivity values for divides, D_d, and channels, D_c.

The mixing/dilution processes implemented in Steps 1 – 5 above are assumed to occur instantaneously after the potentially contaminated tephra is deposited on the ground surface after a volcanic eruption. To simplify the model conceptualization, the diffusion process in Step 6 is the only process considered to be time-dependent in the Tephra Redistribution Submodel. This is a reasonable simplification given the expected relatively short time scale of the mixing processes.

Descriptions of the key input parameters to the Tephra Redistribution Submodel are shown in Table 6.5-5. The results of the Tephra Redistribution Submodel calculations are passed to the Volcanic Ash Exposure Submodel for dose calculations. The results consist of four time series of mass concentration: (1) concentration on divides averaged over the tillage depth; (2) concentration on divides averaged over the resuspendable surface layer; (3) concentration in channels averaged over the tillage depth; and (4) concentration in channels averaged over the resuspendable surface layer. The concentrations on divides and channels are combined using the weighting factor, F, for the fraction of the alluvial fan composed of channels (and $1-F$ for the

fraction of the alluvial fan composed of divides) to yield one concentration for the resuspendable surface layer and one concentration for the tillage depth for use by the Volcanic Ash Exposure Submodel in dose calculations.

6.5.2.1.4 Volcanic Ash Exposure Submodel

The Volcanic Ash Exposure Submodel provides the calculation of annual dose for the Volcanic Eruption Modeling Case. Details of the dose calculation are provided with the Biosphere Model Component description in Section 6.3.11. Implementation of the Volcanic Eruption Modeling Case for the TSPA-SEIS includes the determination of both the probability of the event and its consequences.

During the atmospheric transport and redistribution on the ground surface, radionuclide concentrations in the waste are proportional to those in the waste inventory that combine each type of WP hit, with consideration of radionuclide decay. The calculated radionuclide concentrations in volcanic tephra or in a soil/tephra mixture using the redistribution submodel provide the radioactive source term for calculating annual dose to the RMEI. A set of the BDCFs appropriate to the Volcanic Eruption Modeling Case is developed according to the Biosphere Model Component described in Section 6.3.11. The annual dose associated with the radioactive source is calculated by multiplying radionuclide concentrations by the volcanic ash BDCFs.

6.5.2.2 Implementation in the TSPA-SEIS

This subsection describes the inputs, feeds, software, and model calculations required for the Volcanic Eruption Modeling Case. The Volcanic Eruption component of the TSPA-SEIS is implemented as a separate, stand-alone GoldSim model file.

The determination of atmospheric dispersal and deposition of ash and waste fuel particles from a hypothetical volcanic eruption that intersects the repository is accomplished using the ASHPLUME_DLL_LA V.2.1 code, which is dynamically coupled to the TSPA-SEIS. The ASHPLUME DLL requires input parameters that define the characteristics of the eruptive event, the environmental conditions, and the mass of the waste to be included in the event. The key ASHPLUME input parameters are shown in Table 6.5-4. The mass of waste to be included in the eruptive event is calculated based on the proportion of CSNF WPs to CDSP WPs in the repository, a sampled parameter that selects the number of WPs affected by the eruptive event, and a factor that accounts for the proportion of waste-contaminated magma that is erupted into the tephra column. Note that this is the total mass of waste that the ASHPLUME code uses, and not a mass vector by radionuclide species. These inputs to the ASHPLUME code are located in the ASHPLUME_DLL input container in the TSPA-SEIS. GoldSim (GoldSimV.9.60.100, STN 10344-9.60-01 [DIRS 181903]) first samples the input parameters that are probability distributions, and then passes all parameters to the ASHPLUME code. The ASHPLUME code then calculates the waste and ash deposition results (g/cm^2) at the RMEI location, followed by an additional calculation (using the same input parameters) at many grid points covering the Fortymile Wash watershed.

The TSPA-SEIS then performs calculations for the Tephra Redistribution Submodel. The consequences of a volcanic eruption include the potential increase in dose at the location of the RMEI from the transport of radioactive waste-contaminated ash through hillslope and fluvial transport mechanisms. The Tephra Redistribution Submodel accounts for this effect at the location of the RMEI for both interchannel divides and distributary channels. The volcanic ash redistribution calculations are performed using the computer code FAR V1.2 (STN: 11190-1.2-00 [DIRS 182225]). Inputs to this DLL define such parameters as directly deposited ash and waste concentrations at the RMEI location and at grid points covering the Fortymile Wash watershed; critical gradient and drainage density for tephra mobilization; scour depth; diffusion parameters; and Biosphere Model Component inputs. GoldSim samples those inputs that are probability distributions and then passes all inputs to FAR V1.2, which uses these inputs to calculate the time dependent waste concentration on interchannel divides and distributary channels. The TSPA-SEIS takes these ash redistribution results and, using the areal weighting factor, F (Table 6.5-5), for interchannel divides and distributary channels, determines the source terms for:

- Ingestion and radon exposure for the interchannel divides and distributary channels
- Long-term inhalation exposure for interchannel divides and distributary channels
- Short-term inhalation exposure for interchannel divides and distributary channels.

The TSPA-SEIS then converts the source terms back into the masses of the individual radionuclide species based on total repository inventory and accounts for radioactive decay. As described in Section 6.3.11, these source terms are then multiplied by the corresponding BDCFs to determine dose.

To provide the capability to evaluate model sensitivity as well as to compute mean annual dose, the Volcanic Eruption Model File provides the option to calculate annual dose as a function of time, $D(\tau)$, in one of the following two ways: (1) either as the dose consequence, D_{VE}, of single eruptive event that occurs at a specified future time, T:

$$D(\tau) = D_{VE}(\tau \mid T) \qquad \text{(Eq. 6.5.2-1)}$$

or (2) as the mean annual dose at time τ due to all possible volcanic events occurring at time T prior to time τ:

$$D(\tau) = \lambda_E \int_0^{\tau} D_{VE}(\tau \mid T) dT \qquad \text{(Eq. 6.5.2-2)}$$

where λ_E is the frequency of occurrence of an eruptive event intersecting the repository.

The TSPA-SEIS calculates the mean annual dose for the Volcanic Eruption Modeling Case using a three-step process. First, an LHS of epistemically uncertain TSPA-SEIS parameters is generated. Each element in the LHS defines a value for the epistemic parameters listed in Table 6.5-4. For each element in the LHS, a number of annual dose histories are computed using GoldSim. Each annual dose history is associated with a single volcanic eruption occurring at a specified time and with specified characteristics, and with specified wind conditions. The characteristics of each eruption (e.g. eruptive power, eruptive height, etc.) and the wind

conditions at the time of the eruption are specified by elements of a separate LHS for the aleatory parameters listed in Table 6.5-4. Using these inputs, the amount of waste entrained in the eruptive plume, its deposition and redistribution are evaluated using the models described above, to produce a single annual dose history.

Second, for each element of the LHS of epistemic parameters, the expected annual dose history is calculated by Equation 6.5.2-1, using the annual dose histories computed for that realization. The integral in Equation 6.5.2-2 accounts for the aleatory uncertainty in the time and characteristics of the eruption and the wind conditions, as well as the uncertainty in the frequency of igneous events, and is evaluated numerically by EXDOC (Section 6.1.5). The frequency of igneous events is sampled from the probability distribution described in Table 6.5-2. Finally, the mean annual dose history is calculated as the average of the expected annual dose histories from the set of realizations.

6.5.2.3 Evaluation of Implementation Provisions for the TSPA-SEIS

Differences in assumptions and parameter sets in the TSPA-SEIS have arisen in the development of the supporting information. Most of these differences are due to the use of conservative submodels when there is uncertainty that is difficult to quantify. Those differences that may have an impact on dose can be shown to result in a conservative estimation of dose. To enhance understanding of the complex interactions within the TSPA-SEIS, a discussion of consistency among model components and submodels, and identification of TSPA-SEIS conservatisms in submodels and abstractions specific to the Volcanic Eruption Modeling Case, are discussed below.

6.5.2.3.1 Model Component Integration

Volcanic Ash Particle Size—The size distribution of ash particles transported by the ASHPLUME code is generally much larger than the particle size used to calculate the inhalation BDCFs. The ASHPLUME model is appropriate for particles of mean diameter greater than 15-30 μm (Jarzemba et al. 1997 [DIRS 100987], p. 2-2). The dose coefficients for inhalation are for particles with activity median aerodynamic diameter of 1 μm (BSC 2005 [DIRS 172827], Section 6.5.3.1.) An analysis was conducted in BSC 2005 [DIRS 172827] Section 6.5.5.2 regarding the effects of the size distribution of ash particles transported by the ASHPLUME code being generally much larger than the particle size used to calculate the inhalation BDCFs. It was concluded from that analysis that the application of dose coefficients for particles with activity median aerodynamic diameter of 1 μm will not underestimate the doses from inhalation of resuspended material and that the dose coefficients are adequate for use in the biosphere model.

6.5.2.3.2 Identification of Conservatisms in Submodels and Abstractions

Radionuclide Waste Form Completely Destroyed—As described in *Atmospheric Dispersal and Deposition of Tephra from a Potential Volcanic Eruption at Yucca Mountain, Nevada*, (SNL 2007 [DIRS 177431], Section 5.1.2) , WP failure and entrainment of fragmented waste within rising magma is assumed to occur due to the intersection of an eruptive conduit with WPs. In the TSPA-SEIS implementation, the WPs hit are assumed to be completely destroyed and all of the

waste contained in the WPs is available to be erupted. This conservative assumption tends to maximize the release of radionuclides from the EBS.

6.5.2.4 Alternative Conceptual Model(s) for the Volcanic Eruption Modeling Case

An ACM for the volcanic eruption phase dose is evaluated below. This ACM was not included in the Volcanic Eruption Modeling Case of the Igneous Scenario Class in the TSPA-SEIS based on the results of this analysis showing that the eruption phase dose is insignificant compared the post-eruption phase dose.

Volcanic Eruption Phase Dose ACM—This subsection describes the calculation of the radiation dose received by a receptor that does not leave the region during a volcanic eruption. The result of this calculation is used as the basis for excluding the potential eruption phase dose in the TSPA-SEIS. Because a high concentration of airborne radioactive particulates is expected during this phase, inhalation of airborne contaminated ash particles is the only pathway considered, as described in SNL (2007 [DIRS 177399], Section 6.15.2). The receptor has the same inhalation characteristics as those for the RMEI discussed in Section 6.3.11.

The eruption phase of a volcanic event refers to the conditions that exist during the volcanic eruption before the deposition of volcanic ash on the ground is completed. The dose factors for determining inhalation dose during a volcanic eruption are different from the BDCFs used for the time period after the deposition of volcanic ash on the ground. To calculate the daily dose from inhaling a specific radionuclide during a volcanic eruption, the activity concentration of that radionuclide in air is multiplied by the appropriate dose factor. The total inhalation dose from concentrations of primary radionuclides in air is then calculated as (SNL 2007 [DIRS 177399], Section 6.15.2.2, Equation 6.15-9)

$$D_{inh} = \sum_i D_{inh,i} = \sum_i DF_i \times Ca_i \qquad \text{(Eq. 6.5.2-3)}$$

where

D_{inh} = total inhalation dose rate for all radionuclides (Sv/day)

$D_{inh,\,i}$ = inhalation dose rate for a primary radionuclide i (Sv/day)

DF_i = dose factor for a primary radionuclide i (Sv/day per Bq/m^3)

Ca_i = activity concentration of a primary radionuclide i in air (Bq/m^3) (Equation 6.5.2-7).

The total inhalation dose during a volcanic eruption can then be calculated by multiplying the inhalation dose rate by the duration of the volcanic eruption:

$$D = D_{inh} \times t_{vol} \qquad \text{(Eq. 6.5.2-4)}$$

where

D = total inhalation dose during volcanic eruption (Sv)

t_{vol} = duration of volcanic eruption, or volcanic eruption time (day).

The probability-weighted annual dose from the volcanic eruption phase can be calculated as

$$D_{prob} = D \times \rho_{event} \times \rho_{center} \quad \text{(Eq. 6.5.2-5)}$$

where

D_{prob} = probability-weighted annual dose from the volcanic eruption (Sv)

ρ_{event} = annual frequency of an intersection of the repository by a volcanic dike (1/yr)

ρ_{center} = probability of one or more eruptive centers intersecting the repository in an igneous event.

The activity concentration of a radionuclide in air, Ca_i, is proportional to the volcanic ash concentration in air, which can vary with time during the eruption phase. To estimate the activity concentration in air, it is assumed that the ratio of waste to ash in volcanic ash does not change between the time it was in the air and the time it was deposited on the ground:

$$Ca_{waste\_air} = Ca_{ash\_air} \times \frac{C_{waste\_dep}}{C_{ash\_dep}} \quad \text{(Eq. 6.5.2-6)}$$

where

Ca_{waste_air} = mass concentration of waste in air (g/m^3)

Ca_{ash_air} = mass concentration of volcanic ash in air (g/m^3) (Equation 6.5.2-9)

C_{waste_dep} = mass concentration of waste deposited on the ground (g/m^2)

C_{ash_dep} = mass concentration of volcanic ash deposited on the ground (g/m^2).

Both mass concentrations of waste and volcanic ash deposited at the location of the RMEI on the ground can be obtained from the results of the TSPA-SEIS for the Igneous Scenario Class. By using the mass concentration of waste in air, activity concentrations of individual radionuclides can be calculated as:

$$Ca_i = Ca_{waste\_air} \times f_i \times SA_i \quad \text{(Eq. 6.5.2-7)}$$

where

f_i = fraction of an individual radionuclide, i, among the total waste mass, dimensionless (Equation 6.5.2-8)

SA_i = specific activity for the individual radionuclide, i, (pCi/g).

The fraction of an individual radionuclide should be weighted by the number of CSNF and CDSP WPs hit, as follows:

$$f_i = \frac{N_{CSNF} \times m_{CSNF,i} + N_{CDSP} \times (m_{HLW,i} + m_{DSNF,i})}{\sum_i [N_{CSNF} \times m_{CSNF,i} + N_{CDSP} \times (m_{HLW,i} + m_{DSNF,i})]} \quad \text{(Eq. 6.5.2-8)}$$

where

N_{CSNF} = number of CSNF WPs hit by volcanic eruption

N_{CDSP} = number of CDSP WPs hit by volcanic eruption

$m_{CSNF,i}$ = mass of radionuclide, i, per CSNF WP (g)

$m_{HLW,i}$ = mass of radionuclide, i, for HLW per CDSP WP (g)

$m_{DSNF,i}$ = mass of radionuclide, i, for DSNF per CDSP WP (g).

As mentioned before, the mass concentration of volcanic ash may vary with time during the eruption phase. However, the average mass concentration of volcanic ash in air, Ca_{ash_air}, can be calculated using the amount of ash deposited on the ground, ash settling velocity, and volcanic eruption time:

$$Ca_{ash\_air} = \frac{C_{ash\_dep}}{0.01 \times V_0 \times 86{,}400 \times t_{vol}} \quad \text{(Eq. 6.5.2-9)}$$

where

V_0 = settling velocity for volcanic ash (cm/sec) (Equation 6.5.2-10)

t_{vol} = eruption duration (days)

0.01 = unit conversion (m/cm)

86,400 = unit conversion (sec/day).

The settling velocity of volcanic ash can be calculated, and its equation and inputs are given in *Atmospheric Dispersal and Deposition of Tephra from a Potential Volcanic Eruption at Yucca Mountain, Nevada,* (SNL 2007 [DIRS 177431], Section 6.5.1 Equation 6-4 and Table 8-2):

$$V_0 = \frac{\psi_p g d^2}{9\eta_a F^{-0.32} + \sqrt{81\eta_a^2 F^{-0.64} + \frac{3}{2}\psi_p \psi_a g d^3 \sqrt{1.07 - F}}} \quad \text{(Eq. 6.5.2-10)}$$

where

Ψ_a = density of air (0.001734 g/cm^3 used in TSPA-SEIS)

Ψ_p = density of particles, dependent on particle size (g/cm^3) (Equation 6.5.2-11)

g = gravitational acceleration constant (980 cm/s^2)

η_a = viscosity of air (0.000185 g/cm-s used in TSPA-SEIS)

F = shape factor for particles (0.5 used in TSPA-SEIS)

d = mean particle diameter (cm).

The particle density, Ψ_p, depends on the particle size, and larger particles are less dense because of the incorporation of more gas bubbles. Particle density is a function of the particle log-diameter, ρ_a in cm, as follows (SNL 2007 [DIRS 177431], Section 6.5.1, Equation 6-5):

$$\Psi_p = \Psi_p^{high} \quad \text{for } \rho_a < \rho_a^{low}$$
$$\Psi_p = \Psi_p^{low} + (\Psi_p^{high} - \Psi_p^{low})(\rho_a^{high} - \rho_a)/(\rho_a^{high} - \rho_a^{low}) \quad \text{for } \rho_a^{low} < \rho_a < \rho_a^{high} \quad \text{(Eq. 6.5.2-11)}$$
$$\Psi_p = \Psi_p^{low} \quad \text{for } \rho_a > \rho_a^{high}$$

where

Ψ_p^{high} = ash particle density at minimum particle size (2.08 g/cm^3 used in TSPA-SEIS)

Ψ_p^{low} = ash particle density at maximum particle size (1.04 g/cm^3 used in TSPA Model)

ρ_a^{low} = log ash particle size in cm at maximum ash density (-3 used in TSPA-SEIS)

ρ_a^{high} = log ash particle size in cm at minimum ash density (0 used in TSPA-SEIS)

ρ_a = log(d), log particle diameter in cm.

The mass of radionuclides in CSNF, DSNF, and HLW ($m_{CSNF,\,i}$, $m_{DSNF,\,i}$ and $m_{DSNF,\,i}$), changes with time due to decay and ingrowth in the radioactive waste. This causes the probability-weighted mean annual dose during the eruption phase to decrease with time if a volcano occurs at a later time. A calculation was conducted using the GoldSim software to implement Equations 6.5.2-1 to 6.5.2-9. The input values for these equations were taken directly from the Volcanic Eruption Modeling Case of the Igneous Scenario Class in the TSPA-SEIS. The calculation results of 1,000 realizations using the GoldSim software are shown on Figure 6.5-14, which includes a comparison between the probability-weighted mean annual doses to the RMEI during the volcanic eruptive phase and post-eruption processes (Volcanic Eruption Modeling Case). The probability-weighted mean annual dose from the volcanic eruption phase is small compared to the probability-weighted mean annual dose caused by volcanic ash deposited on the ground calculated in the TSPA-SEIS. Because of its relative insignificance to the annual dose, the contribution from this eruptive phase dose ACM is not included in the TSPA-SEIS.

Table 6.5-1. Waste Form Temperatures Inside Intrusive Body

Time Since Igneous Event	For an Intrusion into a Repository at 25°C		For an Intrusion into a Repository at 50°C		For an Intrusion into a Repository at 100°C		For an Intrusion into a Repository at 150°C		For an Intrusion into a Repository at 200°C	
Years	WP	Drift Wall	WP	Drift Wall	WP	Drift Wall	WP	Drift Wall	WP	Drift Wall
0	1,150	1,150	1,150	1,150	1,150	1,150	1,150	1,150	1,150	1,150
0.1	977	592	1,006	620	1,012	644	1,019	668	1,026	692
0.2	702	462	749	494	768	524	786	553	804	583
0.3	530	382	577	416	603	449	629	483	655	516
0.4	422	326	467	360	498	396	529	432	560	468
0.5	351	284	394	318	428	356	462	394	497	431
0.6	301	252	341	286	378	325	415	364	452	403
0.7	264	226	303	260	341	300	380	341	418	381
0.8	236	206	273	239	313	281	353	322	392	363
0.9	213	189	249	222	290	264	331	306	372	349
1	195	175	230	208	272	251	314	293	356	336
2	111	106	142	136	187	182	233	228	279	274
3	82.8	80.4	111	109	158	156	206	203	253	251
4	68.4	67.0	96.0	94.5	144	142	192	190	240	238
5	59.7	58.9	86.8	85.8	135	134	183	183	232	231
6	54.0	53.4	80.7	80.0	129	129	178	177	227	226
7	49.8	49.4	76.3	75.8	125	125	174	173	223	222
8	46.7	46.4	73.0	72.6	122	122	171	171	220	220
9	44.3	44.0	70.5	70.2	120	119	169	168	218	217
10	42.4	42.2	68.4	68.2	118	117	167	167	216	216
20	33.7	33.6	59.2	59.2	109	109	158	158	208	208
30	30.8	30.8	56.1	56.1	106	106	156	156	205	205
40	29.3	29.3	54.6	54.6	104	104	154	154	204	204
50	28.5	28.5	53.7	53.7	104	104	153	153	203	203
60	27.9	27.9	53.1	53.1	103	103	153	153	203	203
70	27.5	27.5	52.6	52.6	103	103	152	152	202	202
80	27.2	27.2	52.3	52.3	102	102	152	152	202	202
90	26.9	26.9	52.0	52.0	102	102	152	153	202	202
100	26.7	26.7	51.8	51.8	102	102	152	152	202	202

Sources: DTN: LA0702PADE01EG.001 [DIRS 179495].
Modified from Table 6-13 in *Dike/Drift Interactions* (SNL 2007 [DIRS 177430], Section 6.4.6).

Table 6.5-2. Annual Frequencies of Intersection of Repository by a Dike for the Repository Footprint

Hazard Level (%)	Annual Frequency of Intersection of Repository by a Dike
Mean	1.69×10^{-8}
5	7.41×10^{-10}
10	1.48×10^{-9}
15	2.29×10^{-9}
20	3.02×10^{-9}
30	4.57×10^{-9}
40	6.92×10^{-9}
50	1.00×10^{-8}
60	1.45×10^{-8}
70	2.04×10^{-8}
80	2.69×10^{-8}
85	3.31×10^{-8}
90	4.07×10^{-8}
95	5.50×10^{-8}

Sources: DTN: LA0307BY831811.001_R0 [DIRS 164713].
Composite frequency results from full enumeration of the expert elicitation, excerpted from Table 6-8 in *Characterize Framework for Igneous Activity at Yucca Mountain, Nevada* (BSC 2004 [DIRS 169989], Section 6.5.3.1).

Table 6.5-3. Cumulative Distribution Function for the Number of Waste Packages Hit by Conduits

Number of WPs Hit	CDF Value
0	0.703
1	0.710
2	0.748
3	0.806
4	0.942
5	0.981
6	0.994
7	1.000

Source: DTN: SN0701PAWPHIT1.001_R2 [DIRS 182961].

Table 6.5-4. Key Parameters for the ASHPLUME Code

TSPA-SEIS Parameter Name	Description	Distribution Type	Uncertainty Type	Value(s)
C	Constant relating eddy diffusivity and particle fall time ($cm^2/s^{5/2}$)	Point value	Fixed value	400
Erupt_Power_a	Eruptive power (W)	Log uniform	Aleatory	Min = 1.0×10^9 Max = 1.0×10^{12}
Beta_Dist_a	Column diffusion constant	Uniform	Epistemic	Min = 0.01 Max = 0.5
Erupt_Velocity_a	Initial rise velocity (cm/s)	Uniform	Aleatory	Min = 1 Max = 1.0×10^4
AirDen	Density of air (g/cm^3)	Point value	Fixed value	0.001734
AirVis	Viscosity of air (g/cm-s)	Point value	Fixed value	0.000185
Fshape	Ash particle shape factor	Point value	Fixed value	0.5
Dash_Mean_a	Mean ash particle diameter (cm)	Log triangular	Epistemic	Min = 0.001 Mode = 0.01 Max = 0.1
Dash_sigma_a	Ash particle diameter standard deviation (log cm)	Uniform	Epistemic	Min = 0.301 Max = 0.903
Dmax_trans	Maximum particle diameter for transport (cm)	Point value	Fixed value	10
AshDen_maxD	Ash particle density at minimum particle size (g/cm^3)	Point value	Fixed value	2.08
AshDen_MinD	Ash particle density at maximum particle size (g/cm^3)	Point value	Fixed value	1.04
LogD_minDen	Log ash particle size at minimum ash density (log(cm))	Point value	Fixed value	0
LogD_maxDen	Log ash particle size at maximum ash density (log(cm))	Point value	Fixed value	–3
D_min	Minimum waste particle diameter (cm)	Point value	Fixed value	0.0001
D_mode	Mode of waste particle diameter (cm)	Point value	Fixed value	0.0013
D_max	Maximum waste particle diameter (cm)	Point value	Fixed value	0.2

Table 6.5-4. Key Parameters for the ASHPLUME Code (Continued)

TSPA-SEIS Parameter Name	Description	Distribution Type	Uncertainty Type	Value(s)
Rhocut	Waste incorporation ratio	Point value	Fixed value	0.0
Erupt_Time_a	Eruption duration (seconds)	Log uniform	Aleatory	DTN: LA0702PADE03GK.002 [DIRS 179980]
Wind_Direction	Wind direction (degrees)	Empirical	Aleatory	DTN: MO0408SPADRWSD.002 [DIRS 171751]
Wind_Speed	Wind speed (cm/s)	Empirical	Aleatory	DTN: MO0408SPADRWSD.002 [DIRS 171751]
A_cutoff	Threshold limit on ash accumulation (g/cm^2)	Point value	Fixed value	1×10^{-10}
Magma_Partitioning_a	Fractional multiplier on waste mass to account for waste-containing magma erupted in scoria cone and lava flows	Uniform	Aleatory	Min = 0.1 Max = 0.5

Table 6.5-5 Key Input Parameters to the Tephra Redistribution Submodel

TSPA Parameter Name	Parameter Description	Distribution type	Uncertainty Type	Value (s)
Critical_Slope_a	Critical gradient for tephra mobilization from hillslopes	Uniform	Epistemic	0.21 – 0.47
Drainage_Density_a	Average drainage density for the Fortymile Wash drainage basin	Uniform	Epistemic	17 – 25 km^{-1}
Scour_Depth_a	Scour depth in Fortymile Wash at the fan apex	Uniform	Epistemic	73 – 122 cm
RMEI_Area	Area of the Fortymile Wash fan	Constant	fixed value	33 km^2
Fraction_Channel_a	Fraction, *F*, of the Fortymile Wash fan subject to fluvial activity	Uniform	Epistemic	0.09 – 0.54
L_Channels_a	Depth of permeable soil on channels, L_c, of the Fortymile Wash fan (RMEI location)	Constant	fixed value	200 cm
L_Divides_a	Depth of permeable soil on divides, L_d, of the Fortymile Wash fan (RMEI location)	Uniform	Epistemic	102 – 140 cm
D_Channels_a	Diffusivity of waste in channels, D_c, of the Fortymile Wash fan (RMEI location)	Uniform	Epistemic	0.035 – 0.266 cm^2/yr
D_Divides_a	Diffusivity of waste in divides, D_d, of the Fortymile Wash fan (RMEI location)	Uniform	Epistemic	0.001 – 0.095 cm^2/yr
Ash_Density_a	Tephra settled density	Truncated normal	Epistemic	300 – 1,500 kg/m^3 mean = 1,000 kg/m^3 std. dev. = 100 kg/m^3
b_Tillage	Tillage depth	Uniform	Epistemic	0.05 – 0.30 m

Source: DTNs: MO0702PAFARDAT.001_R3 [DIRS 182578];
LA0612DK831811.001_R1 [DIRS 179987] (Tephra Density);
MO0702PAVBPDCF.000_R0 [DIRS 179330] (Tillage depth).

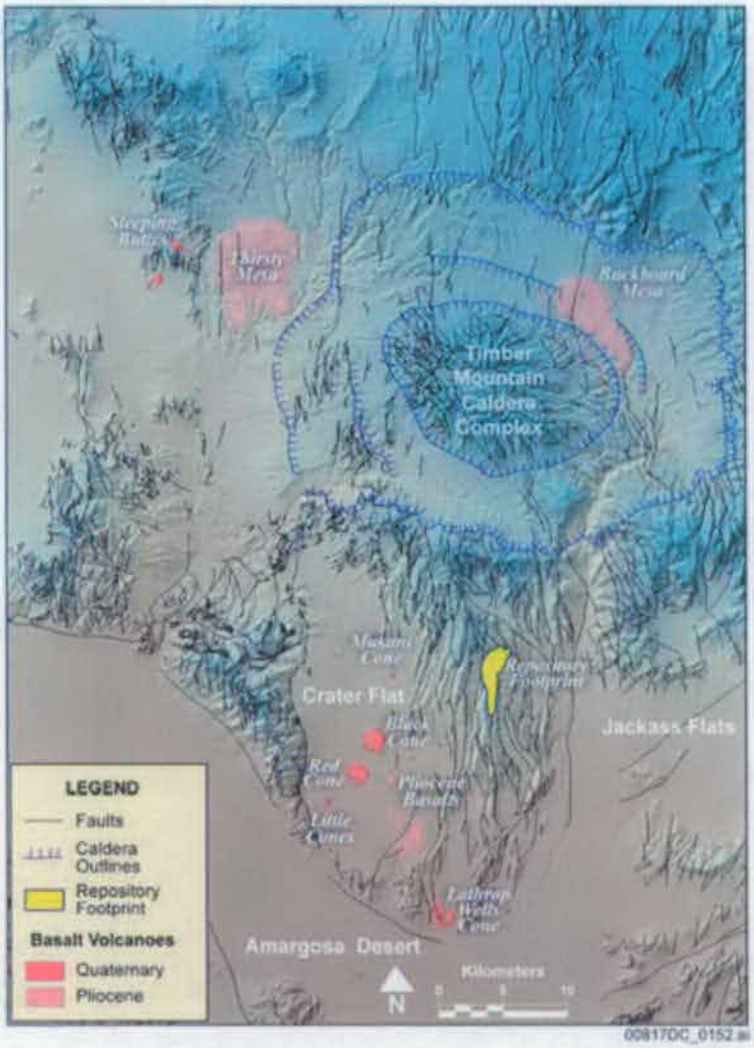

Source: Modified from (CRWMS M&O 1998 [DIRS 123196], Figure 2.1)

Figure 6.5-1. Location and Age of Post-Miocene (less than 5.3 million years) Volcanoes (or clusters where multiple volcanoes have indistinguishable ages) in the Yucca Mountain Region

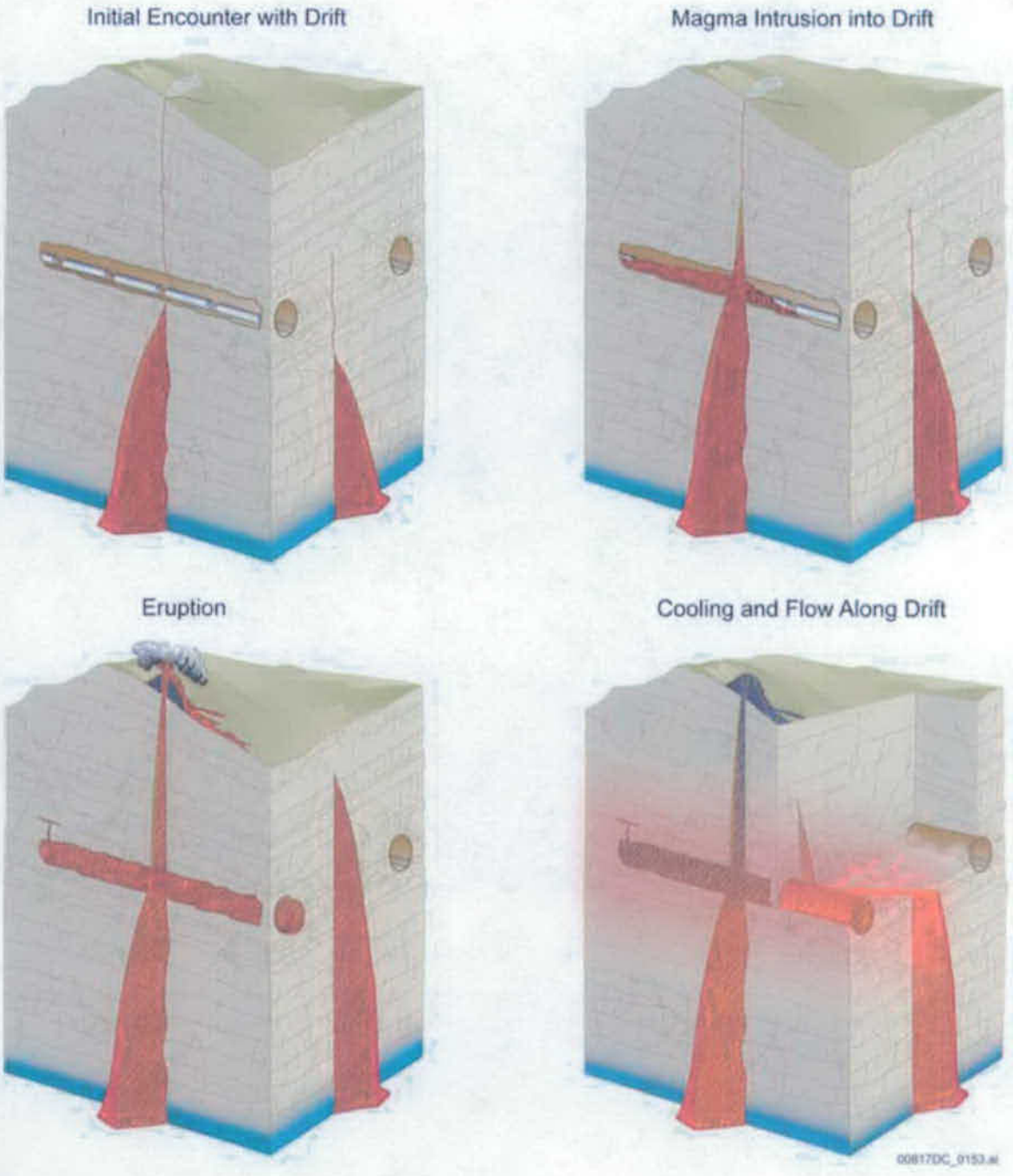

Source: Modified from (SNL 2007 [DIRS 177430], Figure 1-1)

Figure 6.5-2. Schematic Drawing of the Processes Associated with a Dike Intrusion or Eruption through the Repository

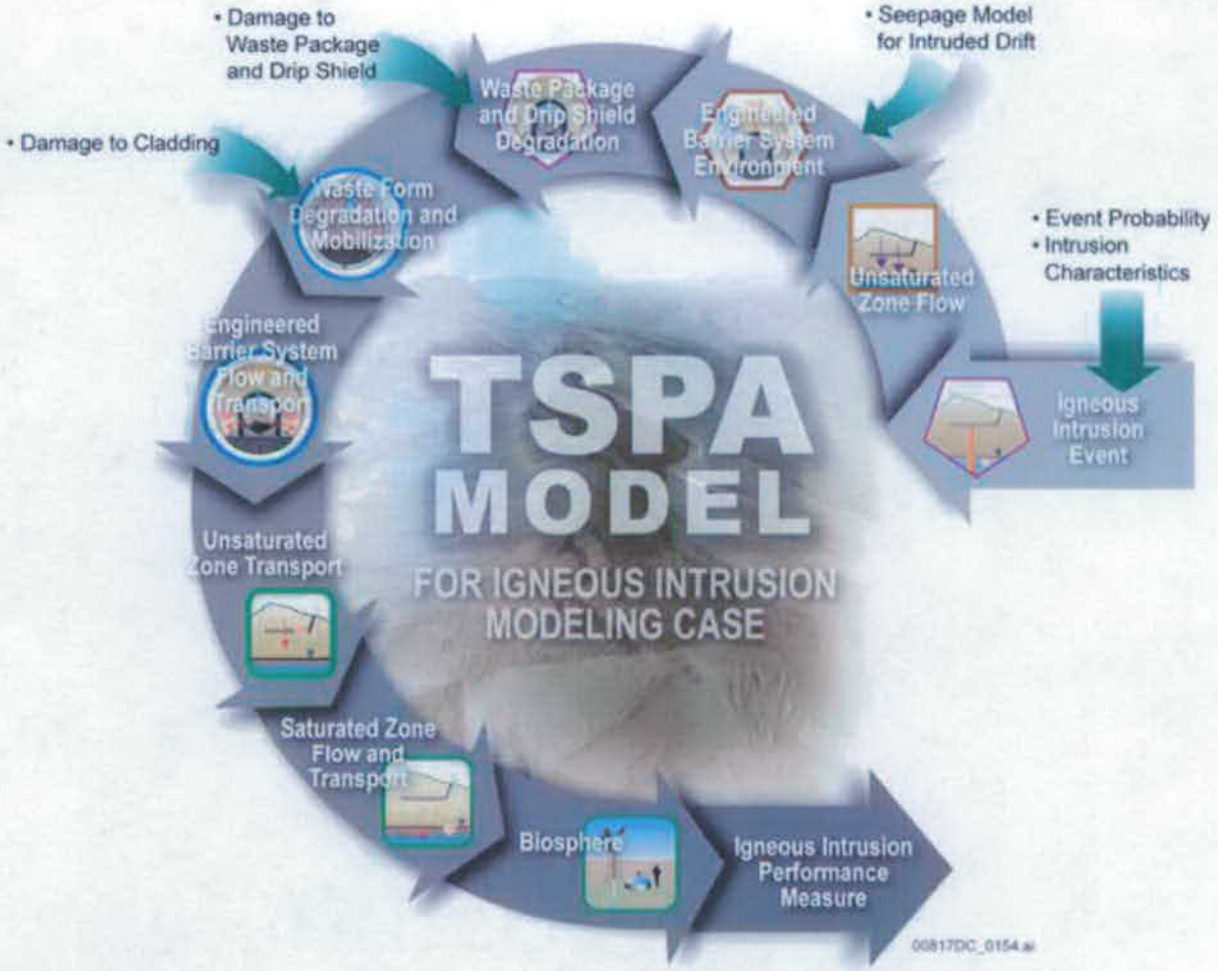

Figure 6.5-3. TSPA-SEIS Components for the Igneous Intrusion Modeling Case

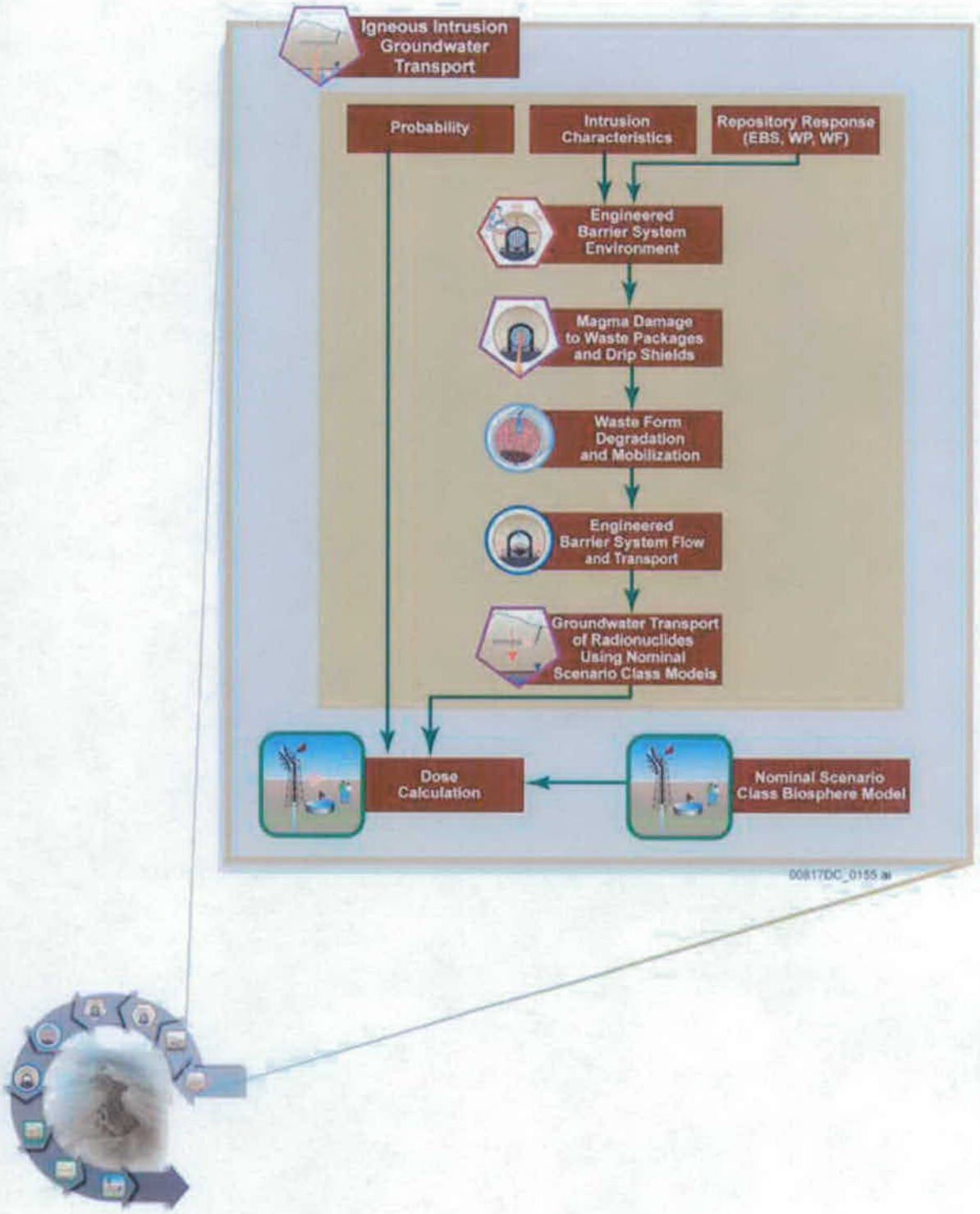

Figure 6.5-4. Information Flow Diagram for the TSPA-SEIS Igneous Intrusion Modeling Case

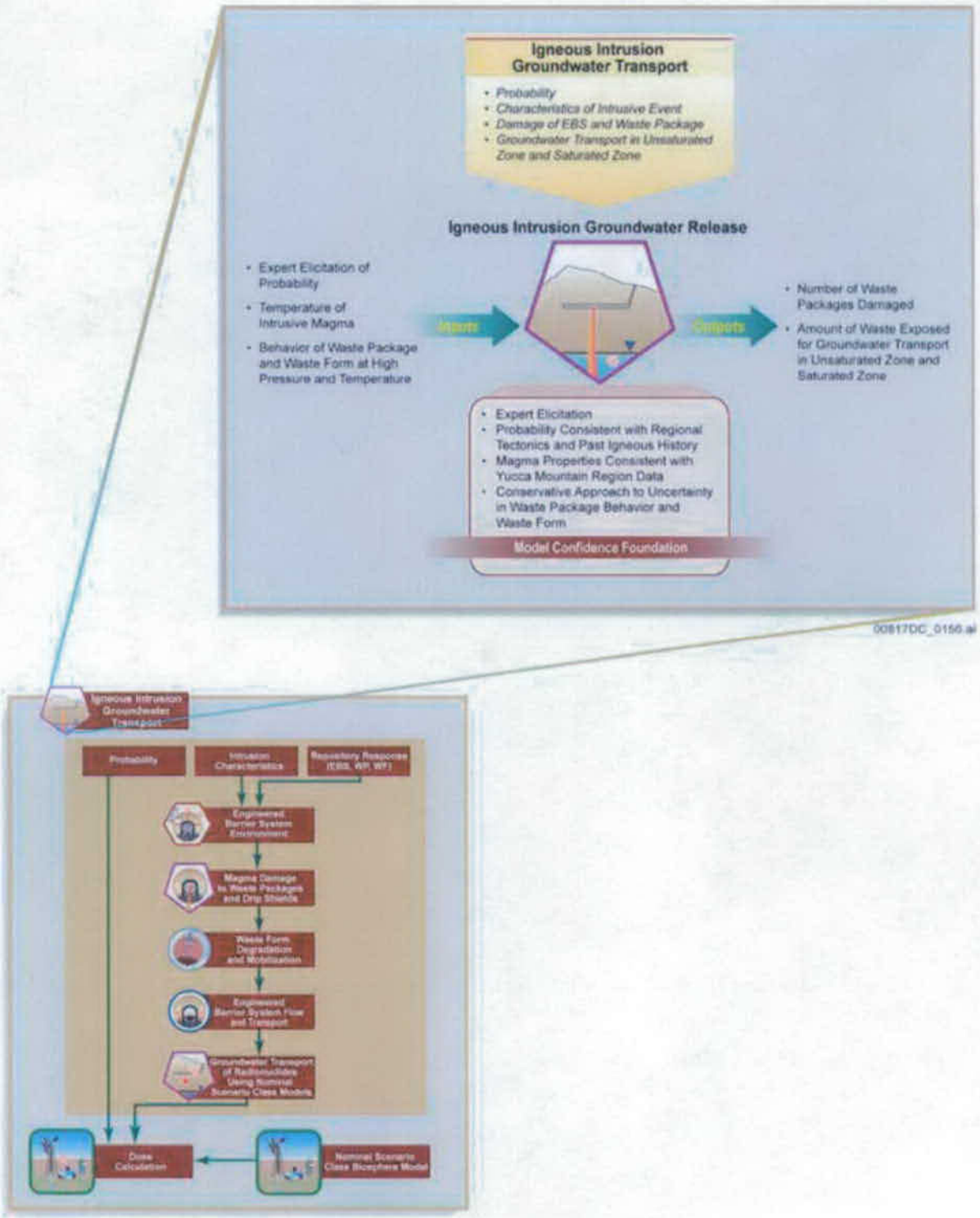

Figure 6.5-5. Inputs, Outputs, and Basis for Model Confidence for the TSPA-SEIS Igneous Intrusion Modeling Case

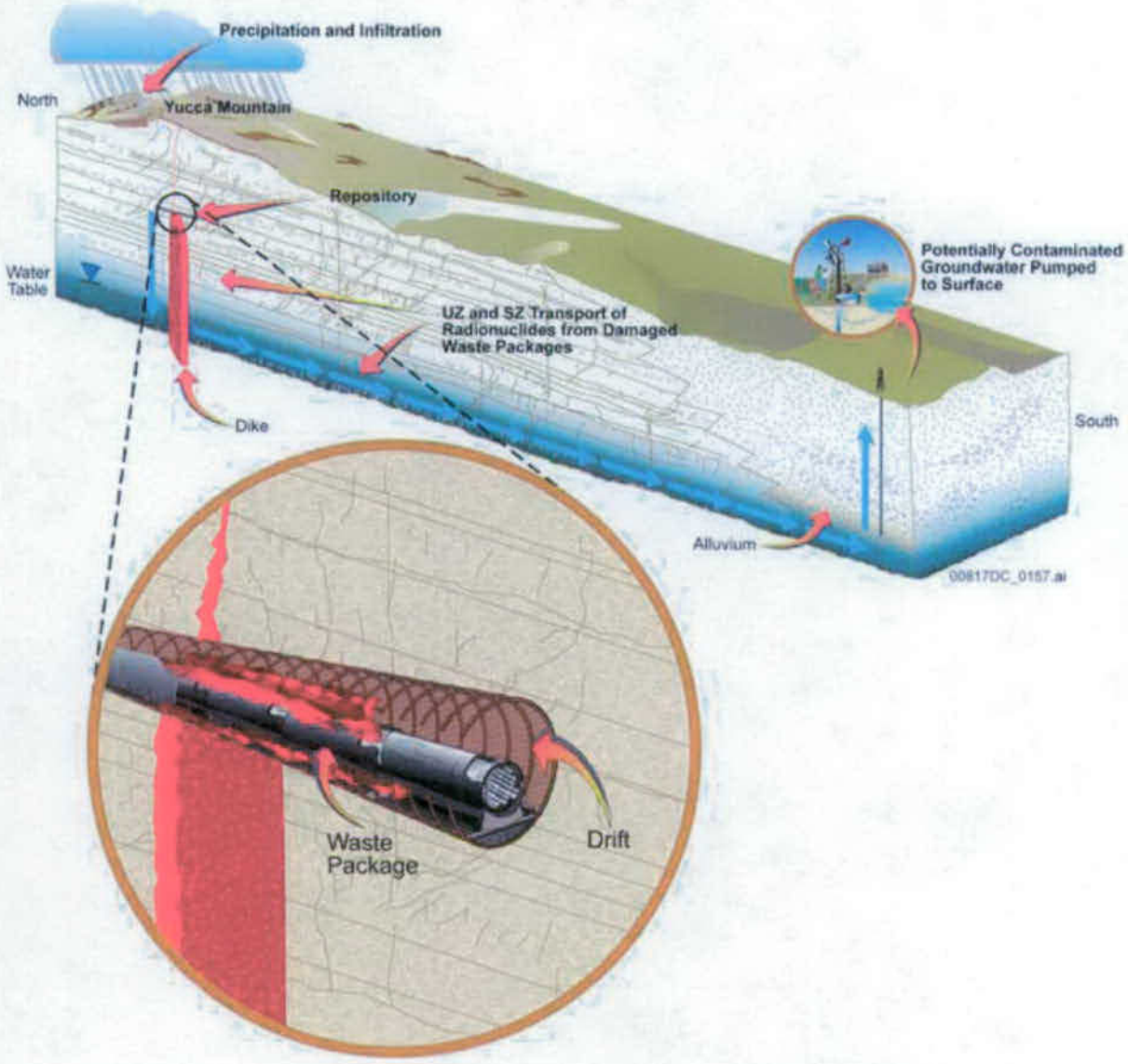

Figure 6.5-6. Schematic Diagram of the Intersection of an Igneous Dike with the Repository and Waste Packages

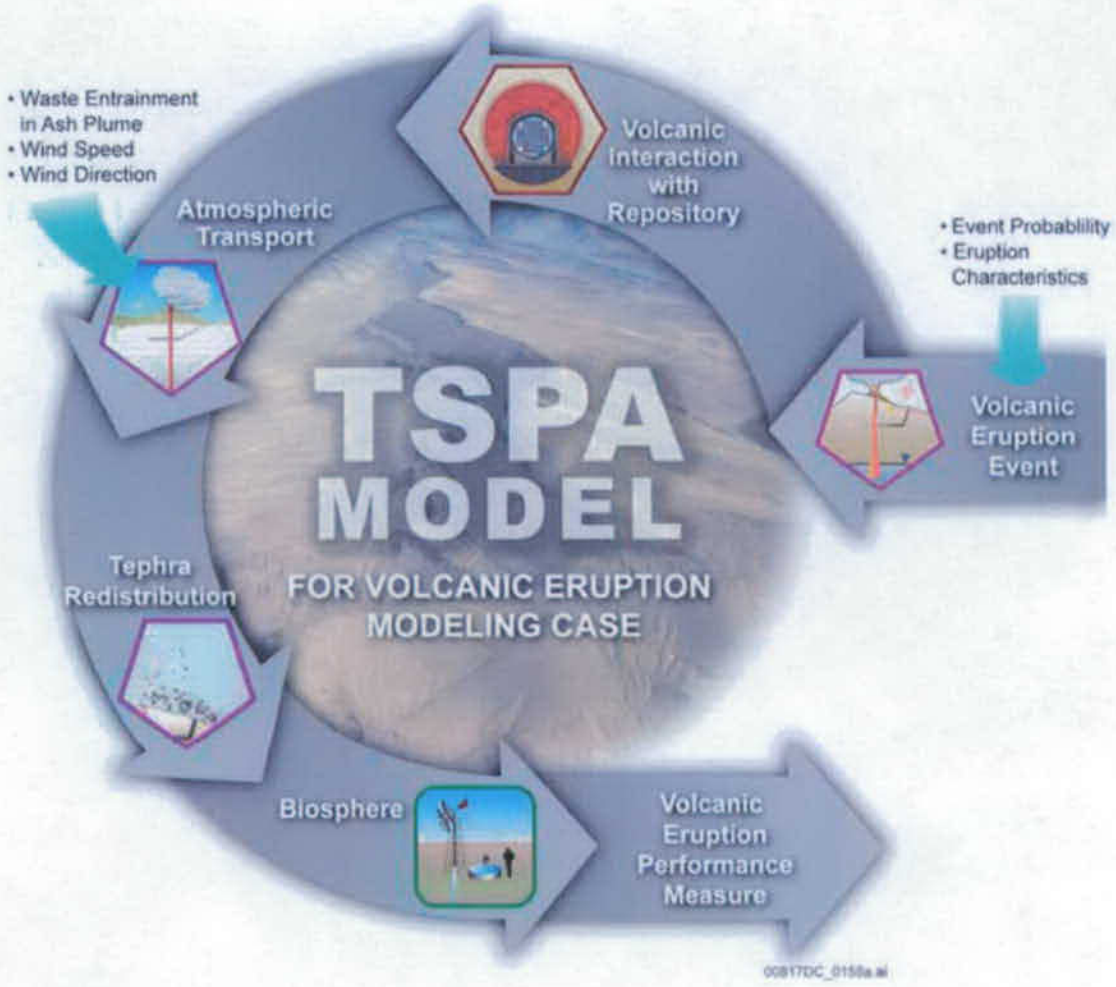

Figure 6.5-7. TSPA-SEIS Components for the Volcanic Eruption Modeling Case

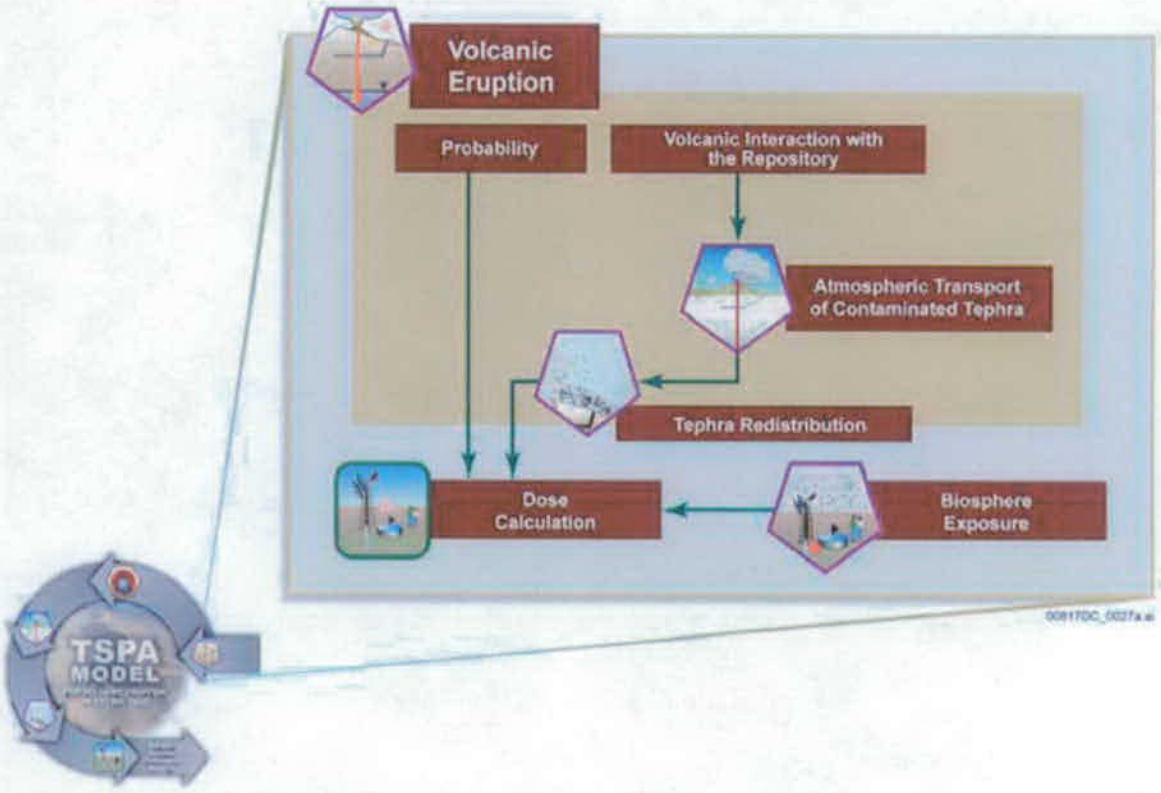

Figure 6.5-8. Information Flow Diagram for the TSPA-SEIS Volcanic Eruption Modeling Case

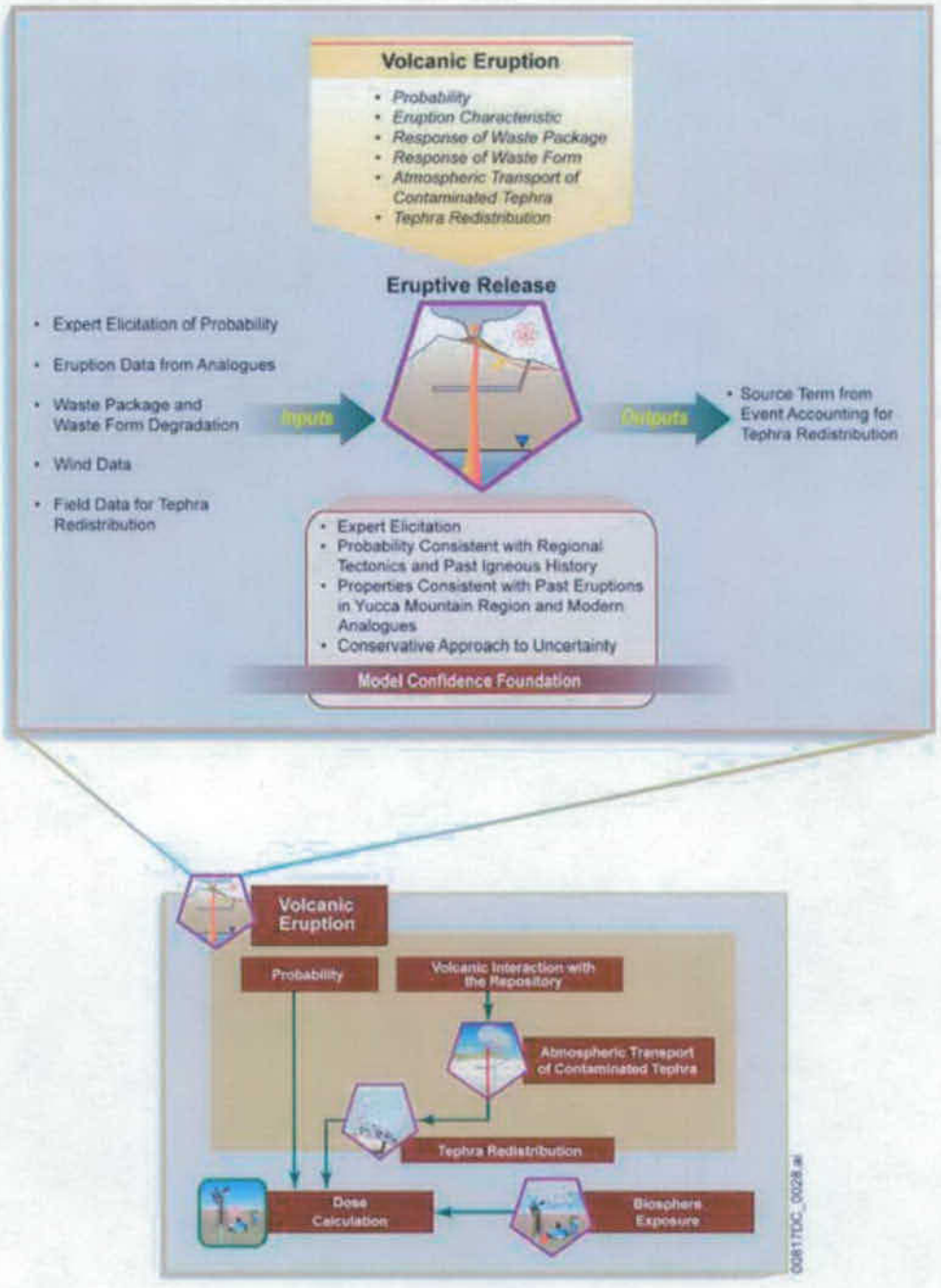

Figure 6.5-9. Inputs, Outputs, and Basis for Model Confidence for the TSPA-SEIS Volcanic Eruption Modeling Case

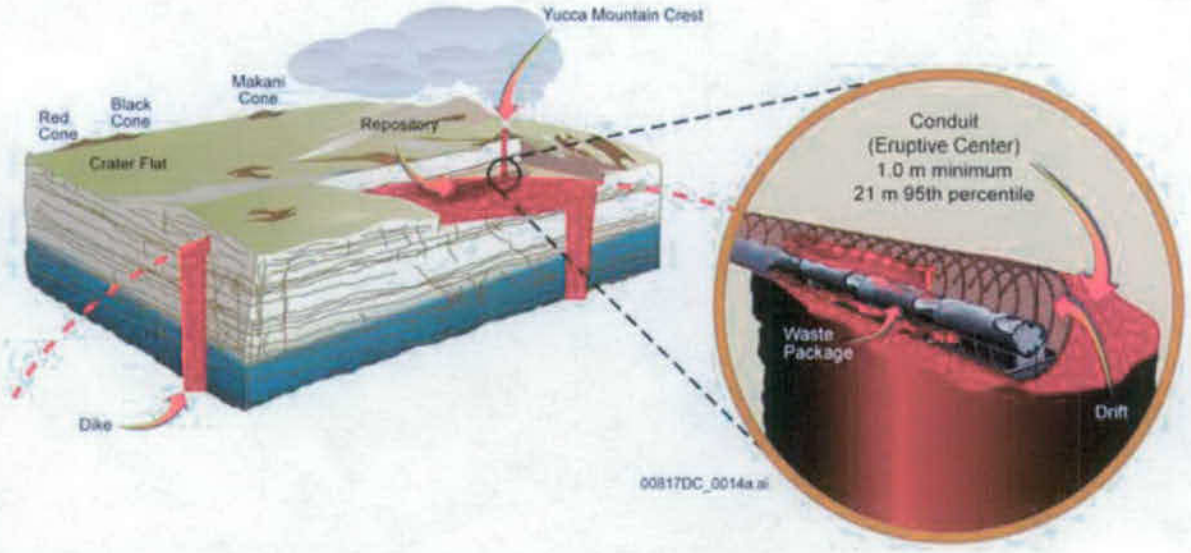

Figure 6.5-10. Schematic Diagram of the Intersection of an Igneous Dike and Eruptive Conduit with the Repository

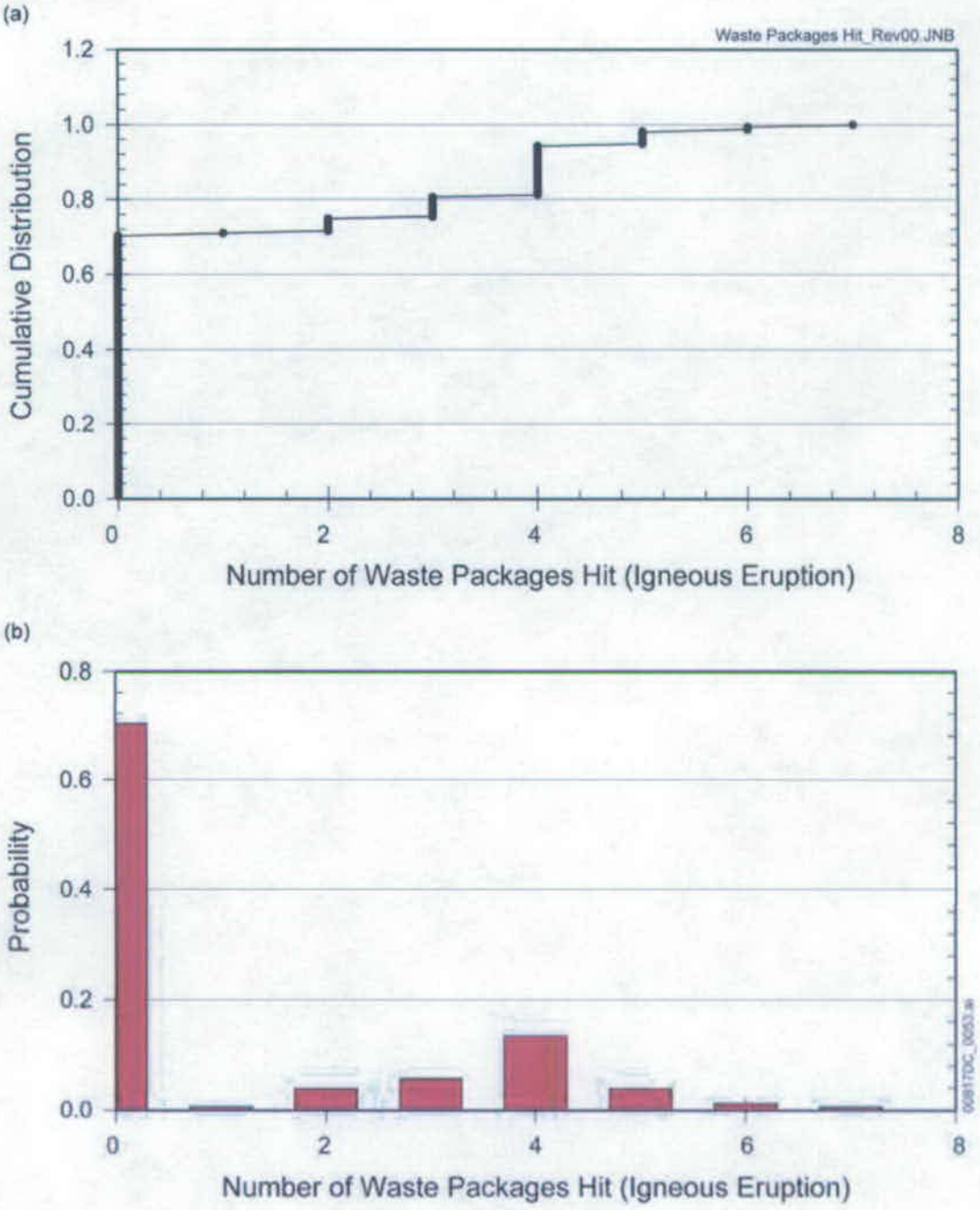

Source: DTN: SN0701PAWPHIT1.001_R2 [DIRS 182961]

Figure 6.5-11. Number of Waste Packages Hit by Conduits from a Volcanic Eruption

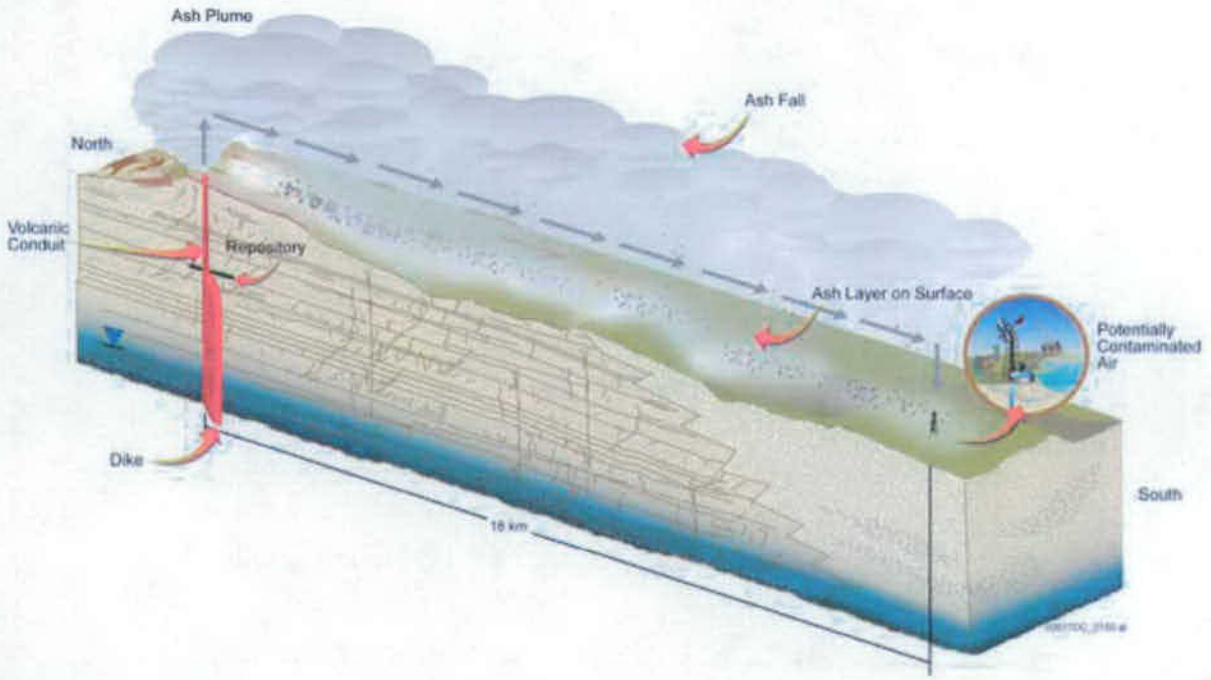

Figure 6.5-12. Schematic Representation of a Volcanic Eruption at Yucca Mountain, Showing Transport of Radioactive Waste in a Tephra Plume

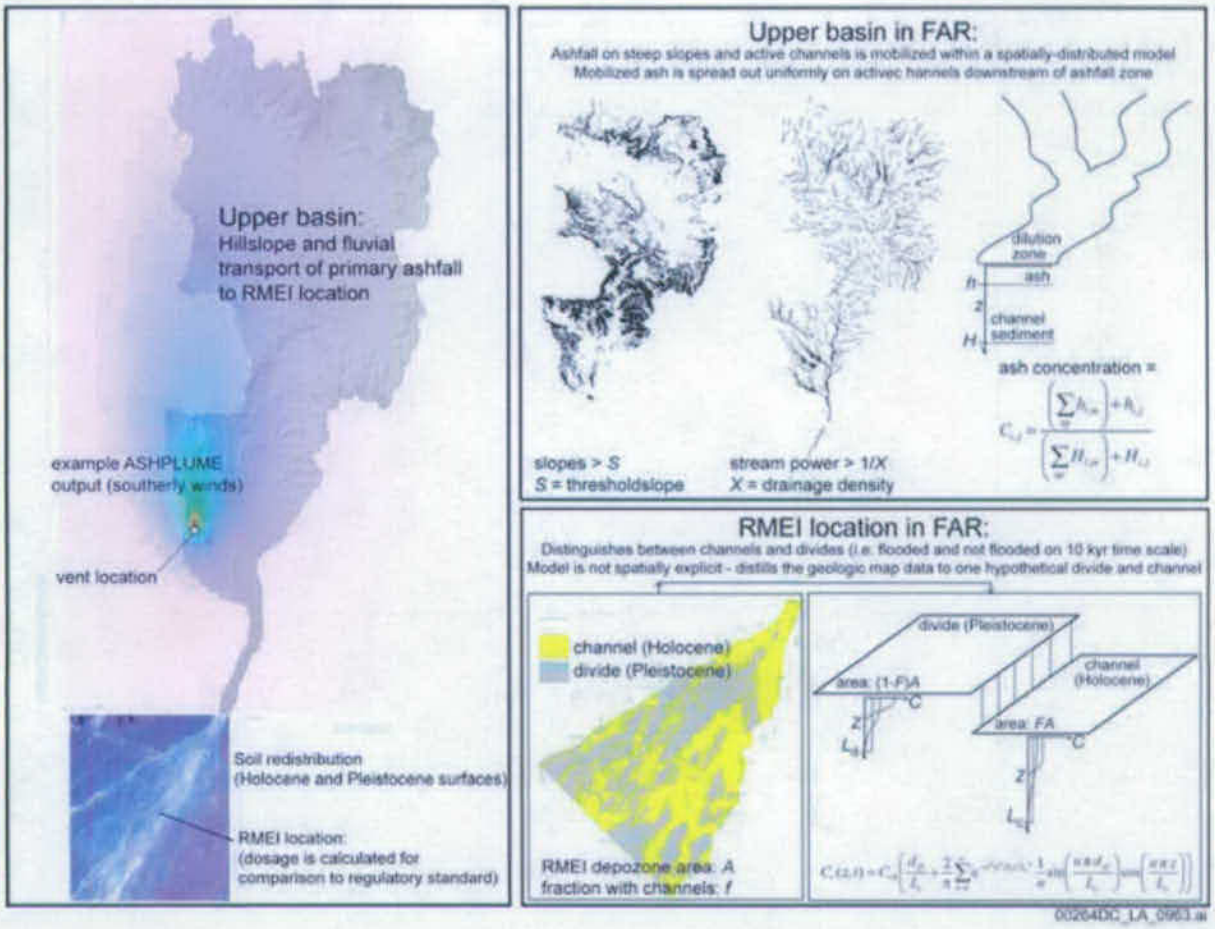

Source: (SNL 2007 [DIRS 180667], Figure 5-1)

Figure 6.5-13. Schematic Diagram of Tephra Redistribution Model

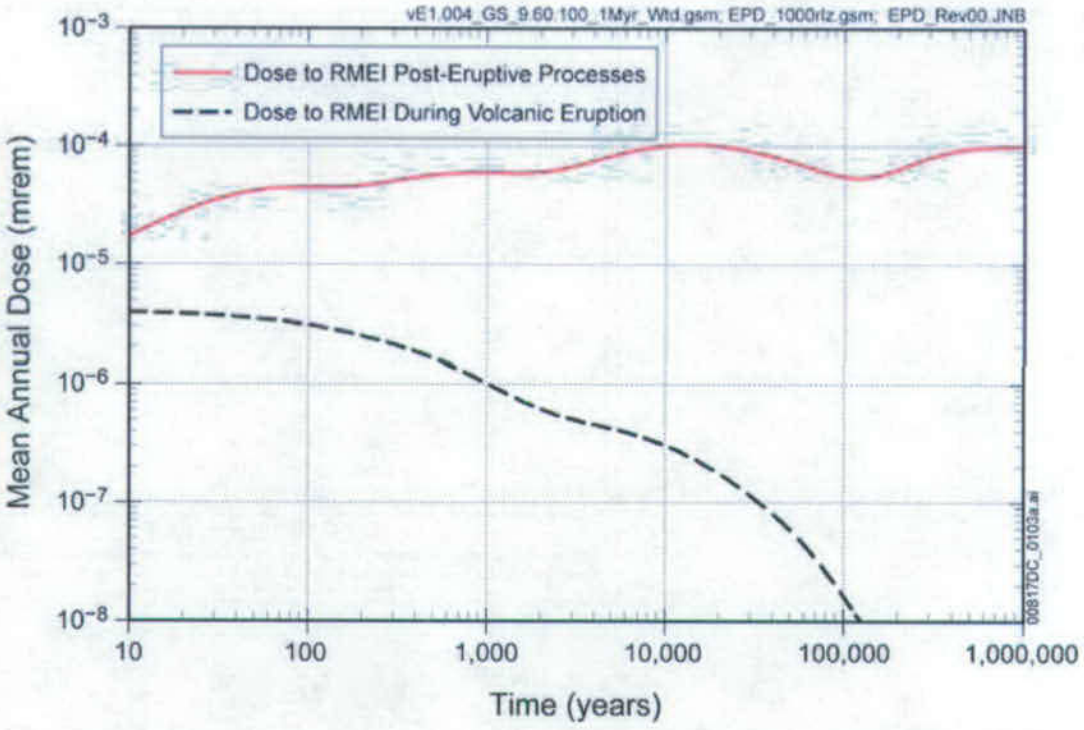

Figure 6.5-14. Comparison of Dose to the RMEI for Post-Eruptive Processes and Dose to the RMEI During a Volcanic Eruption

6.6 TSPA-SEIS MODEL FOR THE SEISMIC SCENARIO CLASS

The Seismic Scenario Class describes future performance of the repository system in the event of seismic activity that could disrupt the repository system. The Seismic Scenario Class represents the direct effects of vibratory ground motion and fault displacement associated with seismic activity. Indirect effects of drift collapse and rockfall induced by vibratory ground motion are also considered in this scenario class. The Seismic Scenario Class considers the effects of the seismic hazards on DSs and WPs because damage to or failure of these components has the potential to initiate or increase releases of radionuclides by forming new diffusive or advective transport pathways. The Seismic Scenario Class also takes into account changes in seepage and drift wall condensation, WP and DS degradation, and in-drift thermal environment that might be associated with a seismic event. The conceptual models and abstractions for the mechanical response of EBS components to seismic hazards at a geologic repository are documented in *Seismic Consequence Abstraction* (SNL 2007 [DIRS 176828]). The structural response calculations and rockfall calculations that provide the basis for the seismic damage abstractions are documented in *Mechanical Assessment of Degraded Waste Packages and Drip Shields Subject to Vibratory Ground Motion* (SNL 2007 [DIRS 178851]).

The Seismic Scenario Class estimates the annual dose due to seismic activity by accounting for the probability of occurrence of activity, expressed in terms of its mean annual exceedance frequency (SNL 2007 [DIRS 176828], Section 6.1.7), and the associated consequences to EBS components. The estimate of annual dose takes into account the relevant processes that affect system performance. The Seismic Scenario Class is represented by two modeling cases. The first modeling case includes those WPs that fail solely due to the ground motion damage associated with the seismic event and it is denoted as the Seismic GM Modeling Case. Because nominal corrosion processes have the potential to alter the repository's susceptibility to damage during a seismic ground motion event, the Seismic GM Modeling Case includes these nominal processes when calculating consequences. The second modeling case includes only those WPs that fail due to fault displacement damage and it is denoted as the Seismic FD Modeling Case. Nominal corrosion processes are not included in the Seismic FD Modeling Case because the damage abstraction for fault displacement is based on a comparison of clearances between EBS components with fault displacements, independent of the thickness of EBS components. The mean annual dose calculated by the two modeling cases (Section 6.6.1.3.1) is the parameter that will be compared to regulatory limits, as required by the NRC proposed rule, 10 CFR 63.321(b) [DIRS 178394].

The two modeling cases in the Seismic Scenario Class have the same framework as the Nominal Scenario Class Modeling Case. This framework includes the TSPA-SEIS Model components that evaluate the mobilization and transport of radionuclides from the repository to the location of the RMEI. In other words, the mobilization of radionuclides in seeping water, the release of these radionuclides from the EBS, and the transport of these radionuclides through the UZ and SZ to the RMEI are based on the same model components for the Nominal Scenario Class as described in Section 6.3. The effects of the seismic event are taken into account in the changing state of the EBS components, as required by the NRC proposed rule, 10 CFR 63.342(c)(i) [DIRS 178394] and 10 CFR 63.102(j) [DIRS 180319], but not in the natural system components, which have been screened out by the FEPs screening process.

The calculational approach for the two Seismic Scenario Class modeling cases is discussed in Section 6.1.2.4.4.

Section 6.6 is organized as follows. Section 6.6.1 summarizes the model components and submodels of the Seismic Scenario Class. Sections 6.6.1.1 through 6.6.1.3 describe the ground motion damage and fault displacement damage conceptual models, the corresponding abstraction models, and their implementation in the TSPA-SEIS Model. Section 6.6.2 discusses the changes to other TSPA-SEIS Submodels that occur as a result of a seismic event. These include changes to the Drift Seepage Submodel and Drift Wall Condensation Submodel (Section 6.6.2.1), changes to the EBS TH Environment Submodel (Section 6.6.2.2), changes to the WP and DS Degradation Submodel (Section 6.6.2.3), and the potential effect of crown-seepage induced localized corrosion (Section 6.6.2.4). Model component consistency and conservatisms in assumptions and parameters are discussed in Section 6.6.3. In Section 6.6.4, alternative conceptual models (ACMs) are considered.

6.6.1 TSPA-SEIS Model Components and Submodels for the Seismic Scenario Class

The Seismic Scenario Class considers seismic events in the mean annual exceedance frequency range of 4.287×10^{-4} to 10^{-8} per year. The upper bound on the mean annual exceedance frequency is based on the minimum peak ground velocity (PGV) threshold for the onset of kinematic damage (SNL 2007 [DIRS 176828]), Section 6.4.3) and the lower bound is dictated by regulation (NRC proposed rule 10 CFR 63.342(b) [DIRS 178394]). If a seismic event breaches the WPs, radionuclides are mobilized and transported from the EBS into the repository host rock. The mobilized radionuclides can then be transported by water percolating through the UZ to the water table, and then to the accessible environment by flow and transport processes in the SZ.

The model components and submodels of the TSPA-SEIS Model for the Seismic Scenario Class are shown on Figure 6.6-1. Figure 6.6-2 shows the information flow within the TSPA-SEIS Model associated with the Seismic Scenario Class. Figure 6.6-3 indicates the major inputs and outputs of the model components and submodels of the Seismic Scenario Class, the processes included in the Seismic Scenario Class, and the foundation for confidence in the TSPA-SEIS Model. These figures indicate that the TSPA-SEIS Model framework for the Seismic Scenario Class is similar to that of the Nominal Scenario Class. However, some of the model components and submodels differ from those described in Section 6.3. These include the following:

- WP and DS Degradation Model Component
- Drift Seepage Submodel and Drift Wall Condensation Submodel of the UZ Flow Model Component
- EBS TH Environment Submodel of the EBS Environment Model Component.

Figure 6.6-4 provides a schematic illustration of the various elements of the Seismic Scenario Class. The figure shows the likely seismic effects within an emplacement drift of the repository, the subsequent radionuclide releases to the SZ, and their transport to the accessible environment.

In order to provide a complete description of the model components and submodels needed for the Seismic Scenario Class modeling cases, the model components and submodels that differ from those described in Section 6.3 are described in the following sections, according to their effects on repository performance.

6.6.1.1 Conceptual Model for Seismic Response of the Engineered Barrier System

The conceptual model for mechanical damage to the EBS associated with seismic activity is documented in *Seismic Consequence Abstraction* (SNL 2007 [DIRS 176828], Section 6). The conceptual model for the mechanical response of the EBS components is summarized in the following sections.

6.6.1.1.1 Conceptual Model for Rockfall from Ground Motion

Rockfall induced by vibratory ground motion has the potential to fill the emplacement drifts during the period of geologic stability for dose assessment as defined at NRC proposed rule 10 CFR 63.302 [DIRS 178394]. Rockfall refers to the large rock blocks that may be ejected from the nonlithophysal units of the repository during vibratory ground motion. Rockfall also refers to the fractured and rubblized material that may surround the DS and fill the drifts during partial or complete collapse of drifts in lithophysal units of the repository. Detailed rockfall analyses have been performed for both lithophysal and nonlithophysal rock, under vibratory ground motion.

In the lithophysal zones, the rock mass has very low compressive strength and is permeated with void spaces of varying size (SNL 2007 [DIRS 176828], Section 6.7.1). The drifts in the lithophysal zone are predicted to collapse into small fragments with particle sizes of centimeters to decimeters under the loads imposed by vibratory ground motion. In the nonlithophysal zones, large rock blocks may be shaken loose from the drift walls and fall onto DSs in response to vibratory ground motion.

Drift collapse impacts the temperature and relative humidity of the outer surface of a WP in lithophysal regions of the repository because rubble fills the collapsed drift, essentially forming a thermal blanket covering the DSs and possibly the WPs if the DSs have failed as a barrier to rockfall. Drift collapse also impacts seepage flux and DWC in the emplacement drifts in the lithophysal zones. The abstraction and implementation of the effect of drift collapse on temperature and seepage are discussed in more detail in Sections 6.6.2.2 and 6.6.2.1.

6.6.1.1.2 Conceptual Model for Drip Shield and Waste Package Failure from Ground Motion

The components of the EBS are illustrated on Figure 1-11. Mechanical processes that occur during a significant seismic event (i.e., an event with the capacity to degrade or rupture WPs and/or DSs) have the potential to compromise the functionality of the DSs as barriers to seepage and rockfall and of the WPs as barriers to radionuclide release. For significant vibratory ground motions, impacts can occur between adjacent WPs and between a WP and its emplacement pallet, the surrounding DS, and the invert. Impacts can also occur between DSs and emplacement pallets, the invert, and the drift wall. Dynamic loads induced by vibratory ground motions can result in impacts on DSs in the postclosure period. Lithophysal and nonlithophysal rockfall induced by vibratory ground motion can result in static loads on DSs from the

surrounding mass of rubblized rock. Finally, mechanical loads may be generated by fault displacement within the repository block. In this case, EBS components may become sheared if fault displacement is greater than the available clearances between or around components.

DS Failure Mechanisms—The mechanical response of DSs to vibratory ground motion, which could adversely affect the ability of a DS to prevent flow from reaching a WP, was examined in *Seismic Consequence Abstraction* (SNL 2007 [DIRS 176828], Sections 6.8 and 6.10) and is described as follows:

- The static load from rockfall combined with the dynamic load during a seismic event may buckle the DS framework or rupture DS plates. Buckling or rupture compromises the capacity of a DS to deflect seepage and rockfall away from a WP. Quasi-static and dynamic calculations were performed to define the failure mode (i.e., buckling) of the DS framework (SNL 2007 [DIRS 176828], Section 6.8.3.1).

- The static load from rockfall combined with the dynamic load during a seismic event may deform the plates on the crown of a DS. High levels of residual tensile stress may lead to accelerated degradation processes like SCC. The damaged or deformed area that exceeds a residual stress threshold is conceptualized to result in a tightly spaced network of stress corrosion cracks, providing a potential pathway for radionuclide transport and release (SNL 2007 [DIRS 176828], Sections 6.3 and 6.10).

- Impacts by large rock blocks in unfilled or partly filled drifts in nonlithophysal units may deform DSs or fail plates and axial stiffeners on the crown of a DS. Failed DS plates provide a potential pathway for seepage to contact the WPs (SNL 2007 [DIRS 176828] Section 6.10.2).

- Large displacements on known faults in the repository block have the potential to shear DSs if they become pinned by the fault response. The response of EBS components to fault displacement is discussed in Sections 6.6.1.1.3 and 6.6.1.2.3.

WP Failure Mechanisms—The potential failure mechanisms for the response of WPs to vibratory ground motion were examined in *Seismic Consequence Abstraction* (SNL 2007 [DIRS 176828], Sections 6.5, 6.6, and 6.9) and were described as follows.

- Dynamic loads may dent WPs, resulting in permanent structural deformation with residual tensile stress. The damaged or deformed area that exceeds a residual tensile stress threshold is conceptualized to result in a tightly spaced network of stress corrosion cracks. WP structural response was evaluated for three values of the residual tensile stress threshold for Alloy 22: 90 percent, 100 percent, and 105 percent of the yield strength of Alloy 22. The network of stress corrosion cracks is considered to immediately form once the residual tensile stress threshold is exceeded, providing potential pathways for radionuclide transport and release (SNL 2007 [DIRS 181953], Section 6.7). For WPs subject to SCC damage, the effective transport area for a damaged WP is much smaller than the damaged area because advection and diffusion occurs through a network of stress corrosion cracks, rather than through the total damaged area that exceeds the residual stress threshold. The effective area for flow and transport is

based on the crack density model and associated scaling factor for Alloy 22 developed in *Stress Corrosion Cracking of Waste Package Outer Barrier and Drip Shield Materials* (SNL 2007 [DIRS 181953], Section 6.7). The distribution representing the scaling factor has a mean value of 0.00819 (Section 6.6.1.3.7).

- Dynamic loads on WPs free to move during a seismic event have the potential to result in a rupture (tear) of a WP if the local strain exceeds the ultimate tensile strain. Dynamic loading from a single impact may not produce tensile strains in the Alloy 22 (UNS N06022) outer corrosion barrier that exceed the ultimate tensile strain. However, the extreme deformation from a major seismic event could weaken the outer corrosion barrier, potentially resulting in a ruptured outer corrosion barrier from a subsequent extreme seismic event (SNL 2007 [DIRS 176828], Section 6.1.2). WPs that have been ruptured provide potential pathways for seepage and for radionuclide transport and release. An abstraction for WP rupture from kinematic impacts has been included in the Seismic Scenario Class (Section 6.6.1.2.2.2). WP rupture occurs only for WPs free to move under intact DSs.

- The probability of rupture for WPs with degraded internals surrounded by rubble is zero because the strain on the outer corrosion barrier is always below the ultimate tensile strain for Alloy 22 (SNL 2007 [DIRS 178851] Section 6.5.1). However, a severely deformed outer corrosion barrier may be punctured by the sharp edges of fractured or partly degraded internal components. The WP internals are assumed to degrade as structural elements after the outer corrosion barrier is first breached. Extreme deformation of the cylindrical outer corrosion barrier can eliminate the free volume within the outer corrosion barrier, allowing the sharp corners or sharp edges from degraded internal elements to puncture the outer corrosion barrier when it is surrounded by lithophysal rubble (SNL 2007 [DIRS 176828], Section 6.1.2). The punctured area is conceptualized to be a small patch on the surface of the outer corrosion barrier (SNL 2007 [DIRS 176828], Section 6.9.1). WPs that have been punctured provide potential pathways for seepage and for radionuclide transport and release. An abstraction for puncture of WPs surrounded by rubble has been included in the Seismic Scenario Class (Section 6.6.1.2.2.2). WP puncture occurs only for WPs with degraded internals, surrounded by lithophysal rubble.

- Large displacements on known faults in the repository block have the potential to shear WPs if they become pinned by the fault response (SNL 2007 [DIRS 176828], Section 6.11). The response of EBS components to fault displacement is discussed in Sections 6.6.1.1.3 and 6.6.1.2.3.

6.6.1.1.3 Fault Displacement Conceptual Model

The conceptual model for fault displacement was developed using data from known and hypothetical faults in the repository. The expected number of WP failures that could occur due to fault displacement is a small fraction of the total number of WPs in the repository. The number of failed WPs is estimated based on an understanding of the displacements that could occur on these faults and geometrical considerations, as described in *Seismic Consequence Abstraction* (SNL 2007 [DIRS 176828], Section 6.11). A fault displacement that occurs in an

emplacement drift may cause a sudden discontinuity in the profile of the drift. This could result in one portion of the drift being displaced vertically relative to the adjacent section. Such a discontinuity in the drift could cause shearing of the WP and DS located over the fault if the fault displacement exceeds the available clearance in the EBS. The comparison of fault displacements with available clearances defines the potential for damage to EBS components from fault displacement.

Two distinct cases were considered in analyzing the clearances between EBS components: (1) an intact DS, and (2) a failed DS. The first case represents the as-emplaced configuration of the EBS, shortly after repository closure, and is expected to be applicable to the first 10,000 years after repository closure. The second case represents the late time response of the EBS after DS framework and DS plates have failed and rockfall has partly filled the emplacement drifts and surrounded WPs with rubble. The results of the analyses representing failed DSs with WPs surrounded by rubble were deemed appropriate for use in TSPA-SEIS model, since they are conservative relative to unfailed DS results (SNL 2007 [DIRS 176828], Section 6.11.1.3).

Given the complexity of the response of EBS components and the invert to a fault displacement, a simplified failure criterion was applied to determine shear failure in a collapsed drift. If the fault displacement exceeds one-quarter of the outer diameter of the outer corrosion barrier (about 0.4 meters to 0.5 meters), the WP fails from shear (SNL 2007 [DIRS 176828], Section 6.11.1.2). This simple failure criterion is appropriate because shear failure from fault displacement only occurs from extremely low-frequency, high-amplitude fault displacements, corresponding to a mean annual exceedance frequency of less than or equal to 2.5×10^{-7} per year (SNL 2007 [DIRS 176828], Table 6-67). Fault displacement in excess of these values is conservatively considered to fail WPs and the overlying DSs through direct shearing, allowing advective flow through the sheared components. The cladding within the affected WPs would also be failed, but cladding failure is not analyzed because the TSPA-SEIS is not taking credit for the cladding.

6.6.1.2 Abstraction Model for Seismic Response of the Engineered Barrier System

The mechanical response of EBS components to a seismic event will be highly dependent on the in-drift configuration of EBS components and on the structural integrity of the EBS components at the time of the seismic event. The future configuration of the EBS components has been represented by three idealized configurations, as shown on Figure 6.6-5. Figure 6.6-5 (a) represents the as-emplaced EBS configuration, with an intact DS and minimal rockfall in the drifts. In this configuration, WPs can move freely beneath DSs. Figure 6.6-5 (b) represents an intermediate state of the system where the legs of a DS have buckled under combined rockfall/seismic load (i.e., DS framework failed), but DS plates remain intact. In this configuration, a DS may collapse onto a WP, inhibiting free movement of the WP and emplacement pallet during the seismic event. Figure 6.6-5 (c) represents the end state of the system, in which rubble surrounds WPs after failure of DS plates. The transition between these configurations is determined by fragility curves for DS framework and plates, based on the intensity of the seismic event and on the thickness of DS components and accumulated rockfall load at the time of the seismic event. The structural integrity of the DS is determined by structural response calculations (SNL 2007 [DIRS 178851], Sections 6.4.3 and 6.4.4).

This potential for DS failure leads to three distinct damage mechanisms for WPs. The first mechanism, referred to as kinematic damage, exists when WPs are free to move beneath DSs (Figure 6.6-5(a)). The second and third damage mechanisms occur when the motion of WPs is restricted and are shown on Figure 6.6-5(b) and Figure 6.6-5(c). These mechanisms are referred to as damage for a WP beneath (loaded by) a buckled DS and damage for a WP surrounded by rubble, respectively.

The future state of the internal structures within WPs is also important for the damage mechanisms. This internal structure includes a 2-inch thick inner vessel of stainless steel, a TAD canister (for CSNF), and the basket structure that supports the fuel rod assemblies within the WPs. The internal structures add structural strength to the SPs. These internal structures may degrade much faster than Alloy 22, depending on the in-package chemical environment, the residual stress near welds in the inner vessel, and the potential for galvanic contact between the Alloy 22 outer corrosion barrier and the stainless steel inner vessel. Given the uncertainties related to these long-term degradation processes, the future state of the internals is represented as either intact or degraded. The internals remain intact structurally until the first breach of the outer corrosion barrier, after which time they are treated as a degraded material with minimal strength and minimal cohesion. Breach refers to any penetration of the outer corrosion barrier. First breach will usually occur from SCC in the lid welds or in response to seismic events (SNL 2007 [DIRS 176828], Section 6.1.3).

The timing of the first seismic event that breaches the WP is a strong function of WP type. The CSNF WP has two independent stainless steel vessels, the inner vessel and its lids and the TAD canister. The CDSP WP has only the inner vessel and its lids. The CSNF WP is demonstrably more robust based on a comparison of the probabilities of damage to WPs with intact internals (Figures 6.6-10 and 6.6-11).

The assumption (SNL 2007 [DIRS 176828], Assumption 5.4) that the internal structures degrade by the time of the next seismic event after the outer corrosion barrier is first breached adds conservatism to the seismic WP damage abstraction. Since the Poisson frequency of seismic events is 4.287×10^{-4} per year (Section 6.6.1.3.2), the typical time interval between seismic events is about 2,300 years. However, stainless steel internal structures may remain structurally intact for much more than 2,300 years if in-package chemical conditions remain similar to a fresh water environment, which is the expected condition until after DS failure (SNL 2007 [DIRS 176828], Section 6.1.3). Because seismic damage to a WP is much greater when the internals are degraded, due to the much lower structural strength, this nearly instantaneous degradation of the internals maximizes seismic-related damage to the WP.

A probabilistic seismic hazard analysis (PSHA) was performed to assess the seismic hazards of vibratory ground motion and fault displacement at Yucca Mountain. The PSHA (CRWMS M&O 1998 [DIRS 103731]) provides quantitative hazard results to support an assessment of the repository's long-term performance and to form the basis for developing seismic design criteria. The PSHA methodology for vibratory ground motions is standard practice for deriving vibratory ground motion hazards for design purposes. In addition, probabilistic fault displacement analyses were conducted to provide quantitative assessments of the location and amount of differential ground displacement that might occur. Both analyses provide hazard curves, which express the annual frequency of exceeding various amounts of ground motion (or fault

displacement) (SNL 2007 [DIRS 176828], Section 6.4.1). The Seismic Scenario Class for the TSPA-SEIS uses the mean hazard curves for PGV and fault displacement. Each mean hazard curve, which is defined as the mean estimate or average of a distribution of hazard curves, typically lies above the 80th percentile of the distribution because the average is dominated by the larger values of the distribution. The use of mean hazard curves is conservative relative to median hazard curves, and provides an accurate representation for the mean dose. The mean hazard curve for ground motion defines the relationship between the estimate of mean annual exceedance frequency, and the amplitude of the vibratory ground motion, measured by the PGV of the first horizontal component of the ground motion, denoted as PGV (SNL 2007 [DIRS 176828], Section 1.1, footnote 1, p. 1-2). Analysis of the limits for maximum shear strain in the lithophysal rock typical of geologic conditions at Yucca Mountain led to a determination of a mean bounded hazard curve for horizontal PGV at the repository emplacement level. Figure 6.6-6 shows the mean bounded hazard curve. The effect of fault displacement on the EBS is evaluated in terms of mean fault displacement hazard curves developed for faulting conditions mapped within the immediate vicinity of Yucca Mountain (SNL 2007 [DIRS 176828], Section 6.11.3).

6.6.1.2.1 Abstraction for Rockfall Volume from Ground Motion

The probability of lithophysal rockfall from a seismic event was abstracted, based on computational results for 15 ground motions at the 0.4 m/s, 1.05 m/s, and 2.44 m/s PGV levels and five rock mass categories (SNL 2007 [DIRS 176828], Section 6.7.1.1, Table 6-28). The probability of rockfall was calculated based on a weighted average of the results for each rock mass category, since the rock mass categories are not equally probable. The resulting piecewise linear definition for the probability of rockfall is given in *Seismic Consequence Abstraction* (SNL 2007 [DIRS 176828], Equation 6.7-1):

$$P_{rockfall} = Min(1.0, Max(0.0, (1.288)PGV - 0.353)) \qquad \text{(Eq. 6.6-1)}$$

When rockfall occurs, the volume of lithophysal rock that collapses per meter of drift length is represented by a gamma distribution with mean and standard deviations (SDs) that are quadratic functions of PGV (Figure 6.6-7).

The lithophysal rock volume from multiple seismic events is defined as the sum of the volumes from the individual seismic events. Examination of the mean volume on Figure 6.6-7 shows that rock volume in the lithophysal units will accumulate fairly rapidly. The total rock volume from multiple seismic events is an important parameter because it defines the static load of rubble based on the fraction of the drift filled by rubble. This fraction is defined as the total rubble volume (from multiple seismic events) divided by the rubble volume needed to fill a drift (the effective drift volume after collapse). The effective drift volume after collapse is estimated to be 30 m^3/m to 120 m^3/m for both lithophysal and nonlithophysal zones (SNL 2007 [DIRS 176828], Section 6.7.1.5).

Calculations for the nonlithophysal zones evaluated the response of a 21.74-meter-long section of drift in nonlithophysal rock for the 1.05 m/s, 2.44 m/s, and 5.35 m/s PGV levels. The volume of nonlithophysal rock that collapses per meter of drift length was represented by a gamma distribution with mean and SD that are quadratic functions of PGV. The mean and SD are shown

on Figure 6.6-7. Examination of the mean curves shows that the mean rockfall volume in the lithophysal rock is a factor of 32 to 188 greater than the mean rockfall volume in the nonlithophysal rock for the 1.05 m/s and 2.44 m/s PGV levels, respectively (SNL 2007 [DIRS 176828], Section 6.7.2.1).

The results for nonlithophysal rockfall show probabilities of rockfall that are similar to those for rockfall in the lithophysal zones, except at the 0.4 m/s level, where the calculations could not be compared (SNL 2007 [DIRS 176828], Section 6.7.2.2). Therefore, the probability of rockfall in the nonlithophysal zones is set to be the same as the probability of rockfall in the lithophysal zones, based on the comparison at higher PGV levels than 0.4 m/s.

6.6.1.2.2 Abstraction for Drip Shield and Waste Package Degradation from Ground Motion

Three types of calculations form the basis of the seismic damage abstractions for the WP and DS. The three types of calculation are: (1) three-dimensional kinematic calculations for EBS damage due to vibratory ground motion, appropriate for the early postclosure period, when the DSs are intact and the WPs can move freely beneath the DSs; (2) calculations for deformation and damage of a DS under static and dynamic conditions with intact and degraded EBS components; and (3) calculations for a WP surrounded by rubble that estimate damage after the DS plates have failed(SNL 2007 [DIRS 178851], Section 7.2.1).

Three-dimensional kinematic calculations are used to examine the motion and impact of multiple WPs, pallets, and DSs in an emplacement drift. The objective of these analyses is to define the history of impact parameters for collisions of the WPs, pallets, and DSs as a function of the applied ground motion time histories, and to determine the associated probability of rupture and damaged areas on a WP. Seventeen separate ground motion time histories are used at each of four different PGV levels. A separate kinematic calculation is performed for each ground motion time history at each PGV level, and separate kinematic models are used for CSNF WPs and CDSP WPs. The kinematic calculations are appropriate when the DS is intact and the WP can move freely beneath the DS. At late times, when the degraded DS plates may fail from rockfall and seismic loads, the WP will be surrounded by rubble. The direct loads from this rubble may cause damage to the WP in response to vibratory ground motion. Rubble in the lithophysal zone is most relevant here because the small particle size of the lithophysal rubble means it can more easily slip or fall through gaps or tears in the plates of the DS and because the lithophysal zones encompass approximately 80 to 85 percent of the emplacement drifts in the repository. The damage induced by the rubble surrounding the WP is based on the two-dimensional coupled rockfall/structural response of the Alloy 22 outer barrier during vibratory ground motion. Damage is determined directly from the finite-difference output for the stress and strain state of the outer barrier; additional look-up tables are not required. The input data for the calculations of a single WP surrounded by rubble include 17 ground motion time histories at four PGV levels, elastic and plastic properties of the outer barrier, and the bulk properties of degraded WP internals (SNL 2007 [DIRS 178851], Section 6.5.1.1).

6.6.1.2.2.1 Drip Shield Fragility Abstraction

The fragility analysis for DSs defines the probability of failure as a function of the thickness and plastic load capacity of DS components, the static rockfall load on DSs, and the vertical component of peak ground acceleration (PGA) for the seismic event (SNL 2007 [DIRS 176828], Section 6.8). Fragility curves were developed for two modes of failure: (1) rupture or tearing of DS plates, and (2) buckling or collapse of the sidewalls and/or crown of a DS. A third failure mode, from lateral WP impacts to the DS or from longitudinal impacts of the WP on the bulkhead support beams, was considered but not incorporated into the TSPA-SEIS Model. This third failure mode is not represented in the TSPA-SEIS Model for two reasons. First, lateral impact of the WP on the DS does not cause catastrophic failure of the DS. Second, high velocity longitudinal impacts of the WP on the bulkhead support beams exposed on the underside of the crown of the DS occur infrequently, even at the 4.07 m/s PGV level (SNL 2007 [DIRS 176828], Section 6.8.5).

The fragility analysis is based on the vertical component of PGA because the average loads on the crown are significantly greater than the average loads on the sidewalls of a DS, indicating that vertical loads are likely to be the critical loads for failure. The vertical component of PGA is defined by a probability distribution that is conditional on the PGV level for a seismic event. The static load from rockfall was based on lithophysal rubble. Rockfall in lithophysal rock has significantly greater volume (SNL 2007 [DIRS 176828], Section 6.7.2.1) than rockfall in nonlithophysal rock, resulting in greater static loads from lithophysal rock than from nonlithophysal rubble. The load from lithophysal rubble was treated as uniform on the crown on a DS because the typical particulate sizes in the lithophysal rubble are less than the typical dimensions of DS plates.

Plate Failure

Finite-element calculations were performed to define the plastic (nonlinear) load-bearing capacity of the curved plates on the crown of a DS (SNL 2007 [DIRS 176828], Section 6.8.2.1). These calculations defined the magnitude of the uniform load that causes an element of the plate to exceed the failure criteria for Titanium Grade 7, which are based on both accumulated plastic strain and maximum stress (SNL 2007 [DIRS 178851], Section 6.4.3.1.3). For these calculations, the ultimate plastic load capacity of a DS was determined as a function of plate thickness, the static load from rubble in the drift, and the vertical PGA. Calculations to represent degraded states of the system were performed for 15-mm-, 10-mm-, and 5-mm-thick plates. The plate thicknesses correspond to 0-mm, 5-mm, 10-mm and 13-mm thickness reductions from the initial plate thickness of 15-mm. The probability of DS plate failure as a function of PGV is illustrated on Figure 6.6-8, for 10 percent, 50 percent, and 100 percent rockfall load (i.e., for drifts that are 10 percent, 50 percent, and 100 percent filled with rubble).

If DS plates fail from a seismic event, then all DSs fail as a barrier to seepage (no spatial variability) and this failure is a permanent change for the rest of the realization. See Section 6.6.3.2 for a discussion of spatial variability.

After DS plate failure, the mechanical response of WPs to seismic events is determined by the abstraction, discussed below, for a WP surrounded by rubble.

Framework Failure

A series of dynamic calculations was performed, using selected ground motions for the 2.44 m/s and 4.07 m/s PGV levels, to determine the failure modes of DS framework. Based on these results, the failure mode for the fragility analysis for DS framework was determined to be buckling or collapse of the sidewalls of a DS. Finite-element calculations were carried out to define the plastic (nonlinear) load-bearing capacity of DS framework with intact plates. These calculations defined the magnitude of the load on the crown that caused the side or leg of a DS to buckle. The thickness of all DS components, including the plates and the individual structural members in the framework, was reduced by a constant value of 0-mm, 5-mm, or 10-mm for these calculations. The thickness reduction was taken in the smaller dimension for each structural member in the framework (SNL 2007 [DIRS 176828], Section 6.8.3.2). The probability of DS framework failure as a function of PGV is illustrated on Figure 6.6-9, for 10 percent, 50 percent and 100 percent rockfall load. Comparison with Figure 6.6-8 shows that the probability of framework failure is always higher than the probability of plate failure, for a given rockfall load and PGV. The framework is expected to collapse before the plates rupture (SNL 2007 [DIRS 176828], Section 6.12.2, Step 13(c)).

If DS framework fails for a seismic event, then DSs do not fail as a barrier to seepage. Plate failure must subsequently occur for seepage to pass through the DS. There is no spatial variability (Section 6.6.3.2) for DS collapse (all DSs collapse), and the framework remains collapsed for the rest of the realization. After DS failure, the mechanical response of WPs to seismic events is a function of the state of the internals. If the internals are intact, the abstraction for a WP surrounded by rubble applies as given below. If the internals are degraded, the kinematic damage abstraction for a WP, under an intact DS but with degraded internals, applies.

Abstraction for Drip Shield Damage from Rockfall Loading

Before DS plates fail, DSs accumulate damage from vibratory ground motion and from rockfall induced by vibratory ground motion. In the lithophysal units, the accumulation of rubble from multiple seismic events and the dynamic motion during a seismic event can generate SCC damaged areas on DSs. These damaged areas are regions that exceed the residual (tensile) stress threshold for DS plates, potentially leading to a network of stress corrosion cracks. The damaged area occurs on the crown of a DS; damage to the sides was not abstracted because any seepage through the sides is considered unlikely to drip onto a WP. The damaged areas in the lithophysal zones were analyzed as a function of the thickness of DS plates, the rockfall load on DSs, and the vertical component of PGA for the seismic event. The abstraction for damaged area on DSs in the lithophysal zones is discussed in Section 6.10.1 of *Seismic Consequence Abstraction* (SNL 2007 [DIRS 176828]). Because DS damage in lithophysal zones is in the form of a network of stress corrosion cracks and because advective flow through stress corrosion cracks in DSs has been screened out, the abstraction for DS damage due to rockfall loading in the lithophysal units has not been included in the TSPA-SEIS Model file.

Abstraction for Drip Shield Damage from Rock Block Impacts

Before DSs fail in the nonlithophysal units, rock blocks can impact DSs in an unfilled or partially filled drift. Rock block impacts may result in damaged areas on DS plates and, in more

extreme cases, may result in tearing or rupture of the plates and failure of the axial stiffeners beneath the crown of a DS. The damaged areas and potential for plate or stiffener failure were analyzed as a function of the thickness of DS plates and framework, the rockfall load on DSs, and the vertical component of PGA for the seismic event. Section 6.10.2 of *Seismic Consequence Abstraction* (SNL 2007 [DIRS 176828]) discusses the abstraction for damaged area and plate failures for DSs in unfilled or partly filled drifts in the nonlithophysal units of the repository. The abstraction for DS damage due to rock block impacts in the nonlithophysal units has not been included in the TSPA-SEIS Model file. An analysis was conducted to show that the impact of this damage mechanism is small.

6.6.1.2.2.2 Waste Package Damage Abstraction

Throughout this section reference is made to damage estimates for WPs based on calculations for an outer corrosion barrier at two thicknesses, 23 mm and 17 mm. The 23-mm thick outer corrosion barrier provides representation of an intact or almost intact WP. The 17-mm thick outer corrosion barrier provides a representation for a degraded WP at late times after repository closure. If the outer corrosion barrier thickness is between 17 mm and 23 mm, linear interpolation is used to define the damaged area (i.e., the area that exceeds the residual stress threshold) within the damage abstractions. If the outer corrosion barrier thickness is greater than 23 mm, damage estimates at 23 mm are used. If the outer corrosion barrier thickness is less than 17 mm, damage estimates at 17 mm are used.

A 17-mm-thick outer corrosion barrier is appropriate for late times after repository closure. The median corrosion rate of Alloy 22 at 60°C is less than 7 nm/yr, based on a medium uncertainty level in the distributions for general corrosion rate (SNL 2007 [DIRS 178519] Figure 6-23). The value of 60°C is appropriate because it is an upper bound on OCB temperature beyond 10,000 years after repository closure (SNL 2007 [DIRS 178851], Figure 1-3) and because it is consistent with the structural response calculations for the seismic scenario (SNL 2007 [DIRS 178851] Assumption 5.7, Section 5). The 17-mm-thick OCB, which corresponds to an 8.4-mm ≈ 8-mm thickness reduction, will occur at a time of $(8 \times 10^{-3}\ \text{m})/(7 \times 10^{-9}\ \text{m/yr}) \approx 1{,}100{,}000$ years. More detailed corrosion calculations require a probabilistic analysis, but this estimate indicates that the 17-mm-thick OCB provides a reasonable representation for seismic response at the end of the period for assessment of repository performance.

The adequacy of the 17-mm thick outer corrosion barrier to represent the degraded states that may occur up to one million years after repository closure has been confirmed by a stand-alone probabilistic analysis of WP degradation. The stand-alone analysis model is a modified version of the TSPA-SEIS compliance model. The model components not pertaining to WP and DS degradation have been removed, to allow increased computational speed and to allow more detailed results to be saved. All epistemically uncertain parameters have been retained and all aleatory parameters related to WP and DS degradation have been retained. The sampling sequence is identical to the TSPA-SEIS model 300-realization unified sampling Seismic GM Modeling Case (Section 6.6.1.3.1).

SCC Damage to CSNF and CDSP Waste Packages under Intact Drip Shields

Kinematic and structural response calculations were performed to develop damage estimates for the failed WP surface area for CSNF and CDSP WPs under intact DSs (SNL 2007 [DIRS 176828], Sections 6.5.1 through 6.5.4 and 6.6.1 through 6.6.4). As described in SNL 2007 ([DIRS 176828], Sections 6.5 and 6.6), kinematic damage abstractions were developed for three future states of CSNF and CDSP WPs:

- 23-mm-thick outer corrosion barrier with intact internals
- 23-mm-thick outer corrosion barrier with degraded internals
- 17-mm-thick outer corrosion barrier with degraded internals.

The probability of damage to CSNF or CDSP WPs for the j^{th} seismic event is defined as a function of (1) the state of the internals (intact or degraded), (2) the PGV for the j^{th} seismic event, (3) the value of residual stress threshold for the i^{th} realization, and (4) the outer corrosion barrier thickness (SNL 2007 [DIRS 176828], Sections 6.5.1.2, 6.5.2.2, 6.6.1.2, and 6.6.2.2). Figures 6.6-10 and 6.6-11 illustrate these probabilities, for the three states of the WP (23-mm, intact; 23-mm, degraded; and 17-mm, degraded). When the WP internals are intact the probability of damage is much lower for CSNF WPs, than for CDSP WPs.

If CSNF or CDSP WPs are damaged by the j^{th} seismic event, then their conditional damaged area is represented by a gamma distribution. Separate gamma distributions were defined for three states of WPs: (1) 23-mm-thick outer corrosion barrier with intact internals, (2) 23-mm-thick outer corrosion barrier with degraded internals, and (3) 17-mm-thick outer corrosion barrier with degraded internals. The values for the mean and SD of these gamma distributions are derived in Sections 6.5.1.3, 6.5.2.3, 6.6.1.3, and 6.6.2.3 of Seismic Consequence Abstraction (SNL 2007 [DIRS 176828]). Figures 6.6-12 and 6.6-13 illustrate the quadratic fits for mean damaged area for the CSNF and CDSP WPs, respectively. The means are a function of PGV and there is a separate gamma distribution for the three values of residual stress threshold (90 percent, 100 percent, and 105 percent of yield strength). For CSNF and CDSP WPs with degraded internals, the damage abstractions show consistently higher SCC damage for the CSNF WPs, compared to the CDSP WPs.

Note that for the CSNF WP with intact internals damage occurs only at the 4.07 m/s PGV level (the probability is zero for all other PGVs – Figure 6.6-10). In this particular case, the single point results are conservative for all values of PGV less than 4.07 m/s and all values of the residual stress threshold greater than 90 percent. In addition, the magnitude of the conditional damaged area is less than 0.006 which is a very small fraction of the cylindrical surface area of the CSNF WP of 33.64 m^2 (SNL 2007 [DIRS 176828], Sections 6.5.1.3). Therefore, the conditional damage at 4.07 m/s and 90 percent residual stress threshold is considered to represent the damage at all values of PGV and residual stress threshold in TSPA-SEIS Model (SNL 2007 [DIRS 176828], Section 6.5.1.3).

For either intact or degraded internals, there is no WP-to-WP spatial variability for the conditional damaged area (Section 6.6.3.2). For a single package, the damaged area is randomly located on the cylindrical surface of the outer corrosion barrier. The total damaged area increases

with each seismic event that causes damage to the WP outer corrosion barrier. Damaged area cannot exceed the total surface area of a CSNF or CDSP WP.

Rupture of CSNF and CDSP Waste Packages under Intact Drip Shields

CSNF or CDSP WPs that can move freely beneath a DS can rupture from the accumulation of severe deformation due to multiple impacts, which can accumulate in either one seismic event or multiple seismic events. The probability of rupture for the 23-mm-thick outer corrosion barrier with intact internals was determined to be zero (SNL 2007 [DIRS 176828], Sections 6.5.1.1 and 6.6.1.1). However, for CSNF or CDSP WPs with degraded internals, the effect of multiple WP-to-pallet impacts was assessed by evaluating the severity of accumulated deformation. The degree of deformation was used to define the probability of rupture. A minor degree of deformation indicated that no rupture occurred, consistent with the observation that the strain in the outer corrosion barrier is below the ultimate tensile strain for Alloy 22 for individual impacts. A significant degree of deformation was interpreted as causing an incipient rupture, in the sense that a second severe impact, during a subsequent seismic event, would have the potential to cause rupture. Finally, if two severe impacts occurred during the same seismic event, then the accumulation of severe deformation was interpreted as causing immediate rupture in the outer corrosion barrier. The probability of incipient rupture and the probability of (immediate) rupture for CSNF or CDSP WPs with degraded internals are abstracted as power laws in Sections 6.5.2.1 and 6.6.2.1 of *Seismic Consequence Abstraction* (SNL 2007 [DIRS 176828]). Figure 6.6-14 compares the probability for incipient and immediate rupture of the CSNF and CDSP WPs. Note that for a given PGV, CSNF WPs have a higher rupture probability.

When a WP is ruptured, the failed area is determined by sampling a uniform distribution for failed area, with a lower bound of 0 m^2 and an upper bound equal to the cross-sectional area of the WP outer corrosion barrier. This failed area allows advective flow through and advective and diffusive transport out of ruptured CSNF or CDSP WPs. Once the WP is ruptured, there is no further damage from rupture in successive events, and the WPs remain ruptured for the remainder of the realization

SCC Damage to CSNF and CDSP Waste Packages Surrounded by Rubble

Structural response calculations were performed to develop damage estimates for the failed WP surface area of a CSNF WP surrounded by rubble (SNL 2007 [DIRS 176828], Sections 6.9.1 through 6.9.9). Two damage abstractions were developed for a WP with degraded internals that is surrounded by lithophysal rubble:

- 23-mm-thick outer corrosion barrier with degraded internals
- 17-mm-thick outer corrosion barrier with degraded internals.

Damage for WPs with intact internals was not calculated for WPs surrounded by rubble. A WP becomes surrounded by rubble after DS framework and DS plates have failed during a seismic event. This is expected to occur at late times after repository closure. For CDSP WPs the outer corrosion barrier is likely to be breached by SCC at these times, resulting in degraded internals. In contrast, the probability of SCC damage to CSNF WPs with intact internals under intact DSs is zero except at 4.07 m/s PGV levels. Therefore, CSNF WPs are not likely to have degraded

internals at the time of DS failure. Regardless of the time scale, the damage abstractions for degraded internals will result in greater damaged area relative to the response with intact internals, so this approach is conservative. Separate abstractions were not developed for CSNF and CDSP WPs surrounded by rubble because it was considered that the results for the CSNF WPs provide a reasonable estimate of damage to the CDSP WP (SNL 2007 [DIRS 176828], Sections 6.9.10).

Lithophysal rubble was selected for the dynamic load on WPs. The analysis acknowledges that large rock blocks would tend to have point loading contacts in localized areas on a WP, but the cumulative loading from the lithophysal rubble is expected to be significantly greater because the volume of lithophysal rubble is much greater than the volume of nonlithophysal rockfall (SNL 2007 [DIRS 176828], Table 6-32 and Figure 6-58).

The probability of damage for the j^{th} seismic event was abstracted as a function of the value of PGV for the j^{th} seismic event, the value of residual stress threshold for the i^{th} realization, and of the outer corrosion barrier thickness (SNL 2007 [DIRS 176828]), Section 6.9.2). Figure 6.6-15 illustrates these probabilities, for the two states of the WP (23-mm degraded and 17-mm degraded).

If WPs are damaged by the j^{th} seismic event, then the conditional damaged area is represented by a gamma distribution. Separate gamma distributions were defined for two states of WPs: (1) 23-mm-thick outer corrosion barrier with degraded internals, and (2) 17-mm-thick outer corrosion barrier with degraded internals. The mean and SD of the gamma functions are quadratic equations in residual stress threshold (SNL 2007 [DIRS 176828], Section 6.9.3). For the 23-mm thick and the 17-mm thick outer corrosion barrier, relatively few data points showed SCC damage (SNL 2007 [DIRS 176828], Sections 6.9.3 and 6.9.5). Therefore, the abstraction for damage was done at a single PGV level (4.07 m/s). It was considered to be conservative to use the conditional damage at the 4.07 m/s PGV level for all values of PGV (SNL 2007 [DIRS 176828], Section 6.9.3). Figure 6.6-16 shows the quadratic fit for the mean damage area as a percent of the total surface area, for the 23-mm and 17-mm thick outer corrosion barrier.

There is no WP-to-WP spatial variability for the conditional damaged area (SNL 2007 [DIRS 176828], Section 6.9.9). Spatial variability is also discussed in Section 6.6.3.2. For a single package, the damaged is randomly located on the cylindrical surface of the outer corrosion barrier. The total damaged area increases with each seismic event that causes damage to the outer corrosion barrier. The damaged area cannot exceed the total surface area of a CSNF or CDSP WP.

Puncture of CSNF and CDSP Waste Packages Surrounded by Rubble

For a WP surrounded by rubble, loss of WP integrity is conceptualized to occur from puncture by sharp internal fragments, rather than rupture of the outer corrosion barrier due to impact with other EBS components. The probability of puncture for the 23-mm-thick and 17-mm-thick outer corrosion barriers is abstracted as a power law in PGV (SNL 2007 [DIRS 176828], Section 6.9.1). Figure 6.6-17 shows the probability of puncture for 23-mm and 17-mm outer corrosion barriers. Comparison with Figure 6.6-14 shows that puncture can be more likely than rupture, particularly for 17-mm outer corrosion barriers and at lower PGVs.

When WPs are punctured, the failed area is determined by sampling a uniform distribution, with a lower bound of 0 m^2 and an upper bound of 0.10 m^2. The upper bound of the uniform distribution is based on two estimates for the area of a hypothetical puncture. If the puncture occurs from a sharp fragment of a fuel rod, the corresponding hole is likely to be quite small. In the second estimate, one of the fuel basket plates is conceptualized to form a lengthwise slice through the outer corrosion barrier (SNL 2007 [DIRS 176828], Section 6.9.1). The upper bound of 0.10 m^2 represents the maximum estimated area from either mechanism. This failed area allows advective flow through punctured WPs and advective and diffusive transport out of the punctured WPs. Once a WP is penetrated, there is no further damage from penetrations in successive events and the WPs remain punctured for the remainder of the realization.

6.6.1.2.3 Fault Displacement Abstraction

In addition to the damage from vibratory ground motion, it is possible that WP and DS failures may occur due to fault displacement. Damage to WPs by fault displacement occurs when the fault displacement exceeds the available clearances between or around EBS components. Two distinct cases were considered in analyzing the clearances between EBS components (Section 6.6.1.1.3). The maximum allowable displacement, for six different package types (SNL 2007 [DIRS 176828], Tables 6-58 and 6-59), was determined for the two cases, one with an intact DS and a second with a failed DS. The values corresponding to the second case (failed DSs) are used for the TSPA-SEIS Model because these values result in more failures than for the first case, with an intact drip shield. Fault displacement hazard curves for 15 faulting conditions mapped within the immediate vicinity of Yucca Mountain were used to provide displacement values as a function of the mean annual exceedance frequency (SNL 2007 [DIRS 176828], Section 6.11.3). The inventory of WP types was split into two groups (CSNF and CDSP WP). WPs of similar design and similar waste type were grouped together. The WP designs with the smallest diameter in the group are chosen to represent the clearance for all packages in that group. The clearance is given by one-quarter of the outer diameter of the outer corrosion barrier, so the smallest diameter results in the least clearance for all WPs in the group. The probability of finding a WP in each group on a fault was calculated based on the total length of the WP types in the group versus the total length of all emplaced WPs (rather than the number of each type of WP divided by the total number of WPs). The hazard curve data is combined with the clearance data and the probability of find a WP from each group on a fault to give the expected number of WP failures as a function of mean annual exceedance frequency. The expected number of WPs that could fail from fault displacement was found to be a small fraction of the total number of WPs in the repository. If a WP fails from fault displacement, then the surrounding DS also fails from fault displacement (if it hasn't already failed in a previous seismic event). The results are summarized in Table 6.6-1. The table indicates that damage to WPs and DSs from fault displacement is not expected if the mean annual frequency of occurrence is greater than 2.5×10^{-7} per year.

Shearing of the WP and DS over the fault can occur if the fault exceeds the available clearance in the EBS (SNL 2007 [DIRS 176828], Section 6.11). When a WP fails by fault displacement, the failed area is determined by sampling a uniform distribution with a lower bound of zero and an upper bound equal to the area of a WP lid. The lower bound is appropriate for mean annual exceedance frequencies near 10^{-7} per year because a WP that is minimally pinned from fault displacement is expected to have only minor crimping and is unlikely to rupture. The upper

bound is appropriate for a large fault displacement that shears a WP near its lid. In this case, the lid welds have the potential to fracture, separating the lid from the package and potentially exposing the entire waste form to seepage and release (SNL 2007 [DIRS 176828], Section 6.11.5). The use of a uniform distribution is appropriate because reasonable upper and lower bounds can be defined and because the use of this type of distribution maintains the uncertainty in the damaged area for this abstraction.

In the TSPA model the failed area is conceptualized to be a shear that lies in a plane normal to the central axis of a WP. The failed area can be represented as a circumferential band around a WP for transport calculations in the TSPA. Once WPs fail in shear, there is no further damage on successive events and WPs remain failed for the remainder of the realization. The resulting damage is assumed to allow flow into WPs (if seepage is present) and allow advective and diffusive transport out of WPs. When a WP fails from fault displacement, the associated DS is also presumed to fail, causing damage to the total surface area of the DS. A sheared DS will allow all seepage to pass through no flux splitting (SNL 2007 [DIRS 176828], Section 6.11.5). A damage abstraction for the cladding in a fault-failed WP was not developed because the TSPA-SEIS Model does not take credit for cladding as a barrier to radionuclide releases (SNL 2007 [DIRS 180616], Section 6.2.1.2[a]).

6.6.1.2.4 Treatment of Uncertainty

The TSPA-SEIS Model includes parameter uncertainty in the Seismic Scenario Class at two levels: in the implementation of the abstraction in the TSPA-SEIS model, and in the underlying process models used in the development of the Seismic Consequences Abstraction.The term parameter uncertainty encompasses uncertainty in input parameters for process level models (like ground motions) and uncertainty in random variables for seismic damage, such as the damaged areas.

Uncertainty can be characterized as epistemic (representing limited data and knowledge) or aleatory (representing variability or natural randomness in a process). Uncertainty in the Seismic Scenario Class is directly represented in the TSPA-SEIS Model by defining uncertain parameters that are sampled either once per realization (epistemic parameters) or multiple times per realization, i.e. at the occurrence of each seismic event (aleatory parameters). Table 6.6-2 lists the parameters that represent uncertainty in the Seismic Scenario Class. In this table the parameters are categorized according to whether they represent epistemic or aleatory uncertainty.

The uncertainty in the input parameters to the underlying process models, and its propagation in the TSPA-SEIS Model, is discussed in Section 8.2 of Seismic Consequence Abstraction (SNL 2007 [DIRS 176828]), and summarized as follows:

- The structural response calculations for the responses of WPs that are affected by vibratory ground motion include three principal sources of uncertainty: (1) the ground motion time histories (aleatory uncertainty); (2) the metal-to-metal friction coefficient (epistemic uncertainty); and (3) the metal-to-rock friction coefficient (epistemic uncertainty) (SNL 2007 [DIRS 176828], Section 8.2, Acceptance Criterion 3). The variations of these uncertain input parameters are simultaneously included in the 17 structural response calculations at each seismic hazard level. This is accomplished by a

Latin Hypercube procedure that ensures robust sampling of the uncertain parameters over their full ranges (SNL 2007 [DIRS 178851]), Sections 6.3.1, 6.4.4.5, and 6.5.1.1).

- All rockfall analyses include the ground motion time histories as a major source of aleatory uncertainty. Fifteen ground motions represent the uncertainty in the seismic forcing functions. Note that the rockfall calculations predate the WP calculations and for these earlier calculations only 15 of the 17 ground motion histories were used (SNL 2007 [DIRS 176828], Section 6.1.3). In the lithophysal units, the rock compressive strength is an uncertain input parameter that is represented as five discrete levels of rock strength. The computational results for probability of lithophysal rockfall are based on 15 realizations with Latin Hypercube sampling for the ground motion histories and the rock strengths. In the nonlithophysal units, the synthetic fracture pattern that defines the fracture geometry is an uncertain input parameter that is used in the rockfall analyses for the nonlithophysal units. The nonlithophysal analysis evaluated the response of a 25-meter long section of drift in nonlithophysal rock with randomly selected fracture patterns paired with randomly selected ground motion time histories (BSC 2004 [DIRS166107] Section 6.3.1).

- The calculations of damaged areas on WPs that are due to vibratory ground motion exhibit substantial variability (primarily aleatory uncertainty) induced by the uncertainties in seismic ground motions and other input parameters. This variability in damaged area is represented as conditional probability distributions that are provided to and sampled in the TSPA-SEIS model.

6.6.1.3 Implementation in the TSPA-SEIS Model

The potential for deformation and rupture/puncture of EBS components from multiple seismic events within a given realization of the TSPA-SEIS Model is described in the following sections. These sections are aligned with the separate elements of the seismic damage abstractions. A realization of the TSPA-SEIS model represents one of many future potential histories of the repository. Each realization generally has a unique value for each random variable that represents epistemic (knowledge) uncertainty, such the residual stress threshold (RST) for initiation of potential stress corrosion cracking. Each realization also has a unique sequence of seismic events whose timing and intensity capture the aleatory uncertainty (i.e., the randomness) in the seismic process.

6.6.1.3.1 TSPA-SEIS Modeling Cases

The implementation of the Seismic Damage Abstraction involves two modeling cases, the Seismic GM Modeling Case and the Seismic FD Modeling Case.

Seismic GM Modeling Case

The Seismic GM Modeling Case calculates mean annual dose due to damage to WPs resulting from vibratory ground motion. This modeling case also accounts for fragility of the DSs under the combined loads from vibratory ground motion and accumulated rockfall around the DS.. In addition, corrosion processes are included in the Seismic GM Modeling Case calculation for

1,000,000 years, and the dose due to corrosion processes is calculated as part of the Seismic GM Modeling Case for 1,000,000 years. The Seismic GM Modeling Case does not include damaged areas (due to SCC) on the DS because advective flow through the DS has been screened out. This modeling case also does not include failure of the DSs from large rock block impacts in nonlithophysal units because these processes have been screened out.

The Seismic GM Modeling Case for 10,000 years and the Seismic GM Modeling Case for 1,000,000 years use different numerical techniques to calculate mean annual dose. These are described in the following paragraphs. The TSPA-SEIS Model calculates the mean annual dose for the Seismic GM Modeling Case for 10,000 years using a three-step process. First, a Latin Hypercube Sample (LHS) of uncertain TSPA-SEIS Model parameters is generated. Each element of the LHS is a vector, specifying a value for each epistemically uncertain parameter. For each element in the LHS, a number of annual dose histories are computed using GoldSim. Each annual dose history represents a single seismic ground motion event, which occurs at a specified time, and results in a specified damage area to each WP simulated. The mobilization and transport of radionuclides is evaluated using the Nominal Scenario Class submodels for radionuclide transport in the EBS, UZ, and SZ.

Second, for each element in the LHS, the expected annual dose history is calculated by Equation 6.1.2-22, using the annual dose histories computed for each element of the LHS. The integral in Equation 6.1.2-22 accounts for the uncertainty in the number of seismic events, the time of each event, and the damaged area. The integral is evaluated numerically by EXDOC software (Section 6.1.5). The mean annual dose history is calculated as the average of the expected annual dose histories from the set of realizations.

Because relatively few seismic events (approximately 5) occur within 10,000 years, and the probability of damage to CDSP WPs is much greater than that of damage to the CSNF WPs, the expected dose for the Seismic GM Modeling Case for 10,000 years relies on a number of simplifying approximations:

- Corrosion of WP and DS materials is bounded by a 2 mm thickness reduction to the WP and a 2 mm thickness reduction to the DS
- Only CDSP WPs are considered because the probability of damageing the CSNF WP is very low during the first 10,000 years
- Rupture and puncture events are not considered
- The DS remains intact and functional
- Seepage and temperature are not altered due to rockfall.

Calculation of the mean annual dose for the Seismic GM Modeling Case for 1,000,000 years also begins by generating an LHS of uncertain TSPA-SEIS Model parameters. For each element in the LHS, a number of annual dose histories are computed using GoldSim. Each annual dose history is associated with a sequence of seismic events generated by GoldSim. The effects of corrosion on EBS components are included, and rockfall and damage to EBS components are

accumulated as seismic events occur. The mobilization and transport of radionuclides is evaluated using the Nominal Scenario Class submodels for radionuclide transport in the EBS, UZ, and SZ.

The expected annual dose history is calculated by Equation 6.1.2-24, using the annual dose histories computed for each element of the LHS. The mean annual dose history is calculated as the average of the expected annual dose histories from the set of realizations.

Seismic FD Modeling Case

The Seismic FD Modeling Case calculates mean annual dose due to damage caused by fault displacements. This modeling case accounts for damage to WPs and DSs through direct shearing which allows advective flow through the sheared components. Corrosion processes are not included in the Seismic FD Modeling Case. The modeling case considers a single seismic event. This modeling case does not consider rockfall accumulation in the drifts, however, after the seismic event occurs drifts are considered to be filled with rockfall. Calculation of the mean annual dose for the Seismic FD Modeling Case for either 10,000 years or 1,000,000 years also begins by generating an LHS of uncertain TSPA-SEIS Model parameters, and, for each element of the LHS, computing a number of annual dose histories using GoldSim. Each annual dose history is associated with a single seismic fault displacement event occurring at a specified time, and resulting in a specified damage area to each WP represented. The effects of the fault displacement are applied to the DS and to the drift, and the mobilization and transport of radionuclides is evaluated using the Nominal Scenario Class submodels for radionuclide transport in the EBS, UZ, and SZ.

The expected annual dose history is calculated by Equation 6.1.2-25, using the annual dose histories computed for each element of the LHS. The integral in Equation 6.1.2-25 accounts for the uncertainty in the time of the seismic fault displacement event, the uncertainty in the damaged area caused by the seismic event, and the number of WPs affected; this equation is evaluated numerically by EXDOC (Section 6.1.5). The mean annual dose history is calculated as the average of the expected annual dose histories from the set of realizations. Table 6.6-4 summarizes the calculations for the modeling cases.

6.6.1.3.2 Seismic Event Time and Magnitude Calculations for the 1,000,000 Year Ground Motion Case

For the Seismic GM Modeling Case 1,000,000-year simulation, each realization includes multiple seismic events. In the discussions that follow, a particular seismic event, the j^{th} event, will be considered representative of all seismic events in a particular Monte Carlo realization. The time of the j^{th} event is determined by GoldSim's random time internal (Poisson) event generator (GoldSim Technology Group 2007 [DIRS 181727], Appendix B) using a Poisson frequency of $(\lambda_{max} - \lambda_{min})$. The values of λ_{min} and λ_{max} are set to 1×10^{-8} per year and 4.287×10^{-4} per year, respectively. The Poisson frequency is then given by (4.287×10^{-4} per year $- 1 \times 10^{-8}$ per year) = 4.287×10^{-4} per year.

The mean annual exceedance frequency for the j^{th} event is sampled from a uniform distribution between λ_{min} and λ_{max}. The bounds are chosen to encompass all mean annual exceedance

frequencies with the potential to result in significant damage to DSs or WPs. The range of mean annual exceedance frequencies, spans the response of the system from no damage to the regulatory probability limit at 10^{-8} per year.

After the value of the mean annual exceedance frequency has been determined for the j^{th} event, the corresponding value of the PGV is calculated. The relationship between the PGV and the mean annual exceedance frequency (bounded hazard curve) is represented in the model by a one-dimensional table. Interpolation between points on the hazard curve is based on a piecewise linear interpolation with the values of $\log(\lambda)$ and log (PGV) at the individual points.

6.6.1.3.3 Methodology for Damage Abstraction Implementation

The seismic damage abstractions are generally based on a three-part approach:

1. The probabilities of incipient rupture, (immediate) rupture, or puncture are defined as a function of horizontal PGV and the thickness of the OCB. If rupture or puncture occurs, the resulting rupture area or puncture area is defined using a bounding, uniform distribution. The probabilities of incipient rupture, (immediate) rupture, or puncture are represented as a power-law function of PGV. The rationale for two types of rupture, incipient and immediate, is explained in Section 6.6.1.2.2.2.

2. The probability of damage is defined as a function of PGV, RST, and the thickness of the WP. Damaged area is defined as the area that exceeds the RST and is thereby susceptible to potential SCC. Damaged area represents the physical area of a dented region with high residual stress. Damaged area is significantly greater than the effective area for transport through a network of stress corrosion cracks, as explained in Section 6.6.1.1.2.

3. The probability of nonzero damaged area, or more simply the probability of damage, is usually represented as a lookup table that uses PGV and RST as the independent variables. The typical lookup table for probability of damage at a given OCB thickness has 12 entries defined by four values of PGV (0.4 m/s, 1.05 m/s, 2.44 m/s, and 4.07 m/s) and by three values of RST (90% , 100%, and 105% of the yield strength of Alloy 22). A piecewise linear interpolation scheme is used between the points in the lookup table, avoiding the need for a functional fit to a probability surface.

4. When nonzero damaged area occurs, a conditional probability distribution for the magnitude of the conditional damaged area is defined as a function of PGV, RST, and the thickness of the OCB. The conditional damaged areas are always nonzero areas, by definition.

This approach is useful because it eliminates zero values from the conditional probability distributions in Step 3. A similar approach is applied for rockfall induced by a seismic event, based on Steps 2 and 3, as described in the next section.

6.6.1.3.4 Implementation of Rockfall for the 1,000,000 Year Ground Motion Case

Lithophysal Rockfall Calculation

The probability of rockfall was abstracted as a linear function of PGV (Equation 6.6-1). The occurrence of rockfall is determined by comparing the calculated probability of rockfall for the j^{th} seismic event, $P_{rockfall}$, to a random number between 0 and 1, R_j , corresponding to the j^{th} seismic event

$$If \quad R_j \le P_{rockfall} \quad \text{then } RV_{LITH,j} > 0 \qquad \text{(Eq. 6.6-2)}$$

$$else \quad RV_{LITH,j} = 0$$

where $RV_{LITH,\,j}$ is the volume of lithophysal rockfall. The random number is resampled for each seismic event because the uncertainty in the probability of rockfall is related to the aleatory uncertainty in 17 ground motion time histories.

For each seismic event where rockfall occurs, the volume of lithophysal rock that collapses per meter of drift length is represented by a gamma distribution with mean (μ) and SD (σ) that are quadratic functions of PGV. If the PGV determined from the bounded hazard curve is less than 0.4 m/s, then the values at 0.4 m/s are used in the volume calculations, since Equations 6.6-4 and 6.6-5 may produce nonphysical values of the mean and SD for PGVs less than 0.4 m/s.

$$PGV_{rf} = MAX(PGV, 0.4m/s), \qquad \text{(Eq. 6.6-3)}$$

$$\mu = (20.307)(PGV_{rf})^2 - (18.023)PGV_{rf} + 4.0102, \qquad \text{(Eq. 6.6-4)}$$

$$\sigma = -(3.5613)(PGV_{rf})^2 + (18.018)PGV_{rf} - 6.6202. \qquad \text{(Eq. 6.6-5)}$$

The total volume of lithophysal rock that collapses per meter of drift length after the j^{th} seismic event, $TV_{LITH\,j}$, is the sum of the volumes for the first j seismic events.

$$TV_{LITH,\,j} = \sum_{k=1}^{j} RV_{LITH,k} \qquad \text{(Eq. 6.6-6)}$$

The volume of lithophysal rock that must collapse to fill the drift ($V_{L,i}$) is defined as a uniform distribution between 30 m^3 per meter to 120 m^3 per meter of drift length. This parameter is sampled once per realization.

The fraction of the drift that is filled after the j^{th} seismic event, FD_j, is defined as the ratio of the total volume of collapsed lithophysal rock after the j^{th} seismic event to the volume that is required to fill the drift ($V_{L,i}$), for the i^{th} realization.

$$FD_{LITH,j} = MIN\left(\frac{TV_{LITH,j}}{V_{L,i}}, 1.0\right) \quad \text{(Eq. 6.6-7)}$$

The fraction of drift filled by lithophysal rubble ($FD_{LITH,j}$) is a parameter used in DS fragility calculations.

Nonlithophysal Rockfall Calculation

The probability of nonlithophysal rockfall has been abstracted to be the same as the probability of lithophysal rockfall (Section 6.6.1.2.1). Thus the probability of occurrence of nonlithophysal rockfall is given in Equation 6.6-2.

For each seismic event where rockfall occurs, the volume of nonlithophysal rock that collapses per meter of drift length is represented by a gamma distribution with mean (μ) and SD (σ) that are quadratic functions of PGV :

$$\mu = (-0.0142)(PGV)^2 + (0.2064)PGV + 0.0387 \quad \text{(Eq. 6.6-8)}$$

$$\sigma = (-0.037)(PGV)^2 + (0.3057)PGV + 0.0696. \quad \text{(Eq. 6.6-9)}$$

The total volume of nonlithophysal rock that collapses per meter of drift length after the j^{th} seismic event, the volume of nonlithophysal rock that must collapse to fill a drift, and the fraction of the drift that is filled after the j^{th} seismic event are all defined in an analogous fashion to the definitions for lithophysal rockfall.

The fraction of a drift filled by nonlithophysal rubble is a parameter used by the drift seepage abstraction (Section 6.6.2.1) for the Seismic GM Modeling Case for 1,000,000 years.

6.6.1.3.5 Implementation of Drip Shield Plate and Framework Damage from Ground Motion

Plate Fragility

DS plate fragility is defined as the probability of rupturing a plate during a seismic event. Plate fragility is a function of *PGV* for the j^{th} seismic event, of the thickness of DS plates, and of the static load on plates from rockfall. The thickness of DS plates is a feed from WP and DS Degradation Model Component (Section 6.3.5) of the TSPA-SEIS Model, based on the time of the event, the top-side (upper surface of the DS) and bottom-side (lower surface of the DS) corrosion rates for Titanium Grade 7, and the initial plate thickness. The static load is defined by the fraction of the drift that is filled with lithophysal rubble ($FD_{LITH,j}$), as discussed in Section 6.6.1.3.4 and the resulting failure probability is applied to all zones of the repository.

Four two-dimensional look-up tables represent the probability of failure of DS plates at 0 percent, 10 percent, 50 percent, and 100 percent rockfall load (Figure 6.6-8). Each of these tables is a function of PGV and DS plate thickness. A two-stage linear interpolation process is used to determine the probability. The first step in this interpolation is to linearly interpolate

within each of the four sections of the supporting information using the values of PGV for the j^{th} event and of the plate thickness at the time of the j^{th} event. This first interpolation produces four failure probabilities for drifts that are 0 percent, 10 percent, 50 percent, and 100 percent filled with rubble. A second linear interpolation using the value of $FD_{LITH,j}$ (Equation 6.6-7) for the j^{th} event versus the failure probabilities at these four points determines the probability of DS plate failure. Plate failure is determined by comparing the calculated probability of failure for the j^{th} seismic event to a random number between 0 and 1, R_j, corresponding to the j^{th} seismic event :

$$\textit{If} \quad R_j \leq P_{\textit{plate failure}} \quad \textit{then} \quad \textit{Plate Failure} = \textit{true}$$

$$\textit{else} \quad \textit{Plate Failure} = \textit{false}$$

Note that the same random number was used in Section 6.6.1.3.4 for the determination of the occurrence of rockfall. This random number is also used for the determination of DS framework failure and WP damage. The reason for this is that a more intense ground motion is likely to simultaneously cause rockfall, WP damage, and DS failure because the intensity of the ground motion for a given PGV level is the major driver of system response. The probabilities of rockfall, WP damage, and DS failure are therefore expected to be highly correlated, rather than independent random variables. This random number is resampled for each event because the uncertainty in these probabilities is primarily caused by the aleatory uncertainty in the ground motions.

The consequence of plate failure is that all DSs fail as a barrier to seepage for the remainder of the simulation. In addition, the damage abstraction for WPs under failed DSs (Section 6.6.1.2.2.2) will be applied to all WPs for the remainder of the simulation.

Framework Fragility

DS framework fragility is defined as the probability of collapsing the sides of a DS during a seismic event. Framework fragility is a function of PGV for the j^{th} seismic event, of the reduction in thickness of DS framework, and of the static load on the crown of a DS from rockfall. The reduction in thickness of DS plates is a feed from the WP and DS Degradation Model Component (Section 6.3.5) of the TSPA-SEIS Model, based on the time of the event, the external (upper surface of the DS) corrosion rate for Titanium Grade 7, and the corrosion rate multiplier that converts the Titanium Grade 7 corrosion rate to a corrosion rate appropriate for Titanium Grade 29 corrosion rate is appropriate because the predicted failure mode for the DS framework is collapse of the legs, and the supporting bulkheads on the sides of the DS are located on the exterior side of the DS plates. The external (upper surface) corrosion rate is applied to both sides of the framework components (double-sided corrosion). Double-sided corrosion is considered appropriate since the width of the bulkheads and stiffeners in the axial direction of the DS is usually less than the depth of the bulkheads and stiffeners normal to the plates. In this geometry, the thickness reduction of the width is the important parameter for buckling of the legs. Both sides of the bulkhead or stiffener that are perpendicular to the width will be exposed to the in-drift environment and experience general corrosion (SNL 2007 [DIRS 176828], Section 6.8.3.3). The static load is defined by the fraction of the drift that is filled with lithophysal rubble.

The calculation of probability of framework failure (i.e. buckling of the sidewalls) is analogous to that for plate failure. The probability is represented by four look-up tables, each a function of PGV and framework thickness reduction (Figure 6.6-9). A two-stage linear interpolation process is used to determine the probability of framework failure. The first step in this interpolation is to linearly interpolate using the values of PGV for the j^{th} event and of the reduction in framework thickness at the time of the j^{th} event. This first interpolation produces four conditional failure probabilities, for drifts that are 0 percent, 10 percent, 50 percent, and 100 percent filled with rubble. A second linear interpolation using the value of $FD_{LITH,j}$ for the j^{th} event versus the failure probabilities at these four points determines the probability of collapse. Framework failure is determined by comparing the calculated probability for the j^{th} seismic event to the same random number used to determine DS plate failure.

If DS framework fails, DSs are considered collapsed but are not considered failed as a barrier to seepage. Two calculations were done to represent the response of CSNF (TAD-bearing) WPs, one with intact internals and one with degraded internals (SNL 2007 [DIRS 176828], Section 6.8.4). The expected damage for a CSNF WP surrounded by rubble was found to provide an upper bound for the damage to a CSNF WP with intact internals loaded by a collapsed DS. The results for degraded internals showed a higher level of damage which was consistent with the kinematic damage abstractions for CSNF WPs with degraded internals. Separate calculations were not performed for CDSP WPs loaded by collapsed DSs. Since the calculations for the CSNF WPs were performed quasi-statically, it was anticipated that the response of the CDSP WPs would be very similar (SNL 2007 [DIRS 176828], Section 6.8.4). Therefore, after DS framework failure but before DS plate failure the damage abstractions for WPs surrounded by rubble are applied, if the WP internals are still intact. When the WP internals become degraded (after the first damage-causing event), the damage abstractions for WPs under intact DSs, but with degraded internals, apply until the DS plates also fail.

6.6.1.3.6 Implementation of WP Rupture and Puncture from Ground Motion

The rupture of a CSNF or CDSP WP that can move freely beneath a DS can occur only up until the time of DS plate failure. After DS plate failure, WPs are surrounded by rubble and the failure mechanism is abstracted to be WP puncture.

Ruptured WPs

The probability of rupture for CSNF or CDSP WPs with intact internals is zero. For WPs with degraded internals, two rupture probabilities are calculated; one for incipient rupture, one for immediate rupture. For both CSNF and CDSP WPs, they are given by power laws in PGV. There are three possible rupture states: immediate rupture, PR_{immed}; incipient rupture, PR_{incip}; and no rupture, PR_{none} (given by one minus the sum of the two rupture probabilities). The appropriate state is determined using a random number R_{ruptue}, and a counter, C, with the following logic:

If	$R_{rupture} < PR_{none}$	*then*	$C = 0$
else if	$R_{rupture} < PR_{none} + PR_{incip}$	*then*	$C = 1$
else			$C = 2$

A counter value of 1 indicates an incipient condition for rupture after a single severe impact. A counter value of 2 indicates immediate rupture. The value of the counter is retained, so if an event is deemed to be incipient (C=1) and a subsequent seismic event is also deemed to be incipient, then a rupture condition exists for that seismic event. Independent random numbers (not correlated) are used for the determination of rupture for CSNF and CDSP WPs.

When a WP is ruptured, the failed area is determined by sampling a uniform distribution with a lower bound of 0 m^2 and an upper bound equal to the cross-sectional area, 2.78 m^2 and 3.28 m^2 for CSNF and CDSP WPs, respectively. This failed area allows advective flow into and advective and diffusive transport out of ruptured CSNF or CDSP WPs.

Punctured WPS

The probability of rupture for a WP surrounded by rubble is represented by two power laws in PGV, one that applies to WPs with 23-mm-thick outer corrosion barriers and one that applies to WPs with 17-mm-thick outer corrosion barriers. For thicknesses greater than 23 mm or less than 17-mm, the 23-mm power law and 17-mm power law are used, respectively, for the probabilities of puncture. For intermediate thicknesses, linear interpolation is used.

The determination of the occurrence of puncture is done by comparing the calculated probability of puncture to a random number between 0 and 1. This random number is not correlated with any of the other random numbers used either for assessing the probability of rockfall, WP crack damage, or rupture (Section 6.6.1.3.4). If the random number is less than or equal to the calculated probability of puncture, then all CSNF or CDSP WPs are punctured by this seismic event. Note that the evaluation of puncture is done separately for CSNF and CDSP WPs because the probability depends on WP outer corrosion barrier thickness, which in turn depends on general corrosion rate.

When WPs are punctured, the failed area is determined by sampling a uniform distribution with a lower bound of 0 m^2 and an upper bound of 0.1 m^2. This failed area allows advective flow through the punctured WP and advective and diffusive transport out of the punctured WP.

6.6.1.3.7 Implementation of Waste Package SCC Damage from Ground Motion

The damage to WP outer corrosion barrier surface has been abstracted to occur as a dense network of stress corrosion cracks (Sections 6.6.1.2.3 and 6.6.1.2.4). Both the probability of WP damage and the conditional probability distributions for the amount of damage have been abstracted to be functions of the PGV level for the seismic event and of the residual stress threshold for Alloy 22. Residual stress threshold for Alloy 22 is a random variable that is sampled once per realization from a uniform distribution between 90 and 105 percent of the yield strength of Alloy 22. The random variable is sampled once per realization because it represents the epistemic uncertainty in the residual stress threshold.

The abstractions for probability of WP damage and for the conditional damaged area are functions of whether or not the WP internals are degraded. The internals are considered intact until the first event that causes damage, or breach by nominal general corrosion processes, if this occurs first. After this time, WPs are considered to have degraded internals and the probability and damage abstractions for degraded internals are used.

Probability of WP Damage

The probability of WP damage is represented as a look-up table that uses PGV and residual stress threshold as the independent variables. The typical look-up table for probability of damage at a given WP outer corrosion barrier thickness has up to six values of PGV (forming the rows of the table) and three values of residual stress threshold (90 percent, 100 percent, and 105 percent of the yield strength of Alloy 22). A piecewise linear interpolation scheme is used between the points in each look-up table, avoiding the need for a functional fit to a probability surface. Figures 6.6-10, 6.6-11, and 6.6-15 illustrate these probabilities.

The determination of damage is done by comparing the calculated probability of damage to a random number between 0 and 1. The random number (R_j) is the same random number used for the determination of rockfall and DS fragility (Sections 6-6.1.3.4 and 6.6.1.3.5). If the random number is less than or equal to the calculated probability of damage, then all CSNF or CDSP WPs are damaged by the j^{th} seismic event and the internals of CSNF or CDSP WPs are considered degraded for all subsequent seismic events.

Probability of Damage to CSNF and CDSP Waste Packages under Intact Drip Shields

For WPs under an intact DS, with intact internals, two look-up tables represent the probability of damage to a WP with outer corrosion barrier thickness 23 mm. One table represents the CSNF WPs and one represents the CDSP WPs. A single table look-up is done in each table to obtain the probability of damage.

For WPs under an intact DS, with degraded internals, there are four look-up tables that represent the probability of damage to WPs, two representing CSNF and CDSP WPs at outer corrosion barrier thickness 23 mm and two representing CSNF and CDSP WPs at outer corrosion barrier thickness 17 mm. The current WP thickness is used to interpolate between the values from the look-up tables at 23 mm and 17 mm. The probability of damage is set equal to the value at 23 mm if the average outer corrosion barrier thickness is greater than 23 mm. The probability is set equal to the value at 17 mm if the average outer corrosion barrier thickness is less than 17 mm.

Probability of Damage to CSNF and CDSP Waste Packages Surrounded by Rubble

For WPs surrounded by rubble, four look-up tables represent the probability of damage to CSNF and CDSP WPs of thickness 23 mm and 17 mm with degraded internals. Two tables represent the probability of CSNF WP failure at 23 mm and 17 mm outer corrosion barrier thicknesses and two tables represent the probabilities of CDSP WP failure at 23 mm and 17 mm outer corrosion barrier thicknesses. The current WP thickness is used to interpolate between the values from the look-up tables at 23 and 17 mm. If the current WP thickness lies outside this range, the 23 mm or 17 mm table values are used.

Calculation of WP Damage Area

The conditional (nonzero) damaged areas are represented by gamma distributions. The parameters for the gamma distributions are their mean and SDs. All gamma distributions are resampled for each event.

The damage abstractions for WPs with degraded internals are derived for two different thicknesses of the WP outer corrosion barrier, 23 mm and 17 mm. These are both represented by gamma distributions that must be sampled at the same level of probability (i.e., in a correlated manner) to allow interpolation between the two thicknesses. Three independent random numbers are used to maintain this correlation, one for damage to CSNF WPs under intact DSs, one for CDSP WPs under intact DSs, and one for damage to WPs surrounded by rubble. These random numbers are resampled for each event to represent the aleatory uncertainty in the ground motions.

If the outer corrosion barrier thickness is greater than 23 mm, the damaged area is conservatively set equal to the value at 23 mm. The damaged area is set equal to the value at 17 mm if the average outer corrosion barrier thickness is less than 17 mm.

The total damaged area increases with each seismic event that causes damage to the outer corrosion barrier. Total damaged area for CSNF or the CDSP WPs is the sum of the damaged areas for the first through j^{th} seismic events. Total damaged area cannot exceed the total surface area of a CSNF or CDSP WP, respectively.

Seismically damaged areas are represented as a dense network of stress corrosion cracks. The effective area for transport through the crack network is determined by the product of the total damaged area and the crack density per unit surface area. The crack density model developed for Alloy 22 was abstracted as a uniform distribution between 0.00327 and 0.0131. This parameter represents epistemic uncertainty and is sampled once per realization.

Damage Area for CSNF and CDSP Waste Packages under Intact Drip Shields

The mean and SDs of the gamma distribution for damaged area for CDSP WPs with intact internals under intact DSs are quadratic functions in PGV and have coefficients that are linear in residual stress threshold. The parameters for CSNF WPs with intact internals under intact DSs are based on computational results at PGV = 4.07 m/s and residual stress threshold = 90 percent, which will have the maximum damaged area and apply to all values of PGV and residual stress threshold. In spite of this conservatism, damage will still be zero at most values of PGV and residual stress threshold because the damage is conditional on the probability of damage, and this probability is 0 except for a single point in the first five lines of Table 1-6 in Step 13(a). There are two pairs of gamma distributions representing the damaged area for CSNF and CDSP WPs with degraded internals under intact DSs. One pair represents CSNF WPs and one pair represents CDSP WPs. Their means and SDs are quadratic functions in PGV and have coefficients that are linear in residual stress threshold (Figure 6.6-13).

Damage Area for CSNF and CDSP Waste Packages Surrounded by Rubble

There are two gamma distributions representing the conditional damaged area for CSNF WPs with 23-mm and 17-mm thick outer corrosion barriers surrounded by rubble (degraded DSs). Their means and SDs are quadratic functions of residual stress threshold, with no PGV dependence (Section 6.6.1.2.3) (Figure 6.6-16). The damage to CDSP WPs is represented by the same gamma distributions as those used for CSNF WPs, although the thicknesses of the OCBs for the CDSP and CSNF waste packages may be different at the time of the j^{th} seismic event.

6.6.1.3.8 Waste Package Thickness Calculations

WPs and overlying DSs are partitioned among the five percolation subregions according to the partitioning described in Section 6.3.2.2.1. In the Seismic GM Modeling Case, the calculations for the probability and damaged area are a function of WP outer corrosion barrier thickness, which depends on the general corrosion rate of Alloy 22. The general corrosion calculation depends on temperature, and other that parameters vary at the percolation subregion level and with fuel type (Section 6.3.5.1.2). Therefore, the time-dependent WP outer corrosion barrier thickness will be different for each of the five percolation subregions and for each of the two fuel types.

The general corrosion rate of the Titanium Grade 7 DSs is given by a distribution that is independent of percolation subregion parameters and will be the same for all DSs (Section 6.3.5.1.2).

The abstractions for WP degradation used in the Seismic GM Modeling Case require the spatially-averaged thickness of the WP outer corrosion barrier as a function of time. This calculation is done as part of the WP and DS Degradation Submodel calculations. The WAPDEG v4.07 software is run 10 times, once for each percolation subregion and fuel type, to produce a time history of WP thickness. This calculation is done separately from the calculation of WP breach used to feed the EBS Flow and Transport Model Component (Sections 6.3.6 and 6.3.8) for nominal corrosion processes. The general corrosion rate used for the feed to the Seismic GM Modeling Cases is done with an average rate rather than an extreme patch approximation to the general corrosion rate discussed in Section 6.3.5.1.2. The method discussed in Section 6.3.5.1.2 used the highest of four sampled corrosion rates (from the two-parameter Weibull distribution) to analyze general corrosion of the WP patch. For the purposes of the seismic abstractions, the average of the four sampled corrosion rates was used to generate the general corrosion rate fed to the WAPDEG v4.07 software. The GetThk_LA v1.0 (STN: 11229-1.0-00 [DIRS 181040]) software was used to post-process the thickness file output by the WAPDEG v4.07 software and generate a one-dimensional table of mean WP outer corrosion barrier thickness versus time. This mean thickness is a spatially-averaged WP outer corrosion barrier thickness over all the WPs in a particular percolation subregion for each fuel type.

Since the nominal corrosion processes calculated by the WAPDEG V4.07 software calculations are included in the Seismic GM Modeling Case, the inside-out corrosion that occurs after a seismic event has damaged a WP must be accounted for. The mean time of the first seismic event that causes WP damage must be passed as an input to the WAPDEG V4.07 calculations. However, the WAPDEG 4.07 calculations are done at the beginning of the simulation, before any seismic calculations are done. Therefore, a separate *a priori* calculation of the time that WPs are first damaged by a seismic event is carried out.

CSNF and CDSP WPs are considered to have intact internals before the first seismic damage event and the probability of damage for WPs with intact internals under intact DSs is not a function of WP thickness (Figures 6.6-10 and 6.6-11). However, for CSNF WPs, damage is not likely to occur before DS failure. In this case, the abstraction for the probability of damage for WPs surrounded by rubble with a 17 mm thickness is used as a conservative estimate of the

probability of first failure time (Figure 6.6-15). This estimate is conservative because it gives the highest possible probability of failure for a WP surrounded by rubble. The same approximation is used for CDSP WPs if the WP damage does not occur before DS failure. However, in the case of CDSP WPs, the probability of WP damage under intact DSs is higher (Figures 6.6-11).

6.6.1.3.9 Implementation of Fault Displacement Damage

The two simulations for Seismic FD Modeling Case are both run using pre-specified parameters. The fraction of damage is set at 0.028, 0.056, or 0.084, for CSNF WPs, and at 0.0335, 0.067, or 0.101, for CDSP WPs. These values represent 1/3, 2/3, 3/3 of the ratio of lid area to WP surface area, for CSNF and CDSP WPs respectively.

The time of the seismic event is set to be 1,000 years, 20,000 years, 80,000 years, 200,000 years, 400,000 years, or 800,000 years, for the 1,000,000-year Seismic FD Modeling Case. For the 10,000-year Seismic FD Modeling Case, the time of the seismic event is set to be either 200 years, 800 years, 2,000 years, 4,000 years, 8,000 years, or 18,000 years.

The time at which the drifts fill with rubble is set to be the time of the seismic event.

The number of failed WPs is set to 100. This number is chosen so that there will be failed WPs in each percolation subregion. The dose calculation is then scaled by the ratio of the expected number of WP failures divided by 100 (Section 6.1.2.4.3, Equation 6.1.2-24).

The expected number of WP failures due to fault displacement is extracted from a table over a series of mean annual exceedance frequency intervals for each of two WP groups and is rounded to the nearest integer. Note that inspection of the failure numbers shows that the maximum number of failures for the CSNF and CDSP WP groups is approximately 159 and 53, respectively.

The DSs and cladding corresponding to fault-failed WPs are also considered to be completely failed .

6.6.2 Interaction of Seismic Scenario Class Submodels with other TSPA-SEIS Submodels

The rockfall accumulation calculations described in Section 6.6.1.3.4 have consequences with respect to other TSPA-SEIS submodels.

6.6.2.1 Drift Seepage Submodel and Drift Wall Condensation Submodel Modifications for Seismic Disruption

The Drift Seepage Submodel's (Section 6.3.3.1) drift seepage simulations produce response surfaces in the form of look-up tables for the seepage flux into the degraded drifts. The independent variables in the look-up tables are local percolation flux, permeability, and capillary strength. For the Seismic Scenario Class, drift collapse occurs in both lithophysal and nonlithophysal zones. Partial collapse, followed by full collapse, can occur in the lithophysal units. The switch from noncollapsed to collapsed conditions depends on rockfall volume in the drift. For lithophysal rock, if rockfall volumes in the drift are less than or equal to 5 m^3/m of drift length, the intact drift seepage response surface table is utilized in the analysis. If rockfall

volumes in the drift are greater than 60 m^3/m of drift length, the collapsed drift seepage response surface is utilized in the analysis. If rockfall volumes (per unit drift length) in the drift are between 5 m^3/m and 60 m^3/m, seepage values are linearly interpolated between the two response surfaces (Section 6.3.3.1.3). In the nonlithophysal units, once a specified degree of drift collapse has occurred, the intact-drift seepage model is no longer appropriate. Therefore, in the nonlithophysal zone, if rockfall volumes in the drift are less than or equal to 0.5 m^3/m, the intact drift seepage response surface is utilized; if not, the percolation rates are utilized instead of seepage rates (Section 6.3.3.1.3).

The rockfall volume in the drift is a feed from the seismic rockfall calculations to the drift seepage calculations. The rockfall volumes in the lithophysal and nonlithophysal zones are calculated as described in Section 6.6.1.3.4, for the Seismic GM Modeling Case 1,000,000–year simulation, which uses GoldSim-sampled event sequences. For the 1,000,000-year Seismic FD Modeling Case and the 10,000-year Seismic FD Modeling Case simulations, rockfall volumes are pre-specified (Table 6.6-4). The Drift Wall Condensation Abstraction (Section 6.3.3.2.2) calculates a probability of condensation occurrence on the drift walls at a WP location and, if condensation occurs, a rate of condensation. For the Seismic Scenario Class, drift collapse is expected in the lithophysal regions but is not expected in the nonlithophysal units. Condensation occurs on drift walls above DSs in the nonlithophysal units at all times. In contrast, there is no condensation in the lithophysal units after drift collapse. The Seismic Scenario Class modeling cases calculate the time of drift collapse in terms of the time at which rubble fills the lithophysal drifts. For the Seismic GM Modeling Case 1,000,000-year simulation, this calculation is described in Section 6.6.1.3.4. For the 1,000,000-year Seismic FD Modeling Case and the 10,000-year Seismic FD Modeling Case simulations, drift collapse times are pre-specified (Section 6.6-4) and are set to either the time of the first seismic event or are set to be non collapsed.

6.6.2.2 Engineered Barrier System Thermal-Hydrologic Environment Submodel Modifications for Seismic Disruption

Seismically induced ground motion can cause drift collapse in the lithophysal zones, requiring an adjustment to the temperature and relative humidity histories to account for the presence of rubble on WPs. The adjusted temperature and relative humidity histories for the Seismic Scenario Class modeling cases are provided by a supplemental analysis performed on the EBS TH Environment Submodel thermal-hydrology data. The data tracking number provides eight files containing time-dependent temperature adjustments and eight files containing time-dependent relative humidity adjustments: one file for each of the six representative CSNF and two representative CDSP WP/DS pairs (Section 6.3.2.2). Each file contains two types of temperature/relative humidity adjustments, one associated with a collapsed drift with low thermal-conductivity rubble and one associated with a collapsed drift with high thermal-conductivity rubble. The assignment of a low or high thermal-conductivity adjustment is based on sampling a discrete distribution with equal probability for high or low (SNL 2007 [DIRS 181383], Section 6.2.10.3).

The Seismic GM and FD Modeling Cases calculate the time required to fill the drift with rockfall, after which the adjustments apply. For the Seismic GM Modeling Case 1,000,000-year simulation, this time is based on the calculations described in Section 6.6.1.3.4. For the

1,000,000-year Seismic FD Modeling Case and the 10,000-year Seismic FD Modeling Case simulations, drift fill times are pre-specified (Section 6.6.1.3.9and are set to either the time of the first seismic event or the end of the simulation. The adjusted temperature and relative humidity values are used for both lithophysal and nonlithophysal zones in the TSPA-SEIS Model because the TSPA-SEIS Model does not distinguish between the lithophysal and nonlithophysal components of a percolation subregion.

6.6.2.3 Waste Package and Drip Shield Degradation Submodel Modifications for Seismic Disruption

Nominal corrosion processes are included in the Seismic GM Modeling Case when calculating consequences after 10,000 years. When WPs are first damaged by a seismic event, the resulting cracks will impact the nominal corrosion processes. In particular, corrosion on the inner surface of a WP outer corrosion barrier (inside-out corrosion) will be initiated. An *a priori* calculation is done to determine the time of the first seismic event that causes WP damage and this time is fed to the input vector for the WAPDEG V4.07 software. This time will be different for CSNF and CDSP WPs. The WAPDEG V4.07 software will initiate an inside-out corrosion event at that time, thus accelerating the corrosion processes that ultimately lead to WP breach. This effect is also included in the separate WAPDEG V4.07 calculations that determine mean WP thickness for each percolation subregion. These calculations are used by the Seismic GM Modeling Case as input to the WP damage calculations (Section 6.6.1.3.8).

6.6.2.4 Waste Package Localized Corrosion Initiation Submodel for Seismic Disruption

The Seismic Scenario Class does not include the potential effect of crown-seepage initiated localized corrosion on the WP outer surface. Although crown-seepage induced localized corrosion is possible for both the Seismic GM and FD Modeling Cases, a stand-alone localized corrosion initiation analysis has been carried out to determine that the environmental conditions required for localized corrosion initiation are present only for the first 4,000 years after repository closure. Beyond this time, the chemistry of the seepage water is benign and localized corrosion no longer initiates. This stand-alone analysis is documented in Section 6.3.5.2. The temperature, pH, chloride-ion concentration, and nitrate-ion concentrations in aqueous solutions on the WP outer surface are the primary factors that determine the potential for initiating localized corrosion. In addition, localized corrosion can only occur if crown seepage water contacts the WP outer surface, i.e. if the DS is failed. In the Seismic GM Modeling Case simulations, there is a low probability of DS plate failure occurring before 4,000 years. In the Seismic FD Modeling Case simulations, DS can be failed at early times, where environmental conditions are suitable for localized corrosion initiation. However, it is assumed that the advective damage due to the fault displacement is sufficient to account for the effects of localized corrosion. This assumption has been verified by simulation runs which show that the dose is insensitive to increasing the fraction of damaged area beyond 1/3 of the WP cross-sectional area.

A description of localized corrosion of the WP outer surface is provided in Section 6.3.5.2. Section 6.3.5.2 describes the Localized Corrosion Initiation Analysis and Localized Corrosion Penetration Rate Abstraction that form the components of the Localized Corrosion Initiation

Submodel. Section 6.3.5.2.1 provides the conceptual models for these localized corrosion processes, and Section 6.3.5.2.2 describes the model abstractions.

For the localized corrosion initiation analysis, a temperature constraint is applied to the seepage flux after drift collapse in the lithophysal zones. Specifically, seepage onto WPs is set to zero for the period of above-boiling temperatures by using a 100°C threshold temperature at a WP surface. This constraint implies that seepage can enter the drift and be diverted through the rubble to the invert beneath a WP, but it cannot contact a WP surface until the surface temperature drops to less than 100°C. This threshold temperature is based on a sensitivity study of seepage arrival times at a DS crown for a collapsed drift that is filled with rubble (SNL 2007 [DIRS 181383], Section 6.3.7.3 and Table 6.3-44). This study considers rubble with high and low values of thermal conductivity and seepage magnitudes that vary between 10 liter/yr/WP and 1,000 liter/yr/WP. The temperature threshold of 100°C is a reasonable upper bound to the ranges of WP temperatures that significantly delay the arrival of seepage at a DS crown. A 100°C temperature is, therefore, an appropriate threshold to limit the presence of liquid seepage in a rubble-filled drift. This temperature constraint on seepage flux after drift collapse is applied only in the Localized Corrosion Initiation and Propagation Analysis. The constraint is not applied to the calculation of seepage flux in the Drift Seepage Submodel (Section 6.3.3.1).

The Localized Corrosion Initiation Analysis also accounts for changes in temperature and relative humidity due to the presence of rubble after a seismic event. The Localized Corrosion Initiation Analysis uses the same eight WP emplacement configurations to calculate temperature and relative humidity adjustments discussed in Section 6.6.2.2, for the purposes of localized corrosion initiation. The rubble fill time is based on the calculations described in Section 6.6.1.3.4 for the lithophysal zones. In addition, the Localized Corrosion Initiation Analysis does distinguish between lithophysal and nonlithophysal regions and, therefore, the temperature and relative humidity adjustments are applied only when a WP location lies in the lithophysal zone. For the nonlithophysal zones, examination of Tables 6-30 and 6-31 in *Seismic Consequence Abstraction* (SNL 2007 [DIRS 176828]) shows that all of the calculated rockfall volumes are significantly less than those in the lithophysal zones at the same PGV level. Therefore, the temperature and relative humidity adjustments are not applied in the nonlithophysal zones.

6.6.3 Model Component Consistency and Conservatisms in Assumptions and Parameters

To enhance understanding of the complex interactions within the TSPA-SEIS Model, a discussion of consistency among model components and submodels and identification of conservative assumptions in abstractions, process models, and parameter sets supporting the Seismic Scenario Class are discussed below.

6.6.3.1 Consistency of Assumptions

Degradation of the Internal Structures After Breach of Outer Corrosion Barrier—In the Seismic GM Modeling Case calculations once the outer corrosion barrier is breached due to seismic damage it is assumed that the internal structure of the WP would degrade as a structural element, quickly leading to an overall loss of WP structural strength by the time of next seismic event. As a result the damage abstractions for the fully degraded internals are applied after the

WP is breached for the first time. This is a conservative assumption and inconsistent with the slow degradation of steel internals modeled in the EBS Transport model, where the stainless steel is expected to last for tens of thousands of years on average thus maintaining the integrity of the WP for much longer duration than the time to the next seismic event.

Effect on the TSPA-SEIS Model—Using the WP damage abstraction for the fully degraded internals subsequent to the seismic event that leads to the first breach is conservative as it would lead to larger damage area on the WP due to lower structural strength of the WP. This would likely result in a greater diffusive release rate out of the WP.

6.6.3.2 Identification of Conservatisms in Submodels and Abstractions

Conservatism in Ground Motion Calculations—The use of a bounded hazard curve for PGV does not mean that all three components of a ground motion are bounded. Only one horizontal component of the ground motion is scaled to a given PGV value on the bounded hazard curve (SNL 2007 [DIRS 176828], Section 6.4.3). In developing the time histories used in the kinematic and structural response calculations, the second horizontal component and the vertical component are not directly scaled, but rather are allowed to vary to maintain the inter-component variability of the original accelerogram. This means that these components can vary substantially even when the PGV for the first horizontal component is at a fixed value. This inter-component variability reflects the aleatory uncertainty inherent in vibratory ground motions. In some cases, this results in PGV values for these components that exceed the maximum scaled value for the first horizontal component. Thus, the damage abstractions, although parameterized using one horizontal component, in some cases represent damage associated with larger PGVs on the other components. Thus, although the hazard curve for horizontal PGV is bounded, the damage abstractions include larger, unbounded PGVs on the other components as given in Acceptance Criterion 3, Propagation of Uncertainty into TSPA (SNL 2007 [DIRS 176828], Section 8.2). Alternate ground motions with bounded components are not available to quantify this conservatism.

Seismic Failure Criteria—The seismic abstractions for WPs and DSs make use of two failure criteria: a residual stress threshold and the ultimate tensile strain. If the residual stress from mechanical damage exceeds the stress threshold for the barrier, then the affected area(s) are represented as a network of stress corrosion cracks. The residual stress threshold for WPs is based on a uniform distribution between 90 percent and 105 percent of the yield strength for Alloy 22. The residual stress threshold for Titanium Grade 7 is conservatively set to a constant value of 80 percent of its yield strength (and for Titanium Grade 29 at 50 percent of its yield strength). These thresholds are conservative estimates for the initiation of SCC (SNL 2007 [DIRS 181953], Sections 6.2.2 (Alloy 22), 6.8.3.1.3 (Titanium Grade 7), and 6.8.3.2.3 (Titanium Grades 25 and 29)). The potential for tearing or rupture of EBS components is based on the ultimate tensile strain for Alloy 22 and Titanium Grade 7, with a conservative knockdown factor of 2 (the maximum value), which adjusts the uniaxial data for ultimate tensile strain in a multidimensional stress field .

Spatial Variability—Spatial variability in the mechanical response of EBS components to vibratory ground motion has not been represented in the TSPA-SEIS Model. Damage to the WP and DS from vibratory ground motion is constant throughout the repository for each seismic

event. Although spatial variability is not included within the TSPA-SEIS Model, it has been included in the kinematic calculations through the variability of friction factors on a package-by-package basis and in the abstraction of damaged areas for the two or three central WPs in the kinematic calculations. Lack of spatial variability is not important for estimating the mean annual dose from the Seismic Scenario Class. The mean dose is accurately estimated because the sum of the mean doses from groups of WPs with different damage levels is equal to the mean of the sum of the doses from the individual groups. Using a constant mean value for the damage is an accurate approach for calculating the mean annual dose from the repository (SNL 2007 [DIRS 176828], Section 1.2).

Conservatism in Hazard Curve—The development of hazard curves for vibratory ground motion and fault displacement included an expert elicitation—(*Probabilistic Seismic Hazard Analyses for Fault Displacement and Vibratory Ground Motion at Yucca Mountain, Nevada,* Milestone SP32IM3, September 23, 1998 (CRWMS M&O 1998 [DIRS 103731]). Evaluations by multiple experts were made within a structured process designed to minimize uncertainty due to uneven or incomplete knowledge and understanding (Budnitz et al. 1997 [DIRS 103635]). The weighted alternative interpretations were expressed by the use of logic trees. Each pathway through the logic tree represented a weighted interpretation of the seismotectonic environment of the site for which a seismic hazard curve was computed. The result of computing the hazard for all relevant pathways was a distribution of hazard curves representing the full variability and uncertainty in the hazard at Yucca Mountain. The Seismic Scenario Class for the TSPA-SEIS Model uses the mean hazard curves for PGV and for fault displacement. Each mean hazard curve is defined as an average of the distribution of hazard curves and each typically lies above the 80th percentile of the distribution for high intensity ground motions (i.e. at low annual exceedance frequencies) because the average is dominated by the larger values of the distribution (SNL 2007 [DIRS 176828], Section 6.4.1). The use of the mean hazard curves ensures a conservative representation of the seismic hazard in the TSPA-SEIS Model.

Conservatism in Initiation of Inside-Out Corrosion Processes—Corrosion on the inner surface of a WP outer corrosion barrier (inside-out corrosion) is initiated at the time of the first seismic event that causes WP damage. An *a priori* calculation is done to determine the time of the first seismic event that causes WP damage. The probability that a CSNF WP with intact internals under intact DSs will be damaged by a seismic event is small (Figure 6.6-10). Therefore, DS failure is likely to occur before a damaging seismic event occurs. If such a WP has not been damaged, its internals will still be intact even though it is under a failed DS and surrounded by rubble. However, there is no abstraction for probability of damage for a CSNF WP with intact internals under a failed DS. Such a WP is also likely to have a reduced shell thickness. Therefore the probability of damage to a CSNF WP with degraded internals and an outer corrosion barrier thickness of 17 mm is used as a surrogate to the damage on a CSNF WP with intact internals under a failed DS. This is a conservative assumption, as can be seen from an examination of Figure 6.6-15.

6.6.4 Alternative Conceptual Model(s) for Seismic Scenario Modeling Cases

A brief description of the Seismic Scenario Class ACMs is presented below. The Seismic Scenario Class ACMs are also summarized in Table 6.6-3.

Lithophysal and Nonlithophysal Rock—Alternative modeling approaches were evaluated for the conceptual and computational models of lithophysal and nonlithophysal rockfall (BSC 2004 [DIRS 166107], Section 7.4). A standard approach for solving excavation stability problems is the use of numerical models based on continuum mechanics. Continuum models use constitutive relations to describe the mechanical behavior of a material. The use of a continuum model requires that the mechanical effects of fractures be lumped into the constitutive relationships. Continuum models are unable to predict instabilities such as fracture and rockfall (BSC 2004 [DIRS 166107], Section 7.4.1).

The ACM based on continuum mechanics (BSC 2004 [DIRS 166107], Section 7.4.1) was not used to represent rockfall. The estimation of rockfall requires that the modeling technique and mechanical material model be capable of representing fracture of the rock mass and separation of the intact rock mass into blocks. The discontinuum approach is more suitable for these purposes and was therefore adopted for modeling the drift degradation processes that occur after a seismic event (BSC 2004 [DIRS 166107], Section 7.4.2).

Fault Displacement WP Damage Abstraction—The damage abstraction for fault displacement was compared to an ACM proposed by Waiting et al., described in *Seismic Consequence Abstraction* (SNL 2007 [DIRS 176828], Section 6.11.6). The ACM considered the probability-weighted number of WP failures from fault displacement and the number of fault intersections with emplacement drifts. The ACM, based on the use of historical data for fault displacement in the western United States, provided results that are consistent with the base case model for both the probability weighted number of WP failures and the number of fault intersections with the emplacement drifts (SNL 2007 [DIRS 176828], Section 6.11.6).

The ACM based on historical western United States data was not used in the TSPA-SEIS Model. The damage abstraction used in the TSPA-SEIS Model is based on hazard curves specific to Yucca Mountain. Nevertheless, the agreement between the two models is very good and this adds confidence to the TSPA-SEIS Model damage abstraction.

Effective Cross-sectional Area for Transport—The effective cross-sectional area for transport out of Alloy 22 WPs through a network of stress corrosion cracks is given by a crack area density based on two conceptual models (SNL 2007 [DIRS 181953], Section 6.7.3). The first conceptual model is based on a hexagonal array of randomly oriented cracks, while the second conceptual model is based on a hexagonal array of cracks in parallel rows. The distribution for crack area density used in the TSPA-SEIS Model is based on both conceptual models. An alternative conceptual model for crack area density is presented in *Stress Corrosion Cracking of Waste Package outer barrier and Drip Shield Materials* (SNL 2007 [DIRS 181953] Section 6.7.4). The alternative model considers a circular geometry circumscribed by a single through-wall crack.

The ACM was not used for the TSPA-SEIS Model implementation of seismic crack density. The hexagonal geometry represents a high effective density of individual cracks and the two hexagonal geometry conceptual models are considered conservative representations. The ACM analysis which uses circular geometry is considered a limiting realistic case (SNL 2007 [DIRS 181953], Section 6.7.2).

Conditional Probability Distributions for Damaged Areas—The seismic consequence abstractions have considered ACMs for the conditional probability distributions representing damaged areas on the WP, damaged areas on the DS, and the volume of rockfall from a seismic event. These alternate distributions include the gamma, normal, log-normal, Weibull and triangular distributions, as presented in Sections 6.5.1.4, 6.5.2.4, 6.6.1.4, 6.6.2.4, 6.7.1.3, 6.7.2.4, 6.9.4, and 6.10.2.8 of *Seismic Consequence Abstraction* (SNL 2007 [DIRS 176828]). Gamma distributions generally provided simpler and more accurate representations of the statistical observations than normal, log-normal, log-triangular, and Weibull distributions. The exception to the use of gamma distributions is that the fragility analyses (for DS plates and framework) have used log-normal representations to simplify manipulation of products and quotients of random variables.

The alternative conditional probability distributions for WP damaged areas were investigated, in the sections noted above, but not used since gamma distributions provided the simplest and most accurate representation of the data.

INTENTIONALLY LEFT BLANK

Table 6.6-1. Expected Waste Package Failure Due to Fault Displacement

Annual Exceedance Frequency (1/yr)	Expected Number of Failures – CSNF (TAD) Group	Annual Exceedance Frequency (1/yr)	Expected Number of Failures – CDSP Group
$> 2.2 \times 10^{-7}$	0	$> 2.5 \times 10^{-7}$	0
1.4×10^{-7} to 2.2×10^{-7}	19.5	1.6×10^{-7} to 2.5×10^{-7}	6.5
7.8×10^{-8} to 1.4×10^{-7}	27.7	8.6×10^{-8} to 1.6×10^{-7}	9.3
2.6×10^{-8} to 7.8×10^{-8}	30.7	2.9×10^{-8} to 8.6×10^{-8}	10.3
1×10^{-8} to 2.6×10^{-8}	158.8	1×10^{-8} to 2.9×10^{-8}	53.2

Source: DTN: MO0703PASEISDA.002_R4 [DIRS 183156], Table 1-14.

NOTE: TAD = transportation, aging, and disposal (canister); CSNF = commercial spent nuclear fuel; CDSP = co-disposed (waste package).

Table 6.6-2. Uncertain Inputs Used in the Seismic Scenario Class

TSPA Parameter Name	Description	Units	Distribution
Epistemic Parameters			
Stress_Thresh_A22_a	Residual stress threshold of Alloy 22.		Uniform(90,105)
Vol_Rubble_Max_Lith_a (MAX_RUBBLE_VOLUME)	Volume of lithophysal rock that must fall to fill the drift.	m^3/m	Uniform(30,120)
Vol_Rubble_Max_NonLith_a (MAX_BLOCK_VOLUME)	Volume of nonlithophysal rock that must fall to fill the drift.	m^3/m	Uniform(30,120)
DS_Crack_Area_Density_a	Crack area per unit of seismic DS damage.		Uniform(0.00467, 0.01875)
WP_Crack_Area_Density_a	Crack area per unit area of seimic WP damage.		Uniform(0.00327, 0.0131)
Aleatory Parameters			
Exceedance_Frequency_a	Annual exceedance frequency for the seismic hazard.	1/yr	Uniform(Seismic_Lambda_Min, Seismic_Lambda_Max) Seismic_Lambda_Min=$1x10^{-8}$ Seismic_Lambda_Max=$4.287x10^{-4}$
Rubble_Vol_Lith_a	Distribution used to calculate the rubble area deposited around the DS / WP in the last seismic event.	m^3/m	Gamma Distribution Mean: function of seismic event PGV SD: function of seismic event PGV
Rubble_Vol_NonLith_a	Distribution used to calculate the rubble volume deposited around the DS / WP in the last seismic event (nonlithophysal zones).	m^3/m	Gamma Distribution Mean: function of seismic event PGV SD: function of seismic event PGV
Ln_Dyn_Load_DS	Dynamic load on the DS due to a seismic event.		Normal Distribution Mean: function of seismic event PGV and lithophysal rubble volume SD: 0.536
Corr_TAD_Dam_DS_Intact_a	Random number for maintaining correlation while sampling the TAD-bearing WP damage gamma distributions for intact DSs.		Uniform(0,1)
Corr_CDSP_Dam_DS_Intact_a	Random number for maintaining correlation while sampling the CDSP WP damage gamma distributions for intact DSs.		Uniform(0,1)
Corr_WP_Dam_DS_Failed_a	Random number for maintaining correlation while sampling the WP (CDSP and TAD) damage gamma distributions for failed DSs.		Uniform(0,1)
Gamma_A_Intact_TAD	Damage to a TAD-bearing WP of thickness 23 mm with intact internals under an intact DS.	m^2	Gamma Distribution Mean: 0.00408 SD: 0.0013

Table 6.6-2. Uncertain Inputs Used in the Seismic Scenario Class (Continued)

TSPA Parameter Name	Description	Units	Distribution
Gamma_A_Degrdd_TAD	Damage to a TAD-bearing WP of thickness 23 mm with degraded internals under an intact DS.	m^2	Gamma Distribution Mean: quadratic in seismic event PGV with coefficients a function of residual stress threshold SD: quadratic in seismic event PGV with coefficients a function of residual stress threshold
Gamma_B_Degrdd_TAD	Damage to a TAD-bearing WP of thickness 17 mm with degraded internals under an intact DS.	m^2	Gamma Distribution Mean: quadratic in seismic event PGV with coefficients a function of residual stress threshold SD: quadratic in seismic event PGV with coefficients a function of residual stress threshold
Gamma_A_Intact_CDSP	Damage to a CDSP WP of thickness 23 mm with degraded internals under an intact DS.	m^2	Gamma Distribution Mean: quadratic in seismic event PGV with coefficients a function of residual stress threshold SD: quadratic in seismic event PGV with coefficients a function of residual stress threshold
Gamma_A_Degrdd_CDSP	Damage to a CDSP WP of thickness 23 mm with degraded internals under an intact DS.	m^2	Gamma Distribution Mean: quadratic in seismic event PGV with coefficients a function of residual stress threshold SD: quadratic in seismic event PGV with coefficients a function of residual stress threshold
Gamma_B_Degrdd_CDSP	Damage to a CDSP WP of thickness 17 mm with degraded internals under an intact DS.	m^2	Gamma Distribution Mean: quadratic in seismic event PGV with coefficients a function of residual stress threshold SD: quadratic in seismic event PGV with coefficients a function of residual stress threshold
Gamma_A_Degrdd_WP_NoDS	Damage to a CDSP WP of thickness 23 mm with degraded internals under a degraded DS.	m^2	Gamma Distribution Mean: quadratic in residual stress threshold SD: quadratic in residual stress threshold
Gamma_B_Degrdd_WP_NoDS	Damage to a CDSP WP of thickness 17 mm with degraded internals under a degraded DS.	m^2	Gamma Distribution Mean: quadratic in residual stress threshold SD: quadratic in residual stress threshold
RN_DSF_a (RN_DSF)	Random number to determine rockfall damage, WP damage, and drip shield plate and/or framework failure.		Uniform(0,1)

Table 6.6-2. Uncertain Inputs Used in the Seismic Scenario Class (Continued)

TSPA Parameter Name	Description	Units	Distribution
RN_ _Rupture_TAD_a	Random number used to determine rupture TAD of WPs under intact DSs, due to multiple impacts.		Uniform(0,1)
RN_Rupture_CDSP_a	Random number used to determine rupture of CDSP WPs under intact DSs, due to multiple impacts.		Uniform(0,1)
RN_Puncture_a	Random number used to determine puncture of WPs under failed DSs, due to multiple impacts.		
TAD_Rupture_Area_a (RUPAREA_TAD)	Failed area of the TAD-bearing WP due to WP rupture damage.	m^2	Uniform(0, 2.78)
CDSP_Rupture_Area_a (RUPAREA_CDSP)	Failed area of the CDSP WP due to WP rupture damage.	m^2	Uniform(0, 3.28)
Puncture_Area_a	Failed area when WPs surrounded by rubble are punctured.	m^2	Uniform(0, 0.1)
TAD_Failed_Area_a (FAILED_AREA_TAD)	Cross-sectional area of the TAD-bearing WP.	m^2	Uniform(0,2.78)
CDSP_Failed_Area_a (FAILED_AREA_CDSP)	Failed area of the CDSP WP due to fault displacement damage.	m^2	Uniform(0,3.28)

Source: DTN: MO0703PASEISDA.002_R4 [DIRS 183156], Table 1-15.

NOTE: CDSP (WP) = co-disposed; TAD (WP) = transportation, aging, and disposal (canister); PGV = peak ground velocity; SD = standard deviation.

Table 6.6-3. Alternative Conceptual Models Considered for the Seismic Scenario Class

Alternative Conceptual Models	Key Assumptions	Assessment and Basis
Alternative modeling approaches were evaluated for the conceptual and computational models of lithophysal and nonlithophysal rock (BSC 2004 [DIRS 166107], Section 7.4).	A standard approach for solving excavation stability problems is the use of numerical models based on continuum mechanics. Continuum models use constitutive relations to describe the mechanical behavior of a material. The use of a constitutive model requires that the mechanical effects of fractures be lumped into the constitutive relationships.	Continuum models are unable to predict instabilities, such as fracture and rockfall (BSC 2004 [DIRS 166107], Section 7.4.1). The discontinuum approach is more suitable for representing fracture of the rock mass and separation of the intact rock mass into blocks and was therefore adopted for modeling the drift degradation processes that occur after a seismic event (BSC 2004 [DIRS 166107], Section 7.4.2).
An alternative damage abstraction for fault displacement damage was proposed by Waiting et al., described in *Seismic Consequence Abstraction* (SNL 2007 [DIRS 176828], Section 6.11.6).	The ACM considered the probability-weighted number of waste package failures from fault displacement and the number of fault intersections with emplacement drifts. The ACM, based on the use of historical data for fault displacement in the western United States.	The results provided by the ACM are consistent with the base-case model for both the probability-weighted number of WP failures and the number of fault intersections with the emplacement drifts (SNL 2007 [DIRS 176828], Section 6.11.6).
An alternative conceptual model for crack area density was presented in Section 6.7.4 (SNL 2007 [DIRS 181953]).	The alternative model considered a circular geometry circumscribed by a single through-wall crack. The base case model combines two conceptual models based on hexagonal geometry (SNL 2007 [DIRS 181953], Section 6.7.3).	The hexagonal geometry represents a high effective density of individual cracks and the two hexagonal geometry conceptual models are considered conservative representations. The ACM analysis which uses circular geometry is considered a limiting realistic case (SNL 2007 [DIRS 181953], Section 6.7.2).
Alternative conceptual models for the conditional probability distributions representing damaged areas on the waste package, damaged areas on the drip shield, and the volume of rockfall from a seismic event were considered.	These alternate distributions included the gamma, normal, log-normal, Weibull and triangular distributions, as presented in Sections 6.5.1.4, 6.5.2.4, 6.6.1.4, 6.6.2.4, 6.7.1.3, 6.7.2.4, 6.9.4, and 6.10.2.8 of *Seismic Consequence Abstraction* (SNL 2007 [DIRS 176828]).	Gamma distributions generally provided simpler and more accurate representations of the statistical observations than normal, log-normal, log-triangular, and Weibull distributions. The exception to the use of gamma distributions is that the fragility analyses (for drip shield plates and framework) have used log-normal representations to simplify manipulation of products and quotients of random variables.

Table 6.6-4. Seismic Ground Motion and Fault Displacement Modeling Cases Using Pre-Specified Parameters

Modeling Case	Seismic Event Time (yr)	CSNF WP Damage	CDSP WP Damage	Number of Failed CSNF WPs	Number of Failed CDSP WPs	Rubble Volume (m^3/m)	Rubble Fill Time (yr)	DS Damage Fraction
Seismic 1M yr FD Case	1,000 20,000 80,000 200,000 400,000 800,000	0.028 0.056 0.084	0.0335 0.067 0.101	0 100	100 0	120	Seismic Event Time	1.0
Seismic 10k yr FD Case	200 800 2,000 4,000 8,000 18,000	0.028 0.056 0.084	0.0335 0.067 0.101	0 100	100 0	120	Seismic Event Time	1.0
Seismic 10k yr GM Case	100 1,000 3,000 6,000 12,000 18,000	0	1.00×10^{-7} 1.00×10^{-6} 0.00001 0.001	0	3416	0	2,000,000	0.0
Seismic 1M yr GM Case	Section 6.6.1.3.1	Section 6.6.1.3.4	Section 6.6.1.3.4	Section 6.6.1.3.4	Section 6.6.1.3.4	Section 6.6.1.3.2	Section 6.6.1.3.2	Section 6.6.1.3.3

Source: DTN: MO0708TSPAGENT.000 [DIRS 183000], DL-TSPA-DTN-8.doc, DL-TSPA-DTN-9.doc.

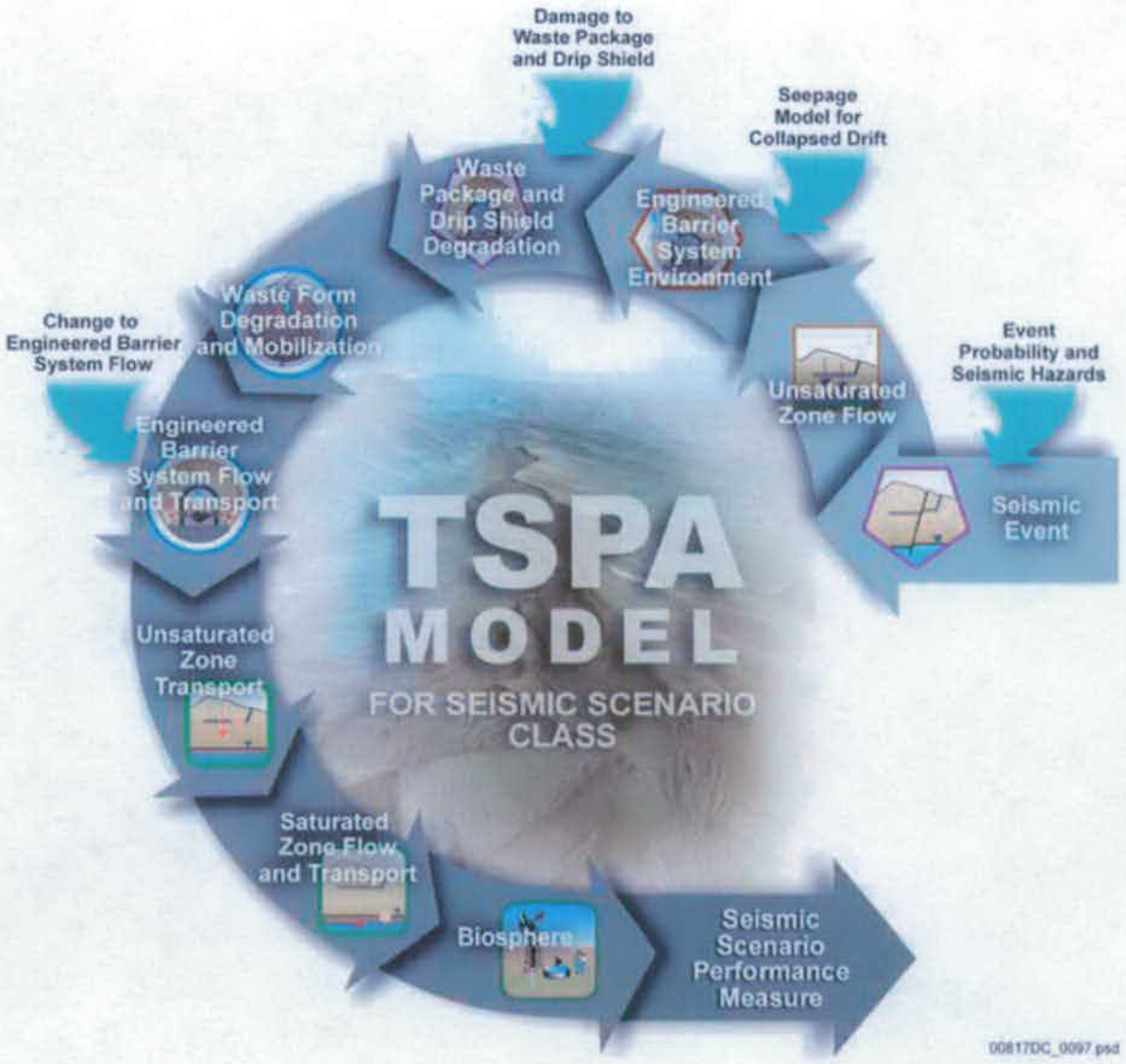

Figure 6.6-1. Schematic Representation of the TSPA-SEIS Model Components for the Seismic Scenario Class

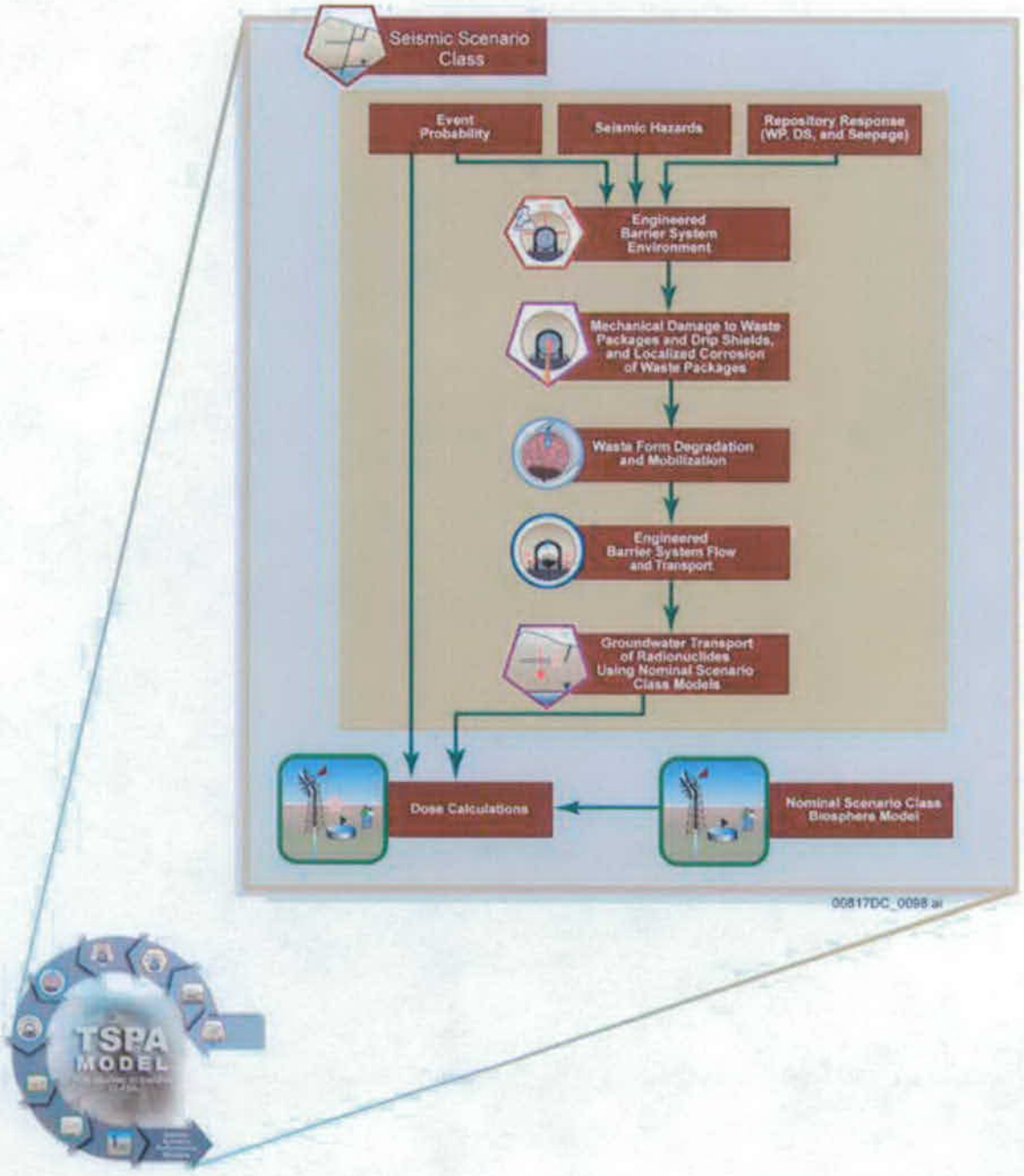

Figure 6.6-2. Information Flow Diagram for the Seismic Scenario Class in the TSPA-SEIS Model

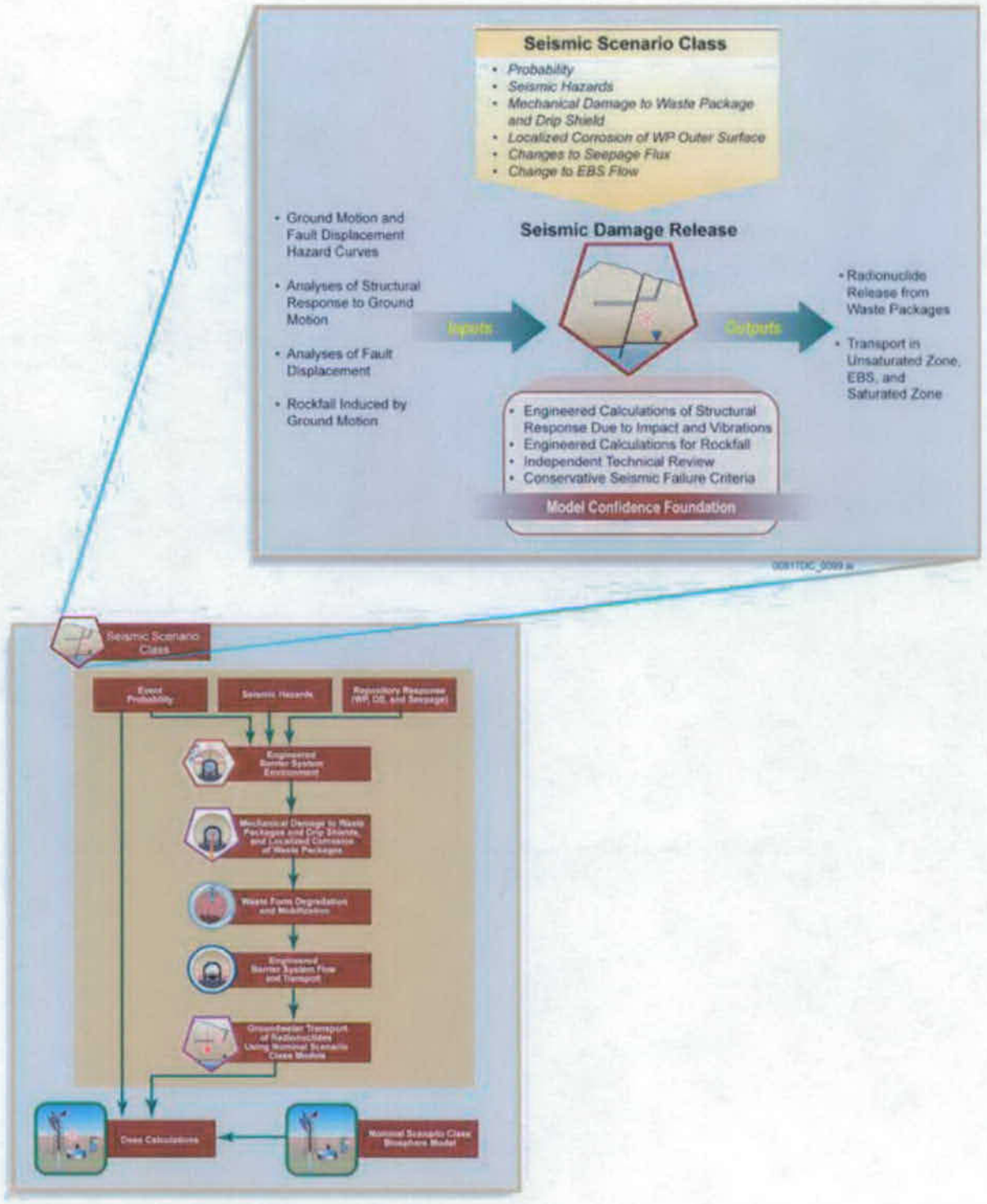

Figure 6.6-3. Inputs, Outputs, and Basis for Model Confidence for the Seismic Scenario Class

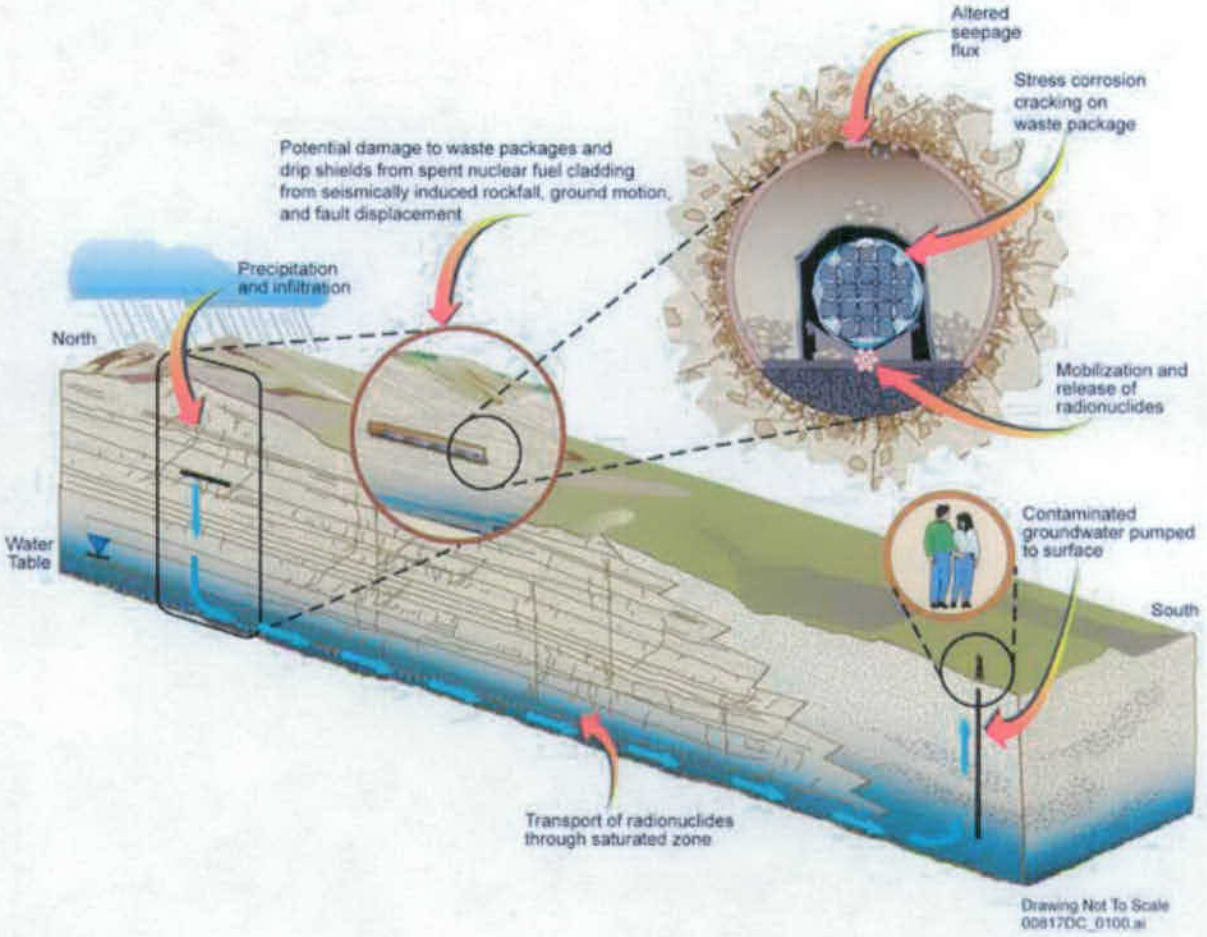

Figure 6.6-4. Schematic Illustration of the Seismic Scenario Class, the Seismic Effects within a Drift, and Subsequent Radionuclide Releases to the Accessible Environment

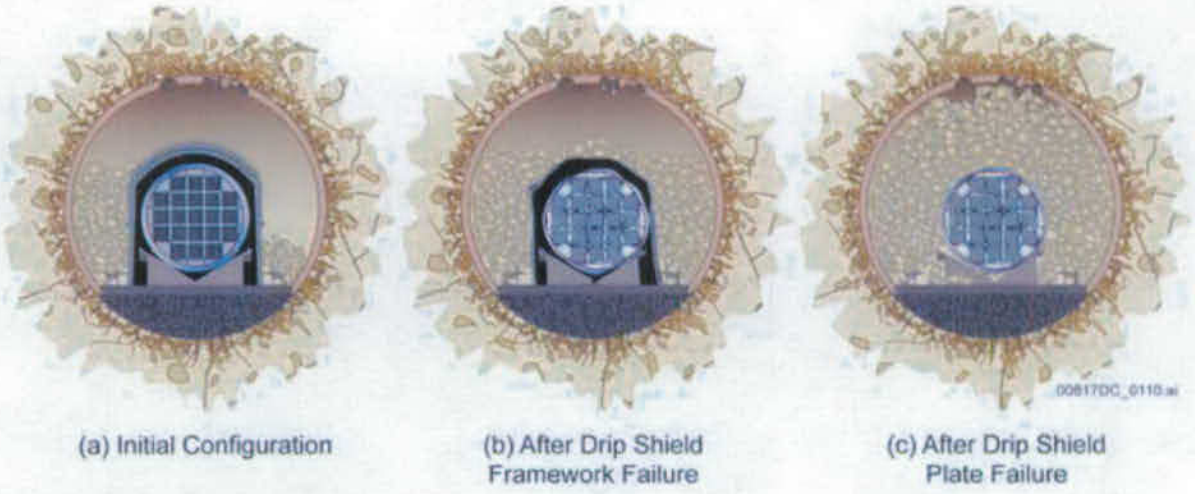

Figure 6.6-5. Schematic Representation of Future Configurations of EBS Components for Seismic Damage Abstraction

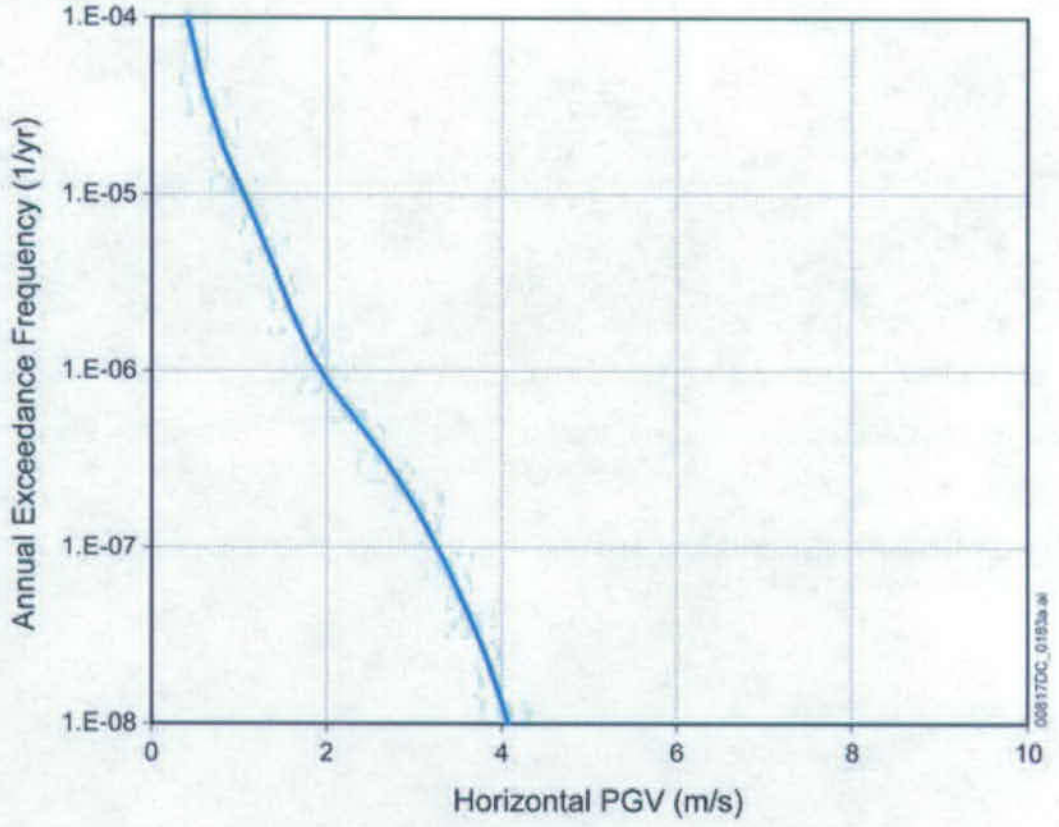

Source: DTN: MO0501BPVELEMP.001 [DIRS 172682], *Bounded Horizontal Peak Ground Velocity Hazard at the Repository Waste Emplacement Level.xls.*

NOTE: Data is plotted on a linear scale for the Horizontal PGV.

Figure 6.6-6. Hazard Curve for Seismic Scenario Class

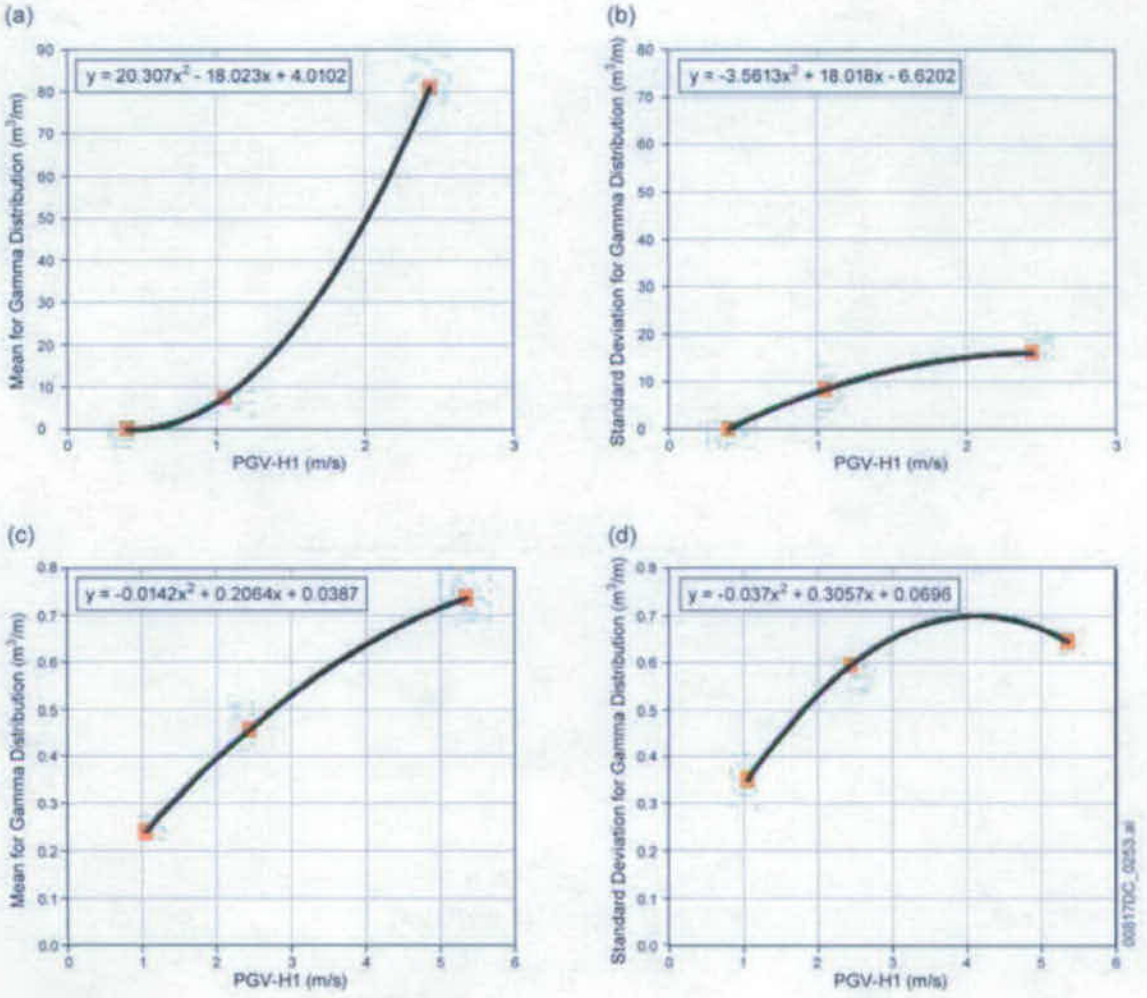

Source: DTN: MO0703PASDSTAT.001_R3 [DIRS 182878], *Lith Rubble Abstraction.xls* (a and b) and *Nonlith Rockfall Abstraction.xls* (c and d).

Figure 6.6-7. Comparison of Mean Rockfall Volumes for Lithophysal (a and b) and Nonlithophysal (c and d) Zones

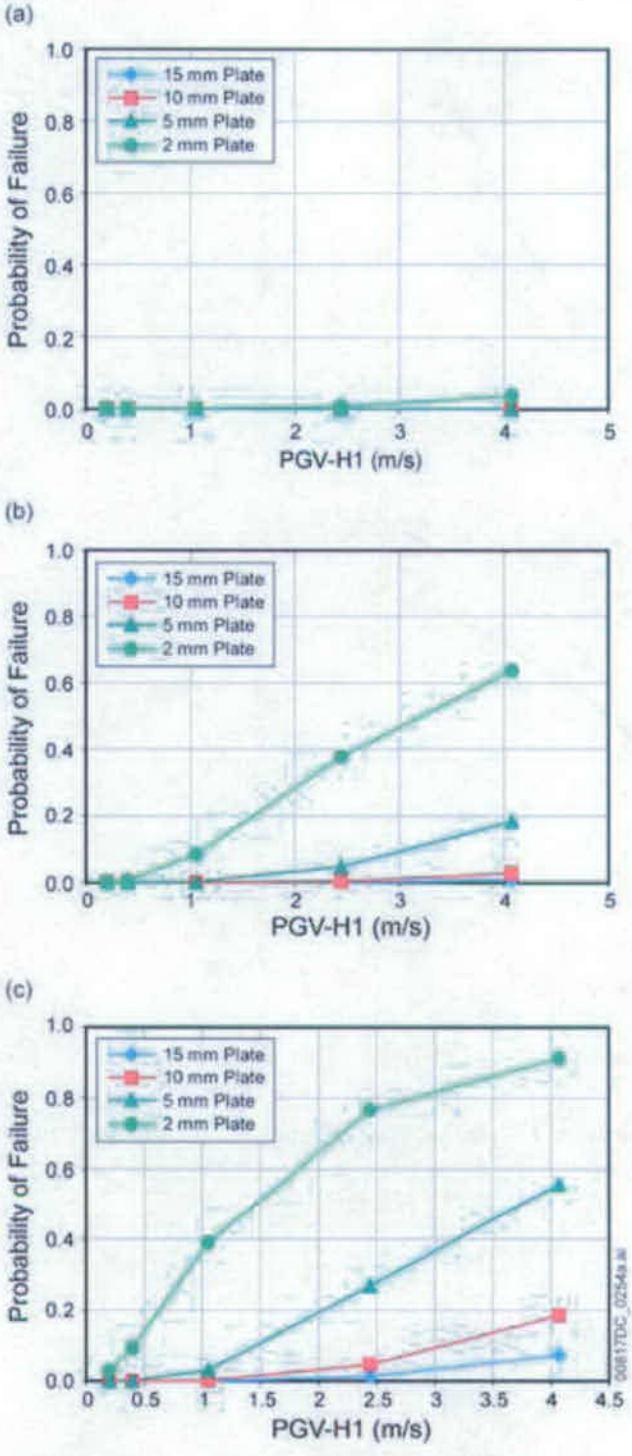

Source: DTN: MO0703PASDSTAT.001_R3 [DIRS 182878], *Plate Fragility Analysis.xls*.

Figure 6.6-8. Drip Shield Plate Fragility as a Function of Rockfall Load: (a) 10 Percent, (b) 50 Percent, and (c) 100 Percent

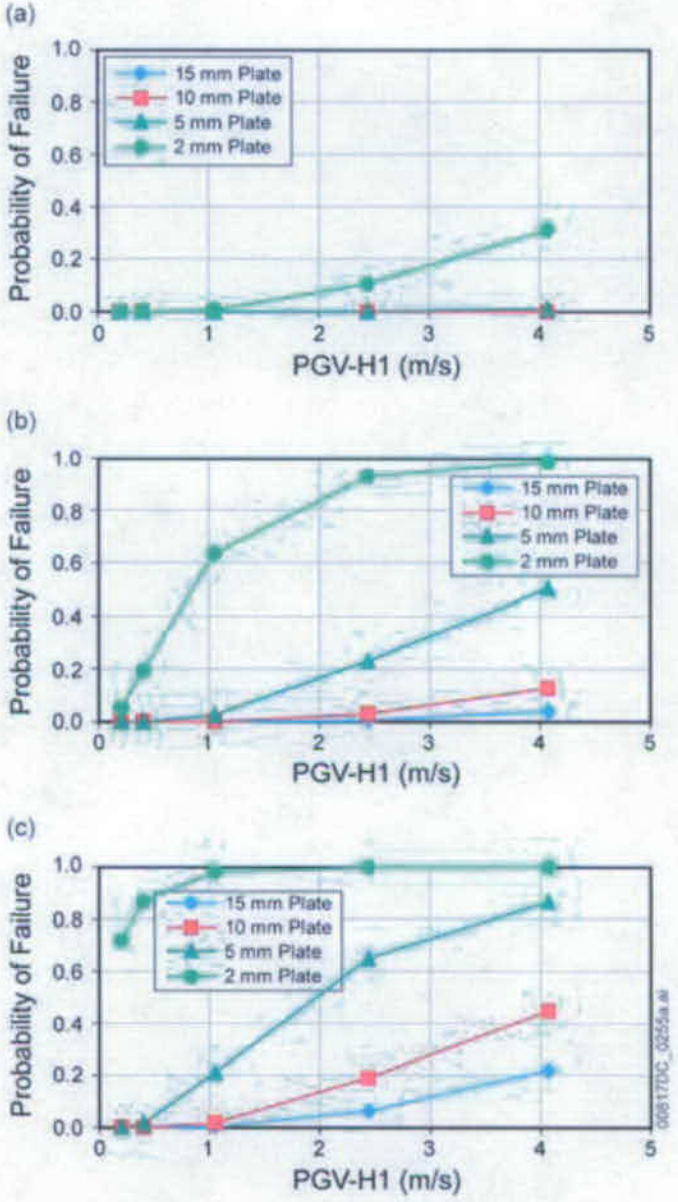

Source: DTN: MO0703PASDSTAT.001_R3 [DIRS 182878], *Frame Fragility Analysis.xls*.

Figure 6.6-9. Drip Shield Framework Fragility as a Function of Rockfall Load: (a) 10 Percent, (b) 50 Percent, and (c) 100 Percent

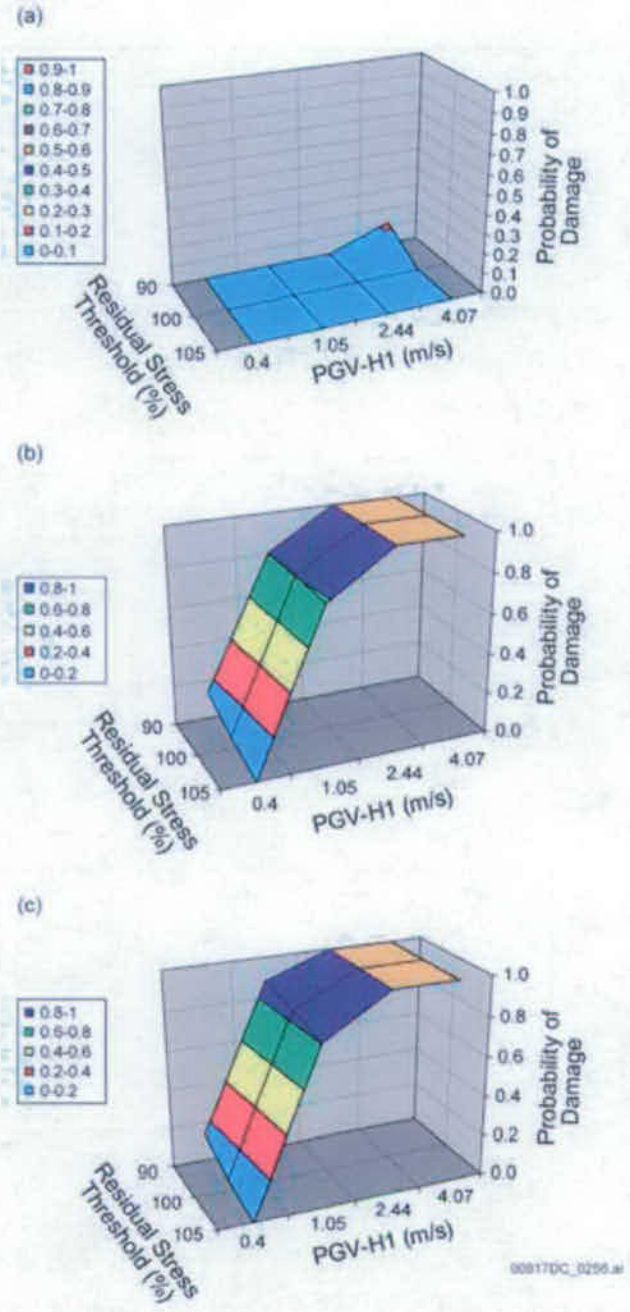

Source: DTN: MO0703PASDSTAT.001_R3 [DIRS 182878], *CDSP Kinematic Damage Abstraction 23-mm Intact.xls, CDSP Kinematic Damage Abstraction 23-mm Degraded.xls, and CDSP Kinematic Damage Abstraction 17-mm Degraded.xls.*

NOTE: Orange represents a probability of 1.0.

Figure 6.6-10. Probability of Damage for a CSNF WP under and Intact Drip Shield: (a) 23 mm OCB with Intact Internals, (b) 23 mm OCB with Degraded Internals, and (c) 17 mm OCB with Degraded Internals

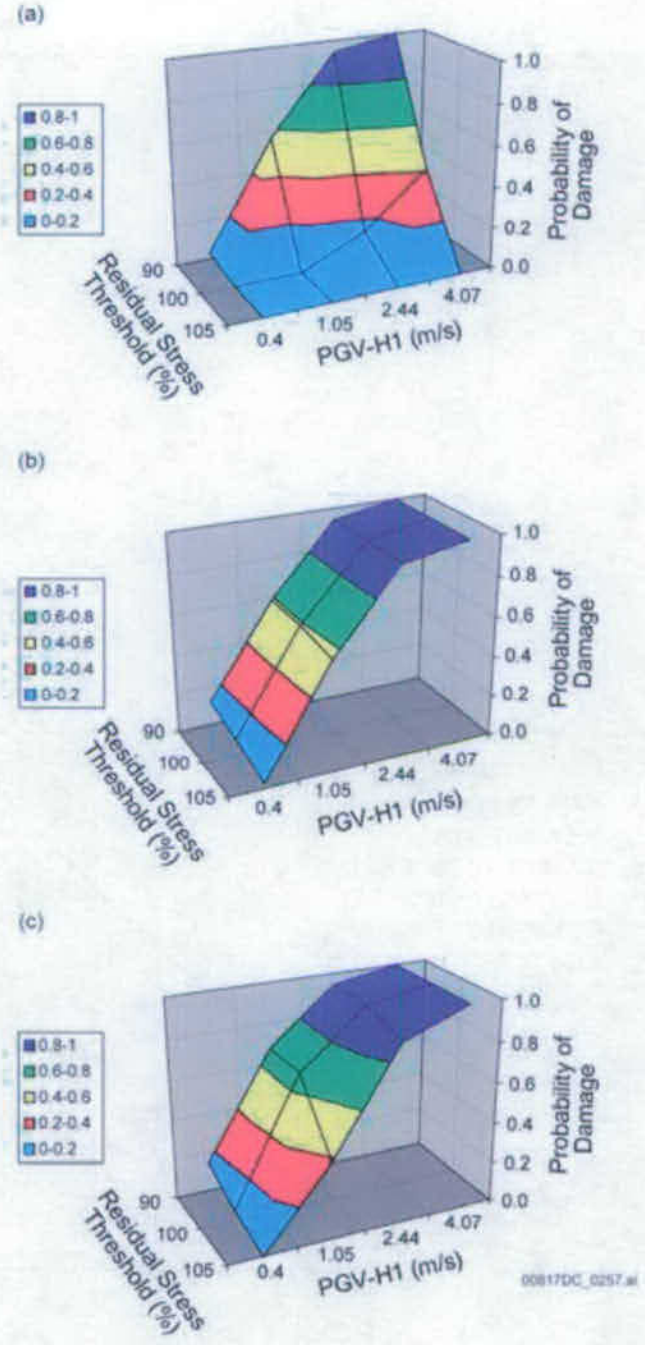

Source: DTN: MO0703PASDSTAT.001_R3 [DIRS 182878], *CDSP Kinematic Damage Abstraction 23-mm Intact.xls, CDSP Kinematic Damage Abstraction 23-mm Degraded.xls, and CDSP Kinematic Damage Abstraction 17-mm Degraded.xls.*

Figure 6.6-11. Probability of Damage for a CDSP WP under an Intact Drip Shield: (a) 23 mm OCB with Intact Internals, (b) 23 mm OCB with Degraded Internals, and (c) 17 mm OCB with Degraded Internals

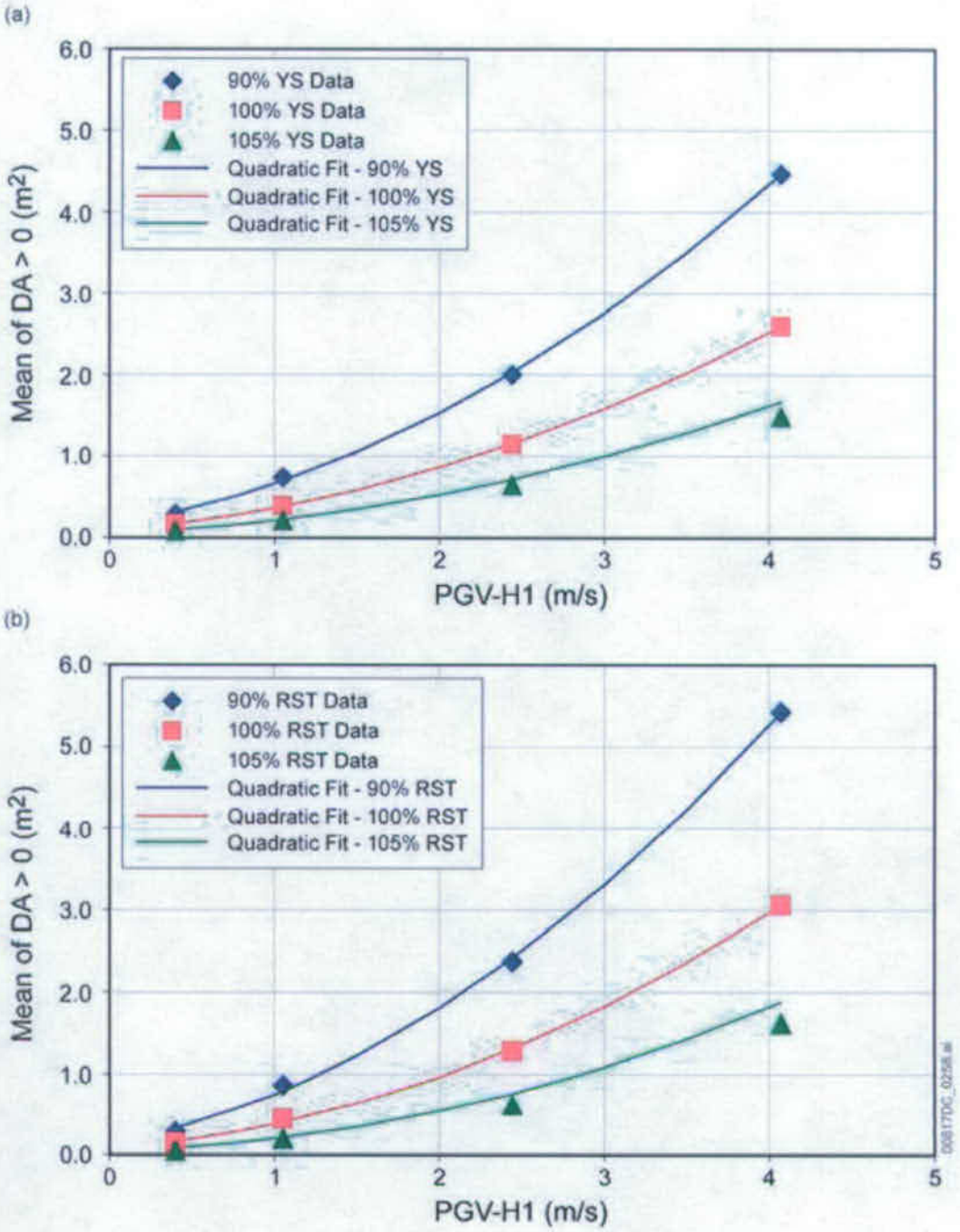

Source: DTN: MO0703PASDSTAT.001_R3 [DIRS 182878], *Kinematic Damage Abstraction 23-mm Degraded.xls* and *Kinematic Damage Abstraction 17-mm Degraded.xls*.

Figure 6.6-12. Quadratic Fit for Mean Damaged Area on a CSNF WP with Degraded Internals under an Intact Drip Shield: (a) 23 mm OCB and (b) 17 mm OCB

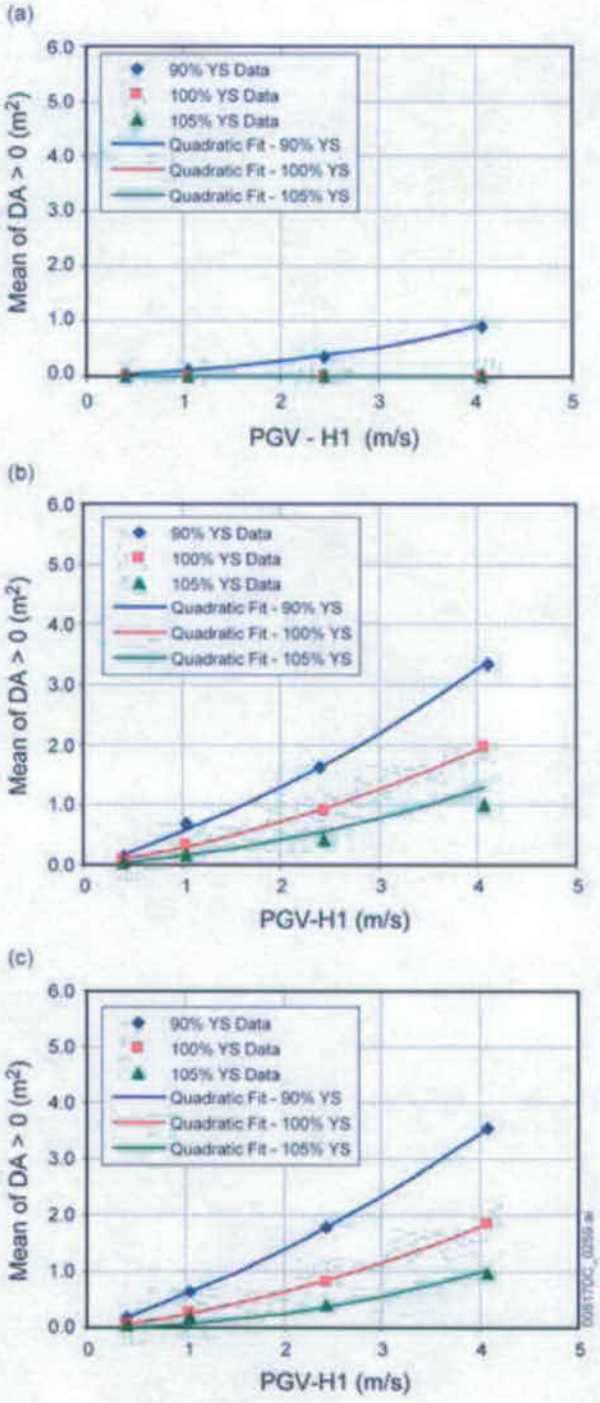

Source: DTN: MO0703PASDSTAT.001_R3 [DIRS 182878], CDSP *Kinematic Damage Abstraction 23-mm Intact.xls*, *CDSP Kinematic Damage Abstraction 23-mm Degraded.xls*, and *CDSP Kinematic Damage Abstraction 17-mm Degraded.xls*.

Figure 6.6-13. Quadratic Fit for Mean Damaged Area on a CDSP WP under an Intact Drip Shield: (a) 17 mm OCB with Degraded Internals, (b) 23 mm OCB with Degraded Internals, and (c) 23 mm OCB with Intact Internals

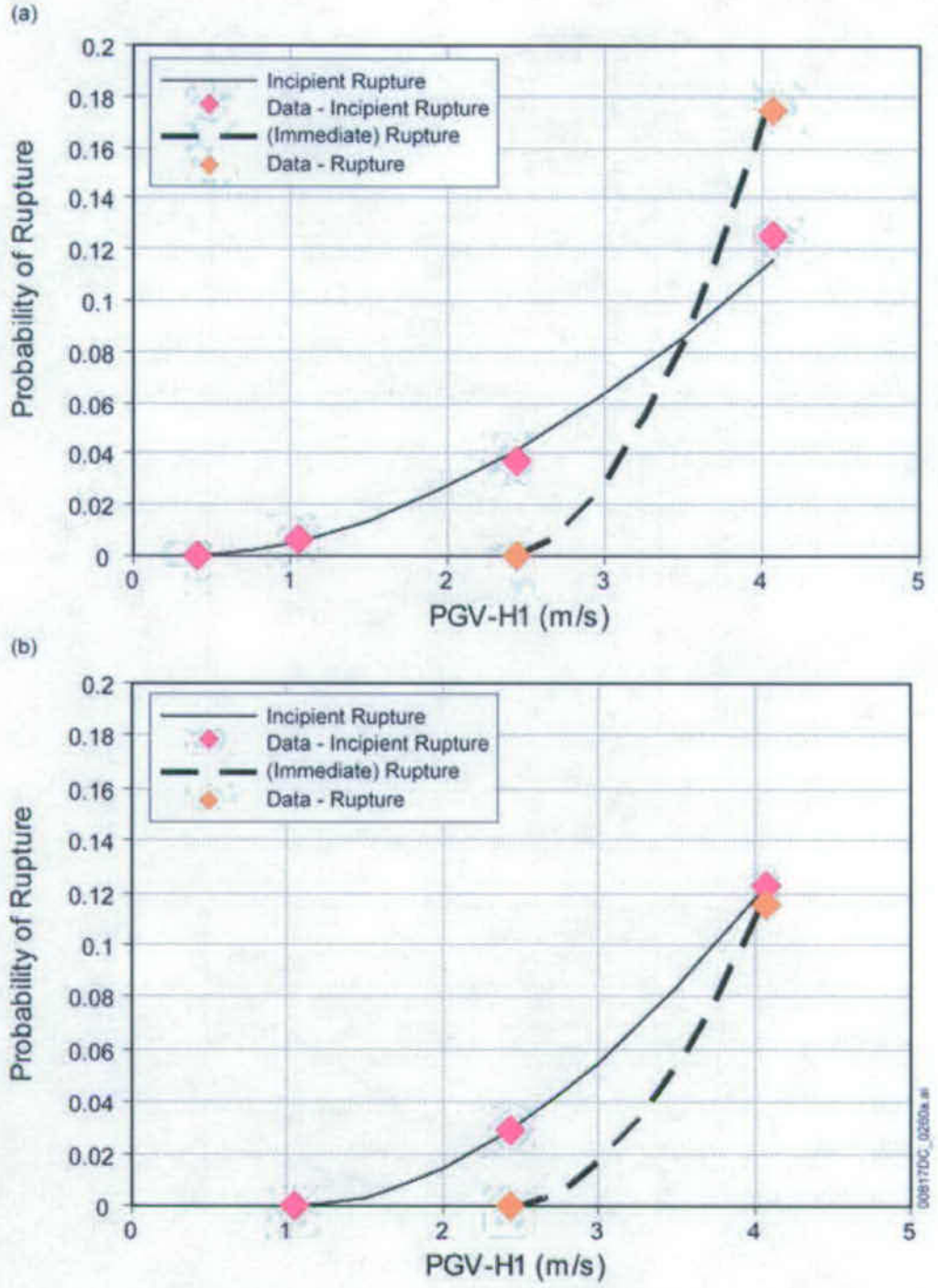

Source: DTN: MO0703PASDSTAT.001_R3 [DIRS 182878], *Rupture and Puncture Abstractions.xls*.

Figure 6.6-14. Probability of Incipient and Immediate Rupture for (a) CSNF and (b) CDSP WPs under Intact Drip Shields

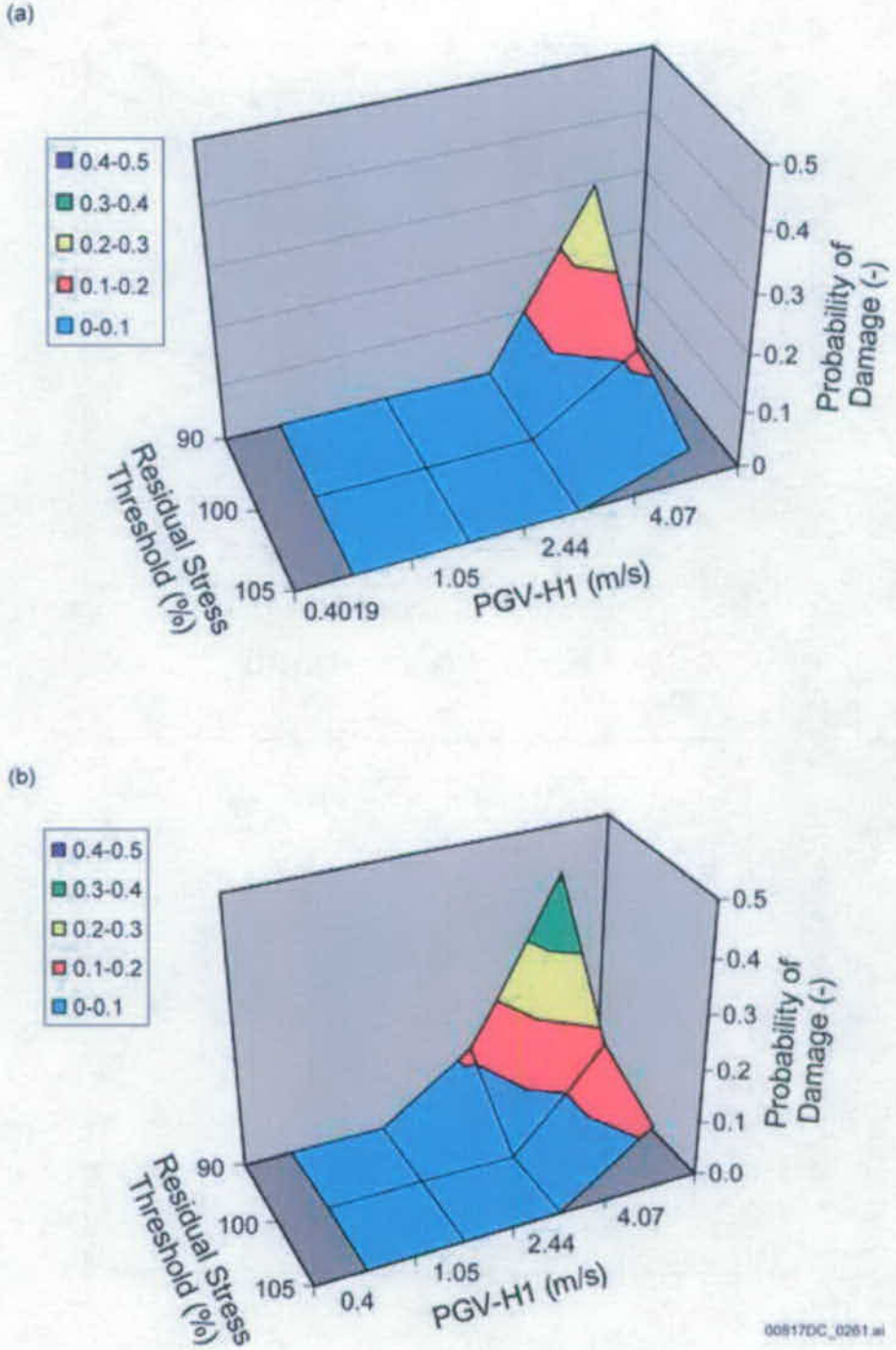

Source: DTN: MO0703PASDSTAT.001_R3 [DIRS 182878], *WP-Rubble Damage Abstraction 23-mm Degraded.xls* and *WP-Rubble Damage Abstraction 17-mm Degraded.xls*.

Figure 6.6-15. Probability of Damage for a CSNF WP Surrounded by Rubble: (a) 23 mm and (b) 17 mm

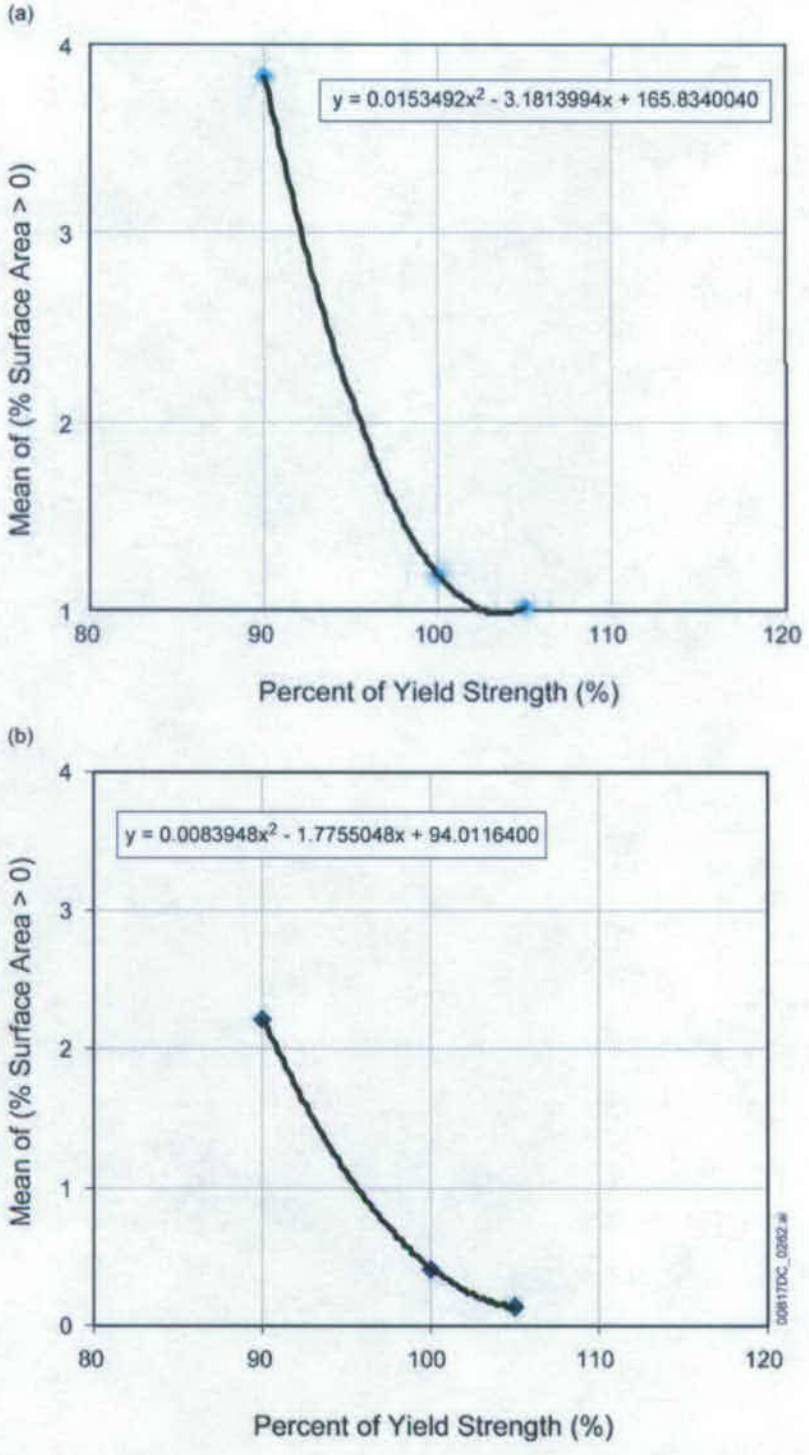

Source: DTN: MO0703PASDSTAT.001_R3 [DIRS 182878], *WP-Rubble Damage Abstraction 23-mm Degraded.xls* and *WP-Rubble Damage Abstraction 17-mm Degraded.xls*.

Figure 6.6-16. Quadratic Fit for Mean Damage Area on a CSNF WP with Degraded Internals Surrounded by Rubble: (a) 23 mm and (b) 17 mm

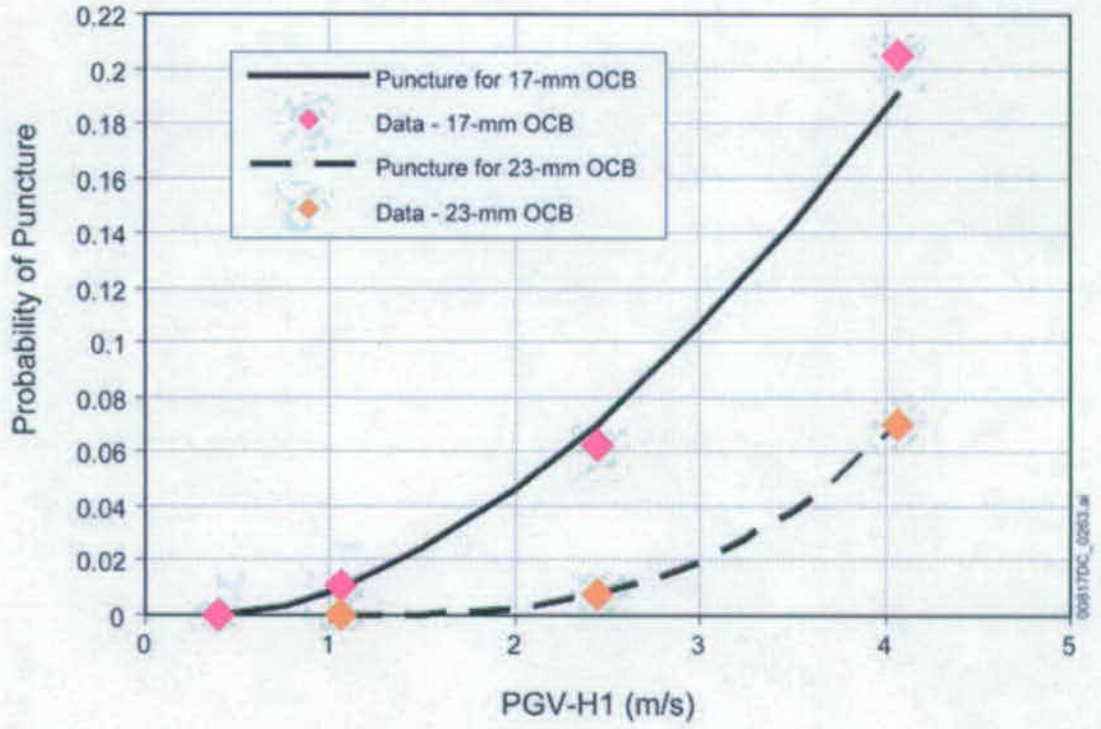

Source: DTN: MO0703PASDSTAT.001_R3 [DIRS 182878], *Rupture and Puncture Abstractions.xls*.

Figure 6.6-17. Probability of Puncture for a CSNF WP Surrounded by Rubble

INTENTIONALLY LEFT BLANK

6.7 TSPA-SEIS FOR THE HUMAN INTRUSION SCENARIO

The Human Intrusion Modeling Case is based on the stylized Human Intrusion Scenario at NRC proposed rule at 10 CFR 63.322 [DIRS 180319], and the individual protection standard for a human intrusion of the repository at proposed 10 CFR 63.321 [DIRS 178394]. The TSPA-SEIS stylized Human Intrusion Scenario is based on NRC proposed rule at 10 CFR 63.322 [DIRS 180319] as follows:

"For the purposes of the analysis of human intrusion, DOE must make the following assumptions:

(a) There is a single human intrusion as a result of exploratory drilling for ground water;

(b) The intruders drill a borehole directly through a degraded waste package into the uppermost aquifer underlying the Yucca Mountain repository;

(c) The drillers use the common techniques and practices that are currently employed in exploratory drilling for ground water in the region surrounding Yucca Mountain;

(d) Careful sealing of the borehole does not occur, instead natural degradation processes gradually modify the borehole;

(e) No particulate waste material falls into the borehole;

(f) The exposure scenario includes only those radionuclides transported to the saturated zone by water (e.g., water enters the waste package, releases radionuclides, and transports radionuclides by way of the borehole to the saturated zone); and

(g) No releases are included which are caused by unlikely natural processes and events."

In addition NRC proposed rule at 10 CFR 63.321 [DIRS 178394] specifies the individual protection standard for human intrusion as follows:

"(a) DOE must determine the earliest time after disposal that the waste package would degrade sufficiently that a human intrusion (see § 63.322) could occur without recognition by the drillers.

(b) DOE must demonstrate that there is a reasonable expectation that the reasonably maximally exposed individual receives, as a result of human intrusion, no more than the following annual dose:

(1) 0.15 mSv (15 mrem) for 10,000 years following disposal; and

(2) 3.5 mSv (350 mrem) after 10,000 years, but within the period of geologic stability.

(c) DOE's analysis must include all potential environmental pathways of radionuclide transport and exposure, subject to the requirements at § 63.322."

Section 6.7 is organized as follows. Section 6.7.1 summarizes the model components and submodels of the Human Intrusion Scenario. The earliest time at which a WP is expected to be breached by an inadvertent drilling event is discussed in Section 6.7.2. Section 6.7.2.1 describes the TSPA-SEIS analysis for drip shield (DS) and WP degradation. Section 6.7.2.2 discusses the unlikely events-related damage mechanisms. Section 6.7.2.3 describes the potential for WP penetration by a drilling event. Implementation and the process for estimating the mean annual dose for the Human Intrusion Scenario is discussed in Section 6.7.3. The model component and submodel integration points, as well as conservatisms in submodels and abstraction models, are discussed in Section 6.7.4. In Section 6.7.5, alternative conceptual models (ACMs) are considered.

6.7.1 TSPA-SEIS Components and Submodels for the Human Intrusion Scenario

The Human Intrusion Scenario describes performance of the repository system in the event that exploratory drilling disrupts the repository. Human intrusion disruption of the repository is addressed by a single modeling case.

The Human Intrusion Modeling Case, based upon NRC proposed rule 10 CFR 63.322 [DIRS 180319], assumes that exploratory drilling activities intersect the repository and destroy a single DS and WP without recognition by the drillers. After penetrating a thinned DS and WP, the drillers continue to bore a conduit through to the SZ. The drillers penetrate a DS and WP with an opening the size of the drill bit and water enters the WP, mobilizing radionuclides. The released radionuclides may then be transported out of the repository, move down through the borehole to the SZ, and then be transported through the SZ to the accessible environment. The TSPA-SEIS components and submodels needed to calculate total system performance for the Human Intrusion Modeling Case include the following, given that a certain WP is destroyed by the intrusion:

- UZ Flow
- EBS Environment
- Waste Form Degradation and Mobilization
- EBS Flow and Transport
- SZ Flow and Transport
- Biosphere.

The model components and submodels of the TSPA-SEIS for the Human Intrusion Scenario are shown on Figure 6.7-1. Figure 6.7-2 shows the information flow within the model for the Human Intrusion Scenario in the TSPA-SEIS. Figure 6.7-3 indicates the major inputs and outputs of the model components and submodels included in the Human Intrusion Scenario and the foundation for confidence in the TSPA-SEIS. The TSPA-SEIS framework for the Human Intrusion Scenario is similar to that of the Nominal Scenario Class. However, some of the submodels differ from those described in Section 6.3. These include the following:

- Mechanical damage to WPs, DSs, and cladding
- Drift seepage for the Human Intrusion Scenario
- UZ Transport for the Human Intrusion Scenario
- EBS flow for the Human Intrusion Scenario.

The WP and DS Degradation Submodel is not used to calculate the corrosion failure of WPs prior to penetration time in the Human Intrusion Modeling Case. It is conservatively assumed that the WP could be penetrated without detection by the drillers. The WP and DS Degradation Submodel is not used to calculate corrosion failure of undisrupted WPs after the disruption occurs in the Human Intrusion Modeling Case. Instead, these WPs are accounted for in the Nominal Modeling Case.

6.7.2 Evaluation of the Earliest Time of Waste Package Penetration by Human Intrusion

The Human Intrusion Scenario considers the effects of a single well drilled from the land surface above the repository, which penetrates the repository and passes through a single DS and WP, and into the underlying SZ. To determine the earliest time after disposal that a WP would degrade sufficiently that a human intrusion could occur without recognition by the drillers, the degradation mechanisms for DSs and WPs were evaluated and the earliest time at which a WP could be breached without recognition by the drillers was conservatively selected. The following discussion considers all the degradation states for a WP and DS considered for the TSPA-SEIS. Because degradation of WPs and DSs occurs gradually with time, the probability that a human intrusion could occur without recognition by the drillers increases with time.

6.7.2.1 General Corrosion of the Waste Package and Drip Shield

The EBS design includes Titanium Grade 7 DS supported by a Titanium Grade 29 framework, which is placed over the waste packages (SNL 2007 [DIRS 179354] Section 4.2.1). As long as they remain substantially intact, the DS will divert an inadvertent drilling event (Section 6.7.2.3) away from the WP and preclude damage to a WP. The TSPA-SEIS for general corrosion is the only DS corrosion mechanism modeled. This degradation mode and abstraction model is described in Section 6.3.5. This process is modeled as being independent of temperature and relative humidity and is initiated at the time of repository closure. Because of the low corrosion rate of titanium alloy used for the DSs, the initial breaches of the DSs are not expected to occur until well after 10,000 years; more specifically, analyses predict that initial breaches of the DSs will not occur under nominal conditions until after approximately 230,000 years post closure (Section 6.3.5.1.3). General corrosion is modeled separately for the topside and underside surfaces of the DSs. The mean Titanium DS corrosion rates are the sum of the topside surface corrosion rate plus the underside surface corrosion rate. The benign chemistry DS corrosion rates are applied to both the topside and underside of the DS for DSs that are not exposed to dripping water. Considering the only DSs that are exposed to dripping, from the tabulated data, the sum of the Expected Case (50 percent) for the Aggressive Condition (topside) plus the Benign Condition (underside) yields total corrosion rates of approximately 50.59 nm/yr, 37.33 nm/yr, and 75.44 nm/yr for the median (0.5 quantile), minimum (0.001 quantile), and maximum (0.999 quantile) values, respectively. Even applying the maximum predicted titanium corrosion rate (0.999 quantiles for the topside and underside), the first failures of the DSs due to general corrosion are not likely to occur until approximately 200,000 years after repository closure under nominal conditions (using a DS thickness of 15 mm (SNL 2007 [DIRS 179354], Table 4-2, Parameter Number 07-04A).

The TSPA-SEIS for WP degradation includes four degradation modes: general corrosion, microbially influenced corrosion (MIC), stress corrosion cracking (SCC), and localized

corrosion. These degradation modes and their abstractions are described in Section 6.3.5. The WPs have a dual-metal design consisting of an inner vessel and outer barrier. The inner vessel is composed of a 50.8-mm-thick layer of Stainless Steel Type 316 (material type SA-240 (UNS S31600)). The outer shell (i.e., outer corrosion barrier) is a 25-mm-thick layer of Alloy 22 (material type SB-575 (UNS N06022)), a corrosion-resistant, nickel-based alloy surrounding transportation, aging, and disposal (TAD) canister made of a 300-series stainless steel such as Stainless Steel Type 316; (SNL 2007 [DIRS 179394], Table 4-3; and SNL 2007 [DIRS 179567], Tables 4-6 through 4-10). Alloy 22 protects the Stainless Steel Type 316 inner vessel from corrosion, and the Stainless Steel Type 316 inner vessel provides structural support for the thinner Alloy 22 outer shell. Because the WP outer shell is highly corrosion resistant, WPs will not be breached by corrosion processes during the 10,000-year modeling period in the absence of localized corrosion (SNL 2007 [DIRS 178519], Section 8.1). The corrosion rate results for the WP degradation analyses are used to approximate a conservative WP failure time due to general corrosion, MIC, and SCC. The actual WP degradation profiles used in the TSPA-SEIS will make use of the actual thermal hydrologic history files appropriate for the repository, as well as uncertainty in the exact calculated timing of the first WP failure (Section 6.3.5).

The WP Localized Corrosion Initiation and Propagation Analysis for the WP outer surface is based on the Localized Corrosion Initiation Abstraction developed in *General Corrosion and Localized Corrosion of Waste Package Outer Barrier* (SNL 2007 [178519], Section 6.4.4). The primary factors that determine the potential for initiating localized corrosion are sample configuration, metallurgical conditions, and exposure conditions including temperature, pH, chloride-ion concentration, and nitrate-ion concentration, which are obtained from the EBS TH Environment Submodel (Section 6.3.2) and the EBS Chemical Environment Submodel (Section 6.3.4). Localized corrosion requires the presence of seepage water on the WP surface. The potential effects of localized corrosion on the WPs during the initial 10,000-year period are, therefore, conditional on a DS failure (Section 6.3.5.2). Until a breach of the DS occurs, the WP itself is not susceptible to localized corrosion. Therefore, under nominal conditions, localized corrosion of WPs will not occur because DS failures are not expected until well after the chemical environment necessary for localized corrosion initiation has subsided (Section 6.3.5.2).

General corrosion of DSs and WPs occurs gradually over time. The general corrosion process is a surface phenomenon and the underlying metal retains its integrity and resistance to drilling until a significant amount of material has been corroded and the remaining DS or WP thickness is insufficient to prevent penetration by a drill bit. Nominal WP and DS degradation processes are insufficient to significantly degrade the titanium DS in 10,000 years. Given the slower relative degradation rates of the WPs and barring disruptive events of large magnitude, until there is a DS failure, the structural integrity of a WP is maintained and provides an additional barrier to borehole drill penetration.

6.7.2.2 Occurrence of Unlikely Events

In NRC proposed rule at 10 CFR 63.342(b) [DIRS 178394], the NRC specifies that, the human intrusion standards "*...shall exclude the unlikely features, events, and processes, or sequences of events and processes, i.e., those that are estimated to have less than one chance in 10 and at least one chance in 10,000 of occurring within 10,000 years...*" (i.e., an annual frequency of 10^{-5} (1/yr) to 10^{-8} (1/yr)). Therefore, FEPs that have at least one chance in 10 of occurring within

10,000 years (i.e., a probability of occurrence greater than or equal to 1×10^{-5} per year) need to be considered for the human intrusion calculations. The following FEPs are discussed below in terms of their probability of occurrence: early failure of DSs, igneous events, and seismic events.

Early Failed Drip Shield

Although the TSPA-SEIS's results show some DS failures at an early time, these failures are the result of manufacturing defects that increase susceptibility to SCC (SNL 2007 [DIRS 178765], Section 6.4). The probability of DS early failure (i.e., having an undetected defect that could cause an early failure) is determined from the DS cumulative uncertainty distribution for undetected DS defects (SNL 2007 [DIRS 178765], Table 6-10). This cumulative distribution function (CDF) gives the probability of having an undetected defect for a given DS. Considering that only a single WP and DS are penetrated during a human intrusion event, the probability of a human intrusion event intersecting a WP location that has an early failed DS can be determined by the probability of a DS defect occurring at that location. To evaluate the likelihood of this scenario, a conservative DS defect probability was chosen at the 0.99 quantile value of 3.106×10^{-5} from the DS cumulative uncertainty distribution for undetected DS defects (SNL 2007 [DIRS 178765], Table 6-10). Therefore, the probability of an early failed DS at the location of a human intrusion is 3.106×10^{-5}. There is no time dependency on this probability. However, it can be excluded from consideration as an unlikely event as it is an event with less than one chance in 10 in 10,000 years as defined by the NRC proposed rule at 10 CFR 63.342 (b) [DIRS 178394] and 10 CFR 63.322 (g) [DIRS 180319]. Even in the unlikely event that the human intrusion event were to intersect a location with an early failed DS, the likelihood of the WP being failed at the same location as a DS is even smaller. The joint probability (using the 0.9999 quantiles for DS and WP defects) for DS and WP early failure occurring at the same location is approximately 4.2×10^{-7} (SNL 2007 [DIRS 178765], Section 6.5.1, Table 6-11).

Similarly, potential effects of localized corrosion on the WPs during the initial 10,000-year period are conditional on a DS failure (Section 6.3.5.2). Given the probability of a human intrusion event at a location with an early failed DS (at a 0.99 quantile value) is 3.106×10^{-5}; a human intrusion event intersecting a WP failed by localized corrosion can be excluded as an unlikely event (events with less than one chance in 10) per NRC proposed rule at 10 CFR 63.342 (b) [DIRS 178394] and 63.322 (g) [DIRS 180319].

Igneous Disruptive Events

Igneous disruptive events capable of causing significant damage are unlikely (i.e., igneous intrusion of the repository footprint has an annual probability of exceedance of less than 10^{-5} but greater than 10^{-8}). Therefore, further consideration of an igneous event in consort with a human intrusion stylized analysis is excluded from consideration. The exclusion is consistent with requirements of the NRC proposed rule at 10 CFR 63.342 (b) [DIRS 178394] and 10 CFR 63.322 (g) [DIRS 180319], which exclude consideration of unlikely events (events with less than one chance in 10 in 10,000 years [i.e., an annual frequency of 10^{-5} 1/yr]) in consort with a human intrusion event.

Seismic Disruptive Events

The analyses for seismic damage to DSs and WPs are documented in *Seismic Consequence Abstraction* (SNL 2007 [DIRS 176828]. The analyses provide a description of the damage that may occur to DSs and WPs from the mechanical response of EBS components to seismic hazards at the proposed repository horizon. The seismic induced damage to WPs and DSs includes the effects from fault displacement along faults that intersect the repository, seismic ground motion induced mechanical damage, or by rock fall, via imposed residual stresses in DSs and WPs (Section 6.6). The effect of fault displacement on the EBS is evaluated in terms of mean fault displacement hazard curves developed for faulting conditions mapped within the immediate vicinity of Yucca Mountain (SNL 2007 [DIRS 176828], Section 6.11 and Table 6-61). The Seismic FD Modeling Case includes disruption of the DSs and breach of the WPs affected by the displacement of faults, as well as nominal failures of DSs and WPs (Section 6.6.1.3). The expected number of WPs and DSs that fail from fault displacement is small because the number of WPs lying on known and generic faults is estimated to be 212, which is a small fraction of the approximately 11,000 WPs in the repository (SNL 2007 [DIRS 176828], Section 6.12.2, Item 27, p. 6-254). Seismic events capable of causing significant damage from fault displacement are unlikely (i.e., WP failure due to fault displacement along faults intersecting the repository footprint has an annual probability of exceedance less than 2.2×10^{-7} [1/yr] for TAD canisters and less than 2.5×10^{-7} [1/yr] for co-disposed WPs (CDSP WPs) (SNL 2007 [DIRS 179652] Table 1-8). Therefore, further consideration of a seismic fault displacement event in combination consort with a human intrusion stylized analysis is excluded from consideration. The exclusion is consistent with requirements of the NRC proposed rule at 10 CFR 63.342 (b) [DIRS 178394] and 10 CFR 63.322 (g) [DIRS 180319], which exclude consideration of unlikely events.

For the seismic ground motion analysis, the threshold for considering the potential for damage to WPs and DSs is reached if the residual stress from mechanical damage exceeds the residual stress threshold for the barrier. The presence of residual stress induced by seismic events and/or related rock fall may result in local barrier degradation from accelerated SCC or rupture of the WPs and/or DSs (SNL 2007 [DIRS 176828], Sections 6.1.3 and 6.1.4). While SCC is appropriate for consideration of EBS flow and transport, it does not necessarily reflect changes to the effective material properties and may not constitute failure with respect to recognition of a change in conditions while drilling. Even with an imposed residual stress and minor amounts of corrosion and cracking, a rotating drill bit that encounters a metallic object will behave significantly different than when encountering naturally occurring geologic materials (Section 6.7.2.3). However, DS rupture, or plate fragility, is defined as the probability of rupturing or puncturing the DS plate during a seismic event (Section 6.6.1.2.2). For the evaluation of a human intrusion event, the DS rupture (plate fragility abstraction) is evaluated with respect to the earliest time a WP could be penetrated without recognition by the drillers.

The plate fragility abstraction is a function of peak ground velocity (PGV), the thickness of the DS plate, and the static load on the plates from rock fall (Section 6.6.1.2.2) (SNL 2007 [DIRS 176828], Section 6.8 and Table 6-36). Applying the maximum DS general corrosion rates over a 10,000-year period would reduce the original DS thickness of 15 mm by approximately 0.75 mm (using the 0.999 quantiles for the underside and topside of the DS as discussed in Section 6.7.2.1). Given this conservative DS thickness (14.25 mm), there is a very

small probability ($p<0.001$) for DS rupture to occur in a seismic event with a PGV of 1.05 (m/s). This evaluation assumes the probability of DS plate failure for a drift 100 percent filled with rubble (i.e., maximum static loading) and linear interpolating between a 10 mm and a 15 mm DS thickness (SNL 2007 [DIRS 176828], Table 6-36). A PGV of 1.05 m/s corresponds to an annual probability of exceedance of 9.955×10^{-6} (1/yr) (SNL 2007 [DIRS 176828], Table 6-3). Given an annual probability of exceedance of 9.955×10^{-6} (1/yr), seismic disruptive events capable of causing DS rupture are unlikely. Similarly, the rupture of a WP that can move freely beneath the DS is conceptualized to occur from the accumulation of severe deformation due to multiple impacts (SNL 2007 [DIRS 176828], Section 6.5.2.1 and Section 6.6.2.1). WPs with a 23-mm thick outer corrosion barrier (i.e., degraded from 25 mm) and intact internals are not ruptured by multiple impacts (SNL 2007 [DIRS 176828] Section 6.5.1.1 and Section 6.6.1.1). There is a small probability for rupture to WPs with degraded internals that have been exposed to severe deformation due to multiple impacts (SNL 2007 [DIRS 176828] Section 6.5.2 and Section 6.6.2). The internals are considered degraded only after the WP has been breached due to SCC, general corrosion, or seismic damage (SNL 2007 [DIRS 176828] Section 5.4 and Section 6.6.1.3.3). For a CDSP WP with intact internals, there is a probability of 0.029 of WP damage (cracking) which would result in degraded internals, given a seismic event with a PGV of 0.40 m/s (SNL 2007 [DIRS 176828] Table 6-14). However in order to rupture a CDSP WP with degraded internals, one or more additional seismic events with a PGV of 1.05 (m/s) or greater must occur (SNL 2007 [DIRS 176828] Table 6-20 and Table 6-21). Given an annual exceedance frequency of 9.955×10^{-6} (1/yr) for a PGV of 1.05 (m/s) (SNL 2007 [DIRS 176828], Table 6-3), seismic disruptive events capable of causing CDSP WP rupture are unlikely. For a TAD-bearing WP with intact internals, damage from ground motion (cracking) which would result in degraded internals requires a seismic event with a PGV of 4.07 (m/s) or larger (SNL 2007 [DIRS 176828] Table 6-4). Given an annual exceedance frequency of approximately 1.0×10^{-8} (1/yr) for a PGV of 4.07 (m/s) (SNL 2007 [DIRS 176828], Table 6-3), seismic disruptive events capable of causing TAD-bearing WP rupture are unlikely.

Consequently, with regard to the human intrusion stylized analysis in combination with a seismic event, it is concluded that seismic ground motion events are insufficient to significantly alter material properties of the DS to a sufficient degree that it would not be noticed by a driller in 10,000 years.

6.7.2.3 Potential for Waste Package Penetration by Drilling

The NRC, in the discussion regarding the timing and frequency of human intrusion (66 FR 55732 [DIRS 156671], p. 55761), states that "some evaluations of resource potential of the site suggest that Yucca Mountain (and the area immediately around it) does not represent an attractive candidate for either random or systematic exploratory drilling at this time...". A list of citations for those studies is available in the regulation. Furthermore, the elevation of the mountain, with the resultant greater depth to water compared to shallower groundwater wells that would be drilled to the south of the mountain, decreases the likelihood of groundwater exploration through the repository footprint. Regardless, the regulations specify evaluation of the timing of a human intrusion event and consideration of a stylized human intrusion assuming exploratory drilling for groundwater in the region surrounding Yucca Mountain (10 CFR 63.322(c) [DIRS 180319]). The following discussion presents several lines of evidence relevant to estimating the time when a human intrusion could occur, based upon the earliest time that

current technology and practices used for groundwater exploration could lead to WP penetration without recognition by a driller.

There are a number of operational parameters that would indicate to a driller that a change in down-hole conditions would merit additional investigation, including a bit run (the removal of the bit from the hole for review and grading). These down-hole conditions could include loss of circulation, decreased penetration rate, increased drill string and bit instability, and increased drill string torque caused by differing material properties.

6.7.2.3.1 Initial Bit Selection and Drilling Principles

The bases for the following discussions are focused on typical practices used in drilling water wells in the southwestern United States. Generally speaking, the drill string assembly consists of the drill bit, drill collar, drill pipe, and in some instances, the use of stabilizers.

As described in Driscoll (1986 [DIRS 116801], pp. 278 to 286) and Bourgoyne et al. (1986 [DIRS 155233], Section 5.1), roller bits are typically used in drilling water wells due to their low cost and wide range of operational flexibility. Polycrystalline diamond cutter and diamond cutter drag bits typically are not used in water well drilling because of the high costs of these drill bits. Direct circulation down-hole hammer drills are sometimes used to drill brittle competent rock, such as welded volcanic tuff, but they typically are inefficient in unconsolidated alluvium or incompetent rock formations. This limitation reduces the use of these drills in typical water well drilling. The discussions provided herein would be generally applicable to roller or hammer bits.

The initial selection of bit type is typically based on what is known about the formation characteristics. The terms usually used by drilling engineers to describe the formation characteristics are drillability and abrasiveness. The drillability of the formation is a measure of how easy the rock formation is to drill. It is inversely related to the compressive strength of the rock, although other factors are also important. The abrasiveness of the formation is a measure of how rapidly the cutting surface of a bit will wear when drilling the formation. Although there are some exceptions, the abrasiveness tends to increase as the drillability decreases (Bourgoyne et al. 1986 [DIRS 155233], Chapter 5).

The International Association of Drilling Contractors (IADC 1992 [DIRS 155232]) has developed a classification chart for selection of roller bits. Using this classification chart, roller bits with characteristics of 7-1 or 7-2 (hard semi-abrasive and abrasive formations) would be selected for drilling through the welded geologic units at Yucca Mountain, based on geomechanical properties. Roller bits are designed to take advantage of brittle failure of the rock matrix to crush, break, and remove the rock in an efficient manner. The volume of rock that is newly fractured by a tooth depends on the geometry, rock properties, and tooth penetration depth below the rock surface. The force applied to the tooth is supplied by the drill string torque and weight on the bit. The force applied to a particular situation determines the tooth penetration depth. The bit tooth penetrates into the rock until the resistant force offered back by the rock equals the force applied to the tooth. As a load is applied to a bit tooth, the pressure beneath the tooth increases until it exceeds the crushing strength of the rock and a wedge of finely powered rock is formed beneath the tooth.

As the force of the tooth increases, the material in the wedge compresses and exerts high lateral forces on the solid rock surrounding the wedge until the shear stress exceeds the shear strength of the solid rock and the rock fractures. The rock may also exhibit ductility such that a greater tooth penetration is required to cause sufficient strain for chipping to occur (Warren 1987 [DIRS 155234]). The tooth will penetrate until the shear stress on the tooth is balanced by the shear strength of the rock.

These forces generate fractures that propagate along a maximum shear surface. As the force of the tooth increases above the threshold value, subsequent fracturing occurs in the region above the initial fracture, forming a zone of broken rock. The bit tooth moves forward until it reaches the margins of the wedge and/or fracture zone, and the process repeats (Bourgoyne et al. 1986 [DIRS 155233], Chapter 5). The crushed and broken material is then removed from the boring using circulated drilling fluids (air, water, or admixtures thereof) that also provide cooling and cleaning for the drill bit.

The drill collar is a heavy-walled length of drill pipe with a diameter less than the borehole diameter. If too much force is applied at the top of the drill stem, the drill pipe will bow and tend to cause the bit to cut off-center and, thereby, cause deviations in the borehole alignment. To compensate, drill collars are used to add weight to the lower part of the drill string assembly. This concentration of weight and the increased rigidity of the collars helps to keep the lower part of the drill assembly in alignment and provide weight to the bit to maintain appropriate penetration rate (Driscoll 1986 [DIRS 116801], p. 281). Drill collars may also be fitted with stabilizer devices that contact the borehole walls. The drill collars and stabilizers are used to maintain alignment of the drill string within the borehole and reduce vibration or wobble of the bit and drill pipe that transfers the torque from the surface to the drill bit.

6.7.2.3.2 Bit Operating Conditions and Change-in-Conditions

Bit operating conditions (i.e., drilling fluid properties and circulation rates, drill string stability, bit weight, and rotary speed) affect the rate of penetration and vibrations felt on the drill rig. These factors would be affected by the drilling assembly's entry into the emplacement drift, and the bit operating conditions would be significantly affected by the rounded geometry of the emplacement drift, DS, and WP.

The loss of drilling fluid circulation and sudden drop in weight on the bit when the drill bit breaks through the top of the emplacement drift would provide initial indications that conditions had changed significantly. The loss of circulation would occur because of the flow of drilling fluids from the borehole and into the emplacement drift which, at 5.5 m diameter and on the scale of a kilometer (km) in length, represents an essentially instantaneous increase in volume compared to the borehole volume. At that point, the driller would either try to continue drilling without compensating for the fluid loss in the hope of passing through the loss zone, would try various additives in the drilling fluid to try to seal the formation (Driscoll 1986 [DIRS 116801], p. 360), or would have to pull the drill assembly and either change drilling methods or install temporary or permanent casing to seal off the cavity. In the event of continued drilling, encountering of the DS or WP would prevent progress, and the lack of cooling from circulated fluids would eventually destroy the drilling bit and result in the drilling assembly being pulled from the hole (or otherwise cause the driller to consider alternative courses of action). Given the

volume difference between the borehole and emplacement drift, it is implausible that any amount of additive would resolve the lost circulation problem, again leading the driller to some alternative course of action. Alternative courses of action, such as spot cementing through the loss zone or setting casing through the cavity, would involve pulling the drilling assembly from the borehole. In either scenario, the driller would then encounter continued volumetric problems or would encounter problems in trying to set casing due to the presence of the DS or WP within the emplacement drift.

In addition to loss of circulation, the space between the crown or sides of the emplacement drift (5.5 m) and the DS would cause the operating conditions to become unstable and would evidence themselves with a sudden increase in rotation speed as the weight on the drill bit was unloaded, followed by a sudden drop in the drill assembly (i.e., essentially free fall until the DS or invert of the drift was encountered), and/or a significant increase in the amount of vibration at the surface. Any of these conditions would cause the destabilization of the drill bit (i.e., tend to allow the bit to change direction from the original concentric alignment) and would trigger a response by the driller to address the change in conditions. This is particularly true as drilling conditions would noticeably change (due to the difference in rock and alloy material properties) if the drilling assembly came in contact with the DS material (Section 6.7.2.3.4).

These various scenarios and alternatives assume that the drift has not collapsed. However, the lithophysal and fractured nature of some the Topopah Spring Tuff rock units could provide similar indications, or a rubble accumulation at a collapse point could limit the degree of lost circulation, and the various alternatives discussed above might allow the borehole to progress. Rubble material in a collapsed drift could reduce the degree of the effects on drilling but would likely not eliminate them. The drift stability through time has been examined in *Drift Degradation Analysis* (BSC 2004 [DIRS 166107]). The analysis indicates that during the regulatory period of 10,000 years, the ground support will completely lose its integrity, and drift degradation will occur due to strength decay of the rock mass within the lithophysal zone (SNL 2007 [DIRS 166107], p.188). However, the collapse results in the bulking of, or increase in, the volume of the rock as the rock mass disintegrates into a number of pieces resulting in increased porosity and overall volume. The resulting bulk properties of the fill are different from that of the intact rock mass. Loss of drilling fluid circulation would still occur but perhaps could be accommodated by the driller. Additionally, the rubble pile of rocks would tend to move or shift under small loads, and the uneven loading on the drill bit would increase the lateral deviation forces (Bourgoyne et al. 1986 [DIRS 155233], Chapter 5). As such, even if the drifts collapse, the character of the rubble would be insufficient to stabilize the drill string. Severe wobbling bit action would result as the bit is rotated if the drill collars or stabilizers above the bit are not held in a concentric position in the borehole.

6.7.2.3.3 Penetration of the Drip Shield and Waste Package

To have any possibility of penetrating the DS or WP, the drilling assembly would have to contact the surfaces in an essentially perpendicular orientation. In general, deviation in alignment may be caused by the character of the subsurface material. This is because lateral deviation forces increase with relatively small changes in the contact angle between the bit and drilled material (Bourgoyne et al. 1986 [DIRS 155233], Chapter 5). Deviations may also be caused by too much or too little weight on the drill bit and differences in the pull-down force applied to the drill pipe

during rotary drilling. Additionally, the varying hardness of different materials being penetrated deflects the bit from a consistent alignment.

Given that the top of the DS is curved and that most groundwater exploration holes are drilled in a near-vertical orientation (i.e., angle and directional drilling are possible but are not typically used for groundwater exploration purposes due to increased difficulty and cost), the drill bit would have to make contact at the relatively small areas that make up the apex of the DS or WP, where the surfaces are essentially perpendicular to the drill bit orientation. Only the apex of the DS or WP provides a perpendicular surface for which DS and WP geometry would not increase the lateral deviation forces.

If the drilling assembly contacts any location other than the relatively small areas that make up the apex of the DS or WP, then the relatively small drill bit diameter and high rotational speeds and the increased strength of material used for the DS and WP compared to the geologic materials would result in large lateral deviation forces and uneven loading on the bit. In turn, this would lead to drilling assembly instability and the bit would essentially bounce and slide on the top or side of the engineered barriers and potentially cause the drill bit to slip off of the DS or WP apex. Consequently, no penetration of the WP would occur. Furthermore, any non-slip contact with the DS or WP would be accompanied by a noticeable increase in drill string torque and reduced rate of penetration as the bit teeth contacted the metallic alloy. At the surface, the driller would recognize these conditions as a lack of drill bit penetration and excessive vibration. High levels of vibration and correspondingly low rates of penetration, such as these observed with poorly designed bits when crossing hard and abrasive formations would prompt the driller to adjust the rotary speed and weight on bit that eliminates shock. In some cases, this could include removing the drilling assembly from the borehole to inspect the bit condition (Putot et al. 2000 [DIRS 167791], p. 118), which would increase the chance for recognition of excessive bit wear and possible recognition that a metallic object had been encountered.

The ability of the drill string to penetrate a waste package as a result of a sudden drop when the drill bit breaks through the top of the emplacement drift and the weight of the drill string free falls and potentially impacts the apex of the engineered barriers was considered. Impacts to a WP and DS and resulting damaged area and rupture condition are determined for the OCB of the waste package as documented in *Mechanical Assessment of Degraded Waste Packages and Drip Shields Subject to Vibratory Ground Motion* (SNL 2007, [DIRS 178851], Section 6.3.2.2). Estimates of impact induced damage to the waste package is a function of impact parameters such as location, angle, and velocity using rigid body analyses (SNL 2007, [DIRS 178851], Section 6.3.2.1). These detailed analyses are used to produce lookup tables of damage values as a function of impact parameters. Results for the TAD-bearing waste package are summarized in Table 6-38 to Table 6-63 of *Mechanical Assessment of Degraded Waste Packages and Drip Shields Subject to Vibratory Ground Motion* (SNL 2007, [DIRS 178851]). Results for the CDSP waste package are summarized in Table 6-64 to Table 6-93 of *Mechanical Assessment of Degraded Waste Packages and Drip Shields Subject to Vibratory Ground Motion* (SNL 2007, [DIRS 178851]).

The rupture condition of a waste package is determined by comparing the maximum effective strain from all elements on the outer and inner surfaces of the OCB to the ultimate tensile strain limit (SNL 2007, [DIRS 178851], Section 6.3.3, Appendix A). For uniaxial tension, the

maximum effective strain limit is 0.57; and for biaxial tension, the maximum effective strain limit can be as low as 0.285, based on a triaxiality factor of 2.0 (SNL 2007, [DIRS 178851], Section 6.3.3, Appendix A). The procedure for determining the rupture condition is described in Section 6.3.2.2.5 (SNL 2007, [DIRS 178851], Section 6.3.2.2.5, Figure 6-25). The maximum effective strain and rupture conditions for waste package-to-pallet damage analyses evaluated over a range of impact velocities are provided (SNL 2007, [DIRS 178851], Tables 6-55 through 6-63 and 6-83 through 6-93). The WP rupture is evaluated for a fully loaded waste package impacting a stationary pallet for impact velocities of 1.00 m/s, 2.00 m/s, 3.00 m/s, 5.00 m/s, 7.00 m/s, and 10.00 m/s (SNL 2007, [DIRS 178851], Section 6.3.2.2.7). For both TAD-bearing and codisposal waste packages, the deformation is insignificant for intact internals, even at the largest impact velocities (SNL 2007, [DIRS 178851], Section 6.3.3.2). There is no rupture calculated for waste packages with intact internals. For WP with degraded internals for both TAD-bearing and codisposal waste packages, an impact velocity of greater than 3.00 m/s is needed to cause severe enough damage to lead to rupture after multiple impacts at that level or greater (SNL 2007, [DIRS 178851], Section 6.3.3.2). Since a typical weight of the drill string is much less than the weight of a fully loaded WP, a ratio of the weight of the drill string to the weight of the waste package is calculated so that the drill string impact can be properly mapped to the appropriate impact velocity evaluated in the seismic analyses. A drill string assembly consisting of the drill bit, drill collar, drill pipe, can be estimated to be approximately 14 mT at a depth of 300 m (Table 6.7-1). The ratio of the drill string weight to the TAD-bearing WP is 14 mT divided by 73.5 mT or approximately 0.19 (Table 6.7-2). For the CDSP WP the ratio is 0.24 (14 mT divided by 58 mT, Table 6.7-2).Using Torricelli's equation (Eq. 6.7-2), the peak impact velocity for the drill string at the waste package outer barrier would be approximately 5.9 m/s for a TAD-bearing WP and 5.7 m/s for a CDSP WP given a drop distance of 1.8 m and 1.6 m respectively (Table 6.7-2).

$$v_f^2 = v_i^2 + 2a\Delta d \qquad \text{(Eq. 6.7-2)}$$

where

v_f = final velocity (or impact velocity of the drill string)

v_i = the initial velocity (0 m/s)

a = acceleration due to gravity (9.8 m/s)

Δd = distance from drift crown to the top of the waste package (Table 6.7-2)

Therefore the equivalent WP velocity for a waste package to pallet impact is the ratio of the weight of the drill string to the weight of the waste package times the velocity of the drill string at impact. An equivalent velocity of approximately 1.0 m/s was calculated for both the TAD-bearing WP and CDSP WP. Given an equivalent impact velocity for the drill string of 1.0 m/s is less than the velocity at which rupture is expected to occur, no penetration of the WP would occur.

6.7.2.3.4 Comparative Material Strength

Assuming that the drilling assembly does not slide off the apex of the DS, then a significant change in down-hole conditions would also be recognized because the failure mechanisms of brittle rock (such as that present at the repository host horizon) and ductile alloys (such as the materials used for the DS and WPs) differ significantly. These changes in failure mechanisms are so significant that specialized down-hole techniques and tools are used to drill through metal. Milling (a technique used for drilling through metal) produces a different failure mechanism than brittle failure that roller bits and hammer bits typically produce. Bits designed for drilling rock would not be efficient for drilling through metal and would likely be seriously damaged, and the milling techniques needed to bore metals (Avallone 1987 [DIRS 103508], pp. 13-63 to 13-64) are not used in rock drilling unless required for specialized applications (e.g., Driscoll 1986 [DIRS 116801], pp. 316 to 319, Figure 10.10 and Figure 10.54).

Brittle materials are characterized by the fact that rupture occurs without any noticeable prior change in the rate of elongation. Thus, for brittle materials under tension, there is no difference between the ultimate strength and breaking strength. Also, under tension, the strain at the time of rupture is much smaller for brittle than for ductile materials (Beer and Johnston 1981 [DIRS 166708], p. 36). In general, brittle materials are weaker in tension than in shear (Beer and Johnston 1981 [DIRS 166708], p. 101), and brittle materials are significantly stronger in compression than in tension (e.g., the tensile strength of concrete is about 10 to 20 percent of its compressive strength; also see Table 6.7-3 for a comparison of rock strength in compression and tension). For brittle materials, strength is typically reported as compressive strength rather than tensile strength, while ductile material strengths are typically determined in tension.

The ductility of a material, such as the alloys used for the DSs and WPs, is usually measured as the percent reduction in area (or the elongation that occurs during a tensile test). Ductile materials, with a minimum elongation in tensile testing, will not fail in service through brittle fracture (Boyer and Gall 1984 [DIRS 155318]), which is the failure mode exhibited by the repository host horizon materials. Also, for ductile metals, the compression strength is generally assumed equal to the tensile strength (Beer and Johnson 1981 [DIRS 166708], p. 584). Generally speaking, values obtained for the yield strength and ultimate strength of a given material are only about half as large in shear as they are in tension, and the shear modulus is generally less than one-half, but more than one-third, of the modulus of elasticity of that material (Beer and Johnston 1981 [DIRS 166708], pp. 68 and 69).

Therefore, if the differences between milling and rotary drilling tools are ignored and rotary bits could be used to penetrate the engineered barriers, a measure for comparing strength properties between brittle and ductile materials is needed. One such parameter is a comparison of the modulus of elasticity of these differing materials. Because of the lack of elongation, the stress-strain diagram for brittle materials is generally linear, and the modulus of elasticity provides a convenient method for comparing material properties between brittle and ductile materials. This also suggests that comparison of tensile strength of brittle materials to yield strength of ductile materials may also be appropriate. Comparison of the compressive strength of rock materials and tensile strength of alloy is also appropriate. Furthermore, the reported shear modulus could be compared (if available) or a value of twice to three times the shear modulus could be compared to the modulus of elasticity.

Various rock properties for materials at Yucca Mountain are shown on Figure 6.7-4 and in Table 6.7-3, including uniaxial compressive strength, tensile strength, and modulus of elasticity (Young's modulus). Based on the design drawings and data tracking numbers (DTNs) cited, the yield strength, tensile strength, and modulus of elasticity for the DS and WP materials are shown in Table 6.7-4.

Studies that have been conducted to correlate operational parameters to the rate of penetration of the drill bit indicate that the rate of penetration may range from inversely proportional to the square of the strength of the material being drilled to inversely proportional to the strength of the material, all other factors being equal (Bourgoyne et al. 1986 [DIRS 155233], Equation 5-19; Kahraman 2000 [DIRS 167761], Equations 8, 12, and 14). Putot et al. 2000 [DIRS 167791], p. 123) suggests, at least for balling tendencies in shales and for a given weight on the bit, that drilling performance collapses upon a doubling of the rotary speed. Assuming that a change in the penetration rate by a factor of 1.5 or greater (increase) or 0.66 or less (decrease) (i.e., some condition occurring before performance collapse) would be sufficient to be noticed by a driller, a change in compressive strength of materials by a factor of 1.5 (or possibly less if one assumes the inverse square relationship presented by Bourgoyne et al. 1986 [DIRS 155233]) would cause a significant change in drilling conditions that would be recognized by the driller.

Table 6.7-3 indicates that the mean compressive strength of the rock material ranges from 19.3 MPa to 188.8 MPa. At room temperature, the tensile strength of the DS materials ranges from 345 MPa to 895 MPa (Table 6.7-4). Thus, the factor of compressive strengths ranges from about 1.8 (345/188.8) to as great as 46 (895/19.3). The tensile strength of the WP material at room temperature ranges from 550 MPa to 802 MPa (Table 6.7-4). This represents factors of 2.9 (550/188.8) to as great as 42 (802/19.3). If one conservatively assumes the yield strength of the engineered barrier materials is comparable to rock compressive strength, the factors decrease. For the DS material at room temperature, the factor ranges from 1.5 (275/188.8) to 23 (450/19.3). For the WP material at room temperature, the factors range from 1.3 (240/188.8) to as great as 21 (403/19.3). However, given that all WPs include Alloy 22 (UNS N06022) material in the outer barrier, the lower end of the range is bounded at a factor of 1.9 (358/188.8). Therefore, at room temperature, there is a minimum factor of 1.9 for the WPs and 1.5 for the DSs. If one assumes an inverse proportionality of rock strength to rate of penetration, the penetration rates would decrease to less than 67 percent of the rock penetration rate when intersecting a DS and to less than 53 percent of the rock penetration rate when intersecting a WP and, therefore, be recognizable, as previously discussed.

At elevated temperatures, such as those during the thermal period (e.g., 200°C); the strength properties of the DS material are reduced. The factor reduces in range from 1.1 (207/188.8) to as great as 12 (228/19.3), based on compressive strength. However, the properties of the Alloy 22 (UNS N06022) outer barrier are not as significantly reduced. The factor for compressive strengths for the elevated temperature ranges from 3.5 (662/188.8) to 36 (701/19.3). The minimum factor of 1.1 for the DS and rock strength comparison at elevated temperature would not by itself produce a sufficient change in penetration rate to be noticed by a driller. However, further penetration to a WP, with a larger compressive strength change, would produce a sufficiently reduced penetration rate.

Furthermore, the mean tensile strength of the brittle rock units is reported to range from 7.9 MPa to 10.9 MPa (or approximately 6 percent of the corresponding mean compressive strength). These rock tensile strengths are at least a factor of 19 less than those of the ductile engineered barrier materials, even at elevated temperatures. Even conservatively assuming an equivalence of the yield strength of a ductile material to tensile strength of brittle material generates a difference of a factor of 13.

Similarly, the mean modulus of elasticity for the rock materials is on the order of 6.9 to 33.6 GPa. By contrast, for the ductile alloys, the modulus of elasticity ranges from 107 to 206 GPa, representing a minimum factor of 3.2 different from the rock properties. These differences in tensile strength and modulus of elasticity between the brittle rock and ductile engineered barrier materials would further contribute to lack of drill bit penetration and excessive vibration.

Finally, the recognizable differences in penetration rate or vibrations are only applicable in the improbable situation of a rock drill bit hitting sufficiently near the engineered barrier apex to avoid bouncing or sliding (such as by impacting a metal crack) to initiate penetration into the engineered barrier. It is more likely that rotary bits for rock, which are not designed for drilling in metal, would simply bounce and slip off either the DS or WP.

The discussion provided above would be applicable even if the DS or one of the materials used in the WP were degraded to the point where structural integrity were lost or, in the case of the DS, the interlock mechanism were bent and penetrated by the drilling assembly.

Summary of Waste Package Penetration by Drilling Analysis

Selection of a bit for drilling involves knowledge of the characteristics of the rock. As indicated in Tables 6.7-1-1 and 6.7-2-2, there are significant differences between the tensile strengths and other material properties of the geologic units at Yucca Mountain and the materials for the DS and WP. Because the materials used in the DSs and WPs have high tensile strengths, yield strengths, and increased modulus of elasticity compared to the host rock properties, the tooth of a roller bit cannot penetrate enough to cause sufficient strain for chipping to occur. Rather, if contact with the DS occurs, the rotation of the bit would result in a tearing or shearing action with associated and recognizable high torque values. Consequently, the ductility of the metals makes them nearly impenetrable by techniques used in drilling rock. Boring in metals typically utilizes a milling technique. The down-hole milling tools needed to penetrate the DS and WP are not typically used in groundwater exploration, and use of such tools would be a clear indicator of recognition of penetration of some type of metallic, anthropogenic structure.

6.7.2.4 Earliest Time of Waste Package Penetration by Human Intrusion

Conclusions based on information presented above suggest that a human intrusion event, if it were to occur before the WPs and DSs had sufficiently degraded, would not happen without recognition by the drillers. General corrosion of the DS is not expected to thin the DS plates significantly before 230,000 years (Section 6.7.2.1) and seismic ground motion cracks are not expected to affect a rotating drill bit because the failure mode and drill bit interaction are significantly different for rock and metals, as discussed in Section 6.7.2.3. In general, until a

breach of the DS occurs, the structural integrity of the WP is maintained, providing an additional barrier to drill-bit penetration. The analysis provided in this section indicates that an unrecognized intrusion will not occur prior to 10,000 years following closure of the repository. For the TSPA-SEIS Human Intrusion Scenario, the WP degradation is conservatively ignored and the human intrusion event time, based on DS corrosion and observable effect on the drilling system is taken to be no less than 200,000 years. Figure 6.7-5 shows the calculated probability that a DS has failed by a given time (t) including the general corrosion and DS plate fragility (DS rupture) failure modes as documented from the TSPA-SEIS results. Figure 6.7-5 indicates a greater than 1 in 10 probability of DS failure after approximately 200,000 years post closure. Although some uncertainty exists about the timing of when penetrating a WP would not be detected, an assumption of penetration at 200,000 years is appropriate since WP degradation models under nominal conditions indicate that it is unlikely that the time to initial breaching of the WPs will occur before 225,000 years post closure. Therefore, for the stylized Human Intrusion Scenario, the WP corrosion is conservatively ignored and the assumed DS failure at 200,000 years is considered to be the earliest time a driller could penetrate a WP without recognition.

6.7.3 TSPA-SEIS Implementation

The stylized Human Intrusion Scenario is based on the human intrusion scenario at NRC proposed rule at 10 CFR 63.322 [DIRS 180319], and the individual protection standard for a human intrusion of the repository at 10 CFR 63.321 [DIRS 178394].

6.7.3.1 EBS Transport for Human Intrusion

Conceptual Model—The human intrusion borehole is assumed to be drilled from the ground surface (at a random location within the footprint of the repository), through the DS and a single WP (top and bottom) to the water table. All cladding, either CSNF or DSNF, is assumed destroyed when drilling intersects a WP. The initial fraction of failed cladding and the fraction of fuel available for corrosion (Fuel_Split_Fraction) are set to one. The WP type is randomly selected, either CDSP WP or CSNF WP. The location of the intrusion is also unknown and is therefore randomly placed in one of the five repository percolation subregions. After penetration of the WP via a drilling event, water will flow into the WP and the waste form degradation and mobilization will occur. Nominal Scenario Class submodels for Waste Form Degradation and Mobilization (Section 6.3.7) and EBS TH Environment (Section 6.3.2) were applied in the Human Intrusion Scenario. Radionuclide mass is released from the intruded WP to the EBS Transport submodel (described in Section 6.3.8).

Implementation—For a Human Intrusion event, the WP type (CSNF or CDSP) and WP location within the repository footprint need to be characterized. These two properties, WP type and WP location, are treated as aleatory uncertainties and randomly selected from assigned probability weights:

- The WP type is sampled randomly by assigning probability for a CSNF WP equal to the fraction of CSNF WPs in the repository to the total number of WPs in the repository (combined CSNF and CDSP WPs). The probability of CDSP WP is assigned the remaining percentage. The number of WPs projected to be emplaced in the repository

is 11,629 (Section 6.3.7, Table 6.3.7-1). There are 8,213 CSNF WPs (including approximately 200 Naval SNF WPs) and 3,416 CDSP WPs (Section 6.3.7, Table 6.3.7-1). Thus, there is about 70 percent probability the intruded WP is a CSNF WP type and about 30 percent probability the intruded WP is a CDSP type.

- The location of the WP intersected by a Human Intrusion drilling event can be randomly selected based upon the areal distribution of the five percolation subregions that have been defined over the repository horizon as defined by the EBS TH Environment Model Component described in Section 6.3.1. The mean infiltration, glacial-transition climate percolation flux values at the base of the PTn for each of the 3,264 MSTHM Process Model subdomains are used to group each of the subdomains into one of five repository percolation subregions (Section 6.3.2). The probability of an event (e.g., Human Intrusion failed WP) occurring in any of the five percolation subregions is the same as the quantile distribution used to define the percolation subregions (i.e., 5 percent, 25 percent, 40 percent, 25 percent, and 5 percent).

Once the WP type and percolation subregion are selected, the representative temperature and relative humidity time histories are applied for calculating the waste form degradation rate, in-package chemistry, and transport properties in the EBS. The seepage flux through the intruded WP is applied by taking the percolation flux at the base of the PTn (supplied by the MSTHM; Section 6.3.2) for the selected percolation subregion. The percolation rates at the base of the PTn are generally higher than the calculated seepage rates which include the effects of the drift. The Seepage DLL, used to compute the drift-scale seepage, is exercised using the same method as the igneous intrusion modeling case to get the percolation flux without flow focusing effects at the drift boundary (Section 6.5.1). Potential flow focusing effects of the borehole are not included. The percolation flux (a Darcy flux) is converted into a volumetric flux by multiplying the percolation flux with a borehole cross-sectional area calculated using a 20.3-cm-borehole diameter (an assumption that is derived from a borehole area of 0.0324 m^2, based on current drilling practices for a typical water well (Driscoll 1986 [DIRS 116801])). The entire calculated volumetric flux is used as the flow through the WP for the advective component of the EBS transport calculation. For the diffusive component of the EBS transport calculation, the diffusive area is set equal to the cross-sectional area of the borehole. And the downstream concentration boundary condition is set as a zero concentration to maximize diffusion out of the WP. This is done by giving the invert a very large water volume. The borehole flux was assumed to flow directly into the penetrated WP; no diversion of the water by the DS or WP is considered. This is a mathematical construct used to maximize diffusion. The concentration flowing to the UZ borehole is not zero, but that the mass flux to the UZ borehole is calculated by the sum of the advective and diffusive mass that is leaves the WP boundary.

For the expected dose calculations, 9,000 realizations are run for each combination of 30 aleatory inputs and 300 Monte Carlo samples of epistemic parameters. There are three parameters subject to epistemic uncertainty, WP type, percolation subregion, and SZ source region The 300 epistemic samples match the development Nominal Scenario Class v5.000 model run, which is also performed for 300 realizations. The 30 aleatory configurations apply 30 different human intrusion futures for each epistemic sample. The futures are determined by sampling uncertainty distributions.

6.7.3.2 UZ Transport for Human Intrusion

Conceptual Model—The radionuclide mass (both dissolved and colloidal) released from the WP was assumed to be transported down the human intrusion borehole to the water table. The borehole transport pathway was assumed to be a degraded, uncased borehole, with properties similar to a fault pathway in the UZ. The implementation of the borehole transport pathway below the potential repository in the Human Intrusion Scenario is a one-dimensional pipe pathway. The mass released from the intruded WP is passed to the one-dimensional pipe that simulates the borehole in the UZ beneath the WP. The properties that define the borehole fill are chosen to stay consistent with the near-drift rock properties described in the UZ Transport Model (described in Section 6.3.9). The volumetric flux was assumed to be the same as in the WP. The transport path length through the borehole is determined to be the vertical path length between the repository and the future water table. Because the repository host rock and water table elevations change over the UZ and SZ transport domains, the shortest possible transport path length is conservatively chosen.

Implementation—A schematic cross-section of a borehole bisecting the repository system and intruding through the underlying UZ to the water table is shown on Figure 6.7-6. The borehole is conceptualized to be filled with the rubble of collapsed matrix blocks that have preferential pathways such as fractures similar to the fractures in the undisturbed host rock near the drift (Figure 6.7-7). The fracture properties such as fracture aperture, porosity, and frequency (Table 6.7-5) are assumed to be the same as that for the rock type near the drift (such as the TSw unit) and to be consistent with the property sets used by the UZ Transport Model.. For model simplification, these values do not vary with penetration depth, although the surrounding rock properties may change. Table 6.7-6 identifies and defines calculated fracture properties associated with the conceptualized fracture geometry relative to the borehole that was used for the transport through the Human Intrusion borehole pathway. The number of vertical fractures that cut through the borehole is determined by considering the fracture frequency (calculated to be about four fractures per meter) and comparing it to the diameter of the borehole (about 0.2 m), which is derived from the circular drill area of 0.0324 m^2, based on current drilling practices (Driscoll 1986 [DIRS 116801]). This results in less than one fracture per borehole diameter, which is rounded up to be one fracture for the borehole. Assumption of vertical orientation of the fractures is consistent with the conceptualization of fractures in the UZ Transport model using finite-element, heat and mass transfer code (FEHM) (Section 6.3.9). The width of the fracture is calculated by assuming that the fracture cuts across the borehole and, depending on where it cuts through the borehole, the width could be as much as the diameter and as small as to be nearly zero. Thus, an average width is calculated by dividing the drill area by the diameter. The fracture aperture and fracture porosity (fraction of the area occupied by the fracture) is considered fixed at 0.00264 m and 0.0105, respectively, which are average values for Group 8 rock type. No uncertainty is applied to these parameters as it is not currently known how the range of uncertainty would be affected by a borehole that cuts across several lithologic units. The collapsed matrix blocks fill up most of the borehole volume (about 99 percent). Diffusion of radionuclides from the fractures into the matrix blocks can occur. The diffusive distance between the fracture and matrix is set equal to half the distance between two fractures (about 0.125 m), and the entire surface of the fracture wall (equal to the perimeter) is assumed to be wetted for diffusive transfer to the matrix (Figure 6.7-7). All of the water flowing through the borehole is passed through the vertical fracture, which is the most conductive zone in the

borehole. The fractures are assumed to be free flowing with no infill or obstructions that could potentially retard radionuclide transport through the fractures. A fracture dispersivity value of 10 m is assumed in the fracture that is consistent with the values used in the UZ Transport Model (SNL 2007 [DIRS 181006], Section 4.1.6).

The saturation values for the fracture and matrix along with the matrix density and porosity are taken from the EBS-UZ Interface Model described in Section 6.3.8. Within the matrix media, the radionuclides are given the devitrified UZ Kd values as representative for the entire pathway, while there is no retardation modeled for the mass transported irreversibly on colloids. No radionuclide sorption is modeled in the fractures.

A flat lying water table beneath the repository is estimated to be located at about an 850 m elevation, based on the water table rise estimated to occur during the glacial transition climate period (SNL 2007 [DIRS 181006], Section 6.4.8). For the repository elevation, a value of 1,040 m is assumed as all repository drifts are at elevations of 1,039 m or higher (SNL 2007 [DIRS 179466], parameter 01-02). Thus, the path length of the borehole from the repository to the SZ is set at 190 m.

6.7.3.3 SZ Transport for Human Intrusion

Conceptual Model—The transport of radionuclides through the SZ in the Human Intrusion Scenario was identical to the Nominal Scenario Modeling Case, with one exception. From the borehole, the radionuclides are passed to one of the four SZ source regions (SZ region). One of each of the four SZ source regions is selected that corresponds to the EBS percolation subregion intersected during the human intrusion event.

Implementation—In order to apply spatial correlation between the EBS percolation subregions (where the radionuclides enter the borehole) and SZ source regions (where the radionuclides exit the borehole), the five EBS percolation subregions are mapped to the four SZ source regions. The relative areal fraction of the five EBS percolation subregions within the four SZ source regions is determined and represents the probability of each SZ source region to accept the radionuclides released from the borehole. A more detailed description of the four SZ source regions (quadrants) can be found in *Particle Tracking Model and Abstraction of Transport Processes* (SNL 2007 [DIRS 181006] Section 6.5.16).

There is a mapping of the UZ nodes at the repository horizon with the five percolation subregions. There are 560 UZ nodes included in the five percolation subregions, along with their geographic locations in UTM coordinates. The 560 UZ node locations sorted by percolation subregion are mapped to the SZ quadrants, and the fraction of each of the five percolation subregions to the four SZ regions is calculated (Table 6.7-7).

6.7.3.4 Mean Annual Dose Submodel for the Human Intrusion Scenario

A schematic illustration of the implementation of human intrusion in the TSPA-SEIS is provided in Figure 6.7-8. The TSPA-SEIS calculates the mean annual dose for the Human Intrusion Scenario using a two-step process. First, the TSPA-SEIS generates a set of realizations and each realization results in an annual dose history for a single human intrusion event. In the second

step, the mean annual dose history is calculated using a sum of the annual dose histories from the set of realizations generated in the first step.

In Step 1, the annual dose history is evaluated for each set of realizations. Each realization is associated with a single human intrusion occurring at a specified time (200,000 years postclosure). For each realization, TSPA-SEIS parameter values are selected for each of the processes affecting the estimate of annual dose. The seepage water chemistry and thermal-hydrologic properties are used to calculate waste form degradation and radionuclide mobilization. Using these inputs, the fate of the mobilized radionuclides is evaluated using the Nominal Scenario Class submodels for radionuclide transport in the EBS and SZ and Biosphere. In Step 2, the sum accounts for both aleatory uncertainty associated with the randomness of the location of an event and their impacts on the repository system and epistemic uncertainty in the parameters describing these impacts (Section 6.1.3).

6.7.4 Model Component Consistency and Conservatism in Assumptions and Parameters

To enhance understanding of the complex interactions within the TSPA-SEIS, a discussion of consistency among model components and submodels and identification of conservative assumptions in abstractions, process models, and parameter sets supporting the Human Intrusion Scenario are discussed below. Many of the nominal abstractions, process models, and parameter sets are used in the Human Intrusion Scenario and, therefore, many of the discussions of the implementation provisions in Section 6.3 apply to the Human Intrusion Scenario.

6.7.4.1 Consistency of Assumptions

WP and DS Material Corrosion in the Human Intrusion Scenario—General corrosion and SCC of the WP and DS materials are not applied to the WP/DS pair penetrated by a human intrusion event. The WP/DS general corrosion and SCC submodels are turned off for the Human Intrusion Modeling Case.

Effect on the TSPA-SEIS—The early penetration time of a WP/DS pair of 200,000 years postclosure during a Human Intrusion Scenario event is a conservative assumption. After the WP is penetrated, the entire waste form is exposed to the water flux through the WP. Applying the general corrosion model would not result in an earlier failure time (as demonstrated in Section 6.7.2). The radionuclide releases will be predominately via advective transport. Additional SCC cracks or general corrosion patches would not increase the volumetric water flux or mass flux of radionuclides released from the WP. This assumption will have no effect on the results of the Human Intrusion Scenario Modeling Case.

6.7.4.2 Identification of Conservatisms in Submodels and Abstractions

Human Intrusion Event Time—The probability associated with a human intrusion event time of 200,000 years postclosure assumes a WP would be degraded sufficiently to be undetected by drillers using the common techniques and practices that are currently employed in exploratory drilling for ground water in the region surrounding Yucca Mountain (NRC Proposed Rule 10 CFR 63.322(c) [DIRS 180319]). Assuming an early event time is conservative in respect to the probability of WP failure.

UZ Borehole as a Fracture Pathway—This fracture is conceived to be a highly conductive zone with elevated flow velocities through the fracture void space. Matrix diffusion into the host rock occurs and depends on fracture frequency. Using the fracture frequency for the UZ host rock (~ 4 per meter) yields only one fracture, given the diameter of the borehole. Matrix diffusion over the length is calculated as half the distance from the nearest fracture. Therefore, a limited amount of matrix medium is used to define the matrix diffusion zone between fractures in the pipe pathway.

Fewer fractures result in less surface area in the pipe pathway. A smaller surface area results in less sorption into the UZ rock matrix as the radionuclides travel through the UZ pipe pathway.

UZ Borehole Pathway Length—The Human Intrusion Scenario assumes the shortest possible transport path length. The conservative estimate for future water table rise places a flat water table at an 850 m elevation, reached during the glacial transition climate period (SNL 2007 [DIRS 181006], Section 6.4.8). Based on elevations reported in *Repository Design, Repository/PA IED Subsurface Facilities* (BSC 2003 [DIRS 161727]), a value of 1,040 m is assumed for the repository drift elevation (all repository drifts are at elevations of 1,039 m or higher).

A conservative length of the borehole from the repository to the SZ is set at 190 m. This conservatism tends to shorten radionuclide transport times.

6.7.5 Alternative Conceptual Model(s) for the Human Intrusion Scenario for TSPA-SEIS

An important reason for considering ACMs is to help build confidence that plausible changes in modeling assumptions or simplifications will not change the conclusions regarding subsystem and total system performance. Section 6.2 outlines the general consideration and treatment of ACMs used to support the TSPA-SEIS. Conservatism at the subsystem level was used to select the best ACM rather than quantitatively propagate multiple ACMs to the TSPA-SEIS. Generally, additional uncertainty is incorporated into the selected conceptual model if more than one ACM is deemed appropriate for use rather than considering multiple ACMs in the TSPA-SEIS. If an ACM appears to be significant at the subsystem level, then an appropriate abstraction is developed for that ACM for consideration within the TSPA-SEIS. The result of the process is documented within the individual analysis and model reports. It is important to note that treatment of ACMs within the individual analysis and model reports may differ significantly to be consistent with available data and current scientific understanding. ACMs related to individual submodels used in the Human Intrusion Scenario calculations are discussed in relevant Section 6.3 sections. There are no ACMs specific to the stylized Human Intrusion Scenario.

INTENTIONALLY LEFT BLANK

Table 6.7-1. Specifications of Drilling Components

Parameter		Source	Description
Length of Drill String	300 m	SNL 2007 [DIRS 179466], Table 4-1	Assumed depth from the surface to the repository horizon. Based upon design information for minimum standoff distance from repository to water table.
Weight of Drill Steel	20 lb/ft (29.8 kg/m)	American Petroleum Institute 1992. Specification for Drill Pipe. API Spec. 5D, 3rd Edition, Table 6-1, 4.5-in drill pipe.	Drill pipe weight for standard 4.5 inch OD well pipe.
Length of Drill Collar	30 ft (9.1 m)	http://www.grantprideco.com/drilling/catalog/drilling_Catalogs.asp , drill_collars.pdf, p. 99, drill collar number NC 44-62	Typical drill collar length for 6.25 inch OD drill collar.
Number of Drill Collars	4	NA	Assumed 100 ft of drill collar (10% of depth), based on common drilling practices.
Weight of Drill Collar	90.52 lbs (41.0 kg)	http://www.grantprideco.com/drilling/catalog/drilling_Catalogs.asp , drill_collars.pdf, p. 99, drill collar number NC 44-62	Typical weight for 6.5 inch OD drill collar.
Weight of Drill Bit	38 kg (83 lb)	http:// www.varelintl.com/content/released/Varel_2006_RollerconeCatalog-FINAL.pdf : Bit Weights Table, p.27, 8.5 " bit	Assumed approximately 8" borehole diameter assumption that is derived from the circular drill area of 0.0324 m^2, based on current drilling practices for a typical water well (Driscoll 1986 [DIRS 116801]).
Total Weight of Drill String Assembly	13.8 mT	NA	(Length of Drill Sting × Weight of Drill Steel) + (Length of Drill Collar × Number of Drill Collars × Weight of Drill Collar)+ Weight of Drill Bit

Table 6.7-2. Waste Package Specification and Design Dimensions.

Parameter		Source	Description
Drop Height (TAD-bearing)	1.80 m	SNL 2007 [DIRS 179354], Figure 4-1, *In-Drift Configuration.*	Distance from drift crown to top of DS plus the distance from the DS to the top of WP.
Drop Height (CDSP WP)	1.63 m		
Nominal loaded mass for TAD-bearing waste package	162,055 lbm (73.5 mT)	SNL 2007 [DIRS 179394], Table 4-3	
Nominal loaded mass for CDSP waste package	127,870 lbm (58 mT)	SNL 2007 [DIRS 179567], Table 4-9	

Table 6.7-3. Uniaxial Compressive Strength and Young's Moduli by Rock Unit

Rock Unit	Uniaxial Compressive Strength Mean (MPa)	Tensile Strength Mean; Range (MPa)	Shear Modulus (GPa)	Elasticity (Young's Modulus) Mean; Range (GPa)
Topopah Springs Tuff – upper lithophysal zone (Tptpul)	19.3	–	–	13.0; 5.0–21.5
Topopah Springs Tuff – lower lithophysal zone (Tptpll)	23.8	8.3; 3.2–14.3	0.80–8.21	6.9; 5.0–9.2
Topopah Springs Tuff – middle nonlithophysal zone (Tptpmn)	188.8	10.9; 4.3–16.8	–	33.6; 13.4–47.3
Topopah Springs Tuff – lower nonlithophysal zone (Tptpln)	129.9	7.9; 4.8–13.7	–	33.6; 13.4–47.3

Sources: Mean Uniaxial Compressive Strength data (also referred to as Ultimate Strength) for the Tptpul and Tptpll are calculated as the mean of the strength data from SNL (2007 [DIRS 166107], Table E-9). The Mean Uniaxial Compressive Strength of the Tptpmn unit is from SNL (2007 [DIRS 166107], Table E-14). The Mean Uniaxial Compressive Strength of the Tptpln is calculated as the mean of the strength data from DTN: MO0408MWDDDMIO.002 [DIRS 171483], Calculation Files\Material property\rock mass strength v2.xls, worksheet Intact Strength (using Ultimate Differential Strength data with a Confining Pressure of either 0 or 0.1 MPa).

Tensile Strength taken from (SNL 2007 [DIRS 166107], Table E-70).

Shear Modulus estimated for rock mass qualities 1 through 5 and taken from (SNL 2007 [DIRS 166107], Table E-10).

Mean for Elastic Modulus (Young's Modulus) based on data from (SNL 2007 [DIRS 166107], Tables E-6 and E-9).

Table 6.7-4. Material Properties for Drip Shield and Waste Package Fabrication

Engineered Barrier Material	Use	Yield Strength at 0.2% Offset (MPa)	Tensile Strength (MPa)	Modulus of Elasticity (GPa)
Titanium Grade 7[a] and Grade 16 (at room temperature)	Drip Shield	275–450	345	106.87
Titanium Grade 7[a] and Grade 16 (at 400°F/204°C)	Drip Shield	138–152	207–228	- -
Titanium Grade 24	Drip Shield	–	895[b]	113.8[c]
Alloy 22 (UNS N06022) (at room temperature)[d]	Waste Package	358–403	765–802	206
Alloy 22 (UNS N06022) (at 400°F/204°C)[d]	Waste Package	262–303	662–701	196
Type 316 N Grade Stainless Steel (minimum properties)[e]	Waste Package	240	550	196

[a]DTN: MO0003RIB00073.000 [DIRS 152926] for Titanium Grades 7 and 16.
[b]Tensile strength for Titanium Grade 24 (ASME 1998 [DIRS 145103], Section II, Table 1).
[c]Modulus of Elasticity for Titanium Grade 24 (ASM International 1990 [DIRS 141615], p. 621).
[d]DTN: MO0003RIB00071.000 [DIRS 148850] for Alloy 22 (UNS N06022).
[e]DTN: MO0003RIB00076.000 [DIRS 153044] for Type 316N.

Table 6.7-5. Borehole Properties used in UZ Flow and Transport Calculations

Parameter Name	Description	Parameter Value	Reference
HI_UZ_Borehole_Length	Distance between the repository horizon elevation and the estimated maximum water table elevation during the Glacial Transition Climate.	190 m	(SNL 2007 [DIRS 181006], Section 6.4.8) and (BSC 2003 [DIRS 161727])
HI_UZ_Borehole_Disp	UZ borehole fracture dispersivity.	10 m	(SNL 2007 [DIRS 181006], Section 4.1.6)
HI_UZ_Fracture_Aperture	Distance between fracture openings in UZ borehole. Aperture, 2b (m), is calculated using fracture porosity and frequency distribution for rock units closest to the repository horizon (Group 8 or tswF[4,5]).	0.00264 m	(SNL 2007 [DIRS 181006], Table 6-15)
HI_Drill_Patch_Area	Borehole cross-sectional (circular) area. Also referred to as the drill patch area which is the area assumed to be affected by the intruding drill bit.	0.0034 m^2	(Driscoll 1986 [DIRS 116801])
HI_UZ_Fracture_Porosity	Half the distance between two fractures in the UZ borehole for rock units closest to the repository horizon (Group 8 or tswF[4,5]). Also equal to HI_UZ_Fracture_Fraction.	0.0105	(SNL 2007 [DIRS 181006], Table 6-15)

Table 6.7-6 Borehole Fracture Properties used in UZ Flow and Transport Calculations

Parameter Name	Description	Parameter Value
HI_UZ_Frac_Freq	The number of fractures per meter in host rock. Value is used as estimate of fractures in borehole and is calculated as fracture porosity divided by fracture aperture.	~4 1/m
Diff_Distance_To_Matrix	The distance between the fracture and matrix set equal to half the distance between two fractures.	~0.125 m
Radius_Drill_Patch	Radius of the borehole equal to the square root of the circular borehole cross-sectional area (drill patch area) divided by pi.	~0.101 m
Avg_Width_Fracture	Assuming the fracture is vertical in orientation and is cross-cutting the borehole, the fracture width is a function of the bisecting location relative to borehole center (Figure 6.7-7). This width can vary from a minimum value approaching zero to a maximum value equal to the borehole diameter (~0.2 m). Therefore, an average width is calculated by dividing the drill patch area by the borehole diameter.	~ 0.160 m
Fracture_Plan_Area	Cross-sectional (rectangular) area of the fracture. Equal to the product of the fracture aperture and average fracture width.	~0.0004 m^2
Fracture_Perimeter	The length of all sides of the rectangle created by fracture aperture and fracture width.	~0.324 m

Source: UZ Transport model parameters used to calculate the values listed in the table taken from DTN: LA0701PANS02BR.003_R2 [DIRS 180497].

Table 6.7-7. Fraction of Percolation Subregion Bin Assignments by SZ Source Region

Fraction of Percolation Subregion Bin Assignments by SZ Source Region					
	B1	B2	B3	B4	B5
SZ1	0.1071	0.3786	0.3973	0.4929	0.6071
SZ2	0.8929	0.4571	0.2857	0.1000	0.0000
SZ3	0.0000	0.1357	0.3125	0.4071	0.3929
SZ4	0.0000	0.0286	0.0045	0.0000	0.0000
Total	1	1	1	1	1

Source: Calculation file *PS_EBSmaptoSZ.xls*.
DTN: MO0708TSPAGENT.000 [DIRS 183000].

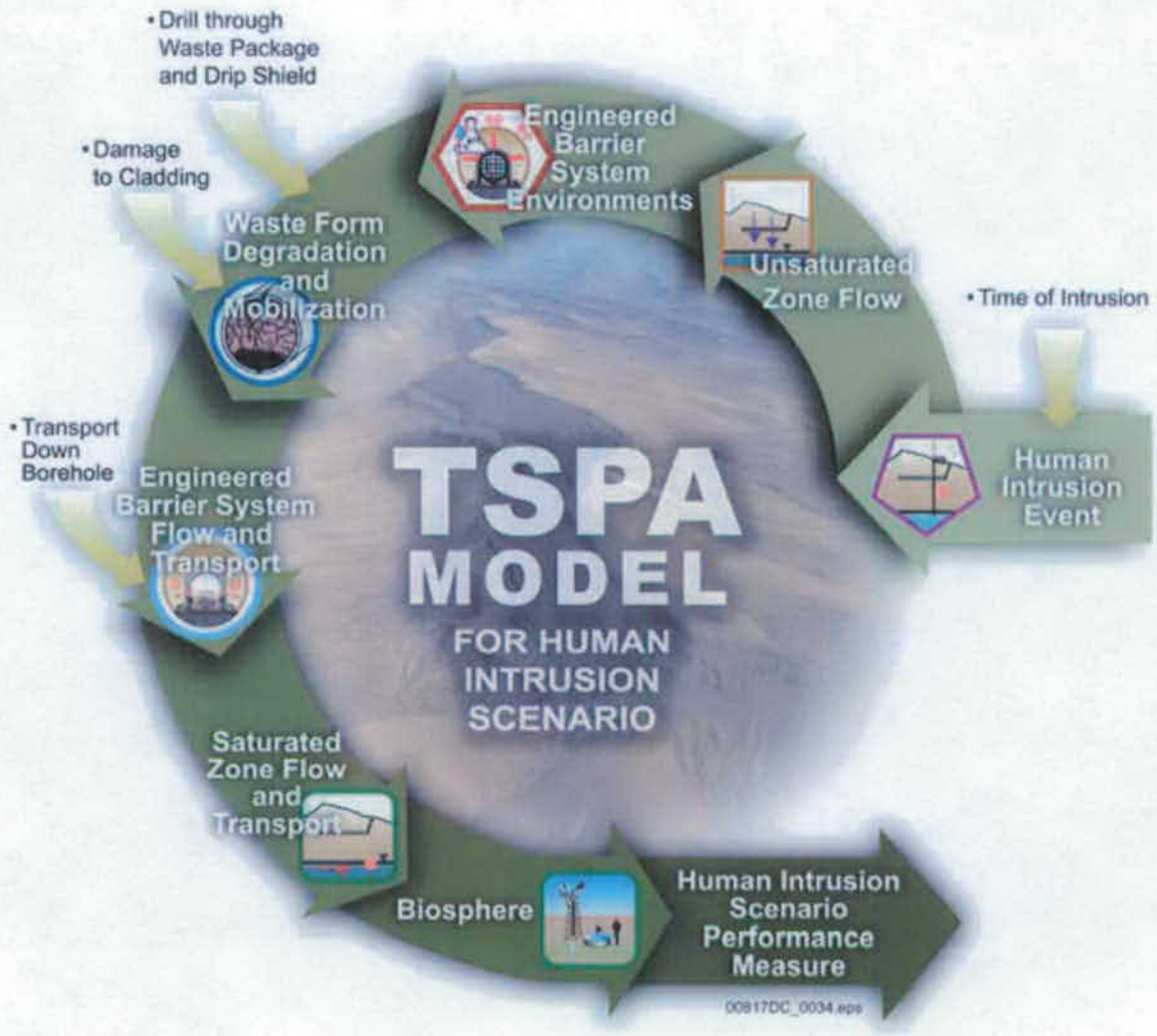

Figure 6.7-1. Schematic Representation of the TSPA-SEIS Components for the Human Intrusion Scenario

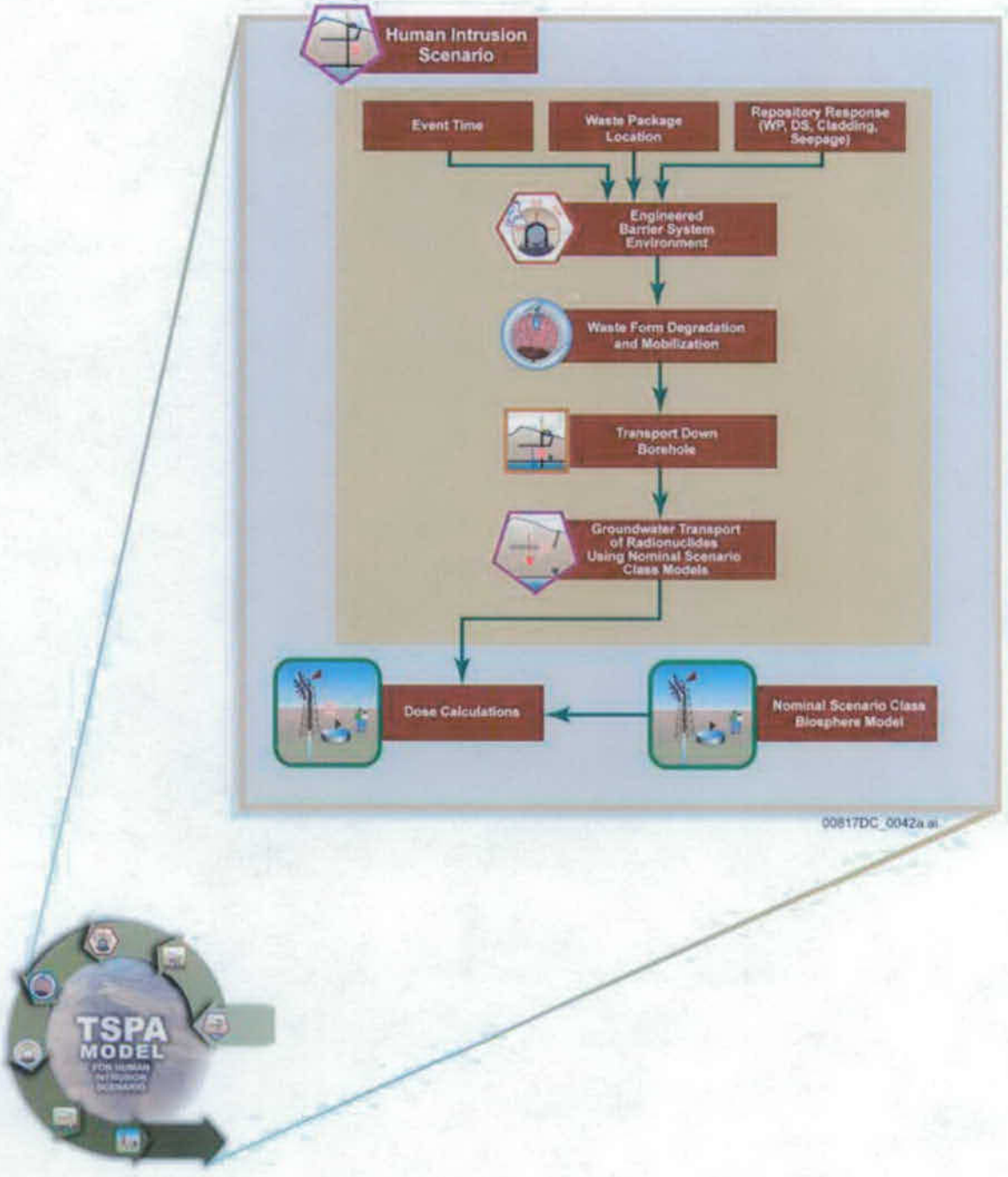

Figure 6.7-2. Information Flow Diagram for the Human Intrusion Scenario in the TSPA-SEIS

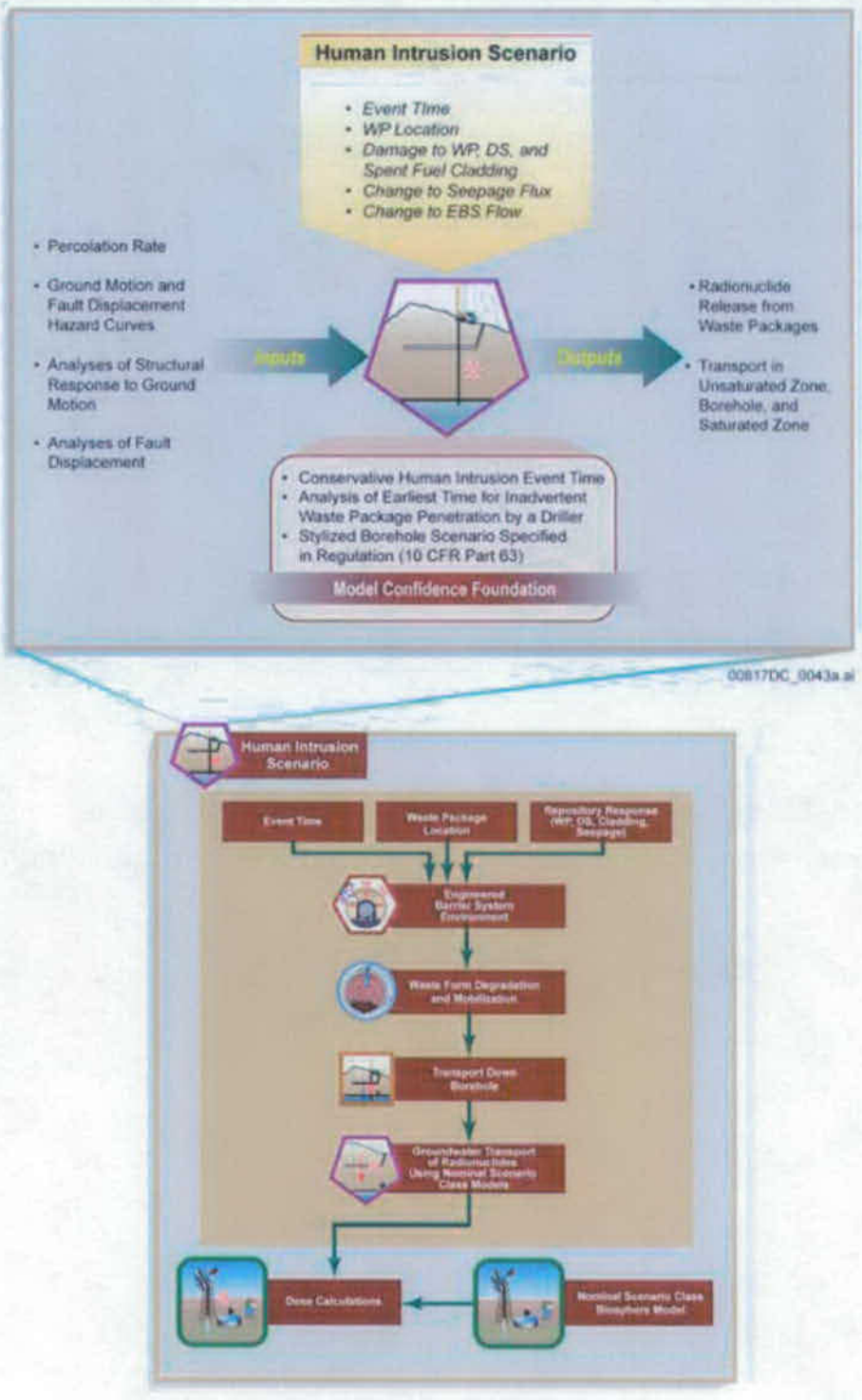

Figure 6.7-3. Inputs, Outputs, and Basis for Model Confidence for the Human Intrusion Scenario

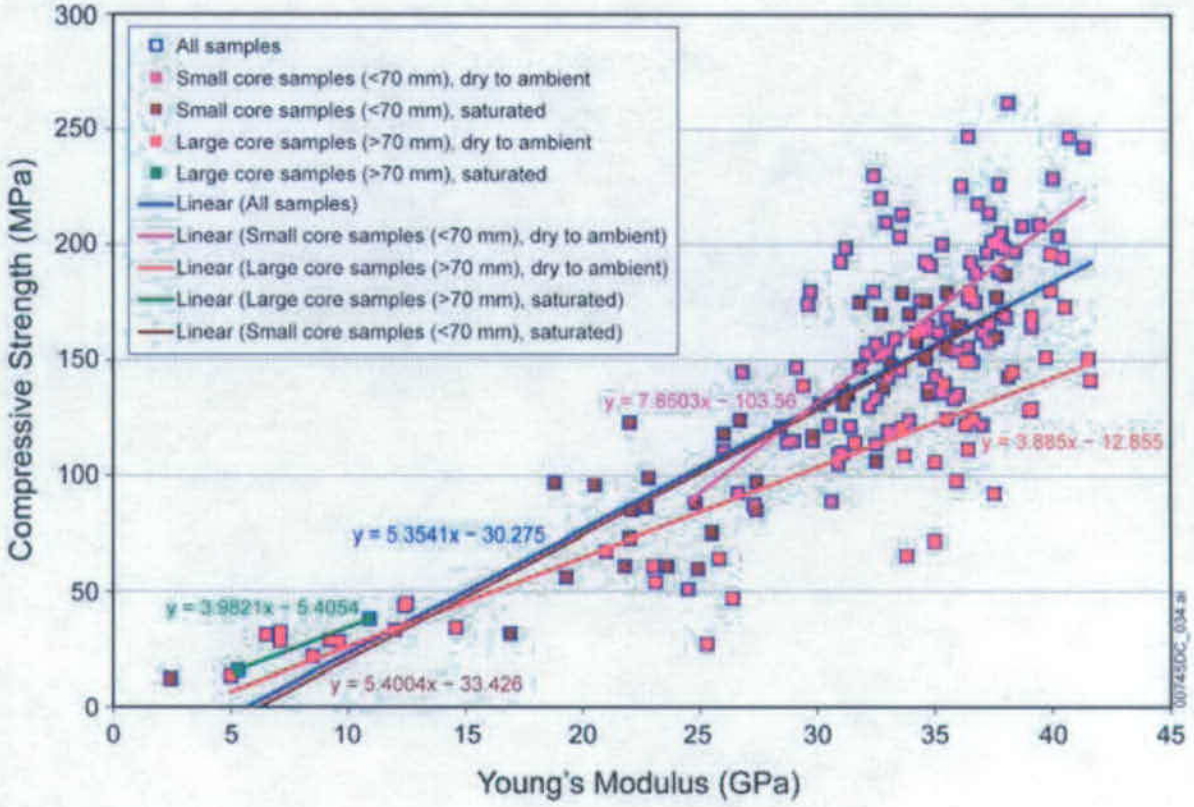

Source: (BSC 2007 [DIRS 178693], Figure 6-37).

Figure 6.7-4. Unconfined Compressive Strength versus Young's Modulus in Tptpll Zone

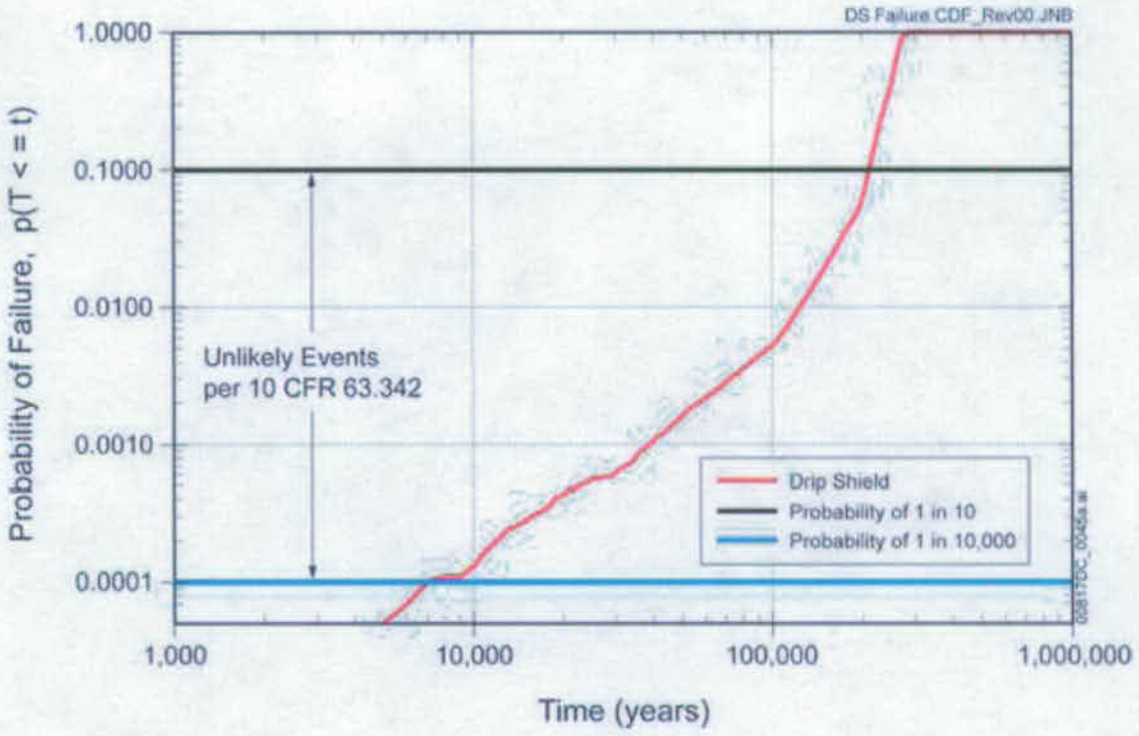

Sources: DTNs: SN0704PADSGCMT.001_R2 [DIRS 182122] and MO0703PASDSTAT.001_R3 [DIRS 183148].

Figure 6.7-5. Probability of Drip Shield Failure over Time including General Corrosion and the Probability of Failure of the Drip Shield Plates

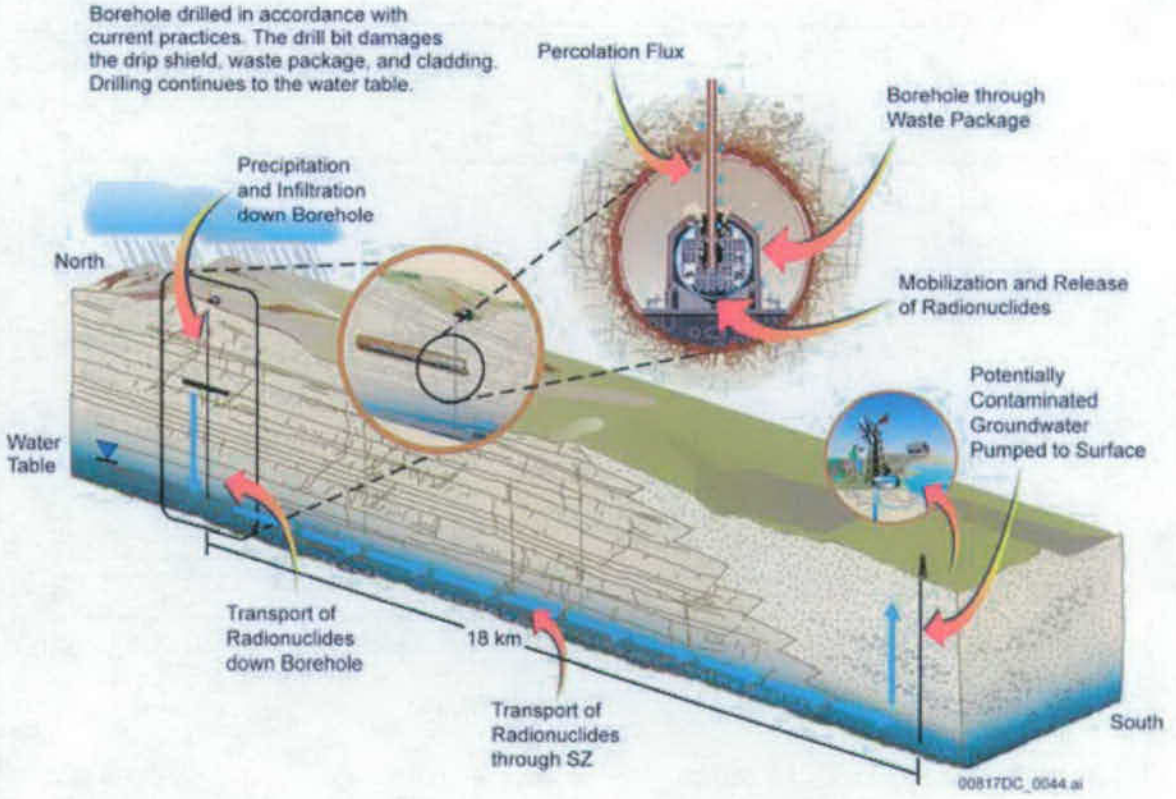

Figure 6.7-6. Conceptualization of the Human Intrusion Scenario for the TSPA-SEIS and Subsequent Radionuclide Releases to the Accessible Environment

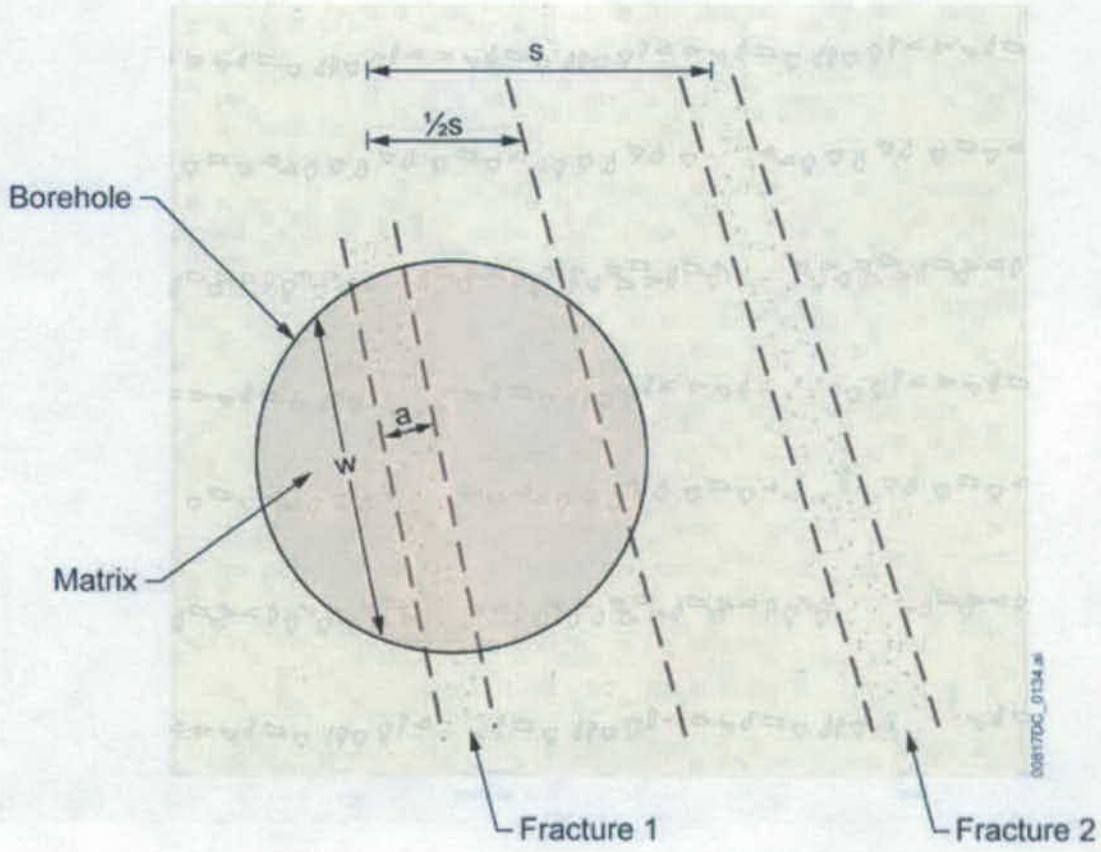

w = fracture width
s = fracture spacing
a = fracture aperture
½s = diffusion length between fracture and matrix
Borehole = Drill Patch Area = 0.0324 m^2

Figure 6.7-7. Schematic Depiction of Borehole (map view) with a Bisecting Fracture

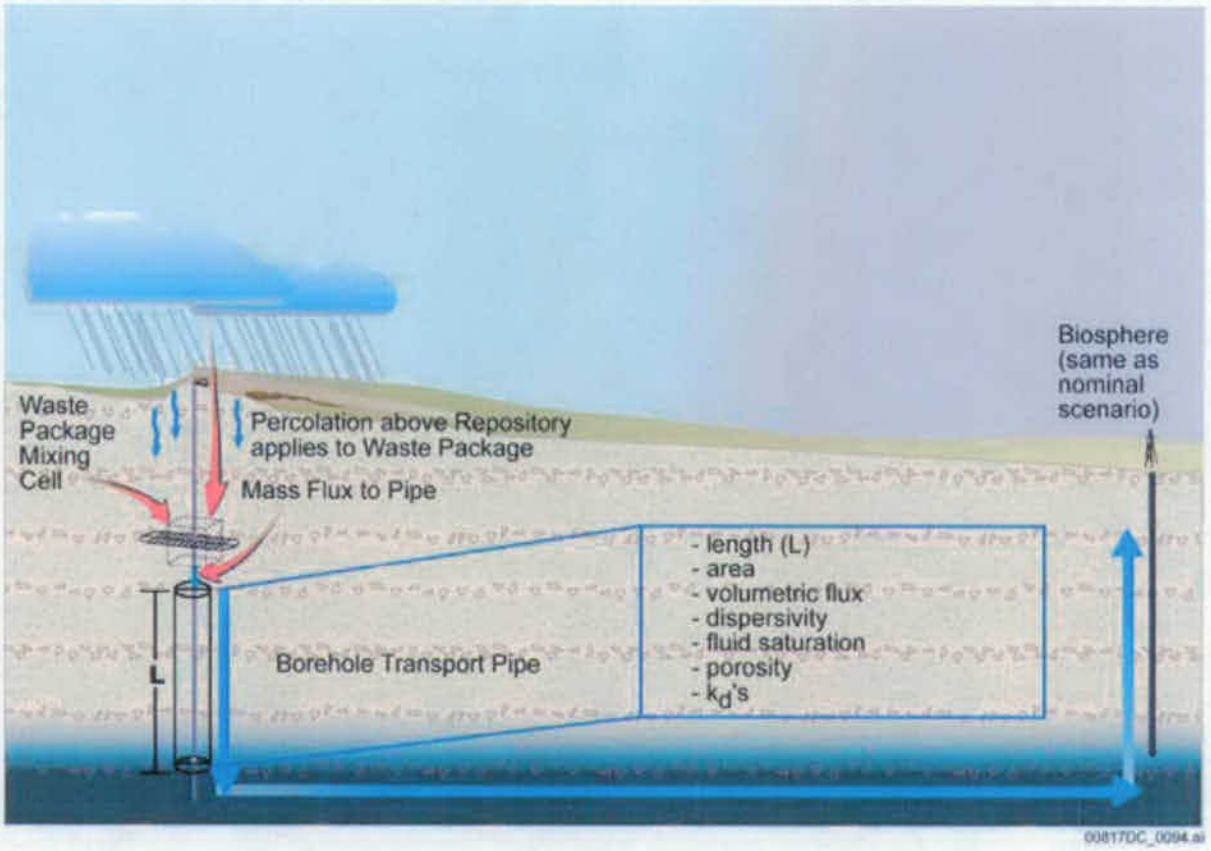

Figure 6.7-8. Schematic Illustration of the Implementation of Human Intrusion in TSPA-SEIS

DIRS Database

Master Reference List – 10_02_07_8:00p

TDR-WIS-PA-000014 Rev. 00
TSPA INFORMATION PACKAGE FOR THE DRAFT SEIS

10 CFR 63. 2007. Energy: Disposal of High-Level Radioactive Wastes in a Geologic Repository at Yucca Mountain, Nevada. Internet Accessible. **180319**

66 FR 32074. 40 CFR Part 197, Public Health and Environmental Radiation Protection Standards for Yucca Mountain, NV; Final Rule. ACC: MOL.20050418.0113. **155216**

66 FR 55732. Disposal of High-Level Radioactive Wastes in a Proposed Geologic Repository at Yucca Mountain, NV, Final Rule. 10 CFR Parts 2, 19, 20, 21, 30, 40, 51, 60, 61, 63, 70, 72, 73, and 75. ACC: MOL.20050324.0102; MOL.20050418.0124. **156671**

70 FR 49014. Public Health and Environmental Radiation Protection Standards for Yucca Mountain, NV. Internet Accessible. **177357**

70 FR 53313. Implementation of a Dose Standard After 10,000 Years. Internet Accessible. **178394**

Anderson, T.W. 1984. *An Introduction to Multivariate Statistical Analysis.* 2nd Edition. New York, New York: John Wiley & Sons. TIC: 244809. **169668**

ASHPLUME_DLL_LA V. 2.0. 2003. WINDOWS 2000. STN: 11117-2.0-00. **181034**

ASHPLUME_DLL_LA V. 2.1. 2003. WinDOWS 2000/XP. STN: 11117-2.1-00. **181035**

ASHPLUME_DLL_LA V. 2.1. 2007. WINDOWS 2003. STN: 11117-2.1-01. **180147**

ASM International 1990. *Properties and Selection: Nonferrous Alloys and Special-Purpose Materials.* Volume 2 of *ASM Handbook.* Formerly Tenth Edition, Metals Handbook. 5th Printing 1998. [Materials Park, Ohio]: ASM International. TIC: 241059. **141615**

ASM International. 1987. *Corrosion.* Volume 13 of *ASM Handbook.* Formerly 9th Edition, Metals Handbook. [Materials Park, Ohio]: ASM International. TIC: 240704. **133378**

ASME (American Society of Mechanical Engineers) 1998. *1998 ASME Boiler and Pressure Vessel Code.* 1998 Edition with 1999 and 2000 Addenda. New York, New York: American Society of Mechanical Engineers. TIC: 247429. **145103**

Avallone, E.A. and Baumeister, T., III, eds. 1987. *Marks' Standard Handbook for Mechanical Engineers.* 9th Edition. New York, New York: McGraw-Hill. TIC: 206891. **103508**

Aziz, P.M. 1956. "Application of the Statistical Theory of Extreme Values to the Analysis of Maximum Pit Depth Data for Aluminum." *Corrosion, 12,* (10), 35-46. Houston, Texas: National Association of Corrosion Engineers. TIC: 241560. **159379**

Beer, F.P. and Johnston, E.R., Jr. 1981. *Mechanics of Materials.* New York, New York: McGraw-Hill. TIC: 255414. **166708**

Beven, K. and Binley, A. 1992. "The Future of Distributed Models: Model Calibration and Uncertainty Prediction." *Hydrological Processes, 6,* (3), 279-298. [New York, New York]: John Wiley & Sons. TIC: 258993. **179079**

BIOMASS (Biosphere Modelling and Assessment) 2003. *"Reference Biospheres" for Solid Radioactive Waste Disposal, Report of BIOMASS Theme 1 of the BIOsphere Modelling and ASSessment (BIOMASS) Programme, Part of the IAEA Co-ordinated Research Project on Biosphere Modelling and Assessment (BIOMASS).* IAEA-BIOMASS-6. Vienna, Austria: International Atomic Energy Agency, Waste Safety Section. TIC: 255411. **168563**

BIOMASS (Biosphere Modelling and Assessment) 2000. *Example Reference Biosphere 2A: Agricultural Well, Constant Biosphere.* Draft TECDOC. BIOMASS/T1/WD08. Vienna, Austria: International Atomic Energy Agency, Division of Radiation and Waste Safety. TIC: 249456. **154522**

Bourgoyne, A.T., Jr.; Millheim, K.K.; Chenevert, M.E.; and Young, F.S., Jr. 1986. "Rotary Drilling Bits." *Applied Drilling Engineering.* [SPE Textbook Series Volume 2]. Pages 190-245. Richardson, Texas: Society of Petroleum Engineers. TIC: 250085. **155233**

Boyer, H.E. and Gall, T.L., eds. [1984]. *Metals Handbook.* Desk Edition. 10th Printing 1997. Metals Park, Ohio: American Society for Metals. TIC: 250192. **155318**

BSC (Bechtel SAIC Company) 2001. *MKTABLE Software Management Report.* SDN: 10505-SMR-1.00-00. Las Vegas, Nevada: Bechtel SAIC Company. ACC: MOL.20010712.0055. **167572**

BSC (Bechtel SAIC Company) 2002. *Design Document for WAPDEG 4.07.* SDN: 10000-DD-04.07-00. Las Vegas, Nevada: Bechtel SAIC Company. ACC: MOL.20030409.0229; MOL.20040427.0343. **167547**

BSC (Bechtel SAIC Company) 2002. *Installation Test Plan for WAPDEG 4.07.* SDN: 10000-ITP-4.07-01. Las Vegas, Nevada: Bechtel SAIC Company. ACC: MOL.20030409.0231; MOL.20040427.0343. **167548**

BSC (Bechtel SAIC Company) 2002. *Requirements Document for WAPDEG 4.07.* SDN: 10000-RD-4.07-00. Las Vegas, Nevada: Bechtel SAIC Company. ACC: MOL.20030409.0228; MOL.20040427.0343. **167545**

BSC (Bechtel SAIC Company) 2002. *Users' Manual for WAPDEG 4.07.* SDN: 10000-UM-4.07-00. Las Vegas, Nevada: Bechtel SAIC Company. ACC: MOL.20030409.0233; MOL.20040427.0343. **162606**

BSC (Bechtel SAIC Company) 2002. *Validation Test Plan for WAPDEG 4.07.* SDN: 10000-VTP-4.07-00. Las Vegas, Nevada: Bechtel SAIC Company. ACC: MOL.20030409.0232; MOL.20040427.0343. **167542**

BSC (Bechtel SAIC Company) 2002. *Validation Test Report for WAPDEG 4.07.* SDN: 10000-VTR-4.07-00. Las Vegas, Nevada: Bechtel SAIC Company. ACC: MOL.20030409.0234; MOL.20040427.0343. **167554**

BSC (Bechtel SAIC Company) 2003. *Repository Design, Repository/PA IED Subsurface Facilities.* 800-IED-EBS0-00402-000-00B. Las Vegas, Nevada: Bechtel SAIC Company. ACC: MOL.20030109.0146. **161727**

BSC (Bechtel SAIC Company) 2004. *Analysis of Hydrologic Properties Data.* ANL-NBS-HS-000042 REV 00. Las Vegas, Nevada: Bechtel SAIC Company. ACC: DOC.20041005.0004; DOC.20050815.0003. **170038**

BSC (Bechtel SAIC Company) 2004. *Analysis of Mechanisms for Early Waste Package/Drip Shield Failure.* CAL-EBS-MD-000030 REV 00C. Las Vegas, Nevada: Bechtel SAIC Company. ACC: DOC.20040913.0006; DOC.20050606.0005; DOC.20050830.0002. **170024**

BSC (Bechtel SAIC Company) 2004. *Characterize Framework for Igneous Activity at Yucca Mountain, Nevada.* ANL-MGR-GS-000001 REV 02. Las Vegas, Nevada: Bechtel SAIC Company. ACC: DOC.20041015.0002; DOC.20050718.0007. **169989**

BSC (Bechtel SAIC Company) 2004. *Conceptual Model and Numerical Approaches for Unsaturated Zone Flow and Transport.* MDL-NBS-HS-000005 REV 01. Las Vegas, Nevada: Bechtel SAIC Company. ACC: DOC.20040922.0006; DOC.20050307.0009. **170035**

BSC (Bechtel SAIC Company) 2004. *CSNF Waste Form Degradation: Summary Abstraction.* ANL-EBS-MD-000015 REV 02. Las Vegas, Nevada: Bechtel SAIC Company. ACC: DOC.20040908.0001; DOC.20050620.0004. **169987**

BSC (Bechtel SAIC Company) 2004. *Defense HLW Glass Degradation Model.* ANL-EBS-MD-000016 REV 02. Las Vegas, Nevada: Bechtel SAIC Company. ACC: DOC.20041020.0015; DOC.20050922.0002. **169988**

BSC (Bechtel SAIC Company) 2004. *Drift Degradation Analysis.* ANL-EBS-MD-000027 REV 03. Las Vegas, Nevada: Bechtel SAIC Company. ACC: DOC.20040915.0010; DOC.20050419.0001; DOC.20051130.0002; DOC.20060731.0005. **166107**

BSC (Bechtel SAIC Company) 2004. *Drift-Scale Radionuclide Transport.* MDL-NBS-HS-000016 REV 01. Las Vegas, Nevada: Bechtel SAIC Company. ACC: DOC.20040927.0031; DOC.20050927.0003. **170040**

BSC (Bechtel SAIC Company) 2004. *DSNF and Other Waste Form Degradation Abstraction.* ANL-WIS-MD-000004 REV 04. Las Vegas, Nevada: Bechtel SAIC Company. ACC: DOC.20041201.0007. **172453**

BSC (Bechtel SAIC Company) 2004. *Future Climate Analysis.* ANL-NBS-GS-000008 REV 01. Las Vegas, Nevada: Bechtel SAIC Company. ACC: DOC.20040908.0005. **170002**

BSC (Bechtel SAIC Company) 2004. *Natural Analogue Synthesis Report.* TDR-NBS-GS-000027 REV 01. Las Vegas, Nevada: Bechtel SAIC Company. ACC: DOC.20040524.0008. **169218**

BSC (Bechtel SAIC Company) 2004. *Saturated Zone Colloid Transport.* ANL-NBS-HS-000031 REV 02. Las Vegas, Nevada: Bechtel SAIC Company. ACC: DOC.20041008.0007; DOC.20051215.0005. **170006**

BSC (Bechtel SAIC Company) 2004. *Seepage Model for PA Including Drift Collapse.* MDL-NBS-HS-000002 REV 03. Las Vegas, Nevada: Bechtel SAIC Company. ACC: DOC.20040922.0008; DOC.20051205.0001. **167652**

BSC (Bechtel SAIC Company) 2004. *WAPDEG Analysis of Waste Package and Drip Shield Degradation.* ANL-EBS-PA-000001 REV 02. Las Vegas, Nevada: Bechtel SAIC Company. ACC: DOC.20041004.0005. **169996**

BSC (Bechtel SAIC Company) 2004. *Yucca Mountain Site Description.* TDR-CRW-GS-000001 REV 02 ICN 01. Two volumes. Las Vegas, Nevada: Bechtel SAIC Company. ACC: DOC.20040504.0008. **169734**

BSC (Bechtel SAIC Company) 2005. *Characteristics of the Receptor for the Biosphere Model.* ANL-MGR-MD-000005 REV 04. Las Vegas, Nevada: Bechtel SAIC Company. ACC: DOC.20050405.0005. **172827**

BSC (Bechtel SAIC Company) 2005. *Development of the Total System Performance Assessment-License Application Features, Events, and Processes.* TDR-WIS-MD-000003 REV 02. Las Vegas, Nevada: Bechtel SAIC Company. ACC: DOC.20050829.0004. **173800**

BSC (Bechtel SAIC Company) 2005. *Drift-Scale Coupled Processes (DST and TH Seepage) Models.* MDL-NBS-HS-000015 REV 02. Las Vegas, Nevada: Bechtel SAIC Company. ACC: DOC.20050114.0004; DOC.20051115.0002. **172232**

BSC (Bechtel SAIC Company) 2005. *Mountain-Scale Coupled Processes (TH/THC/THM) Models.* MDL-NBS-HS-000007 REV 03. Las Vegas, Nevada: Bechtel SAIC Company. ACC: DOC.20050825.0007. **174101**

BSC (Bechtel SAIC Company) 2006. *Basis of Design for the TAD Canister-Based Repository Design Concept.* 000-3DR-MGR0-00300-000-000. Las Vegas, Nevada: Bechtel SAIC Company. ACC: ENG.20061023.0002; ENG.20061121.0005; ENG.20061116.0005; ENG.20061204.0002; ENG.20061218.0003; ENG.20061218.0004; ENG.20070220.0010; ENG.20070220.0011; ENG.20070220.0012; ENG.20070314.0009; ENG.20070412.0002; ENG.20070222.0007; ENG.20070222.0008; ENG.20070221.0010; ENG.20070222.0009; ENG.20070308.0029; ENG.20070501.0009; ENG.20070507.0028; ENG.20070608.0019. **177636**

BSC (Bechtel SAIC Company) 2006. *Inhalation Exposure Input Parameters for the Biosphere Model.* ANL-MGR-MD-000001 REV 04. Las Vegas, Nevada: Bechtel SAIC Company. ACC: DOC.20060605.0011. **177101**

BSC (Bechtel SAIC Company) 2006. *Technical Work Plan for: Igneous Activity Assessment for Disruptive Events.* TWP-WIS-MD-000007 REV 09 ICN 01. Las Vegas, Nevada: Bechtel SAIC Company. ACC: DOC.20060814.0018. **178448**

BSC (Bechtel SAIC Company) 2007. *Subsurface Geotechnical Parameters Report.* ANL-SSD-GE-000001 REV 00. Las Vegas, Nevada: Bechtel SAIC Company. ACC: ENG.20070115.0006. **178693**

Budnitz, R.J.; Apostolakis, G.; Boore, D.M.; Cluff, L.S.; Coppersmith, K.J.; Cornell, C.A.; and Morris, P.A. 1997. *Recommendations for Probabilistic Seismic Hazard Analysis: Guidance on the Uncertainty and Use of Experts.* NUREG/CR-6372. Two volumes. Washington, D.C.: U.S. Nuclear Regulatory Commission. TIC: 235076; 235074. **103635**

Bureau of the Census. 2002. "2000 Summary File 3 (SF 3) Sample Data, Amargosa Valley CCD, Nye County, Nevada." Washington, D.C.: U.S. Department of Commerce, Bureau of the Census. Accessed August 28, 2002. TIC: 253098. URL: http://factfinder.census.gov/servlet/DTTable?_ts=48597952130 **159728**

Cranwell, R.M.; Guzowski, R.V.; Campbell, J.E.; and Ortiz, N.R. 1990. *Risk Methodology for Geologic Disposal of Radioactive Waste, Scenario Selection Procedure.* NUREG/CR-1667. Washington, D.C.: U.S. Nuclear Regulatory Commission. ACC: NNA.19900611.0073. **101234**

CRWMS M&O 1998. "Geology and Geochronology of Basaltic Volcanism in the Yucca Mountain Region." Chapter 2 of *Synthesis of Volcanism Studies for the Yucca Mountain Site*

Characterization Project. Deliverable 3781MR1. Las Vegas, Nevada: CRWMS M&O. ACC: MOL.19990511.0400. **123196**

CRWMS M&O 1998. *Probabilistic Seismic Hazard Analyses for Fault Displacement and Vibratory Ground Motion at Yucca Mountain, Nevada.* Milestone SP32IM3, September 23, 1998. Three volumes. Las Vegas, Nevada: CRWMS M&O. ACC: MOL.19981207.0393. **103731**

CRWMS M&O 1998. *Synthesis of Volcanism Studies for the Yucca Mountain Site Characterization Project.* Deliverable 3781MR1. Las Vegas, Nevada: CRWMS M&O. ACC: MOL.19990511.0400. **105347**

CRWMS M&O 1998. *Waste Package Degradation Expert Elicitation Project.* Rev. 1. Las Vegas, Nevada: CRWMS M&O. ACC: MOL.19980727.0002. **100349**

CRWMS M&O 2000. *Comparison of ASHPLUME Model Results to Representative Tephra Fall Deposits.* CAL-WIS-MD-000011 REV 00. Las Vegas, Nevada: CRWMS M&O. ACC: MOL.20001204.0032. **152998**

CRWMS M&O 2000. *SCCD Software Routine Report.* SDN: 10343-SRR-2.01-00. Las Vegas, Nevada: CRWMS M&O. ACC: MOL.20010205.0113. **152499**

CRWMS M&O 2000. *Total System Performance Assessment for the Site Recommendation.* TDR-WIS-PA-000001 REV 00 ICN 01. Las Vegas, Nevada: CRWMS M&O. ACC: MOL.20001220.0045. **153246**

CWD V. 2.0. 2003. WINDOWS 2000. STN: 10363-2.0-00. **162809**

CWD V. 2.0. 2007. WINDOWS 2003. STN: 10363-2.0-01. **181037**

D'Agnese, F.A.; Faunt, C.C.; Turner, A.K.; and Hill, M.C. 1997. *Hydrogeologic Evaluation and Numerical Simulation of the Death Valley Regional Ground-Water Flow System, Nevada and California.* Water-Resources Investigations Report 96-4300. Denver, Colorado: U.S. Geological Survey. ACC: MOL.19980306.0253. **100131**

Day, W.C.; Dickerson, R.P.; Potter, C.J.; Sweetkind, D.S.; San Juan, C.A.; Drake, R.M., II; and Fridrich, C.J. 1998. *Bedrock Geologic Map of the Yucca Mountain Area, Nye County, Nevada.* Geologic Investigations Series I-2627. Denver, Colorado: U.S. Geological Survey. ACC: MOL.19981014.0301. **100027**

DOE (U.S. Department of Energy) 2003. *Design Document for: SZ_CONVOLUTE Version 3.0.* 10207-DD-3.0-00. Las Vegas, Nevada: U.S. Department of Energy, Office of Repository Development. ACC: MOL.20030717.0479. **167588**

DOE (U.S. Department of Energy) 2003. *Installation Test Process for: SZ_CONVOLUTE Version 3.0.* 10207-ITP-3.0-00. Las Vegas, Nevada: U.S. Department of Energy, Office of Repository Development. ACC: MOL.20030717.0480. **167590**

DOE (U.S. Department of Energy) 2003. *Requirements Document for: ASHPLUME_DLL_LA, V2.0, Rev. No. 00.* Document ID: 11117-RD-2.0-00. Las Vegas, Nevada: U.S. Department of Energy, Office of Repository Development. ACC: MOL.20031212.0438. **167601**

DOE (U.S. Department of Energy) 2003. *Requirements Document for: SZ_CONVOLUTE Version 3.0.* 10207-RD-3.0-00. Las Vegas, Nevada: U.S. Department of Energy, Office of Repository Development. ACC: MOL.20030717.0478. **167587**

DOE (U.S. Department of Energy) 2003. *Software Management Report, MFCP_LA, V1.0.* DI: 11071-SMR-1.0-00. Las Vegas, Nevada: U.S. Department of Energy, Office of Repository Development. ACC: MOL.20030529.0258. **167597**

DOE (U.S. Department of Energy) 2003. *Software Management Report: CWD Version Number 2.0.* Document ID: 10363-SMR-2.0-00. Las Vegas, Nevada: U.S. Department of Energy, Office of Repository Development. ACC: MOL.20030501.0182. **167564**

DOE (U.S. Department of Energy) 2003. *User's Manual for: ASHPLUME_DLL_LA Version 2.0, UM Rev. No.: 00.* Document ID: 11117-UM-2.0-00. Las Vegas, Nevada: U.S. Department of Energy, Office of Repository Development. ACC: MOL.20031212.0444. **167607**

DOE (U.S. Department of Energy) 2003. *Users Manual, SZ_CONVOLUTE Version 3.0.* 10207-UM-3.0-00. Las Vegas, Nevada: U.S. Department of Energy, Office of Repository Development. ACC: MOL.20030717.0483. **167591**

DOE (U.S. Department of Energy) 2003. *Validation Test Process for: ASHPLUME_DLL_LA Version 2.0.* Document ID: 11117-VTP-2.0-01. Las Vegas, Nevada: U.S. Department of Energy, Office of Repository Development. ACC: MOL.20031212.0441. **167604**

DOE (U.S. Department of Energy) 2003. *Validation Test Process for: SZ_CONVOLUTE Version 3.0.* 10207-VTP-3.0-00. Las Vegas, Nevada: U.S. Department of Energy, Office of Repository Development. ACC: MOL.20030717.0481. **167589**

DOE (U.S. Department of Energy) 2003. *Validation Test Report for: SZ_CONVOLUTE.* 10207-VTR-3.0-0.0. Las Vegas, Nevada: U.S. Department of Energy, Office of Repository Development. ACC: MOL.20030717.0484. **167593**

DOE (U.S. Department of Energy) 2004. *Software Management Report for: PassTable1D_LA, V1.0.* Document ID: 11142-SMR-1.0-00. Las Vegas, Nevada: U.S. Department of Energy, Office of Repository Development. ACC: MOL.20040310.0105. **168978**

DOE (U.S. Department of Energy) 2004. *Software Management Report for: PassTable3D_LA, V1.0, SMR Rev. No.: 00.* Document ID: 11143-SMR-1.0-00. Las Vegas, Nevada: U.S. Department of Energy, Office of Repository Development. ACC: MOL.20040317.0127. **168981**

DOE (U.S. Department of Energy) 2004. *Software Management Report for: SOILEXP_LA, V1.0, SMR REV. NO.: 00.* Document ID: 10933-SMR-1.0-00. Las Vegas, Nevada: U.S. Department of Energy, Office of Repository Development. ACC: MOL.20040227.0046. **168977**

DOE (U.S. Department of Energy) 2004. *Software Management Report, INTERPZDLL_LA, V1.0, STN: 11107-1.0-00, Rev. 00.* Document ID: 11107-SMR-1.0-00. Las Vegas, Nevada: U.S. Department of Energy, Office of Repository Development. ACC: MOL.20040130.0403. **168988**

DOE (U.S. Department of Energy) 2005. *Design Document for: MVIEW V4.0.* Document ID: 10072-DD-4.0-00. Las Vegas, Nevada: U.S. Department of Energy, Office of Repository Development. ACC: MOL.20050712.0025. **174594**

DOE (U.S. Department of Energy) 2005. *Requirements Document for: MVIEW V4.0.* Document ID: 10072-RD-4.0-01. Las Vegas, Nevada: U.S. Department of Energy, Office of Repository Development. ACC: MOL.20050712.0023. **174593**

DOE (U.S. Department of Energy) 2005. *User Information for: MVIEW 4.0.* Document ID: 10072-UID-4.0-00. Las Vegas, Nevada: U.S. Department of Energy, Office of Repository Development. ACC: MOL.20050712.0027. **174595**

DOE (U.S. Department of Energy) 2006. *Design Document for SZ_CONVOLUTE Version 3.10.* Document ID: 10207-DD-3.10-00. Las Vegas, Nevada: U.S. Department of Energy, Office of Repository Development. ACC: MOL.20061106.0219. **181286**

DOE (U.S. Department of Energy) 2006. *Design Document for: GetThk_LA v1.0.* Document ID: 11229-DD-1.0-00. Las Vegas, Nevada: U.S. Department of Energy, Office of Repository Development. ACC: MOL.20060915.0165. **181101**

DOE (U.S. Department of Energy) 2006. *Design Document for: MkTable_LA v1.0.* Document ID: 11217-DD-1.0-00. Las Vegas, Nevada: U.S. Department of Energy, Office of Repository Development. ACC: MOL.20060413.0351. **181115**

DOE (U.S. Department of Energy) 2006. *Design Document for: PREWAP_LA v1.1.* Document ID: 10939-DD-1.1-00. Las Vegas, Nevada: U.S. Department of Energy, Office of Repository Development. ACC: MOL.20060418.0165. **181128**

DOE (U.S. Department of Energy) 2006. *Design Document for: SEEPAGEDLL_LA V1.3.* Document ID: 11076-DD-1.3-00. Las Vegas, Nevada: U.S. Department of Energy, Office of Repository Development. ACC: MOL.20060525.0296. **181132**

DOE (U.S. Department of Energy) 2006. *Requirements Document for SZ_CONVOLUTE V. 3.10.* Document ID: 10207-RD-3.10-00. Las Vegas, Nevada: U.S. Department of Energy, Office of Repository Development. ACC: MOL.20061106.0218. **181284**

DOE (U.S. Department of Energy) 2006. *Requirements Document for: FEHM V2.24.* Document ID: 10086-RD-2.24-00-00. Las Vegas, Nevada: U.S. Department of Energy, Office of Repository Development. ACC: MOL.20061127.0272. **181094**

DOE (U.S. Department of Energy) 2006. *Requirements Document for: GetThk_LA v1.0.* Document ID: 11229-RD-1.0-00. Las Vegas, Nevada: U.S. Department of Energy, Office of Repository Development. ACC: MOL.20060915.0163. **181100**

DOE (U.S. Department of Energy) 2006. *Requirements Document for: MkTable_LA v1.0.* Document ID: 11217-RD-1.0-00. Las Vegas, Nevada: U.S. Department of Energy, Office of Repository Development. ACC: MOL.20060413.0349. **181114**

DOE (U.S. Department of Energy) 2006. *Requirements Document for: PREWAP_LA v1.1.* Document ID: 10939-RD-1.1-00. Las Vegas, Nevada: U.S. Department of Energy, Office of Repository Development. ACC: MOL.20060418.0163. **181127**

DOE (U.S. Department of Energy) 2006. *Requirements Document for: SEEPAGEDLL_LA V1.3.* Document ID: 11076-RD-1.3-00. Las Vegas, Nevada: U.S. Department of Energy, Office of Repository Development. ACC: MOL.20060525.0294. **181131**

DOE (U.S. Department of Energy) 2006. *Software Validation Report for: GetThk_LA v1.0.* Document ID: 11229-SVR-1.0-00-WIN2000. Las Vegas, Nevada: U.S. Department of Energy, Office of Repository Development. ACC: MOL.20060915.0173. **181104**

DOE (U.S. Department of Energy) 2006. *Software Validation Report for: GetThk_LA v1.0.* Document ID: 11229-SVR-1.0-00-WIN2003. Las Vegas, Nevada: U.S. Department of Energy, Office of Repository Development. ACC: MOL.20060915.0171. **181105**

DOE (U.S. Department of Energy) 2006. *Software Validation Report for: MFCP_LA v1.0.* Document ID: 11071-SVR-1.0-01-WIN2003. Las Vegas, Nevada: U.S. Department of Energy, Office of Repository Development. ACC: MOL.20061218.0126. **181113**

DOE (U.S. Department of Energy) 2006. *Software Validation Report for: MkTable_LA v1.0.* Document ID: 11217-SVR-1.0-00-WIN2000. Las Vegas, Nevada: U.S. Department of Energy, Office of Repository Development. ACC: MOL.20060413.0357. **181117**

DOE (U.S. Department of Energy) 2006. *Software Validation Report for: PASSTABLE1D_LA v1.0.* Document ID: 11142-SVR-1.0-01-WIN2003. Las Vegas, Nevada: U.S. Department of Energy, Office of Repository Development. ACC: MOL.20061218.0107. **181120**

DOE (U.S. Department of Energy) 2006. *Software Validation Report for: PREWAP_LA v1.1.* Document ID: 10939-SVR-1.1-00-WIN2000. Las Vegas, Nevada: U.S. Department of Energy, Office of Repository Development. ACC: MOL.20060418.0171. **181130**

DOE (U.S. Department of Energy) 2006. *Software Validation Report for: SEEPAGEDLL_LA V1.3.* Document ID: 11076-SVR-1.3-00-WIN2000. Las Vegas, Nevada: U.S. Department of Energy, Office of Repository Development. ACC: MOL.20060525.0302. **181134**

DOE (U.S. Department of Energy) 2006. *Software Validation Report for: TSPA_Input_DB v2.2.* Document ID: 10931-SVR-2.2-00-WIN2000. Las Vegas, Nevada: U.S. Department of Energy, Office of Repository Development. ACC: MOL.20060222.0422. **181139**

DOE (U.S. Department of Energy) 2006. *Software Validation Report for: TSPA_Input_DB v2.2.* Document ID: 10931-SVR-2.2-01-WIN2003. Las Vegas, Nevada: U.S. Department of Energy, Office of Repository Development. ACC: MOL.20061011.0198. **181140**

DOE (U.S. Department of Energy) 2006. *User Information Document for: GetThk_LA v1.0.* Document ID: 11229-UID-1.0-00. Las Vegas, Nevada: U.S. Department of Energy, Office of Repository Development. ACC: MOL.20060915.0169. **181102**

DOE (U.S. Department of Energy) 2006. *User Information Document for: MkTable_LA v1.0.* Document ID: 11217-UID-1.0-00. Las Vegas, Nevada: U.S. Department of Energy, Office of Repository Development. ACC: MOL.20060413.0354. **181116**

DOE (U.S. Department of Energy) 2006. *User Information Document for: PREWAP_LA v1.1.* Document ID: 10939-UID-1.1-00. Las Vegas, Nevada: U.S. Department of Energy, Office of Repository Development. ACC: MOL.20060418.0169. **181129**

DOE (U.S. Department of Energy) 2006. *User Information Document for: SEEPAGEDLL_LA V1.3.* Document ID: 11076-UID-1.3-00. Las Vegas, Nevada: U.S. Department of Energy, Office of Repository Development. ACC: MOL.20060525.0300. **181133**

DOE (U.S. Department of Energy) 2006. *User Information Document for: TSPA_Input_DB Version 2.2.* Document ID: 10931-UID-2.2-00. Las Vegas, Nevada: U.S. Department of Energy, Office of Repository Development. ACC: MOL.20060222.0419. **181137**

DOE (U.S. Department of Energy) 2007. *Design Document for: EXDOC_LA Version 2.0.* Document ID: 11193-DD-2.0-00. Las Vegas, Nevada: U. S. Department of Energy, Office of Repository Development. ACC: MOL.20070723.0255. **183126**

DOE (U.S. Department of Energy) 2007. *Design Document for: FAR Version 1.1.* Document ID: 11190-DD-1.1-00. Las Vegas, Nevada: U.S. Department of Energy, Office of Repository Development. ACC: MOL.20070323.0328. **181081**

DOE (U.S. Department of Energy) 2007. *Design Document for: FEHM V2.24-01.* Document ID: 10086-DD-2.24-01-00. Las Vegas, Nevada: U.S. Department of Energy, Office of Repository Development. ACC: MOL.20070309.0032. **181095**

DOE (U.S. Department of Energy) 2007. *Design Document for: GoldSim v9.60.* Document ID: 10344-DD-9.60-01. Las Vegas, Nevada: U.S. Department of Energy, Office of Repository Development. ACC: MOL.20070416.0338. **181107**

DOE (U.S. Department of Energy) 2007. *Design Document for: PassTable1D_LA version 2.0.* Document ID: 11142-DD-2.0-01. Las Vegas, Nevada: U.S. Department of Energy, Office of Repository Development. ACC: MOL.20070420.0359. **181122**

DOE (U.S. Department of Energy) 2007. *Quality Assurance Requirements and Description.* DOE/RW-0333P, Rev. 19. Washington, D. C.: U.S. Department of Energy, Office of Civilian Radioactive Waste Management. ACC: DOC.20070717.0006. **182051**

DOE (U.S. Department of Energy) 2007. *Requirements Document for: EXDOC_LA Version 2.0.* Document ID: 11193-RD-2.0-01. Las Vegas, Nevada: U. S. Department of Energy, Office of Repository Development. ACC: MOL.20070723.0260. **182906**

DOE (U.S. Department of Energy) 2007. *Requirements Document for: FAR Version 1.1.* Document ID: 11190-RD-1.1-00. Las Vegas, Nevada: U.S. Department of Energy, Office of Repository Development. ACC: MOL.20070323.0326. **181080**

DOE (U.S. Department of Energy) 2007. *Requirements Document for: GoldSim v9.60.* Document ID: 10344-RD-9.60-00. Las Vegas, Nevada: U.S. Department of Energy, Office of Repository Development. ACC: MOL.20070416.0330. **181106**

DOE (U.S. Department of Energy) 2007. *Requirements Document for: PassTable1D_LA Version 2.0.* Document ID: 11142-RD-2.0-01. Las Vegas, Nevada: U.S. Department of Energy, Office of Repository Development. ACC: MOL.20070420.0357. **181121**

DOE (U.S. Department of Energy) 2007. *Software Validation Report for: ASHPLUME_DLL_LA Version 2.1 Operating in GoldSim under the Windows Server 2003 Environment.* Document ID: 11117-SVR-2.1-01-Win2003. Las Vegas, Nevada: U.S. Department of Energy, Office of Repository Development. ACC: MOL.20070223.0261. **181275**

DOE (U.S. Department of Energy) 2007. *Software Validation Report for: CWD v2.0.* Document ID: 10363-SVR-2.0-01-WIN2003. Las Vegas, Nevada: U.S. Department of Energy, Office of Repository Development. ACC: MOL.20070209.0021. **181079**

DOE (U.S. Department of Energy) 2007. *Software Validation Report for: EXDOC_LA Version 2.0.* Document ID: 11193-SVR-2.0-00-WIN2000. Las Vegas, Nevada: U. S. Department of Energy, Office of Repository Development. ACC: MOL.20070723.0266. **182909**

DOE (U.S. Department of Energy) 2007. *Software Validation Report for: EXDOC_LA Version 2.0.* Document ID: 11193-SVR-2.0-00-WIN2003. Las Vegas, Nevada: U.S. Department of Energy, Office of Repository Development. ACC: MOL.20070723.0268. **182910**

DOE (U.S. Department of Energy) 2007. *Software Validation Report for: FAR Version 1.1.* Document ID: 11190-SVR-1.1-00-Win2000. Las Vegas, Nevada: U.S. Department of Energy, Office of Repository Development. ACC: MOL.20070417.0338. **181085**

DOE (U.S. Department of Energy) 2007. *Software Validation Report for: FAR Version 1.1.* Document ID: 11190-SVR-1.1-00-Win2003. Las Vegas, Nevada: U.S. Department of Energy, Office of Repository Development. ACC: MOL.20070417.0340. **181087**

DOE (U.S. Department of Energy) 2007. *Software Validation Report for: FAR Version 1.2.* Document ID: 11190-SVR-1.2-00-Win2003. Las Vegas, Nevada: U.S. Department of Energy, Office of Repository Development. ACC: MOL.20070919.0336. **183121**

DOE (U.S. Department of Energy) 2007. *Software Validation Report for: FEHM V2.24-01.* Document ID: 10086-SVR-2.24-01-00-Win2003. Las Vegas, Nevada: U.S. Department of Energy, Office of Repository Development. ACC: MOL.20070309.0045. **181098**

DOE (U.S. Department of Energy) 2007. *Software Validation Report for: FEHM V2.24-01.* Document ID: 10086-SVR-2.24-01-00-Win2000. Las Vegas, Nevada: U.S. Department of Energy, Office of Repository Development. ACC: MOL.20070309.0047. **181097**

DOE (U.S. Department of Energy) 2007. *Software Validation Report for: GoldSim v9.60 on Window XP.* Document ID: 10344-SVR-9.60-00-WINXP. Las Vegas, Nevada: U.S. Department of Energy, Office of Repository Development. ACC: MOL.20070416.0345. **181111**

DOE (U.S. Department of Energy) 2007. *Software Validation Report for: GoldSim v9.60 on Windows 2000.* Document ID: 10344-SVR-9.60-00-WIN2000. Las Vegas, Nevada: U.S. Department of Energy, Office of Repository Development. ACC: MOL.20070416.0341. **181109**

DOE (U.S. Department of Energy) 2007. *Software Validation Report for: GoldSim v9.60 on Windows Server 2003.* Document ID: 10344-SVR-9.60-00-WIN2003. Las Vegas, Nevada: U.S. Department of Energy, Office of Repository Development. ACC: MOL.20070416.0343. **181110**

DOE (U.S. Department of Energy) 2007. *Software Validation Report for: GoldSim Version 9.60.100 on Windows 2000.* Document ID: 10344-SVR-9.60-01-WIN2000. Las Vegas, Nevada:

U.S. Department of Energy, Office of Repository Development. ACC: MOL.20070711.0250. **182913**

DOE (U.S. Department of Energy) 2007. *Software Validation Report for: GoldSim Version 9.60.100 on Windows XP.* Document ID: 10344-SVR-9.60-01-WINXP. Las Vegas, Nevada: U. S. Department of Energy, Office of Repository Development. ACC: MOL.20070711.0254. **182915**

DOE (U.S. Department of Energy) 2007. *Software Validation Report for: GoldSim Version 9.60.100 Windows Server 2003.* Document ID: 10344-SVR-9.60-01-WIN2003. Las Vegas, Nevada: U.S. Department of Energy, Office of Repository Development. ACC: MOL.20070711.0252. **182914**

DOE (U.S. Department of Energy) 2007. *Software Validation Report for: INTERPZDLL_LA v1.0.* Document ID: 11107-SVR-1.0-01-WIN2003. Las Vegas, Nevada: U.S. Department of Energy, Office of Repository Development. ACC: MOL.20070220.0471. **181092**

DOE (U.S. Department of Energy) 2007. *Software Validation Report for: MkTable_LA v1.0.* Document ID: 11217-SVR-1.0-01-WIN2003. Las Vegas, Nevada: U.S. Department of Energy, Office of Repository Development. ACC: MOL.20070208.0274. **181118**

DOE (U.S. Department of Energy) 2007. *Software Validation Report for: MView 4.0.* Document ID: 10072-SVR-4.0-01-WinXP. Las Vegas, Nevada: U.S. Department of Energy, Office of Repository Development. ACC: MOL.20070417.0382. **181119**

DOE (U.S. Department of Energy) 2007. *Software Validation Report for: PassTable1D_LA v2.0.* Document ID: 11142-SVR-2.0-00-WIN2000. Las Vegas, Nevada: U.S. Department of Energy, Office of Repository Development. ACC: MOL.20070420.0363. **181124**

DOE (U.S. Department of Energy) 2007. *Software Validation Report for: PassTable1D_LA Version 2.0.* Document ID: 11142-SVR-2.0-00-WIN2003. Las Vegas, Nevada: U.S. Department of Energy, Office of Repository Development. ACC: MOL.20070420.0365. **181125**

DOE (U.S. Department of Energy) 2007. *Software Validation Report for: PassTable3D_LA v1.0.* Document ID: 11143-SVR-1.0-01-WIN2003. Las Vegas, Nevada: U.S. Department of Energy, Office of Repository Development. ACC: MOL.20070208.0286. **181126**

DOE (U.S. Department of Energy) 2007. *Software Validation Report for: SCCD v2.01.* Document ID: 10343-SVR-2.01-01-WIN2003. Las Vegas, Nevada: U.S. Department of Energy, Office of Repository Development. ACC: MOL.20070209.0013. **181277**

DOE (U.S. Department of Energy) 2007. *Software Validation Report for: SEEPAGEDLL_LA V1.3.* Document ID: 11076-SVR-1.3-01-WIN2003. Las Vegas, Nevada: U.S. Department of Energy, Office of Repository Development. ACC: MOL.20070223.0249. **181135**

DOE (U.S. Department of Energy) 2007. *Software Validation Report for: WAPDEG v4.07.* Document ID: 10000-SVR-4.07-01-WIN2003. Las Vegas, Nevada: U.S. Department of Energy, Office of Repository Development. ACC: MOL.20070417.0371. **181141**

DOE (U.S. Department of Energy) 2007. *Software Validation Report, SZ_Convolute Version 3.10.01.* Document ID: 10207-3.10.01-00-Win2003. Las Vegas, Nevada: U.S. Department of Energy, Office of Repository Development. ACC: MOL.20070501.0394. **181290**

DOE (U.S. Department of Energy) 2007. *User Information Document for: EXDOC_LA Version 2.0.* Document ID: 11193-UID-2.0-00. Las Vegas, Nevada: U. S. Department of Energy, Office of Repository Development. ACC: MOL.20070723.0264. **182908**

DOE (U.S. Department of Energy) 2007. *User Information Document for: FAR Version 1.1.* Document ID: 11190-UID-1.1-00. Las Vegas, Nevada: U.S. Department of Energy, Office of Repository Development. ACC: MOL.20070417.0336. **181084**

DOE (U.S. Department of Energy) 2007. *User Information Document for: FAR Version 1.2.* Document ID: 11190-UID-1.2-00. Las Vegas, Nevada: U.S. Department of Energy, Office of Repository Development. ACC: MOL.20070919.0332. **183116**

DOE (U.S. Department of Energy) 2007. *User Information Document for: FEHM V2.24-01.* Document ID: 10086-UID-2.24-01-00. Las Vegas, Nevada: U.S. Department of Energy, Office of Repository Development. ACC: MOL.20070309.0037. **181096**

DOE (U.S. Department of Energy) 2007. *User Information Document for: GoldSim Version 9.60.* Document ID: 10344-UID-9.60-00. Las Vegas, Nevada: U.S. Department of Energy, Office of Repository Development. ACC: MOL.20070416.0339. **181108**

DOE (U.S. Department of Energy) 2007. *User Information Document for: PassTable1D_LA Version 2.0.* Document ID: 11142-UID-2.0-00. Las Vegas, Nevada: U.S. Department of Energy, Office of Repository Development. ACC: MOL.20070420.0361. **181123**

DOE (U.S. Department of Energy) 2007. *User Information Document for: SZ_Convolute V. 3.10.* Document ID: 10207-UID-3.10-00. Las Vegas, Nevada: U.S. Department of Energy, Office of Repository Development. ACC: MOL.20070223.0313. **181288**

DOE (U.S. Department of Energy) 2003. *Design Document for: ASHPLUME_DLL_LA Version 2.0, Rev. No. 00.* Document ID: 11117-DD-2.0-00. Las Vegas, Nevada: U.S. Department of Energy, Office of Repository Development. ACC: MOL.20031212.0439. **167603**

DOE (U.S. Department of Energy) 2003. *Installation Test Process for: ASHPLUME_DLL_LA Version 2.0.* Document ID: 11117-ITP-2.0-00. Las Vegas, Nevada: U.S. Department of Energy, Office of Repository Development. ACC: MOL.20031212.0440. **167606**

DOE (U.S. Department of Energy) 2003. *Validation Test Report for: ASHPLUME_DLL_LA Version 2.0.* 11117-VTR-2.0-00. Las Vegas, Nevada: U.S. Department of Energy, Office of Repository Development. ACC: MOL.20031212.0443. **166506**

DOE (U.S. Department of Energy) 2005. *Design Document for: FEHM V2.23.* Document ID: 10086-DD-2.23-00. Las Vegas, Nevada: U.S. Department of Energy, Office of Repository Development. ACC: MOL.20050301.0043. **173440**

DOE (U.S. Department of Energy) 2005. *Design Document for: SEEPAGEDLL_LA V1.2.* Document ID: 11076-DD-1.2-00. Las Vegas, Nevada: U.S. Department of Energy, Office of Repository Development. ACC: MOL.20050406.0440. **173464**

DOE (U.S. Department of Energy) 2005. *Design Document for: TSPA_Input_DB Version 2.0.* Document ID: 10931-DD-2.0-00. Las Vegas, Nevada: U.S. Department of Energy, Office of Repository Development. ACC: MOL.20050131.0430. **173450**

DOE (U.S. Department of Energy) 2005. *Requirements Document for: FEHM V2.23.* Document ID: 10086-RD-2.23-00. Las Vegas, Nevada: U.S. Department of Energy, Office of Repository Development. ACC: MOL.20050301.0040. **174616**

DOE (U.S. Department of Energy) 2005. *Requirements Document for: SEEPAGEDLL_LA V1.2.* Document ID: 11076-RD-1.2-00. Las Vegas, Nevada: U.S. Department of Energy, Office of Repository Development. ACC: MOL.20050406.0437. **173465**

DOE (U.S. Department of Energy) 2005. *Requirements Document for: TSPA_Input_DB Version 2.0.* Document ID: 10931-RD-2.0-00. Las Vegas, Nevada: U.S. Department of Energy, Office of Repository Development. ACC: MOL.20050131.0427. **173449**

DOE (U.S. Department of Energy) 2005. *Software Validation Report for: FEHM V2.23.* Document ID: 10086-SVR-2.23-00 Win2000. Las Vegas, Nevada: U.S. Department of Energy, Office of Repository Development. ACC: MOL.20050301.0049. **173442**

DOE (U.S. Department of Energy) 2005. *Software Validation Report for: SEEPAGEDLL_LA V1.2.* Document ID: 11076-SVR-1.2-00. Las Vegas, Nevada: U.S. Department of Energy, Office of Repository Development. ACC: MOL.20050406.0429. **173462**

DOE (U.S. Department of Energy) 2005. *User Information Document for: SEEPAGEDLL_LA V1.2.* Document ID: 11076-UID-1.2-00. Las Vegas, Nevada: U.S. Department of Energy, Office of Repository Development. ACC: MOL.20050406.0425. **173463**

DOE (U.S. Department of Energy) 2005. *User Information for: FEHM V2.23.* Document ID: 10086-UID-2.23-00. Las Vegas, Nevada: U.S. Department of Energy, Office of Repository Development. ACC: MOL.20050301.0046. **173441**

DOE (U.S. Department of Energy) 2006. *Design Document for: ASHPLUME_DLL_LA V2.1.* Document ID: 11117-DD-2.1-00. Las Vegas, Nevada: U.S. Department of Energy, Office of Repository Development. ACC: MOL.20061106.0387. **181075**

DOE (U.S. Department of Energy) 2006. *Requirements Document for: ASHPLUME_DLL_LA V2.1.* Document ID: 11117-RD-2.1-00. Las Vegas, Nevada: U.S. Department of Energy, Office of Repository Development. ACC: MOL.20061106.0385. **181073**

DOE (U.S. Department of Energy) 2006. *Software Validation Report for: ASHPLUME_DLL_LA Version 2.1 Operating in GoldSim under the Windows 2000 Environment.* Document ID: 11117-SVR-2.1-00-Win2000. Las Vegas, Nevada: U.S. Department of Energy, Office of Repository Development. ACC: MOL.20070102.0246. **181077**

DOE (U.S. Department of Energy) 2006. *User Information Document for: ASHPLUME_DLL_LA Version 2.1.* Document ID: 11117-UID-2.1-00. Las Vegas, Nevada: U.S. Department of Energy, Office of Repository Development. ACC: MOL.20070102.0242. **181076**

DOE (U.S. Department of Energy) 2007. *Design Document for: EXDOC_LA Version 2.0.* Document ID: 11193-DD-2.0-01. Las Vegas, Nevada: U. S. Department of Energy, Office of Repository Development. ACC: MOL.20070723.0262. **182907**

DOE (U.S. Department of Energy) 2007. *Design Document for: FAR Version 1.2.* Document ID: 11190-DD-1.2-00. Las Vegas, Nevada: U.S. Department of Energy, Office of Repository Development. ACC: MOL.20070919.0327. **183118**

DOE (U.S. Department of Energy) 2007. *Design Document for: PassTable3D_LA Version 2.0.* Document ID: 11143-DD-2.0-00. Las Vegas, Nevada: U. S. Department of Energy, Office of Repository Development. ACC: MOL.20070816.0247. **182917**

DOE (U.S. Department of Energy) 2007. *Requirements Document for: EXDOC_LA Version 2.0.* Document ID: 11193-RD-2.0-00. Las Vegas, Nevada: U. S. Department of Energy, Office of Repository Development. ACC: MOL.20070723.0253. **183125**

DOE (U.S. Department of Energy) 2007. *Requirements Document for: FAR Version 1.2.* Document ID: 11190-RD-1.2-00. Las Vegas, Nevada: U. S. Department of Energy, Office of Repository Development. ACC: MOL.20070919.0325. **183117**

DOE (U.S. Department of Energy) 2007. *Requirements Document for: PassTable3D_LA Version 2.0.* Document ID: 11143-RD-2.0-00. Las Vegas, Nevada: U.S. Department of Energy, Office of Repository Development. ACC: MOL.20070816.0245. **182916**

DOE (U.S. Department of Energy) 2007. *Software Validation Report for: EXDOC_LA Version 2.0.* Document ID: 11193-SVR-2.0-00-WINXP. Las Vegas, Nevada: U. S. Department of Energy, Office of Repository Development. ACC: MOL.20070723.0270. **182911**

DOE (U.S. Department of Energy) 2007. *Software Validation Report for: FAR Version 1.2.* Document ID: 11190-SVR-1.2-00-Win2000. Las Vegas, Nevada: U.S. Department of Energy, Office of Repository Development. ACC: MOL.20070919.0334. **183120**

DOE (U.S. Department of Energy) 2007. *Software Validation Report for: PassTable3D_LA Version 2.0.* Document ID: 11143-SVR-2.0-00-WIN2000. Las Vegas, Nevada: U.S. Department of Energy, Office of Repository Development. ACC: MOL.20070816.0254. **182919**

DOE (U.S. Department of Energy) 2007. *Software Validation Report for: PassTable3D_LA Version 2.0.* Document ID: 11143-SVR-2.0-00-WIN2003. Las Vegas, Nevada: U. S. Department of Energy, Office of Repository Development. ACC: MOL.20070816.0256. **182920**

DOE (U.S. Department of Energy) 2007. *Software Validation Report, SZ_CONVOLUTE Version 3.10.01.* Document ID: 10207-SVR-3.10.01-00-Win2000. Las Vegas, Nevada: U.S. Department of Energy, Office of Repository Development. ACC: MOL.20070501.0392. **181289**

DOE (U.S. Department of Energy) 2007. *User Information Document for: PassTable3D_LA Version 2.0.* Document ID: 11143-UID-2.0-00. Las Vegas, Nevada: U. S. Department of Energy, Office of Repository Development. ACC: MOL.20070816.0252. **182918**

Driscoll, F.G. 1986. *Groundwater and Wells.* 2nd Edition. St. Paul, Minnesota: Johnson Filtration Systems. TIC: 217555. **116801**

Duan, N. 1982. "Models for Human Exposure to Air Pollution." *Environment International, 8,* 305-309. [New York, New York]: Pergamon Press. TIC: 250558. **162466**

EPA (U.S. Environmental Protection Agency) 2002. *Federal Guidance Report 13, CD Supplement, Cancer Risk Coefficients for Environmental Exposure to Radionuclides, EPA.* EPA-402-C-99-001, Rev. 1. [Washington, D.C.]: U.S. Environmental Protection Agency. ACC: MOL.20051013.0016. **175544**

EPA (U.S. Environmental Protection Agency) 1997. *Activity Factors.* Volume III of *Exposure Factors Handbook.* EPA/600/P-95/002Fc. Washington, D.C.: U.S. Environmental Protection Agency. TIC: 241062. **116135**

EQ3/6 V. 8.0. 2003. WINDOWS 2000, WIN NT 4.0, WIN 98, WIN 95. STN: 10813-8.0-00. **162228**

EQ6 V. 7.2bLV. 2002. WINDOWS 2000, NT. STN: 10075-7.2bLV-02. **159731**

Evans, M.; Hastings, N.; and Peacock, B. 1993. *Statistical Distributions.* 2nd Edition. New York, New York: John Wiley & Sons. TIC: 246114. **112115**

EXDOC_LA V. 2.0. 2007. WINDOWS XP, WINDOWS 2000 & WINDOWS 2003. STN: 11193-2.0-00. **182102**

FAR V. 1.1. 2007. WINDOWS 2000 & 2003. STN: 11190-1.1-00. **180002**

FAR V. 1.2. 2007. WINDOWS 2000 & WINDOWS 2003. STN: 11190-1.2-00. **182225**

FEHM V. 2.23. 2005. WINDOWS 2000. STN: 10086-2.23-00. **173139**

FEHM V. 2.24-01. 2007. WIN2003, 2000, & XP, Red Hat Linux 2.4.21, OS 5.9. STN: 10086-2.24-01-00. **179419**

FEPS Database Software Program V.2. 2002. WINDOWS 2000. STN: 10418-.2-00. **159684**

FLUENT V. 6.0.12. 2003. Redhat Linux V7.3. STN: 10550-6.0.12-01. **164315**

Forester, R.M.; Bradbury, J.P.; Carter, C.; Elvidge-Tuma, A.B.; Hemphill, M.L.; Lundstrom, S.C.; Mahan, S.A.; Marshall, B.D.; Neymark, L.A.; Paces, J.B.; Sharpe, S.E.; Whelan, J.F.; and Wigand, P.E. 1999. *The Climatic and Hydrologic History of Southern Nevada During the Late Quaternary.* Open-File Report 98-635. Denver, Colorado: U.S. Geological Survey. TIC: 245717. **109425**

Frankel, J.J. 1967. "Forms and Structures of Intrusive Basaltic Rocks." *Basalts, the Poldervaart Treatise on Rocks of Basaltic Composition.* Volume 1. Hess, H.H. and Poldervaart, A., eds. Pages 63-102. New York, New York: Interscience Publishers. TIC: 254505. **168717**

Freeze, G.A.; Brodsky, N.S.; and Swift, P.N. 2001. *The Development of Information Catalogued in REV00 of the YMP FEP Database.* TDR-WIS-MD-000003 REV 00 ICN 01. Las Vegas, Nevada: Bechtel SAIC Company. ACC: MOL.20010301.0237. **154365**

George-Aniel, B.; Leroy, J.L.; and Poty, B. 1991. "Volcanogenic Uranium Mineralizations in the Sierra Pena Blanca District, Chihuahua, Mexico: Three Genetic Models." *Economic Geology, 86,* (2), 233-248. El Paso, Texas: Economic Geology Publishing. TIC: 237050. **105636**

GetThk_LA V. 1.0. 2006. WINDOWS 2000 & WINDOWS 2003. STN: 11229-1.0-00. **181040**

GoldSim Technology Group 2007. *User's Guide, GoldSim Probabilistic Simulation Environment.* Version 9.60. Two volumes. Issaquah, Washington: GoldSim Technology Group. TIC: 259221. **181727**

GoldSim V. 9.60. 2007. WINDOWS 2000, WINDOWS XP, WINDOWS 2003. STN: 10344-9.60-00. **180224**

Goldsim V. 9.60.100. 2007. WIN 2000, 2003, XP. STN: 10344-9.60-01. **181903**

Goldstein, S.J.; Luo, S.; Ku, T.L.; and Murrell, M.T. 2006. "Uranium-Series Constraints on Radionuclide Transport and Groundwater Flow at the Nopal I Uranium Deposit, Sierra Peña Blanca, Mexico." *International High-Level Radioactive Waste Management Conference (IHLRWM), April 30-May 4, 2006, Las Vegas, Nevada.* Pages 215-222. La Grange Park, Illinois: American Nuclear Society. TIC: 258345. **181364**

GS000308315121.003. Meteorological Stations Selected to Represent Future Climate States at Yucca Mountain, Nevada. Submittal date: 03/14/2000. **151139**

Haukwa, C.; Wu, Y.S.; Hinds, J.J.; Zhang, W.; Ritcey, A.C.; Pan, L.H.; Simmons, A.M.; and Bodvarsson, G.S. 1998. *Results of Sensitivity Studies of Thermo-Hydrologic Behavior Conducted on Hydrologic Parameter Sets.* Milestone SP3CK5M4. Berkeley, California: Lawrence Berkeley National Laboratory. ACC: MOL.19980918.0001. **117826**

Hoffman, F.O. and Hammonds, J.S. 1994. "Propagation of Uncertainty in Risk Assessments: The Need to Distinguish Between Uncertainty Due to Lack of Knowledge and Uncertainty Due to Variability." *Risk Analysis, 14,* (5), 707-712. New York, New York: Plenum. TIC: 246313. **107502**

IADC (International Association of Drilling Contractors) 1992. *Drilling Manual.* 11th Edition. [Houston, Texas]: International Association of Drilling Contractors. TIC: 232344. **155232**

ICRP (International Commission on Radiological Protection) 1994. *Human Respiratory Tract Model for Radiological Protection.* Volume 24, Nos. 1-3 of *Annals of the ICRP.* Smith, H., ed. ICRP Publication 66. [New York, New York]: Pergamon. TIC: 249223. **153705**

Iman, R.L. and Conover, W.J. 1982. "A Distribution-Free Approach to Inducing Rank Correlation Among Input Variables." *Communications in Statistics, Simulation and Computation, 11,* (3), 311-334. New York, New York: Marcel Dekker. TIC: 243311. **124158**

Incropera, F.P. and DeWitt, D.P. 2002. *Fundamentals of Heat and Mass Transfer.* 5th Edition. [New York, New York]: John Wiley & Sons. TIC: 254280. **163337**

InterpZdll_LA V. 1.0. 2004. WINDOWS 2000. STN: 11107-1.0-00. **167885**

InterpZdll_LA V. 1.0. 2007. WINDOWS 2003. STN: 11107-1.0-01. **181043**

Jarzemba, M.S.; LaPlante, P.A.; and Poor, K.J. 1997. *ASHPLUME Version 1.0—A Code for Contaminated Ash Dispersal and Deposition, Technical Description and User's Guide.* CNWRA

97-004, Rev. 1. San Antonio, Texas: Center for Nuclear Waste Regulatory Analyses. ACC: MOL.20010727.0162. **100987**

Kahraman, S.; Balci, C.; Yazici, S.; and Bilgin, N. 2000. "Prediction of the Penetration Rate of Rotary Blast Hole Drills Using a New Drillability Index." *International Journal of Rock Mechanics and Mining Sciences, 37,* ([5]), 729-743. [New York, New York]: Pergamon. TIC: 255709. **167761**

Klepeis, N.E. 1999. "An Introduction to the Indirect Exposure Assessment Approach: Modeling Human Exposure Using Microenvironmental Measurements and the Recent National Human Activity Pattern Survey." *Environmental Health Perspectives, 107,* (Supplement 2), 365-374. [Research Park Triangle, North Carolina: National Institute of Environmental Health Sciences, National Institutes of Health]. TIC: 250567. **160094**

LA0303HV831352.003. Fraction of Colloids that Travel Unretarded. Submittal date: 03/31/2003. **165624**

LA0307BY831811.001. Characterize Igneous Framework Additional Output. Submittal date: 07/29/2003. **164713**

LA0408AM831341.001. Unsaturated Zone Distribution Coefficients (Kds) for U, Np, Pu, Am, Pa, Cs, Sr, Ra, and Th. Submittal date: 08/24/2004. **171584**

LA0612DK831811.001. Magma and Eruption Properties for Potential Volcano at Yucca Mountain. Submittal date: 03/23/2007. **179987**

LA0701PANS02BR.003. UZ Transport Parameters. Submittal date: 04/23/2007. **180497**

LA0702AM150304.001. Probability Distribution Functions and Cross-Radionuclide Correlations for Sampling of Sorption Coefficient Probability Distributions in the SZ at the YM. Submittal date: 08/16/2007. **182480**

LA0702PADE01EG.001. Igneous Temperatures. Submittal date: 02/01/2007. **179495**

LA0702PADE01EG.002. EBS Failure Fractions. Submittal date: 02/02/2007. **179496**

LA0702PADE03GK.002. Input Parameter Values for the ASHPLUME V2.1_DLL_LA Model for TSPA. Submittal date: 03/23/2007. **179980**

LA0702PANS02BR.001. Repository and Water Table Bins. Submittal date: 04/16/2007. **180322**

LA0705PR150304.001. Colloid Diversity Model Parameters. Submittal date: 05/18/2007. **181744**

LANL (Los Alamos National Laboratory) 2003. *Software Users Manual (UM) for the FEHM Application Version 2.21.* Document ID: 10086-UM-2.21-00. Los Alamos, [New Mexico]: Los Alamos National Laboratory. ACC: MOL.20031031.0266. **167579**

LB03033DSSFF9I.001. 3-D Site Scale UZ Flow Fields for 9 Infiltration Scenarios: Simulations Using Alternative Hydraulic Properties. Submittal date: 03/28/2003. **163047**

LB0310AMRU0120.002. Mathcad 11 Spreadsheets for Probabilistic Seepage Evaluation. Submittal date: 10/23/2003. **166116**

LB0407AMRU0120.001. Supporting Calculations and Analysis for Seepage Abstraction and Summary of Abstraction Results. Submittal date: 07/29/2004. **173280**

LB0610UZDSCP30.001. Drift-Scale Calibrated Property Set for the 30-Percentile Infiltration Map. Submittal date: 11/02/2006. **179180**

LB0611MTSCHP10.001. Mountain Scale Calibrated Property Set for the 10-Percentile Infiltration Map. Submittal date: 11/28/2006. **178586**

LB0611MTSCHP30.001. Mountain Scale Calibrated Property Set for the 30-Percentile Infiltration Map. Submittal date: 11/28/2006. **180293**

LB0612MTSCHP50.001. Mountain Scale Calibrated Property Set for the 50-Percentile Infiltration Map. Submittal date: 12/19/2006. **180294**

LB0612MTSCHP90.001. Mountain Scale Calibrated Property Set for the 90-Percentile Infiltration Map. Submittal date: 12/20/2006. **180295**

LB0612MTSCHPFT.001. Calibrated UZ Fault Property Sets. Submittal date: 12/07/2006. **180296**

LB0612PDFEHMFF.001. Flow-Field Conversions from TOUGH2 to FEHM Format for Present Day 10-, 30-, 50-, and 90-Percentile Infiltration Maps. Submittal date: 12/19/2006. **179296**

LB0701GTFEHMFF.001. Flow-Field Conversions from TOUGH2 to FEHM Format for Glacial Transition Climate 10th-, 30th-, 50th-, and 90th-Percentile Infiltration Maps. Submittal date: 01/05/2007. **179160**

LB0701MOFEHMFF.001. Flow-Field Conversions from TOUGH2 to FEHM Format for Monsoon Climate 10th-, 30th-, 50th-, and 90th-Percentile Infiltration Maps. Submittal date: 01/05/2007. **179297**

LB0701PAKDSESN.001. Unsaturated Zone Sorption Coefficients for Selenium and Tin. Submittal date: 01/31/2007. **179299**

LB0701PAWFINFM.001. Weighting Factors for Infiltration Maps. Submittal date: 01/25/2007. **179283**

LB0702PAFEM10K.002. Flow Field Conversions to FEHM Format for Post 10,000 Year Peak Dose Fluxes in the Unsaturated Zone for Four Selected Infiltration Rates. Submittal date: 02/15/2007. **179507**

LB0702PASEEP01.001. New Extended-Range Seepage Look-Up Tables for Intact and Collapsed Drifts Plus Supporting Files. Submittal date: 02/20/2007. **179511**

LB0702PASEEP02.001. Seepage Abstraction for Degraded Drifts. Submittal date: 06/29/2007. **181635**

LB0702PAUZMTDF.001. Unsaturated Zone Matrix Diffusion Coefficients. Submittal date: 05/10/2007. **180776**

Leigh, C.D.; Thompson, B.M.; Campbell, J.E.; Longsine, D.E.; Kennedy, R.A.; and Napier, B.A. 1993. *User's Guide for GENII-S: A Code for Statistical and Deterministic Simulations of Radiation Doses to Humans from Radionuclides in the Environment.* SAND91-0561. Albuquerque, New Mexico: Sandia National Laboratories. ACC: MOL.20010721.0031. **100464**

Lichtner, P.C.; Keating, G.; and Carey, B. 1999. *A Natural Analogue for Thermal-Hydrological-Chemical Coupled Processes at the Proposed Nuclear Waste Repository at Yucca Mountain, Nevada.* LA-13610-MS. Los Alamos, New Mexico: Los Alamos National Laboratory. TIC: 246032. **121006**

Liu, H.H.; Doughty, C.; and Bodvarsson, G.S. 1998. "An Active Fracture Model for Unsaturated Flow and Transport in Fractured Rocks." *Water Resources Research, 34,* (10), 2633-2646. Washington, D.C.: American Geophysical Union. TIC: 243012. **105729**

LL0702PA027MST.082. Output for ANL-EBS-MD-000049 Multiscale Thermohydrologic Model for the Mean Host-Rock Thermal Conductivity, 10-Percentile Percolation Flux, Collapsed-Drift, High and Low Rubble Thermal Conductivity Cases. Submittal date: 02/15/2007. **179590**

LL0703PA011MST.006. Output for ANL-EBS-MD-000049 REV 04 Multiscale Thermohydrologic Model for the Mean Host-Rock Thermal Conductivity, 10-Percentile Percolation Flux Case. Submittal date: 03/07/2007. **179853**

LL0703PA012MST.007. Output for ANL-EBS-MD-000049 REV 04 Multiscale Thermohydrologic Model for the Mean Host-Rock Thermal Conductivity, 30-Percentile Percolation Flux Case. Submittal date: 03/13/2007. **179854**

LL0703PA013MST.008. Output for ANL-EBS-MD-000049 REV 04 Multiscale Thermohydrologic Model for the Mean Host-Rock Thermal Conductivity, 50-Percentile Percolation Flux Case. Submittal date: 03/13/2007. **179855**

LL0703PA014MST.009. Output for ANL-EBS-MD-000049 REV 04 Multiscale Thermohydrologic Model for the Mean Host-Rock Thermal Conductivity, 90-Percentile Percolation Flux Case. Submittal date: 03/13/2007. **179856**

LL0703PA015MST.010. Output for ANL-EBS-MD-000049 REV 04 Multiscale Thermohydrologic Model for the Low Host-Rock Thermal Conductivity, 10-Percentile Percolation Flux Case. Submittal date: 03/13/2007. **179857**

LL0703PA016MST.011. Output for ANL-EBS-MD-000049 REV 04 Multiscale Thermohydrologic Model for the High Host-Rock Thermal Conductivity, 90-Percentile Percolation Flux Case. Submittal date: 03/13/2007. **179858**

LL0703PA017MST.012. Output for ANL-EBS-MD-000049 REV 04 Multiscale Thermohydrologic Model for the High Host-Rock Thermal Conductivity, 10-Percentile Percolation Flux Case. Submittal date: 03/13/2007. **179859**

LL0703PA026MST.013. Weighting Factors for Low (10-Percentile), Mean, and High (90-Percentile) Host-Rock Thermal Conductivity Cases for ANL-EBS-MD-000049 Multiscale Thermohydrologic Model. Submittal date: 03/28/2007. **179981**

LL0703PA034MST.016. Output for ANL-EBS-MD-000049 Multiscale Thermohydrologic Model for the Low Host-Rock Thermal Conductivity, 30-Percentile Percolation Flux (P30L) Case. Submittal date: 03/22/2007. **179982**

LL0703PA035MST.017. Output for ANL-EBS-MD-000049 Multiscale Thermohydrologic Model for the High Host-Rock Thermal Conductivity, 30-Percentile Percolation Flux (P30H) Case. Submittal date: 03/22/2007. **179985**

LL0703PA036MST.018. Output for ANL-EBS-MD-000049 Multiscale Thermohydrologic Model for the Low Host-Rock Thermal Conductivity, 50-Percentile Percolation Flux (P50L) Case. Submittal date: 03/22/2007. **179986**

LL0703PA037MST.019. Output for ANL-EBS-MD-000049 Multiscale Thermohydrologic Model for the High Host-Rock Thermal Conductivity, 50-Percentile Percolation Flux (P50H) Case. Submittal date: 03/22/2007. **179989**

LL0703PA038MST.020. Output for ANL-EBS-MD-000049 Multiscale Thermohydrologic Model for the Low Host-Rock Thermal Conductivity, 90-Percentile Percolation Flux (P90L) Case. Submittal date: 03/22/2007. **179992**

Lu, N.; Conca, J.; Parker, G.R.; Leonard, P.A.; Moore, B.; Strietelmeier, B.; and Triay, I.R. 2000. *Adsorption of Actinides onto Colloids as a Function of Time, Temperature, Ionic Strength, and Colloid Concentration, Waste Form Colloids Report for Yucca Mountain Program (Colloid Data Summary from 1999 to 2000 Research).* LA-UR-00-5121. Los Alamos, New Mexico: Los Alamos National Laboratory. ACC: MOL.20031204.0108. **166315**

Mage, D.T. 1985. "Concepts of Human Exposure Assessment for Airborne Particulate Matter." *Environment International, 11,* 407-412. [New York, New York]: Pergamon Press. TIC: 250582. **162465**

Martinez, L.J.; Meertens, C.M.; and Smith, R.B. 1998. "Rapid Deformation Rates Along the Wasatch Fault Zone, Utah, from First GPS Measurements with Implications for Earthquake Hazard." *Geophysical Research Letters, 25,* (4), 567-570. [Washington, D.C.]: American Geophysical Union. TIC: 246585. **159031**

MFCP_LA V. 1.0. 2003. WINDOWS 2000. STN: 11071-1.0-00. **167884**

MFCP_LA V. 1.0. 2006. WINDOWS 2003. STN: 11071-1.0-01. **181045**

Miller, G.A. 1977. *Appraisal of the Water Resources of Death Valley, California-Nevada.* Open-File Report 77-728. Menlo Park, California: U.S. Geological Survey. ACC: HQS.19880517.1934. **105462**

MkTable V. 1.00. 2003. WINDOWS 2000. STN: 10505-1.00-00. **174528**

MkTable_LA V. 1.0. 2006. WINDOWS 2000. STN: 11217-1.0-00. **181047**

MkTable_LA V. 1.0. 2007. WINDOWS 2003. STN: 11217-1.0-01. **181048**

MO0003RIB00071.000. Physical and Chemical Characteristics of Alloy 22. Submittal date: 03/13/2000. **148850**

MO0003RIB00073.000. Physical and Chemical Characteristics of Ti Grades 7 and 16. Submittal date: 03/13/2000. **152926**

MO0003RIB00076.000. Physical and Chemical Characteristics of Type 316N Grade. Submittal date: 03/14/2000. **153044**

MO0010SPANYE00.001. Cleaned Nye County Food Consumption Frequency Survey. Submittal date: 10/10/2000. **154976**

MO0310SPANGRAC.000. Natural Gross Alpha Concentration in Amargosa Valley Groundwater. Submittal date: 10/23/2003. **169456**

MO0404ANLSF001.001. CSNF Radionuclide Release Model. Submittal date: 04/09/2004. **169007**

MO0408MWDDDMIO.002. Drift Degradation Model Inputs and Outputs. Submittal date: 08/31/2004. **171483**

MO0408SPADRWSD.002. Desert Rock Wind Speed and Wind Direction Analyses for Years 1978 - 2003. Submittal date: 08/19/2004. **171751**

MO0411SPACLDDG.003. Updated TSPA-LA Parameters from Clad Degradation-Summary and Abstraction for LA, ANL-WIS-MD-000021 REV 03. Submittal date: 05/10/2007. **180755**

MO0501BPVELEMP.001. Bounded Horizontal Peak Ground Velocity Hazard at the Repository Waste Emplacement Level. Submittal date: 01/11/2005. **172682**

MO0502ANLGAMR1.016. HLW Glass Degradation Model. Submittal date: 02/08/2005. **172830**

MO0502SPAINPCA.000. In-Package Chemistry Abstraction. Submittal date: 02/25/2005. **172893**

MO0505SPAROCKM.000. Rock Mass and Invert Properties for TSPA-LA. Submittal date: 05/23/2005. **173893**

MO0508SEPFEPLA.002. LA FEP List and Screening. Submittal date: 08/22/2005. **175064**

MO0605SPAFORTY.000. Fortymile Wash Drainage Basin Dem. Submittal date: 08/02/2007. **182281**

MO0701PACSNFCP.000. CSNF Colloid Parameters. Submittal date: 04/17/2007. **180439**

MO0701PAGLASWF.000. Glass Waste Form Colloid Parameters. Submittal date: 04/17/2007. **180393**

MO0701PAGROUND.000. Groundwater Colloid Concentration Parameters. Submittal date: 01/18/2007. **179310**

MO0701PAIRONCO.000. Colloidal Iron Corrosion Products Parameters. Submittal date: 04/17/2007. **180440**

MO0701PAKDSUNP.000. Colloidal KDS for U, NP, RA and SN. Submittal date: 04/17/2007. **180392**

MO0701PASHIELD.000. Waste Package/Drip Shield Early Failure Probabilities. Submittal date: 04/24/2007. **180508**

MO0701PASORPTN.000. Colloidal Sorption Coefficients for PU, AM, TH, CS, and PA. Submittal date: 04/17/2007. **180391**

MO0701RLTSCRNA.000. Results of Screening Analysis. Submittal date: 01/30/2007. **179334**

MO0702PADISCON.001. Dissolved Concentration Limits of Elements with Radioactive Isotopes. Submittal date: 02/15/2007. **179358**

MO0702PAFARDAT.001. FAR Data. Submittal date: 08/21/2007. **182578**

MO0702PAFLUORI.000. Fluoride Uncertainty Associated with Dissolved Concentration Limits. Submittal date: 06/01/2007. **181219**

MO0702PAGBDCFS.001. Groundwater Biosphere Dose Conversion Factors. Submittal date: 02/09/2007. **179327**

MO0702PAGWPROS.001. Groundwater Protection Standards Conversion Factors. Submittal date: 02/06/2007. **179328**

MO0702PAINHALA.001. Inhalation Dose Factors. Submittal date: 02/15/2007. **179329**

MO0702PALOVERT.000. Condensation Abstraction: Well-Ventilated Drip Shield; Low Invert Transport, (0-10,000 Years). Submittal date: 04/16/2007. **180377**

MO0702PALV010K.000. Condensation Abstraction: Unventilated Drip Shield; Low Invert Transport, (0-10,000 Years). Submittal date: 04/16/2007. **180376**

MO0702PASTREAM.001. Waste Stream Composition and Thermal Decay Histories for LA. Submittal date: 02/15/2007. **179925**

MO0702PASTRESS.002. Output DTN of Model Report, "Stress Corrosion Cracking of Waste Package Outer Barrier and Drip Shield Materials," ANL-EBS-MD-000005. Submittal date: 04/24/2007. **180514**

MO0702PAVBPDCF.000. Volcanic Biosphere Dose Conversion Factors. Submittal date: 02/21/2007. TBV-7840 **179330**

MO0703PAEVSIIC.000. Evaluation of Stage II Condensation. Submittal date: 07/16/2007. **181990**

MO0703PAGENCOR.001. Output from General Corrosion and Localized Corrosion of Waste Package Outer Barrier 2007 Second Version. Submittal date: 07/18/2007. **182029**

MO0703PAHYTHRM.000. Hydrological and Thermal Properties of the Invert. Submittal date: 07/19/2007. **182093**

MO0703PASDSTAT.001. Analyses for Seismic Damage Abstractions. Submittal date: 09/21/2007. **183148**

MO0703PASDSTAT.001. Statistical Analyses for Seismic Damage Abstractions. Submittal date: 09/05/2007. **182878**

MO0703PASEISDA.002. Seismic Damage Abstractions for TSPA Compliance Case. Submittal date: 09/21/2007. **183156**

MO0704PAFEHMBR.001. FEHM Model and Input. Submittal date: 04/26/2007. **180526**

MO0704PAPTTFBR.002. Particle Tracking Transfer Functions. Submittal date: 04/12/2007. **180442**

MO0704PASCOURD.000. Scour Depth. Submittal date: 07/25/2007. **182149**

MO0704PASOLCAP.000. In-Package Solubility "Caps" for Pu, Np, U, Th, Am, and Pa. Submittal date: 04/06/2007. **180389**

MO0707UZKDCORR.000. UZ KD Correlation Matrix for the TSPA Model. Submittal date: 2007. **183003**

MO0707WPDRIPSD.000. TSPA LA Waste Package and Drip Shield Degradation. Submittal date: 2007. **183005**

MO0708TSPAGENT.000. TSPA Generated Inputs and Post Processed Inputs. Submittal date: 2007. **183000**

MSTHAC V. 7.0. 2002. SUN O.S. 5.8. STN: 10419-7.0-00. **164274**

MView V. 4.0. 2007. WINDOWS XP. STN: 10072-4.0-01. **181049**

Napier, B.A.; Peloquin, R.A.; Strenge, D.L.; and Ramsdell, J.V. 1988. *Conceptual Representation.* Volume 1 of *GENII - The Hanford Environmental Radiation Dosimetry Software System.* PNL-6584. Richland, Washington: Pacific Northwest Laboratory. TIC: 252237. **157927**

Napier, B.A.; Strenge, D.L.; Ramsdell, J.V., Jr.; Eslinger, P.W.; and Fosmire, C. 2006. *GENII Version 2 Software Design Document.* PNNL-14584, Rev. 1. [Richland, Washington]: Pacific Northwest National Laboratory. ACC: MOL.20060815.0035. **177331**

National Research Council. 1995. *Technical Bases for Yucca Mountain Standards.* Washington, D.C.: National Academy Press. TIC: 217588. **100018**

NEA (Nuclear Energy Agency) 1999. *An International Database of Features, Events and Processes.* Paris, France: Organisation for Economic Co-operation and Development. TIC: 248820. **152309**

NRC (U.S. Nuclear Regulatory Commission) 2003. *Yucca Mountain Review Plan, Final Report.* NUREG-1804, Rev. 2. Washington, D.C.: U.S. Nuclear Regulatory Commission, Office of Nuclear Material Safety and Safeguards. TIC: 254568. **163274**

NRC (U.S. Nuclear Regulatory Commission) 2007. *Igneous Activity at Yucca Mountain: Technical Basis for Decisionmaking.* [Washington, D.C.]: U.S. Nuclear Regulatory Commission, Advisory Committee on Nuclear Waste and Materials. ACC: LLR.20070725.0023. **182132**

Nuclear Waste Policy Act of 1982. 42 U.S.C. 10101-10133. (1988). Internet Accessible. **131951**

Nuclear Waste Policy Amendments Act of 1987. Public Law No. 100-203, 101 Stat. 1330. TIC: 223717. **100016**

OECD (Organisation for Economic Co-operation and Development) and IAEA (International Atomic Energy Agency) 2002. *An International Peer Review of the Yucca Mountain Project TSPA-SR, Total System Performance Assessment for the Site Recommendation (TSPA-SR).* Paris, France: Organisation for Economic Co-operation and Development, Nuclear Energy Agency. TIC: 252385. **158098**

Ortiz, T.S.; Williams, R.L.; Nimick, F.B.; Whittet, B.C.; and South, D.L. 1985. *A Three-Dimensional Model of Reference Thermal/Mechanical and Hydrological Stratigraphy at Yucca Mountain, Southern Nevada.* SAND84-1076. Albuquerque, New Mexico: Sandia National Laboratories. ACC: MOL.19980602.0331. **101280**

Painter, S.; Cvetkovic, V.; Pickett, D.; and Turner, D.R. 2002. "Significance of Kinetics for Sorption of Inorganic Colloids: Modeling and Experiment Interpretation Issues." *Environmental Science & Technology, 36,* (24), 5369-5375. [Washington, D.C.]: American Chemical Society. TIC: 257438. **174071**

Parrington, J.R.; Knox, H.D.; Breneman, S.L.; Baum, E.M.; and Feiner, F. 1996. *Nuclides and Isotopes, Chart of the Nuclides.* 15th Edition. San Jose, California: General Electric Company and KAPL, Inc. TIC: 233705. **103896**

PassTable1D_LA V. 1.0. 2004. WINDOWS 2000. STN: 11142-1.0-00. **169130**

PassTable1D_LA V. 1.0. 2006. WINDOWS 2003. STN: 11142-1.0-01. **181050**

PassTable1D_LA V. 2.0. 2007. WINDOWS 2000 & WINDOWS 2003. STN: 11142-2.0-00. **181051**

PassTable3D_LA V. 1.0. 2004. WINDOWS 2000. STN: 11143-1.0-00. **168980**

PassTable3D_LA V. 1.0. 2007. WINDOWS 2003. STN: 11143-1.0-01. **181052**

PassTable3D_LA V. 2.0. 2007. WINDOWS 2000 & WINDOWS 2003. STN: 11143-2.0-00. **182556**

Pearcy, E.C.; Prikryl, J.D.; Murphy, W.M.; and Leslie, B.W. 1993. *Uranium Mineralogy of the Nopal I Natural Analog Site, Chihuahua, Mexico.* CNWRA 93-012. San Antonio, Texas: Center for Nuclear Waste Regulatory Analyses. TIC: 246628. **151774**

Press, W.H.; Teukolsky, S.A.; Vetterling, W.T.; and Flannery, B.P. 1992. *Numerical Recipes in Fortran 77, The Art of Scientific Computing.* Volume 1 of *Fortran Numerical Recipes.* 2nd Edition. Cambridge, United Kingdom: Cambridge University Press. TIC: 243606. **103316**

PREWAP_LA V. 1.1. 2006. WINDOWS 2000. STN: 10939-1.1-00. **181053**

Putot, C.J.M.; Guesnon, J.; Perreau, P.J.; and Constantinescu, A. 2000. "Quantifying Drilling Efficiency and Disruption: Field Data vs. Theoretical Model." *SPE Drilling & Completion, 15,* (2), 118-125. [Richardson, Texas]: Society of Petroleum Engineers. TIC: 255897. **167791**

Rai, D.; Moore, D.A.; Felmy, A.R.; Choppin, G.R.; and Moore, R.C. 2001. "Thermodynamics of the PuO{subscript 2}{superscript +}-Na{superscript +}-OH{superscript -}-Cl{superscript -}-ClO{subscript 4}{superscript -}-H{subscript 2}O System: Use of NpO{subscript 2}{superscript +} Pitzer Parameters for PuO{subscript 2}{superscript +}." *Radiochimica Acta, 89,* ([8]), 491-498. München, Germany: Oldenbourg Wissenschaftsverlag. TIC: 255398. **168392**

Reamer, C.W. 2001. "U.S. Nuclear Regulatory Commission/U.S. Department of Energy Technical Exchange and Management Meeting on Total System Performance Assessment and Integration (August 6 through 10, 2001)." Letter from C.W. Reamer (NRC) to S. Brocoum (DOE/YMSCO), August 23, 2001, with enclosure. ACC: MOL.20011029.0281. **158380**

Rechard, R.P., ed. 1993. *Initial Performance Assessment of the Disposal of Spent Nuclear Fuel and High Level Waste Stored at Idaho National Engineering Laboratory.* SAND93-2330. Volumes 1 and 2. Albuquerque, New Mexico: Sandia National Laboratories. TIC: 247212. **147343**

Reimus, P.W.; Callahan, T.J.; Ware, S.D.; Haga, M.J.; and Counce, D.A. 2007. "Matrix Diffusion Coefficients in Volcanic Rocks at the Nevada Test Site: Influence of Matrix Porosity, Matrix Permeability, and Fracture Coating Minerals." *Journal of Contaminant Hydrology, 93,* 85-95. [New York, New York]: Elsevier. TIC: 259673. **179246**

Runde, W.; Neu, M.P.; Conradson, S.D.; Clark, D.L.; Palmer, P.D.; Reilly, S.D.; Scott, B.L.; and Tait, C.D. 1997. "Spectroscopic Investigation of Actinide Speciation in Concentrated Chloride Solution." *Scientific Basis for Nuclear Waste Management XX, Symposium held December 2-6 1996, Boston Massachusetts.* Gray, W.J. and Triay, I.R., eds. *465,* 693-703. Pittsburgh, Pennsylvania: Materials Research Society. TIC: 238884. **182190**

Sawyer, D.A.; Fleck, R.J.; Lanphere, M.A.; Warren, R.G.; Broxton, D.E.; and Hudson, M.R. 1994. "Episodic Caldera Volcanism in the Miocene Southwestern Nevada Volcanic Field: Revised Stratigraphic Framework, {superscript 40}Ar/{superscript 39}Ar Geochronology, and Implications for Magmatism and Extension." *Geological Society of America Bulletin, 106,* (10), 1304-1318. Boulder, Colorado: Geological Society of America. TIC: 222523. **100075**

SCCD V. 2.01. 2003. WINDOWS 2000. STN: 10343-2.01-00. **181157**

SCCD V. 2.01. 2007. WINDOWS 2003. STN: 10343-2.01-01. **181054**

SEEPAGEDLL_LA V. 1.2. 2005. WINDOWS 2000. STN: 11076-1.2-00. **173435**

SEEPAGEDLL_LA V. 1.3. 2006. WINDOWS 2000. STN: 11076-1.3-00. **180318**

SEEPAGEDLL_LA V. 1.3. 2007. WINDOWS 2003. STN: 11076-1.3-01. **181058**

Sharpe, S. 2003. *Future Climate Analysis—10,000 Years to 1,000,000 Years After Present.* MOD-01-001 REV 01. [Reno, Nevada: Desert Research Institute]. ACC: MOL.20030407.0055. **161591**

Sheppard, M.I.; Sheppard, S.C.; and Amiro, B.D. 1991. "Mobility and Plant Uptake of Inorganic {superscript 14}C and {superscript 14}C-Labelled PCB in Soils of High and Low Retention." *Health Physics, 61,* (4), 481-492. New York, New York: Pergamon Press. TIC: 252687. **159545**

Shibata, T. 1996. "Statistical and Stochastic Approaches to Localized Corrosion." *Corrosion, 52,* (11), 813-830. Houston, Texas: National Association of Corrosion Engineers. TIC: 236691. **119589**

Singh, B. 2002. "Nuclear Data Sheets for A = 79." *Nuclear Data Sheets, 96,* (1), 1-240. San Diego, California: Elsevier. TIC: 254728. **164741**

Smyth, J.R. 1982. "Zeolite Stability Constraints on Radioactive Waste Isolation in Zeolite-Bearing Volcanic Rocks." *Journal of Geology, 90,* (2), 195-201. Chicago, Illinois: University of Chicago Press. TIC: 221104. **119483**

SN0308T0503100.008. Revised Frequency Distributions for Net Infiltrations and Weighting Factors Applied to Lower, Mean, and Upper Climates. Submittal date: 08/28/2003. **165640**

SN0310T0505503.004. Initial Radionuclide Inventories for TSPA-LA. Submittal date: 10/27/2003. **168761**

SN0609T0502404.012. Pitzer Thermodynamic Database (DATA0.YP2). Submittal date: 09/28/2006. **179067**

SN0701PAEBSPCE.001. PCE TDIP Potential Seepage Water Chemistry Lookup Tables. Submittal date: 04/25/2007. **180523**

SN0701PAEBSPCE.002. PCE TDIP PCO2 and Total Carbon Lookup Tables. Submittal date: 01/30/2007. **179425**

SN0701PAWPHIT1.001. Number of Waste Packages Hit by Igneous Events. Submittal date: 09/13/2007. **182961**

SN0702PAIPC1CA.001. In-Package Chemistry Calculations and Abstractions. Submittal date: 04/19/2007. **180451**

SN0702PASZFTMA.001. Saturated Zone Flow and Transport Model Abstraction. Submittal date: 02/06/2007. **179504**

SN0702PASZFTMA.002. Saturated Zone 1-D Transport Model. Submittal date: 02/15/2007. **179494**

SN0703PAEBSPCE.006. Physical and Chemical Environment (PCE) TDIP Water-Rock Interaction Parameter Table and Salt Separation Tables with Supporting Files. Submittal date: 06/27/2007. **181571**

SN0703PAEBSPCE.007. Physical and Chemical Environment (PCE) TDIP Uncertainty Evaluations and Supporting Files. Submittal date: 04/06/2007. **180177**

SN0703PAEBSRTA.001. Inputs Used in the Engineered Barrier System (EBS) Radionuclide Transport Abstraction. Submittal date: 09/28/2007. **183217**

SN0704PADSGCMT.001. Drip Shield General Corrosion Models Based on 2.5-Year Titanium Grade 7 Corrosion Rates. Submittal date: 07/24/2007. **182122**

SN0704PADSGCMT.002. Drip Shield General Corrosion Rate Multiplier for Titanium Grade 29. Submittal date: 07/27/2007. **182188**

SN0706PAEBSPCE.016. P&CE Invert Relative Humidity (RH) Boundary Table. Submittal date: 06/28/2007. **181837**

SNL (Sandia National Laboratories) 2006. *Data Analysis for Infiltration Modeling: Extracted Weather Station Data Used to Represent Present-Day and Potential Future Climate Conditions in the Vicinity of Yucca Mountain.* ANL-MGR-MD-000015 REV 00. Las Vegas, Nevada: Sandia National Laboratories. ACC: DOC.20070109.0002. **177081**

SNL (Sandia National Laboratories) 2007. *Abstraction of Drift Seepage.* MDL-NBS-HS-000019 REV 01 ADD 01. Las Vegas, Nevada: Sandia National Laboratories. ACC: DOC.20070807.0001. **181244**

SNL (Sandia National Laboratories) 2007. *Analysis of Dust Deliquescence for FEP Screening.* ANL-EBS-MD-000074 REV 01 AD 01. Las Vegas, Nevada: Sandia National Laboratories. ACC: DOC.20070911.0004. **181267**

SNL (Sandia National Laboratories) 2007. *Analysis of Mechanisms for Early Waste Package/Drip Shield Failure.* ANL-EBS-MD-000076 REV 00. Las Vegas, Nevada: Sandia National Laboratories. ACC: DOC.20070629.0002. **178765**

SNL (Sandia National Laboratories) 2007. *Atmospheric Dispersal and Deposition of Tephra from a Potential Volcanic Eruption at Yucca Mountain, Nevada.* MDL-MGR-GS-000002 REV 03. Las Vegas, Nevada: Sandia National Laboratories. **177431**

SNL (Sandia National Laboratories) 2007. *Biosphere Model Report.* MDL-MGR-MD-000001 REV 02. Las Vegas, Nevada: Sandia National Laboratories. ACC: DOC.20070830.0007. **177399**

SNL (Sandia National Laboratories) 2007. *Calibrated Unsaturated Zone Properties.* ANL-NBS-HS-000058 REV 00. Las Vegas, Nevada: Sandia National Laboratories. ACC: DOC.20070530.0013. **179545**

SNL (Sandia National Laboratories) 2007. *Characterize Eruptive Processes at Yucca Mountain, Nevada.* ANL-MGR-GS-000002 REV 03. Las Vegas, Nevada: Sandia National Laboratories. ACC: DOC.20070301.0001. **174260**

SNL (Sandia National Laboratories) 2007. *Cladding Degradation Summary for LA.* ANL-WIS-MD-000021 REV 03 ADD 01. Las Vegas, Nevada: Sandia National Laboratories. ACC: DOC.20050815.0002; DOC.20070614.0002. **180616**

SNL (Sandia National Laboratories) 2007. *Dike/Drift Interactions.* MDL-MGR-GS-000005 REV 02. Las Vegas, Nevada: Sandia National Laboratories. **177430**

SNL (Sandia National Laboratories) 2007. *Dissolved Concentration Limits of Elements with Radioactive Isotopes.* ANL-WIS-MD-000010 REV 06. Las Vegas, Nevada: Sandia National Laboratory. ACC: DOC.20070918.0010. **177418**

SNL (Sandia National Laboratories) 2007. *Drift-Scale THC Seepage Model.* MDL-NBS-HS-000001 REV 05. Las Vegas, Nevada: Sandia National Laboratories. **177404**

SNL (Sandia National Laboratories) 2007. *EBS Radionuclide Transport Abstraction.* ANL-WIS-PA-000001 REV 03. Las Vegas, Nevada: Sandia National Laboratories. **177407**

SNL (Sandia National Laboratories) 2007. *Engineered Barrier System: Physical and Chemical Environment.* ANL-EBS-MD-000033 REV 06. Las Vegas, Nevada: Sandia National Laboratories. ACC: DOC.20070907.0003. **177412**

SNL (Sandia National Laboratories) 2007. *General Corrosion and Localized Corrosion of the Drip Shield.* ANL-EBS-MD-000004 REV 02 ADD 01. Las Vegas, Nevada: Sandia National Laboratories. ACC: DOC.20060427.0002; DOC.20070807.0004. **180778**

SNL (Sandia National Laboratories) 2007. *General Corrosion and Localized Corrosion of Waste Package Outer Barrier.* ANL-EBS-MD-000003 REV 03. Las Vegas, Nevada: Sandia National Laboratories. ACC: DOC.20070730.0003; DOC.20070807.0007. **178519**

SNL (Sandia National Laboratories) 2007. *In-Drift Natural Convection and Condensation.* MDL-EBS-MD-000001 REV 00 AD 01. Las Vegas, Nevada: Sandia National Laboratories. ACC: DOC.20041025.0006; DOC.20050330.0001; DOC.20051122.0005; DOC.20070907.0004. **181648**

SNL (Sandia National Laboratories) 2007. *In-Drift Precipitates/Salts Model.* ANL-EBS-MD-000045 REV 03. Las Vegas, Nevada: Sandia National Laboratories. ACC: DOC.20070306.0037. **177411**

SNL (Sandia National Laboratories) 2007. *In-Package Chemistry Abstraction.* ANL-EBS-MD-000037 REV 04 ADD 01. Las Vegas, Nevada: Sandia National Laboratories. ACC: DOC.20051130.0007; DOC.20070816.0004. **180506**

SNL (Sandia National Laboratories) 2007. *Initial Radionuclides Inventory.* ANL-WIS-MD-000020 REV 01 ADD 01. Las Vegas, Nevada: Sandia National Laboratories. ACC: DOC.20050927.0005; DOC.20070801.0001. **180472**

SNL (Sandia National Laboratories) 2007. *Mechanical Assessment of Degraded Waste Packages and Drip Shields Subject to Vibratory Ground Motion.* MDL-WIS-AC-000001 REV 00. Las Vegas, Nevada: Sandia National Laboratories. ACC: DOC.20070917.0006. **178851**

SNL (Sandia National Laboratories) 2007. *MOX Spent Nuclear Fuel and LaBS Glass for TSPA-LA.* ANL-WIS-MD-000022 REV 01. Las Vegas, Nevada: Sandia National Laboratories. ACC: DOC.20070220.0007. **177422**

SNL (Sandia National Laboratories) 2007. *Multiscale Thermohydrologic Model.* ANL-EBS-MD-000049 REV 03 ADD 01. Las Vegas, Nevada: Sandia National Laboratories. ACC: DOC.20070831.0003. **181383**

SNL (Sandia National Laboratories) 2007. *Number of Waste Packages Hit by Igneous Events.* ANL-MGR-GS-000003 REV 03. Las Vegas, Nevada: Sandia National Laboratories. ACC: DOC.20071002.0001. **177432**

SNL (Sandia National Laboratories) 2007. *Particle Tracking Model and Abstraction of Transport Processes.* MDL-NBS-HS-000020 REV 02 ADD 01. Las Vegas, Nevada: Sandia National Laboratories. ACC: DOC.20070823.0005. **181006**

SNL (Sandia National Laboratories) 2007. *Radionuclide Screening.* ANL-WIS-MD-000006 REV 02. Las Vegas, Nevada: Sandia National Laboratories. ACC: DOC.20070326.0003. **177424**

SNL (Sandia National Laboratories) 2007. *Radionuclide Transport Models Under Ambient Conditions.* MDL-NBS-HS-000008 REV 02 ADD 01. Las Vegas, Nevada: Sandia National Laboratories. ACC: DOC.20050823.0003; DOC.20070718.0003. **177396**

SNL (Sandia National Laboratories) 2007. *Redistribution of Tephra and Waste by Geomorphic Processes Following a Potential Volcanic Eruption at Yucca Mountain, Nevada.* MDL-MGR-GS-000006 REV 00. Las Vegas, Nevada: Sandia National Laboratories. **179347**

SNL (Sandia National Laboratories) 2007. *Saturated Zone Flow and Transport Model Abstraction.* MDL-NBS-HS-000021 REV 03 AD 01. Las Vegas, Nevada: Sandia National Laboratories. ACC: DOC.20050808.0004; DOC.20070913.0002. **181650**

SNL (Sandia National Laboratories) 2007. *Saturated Zone Site-Scale Flow Model.* MDL-NBS-HS-000011 REV 03. Las Vegas, Nevada: Sandia National Laboratories. ACC: DOC.20070626.0004. **177391**

SNL (Sandia National Laboratories) 2007. *Seismic Consequence Abstraction.* MDL-WIS-PA-000003 REV 03. Las Vegas, Nevada: Sandia National Laboratories. ACC: DOC.20070928.0011. **176828**

SNL (Sandia National Laboratories) 2007. *Simulation of Net Infiltration for Present-Day and Potential Future Climates.* MDL-NBS-HS-000023 REV 01 AD 01. Las Vegas, Nevada: Sandia National Laboratories. **182145**

SNL (Sandia National Laboratories) 2007. *Simulation of Net Infiltration for Present-Day and Potential Future Climates.* MDL-NBS-HS-000023 REV 01. Las Vegas, Nevada: Sandia National Laboratories. ACC: DOC.20070530.0014. **174294**

SNL (Sandia National Laboratories) 2007. *Site-Scale Saturated Zone Transport.* MDL-NBS-HS-000010 REV 03. Las Vegas, Nevada: Sandia National Laboratories. ACC: DOC.20070822.0003. **177392**

SNL (Sandia National Laboratories) 2007. *Soil-Related Input Parameters for the Biosphere Model.* ANL-NBS-MD-000009 REV 03 AD 01. Las Vegas, Nevada: Sandia National Laboratories. ACC: DOC.20070927.0004. **179993**

SNL (Sandia National Laboratories) 2007. *Stress Corrosion Cracking of Waste Package Outer Barrier and Drip Shield Materials.* ANL-EBS-MD-000005 REV 04. Las Vegas, Nevada: Sandia National Laboratories. ACC: DOC.20070913.0001. **181953**

SNL (Sandia National Laboratories) 2007. *Technical Work Plan for: Igneous Activity Assessment for Disruptive Events.* TWP-WIS-MD-000007 REV 10. Las Vegas, Nevada: Sandia National Laboratories. ACC: DOC.20070830.0002. **182219**

SNL (Sandia National Laboratories) 2007. *Total System Performance Assessment (TSPA) Data Input Package for Tephra Redistribution.* TDR-TDIP-DE-000005 REV 00. Las Vegas, Nevada: Sandia National Laboratories. ACC: DOC.20070502.0014. **180667**

SNL (Sandia National Laboratories) 2007. *Total System Performance Assessment (TSPA) Data Input Package for Unsaturated Zone Radionuclide Transport Parameters Matrix Diffusion and Sorption.* TDR-TDIP-NS-000003 REV 00. Las Vegas, Nevada: Sandia National Laboratories. ACC: DOC.20070418.0009. **179301**

SNL (Sandia National Laboratories) 2007. *Total System Performance Assessment Data Input Package for Requirements Analysis for DOE SNF/HLW and Naval SNF Waste Package Physical*

Attributes Basis for Performance Assessment. TDR-TDIP-ES-000009 REV 00. Las Vegas, Nevada: Sandia National Laboratories. ACC: DOC.20070921.0009. **179567**

SNL (Sandia National Laboratories) 2007. *Total System Performance Assessment Data Input Package for Requirements Analysis for Engineered Barrier System In-Drift Configuration.* TDR-TDIP-ES-000010 REV 00. Las Vegas, Nevada: Sandia National Laboratories. ACC: DOC.20070921.0008. **179354**

SNL (Sandia National Laboratories) 2007. *Total System Performance Assessment Data Input Package for Requirements Analysis for Subsurface Facilities.* TDR-TDIP-PA-000001 REV 00. Las Vegas, Nevada: Sandia National Laboratories. ACC: DOC.20070921.0007. **179466**

SNL (Sandia National Laboratories) 2007. *Total System Performance Assessment Data Input Package for Requirements Analysis for Transportation Aging and Disposal Canister and Related Waste Package Physical Attributes Basis for Performance Assessment.* TDR-TDIP-ES-000006 REV 00. Las Vegas, Nevada: Sandia National Laboratories. ACC: DOC.20070918.0005. **179394**

SNL (Sandia National Laboratories) 2007. *Total System Performance Assessment Data Input Package for Seismic Consequence Abstraction.* TDR-TDIP-ES-000002 REV 00. Las Vegas, Nevada: Sandia National Laboratories. ACC: DOC.20070529.0008. **179652**

SNL (Sandia National Laboratories) 2007. *Total System Performance Assessment Data Input Package for Site-Scale Saturated Zone Breakthrough Curves.* TDR-TDIP-NS-000005 REV 00. Las Vegas, Nevada: Sandia National Laboratories. ACC: DOC.20070423.0004. **179412**

SNL (Sandia National Laboratories) 2007. *Total System Performance Assessment Data Input Package for Waste Form and In-Drift Colloids.* TDR-TDIP-NF-000002 REV 00. Las Vegas, Nevada: Sandia National Laboratories. ACC: DOC.20070515.0010. **180679**

SNL (Sandia National Laboratories) 2007. *UZ Flow Models and Submodels.* MDL-NBS-HS-000006 REV 03. Las Vegas, Nevada: Sandia National Laboratories. ACC: DOC.20070907.0001. **175177**

SNL (Sandia National Laboratories) 2007. *Waste Form and In-Drift Colloids-Associated Radionuclide Concentrations: Abstraction and Summary.* MDL-EBS-PA-000004 REV 03. Las Vegas, Nevada: Sandia National Laboratories. **177423**

Snow, J.K. and Wernicke, B.P. 2000. "Cenozoic Tectonism in the Central Basin and Range: Magnitude, Rate, and Distribution of Upper Crustal Strain." *American Journal of Science, 300,* (9), 659-719. New Haven, Connecticut: Yale University, Kline Geology Laboratory. TIC: 253039. **159400**

Software Code: EQ3/6 V. 7.2b. 1999. UCRL-MA-110662 (LSCR198). **153964**

Software Code: SZ_Convolute V. 3.0. 2003. PC, Windows 2000. 10207-3.0-00. **164180**

Soilexp_LA V. 1.0. 2004. WINDOWS 2000. STN: 10933-1.0-00. **167883**

Suzuki, T. 1983. "A Theoretical Model for Dispersion of Tephra." *Arc Volcanism: Physics and Tectonics, Proceedings of a 1981 IAVCEI Symposium, August-September, 1981, Tokyo and Hakone.* Shimozuru, D. and Yokoyama, I., eds. Pages 95-113. Tokyo, Japan: Terra Scientific Publishing Company. TIC: 238307. **100489**

SZ_CONVOLUTE V. 3.10.01. 2007. WINDOWS 2000 & WINDOWS 2003. STN: 10207-3.10.01-00. **181060**

Thatcher, W.; Foulger, G.R.; Julian, B.R.; Svarc, J.; Quilty, E.; and Bawden, G.W. 1999. "Present-Day Deformation Across the Basin and Range Province, Western United States." *Science, 283,* (5408), 1714-1718. Washington, D.C.: American Association for the Advancement of Science. TIC: 246227. **119053**

TOUGH2 V. 1.6. 2003. DOS Emulation (win95/98), SUN OS 5.5.1., OSF1 V4.0. STN: 10007-1.6-01. **161491**

TSPA_Input_DB V. 2.2. 2006. WINDOWS 2000. STN: 10931-2.2-00. **181061**

TSPA_Input_DB V. 2.2. 2006. WINDOWS 2003. STN: 10931-2.2-01. **181062**

USDA (U.S. Department of Agriculture) 2000. *Food and Nutrient Intakes by Individuals in the United States, 1994-1996.* Nationwide Food Surveys Report No. 96-3. Two volumes. [Washington, D.C.: U.S. Department of Agriculture]. TIC: 249498. **154158**

Waiting, D.J.; Stamatakos, J.A.; Ferrill, D.A.; Sims, D.W.; Morris, A.P.; Justus, P.S.; and Ibrahim, A.K. 2003. "Methodologies for the Evaluation of Faulting at Yucca Mountain, Nevada." *Proceedings of the 10th International High-Level Radioactive Waste Management Conference (IHLRWM), March 30-April 2, 2003, Las Vegas, Nevada.* Pages 377-387. La Grange Park, Illinois: American Nuclear Society. TIC: 254559. **164449**

WAPDEG V. 4.07. 2002. WINDOWS NT 4.0. STN: 10000-4.07-00. **161240**

WAPDEG V. 4.07. 2003. Windows 2000. STN: 10000-4.07-00. **181774**

WAPDEG V. 4.07. 2007. WINDOWS SERVER 2003. STN: 10000-4.07-01. **181064**

Warren, T.M. 1987. "Penetration-Rate Performance of Roller-Cone Bits." *Drilling.* SPE Reprint Series No. 22. Richardson, Texas: Society of Petroleum Engineers. TIC: 250084. **155234**

Williams, N.H. 2001. "Contract No. DE-AC08-01RW12101 – Total System Performance Assessment – Analyses for Disposal of Commercial and DOE Waste Inventories at Yucca Mountain – Input to Final Environmental Impact Statement and Site Suitability Evaluation REV 00 ICN 02." Letter from N.H. Williams (BSC) to J.R. Summerson (DOE/YMSCO), December 11, 2001, RWA:cs-1204010670, with enclosure. ACC: MOL.20011213.0056. **157307**

Williams, N.H. 2001. "Contract No. DE-AC08-01RW12101 – Uncertainty Analyses and Strategy Letter Report, REV 00, Activity #SA011481M4." Letter from N.H. Williams (BSC) to S.J. Brocoum (DOE/YMSCO), November 19, 2001, JM:cs-1116010483, with enclosure. ACC: MOL.20020109.0064. **157389**

Wittman, R.S.; Buck, E.C.; and Hanson, B.D. 2005. *Data Analysis of Plutonium Sorption on Colloids in a Minimal Kinetics Model.* PNNL-15285. Richland, Washington: Pacific Northwest National Laboratory. ACC: MOL.20050811.0087. **174895**

Yu, C.; Zielen, A.J.; Cheng, J.-J.; LePoire, D.J.; Gnanapragasam, E.; Kamboj, S.; Arnish, J.; Wallo, A., III; Williams, W.A.; and Peterson, H. 2001. *User's Manual for RESRAD Version 6.* ANL/EAD-4. Argonne, Illinois: Argonne National Laboratory. TIC: 252702. **159465**